

**Efforts Towards the Synthesis of Fully N-Differentiated Heparin-like Glycosaminoglycans
and
Investigations into the Mechanism of Inactivation of RTPR by Gemcitabine Triphosphate**

by

Gregory J. S. Lohman

B.S. Chemistry/B.S. Biology
Case Western Reserve University, 2000

Submitted to the Department of Chemistry
in Partial Fulfillment of the Requirements for the Degree of

Doctor of Philosophy in Organic Chemistry

at the

MASSACHUSETTS INSTITUTE OF TECHNOLOGY

[February 2007]
December 2006

© 2006 Massachusetts Institute of Technology

All rights reserved

Signature of Author: _____

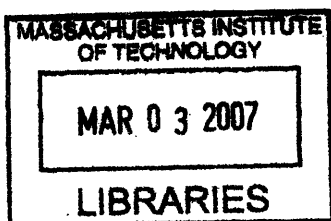
Department of Chemistry
December 1, 2006

Certified by: _____

Professor JoAnne Stubbe
Thesis Supervisor

Accepted by: _____

Professor Robert W. Field
Chairman, Departmental Committee on Graduate Students




ARCHIVES

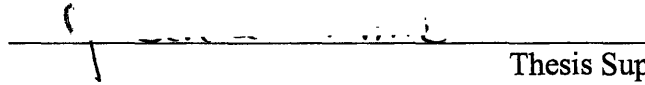
V.1

This doctoral thesis has been examined by a Committee of the Department of Chemistry as follows:

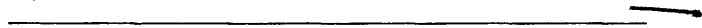
Professor ~~Richard~~ Danheiser


Chairperson

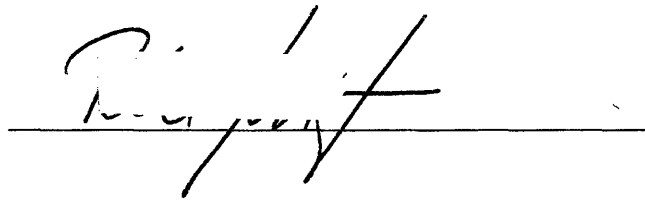
Professor JoAnne Stubbe


Thesis Supervisor

Professor Catherine Drennan



Professor Peter Seeberger



To my father and mother

Acknowledgements

I would like to thank my family for supporting me, not just in graduate school, but throughout my life. I'd like to thank my father in particular for all he's done to encourage my interest in science—without that basement greenhouse in 8th grade, I wouldn't be here today—and my mother for reading countless thousands of pages of book reports, history papers, lab reports and more, and my sister for being such a good friend.

I would like to thank my grandparents for all the wonderful things they gave me in life. I wish you could be here today.

I would like to thank my advisors in graduate school: Peter, for bring me to MIT in the first place, giving me an exciting project and making me the organic chemist I am today; and JoAnne, who took me in when I needed a new lab and taught me to think about mechanism and the scientific process in a whole new way.

I would like to thank all the members of the Seeberger and Stubbe laboratories with whom I worked with throughout the years, and those who came before me but without whom I could not have accomplished this work. In particular, I would like to thank Dan and Aaron, who both taught me so much, who were always willing to go over problems with me, and who have done more than anyone to keep me in good spirits.

I would like to thank Professors Drennan, Danheiser, and Licht for helpful discussions, advice, and support.

I would like to thank all my friends, especially Dan, Graham, Aaron, Diana, and Laura for keeping me sane, happy and social, and making sure I got out of the lab now and again! Particular thanks to Graham, who got me involved in music again.

Efforts towards the Synthesis of Fully *N*-Differentiated Heparin-like Glycosaminoglycans

By

Gregory J. S. Lohman

Submitted to the Department of Chemistry in December, 2006 in Partial Fulfillment of the Requirements for the Degree of Doctor of Philosophy in Organic Chemistry

ABSTRACT

Heparin-like glycosaminoglycans (HLGAGs) are complex information-carrying biopolymers and are an important component of the coagulation cascade. They have also been implicated in interactions with growth factors, cytokines, virus entry, and other functions. Currently, no general synthesis of arbitrary HLGAG sequences has been demonstrated. The modular synthesis of glycosaminoglycans requires straightforward methods for the production of large quantities of protected uronic acid building blocks. An efficient route to methyl 3-*O*-benzyl-1,2-*O*-isopropylidene- α -L-idopyranosiduronate from diacetone glucose in nine steps and 36% overall yield is described. Additionally, a general method for the conversion of glycols to the corresponding 1,2-*cis*-isopropylidene- α -glycosides is reported. Epoxidation of glycols with dimethyldioxirane followed by ZnCl₂-catalyzed addition of acetone converted a variety of protected glycols into 1,2-*cis*-isopropylidene- α -glycosides in good yield. The reaction is compatible with a range of protecting groups, as well as free hydroxyl groups. This method has been applied to develop a synthesis of 3-*O*-benzyl-1,2-*O*-isopropylidene- β -D-glucopyranosiduronate in seven steps and 32% overall yield. These compounds are useful as glycosyl acceptors and as intermediates that may be further elaborated into uronic acid trichloroacetimidate glycosyl donors for the assembly of glycosaminoglycan structures.

The glucosamine residues in HLGAGs have been found to exist as amines, acetamides, and *N*-sulfonates. In order to develop a completely general, modular synthesis of heparin, three degrees of orthogonal nitrogen protection are required. Reported is a strategy for the synthesis of fully *N*-differentiated heparin oligosaccharides in the context of target octasaccharide **3-1**, which contains an *N*-acetate, *N*-sulfonates, and a free amine. The protecting group scheme used in the synthesis blocked the *N*-acetate as a *N*-diacetate, the *N*-sulfonates as azido groups, and the amine as a *N*-CBz; free hydroxyls were masked as benzyl ethers and *O*-sulfonates as acetate esters. Disaccharide and tetrasaccharide modules were synthesized using this strategy; however, the union of tetrasaccharide trichloroacetimidate **3-4** with disaccharide acceptor **3-5** unexpectedly formed the undesired β -linked glycoside in addition to the α -linkage anticipated for iduronic acid nucleophiles, resulting in an inseparable 6:1 α : β mixture of products. Detailed studies into the basis for this unexpected result were conducted and are also reported.

Thesis Supervisor: Peter H. Seeberger

Title: Professor for Organic Chemistry, ETH, Zurich

Investigations into the Mechanism of Inactivation of RTPR by Gemcitabine Triphosphate

By

Gregory J. S. Lohman

Submitted to the Department of Chemistry in December, 2006 in Partial Fulfillment of the Requirements for the Degree of Doctor of Philosophy in Organic Chemistry

ABSTRACT

Ribonucleoside triphosphate reductase (RTPR) is an adenosylcobalamin (AdoCbl) dependant enzyme that catalyzes the conversion of nucleoside triphosphates to deoxynucleoside triphosphates via controlled radical chemistry. The antitumor agent 2',2'-difluoro-2'-deoxycytidine (gemcitabine, F₂C) has been shown to owe some of its *in vivo* activity to inhibition of human RNR by the 5'-diphosphate (F₂CDP). Previous studies have shown that RTPR is rapidly inactivated by one equivalent of 2',2'-difluoro-2'-deoxycytidine 5'-triphosphate (F₂CTP). This inactivation is associated with the release of two equivalents of fluoride and modification of RTPR by a Co—S bond between C419 and the cobalamin cofactor. In order to further characterize this inactivation, isotopically labeled derivatives of F₂CTP were synthesized: radiolabeled 1'-[³H]-F₂C and mass labeled 1'-[²H]-F₂C and 3'-[²H]-F₂C. These compounds were converted to F₂CTP through a set of enzymatic phosphorylation steps which overcome difficulties found using traditional, chemical methods.

Biochemical investigations were performed using these labeled derivatives to track the fate of the base and sugar during RTPR inactivation by F₂CTP. The release of cytosine base, previously overlooked in this system, was detected utilizing 5-[³H]-F₂CTP: 0.7 equiv. of cytosine were released, with 0.15-0.2 equiv. of unreacted F₂CTP remaining. Size exclusion chromatography (SEC) was used to quantify covalent labeling of RTPR by F₂CTP: 0.15 equiv. were detected using 5-[³H]-F₂CTP, 0.45 equiv. were detected using 1'-[³H]-F₂CTP. A small molecule nucleotide product was identified in inactivation mixtures quenched with NaBH₄ and identified as an isomer of cytidine, indicating the loss of both fluorides and the addition of an oxygen at the 2' carbon. RTPR inactivated with 1'-[³H]-F₂CTP was digested with trypsin and peptides containing radioactivity purified. Identical peptides were prepared using partially deuterated F₂CTP, allowing identification by MALDI-MS. Post source decay (PSD) MS/MS methods were used to further characterize these peptides, identifying the site of label as the C-terminal tryptic peptide of RTPR at C731 and C736. The cysteines were labeled through conjugate addition with a furanone-like precursor that had lost cytosine, triphosphate, and both fluorines. The results of these studies have allowed for the first time the proposal of a mechanistic hypothesis for RTPR inactivation by F₂CTP.

Thesis Supervisor: JoAnne Stubbe

Title: Novartis Professor of Chemistry and Biology

Preface

Portions of the work presented in Chapters 2 and 3 have appeared in the following publications:

1. Lohman, G. J. S.; Seeberger, P. H. "A Stereochemical Surprise at the Late Stage of the Synthesis of Fully *N*-Differentiated Heparin Oligosaccharides Containing Amino, Acetamido, and *N*-Sulfate Groups." *J. Org. Chem.* **2004**, *69*, 4081-4093.
2. Lohman, G. J. S.; Seeberger, P. H. "The one pot conversion of glycals to *cis*-1,2-isopropylidene- α -glycosides." *J. Org. Chem.* **2003**, *68*, 7541-7543.
3. Lohman, G. J. S.; Hunt, D. K.; Högermeier, J. A. Seeberger, P. H. "Synthesis of Iduronic Acid Building Blocks for the Modular Assembly of Glycosaminoglycans." *J. Org. Chem.* **2003**, *68*, 7559-7561.

Table of Contents

Acknowledgements	4
Abstract of Part I	5
Abstract of Part II	6
Preface	7
Table of Contents	8
List of Figures	11
List of Tables	15
List of Schemes	16
List of Abbreviations	18
Part I. Efforts Towards the Synthesis of Heparin-like Glycosaminoglycans	21
Chapter 1. The Synthesis of Heparin-like Glycosaminoglycans	23
1.1 Introduction	24
1.2 Structure and Conformation of Heparin and Heparan Sulfate	28
1.3 Biosynthesis	31
1.4 Heparin-Protein Interactions	32
1.5 The Chemical Synthesis of HLGAGs	39
1.6 Conclusions	66
1.7 References	66
Chapter 2. The Synthesis of Fully Differentiated Uronic Acid Monosaccharide Building Blocks for the Synthesis of Heparin-like Glycosaminoglycans	77
2.1 Introduction	78
2.2 Experimental	80
2.3 Results and Discussion	101
2.4 References	110

Chapter 3. A Stereochemical Surprise at the Late Stage of the Synthesis of Fully <i>N</i>-Differentiated Heparin Oligosaccharides Containing Amino, Acetamido, and <i>N</i>-Sulfonate Groups	115
3.1 Introduction	116
3.2 Experimental	119
3.3 Results and Discussion	144
3.4 References	157
Part II. Investigations into the Mechanism of Inactivation of RTPR by Gemcitabine Triphosphate	163
Chapter 4. Ribonucleotide Reductases: Mechanism and Inhibition	165
4.1 Overview	166
4.2 Ribonucleotide Reductases	169
4.3 Inhibitors of RNRs	183
4.4 Summary	206
4.5 References	207
Chapter 5. Synthesis of Isotopically-Labeled Gemcitabine (F2C) 5'-Phosphates	221
5.1 Introduction	222
5.2 Experimental	230
5.3 Results and Discussion	245
5.4 References	255
Chapter 6. Products of the Inactivation of Ribonucleoside Triphosphate Reductase by Gemcitabine Triphosphate	261
6.1 Introduction	262
6.2 Experimental	274

6.3 Results	288
6.4 Discussion	348
6.5 References	355
Appendix 1. Supporting Information for Part I	367
Appendix 2. Supporting Information for Part II	529
Curriculum Vitae	591

List of Figures

Figure 1-1. Features of carbohydrates.	25
Figure 1-2. Major disaccharide repeat units of the glycosaminoglycans.	26
Figure 1-3. The structure and sequence variability of HLGAGs.	29
Figure 1-4. Linker region tetrasaccharide.	29
Figure 1-5. Conformations of HLGAG-chain monosaccharides.	30
Figure 1-6. The high affinity ATIII binding sequence.	34
Figure 1-7. HSV-binding heparin octasaccharide sequence.	37
Figure 1-8. Challenges in the synthesis of HLGAGs.	40
Figure 1-9. Orthoester linkages.	41
Figure 1-10. Conformationally locked uronic acid acceptors.	50
Figure 1-11. First synthetic strategy for FGF binding HLGAGS.	57
Figure 1-12. Synthesis of FGF binding HLGAGS.	58
Figure 1-13. Modular strategy for HLGAG synthesis.	60
Figure 1-14. Modular synthesis of HLGAGs with a late-stage oxidation.	62
Figure 1-15. Modular synthesis of HLGAGs using a growing donor chain strategy.	63
Figure 2-1. Uronic acid acceptors for the synthesis of HLGAGs.	78
Figure 3-1. Target structure.	117
Figure 3-2. Retrosynthetic analysis.	119
Figure 3-3. Orthoester byproduct.	147
Figure 3-4. Glucosamine CBz acceptor.	148
Figure 3-5. Rearranged trichloroacetimidate donors.	150
Figure 3-6. HSQC spectrum of the anomeric region.	152

Figure 3-7. Rearrangement of alloc protected iduronates.	154
Figure 3-8. Proposed modular synthesis of HLGAGs.	155
Figure 3-9. Alternate disconnection of HSV binding octasaccharide.	156
Figure 4-1. The ribonucleotide reduction reaction.	167
Figure 4-2. Crystal structures of <i>E. coli</i> class I and <i>L. leichmannii</i> class II RNR.	171
Figure 4-3. A comparison of the α/β barrel fold found in the three classes of RNR.	171
Figure 4-4. The active site of <i>E. coli</i> class I and <i>L. leichmannii</i> class II RNR.	173
Figure 4-5. The active site of <i>S. cerevisiae</i> class I with ADP bound.	174
Figure 4-6. Generation of the thiyl radicals in the active site of RNRs.	177
Figure 4-7. Proposed mechanism of nucleotide reduction by RNR.	179
Figure 4-8. One electron oxidation of ethylene glycol.	180
Figure 4-9. Selenocarbonyl nucleotide model system of Giese and coworkers.	181
Figure 4-10. Disulfide interchange from the active site to the C-terminal tail.	182
Figure 4-11. Some nucleoside analog inhibitors of RNR.	184
Figure 4-12. Inhibition of RNR by 2' halonucleotides.	185
Figure 4-13. Reaction catalyzed by diol dehydratase.	186
Figure 4-14. 9 GHz EPR of the radical detected upon inactivation of RDPR with F ₂ CDP.	190
Figure 4-15. 140 GHz EPR of the radical detected upon inactivation of RDPR with F ₂ CDP.	191
Figure 4-16. Inactivation mechanism of F ₂ CDP and RDPR based on DFT calculations.	195
Figure 4-17. Crystal structure of CDP and F ₂ CDP in active site of yeast RDPR.	197
Figure 4-18. Products of inhibition of RNR by 2'-azido-2'-deoxynucleotides.	198
Figure 4-19. Inhibition of RNR by 2' azidonucleotides.	199
Figure 4-20. Inhibition of RNR by 2' fluoromethylene cytidine.	201
Figure 4-21. Proposed mechanism of inhibition of RNR by 2' mercapto-CDP.	203

Figure 4-22. RNR inhibitors that bind to the effector and activity sites.	204
Figure 4-23. Radical scavengers and iron chelators applied to the inhibition of RNR.	205
Figure 4-24. Structures of some RNR subunit-subunit interaction inhibitors.	206
Figure 5-1. Gemcitabine (F ₂ C).	222
Figure 5-2. Apparatus for production of BH ₃ :THF.	235
Figure 5-3. Anion exchange chromatography of the reaction of F ₂ CMP reaction.	250
Figure 6-1. Gemcitabine (F ₂ C).	262
Figure 6-2. Cellular metabolism of F ₂ C.	267
Figure 6-3. Proposed mechanism of F ₂ CTP inhibition of RTPR, “alkylative” pathway.	270
Figure 6-4. Proposed mechanism of F ₂ CTP inhibition of RTPR, “non-alkylative” pathway.	272
Figure 6-5. Outline of purification of labeled RTPR peptides and recoveries at each stage.	287
Figure 6-6. Time dependent inactivation of RTPR with F ₂ CTP (1 equiv.).	289
Figure 6-7. Analysis of cytosine release from RTPR/5-[³ H]-F ₂ CTP.	293
Figure 6-8. Analysis of small molecule products from RTPR/1'-[³ H]-F ₂ CTP.	297
Figure 6-9. Small molecule products from RTPR/1'-[³ H]-F ₂ CTP, NaBH ₄ treatment.	298
Figure 6-10. Isolation of small molecule products from RTPR/F ₂ CTP, NaBH ₄ treatment.	301
Figure 6-11. ¹ H-NMR of new products isolated from NaBH ₄ quench of RTPR/F ₂ CTP.	303
Figure 6-12. ¹ H-NMR of new products isolated from NaBH ₄ quench of RTPR/F ₂ CTP.	304
Figure 6-13. ¹ H-NMR of new products isolated from NaBH ₄ quench of RTPR/F ₂ CTP.	305
Figure 6-14. Isolation of small molecule products from RTPR/F ₂ CTP, NaBD ₄ treatment.	307
Figure 6-15. Deuterium incorporation at 2' and 3'.	309
Figure 6-16. Standards of cobalamin compounds at 25 μM.	310
Figure 6-17. UV-vis spectra of peptide-bound and solution phase products.	313

Figure 6-18. UV-vis spectra of peptide bound products.	316
Figure 6-19. UV-vis spectra of small molecules fraction.	317
Figure 6-20. UV-vis spectra of small molecules fraction. Subtraction spectra.	318
Figure 6-21. Summary of inactivation stoichiometry.	320
Figure 6-22. Stability of 1'-[³ H]F ₂ CTP-derived label on RTPR.	321
Figure 6-23. Separation of peptides from RTPR/1'-[³ H]-F ₂ CTP digested with trypsin.	323
Figure 6-24. Separation of peptides, RTPR/1'-[³ H]-F ₂ CTP, NaBH ₄ , digested w/ trypsin.	327
Figure 6-25. Predicted distribution of masses for the RTPR C-terminal peptide.	328
Figure 6-26. Full MALDI of Region I from the trypsin digest of RTPR/F ₂ CTP.	329
Figure 6-27. MALDI of Region I from the trypsin digest of RTPR/F ₂ CTP, expansion.	329
Figure 6-28. MALDI feature at 2004 Da.	330
Figure 6-29. MALDI feature at 2063 Da.	331
Figure 6-30. Reduction of ketones by NaBD ₄ .	334
Figure 6-31. Annotated MS/MS spectrum of the 2020 Da peptide.	336
Figure 6-32. PSD fragmentation along the peptide-bonds to give b type and y type ions.	336
Figure 6-33. MS/MS of peak at 2063 Da.	339
Figure 6-34. MS/MS of peak at 2004 Da.	340
Figure 6-35. Proposal for label structure and mechanism of formation.	343
Figure 6-36. Alternate proposal for label structure.	344

List of Tables

Table 2-1. Optimization of isoproylidenation reaction conditions.	107
Table 2-2. Substrate scope of isoproylidenation reaction.	108
Table 6-1. SEC of RTPR inactivated with 1'-[³ H] and 5-[³ H]-F ₂ CTP.	290
Table 6-2. Masses of the C-terminal tryptic peptide of RTPR.	333

List of Schemes

Scheme 1-1. Preparation of fully differentiated glucosamine derivatives.	43
Scheme 1-2. Approaches to the preparation of ido-configured sugars.	46
Scheme 1-3. Synthesis of iduronic acid glycosyl donors.	47
Scheme 1-4. Other methods for the preparation of iduronic synthons.	48
Scheme 1-5. Synthesis of idose and iduronic acid derivatives from diacetone glucose.	49
Scheme 1-6. Early syntheses of a HLGAG trisaccharide.	51
Scheme 1-7. Synthesis of an ATIII binding pentasaccharide.	53
Scheme 1-8. Second of the ATIII binding pentasaccharide.	54
Scheme 1-9. Synthesis of an ATIII binding pentasaccharide.	55
Scheme 1-10. Chemoenzymatic preparation of heparin chains.	65
Scheme 2-1. Synthesis of iduronic acid acceptor.	102
Scheme 2-2. Protection of the 4-OH of 2-1.	103
Scheme 2-3. Synthesis of iduronic trichloroacetimidates by selective ester cleavage.	104
Scheme 2-4. Synthesis of iduronic trichloroacetimidates via selective silylation.	105
Scheme 2-5. Conversion of glucals to 1,2-isopropylidenes.	106
Scheme 2-6. Synthesis of glucuronic acid acceptor.	109
Scheme 3-1. Synthesis of non-reducing end disaccharide.	144
Scheme 3-2. Synthesis of middle tetrasaccharide.	145
Scheme 3-3. Synthesis of reducing end disaccharide.	146
Scheme 3-4. Synthesis of second reducing end disaccharide	147
Scheme 3-5. Block coupling of tetrasaccharide donor and reducing end disaccharide.	149
Scheme 3-6. Model trisaccharide.	151

Scheme 5-1. First reported synthesis of F ₂ C.	224
Scheme 5-2. Second generation F ₂ C synthesis.	225
Scheme 5-3. Alternative synthesis of protected difluororibose.	227
Scheme 5-4. Isotopic labeling of F ₂ C.	228
Scheme 5-5. Chemical phosphorylation of F ₂ C.	229
Scheme 5-6. Enzymatic phosphorylation of F ₂ C.	229
Scheme 5-7. Purification and recovery of 5-14a .	245
Scheme 5-8. Synthesis of F ₂ C.	247
Scheme 5-9. Enzymatic phosphorylation of F ₂ C.	249
Scheme 5-10. Destruction of ADP by periodate cleavage.	250
Scheme 5-11. Synthesis of 3'-[² H]-F ₂ C.	255

List of Abbreviations

A	adenosine	ENDOR	electron-nuclear double resonance
Ac	acetate	EPR	electron paramagnetic resonance
AcOH	acetic acid	ESI	electrospray ionization
AdoCbl	adenosylcobalamin	ESEEM	electron spin echo envelope modulation
All	allyl	Et	ethyl
AMPPNP	adenosine 5'-(β,γ -imido)triphosphate	ET	electron transfer
ATIII	antithrombin III	Et ₂ O	diethylether
ATP	adenosine triphosphate	EtOAc	ethyl acetate
BME	β -mercaptoethanol	EVE	ethyl vinyl ether
Bn	benzyl	F ₂ C	2',2'-difluoro-2'-deoxycytidine
BSA	bovine serum albumin	FGF	fibroblast growth factor
Bu	butyl	FGFR	fibroblast growth factor receptor
Bz	benzoyl	FMC	2'-fluoromethylene-2'-deoxycytidine
C	cytidine	FT	Fourier transform
CBz, Z	<i>N</i> -Benzyloxycarbonyl	FU	fluorouridine
CIU	chlorouridine	F ₂ U	2',2'-difluoro-2'-deoxyuridine
CoA	coenzyme A	g	gravity
Cp	cyclopentenyl	G	guanosine
CS	chondroitin sulfate	GAG	glycosaminoglycan
CSA	camphor sulfonic acid	GalNAc	<i>N</i> -acetylgalactosamine
cv	column volume	gCOSY	gradient correlation spectroscopy
d	doublet	Glc	glucose
5'-dA	5'-deoxyadenosine	GlcA	glucuronic acid
DAST	(diethylamino)sulfur trifluoride	GlcNAc	<i>N</i> -acetylglucosamine
DBU	Diaza(1,3)bicyclo[5.4.0]undecane	GSCbl	glutathionyl cobalamin
DCC	<i>N,N'</i> -dicyclohexylcarbodiimide	HA	hyaluronic acid
dCK	deoxycytidine kinase	hCNT	human concentrative nucleoside transporter
DEAE	diethylaminoethyl	hENT	human equilibrative nucleoside transporter
DFO	desferoxamine	HEPES	4-(2-hydroxyethyl)-1-piperazineethanesulfonic acid
DFT	density functional theory	HMBC	heteronuclear multiple bond correlation
DIBAL-H	diisobutylaluminium hydride	HIV	human immunodeficiency virus
DIPC	diisopropylcarbodiimide	HLGAG	heparin-like glycosaminoglycan
DMAP	4-dimethylaminopyridine	HMDS	hexamethyldisilazane
DMDO	dimethyldioxirane	HOCbl	hydroxycobalamin
DMF	dimethylformamide	HSQC	heteronuclear single quantum correlation
DMT	dimethoxytrityl		
DNA	deoxyribonucleic acid		
dN	deoxynucleoside		
DP	diphosphate		
DS	dermatin sulfate		
DTT	dithiothreitol		
EDTA	ethylenediaminetetraacetic acid		

HPLC	high performance liquid chromatography	RFQ	rapid-freeze quench
HS	heparan sulfate	RNA	ribonucleic acid
HSV	herpes simplex virus	RNR	ribonucleotide reductase
HU	hydroxyurea	RTPR	ribonucleoside triphosphate reductase
IdoA	iduronic acid	s	singlet
IR	infrared	S•	thiyl radical
KS	keratin sulfate	SA	specific activity
Lev	levulinate	SAM	<i>S</i> -adenosylmethionine
m	multiplet	SEC	size exclusion chromatography
<i>m/z</i>	mass/charge ratio	Sia	siamyl
MALDI	matrix-assisted laser desorption/ionisation	t	triplet
MCA	monochloroacetate	T	thymidine
Me	methyl	TBAI	tetrabutylammonium iodide
MMT	monomethoxytrityl	TBAF	tetrabutylammonium fluoride
MP	monophosphate	TBDMS	<i>tert</i> -butyldimethylsilyl
Ms	methanesulfonate	TBAB	triethyl ammonium bicarbonate
MS	mass spectrometry	TBAP	tetrabutylammonium phosphate
MWCO	molecular weight cut-off	TCA	trichloroacetimidate
N	nucleoside	TDS	thexyldimethyl silyl
NADPH	nicotinamide adenine dinucleotide phosphate reduced form	TEMPO	2,2,6,6-tetramethylpiperidine-1-oxyl
NBS	<i>N</i> -bromosuccinimide	Tf	Trifluoromethanesulfonate
NDP	nucleoside diphosphate	TFA	trifluoroacetic acid
NMR	nuclear magnetic resonance	THF	tetrahydrofuran
NRE	non-reducing end	TIPS	tri- <i>iso</i> -propylsilyl
NTP	nucleoside triphosphate	TMS	trimethylsilyl
N ₃ U	azidouridine	TMSOTf	trimethylsilyl trifluoromethanesulfonate
PAPS	phosphoadenine-5'-phosphosulfate	TR	thioredoxin
PCC	pyridinium chlorochromate	Tris	trishydroxymethylaminomethane
PCET	proton-coupled electron transfer	TRR	thioredoxin reductase
PEP	phosphoenolpyruvate	Ts	toluene-4-sulfonate
PF	platelet factor	TLC	thin-layer chromatography
Ph	phenyl	TOF	time of flight
P _i	inorganic phosphate	TP	triphosphate
Piv	pivaloyl	U	units
PK	pyruvate kinase	U	uridine
PMB	<i>p</i> -methoxybenzyl	UA	uronic acid
PMP	<i>p</i> -methoxyphenyl	UDP	uridine diphosphate
PSD	post-source decay	UV	ultraviolet
pyr	pyridine	vis	visible
RDPR	ribonucleoside diphosphate reductase	Y•	tyrosyl radical
RE	reducing end		
Rf	resolution factor		

PART I:
**Efforts Towards the Synthesis of Fully *N*-Differentiated Heparin-like
Glycosaminoglycans**

Chapter 1
The Synthesis of Heparin-Like Glycosaminoglycans

1.1 Introduction

Carbohydrates in natural products

Carbohydrates, along with nucleic acids and proteins, are key information-carrying and structural polymers in biological systems. The biological and organic chemistry of carbohydrates is a field more than a century old, and comes with its own particular nomenclature (Figure 1-1).⁽¹⁾ Apart from nucleic acids, most monosaccharides involved in natural products are six-carbon hexoses. Hexoses exist almost entirely in their cyclic, pyranose (six-membered ring) forms, though they can also cyclize to a furanose (five-membered ring). Cyclization creates a new stereogenic center at this position, and each carbohydrate has α and β “anomers” as a result. The assignment of the α or β designation is based on the highest numbered asymmetric center; for glucose and its derivatives, the α anomer projects the substituent axially. In general, α has the C1 and C5 substituents on opposite faces of the sugar ring, β on the same face. These anomers can interconvert if the C1 hydroxyl is unmodified through a ring-opening and closing equilibrative process known as mutarotation.

Oligosaccharide chains often show a greater level of complexity than other biopolymers, as they can be branched and each sugar may be added to a different hydroxyl. When describing carbohydrate chains, the “reducing end” refers to the end of the chain possessing an unglycosylated C1 hydroxyl, the “non-reducing end,” the opposite. Linkages between sugars are noted with the anomeric stereochemistry and the connectivity: Glc $\alpha(1\rightarrow4)$ Glc means a glucose disaccharide connected with an α -linkage from the C1 of one glucose to the C4 of the other.

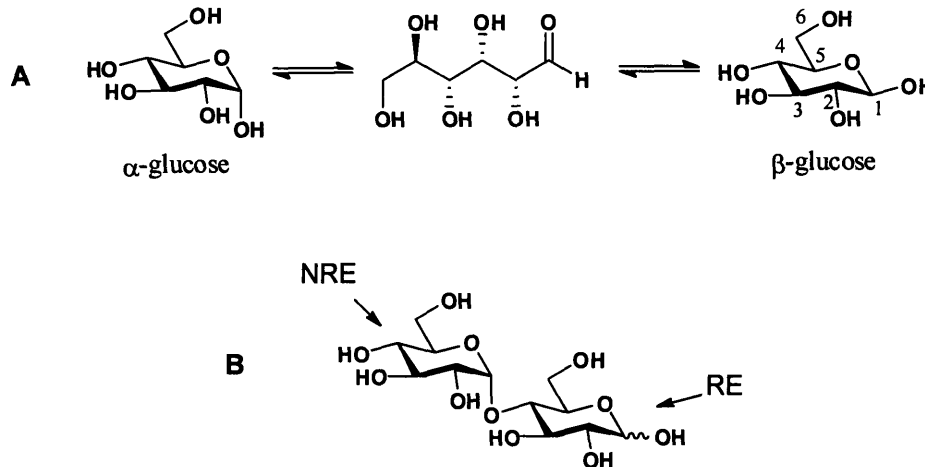


Figure 1-1. Features of carbohydrates. A) glucose—anomeric stereochemistry, mutarotation, and carbon numbering. B) Glc $\alpha(1 \rightarrow 4)$ Glc, with the reducing end (RE) and non-reducing ends (NRE) indicated.

Heparin and the glycosaminoglycans

Heparin and heparan sulfate (HS) are complex linear carbohydrates in the glycosaminoglycan family, found ubiquitously in the extracellular matrix and free in the plasma. In addition to heparin and HS, the glycosaminoglycans (GAGs) include keratan sulfate (KS), dermatin sulfate (DS), chondroitin sulfate (CS), and hyaluronic acid (HA).⁽²⁻⁴⁾ All these polymers consist of a repeating disaccharide structure, consisting of a hexosamine (galactosamine in the case of DS and CS, glucosamine for KS, HA, and HS) alternating with a hexauronic acid (glucuronic acid or iduronic acid). Excepting HA, all classes are additionally sulfated to varying degrees, and are among the most highly charged biopolymers. The repulsion due to this densely-packed negative charge lends these polymers rigidity, and several GAGs play important structural roles in the extracellular matrix. All are found conjugated to proteins bound to the extracellular matrix, generally to serine residues of proteoglycan core proteins. Unconjugated heparin and HA are found free in the plasma, and GAGs may also be found in intracellular granules and at the cell surface.

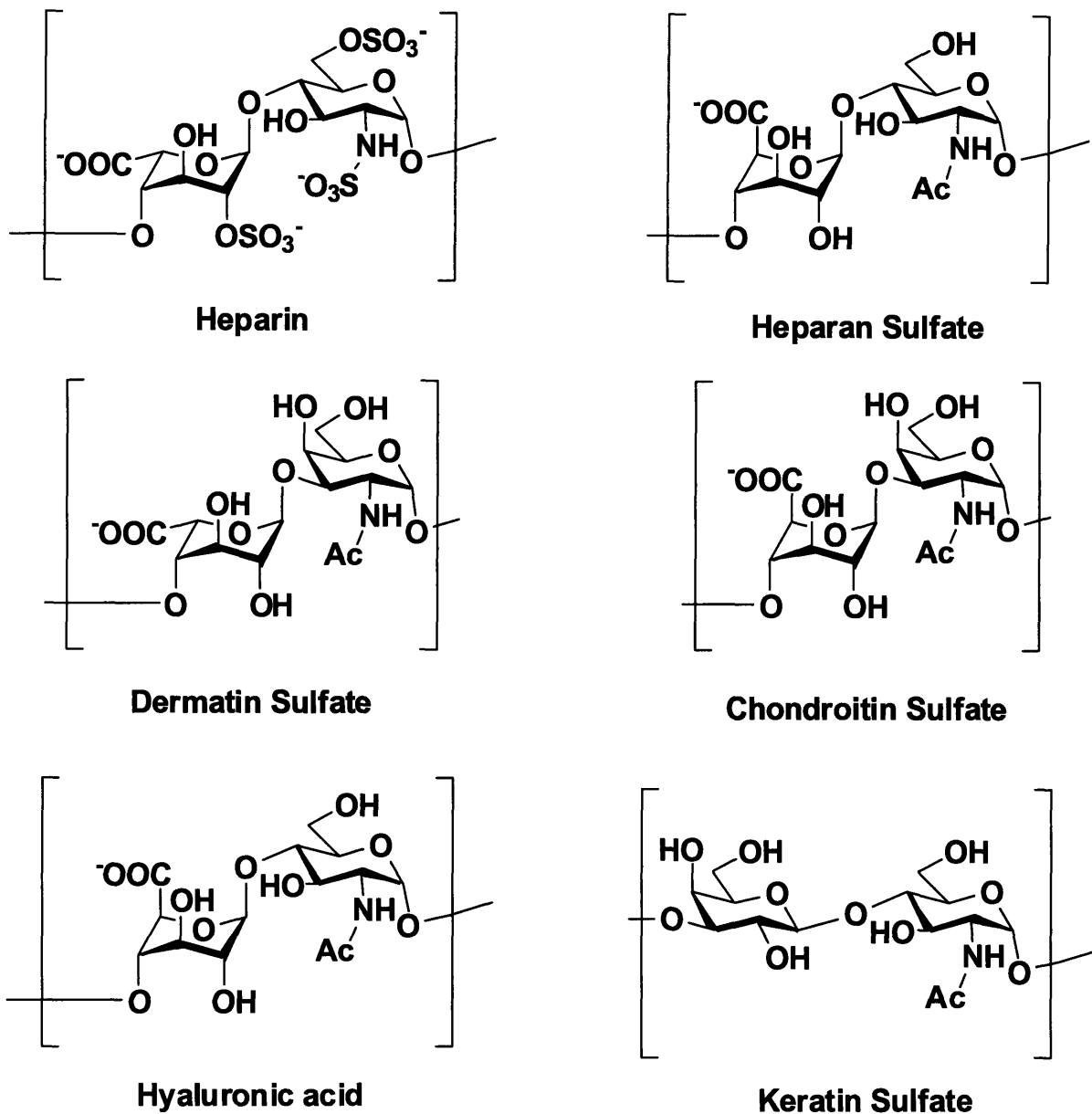


Figure 1-2. Major disaccharide repeat units of the glycosaminoglycans; all but heparin contain primarily unsulfated backbones as shown. In their variable sequences, heparin, HS, and DS may contain either iduronic or glucuronic acid. Heparin/HS may be sulfated, acetylated, or unmodified at the amine; Heparin/HS may be sulfated at the uronic acid 2OH or the glucosamine 3OH or 6OH; DS maybe sulfated at the galactosamine 4OH and CS at the galactosamine 4OH or 6OH and both at either uronic acid OH; KS at the 3OH or 6OH of the glucosamine.

GAGs are implicated in a variety of cellular functions aside from simple structural roles, including adhesion, motility, cell-cell recognition, proliferation, and tissue differentiation. Further, many sequences have been shown to act as specific ligands for protein receptors. While each class of GAG has a predominant disaccharide repeat “monomer” (Figure 1-2) that defines

the structure, most proteoglycan chains show variability in sulfation and acetylation patterns. CS and DS consist primarily of *N*-acetylgalactosamine (GalNAc)→uronic acid (UA) repeats, but variable sulfation and the presence of both iduronic acid (IdoA) and glucuronic acid (GlcA) result in nine possible disaccharide units. Heparin and heparan sulfate chains are even more variable, with the core *N*-acetyl glucosamine (GlcNAc) → UA structure differentiated through sulfation, acetylation and the selection of iduronic or glucuronic acid to give rise to as many as 48 different disaccharides. This sequence variability can grant proteoglycans a very high information density, enabling many different protein-GAG interactions that result in the diverse biological functions of GAGs.

Heparin and heparan sulfate are extremely closely related polymers in structure, function, and biogenesis, and are often considered variations on the same biopolymer class.(2, 5-13) Collectively, these carbohydrates are known as heparin-like glycosaminoglycans (HLGAGs) and will often be considered together in this document. Heparin, named after the hepatic tissue from which it is isolated, was originally discovered in 1916 and has been used therapeutically for its anti-coagulant effects since the 1930s.(14, 15) Heparan sulfate was first identified as an impurity in heparin preparations, and its close structural similarity to heparin was not determined for several decades. In addition to differences in the primary disaccharide repeat, heparin and HS vary on a few other points. Heparin is found bound to a proteoglycan core protein (serglycin) only in mastocytes and is cleaved from this protein and secreted into the serum as a glycosaminoglycan chain. Its uronic acid is predominantly (90%) iduronic acid, and it possesses a very high degree of sulfation (2.7 sulfates per disaccharide on average).(9) By contrast, heparan sulfate is found ubiquitously in the extracellular matrix throughout the body, possesses

approximately equal fractions of glucuronic to iduronic acid, and is significantly less sulfated than heparin.

Together, the HLGAGs are the best studied class of glycosaminoglycans. In addition to their clinical relevance as inhibitors of the coagulation cascade, HLGAGs have been implicated in interactions with growth factors, cytokines, virus entry, and other functions.(2, 7-9, 16) Biological study of these polymers has long been hampered by a lack of defined sequences for study; heparin isolated from animal systems is very heterogeneous and difficult or impossible to purify into defined sequences. Sequencing and structure identification is also difficult, further complicating attempts to define sequence-function relationships in heparin. Consequently, there has been much effort to devise synthetic strategies for defined heparin sequences—initially for individual structures, but increasingly with an eye towards a general, modular synthesis of the polymer. The remainder of this chapter will present an overview of HLGAGs structure and biological interactions, followed by an extensive review of the synthesis of HLGAGs and related compounds in the literature.

1.2 Structure and Conformation of Heparin and Heparan Sulfate

Heparin and heparan sulfate consist of the repeating 1→4 linked disaccharide structure shown in Figure 1-3. All glucosamines in the structures are $\alpha(1\rightarrow4)$ linked to a uronic acid; the acids are similarly 1→4 linked to the next glucosamine in the sequence. The anomeric stereochemistry of the uronic acids is 1,2-*trans*, which is defined as β for glucuronic acid and α for iduronic acid. As shown in Figure 1-3, in addition to the variability in stereochemistry at C5 of the uronic acids, HLGAG disaccharides may be sulfated at the 2 position of the uronic acids and at the 3 or 6 positions of the glucosamines. The amine may also be sulfated, acetylated, or,

rarely, unmodified,(17) giving a total of 48 possible disaccharide units, though only about half of these have been observed in natural structures.(18)

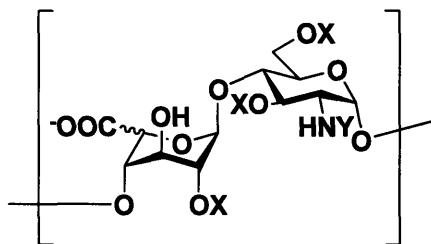


Figure 1-3. The structure and sequence variability of HLGAGs. X = H or SO₃⁻, Y = Ac, H, or SO₃⁻. The stereochemistry of the uronic acid may be *gluco* or *ido*.

HLGAG chains may be dozens to hundreds of these disaccharide units in length, ranging in molecular weight from 5 to 50 kDa with an average of ~12 kDa for free heparin and ~30 kDa for protein-conjugated HS chains.(6) In general, they are structured in a block-polymer fashion, with long stretches of the major repeat disaccharide interspersed with “variable regions” that display a greater heterogeneity in sulfation. Heparin chains primarily consist of the triply-sulfated disaccharide shown in Figure 1-3. With an average charge of -75, heparin chains are the most densely charged natural polyelectrolyte known. HS chains are generally found conjugated to proteoglycan core proteins through a defined linker region tetrasaccharide (Figure 1-4).(19) The HS chain is attached to the 4-OH of the glucuronic acid.

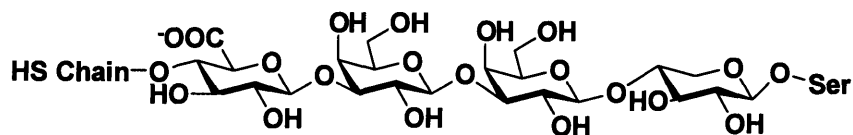


Figure 1-4. Linker region HS-GlcA-Gal-Gal-Xyl-PG.

In heparin, the glucosamine and glucuronic acid residues are expected to take the ⁴C₁ conformation in solution, placing the majority of substituents equatorial (Figure 1-5).(20-25) Conformational dynamics studies indicate that iduronic acid possesses two conformations of approximately equal energy, the ¹C₄ chair and ²S₀ skew-boat conformations.(26, 27) The

preferred conformation of the iduronic residues is believed to be strongly influenced by the sulfation pattern of surrounding glucosamine residues. The specific conformation of iduronic residues has been implicated in protein binding, and protein-bound heparin sequences may favor one conformation over the other.(21, 28-31)

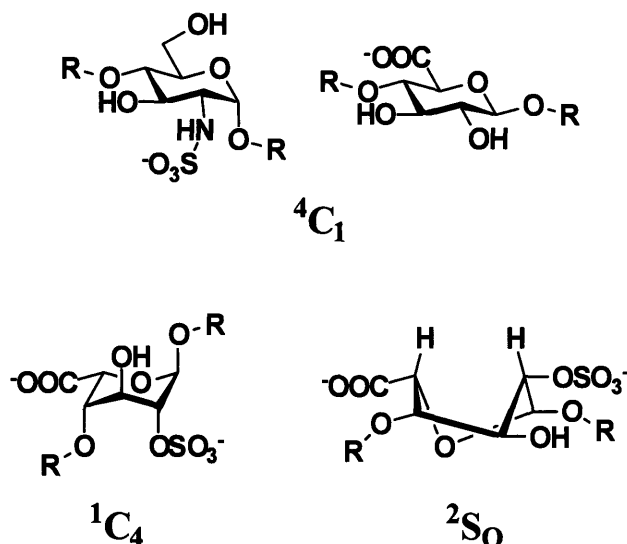


Figure 1-5. Conformations of HLGAG-chain monosaccharides.

Heparin does not fold into stable, complex secondary structures as do proteins and RNA: the general secondary structure of highly charged heparin chains is an α -helical structure with a turn every 5 residues.(23, 24, 32) The iduronic acids in these structures may be in either the 1C_4 or 2S_0 conformations without affecting the overall chain structure, and inter-conversion between these forms is allowed within a helix. The secondary structure of HS is less well defined—while the individual glucosamine and glucuronic acid residues are expected to maintain the 4C_1 conformation, the lack of dense charge in extended regions means that the rotation about the glycosidic bonds is relatively unhindered. The secondary structures of HLGAGs are flexible, and the polymers have been shown to adopt more rigid conformers upon interaction with protein ligands.(28, 33)

1.3 Biosynthesis

Extensive reviews of HLGAG biosynthesis and the enzymes involved have been published;(7, 11, 18, 34) a brief overview is presented here. Assembly of HS chains takes place within the Golgi apparatus as a non-template-driven process. Initiation of biosynthesis takes place by assembly of the linker region (Figure 1-4) on serine residues on the core proteins. The initial reaction is the glycosylation of a protein serine residue with UDP-xylose. Two galactose units are added sequentially, each by a different galactosyl transferase. Finally, UDP-glucuronic acid is added by glucuronyl transferase I. The linkage-region tetrasaccharide is assembled identically for both HS and CS chains. It is believed that the next glycosylation determines the identity of the growing chain. In the case of HS, *N*-acetylglucosaminyl transferase I attaches an *N*-acetylglucosamine $\alpha(1\rightarrow4)$ to the terminal glucuronic acid of the linkage tetrasaccharide.

Chain elongation is controlled by two enzymes: glucuronyl transferase II and *N*-acetylglucosaminyl transferase II. The HS chain is elongated through alternating $\beta(1\rightarrow4)$ glucuronic acid and $\alpha(1\rightarrow4)$ *N*-acetylglucosamine monosaccharides. A number of other enzymes act on the elongating polysaccharide chain to elaborate it into the final complex, heterogeneous structure. This process is not random and it appears that the actions of each enzyme generate sequence-specific binding sites for later enzymes. The initial modification is by *N*-acetylglucosamine deacetylase/*N*-sulfotransferase, which cleaves some of the *N*-acetyl groups and replaces them with *N*-sulfonates. Unmodified glucosamines are likely the result of “missed” sulfations by this enzyme. Following the *N*-deacetylase/sulfotransferase, a C5-glucuronyl epimerase acts to introduce iduronic acids to the chain. Iduronic acid is only incorporated via this method, as no iduronyl-UDP or iduronyl transferases are known to exist in nature. Finally, a group of *O*-sulfotransferases act to add sulfates at the 2-OH of glucuronic acid

or iduronic acid, or at the 3- and 6-OH positions of the glucosamines; different enzymes catalyze the sulfation of each sugar.

The variation in structure and sulfation patterns itself comes from the presence of multiple isoforms of each of the basic sulfation enzymes, each with different substrate specificity. In addition, the epimerase specificity seems to be strongly affected by the presence of *O*-sulfates both on the glucuronic acid and on neighboring glucosamines. Likewise, the specificity of some sulfotransferase enzymes is influenced by both the uronic acid stereochemistry and the existing sulfation patterns. This complex and, as yet, incompletely understood biosynthetic pathway gives rise to the incredible diversity of HLGAG structures, and allows the assembly of specific binding sites for protein interactions.

1.4 Heparin-Protein Interactions

Heparin and HS sequences have been shown to interact with a range of protein targets fulfilling diverse biological functions.(5-9, 13, 35, 36) Heparin binding sites on proteins are characterized by collections of basic residues in shallow channels on the surface of the proteins. Early work suggested heparin consensus binding sequences of XBBXBX and XBBBXXBX (where B is a basic amino acid and X is a hydrophobic residue).(16) Subsequent work showed many heparin-binding proteins do not possess these motifs—instead, binding sites are assembled from spatially-arranged basic residues that are distant in primary sequence.(16)

Proteins can bind heparin in non-specific modes defined primarily by ionic interactions, with regions of positively-charged basic amino acids interacting with heparin as a polyanion. Several studies, particularly of the thrombin-heparin binding domain,(37) have shown that some proteins will strongly bind other polymers carrying high negative charge such as sulfated(38, 39)

or phosphorylated(40, 41) derivatives of polyglucose, sulfated sucrose derivatives,(42) and even non-carbohydrate polyanions such as polyacrylic acids.(43) Other interactions between HLGAGs and protein binding sites are highly specific, with proteins recognizing only particular sulfation patterns and uronic acid stereochemistry and conformation.

Thrombin/Antithrombin and the coagulation cascade

The clinical effectiveness of heparin as an anticoagulant derives from its role in the activation of antithrombin III (ATIII), a key player in the coagulation cascade.(14, 15) The coagulation cascade requires sequential activation of a number of proteins.(2, 7, 9) Factor Xa is a serine protease that converts pro-thrombin into active thrombin, which is itself a protease that converts fibrinogen into fibrin monomers that crosslink into insoluble fibers within the clot. The protein antithrombin III (ATIII) inhibits both proteases in a heparin-dependant manner. Binding to short heparin structures triggers a conformational change that allows ATIII to inhibit the action of factor Xa. Binding to longer sequences allows the formation of a ternary ATIII-heparin-thrombin complex where ATIII inhibits the action of thrombin. Once brought into close proximity by the templating of the heparin strand, ATII binds to and inhibits thrombin with 2000-fold greater efficiency than in the absence of heparin. The heparin strand can be released back into circulation, leaving the inhibitor-protease complex intact.(44, 45)

ATIII binds with high affinity to a specific pentasaccharide sequence (Figure 1-6), initially identified through the chemical synthesis of several HLGAG structures.(46) A crystal structure of ATIII bound to this synthetic pentasaccharide confirmed the specific interaction of the protein to this ligand.(45) Binding to this pentasaccharide causes a conformational change that increases ATIII's affinity for factor Xa, but not towards thrombin. Much longer sequences

(at least 15-16 saccharides) are required to initiate thrombin inhibition.(39, 47) A recent crystal structure of a thrombin-ATIII-heparin mimetic complex(48) confirmed that this requirement relates to the template-driven association of these two proteins by one heparin strand. ATIII binds specifically to the pentasaccharide, while thrombin binds non-specifically to a length of heparin carrying high charge.(37) In the case of many synthetic therapeutics, a highly sulfated or phosphorylated polyglucose structure is substituted for heparin.(47) A flexible spacer region 56 atoms in length between the pentasaccharide and the charged region gave optimal binding.

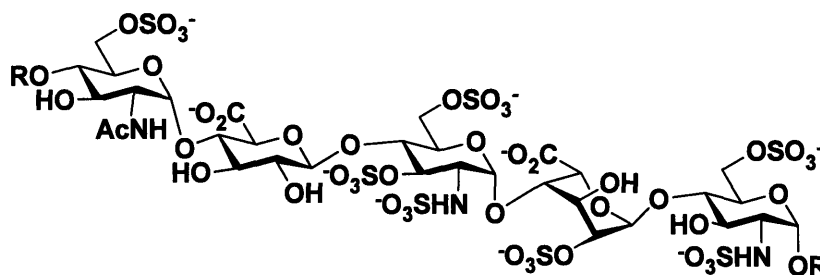


Figure 1-6. The high affinity ATIII binding sequence. R = the continuation of the HLGAG chain.

The pentasaccharide-ATIII crystal structure shows some interesting features of the specific interaction.(45) The helix is “overwound,” resulting in a bend which maximizes van der Waals contact. Further, the iduronic acid moiety is bound in the 2S_0 conformation.(25, 29) Binding studies with synthetic compounds locking the iduronic acid ring in either the 1C_4 or 2S_0 conformation confirm that this conformation is required for maximal binding.(30, 31) Finally, many interactions are evident between the 3-*O*-sulfate and the protein, indicating a key role in binding for this moiety. Structure-function studies have confirmed that this modification is necessary for binding,(44, 49) and its addition to heparin strands is the key biosynthetic event that creates the ATIII binding site.(50, 51)

Fibroblast growth factor

Another extremely well-studied HLGAG interaction is with the acidic (FGF-1) and basic (FGF-2) fibroblast growth factors.(2, 7, 9, 13) The fibroblast growth factors are a set of more than twenty related proteins involved in intercellular signaling, regulating cell differentiation and proliferation and expressed primarily during embryonic development.(52) The binding of FGFs to receptors (FGFR) on the cell surface triggers changes in gene expression mediated through a cytosolic tyrosine kinase domain on the FGFR proteins. The binding of HLGAGs to FGF proteins potentiates their activities, and increases binding affinity for their receptors by a hundred fold or more.

Several crystal structures of FGF co-crystallized with HLGAG structures have been reported.(53-56) Evidence from these structures indicates that a single HLGAG chain can bridge two FGF-1-FGFR interactions in a 2:2:1 FGF-1:FGFR:HS complex, while FGF-2 forms a 2:2:2 FGF-2:FGFR:HS complex.(57) The HS sequences associated with FGF proteins in the crystal structures were made up of the standard heparin disaccharide repeat [IdoA2S-GlcNS6S]_n (Figure 1-2) where n=2-7. Tetra and hexasaccharides will bind FGF-1 and FGF-2 with high affinity, but at least an octasaccharide is required to form the FGF-FGFR complexes. The crystal structures generally show the iduronic acid residues in the ²S_O conformation, though NMR evidence suggests that the iduronic acid in heparin structures bound to FGF may exist in either the ¹C₄ or ²S_O conformations and interconvert between the two.(58)

The FGF-2-HS-FGFR complex is thought to form near the non-reducing end of HS chains.(59) One FGF-2 and one FGFR bind, mediated by a single HS chain in a 1:1:1 complex. Two of these units then associate, forming a 2:2:2 complex. In proposed models of FGF-1-FGFR complex formation, the apparent 2:2:1 ratio is invoked to explain why FGF binding of

short HLGAG sequences does not allow complex formation—two FGFs must bind to a dimer of FGFR proteins, requiring HLGAG chains long enough to simultaneously bind two FGF molecules. (57)

While most crystal structures show FGF binding to an extended disaccharide repeat, evidence exists that FGF and FGFR have varying specificities for different HS structures. For example, while a decasaccharide of this repeat is also the minimum length necessary for biological activity, shorter sequences prepared synthetically have been shown to activate the complex *in vitro* as well.(60) Studies involving tissue-derived HS fractions have shown markedly larger increases in complex formation than treatment with heparin preparations, indicating tissue and protein related differences in the specificity of FGF family members for various HLGAG structures. Binding specificity has been hypothesized to relate closely to van der Waals contact between the protein and HLGAG chains, not simply ionic interactions, and specific binding is associated with a formation of a “kink” in the helical heparin secondary structure.(28)

Virus entry into cells

Heparan sulfate chains in the extracellular matrix have been implicated in the initial attachment of a number of viruses to potential host cells.(8, 9, 35, 61) The initial recognition/binding step often results from the interaction of a viral coat protein and a ligand on the surface of the target cell. Heparan sulfate is found on the surface of most mammalian cells and the specific sulfation patterns are expressed in a tissue specific manner.(3, 10) Unsurprisingly, it is a common ligand for recognition and binding of targets by virus particles. Heparan sulfate has been implicated in the binding and cell entry in a wide range of pathogens,

including herpes simplex virus (HSV), dengue virus, human immunodeficiency virus, Epstein-Barr virus, cytomegalovirus, vaccinia virus, hepatitis C, human papillomavirus and others,(61) as well as non-viral pathogens such as the malaria parasite *Plasmodium falciparum*.(9, 62)

The infection of cells by the herpes simplex virus types 1 and 2 (HSV-1 and HSV-2) is a particularly well characterized interaction involving the HS-binding event.(63, 64) Initial contact and cell binding is facilitated by two viral coat proteins, gB and gC. These proteins bind to cell-surface HS and greatly enhance infectivity, but are not required for infection. Deletion of gC results in a 10-fold lower infectivity. Deletion of gB eliminates infectivity, but only because it plays a role in later entry events—elimination of the HS binding domain also reduces but does not eliminate infectivity. The identity and specificity of the HS sequences bound by gB and gC are not yet known, but appear to differ for each protein and between HSV-1 and HSV-2. The key HS-binding event for cell entry is the interaction with another coat protein, gD, and a specific HS octasaccharide sequence.(65-67) As in a number of other heparin-protein interactions, the action of the 3-*O*-sulfotransferase that adds the reducing-end 3-*O*-sulfate is key to the generation of a tight-binding sequence.(67)

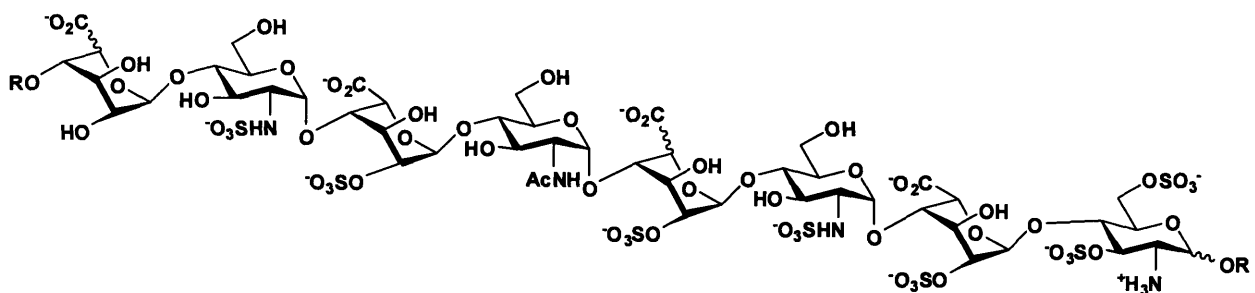


Figure 1-7. HSV-binding heparin octasaccharide sequence involved in viral cell entry, UA-GlcNS-IdoUA2S-GlcNAc-UA2S-GlcNS-IdoUA2S-GlcNH₂3S6S. Counter ions are typically sodium. The stereochemistry of two of the uronic acids is unknown due to artifacts of the sequencing procedure.(66)

HS-binding also plays several roles in human immunodeficiency virus infection.(9, 61, 68) Heparin binds the HIV coat protein gp120, assisting in association and cell-entry of the

virus. T cells treated with heparinase showed substantially lower association with viral particles. HS also binds the Tat protein, a factor released by HIV and believed to prime cells for infection. It is speculated that HS binding is responsible for Tat protein entry into cells. The Dengue virus has also been shown to interact with HS in a sequence specific manner,(69) as has the virus responsible for foot and mouth disease.(70) It is clear that HS is a key player in a wide range of infection processes. Consequently, heparin-like therapeutics may be valid anti-viral lead compounds.

Chemokines, Annexins, and other interactions

HLGAGs have been shown to play key roles in the regulation of several other protein systems. Chemokines are signaling proteins involved in many processes, particularly those associated with inflammation and wound repair.(7, 9, 36) Many chemokines bind HLGAGs, and these interactions seem to play a particular role in cell migration by maintaining chemokine gradients and giving specific directionality to cell migration. Mutant chemokines with reduced HLGAG binding ability were shown to be unable to initiate cell migration *in vivo*.(71) A number of HS sequences that bind chemokines have been identified, and tend to consist of a stretch of highly sulfated residues (6-12 sugars long, depending on the chemokine) separated by a variable, *N*-acetylated linker region. Chemokine interactions can have important clinical consequences as well: interaction of heparin with the chemokine platelet factor PF-4 can trigger a loss of platelets. This interaction is the cause of heparin-induced thrombocytopenia, a dangerous condition that can result from the administration of heparin as an anticoagulant.

Annexins are another family of HLGAG-binding proteins found bound to cell membranes in a Ca^{+2} -dependant manner and implicated in a range of cellular signaling

functions.(6, 9, 72) Heparin binds to annexin V by wrapping around the protein, making contact with three separate heparin-binding domains.(72) This complex in turn plays a role in an antithrombic (anticoagulant) array on the cell surface. Other characterized heparin-protein interactions include binding to apolipoprotein E, a range of extracellular matrix proteins, and numerous lipases and proteases in addition to antithrombin. The details of many HLGAG-protein interactions are poorly understood, and the area remains one of active research.

1.5 The Chemical Synthesis of HLGAGs

The organic chemistry of carbohydrates

The synthesis of oligosaccharides and carbohydrate-containing natural products involves many challenges particular to the molecules.(1, 73-76) Synthesis of carbohydrates with well defined connectivity and stereochemistry requires selective protection of 3-5 hydroxyls on each sugar.(77) Through taking advantage of reactivity differences between the hydroxyls, such as the primary hydroxyl versus the secondary hydroxyls, or the altered acidity of the anomeric hydroxyl, one may generate a carbohydrate differentially protected at each position. Protecting groups are often described as “permanent,” groups to be removed only in the final stages of the synthesis, and “temporary,” those installed and removed during the selective protection of the monosaccharides or used to block positions to be glycosylated when forming polysaccharides.

Further, one must plan how to assemble the molecule. Much of modern chemical synthesis favors a convergent model, where the molecule is divided into fragments of approximately equal size and synthetic complexity, and assembled in the end via a few block couplings of these fragments. In carbohydrate chemistry, it is often more convenient and practical to assemble the molecule in a linear fashion, adding mono- or disaccharide units onto a

growing chain similar to the method commonly employed in DNA and protein synthesis. This construction may proceed in either direction. Glycosyl “donors,” sugars with a reactive leaving group at C1, may be added to the non-reducing end. Removing a temporary protecting group from the product will generate a new glycosyl “acceptor,” a carbohydrate with a free hydroxyl that can react with another donor. Alternatively, monosaccharide acceptors may be reacted with a long-chain donor, and a temporary protecting group removed from C1 at each stage to generate a new donor.

Challenges of HLGAG synthesis

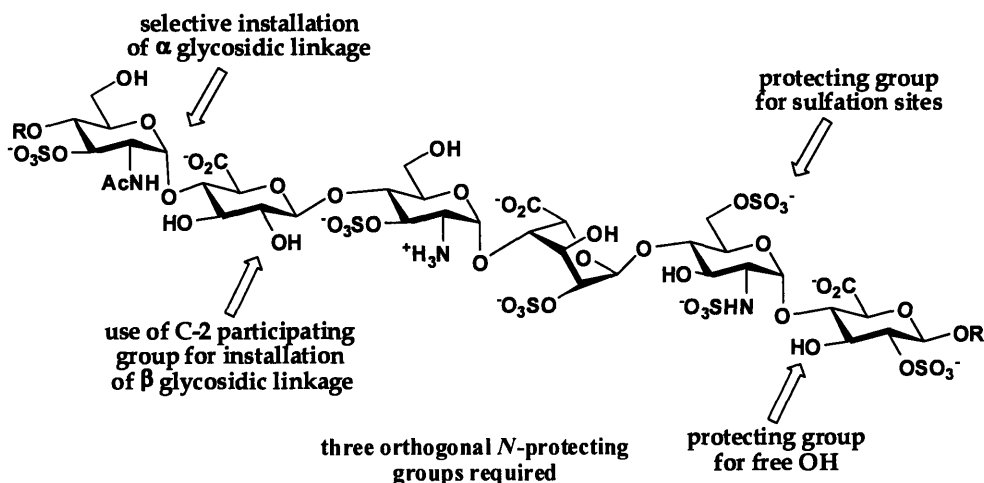


Figure 1-8. Challenges in the synthesis of HLGAGs.

The synthesis of HLGAGs in particular, though an active area of research for over twenty years, remains a daunting task with many synthetic challenges to overcome.^(5, 19, 46, 47, 78, 79) Figure 1-8 illustrates the features of a HLGAG of particular interest to the synthetic chemist. While HLGAGs are linear polymers, they possess an additional level of complexity in the wide variety of sulfation patterns possible. Any synthesis of HLGAGs must include two types of orthogonally-cleavable permanent protecting groups—one to mask free hydroxyls, and one that blocks positions to be sulfated. Further, syntheses must incorporate *three* orthogonal degrees of

nitrogen protection, to allow for the installation of *N*-sulfonates, *N*-acetates, and unmodified amines in the final structures. This problem had not yet been addressed in any published synthesis of HLGAGs at the time of the work described in Chapters 2 and 3.

Additional constraints on the choice of protecting groups in HLGAG synthesis are added by the need to control the stereochemistry of each glycosyl coupling. All the uronic acid residues possess 1,2-*trans* stereochemistry, meaning use of a “participating” ester or carbonate protecting group on the 2-OH should allow selective installation of this geometry via anchimeric assistance. However, iduronic acids in particular are prone to the formation of stable orthoesters rather than the desired glycosyl linkage (Figure 1-9).⁽⁸⁰⁻⁸³⁾ More difficult still is the selective installation of the glucosamine α -linkage. Allowing a 1,2-*cis* linkage requires the use of a non-participating protecting group at C2, drastically restricting the chemistries available. All HLGAG syntheses to date have used an azide at this position. Next, careful choice of donor chemistry, acceptor conformation, or other reaction conditions must be applied to favor the α -isomer—while the anomeric effect generally favors the axial isomer, the production of any quantity of the β isomer is likely to mean a difficult separation and loss of material at each coupling step.

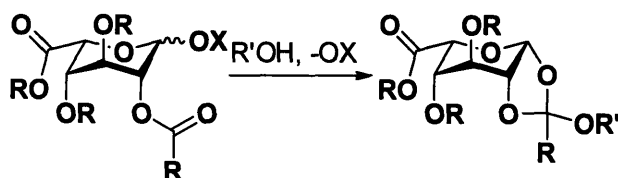


Figure 1-9. Orthoester linkages.

Finally, the order of assembly must be carefully chosen. HLGAG chains could be assembled by alternate couplings of uronic acid and glucosamine glycosyl donors, or through disaccharide “monomers” with either the uronic acid or glucosamine at the reducing end. Block couplings between larger precursors are also possible, and as in any carbohydrate synthesis, one

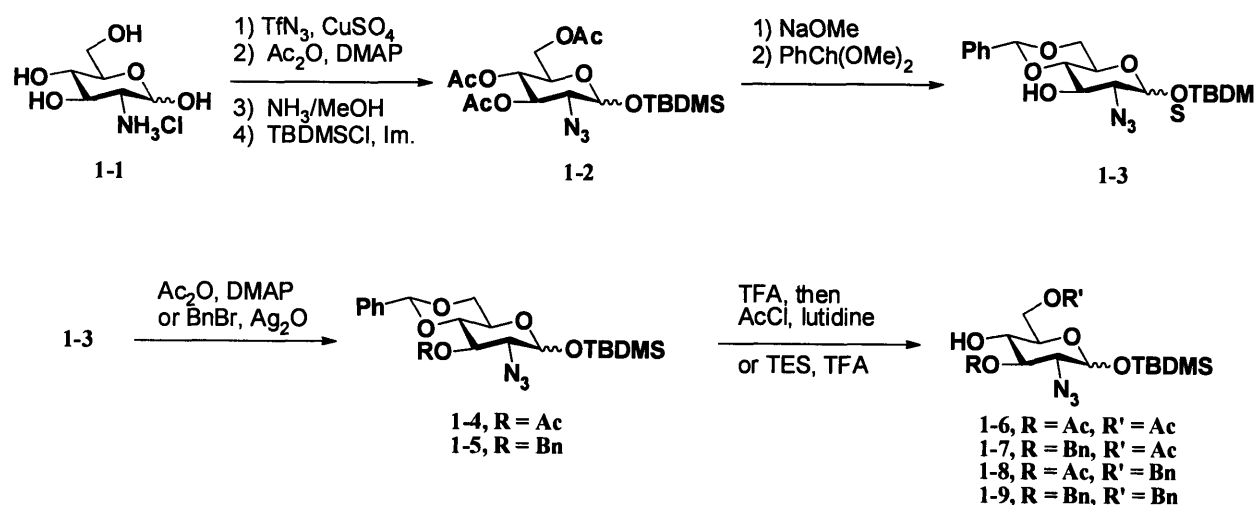
may define the growing carbohydrate chain as a glycosyl donor or acceptor. Each of these choices adds constraints to the type of temporary protecting groups used, and the type of donor chemistry employed.

Synthesis of glucosamine donors and acceptors

A large body of work on the synthesis of differentially protected derivatives of glucosamine exists,(84) and the basic scheme of glucosamine monosaccharide donors and acceptors used in heparin synthesis has been largely established. For any synthesis of glucosamine derivatives for the general synthesis of glycosaminoglycans, it is desirable to be able to produce the glycosyl donors and acceptors in large quantity from readily available starting materials. Glucose 2-azides have long been the derivative of choice for heparin synthesis, providing a non-participating amine equivalent that is stable to a wide range of chemistries, but may itself be selectively reacted to the amine through a range of specialized chemistries.(85) Azide-masked glucosamine trichloroacetimidate donors also have the advantage of providing good α -selectivity, especially in coupling to iduronic acid monosaccharide(86) and disaccharide acceptors, and to conformationally “locked” glucuronic acid derivatives.(83) Other 2-azidoglucose donor strategies have been employed, including fluoro(87) and other halo(46) donors, and recently the free hydroxyl,(88) with variable degrees of success at α -selectivity.

Glucosamine azide can be readily prepared in large quantity through published procedures,(89) and a recent report outlined the synthesis of differentially protected glucose-azide derivatives for HLGAG synthesis from common intermediates.(83) Here, as in most heparin syntheses,(5, 19, 47, 79) acetates were used as the permanent protecting group to block

sites of sulfation, and benzyl ethers were used as the permanent protecting group for free hydroxyls. Glucosamine (1-1) is converted to the azide and the product peracetylated. The anomeric acetate is selectively cleaved and the anomeric position protected with TBDMS ether to give 1-2. Cleavage of the acetates followed by installation of a 4,6-benzylidene acetal gave 1-3, the key common intermediate. The compound could be acetylated or reacted to the benzyl ether to give 1-4 and 1-5, respectively. The benzylidene acetal could be cleaved and the 6-OH selectively esterified to yield the 6-acetyl compounds 1-6 and 1-7, or the benzylidene could be reductively ring-opened to give 1-8 and 1-9. These compounds were suitable as 4-OH glycosyl acceptors, or could be blocked with a temporary protecting group at C4 and the anomeric TBDMS ether cleaved and reacted to a trichloroacetimidate donor. Variations on this synthetic plan could produce glucosamine azide donors/acceptors with almost any protecting groups or donor chemistry desired.



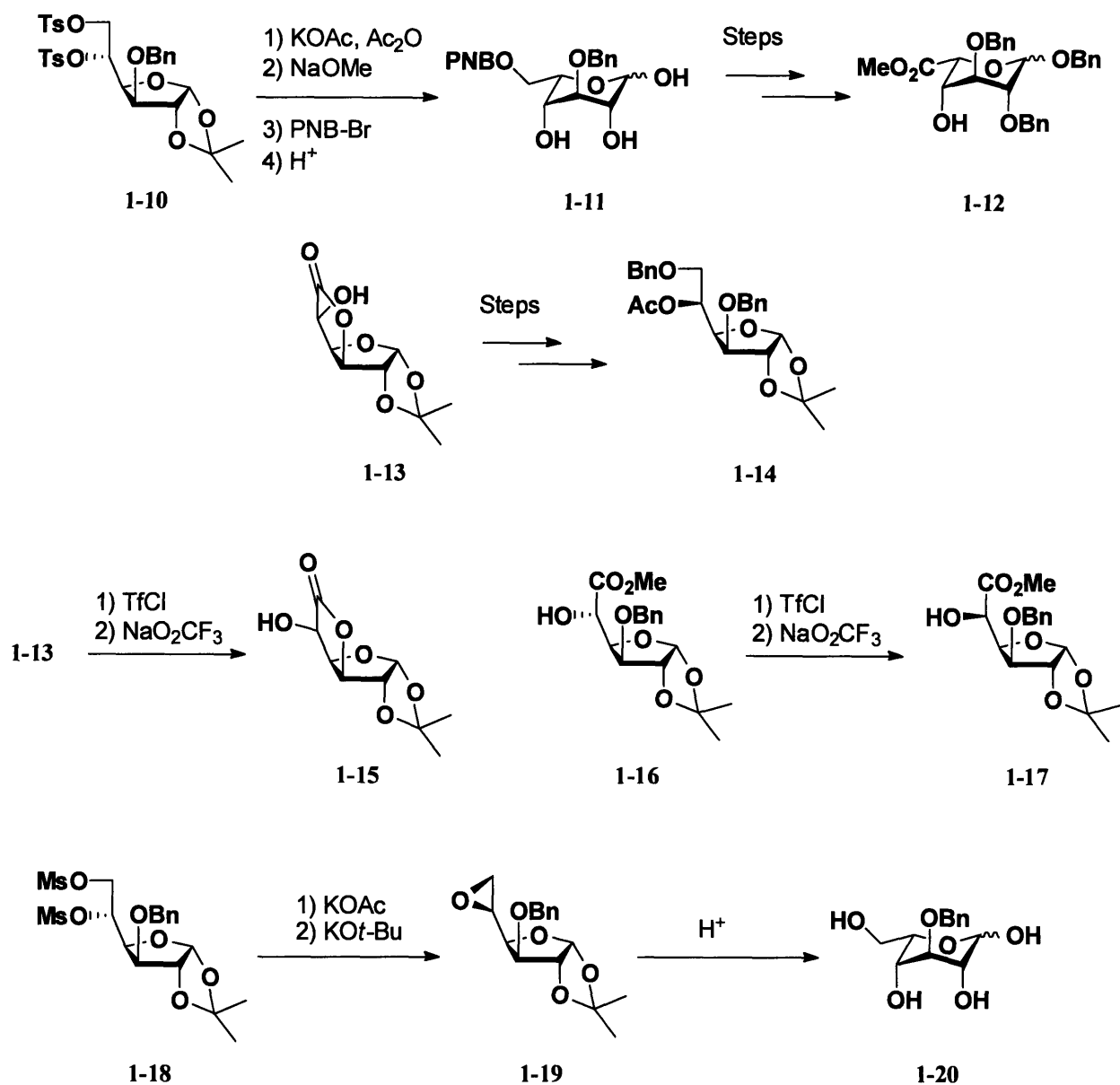
Scheme 1-1. Preparation of fully differentiated glucosamine derivatives.

Synthesis of glucuronic and iduronic acid donors and acceptors

One of the most difficult problems in heparin synthesis has long been the synthesis of fully-differentiated uronic acid donors and acceptors. Uronic acids have the additional complication of the 6-carboxylic acid moiety, which changes the reactivity and conformation of these monosaccharides relative to more commonly used hexoses. A wide range of chemistries have been reported in the synthesis of uronic acid derivatives. Glucuronic acid synthons are readily prepared from oxidation of glucose derivatives.(90, 91) Iduronic acid is more of a challenge, as idose and iduronic acid are not readily available as starting materials. Nevertheless, many syntheses of iduronic acid and idose derivatives have been reported, starting from derivatives of glucose,(92-97), trehalose,(98) glucuronic acid 3,6 lactone,(99-102) glucuronic acid through epimerization,(81, 103), glucuronic acid through radical bromination,(104, 105) Δ^4 -uronic acids,(106) *exo*-glucals,(107) xylose,(108) glycuronolactams,(109) and uronic acid glycals.(110)

Some specific approaches to the preparation of iduronic acid are shown in Scheme 1-2. One of the earliest reported methods utilizes substituted glucofuranose 1-10.(92, 93) Treatment with potassium acetate in acetic anhydride effected the displacement of both tosyl groups, with inversion at C5. Cleavage of the acetates, selective primary protection as a *p*-methoxybenzyl ether and hydrolysis of the isopropylidene gave substituted idose 1-11. Further manipulation, finishing with selective oxidation of the primary OH with O₂ and Pt catalyst and treatment with diazomethane gave 1-12. A similar inversion method started with the 6,3-glucuronolactone derivative 1-13.(99) The 5-OH was converted to the tosylate, the lactone reduced with LiAlH₄, the resultant diol protected with benzyl ethers and the 5-OH inverted by treatment with KOAc. The idose derivative 1-14 that results can be converted into idofuranose derivatives in a similar

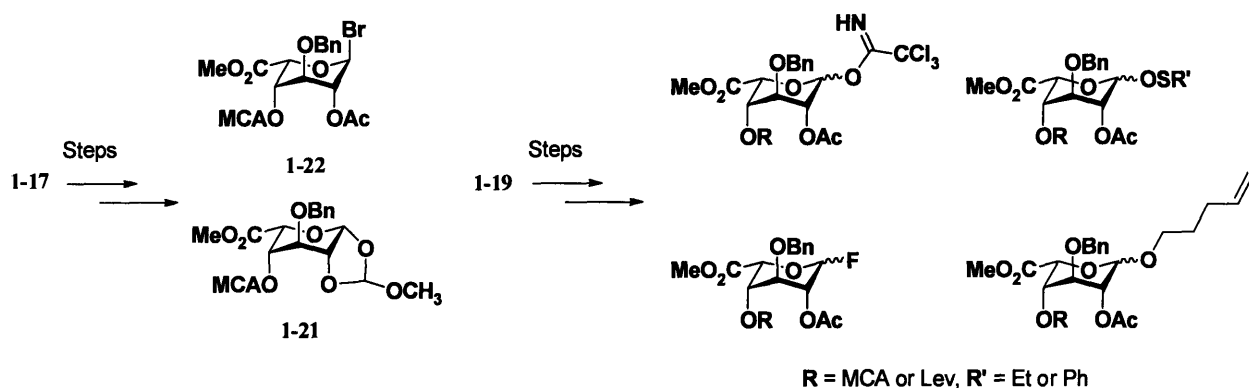
manner to the previous case. A later refinement(100) greatly simplified the preparation of idose derivatives by reacting the 5-triflate derivative of **1-13** with sodium trifluoroacetate. The trifluoroacetyl group is lost upon workup, to yield **1-15** directly in good yield, with little cleavage of the lactone. This chemistry was later applied to the glucuronic furanose derivative **1-16**, yielding the iduronic furanose **1-17**. Another C5 inversion method was described starting from **1-18**.(111) Treatment with KOAc in the presence of a crown ether selectively reacted the primary mesylate; treatment with potassium *t*-butoxide cleaved the ester and caused elimination of the second mesylate to form the epoxide **1-19**. Acidic hydrolysis opens the epoxide with retention of C5 and cleaves the isopropylidene to give 3-*O*-benzyl idose **1-20**. These last two chemistries have in general been the preferred methods for the production of iduronic derivatives in the literature.(81, 102, 112-115)



Scheme 1-2. Approaches to the preparation of ido-configured sugars.

Iduronic acid glycosyl donors were prepared from 1-17 (Scheme 1-3). Hydrolysis of the isopropylidene followed by peracetylation yielded a mixture of both anomers of both the furanose and pyranose sugars. The desired α -pyranose was isolated, and converted into the orthoester 1-21.(81) Both this compound and the related anomeric bromide 1-22(116) were used as iduronic glycosyl donors. Refinements and generalization of this chemistry allowed

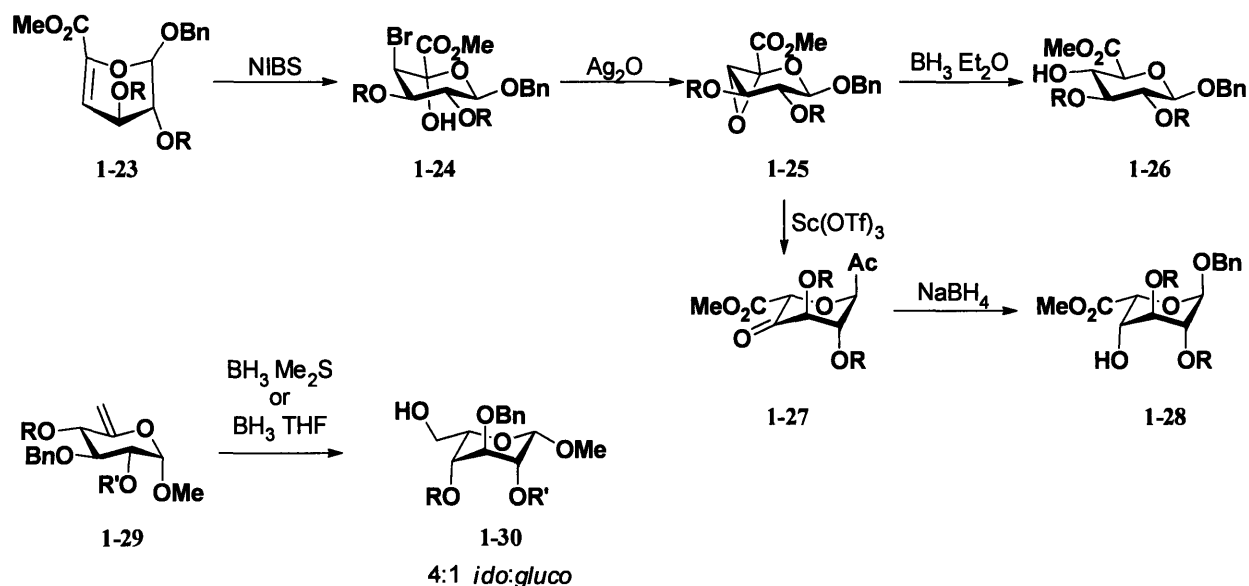
preparation of a range of fully-differentiated iduronic glycosyl donors, including trichloroacetimidates,(112) thiosugars, fluorosugars, and *n*-pentenyl glycosides from 1-19.(113)



Scheme 1-3. Synthesis of iduronic acid glycosyl donors.

By late 1990's, successful synthesis of ATIII binding pentasaccharides(46) had rekindled interest in developing an efficient and inexpensive procedure for the production of iduronic synthons, and a host of new methods appeared in the literature. Preparation of uronic acid donors from the Δ^4 -uronic acid(106, 117) 1-23 (Scheme 1-4) preceded by protection of the two free hydroxyls (several differentially protected derivatives were used) followed by NBS hydrobromination and isolation of the major product 1-24. This compound was closed to the epoxide 1-25 which could be reductively opened with $\text{BH}_3 \cdot \text{Et}_2\text{O}$ to glucuronic derivatives (1-26), or rearranged to the 4-ulose 1-27 (as well as contaminating 5-ulose) that could be reduced with NaBH_4 to give the ido derivatives 1-28. This methodology allows for a greater variability in the protection scheme, but suffers from multiple steps that give mixtures of isomeric products. Another route converts *exo*-glycals of the form 1-29 to *ido*-configured sugars (1-30) using $\text{BH}_3 \cdot \text{Me}_2\text{S}$ or $\text{BH}_3 \cdot \text{THF}$. The products were predominantly *ido* (4:1 as long as R was not a bulky group such as TBDMS), and could be separated from the contaminating *gluco* products. Still other routes produce idose from xylose,(108) 5-uloses of open chain glucose,(94) glyconolactones,(109) and glucuronic acid glycals,(110) and unprotected iduronic acid from

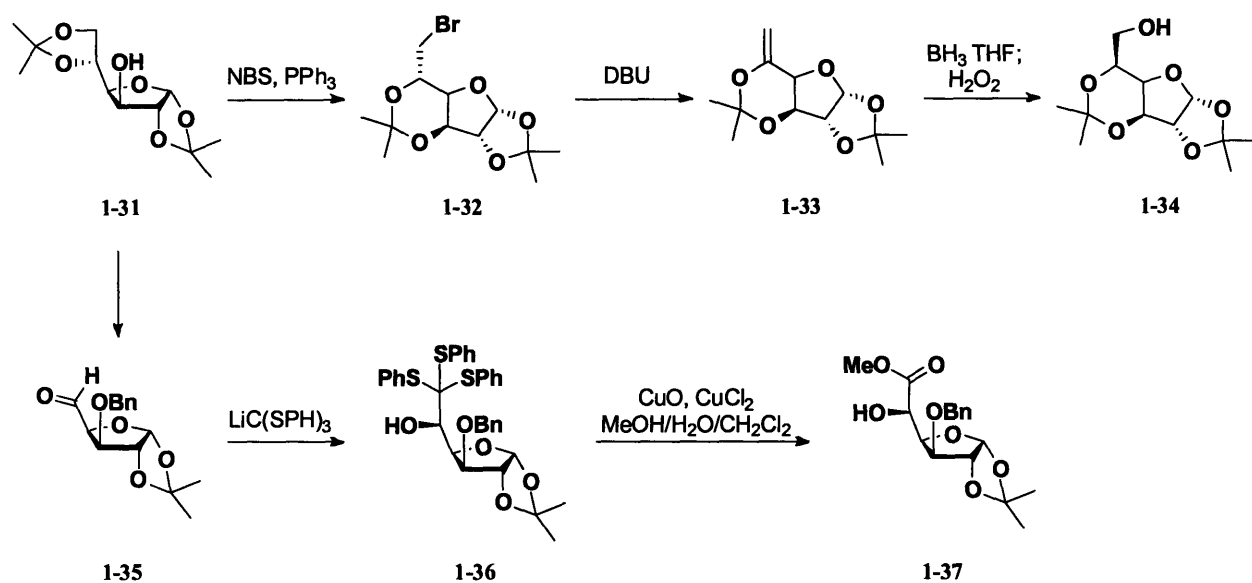
trehalose.(98) A recent report outlines a short synthesis of fully-differentiated glucuronic and iduronic thiosugars via an aldol condensation of protected aldehydes and silyl enol ethers.(118) All of these routes to idose and iduronic derivatives also suffer from the need to separate diastereomeric products at one or more steps.



Scheme 1-4. Other methods for the preparation of iduronic synthons.

Two recent reports outline short, highly selective syntheses of iduronic acid derivatives starting from diacetone glucose (Scheme 1-5).(95, 96) In the first, (95) commercially available diacetone glucose (1-31) was converted to the 6-Br derivative 1-32 by reaction with PPh_3 and NBS. Treatment with the hindered base DBU created a compound with an exocyclic double bond (1-33); hydroboration with $\text{BH}_3 \cdot \text{THF}$ produced exclusively the *ido*-configured derivative 1-34 in high (90%) yield. Acidic hydrolysis of the isopropylidenes gives L-idose. In the second report, 1-31 was converted to its benzyl ether, and the 5,6-isopropylidene cleaved. The diol was converted to the aldehyde 1-35 by treatment with NaIO_4 , and this aldehyde was reacted with a number of C-nucleophiles. The methyl ester equivalent $\text{LiC}(\text{SPh})_3$ gave a high yield (>90%) of

the *ido* product **1-36** with none of the *gluco* isomer detected, and could be converted to the methyl ester **1-37** in near quantitative yield.



Scheme 1-5. Synthesis of idose and iduronic acid derivatives from diacetone glucose.

Recent attempts to control the stereoselectivity of the formation of the glucosamine α -linkage have focused on the use of acceptor stereochemistry to control the outcome of the coupling.^(115, 119) It has long been known that couplings of 2-azido trichloroacetimidates to the 4-OH of iduronic acid acceptors produced exclusively the α -linkage. Reasoning this selectivity was being influenced by acceptor conformation, Seeberger and coworkers prepared the glucuronic acid derivative **1-38** by reaction of 3-*O*-benzyl glucuronic acid methyl ester with the isopropylidene equivalent 2-methoxypropene. Compound **1-38** (Figure 1-10) is expected to take an iduronic-like ¹C₄ conformation in solution, and could be coupled to a range of 2-azidoglucose trichloroacetimidates and fluorides to give exclusively the α -linkage. The major drawback to this synthon (and the related *ido*-compound **1-39**) arose in the installation of the 1,2-isopropylidene. The reaction with the lactol inevitably produces mixtures of the pyranose and furanose forms, and of mixed, acyclic acetals that decompose upon workup. This feature led to

variable and often low yields, especially for 1-38. Recent efforts to produce similarly locked glucuronic and iduronic acceptors have been reported, using a 1,2-ethylidene installed by reduction of a 2-*O*-acetyl anomeric bromide.(120) In this case, the problem of equilibrating between pyranose and furanose forms is avoided. The results of other efforts to improve the selectivity and yields of the 1,2-isopropylidene and the reaction of 1-38 and 1-39 to fully differentiated uronic acid donors are described in detail in the next chapter.(121, 122)

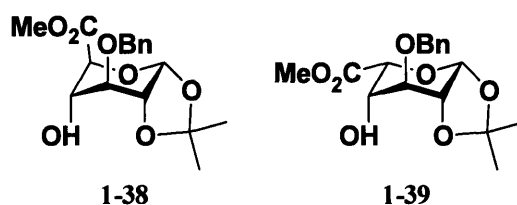


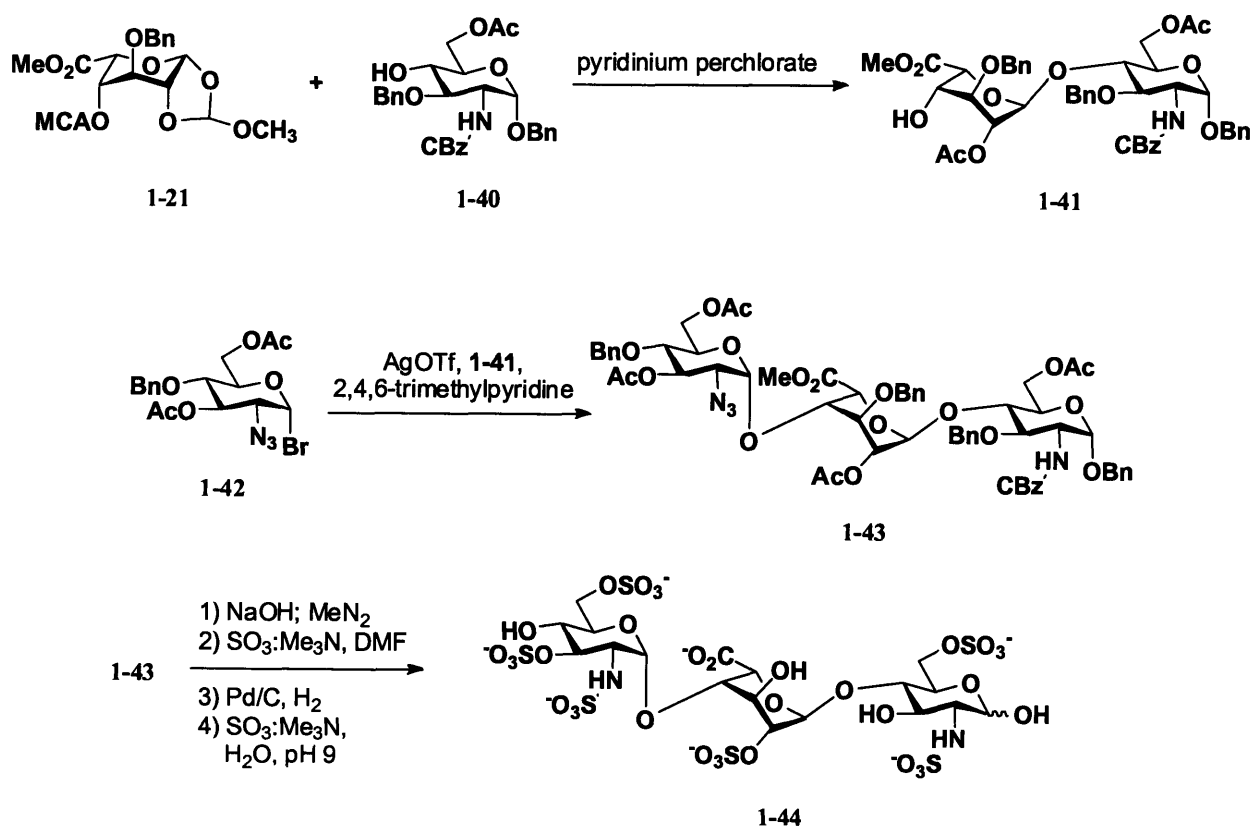
Figure 1-10. Conformationally locked uronic acid acceptors.

Synthesis of defined HLGAG sequences: the ATIII binding site and related oligosaccharides

The earliest work in the synthesis of defined HLGAG sequences centered on the production of the high-affinity ATIII binding pentasaccharide. These efforts were undertaken both as a validation of the structure assigned the binding sequence, and the start of a program to develop synthetic anticoagulant drugs based on heparin.(46, 47) Application of previous work to produce iduronic acid derivatives, development of new coupling procedures, and the first schemes for deprotection and elaboration of HLGAG compounds were laid out in these syntheses, and many of the procedures developed still see use today.

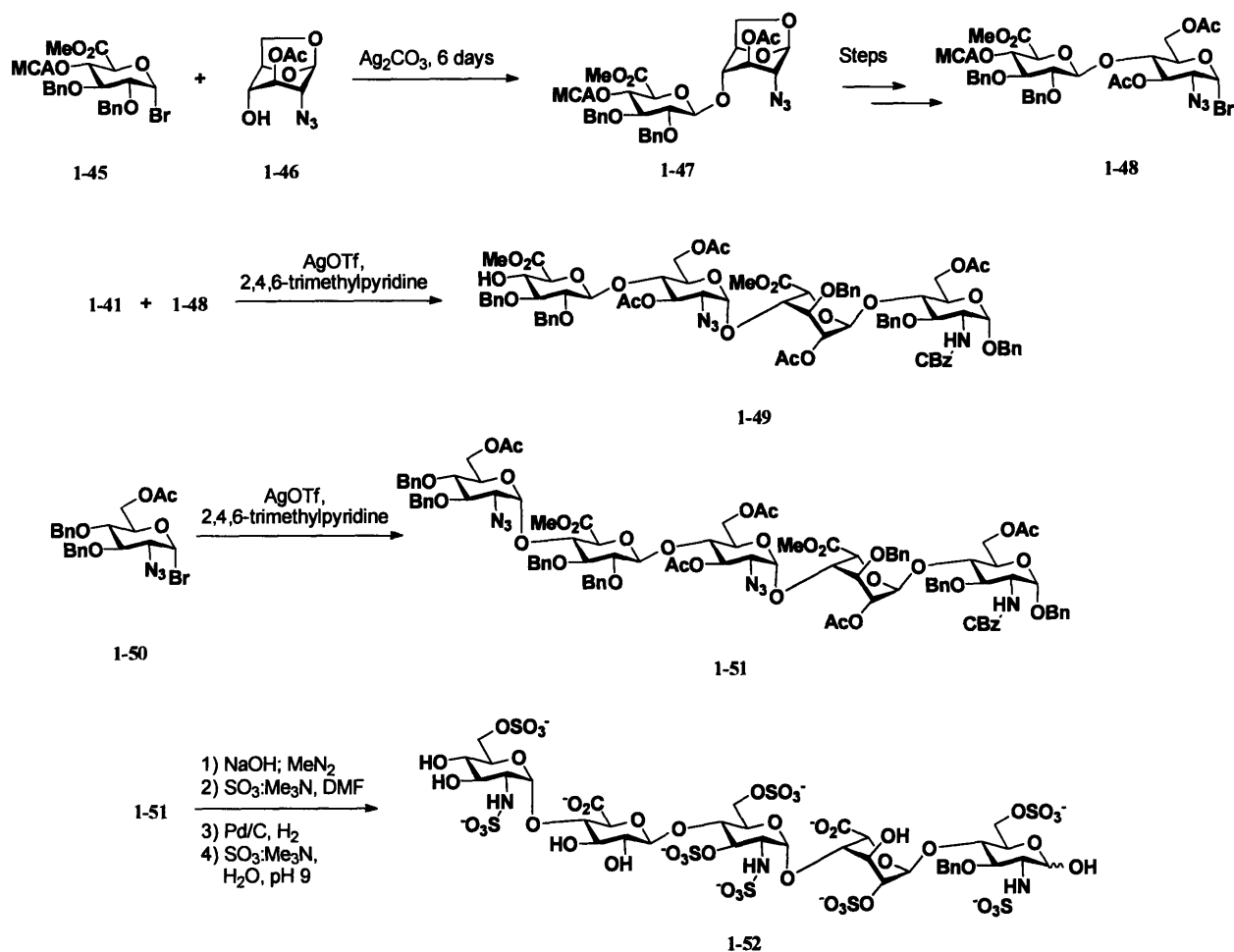
Early work to produce heparin-like disaccharides(92, 123) had produced both glucuronic acid $\beta(1\rightarrow4)$ glucosamine and glucosamine $\alpha(1\rightarrow4)$ glucuronic acid derivatives from similar starting materials. These early routes used 1,2-gluco or glucurono epoxides as the glycosyl donor, and installed the amine functionality by first forming a 2,3-epoxide and installing the

amine by aminolysis. The first sulfated heparin trisaccharide was prepared some years later by the methods shown in Scheme 1-6.(81) The iduronic acid orthoester **1-21** was coupled with the 4-OH glucosamine acceptor **1-40** using 2,6-dimethylpyridinium perchlorate and the MCA cleaved to give **1-41**. Poor yields (40%) were obtained even with a four-fold excess of the acceptor. This disaccharide could be coupled to the azido glucose bromo-sugar **1-42** in high yield. The trisaccharide product **1-43** was elaborated by cleavage of acetates with sodium hydroxide, reprotection of the carboxyl group with diazomethane, and sulfation of all free hydroxyls with sulfur trioxide-trimethylamine complex in DMF. Removal of benzyl ethers and reduction of the azide by Pd/C with H₂ gas, followed by selective N-sulfation using sulfur trioxide-trimethylamine in water at pH 9 also cleaved the methyl ester to give **1-44**.



Scheme 1-6. Early syntheses of a HLGAG trisaccharide.

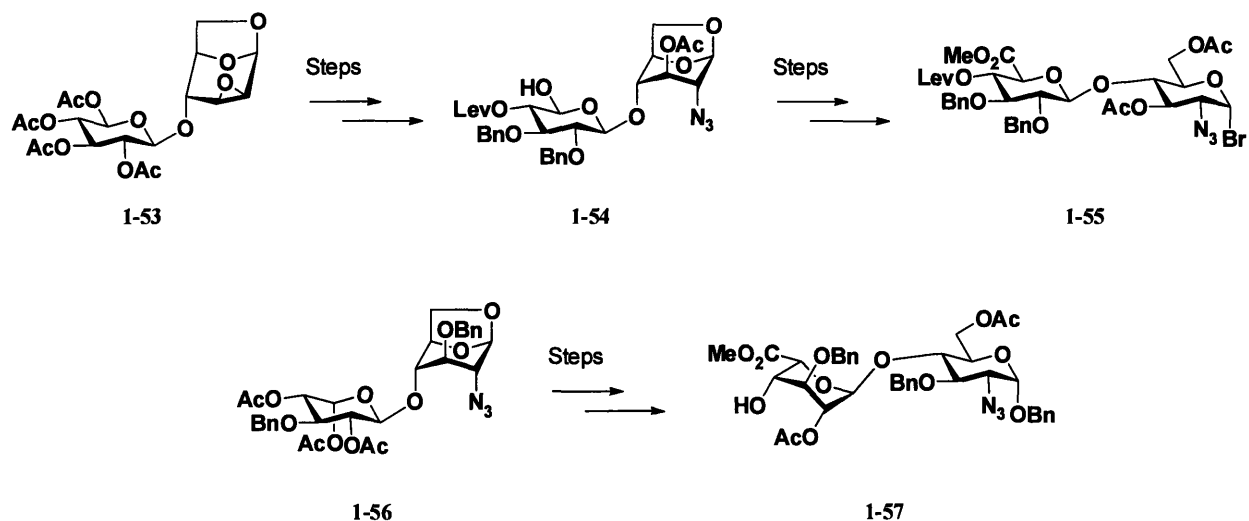
The first reported syntheses of the ATIII binding pentasaccharide by Sinaý and coworkers used the methods developed in the earlier reports (Scheme 1-7).^(80, 124, 125) In the first syntheses, the poly-*N*-sulfonate was prepared rather than the structure with one *N*-acetate at the non-reducing end (Figure 1-6) to simplify the protocol. This variant was shown to bind ATIII with high affinity as well. In order to install the glucosamine α -linkages selectively, anomerically pure azido-glucosamine 1-bromides were prepared, and reacted with glucuronic and iduronic acceptors under conditions to favor formation of the α -anomer. The reducing end disaccharide **1-41** was prepared as previously described.⁽⁸¹⁾ The glucuronic acid derivative **1-45** was prepared from glucose, and reacted with the 1,6-anhydro-2-azido-glucose derivative **1-46**. The disaccharide product **1-47** was subjected to acidolysis in Ac₂O followed by treatment with titanium tetrabromide to give **1-48** in ~40% yield. This disaccharide glycosyl donor was condensed with **1-41** using silver triflate to give the tetrasaccharide **1-49** after removal of the MCA protecting group. This tetrasaccharide was coupled with the azido-glucose anomeric bromide **1-50** to give the protected pentasaccharide **1-51**. Deprotection using the previously described conditions gave the ATIII binding pentasaccharide **1-52**.



Scheme 1-7. Synthesis of an ATIII binding pentasaccharide.

An alternate method for assembly of the pentasaccharide is outlined in Scheme 1-8.(111) In this synthesis, yields were improved by installation of the azides and oxidation to uronic acids at the disaccharide stage. Initial disaccharide 1-53 was converted to the disaccharide 1-54 over several steps; after protecting group manipulation of the NRE glucose, the epoxide was selectively opened with azide as previously described.(92, 123) The NRE glucose was selectively oxidized and the glucose azide converted to the bromosugar, giving disaccharide 1-55, very similar to 1-48 in the prior synthesis with the only difference being the use of the levonyl (lev) ester instead of MCA as a temporary protecting group. Similarly, idose-containing disaccharide 1-56 was prepared and converted to 1-57 through selective oxidation and reaction to

the anomeric benzyl ether. These disaccharides were assembled as in the previous synthesis to the corresponding tetrasaccharide and finally coupled with the same non-reducing end azido glucose bromosugar to give a protected pentasaccharide.

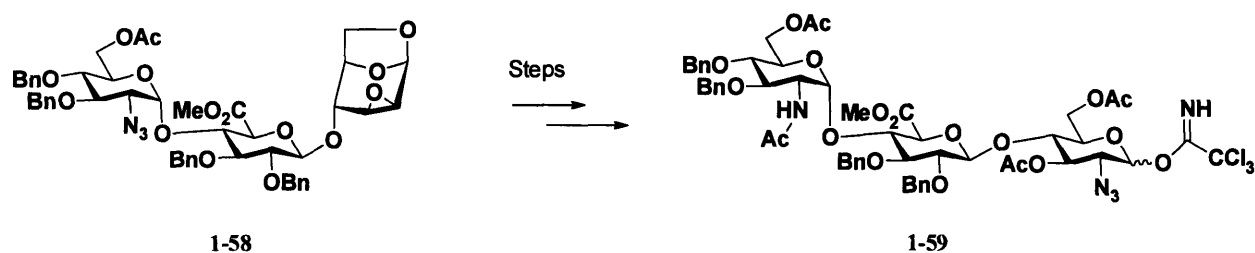


Scheme 1-8. Second of the ATIII binding pentasaccharide.

Later refinements to the initial synthesis improved yields and changed to the anomeric methyl glycoside (rather than the free lactol revealed by the anomeric benzyl ether of the original synthesis), but did not change the key methodological features.⁽¹²⁵⁾ Similar methods were employed to produce variants of the ATIII structure with different sulfation patterns,⁽¹²⁶⁻¹³²⁾ and for variations on the synthesis with different starting materials.^(133, 134)

The ATIII binding site containing the NRE *N*-acetyl moiety was synthesized using the strategy shown in Scheme 1-9.⁽¹³⁵⁾ In this case, trisaccharide **1-58** was assembled analogously to previous syntheses. The azide was reduced and converted to the *N*-acetate, and the trisaccharide further modified to the trichloroacetimidate donor **1-59**. Coupling to a RE disaccharide and subsequent deprotection and elaboration produced the first synthetic ATIII pentasaccharide with all the features of the natural product installed. The coupling of the trisaccharide and RE disaccharide proceeded in poor yield, however, likely due to the presence

of the *N*-acetyl group.(136, 137) The trichloroacetimidate chemistry was later used to assemble ATIII variants with 3-deoxy iduronic acid(138) and a 2,5-bridged iduronic acid simulating the skew-boat ²S₀ conformation.(30) These structures were used as probes in the binding contribution from different iduronic acid conformations. Trichloroacetimidate donors were also used in the synthesis of ATIII binding site fragments used for investigations into platelet binding.(132, 139)



Scheme 1-9. Synthesis of an ATIII binding pentasaccharide containing an *N*-acetyl group.

The synthetic pentasaccharides produced allowed detailed structure-function studies and determination of the contribution to binding of each moiety within the molecule. The syntheses allowed for the production of several constructs possessing the full ATIII activating/thrombin inhibiting anticoagulant properties of heparin, some of which are now clinically used drugs.(39, 47, 140-148) These conjugates typically combined a synthetic ATIII binding pentasaccharide domain to a charged, sulfated polyglucose region (the thrombin-binding domain) connected by a flexible linker.

The total synthesis of ATIII paved the way for future synthetic work, providing schemes for the preparation of monosaccharides and documenting the difficulties in HLGAG synthesis. A critical observation in this early work(46) and subsequent syntheses(149) was that the couplings of glucose-azide halo and trichloroacetimidate donors to iduronic acid derivatives were highly α -selective, but couplings to the 4-OH of glucuronic derivatives produced α/β mixtures.(125, 135, 150) Recent results have shown that the coupling to the 4-OH of iduronic

acid acceptors with glucose azide donors are not always α -selective.(82, 136) Block couplings between glycosylated glucose azide trichloroacetimidates and iduronic acid terminated acceptors show significant erosion of this selectivity.

Modular approaches to syntheses of HLGAGs

Subsequent syntheses of HLGAGs began to move away from the iduronic orthoester/glucose azide bromosugar strategy and convergent synthetic plan employed in the original ATIII synthesis. In the production of heparin oligosaccharides related to the linkage region of HS, Nillson, Westman and Svahn report use of uronate bromo-sugars and azido-glucose thioglycosides as donors.(151, 152) The glucosamine α -linkage was installed successfully with the thiosugar chemistry in good yields onto glucuronic acid acceptors, though no comment was given as to anomeric selectivity. Reactivity problems were encountered with glucuronic bromosugars: coupling to acceptors larger than a monosaccharide gave variable, generally poor yields. Later work with glucuronyl trichloroacetimidates(153) allowed the assembly of short, glucuronic acid containing HLGAG sequences with the glucuronic acid $\beta(1\rightarrow4)$ glucosamine linkage installed rapidly, though only in moderate ($\sim 50\%$) yield.

The first efforts in what could be called a “modular” synthetic strategy for HLGAGs were in production of the FGF binding structure. The basic FGF binding structure is made of a disaccharide repeat, and syntheses of FGF-binding structure have attempted to assemble the structure by sequential glycosylations of protected disaccharides.(86, 154-159) The first strategy devised used protected iduronic acid $\alpha(1\rightarrow4)$ azidoglucose trichloroacetimidate disaccharides (Figure 1-11),(154-156) and formed the α -glucosamine linkages by taking advantage of the known stereoselectivity of the coupling of azidoglucose donors and 4-OH iduronic acceptors. In

this and subsequent FGF syntheses, the permanent protecting group and deprotection scheme used were the same as in the original ATIII synthesis: acetates mask sites to be sulfated, benzyl ethers mask sites to be unmodified hydroxyls, and azides are transformed into sulfated amines. In preparation of FGF binding structures, the “repeat” disaccharide is first coupled to a terminal reducing end unit, either an iduronic acid monosaccharide or simple alcohol. The temporary protecting group (levulinyl in this case) is removed, and the next disaccharide attached. The final coupling is to the “cap” disaccharide. Though the couplings proceeded in moderate to good yields with high selectivity, incorporation of glucuronate-containing disaccharides was problematic as the contaminating β -coupled products produced would have to be separated after each glycosylation. Consequently, only structures with a terminal non-reducing end glucuronic acid were produced.

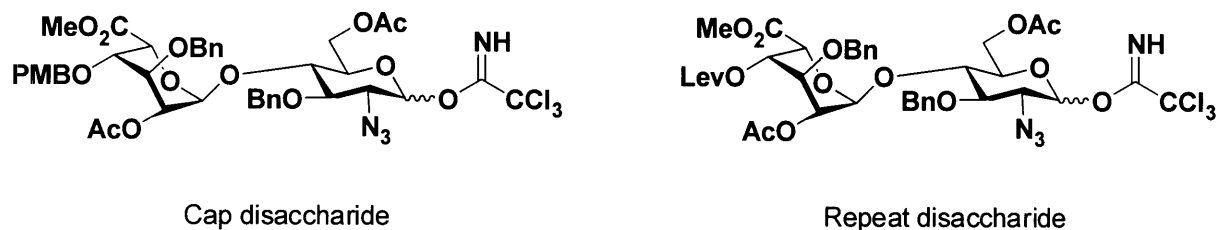


Figure 1-11. First synthetic strategy for FGF binding HLGAGS.

The next-generation strategy employed for the synthesis of FGF-binding structures reversed the order of the disaccharide unit.^(86, 157-159) In this case, disaccharides of the form azidoglucose $\alpha(1 \rightarrow 4)$ iduronic acid were prepared (Figure 1-12). The disaccharides could be prepared with the α -linkage with complete selectivity. Glucuronate-containing disaccharides could presumably be synthesized as a mixture and separated from the β -anomer on the protected disaccharide stage, though no glucuronic building blocks have been reported as part of this strategy. The protecting group on the 2 position was typically benzoate or pivaloate; these esters have reduced electrophilicity at the carbonyl, and thus discourage orthoester formation. They

can, however, create problems with incomplete deprotection in the final stages of the synthesis. Using this strategy, FGF binding tetra, hexa, and octasaccharides been prepared. Variants of this strategy using 2-levulinyl esters as temporary protecting groups to mask sites that are to be free hydroxyls in the final structure, and using 4,6-benzylidene as the temporary protecting group on the azido glucose residues have been reported.

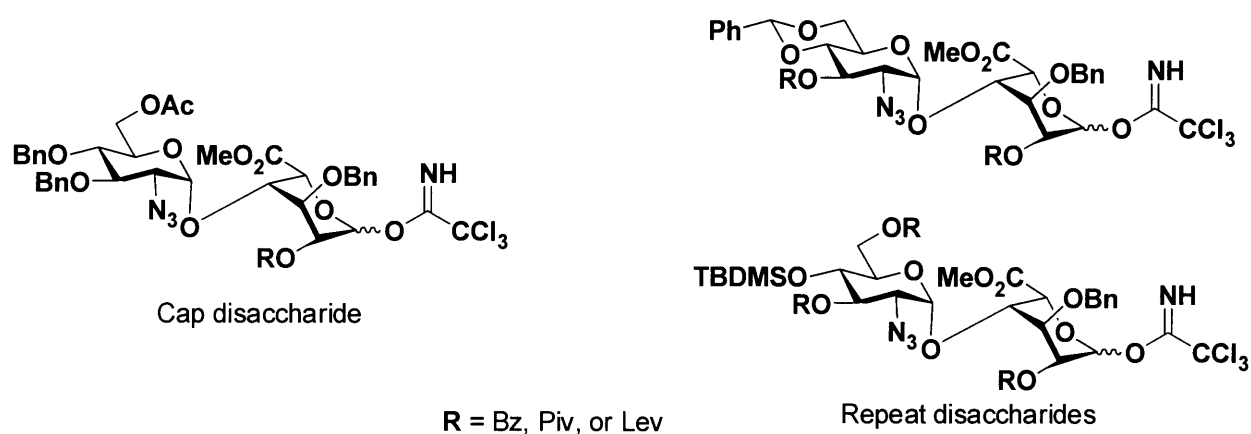
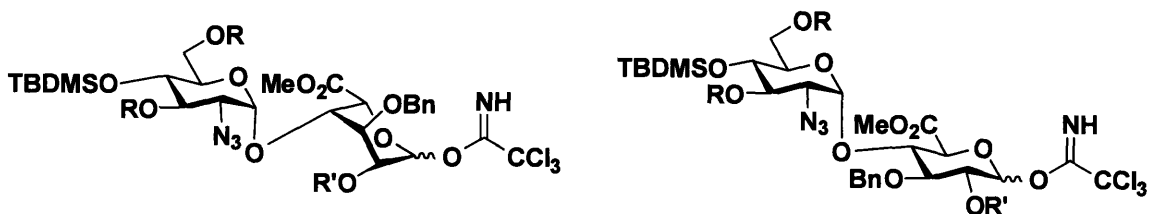


Figure 1-12. Synthesis of FGF binding HLGAGS.

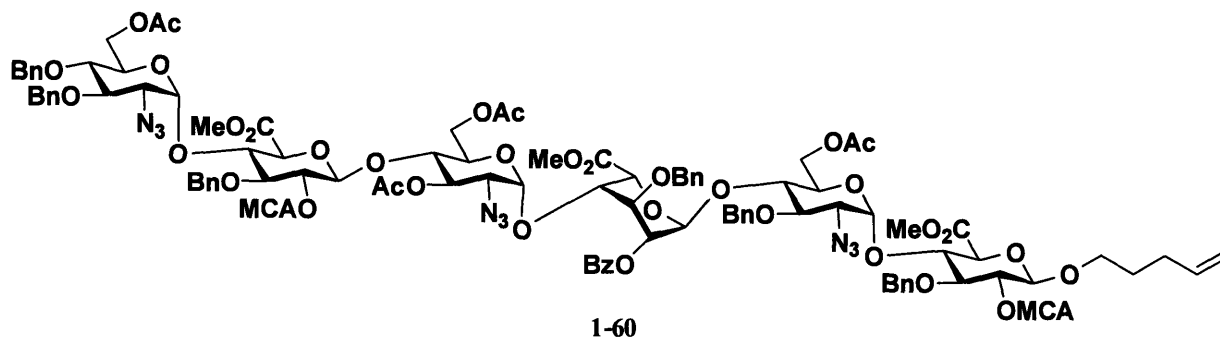
Seeberger and coworkers reported a detailed modular strategy for the synthesis of HLGAGs, outlined in Figure 1-13. The key feature of this strategy is the production of disaccharide units of an azidoglucose $\alpha(1\rightarrow4)$ uronic acid structure from common intermediates. The permanent protecting group strategy employed is very similar to previous routes, with *O*-acetylated blocking sites to be sulfated, azides masking *N*-sulfonates, and benzyl ethers blocking sites that will be unmodified hydroxyls. MCA esters are used as temporary protecting groups on the C2 hydroxyl of uronic acids that are to be free hydroxyls in the final structure—these are used to direct the 1,2-trans geometry of coupling reactions, then cleaved and replaced with benzyl ethers on the growing HLGAG chain. TBDMS ethers were used as the temporary protecting group on the 4-OH of the azidoglucose residues, and trichloroacetimidates were used as the donors of choice. The question of nitrogen differentiation was not directly addressed in

this publication, but the ability to selectively reduce azides(85) should allow for conversion of the azide to other masked amino groups on the disaccharide stage.

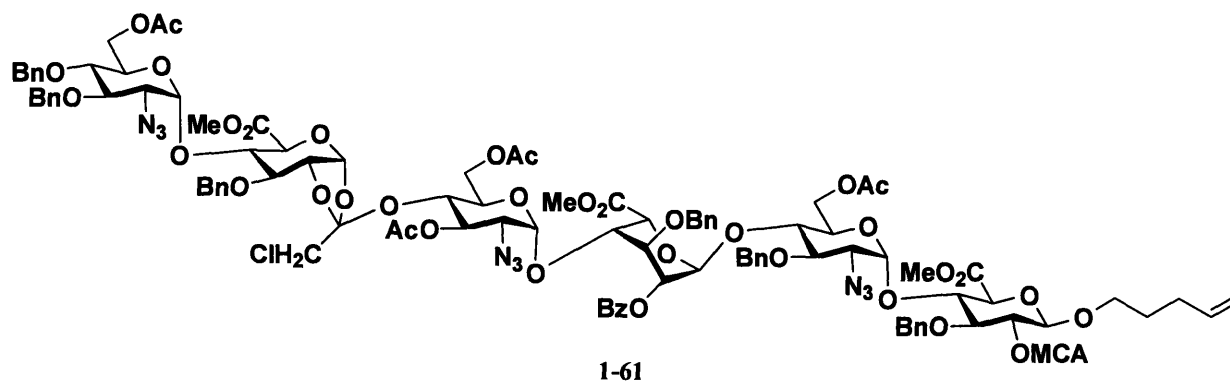
Selectively protected glucosamine derivatives (Scheme 1-1) were used as precursors for 4-*O*-TBMDS ether, 2-azido glucose trichloroacetimidates. These were coupled with the glucuronic and iduronic acceptors **1-38** and **1-39**. These couplings were shown to occur with complete α -selectivity in high (70-90%) yields. Cleavage of the isopropylidene and esterification with either acetate or MCA groups, selective removal of the anomeric ester, and reaction to the trichloroacetimidate gave all disaccharide units proposed.



Disaccharide Building Blocks. R = Ac or Bn. R' = MCA or Ac



1-60



1-61

Figure 1-13. Modular strategy for HLGAG synthesis utilizing azidoglucose $\alpha(1\rightarrow4)$ uronic acid disaccharides.

The protected hexasaccharide **1-60**, based on the ATIII binding structure, was selected as a target for validation of this strategy. While several different tetrasaccharides were synthesized in excellent (86-91%) yield, attempts to couple to the next disaccharide donor uniformly failed, regardless of the protecting groups on the acceptor or the C2 protecting group on the iduronic acid portion of the donor. It appeared that the formation of orthoesters or orthocarbonates was more favorable than the coupling of the deactivated donor disaccharide with the hindered tetrasaccharide acceptor—in the case of the C2 MCA protected disaccharide, a 30% yield of the orthoester product **1-61** was isolated. The target hexasaccharide was synthesized through the

coupling of a trisaccharide donor terminated in an azidoglucose trichloroacetimidate and a 4-OH iduronic acid terminated acceptor trisaccharide, themselves produced through the chemistry outlined in the paper. The tetrasaccharides produced in the original synthetic plan were also deprotected and sulfated using the strategy outlined in the original ATIII synthesis.⁽⁴⁶⁾ While selectivities were excellent at every stage and yields were high for both the synthesis of the disaccharide units and for the initial disaccharide plus disaccharide coupling, the failure of the disaccharide donor to couple with a tetrasaccharide acceptor indicates a serious problem with this strategy, and it is unclear whether the problem lay in the nature of the donor, the acceptor, or both.

Several other modular synthesis proposals exist, and have generally focused on the development of disaccharide moieties, with only a few syntheses of non-FGF structures reported. Boons and coworkers have proposed a strategy based on a late-stage oxidation of the uronic acid residues, incorporating 6-OH benzyl ether blocked glucose and idose, and 6-OH silyl ether protected azido-glucosamines in the preparation of disaccharide units^(87, 160, 161) (a similar plan has also been presented by an unrelated group).⁽¹⁶²⁾ This synthetic plan depends on adding a global, primary hydroxyl-selective oxidation step to the deprotection/elaboration scheme, followed by removal of the silyl ethers or other protecting group from the 6-OH of the glucosamine residues. The initial report on this strategy outlined the successful synthesis and selective oxidation of unsulfated trisaccharide **1-62** and the monosulfated disaccharide **1-63**. Some difficulty was found with cleavage of the sulfate during oxidation—the pH had to be carefully maintained below 10. Further, the yields of the oxidation and silyl ether cleavage were low, only ~65% per step in the case of **1-63**. In the case of a HLGAG oligosaccharide, these low yields could translate to incomplete oxidation or silyl ether cleavage. Later reports^(160, 161)

show improved yields and alternate protecting strategies, but no syntheses larger than a trisaccharide have yet been reported. Additionally, the question of α -selectivity in couplings to glucosamine derivatives is not addressed. The azido glucose terminated donors described would be expected to give anomeric mixtures upon coupling to the 4-OH of glucose and idose.

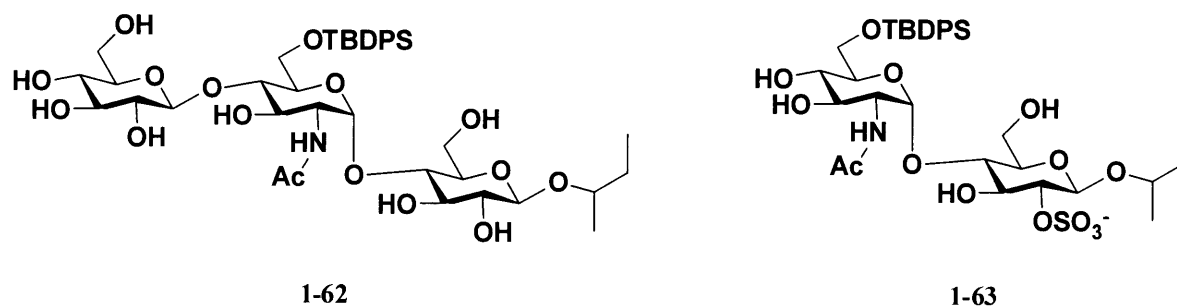


Figure 1-14. Modular synthesis of HLGAGs with a late-stage oxidation.

A very recent proposal for a modular strategy utilizes sequential glycosylations of monosaccharide acceptors with a growing oligosaccharide chain terminated by a deactivated donor group (Figure 1-15).⁽⁸⁸⁾ Uronic acid thio donors were chosen, which have the advantage of being stable under most conditions, but become glycosyl donors when treated with strong activators—thus eliminating the need for deprotection and conversion to a new donor after each glycosylation. Glucose azide acceptors were used, protected as 1,6-anhydrosugars. These were deprotected to the 6-acetate, 1-lactol at each step, and the lactols themselves used as the glycosyl donors. The use of these low reactivity donors in couplings to the hindered 4-OH of uronic acids allowed stereochemistry to be controlled thermodynamically, granting the α -linkage exclusively for many donor-acceptor pairs. Significantly, this included most pairings with glucuronic acceptors. This selectivity comes at the cost of yield in each step, with couplings typically only producing 50-60% yields per step.

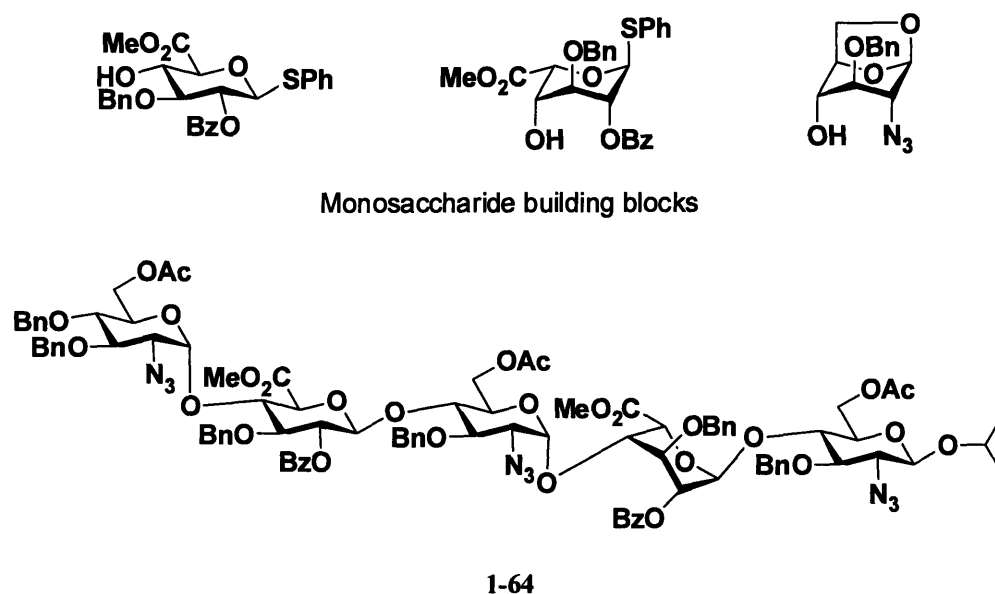


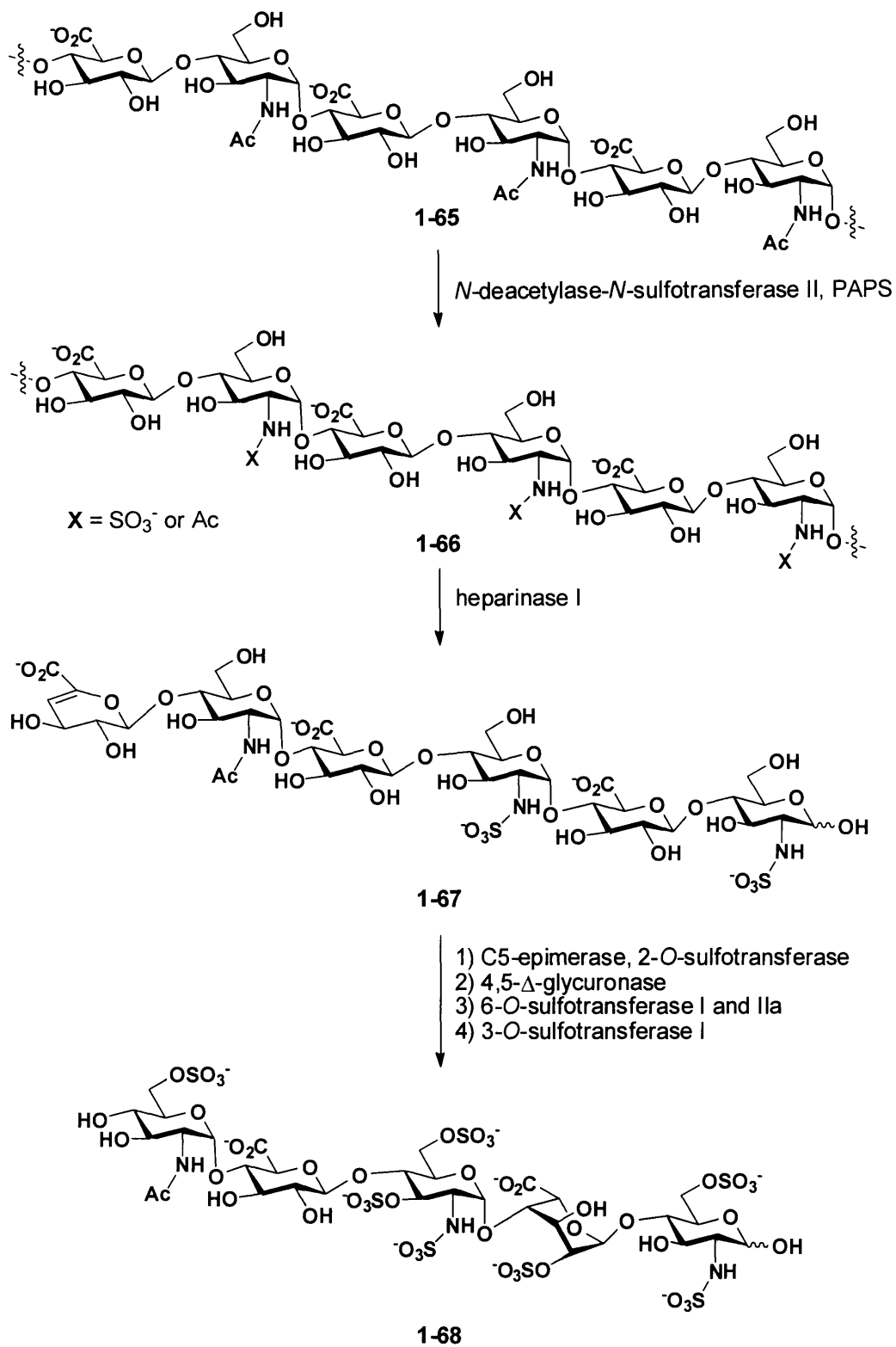
Figure 1-15. Modular synthesis of HLGAGs using a monosaccharide acceptor, growing donor chain strategy.

The pentasaccharide **1-64** was assembled using this strategy, with excellent stereoselectivity in each coupling, but with stepwise yields of <60% for all couplings but one. Such low yields may be a barrier to application of this strategy for the production of larger sequences, but the demonstration of thermodynamic control of formation of the α -glucosamine linkages may well represent a general solution to this selectivity problem. The method also benefits from a low number of monomers and minimization of deprotection/activation steps. Nitrogen differentiation is not addressed—in this strategy, azides would have to be reduced and deprotected after each glycosylation to provide access to structures other than poly-*N*-sulfonates.

Enzymatic semisynthesis of HLGAGs

As an alternative to the total synthesis of HLGAGs, some efforts have been undertaken to apply the natural biosynthetic enzymes to the synthesis of defined heparin sequences (Scheme 1-10).^(51, 163, 164) Compound **1-65**, a polyglucuronic acid/*N*-acetyl glucosamine resembling the heparin backbone, was used as the starting material. Treatment of this polymer with NaOH

followed by sulfur trioxide-trimethylamine complex in water produced the poly *N*-sulfonated compound **1-66**.⁽¹⁶³⁾ In addition, the enzyme *N*-deacetylase-*N*-sulfotransferase II was used to produce the predominantly *N*-sulfonated structure with 30% of the initial *N*-acetates remaining.⁽⁵¹⁾ For this step and subsequent sulfations, the natural sulfate donor 3'-phosphoadenine-5'-phosphosulfate (PAPS) was used. The polymers were subjected to partial cleavage with heparinase I, and the hexasaccharide **1-67** purified to homogeneity from the mixtures of products. Sequential treatment of **1-67** by C5-epimerase and 2-*O*-sulfotransferase I, 6-*O*-sulfotransferases I and IIa, Δ -4,5-glycuronidase, and 3-*O*-sulfotransferase I elaborated the hexasaccharide into the ATIII binding pentasaccharide **1-68**. Purity and identity of this final product was established by standard sequencing methods, use of radioactive sulfur in sulfation steps, and binding assays with ATIII. While an elegant use of enzymatic methods to produce a fully elaborated ATIII binding-pentasaccharide, the method suffers from the need to know the detailed substrate specificity of each enzyme to be used. As much of the efforts in producing defined heparin sequences are geared towards producing substrates to learn more about biosynthesis enzyme specificity and to produce defined sequences to confirm protein binding specificity, these methods are unlikely to displace purely chemical synthesis of defined HLGAGs.



Scheme 1-10. Chemoenzymatic preparation of heparin chains containing the high-affinity ATIII binding pentasaccharide sequence.

1.6 Conclusions

HLGAGs are a complex class of biopolymers with a broad range of biological interactions, key players in many signaling and recognition pathways, and important as anti-coagulant therapeutics. While the total syntheses of several defined sequences have been achieved, a truly general, modular synthesis of any arbitrary heparin sequence remains elusive. Many strategies have been attempted, but no general synthetic strategy exists that allows production of HLGAG chains longer than tetrasaccharides. The synthesis of these oligosaccharides remains an important goal, as the potential benefits of access to any heparin structure for the biochemical and pharmacological study of heparin derivatives would be immense. A general, modular strategy could also be extended to solid-phase and automated synthesis methods,^(165, 166) allowing access to defined heparin oligosaccharides with the same ease we now produce synthetic peptides and nucleic acids.

1.7 References

- (1) Collins, P., and Ferrier, R. (1995) *Monosaccharides: Their Chemistry and Their Roles in Natural Products*, John Wiley & Sons, New York.
- (2) Raman, R., Sasisekharan, V., and Sasisekharan, R. (2005) Structural insights into biological roles of protein-glycosaminoglycan interactions. *Chem. Biol.* 12, 267–277.
- (3) Kjellén, L., and Lindahl, U. (1991) Proteoglycans: structures and interactions. *Annu. Rev. Biochem.* 60, 443-475.
- (4) Iozzo, R. V. (1998) Matrix proteoglycans: from molecular design to cellular function. *Annu. Rev. Biochem.* 67, 609-652.
- (5) Noti, C., and Seeberger, P. H. (2005) Chemical approaches to define the structure-activity relationship of heparin-like glycosaminoglycans. *Chem. Biol.* 12, 731-756.
- (6) Linhardt, R. J. (2003) 2003 Claude S. Hudson Award address in carbohydrate chemistry. Heparin: structure and activity. *J. Med. Chem.* 46, 2551-2564.
- (7) Whitelock, J. M., and Iozzo, R. V. (2005) Heparan sulfate: a complex polymer charged with biological activity. *Chem. Rev.* 105, 2745-2764.
- (8) Coombe, D. R., and Kett, W. C. (2005) Heparan sulfate-protein interactions: therapeutic potential through structure-function insights. *Cell. Mol. Life Sci.* 62 410-424.
- (9) Capila, I., and Linhardt, R. J. (2002) Heparin-protein interactions. *Angew. Chem. Int. Ed.* 41, 390-412.

- (10) Bernfield, M., Götte, M., Park, P. W., Reizes, O., Fitzgerald, M. L., Lincecum, J., and Zako, M. (1999) Functions of cell surface heparan sulfate proteoglycans. *Annu. Rev. Biochem.* 68, 729-777.
- (11) Esko, J. D., and Lindahl, U. (2001) Molecular diversity of heparan sulfate. *J. Clin. Invest.* 108, 169-173.
- (12) Lindahl, U., Kusche-Gullberg, M., and Kjelle, L. (1998) Regulated diversity of heparan sulfate. *J. Biol. Chem.* 273, 24979-24982.
- (13) Casu, B., and Lindahl, U. (2001) Structure and biological interactions of heparin and heparan sulfate. *Adv. Carbohydr. Chem. Biochem.* 57, 159-206.
- (14) Chong, B. H. (1992) Heparin-induced thrombocytopenia. *Aust. N. Z. J. Med.* 22, 145-152.
- (15) Engelberg, H. (1984) Heparin and the atherosclerotic process. *Pharm. Rev.* 36, 91-110.
- (16) Hileman, R. E., Fromm, J. R., Weiler, J. M., and Linhardt, R. J. (1998) Glycosaminoglycan-protein interactions: definition of consensus sites in glycosaminoglycan binding proteins. *BioEssays* 20, 156-167.
- (17) Westling, C., and Lindahl, U. (2002) Location of *N*-unsubstituted glucosamine residues in heparan sulfate. *J. Biol. Chem.* 277, 49247-49255.
- (18) Esko, J. D., and Selleck, S. B. (2002) Order out of chaos: assembly of ligand binding sites in heparan sulfate. *Annu. Rev. Biochem.* 71, 435-471.
- (19) Karst, N. A., and Linhardt, R. J. (2003) Recent chemical and enzymatic approaches to the synthesis of glycosaminoglycan oligosaccharides. *Curr. Med. Chem.* 10, 1993-2031.
- (20) Verli, H., and Guimarães, J. A. (2004) Molecular dynamics simulation of a decasaccharide fragment of heparin in aqueous solution. *Carbohydr. Res.* 339, 281-290.
- (21) Cros, S., Petitou, M., Sizun, P., Pérez, S., and Imberty, A. (1997) Combined NMR and molecular modeling study of an iduronic acid-containing trisaccharide related to antithrombotic heparin fragments. *Bioorg. Med. Chem.* 5, 1301-1309.
- (22) Becker, C. F., Guimarães, J. A., and Verli, H. (2005) Molecular dynamics and atomic charge calculations in the study of heparin conformation in aqueous solution. *Carbohydr. Res.* 340, 1499-1507.
- (23) Imberty, A., and Pérez, S. (2000) Structure, conformation, and dynamics of bioactive oligosaccharides: theoretical approaches and experimental validations. *Chem. Rev.* 100, 4567-4588.
- (24) Mulloy, B., and Forster, M. J. (2000) Conformation and dynamics of heparin and heparan sulfate. *Glycobiology* 10, 1147-1156.
- (25) Hrincovini, M., Guerrini, M., Bisio, A., Torri, G., Petitou, M., and Casu, B. (2001) Conformation of heparin pentasaccharide bound to antithrombin III. *Biochem. J.* 359, 265-272.
- (26) Ernst, S., Venkataraman, G., Sasisekharan, V., Langer, R., Cooney, C. L., and Sasisekharan, R. (1998) Pyranose ring flexibility. Mapping of physical data for iduronate in continuous conformational space. *J. Am. Chem. Soc.* 120, 2099-2107.
- (27) Ferro, D. R., Provasoli, A., Ragami, M., Torri, G., Casu, B., Gatti, G., Jacquinet, J.-C., Sinaÿ, P., Petitou, M., and Choay, J. (1986) Evidence for conformational equilibrium of the sulfated L-iduronate residue in heparin and in synthetic heparin mono- and oligosaccharides: NMR and force-field studies. *J. Am. Chem. Soc.* 108, 6773-6778.

- (28) Raman, R., Venkataraman, G., Ernst, S., Sasisekharan, V., and Sasisekharan, R. (2003) Structural specificity of heparin binding in the fibroblast growth factor family of proteins. *Proc. Nat. Acad. Sci. USA* 100, 2357-2362.
- (29) Kovensky, J., Mallet, J.-M., Esnault, J., Driguez, P.-A., Sizun, P., Héroult, J.-P., Herbert, J.-M., Petitou, M., and Sinaÿ, P. (2002) Further evidence for the critical role of a non-chair conformation of L-iduronic acid in the activation of antithrombin. *Eur. J. Org. Chem.*, 3595-3603.
- (30) Das, S. K., Mallet, J.-M., Esnault, J., Driguez, P.-A., Duchaussoy, P., Sizun, P., Héroult, J.-P., Herbert, J.-M., Petitou, M., and Sinaÿ, P. (2001) Synthesis of conformationally locked carbohydrates: a skew-boat conformation of L-iduronic acid governs the antithrombotic activity of heparin. *Angew. Chem. Int. Ed.* 40, 1670-1673.
- (31) Das, S. K., Mallet, J.-M., Esnault, J., Driguez, P.-A., Duchaussoy, P., Sizun, P., Héroult, J.-P., Herbert, J.-M., Petitou, M., and Sinaÿ, P. (2001) Synthesis of conformationally locked L-iduronic acid derivatives: direct evidence for a critical role of the skew-boat 2S_0 conformer in the activation of antithrombin by heparin. *Chem. Eur. J.* 7, 4821-4834.
- (32) Mulloy, B., Forster, M. J., Jones, C., and Davies, D. B. (1993) NMR and molecular-modelling studies of the solution conformation of heparin. *Biochem. J.* 293, 849-858.
- (33) Kan, M., Wang, F., Xu, J., Crabb, J. W., Hou, J., and McKeenan, W. L. (1993) An essential heparin-binding domain in the fibroblast growth factor receptor kinase. *Science* 259, 1918-1921.
- (34) Lindahl, U., Feingold, D. S., and Roden, L. (1986) Biosynthesis of heparin. *Trends Biochem. Sci.* 11, 221-225.
- (35) Conrad, H. E. (1998) *Heparin-Binding Proteins*, Academic Press, San Diego.
- (36) Handel, T. M., Johnson, Z., Crown, S. E., Lau, E. K., Sweeney, M., and Proudfoot, A. E. (2005) Regulation of protein function by glycosaminoglycans—as exemplified by chemokines. *Annu. Rev. Biochem.* 74, 385-410.
- (37) Carter, W. J., Cama, E., and Huntington, J. A. (2005) Crystal structure of thrombin bound to heparin. *J. Biol. Chem.* 280, 2745-2749.
- (38) Lucas, H., Basten, J. E. M., Konradsson, P., and van Boeckel, C. A. A. (1993) A short synthetic route towards a biologically active heparin-like pentasaccharide with a pseudo-alternating sequence. *Angew. Chem. Int. Ed. Engl.* 32, 434-436.
- (39) Petitou, M., Héroult, J.-P., Bernat, A., Driguez, P.-A., Duchaussoy, P., Lormeau, J.-C., and Herbert, J.-M. (1999) Synthesis of thrombin inhibiting heparin mimetics without side effects. *Nature* 398, 417-422.
- (40) Buijsman, R. C., Basten, J. E. M., Dreef-Tromp, C. M., van der Marel, G. A., van Boeckel, C. A. A., and van Boom, J. H. (1999) Synthesis of heparin-like antithrombotics having perphosphorylated thrombin binding domains. *Bioorg. Med. Chem.* 7, 1881-1890.
- (41) Buijsman, R. C., Basten, J. E. M., van Dinther, T. G., van der Marel, G. A., van Boeckel, C. A. A., and van Boom, J. H. (1999) Design and synthesis of a novel synthetic NAPAP-pentasaccharide conjugate displaying a dual antithrombotic action. *Bioorg. Med. Chem. Lett.* 9, 2013-2018.
- (42) Polat, T., Mohammadi, M., and Linhardt, R. J. (2002) Synthesis of sulfosucrose derivatives for evaluation as regulators of fibroblast growth factor activity. *Tetrahedron Lett.* 43, 8047-8049.
- (43) Monien, B. H., and Desai, U. R. (2005) Antithrombin activation by nonsulfated, non-polysaccharide organic polymer. *J. Med. Chem.* 48, 1269-1273.

- (44) Desai, U. R., Petitou, M., Bjork, I., and Olson, S. T. (1998) Mechanism of heparin activation of antithrombin - Role of individual residues of the pentasaccharide activating sequence in the recognition of native and activated states of antithrombin. *J. Biol. Chem.* 273, 7478-7487.
- (45) Jin, L., Abrahams, J. P., Skinner, R., Petitou, M., Pike, R. N., and Carrell, R. W. (1997) The anticoagulant activation of antithrombin by heparin. *Proc. Nat. Acad. Sci. USA* 94, 14683-14688.
- (46) van Boeckel, C. A. A., and Petitou, M. (1993) The unique antithrombin III binding domain of heparin: a lead to new synthetic antithrombotics. *Angew. Chem. Int. Ed. Engl.* 32, 1671-1690.
- (47) Petitou, M., and van Boeckel, C. A. A. (2004) A synthetic antithrombin III binding pentasaccharide is now a drug! What comes next? *Angew. Chem. Int. Ed.* 43, 3118-3133.
- (48) Li, W., Johnson, D. J., Esmon, C. T., and Huntington, J. A. (2004) Structure of the antithrombin-thrombin-heparin ternary complex reveals the antithrombotic mechanism of heparin. *Nat. Struct. Mol. Biol.* 11, 857-862.
- (49) Atha, D. H., Lormeau, J.-C., Petitou, M., Rosenberg, R. D., and Choay, J. (1985) Contribution of monosaccharide residues in heparin binding to antithrombin III. *Biochemistry* 24, 6723-6729.
- (50) Lindahl, U., Backström, G., Thunberg, L., and Leder, I. G. (1980) Evidence for a 3-O-sulfated D-glucosamine residue in the antithrombin binding sequence of heparin. *Proc. Natl. Acad. Sci. U.S.A.* 77, 6551-6555.
- (51) Kuberan, B., Lech, M. Z., Beeler, D. L., Wu, Z. L., and Rosenberg, R. D. (2003) Enzymatic synthesis of antithrombin III-binding heparan sulfate pentasaccharide. *Nat. Biotech.* 21, 1343-1346.
- (52) Burgess, W. H., and Maciag, T. (1989) The heparin-binding (fibroblast) growth factor family of proteins. *Annu. Rev. Biochem.* 58, 575-606.
- (53) Schlessinger, J., Plotnikov, A. N., Ibrahimi, O. A., Eliseenkova, A. V., Yeh, B. K., Yayon, A., Linhardt, R. J., and Mohammadi, M. (2000) Crystal structure of a ternary FGF-FGFR-heparin complex reveals a dual role for heparin in FGFR binding and dimerization. *Mol. Cell* 3, 743-750.
- (54) Pellegrini, L., Burke, D. F., von Delft, F., Mulloy, B., and Blundell, T. L. (2000) Crystal structure of fibroblast growth factor receptor ectodomain bound to ligand and heparin. *Nature* 407, 1029-1034.
- (55) DiGabriele, A. D., Lax, I., Chen, D. I., Svahn, C. M., Jaye, M., Schlessinger, J., and Hendrickson, W. A. (1998) Structure of a heparin-linked biologically active dimer of fibroblast growth factor. *Nature* 393, 812-817.
- (56) Faham, S., Hileman, R. E., Fromm, J. R., Linhardt, R. J., and Rees, D. C. (1996) Heparin structure and interactions with basic fibroblast growth factor. *Science* 271, 1116-1120.
- (57) Wu, Z. L., Zhang, L., Yabe, T., Kuberan, B., Beeler, D. L., Love, A., and Rosenberg, R. D. (2003) The involvement of heparan sulfate (HS) in FGF1/HS/FGFR1 signaling complex. *J. Biol. Chem.* 278, 17121-17129.
- (58) Canales, A., Angulo, J., Ojeda, R., Bruix, M., Fayos, R., Lozano, R., Giménez-Gallego, G., Martín-Lomas, M., Nieto, P. M., and Jiménez-Barbero, J. (2005) Conformational flexibility of a synthetic glycosylaminoglycan bound to a fibroblast growth factor. FGF-1 recognizes both the ¹C₄ and ²S_O conformations of a bioactive heparin-like hexasaccharide. *J. Am. Chem. Soc.* 127, 5778-5779.

- (59) Wu, Z. L., and Lech, M. (2005) Characterizing the non-reducing end structure of heparan sulfate. *J. Biol. Chem.* 280, 33749-33755.
- (60) Angulo, J., Ojeda, R., de Paz, J.-L., Lucas, R., Nieto, P. M., Lozano, R. M., Redondo-Horcajo, M., Giménez-Gallego, G., and Martín-Lomas, M. (2004) The activation of fibroblast growth factors (FGFs) by glycosaminoglycans: influence of the sulfation pattern on the biological activity of FGF-1. *ChemBioChem* 5, 55-61.
- (61) Liu, J., and Thorp, S. C. (2002) Cell surface heparan sulfate and its roles in assisting viral infections. *Med. Res. Rev.* 22, 1-25.
- (62) Lyon, M., Deakin, J. A., and Gallagher, J. T. (1994) Liver heparan sulfate structure. A novel molecular design. *J. Biol. Chem.* 269, 11208-11215.
- (63) Spear, P. G., and Longnecker, R. (2003) Herpesvirus entry: an update. *J. Virol.* 77, 10179-10185.
- (64) Spear, P. G. (2004) Herpes simplex virus: receptors and ligands for cell entry. *Cellular Microbiology* 6, 401-410.
- (65) Feyzi, E., Trybala, E., Bergström, T., Lindahl, U., and Spillmann, D. (1997) Structural requirement of heparan sulfate for interaction with herpes simplex virus type 1 virions and isolated glycoprotein C. *J. Biol. Chem.* 272, 24850-24857.
- (66) Liu, J., Shriver, Z., Pope, R. M., Thorp, S. C., Duncan, M. B., Copeland, R. J., Raska, C. S., Yoshida, K., Eisenberg, R. J., Cohen, G., Linhardt, R. J., and Sasisekharan, R. (2002) Characterization of a heparan sulfate octasaccharide that binds to herpes simplex virus type 1 glycoprotein D. *J. Biol. Chem.* 277, 33456-33467.
- (67) Shukla, D., Liu, J., Blaiklock, P., Shworak, N. W., Bai, X., Esko, J. D., Cohen, G. H., Eisenberg, R. J., Rosenberg, R. D., and Spear, P. G. (1999) A novel role for 3-O-sulfated heparan sulfate in herpes simplex virus 1 entry. *Cell* 99, 13-22.
- (68) Ugolini, S., Mondor, I., and Sattentau, Q. J. (1999) HIV-1 attachment: another look. *Trends Microbiol.* 7, 144-149.
- (69) Marks, R. M., Lu, H., Sundaresan, R., Toida, T., Suzuki, A., Imanari, T., Hernáiz, M. J., and Linhardt, R. J. (2001) Probing the interaction of dengue virus envelope protein with heparin: assessment of glycosaminoglycan-derived inhibitors. *J. Med. Chem.* 44, 2178-2187.
- (70) Fry, E. E., Lea, S. M., Jackson, T., Newman, J. W. I., Ellard, F. M., Blakemore, W. E., Abu-Ghazaleh, R., Samuel, A., King, A. M. Q., and Stuart, D. I. (1999) The structure and function of a foot-and-mouth disease virus-oligosaccharide receptor complex. *EMBO J.* 18, 543-554.
- (71) Proudfoot, A. E. I., Handel, T. M., Johnson, Z., Lau, E. K., LiWang, P., Clark-Lewis, I., Borlat, F., Wells, T. N. C., and Kosco-Vilbois, M. H. (2003) Glycosaminoglycan binding and oligomerization are essential for the *in vivo* activity of certain chemokines. *Proc. Nat. Acad. Sci. USA* 100, 1885-1890.
- (72) Capila, I., Hernaiz, M. J., Mo, Y. D., Mealy, T. R., Campos, B., Dedman, J. R., Linhardt, R. J., and Seaton, B. A. (2001) Annexin V-heparin oligosaccharide complex suggests heparan sulfate-mediated assembly on cell surfaces. *Structure* 9, 57-64.
- (73) Osborn, H. M. I. (2003) *Carbohydrates*, Academic Press, Boston.
- (74) Wong, C.-H. (2003) *Carbohydrate-based drug discovery*, Wiley-VCH, New York.
- (75) Boons, G.-J., and Hale, K. J. (2000) *Organic synthesis with carbohydrates*, Blackwell Science, Malden.

- (76) (1996) *Modern Methods in Carbohydrate Synthesis*, Harwood Academic Publishers, Netherlands.
- (77) Green, T. W., and Wuts, P. G. M. (1999) *Protective Groups in Organic Synthesis*, 3rd ed., John Wiley and Sons, New York.
- (78) Yeung, B. K. S., Chong, P. Y. C., and Petillo, P. A. (2002) Synthesis of glycosaminoglycans. *J. Carbohydr. Chem.* 21, 799-865.
- (79) Poletti, L., and Lay, L. (2003) Chemical contributions to understanding heparin activity: synthesis of related sulfated oligosaccharides. *Eur. J. Org. Chem.*, 2999-3024.
- (80) Sinaÿ, P., Jacquinet, J.-C., Petitou, M., Duchaussoy, P., Lederman, I., Choay, J., and Torri, G. (1984) Total synthesis of a heparin pentasaccharide fragment having high affinity for antithrombin III. *Carbohydr. Res.* 132, C5-C9.
- (81) Jacquinet, J.-C., Petitou, M., Duchaussoy, P., Lederman, I., Choay, J., Torri, G., and Sinaÿ, P. (1984) Synthesis of heparin fragments. A chemical synthesis of the trisaccharide *O*-(2-deoxy-2-sulfamido-3,6-di-*O*-sulfo- α -D-glucopyranosyl)-(1 \rightarrow 4)-*O*-(2-*O*-sulfo- α -L-idopyranosyluronic acid)-(1 \rightarrow 4)-2-deoxy-2-sulfamido-6-*O*-sulfo-D-glucopyranose heptasodium salt. *Carbohydr. Res.* 130, 221-241.
- (82) Lohman, G. J. S., and Seeberger, P. H. (2004) A stereochemical surprise at the late stage of the synthesis of fully *N*-differentiated heparin oligosaccharides containing amino, acetamido, and *N*-sulfonate groups. *J. Org. Chem.* 69, 4081-4093.
- (83) Orgueira, H. A., Bartolozzi, A., Schell, P., Litjens, R. E. J. N., Palmacci, E. R., and Seeberger, P. H. (2003) Modular synthesis of heparin oligosaccharides. *Chem. Eur. J.* 9, 140-169.
- (84) Debenham, J., Rodebaugh, R., and Fraser-Reid, B. (1997) Recent advances in *N*-protection for amino sugar synthesis. *Liebigs Ann./Recueil*, 791-802.
- (85) Amantini, D., Fringuelli, F., Pizzo, F., and Vaccaro, L. (2002) Selected methods for the reduction of the azido group. *Org. Prep. and Proc.* 34, 109-147.
- (86) de Paz, J.-L., Angulo, J., Lassaletta, J.-M., Nieto, P. M., Redondo-Horcajo, M., Lozano, R. M., Giménez-Gallego, G., and Martín-Lomas, M. (2001) The activation of fibroblast growth factors by heparin: synthesis, structure, and biological activity of heparin-like oligosaccharides. *ChemBioChem* 2, 673-685.
- (87) Haller, M., and Boons, G.-J. (2001) Towards a modular approach for heparin synthesis. *J. Chem. Soc., Perkin Trans. 1*, 814-822.
- (88) Codée, J. D. C., Stubba, B., Schiattarella, M., Overkleeft, H. S., van Boeckel, C. A. A., van Boom, J. H., and van der Marel, G. A. (2005) A modular strategy toward the synthesis of heparin-like oligosaccharides using monomeric building blocks in a sequential glycosylation strategy. *J. Am. Chem. Soc.* 127, 3767-3773.
- (89) Alper, P. B., Hung, S.-C., and Wong, C.-H. (1996) Metal catalyzed diazo transfer for the synthesis of azides from amines. *Tetrahedron Lett.* 37, 6029-6032.
- (90) Davis, N. J., and Flitsch, S. L. (1993) Selective oxidation of monosaccharide derivatives to uronic acids. *Tetrahedron Lett.* 34, 1181-1184.
- (91) Pews-Davtyan, A., Pirojan, A., Shaljyan, I., Awetissjan, A. A., Reinke, H., and Vogel, C. (2003) Comparison of several glucuronate glycosyl donors. *J. Carbohydr. Chem.* 22, 939-962.
- (92) Kiss, J., and Wyss, P. C. (1976) Synthesis of heparin saccharides-V. Anomeric *O*-benzyl derivatives of L-idopyranosyluronic acid. *Tetrahedron* 32, 1399-1402.

- (93) Kiss, J., and Wyss, P. C. (1973) Synthesis of heparin saccharides. Part II. Synthesis and stereochemical aspects of anomeric methyl (benzyl 2,3-di-*O*-benzyl-L-idopyranosid)uronates. *Carbohydr. Res.* 27, 282-285.
- (94) Adinolfi, M., Barone, G., Lorenzo, F. D., and Iadonisi, A. (1999) Intramolecular Tishchenko reactions of protected hexos-5-uloses: a novel and efficient synthesis of L-idose and L-altrose. *Synlett*, 336-338.
- (95) Hung, S.-C., Puranik, R., and Chi, F.-C. (2000) Novel synthesis of 1,2:3,5-di-*O*- β -L-idofuranoside and its derivatives at C6. *Tetrahedron Lett.* 41, 77-80.
- (96) Lubineau, A., Gavard, O., Alais, J., and Bonnaffé, D. (2000) New accesses to L-iduronyl synthons. *Tetrahedron Lett.* 41, 307-311.
- (97) Lee, J.-C., Lu, X.-A., Kulkarni, S. S., Wen, Y.-S., and Hung, S.-C. (2004) Synthesis of heparin oligosaccharides. *J. Am. Chem. Soc.* 126, 476-477.
- (98) Hinou, H., Kurosawa, H., Matsuoka, K., Terunuma, D., and Kuzuhara, H. (1999) Novel synthesis of L-iduronic acid using trehalose as the disaccharidic starting material. *Tetrahedron Lett.* 40, 1501-1504.
- (99) Dax, K., Macher, I., and Weidmann, H. (1974) Reactionen der D-glucuronsäure. *J. Carbohydr. Nucleosides and Nucleotides* 1, 323-334.
- (100) Csuk, R., Hömig, H., Nimpf, J., and Weidmann, H. (1980) A facile synthesis of 1,2-*O*-isopropylidene- β -L-idofuranurono-6,3-lactone. *Tetrahedron Lett.* 21, 2135-2136.
- (101) Vlahov, I. R., and Linhardt, R. J. (1995) Regioselective synthesis of derivatives of idopyranuronic acid: A key constituent of glycosaminoglycans. *Tetrahedron Lett.* 36, 8379-8382.
- (102) Du, Y., Lin, J., and Linhardt, R. J. (1997) Regioselective synthesis of L-idopyranuronic acid derivatives: intermolecular aglycon transfer of dithioacetal under standard glycosylation conditions. *J. Carbohydr. Chem.* 16, 1327-1344.
- (103) Baggett, N., and Smithson, A. (1982) Synthesis of L-iduronic acid derivatives by epimerisation of anomeric D-glucuronic acid analogues. *Carbohydr. Res.* 108, 59-70.
- (104) Chiba, T., and Sinay, P. (1986) Application of a radical reaction to the synthesis of L-iduronic acid derivatives from D-glucuronic acid analogues. *Carbohydr. Res.* 151, 379-389.
- (105) Medaković, D. (1994) An efficient synthesis of methyl 1,2,3,4-tetra-*O*-acetyl- β -L-idopyranuronate. *Carbohydr. Res.* 253, 299-300.
- (106) Bazin, H. G., Kerns, R. J., and Linhardt, R. J. (1997) Regio and stereoselective conversion of Δ^4 -uronic acids to L-ido- and D-glucopyranosiduronic acids. *Tetrahedron Lett.* 38, 923-926.
- (107) Rochepeau-Jobron, L., and Jacquinet, J.-C. (1997) Diastereoselective hydroboration of substituted *exo*-glucals revisited. A convenient route for the preparation of L-iduronic acid derivatives. *Carbohydr. Res.* 303, 395-406.
- (108) Dromowicz, M., and Köll, P. (1998) A convenient synthesis of D-idose. *Carbohydr. Res.* 308, 169-171.
- (109) Takahashi, H., Hitomi, Y., Iwai, Y., and Ikegami, S. (2000) A novel and practical synthesis of L-hexoses from D-glycono-1,5-lactones. *J. Am. Chem. Soc.* 122, 2995-3000.
- (110) Schell, P., Orgueira, H. A., Roehrig, S., and Seeberger, P. H. (2001) Synthesis and transformations of D-glucuronic and L-iduronic acid glycals. *Tetrahedron Lett.* 42, 3811-3814.

- (111) van Boeckel, C. A. A., Beetz, T., Vos, J. N., de Jong, A. J. M., van Aelst, S. F., van den Bosch, R. H., Mertens, J. M. R., and van der Vlugt, F. A. (1985) Synthesis of a pentasaccharide corresponding to the antithrombin III binding fragment of heparin. *J. Carbohydr. Chem.* *4*, 293-321.
- (112) Marra, A., Dong, X., Petitou, M., and Sinaÿ, P. (1989) Synthesis of disaccharide fragments of dermatan sulfate. *Carbohydr. Res.* *195*, 39-50.
- (113) Tabeur, C., Machetto, F., Mallet, J.-M., Duchaussoy, P., Petitou, M., and Sinaÿ, P. (1996) L-Iduronic acid derivatives as glycosyl donors. *Carbohydr. Res.* *281*, 253-276.
- (114) Ojeda, R., de Paz, J. L., Martín-Lomas, M., and Lassaletta, J. M. (1999) A new route to L-iduronate building-blocks for the synthesis of heparin-like oligosaccharides. *Synlett*, 1316-1318.
- (115) Cid, M. B., Alfonso, F., and Martín-Lomas, M. (2005) A study on the influence of the structure of the glycosyl acceptors on the stereochemistry of the glycosylation reactions with 2-azido-2-deoxy-hexopyranosyl trichloroacetimidates. *Chem. Eur. J.* *11*, 928-938.
- (116) Chiba, T., Jacquinet, J.-C., and Sinaÿ, P. (1988) Chemical synthesis of L-iduronic acid-containing disaccharidic fragments of heparin. *Carbohydr. Res.* *174*, 253-264.
- (117) Bazin, H. G., Wolff, M. W., and Linhardt, R. J. (1999) Regio- and stereoselective synthesis of β -D-gluco-, α -L-ido-, and α -L-altropyranosiduronic acids from Δ^4 -uronates. *J. Org. Chem.* *64*, 144-152.
- (118) Timmer, M. S. M., Adibekian, A., and Seeberger, P. H. (2005) Short *de novo* synthesis of fully functionalized uronic acid monosaccharides. *Angew. Chem. Int. Ed.* *44*, 7605-7607.
- (119) Orgueira, H. A., Bartolozzi, A., Schell, P., and Seeberger, P. H. (2002) Conformational locking of the glycosyl acceptor for stereocontrol in the key step in the synthesis of heparin. *Angew. Chem. Int. Ed.* *41*, 2128-2131.
- (120) Yu, H. N., Furukawa, J., Ikeda, T., and Wong, C.-H. (2004) Novel efficient routes to heparin monosaccharides and disaccharides achieved via regio- and stereoselective glycosidation. *Org. Lett.* *6*, 723-726.
- (121) Lohman, G. J. S., and Seeberger, P. H. (2003) One-pot conversion of glycals to *cis*-1,2-isopropylidene- α -glycosides. *J. Org. Chem.* *68*, 7541-7543.
- (122) Lohman, G. J. S., Hunt, D. K., Högermeier, J. A., and Seeberger, P. H. (2003) Synthesis of iduronic acid building blocks for the modular assembly of glycosaminoglycans. *J. Org. Chem.* *68*, 7559-7561.
- (123) Kiss, J., and Taschner, P. (1977) Synthesis of heparin saccarides VI. *J. Carbohydr. Nucleosides and Nucleotides* *4*, 101-119.
- (124) Petitou, M., Duchaussoy, P., Lederman, I., Choay, J., Sinaÿ, P., Jacquinet, J.-C., and Torri, G. (1986) Synthesis of heparin fragments. A chemical synthesis of the pentasaccharide *O*-(2-deoxy-2-sulfamido-6-*O*-sulfo- α -D-glucofuranosyl)-(1 \rightarrow 4)-*O*-(β -D-glucofuranosyluronic acid)-(1 \rightarrow 4)-*O*-(2-deoxy-2-sulfamido-3,6-di-*O*-sulfo- α -D-glucofuranosyl)-(1 \rightarrow 4)-*O*-(2-*O*-sulfo-(α -L-idopyranosyluronic acid)-(1 \rightarrow 4)-2-deoxy-2-sulfamido-6-*O*-sulfo-D-glucofuranose decasodium salt, a heparin fragment having high affinity for antithrombin III. *Carbohydr. Res.* *147*, 221-236.
- (125) Petitou, M., Duchaussoy, P., Lederman, I., Choay, J., Jacquinet, J.-C., Sinaÿ, P., and Torri, G. (1987) Synthesis of heparin fragments: a methyl α -pentaoside with high affinity for antithrombin III. *Carbohydr. Res.* *167*, 67-75.

- (126) Beetz, T., and van Boeckel, C. A. A. (1986) Synthesis of an antithrombin binding heparin-like pentasaccharide lacking 6-*O* sulphate at its reducing end. *Tetrahedron Lett.* 27, 5889-5892.
- (127) Weissman, B., and Chao, H. (1986) Heparin trisaccharides with nonreducing 2-amino-2-deoxy- α -D-glucopyranosyl end-groups suitable as substrates for catabolic enzymes. *Carbohydr. Res.* 154, 217-228.
- (128) van Boeckel, C. A. A., Basten, J. E. M., Lucas, H., and van Aelst, S. F. (1988) A synthetic heparin-like compound which still activates antithrombin III although it contains an open chain fragment instead of α -L-idopyranuronate. *Angew. Chem. Int. Ed. Engl.* 27, 1177-1178.
- (129) van Boeckel, C. A. A., Beetz, T., and van Aelst, S. F. (1988) Synthesis of a potent antithrombin activating pentasaccharide: a new heparin-like fragment containing two 3-*O*-sulphated glucosamines. *Tetrahedron Lett.* 29, 803-806.
- (130) Lucas, H., Basten, J. E. M., van Dinther, T. G., Meuleman, D. G., van Aelst, S. F., and van Boeckel, C. A. A. (1990) Syntheses of heparin-like pentamers containing "opened" uronic acid moieties. *Tetrahedron* 46, 8207-8228.
- (131) Jaurand, G., Tabeur, C., and Petitou, M. (1994) Synthesis of the basic disaccharide unit of heparin. *Carbohydr. Res.* 255, 295-301.
- (132) Koshida, S., Suda, Y., Sobel, M., Ormsby, J., and Kusumoto, S. (1999) Synthesis of heparin partial structures and their binding activities to platelets. *Bioorg. Med. Chem. Lett.* 9, 3127-3132.
- (133) Ichikawa, Y., Monden, R., and Kusuhara, H. (1986) Synthesis of a heparin pentasaccharide fragment with a high affinity for antithrombin III employing cellobiose as a key starting material. *Tetrahedron Lett.* 27, 611-614.
- (134) Ichikawa, Y., Monden, R., and Kuzuhara, H. (1988) Synthesis of methyl glycoside derivatives of tri- and pentasaccharides related to the antithrombin III-binding sequence of heparin, employing cellobiose as a key starting material. *Carbohydr. Res.* 172, 37-64.
- (135) Duchaussoy, P., Leih, P. S., Petitou, M., Sinaÿ, P., Lormeau, J. C., and Choay, J. (1991) The first total synthesis of the antithrombin III binding site of porcine mucosa heparin. *Bioorg. Med. Chem. Lett.* 1, 99-102.
- (136) Lucas, R., Hamza, D., Lubineau, A., and Bonnaffe, D. (2004) Synthesis of glycosaminoglycan oligosaccharides — an unexpected inhibitory effect of a remote *N*-acetyl group upon trichloroacetimidate-mediated couplings. *Eur. J. Org. Chem.*, 2107-2117.
- (137) Castro-Palomino, J. C., and Schmidt, R. R. (1995) *N,N*-Diacetyl-glucosamine and -galactosamine derivatives as glycosyl donors. *Tetrahedron Lett.* 36, 6871-6874.
- (138) Lei, P.-S., Duchaussoy, P., Sizun, P., Mallet, J.-M., Petitou, M., and Sinaÿ, P. (1998) Synthesis of a 3-deoxy-L-iduronic acid containing heparin pentasaccharide to probe the conformation of the antithrombin III binding sequence. *Bioorg. Med. Chem.* 6, 1337-1346.
- (139) Koshida, S., Suda, Y., Sobel, M., and Kusumoto, S. (2001) Synthesis of oligomeric assemblies of a platelet-binding key disaccharide in heparin and their biological activities. *Tetrahedron Lett.* 42, 1289-1292.
- (140) Westerduin, P., Basten, J. E. M., Broekhoven, M. A., de Kimpe, V., Kuijpers, W. H. A., and van Boeckel, C. A. A. (1996) Synthesis of tailor-made glycoconjugates showing

- ATIII-mediated inhibition of blood coagulation factors Xa and thrombin. *Angew. Chem. Int. Ed.* 35, 331-333.
- (141) Petitou, M., Duchaussoy, P., Bemat, A., Hoffmann, P., and Herbert, J. M. (1997) A synthetic heparin/heparan sulfate-like decasaccharide releases lipase activity *in vivo*. Chemical synthesis and biological activity. *Bioorg. Med. Chem. Lett.* 7, 2067-2070.
- (142) Basten, J. E. M., Dreef-Tromp, C. M., de Wijs, B., and van Boeckel, C. A. A. (1998) *In vitro* evaluation of synthetic heparin-like conjugates comprising different thrombin binding domains. *Bioorg. Med. Chem. Lett.* 8, 1201-1206.
- (143) Petitou, M., Duchaussoy, P., Driguez, P.-A., Jaurand, G., Hérault, J.-P., Lormeau, J.-C., van Boeckel, C. A. A., and Herbert, J.-M. (1998) First synthetic carbohydrates with the full anticoagulant properties of heparin. *Angew. Chem. Int. Ed.* 37, 3009-3014.
- (144) Duchaussoy, P., Jaurand, G., Driguez, P.-A., Lederman, I., Ceccato, M.-L., Gourvenec, F., Strassel, J.-M., Sizun, P., Petitou, M., and Herbert, J.-M. (1999) Assessment through chemical synthesis of the size of the heparin sequence involved in thrombin inhibition. *Carbohydr. Res.* 317, 85-99.
- (145) Petitou, M., Driguez, P.-A., Duchaussoy, P., Hérault, J.-P., Lormeau, J.-C., and Herbert, J.-M. (1999) Synthetic oligosaccharides having various functional domains: potent and potentially safe heparin mimetics. *Bioorg. Med. Chem. Lett.* 9, 1161-1166.
- (146) Petitou, M., Duchaussoy, P., Driguez, P.-A., Hérault, J.-P., Lormeau, J.-C., and Herbert, J.-M. (1999) New synthetic heparin mimetics able to inhibit thrombin and factor Xa. *Bioorg. Med. Chem. Lett.* 9, 1155-1160.
- (147) Driguez, P.-A., Lederman, I., Strassel, J.-M., Herbert, J.-M., and Petitou, M. (1999) Synthetic carbohydrate derivatives as low sulfated heparin mimetics. *J. Org. Chem.* 64, 9512-9520.
- (148) Papy-Garcia, D., Barbier-Chassefière, V., Rouet, V., Kerros, M.-E., Klochendler, C., Tournaire, M.-C., Barritault, D., Caruelle, J.-P., and Petit, E. (2005) Nondegradative sulfation of polysaccharides. Synthesis and structure characterization of biologically active heparan sulfate mimetics. *Macromolecules* 38, 4647-4654.
- (149) Westman, J., Nilsson, M., Ornitz, D. M., and Svahn, C.-M. (1995) Synthesis and fibroblast growth factor binding of oligo-saccharides related to heparin and heparan sulphate. *J. Carbohydr. Chem.* 14, 95-113.
- (150) Suda, Y., Bird, K., Shiyama, T., Koshidan, S., Marques, D., Fukase, K., Sobel, M., and Kusumoto, S. (1996) Synthesis and biological activity of a model disaccharide containing a key unit in heparin for binding to platelets. *Tetrahedron Lett.* 37, 1053-1056.
- (151) Nilsson, M., Svahn, C.-M., and Westman, J. (1993) Synthesis of the methyl glycosides of a tri- and a tetra-saccharide related to heparin and heparan sulphate. *Carbohydr. Res.* 246, 161-172.
- (152) Nilsson, M., Westman, J., and Svahn, C.-M. (1993) Synthesis of tri- and tetrasaccharides present in the linkage region of heparin and heparan sulphate. *J. Carbohydr. Chem.* 12, 23-37.
- (153) Cipolla, L., Nicotra, F., Lay, L., Lindahl, U., Panza, L., and Russo, G. (1996) Synthesis of the disaccharides methyl 4-*O*-(2'/3'-*O*-sulfo- β -D-glucopyranosyluronic acid)-2-amino-2-deoxy- α -D-glucopyranoside disodium salts, related to heparin biosynthesis. *Glycoconjugate Journal* 13, 995-1003.

- (154) Kovensky, J., Duchaussoy, P., Petitou, M., and Sinaÿ, P. (1996) Binding of heparan sulfate to fibroblast growth factor-2 total synthesis of a putative pentasaccharide binding site. *Tetrahedron: Asymmetry* 7, 3119-3128.
- (155) Kovensky, J., Duchaussoy, P., Bono, F., Salmivirta, M., Sizun, P., Herbert, J.-M., Petitou, M., and Sinaÿ, P. (1999) A synthetic heparan sulfate pentasaccharide, exclusively containing L-iduronic acid, displays higher affinity for FGF-2 than its D-glucuronic acid-containing isomers. *Bioorg. Med. Chem.* 7, 1567-1580.
- (156) Tabeur, C., Mallet, J.-M., Bono, F., Herbert, J.-M., Petitou, M., and Sinaÿ, P. (1999) Oligosaccharides corresponding to the regular sequence of heparin: chemical synthesis and interaction with FGF-2. *Bioorg. Med. Chem.* 7, 2003-2012.
- (157) Poletti, L., Fleischer, M., Vogel, C., Guerrini, M., Torri, G., and Lay, L. (2001) A rational approach to heparin-related fragments—synthesis of differently sulfated tetrasaccharides as potential ligands for fibroblast growth factors. *Eur. J. Org. Chem.*, 2727-2734.
- (158) de Paz, J.-L., Ojeda, R., Reichardt, N., and Martín-Lomas, M. (2003) Some key experimental features of a modular synthesis of heparin-like oligosaccharides. *Eur. J. Org. Chem.*, 3308-3324.
- (159) de Paz, J. L., and Martín-Lomas, M. (2005) Synthesis and biological evaluation of a heparin-like hexasaccharide with the structural motifs for binding to FGF and FGFR. *Eur. J. Org. Chem.*, 1849-1858.
- (160) Haller, M. F., and Boons, G.-J. (2002) Selectively protected disaccharide building blocks for modular synthesis of heparin fragments. *Eur. J. Org. Chem.*, 2033-2038.
- (161) Prabhu, A., Venot, A., and Boons, G.-J. (2003) New set of orthogonal protecting groups for the modular synthesis of heparan sulfate fragments. *Org. Lett.* 5, 4975-4978.
- (162) Hassan, H. H. A. M. (2005) Preparation of a set of selectively protected disaccharides for modular synthesis of heparan sulfate fragments: toward the synthesis of several O-sulfonated [-D-GlcUA-(1→4)-D-GlcNAc]OPr types. *Central Eur. J. Chem.* 3, 803-829.
- (163) Kuberan, B., Beeler, D. L., Lech, M., Wu, Z. L., and Rosenberg, R. D. (2003) Chemoenzymatic synthesis of classical and non-classical anticoagulant heparan sulfate polysaccharides. *J. Biol. Chem.* 278, 52613-52621.
- (164) Kuberan, B., Beeler, D. L., Lawrence, R., Lech, M., and Rosenberg, R. D. (2003) Rapid two-step synthesis of mitrin from heparosan: a replacement for heparin. *J. Am. Chem. Soc.* 125, 12424-12425.
- (165) Werz, D. B., and Seeberger, P. H. (2005) Carbohydrates as the next frontier in pharmaceutical research. *Chem. Eur. J.* 11, 3194-3206.
- (166) Seeberger, P. H., and Werz, D. B. (2005) Automated synthesis of oligosaccharides as a basis for drug discovery. *Nat. Rev. Drug Disc.* 4, 751-763.

Chapter 2

The Synthesis of Fully Differentiated Uronic Acid Monosaccharide Building Blocks for the Synthesis of Heparin-like Glycosaminoglycans

2.1 Introduction

Glycosaminoglycan synthesis(1-5) requires large quantities of differentially protected uronic acid and glucosamine derivatives, necessitating concise and efficient methods for the production of these synthons. In particular, much effort has been expended in the development of uronic acid synthons and methodology for the formation of the glucosamine $\alpha(1\rightarrow4)$ uronic acid bond with high anomeric selectivity. Since iduronic acid itself is not commercially available, syntheses of iduronic acid derivatives from a variety of starting materials, including glucose,(6-11) glycals,(12) and glucuronic acid,(13-19) and other starting materials(20-24) have been developed. While L-idose is very costly, rendering it an undesirable starting material, syntheses using other starting materials require the inversion of the C-5 stereocenter on a D-gluco sugar. Few methods reported for this inversion have realized full selectivity for the desired configuration.(9, 10) Syntheses from idose to procure iduronic acid building blocks used in the synthesis of large heparin structures have been reported, but remain lengthy and involve several steps that produce multiple products.(25) Methods for the completely selective conversion of 5-aldopentoses to iduronic acid derivatives(10) and for the selective silylation of the anomeric hydroxyl of iduronic acids(26) have been described, but have not been incorporated into the synthesis of iduronic acid monosaccharide building blocks.

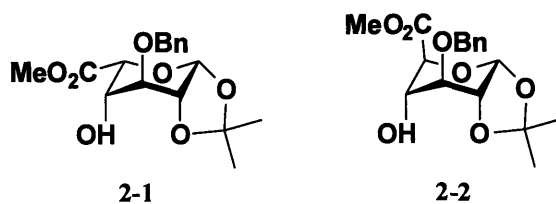


Figure 2-1. Uronic acid acceptors for the synthesis of HLGAGs.

Differentially protected uronic acids 2-1 and 2-2 (Figure 2-1) are key building blocks in the modular synthesis of heparin.(27, 28) The 1,2-isopropylidene group has been shown to lock

2-2 in the 1C_4 conformation naturally taken by iduronic derivatives in solution, forcing the C4 hydroxyl into an axial position. Glycosylation of this axial hydroxyl group with C2 azido-protected glucosamine trichloroacetimidates resulted in the formation of the glycosidic bond with complete α -selectivity for both **2-1** and **2-2**.⁽²⁸⁾ The syntheses of **2-1** and **2-2** previously described relied on the interconversion of the furanose and pyranose forms of the sugars, resulting in a mixture of products and variable yields of the desired compound, particularly for **2-2**.⁽²⁸⁾

Glycals are versatile intermediates in the synthesis of oligosaccharides and other natural products.⁽²⁹⁾ The challenge of differential protection of carbohydrates is significantly simplified in glycals as only three, rather than five, hydroxyl groups need to be distinguished. Glycals have previously served as starting materials for the synthesis of differentiated glucuronic acid building blocks, important synthons for the modular assembly of glycosaminoglycans,⁽¹²⁾ though syntheses of large GAG structures have not yet involved glycals in the production of glucuronic acid monomers. Direct conversion of a protected glycal to the 1,2- isopropylidene- α -glycoside would avoid the problem of furanose-pyranose conversion and potentially provide more convenient access to **2-2**. The reaction of glycals, enol ethers, or enol ether epoxides to isopropylidene-protected diols has not been previously described.

This chapter outlines a short synthetic route to iduronic acid building blocks through the conversion of diacetone glucose to the key intermediate methyl 3-*O*-benzyl-1,2-*O*-isopropylidene- α -L-idopyranosiduronate **2-1**. This iduronic acid derivative can serve as a glycosyl acceptor or can be readily converted to fully differentiated iduronic acid trichloroacetimidate glycosyl donors. The synthesis described incorporates a number of past chemistries through improved and simplified procedures, and requires only a few purification

steps. Further, the development of a new reaction for the conversion of glycols to 1,2-isopropylidenes is described, and applied to the synthesis of **2-2**.

2.2 Experimental

Materials and Methods. All commercial materials were used without purification, unless otherwise noted. CH₂Cl₂, THF, and diethyl ether were passed through neutral alumina columns prior to use. Toluene was passed through neutral alumina and copper (II) oxide columns before use. Methanol and DMF were purchased anhydrous and used without further purification. Analytical thin-layer chromatography was performed on E. Merck silica gel 60 F254 plate (≤ 0.25 mm). Compounds were visualized by cerium sulfate-ammonium molybdate stain and heating. Liquid chromatography was performed using forced flow of the indicated solvent on silica (230-400 Mesh).

3-O-benzyl-1,2-isopropylidene- α -D-glucofuranoside (2-4). Commercially-available diacetone glucose **2-3** (16.6 g, 63.8 mmol) was dissolved in THF (160 mL) and NaH (60% in mineral oil) (3.1 g, 77 mmol) was added in portions. After evolution of hydrogen ceased, tetrabutylammonium iodide (160 mg, 0.43 mmol) and benzyl bromide (8 mL, 67.2 mmol) were added and the mixture stirred for 14 h at room temperature. Water was added slowly to the reaction mixture and the organic layer evaporated under reduced pressure. The aqueous phase was extracted with ethyl acetate (3 x 250 mL) and the organic phases combined and dried over MgSO₄, filtered through a plug of silica, and the solvent removed under reduced pressure.

Aqueous acetic acid (66%, 100 mL) was added to the resulting oil and stirred 16 h at room temperature. The reaction mixture was evaporated under reduced pressure and the residue dissolved in CH₂Cl₂ and washed with saturated aq. NaHCO₃. The aqueous phase was extracted

with CH₂Cl₂ (2 x 250 mL) and the combined organic phases dried over MgSO₄ and the solvent removed under reduced pressure. Flash silica gel column chromatography gel (hexanes-ethyl acetate 9:1 → 1:1) yielded **2-4** (17.8 g, 57.4 mmol, 90%). Spectra were consistent with previously reported data.^(30, 31)

Methyl 3-O-benzyl-1,2-isopropylidene-β-L-idofuranosiduronate (2-5). To a suspension of silica gel (150 g) in CH₂Cl₂ (1.2 L) was added a solution of NaIO₄ (16.12 g, 74.5 mmol) in water (100 mL). The suspension was stirred vigorously for 30 minutes, followed by addition of a solution of **2-4** (17.8 g, 57.3 mmol) in CH₂Cl₂ (200 mL). The reaction was stirred for 1.5 h, followed by filtration through Celite and concentration under reduced pressure. The residue was dried under vacuum over P₂O₅ and used without further purification.

To a flame-dried three-necked flask was added tris(phenylthio)orthoformate (23.4 g, 68.6 mmol), followed by THF (110 mL). The reaction vessel was cooled to -78 °C and *n*-butyl lithium (1.6 M in hexanes, 39.4 mL, 63 mmol) was added dropwise. The bright yellow solution was allowed to warm slowly to -50 °C over 1 h, then cooled to -78 °C and stirred for 30 minutes. Crude aldehyde **2-6** from the previous step (~57.3 mmol) was dissolved in THF (160 mL) and added dropwise via cannula to the reaction flask over 15 min. The reaction was stirred at -78 °C for 1 h, allowed to warm to room temperature over 30 min, then quenched with saturated aqueous NH₄Cl (500 mL). The aqueous phase was extracted with EtOAc (3 x 500 mL), and the combined organic phases were dried over MgSO₄, filtered, concentrated under reduced pressure, and dried under vacuum. The crude product was used without further purification.

To CuCl₂ (46.9 g, 275 mmol) and CuO (79.95 g, 114.6 mmol) suspended in methanol:water (12:1, 650 mL) was added crude material from the previous step in CH₂Cl₂ (200 mL). The reaction was stirred at ambient temperature for 5 min and then the solvent was

evaporated under reduced pressure with gentle heat. The resulting green-white solid was dissolved in EtOAc (1 L) and washed with 1 N HCl (2 x 500 mL), brine (2 x 500 mL), and saturated aqueous NaHCO₃ (500 mL). The combined organic layers were dried over MgSO₄, filtered, concentrated under reduced pressure, and dried under vacuum for 1 h. The resulting oil was dissolved in CH₂Cl₂ (525 mL) and methanol (75 mL) and K₂CO₃ (2 g, 14.3 mmol) was added. The reaction was stirred at ambient temperature for 1.5 h, then the solution filtered through Celite and concentrated under reduced pressure. Purification via flash silica gel column chromatography (5%→30% EtOAc/hexanes) afforded **2-5** (15.4 g, 79%) as a light yellow oil. Spectra were consistent with reported data.(10)

Methyl 3-O-benzyl-1,2-isopropylidene-β-L-idopyranosiduronate (2-1). Compound **2-5** (15.4 mg, 45.4 mmol) was dissolved in 90% aqueous trifluoroacetic acid (40 mL) and stirred at ambient temperature for 35 min. The reaction solvent was removed and the crude product was crystallized from 4:1 Et)Ac:hexanes to give 10.4 g of a white solid. This material was coevaporated with toluene (5 x 25 mL), and dried under vacuum for 18 h. The resulting white solid **2-7** was dissolved in 2-methoxypropene (70 mL) and cooled to 0°C. To the cooled reaction mixture was added (+)-camphorsulfonic acid (838 mg, 3.62 mmol) dissolved in DMF (8.5 mL). The reaction was stirred at 0 °C for 3 h, then quenched with NEt₃ (2 mL) and allowed to warm to room temperature. The reaction solvent was removed under reduced pressure and the reaction mixture was dried under vacuum 18 h. The crude product was dissolved in methanol (250 mL), washed Dowex acidic resin (5 g) was added, and the reaction stirred at ambient temperature 20 min. The resin was filtered off, the reaction concentrated under reduced pressure and purified via flash silica gel column chromatography to afford product **2-1** (7.68 g, 50%) and recovered triol **2-7** (1.95 g, 12.5%). Spectra were in agreement with reported data.(27)

Methyl 4-*O*-allyl-3-*O*-benzyl-1,2-isopropylidene- β -L-idopyranosiduronate (2-8). Compound **2-1** (350 mg, 1.03 mmol) was coevaporated three times with toluene. The compound was dissolved in CH₂Cl₂ (4 mL) and allyl bromide (1 mL, 12.36 mmol), passed through a plug of basic alumina before use, and freshly activated 4Å molecular sieves (700 mg) were added. After stirring for 30 min, Ag₂O (720 mg, 3.1 mmol) was added and the reaction stirred for 3 days under N₂ and exclusion of light. The reaction mixture was filtered through Celite and the solvent removed under reduced pressure. Flash silica gel column chromatography (toluene:EtOAc 30:1) afforded **2-8** (270 mg, 0.72 mmol, 70%) as a clear oil. Rf. 0.32 (hexanes:ethyl acetate 2:1). $[\alpha]_D^{24}$: -40.9, (c = 1.27). IR (thin film, NaCl plate) 2986, 1766, 1736, 852, 752 cm⁻¹. ¹HNMR (500 MHz, CDCl₃) δ 7.32-7.4 (m, 5H), 5.75-5.83 (m, 1H), 5.35 (d, *J* = 2.6 Hz, 1H), 5.21 (d², *J* = 1.6 Hz, 17 Hz), 5.13 (d², *J* = 1.7 Hz, 10.4 Hz, 1H), 4.68 (d, *J* = 11.9 Hz, 1H), 4.65 (d, *J* = 11.9 Hz, 1H), 4.43 (d, *J* = 1.7 Hz, 1H), 3.98-4.06 (m, 3H), 3.88-3.92 (m, 1H), 3.82 (m, 1H), 3.8 (s, 3H), 1.6 (s, 3H), 1.4 (s, 3H). ¹³CNMR (125 MHz, CDCl₃) δ 169.7, 137.4, 134.6, 128.8, 128.4, 128.1, 117.3, 112.4, 97.0, 75.5, 73.0, 72.7, 71.9, 71.1, 52.5, 28.0, 26.7. ESI MS (C₂₀H₂₆O₇) *m/z* (M + Na⁺) calcd 401.1571, obsd 401.1571.

Methyl 3,4-di-*O*-benzyl-1,2-isopropylidene- β -L-idopyranosiduronate (2-9). Compound **2-1** (183 mg, 0.54 mmol) was coevaporated three times with toluene and dissolved in CH₂Cl₂ (2 mL). Benzyl bromide (640 μ L, 5.4 mmol), passed through a plug of basic alumina before use, and freshly activated 4Å molecular sieves (360 mg) were added. After 30 min, Ag₂O (500 mg, 2.16 mmol) was added and the reaction stirred for 3 days under N₂ and exclusion of light. The reaction mixture was filtered through Celite and the solvent removed under reduced pressure. Flash silica gel column chromatography on (toluene:ethyl acetate 30:1) afforded **2-9** (179 mg, 0.42 mmol, 77%) as a clear oil. Rf. 0.32 (hexanes:ethyl acetate 2:1). $[\alpha]_D^{24}$: -26.8, (c = 1.00).

IR (thin film, NaCl plate) 2916, 1768, 1735, 738, 698 cm^{-1} . ^1H NMR (500 MHz, CDCl_3) 7.26-7.39 (m, 10H), 5.36 (d, $J = 2.6$ Hz, 1H), 4.58-4.62 (m, 3H), 4.43 (m, 2H), 4.09 (t, $J = 2.32$ Hz, 1H), 3.99 (d, $J = 3.2$ Hz, 1H), 3.85 (m, 1H), 3.73 (s, 3H), 1.61 (s, 3H), 1.41 (s, 3H). ^{13}C NMR (125 MHz, CDCl_3) δ 169.7, 138.0, 137.3, 128.8, 128.41, 128.39, 128.0, 127.8, 112.5, 97.0, 75.5, 73.2, 72.7, 72.0, 71.9, 71.8, 52.5, 28.1, 28.7. ESI MS ($\text{C}_{24}\text{H}_{28}\text{O}_7$) m/z ($\text{M} + \text{Na}^+$) calcd 451.1727, obsd 451.1736.

Methyl 3-*O*-benzyl-1,2-isopropylidene-4-*O*-levulinyl- α -L-idopyranosiduronate (2-10).

Compound **2-1** (2.69 g, 7.95 mmol) was dissolved in CH_2Cl_2 (50 mL) and cooled to 0 $^\circ\text{C}$. To this solution were added levulinic acid (1.34 mL, 12.7 mmol), DIPC (1.87 mL, 11.9 mmol), and DMAP (1.56 g, 12.8 mmol), and light was excluded. The reaction was allowed to warm to room temperature and was stirred for 11 h. The reaction mixture was diluted with EtOAc:hexanes (1:1), run through a silica plug, and concentrated under reduced pressure. Purification via flash silica gel column silica gel column chromatography (30% \rightarrow 50% EtOAc/hexanes) afforded **2-10** (3.44 g, 98%) as a yellow oil. $[\alpha]_{\text{D}}^{24}$: -32.0, ($c=1.00$). IR (thin film, NaCl plate) 2934, 1766, 1742, 1721 cm^{-1} . ^1H NMR (500 MHz, CDCl_3) δ 7.39-7.33 (m, 5H), 5.37 (d, $J = 2.61$ Hz, 1H), 5.20 (m, 1H), 4.82 (d, $J = 1.6$ Hz, 1H), 4.68 (d, $J = 1.6$ Hz, 1H), 4.53 (d, $J = 1.5$ Hz, 1H), 4.08 (wt, $J = 2.1$ Hz, 1H), 3.93 (m, 1H), 3.8 (s, 3H), 2.75 (m, 2H), 2.56 (t, $J = 6.4$ Hz, 2H), 2.18 (s, 3H), 1.62 (s, 3H), 1.38 (s, 3H). ^{13}C NMR (125 MHz, CDCl_3) δ 206.9, 172.5, 168.9, 137.7, 129.3, 128.9, 128.6, 112.7, 97.2, 75.8, 73.5, 72.8, 70.7, 67.8, 38.5, 30.4, 28.7, 28.6, 26.9. ESI MS ($\text{C}_{22}\text{H}_{28}\text{O}_9$) m/z ($\text{M} + \text{Na}^+$) calcd 459.1626, obsd 459.1617.

Methyl 1,2-di-*O*-acetyl-4-*O*-allyl-3-*O*-benzyl-L-idopyranosiduronate (2-11a/b).

Monosaccharide **2-8** (575 mg, 1.52 mmol) was dissolved in TFA (90% aq., 3 mL) and stirred for

30 min. The solvent was removed under reduced pressure and the residue coevaporated with toluene until the odor of TFA could no longer be detected.

The resultant oil was dissolved in CH₂Cl₂ (13 mL) and pyridine (1.8 mL). Acetic anhydride (575 μL, 6.08 mmol) and DMAP (36 mg, 0.3 mmol) were added and the reaction was stirred under N₂ overnight. Water (1 mL) was added, the mixture stirred 30 min and poured into 200 mL ethyl acetate. The combined organic phases were washed with 1N HCl, brine, and saturated aq. NaHCO₃. The organic phase was dried over MgSO₄, filtered, and the solvent removed under reduced pressure. Flash silica gel column chromatography (hexanes:ethyl acetate 3:1) yielded **2-11a/b** as a clear oil (628 mg, 1.44 mmol, 98%, 1:2 α:β) **2-11a** (α) Rf. 0.17 (hexanes:ethyl acetate 2:1). [α]²⁴_D: -64.0, (c = 0.60). IR (thin film, NaCl plate) 2361, 1750, 1745, 1735 cm⁻¹. ¹HNMR (500 MHz, CDCl₃) δ 7.31-7.39 (m, 5H, aromatics), 6.27 (s, 1H, H1), 5.75 (m, 1H, -OCH₂CH=CH₂), 5.16 (m, 1H, -OCH₂CH=CHH), 5.13 (m, 1H, -OCH₂CH=CHH), 4.93 (s, 1H, H2), 4.86 (d, ³J_{H5-H4} = 2.5 Hz, 1H, H5), 4.76 (d, ²J = 11.9, 1H, benzyl CH₂), 4.68 (d, ²J = 11.9, 1H, benzyl CH₂), 3.98 (d², ²J = 12.8 Hz, ³J = 5.7 Hz, 1H, -OCHHCH=CH₂), 3.91 (d², ²J = 12.8 Hz, ³J = 5.9 Hz, 1H, -OCHHCH=CH₂), 3.89 (ψt, J = 3.3 Hz, 1H, H3), 3.85 (d, J = 2.5 Hz, 1H, H4), 3.81 (s, 3H, -OCH₃), 2.08 (s, 3H, O2-acetate), 2.05 (s, 3H, O1-acetate). ¹³CNMR (125 MHz, CDCl₃) δ 170.2 (O2 acetate carbonyl), 169.4 (C6), 168.9 (O1 acetate carbonyl), 137.7 (aromatic quat.), 134.1 (-OCH₂CH=CH₂), 128.7 (aromatic C), 128.2 (aromatic C), 127.9 (aromatic C), 118.0 (-OCH₂CH=CH₂), 92.0 (C1), 74.2 (C4), 72.6 (benzyl CH₂), 71.8 (-OCH₂CH=CH₂), 71.3 (C3), 70.2 (C5), 66.7 (C2), 52.6 (-OCH₃), 21.7 (O2 acetate), 21.1 (O1 acetate). ESI MS (C₂₁H₂₆O₉) m/z (M + Na⁺) calcd 445.1469, obsd 445.1472. **2-11b** (β) Rf. 0.11 (hexanes:ethyl acetate 2:1). [α]²⁴_D: -7.86, (c = 1.43). Mp 96-98°C. IR (thin film, NaCl plate) 2361, 1761, 1742, 1739, 1064 cm⁻¹. ¹HNMR (500 MHz, CDCl₃) δ 7.32-7.4 (m, 5H, aromatics),

6.08 (d, $^3J_{H1-H2} = 1.7$ Hz, 1H, H1), 5.71 (m, 1H, O-CH₂CH=CH₂), 5.14 (m, 1H, O-CH₂CH=CHH), 5.09 (m, 1H, O-CH₂CH=CHH), 4.99 (m, 1H, H2), 4.76 (d, $^2J = 11.9$ Hz, 1H, benzyl CH₂), 4.67 (d, $^3J_{H4-H5} = 2.2$ Hz, 1H, H5), 4.64 (d, $^2J = 11.9$ Hz, 1H, benzyl CH₂), 3.99 (ψt, $J = 3$ Hz, 1H, H3), 3.89 (m, 1H, O-CHHCH=CH₂), 3.84 (m, 1H, O-CHHCH=CH₂), 3.79 (s, 3H, -OCH₃), 3.72 (ψt, $J = 2.2$ Hz, 1H, H4), 2.12 (s, 3H, O1 acetate), 2.11 (s, 3H, O2 acetate).

¹³CNMR (125 MHz, CDCl₃) δ 171.0 (O2-acetate carbonyl), 169.0 (O1-acetate carbonyl), 168.6 (C6), 137.1 (benzyl quat.), 134.1 (O-CH₂CH=CH₂), 128.8 (aromatic C), 128.5 (aromatic C), 128.2 (aromatic C), 117.6 (O-CH₂CH=CH₂), 90.2 (C1), 75.1 (C5), 73.7 (C4), 72.9 (benzyl CH₂), 71.7 (O-CH₂CH=CH₂), 71.8 (C3), 66.7 (C2), 52.5 (-OCH₃), 21.2 (O1-acetate), 21.1 (O2-acetate). ESI MS (C₂₁H₂₆O₉) m/z (M + Na⁺) calcd 445.1469, obsd 445.1451.

Methyl 2-O-acetyl-4-O-allyl-3-O-benzyl-L-idopyranosiduronate trichloroacetimidate (2-12).

Procedure A. Compound **2-11a** (117 mg, 0.277 mmol) was coevaporated three times with toluene and dissolved in THF (2.8 mL). Benzyl amine (182 μL, 1.66 mmol) was added and the reaction was stirred 4 h and monitored by TLC. The reaction was poured into 1N HCl and the aqueous phase was extracted with ethyl acetate (2 x 100 mL). The combined organic phases were dried over MgSO₄, filtered, and the solvent removed under reduced pressure. Flash silica gel column chromatography (hexanes:ethyl acetate 6:4) afforded the lactol (78 mg, 0.205 mmol, 74%) as a clear oil.

Procedure B. Compound **2-11b** (262 mg, 0.62 mmol) was coevaporated three times with toluene and dissolved in THF (6 mL). Benzyl amine (237 μL, 2.17 mmol) was added and the reaction was stirred 5.5 h and monitored by TLC. The reaction was poured into 1N HCl and the aqueous phase was extracted with ethyl acetate (2 x 150 mL). The combined organic phases were dried over MgSO₄, filtered, and the solvent removed under reduced pressure. Flash silica

gel column chromatography (hexanes:ethyl acetate 6:4) afforded lactol (200 mg, 0.53 mmol, 85%) as a clear oil.

Lactol (785 mg, 2.06 mmol) was coevaporated three times with toluene and dissolved in CH₂Cl₂ (16 mL) under N₂. The solution was cooled to 0°C and trichloroacetonitrile (3.1 mL, 31 mmol) and DBU (58 μL) were added. The reaction was stirred for 30 min, then allowed to warm to room temperature. The solvent was removed under reduced pressure and the residue was purified by flash silica gel column chromatography (hexanes:ethyl acetate 7:3) to afford **2-12** (1.0 g, 1.91 mmol, 92%, 3:2 mixture of anomers) as a yellow oil. Rf. 0.29, 0.37 (hexanes:ethyl acetate 2:1). IR (thin film, NaCl plate) 2920, 1772, 1736, 1675, 1064 cm⁻¹. ¹H NMR (500 MHz, CDCl₃) δ 8.66 (s, 1H), 7.29-7.39 (m, 5H), 6.43 (s, 0.6H), 6.23 (d, *J* = 2 Hz, 0.4H), 5.71-5.78 (m, 1H), 5.75 (m, 0.4H), 5.09-5.74 (m, 2H), 4.98 (d, *J* = 2.2 Hz, 0.6H), 4.65-4.81 (m, 3H), 3.80-4.06 (m, 7H), 2.10 (s, 2H), 2.09 (s, 1.5H). ¹³C NMR (125 MHz, CDCl₃) δ 170.9, 170.2, 169.3, 168.4, 160.7, 160.3, 137.5, 137.1, 134.1, 128.7, 128.6, 128.5, 128.4, 128.2, 128.1, 118.2, 118.0, 95.6, 94.6, 91.0, 90.7, 75.1, 73.8, 73.7, 72.9, 72.7, 72.1, 71.8, 71.7, 70.5, 69.9, 66.1, 65.5, 52.7, 52.6, 21.2, 21.5. ESI MS (C₂₁H₂₄Cl₃NO₈) *m/z* (M + Na⁺) calcd 546.0460, obsd 546.0433.

Methyl (t-butyldimethylsilyl 3,4-di-O-benzyl-β-L-idopyranosid)uronate (2-13).

Monosaccharide **2-9** (179 mg, 0.42 mmol) was dissolved in TFA (90% aq., 1 mL) and stirred for 30 min. The solvent was removed under reduced pressure and the residue coevaporated three times with toluene. The crude material was dissolved in CH₂Cl₂ (420 μL) and cooled to -25°C under N₂. TBDMS-Cl (95 mg, 0.63 mmol) and imidazole (114 mg, 1.67 mmol) were added and the reaction was stirred for 14 h at -25°C. Methanol (2 mL) was added and the mixture stirred 30 min, the poured into ethyl acetate. The organic phase was washed with 1N HCl, brine, and saturated aq. NaHCO₃. The organic phase was dried over MgSO₄ and solvent removed under

reduced pressure. Flash silica gel column chromatography (hexanes:ethyl acetate 9:1) afforded **2-13** (166 mg, 0.33 mmol, 79%) as a clear oil (9:1 β : α). Rf. 0.53 (hexanes:ethyl acetate 2:1). IR (thin film, NaCl plate) 3527, 2928, 2857, 1772, 1734, 838, 780 cm^{-1} . ^1H NMR (500 MHz, CDCl_3) 7.15-7.4 (m, 10H (α/β)), 5.34(s, 1H (α)), 5.03 (d, $J = 1$ Hz, 1H (β)), 4.92 (d, $J = 1.9$ Hz, 1H (α)), 4.42-4.7 (m, 5H (α/β)), 3.98 (m, 1H (α)), 3.92 (m, 1H (β)), 3.86 (m, 1H, (α)), 3.80 (m, 1H (β)), 3.71 (s, 3H (α)), 3.70 (s, 3H, (β)), 3.65 (m, 1H (α/β)), 3.4 (m, 1H (α)), 3.08 (bs, 1H, (β)), 0.94 (s, 9H (β)), 0.87 (s, 9H (α)), 0.20 (s, 3H, (β)), 0.16 (s, 3H, (β)), 0.14 (s, 3H (α)), 0.12 (s, 3H (α)). ^{13}C NMR (125 MHz, CDCl_3) β : δ 1.69.3, 137.5, 137.0, 128.8, 128.7, 128.6, 128.4, 128.3, 94.7, 74.4, 74.0, 73.7, 72.8, 72.5, 69.0, 52.2, 26.0, 28.4, -3.9, -4.9. α : δ 170.5, 138.0, 136.9, 129.2, 128.9, 128.5, 128.4, 128.2, 127.6, 96.0, 75.4, 73.1, 71.8, 67.6, 67.4, 52.4, 25.7, 18.0, -4.4, -5.4. ESI MS ($\text{C}_{27}\text{H}_{38}\text{O}_{7\text{Si}}$) m/z ($\text{M} + \text{Na}^+$) calcd 525.2284, obsd 525.2269.

Methyl (t-butyldimethylsilyl 3,4-di-O-benzyl-2-O-levulinoyl- β -L-idopyranosid)uronate (2-14). Compound **2-13** (58 mg, 0.115 mmol) was coevaporated three times with toluene and dissolved in CH_2Cl_2 (1 mL). DMAP (56 mg, 0.46 mmol) and levulinic anhydride (74 mg, 0.345 mmol) were added and the reaction was stirred overnight under N_2 with exclusion of light. The reaction mixture was poured into ethyl acetate (50 mL) and washed with 1N HCl, brine, and saturated aq. NaHCO_3 . The organic phase was dried over MgSO_4 , filtered, and the solvent removed under reduced pressure. Flash silica gel column chromatography on a Biotage automated chromatograph (hexanes:ethyl acetate 3:1) afforded **2-14** (55 mg, 0.092 mmol, 80%) as a clear oil. Rf. 0.4 (hexanes:ethyl acetate 2:1). $[\alpha]_D^{24}$: +10.6, ($c = 0.89$). IR (thin film, NaCl plate) 2928, 2857, 1770, 1736, 1721, 839 cm^{-1} . ^1H NMR (500 MHz, CDCl_3) δ 7.21-7.46 (m, 10H, aromatics), 5.07 (d, $^3J_{\text{H1-H2}} = 1.7$ Hz, 1H, H1), 4.92 (m, 1H, H2), 4.64 (d, $^2J = 11.9$ Hz, 1H, O3-benzyl CH_2), 4.54 (d, $^2J = 11.9$ Hz, 1H, O3-benzyl CH_2), 4.51 (d, $^2J = 12$ Hz, 1H, O4-benzyl

CH₂), 4.48 (d, $J = 2.2$, 1H, H5), 4.39 (d, $^2J = 12$ Hz, 1H, O4-benzyl CH₂), 3.88 (ψt, $J = 2.9$ Hz, 1H, H3), 3.73 (m, 1H, H4), 3.72 (s, 3H, -OCH₃), 2.56-2.76 (m, 4H, Lev CH₂), 2.13 (s, 3H, Lev -COCH₃), 0.89 (s, 9H TBDMS butyl CH₃), 0.18 (s, 3H, TBDMS methyl), 0.15 (s, 3H TBDMS methyl). ¹³CNMR (125 MHz, CDCl₃) δ 206.7, 172.8, 169.2 (C6), 137.8 (O4-benzyl quat.), 137.5 (O3-benzyl quat.), 128.8 (aromatic C), 128.5 (aromatic C), 128.4 (aromatic C), 128.3 (aromatic C), 128.1 (aromatic C), 93.1 (C1), 74.3 (C5), 73.3(C4), 73.0 (C3), 72.9 (O3-benzyl CH₂), 72.6 (O4-benzyl CH₂), 68.2 (C2), 52.2 (-OCH₃), 38.0 (Lev CH₂), 30.1 (Lev COCH₃), 28.4 (Lev CH₂) 25.1 (TBDMS butyl CH₃), 18.2 (TBDMS quat.), -3.8 (TBDMS methyl), -5.3 (TBDMS methyl). ESI MS (C₃₂H₄₄O₉Si) m/z (M + Na⁺) calcd 623.2647, obsd 623.2618.

Methyl 3,4-di-O-benzyl-2-O-levulinoyl-L-idopyranosiduronate trichloroacetimidate (2-15).

Monosaccharide **2-14** (65 mg, 0.108 mmol) was coevaporated three times with toluene and dissolved in THF (1 mL). The solution was cooled to 0°C and acetic acid (7 μL) was added followed by TBAF (1.0 M in THF, 119 μL, 0.119 mmol). After 1 h, the reaction was poured into ethyl acetate (100 mL) and washed twice with brine. The organic phase was dried over MgSO₄, filtered, and the solvent removed under reduced pressure.

The residue was coevaporated three times with toluene and dissolved in CH₂Cl₂ (1 mL) under N₂. The solution was cooled to 0°C and trichloroacetonitrile (162 μL) and DBU (3 μL) were added. The reaction was stirred for 30 min then allowed to warm to room temperature. Solvent was evaporated and the residue purified by flash silica gel column chromatography (silica quenched with 1% NEt₃ in toluene, eluted with toluene:ethyl acetate 19:1) afforded **2-15** (65 mg, 0.102 mmol, 95%, 1:1 α:β) as a yellow oil. α: Rf. 0.09, (hexanes:ethyl acetate 2:1). $[\alpha]_D^{24}$: -37.3, (c = 1.42). IR (thin film, NaCl plate) 3339, 1774, 1741, 1723, 1673 cm⁻¹. ¹HNMR (500 MHz, CDCl₃) δ 8.66 (s, 1H), 7.14-7.38 (m, 10H), 6.43 (s, 1H), 5.15 (m, 1H), 4.96 (d, $J =$

1.9 Hz, 1H), 4.78 (d, $J = 11.7$ Hz, 1H), 4.62 (d, $J = 11.9$ Hz, 1H), 4.57 (d, $J = 11.6$ Hz, 1H), 4.45 (d, $J = 11.7$ Hz, 1H), 3.91-3.93 (m, 2H), 3.73 (s, 3H), 2.74-2.80 (m, 1H), 2.54-2.66 (m, 3H), 2.16 (s, 3H). ^{13}C NMR (125 MHz, CDCl_3) δ 206.5, 172.1, 165.3, 160.3, 137.52, 137.5, 128.7, 128.6, 128.3, 128.2, 128.15, 128.1, 95.6, 91.1, 73.6, 72.5, 72.4, 70.5, 69.9, 65.6, 52.6, 37.9, 30.0, 28.5. ESI MS ($\text{C}_{28}\text{H}_{30}\text{Cl}_3\text{NO}_9$) m/z ($\text{M} + \text{Na}^+$) calcd 652.0878, obsd 652.0889. β : Rf. 0.21 (hexanes:ethyl acetate 2:1). $[\alpha]_D^{24}$: -3.66, ($c = 1.12$). IR (thin film, NaCl plate) 3031, 1772, 1739, 1717, 1674 cm^{-1} . ^1H NMR (500 MHz, CDCl_3) δ 8.66 (s, 1H), 7.21-7.40 (m, 10H), 6.22 (d, $J = 1.9$ Hz, 1H), 5.25 (m, 1H), 4.72 (d, $J = 11.7$, 1H), 4.69 (d, $J = 2.4$, 1H), 4.59 (d, $J = 11.7$ Hz, 1H), 4.55 (d, $J = 11.8$, 1H), 4.41 (d, $J = 11.7$, 1H), 4.03 (t, $J = 2.4$, 1H), 3.81 (m, 1H), 3.73 (s, 3H), 2.58-2.71 (m, 4H), 2.14 (s, 3H). ^{13}C NMR (125 MHz, CDCl_3) δ 206.5, 172.6, 168.3, 160.6, 137.4, 137.1, 128.8, 128.7, 128.5, 128.4, 128.3, 128.2, 94.6, 90.7, 75.2, 73.6, 73.0, 72.8, 72.3, 66.1, 52.5, 37.9, 30.0, 28.3. ESI MS ($\text{C}_{28}\text{H}_{30}\text{Cl}_3\text{NO}_9$) m/z ($\text{M} + \text{Na}^+$) calcd 652.0878, obsd 652.0874.

Methyl (dimethylhexylsilyl-3-*O*-benzyl-4-*O*-levulinoyl-*L*-idopyranosid)uronate (2-16).

Compound 2-10 (503 mg, 1.15 mmol) was dissolved in 90% aqueous trifluoroacetic acid (10 mL) and stirred at ambient temperature for 15 min. The reaction solvent was removed *in vacuo* and the resulting oil coevaporated with toluene (5 x 10 mL), and dried under vacuum 18 h. The resulting brown oil was dissolved in CH_2Cl_2 (1.2 mL) and imidazole (304 mg, 4.4 mmol) was added. The solution was cooled to -20 °C and dimethylhexylsilyl chloride (0.290 mL, 1.5 mmol) was added. The reaction was stirred at -20 °C for 41 h, when it was quenched with saturated aq. NaHCO_3 (1 mL) and allowed to warm to room temperature. The reaction was diluted with CH_2Cl_2 and washed with brine. The aqueous layer was extracted with CH_2Cl_2 and the combined organic phases were dried over MgSO_4 , filtered, concentrated under reduced

pressure, and purified via flash silica column chromatography (33%→50% EtOAc/hexanes) to afford **2-16** (500 mg, 80%, α : β 1:2.5) as a clear oil. α : $[\alpha]_D^{24} = -54.9^\circ$ (c 2.35, CH₂Cl₂). IR (thin film, NaCl plate) 1744, 1719, 1364, 1153, 1054 cm⁻¹. ¹H NMR (500 MHz) δ 7.39-7.28 (m, 5H, aromatics), 5.31 (s, 1H, h1), 5.27 (at, $J = 2.8$ Hz, 1H, H4), 4.97 (d, $J = 2.4$ Hz, 1H, H5), 4.67 (dd, $J = 11.6, 14.0$ Hz, 2H, O3-benzyl CH₂), 3.78 (s, 3H, OMe), 3.76 (at, $J = 2.4$ Hz, 1H, H3), 3.60 (bd, $J = 10.1$ Hz, 1H, H2), 2.73 (t, $J = 10.0$ Hz, 2H, Lev CH₂), 2.58-2.48 (m, 3H, Lev CH₂, OH), 2.17 (s, 3H, Lev CH₃), 1.60-1.56 (m, 1H, SiC(CH₃)₂C(CH₃)₂-H), 0.83-0.81 (m, 12H, SiC(CH₃)₂C(CH₃)₂-H), 0.17 (s, 3H, Si-CH₃), 0.14 (s, 3H, Si-CH₃). ¹³C NMR (125 MHz) δ 206.4, 171.4, 169.4, 137.9, 128.4, 127.9, 127.7, 96.0, 75.0, 72.6, 69.3, 69.0, 66.5, 52.6, 38.0, 34.1, 29.8, 28.1, 25.0, 20.2, 20.1, 18.6, 18.6, -2.3, -3.5. ESI MS m/z (M + Na⁺) calculated 561.2490, found 561.2488. β : $[\alpha]_D^{24} = +8.65^\circ$ (c 1.90, CH₂Cl₂). IR (thin film, NaCl plate) 1768, 1742, 1721, 1154, 1048 cm⁻¹. ¹H NMR (500 MHz) δ 7.38-7.32 (m, 5H, aromatics), 5.17 (s, 1H, H4), 5.04 (as, 1H, H1), 4.77 (d, $J = 11.9$ Hz, 1H, O3-benzyl CH₂), 4.63 (d, $J = 11.9$ Hz, 1H, O3-benzyl CH₂), 4.60 (as, 1H, H5), 3.92-3.91 (m, 1H, H3), 3.80 (s, 3H, OMe), 3.58 (s, 1H, H2), 2.74-2.71 (m, 2H, Lev CH₂), 2.60-2.52 (m, 2H, Lev CH₂), 2.43 (d, $J = 4.9$ Hz, 1H, OH), 2.18 (s, 3H, Lev Me), 1.67-1.64 (m, 1H, SiCMe₂CMe₂-H), 0.91-0.88 (m, 12H, SiCMe₂CMe₂-H), 0.26 (s, 3H, Si-Me), 0.19 (s, 3H, Si-Me). ¹³C NMR (125 MHz) δ 206.4, 171.9, 168.1, 137.5, 128.7, 128.3, 128.0, 94.3, 75.2, 72.9, 72.7, 68.8, 67.5, 52.6, 38.0, 34.2, 29.9, 28.3, 25.1, 20.4, 20.2, 18.8, 18.6, -1.7, -3.3. ESI MS m/z (M + Na⁺) calculated 561.2490, found 561.2473.

Methyl (dimethylthexylsilyl 3-O-benzyl-4-O-levulinoyl-2-O-pivaloyl-L-

idopyranosid)uronate (2-17). Compound **2-16** (541 mg, 1.00 mmol) was dissolved in CH₂Cl₂ (10 mL) and pivaloyl chloride (0.250 mL, 2.01 mmol) and DMAP (227 mg, 1.86 mmol) were added. The reaction was stirred at ambient temperature for 48 h, then diluted with 1:1

EtOAc:hexanes and run through a silica plug. The solution was then concentrated under reduced pressure and purified via flash silica column chromatography (50% EtOAc/hexanes) to afford **2-17** (588 mg, 94%) as a clear oil. (α : β 1:0.3) IR (thin film, NaCl plate) 1741, 1368, 1152, 1053, 837 cm^{-1} . ^1H NMR (500 MHz) δ 7.39-7.32 (m, 6.5H), 5.26 (as, 0.3H), 5.24 (as, 0.3H), 5.07 (m, 1H), 4.99 (d, $J = 2.0$ Hz, 0.3H), 4.98-4.97 (m, 1H), 4.78-4.70 (m, 3.6H), 4.57 (as, 1H), 3.80-3.78 (m, 3.9H), 3.71 (as, 0.3H), 2.78-2.68 (m, 2.6H), 2.56-2.53 (m, 2.6H), 2.19 (as, 3.9H), 1.63-1.59 (m, 1.3H), 1.26-1.21 (m, 11.7H), 0.87-0.82 (m, 15.6H), 0.22-0.15 (m, 7.8H). ^{13}C NMR (125 MHz) δ 206.2, 206.2, 177.8, 177.7, 172.2, 172.0, 169.3, 168.0, 137.7, 137.4, 128.7, 128.5, 128.3, 127.9, 127.7, 93.6, 93.4, 75.3, 73.7, 73.1, 72.8, 72.6, 68.5, 68.2, 67.3, 66.1, 52.7, 52.5, 39.1, 37.9, 37.9, 34.2, 34.1, 30.0, 29.9, 28.1, 28.1, 27.4, 27.3, 26.7, 25.1, 25.0, 20.2, 20.1, 18.7, 18.7, 18.7, 18.6, -1.7, -2.4, -3.4, -3.5. ESI MS m/z ($\text{M} + \text{Na}^+$) calculated 645.3065, found 645.3080.

Methyl (dimethylhexylsilyl 2-O-acetyl-3-O-benzyl-4-O-levulinoyl-L-idopyranosid)uronate (2-18). Compound **2-16** (345 mg, 0.641 mmol) was dissolved in CH_2Cl_2 (6 mL) and acetic anhydride (0.120 mL, 1.28 mmol) and DMAP (130 mg, 1.07 mmol) were added. The reaction was stirred at ambient temperature for 2 h, followed by concentration under reduced pressure and purification via flash silica column chromatography (33% EtOAc/hexanes) to afford **2-18** (363 mg, 97%) as a clear oil. (α : β 1:2) IR (thin film, NaCl plate) 1744, 1720, 1231, 1156, 1055 cm^{-1} . ^1H NMR (500 MHz) δ 7.40-7.28 (m, 7.5H), 5.30 (s, 0.5H), 5.19 (as, 0.5H), 5.14 (as, 1H), 5.00-4.98 (m, 1.5H), 4.79-4.70 (m, 3.5H), 4.62 (d, $J = 1.8$ Hz, 1H), 3.87 (t, $J = 2.8$ Hz, 1H), 3.80-3.78 (m, 5H), 2.83-2.77 (m, 1.5H), 2.68-2.49 (m, 4.5H), 2.21-2.19 (m, 4.5H), 2.11-2.09 (m, 4.5H), 1.64-1.58 (m, 1.5H), 0.88-0.82 (m, 18H), 0.24-0.15 (m, 9H). ^{13}C NMR (125 MHz) δ 206.3, 172.1, 172.0, 170.5, 170.2, 169.4, 168.1, 137.7, 137.3, 128.8, 128.5, 128.3, 128.0, 127.9, 127.7, 93.3, 93.2, 77.5, 74.2, 73.1, 72.9, 72.7, 72.6, 68.6, 68.3, 67.7, 67.4, 66.1, 52.7, 52.6, 37.8, 37.8,

34.2, 34.2, 30.0, 30.0, 28.1, 28.1, 25.1, 25.0, 21.2, 21.2, 20.4, 20.2, 20.1, 20.0, 18.8, 18.7, 18.7, 18.6, -1.7, -2.4, -3.4, -3.5. ESI MS m/z ($M + Na^+$) calculated 603.2596, found 603.2600.

Methyl 3-*O*-benzyl-4-*O*-levulinoyl-2-*O*-pivaloyl-L-idopyranosiduronate

trichloroacetimidate (2-19). Compound 2-17 (588 mg, 0.94 mmol) was dissolved THF (8 mL), and HF•pyridine (70% solution, 0.7 mL) was added. The reaction was stirred at room temperature for 28 h, then diluted with water, extracted with CH₂Cl₂ (3 x 40 mL), dried over MgSO₄, filtered, and concentrated under reduced pressure. Purification via flash silica column chromatography (50% EtOAc/hexanes) provided the deprotected lactol. The lactol was dissolved in CH₂Cl₂ and trichloroacetonitrile (1:1, 7 mL) and cooled to 0°C. DBU (4 μL) was added to the cooled reaction mixture, and the reaction allowed to warm to room temperature over 30 min. The reaction was concentrated under reduced pressure and purified via flash silica gel column chromatography (35% EtOAc/hexanes) to afford 2-19 (398 mg, 68%) as a white foam. (α : β 1:1) IR (thin film, NaCl plate) 1769, 1741, 1722, 1677, 1144, 1064 cm⁻¹. ¹H NMR (500 MHz) δ 8.72 (s, 1H), 8.70 (s, 1H), 7.38-7.29 (m, 10H), 6.38 (s, 1H), 6.23 (as, 1H), 5.32 (s, 1H), 5.28-5.26 (m, 2H), 5.13 (s, 1H), 5.04 (s, 1H), 4.84-4.72 (m, 5H), 3.94 (t, J = 3.0 Hz, 1H), 3.83-3.80 (m, 7H), 2.79-2.68 (m, 4H), 2.57-2.53 (m, 4H), 2.19 (as, 6H), 1.25-1.23 (m, 18H). ¹³C NMR (125 MHz) δ 206.0, 177.5, 177.2, 171.9, 171.8, 168.1, 167.2, 160.6, 160.0, 137.2, 137.0, 128.7, 128.4, 128.3, 127.9, 127.9, 127.7, 95.1, 94.3, 74.6, 73.3, 73.2, 72.6, 72.3, 67.8, 67.5, 67.5, 65.8, 65.0, 52.8, 52.7, 39.1, 38.9, 37.8, 29.8, 28.0, 27.3, 27.1. ESI MS m/z ($M + Na^+$) calculated 646.0984, found 646.0996.

Methyl 2-*O*-acetyl-3-*O*-benzyl-4-*O*-levulinoyl-L-idopyranosiduronate trichloroacetimidate (2-20). Compound 2-18 (890 mg, 1.53 mmol) was dissolved in THF (15 mL), and HF•pyridine (70% solution, 1.0 mL) was added. The reaction was stirred at room temperature for 28 h, then

diluted with water, extracted with CH₂Cl₂ (2 x 50 mL), dried over MgSO₄, filtered, and concentrated under reduced pressure. Purification via flash silica column chromatography (35%→60% EtOAc/hexanes) provided the deprotected lactol. The lactol was dissolved in CH₂Cl₂ and trichloroacetonitrile (1:1, 10 mL) and cooled to 0°C. DBU (5 μL) was added to the cooled reaction mixture, and the reaction allowed to warm over 30 min. The reaction was concentrated under reduced pressure and purified via flash silica gel column chromatography (50% EtOAc/hexanes) to afford **2-20** (662 mg, 74%) as a white foam. Spectra corresponded to published data.(25)

Conversion of glycols to 1,2-*cis*-isopropylidenes (General Procedure). Glycol (0.1 mmol) was dried by coevaporation with toluene and dissolved in CH₂Cl₂ (250 μL) under N₂. The solution was cooled to 0°C and dimethyldioxirane (DMDO) (1.5 mL, ~0.08 M in acetone) was added. The reaction mixture was stirred for 10 min, ethyl vinyl ether (10 μL, 0.1 mol) was added and the reaction mixture stirred for an additional 10 min. Zinc (II) chloride (20 μL, 0.5 M in Et₂O) was added, the reaction mixture was allowed to warm to room temperature and stirred for 18 h. The reaction mixture was poured into water (50 mL) and the aqueous phase extracted with CH₂Cl₂ (3 x 50 mL). The combined organic layers were dried over MgSO₄, filtered, and the solvent removed under reduced pressure. Products were purified via flash silica gel column chromatography (between 10:1 and 20:1 hexanes:ethyl acetate).

1,2-*O*-isopropylidene-3,4,6-tri-*O*-benzyl- α -D-glucopyranoside (2-21b). Followed general procedure to yield: 33 mg, 67%. Spectra were consistent with reported data.(32)

1,2-*O*-isopropylidene-3,4,6-tri-*O*-acetyl- α -D-glucopyranoside (2-22b). Followed general procedure to yield: 7 mg, 20%. Spectra were consistent with reported data.(33)

6-*O*-*t*-Butyldiphenylsilyl-3,4-di-*O*-pivoalyl-D-glucal (2-23a) 6-*O*-*t*-Butyldiphenylsilyl-D-glucal(34) (278 mg, 0.72 mmol) was dissolved in CH₂Cl₂ (6 mL) and pyridine (0.93 mL). DMAP (17.5 mg, 0.14 mmol) and trimethylacetyl chloride (360 μL, 2.9 mmol) were added and the reaction mixture was stirred for 18 h at room temperature. Water (2 mL) was added and the reaction mixture stirred for 3 h to quench the acid chloride. The reaction mixture was poured into ethyl acetate (100 mL) and the organic layer was extracted with saturated NaHCO₃ (50 mL) and brine (50 mL). The organic layer was dried over MgSO₄, filtered, and the solvent removed under reduced pressure. Flash silica gel column chromatography (hexanes-ethyl acetate 30:1) yielded **2-23a** (210 mg, 0.38 mmol, 52.5%) as a clear oil. Rf. 0.44 (hexanes:ethyl acetate 9:1). [α]²⁴_D: -10.0, (c = 0.87). IR (thin film, NaCl plate) 2962, 1732, 1651 cm⁻¹. ¹HNMR (500 MHz, CDCl₃) δ 7.60-7.70 (m, 4H), 7.36-7.45 (m, 6H), 6.44 (d², *J* = 6.1, 1.2 Hz, 1H), 5.29-5.31 (m, 1H), 5.23-5.25 (m, 1H), 4.75 (d², *J* = 6.1, 3.2 Hz, 1H), 4.15-4.18 (m, 1H), 3.85 (d², *J* = 11.5, 6.1 Hz, 1H), 3.77 (d², *J* = 11.5, 2.8 Hz, 1H), 1.13 (s, 9H), 1.10 (s, 9H), 1.07 (s, 9H). ¹³CNMR (125 MHz, CDCl₃) δ 178.0, 176.7, 146.0, 135.9, 133.4, 133.3, 129.9, 129.85, 127.9, 98.6, 77.2, 67.7, 67.0, 62.2, 38.9, 38.8, 27.2, 27.19, 26.9, 19.4. ESI MS (C₃₂H₄₄O₆Si) *m/z* (M + Na⁺) calcd 575.2799, obsd 575.2812.

6-*O*-*t*-Butyldiphenylsilyl-1,2-*O*-isopropylidene-3,4-di-*O*-pivoalyl-α-D-glucopyranoside (2-23b). Followed general procedure to yield: 37 mg, 60%. Rf. 0.54 (hexanes:ethyl acetate 4 :1). [α]²⁴_D: +9.72, (c = 1.23). IR (thin film, NaCl plate) 2963, 1739 cm⁻¹. ¹HNMR (500 MHz, CDCl₃) δ 7.72 (ψt, 2H), 7.70 (ψt, 2H), 7.35-7.67 (m, 6H), 5.64 (d, *J* = 4.8 Hz, 1H), 5.12-5.15 (m, 2H), 4.16-4.18 (m, 1H), 3.96-3.99 (m, 1H), 3.80 (d², *J* = 11.5, 2.3 Hz, 1H), 3.70 (d², *J* = 11.5, 4.5 Hz, 1H), 1.59 (s, 3H), 1.37 (s, 3H), 1.23 (s, 9H), 1.13 (s, 9H), 1.06 (s, 9H). ¹³CNMR (125 MHz, CDCl₃) δ 177.1, 177.0, 135.9, 135.8, 133.45, 133.4, 129.85, 129.8, 127.9, 109.8, 97.1, 73.4, 70.5,

69.8, 67.5, 63.3, 38.9, 38.8, 27.2, 27.1, 27.0, 26.5, 25.9, 19.5. ESI MS ($C_{35}H_{50}O_8Si$) m/z ($M + Na^+$) calcd 649.3167, obsd 649.3144.

3,4-Di-*O*-acetyl-6-*O*-triisopropylsilyl-D-glucal (2-24a) 6-*O*-Triisopropylsilyl-D-glucal(35) (91 mg, 0.3 mmol) was dissolved in CH_2Cl_2 (2.5 mL) and pyridine (0.5 mL). DMAP (4 mg, 0.03 mmol) and acetyl chloride (113 μ L, 1.2 mmol) were added and the reaction mixture was stirred for 3 h at room temperature. Water (1 mL) was added and the reaction mixture stirred for 1 h to quench the acid chloride. The reaction mixture was poured into ethyl acetate (100 mL) and the organic layer was extracted with saturated $NaHCO_3$ (50 mL) and brine (50 mL). The organic layer was dried over $MgSO_4$, filtered, and the solvent removed under reduced pressure. Flash silica gel column chromatography (hexanes-ethyl acetate 10:1) yielded **2-24a** (92 mg, 0.24 mmol, 80%) as a clear oil. Rf. 0.46 (hexanes:ethyl acetate 4:1). $[\alpha]_D^{24}$: -2.33, ($c = 1.27$). IR (thin film, NaCl plate) 2944, 2867, 1743, 1651 cm^{-1} . 1H NMR (500 MHz, $CDCl_3$) δ 6.47 (d, $J = 5.8$ Hz, 1H), 5.31 (m, 2H), 4.75 (m, 1H), 4.13 (m, 1H), 3.90 (d, $J = 4.8$ Hz, 2H), 2.07 (s, 3H), 2.04 (s, 3H), 1.02-1.13 (m, 21H). ^{13}C NMR (125 MHz, $CDCl_3$) δ 170.3, 169.6, 146.2, 98.3, 67.7, 67.5, 61.6, 21.3, 21.1, 18.1, 18.05, 12.1. ESI MS ($C_{19}H_{34}O_6Si$) m/z ($M + Na^+$) calcd 409.2017, obsd 409.2014.

3,4-Di-*O*-acetyl-1,2-*O*-isopropylidene-6-*O*-triisopropylsilyl- α -D-glucopyranoside (2-24b).

Followed general procedure to yield: 31 mg, 75%. Rf. 0.29 (hexanes:ethyl acetate 4:1). $[\alpha]_D^{24}$: +14.6, ($c = 1.25$). IR (thin film, NaCl plate) 2943, 2867, 1751 cm^{-1} . 1H NMR (500 MHz, $CDCl_3$) δ 5.61 (d, $J = 4.8$ Hz, 1H), 5.20 (ψ t, 1H), 5.04 (m, 1H), 4.18 (m, 1H), 3.94 (m, 1H), 3.86 (d^2 , $J = 11.2, 2.7$ Hz, 1H), 2.10 (s, 3H), 2.07 (s, 3H), 1.60 (s, 3H), 1.35 (s, H), 0.97-1.14 (m, 21H). ^{13}C NMR (125 MHz, $CDCl_3$) δ 169.9, 169.7, 109.8, 97.0, 73.5, 71.1, 70.0, 68.5, 63.5, 26.5, 25.8,

21.15, 21.1, 18.1, 1, 18.10, 12.1. ESI MS ($C_{22}H_{40}O_8Si$) m/z ($M + Na^+$) calcd 483.2385, obsd 483.2376.

3-*O*-Benzyl-4-*O*-*t*-butyldimethylsilyl-6-*O*-triisopropylsilyl- β -D-glucal (2-25a) 3-*O*-Benzyl-6-*O*-triisopropylsilyl- β -D-glucal.(12) (516 mg, 1.31 mmol) was coevaporated three times with toluene and dissolved in DMF (3mL). Imidazole (178 mg, 2.6 mmol) and TBDMS-Cl (217 mg, 1.44 mmol) were added and the reaction mixture stirred 16 h at room temperature. The reaction mixture was poured into ethyl acetate (200 mL) and washed with water, brine, and saturated $NaHCO_3$ (50 mL each). The organic layer was dried over $MgSO_4$, filtered, and the solvent removed under reduced pressure. Flash silica gel column chromatography (hexanes-ethyl acetate 50:1) yielded **2-25a** (564 mg, 1.11 mmol, 85%) as a clear oil. Rf. 0.63 (hexanes:ethyl acetate 10:1). $[\alpha]_D^{24}$: -21.1, ($c = 0.88$). IR (thin film, NaCl plate) 2944, 2866, 1652 cm^{-1} . 1H NMR (500 MHz, $CDCl_3$) δ 7.26-7.37 (m, 5H), 6.40 (d^2 , $J = 6.1, 1.1$ Hz, 1H), 4.82 (d^2 , $J = 6.1, 2.8$ Hz, 1H), 4.61 (d, $J = 11.6$ Hz, 1H), 4.51 (d, $J = 11.6$ Hz, 1H), 4.00-4.05 (m, 2H), 3.87-3.95 (m, 3H), 1.05-1.15 (m, 21H), 0.88 (s, 9H), 0.10 (s, 3H), 0.08 (s, 3H). ^{13}C NMR (125 MHz, $CDCl_3$) δ 144.9, 138.7, 128.5, 127.9, 127.6, 98.9, 80.0, 76.6, 70.2, 68.1, 62.5, 26.1, 18.4, 18.2, 18.15, 12.2, -4.0, -4.7. ESI MS ($C_{28}H_{50}O_4Si_2$) m/z ($M + Na^+$) calcd 529.3140, obsd 529.3150.

3-*O*-Benzyl-4-*O*-*t*-butyldimethylsilyl-1,2-*O*-isopropylidene-6-*O*-triisopropylsilyl- α -D-glucopyranoside (2-25b). Followed general procedure to yield: 43 mg, 75%. Rf. 0.48 (hexanes:ethyl acetate 9:1). $[\alpha]_D^{24}$: +7.42, ($c = 1.20$). IR (thin film, NaCl plate) 2940, 2866 cm^{-1} . 1H NMR (500 MHz, $CDCl_3$) δ 7.28-7.38 (m, 5H), 5.61 (d, $J = 4.9$ Hz, 1H), 4.75 (d, $J = 11.7$ Hz, 1H), 4.61 (d, $J = 11.7$ Hz, 1H), 4.22 (ψ t, 1H), 3.96 (d^2 , $J = 11.2, 2.0$ Hz, 1H), 3.90 (d^2 , $J = 9.0, 4.8$ Hz, 1H), 3.86 (d^2 , $J = 11.2, 4.3$ Hz, 1H), 3.70-3.73 (m, 2H), 1.55 (s, 3H), 1.35 (s, 3H), 1.04-1.14 (s, 21H), 0.87 (s, 9H), 0.08 (s, 3H), 0.04 (s, 3H). ^{13}C NMR (125 MHz, $CDCl_3$) δ 138.3,

128.5, 127.8, 127.75, 109.0, 97.5, 82.0, 76.2, 73.9, 72.0, 68.4, 63.4, 27.1, 26.2, 26.0, 18.2, 18.18, 12.3, -3.9, -4.8. ESI MS ($C_{31}H_{56}O_6Si_2$) m/z ($M + Na^+$) calcd 603.3508, obsd 603.3491.

3-*O*-Benzyl-4,6-*p*-methoxybenzylidene-D-glucal (2-26a) This material was prepared as previously reported.(12)

3-*O*-Benzyl-1,2-*O*-isopropylidene-4,6-*p*-methoxybenzylidene- α -D-glucopyranoside (2-26b).

Followed general procedure to yield: 9.5 mg, 6:1 of an inseparable mixture of diastereomers, 22%. ESI MS ($C_{24}H_{28}O_7$) m/z ($M + Na^+$) calcd 451.1727, obsd 451.1723.

4,6-Di-*t*-butylsilylidene-D-glucal (2-27a) This material was prepared as previously reported.(36)

4,6-Di-*t*-butylsilylidene-1,2-*O*-isopropylidene- α -D-glucopyranoside (2-27b). Followed

general procedure to yield: 6.5 mg, 18%. Rf. 0.28 (hexanes:ethyl acetate 4:1). $[\alpha]_D^{24}$: +22.5, ($c = 0.39$). IR (thin film, NaCl plate) 3431, 2935 cm^{-1} . 1H NMR (500 MHz, $CDCl_3$) δ 5.54 (d, $J = 4.9$ Hz, 1H), 4.19 (m, 1H), 4.09 (d^2 , $J = 6.1, 5.1$ Hz, 1H), 3.85-3.89 (m, 2H), 3.77-3.84 (m, 1H), 3.65-3.69 (m, 1H), 2.67 (d, $J = 1.9$ Hz, 1H), 1.58 (s, 3H), 1.41 (s, 3H), 1.06 (s, 9H), 1.00 (s, 9H). ^{13}C NMR (125 MHz, $CDCl_3$) δ 108.4, 98.0, 77.2, 77.1, 76.2, 67.4, 66.3, 28.2, 27.6, 27.5, 27.1, 22.9, 20.1. ESI MS ($C_{17}H_{32}O_6Si$) m/z ($M + Na^+$) calcd 383.1860, obsd 383.1875.

3,6-Di-*O*-triisopropylsilyl-D-glucal (2-28a) This material was isolated as a byproduct from the synthesis of 6-*O*-Triisopropylsilyl-D-glucal.(35) Rf. 0.41 (hexanes:ethyl acetate 9:1). $[\alpha]_D^{24}$: -10.3, ($c = 0.79$). IR (thin film, NaCl plate) 3496, 2944, 2867, 1645 cm^{-1} . 1H NMR (500 MHz, $CDCl_3$) δ 6.3 (d^2 , $J = 6.1, 1.4$ Hz, 1H), 4.72 (d^2 , $J = 6.2, 2.8$ Hz, 1H), 4.31 (m, 1H), 4.09 (d^2 , $J = 10.9, 5.3$ Hz, 1H), 3.90-3.97 (m, 2H), 3.83 (m, 1H), 2.55 (d, $J = 4.2$ Hz, 1H), 1.03-1.58 (m, 42H). ^{13}C NMR (125 MHz, $CDCl_3$) δ 143.4, 103.5, 78.4, 71.7, 69.5, 63.7, 18.28, 18.27, 18.13, 12.6, 12.1. ESI MS ($C_{24}H_{50}O_4Si_2$) m/z ($M + Na^+$) calcd 481.3140, obsd 481.3128.

1,2-*O*-isopropylidene-3,6-di-*O*-triisopropylsilyl- α -D-glucopyranoside (2-28b). Followed general procedure to yield: 37 mg, 70%. Rf. 0.36 (hexanes:ethyl acetate 9:1). $[\alpha]_D^{24}$: -30.4, (c = 1.13). IR (thin film, NaCl plate) 3508, 2949, 2867 cm^{-1} . ^1H NMR (500 MHz, CDCl_3) δ 5.56 (d, $J = 4.3$ Hz, 1H), 4.16-4.20 (m, 1H), 3.74-4.00 (m, 3H), 2.71 (d, $J = 4.5$ Hz, 1H), 1.59 (s, 3H), 1.36 (s, 3H), 1.03-1.18 (m, 42H). ^{13}C NMR (125 MHz, CDCl_3) δ 109.6, 96.8, 76.8, 73.7, 72.1, 66.1, 26.8, 25.5, 18.2, 18.16, 18.13, 12.4, 12.0. ESI MS ($\text{C}_{27}\text{H}_{56}\text{O}_6\text{Si}_2$) m/z ($\text{M} + \text{Na}^+$) calcd 555.3508, obsd 555.3498.

3-*O*-Benzyl-6-*O*-triisopropylsilyl-D-glucal (2-29a) This material was prepared as previously reported.⁽¹²⁾

3-*O*-Benzyl-1,2-*O*-isopropylidene-6-*O*-triisopropylsilyl- α -D-glucopyranoside (2-29b).

Followed general procedure to yield: 34 mg, 73%. Rf. 0.41 (hexanes:ethyl acetate 4:1). $[\alpha]_D^{24}$: -4.22, (c = 1.02). IR (thin film, NaCl plate) 3495, 2942, 2897 cm^{-1} . ^1H NMR (500 MHz, CDCl_3) δ 7.24-7.40 (m, 5H), 5.60 (d, $J = 4.6$ Hz, 1H), 4.75 (vtd, 2H), 4.29 (vvt, 1H), 4.05 (d², $J = 9.9$, 4.1 Hz, 1H), 3.91-3.95 (m, 1H), 3.97-3.8 (m, 3H), 3.03 (d, $J = 2.9$ Hz, 1H), 1.57 (s, 3H), 1.37 (s, 3H), 1.04-1.18 (m, 21H). ^{13}C NMR (125 MHz, CDCl_3) δ 138.0, 128.6, 128.1, 109.5, 97.3, 80.0, 76.5, 72.3, 71.6, 70.7, 65.7, 27.2, 26.1, 18.1, 12.0. ESI MS ($\text{C}_{25}\text{H}_{42}\text{O}_6\text{Si}$) m/z ($\text{M} + \text{Na}^+$) calcd 489.2643, obsd 489.2640.

1,2-*O*-isopropylidene-3-tri-*O*-benzyl- α -D-galactopyranoside (2-30b). Followed general procedure to yield: 38 mg, 78%. Rf. 0.39 (hexanes:ethyl acetate 4:1). $[\alpha]_D^{24}$: +37.7, (c = 1.23). IR (thin film, NaCl plate) 3031, 2933 cm^{-1} . ^1H NMR (500 MHz, CDCl_3) δ 7.27-7.42 (m, 15H), 5.59 (d, $J = 4.2$ Hz, 1H), 4.93 (d, $J = 11.6$ Hz, 1H), 4.81 (d, $J = 12.2$ Hz, 1H), 4.70 (d, $J = 12.2$ Hz, 1H), 4.62 (d, $J = 11.6$ Hz, 1H), 4.52 (d, $J = 11.9$ Hz, 1H), 4.46 (d, $J = 11.9$ Hz, 1H), 4.33 (d², $J = 6.2$, 4.2 Hz, 1H), 4.09-4.12 (m, 1H), 4.03 (vvt, 1H), 3.61-3.71 (m, 3H), 1.48 (s, 3H), 1.40 (s,

3H). ^{13}C NMR (125 MHz, CDCl_3) δ 138.7, 138.4, 138.1, 128.6, 128.5, 128.45, 128.1, 128.05, 127.9, 127.8, 127.75, 127.7, 109.4, 97.7, 80.8, 78.5, 77.48, 77.2, 77.0, 74.6, 73.7, 73.2, 73.15, 71.6, 68.3, 28.5, 27.3. ESI MS ($\text{C}_{30}\text{H}_{34}\text{O}_6$) m/z ($\text{M} + \text{Na}^+$) calcd 513.2248, obsd 513.2258.

3,4-Carbonate-6-*O*-triisopropylsilyl-D-galactal (2-31a) This material was prepared as previously reported.⁽³⁷⁾

Methyl 3-*O*-benzyl-1,2-*O*-isopropylidene- α -D-glucopyranosiduronate (2-2). Glycal 2-29a (193 mg, 0.51 mmol) was coevaporated three times with toluene and dissolved in CH_2Cl_2 (1 mL). The reaction mixture was cooled to 0°C and DMDO (8 mL, ~ 0.08 M in acetone) was added. The reaction mixture was stirred for 10 min and ethyl vinyl ether (50 μL , 0.5 mol) was added and the reaction mixture stirred an additional 10 min. Zinc (II) chloride (102 μL , 0.5 M in Et_2O) was added, the reaction mixture brought to room temperature and stirred for 18 h. The reaction mixture was poured into water (100 mL) and the aqueous phase extracted with CH_2Cl_2 (2 x 100 mL) and ethyl acetate (2 x 50 mL). The combined organic layers were dried over MgSO_4 , filtered, and the solvent removed under reduced pressure.

The crude material was dissolved in THF (5 mL) and tetrabutylammonium fluoride (560 μL , 1.0 M in THF) was added. The reaction mixture was stirred for 30 min and poured into saturated NH_4Cl . The aqueous phase was extracted with CH_2Cl_2 (2 x 100 mL) and ethyl acetate (2 x 50 mL). The combined organic layers were dried over MgSO_4 , filtered, and the solvent removed under reduced pressure.

The residue was dissolved in CH_2Cl_2 (1 mL) and water (0.5 mL), saturated NaHCO_3 (2 mL), KBr (6 mg, 0.05 mmol), and tetrabutylammonium bromide (8 mg, 0.025 mmol) were added. The reaction mixture was cooled to 0°C and 2,2,6,6-tetramethylpiperidine-1-oxyl (TEMPO) (~ 2 mg) was added. Bleach (2.5 mL) was added in five portions ten minutes apart;

the reaction turned deep yellow. After complete addition of the bleach, the reaction mixture was stirred for 1.5 h at 0°C. Methanol was added until the reaction was decolorized and stirred for 15 min. The reaction mixture was diluted with water (50 mL) and extracted with CH₂Cl₂ (75 mL). The aqueous layer was acidified by dropwise addition of conc. HCl until the pH was less than 2 and extracted with CH₂Cl₂ (3 x 75 mL) and ethyl acetate (50 mL). The combined organic layers were dried over MgSO₄, filtered, and the solvent removed under reduced pressure.

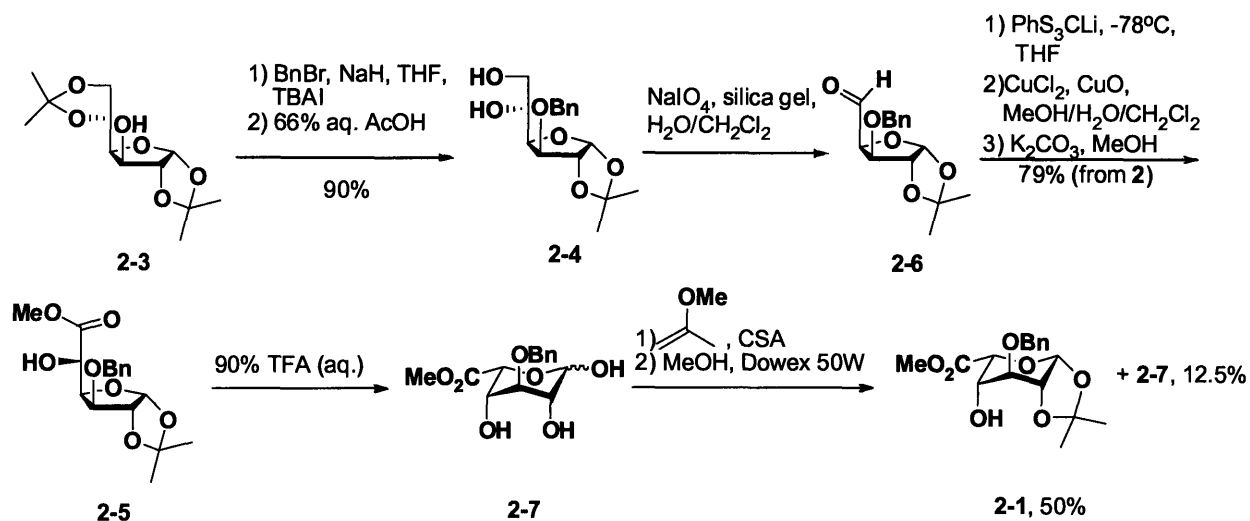
The crude acid was coevaporated twice with toluene and dissolved in DMF (1 mL) under argon. To the reaction mixture was added KHCO₃ (100 mg, 1 mmol) and methyl iodide (63 μL, 1 mmol). The reaction was stirred for 16 h at room temperature. The reaction mixture was diluted with ethyl acetate (100 mL) and washed with water, saturated Na₂S₂O₃, and brine. The organic layer was dried over MgSO₄, filtered, and the solvent removed under reduced pressure. Flash silica gel column chromatography (hexanes-ethyl acetate 85:15) yielded **2-2** (83 mg, 0.245 mmol, 48%) as a clear oil. Spectra were consistent with reported data.(28)

2.3 Results and Discussion

Synthesis of iduronic donors and acceptors

Commercially available diacetone glucose **2-3** was transformed to diol **2-4** through benzylation and selective acetal cleavage (Scheme 2-1).(27) Treatment of **2-4** with aqueous sodium periodate adsorbed onto silica yielded aldehyde **2-6**(38, 39) that was used without purification. Reaction of **2-6** with freshly prepared trithiophenylmethyl lithium afforded L-idose-configured thioorthoester in high yield with no D-glucose product detectable.(10) The reaction products were treated directly with CuCl₂/CuO to effect the cleavage of the thioorthoester to the furanose methyl ester **2-5**, along with small amounts of the corresponding phenylthioester.

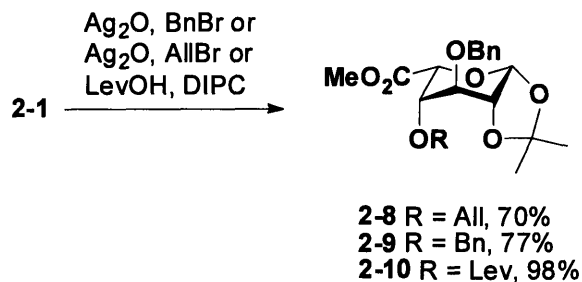
Stirring the crude product mixture with K_2CO_3 in methanol converted this byproduct to the desired methyl ester **2-5**. Purification by flash chromatography gave **2-5** in a total yield of 79% from **2-4**. Removal of the isopropylidene group from furanose **2-5** by reaction with 90% TFA (aq.) yielded the crystalline 3-*O*-benzyl iduronic methyl ester **2-7** in its pyranose form.(28)



Scheme 2-1. Synthesis of **2-1**.

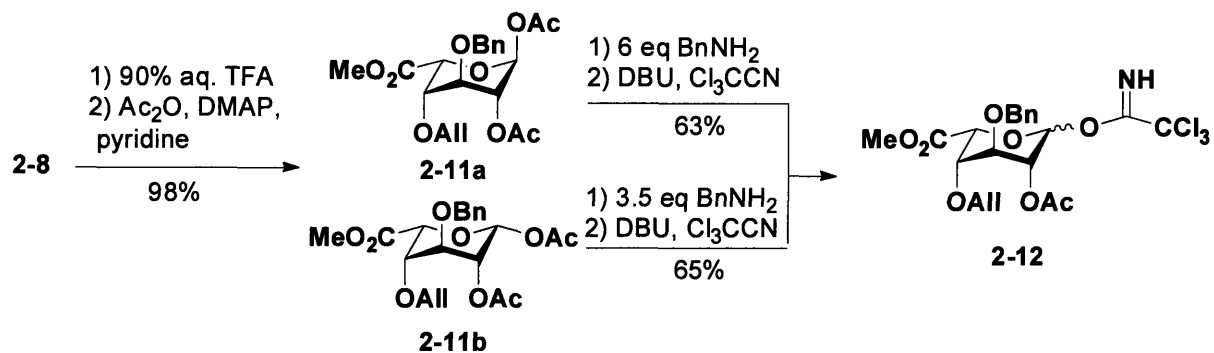
Installation of a 1,2-isopropylidene onto **2-7** locked the sugar in the ¹C₄ pyranose form and afforded key intermediate **2-1**.(28) Use of highly-reactive 2-methoxypropene with catalytic camphorsulfonic acid (CSA)(40, 41) to form the desired isopropylidene acetal prevented opening of the sugar ring and thus the trapping of thermodynamically more stable furanose isomers. Partial hydrolysis of the crude product mixture with acidic resin in methanol produced the desired product **2-1** in 50% yield from **2-5**, along with recovered **2-7** (12.5%). The synthesis of **2-1** from diacetone glucose was achieved in nine steps and 36% overall yield (42% assuming complete resubmission of **2-7**). Only three chromatographic steps were required in this synthetic sequence; additionally, the procedures for the transformation of **2-6** to **2-5** and **2-7** to **2-1** have been simplified from those previously reported and the yields improved.(10, 28)

L-iduronic acid derivative **2-1** may serve as a glycosyl acceptor in the synthesis of disaccharide modules,(27, 28) or may be converted into a variety of iduronic acid trichloroacetimidate glycosyl donors. The introduction of different protecting groups, including silyl ethers, esters, and alkyl ethers, on the C-4 hydroxyl can be readily achieved.(27) Silylation can be effected through the use of silyl triflates, esterification through acid anhydrides and DMAP. Alkylation poses more of a challenge, as the C-5 stereocenter of **2-1** may epimerize in the presence of strong base, but was accomplished using silver oxide and the corresponding alkyl bromide (Scheme 2-2).



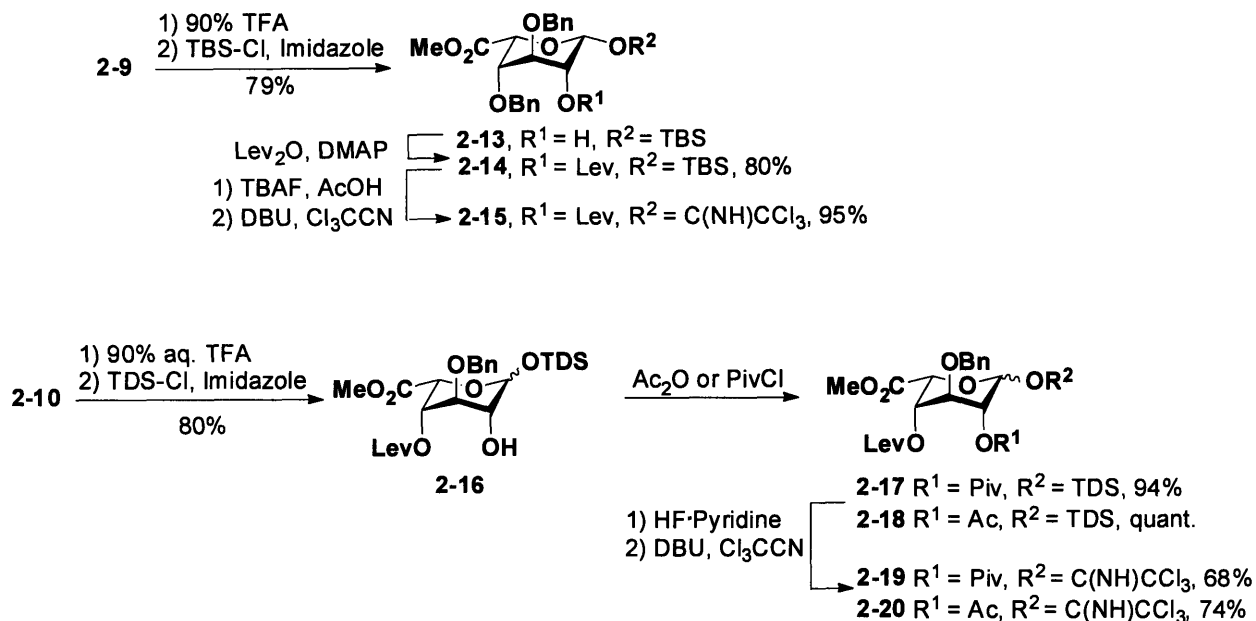
Scheme 2-2. Protection of the 4-OH of **2-1**.

Differential protection of the C-1 and C-2 hydroxyls was achieved through two routes. One option capitalized on the faster rate of cleavage of anomeric acetates over other ester protecting groups.(42) Treatment of **2-8** with aqueous TFA to effect isopropylidene cleavage, followed by acetylation of the crude material, afforded **2-11a** and **2-11b** (Scheme 2-3). These anomers were separated and exposed to benzylamine to cleave the anomeric acetate selectively. Since **2-11a** and **2-11b** react at different rates under these conditions, better yields were obtained by treating these isomers separately. The resultant lactol was transformed to glycosyl trichloroacetimidate **2-12** by reaction with trichloroacetonitrile and DBU.



Scheme 2-3. Synthesis of iduronic trichloroacetimidates by selective ester cleavage.

The second route to differentially protected iduronic acid derivatives from **2-1** was the selective formation of anomeric silyl ethers.⁽²⁶⁾ After protection of the C-4 hydroxyl, the isopropylidene of **2-9** and **2-10** were cleaved using aqueous TFA (Scheme 2-4). The products were exposed to a silyl chloride at low temperature to selectively protect the C-1 hydroxyl and produce **2-13** and **2-16** respectively. The steric bulk of the C-4 protecting group required the adjustment of reaction conditions to achieve good yield and selectivity. The larger benzyl group allowed use of *t*-butyldimethylsilyl chloride (TBDMS-Cl) as the silylating agent. The smaller levulinate ester required lower temperatures and the bulkier hexyldimethylsilyl chloride (TDS-Cl) to achieve good selectivity.



Scheme 2-4. Synthesis of iduronic trichloroacetimidates via selective silylation.

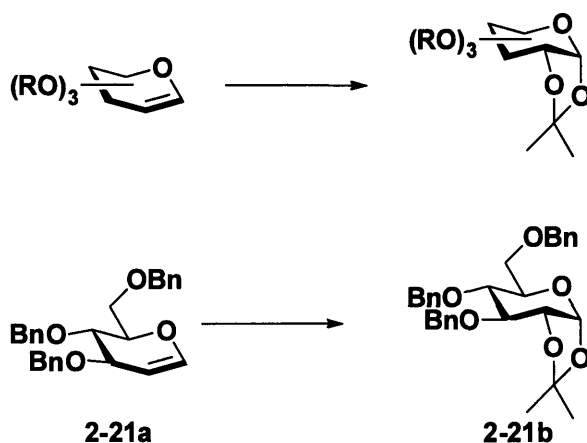
Further elaboration of **2-13** by introduction of a levulinate ester on the C-2 hydroxyl afforded **2-14**. Cleavage of the anomeric silyl ether yielded lactol which was converted to the trichloroacetimidate **2-15**. Similarly, product **2-16** was converted to its pivaloyl ester **2-17** and acetate ester **2-18**. The anomeric TDS ethers were cleaved using HF•pyridine, and the lactols converted to the corresponding trichloroacetimidates **2-19** and **2-20**.

Conversion of glycols to 1,2-isopropylidenes

The nine-step synthesis of **2-2** previously described relied on the interconversion of the furanose and pyranose forms of the sugar, resulting in a mixture of products and variable yields of the desired compound.⁽²⁸⁾ Direct conversion of a protected glycol to the 1,2-isopropylidene- α -glycoside would avoid the problem of furanose-pyranose conversion and provide more convenient access to **2-2**. Several procedures for the direct conversion of aliphatic epoxides to isopropylidenes have been published.⁽⁴³⁻⁵⁰⁾ These procedures called for the treatment of the

epoxide with a Lewis acid (typically AlCl_3 or $\text{BF}_3 \cdot \text{Et}_2\text{O}$) in acetone to effect the ring expansion and were not reported to be diastereoselective.

Glucals are well known to react readily and selectively to 1,2-anhydroglucoses upon treatment with dimethyldioxirane (DMDO) solution in acetone.⁽⁵¹⁾ We anticipated that addition of an acid catalyst to the reaction mixture after complete epoxidation would bring about the ring-expansion of the anhydrosugar to the 1,2-isopropylidene through the addition of acetone (Scheme 1). The desired α -isomer should be favored both by the anomeric effect and the relatively high strain of the 1,2-*trans*- β -acetal.



Scheme 2-5. Conversion of glucals to 1,2-isopropylidenes.

The proposed reaction was initially developed using tribenzyl glucal **2-21a** as the test substrate. Epoxidation of **2-21a** with DMDO is rapid, and the anhydrosugar gives good yields in acid catalyzed ring opening with alcohols.⁽⁵¹⁾ In this case, after complete epoxidation of the substrate, an acid catalyst was added directly to the reaction mixture to effect the addition of acetone to the anhydrosugar. CSA, a protic acid, gave only trace amounts of product while the remainder of the material decomposed. The Lewis acid ZnCl_2 afforded the product **2-21b** in significantly higher yields and the reaction was optimized for time and equivalents of ZnCl_2 (Table 2-1). The yield of this reaction was further improved by quenching the excess oxidant

before addition of the acid, either by evaporation of the solvent followed by dissolving the residue in anhydrous acetone, or by addition of ethyl vinyl ether (EVE) to react the remaining DMDO. Both procedures worked equally well in initial trials; addition of EVE was selected due to the ease of the procedure. Conversion of **2-21a** to **2-21b** by epoxidation with DMDO, followed by addition of EVE to quench the remaining oxidant and subsequent reaction with 0.1 equivalents of ZnCl₂ for 18 h yielded 67% of the desired product. Other Lewis acids (AlCl₃, SnCl₄, and BF₃•Et₂O) gave results similar to ZnCl₂.

Table 2-1. Optimization of reaction conditions.

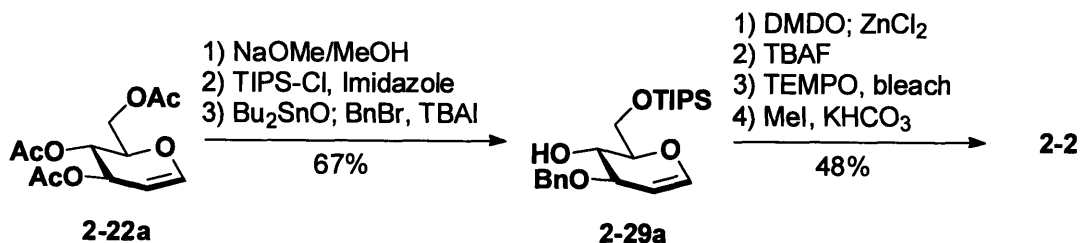
Activator	DMDO Quench	Time (h)	Yield (%)
0.1 eq. CSA	No	18	<5
0.1 eq. ZnCl ₂	No	4	47
1.0 eq. ZnCl ₂	No	20	45
0.1 eq. ZnCl ₂	No	20	55
0.025 eq. ZnCl ₂	No	18	43
0.1 eq. ZnCl₂	EVE	18	67

Table 2-2. Substrate scope. PMP = p-methoxyphenyl, Piv = pivaloyl (trimethylacetyl). The product 2-26b was a 6:1 mixture of compounds, likely diastereomers from epimerization of the benzylidene acetal.

Entry	Substrate (a)	Product (b)	Yield (%)
2-22			20
2-23			60
2-24			75
2-25			75
2-26			22 ^a
2-27			18
2-28			70
2-29			73
2-30			78
2-31			N.D.

Next, the substrate scope and protecting group compatibility of the reaction was explored (Table 2-2). Differentially protected glucals (entries 2-23, 2-24, 2-25, 2-28, and 2-29) and tribenzyl galactal (entry 2-30) reacted smoothly; ester, silyl ether and benzyl groups were tolerated. Glycals with unprotected secondary hydroxyl groups (entries 2-28, and 2-29) were also readily converted into the desired products in good yield. Deactivated tri-*O*-acetyl-D-glucal **2-22a** gave a low yield of isopropylidene **2-22b** due to its poor reactivity with DMDO.^(29, 51) The conversion of glycals containing cyclic protecting groups (entries 2-26, 2-27, and 2-31) also proceeded in poor yield. While epoxidation appeared complete, treatment with ZnCl₂ did not afford the isopropylidene in significant quantities.

Using this new transformation, a short synthesis of the glucuronic acid building block methyl 3-*O*-benzyl-1,2-*O*-isopropylidene- α -D-glucopyranosiduronate **2-2** was developed (Scheme 3). Glycal **2-29a** can be produced in three steps from commercially available **2-22a** via a previously reported route in 67% overall yield.⁽¹²⁾ Epoxidation of **2-29a** with DMDO followed by reaction with ZnCl₂ produced **2-29b**; the crude product mixture was carried on without purification. Treatment of this mixture with tetrabutylammonium fluoride cleaved the silyl ether to reveal the primary hydroxyl group. The crude product was reacted with bleach and catalytic 2,2,6,6-tetramethylpiperidine-1-oxyl (TEMPO) to selectively oxidize the C6-hydroxyl to the carboxylic acid. The crude acid was methylated using methyl iodide and KHCO₃ in DMF. Purification via flash silica gel column chromatography gave **2-2** in 48% yield.



Scheme 2-6. Synthesis of 2-2.

Conclusions

The synthesis of compound **2-1** in 36% overall yield in nine steps from diacetone glucose is significantly shorter than the previous route,⁽²⁷⁾ allowing for the rapid production of multigram quantities of this iduronic acid building block. Key intermediate **2-1** may be elaborated through selective anomeric hydroxyl silylation or selective acetate cleavage to produce a variety of iduronic acid derivatives, including the glycosyl donors **2-12**, **2-15**, **2-19**, and **2-20**, using chemistry readily adaptable to other protecting group schemes. Further, a general methodology for the conversion of differentiated glycals to the corresponding 1,2-*cis*-isopropylidienes via a one-pot procedure was developed. The reaction described is easily executed and tolerates a variety of useful protecting groups, including silyl ethers, benzyl ethers, esters, and free hydroxyls. Glycals containing cyclic protecting groups, such as acetals and internal carbonates, are not useful substrates, as their epoxides do not add acetone readily. This new methodology was applied to the synthesis of glucuronic acid derivative **2-2**, a useful building block in the assembly of glycosaminoglycans, such as heparin. The synthesis of **2-2** was achieved in seven steps and 32% overall yield. The chemistry presented offers for the first time a general, high yielding, and easily scaleable route to uronic acid synthons for glycosaminoglycan assembly, addressing a long-standing obstacle in the convenient production of these compounds.

2.4 References

- (1) Noti, C., and Seeberger, P. H. (2005) Chemical approaches to define the structure-activity relationship of heparin-like glycosaminoglycans. *Chem. Biol.* 12, 731-756.
- (2) Petitou, M., and van Boeckel, C. A. A. (2004) A synthetic antithrombin III binding pentasaccharide is now a drug! What comes next? *Angew. Chem. Int. Ed.* 43, 3118-3133.
- (3) Poletti, L., and Lay, L. (2003) Chemical contributions to understanding heparin activity: synthesis of related sulfated oligosaccharides. *Eur. J. Org. Chem.*, 2999-3024.

- (4) Karst, N. A., and Linhardt, R. J. (2003) Recent chemical and enzymatic approaches to the synthesis of glycosaminoglycan oligosaccharides. *Curr. Med. Chem.* 10, 1993-2031.
- (5) Yeung, B. K. S., Chong, P. Y. C., and Petillo, P. A. (2002) Synthesis of glycosaminoglycans. *J. Carbohydr. Chem.* 21, 799-865.
- (6) Kiss, J., and Wyss, P. C. (1976) Synthesis of heparin saccharides-V. Anomeric *O*-benzyl derivatives of L-idopyranosyluronic acid. *Tetrahedron* 32, 1399-1402.
- (7) Kiss, J., and Wyss, P. C. (1973) Synthesis of heparin saccharides. Part II. Synthesis and stereochemical aspects of anomeric methyl (benzyl 2,3-di-*O*-benzyl-L-idopyranosid)uronates. *Carbohydr. Res.* 27, 282-285.
- (8) Adinolfi, M., Barone, G., Lorenzo, F. D., and Iadonisi, A. (1999) Intramolecular Tishchenko reactions of protected hexos-5-uloses: a novel and efficient synthesis of L-idose and L-altrose. *Synlett*, 336-338.
- (9) Hung, S.-C., Puranik, R., and Chi, F.-C. (2000) Novel synthesis of 1,2:3,5-di-*O*- β -L-idofuranoside and its derivatives at C6. *Tetrahedron Lett.* 41, 77-80.
- (10) Lubineau, A., Gavard, O., Alais, J., and Bonnaffé, D. (2000) New accesses to L-iduronyl synthons. *Tetrahedron Lett.* 41, 307-311.
- (11) Lee, J.-C., Lu, X.-A., Kulkarni, S. S., Wen, Y.-S., and Hung, S.-C. (2004) Synthesis of heparin oligosaccharides. *J. Am. Chem. Soc.* 126, 476-477.
- (12) Schell, P., Orgueira, H. A., Roehrig, S., and Seeberger, P. H. (2001) Synthesis and transformations of D-glucuronic and L-iduronic acid glycals. *Tetrahedron Lett.* 42, 3811-3814.
- (13) Dax, K., Macher, I., and Weidmann, H. (1974) Reactionen der D-glucuronsäure. *J. Carbohydr. Nucleosides and Nucleotides* 1, 323-334.
- (14) Csuk, R., Höning, H., Nimpf, J., and Weidmann, H. (1980) A facile synthesis of 1,2-*O*-isopropylidene- β -L-idofuranurono-6,3-lactone. *Tetrahedron Lett.* 21, 2135-2136.
- (15) Vlahov, I. R., and Linhardt, R. J. (1995) Regioselective synthesis of derivatives of idopyranuronic acid: A key constituent of glycosaminoglycans. *Tetrahedron Lett.* 36, 8379-8382.
- (16) Du, Y., Lin, J., and Linhardt, R. J. (1997) Regioselective synthesis of L-idopyranuronic acid derivatives: intermolecular aglycon transfer of dithioacetal under standard glycosylation conditions. *J. Carbohydr. Chem.* 16, 1327-1344.
- (17) Chiba, T., and Sinaÿ, P. (1986) Application of a radical reaction to the synthesis of L-iduronic acid derivatives from D-glucuronic acid analogues. *Carbohydr. Res.* 151, 379-389.
- (18) Medaković, D. (1994) An efficient synthesis of methyl 1,2,3,4-tetra-*O*-acetyl- β -L-idopyranuronate. *Carbohydr. Res.* 253, 299-300.
- (19) Bazin, H. G., Kerns, R. J., and Linhardt, R. J. (1997) Regio and stereoselective conversion of Δ^4 -uronic acids to L-ido- and D-glucopyranosiduronic acids. *Tetrahedron Lett.* 38, 923-926.
- (20) Rochepeau-Jobron, L., and Jacquinet, J.-C. (1997) Diastereoselective hydroboration of substituted *exo*-glucals revisited. A convenient route for the preparation of L-iduronic acid derivatives. *Carbohydr. Res.* 303, 395-406.
- (21) Dromowicz, M., and Köll, P. (1998) A convenient synthesis of D-idose. *Carbohydr. Res.* 308, 169-171.

- (22) Hinou, H., Kurosawa, H., Matsuoka, K., Terunuma, D., and Kuzuhara, H. (1999) Novel synthesis of L-iduronic acid using trehalose as the disaccharidic starting material. *Tetrahedron Lett.* *40*, 1501-1504.
- (23) Takahashi, H., Hitomi, Y., Iwai, Y., and Ikegami, S. (2000) A novel and practical synthesis of L-hexoses from D-glycono-1,5-lactones. *J. Am. Chem. Soc.* *122*, 2995-3000.
- (24) Timmer, M. S. M., Adibekian, A., and Seeberger, P. H. (2005) Short *de novo* synthesis of fully functionalized uronic acid monosaccharides. *Angew. Chem. Int. Ed.* *44*, 7605-7607.
- (25) Tabeur, C., Machetto, F., Mallet, J.-M., Duchaussoy, P., Petitou, M., and Sinay, P. (1996) L-Iduronic acid derivatives as glycosyl donors. *Carbohydr. Res.* *281*, 253-276.
- (26) Ojeda, R., de Paz, J. L., Martín-Lomas, M., and Lassaletta, J. M. (1999) A new route to L-iduronate building-blocks for the synthesis of heparin-like oligosaccharides. *Synlett*, 1316-1318.
- (27) Orgueira, H. A., Bartolozzi, A., Schell, P., Litjens, R. E. J. N., Palmacci, E. R., and Seeberger, P. H. (2003) Modular synthesis of heparin oligosaccharides. *Chem. Eur. J.* *9*, 140-169.
- (28) Orgueira, H. A., Bartolozzi, A., Schell, P., and Seeberger, P. H. (2002) Conformational locking of the glycosyl acceptor for stereocontrol in the key step in the synthesis of heparin. *Angew. Chem. Int. Ed.* *41*, 2128-2131.
- (29) Danishefsky, S. J., and Bilodeau, M. T. (1996) Glycals in organic synthesis: the evolution of comprehensive strategies for the assembly of oligosaccharides and glycoconjugates of biological consequence. *Angew. Chem. Int. Ed.* *35*, 1380-1419.
- (30) Barroca, N., and Jacquinet, J.-C. (2000) Syntheses of β -D-GalpNAc4SO₃-(1 \rightarrow 4)-L-IdopA2SO₃, a disaccharide fragment of dermatan sulfate, and of its methyl α -L-glycoside derivative. *Carbohydr. Res.* *329*, 667-679.
- (31) Smid, P., Schipper, F. J. M., Broxterman, H. J. G., Boons, G. J. P. H., van de Marel, G. A., and van Boom, J. H. (1993) Use of (chloromethyl)dimethylphenylsilane in sugar chemistry-stereo-controlled approach to destomic acid and 1-deoxy-nojirimycin. *Recl. Trav. Chim. Pays-Bas* *112*, 451-456.
- (32) Crich, D., and Lim, L. B. L. (1991) Diastereoselective free-radical reactions part 3. The methyl glucopyranos-1-yl and the 1,2-*O*-isopropylidene-glucopyranos-1-yl radicals: conformational effects on diastereoselectivity. *J. Chem. Soc., Perkin Trans. 1*, 2209-2214.
- (33) Kozikowski, A. P., Konoike, T., and Ritter, A. (1987) Organometallics in organic synthesis. Applications of a new diorganozinc reaction to the synthesis of C-glycosyl compounds with evidence for an oxonium-ion mechanism. *Carbohydr. Res.* *171*, 109-124.
- (34) Alonso, R. A., Vite, G. D., McDevitt, R. E., and Fraser-Reid, B. (1992) Radical cyclization routes to bridged pyranosides as precursors of densely functionalized cycloalkanes. *J. Org. Chem.* *57*, 573-584.
- (35) Gordon, D. M., and Danishefsky, S. J. (1992) Synthesis of a cyanobacterial sulfolipid: confirmation of its structure, stereochemistry, and anti-HIV-1 activity. *J. Am. Chem. Soc.* *114*, 659-663.
- (36) Mori, Y., and Hayashi, H. (2001) Practical synthesis of 1,3-*O*-di-tert-butylsilylene-protected D- and L-erythritols as a four-carbon chiral building block. *J. Org. Chem.* *66*, 8666-8668.

- (37) Park, T. K., Kim, I. J., Hu, S., Bilodeau, M. T., Randolph, J. T., Kwon, O., and Danishefsky, S. J. (1996) Total synthesis and proof of structure of a human breast tumor (globo-H) antigen. *J. Am. Chem. Soc.* *118*, 11488-11500.
- (38) Krajewski, J. W., Gluzifiski, P., Pakulski, Z., Zamojski, A., Mishnev, A., and Kemme, A. (1994) Synthesis, crystal structure, and conformation of methyl 6-deoxy-2,3-*O*-isopropylidene- α -D-manno-heptofuranoside. *Carbohydr. Res.* *252*, 97-105.
- (39) Stepowska, H., and Zamojski, A. (1999) Elongation of the pentose chain at the terminal carbon atom with grignard C₁ reagents. A study of the homologation reaction. *Tetrahedron* *55*, 5519-5538.
- (40) Gelas, J., and Horton, D. (1981) Acetonation of carbohydrates under kinetic control by use of 2-alkosypropene. *Heterocycles* *16*, 1587-1601.
- (41) Wolfrom, M. L., Diwadkar, A. B., Gelast, J., and Horton, D. (1974) A new method of acetonation. Synthesis of 4,6-*O*-isopropylidene-D-glucopyranose. *Carbohydr. Res.* *35*, 87-96.
- (42) Ernst, B., Hart, G. W., and Sinaÿ, P. (2000) *Carbohydrates in Chemistry and Biology*, Vol. 1, Wiley-VCH, Weinheim, Germany.
- (43) Camps, P., Farrés, X., García, L., Ginesta, J., Paseual, J., Mauleón, D., and Carganico, G. (1995) Stereoselective syntheses of both enantiomers of ketoconazole from (*R*)- and (*S*)-epichlorohydrin. *Tetrahedron: Asymmetry* *6*, 1283-1294.
- (44) Díez, D., Beneitez, M. T., Marcos, I. S., Garrido, N. M., Basabe, P., and Urones, J. G. (2001) Enantioselective synthesis of a 2,3,4-trisubstituted pyrrolidine from 1-hydroxymethyl-4-phenylsulfonylbutadiene. *Synlett*, 655-657.
- (45) Golinski, M., Vasudevan, S., Floresca, R., Brock, C. P., and Watt, D. S. (1993) An enantioselective approach to ring A of taxol using the Wieland-Miescher ketone. *Tetrahedron Lett.* *34*, 55-58.
- (46) Mattay, J., Thünker, W., and Scharf, H.-D. (1981) Synthese von β -oxa- γ,δ -enonen. *Liebigs Ann. Chem.*, 1105-1117.
- (47) Mohammadpoor-Baltork, L., Khosropour, A. R., and Aliyan, H. (2001) Efficient conversion of epoxides to 1,3-dioxolanes catalyzed by bismuth(III) salts. *Synth. Comm.* *31*, 3411-3416.
- (48) Takano, S., Sugihara, T., Satoh, S., and Ogasawara, K. (1988) Enantioselective synthesis of (-)-kainic acid. *J. Am. Chem. Soc.* *110*, 6467-6471.
- (49) Welch, J. T., and Svahn, B.-M. (1985) Synthesis and X-ray crystal structure of methyl D,L-desmethyl-holantosaminide. *J. Carbohydr. Chem.* *4*, 421-427.
- (50) Wershofen, S., and Scharf, H.-D. (1988) Synthesis of side-chain unsaturated *endo*- and *exo*-brevicomins. Representatives of pheromone analogs in the dioxabicyclo[3.2.1]octane series. *Synthesis*, 854-859.
- (51) Halcomb, R. L., and Danishefsky, S. J. (1989) On the direct epoxidation of glycals: application of a reiterative strategy for the synthesis of β -linked oligosaccharides. *J. Am. Chem. Soc.* *111*, 6661-6666.

Chapter 3

A Stereochemical Surprise at the Late Stage of the Synthesis of Fully *N*-Differentiated Heparin Oligosaccharides Containing Amino, Acetamido, and *N*-Sulfonate Groups

3.1 Introduction

Heparin-like glycosaminoglycans (HLGAGs) are a class of polysaccharides found protein-conjugated in the extracellular matrix and free in the circulatory system. HLGAGs are involved in an array of signaling functions, including regulation of the coagulation cascade, growth factor interactions, and viral entry into cells.⁽¹⁻¹²⁾ Heparin fractions isolated from animal sources are used clinically as anti-coagulants,^(13, 14) and several synthetic analogues of heparin have been prepared as anticoagulant drug candidates.⁽¹⁵⁻²⁴⁾

HLGAGs consist of alternating 1,2-anti-(1→4) linked uronic acid residues and α -(1→4) linked glucosamine residues. The polysaccharides exist in a wide variety of *O*- and *N*-sulfonated as well as *N*-acetylated states with a high sequence variability. Due to both the high structural complexity and the difficulty of isolating homogeneous structures from natural sources, heparin is an ideal target for a modular synthetic method. Defined sequences of heparin are needed for biological study, and the ability to generate diverse libraries of heparin would greatly facilitate studies into the structure-activity relationship of HLGAGs. The direct study of heparin biochemistry and the development of HLGAG analytical techniques would benefit from the availability of defined sequences. No completely general method for the production of heparin oligosaccharides exists and substantial synthetic challenges remain to be overcome.^(1, 16, 25-27)

Recent reports describe fully differentiated monosaccharide building blocks for HLGAG synthesis.⁽²⁸⁻³⁶⁾ Several sequences have been produced, including oligomers of the fibroblast growth factor (FGF) disaccharide repeat⁽³⁷⁻⁴³⁾ and several variants and analogues of the antithrombin III (ATIII) binding structure. ^(15, 16, 44-57) The amine group has been masked as an azide in most heparin syntheses to date, allowing access to only poly-*N*-sulfonated structures. One synthesis of the ATIII binding sequence included a non-reducing end GlcNAc residue, ⁽⁵⁷⁾

but the method used was not general and the use of the *N*-acetate as the protecting group resulted in poor coupling yields.(58, 59)

2-Azido glucosyl trichloroacetimidates or halides frequently serve as glycosylating agents to install α -glucosamine linkages. These reagents have shown high α -selectivity when coupled to the C4 hydroxyl group of iduronic acid, but afford mixtures of products when coupled to glucuronic acid.(33, 48, 57, 60) In the recent synthesis of a ATIII-binding hexasaccharide,(32) all α -glucosamine linkages were formed with complete selectivity during the assembly of disaccharide modules via glycosylation of conformationally constrained 1,2-*O*-isopropylidene iduronic or glucuronic acids with 2-azido glucosyl trichloroacetimidates.(33)

The HLGAG octasaccharide 3-1 is known to bind viral coat proteins on herpes simplex virus 1 (HSV-1) and is thought to be involved in viral cell entry.(61, 62) Based on sequencing efforts that combine enzymatic degradation and mass spectrometry, two possible structures (Figure 3-1) have been proposed for the herpes-binding sequence.(63-65) The isolated structures contained 4,5-dehydrouronic acids at the non-reducing end and at the indicated site as a result of the degradation techniques used. The structure contains *N*-sulfonates, an *N*-acetate, and a free amine.

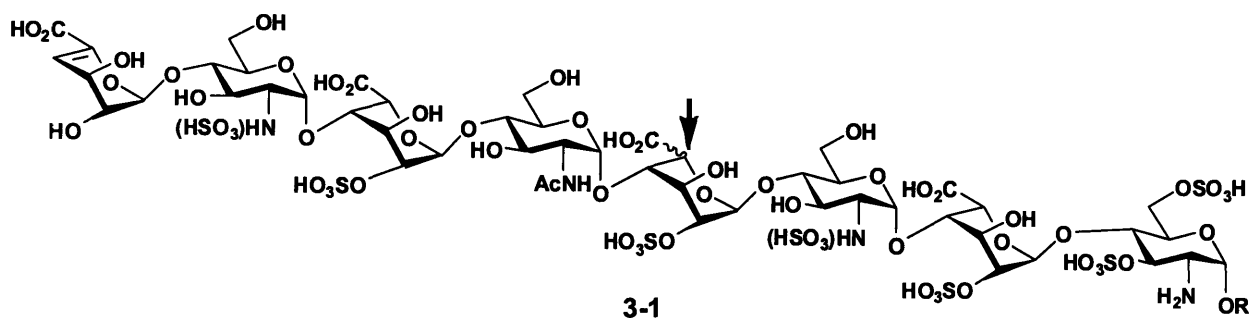


Figure 3-1. Target structure as reported from sequencing studies.(64) The stereochemistry at the indicated site is unknown. Counter ions after oligosaccharide purification are primarily sodium.

This chapter describes a strategy for the synthesis of *N*-differentiated heparin oligosaccharides en route to fully protected target **3-2** (Figure 3-2). Iduronic acid was selected arbitrarily in the two uronic acid positions of unknown stereochemistry to reduce the complexity of the synthetic target. As in previous heparin syntheses, *O*-sulfonates were masked as *O*-acetates, free hydroxyls as *O*-benzyl ethers, carboxylic acids as methyl esters, and *N*-sulfonates as azide groups.(1, 15, 16, 25-27, 32, 37-39, 41-46, 48, 54, 57, 58, 66, 67) An *N*-diacetate masked the *N*-acetate,(59, 68) while the free amine was masked as the benzyl carbamate (CBz, Z). These protecting groups would allow for the deprotection and elaboration of **3-2** through a modification of previously established heparin deprotection protocols.(1, 15, 16, 25-27, 32, 37-39, 41-46, 48, 54, 57, 58, 66, 67) All *O*-acetates and methyl esters, as well as one of the *N*-diacetate amides, could be removed using LiOOH/NaOH. Selective reduction of the azides could be achieved by Staudinger, thiol, SmI₂, or a variety of other selective reduction chemistries.(69) Sulfonation of all hydroxyls and amines with SO₃•NEt₃, followed by Pd/C reductive removal of benzyl ethers and the CBz carbamate, would reveal the fully deprotected and elaborated structure.

Fully protected octasaccharide **3-2** was the proposed target en route to the HSV-1 binding octasaccharide **3-1**. Retrosynthetic analysis of **3-2** revealed that the non reducing end disaccharide **3-3**, the tetrasaccharide **3-4**, and the reducing end disaccharide **3-5** would provide the key modules based on the assumption that 2-azido glucosamines can be coupled to iduronic acid residues with complete α -stereoselectivity. These intermediates can be readily assembled from five previously reported monosaccharide modules: iduronic acid derivatives **3-6**, **3-8**, and **3-9** (Chapter 2)(30) and glucosamine derivatives **3-7**(32) and **3-10**.

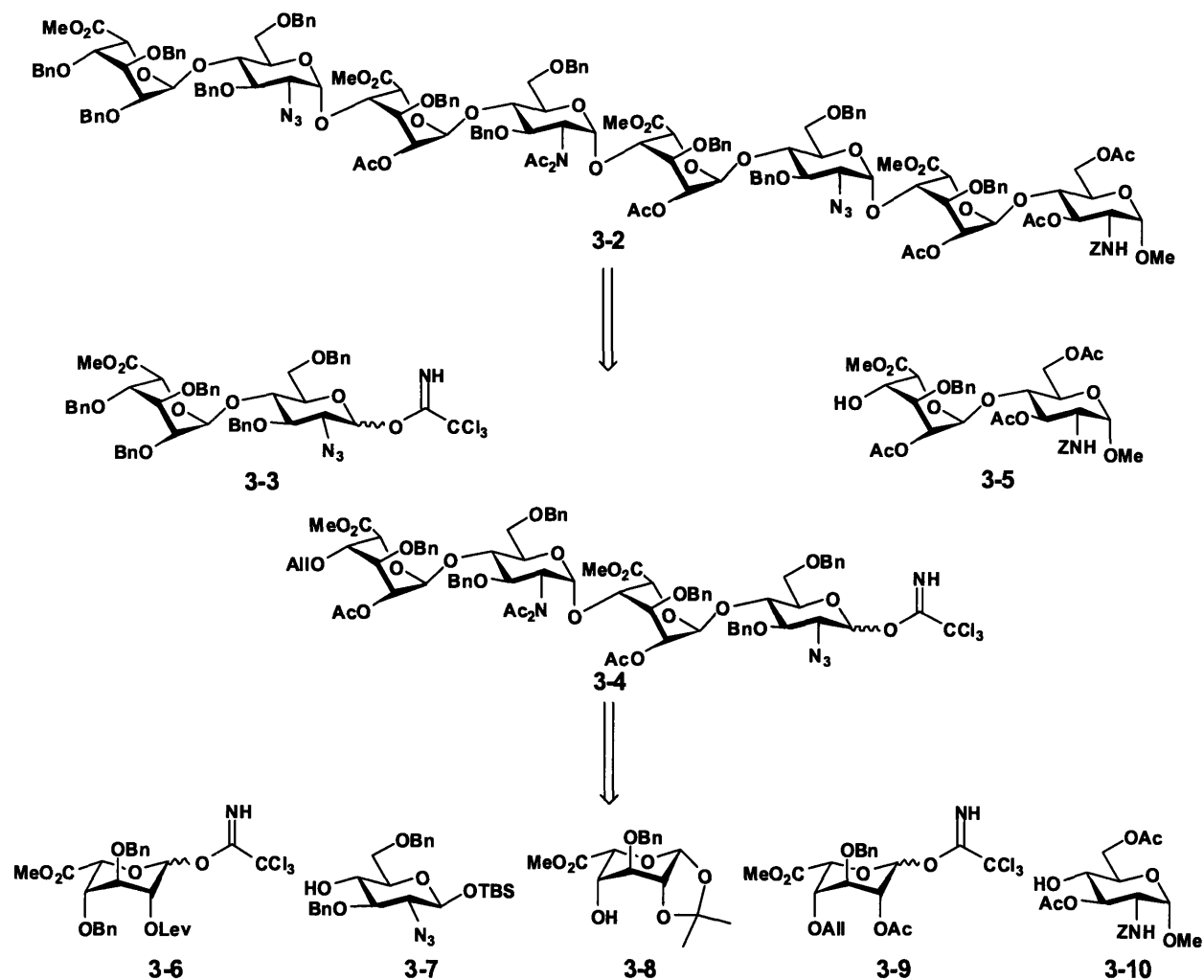


Figure 3-2. Retrosynthetic analysis.

3.2 Experimental

Materials and Methods. All commercial materials were used without purification, unless otherwise noted. CH₂Cl₂, THF, and diethyl ether were passed through neutral alumina columns prior to use. Toluene was passed through neutral alumina and copper (II) oxide columns before use. Methanol and DMF were purchased anhydrous and used without further purification. Analytical thin-layer chromatography was performed on E. Merck silica gel 60 F254 plate (≤0.25 mm). Compounds were visualized by cerium sulfate-ammonium molybdate stain and

heating. Liquid chromatography was performed using forced flow of the indicated solvent on silica (230-400 Mesh).

***t*-Butyldimethylsilyl (methyl 3,4-di-*O*-benzyl-2-*O*-levonuy- α -L-idopyranosiduronate) (1 \rightarrow 4) 2-azido-3,6-di-*O*-benzyl-2-deoxy- β -D-glucopyranoside (3-11).** Trichloroacetimidate 3-6(30) (220 mg, 0.349 mmol) and monosaccharide 3-7(32) (145 mg, 0.29 mmol) were coevaporated three times with anhydrous toluene. The compounds were dissolved in anhydrous CH₂Cl₂ (3 mL) under N₂ and cooled to -15°C. Trimethylsilyl trifluoromethanesulfonate (TMSOTf) (7.5 μ L, 0.042 mmol) was added and the reaction was stirred for 45 min. The reaction was quenched by addition of NEt₃ (0.2 mL) and the solvent was removed under reduced pressure. Flash chromatography on silica (hexanes:ethyl acetate 17:3) afforded recovered 7 (13 mg, 0.026 mmol, 9%). Further elution (hexanes:ethyl acetate 3:1) yielded 3-11 (208 mg, 0.215 mmol, 74%) as a clear oil. Rf. 0.13 (hexanes:ethyl acetate 3:1). $[\alpha]_D^{24}$: -28.3, c = 0.9. IR (thin film, NaCl plates) 2928, 2110, 1745, 1739, 1721 cm⁻¹. ¹H NMR (500 MHz, CDCl₃) δ 7.22-7.39 (m, 20H), 5.31 (d, *J* = 3.6 Hz, 1H), 4.91 (t, *J* = 3.6 Hz, 1H), 4.81 (d, *J* = 3.6 Hz, 1H), 4.69-4.75 (m, 3H), 4.43-4.60 (m, 6H), 4.02 (t, *J* = 9.3 Hz, 1H), 3.87 (t, *J* = 4.1, 1H), 3.81 (t, *J* = 3.9 Hz, 1H), 3.70-3.71 (m, 2H), 3.44 (s, 3H), 3.38 (m, 1H), 3.35 (d², *J* = 7.5 Hz, 10 Hz, 1H), 3.26 (t, *J* = 4.5 Hz, 1H), 2.63 (m, 2H), 2.46 (m, 2H), 2.12 (s, 3H), 0.94 (s, 9H), 0.17 (s, 3H), 0.15 (s, 3H). ¹³C NMR (125 MHz, CDCl₃) δ 206.4, 172.1, 169.8, 138.5, 138.4, 137.9, 137.8, 128.6, 128.5, 128.4, 128.3, 128.1, 128.07, 128.04, 128.0, 127.7, 127.6, 127.4, 97.8, 97.4, 81.0, 75.4, 75.0, 74.9, 74.7, 73.6, 73.4, 73.6, 73.4, 72.9, 72.7, 69.6, 69.3, 68.8, 68.4, 51.9, 37.9, 30.0, 28.1, 25.8, 10.2, -4.0, -5.0. ESI MS (C₅₂H₆₅N₃O₁₃Si) *m/z* (M + Na⁺) calcd 990.4179, obsd 990.4145.

***t*-Butyldimethylsilyl (methyl 3,4-di-*O*-benzyl- α -L-idopyranosiduronate) (1 \rightarrow 4) 2-azido-3,6-di-*O*-benzyl-2-deoxy- β -D-glucopyranoside (3-12).** Disaccharide 3-11 (176 mg, 0.182 mmol)

was dissolved in pyridine (550 μL) and acetic acid (360 μL). Hydrazine hydrate (44 μL , 0.91 mmol) was added and the reaction was stirred for 1 h. The reaction was quenched by addition of acetone (5 mL) and stirred for 30 min. The solution was poured into ethyl acetate (50 mL), washed with 1N HCl, brine, and saturated NaHCO_3 . The organic phase was dried over MgSO_4 and solvent was removed under reduced pressure. Flash chromatography on silica (hexanes:ethyl acetate 17:3) afforded **3-12** (145 mg, 0.167 mmol, 92%) as a clear oil. Rf. 0.21 (hexanes:ethyl acetate 3:1). $[\alpha]_D^{24}$: -47.6, $c = 0.8$. IR (thin film, NaCl plates) 3495, 2929, 2857, 2109, 1776, 1742, 839 cm^{-1} . ^1H NMR (500 MHz, CDCl_3) δ 7.21-7.4 (m, 20H), 5.23 (d, $J = 1.5$ Hz, 1H), 4.90 (d, $J = 2.3$ Hz, 1H), 4.45-4.71 (m, 9H), 3.98 (ψ t, $J = 9.4$ Hz, 1H), 3.83-3.87 (m, 2H), 3.67-3.72 (m, 3H), 3.43 (d, $J = 10.9$ Hz, 1H), 3.35-3.4 (m, 2H), 3.36 (s, 3H), 3.22 (ψ t, $J = 9.5$ Hz, 1H), 0.94 (s, 9H), 0.17 (s, 3H), 0.15 (s, 3H). ^{13}C NMR (125 MHz, CDCl_3) δ 169.9, 138.5, 138.1, 137.9, 136.9, 128.7, 128.6, 128.4, 128.3, 128.2, 128.1, 127.9, 127.4, 101.1, 97.6, 81.2, 75.5, 75.0, 74.3, 73.3, 73.2, 72.3, 68.9, 68.2, 67.2, 52.0, 25.7, 18.2, -4.0, -5.0. ESI MS ($\text{C}_{47}\text{H}_{59}\text{N}_3\text{O}_{11}\text{Si}$) m/z ($\text{M} + \text{Na}^+$) calcd 892.3811, obsd 892.3829.

***t*-Butyldimethylsilyl (methyl 2,3,4-tri-*O*-benzyl- α -L-idopyranosiduronate) (1 \rightarrow 4) 2-azido-3,6-di-*O*-benzyl-2-deoxy- β -D-glucopyranoside (3-13)**. Disaccharide **3-12** (125 mg, 0.144 mmol), was coevaporated three times with anhydrous toluene and dissolved in anhydrous hexanes (1.4 mL) and a minimum amount of anhydrous CH_2Cl_2 to dissolve the compound. Benzyl trichloroacetimidate (54 μL , 0.288 mmol) was added, followed by one drop (~ 1 μL) of trifluoromethanesulfonic acid. After 90 min, the solution was filtered to remove the precipitated trichloroacetamide and the solvent was removed under reduced pressure. Flash chromatography on silica (hexanes:ethyl acetate 9:1) yielded **3-13** (105 mg, 0.109 mmol, 76%) as a clear oil. Rf. 0.53 (hexanes:ethyl acetate 3:1). $[\alpha]_D^{24}$: -20.1, $c = 0.7$. IR (thin film, NaCl plates) 2928, 2110,

1741 cm⁻¹. ¹H NMR (500 MHz, CDCl₃) δ 7.24-7.37 (m, 25H, aryl H), 5.40 (d, ³J_{H1-H2} = 6.4, 1H, IdoA H1), 4.85 (d, ²J = 10.7 Hz, 1H, benzyl CH₂), 4.73 (d, ²J = 11.2 Hz, 1H, benzyl CH₂), 4.72 (m, 1H, benzyl CH₂), 4.71 (m, 1H, benzyl CH₂), 4.70 (m, 1H, benzyl CH₂), 4.68 (d, ²J = 11.5 Hz, 1H, benzyl CH₂), 4.64 (d, ²J = 11.6 Hz, 1H, benzyl CH₂), 4.60 (d, ²J = 11.6 Hz, 1H, benzyl CH₂), 4.58 (d, ³J_{H4-H5} = 5.8, 1H, IdoA H4), 4.54 (d, ²J = 12.4 Hz, 1H, benzyl CH₂), 4.47 (d, ³J_{H1-H2} = 7.4 Hz, 1H, GlcN₃ H1), 4.45 (d, ²J = 12.4 Hz, 1H, benzyl CH₂), 3.98 (m, 1H, GlcN₃ H4), 3.96 (m, 1H, IdoA H3), 3.81 (d², ³J_{H3-H4} = 7.4, ³J_{H4-H5} = 5.8, 1H, IdoA H4), 3.71 (d², ²J = 10.7 Hz, ³J_{H5-H6} = 4.3 Hz, 1H, GlcN₃ H6), 3.66 (d², ²J = 10.7 Hz, ³J_{H5-H6'} = 1.7 Hz, 1H, GlcN₃ H6'), 3.53 (s, 3H, OCH₃), 3.37 (d², ³J_{H1-H2} = 6.4, ³J_{H2-H3} = 7.5, 1H, IdoA H2), 3.34 (m, 1H, GlcN₃ H5), 3.31 (m, 1H, GlcN₃ H2), 3.29 (m, 1H, GlcN₃ H3), 0.95 (s, 9H, TBDMS *t*-butyl), 0.16 (s, 3H, TBDMS methyl), 0.14 (s, 3H, TBDMS methyl). ¹³C NMR (125 MHz, CDCl₃) δ 170.0 (IdoA C6), 138.6 (benzyl quat.), 138.5 (benzyl quat), 138.4 (benzyl quat), 137.9 (benzyl quat), 128.6 (aromatic C), 128.55 (aromatic C), 128.5 (aromatic C), 128.4 (aromatic C), 128.3 (aromatic C), 128.25 (aromatic C), 128.15 (aromatic C), 128.1 (aromatic C), 128.05 (aromatic C), 128.0 (aromatic C), 127.9 (aromatic C), 127.8 (aromatic C), 127.7 (aromatic C), 127.65 (aromatic C), 127.5 (aromatic C), 100.0 (IdoA C1), 97.3 (GlcN₃ C1), 81.1 (GlcN₃ C2), 80.6 (IdoA C2), 79.0 (IdoA C3), 77.2 (IdoA C4), 75.9 (GlcN₃ C4), 75.5 (GlcN₃ C3), 75.0 (benzyl CH₂), 74.9 (benzyl CH₂), 74.6 (benzyl CH₂), 73.4 (benzyl CH₂), 73.35 (benzyl CH₂), 72.0 (IdoA C5), 68.6 (GlcN₃ C5), 68.3 (GlcN₃ C6), 52.0 (OCH₃), 25.8 (TBDMS *t*-butyl CH₃), 18.2 (TBDMS *t*-butyl quat), -4.0 (TBDMS methyl CH₃), -5.0 (TBDMS methyl CH₃). ESI MS (C₅₄H₆₅N₃O₁₁Si) *m/z* (M + Na⁺) calcd 982.4281, obsd 982.4250.

Methyl 2,3,4-tri-*O*-benzyl- α -L-idopyranosiduronate (1 \rightarrow 4) 2-azido-3,6-di-*O*-benzyl-2-deoxy-D-glucopyranoside trichloroacetimidate (3-3). Disaccharide **3-13** (30 mg, 31 μ mol) was

coevaporated three times with anhydrous toluene and dissolved in anhydrous THF (500 μ L).

The solution was cooled to 0°C and acetic acid (2 μ L, 35 μ mol) was added followed by TBAF (34 μ L, 1.0 M in THF). After 1 h, the reaction was poured into ethyl acetate (100 mL) and washed twice with brine. The organic phase was dried over MgSO₄ and the solvent was removed under reduced pressure.

The residue was coevaporated three times with anhydrous toluene and dissolved in anhydrous CH₂Cl₂ (500 μ L) under N₂. The solution was cooled to 0°C and trichloroacetonitrile (47 μ L, 0.47 mmol) and DBU (0.5 μ L, 3 μ mol) added. The reaction was stirred 30 min then allowed to warm to room temperature. The solvent was evaporated and the residue purified by flash chromatography on silica (toluene:ethyl acetate 9:1) to afford **3-3** (24 mg, 24 μ mol, 78%, 1.5:1 α : β) as a yellow oil. Rf. 0.57, 0.63 (hexanes:ethyl acetate 2:1). IR (thin film, NaCl plates) 3030, 2918, 2112, 1761, 1739, 1674 cm⁻¹. ¹H NMR (500 MHz, CDCl₃) δ 8.70 (s, 0.4H), 8.69 (s, 0.6H), 7.12-7.39 (m, 25H), 6.38 (d, J = 3.5 Hz, 0.6H), 5.6 (d, J = 8.4 Hz, 0.4H), 5.44-5.50 (m, 1H), 5.03 (d, J = 10.3 Hz, 0.6H), 4.92 (d, J = 10.7 Hz, 0.4 H), 4.70-4.78 (m, 5H), 4.63-4.67 (m, 2H), 4.51-4.6 (m, 2H), 4.47 (d, J = 12.2 Hz, 0.4H), 4.42 (d, J = 12.0 Hz, 0.6H), 4.24 (t, J = 9.6 Hz, 0.6H), 4.13 (t, J = 9.3 Hz, 0.4 H), 3.91-4.04 (m, 3H), 3.76-3.84 (m, 2H), 3.65-3.71 (m, 1H), 3.35-3.56 (m 6H). ¹³C NMR (125 MHz, CDCl₃) δ 170.6, 170.5, 161.8, 161.3, 139.0, 138.9, 138.85, 138.8, 138.75, 138.7, 138.6, 138.35, 138.30, 129.6, 129.4, 129.15, 129.11, 129.1, 129.07, 129.05, 129.03, 128.9, 128.89, 128.87, 128.85, 128.65, 128.63, 128.60, 128.58, 128.57, 128.55, 128.4, 128.35, 128.1, 100.6, 100.5, 97.4, 15.5, 91.7, 81.75, 81.7, 81.0, 79.9, 79.6, 78.8, 78.1, 77.0, 76.4, 75.9, 75.85, 75.8, 75.7, 75.4, 75.35, 75.1, 74.4, 74.0, 73.9, 73.8, 72.7, 68.0, 67.8, 65.9, 63.1, 52.5, 52.4. MS (C₅₀H₅₁Cl₃N₄O₁₁) m/z (M + Na⁺) calcd 1011.2518, obsd 1011.2507.

***t*-Butyldimethylsilyl (methyl 2-*O*-acetyl-4-*O*-allyl-3-*O*-benzyl- α -L-idopyranosiduronate)**

(1 \rightarrow 4) 2-azido-3,6-di-*O*-benzyl-2-deoxy- β -D-glucopyranoside (3-14). Trichloroacetimidate 3-9(30) (62 mg, 0.118 mmol) and monosaccharide 7(32) (40 mg, 0.079 mmol) were combined and coevaporated three times with anhydrous toluene. The mixture was dissolved in anhydrous CH₂Cl₂ (1 mL) under N₂ and cooled to -15°C. TMSOTf (130 μ L of a 0.1 M solution in CH₂Cl₂) was added and the reaction stirred 30 min at reduced temperature, then allowed to warm to room temperature over 30 min. The reaction was quenched with NEt₃ (0.2 mL) and the solvent was removed under reduced pressure. Flash chromatography on silica (hexanes:ethyl acetate 17:3) afforded 3-14 (60 mg, 0.070 mmol, 88%) as a clear oil. Rf. 0.28 (hexanes:ethyl acetate 3:1). $[\alpha]_D^{24}$: -35.3, c = 0.62. IR (thin film, NaCl plates) 2926, 2110, 1764, 1741 cm⁻¹. ¹H NMR (500 MHz, CDCl₃) δ 7.24-7.39 (m, 15H, aromatics), 5.76 (m, 1H, allyl OCH₂CH=CH₂), 5.30 (d, ³J_{H1H2} = 3.5 Hz, 1H, IdoA H1), 5.17 (d³, J = 17.4 Hz, 3Hz, ⁴J = 1.6 Hz, 1H, allyl OCH₂HCH=CH), 5.13 (d³, J = 10.4 Hz, 3 Hz, ⁴J = 1.1 Hz), 4.89 (ψ t, J = 3.8 Hz, 1H, IdoA H2), 4.79 (d, ³J_{H5H4} = 3.8 Hz, 1H, IdoA H5), 4.76 (d, ²J = 11.1 Hz, 1H, GlcN₃O3 benzyl CH₂), 4.73 (d, ²J = 11.7 Hz, 1H, IdoA O3 benzyl CH₂), 4.71 (d, ²J = 11.1 Hz, 1H, GlcN₃O3 benzyl CH₂), 4.68 (d, ²J = 11.7 Hz, 1H, IdoA O3 benzyl CH₂), 4.60 (d, ²J = 12.3 Hz, 1H, GlcN₃O6 benzyl CH₂), 4.55 (d, ²J = 12.3 Hz, 1H, GlcN₃O6 benzyl CH₂), 4.49 (d, ³J_{H1H2} = 7.5 Hz, 1H GlcN₃ H1), 3.99 (m, 1H, allyl OCHHCH=CH₂), 3.98 (m, 1H, GlcN₃ H4), 3.93 (d² ψ t, J = 1.4 Hz, 5.8 Hz, 12.8 Hz, 1H, allyl OCHHCH=CH₂), 3.84 (ψ t, J = 4.6 Hz, 1H, IdoA H3), 3.74 (ψ t, J = 4.2, 1H, IdoA H4), 3.68 (m, 2H, GlcN₃ H6), 3.51 (s, 3H, -OCH₃), 3.37 (m, 1H, GlcN₃ H5), 3.35 (m, 1H GlcN₃ H2), 3.27 (d², ³J = 9 Hz, 9.8 Hz, GlcN₃ H3), 1.99 (s, 3H, acetate CH₃), 0.96 (s, 9H, TBDMS *t*-butyl), 0.16 (s, 3H, TBDMS methyl), 0.14 (s, 3H, TBDMS methyl). ¹³C NMR (125 MHz, CDCl₃) δ 170.3 (acetate carbonyl), 169.8 (IdoA C6), 138.5 (GlcN₃ O3 benzyl CH₂), 138.3

(GlcN₃O₆ benzyl quat.), 137.9 (IdoA O₃ benzyl quat), 134.4 (allyl OCH₂CH=CH₂), 128.6 (aromatic C), 128.5 (aromatic C), 128.3 (aromatic C), 128.1 (aromatic C), 128.05 (aromatic C), 127.8 (aromatic C), 127.7 (aromatic C), 127.6 (aromatic C), 127.5 (aromatic C), 117.6 (allyl OCH₂CH=CH₂), 98.0 (IdoA C₁), 97.4 (GlcN₃ C₁), 81.1 (GlcN₃ C₃), 75.4 (GlcN₃ C₅), 75.1 (GlcN₃ C₄), 75.1 (IdoA C₄), 74.8 (GlcN₃ O₃ benzyl CH₂), 73.9 (IdoA C₃), 73.5 (GlcN₃O₆ benzyl CH₂), 73.1 (IdoA O₃ benzyl CH₂), 71.8 (allyl OCH₂CH=CH₂), 69.7 (IdoA C₅), 69.4 (IdoA C₂), 68.8 (GlcN₃ C₂), 68.5 (GlcN₃ C₆), 52.0 (OCH₃), 25.8 (TBDMS *t*-butyl CH₃), 21.2 (acetate CH₃), 18.2 (TBDMS *t*-butyl quat.), -4.0 (TBDMS methyl), -5.0 (TBDMS methyl). ESI MS (C₄₅H₅₉N₃O₁₂Si) *m/z* (M + Na⁺) calcd 884.3760, obsd 884.3756.

Methyl (2-*O*-acetyl-4-*O*-allyl-3-*O*-benzyl- α -L-idopyranosid)uronate (1 \rightarrow 4) 2-azido-3,6-di-*O*-benzyl-2-deoxy-D-glucopyranoside trichloroacetimidate (3-15). Disaccharide 3-14 (960 mg, 1.11 mmol) was coevaporated three times with anhydrous toluene and dissolved in anhydrous THF (10 mL). The solution was cooled to 0°C and acetic acid (71 μ L, 1.23 mmol) was added followed by TBAF (1.0 M in THF, 1.23 mL). After 45 min, the reaction was poured into saturated NH₄Cl and the aqueous phase was extracted with ethyl acetate (3 x 150 mL). The organic phases were combined and dried over MgSO₄ and the solvent was removed under reduced pressure.

The residue was coevaporated three times with anhydrous toluene and dissolved in anhydrous CH₂Cl₂ (10 mL) under N₂. The solution was cooled to 0°C and trichloroacetonitrile (1.7 mL, 16.7 mmol) and DBU (32 μ L, 0.22 mmol) was added. The reaction was stirred for 30 minutes then allowed to warm to room temperature. The solvent was evaporated and the residue was purified by flash chromatography on silica (hexanes:ethyl acetate 3:1) to afford 3-15 (950 mg, 1.07 mmol, 96%, 2:1 β : α) as a yellow oil. Rf. 0.14 (hexanes:ethyl acetate 3:1). IR (thin

film, NaCl plates) 3338, 3031, 2876, 2113, 1745, 1739, 1675 cm^{-1} . ^1H NMR (500 MHz, CDCl_3) δ 8.70 (s, 0.67H), 8.69 (s, 0.33H), 7.24-7.38 (m, 15H), 6.40 (d, $J = 3.5$ Hz, 0.33H), 5.74-5.79 (m, 1H), 5.60 (d, $J = 8.3$ Hz, 0.67H), 5.35-5.37 (m, 1H), 5.17-5.21 (m, 2H), 4.51-4.94 (m, 8H), 4.2 (t, $J = 4.4$, 0.33 H), 4.12 (t, 0.66H), 3.83-4.02 (m, 4H), 3.63-3.78 (m, 4H), 3.41-3.59 (m, 2H), 3.52 (s, 2H), 3.51 (s, 1H), 1.97 (s, 2H), 1.96 (s, 1H). ^{13}C NMR (125 MHz, CDCl_3) δ 170.2, 170.19, 169.8, 161.2, 160.9, 138.2, 138.1, 138.0, 137.98, 137.95, 137.92, 134.4, 134.3, 128.66, 128.65, 128.57, 128.48, 128.39, 128.33, 128.18, 128.15, 128.1, 127.98, 127.9, 127.87, 127.77, 127.71, 127.63, 127.6, 117.73, 117.67, 97.9, 96.9, 95.0, 90.7, 78.5, 76.3, 75.3, 75.17, 75.15, 75.0, 75.9, 74.5, 74.2, 74.0, 73.6, 73.5, 73.3, 73.2, 71.95, 71.9, 70.2, 69.9, 69.7, 69.5, 67.8, 67.7, 65.7, 63.1, 52.1, 52.0, 21.22, 21.20. ESI MS ($\text{C}_{41}\text{H}_{45}\text{Cl}_3\text{N}_4\text{O}_{12}$) m/z ($\text{M} + \text{Na}^+$) calcd 913.1992, obsd 913.1996.

Methyl [methyl (2-*O*-acetyl-4-*O*-allyl-3-*O*-benzyl- α -L-idopyranosid)uronate (1 \rightarrow 4) 2-azido-3,6-di-*O*-benzyl-2-deoxy- α -D-glucopyranoside (1 \rightarrow 4) 3-*O*-benzyl-1,2-isopropylidene- β -L-idopyranosid]uronate (3-16). Trichloroacetimidate **3-15** (950 mg, 1.07 mmol) and monosaccharide **3-8**(30, 33) (433 mg, 1.28 mmol) were combined and coevaporated three times with anhydrous toluene. The mixture was dissolved in anhydrous CH_2Cl_2 (10 mL) under N_2 and cooled to -25°C and freshly activated 4Å molecular sieves (1 g) were added and the reaction was stirred for 30 min. TMSOTf (25 μL , 0.107 mmol) was added and the reaction was stirred for 90 minutes at reduced temperature. The reaction was quenched with NEt_3 (1 mL) and the solvent was removed under reduced pressure. Flash chromatography on silica (toluene:ethyl acetate 10:1 \rightarrow 20:3) afforded **3-16** (940 mg, 0.88 mmol, 83%) as a clear oil. Rf. 0.23 (hexanes:ethyl acetate 2:1). $[\alpha]_D^{24}$: -12.5, $c = 1.2$. IR (thin film, NaCl plates) 2932, 2108, 1765, 1741 cm^{-1} . ^1H NMR (500 MHz, CDCl_3) δ 7.24-7.29 (m, 20H), 5.75-5.81 (m, 1H), 5.35 (d, $J = 4.9$ Hz, 1H), 5.32

(d, $J = 2.5$ Hz, 1H), 5.19 (d³, $J = 1.6, 3.2, 17.2$ Hz, 1H), 5.13 (d³, $J = 1.2, 2.8, 10.4$ Hz, 1H), 4.86-4.89 (m, 3H), 4.65-4.74 (m, 6H), 4.61 (d, $J = 12.2$ Hz, 1H), 4.51 (d, $J = 12$ Hz, 1H), 4.40 (d, $J = 1.4$ Hz, 1H), 4.19 (t, $J = 2.3$ Hz, 1H), 3.95-4.08 (m, 5H), 3.86 (t, $J = 6$ Hz, 1H), 3.70-3.77 (m, 4H), 3.64 (s, 3H), 3.61 (d², $J = 1.9, 11.1$ Hz, 1H), 3.51 (s, 3H), 3.43 (d², $J = 3.3, 10.3$ Hz, 1H), 1.96 (s, 3H), 1.58 (s, 3H), 1.37 (s, 3H). ¹³C NMR (125 MHz, CDCl₃) δ 169.9, 161.2, 138.3, 138.15, 138.1, 137.2, 134.4, 128.8, 128.7, 128.5, 128.4, 128.3, 128.2, 128.1, 128.05, 128.0, 127.9, 127.8, 127.5, 117.7, 112.3, 98.3, 97.9, 97.1, 78.3, 75.9, 75.45, 75.4, 75.2, 74.9, 73.6, 73.4, 73.0, 72.8, 72.1, 71.8, 71.4, 70.8, 70.6, 67.5, 63.7, 52.5, 52.0, 28.2, 26.3, 21.2. ESI MS (C₅₆H₆₅N₃O₁₈) m/z (M + Na⁺) calcd 1090.4155, obsd 1090.4123.

Methyl [methyl (2-*O*-acetyl-4-*O*-allyl-3-*O*-benzyl- α -L-idopyranosid)uronate (1 \rightarrow 4) 2-acetamido-3,6-di-*O*-benzyl-2-deoxy- α -D-glucopyranoside (1 \rightarrow 4) 3-*O*-benzyl-1,2-isopropylidene- β -L-idopyranosid]uronate (3-17). Trisaccharide 3-16 (940 mg, 0.88 mmol) was coevaporated three times with anhydrous toluene. The compound was dissolved in anhydrous pyridine (9 mL) under N₂ and cooled to 0°C. Thiolacetic acid (9 mL) was added and the cooling bath removed. The reaction was stirred 12 h and the solvent was removed under reduced pressure. Flash chromatography on silica (hexanes:ethyl acetate 7:3) eluted the side products. Further elution (hexanes:ethyl acetate 1:1) afforded 3-17 (800 mg, 0.74 mmol, 84%) Rf. 0.31 (hexanes:ethyl acetate 1:2). $[\alpha]_D^{24}$: -1.3, $c = 1.03$. IR (thin film, NaCl plates) 3030, 2931, 1767, 1739, 1682 cm⁻¹. ¹H NMR (500 MHz, CDCl₃) δ 7.16-7.41 (m, 20H), 6.53 (d, $J = 9.7$ Hz, 1H), 5.74 (m, 1H), 5.36 (d, $J = 2.3$ Hz, 1H), 5.30 (d, $J = 3.6$ Hz, 1H), 5.16 (d³, $J = 1.6, 3.3, 17.2$ Hz, 1H), 5.10 (d³, $J = 1.3, 3.3, 10.4$ Hz, 1H), 4.89 (t, $J = 4$ Hz, 1H), 4.66-4.74 (m, 6H), 4.57-4.6 (m, 3H), 4.48 (d, $J = 1.4$ Hz, 1H), 4.38 (d, $J = 11.5$ Hz, 1H), 4.36 (dt, $J = 3.7, 10.5$ Hz, 1H), 4.08 (t, $J = 9.5$ Hz, 2H), 3.93-3.99 (m, 4H), 3.88 (t, $J = 2.2$ Hz, 1H), 3.83 (t, $J = 4.8$ Hz,

1H), 3.76 (m, 1H), 3.68 (m, 1H), 3.67 (s, 3H), 3.60 (d², *J* = 2.3, 11 Hz, 1H), 3.52-3.56 (m, 1H), 3.47 (s, 3H), 3.43 (d², *J* = 9.3, 10.5 Hz), 1.93 (s, 3H), 1.8 (s, 3H), 1.55 (s, 3H), 1.36 (s, 3H). ¹³C NMR (125 MHz, CDCl₃) δ 170.2, 170.15, 169.8, 169.1, 138.9, 138.2, 138.0, 136.6, 134.5, 129.0, 128.7, 128.65, 128.5, 128.3, 128.2, 128.1, 128.0, 127.8, 127.7, 127.6, 127.0, 117.5, 112.3, 98.0, 97.7, 96.6, 79.4, 75.3, 75.25, 75.2, 74.7, 74.0, 73.6, 73.25, 73.2, 72.2, 71.9, 71.5, 71.4, 71.35, 69.6, 69.4, 68.1, 52.7, 52.3, 52.0, 28.6, 26.4, 23.1, 21.2. ESI MS (C₅₈H₆₉NO₁₉) *m/z* (M + Na⁺) calcd 1106.4356, obsd 1106.4328.

***t*-Butyldimethylsilyl methyl [methyl (2-*O*-acetyl-4-*O*-allyl-3-*O*-benzyl- α -L-idopyranosid)uronate (1 \rightarrow 4) 2-acetamido-3,6-di-*O*-benzyl-2-deoxy- α -D-glucopyranoside (1 \rightarrow 4) 3-*O*-benzyl- β -L-idopyranosid]uronate (3-18).** Trisaccharide **3-17** (1.66 g, 1.53 mmol) was dissolved in TFA (90% aq., 30 mL) and stirred 20 min. The solvent was removed under reduced pressure and the residue coevaporated five times with anhydrous toluene. The crude material was dissolved in anhydrous CH₂Cl₂ (4 mL) and cooled to -25°C under N₂. TBDMSCl (347 mg, 2.3 mmol) and imidazole (417 mg, 6.12 mmol) were added and the reaction was stirred for 16 h at -5°C. Methanol (1 mL) was added and the mixture stirred 15 min and poured into ethyl acetate (300 mL). The organic phase was washed with 1N HCl, brine, and saturated NaHCO₃. The organic phase was dried over MgSO₄ and solvent was removed under reduced pressure. Flash chromatography on silica (hexanes:ethyl acetate 1:1) afforded **3-18** (1.65 g, 1.43 mmol, 93%) as a clear oil (15:1 β : α). Characterization data is reported for the β isomer only. Rf. 0.28 (hexanes:ethyl acetate 1:2). IR (thin film, NaCl plates) 3336, 3031, 2858, 1767, 1739, 1674 cm⁻¹. ¹H NMR (500 MHz, CDCl₃) δ 7.19-7.41 (m, 20H), 6.71 (d, *J* = 9.6 Hz, 1H); 5.7-5.78 (m, 1H), 5.26 (d, *J* = 3.5 Hz, 1H), 5.14 (d³, *J* = 17.1, 3.2, 1.6 Hz, 1H), 5.09 (d³, *J* = 10.3, 2.9, 1.2 Hz, 1H), 5.02 (d, *J* = 1.3 Hz, 1H), 4.85 (t, *J* = 4 Hz, 1H), 4.76 (d, *J* = 3.8 Hz, 1H), 4.67-4.73 (m,

4H), 4.62 (d, $J = 11.6$ Hz, 1H), 4.51-4.57 (m, 4H), 4.45 (d, $J = 11.6$ Hz, 1H), 4.27-4.32 (m, 1H), 4.05 (t, $J = 9.5$ Hz, 1H), 3.88-3.93 (m, 3H), 3.80 (t, $J = 4.8$ Hz, 1H), 3.74-3.77 (m, 2H), 3.70 (t, $J = 4.3$ Hz, 1H), 3.67 (s, 3H), 3.53-3.67 (m, 4H), 3.48 (s, 3H), 2.68 (s, 1H), 1.94 (s, 3H), 1.73 (s, 3H), 0.96 (s, 9H), 0.24 (s, 3H), 0.19 (s, 3H). ^{13}C NMR (125 MHz, CDCl_3) δ 170.5, 170.1, 169.8, 168.9, 138.9, 138.2, 138.0, 136.9, 134.4, 128.9, 128.65, 128.6, 128.4, 128.16, 128.15, 128.0, 127.9, 127.85, 127.75, 127.6, 127.1, 117.5, 98.0, 97.7, 93.8, 78.3, 75.3, 75.1, 74.4, 74.0, 73.7, 73.5, 73.4, 73.1, 73.0, 72.1, 71.8, 71.7, 69.5, 69.4, 68.7, 68.2, 52.5, 52.2, 51.9, 25.9, 23.1, 21.1, 18.4, -3.9, -5.2. ESI MS ($\text{C}_{61}\text{H}_{79}\text{NO}_{14}\text{Si}$) m/z ($\text{M} + \text{Na}^+$) calcd 1180.4908, obsd 1180.4883.

***t*-Butyldimethylsilyl methyl [methyl (2-*O*-acetyl-4-*O*-allyl-3-*O*-benzyl- α -L-idopyranosid)uronate (1 \rightarrow 4) 2-*N*-acetylacetamido-3,6-di-*O*-benzyl-2-deoxy- α -D-glucopyranoside (1 \rightarrow 4) 2-*O*-acetyl-3-*O*-benzyl- β -L-idopyranosid]uronate (3-19).**

Trisaccharide **3-18** (1.66 g, 1.42 mmol) was coevaporated three times with anhydrous toluene and dissolved in isopropenyl acetate (15 mL) under N_2 . *p*-Toluenesulfonic acid (700 μL , 0.1 M in DMF) was added and the mixture irradiated in a CEM Discover Series Microwave for 5 h at 30 W, 90°C max. The reaction was poured into ethyl acetate (100 mL) and washed with saturated NaHCO_3 . The organic phase was dried over MgSO_4 and the solvent was removed under reduced pressure. Flash chromatography on silica (hexanes:ethyl acetate 7:3) afforded **3-19** (1.52 g, 1.22 mmol, 86%) as a clear oil. Rf. 0.38 (hexanes:ethyl acetate 1:1). $[\alpha]_{\text{D}}^{24}$: +52.9, $c = 0.91$. IR (thin film, NaCl plates) 2952, 1741, 1675 cm^{-1} . ^1H NMR (500 MHz, CDCl_3) δ 7.12-7.39 (m, 20H), 5.74 (m, 1H), 5.34 (d, $J = 3.4$ Hz, 1H), 5.16 (m, 1H), 5.10 (m, 1H), 5.02 (d, $J = 1.9$ Hz, 1H), 5.01 (d, $J = 3.8$ Hz, 1H), 4.99 (m, 1H), 4.92 (ψ t, 1H), 4.78 (d, $J = 11.5$ Hz, 1H), 4.67-4.75 (m, 4H), 4.52-4.62 (m, 5H), 4.45 (d, $J = 1.8$, 1H), 4.33 (d^2 , $J = 4.0, 11$ Hz, 1H), 3.91-4.03 (m, 6H), 3.85 (ψ t, 1H), 3.75 (s, 3H), 3.67-3.74 (m, 3H), 3.49 (s, 3H), 2.20 (s, 6H), 2.03 (s,

3H), 1.98 (s, 3H), 0.87 (s, 9H), 0.14 (s, 3H), 0.09 (s, 3H). ^{13}C NMR (125 MHz, CDCl_3) δ 175.9, 170.3, 170.0, 169.9, 168.8, 139.2, 138.03, 137.97, 137.2, 134.4, 128.8, 128.7, 128.5, 128.4, 128.24, 128.19, 128.06, 127.95, 127.87, 127.2, 127.1, 117.7, 98.0, 95.7, 93.6, 77.5, 76.3, 75.5, 74.7, 73.7, 73.4, 73.1, 72.9, 72.4, 72.3, 71.9, 70.4, 70.2, 70.0, 67.9, 67.7, 59.8, 52.4, 52.0, 26.8, 25.7, 21.2, 21.0, 18.0, -3.9, -5.4. ESI MS ($\text{C}_{65}\text{H}_{83}\text{NO}_{21}\text{Si}$) m/z ($\text{M} + \text{Na}^+$) calcd 1264.5119, obsd 1264.5082.

Methyl [methyl (2-*O*-acetyl-4-*O*-allyl-3-*O*-benzyl- α -L-idopyranosid)uronate (1 \rightarrow 4) 2-*N*-acetylacetamido-3,6-di-*O*-benzyl-2-deoxy- α -D-glucopyranoside (1 \rightarrow 4) 2-*O*-acetyl-3-*O*-benzyl-L-idopyranosid]uronate trichloroacetimidate (3-20). Trisaccharide **3-19** (325 mg, 0.262 mmol) was coevaporated three times with anhydrous toluene and dissolved in anhydrous THF (2.5 mL). The solution was cooled to 0°C and acetic acid (22.5 μL , 0.39 mmol) was added followed by TBAF (1.0 M in THF, 290 μL). After 80 min, the reaction was poured into saturated NH_4Cl and extracted with ethyl acetate (3x200 mL). The organic phase was dried over MgSO_4 and the solvent was removed under reduced pressure.

The residue was coevaporated three times with anhydrous toluene and dissolved in anhydrous CH_2Cl_2 (2.5 mL) under N_2 . The solution was cooled to 0°C and trichloroacetonitrile (394 μL , 3.93 mmol) and DBU (7.4 μL , 0.052 mmol) added. The reaction was stirred for 60 min then allowed to warm to room temperature. The solvent was evaporated and the residue was purified by flash chromatography on silica (elutant toluene:ethyl acetate 3:1) to afford **3-20** (281 mg, 0.22 mmol, 84%, 4:1 mixture of isomers) as a yellow oil. Rf. 0.27, 0.33 (hexanes:ethyl acetate 1:1). IR (thin film, NaCl plates) 3447, 1739, 1674, 1650 cm^{-1} . ESI MS ($\text{C}_{61}\text{H}_{69}\text{Cl}_3\text{N}_2\text{O}_{21}$) m/z ($\text{M} + \text{Na}^+$) calcd 1293.3351, obsd 1293.3347.

***t*-Butyldimethylsilyl (methyl [methyl (2-*O*-acetyl-4-*O*-allyl-3-*O*-benzyl- α -L-idopyranosid)uronate (1 \rightarrow 4) 2-*N*-acetylacetamido-3,6-di-*O*-benzyl-2-deoxy- α -D-glucopyranoside (1 \rightarrow 4) 2-*O*-acetyl-3-*O*-benzyl- α -L-idopyranosid]uronate (1 \rightarrow 4)) 2-azido-3,6-di-*O*-benzyl-2-deoxy- β -D-glucopyranoside (3-21).** Trichloroacetimidate **3-20** (288 mg, 0.226 mmol) and **7** (565 mg, 1.13 mmol) were combined and coevaporated three times with anhydrous toluene. The mixture was dissolved in CH₂Cl₂ (2.25 mL) under N₂ and cooled to -25°C. TMSOTf (4 μ L, 0.023 mmol) was added and the reaction stirred 1.5 h at reduced temperature. The reaction was quenched with NEt₃ (0.1 mL) and the solvent was removed under reduced pressure. Flash chromatography on silica (hexanes:ethyl acetate 9:1) eluted unreacted **7** (480 mg, 0.96 mmol). Further elution (hexanes:ethyl acetate 7:3) afforded **3-21** (259 mg, 0.16 mmol, 71%) as a clear oil. Rf. 0.37 (hexanes:ethyl acetate 1:1). $[\alpha]_D^{24}$: +6.22, c = 1.05. IR (thin film, NaCl plates) 2952, 2111, 1756, 1741, 1675 cm⁻¹. ¹H NMR (500 MHz, CDCl₃) δ 7.13-7.4 (m, 30H), 5.72-5.79 (m, 1H), 5.36 (d, *J* = 4.8 Hz, 1H), 5.16-5.2 (m, 2H), 5.12 (d², *J* = 1.5, 10.5 Hz, 1H), 5.05 (d, *J* = 3.8 Hz, 1H), 4.88-4.93 (m, 2H), 4.47-4.78 (m, 10H), 4.37 (d², *J* = 3.7, 11.1 Hz, 1H), 3.93-4.06 (m, 5H), 3.86-3.90 (m, 2H), 3.77-3.80 (m, 1H), 3.63-3.74 (m, 5H), 3.50 (s, 3H), 3.47 (s, 3H), 3.32-3.37 (m, 2H), 3.24 (ψ t, 1H), 2.14 (s, 6H), 1.97 (s, 3H), 1.94 (s, 3H), 0.94 (s, 9H), 0.17 (s, 3H), 0.15 (s, 3H). ¹³C NMR (125 MHz, CDCl₃) δ 175.6, 170.0, 169.91, 169.9, 169.2, 138.9, 138.4, 138.3, 138.08, 138.03, 137.6, 134.3, 128.7, 128.6, 128.55, 128.5, 128.3, 128.2, 128.15, 128.08, 128.05, 127.9, 127.85, 127.8, 127.7, 127.67, 127.66, 127.5, 127.2, 127.15, 117.75, 98.13, 98.1, 97.4, 96.7, 81.1, 76.7, 76.3, 75.7, 75.4, 75.0, 74.8, 74.7, 73.7, 73.5, 73.4, 73.2, 72.8, 72.0, 71.8, 71.7, 71.2, 70.7, 70.6, 69.0, 68.9, 68.8, 68.4, 67.7, 58.9, 52.1, 52.0, 26.7, 25.8, 21.1, 21.0, 18.1, -4.0, -5.0. ESI MS (C₈₅H₁₀₄N₄O₂₅Si) *m/z* (M + Na⁺) calcd 1631.6651, obsd 1631.6701.

Methyl [methyl (2-*O*-acetyl-4-*O*-allyl-3-*O*-benzyl- α -L-idopyranosid)uronate (1 \rightarrow 4) 2-*N*-acetylacetamido-3,6-di-*O*-benzyl-2-deoxy- α -D-glucopyranoside (1 \rightarrow 4) 2-*O*-acetyl-3-*O*-benzyl- α -L-idopyranosid]uronate (1 \rightarrow 4)) 2-azido-3,6-di-*O*-benzyl-2-deoxy-D-glucopyranoside trichloroacetimidate (3-4). Tetrasaccharide **3-21** (251 mg, 0.156 mmol) was coevaporated three times with anhydrous toluene and dissolved in anhydrous THF (1.5 mL). The solution was cooled to 0°C and acetic acid (10.2 μ L, 0.18 mmol) was added followed by TBAF (1.0 M in THF, 172 μ L). After 30 min, the reaction was poured into saturated NH₄Cl and extracted three times with ethyl acetate. The organic phase was dried over MgSO₄ and the solvent was removed under reduced pressure.

The residue was coevaporated three times with anhydrous toluene and dissolved in anhydrous CH₂Cl₂ (1.5 mL) under N₂. The solution was cooled to 0°C and trichloroacetonitrile (226 μ L, 2.25 mmol) and DBU (4.3 μ L, 0.03 mmol) were added. The reaction was stirred for 45 min, then allowed to warm to room temperature. The solvent was evaporated and the residue was purified by flash chromatography on silica (elutant toluene:ethyl acetate 7:3) to afford **3-4** (228 mg, 0.139 mmol, 89%, 6:1 mixture of isomers) as a yellow oil. Rf. 0.3, 0.375 (hexanes:ethyl acetate 3:2). IR (thin film, NaCl plates) 2926, 2112, 1739, 1675 cm⁻¹. ESI MS (C₈₁H₉₀Cl₃N₅O₂₅) *m/z* (M + Na⁺) calcd 1660.4883, obsd 1660.4913.

Methyl 2-benzyloxycarbonylamino-2-deoxy-3,6-di-*O*-acetyl- α -D-glucopyranoside (3-10).

Compound **3-22(70)** was coevaporated twice with anhydrous toluene and dissolved in 2,4,6-collidine (7 mL, distilled from CaH). The mixture was cooled to -40°C and acetyl chloride (270 μ L, 3.78 mmol) was added. The reaction was stirred overnight under N₂ at -40°C. Water (1 mL) was added and the reaction warmed to room temperature and poured into ethyl acetate (600 mL). The organic phase was washed with 1N HCl, brine, saturated NaHCO₃ and dried over MgSO₄

and the solvent was removed under reduced pressure. Flash chromatography on silica (hexanes:ethyl acetate 7:3) afforded **3-10** (1.17 g, 82%) as a glassy solid. Rf. 0.19 (hexanes:ethyl acetate 1:1). $[\alpha]_D^{24}$: +55.2, $c = 1.26$. Mp = 98.0-99.5°C. IR (thin film, NaCl plates) 3434, 2956, 1739, 1710, 1520 cm^{-1} . ^1H NMR (500 MHz, CDCl_3) δ 7.30-7.36 (m, 5H, CBz aromatic), 5.17 (d, $^3J_{\text{H2-NH}} = 10$ Hz, 1H, carbamate NH), 5.13 (d, $^2J = 12.3$ Hz, 1H Cbz CH_2), 5.06 (d², $^3J_{\text{H3-H4}} = 9.4$ Hz, $^3J_{\text{H2-H3}} = 10.5$ Hz, 1H, H3), 5.02 (d, $^2J = 12.3$ Hz, 1H, Cbz CH_2), 4.71 (d, $^3J_{\text{H1-H2}} = 3.6$ Hz, 1H, H1), 4.44 (d², $^3J_{\text{H5-H6}} = 4.4$ Hz, $^2J_{\text{H6-H6}'} = 12.2$ Hz, 1H, H6), 4.29 (d², $^3J_{\text{H5-H6}'} = 2.2$ Hz, $^2J_{\text{H6-H6}'} = 12.2$ Hz, 1H, H6'), 3.95 (d ψ t, $^3J_{\text{H1-H2}} = 3.6$ Hz, $J = 10.3$ Hz, 1H, H2), 3.77 (d³, $^3J_{\text{H5-H6}'} = 2.2$ Hz, $^3J_{\text{H5-H6}} = 4.4$ Hz, $^3J_{\text{H4-H5}} = 10$ Hz, 1H, H5), 3.57 (ψ t, $J = 9.4$ Hz, 1H, H4), 3.38 (s, 3H, OCH_3), 3.17 (s (b), 1H, OH), 2.11 (s, 3H, 3-*O*-acetate CH_3), 1.94 (s, 6H, 3-*O*-acetate CH_3). ^{13}C -NMR (125 MHz, CDCl_3) δ 172.2 (6-*O*-acetate carbonyl), 171.6 (3-*O*-acetate carbonyl), 156.1 (CBz carbonyl), 136.4 (CBz phenyl quaternary), 128.7 (aromatic C), 128.3 (aromatic C), 128.2 (aromatic C), 98.8 (C1), 74.1 (C3), 70.0 (C5), 68.8 (C4), 67.0 (CBz CH_2), 63.1 (C6), 55.4 (OCH_3), 53.7 (C2), 21.0 (3-*O*-acetate CH_3), 20.9 (6-*O*-acetate CH_3). ESI MS ($\text{C}_{19}\text{H}_{25}\text{NO}_9$) m/z ($\text{M} + \text{Na}^+$) calcd 434.1422, obsd 434.1420.

Methyl methyl 2-*O*-acetyl-4-*O*-allyl-3-*O*-benzyl- α -L-idopyranosiduronate (1 \rightarrow 4) 3,6-di-*O*-acetyl-2-benzyloxycarbonylamino-2-deoxy- α -D-glucopyranoside (3-23). Glycosyl trichloroacetimidate **3-9** (243 mg, 0.46 mmol) and monosaccharide **3-10** (136 mg, 0.33 mmol) were combined and coevaporated three times with anhydrous toluene. The mixture was dissolved in anhydrous CH_2Cl_2 (5 mL) under N_2 and cooled to -15°C . TMSOTf (8 μL , 46 μmol) was added and the mixture was stirred for 3 h at low temperature. The cooling bath was removed and the reaction was stirred for an additional three hours at room temperature, followed by quenching with NEt_3 (0.5 mL). The solvent was removed under reduced pressure. Flash

chromatography on silica (hexanes:ethyl acetate 7:3) afforded **3-23** (143 mg, 0.195 mmol, 59%). Rf. 0.26 (hexanes:ethyl acetate 1:1). $[\alpha]_D^{24}$: +5.75, $c = 1.4$. IR (thin film, NaCl plates) 1739, 1516 cm^{-1} . ^1H NMR (500 MHz, CDCl_3) δ 7.27-7.37 (m, 10H), 5.69-5.76 (m, 1H), 5.19 (d^2 , $J = 9$ Hz, 10.6 Hz, 1H), 5.10-5.15 (m, 3H), 4.99-5.04 (m, 3H), 4.75-4.77 (m, 2H), 4.72 (d, $J = 12.2$ Hz, 1H), 4.70 (d, $J = 3.6$ Hz, 1H), 4.62 (d $J = 12.2$ Hz, 1H), 4.28 (d, $J = 2.8$ Hz, 2H), 3.79-3.99 (m, 5H), 3.78 (s, 3H), 3.74 (m, 2H), 3.36 (s, 3H), 2.13 (s, 3H), 2.06 (s, 3H), 1.92 (s, 3H). ^{13}C NMR (125 MHz, CDCl_3) δ 171.5, 171.1, 170.3, 169.8, 156.1, 137.8, 136.5, 134.2, 128.7, 128.6, 128.4, 128.3, 128.0, 127.8, 118.0, 99.6, 98.7, 76.2, 74.5, 72.7, 72.5, 72.1, 71.8, 69.8, 68.8, 68.7, 67.1, 62.4, 55.5, 54.2, 52.3, 21.3, 21.1, 21.0. ESI MS ($\text{C}_{38}\text{H}_{47}\text{NO}_{16}$) m/z ($\text{M} + \text{Na}^+$) calcd 796.2793, obsd 796.2750.

Methyl (methyl 2-*O*-acetyl-3-*O*-benzyl- α -L-idopyranosiduronate) (1 \rightarrow 4) 3,6-di-*O*-acetyl-2-benzyloxycarbonylamino-2-deoxy- α -D-glucopyranoside (3-5). Disaccharide **3-23** (140 mg, 0.19 mmol) and sodium acetate (600 mg) were combined and dissolved in acetic acid (2.6 mL) and water (150 μL). PdCl_2 (202 mg, 1.14 mmol) was added and the reaction was stirred for 9 h. Palladium black precipitated from solution over the course of the reaction. The reaction mixture was poured into saturated NaHCO_3 (200 mL) and the aqueous layer was extracted with ethyl acetate (3 x 200 mL). The combined organic phases were dried over MgSO_4 and the solvent was removed under reduced pressure. Flash chromatography on silica (1:1 hexanes:ethyl acetate) afforded **5** (113 mg, 0.16 mmol, 86%) as a clear oil. Rf. 0.38 (hexanes:ethyl acetate 1:3). $[\alpha]_D^{24}$: +17.5, $c = 0.99$. IR (thin film, NaCl plates) 3447, 2955, 1743, 1521 cm^{-1} . ^1H NMR (500 MHz, CDCl_3) δ 7.29-7.38 (m, 10H, aromatic H), 5.21 (d^2 , $^3J = 9.0$, 10.6 Hz, 1H, GlcN H3), 5.13 (d, $^2J = 12.2$ Hz, 1H, CBz CH_2), 5.03 (d, $^2J = 12.2$ Hz, 1H, CBz CH_2), 4.98 (d, $^3J_{\text{H}_2-\text{NH}} = 10$ Hz, 1H, CBz NH), 4.94 (s, 1H, IdoA H1), 4.83 (d, $^3J_{\text{H}_5-\text{H}_4} = 1.9$ Hz, 1H, IdoA H5), 4.81, (s, 1H, IdoA

H2), 4.71 (d, $^2J = 12.6$, 1H 3-*O*-benzyl CH₂), 4.70 (d, $^3J_{H1-H2} = 3.9$ Hz, 1H, GlcN H1), 4.62 (d, $^2J = 12.2$, 1H 3-*O*-benzyl CH₂), 4.31 (d², $^2J_{H6-H6'} = 12.3$ Hz, $^3J_{H6-H5} = 3.3$ Hz, 1H, GlcN H6), 4.25 (d², $^2J_{H6-H6'} = 12.3$ Hz, $^3J_{H6'-H5} = 1.8$ Hz, 1H, GlcN H6'), 3.96 (m, 1H, IdoA H4), 3.92 (m, 1H, GlcN H2), 3.80 (s, 3H, methyl ester CH₃), 3.82 (m, 1H, GlcN H4), 3.75 (m, 1H, GlcN H5), 3.68 (ψt, 1H), 3.36 (s, 3H, methyl glycoside CH₃), 2.65 (d, $^3J_{H4-OH} = 11.7$ Hz), 2.13 (s, 3H, 3-*O*-acetate CH₃), 2.10 (s, 3H, 2-*O*-acetate CH₃), 1.93 (s, 3H, 3-*O*-acetate CH₃), . ¹³C NMR (125 MHz, CDCl₃) δ 171.5 (3-*O*-acetate carbonyl), 171.1 (6-*O*-acetate carbonyl), 169.6 (IdoA C6), 169.3 (2-*O*-acetate carbonyl), 156.0 (CBz carbonyl), 137.5 (benzyl quat), 136.5 (CBz quat), 128.7 (aromatic C), 128.6 (aromatic C), 128.4 (aromatic C), 128.3 (aromatic C), 128.1 (aromatic C), 127.6 (aromatic C), 99.8 (IdoA C1), 98.7 (GlcN C1), 77.0 (GlcN C4), 74.0 (IdoA C3), 72.3 (GlcN C3), 71.9 (benzyl CH₂), 68.8 (IdoA C5), 68.7 (GlcN C5), 68.0 (IdoA C4), 67.3 (IdoA C2), 67.1 (CBz CH₂), 62.3 (GlcN C6), 55.6 (methyl glycoside CH₃), 54.2 (GlcN C2), 52.5 (methyl ester CH₃), 21.2 (2-*O*-acetate CH₃), 21.05 (6-*O*-acetate CH₃), 20.9 (3-*O*-acetate CH₃). ESI MS (C₃₅H₄₃NO₁₆) *m/z* (M + Na⁺) calcd 756.2474, obsd 756.2443.

Methyl (*t*-butyldimethylsilyl 4-*O*-allyl-3-*O*-benzyl-*L*-idopyranosid)uronate (3-26).

Monosaccharide 3-25(30) (200 mg, 0.529 mmol) was dissolved in TFA (90% aq., 5 mL) and stirred for 30 min. The solvent was removed under reduced pressure and the residue coevaporated five times with toluene. The crude material was dissolved in CH₂Cl₂ (500 μL) and cooled to -25°C under N₂. TBDMS-Cl (120 mg, 0.794 mmol) and imidazole (144 mg, 2.12 mmol) were added and the reaction was stirred for 16 h at -25°C. Methanol (1 mL) was added and the mixture was stirred 30 min, then diluted into ethyl acetate. The organic phase was washed with 1N HCl, brine, and saturated aq. NaHCO₃. The organic phase was dried over MgSO₄ and the solvent was removed under reduced pressure. Flash silica gel column

chromatography (hexanes:ethyl acetate 85:15) afforded **3-26** (170 mg, 0.376 mmol, 71%) as a clear oil (6:1 mixture of isomers). Rf. 0.37 (hexanes:ethyl acetate 3:1). IR (thin film, NaCl plate) 3519, 2929, 2858, 1770, 1739 cm^{-1} . ^1H NMR (500 MHz, CDCl_3) Major isomer: δ 7.31-7.40 (m, 5H), 5.72-5.80 (m, 1H), 5.14-5.18 (m, 2H), 5.03 (d, $J = 0.8$ Hz, 1H), 4.64 (d, $J = 12$ Hz, 1H), 4.60 (d, $J = 12$ Hz, 1H), 4.52 (d, $J = 1.7$ Hz, 1H), 4.04 (d^2 , $J = 5.9, 12.6$ Hz, 1H), 3.89-3.93 (m, 2H), 3.78 (s, 3H), 3.76 (s, 1H), 3.63-3.65 (m, 1H), 3.04 (d, $J = 10.1$ Hz, 1H), 0.93 (s, 9H), 0.19 (s, 3H), 0.16 (s, 3H). Minor isomer: δ 5.32 (s, 1H), 4.92 (d, $J = 1.8$ Hz, 1H), 3.81 (s, 3H), 3.40 (d, $J = 10$ Hz, 1H), 0.87 (s, 9H), 0.14 (s, 3H), 0.12 (s, 3H). ^{13}C NMR (125 MHz, CDCl_3) Major isomer: δ 169.4, 137.5, 133.9, 128.8, 128.3, 127.9, 116.6, 94.7, 74.3, 74.0, 73.7, 72.5, 72.0, 68.8, 52.3, 26.0, 18.4, -3.9, -4.8. Minor isomer: δ 170.5, 138.0, 133.6, 128.7, 128.3, 127.6, 118.5, 96.4, 74.4, 72.8, 72.1, 71.7, 67.4, 67.3, 52.4, 25.7, 18.0. ESI MS ($\text{C}_{23}\text{H}_{36}\text{O}_7\text{Si}$) m/z ($\text{M} + \text{Na}^+$) calcd 475.2123, obsd 475.2143.

Methyl (*t*-butyldimethylsilyl 4-*O*-allyl-2-*O*-benzoyl-3-*O*-benzyl-L-idopyranosid)uronate (3-27). Compound **3-26** (488 mg, 1.08 mmol) was coevaporated three times with toluene and dissolved in CH_2Cl_2 (10 mL). DMAP (13.5 mg, 0.11 mmol) and benzoyl chloride (250 μL , 2.16 mmol) were added and the reaction was stirred overnight under N_2 with exclusion of light. The reaction mixture was poured into ethyl acetate (200 mL) and washed with 1N HCl, brine, and saturated aq. NaHCO_3 . The organic phase was dried over MgSO_4 , filtered, and the solvent was removed under reduced pressure. Flash silica gel column chromatography (hexanes:ethyl acetate 9:1) afforded **3-27** (464 mg, 0.833 mmol, 77%, 3:1 mixture of isomers) as a clear oil. Rf. 0.33 (hexanes:ethyl acetate 85:15). IR (thin film, NaCl plate) 2929, 2857, 1772, 1723 cm^{-1} . ^1H NMR (500 MHz, CDCl_3) δ 8.11 (d, $J = 7.9$ Hz, 1.5H), 8.06 (s, $J = 8.1$ Hz, 0.5H), 7.53-7.58 (m, 1H), 7.30-7.43 (m, 7H), 5.64-5.80 (m, 1H), 5.48 (s, 0.25H), 5.01-5.23 (m, 4H), 4.93 (d, $J = 2.9$ Hz,

0.25H), 4.80-4.82 (m, 1H), 4.67-4.71 (m, 1H), 4.58 (s, 0.75H), 4.04 (m, 1H), 3.89-3.95 (m, 2H), 3.75-3.80 (m, 4.5 H), 0.87 (s, 2.25H), 0.82 (s, 6.75H), 0.13 (s, 3H), 0.10 (s, 3H). ^{13}C NMR (125 MHz, CDCl_3) Major isomer: δ 169.4, 166.5, 137.5, 134.5, 133.1, 130.3, 128.7, 128.45, 128.4, 128.3, 128.1, 117.6, 93.4, 74.3, 73.6, 73.0, 72.9, 71.6, 68.2, 52.3, 25.8, 18.1, -3.7, -5.0. Minor isomer: δ 170.6, 165.9, 138.0, 134.4, 133.4, 130.4, 130.2, 129.9, 128.5, 128.35, 127.9, 117.4, 93.5, 75.1, 73.2, 72.6, 71.7, 70.0, 69.1, 52.35, 25.7, 18.04, -4.4, -5.4 ESI MS ($\text{C}_{30}\text{H}_{40}\text{O}_8\text{Si}$) m/z ($\text{M} + \text{Na}^+$) calcd 579.2385, obsd 579.2369.

Methyl 4-*O*-allyl-2-*O*-benzoyl-3-*O*-benzyl-L-idopyranosiduronate trichloroacetimidate (3-28). Monosaccharide **27** (303 mg, 0.544 mmol) was coevaporated three times with toluene and dissolved in THF (5 mL). The solution was cooled to 0°C and acetic acid (37.5 μL , 0.653 mmol) was added followed by TBAF (1.0 M in THF, 600 μL). After 30 min, the reaction was poured into ethyl acetate (100 mL) and washed twice with brine. The organic phase was dried over MgSO_4 , filtered, and the solvent was removed under reduced pressure.

The residue was coevaporated three times with toluene and dissolved in CH_2Cl_2 (4 mL) under N_2 . The solution was cooled to 0°C and trichloroacetonitrile (820 μL , 8.16 mmol) and DBU (15 μL , 0.1 mmol) were added. The reaction was stirred for 30 min then allowed to warm to room temperature, and stirred an additional 1.5 h. The solvent was evaporated and the residue was purified by flash silica gel column chromatography (silica quenched with 1% NEt_3 in toluene, eluted with toluene:ethyl acetate 19:1) afforded **3-28** (210 mg, 0.36 mmol, 66%, 3:1 mixture of isomers) as a yellow oil. Rf. 0.3 (hexanes:ethyl acetate 85:15). IR (thin film, NaCl plate) 1723, 1621 cm^{-1} . ESI MS ($\text{C}_{26}\text{H}_{26}\text{Cl}_3\text{NO}_8$) m/z ($\text{M} + \text{Na}^+$) calcd 608.0616, obsd 608.0717.

Methyl methyl 2-*O*-benzoyl-3-*O*-benzyl- α -L-idopyranosiduronate (1 \rightarrow 4) 3,6-di-*O*-acetyl-2-benzyloxycarbonylamino-2-deoxy- α -D-glucopyranoside (3-30). Trichloroacetimidate **3-28** (210 mg, 0.358 mmol) and monosaccharide **3-10** (98 mg, 0.238 mmol) were combined and coevaporated three times with anhydrous toluene. The sugars were dissolved in anhydrous CH₂Cl₂ (2.5 mL) under N₂ and cooled to -15°C. TMSOTf (6.5 μ L, 36 μ mol) was added and the mixture stirred for 1 h, then allowed to warm to room temperature and stirred and additional 30 min. The reaction was quenched by addition of NEt₃ (0.5 mL) and the solvent was removed under reduced pressure. Flash chromatography on silica (hexanes:ethyl acetate 65:35) afforded **3-29** (185 mg, 0.22 mmol, 93%).

Disaccharide **3-29** (34 mg, 40.7 μ mol) and sodium acetate (40 mg) were combined and dissolved in acetic acid (455 μ L) and water (25 μ L). PdCl₂ (42 mg, 0.24 mmol) was added and the reaction was stirred for 8 h. Palladium black precipitated from the solution over the course of the reaction. The reaction mixture was poured into saturated NaHCO₃ (50 mL) and the aqueous layer was extracted with ethyl acetate (3 x 50 mL). The combined organic phases were dried over MgSO₄ and the solvent was removed under reduced pressure. Flash chromatography on silica (4:1 toluene:ethyl acetate) afforded **3-30** (27 mg, 33.9 μ mol, 83%) as a clear oil. Rf. 0.19 (hexanes:ethyl acetate 1:1). $[\alpha]_D^{24}$: +26.0, c = 0.75. IR (thin film, NaCl plates) 3421, 1740 cm⁻¹. ¹H NMR (500 MHz, CDCl₃) δ 7.97 (d, *J* = 7.4 Hz, 2H), 7.61 (t, *J* = 7.5 Hz, 1H), 7.45 (t, *J* = 8.0 Hz, 1H), 7.27-7.38 (m, 10H), 5.24 (d², *J* = 9.3, 10.4 Hz, 1H), 5.13 (ψ t, 2H), 4.99-5.04 (m, 3H), 4.90 (d, *J* = 1.6 Hz, 1H), 4.77 (d, *J* = 12.1 Hz, 1H), 4.70 (d, *J* = 3.5 Hz, 1H), 4.66 (d, *J* = 12.1 Hz, 1H), 4.38 (d², *J* = 3.3, 12.3 Hz, 1H), 4.31 (d, *J* = 10.0 Hz, 1H), 4.04 (d, *J* = 11.4 Hz, 1H), 3.79-3.87 (m, 4H), 3.81 (s, 3H), 3.37 (s, 3H), 2.70 (d, *J* = 11.6 Hz, 1H), 2.13 (s, 3H), 1.92 (s, 3H). ¹³C NMR (125 MHz, CDCl₃) δ 171.5, 171.0, 169.6, 165.1, 156.0, 137.6, 136.4, 134.0,

129.9, 128.9, 128.8, 128.75, 128.7, 128.6, 128.3, 128.2, 128.0, 127.6, 99.8, 98.6, 77.5, 77.0, 74.4, 72.3, 72.1, 68.8, 68.6, 68.1, 68.0, 67.5, 62.3, 55.5, 54.2, 52.4, 21.0, 20.8. ESI MS ($C_{40}H_{45}NO_8$) m/z ($M + Na^+$) calcd 818.2636, obsd 818.2561.

Methyl [methyl (methyl [methyl (2-*O*-acetyl-4-*O*-allyl-3-*O*-benzyl- α -L-idopyranosid)uronate (1 \rightarrow 4) 2-*N*-acetylacetamido-3,6-di-*O*-benzyl-2-deoxy- α -D-glucopyranoside (1 \rightarrow 4) 2-*O*-acetyl-3-*O*-benzyl- α -L-idopyranosid]uronate (1 \rightarrow 4)) 2-azido-3,6-di-*O*-benzyl-2-deoxy-D-glucopyranoside (1 \rightarrow 4) 2-*O*-acetyl-3-*O*-benzyl- α -L-idopyranosid]uronate] (1 \rightarrow 4) 3,6-di-*O*-acetyl-2-benzyloxycarbonylamino-2-deoxy- α -D-glucopyranoside (3-32) In a typical trial, tetrasaccharide **4** (145 mg, 88 μ mol) and disaccharide **3-5** (71 mg, 97 μ mol) were combined and coevaporated three times with anhydrous toluene. The sugars were dissolved in anhydrous CH_2Cl_2 (1 mL) under N_2 and cooled to $-40^\circ C$ and 4 \AA molecular sieves (300 mg) were added and the reaction was stirred for 30 min. TMSOTf (1.6 μ L, 9 μ mol) was added and the mixture was stirred for 1 h. The reaction was quenched by addition of NEt_3 (0.1 mL) and the solvent was removed under reduced pressure. Flash chromatography on silica (hexanes:ethyl acetate 60:40) eluted first a low polarity fraction (61 mg), which contained primarily **3-33** as a 1:1 α : β mixture, followed by a fraction containing **3-32**. Further elution (hexanes:ethyl acetate 40:60) afforded recovered **3-5** (37 mg). The product-containing fraction was further purified by size exclusion chromatography on Biorad Biobeads, 1x crosslinking (40cm x 2.5 cm, toluene elutant) to yield **3-32** (104 mg, 47 μ mol, 53%) as a 6:1 α : β mixture. 1H NMR (500 MHz, $CDCl_3$) major isomer characteristic peaks: δ 5.72-5.79 (m, 1H, allyl $CH=CH_2$), 3.62 (s, 3H, methyl ester), 3.50 (s, 3H, methyl ester), 3.49 (s, 3H, methyl ester), 3.36 (s, 3H, methyl glycoside), 2.13 (s, 3H, acetate), 2.12 (s, 6H, NAc_2), 2.07 (s, 3H, acetate),

1.94 (s, 3H, acetate), 1.92 (s, 3H, acetate), 1.87 (s, 3H, acetate). ESI MS ($C_{114}H_{131}N_5O_{40}$) m/z ($M + Na^+$) calcd 2232.8263, obsd 2232.8263.

***t*-Butyldimethylsilyl 4-*O*-allyl-2-azido-3,6-di-*O*-benzyl-2-deoxy- β -D-glucopyranoside (3-34)**

Compound 3-7(32) (140 mg, 0.28 mmol) was coevaporated three times with anhydrous toluene and dissolved in CH_2Cl_2 (1.5 mL). Freshly activated 4Å molecular sieves (300 mg) and allyl bromide (114 μ L, 1.4 mmol) were added and the reaction stirred 30 min. Silver (I) oxide (227 mg, 0.98 mmol) was added, light was excluded and the reaction was stirred for 40 h. The reaction was filtered through celite, concentrated, and purified via flash column chromatography on silica (elutant 50:1 hexanes:ethyl acetate) to yield 3-34 (114 mg, 0.21 mmol, 75%) as a clear oil. Rf. 0.38 (hexanes:ethyl acetate 10:1). $[\alpha]_D^{24}$: -3.57, $c = 1.15$. IR (thin film, NaCl plates) 2929, 2858, 2110 cm^{-1} . 1H NMR (500 MHz, $CDCl_3$) δ 7.28-7.42 (m, 10H), 5.82-5.90 (m, 1H), 5.21(d^3 , $J = 1.6, 3.3, 17.2$ Hz, 1H), 5.14 ($d_{\psi t}$, $J = 10.4, 1.7$ Hz, 1H), 4.86 (d, $J = 10.9$ Hz, 1H), 4.79 (d, $J = 10.9$ Hz, 1H), 4.64 (d, $J = 12$ Hz, 1H), 4.58 (d, $J = 12$ Hz, 1H), 4.51-4.52 (m, 1H), 4.27-2.31 (m, 1H), 4.07-4.11 (m, 1H), 3.70 (m, 2H), 3.49-3.52 (m, 1H), 3.38-3.41 (m, 1H), 3.31-3.36 (m, 2H), 0.97 (s, 9H), 0.20 (s, 3H), 0.18 (s, 3H). ^{13}C NMR (125 MHz, $CDCl_3$) δ 138.4, 138.3, 134.8, 128.6, 128.5, 128.3, 128.0, 127.8, 127.79, 117.2, 97.4, 83.0, 77.8, 75.6, 75.3, 74.0, 73.7, 69.0, 68.8, 25.8, 18.2, -4.0, -5.0. ESI MS ($C_{29}H_{41}Cl_3N_3O_5Si$) m/z ($M + Na^+$) calcd 562.2708, obsd 562.2681.

4-*O*-Allyl-2-azido-3,6-di-*O*-benzyl-2-deoxy-D-glucopyranoside trichloroacetimidate (3-35)

Monosaccharide 3-34 (155 mg, 0.287 mmol) was coevaporated three times with toluene and dissolved in THF (2.5 mL). The solution was cooled to 0°C and acetic acid (18 μ L, 0.313 mmol) was added followed by TBAF (1.0 M in THF, 299 μ L). After 30 min, the reaction was poured

into saturated NH_4Cl and extracted four times with CH_2Cl_2 . The organic phases were combined and dried over MgSO_4 , filtered, and the solvent was removed under reduced pressure.

The residue was coevaporated three times with toluene and dissolved in CH_2Cl_2 (2.5 mL) under N_2 . The solution was cooled to 0°C and trichloroacetonitrile (409 μL , 4.08 mmol) and DBU (7.5 μL , 0.054 mmol) were added. The reaction was stirred for 30 min, allowed to warm to room temperature, and stirred for an additional 30 min. The solvent was evaporated and the residue was purified by flash silica gel column chromatography (hexanes:ethyl acetate 9:1) afforded **3-35** (133 mg, 0.23 mmol, 81%, ~3:2 α : β mixture) as a yellow oil. Rf. 0.2, 0.3 (hexanes:ethyl acetate 85:15). IR (thin film, NaCl plates) 3340, 2868, 2112, 1675 cm^{-1} . ^1H NMR (500 MHz, CDCl_3) δ 8.75 (s, 0.4H), 8.72 (s, 0.6H), 7.27-7.43 (m, 10H), 6.42 (d, $J = 3.4$ Hz, 0.6H), 5.83-5.86 (m, 1H), 5.62 (d, $J = 8.4$ Hz, 0.4H), 5.14-5.23 (m, 2H), 4.87-4.94 (m, 2H), 4.64 (d, $J = 11.4$ Hz, 1H), 4.50-4.57 (m, 1H), 4.27-4.30 (m, 1H), 3.95-4.09 (m, 2.4H), 3.50-3.79 (m, 5.6H). ^{13}C NMR (125 MHz, CDCl_3) δ 161.3, 160.9, 138.1, 137.95, 137.8, 134.5, 134.4, 128.7, 128.65, 128.6, 128.5, 128.4, 128.3, 128.2, 128.13, 128.1, 128.05, 128.0, 127.9, 117.6, 117.4, 96.9, 95.1, 91.1, 89.5, 83.0, 80.0, 77.6, 77.0, 76.3, 75.8, 75.7, 74.2, 74.0, 73.75, 73.7, 73.6, 68.0, 67.5, 65.8, 63.0. ESI MS ($\text{C}_{25}\text{H}_{27}\text{Cl}_3\text{N}_4\text{O}_5$) m/z ($\text{M} + \text{Na}^+$) calcd 591.0945, obsd 591.0939.

Methyl [methyl (4-*O*-allyl-2-azido-3,6-di-*O*-benzyl-2-deoxy-*D*-glucopyranoside 2-*O*-acetyl-3-*O*-benzyl- α -*L*-idopyranosid)uronate] (1 \rightarrow 4) 3,6-di-*O*-acetyl-2-benzyloxycarbonylamino-2-deoxy- α -*D*-glucopyranoside (3-36) Trichloroacetimidate **3-35** (30 mg, 52 μmol) and disaccharide **3-5** (19 mg, 26 μmol) were combined and coevaporated three times with anhydrous toluene. The sugars were dissolved in anhydrous CH_2Cl_2 (1 mL) under N_2 and cooled to -40°C and 4 \AA molecular sieves (90 mg) were added and the reaction was stirred for 30 min. TMSOTf (1 μL) was added and the mixture was stirred for 2 h. The reaction was quenched by addition of

NEt₃ (0.1 mL) and the solvent was removed under reduced pressure. Flash chromatography on silica (hexanes:ethyl acetate 90:10) eluted **3-38** (22.6 mg, 39 μmol) as a 1:1 α:β mixture. Further elution (hexanes:ethyl acetate 70:30) afforded **3-36** (9 mg) as a ~20:1 α:β mixture.

Characterization data is reported for major isomer only. IR (thin film, NaCl plates) cm⁻¹ 2936, 2108, 1741.5, 15.14. ¹H NMR (500 MHz, CDCl₃) δ 7.31-7.42 (m, 20H), 5.73-5.82 (m, 1H), 4.99-5.24 (m, 8H), 4.93 (d, *J* = 2.3 Hz, 1H), 4.62-4.86 (m, 10H), 4.51 (d, *J* = 12.1 Hz, 1H), 4.20-4.33 (m, 4H), 3.56-4.05 (m, 15H), 3.71 (s, 3H), 3.34 (s, 3H), 3.24 (m, 2H), 2.12 (s, 3H), 2.08 (s, 3H), 1.90 (s, 3H). ¹³C NMR (125 MHz, CDCl₃) δ 171.5, 171.0, 170.2, 169.5, 150.1, 137.94, 137.93, 137.6, 136.5, 134.8, 128.7, 128.68, 128.64, 128.6, 128.5, 128.4, 128.3, 128.14, 128.11, 128.05, 128.0, 127.8, 127.7, 116.5, 99.5, 98.8, 97.3, 79.9, 77.8, 76.4, 75.5, 73.7, 73.69, 73.0, 72.4, 72.2, 72.1, 71.6, 69.0, 68.7, 68.2, 67.9, 67.1, 63.3, 62.3, 55.6, 54.3, 52.3, 21.1, 21.0, 20.9. ESI MS (C₆₁H₆₉Cl₃N₂O₂₁) *m/z* (M + Na⁺) calcd 1163.4325, obsd 1163.4331.

Methyl [methyl (4-*O*-allyl-2-azido-3,6-di-*O*-benzyl-2-deoxy-D-glucopyranoside 2-*O*-benzoyl-3-*O*-benzyl-α-L-idopyranosid)uronate] (1→4) 3,6-di-*O*-acetyl-2-benzyloxycarbonylamino-2-deoxy-α-D-glucopyranoside (3-37) Trichloroacetimidate **3-35** (13 mg, 23 μmol) and disaccharide **3-30** (9 mg, 11 μmol) were combined and coevaporated three times with anhydrous toluene. The sugars were dissolved in anhydrous CH₂Cl₂ (500 μL) under N₂ and cooled to -40°C and 4Å molecular sieves (40 mg) were added and the reaction was stirred for 30 min. TMSOTf (1 μL) was added and the mixture was stirred for 2 h. The reaction was quenched by addition of NEt₃ (0.1 mL) and the solvent was removed under reduced pressure. Flash chromatography on silica (hexanes:ethyl acetate 90:10) eluted **3-38** (8 mg) as a 1:1 α:β mixture. Further elution (hexanes:ethyl acetate 70:30) afforded **3-37** (9 mg, 68%). Characterization data is reported for major isomer only. IR (thin film, NaCl plates) 3032, 2928, 2110, 1767, 1742, 1723 cm⁻¹. ¹H

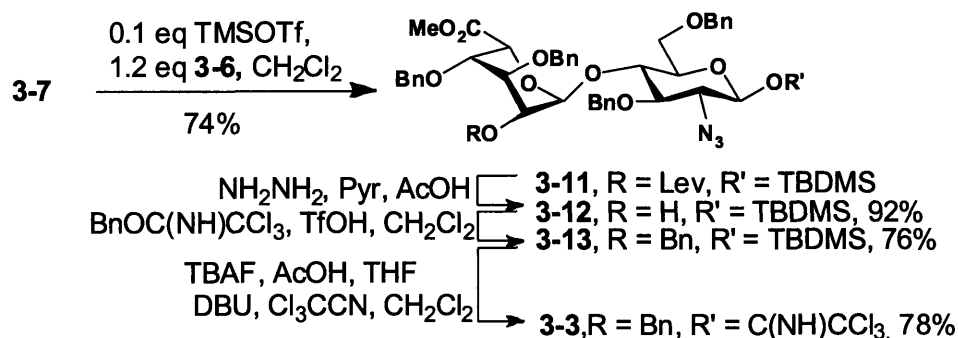
NMR (500 MHz, CDCl₃) Characteristic peaks δ 8.13 (d, J = 8.1 Hz, 2H, benzoate), 7.52 (ψ t, 1H, benzoate), 7.45 (ψ t, 2H, benzoate), 5.77-5.85 (m, 1H, allyl CH=CH₂), 3.75 (s, 3H, methyl ester), 3.35 (s, 3H, methyl glycoside), 2.06 (s, 3H, acetate), 1.90 (s, 3H, acetate). ¹³C NMR (125 MHz, CDCl₃) δ 171.4, 170.8, 169.5, 165.7, 156.1, 138.2, 137.9, 137.7, 136.5, 134.9, 133.6, 133.5, 130.2, 129.9, 129.6, 128.9, 128.7, 128.6, 128.5, 128.41, 128.28, 128.23, 128.13, 128.0, 127.92, 127.84, 127.6, 116.6, 99.9, 99.1, 98.6, 80.2, 77.5, 76.6, 75.2, 74.7, 73.8, 73.7, 72.9, 72.1, 69.4, 69.3, 68.8, 68.0, 67.1 63.6, 63.4, 55.6, 54.3, 52.3, 21.0, 20.9. ESI MS (C₆₁H₆₉Cl₃N₂O₂₁) m/z (M + Na⁺) calcd 1225.4481, obsd 1225.4477.

***N*-(4-*O*-Allyl-2-azido-3,6-di-*O*-benzyl-2-deoxy-D-glucopyranoside) trichloroacetamide (3-38)** This compound was isolated as a byproduct from the synthesis of **3-36** and **3-37** as a 3:2 mixture of anomers. Rf. 0.23, 0.29 (hexanes:ethyl acetate 85:15). IR (thin film, NaCl plates) 3333, 3065, 2917, 2866, 2713, 1709, 1705 cm⁻¹. ¹H NMR (500 MHz, CDCl₃) δ 7.29-7.41 (m, 10H), 7.13 (d, J = 9.1 Hz, 0.6H), 7.01 (d, J = 6.5 Hz, 0.4H), 5.75-5.87 (m, 1H), 5.64 (ψ t, 0.4H), 5.13-5.23 (m, 2H), 4.85-4.98 (m, 2.6H), 4.63-4.67 (m, 1H), 4.50-4.53 (m, 1H), 4.22-4.27 (m, 1H), 4.01-4.09 (m, 1H), 3.87-3.90 (m, 0.4H), 3.42-3.73 (m, 5.6H). ¹³C NMR (125 MHz, CDCl₃) δ 162.1, 161.9, 137.8, 137.6, 137.3, 134.4, 134.2, 128.8, 128.7, 128.61, 128.6, 128.5, 128.45, 128.4, 128.3, 128.2, 128.15, 128.1, 128.0, 117.9, 117.3, 83.9, 81.2, 80.5, 77.5, 77.1, 70.0, 76.0, 75.9, 74.0, 73.95, 73.8, 72.7, 67.9, 67.8, 65.8, 61.7. ESI MS (C₂₅H₂₇Cl₃N₄O₅) m/z (M + Na⁺) calcd 591.0945, obsd 591.0942.

3.3 Results and Discussion

Synthesis of non-reducing end disaccharide trichloroacetimidate 3-3

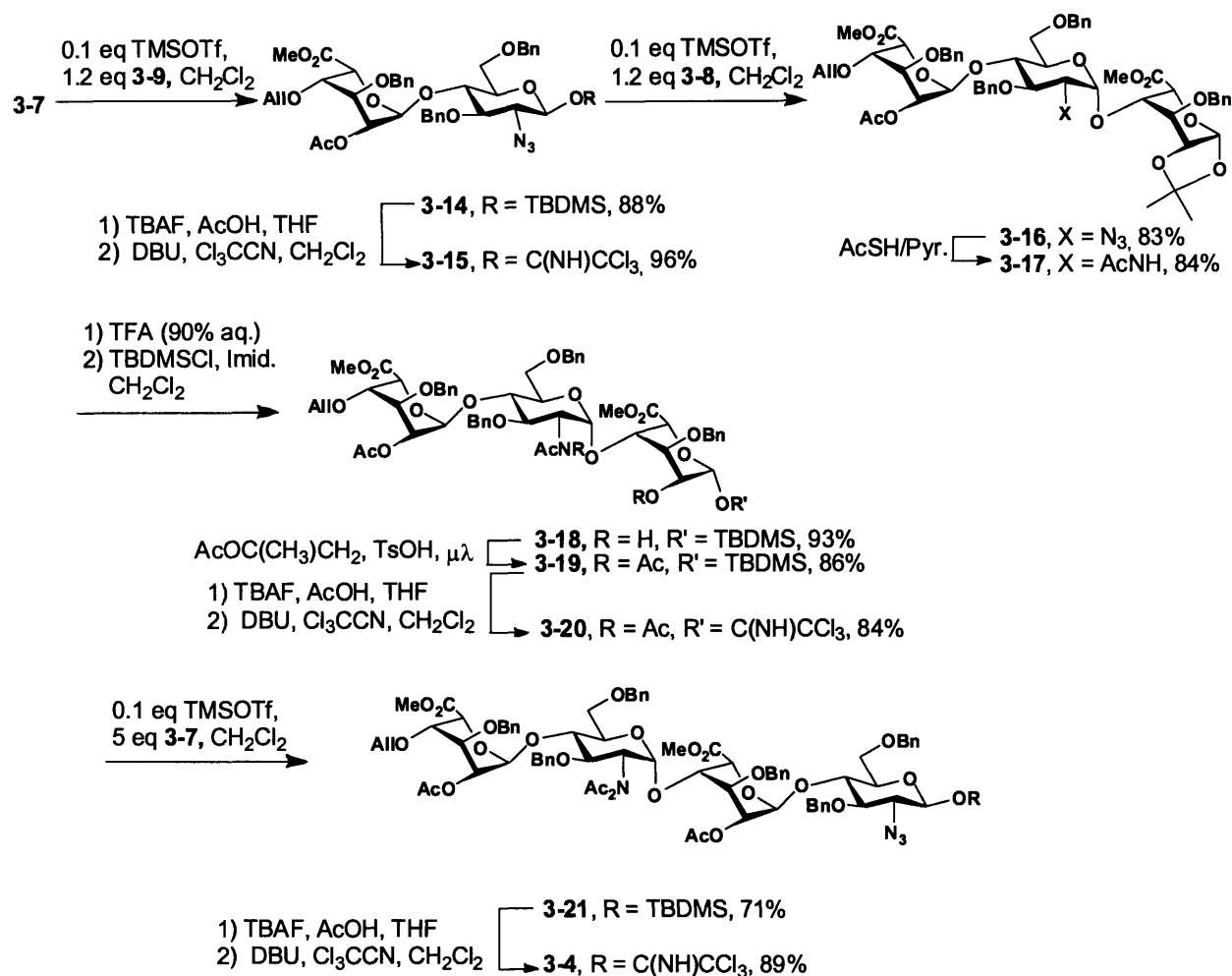
Disaccharide **3-3** was synthesized by coupling iduronic acid trichloroacetimidate **3-6** and glucosamine azide **3-7** to yield the desired disaccharide **3-11** in 74% yield (Scheme 3-1). Removal of the levulinate (Lev) ester with hydrazine proceeded in 92% yield to give **3-12**. This product was converted to its benzyl ether **3-13** in 76% yield using benzyl trichloroacetimidate and trifluoromethanesulfonic acid (TfOH) activator. Cleavage of the anomeric silyl ether with TBAF/AcOH, followed by reaction with DBU/Cl₃CCN yielded 78% of trichloroacetimidate disaccharide building block **3-3**.



Scheme 3-1. Synthesis of non-reducing end disaccharide.

Synthesis of Tetrasaccharide Trichloroacetimidate 3-4

Synthesis of the central tetrasaccharide **3-4** presented more of a challenge (Scheme 3-2). Iduronic acid donor **3-9** and GlcN₃ derivative **3-7** were coupled through TMSOTf activation in 88% yield. Conversion of the product disaccharide **3-14** into glycosyl trichloroacetimidate **3-15** was accomplished by cleavage of the TBDMS group followed by reaction with DBU/Cl₃CCN (96% yield for two steps). Union of **3-15** with iduronic acid derivative **3-8** afforded trisaccharide **3-16** with complete α -selectivity in 83% yield.



Scheme 3-2. Synthesis of middle tetrasaccharide.

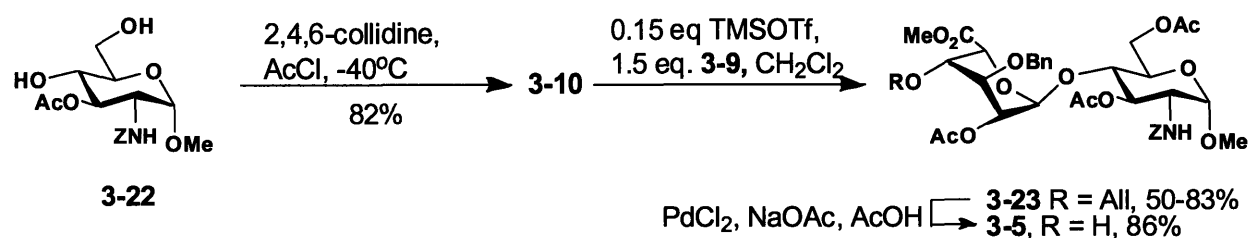
Conversion of the azide moiety in trisaccharide **3-16** to an *N*-acetate was accomplished in one pot and 84% yield by treatment with thiolacetic acid in pyridine.⁽⁷⁰⁾ Removal of the isopropylidene group from product trisaccharide **3-17** with trifluoroacetic acid followed by selective silyl ether formation at the anomeric hydroxyl group⁽⁷¹⁾ furnished **3-18** in a 93% yield. Microwave irradiation of **3-18** in isopropenyl acetate with catalytic *p*-toluene sulfonic acid⁽⁶⁸⁾ simultaneously installed the desired *N*-diacetate and acetylated the free hydroxyl, forming **3-19** in 86% yield. This transformation could not be achieved under a variety of thermal conditions, with only poor yields of **3-19** achieved even after several days. Conversion of **3-19**

to trisaccharide trichloroacetimidate building block **3-20** was achieved in 84% yield by cleavage of the TBDMS ether and reaction with DBU/ Cl_3CCN .

Glycosylating agent **3-20** coupled only poorly with 2-azido-glucose **7** in the presence of catalytic TMSOTf, with mainly hydrolyzed trisaccharide lactol formed instead. Use of a large excess (5 equiv.) of **7** resulted in a 71% conversion to **3-21**; most unreacted **3-7** could be recovered and recycled. Tetrasaccharide **3-21** was converted to glycosyl trichloroacetimidate **3-4** in 89% yield.

Synthesis of Reducing End Disaccharides 3-5 and 3-30.

The reducing end disaccharide **3-5** was synthesized from known 2-*N*-CBz glucosamine **3-22** (Scheme 3-3).⁽⁷²⁾ Selective acetylation of the primary hydroxyl with acetyl chloride in 2,4,6-collidine afforded acceptor **3-10** in 82% yield.⁽⁷³⁾ Glucosamine **3-10** reacted with iduronic acid donor **3-9** under TMSOTf activation to form disaccharide **3-23** in highly variable yields. Close monitoring by TLC revealed that **3-10** was rapidly consumed to form orthoester **3-24** that was identified by $^1\text{H-NMR}$ (Figure 3-3). When left under reaction conditions for several hours **3-24** rearranged to the desired disaccharide **3-23**. Rearrangement and hydrolysis of the orthoester intermediate was highly sensitive to the reaction conditions and resulted in the variability in yield of desired disaccharide **3-23**.



Scheme 3-3. Synthesis of reducing end disaccharide.

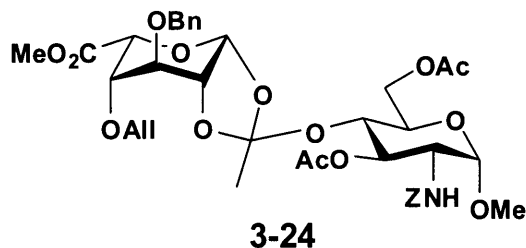
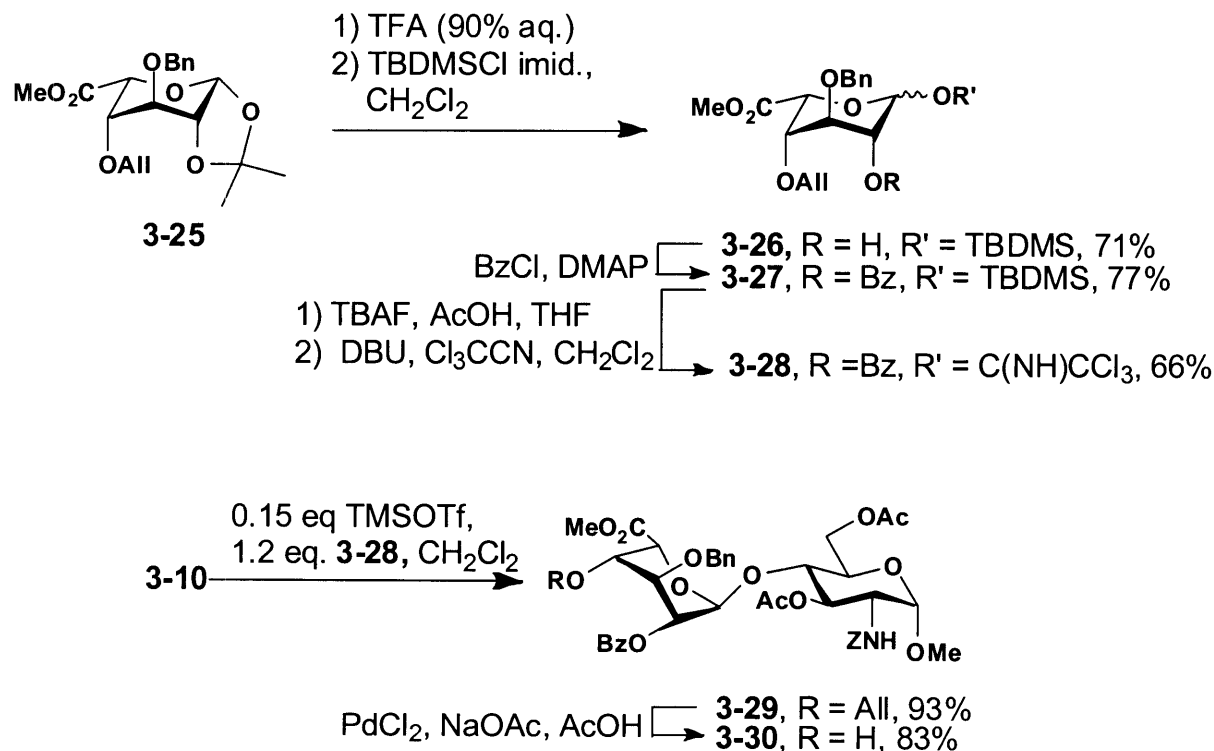


Figure 3-3. Orthoester byproduct.

While sufficient quantities of **3-5** could be produced via PdCl₂-catalyzed allyl ether removal from disaccharide **3-23**, an alternate reducing end disaccharide was also prepared (Scheme 3-4). Synthesis of iduronic acid **3-28** followed established procedures,⁽³⁰⁾ with the exception of the use of a C2 benzoate ester, which was included to reduce orthoester formation. Glycosylating agent **3-28** reacted cleanly with the CBz glucosamine derivative **3-10** to give **3-29** in excellent yield. No orthoester intermediate was observed. This disaccharide was treated with PdCl₂/NaOAc in acetic acid and water to afford disaccharide **3-30** in 83% yield.



Scheme 3-4. Synthesis of second reducing end disaccharide.

The replacement of a C2 acetate with a C2 benzoate group dramatically improved the yield of this coupling reaction. Interestingly, glycosylating agent **3-9** containing a C2 acetate and the *N*-CBz glucosamine *n*-pentenyl glycoside **3-31** (Figure 3-4) coupled in high yield without the formation of orthoester (data not shown). All other couplings of iduronic acid donors reported here proceed in good yields to 1-*O*-TBDMS ether β -glucosamines. Based on these and previous(32) observations it appears that the stereoelectronics of α -glucosamine acceptors can negatively influence the outcome of coupling reactions with uronic acid trichloroacetimidates, greatly favoring orthoester formation. Use of a C2 benzoate protecting group can overcome this effect.

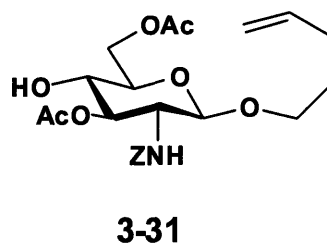
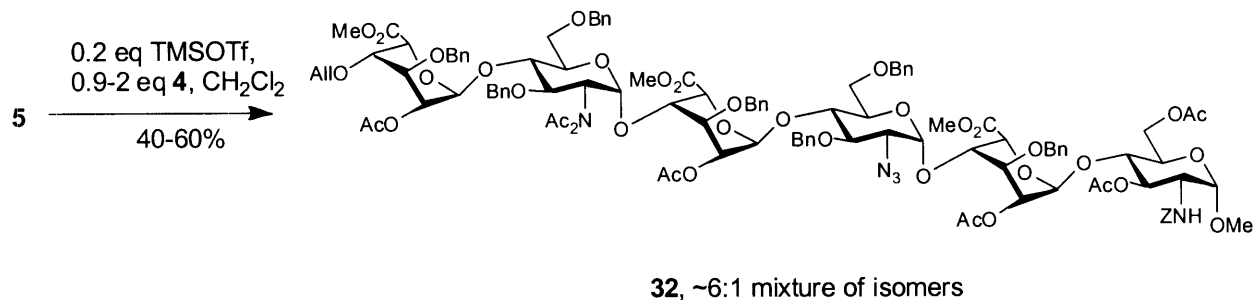


Figure 3-4. Glucosamine CBz acceptor.

Attempted Block Coupling of Tetrasaccharide 3-4 with Reducing End Disaccharides 3-5 and 3-30

With compounds **3-3**, **3-4**, and **3-5** as well as alternate reducing end acceptor **3-30** in hand, assembly of the fully protected target **3-2** was attempted (Scheme 3-5). Coupling of **3-4** and **3-5** under TMSOTf activation proceeded in 59% yield when reacted at -40°C in the presence of molecular sieves. Although the desired α -linked hexasaccharide **3-32** was obtained as the major product, it was contaminated with 17% of an inseparable impurity. Even after purification via normal and reverse phase silica gel HPLC and size exclusion chromatography (Bio-rad Bio-Beads), some of the contaminant always remained.



Scheme 3-5. Block coupling of tetrasaccharide donor and reducing end disaccharide.

Varying the reaction conditions for coupling **3-4** and **3-5** did not prevent formation of the minor product. Variation of reaction temperature (from $-78\text{ }^{\circ}\text{C}$ to $0\text{ }^{\circ}\text{C}$) and activator (TMSOTf and TBDMSOTf) affected the coupling yields, but the isolated product always contained the minor product. Varying the polarity of the reaction solvent through addition of heptanes had no effect on the ratio of the products.

Removal of the allyl protecting group through treatment of the mixture with $\text{PdCl}_2/\text{NaOAc}$ in acetic acid and water and further coupling with disaccharide **3-3** to form the octasaccharide **3-2** did not allow for the separation of the minor product at this later stage of the synthesis. Spectral data indicated that the major isomer did react as desired, but a minor product copurified at each step, suggesting that the contaminant reacted similarly. Finally, coupling of tetrasaccharide **3-4** with disaccharide **3-30** under the best conditions found for the coupling with **3-5** resulted in the formation of a 1:1 mixture of inseparable products.

To identify the minor product contaminating **3-32**, possible reaction byproducts were systematically eliminated. Size exclusion purification ruled out any decomposition products of **3-5**. Small amounts of hydrolyzed **3-4** were detected and separated from the products through silica gel chromatography. Tetrasaccharide **3-33**, formed by rearrangement of **3-4**, was also observed in the crude reaction mixture, but could be readily separated from product **3-2** (Figure 3-5). Acetylation, *N*-diacetylation, and silylation to cap potentially rearranged tetrasaccharides

containing a free hydroxyl group or an *N*-acetamide resulted in re-isolated **3-32** that contained the same contaminant in an unchanged ratio.

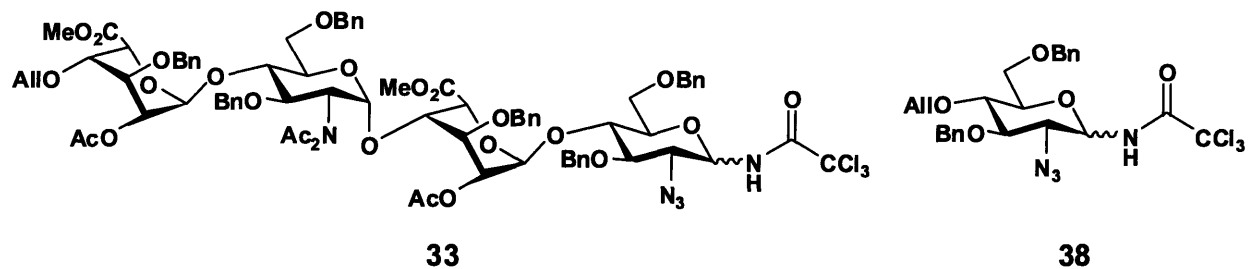
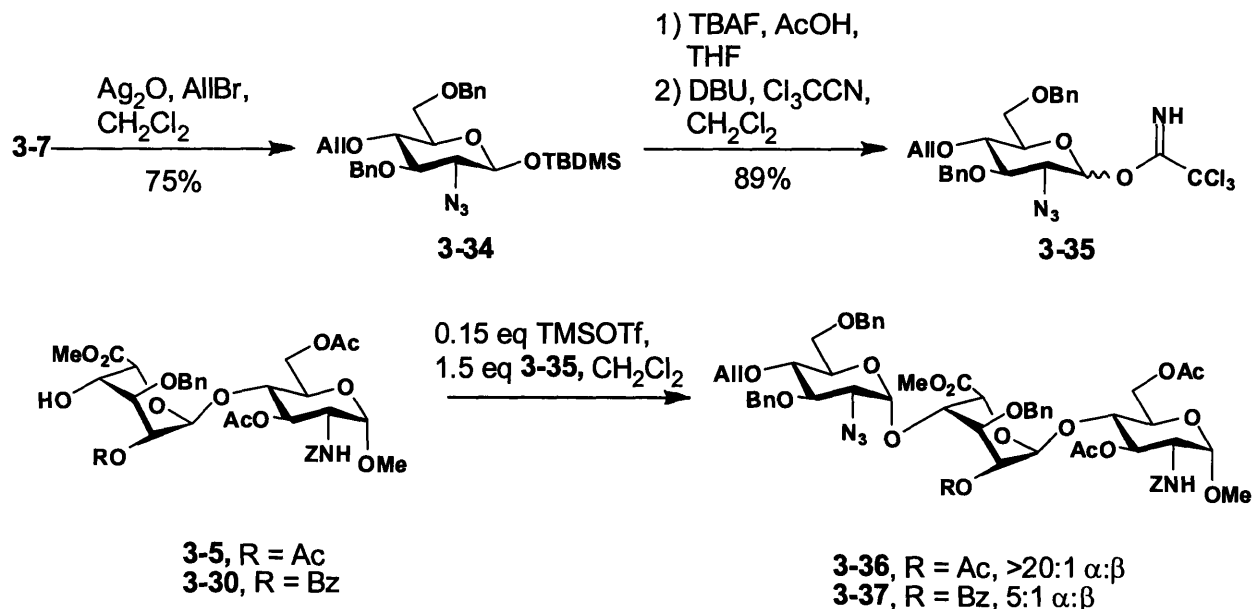


Figure 3-5. Rearranged trichloroacetimidate donors.

Based on these observations, the minor product was likely an isomer of the desired hexasaccharide. Two major possibilities exist: either acceptor **3-5** rearranged under the reaction conditions to result in 1→2 linked hexasaccharide, or an α : β mixture of 1→4 linked isomers was being produced. Treatment of acceptors **3-5** and **3-30** under coupling conditions in the absence of a glycosylating agent resulted exclusively in the re-isolation of unchanged starting materials. Thus, the formation of 1→2 linked regioisomer hexasaccharide could be ruled out. In direct contrast to previous reports,^(33, 48, 57, 60) the coupling of a 2-azido glucosamine donor and the C4 hydroxyl group of iduronic acid seemed to produce an anomeric mixture of products.

Examination of Model Trisaccharides 3-36 and 3-37.



Scheme 3-6. Model trisaccharide.

Since a detailed NMR analysis of the hexasaccharide mixture was difficult due to the large number of overlapping signals, a simplified model system was devised (Scheme 3-6). Alkylation of **3-7** using silver oxide and allyl bromide furnished glucosamine **3-34** in 75% yield. Conversion of **3-34** to trichloroacetimidate **3-35** was achieved in 89% yield. Reaction of monosaccharide trichloroacetimidate **3-35** with **3-5** and **3-30** yielded trisaccharides **3-36** and **3-37** respectively. The structure of rearranged glycosylating agent **3-38** (Figure 3-5) was confirmed by 2-D NMR experiments. Trisaccharide **3-36** contained less than 5% of a contaminating product, while trisaccharide **3-37** was isolated as a 5:1 mixture. Detailed analysis of **3-37** of by NMR and mass spectrometry identified an apparent mixture of trisaccharide isomers. Carbon-proton correlation spectroscopy (HSQC, Figure 3-6), showed that one anomeric cross peak of the minor isomer was consistent with a β -GlcN₃ anomeric cross peak. (74-76)

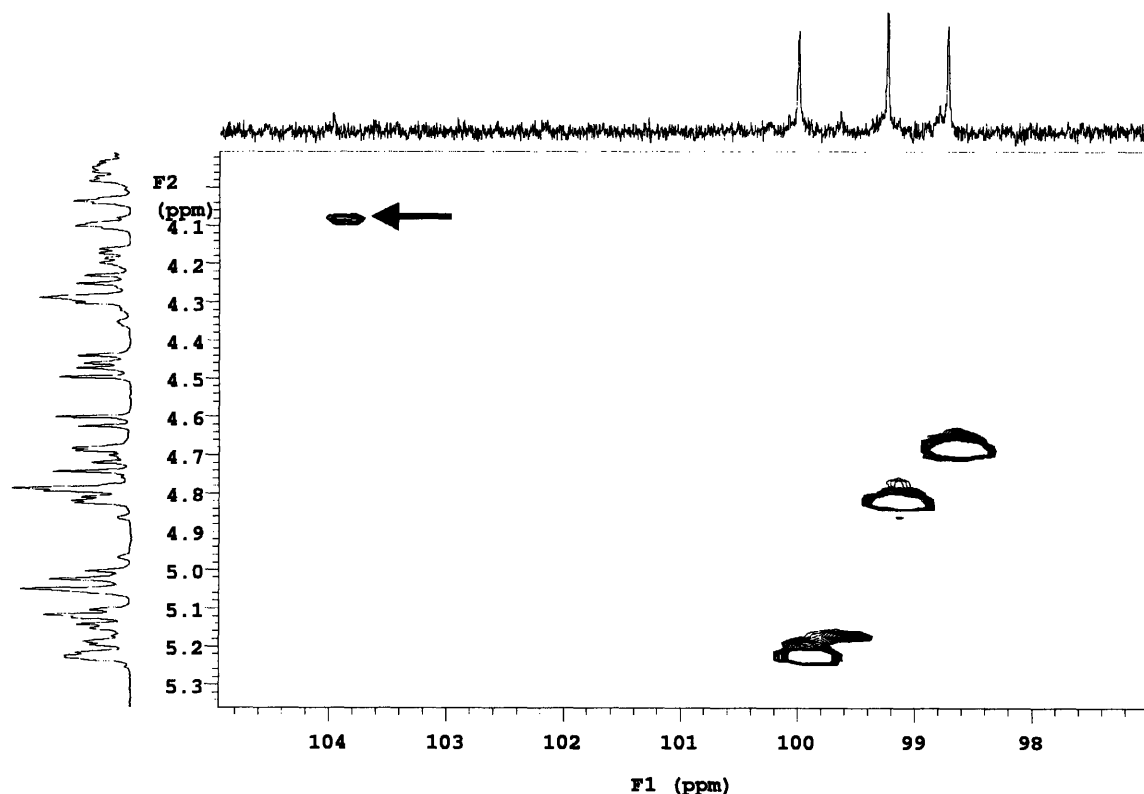


Figure 3-6. HSQC spectrum of the anomeric region of trisaccharide 37. The indicated cross peak arises from the minor isomer and is consistent with a β -glucosamine H1-C1 cross peak.

These observations indicate that the erosion of anomeric selectivity is dependent both on the size of the glycosylating agent and on the exact nature of the nucleophile. The conformation of uronic acid acceptors has a profound influence on the anomeric selectivity of couplings involving such monomers,^(33, 77) whereby the 1C_4 conformation normally adopted by iduronic acid derivatives overwhelmingly favors α -products. This selectivity has also been observed for oligosaccharides containing an iduronic acid at the non-reducing end.

In the case described here, it is hypothesized that the selectivity is eroded due to an altered conformation of the iduronic acid. The 2-*N*-CBz glucosamine residue connected to the anomeric position of the iduronic acid is the major difference between acceptor 3-5 and previously described, α -selective iduronic acid disaccharide acceptors. The nitrogen protecting

group used to differentiate the glucosamine may be responsible for loss of selectivity in the union of 3-4 and 3-5. Presumably the iduronic acid acceptor is forced out of the 1C_4 conformation that appears to allow 2-azido glucosyl trichloroacetimidates to react with complete α -selectivity. The loss of selectivity was apparently exacerbated by the change of the C2 protecting group from acetate to the sterically bulkier benzoate. The C2 substituent is placed axial when the sugar ring is in the 1C_4 conformation; thus larger substituents likely favor the 4C_1 conformation.

Due to the loss of selectivity in this block coupling, and the difficulties encountered with purification, it was judged that the proposed strategy was not useful for producing the target octasaccharide. It is becoming increasingly clear that the coupling of larger oligosaccharide building blocks in the synthesis of heparin-like glycosaminoglycans is greatly influenced by the conformation of the nucleophile. The loss of selectivity in these couplings is a significant obstacle to the general synthesis of HLGAGs. A systematic reevaluation of the protecting group and anomeric leaving group chemistries used in heparin synthesis will greatly facilitate further work on the assembly of larger structures using the modular approach.

Future Directions

These results, showing erosion of selectivity for a GlcN₃ reducing end trichloroacetimidate donor, taken with the previous results in ATIII synthesis showing poor yields (apparently zero) when coupling uronic acid reducing end donors onto polysaccharide acceptors,(32) obviously drastically limit the remaining options for a general, modular synthesis of heparin. The loss of good selectivity when coupling to disaccharides 3-5 and 3-30 suggests that a GlcN₃ reducing end disaccharide approach, used in most previously published syntheses of

large heparin structures, will not work well for general, modular approaches to HLGAG synthesis.

The results shown above (Scheme 3-3, Scheme 3-4) indicate that a return to the original disaccharide strategy may be fruitful if the C2 protecting group on the uronic acid residues is switched to benzoate or another ester with low electrophilicity. In the synthesis of **3-5**, yields were poor due to orthoester formation followed by rearrangement or hydrolysis. Results from previous attempts at a modular synthesis with uronic acid terminated donors(32) also indicated orthoesters formation was a problem when acetate, levulinyl, or monochloroacetate was used as the C2 protecting group on a glucuronic acid trichloroacetimidate. A C2 allyl carbonate did not give product either: while the carbonyl should be less electrophilic, destruction of the donor could occur through the formation of a cyclic carbonate (Figure 3-7), a mechanism previously found to operate for another carbonate group(78). Switching to benzoate has a dramatic effect on the synthesis described in this chapter. In the formation of disaccharide **3-30**, the reaction went cleanly and rapidly to product with no isolatable orthoester found or visualized on TLC.

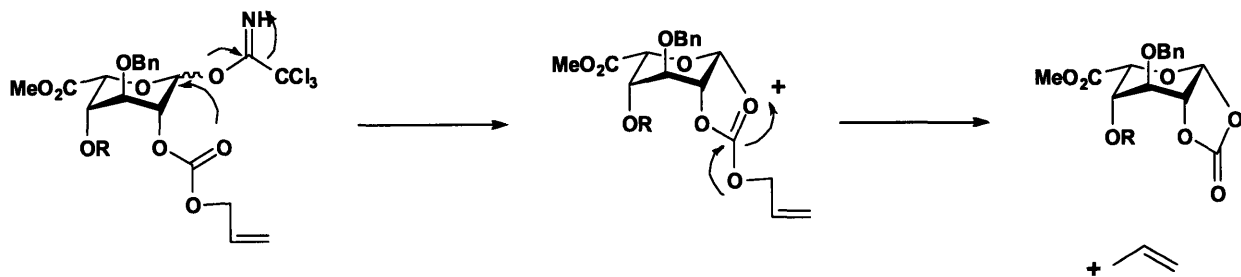


Figure 3-7. Rearrangement of alloc protected iduronates.

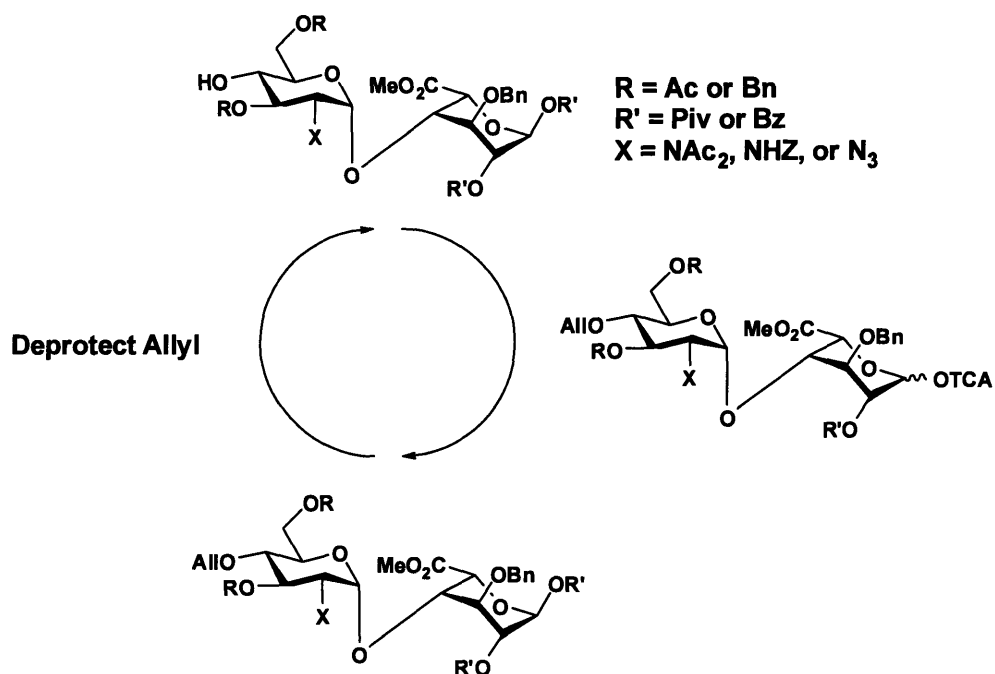


Figure 3-8. Proposed modular synthesis of HLGAGs.

A return to the uronic acid trichloroacetimidate disaccharide strategy may well be promising if benzoyl or pivaloyl esters are employed as C2 protecting groups on the uronic acids (Figure 3-8). In this strategy, the permanent protecting groups on most hydroxyl positions remain unchanged, with acetate masking sites to be sulfated and benzyl ethers masking sites to be unmodified. As presented, the requirement of esters with low electrophilicity does not allow for a temporary uronic acid protecting group, and only C2 sulfated structures could be produced. In order to allow the uronic acid C2 hydroxyls to be unmodified, a new protecting group would be required that had a carbonyl with low electrophilicity, yet could be orthogonally cleaved in the presence of other esters. The uronic acid trichloroacetimidate strategy has the obvious benefits of forming the α -glucosamine linkage with complete selectivity using conformationally locked acceptors,(32, 33) and allows for reduction of the azide and reprotection as in the installation of the *N*-diacetate group in 3-4. This uronic acid donor strategy suggest the

disconnection shown for future attempts at synthesis of the HSV-1 binding octasaccharide (Figure 3-9).

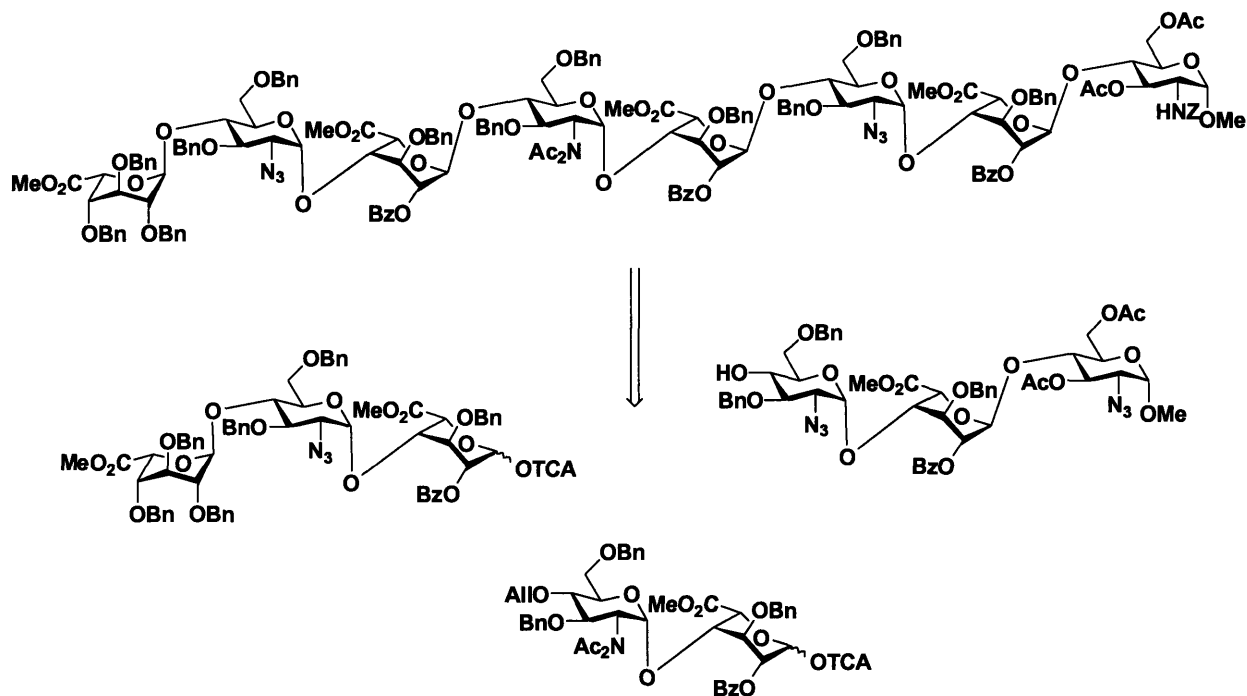


Figure 3-9. Alternate disconnection of HSV binding octasaccharide.

If this strategy is successful at assembling 3-2, the next task will be the implementation of the new deprotection scheme. Briefly, the suggested plan is to cleave all acetate and benzoate esters, deprotect the methyl esters and transform the *N*-diacetate to a *N*-acetate using the standard ester deprotection procedure. Next, selective reduction of the azides using Staudinger chemistry, thiol reagents, Raney Ni, or other chemistry must be examined. Sulfation of all revealed hydroxyls and amines should be achievable by using the $\text{SO}_3:\text{NEt}_3$ reagent employed in the *O*-sulfation step of previous heparin syntheses. Finally, Pd/C reduction should remove all benzyl ethers and CBz groups.

If this strategy does not work, a complete reassessment of the chemistries used will be necessary. One possibility is to try methods involving protected glucose or idose terminated

donors and adding a late stage oxidation to the deprotection/elaboration scheme.(79-81) While adding another reaction step to the deprotection scheme is certainly undesirable, the improvements to coupling chemistry might offset this disadvantage. Alternatively, new donor types will have to be explored. Examining other donor types, such as thio donors and fluoro donors, may make this disconnection feasible. While these chemistries may not be compatible with the solid phase,(82) it may be unnecessarily limiting to allow worries of solid-phase compatibility to prevent the development of any working modular synthesis. The benefits of producing a working solution-phase synthesis alone are great; after accomplishment of this goal the issue of solid phase and automation can be addressed.

3.4 References

- (1) Noti, C., and Seeberger, P. H. (2005) Chemical approaches to define the structure-activity relationship of heparin-like glycosaminoglycans. *Chem. Biol.* 12, 731-756.
- (2) Linhardt, R. J. (2003) 2003 Claude S. Hudson Award address in carbohydrate chemistry. Heparin: structure and activity. *J. Med. Chem.* 46, 2551-2564.
- (3) Whitelock, J. M., and Iozzo, R. V. (2005) Heparan sulfate: a complex polymer charged with biological activity. *Chem. Rev.* 105, 2745-2764.
- (4) Raman, R., Sasisekharan, V., and Sasisekharan, R. (2005) Structural insights into biological roles of protein-glycosaminoglycan interactions. *Chem. Biol.* 12, 267-277.
- (5) Coombe, D. R., and Kett, W. C. (2005) Heparan sulfate-protein interactions: therapeutic potential through structure-function insights. *Cell. Mol. Life Sci.* 62 410-424.
- (6) Handel, T. M., Johnson, Z., Crown, S. E., Lau, E. K., Sweeney, M., and Proudfoot, A. E. (2005) Regulation of protein function by glycosaminoglycans—as exemplified by chemokines. *Annu. Rev. Biochem.* 74, 385-410.
- (7) Esko, J. D., and Selleck, S. B. (2002) Order out of chaos: assembly of ligand binding sites in heparan sulfate. *Annu. Rev. Biochem.* 71, 435-471.
- (8) Kjellén, L., and Lindahl, U. (1991) Proteoglycans: structures and interactions. *Annu. Rev. Biochem.* 60, 443-475.
- (9) Capila, I., and Linhardt, R. J. (2002) Heparin-protein interactions. *Angew. Chem. Int. Ed.* 41, 390-412.
- (10) Iozzo, R. V. (1998) Matrix proteoglycans: from molecular design to cellular function. *Annu. Rev. Biochem.* 67, 609-652.

- (11) Bernfield, M., Götte, M., Park, P. W., Reizes, O., Fitzgerald, M. L., Lincecum, J., and Zako, M. (1999) Functions of cell surface heparan sulfate proteoglycans. *Annu. Rev. Biochem.* 68, 729-777.
- (12) Casu, B., and Lindahl, U. (2001) Structure and biological interactions of heparin and heparan sulfate. *Adv. Carbohydr. Chem. Biochem.* 57, 159-206.
- (13) Chong, B. H. (1992) Heparin-induced thrombocytopenia. *Aust. N. Z. J. Med.* 22, 145-152.
- (14) Engelberg, H. (1984) Heparin and the atherosclerotic process. *Pharm. Rev.* 36, 91-110.
- (15) van Boeckel, C. A. A., and Petitou, M. (1993) The unique antithrombin III binding domain of heparin: a lead to new synthetic antithrombotics. *Angew. Chem. Int. Ed. Engl.* 32, 1671-1690.
- (16) Petitou, M., and van Boeckel, C. A. A. (2004) A synthetic antithrombin III binding pentasaccharide is now a drug! What comes next? *Angew. Chem. Int. Ed.* 43, 3118-3133.
- (17) Rele, S. M., Iyer, S. S., Baskaran, S., and Chaikof, E. L. (2004) Design and synthesis of dimeric heparinoid mimetics. *J. Org. Chem.* 69, 9159-9170.
- (18) Codée, J. D. C., van der Marel, G. A., van Boeckel, C. A. A., and van Boom, J. H. (2002) Probing the heparin-antithrombin III interaction using synthetic-pentasaccharides bearing positively charged groups. *Eur. J. Org. Chem.*, 3954-3965.
- (19) Petitou, M., Héroult, J.-P., Bernat, A., Driguez, P.-A., Duchaussoy, P., Lormeau, J.-C., and Herbert, J.-M. (1999) Synthesis of thrombin inhibiting heparin mimetics without side effects. *Nature* 398, 417-422.
- (20) Petitou, M., Duchaussoy, P., Driguez, P.-A., Héroult, J.-P., Lormeau, J.-C., and Herbert, J.-M. (1999) New synthetic heparin mimetics able to inhibit thrombin and factor Xa. *Bioorg. Med. Chem. Lett.* 9, 1155-1160.
- (21) Petitou, M., Driguez, P.-A., Duchaussoy, P., Héroult, J.-P., Lormeau, J.-C., and Herbert, J.-M. (1999) Synthetic oligosaccharides having various functional domains: potent and potentially safe heparin mimetics. *Bioorg. Med. Chem. Lett.* 9, 1161-1166.
- (22) Buijsman, R. C., Basten, J. E. M., Dreef-Tromp, C. M., van der Marel, G. A., van Boeckel, C. A. A., and van Boom, J. H. (1999) Synthesis of heparin-like antithrombotics having perphosphorylated thrombin binding domains. *Bioorg. Med. Chem.* 7, 1881-1890.
- (23) Petitou, M., Duchaussoy, P., Driguez, P.-A., Jaurand, G., Héroult, J.-P., Lormeau, J.-C., van Boeckel, C. A. A., and Herbert, J.-M. (1998) First synthetic carbohydrates with the full anticoagulant properties of heparin. *Angew. Chem. Int. Ed.* 37, 3009-3014.
- (24) Westerduin, P., Basten, J. E. M., Broekhoven, M. A., de Kimpe, V., Kuijpers, W. H. A., and van Boeckel, C. A. A. (1996) Synthesis of tailor-made glycoconjugates showing ATIII-mediated inhibition of blood coagulation factors Xa and thrombin. *Angew. Chem. Int. Ed.* 35, 331-333.
- (25) Poletti, L., and Lay, L. (2003) Chemical contributions to understanding heparin activity: synthesis of related sulfated oligosaccharides. *Eur. J. Org. Chem.*, 2999-3024.
- (26) Karst, N. A., and Linhardt, R. J. (2003) Recent chemical and enzymatic approaches to the synthesis of glycosaminoglycan oligosaccharides. *Curr. Med. Chem.* 10, 1993-2031.
- (27) Yeung, B. K. S., Chong, P. Y. C., and Petillo, P. A. (2002) Synthesis of glycosaminoglycans. *J. Carbohydr. Chem.* 21, 799-865.
- (28) Ke, W., Whitfield, D. M., Gill, M., Larocque, S., and Yu, S.-H. (2003) A short route to L-iduronic acid building blocks for the syntheses of heparin-like disaccharides. *Tetrahedron Lett.* 44, 7767-7770.

- (29) La Ferla, B., Lay, L., Guerrini, M., Poletti, L., Panza, L., and Russo, G. (1999) Synthesis of disaccharide sub-units of a new series of heparin related oligosaccharides. *Tetrahedron* 55, 9867-9880.
- (30) Lohman, G. J. S., Hunt, D. K., Högermeier, J. A., and Seeberger, P. H. (2003) Synthesis of iduronic acid building blocks for the modular assembly of glycosaminoglycans. *J. Org. Chem.* 68, 7559-7561.
- (31) Lohman, G. J. S., and Seeberger, P. H. (2003) One-pot conversion of glycals to *cis*-1,2-isopropylidene- α -glycosides. *J. Org. Chem.* 68, 7541-7543.
- (32) Orgueira, H. A., Bartolozzi, A., Schell, P., Litjens, R. E. J. N., Palmacci, E. R., and Seeberger, P. H. (2003) Modular synthesis of heparin oligosaccharides. *Chem. Eur. J.* 9, 140-169.
- (33) Orgueira, H. A., Bartolozzi, A., Schell, P., and Seeberger, P. H. (2002) Conformational locking of the glycosyl acceptor for stereocontrol in the key step in the synthesis of heparin. *Angew. Chem. Int. Ed.* 41, 2128-2131.
- (34) Rochepeau-Jobron, L., and Jacquinet, J.-C. (1997) Diastereoselective hydroboration of substituted *exo*-glucals revisited. A convenient route for the preparation of L-iduronic acid derivatives. *Carbohydr. Res.* 303, 395-406.
- (35) Tabeur, C., Machetto, F., Mallet, J.-M., Duchaussoy, P., Petitou, M., and Sinaÿ, P. (1996) L-Iduronic acid derivatives as glycosyl donors. *Carbohydr. Res.* 281, 253-276.
- (36) Yu, H. N., Furukawa, J., Ikeda, T., and Wong, C.-H. (2004) Novel efficient routes to heparin monosaccharides and disaccharides achieved via regio- and stereoselective glycosidation. *Org. Lett.* 6, 723-726.
- (37) Kovensky, J., Duchaussoy, P., Petitou, M., and Sinaÿ, P. (1996) Binding of heparan sulfate to fibroblast growth factor-2 total synthesis of a putative pentasaccharide binding site. *Tetrahedron: Asymmetry* 7, 3119-3128.
- (38) Kovensky, J., Duchaussoy, P., Bono, F., Salmivirta, M., Sizun, P., Herbert, J.-M., Petitou, M., and Sinaÿ, P. (1999) A synthetic heparan sulfate pentasaccharide, exclusively containing L-iduronic acid, displays higher affinity for FGF-2 than its D-glucuronic acid-containing isomers. *Bioorg. Med. Chem.* 7, 1567-1580.
- (39) Tabeur, C., Mallet, J.-M., Bono, F., Herbert, J.-M., Petitou, M., and Sinaÿ, P. (1999) Oligosaccharides corresponding to the regular sequence of heparin: chemical synthesis and interaction with FGF-2. *Bioorg. Med. Chem.* 7, 2003-2012.
- (40) de Paz, J.-L., Angulo, J., Lassaletta, J.-M., Nieto, P. M., Redondo-Horcajo, M., Lozano, R. M., Giménez-Gallego, G., and Martín-Lomas, M. (2001) The activation of fibroblast growth factors by heparin: synthesis, structure, and biological activity of heparin-like oligosaccharides. *ChemBioChem* 2, 673-685.
- (41) Poletti, L., Fleischer, M., Vogel, C., Guerrini, M., Torri, G., and Lay, L. (2001) A rational approach to heparin-related fragments—synthesis of differently sulfated tetrasaccharides as potential ligands for fibroblast growth factors. *Eur. J. Org. Chem.*, 2727-2734.
- (42) de Paz, J.-L., Ojeda, R., Reichardt, N., and Martín-Lomas, M. (2003) Some key experimental features of a modular synthesis of heparin-like oligosaccharides. *Eur. J. Org. Chem.*, 3308-3324.
- (43) de Paz, J. L., and Martín-Lomas, M. (2005) Synthesis and biological evaluation of a heparin-like hexasaccharide with the structural motifs for binding to FGF and FGFR. *Eur. J. Org. Chem.*, 1849-1858.

- (44) van Boeckel, C. A. A., Beetz, T., Vos, J. N., de Jong, A. J. M., van Aelst, S. F., van den Bosch, R. H., Mertens, J. M. R., and van der Vlugt, F. A. (1985) Synthesis of a pentasaccharide corresponding to the antithrombin III binding fragment of heparin. *J. Carbohydr. Chem.* 4, 293-321.
- (45) Jacquinet, J.-C., Petitou, M., Duchaussoy, P., Lederman, I., Choay, J., Torri, G., and Sinaÿ, P. (1984) Synthesis of heparin fragments. A chemical synthesis of the trisaccharide *O*-(2-deoxy-2-sulfamido-3,6-di-*O*-sulfo- α -D-glucopyranosyl)-(1 \rightarrow 4)-*O*-(2-*O*-sulfo- α -L-idopyranosyluronic acid)-(1 \rightarrow 4)-2-deoxy-2-sulfamido-6-*O*-sulfo-D-glucopyranose heptasodium salt. *Carbohydr. Res.* 130, 221-241.
- (46) Sinaÿ, P., Jacquinet, J.-C., Petitou, M., Duchaussoy, P., Lederman, I., Choay, J., and Torri, G. (1984) Total synthesis of a heparin pentasaccharide fragment having high affinity for antithrombin III. *Carbohydr. Res.* 132, C5-C9.
- (47) Petitou, M., Duchaussoy, P., Lederman, I., Choay, J., Sinaÿ, P., Jacquinet, J.-C., and Torri, G. (1986) Synthesis of heparin fragments. A chemical synthesis of the pentasaccharide *O*-(2-deoxy-2-sulfamido-6-*O*-sulfo- α -D-glucopyranosyl)-(1 \rightarrow 4)-*O*-(β -D-glucopyranosyluronic acid)-(1 \rightarrow 4)-*O*-(2-deoxy-2-sulfamido-3,6-di-*O*-sulfo- α -D-glucopyranosyl)-(1 \rightarrow 4)-*O*-(2-*O*-sulfo-(α -L-idopyranosyluronic acid)-(1 \rightarrow 4)-2-deoxy-2-sulfamido-6-*O*-sulfo-D-glucopyranose decasodium salt, a heparin fragment having high affinity for antithrombin III. *Carbohydr. Res.* 147, 221-236.
- (48) Petitou, M., Duchaussoy, P., Lederman, I., Choay, J., Jacquinet, J.-C., Sinaÿ, P., and Torri, G. (1987) Synthesis of heparin fragments: a methyl α -pentaoside with high affinity for antithrombin III. *Carbohydr. Res.* 167, 67-75.
- (49) Lei, P.-S., Duchaussoy, P., Sizun, P., Mallet, J.-M., Petitou, M., and Sinaÿ, P. (1998) Synthesis of a 3-deoxy-L-iduronic acid containing heparin pentasaccharide to probe the conformation of the antithrombin III binding sequence. *Bioorg. Med. Chem.* 6, 1337-1346.
- (50) Das, S. K., Mallet, J.-M., Esnault, J., Driguez, P.-A., Duchaussoy, P., Sizun, P., Hérault, J.-P., Herbert, J.-M., Petitou, M., and Sinaÿ, P. (2001) Synthesis of conformationally locked carbohydrates: a skew-boat conformation of L-iduronic acid governs the antithrombotic activity of heparin. *Angew. Chem. Int. Ed.* 40, 1670-1673.
- (51) Beetz, T., and van Boeckel, C. A. A. (1986) Synthesis of an antithrombin binding heparin-like pentasaccharide lacking 6-*O* sulphate at its reducing end. *Tetrahedron Lett.* 27, 5889-5892.
- (52) Weissman, B., and Chao, H. (1986) Heparin trisaccharides with nonreducing 2-amino-2-deoxy- α -D-glucopyranosyl end-groups suitable as substrates for catabolic enzymes. *Carbohydr. Res.* 154, 217-228.
- (53) van Boeckel, C. A. A., Basten, J. E. M., Lucas, H., and van Aelst, S. F. (1988) A synthetic heparin-like compound which still activates antithrombin III although it contains an open chain fragment instead of α -L-idopyranuronate. *Angew. Chem. Int. Ed. Engl.* 27, 1177-1178.
- (54) van Boeckel, C. A. A., Beetz, T., and van Aelst, S. F. (1988) Synthesis of a potent antithrombin activating pentasaccharide: a new heparin-like fragment containing two 3-*O*-sulphated glucosamines. *Tetrahedron Lett.* 29, 803-806.
- (55) Lucas, H., Basten, J. E. M., van Dinther, T. G., Meuleman, D. G., van Aelst, S. F., and van Boeckel, C. A. A. (1990) Syntheses of heparin-like pentamers containing "opened" uronic acid moieties. *Tetrahedron* 46, 8207-8228.

- (56) Jaurand, G., Tabeur, C., and Petitou, M. (1994) Synthesis of the basic disaccharide unit of heparin. *Carbohydr. Res.* 255, 295-301.
- (57) Duchaussoy, P., Leih, P. S., Petitou, M., Sinaÿ, P., Lormeau, J. C., and Choay, J. (1991) The first total synthesis of the antithrombin III binding site of porcine mucosa heparin. *Bioorg. Med. Chem. Lett.* 1, 99-102.
- (58) Lucas, R., Hamza, D., Lubineau, A., and Bonnaffe, D. (2004) Synthesis of glycosaminoglycan oligosaccharides — an unexpected inhibitory effect of a remote *N*-acetyl group upon trichloroacetimidate-mediated couplings. *Eur. J. Org. Chem.*, 2107-2117.
- (59) Castro-Palomino, J. C., and Schmidt, R. R. (1995) *N,N*-Diacetyl-glucosamine and -galactosamine derivatives as glycosyl donors. *Tetrahedron Lett.* 36, 6871-6874.
- (60) Suda, Y., Bird, K., Shiyama, T., Koshidan, S., Marques, D., Fukase, K., Sobel, M., and Kusumoto, S. (1996) Synthesis and biological activity of a model disaccharide containing a key unit in heparin for binding to platelets. *Tetrahedron Lett.* 37, 1053-1056.
- (61) Spear, P. G., and Longnecker, R. (2003) Herpesvirus entry: an update. *J. Virol.* 77, 10179-10185.
- (62) Spear, P. G. (2004) Herpes simplex virus: receptors and ligands for cell entry. *Cellular Microbiology* 6, 401-410.
- (63) Feyzi, E., Trybala, E., Bergström, T., Lindahl, U., and Spillmann, D. (1997) Structural requirement of heparan sulfate for interaction with herpes simplex virus type 1 virions and isolated glycoprotein C. *J. Biol. Chem.* 272, 24850-24857.
- (64) Liu, J., Shriver, Z., Pope, R. M., Thorp, S. C., Duncan, M. B., Copeland, R. J., Raska, C. S., Yoshida, K., Eisenberg, R. J., Cohen, G., Linhardt, R. J., and Sasisekharan, R. (2002) Characterization of a heparan sulfate octasaccharide that binds to herpes simplex virus type 1 glycoprotein D. *J. Biol. Chem.* 277, 33456-33467.
- (65) Shukla, D., Liu, J., Blaiklock, P., Shworak, N. W., Bai, X., Esko, J. D., Cohen, G. H., Eisenberg, R. J., Rosenberg, R. D., and Spear, P. G. (1999) A novel role for 3-*O*-sulfated heparan sulfate in herpes simplex virus 1 entry. *Cell* 99, 13-22.
- (66) Lee, J.-C., Lu, X.-A., Kulkarni, S. S., Wen, Y.-S., and Hung, S.-C. (2004) Synthesis of heparin oligosaccharides. *J. Am. Chem. Soc.* 126, 476-477.
- (67) Koshida, S., Suda, Y., Sobel, M., Ormsby, J., and Kusumoto, S. (1999) Synthesis of heparin partial structures and their binding activities to platelets. *Bioorg. Med. Chem. Lett.* 9, 3127-3132.
- (68) Demchenko, A. V., and Boons, G.-J. (1998) A novel and versatile glycosyl donor for the preparation of glycosides of *N*-acetylneuraminic acid. *Tetrahedron Lett.* 39, 3065-3068.
- (69) Amantini, D., Fringuelli, F., Pizzo, F., and Vaccaro, L. (2002) Selected methods for the reduction of the azido group. *Org. Prep. and Proc.* 34, 109-147.
- (70) Schwarz, J. B., Kuduk, S. D., Chen, X.-T., Sames, D., Glunz, P. W., and Danishefsky, S. J. (1999) A broadly applicable method for the efficient synthesis of α -*O*-linked glycopeptides and clustered sialic acid residues. *J. Am. Chem. Soc.* 121, 2662-2673.
- (71) Ojeda, R., de Paz, J. L., Martín-Lomas, M., and Lassaletta, J. M. (1999) A new route to L-iduronate building-blocks for the synthesis of heparin-like oligosaccharides. *Synlett*, 1316-1318.
- (72) Fukuda, Y., Sasai, H., and Suami, T. (1982) Synthetic approach toward antibiotic tunicamycins. 3. Methyl 3,4,7,8,-tetra-*O*-acetyl-10-*O*-benzyl-2-

- benzyloxycarbonylamino-2,6-dideoxy-11,12-*O*-isopropylidene- β -L-dodecodialdo-(12*R*)-furanose-(12,9)-pyranosides-(1,5). *Bull. Chem. Soc. Jpn.* 55, 1574-1578.
- (73) Ishihara, K., Kurihara, H., and Yamamoto, H. (1993) An extremely simple, convenient, and selective method for acetylating primary alcohols in the presence of secondary alcohols. *J. Org. Chem.* 58, 3791-3793.
- (74) Bai, Y., Boons, G.-J., Burton, A., Johnson, M., and Haller, M. (2000) Vinyl glycosides in oligosaccharide synthesis (part 6): 3-buten-2-yl 2-azido-2-deoxy glycosides and 3-buten-2-yl 2-phthalimido-2-deoxy glycosides as novel glycosyl donors. *J. Carbohydr. Chem.* 19, 939-958.
- (75) Tai, V. W.-F., and Imperiali, B. (2001) Substrate specificity of the glycosyl donor for oligosaccharyl transferase. *J. Org. Chem.* 66, 6217-6228.
- (76) Westman, J., Nilsson, M., Ornitz, D. M., and Svahn, C.-M. (1995) Synthesis and fibroblast growth factor binding of oligo-saccharides related to heparin and heparan sulphate. *J. Carbohydr. Chem.* 14, 95-113.
- (77) Cid, M. B., Alfonso, F., and Martín-Lomas, M. (2005) A study on the influence of the structure of the glycosyl acceptors on the stereochemistry of the glycosylation reactions with 2-azido-2-deoxy-hexopyranosyl trichloroacetimidates. *Chem. Eur. J.* 11, 928-938.
- (78) Wu, Z. L., Zhang, L., Yabe, T., Kuberan, B., Beeler, D. L., Love, A., and Rosenberg, R. D. (2003) The involvement of heparan sulfate (HS) in FGF1/HS/FGFR1 signaling complex. *J. Biol. Chem.* 278, 17121-17129.
- (79) Haller, M., and Boons, G.-J. (2001) Towards a modular approach for heparin synthesis. *J. Chem. Soc., Perkin Trans. 1*, 814-822.
- (80) Prabhu, A., Venot, A., and Boons, G.-J. (2003) New set of orthogonal protecting groups for the modular synthesis of heparan sulfate fragments. *Org. Lett.* 5, 4975-4978.
- (81) Haller, M. F., and Boons, G.-J. (2002) Selectively protected disaccharide building blocks for modular synthesis of heparin fragments. *Eur. J. Org. Chem.*, 2033-2038.
- (82) Seeberger, P. H., and Werz, D. B. (2005) Automated synthesis of oligosaccharides as a basis for drug discovery. *Nat. Rev. Drug Disc.* 4, 751-763.

PART II:
Investigations into the Mechanism of Inactivation of RTPR by Gemcitabine
Triphosphate.

Chapter 4
Ribonucleotide Reductases: Mechanism and Inhibition

4.1 Overview

Ribonucleotide reductase (RNR) is a key enzyme, found in nearly all organisms—mammals, plants, single-celled eukaryotes and prokaryotes, even some viruses.(1-7) RNR catalyzes the reduction of nucleotides to 2'-deoxynucleotides, generating the pools of these molecules vital to DNA synthesis and repair. RNRs all catalyze the basic reaction shown in Figure 4-1, in which nucleoside di- or triphosphates (NDPs or NTPs) are reduced to the corresponding deoxynucleoside di- or tri-phosphates (dNDPs or dNTPs).(1) In all cases, the nucleotides accepted are adenosine (A), uridine (U), guanosine (G), and cytidine (C). The reaction involves abstraction of the indicated 3' hydrogen, loss of water from the 2' position, and reduction of the intermediate to the deoxynucleotide product.

Nucleotide reductase activity was first observed in living organisms by Rose and coworkers,(8) and identified in cell lysates by Reichard and coworkers.(9) The *E. coli* ribonucleoside diphosphate reductase (RDPR), an iron-dependent enzyme, was later purified by this group.(10, 11) Thelander and coworkers demonstrated that the mammalian RNR is also an iron-dependent enzyme of this type, which became known as class I RNR. Blakley and coworkers discovered an adenosylcobalamin (AdoCbl) dependent ribonucleoside triphosphate reductase (RTPR) in *L. leichmannii*, the class II enzyme.(10, 12) Most recently, the class III, S-adenosylmethionine (SAM) dependent enzyme has been identified as the RNR utilized by strict and facultative anaerobes growing under anaerobic conditions.(13-17) RNRs differ in substrate specificity: all class I enzymes and many class II accept only diphosphates as substrates (ribonucleoside diphosphate reductases, RDPR), while class III and some class II enzymes accept only triphosphates as substrates (ribonucleoside triphosphate reductases, RTPR). All RNRs have been shown to use protein-centered radicals to initiate the radical dependant

nucleotide reduction process. The protein and substrate-based radical intermediates generated by the enzyme are protected from side reactions by the structure of the active site.

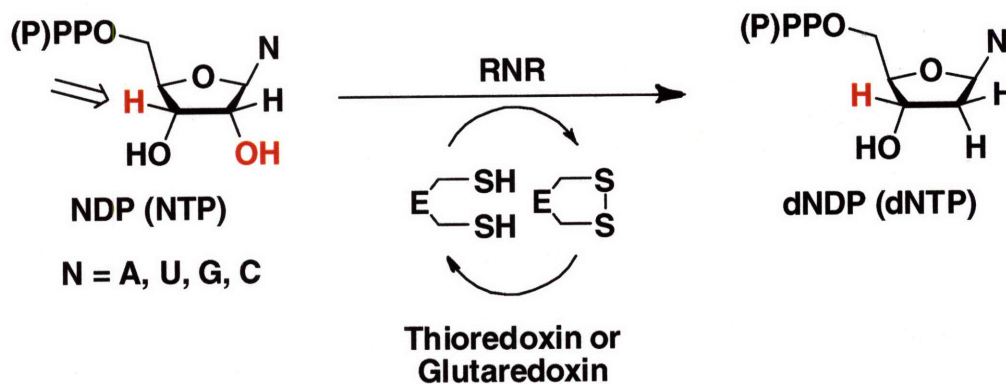


Figure 4-1. The ribonucleotide reduction reaction.

Inhibition of these enzymes has been the subject of a great deal of research.(4, 18-26)

From a medical perspective, RNR has gained prominence as a target for both anti-viral(27) and anti-tumor agents.(18, 25, 28, 29) Inhibitors have also been useful tools for the elucidation of the mechanism of these enzymes.(4) A wide range of strategies have been employed in the inhibition of RNRs, including disruption of subunit-subunit interactions, disruption of the diiron cluster of class I enzymes by chelation of the iron, elimination of the class I tyrosyl radical, and mechanism-based inhibition.(18-22, 25, 30) Mechanism-based inhibitors take advantage of the natural enzymatic reaction to selectively destroy enzyme activity: typically, the enzyme is able to initiate reaction normally with a mechanism-based inhibitor, but the alternate substrate forms a reactive intermediate that eliminates enzyme activity through covalent modification, formation of a tight-binding complex, or other damage to the active site. Understanding the mechanism of reaction of enzymes with substrate analogs can provide insight into the natural mechanism in a manner unachievable using only the normal substrate.

Enzymes utilizing radical chemistry

Free radicals have earned a bad reputation in popular culture as contributors to aging, DNA damage and cancer, and indeed uncontrolled radicals within biological systems can lead to a wide range of oxidative damage. However, the chemistries made possible by the controlled use of radical reactions are diverse and powerful tools in the hands of organic chemists.(31-33) Nature has found many ways of its own to harness the power of free radicals, and over the last thirty years, many enzymatic reactions employing radical chemistry with exquisite specificity have been elucidated.(5, 7, 13, 15, 16, 34-45) Most enzymes utilizing radical chemistry require a metal cofactor, commonly iron, cobalt, manganese or copper, for initial generation of the radical.(36) The most common cofactor is *S*-adenosylmethionine (SAM), which also generates a 5'-deoxyadenosyl radical through one-electron reduction catalyzed by a [4-Fe-4-S] cluster.(13, 15, 39-41, 43, 46-48) In pyruvate-formate lyase, the initial 5'-deoxyadenosyl radical generates a glycy radical on the protein that catalyzes the reaction of pyruvate and coenzyme A to acetyl-CoA and formate. Adenosyl cobalamin (AdoCbl) is a common cofactor for radical reactions, believed to generate a 5'-deoxyadenosyl radical by homolysis of the cobalt-carbon bond. Diol dehydratase and ethanolamine ammonia lyase, which respectively catalyze the transformation of ethylene glycol and ethanolamine to acetaldehyde, are two particularly well characterized examples of AdoCbl-dependent enzymes employing radical rearrangements.(39, 41, 49, 50) Radicals, typically generated by metal cofactors, also play critical roles in respiration and photosynthesis, cyclooxygenases, galactose oxidase and many other reactions within living systems. Some enzymes utilize amino acid radicals for catalysis: common radical harboring residues are glycine, tyrosine, tryptophan, and cysteine.(5, 51) RNRs are the paradigm for enzymes requiring protein radicals, displaying a range of radical initiation chemistries, but a

unifying reaction mechanism involving amino acid-centered radicals.(4-6, 52, 53) The radical chemistry in RNR demonstrates the exquisite control enzymes can hold over these reactive intermediates, and the importance of radical transformations in biology.

4.2 Ribonucleotide Reductases

Nucleoside Metabolism

RNRs play a central role in nucleotide metabolism: most organisms cannot subsist on deoxynucleosides, instead producing dNTPs from nucleotide precursors.(1, 3, 52, 54) RNRs are critical to maintaining the pools of deoxynucleotides in organisms, both the low levels needed for normal maintenance and the larger pools that must be generated in response to DNA damage or for replication.(55-58) The balance and absolute levels of the dNTPs pools are maintained by a complex process of allosteric regulation, where deoxynucleotide triphosphates (dNTPs) and ATP bind to the proteins, altering the active site affinity for various nucleotide bases.(59-62) It has been speculated that an early RNR was the protein that made the transition from an RNA to DNA world possible. The ancestral enzyme has been speculated to be most similar to either the anaerobic class III or the oxygen-independent class II.(63-68) Sequence similarity is low across classes, making it difficult to develop clear phylogenetic trees. Consequently, the evolution of RNRs is a hotly debated area.

Structural features of ribonucleotide reductases

RNRs are complicated enzymes both structurally and mechanistically, and many variations exist in nature.(1, 3, 4, 6, 52-54, 69-72) All RNRs possess a large (80-130 kDa) “ α ” subunit where the catalytic conversion of nucleotides to deoxynucleotides takes place and

containing the five cysteines essential for the reduction process.(73, 74) This subunit also harbors binding sites for allosteric effectors, which control the specificity of the reduction reaction, and the “activity site,” which modulates the rate of nucleotide reduction (Figure 4-2). The source of the radical initiator is the basis for the division of RNRs into their three major classes.(1) The class I enzymes are dependent on a diferric-tyrosyl radical ($Y\cdot$) harbored in a second “ β ” subunit, which is generated in an oxygen and reductant dependent manner. Two major variations of this class are known, designated class Ia and Ib. Eukaryotes all contain enzymes of class Ia, while some bacteria express Ia, some Ib, and some both. Recently, a class Ic has been discovered, which possesses a phenylalanine in place of the widely conserved β -subunit tyrosine, yet has been shown to catalyze nucleotide reduction *in vitro*.(75) Both α and β function as homodimers in this class. The active forms of these enzymes are often designated $\alpha_2\beta_2$, but their precise quaternary structures remain an open question. The class II enzymes are all AdoCbl dependent, and function both in the presence and absence of oxygen. These enzymes are found in certain prokaryotes, and are either α (as is the best known *L. leichmannii* RTPR)(76) or α_2 , with the initiation role of the class I β subunit fulfilled by AdoCbl. Some class II enzymes, including that of *L. leichmannii*, lack an activity site (Figure 4-2 B). The class III enzyme(14, 15, 77) is expressed under anaerobic conditions and utilizes a β unit containing a SAM/[4Fe4S]⁺⁺ cofactor to generate a catalytic glycy radical in the α subunit.(78)

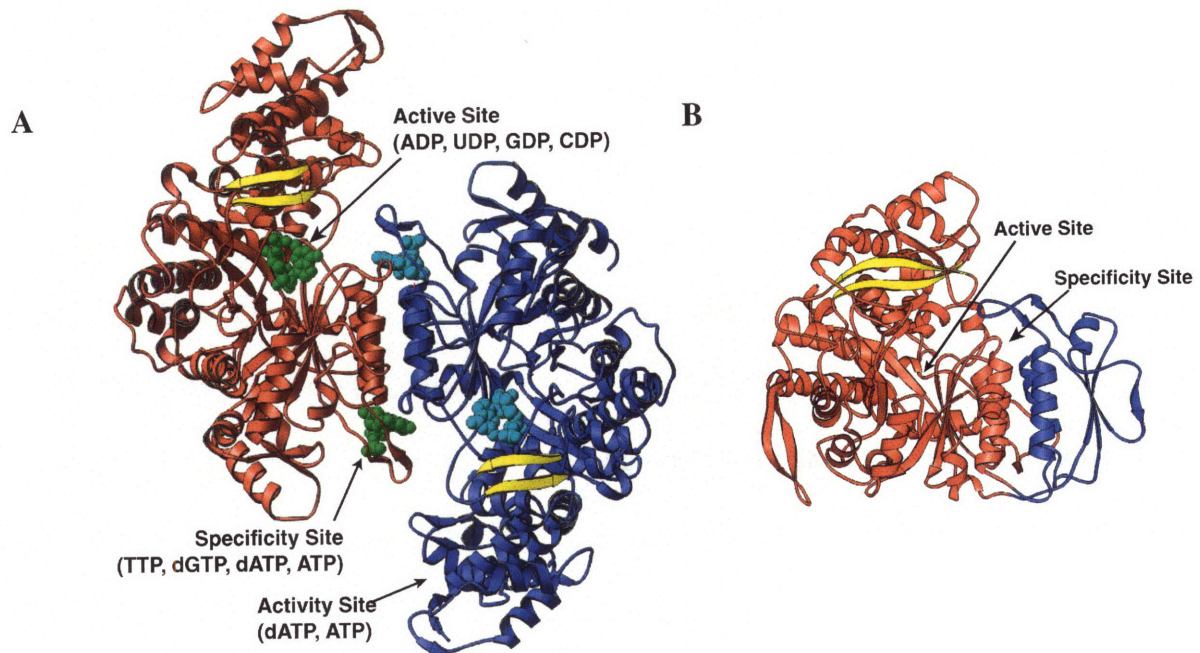


Figure 4-2. Crystal structures of the α subunits of *E. coli* class I (A)(79) and *L. leichmannii* class II (B)(80) RNR. The active site, specificity site, and activity sites are indicated.

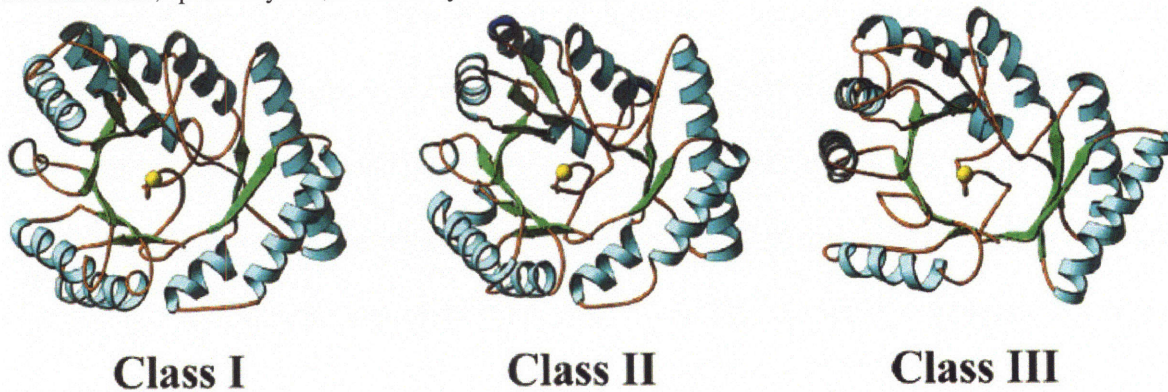


Figure 4-3. A comparison of the α/β barrel fold found in the three classes of RNR.(80) The yellow sphere represents the active site cysteine that is the site of the catalytic thiyl radical.

The crystal structures of at least one representative of each class and subunit have been solved, with the exception of the class III β activating enzyme.(1, 2, 71, 72, 79-89) In the α structures, many common features and a unifying fold are seen (Figure 4-3). Structural homology between members of class I and class II is particularly high.(61, 80) The first α structure solved was of the *E. coli* enzyme(79) and revealed a 10 strand α/β barrel core common to all α structures solved to date.(88) The binding sites for the effector are found on the dimer

interface, and are composed of residues from both α subunits. The ATP binding site is found at the N-terminus of the α subunit, which forms an ATP cone domain. The C-terminal tail is flexible and not visible in any crystal structures.

The *L. leichmannii* class II crystal structure(80) shares many features with the class I α subunit (Figure 4-3 B). The active site is formed by a similar barrel and active site residues are positioned similarly. There is no ATP-binding cone domain, and the effector binding site is created by an appended domain that reproduces the class I dimer interface. The *L. leichmannii* structure with an AdoCbl analog (adeninylpentylcobalamin) bound reveals a unique B₁₂ binding site near the active site (Figure 4-4). This binding site does not resemble AdoCbl binding sites on other B₁₂ enzymes, even those that appear to catalyze similar chemistry to RNR such as diol dehydratase.(80) Instead, the cofactor binds through contacts with two key β strands (residues 570-578 and 602-610 in the *L. leichmannii* structure) that have close structural homology to β strands present in class I structures (residues 641-647 and 650-655 in the *E. coli* enzyme). Thus, it appears that the AdoCbl binding site in class II bears more similarity to regions of the class I structure than to binding sites for the cofactor in other AdoCbl-dependent enzymes.

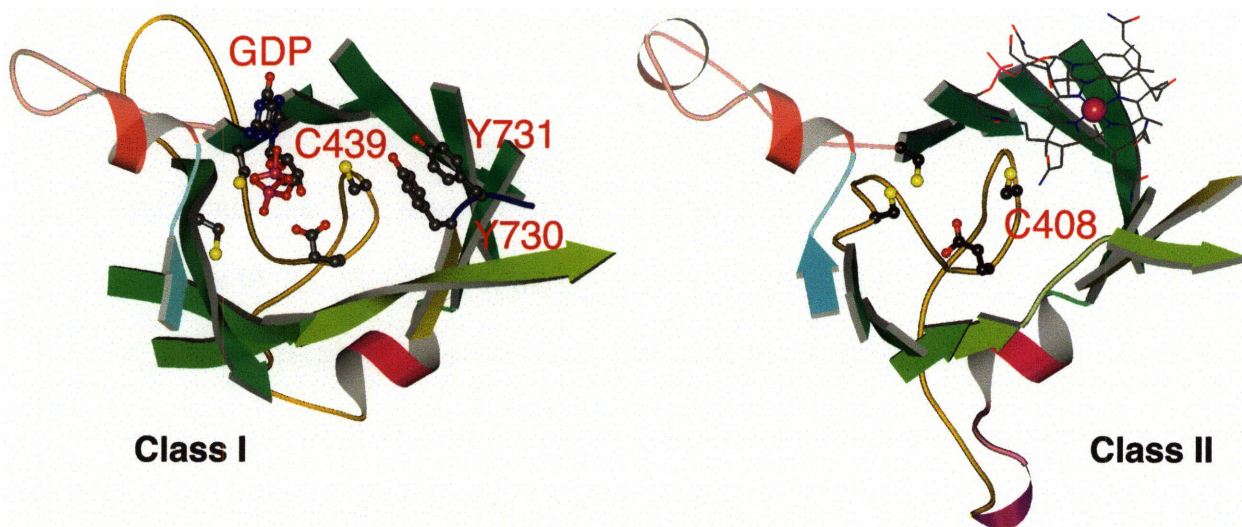


Figure 4-4. The active site of *E. coli* class I(79) and *L. leichmannii* class II(80) RNR. The latter shows the binding site of the AdoCbl cofactor.

Features of the RNR active site

The active sites of the class I and II RNRs are very similar across enzymes (Figure 4-5). Key features are a “top-face” cysteine, positioned above the plane of the ribose ring, (C439 in *E. coli* RDPR, C408 in *L. leichmannii* RTPR), believed to be the site of the thiyl radical that initiates nucleotide reduction, and a pair of “bottom-face” cysteines (C225 and C462 in RDPR, C119 and C419 in RTPR) that provide the reducing equivalents. All three of these cysteines have been shown to be essential for catalysis by mutagenesis studies(90) and are confirmed to be in the active site by multiple crystal structures.(2, 79, 80) The other catalytically essential active site residues are a glutamate (E441 in RDPR, E410 in RTPR) and an asparagine that hydrogen bonds to it.(91, 92) The cysteine that provides the active site thiyl radical, the glutamate and the asparagine lie on a hairpin loop that extends into the active site. The other two essential cysteines lie on β -strands on the inner wall of the α/β barrel. Recent structures of the *S. cerevisiae* class I enzyme with substrate and effector bound show the interactions with the active site residues.(93) The top-face cysteine (C428 in this enzyme) is positioned near the 3' hydrogen on bound nucleotides. One of the bottom-face cysteines is found within hydrogen bonding distance of the substrate 2' and 3' hydroxyls (C218), while the other (C443) is more remote. The essential glutamate (E430) is positioned such that it is hydrogen-bonded to the substrate 3' hydroxyl, as is the essential asparagine (N426).

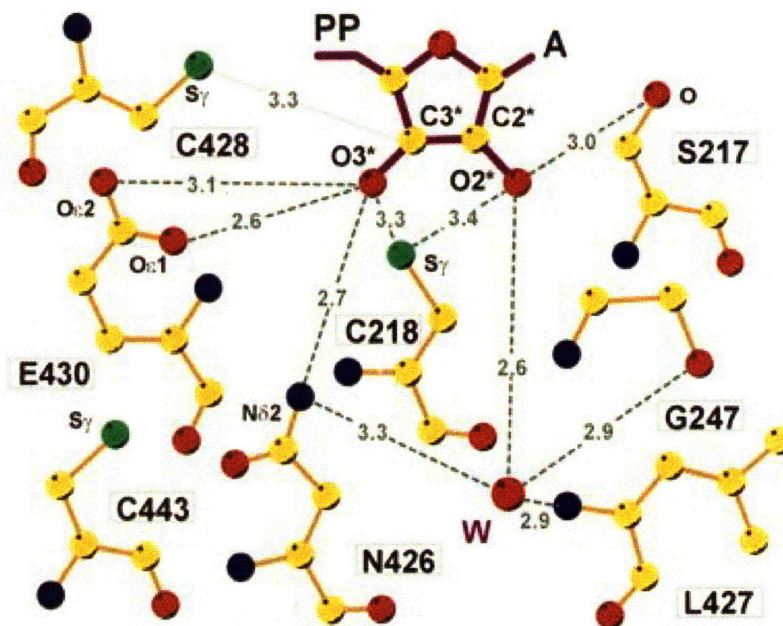


Figure 4-5. The active site of *S. cerevisiae* class I with ADP bound (figure by Dealwis and coworkers),(93) The “top-face” cysteine (C428) is positioned above the plane of the ribose ring, while the “bottom-face” reducing equivalents (C218 and C443) are below it. The residues E430 and N426 are essential for catalysis as well, proposed to be involved in the deprotonation of the nucleotide 3'-OH.

Radical initiation

The initiator of the reduction reaction is a thiyl radical generated in the active site of the enzyme, and the major differences between the classes are the method by which this radical is produced. The $Y\cdot$ essential for radical initiation in class I enzymes begins with the assembly of the diferric cluster in β . The mechanism of cluster assembly is an area of active research, and a detailed discussion of the evidence for each proposed intermediate is beyond the scope of this chapter.(72, 94, 95) During cluster assembly, a nearby tyrosine (β Y122) is oxidized to $Y\cdot$, easily visualized by its distinctive absorbance spectrum with a maximum at 410 nm.

Once the $Y\cdot$ is generated, the radical must somehow reach the active site of the α , $\sim 35\text{\AA}$ away based on docking models using the *E. coli* α and β subunits.(96, 97) This process is kinetically masked, and the EPR and UV-vis spectra of this tyrosyl radical do not disappear during turnover. It has been proposed that the radical is transferred to the active site for each

reaction, then transferred back to the β -subunit tyrosine at the end of each catalytic cycle.(98)

The distance is too great for the radical to tunnel on a rapid enough timescale. Thus, an electron transfer or proton-coupled electron transfer (ET/ PCET) pathway has been proposed, wherein the radical is shuttled to the surface of β through a series of amino acids (β Y122, W48), transferred to the α subunit through the proposed intermediacy of a tyrosyl radical (β Y356) on the C-terminal tail of the β subunit, then continuing through the PCET pathway in the α subunit (α Y731 and Y730).(1, 89, 98) Docking models indicate a distance of 25Å between β W48 and α Y731, and it is proposed that β Y356 transfers the radical through a conformational change that allows it to move from proximity to β W48 to α Y731, carrying the radical with it. Evidence for the importance of β Y356 in the radical transfer is strong, based on the incorporation of unnatural amino acids into this position with altered reduction potentials.(98-103) The use of fluorinated tyrosines in these positions produced enzymes with altered pH-rate profiles related to the pKa of the unnatural amino acid used, and a decrease in reduction activity as the reduction potential of the substituted amino acid increased.(104-106)

In the class II system, AdoCbl is believed to generate the active site thiyl radical directly upon binding to the enzyme.(50) The binding pocket for AdoCbl in *L leichmannii* RTPR is unique amongst AdoCbl enzymes, and binds very weakly. Extensive kinetic studies indicate that the thiyl radical is generated in a coupled fashion, with homolysis of the C-Co bond concurrent with abstraction of a hydrogen atom from the active site cysteine (detailed in the next section).(107) The 5'-deoxyadenosyl radical is not thought to exist as a free species in this transformation. The radical exchange occurs even in the absence of substrate, as evidenced by isotope incorporation from solvent into the deoxyadenosine, the scrambling of stereospecifically deuterated 5'-deoxyadenosine AdoCbl upon incubation with RTPR,(108) and the decomposition

of AdoCbl to hydroxycobalamin (HOCbl) upon addition to RTPR. The homolysis of the C-Co bond is an oxygen independent process, with oxygen neither required as in the class I system or hindering, as in class III, allowing class II enzymes to function under both aerobic and anaerobic conditions.

The class III system is dependent on a $[4Fe4S]^{++}$ cluster to generate a 5'-deoxyadenosyl radical through reduction of a SAM cofactor on the class III β subunit.(14, 15, 77) This radical abstracts a hydrogen atom from a glycine, which in turn generates the active site thiyl radical. Each glycy radical catalyzes many turnovers before regeneration by the activating enzyme. The glycy radical is oxygen sensitive, and is destroyed rapidly under aerobic conditions.

The physical placement of the radical precursors and the active site thiyl radical are very similar across all three classes, lending support to the notion of disparate radical precursors feeding into a common mechanism. Figure 4-6 shows crystal structures from class I, II, and III enzymes overlaid with the top-face cysteines in the same location. In the overlaid structures, it is also clear that the terminal residues of the class I ET pathway (*E. coli* Y731, Y730), the class II AdoCbl, and the class III glycy radical all lie very close in space as well. Upon substrate binding, the thiyl radical initiates a cascade of transformations resulting in nucleotide reduction.

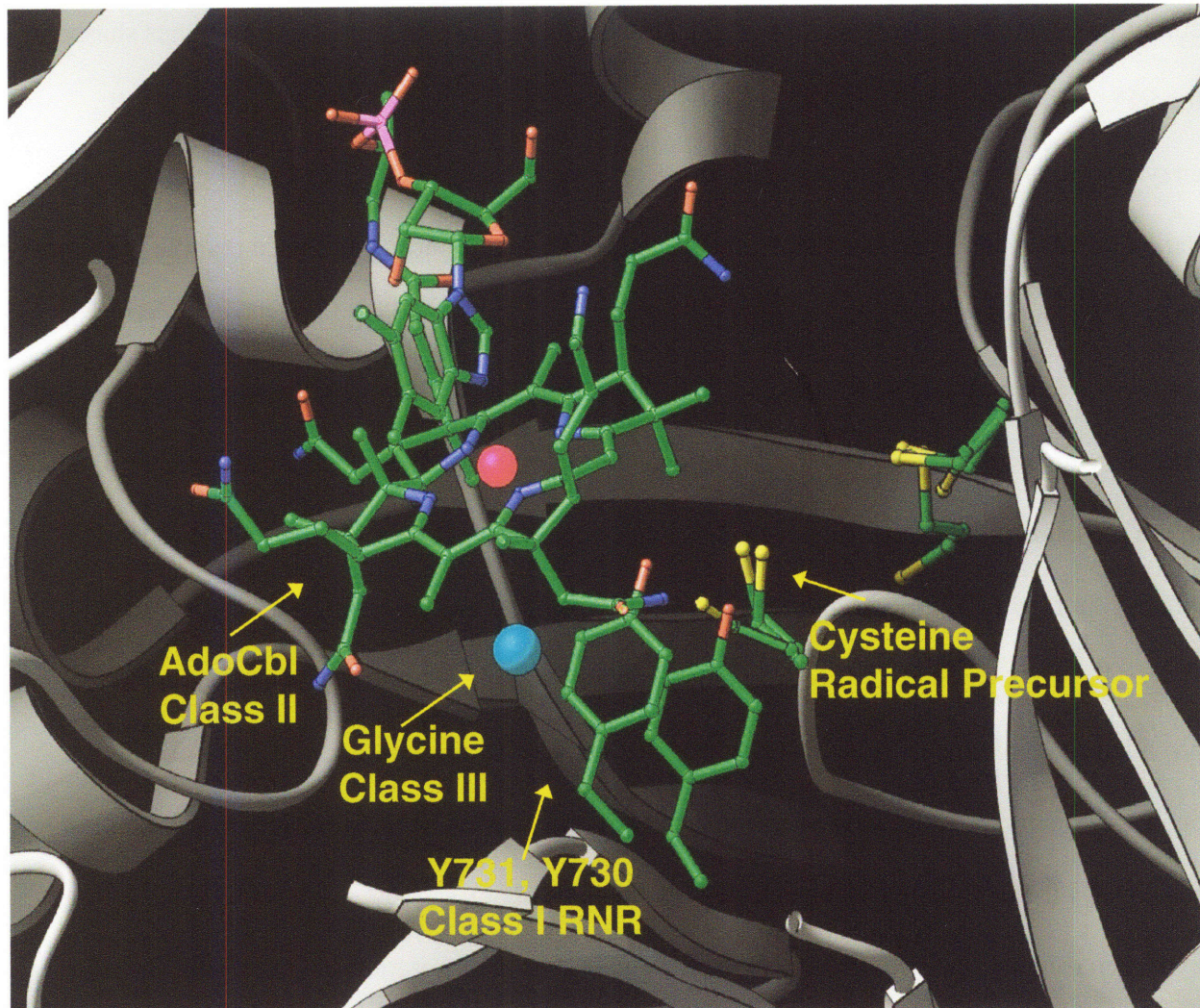


Figure 4-6. Generation of the thiyl radicals in the active site of RNRs.(80)

Mechanism of nucleotide reduction

The mechanism of RNR with its natural substrates is now fairly well established (Figure 4-7).(4, 5, 74, 109, 110) The first step (4-1 to 4-2) is the abstraction of the 3' hydrogen atom: early isotope studies with 3'-[³H]-UDP on the *E. coli* enzyme revealed an isotope effect that varied as a function of buffer pH and the effector used, and that a small amount of [³H]₂O was released during turnover.(111) The abstraction is performed by a top-face thiyl radical; in the class II system, this thiyl radical has been observed by EPR spectroscopy to be exchange-coupled to cobalt and shown to be kinetically competent.(112) Using RTPR grown under

conditions that allow incorporation of β -[^2H] cysteine in place of all normal cysteines sharpens the RFQ-EPR signal of the initial radical formed (at 22 ms) on the *L. leichmannii* class II enzyme, indicating that these deuteriums are coupled to the radical. This Co(II)-coupled thiyl radical forms at the same rate that Co(II) is generated, giving strong evidence that the homolysis of the Co-C bond is giving rise to the new radical. Analogous experiments with 5'-[^2H]-AdoCbl show no effect on the EPR spectrum.(112) The formation of Co(II) and the associated coupled radical occur with k_{obs} of 40 s^{-1} in the presence of effector and absence of substrate, and $>200\text{ s}^{-1}$ in the presence of substrate, making it kinetically competent to catalyze nucleotide reduction, which occurs with a turnover number of $1\text{-}2\text{ s}^{-1}$ depending on substrate/effector pair.(107)

Further evidence for this thiyl radical abstracting the 3' hydrogen of the nucleotide is provided by experiments with 3'- ^3H -UDP that showed no incorporation of [^3H] into 5'-deoxyadenosine (5'-dA) released upon rapid chemical quench of this reaction on the ms time scale.(113) If the 5'-dA radical generated by AdoCbl homolysis were abstracting the substrate hydrogen directly, one would have expected significant incorporation of this tritium into the reduced 5'-dA. Conversely, using 5'-[^3H]-AdoCbl, tritium is washed into the solvent at a calculated rate of 4.8 s^{-1} when incubated with RTPR, dGTP, and TR/TRR/NADPH reductant.(112) This result indicates the Co-C bond homolysis generates a radical through abstraction of a hydrogen atom from a solvent-exchangeable position. When this new radical re-abstracts a hydrogen atom from 5'-dA, a tritium can be taken instead, and exchanged with water. This observation provides further evidence for the formation of an intermediate protein radical by AdoCbl. While this radical has been directly observed only in the case of the *L. leichmannii* enzyme, an isotope effect is also observed when using 3'-[^3H]-NDPs in the *E. coli*, suggesting 3'-C-H bond cleavage is involved in the mechanism.(114, 115)

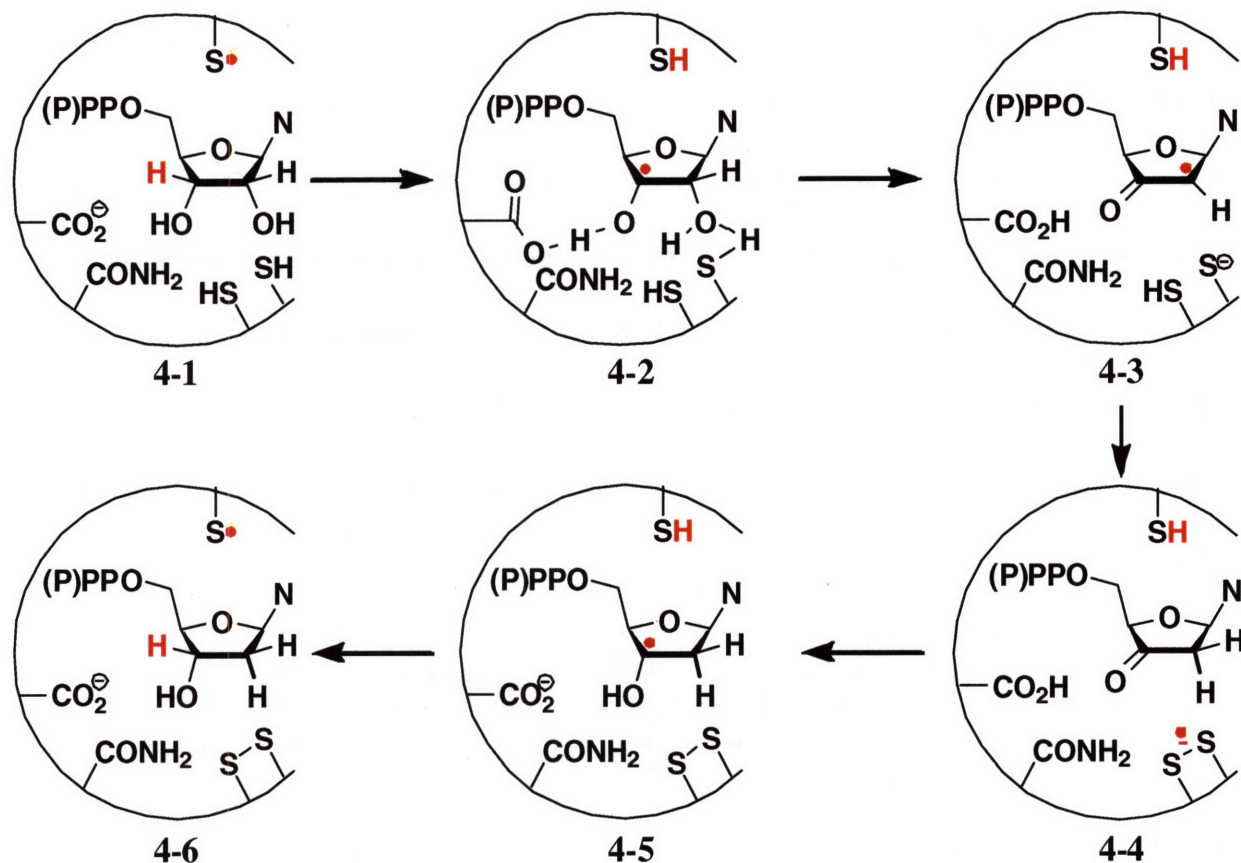


Figure 4-7. Proposed mechanism of nucleotide reduction by RNR.

After generation of 3' radical **4-2**, the next step in the reduction mechanism is loss of the water from the 2' position with protonation from a bottom face cysteine to generate 2' α -keto radical **4-3**. This process is accompanied by deprotonation of the 3' hydroxyl by the active site glutamate. The timing of deprotonation of the 3'-OH and loss of water leads to different chemically plausible mechanisms. The formation of **4-3** could follow radical-anion mechanism, where deprotonation occurs first and loss of the water is driven by the formation of negative charge. Also possible is a radical-cation mechanism, where protonation and loss of the 2'-hydroxyl precedes deprotonation and formation of the α -keto radical. (4, 6, 116) Finally, these steps could be happening in a concerted fashion, with simultaneous deprotonation of the 3' hydroxyl and protonation/loss of the 2'-hydroxyl as water. These possibilities cannot be

distinguished by available experimental data, but several model systems give insight into this process. The one-electron oxidation of ethylene glycol provides a good model for the 2',3'-diol of the nucleotides in reduction by RNR.(116-118) When oxidized with either H₂O₂/photolysis or H₂O₂/titanous ion in the absence of acid, ethylene glycol forms the α-hydroxy radical **4-7** as detected by EPR. In the presence of acid (~pH 2.5) the EPR spectrum changes markedly, indicating the presence of the acetaldehyde radical **4-8**. This result indicates that an acid-catalyzed, radical-cation mechanism can account for the dehydration of this type of radical system.

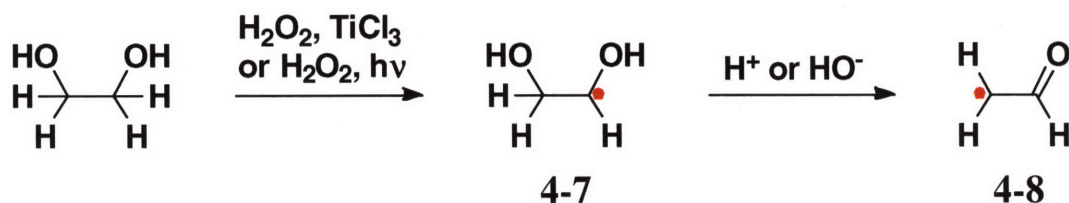


Figure 4-8. One electron oxidation of ethylene glycol.(116-118)

However, it is also apparent that this type of dehydration can be catalyzed by base. A 3'-selenocarbonyl adenosine (Figure 4-9) model system, wherein the radical is generated selectively at the 3' position by photolysis, eliminates the 2' hydroxyl exclusively under basic conditions, and not under acidic conditions.(119) Studies of ethylene glycol radicals generated using pulsed radiolysis demonstrate that the dehydration can be generated both by H⁺ and OH⁻, and are several orders of magnitude faster in each case than the uncatalyzed decomposition.(120, 121) It is clear from studies involving mutant enzymes that neither deprotonation by the glutamate nor protonation by a bottom face cysteine is strictly necessary to catalyze dehydration of the substrate. The *E. coli* E441Q mutant,(91, 92, 122) which would not be expected to be able to undergo base catalysis, and the C225S and C462S mutants (and their RTPR analogs),(90, 123) which should not be able to undergo acid-catalyzed dehydration, both seem to undergo abstraction of the 3'-hydrogen and subsequent dehydration. In all cases, the elimination of base

is seen, indicative of formation of the α -keto radical and reduction to form a 3'-keto, 2' deoxy nucleotide (as in the case of the 2'-monohalo inhibitors discussed below, Figure 4-12). It is plausible that the dehydration may be catalyzed by either mechanism in the active site, or that a concerted 3'-deprotonation, 2' protonation catalyzes the dehydration in the wild type enzyme.(116)

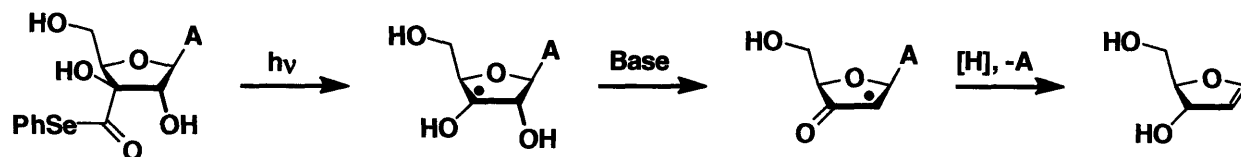


Figure 4-9. Selenocarbonyl nucleotide model system of Giese and coworkers.(119)

Regardless of the mechanism of dehydration, this radical can be reduced by the bottom-face cysteines to generate a 3'-keto nucleoside and a disulfide radical anion (4-4, Figure 4-7). It is proposed that the reduction occurs by single electron transfer from the thiolate generated when water is eliminated from 4-3, either coupled with proton transfer from the other bottom-face cysteine or with direct generation, then rapid protonation of an enolate anion.(4, 124) The reduction of the α -keto acetaldehyde radical by DTT was found to be several orders of magnitude greater at pH 10 than at pH <8.4, indicating the thiolate is the preferred reductant.(124) This reduction would generate a disulfide radical-anion on the bottom face of the nucleotide, allowing reduction of the ketone by the radical-anion with return of the proton from the glutamate (4-5).(116) A buildup of a disulfide radical anion has been detected by EPR spectroscopy in the E441Q mutant of *E. coli* RDPR,(125) and is the only RNR system where this radical has been directly observed. The final step in the mechanism (4-5 to 4-6, Figure 4-7) is return of the same hydrogen atom to the 3' position that was abstracted to initiate the reaction, with regeneration of the top-face thiyl radical (4-6).

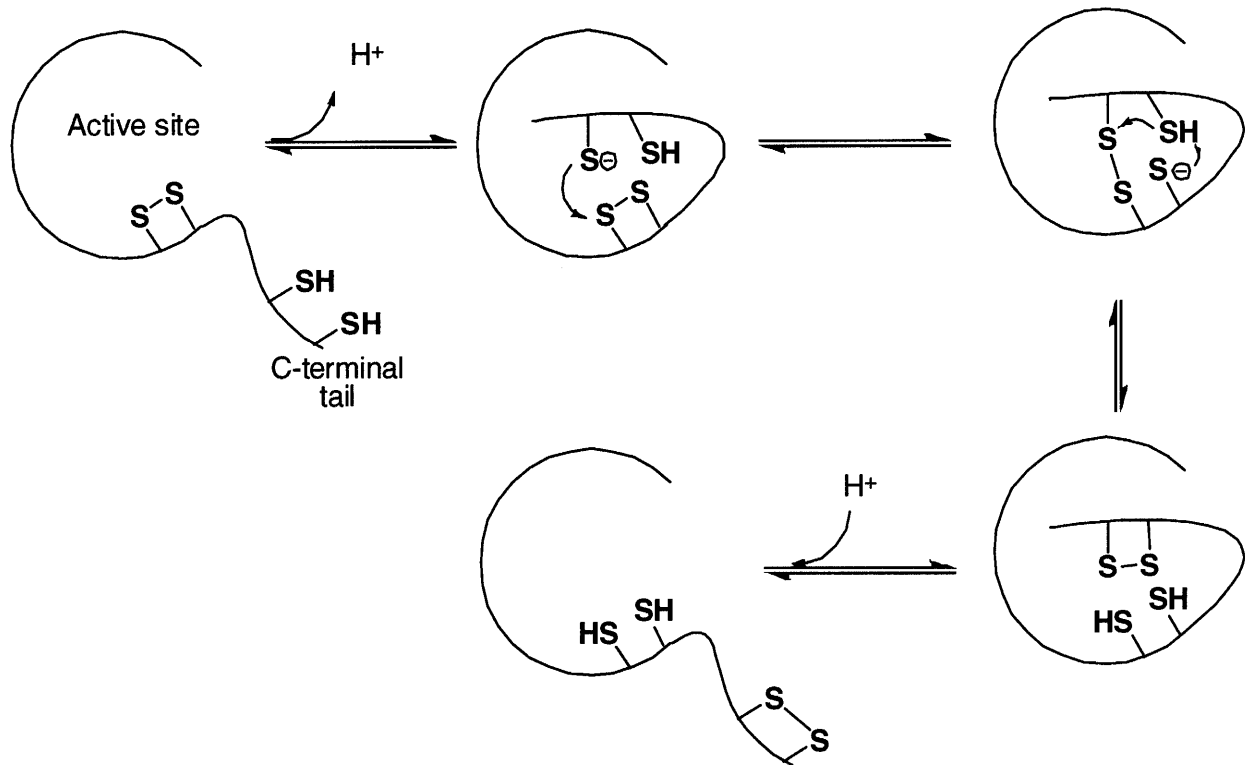


Figure 4-10. Disulfide interchange from the active site to the C-terminal tail. The tail is presumed to enter the active site after turnover, and the disulfide is transferred from the oxidized active site to the tail cysteines.

The initial state of the enzyme is then regenerated by reduction of the disulfide in the active site (Figure 4-10).(73) This reduction is mediated by a second pair of cysteines on the C-terminal tail (C749 and C754 in the *E. coli* RDPR, C733 and C736 *L. leichmannii* RTPR) of the enzymes, which is believed to enter the active site after product release and reduce the active site disulfide by disulfide interchange.(74, 90, 123, 126, 127) The limiting step in turnover of the *L. leichmannii* class II enzyme is believed to be this re-reduction (or a conformational change associated with this chemistry).(128) These C-terminal cysteines are in turn reduced by disulfide interchange with thioredoxin (TR) or glutaredoxin, themselves reduced by thioredoxin reductase and glutaredoxin reductase, respectively. These enzymes are reduced by NADPH, the ultimate source of reducing electrons. The reduction system of class III RNR differs from the others: it

possess only one active-site cysteine apart from the catalytic thiyl radical, does not have a C-terminal cysteine pair, and the reducing equivalents are provided by formate.(1, 3, 129, 130)

4.3 Inhibitors of RNRs

A wide range of strategies have been applied to inhibit RNRs. Many known inhibitors are nucleoside analogues, of which the 5'-diphosphate or 5'-triphosphate forms can act as mechanism-based or competitive inhibitors (Figure 4-11).(109) Nucleotide analogues inactivate RNR through a range of mechanisms: destroying the radical cofactor (Y^{\bullet} , AdoCbl, or G), specific or non-specific alkylation of α , or a combination of α and β inhibition. Mechanism-based inhibitors have been useful probes of the mechanism of RNRs, but few successfully inhibit RNR *in vivo*. However, in the past decade, gemcitabine (2',2'-difluorodeoxycytidine, F₂C) (131-133) and tezacitabine (2'-fluoromethylene cytidine, FMC)(122, 134, 135) have been developed into successful anti-tumor agents.(30)

In addition to mechanism-based inhibitors that bind at the RNR active site, nucleotide analogues (clofarabine) can also compete with effector binding.(18) Other classes of inhibitors target the β subunit of class I RNR exclusively,(18) quenching the tyrosyl radical (hydroxyurea)(136-140) or destroying the diferric cluster (thiosemicarbazones).(141, 142) Finally, disruption of α - β interactions by small molecule peptidomimetics has been successful, as the interaction is largely governed by the 20 amino acid C-terminal tail of β .(22) Species specificity has been achieved as this region is highly diverse between human, bacterial, and viral enzymes. A survey of RNR inhibitors and an examination of their mechanism is discussed in the remainder of this chapter.

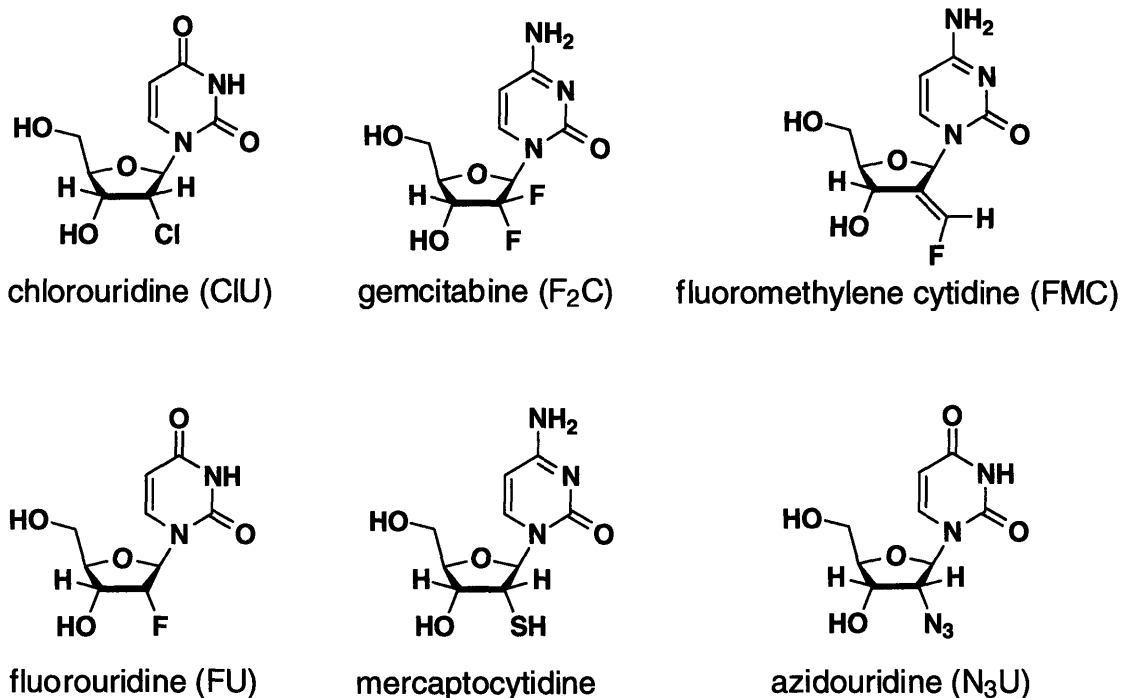


Figure 4-11. Some nucleoside analog inhibitors of RNR. The active inhibitors are the 5'-diphosphates (for RDPR) or triphosphates (for RTPR).

2'-Halonucleotides

Among the first mechanism-based inhibitors studied were the 2'-monohalo-2'-deoxy-nucleotides.⁽¹⁴³⁾ These compounds were shown to irreversibly inhibit α of *E. coli* and mammalian RNRs,^(144, 145) as well as *L. leichmannii* RTPR.^(146, 147) Inactivation of the enzyme is accompanied by the elimination of base and pyrophosphate, and the generation of a new chromophore with an absorption maximum at 320 nm. The mechanism proposed for inhibition by these compounds is shown in Figure 4-12.⁽⁶⁾ Initiation is expected to proceed as in the normal reaction mechanism, with a hydrogen atom abstracted from **4-9** to generate **4-10**. The key difference in the reaction with the 2'-halonucleotides, as compared to the mechanism with the natural substrates (Figure 4-7), comes in the next step. Due to their better leaving group ability and lower pK_a , halides can leave without protonation from the bottom cysteine to give **4-11**. Model studies of the oxidation of 2-chloroethanol with H₂O₂/titanous ion support this

mechanism: 2-chloroethanol can be reacted to the acetaldehyde α -carbonyl radical in the absence of the acid or base catalysis that is required to see rapid elimination of water in the case of ethylene glycol.(117, 118) This system indicates Cl^- can be eliminated without need for leaving group protonation or deprotonation of the alcohol.

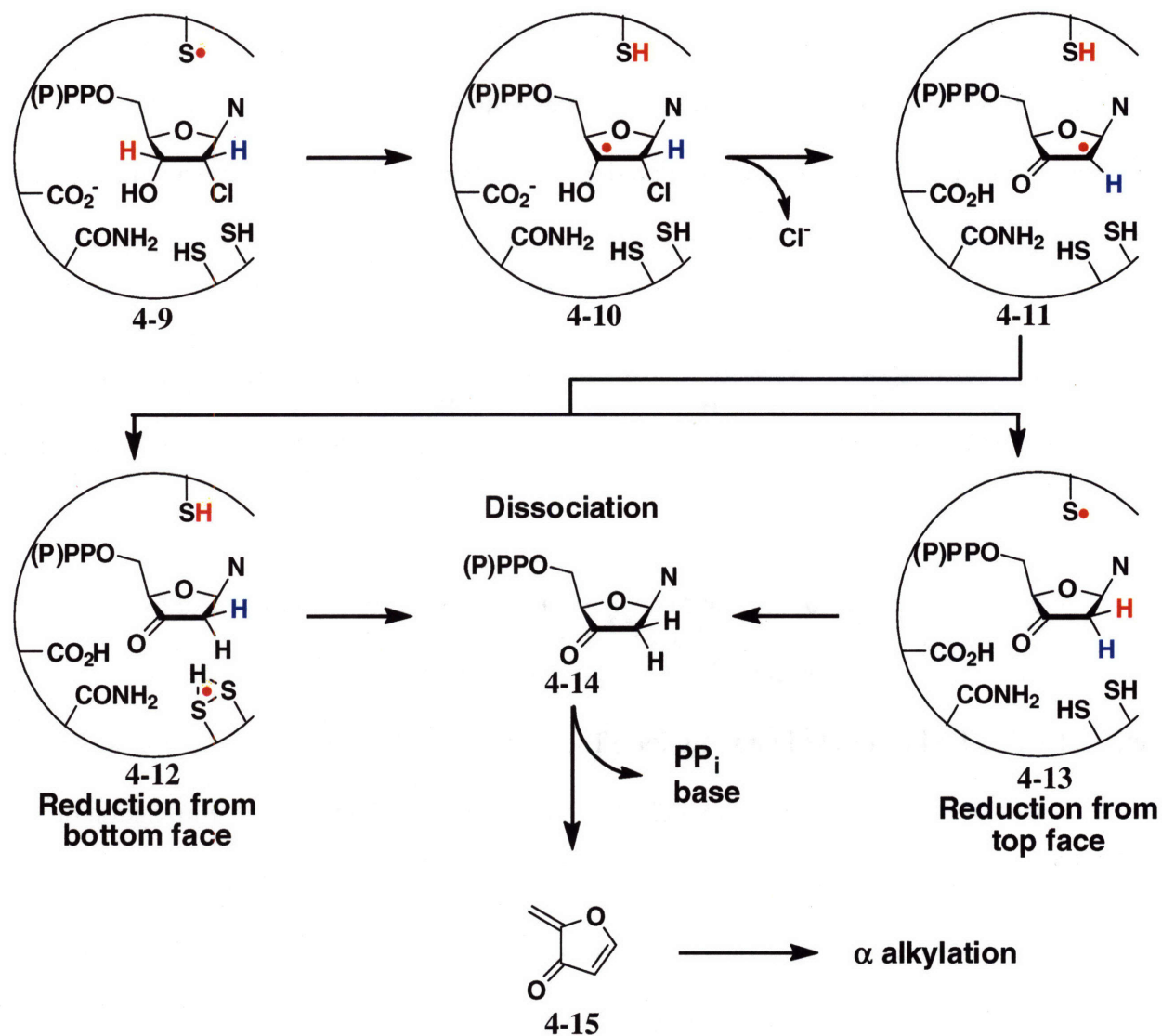


Figure 4-12. Inhibition of RNR by 2' halonucleotides.

From 4-11, reduction must proceed by abstraction of a hydrogen atom from an active site cysteine, rather than by electron transfer from a thiolate, as proposed for the natural substrates. Studies with $3'-[^2\text{H}]\text{-UDP}$ demonstrated that this reduction can occur from the top face cysteine

(**4-12**), as well as the bottom face cysteine (**4-13**).⁽¹⁴⁸⁾ In the former case, the deuterium can be transferred from the 3'-position to the 2'-position, indicating its return by the top face cysteine after its initial abstraction from the 3' carbon. This rearrangement is strikingly similar to more typical AdoCbl-requiring enzymatic reactions,^(49, 149-151) in particular, diol dehydratase and ethanolamine ammonia lyase (Figure 4-13).⁽¹⁵²⁻¹⁵⁴⁾ In these enzymes, the 5'-dA radical generated by AdoCbl homolysis directly abstracts a hydrogen atom from C1 of the substrate, water (or ammonia) is eliminated with formation of a carbonyl at this carbon and a radical on C2. This radical then re-abstracts a hydrogen from 5'-dA, accomplishing a net 1,2-hydrogen shift.

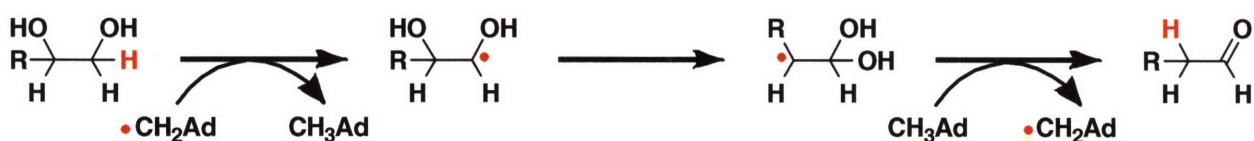


Figure 4-13. Reaction catalyzed by diol dehydratase. The indicated hydrogen atom is abstracted by a 5'-dA radical from C1 and returned to C2.

Whether hydrogen atom transfer occurs from the top face or bottom face of the ribose ring, no disulfide radical anion capable of reducing the carbonyl is produced. The 3'-ketonucleoside **4-14** is released into solution. The ultimate source of inactivation results from the decomposition of the released ketonucleotide to the furanone **4-15** through elimination of inorganic phosphate and base.^(144, 148, 155) This compound inactivates the enzyme through alkylation from solution, forming the characteristic chromophore at 320. This chromophore is believed to result from the reaction of furanone with a C-terminal lysine, and has been observed in both the *E. coli* class I and *L. leichmannii* class II enzymes.⁽¹⁵⁵⁾ Partial loss of the Y• also occurs in class I enzymes; in cases when the hydrogen atom is provided by the bottom face cysteine, the radical cannot return to the β subunit.^(148, 155) In class II enzymes, this pathway would result in the destruction of the AdoCbl cofactor.^(146, 147, 155-157)

Multiple turnovers are required for each α inactivation—use of 3'-[^3H] inhibitors show the release of up to 10 equivalents of [^3H] $_2\text{O}$ for each inactivation event in the absence of exogenous reductants.(157) Reaction in the presence of DTT protects the enzyme from inactivation, presumably through scavenging of the furanone electrophile by DTT, and up to 1000 equivalents of [^3H] $_2\text{O}$ can be released under these conditions. (143-146, 148, 155) Very similar results are observed for a range of 2'-monohalo nucleotides. For RTPR, it was demonstrated that the 2'-chloro, 2'-bromo, 2'-iodo ATP analogs and even the *ara* configured 2'-chloro and 2'-bromo ATP analogs display extremely similar inactivation chemistry to 2'-chloro UTP. Studies of the corresponding 2'-fluoro-2'-deoxy-CTP and UTP analogs (FNTPs) reveal somewhat different behavior.(145, 146) These analogs do inactivate RNRs along with the release of inorganic phosphate, base, fluoride, and formation of the 320 nm chromophore, suggesting a mode of inactivation similar to chloro (Figure 4-12). However, substantial amounts of dNTPs are also produced, and much more fluoride is released than base and phosphate (some deoxynucleotide production can also be observed for 2'-chloro UTP, but with a much lower frequency).(146, 155) This result indicates that FNTPs can sometimes act as the normal substrate. The ratio of turnover to inactivation is dependent on the fluoronucleotide base, the effector, and reductant used. (146, 155) It has been proposed that this partial turnover results from the intermediate leaving group ability of fluoride relative to hydroxide and chloride.(146) The implication is that fluoride sometimes leaves as HF, removing a proton from the bottom face thiol, and sometimes as F $^-$. The former leads to turnover, the latter to inactivation. Partitioning between the two mechanisms seems driven solely by conformational factors, though it has been recently suggested that release of the ketonucleotide to solution (and thus, turnover vs. inactivation) is controlled by the degree of solvation of the leaving group.(158)

Gemcitabine

The 2'-monohalo-2'-deoxynucleotides show low cytotoxicity in tissue culture. It is thus very interesting that the most widely used RNR-targeting nucleoside analog in cancer treatment today, F₂C, differs from these analogs only by the inclusion of a second fluorine at the 2' position. F₂C was designed based on the mechanistic knowledge of inactivation by the 2'-monohalo analogs (159-161) with the assumption that the mechanism of RDPR inactivation by F₂CDP would be similar, but the loss of the second fluoride would make inhibition irreversible.

The first detailed mechanistic study on F₂CDP was carried out on purified *E. coli* RDPR.(159) The studies revealed rapid, irreversible inactivation of the enzyme along with loss of cytosine (detected by HPLC and UV-vis spectroscopy). Approximately two equivalents of cytosine were released per α_2 and any excess F₂C was recovered unreacted (after dephosphorylation). No other nucleoside products were detected. Separation of inactivated protein from small molecules did not allow recovery of activity. The 320 nm chromophore, indicative of furanone alkylation, was not observed and the presence of DTT did not protect RDPR from inactivation. These results gave the first indication that the mechanism of inactivation by difluoronucleotides was distinct from the monohalo derivatives, and that inactivation was not due to alkylation by furanone from solution.

Further efforts to understand the details of the inactivation of *E. coli* RDPR(133) and *L. leichmannii* RTPR(132) were undertaken in the late 1990's in the Stubbe laboratory. The inactivation of RDPR was studied with 5 equivalents of F₂CDP per α_2 , in both the presence of reductants (TR/TRR/NADPH or DTT) or in their absence. Intriguingly, a different inactivation phenotype was observed depending on whether or not reductants were present. In the presence of reductants, complete (>90%) inactivation of α was observed within 2-3 min, concurrent with

20-30% loss of β activity (corresponding to a proportional loss of the tyrosyl radical absorbance peak at 410 nm). The solution phase products of inactivation were characterized, but quantification was difficult as isotopically labeled F_2CDP was not available. Two equivalents of F^- (detected by fluoride electrode) and 1 equivalent of cytosine (detected by UV-vis spectroscopy) were observed per α_2 inactivated. This result contradicts the earlier results showing loss of 2 equiv. of cytosine per α_2 .(159)

In the absence of reductants, β was inactivated due to loss of $Y\cdot$ (95% by 10 min), and α was only partially inactivated. Initially activity fell to 40-50% of the initial rate, then recovered to a steady state with 70% of initial activity. Two equivalents of F^- and 1 equivalent of cytosine were released per $Y\cdot$ consumed, and F^- was released on the same timescale as $Y\cdot$ was lost. Loss of $Y\cdot$ was concomitant with formation of a new organic radical species observed by EPR spectroscopy (9 GHz) (Figure 4-14). This new radical was stable for long time periods, still detectable after 15 min. The spectra of the new radical (Figure 4-14 C) was obtained by subtraction of the spectrum of $Y\cdot$ (Figure 4-14 B), a difficult process due to the overlap of the two spectra. The new spectrum appears to be a pseudo-triplet, indicating the radical is interacting with two similar spin $\frac{1}{2}$ nuclei. Recent results(162) using $1'-[^2H]-F_2CDP$ showed the collapse of this signal to a doublet, indicating that one of the couplings is due to the interaction with the $1'$ hydrogen. When examined by high-field EPR (140 GHz) (Figure 4-15), the radical was found to possess g values consistent with a delocalized, α -keto radical ($g_x = 2.00738$, $g_y = 2.00592$, $g_z = 2.00230$). (162)

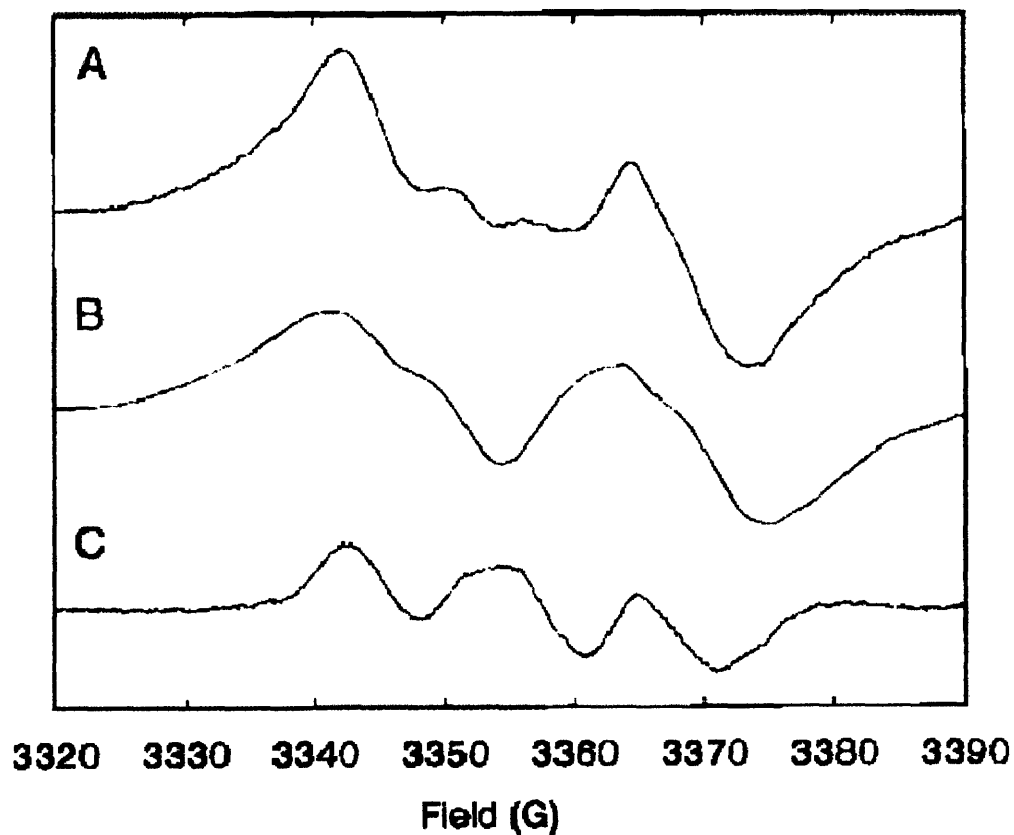


Figure 4-14. Low field (9GHz) EPR of the nucleotide radical detected upon inactivation of RDPR with F_2CDP in the absence of reductants. (A) New radical signal observed during the inactivation. (B) $Y\cdot$ (control) (C) nucleotide radical revealed after subtraction of tyrosyl radical signal.(133)

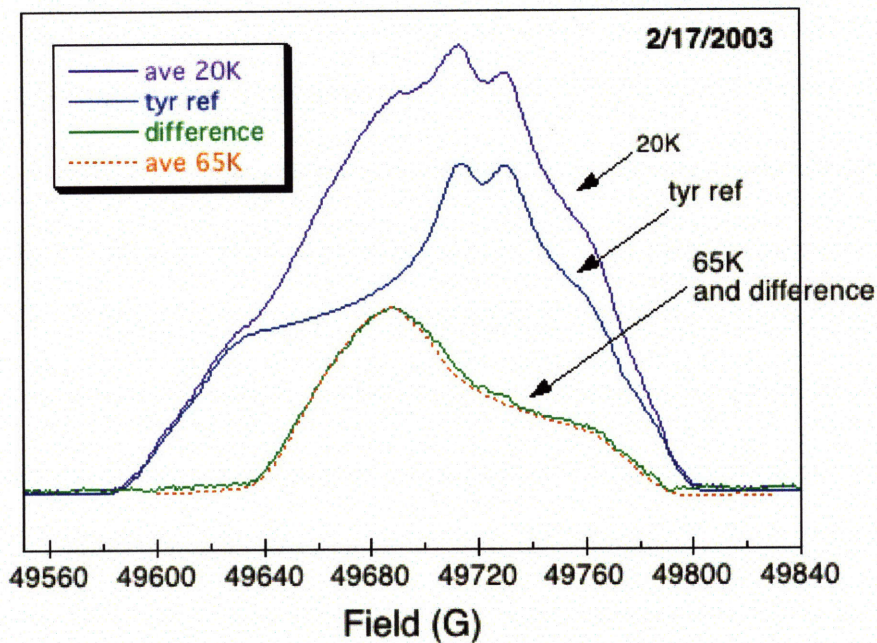


Figure 4-15. High field (140GHz) EPR of the nucleotide radical detected upon inactivation of RDPR with F_2CDP in the absence of reductants.

Detailed studies have also been carried out with RTPR and F_2CTP .⁽¹³²⁾ Incubation of RTPR with 1 equiv F_2CTP resulted in complete (>90%) inactivation within the first time point (< 30s), too fast to accurately measure the rate by the hand-quench method used. Stoichiometric inactivation occurred in the presence and absence of external reductants. The majority of experiments were designed to characterize the end products of RTPR inactivation and were run in the absence of reductants.

Interestingly, alkylation of RTPR by an AdoCbl-derived species was detected.⁽¹³²⁾ Separation of the protein from the solution phase molecules by Sephadex G-50 chromatography in the dark resulted in the co-elution of a red color with a UV-vis spectrum of cobalamin. This species closely resembled the spectrum of glutathionylcobalamin (GSCbl) in its features, and was speculated to be due to loss of the adenosyl ligand and covalent modification to the protein through a Co-S bond, forming on the minute timescale. This assignment was confirmed by

digestion of RTPR with endoproteinase Glu-C and separation of peptides by reverse-phase HPLC; this protease was used over the more common trypsin as it is active at the slightly acidic pH where the corrin-protein bond was found to be the most stable. A peptide containing the cobalamin chromophore was shown to include residues 411-420 of the peptide by N-terminal sequencing, which includes C419, one of the bottom face reducing equivalents. Further, sequencing gave no detected amino acid for the ninth residue, consistent with a modified cysteine. The modified peptides were also analyzed by electrospray ionization (ESI) mass spectrometry. Several peaks were found with m/z consistent with that predicted for the peptide (411-423) conjugated to cobalamin. Further, the kinetics of cleavage of the cobalamin from the peptide using CN^- were examined. They were similar to those observed with CN^- and GSCbl, and the cobalamin product produced was identical. ESI of the product mixture showed m/z peaks consistent with the unmodified 411-423 peptide after CN^- treatment. This data suggested that the primary site of cobalamin modification was at C419 through a Co-S bond.

The small molecule products of this inactivation were also characterized. Two equivalents of F^- were lost per RTPR inactivated, as measured by fluoride electrode. Kinetic studies revealed one equivalent was lost within the dead time of the instrument and a second equivalent lost within one minute. In contrast to RDPR, no base release was detected. Note that experiments described in Chapter 6 indicate that the apparent lack of base release was due to a contaminating cytosine deaminase in the RTPR, and the uracil was overlooked in the original study (a uracil peak is evident in the original HPLC traces from these studies).⁽¹⁶³⁾ It now appears one equivalent of base is released per equivalent of F_2CTP consumed. The release of 5'-dA was also detected: approximately 0.8 equivalents were released per equivalent of F_2CTP /RTPR.

Rapid freeze-quench EPR studies were carried out on F₂CTP inactivations of RTPR. Within the first time point (22 ms) an exchange-coupled thiyl radical-cob(II)alamin species was detected (0.9 equiv based on AdoCbl). RFQ analysis on multiple time points revealed the disappearance of the exchange-coupled thiyl radical and the formation of a new species that was one or more organic radicals coupled to cob(II)alamin with weaker interactions than the initial radical. It was demonstrated that the initially generated thiyl radical was converted to this new radical in a quantitative and kinetically competent fashion. The spin present as a thiyl radical at 22 ms is converted entirely to the new radical by 141 ms, and remains at 255 ms. This radical persists on the minute timescale, with 36% of the initial spin density radical remaining at 20s. It is clear from these studies that the mechanism of inhibition of RNRs by F₂C phosphates is complex and distinct from the monohalonucleotides. However, without radiolabeled F₂CTP, information as to the fate of the ribose ring was lacking and proposal of a mechanism proved difficult.

Recently, DFT computational methods have been applied in an attempt to elucidate this mechanism of F₂CDP with RNR in the absence of exogenous reductants.⁽¹⁶⁴⁾ In these calculations, the active site cysteines were modeled by methanethiols, the glutamate by a formate, and the F₂CDP as only the sugar ring without the base, phosphate or C5'. The structural omissions to make the calculations feasible remove several potentially reactive groups. This omission may be an acceptable approximation, if any elimination of base and inorganic pyrophosphate occur on long timescales, as with furanone-generating RNR inhibitors. The key features of this proposed mechanism are shown in Figure 4-16. The nucleotide is expected to behave normally in the initiation step, with the initial thiyl radical (**4-16**) abstracting of a hydrogen atom from C3' (**4-17**), followed by elimination of one fluorine and formation of an α -

keto radical (**4-18**). The calculations indicated that the fluorine must be protonated to be lost with a reasonable rate, with the proximal bottom-face thiol serving that function. No explanation was provided for previous experimental results on monofluoro nucleotide analogues where dNTP was also detected.(145, 146)

Assuming the fluoride does leave with protonation, the loss of HF would place the bottom face cysteines in the correct protonation states to generate the α -fluoro ketone and a disulfide radical anion (**4-19**), analogously to the reaction mechanism of the normal substrate. It is after the next step, reduction of the ketone to the C3' radical species (**4-20**), that the reaction mechanism would deviate from the normal mechanism of substrate reduction. Rather than the return of a hydrogen atom from the top-face thiol, the calculations reveal that loss of the second fluorine with protonation from the top-face cysteine is more favorable, resulting in loss of a second HF with formation of the α -keto radical (**4-21**). This step would generate the nucleotide radical shown with no abstractable hydrogens nearby.

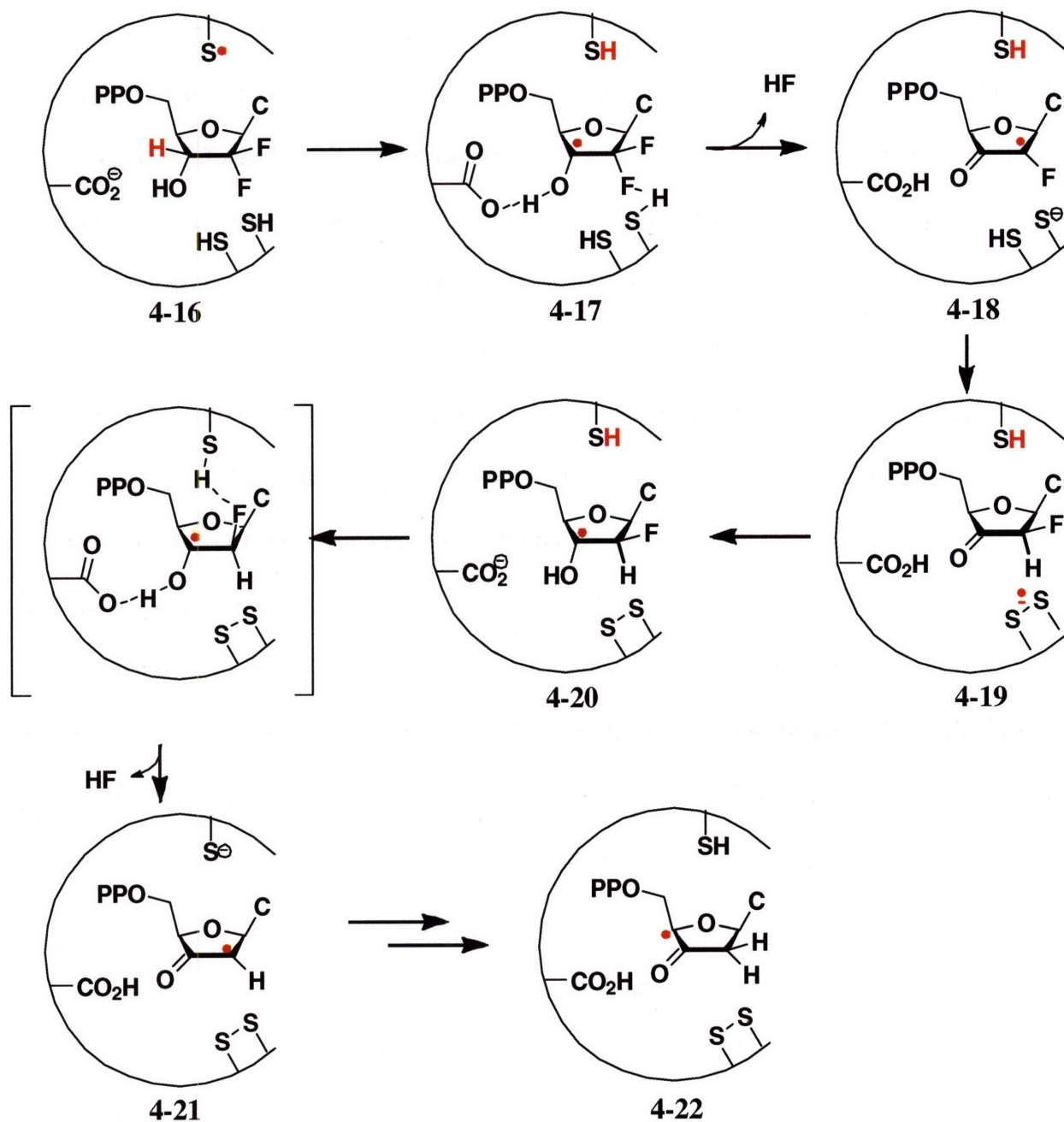


Figure 4-16. Mechanism of reaction of F_2CDP with RDPR in the absence of reductants proposed by Ramos and coworkers. The mechanism is based on DFT calculations modeling only the ribose ring (without base, pyrophosphate, or C5' included) and key active site side chains (cysteines as CH_3SH and the glutamate as formate), not the full active site. (164)

The authors go on to propose a series of rearrangements to generate a stable C4' radical: reprotonation of the top-face cysteine by the glutamate, transfer of a hydrogen atom to C2', and abstraction of the 4' hydrogen atom (4-22). However, crystal structures of RDPR with substrate

bound allow little chance of the top-face cysteine interacting with the opposite face of the ribose ring.(93, 165) Further, it has been shown in the case of the C2'-chloronucleoside that once the 3'-keto nucleotide is formed by transfer of a hydrogen atom from either face of the ring, it is released from the active site and decomposes in solution into furanone.(148) This experimental data rules out the possibility of the 3'-keto nucleotide remaining in the active site long enough for the abstraction of the 4' hydrogen.

Further insight into the inactivation may be gained from comparison of X-ray crystal structures with F₂CDP or CDP bound. Recent structures of *S. cerevisiae* (yeast) class I ribonucleotide reductase show an unusual binding mode of gemcitabine in the enzyme active site.(165) The structures of the yeast α were produced by crystallization in the absence of substrate, then soaking in a solution containing 20 mM DTT, 10 mM MgCl₂, 20 mM adenosine 5'-(β,γ -imido)triphosphate (AMPPNP) and 20 mM of either CDP or F₂CDP. Despite their similar molecular shapes, F₂CDP and CDP exhibit markedly different binding modes (Figure 4-17). The CDP binds such that the 2' and 3' carbons are situated near the catalytically relevant glutamate and asparagine residues (N426 and E430) and the radical initiation and proximal reducing equivalent cysteines (C428 and C218, respectively). In the F₂CDP structure, the ribose ring is rotated up away from the active site, such that C2' is positioned where the cytosine atoms O2, C2, and N3 are located in the CDP structure. This binding mode leaves the 3' hydrogen in approximately the same orientation and position relative to C428, suggesting that chemistry can still be initiated by abstraction of this hydrogen. However, the rotation moves the 2'-OH away from the bottom-face reducing equivalents, and allows two additional waters to bind to the active site, hydrogen-bonded to the ribose. One of these is hydrogen-bonded to the ring oxygen and is situated above the plane of the ring. The cytosine base is further removed from the active site

pocket, and shows interactions with different residues within the base-binding loop 2 relative to CDP. If F₂CDP binds such that initiation proceeds as in the normal mechanism, but is physically removed from the normal reducing equivalents required for turnover, it could have significant mechanistic consequences. It is important to note, however, that these structures may not represent physiologically-relevant binding arrangements.

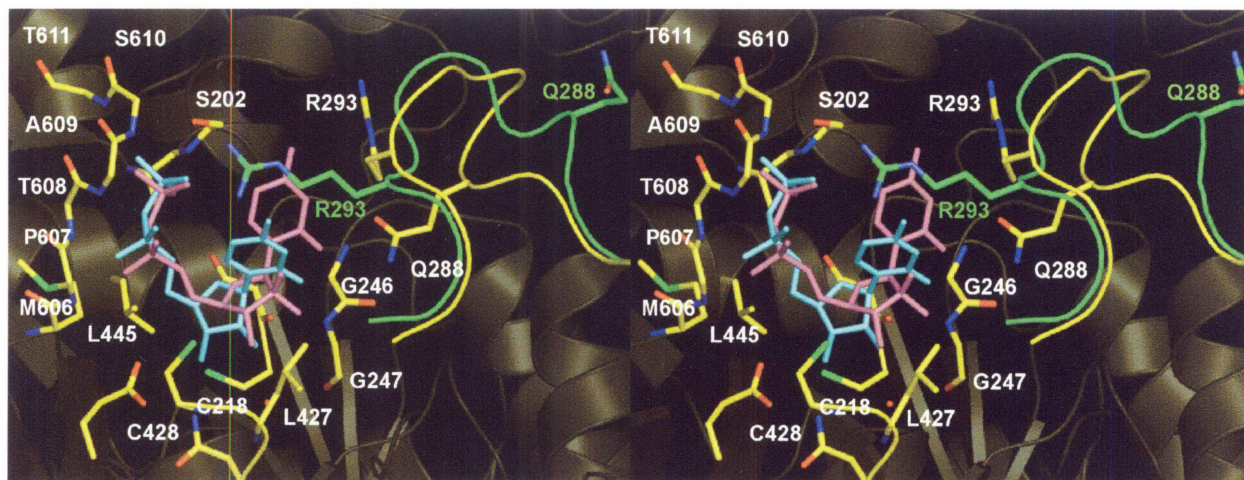


Figure 4-17. Stereoview of crystal structure showing binding of CDP (blue) and F₂CDP (purple) to the active site of yeast RDPR.(165) Figure reprinted with permission of the author.

2'-Azidonucleotides

2'-Azido-2'-deoxynucleotides have also been examined in detail and found to be mechanistically distinct from the 2'-halo-2'-deoxynucleotides.(143) The azide group could be lost from the 3'-hydroxy radical as HN₃ or N₃⁻ to generate the α -keto radical without deprotonation of the bottom face cysteine.(166, 167) In studies using *E. coli* RDPR, the end products on a long (min) timescale were similar to the monohalo case, with both pyrophosphate and base released (Figure 4-18). Azide release was not detected, however, in the case of the wild type enzyme. Instead, N₂ release was observed on a rapid (ms) timescale, and a new, nitrogen centered radical was detected by EPR, forming concomitant with loss of Y \cdot .(166, 168-171) Studies using [¹⁵N]-labeled inhibitor showed that both the radical and the N₂ gas were derived

from the azido group. When oxidized α or the C225S or C462S mutants were used, azide release could be detected, suggesting that interaction with the bottom-face reducing equivalents is leading to alterations in the mechanism of inactivation.(171) Further, the new radical was not detected for the oxidized enzyme or C225S mutant, but was seen for the C462S mutant. To further elucidate the structure of the radical, a range of isotopically labeled inhibitors were used.(169) Studies performed using 1'-, 2'-, 3'-, or 4'-[^2H]- N_3UDP s showed no hyperfine interactions to the radical from these deuterons.(171) Electron spin echo envelope modulation (ESEEM) spectroscopy indicated distances of 3.3 ± 0.2 and 2.6 ± 0.3 Å from the nitrogen centered radical to the 1'- and 4' deuterons, respectively.(171) The use of 2'-[$^{15}\text{N}_3$, ^{13}C]- N_3UDP showed that the 2'-C- N_3 bond is cleaved before formation of the new radical. This data collectively suggested the radical was covalently bonded to the 3' carbon.(171) The EPR spectra were judged to be consistent with a sulfinylamine radical based on model systems, and studies using β -[^2H]-cysteine α showed the sulfur was derived from an active site cysteine.(172) The question of whether the nitrogen was linked directly to the 3' carbon, or by a connecting oxygen, was recently resolved by the use of [^{17}O] labeled N_3UDP and computational analysis. EPR spectroscopy with this inhibitor assigned the structure shown (4-23) based on the hyperfine coupling measured to the ^{17}O .(169)

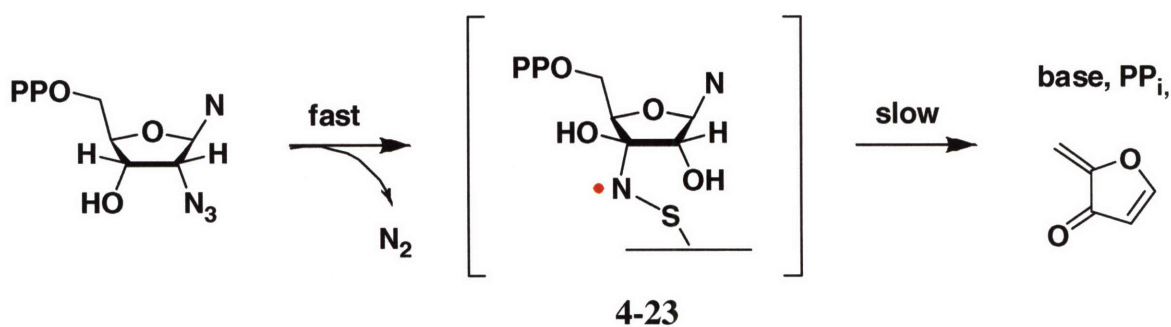


Figure 4-18. Products of inhibition of RNR by 2'-azido-2'-deoxynucleotides.

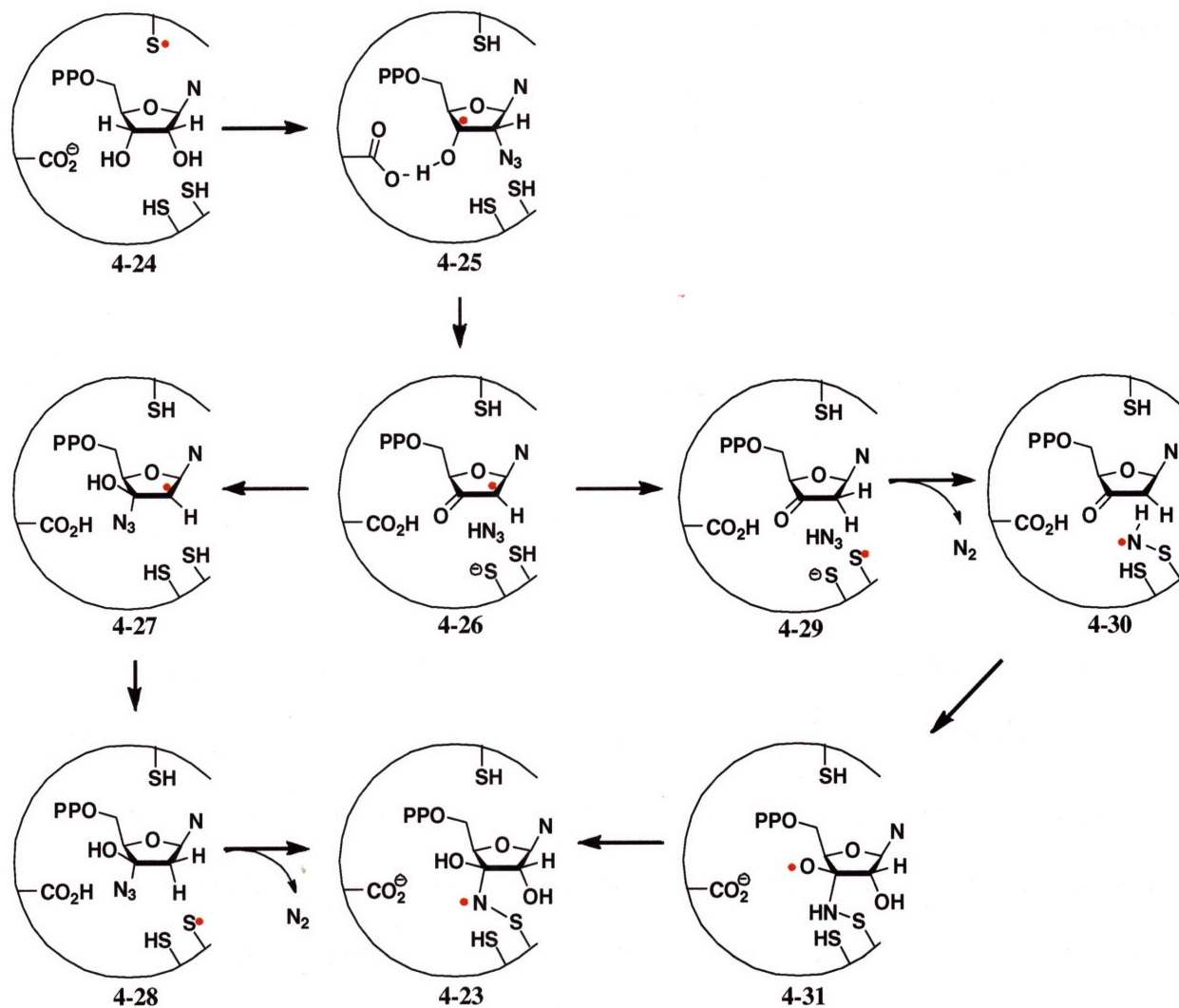


Figure 4-19. Inhibition of RNR by 2' azidonucleotides, and the proposed structure of the stable radical species.

Two mechanisms have been proposed; in both, the initial top face thiyl radical (**4-24**) abstracts the 3'-hydrogen (**4-25**), leading to loss of azide and formation of an α -keto radical (**4-26**). In the first proposal, the released azide attacks the carbonyl of the α -keto radical to give **4-27**, similar to the AdoCbl catalyzed rearrangements discussed above (Figure 4-13). This radical is reduced by the proximal bottom face cysteine (**4-28**), and the resulting sulfur radical attacks the R-N₃ leading to elimination of nitrogen. Alternatively, the keto radical may be reduced by the

cysteine (**4-29**) while HN_3 remains in the active site. The thiyl radical traps the HN_3 with loss of N_2 (**4-30**), and the new nitrogen centered radical attacks the carbonyl (**4-31**). The first mechanism is favored by theoretical studies,⁽¹⁷³⁾ but both are possible and cannot be distinguished based on current experimental data. Destruction of this radical is a slow process occurring on the s to min timescale, and results in release of a 3'-keto nucleotide from the active site that decomposes with elimination of base and PP_i to generate a furanone species. This breakdown is analogous to the 2'-halonucleotide case, and leads to the inactivation of α through alkylation by this furanone.

Fluoromethylene nucleotides

A deoxycytidine analog 2'-substituted with a fluoromethylene group is a potent mechanism-based inhibitor, now in phase III clinical trials.^(18, 135, 174, 175) As with F_2CDP , the diphosphate of this analog is the active species *in vivo*. The reaction requires 1.4 turnovers per inactivation event. Both α and β are inactivated to varying extents, and elimination of fluoride and cytosine accompanies inactivation.^(122, 159, 176) As typical of all mechanism-based inhibitors that inactivate β , $\text{Y}\cdot$ is lost. In this case, this loss is accompanied by the formation of a nucleotide-based radical in the active site of α . This radical has been characterized by EPR spectroscopy of both the unlabeled compound and the isotopically labeled 6'-[^2H]- and 6'-[^{13}C]- derivatives. The EPR spectrum was altered for both isotopically labeled derivatives, providing the first solid evidence of a nucleotide radical in a RNR system, and allowing a structure to be proposed (Figure 4-20).^(134, 177)

In the proposed mechanism for this inactivation, the initial top face thiyl radical (**4-32**) abstracts the 3'-hydrogen, generating an allylic radical stabilized by the fluorine (**4-33** and **4-34**).

Transfer of a hydrogen atom from the bottom-face cysteine would cause loss of radical from the β subunit and result in a system (4-35) that would eliminate fluoride and generate an α,β unsaturated ketone (4-36). This ketone could alkylate a nucleophile through conjugate addition; studies indicate the active site glutamate is the primary site of alkylation (4-37). (122, 177) The radical could also be reduced by transfer of a hydrogen atom from the top face, which would lead to the same electrophile, but return the radical to β . This system can be reduced by the bottom face thiyl radical, forming the nucleotide-based allylic radical (4-38). This radical is believed to be the species observed by EPR spectroscopy in this system.

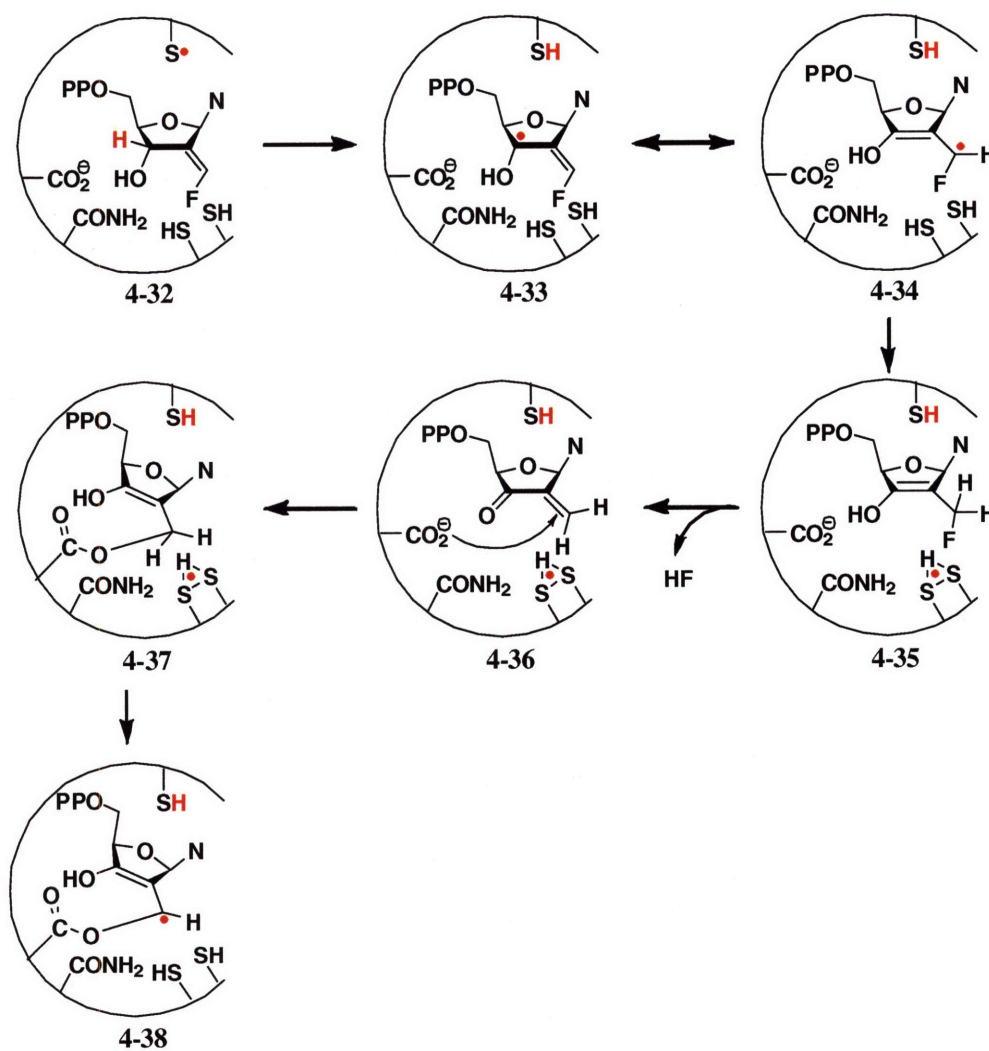


Figure 4-20. Inhibition of RNR by 2' fluoromethylene cytidine, and the proposed structure of the stable radical species.

2'-Mercapto nucleotides

Another inhibitor class that has been investigated are the 2'-mercapto-2'-deoxynucleosides (Figure 4-11).^(178, 179) The 2'-mercapto nucleoside 5'-diphosphate was found to be a potent inhibitor of *E. coli* class I RNR with $K_i = 35 \mu\text{M}$ and $k_{\text{inact}} = 0.18 \text{ s}^{-1}$, but only inactivated RNR in the presence of molecular oxygen.⁽¹⁷⁸⁾ The β subunit was found to be inactivated by $\text{Y}\cdot$ loss. No α inactivation is observed with this inhibitor. During the course of this reaction, a new organic radical was observed by EPR, with g values and hyperfine structure consistent with a perthiyl radical ($\text{RSS}\cdot$). This radical was shown to be on an α subunit cysteine by incorporation of β -[^2H] cysteine into α and the observed loss of hyperfine couplings that resulted.⁽¹⁷⁸⁾ The compound was found to be active *in vivo*; like many of the previously-used *in vivo* inhibitors, the cytidine derivative was the most active in depressing deoxynucleotide pools in cells.⁽¹⁸⁰⁾ Few experimental studies have been performed to investigate this mechanism, and, in particular, the role of molecular oxygen yet to be established. In order to account for the formation of the perthiyl radical on α , it has been proposed that the first step in inhibition (Figure 4-21) requires binding to the active site (**4-39**) and the generation of a disulfide between the nucleotide 2'-thiol and active site cysteine, probably the proximal bottom face cysteine (**4-40**).^(178, 179) Initiation by abstraction of the 3' hydrogen (**4-41**) would trigger elimination of a perthiyl radical (**4-42**). It is not clear how the initial oxidation step would occur specifically, however, or why the enzyme-substrate disulfide would be stable to disulfide exchange with the distal bottom-face cysteine.

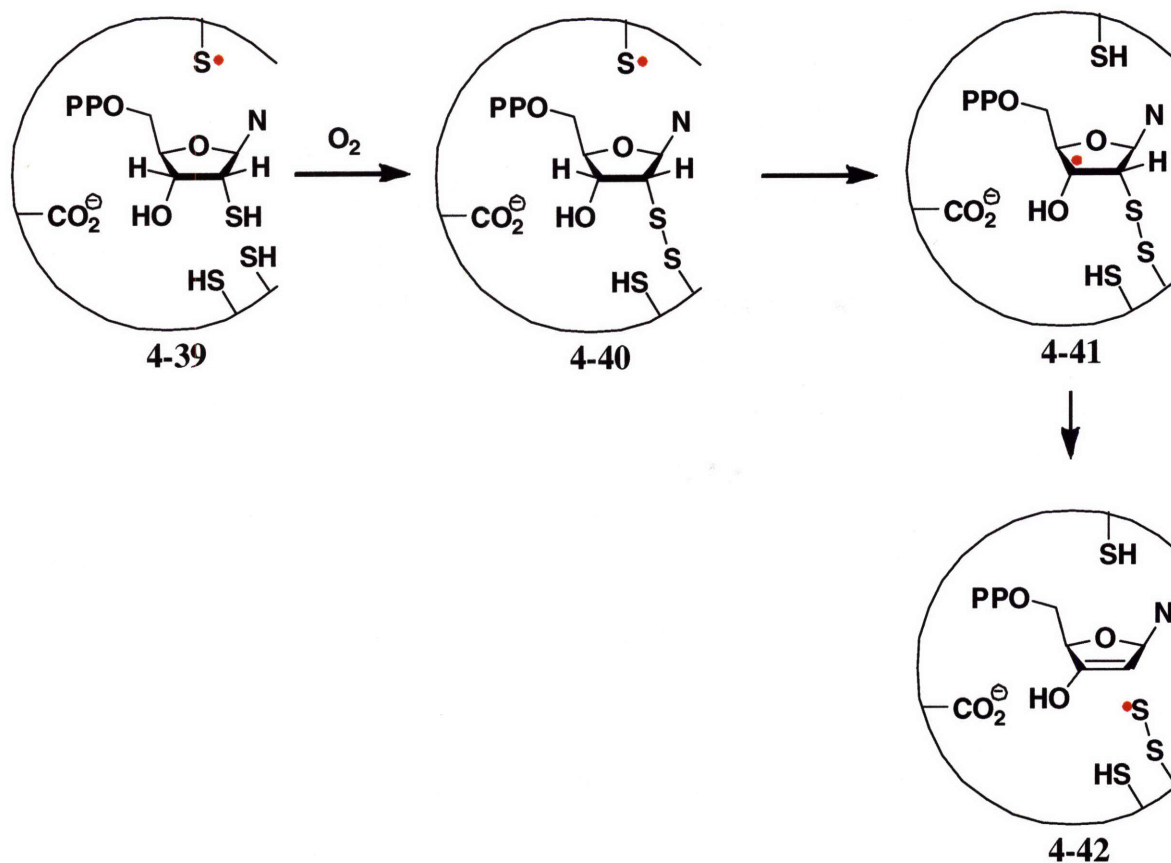


Figure 4-21. Proposed mechanism of inhibition of RNR by 2' mercapto-CDP.

Other nucleoside analogs

The adenosine analogues cladribine, fludarabine, and clofarabine (Figure 4-22) are nucleoside analogues that have seen clinical use as chemotherapeutics.^(18, 29, 181-183) These compounds have complex mechanisms of action *in vivo*. The compounds are inhibitors of DNA synthesis, and can also incorporate into DNA, triggering a cascade of events leading to apoptosis. In addition, the triphosphate derivatives of these compounds have been shown to be inhibitors of RNR *in vitro* in crude cell extracts (IC_{50} of 130 nm for cladribine).^(184, 185) It has been hypothesized that suppression of RNR activity is derived by competition with ATP binding at the effector and activity sites of α .

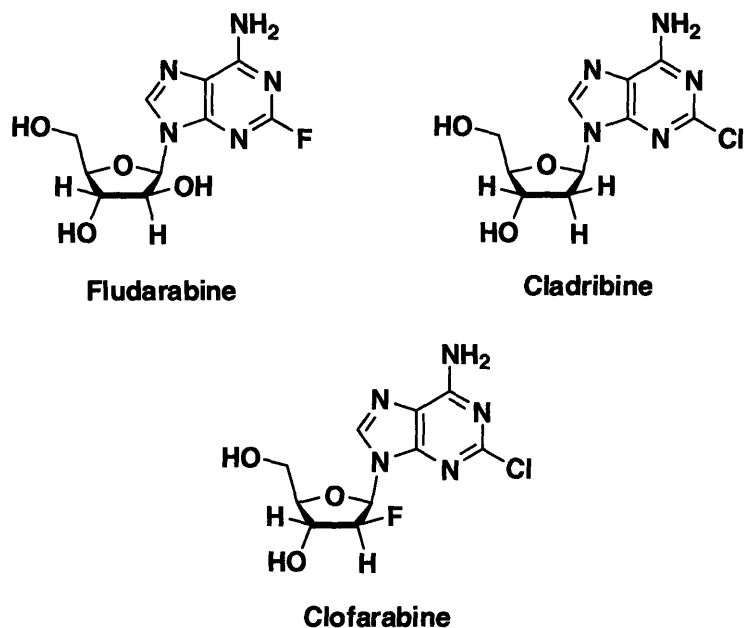


Figure 4-22. RNR inhibitors that bind to the effector and activity sites.

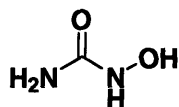
Radical quenchers and metal chelators

Hydroxyurea (HU), the related compounds didiox and trimidox (Figure 4-23), inhibit class I RNRs through reduction of the tyrosyl radical on the β subunit.(140, 186-192) The $Y\cdot$ is deeply buried in the β subunit, and is quenched with a rate several orders of magnitude slower than $Y\cdot$ in solution. The rate of quenching is enhanced more than tenfold when the inactivation is performed in the presence of α , effector and substrate, indicating that the radical becomes more accessible during the transfer to the active site.(191) These radical scavengers inhibit RNR *in vivo* and are useful chemotherapeutics against hematologic cancers, leading to the arrest of DNA synthesis presumably through the polymerases becoming starved for dNTPs.(193)

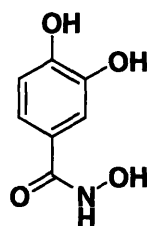
Semicarbazones and thiosemicarbazones such as Triapine are potent iron chelators, and inhibit RNR through destruction of the iron center by an unknown mechanism.(194-197) These compounds appear to associate with β prior to rapid enzyme inactivation, and are believed to inhibit RNR both through radical quenching and by perturbations in iron metabolism that prevent

the formation of the diferric- $Y\cdot$ cofactor on β .(141, 142, 195, 198-200) Other iron-chelating siderophores such as desferoxamine (DFO) have no effect on the tyrosyl radical of active β RNR subunits, but rather are believed to act solely by disruption of iron homeostasis, preventing proper loading of newly translated RNR.(201)

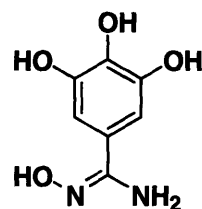
Radical Scavengers



Hydroxyurea

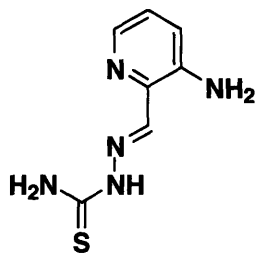


Didiox

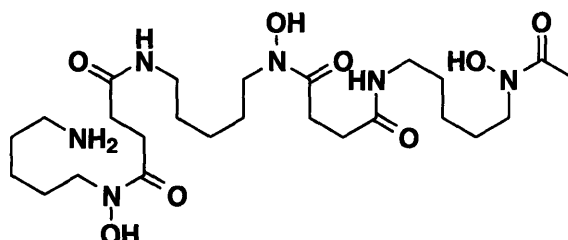


Trimidox

Iron Chelators



Triapine



DFO

Figure 4-23. Structure of radical scavengers and iron chelators applied to the inhibition of RNR.

Inhibitors of subunit-subunit interactions

Class I RNR is one of the few protein systems in which inhibitors of protein-protein interactions have been successfully designed and shown to work *in vivo*.(20, 22, 202-206) This area is of particular interest because the binding interface between the α and β subunits differ in a species dependent manner, creating the opportunity for antibiotic and antiviral RNR inhibitors with little or no effect on mammalian cells.(22, 207-214) Inhibitors designed specifically to disrupt the subunit-subunit interactions in mammalian cells have also been proposed as potential chemotherapeutics that would specifically target nucleotide reduction.(202, 204, 215) The

development of subunit-subunit interaction inhibitors stems from the early observation that the C-terminal peptide of the β subunit can inhibit nucleotide reduction in class I systems.(205, 206, 212, 213, 216) Efforts have also been made to synthesize inhibitors of this interaction based on cyclic peptide or peptidomimetic scaffolds, a necessary step for the use of these inhibitors as therapeutics (Figure 4-24).(217-219) Several compounds developed at Boehringer-Ingelheim to inhibit herpes simplex virus (HSV) RNR. Compounds in this series bind HSV R1 with K_D 's in the 0.2-5 nmol range.(207, 208, 214, 220, 221) Several were quite successful in reducing replication of the virus in culture, and in reducing the severity of symptoms of viral eye infections in murine models.(220)

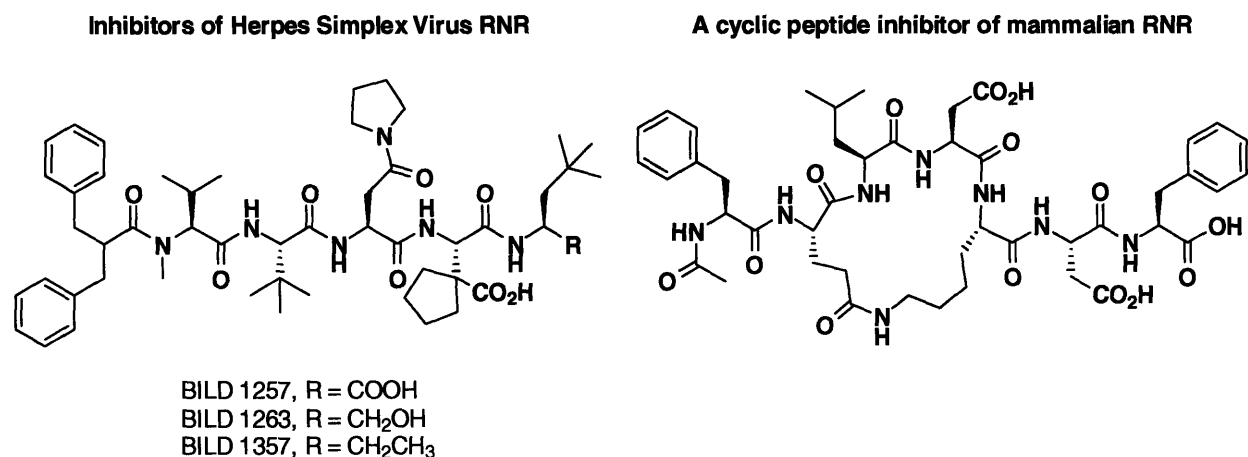


Figure 4-24. Structures of some RNR subunit-subunit interaction inhibitors.

4.4 Summary

Ribonucleotide reductase is a complex, multifaceted enzyme critical to the function of living cells. RNRs are found in nearly all organisms, and though primary sequence may vary considerably, the enzymes share remarkable structural homology across classes. These radical-dependent enzymes utilize a wide range of cofactors for the initial generation of the radical, from oxidation of a tyrosine to reduction of SAM to homolysis of AdoCbl, yet have very similar

active sites that reduce nucleotides through a common mechanism. RNRs central role in nucleotide metabolism has made it an attractive target for both antitumor and antiviral therapeutics, and the strategies devised to inactivate RNR are numerous. An understanding of the mechanism is key to the development of new inhibitors, and data from many inhibitors can give deeper understanding of the mechanism of nucleotide reduction. The study of RNR remains an active area of research—elucidating the evolution of RNR has the potential to give insight on the development of a DNA world, understanding of allosteric regulation will give a clearer picture of nucleotide homeostasis within cells, and development of new inhibitors may improve existing therapies or unlock new ones. Much more remains to be learned about these fascinating enzymes, and their elegant control of a radical reaction within the cell.

4.5 References

- (1) Nordlund, P., and Reichard, P. (2006) Ribonucleotide reductases. *Annu. Rev. Biochem.* 75, 681-706.
- (2) Eklund, H., Uhlin, U., Färnegårdh, M., Logan, D. T., and Nordlund, P. (2001) Structure and function of the radical enzyme ribonucleotide reductase. *Prog. Biophys. Mol. Biol.* 77, 177-268.
- (3) Jordan, A., and Reichard, P. (1998) Ribonucleotide reductases. *Annu. Rev. Biochem.* 67, 71-98.
- (4) Licht, S., and Stubbe, J. (1999) Mechanistic investigations of ribonucleotide reductases, in *Comprehensive Natural Products Chemistry* (Barton, S. D., Nakanishi, K., Meth-Cohn, O., and Poulter, C. D., Eds.) pp 163-203, Elsevier Science, New York.
- (5) Stubbe, J., and van der Donk, W. A. (1998) Protein radicals in enzyme catalysis. *Chem. Rev.* 98, 705-762.
- (6) Stubbe, J., and van der Donk, W. A. (1995) Ribonucleotide reductases: radical enzymes with suicidal tendencies. *Chem. Biol.* 2, 793-801.
- (7) Stubbe, J. (1989) Protein radicals in biological systems. *Annu. Rev. Biochem.* 58, 257-285.
- (8) Rose, I. A., and Schweigert, B. S. (1953) Incorporation of C¹⁴ totally labeled nucleosides into nucleic acids. *J. Biol. Chem.* 202, 635-645.
- (9) Reichard, P., and Rutberg, L. (1960) Formation of deoxycytidine 5'-phosphate from cytidine 5'-phosphate with enzymes from *Escherichia coli*. *Biochim. Biophys. Acta* 37, 554-555.

- (10) Thelander, L., and Reichard, P. (1979) Reduction of ribonucleotides. *Annu. Rev. Biochem.* 48, 133-158.
- (11) Reichard, P. (1995) To be there when the picture is painted. *Annu. Rev. Biochem.* 64, 1-28.
- (12) Blakley, R. L., and Vitols, E. (1968) The control of nucleotide biosynthesis. *Annu. Rev. Biochem.* 37, 201-224.
- (13) Marsh, E. N. G., Patwardhan, A., and Huhta, M. S. (2004) S-Adenosylmethionine radical enzymes. *Bioorg. Chem.* 32, 326-340.
- (14) Fontecave, M., Mulliez, E., and Logan, D. T. (2002) Deoxyribonucleotide synthesis in anaerobic microorganisms: the class III ribonucleotide reductase. *Prog. Nucleic Acid Res.* 72, 95-127.
- (15) Frey, P. A., and Booker, S. J. (2001) Radical mechanisms of S-adenosylmethionine-dependent enzymes. *Adv. Prot. Chem.* 58, 1-45.
- (16) Buckel, W., and Golding, B. T. (1999) Radical species in the catalytic pathways of enzymes from anaerobes. *FEMS Microbiol. Rev.* 22, 523-541.
- (17) Reichard, P. (1992) The anaerobic ribonucleotide reductase from *Escherichia Coli*. *J. Biol. Chem.* 268, 8383-8386.
- (18) Shao, J., Zhou, B., Chu, B., and Yen, Y. (2006) Ribonucleotide reductase inhibitors and future drug design. *Curr. Drug Targets* 6, 409-431.
- (19) Robertson, J. G. (2005) Mechanistic basis of enzyme-targeted drugs. *Biochemistry* 44, 5561-5571.
- (20) Loregian, A., and Palù, G. (2005) Disruption of protein-protein interactions: towards new targets for chemotherapy. *J. Cell. Physiol.* 204, 750-762.
- (21) Cerqueira, N. M. F. S. A., Pereira, S., Fernandes, P. A., and Ramos, M. J. (2005) Overview of ribonucleotide reductase inhibitors: an appealing target in anti-tumor therapy. *Curr. Med. Chem.* 12, 1283-1294.
- (22) Cooperman, B. S. (2003) Oligopeptide inhibition of class I ribonucleotide reductases. *Biopolymers* 71, 117-131.
- (23) Richardson, D. R. (2002) Iron chelators as therapeutic agents for the treatment of cancer. *Crit. Rev. Oncol. Hematol.* 42, 267-281.
- (24) Ingram, G. M., and Kinnaird, J. H. (1999) Ribonucleotide reductase: a new target for antiparasite therapies. *Parasitol. Today* 15, 338-442.
- (25) Nocentini, G. (1996) Ribonucleotide reductase inhibitors: new strategies for cancer chemotherapy. *Crit. Rev. Oncol. Hematol.* 22, 89-126.
- (26) Robins, M. J., Samano, M. C., and Samano, V. (1995) Ribonucleotide reductase targets for chemotherapy: mechanistic aspects and biologically active agents. *Nucleosides Nucleotides* 14, 485-493.
- (27) Szekeres, T., Fritzer-Szekeras, M., and Elford, H. L. (1997) The enzyme ribonucleotide reductase and anti-HIV therapy. *Crit. Rev. Clin. Lab. Sci.* 34, 503-528.
- (28) Cory, J. G. (1988) Ribonucleotide reductase as a chemotherapeutic target. *Adv. Enzyme Regul.* 27, 437-455.
- (29) Lech-Maranda, E., Korycka, A., and Robak, T. (2006) Pharmacological and clinical studies on purine nucleoside analogs-new anticancer agents. *Mini-Rev. Med. Chem.* 6, 575-581.
- (30) Obata, T., Endo, Y., Murata, D., Sakamoto, K., and Sasaki, T. (2003) The molecular targets of antitumor 2'-deoxycytidine analogues. *Curr. Drug Targets* 4, 305-313.

- (31) Tidwell, T. T. (2001) The Gomberg century: free radicals 1900-2000. *Adv. Phys. Org. Chem.* 36, 1-58.
- (32) Zard, S. Z. (2003) *Radical reactions in organic synthesis*, Oxford University Press, Oxford.
- (33) Parsons, A. F. (2000) *An introduction to free radical chemistry*, Blackwell Science, Oxford.
- (34) Stubbe, J. (1989) Protein radical involvement in biological catalysis? *Annu. Rev. Biochem.* 58, 257-285.
- (35) Pedersen, J. Z., and Finazzi-Agrò, A. (1993) Protein-radical enzymes. *FEBS Lett.* 325, 53-58.
- (36) Ochiai, E.-I. (1994) Free radicals and metalloenzymes: general considerations. *Met. Ions Biol. Syst.* 30, 1-24.
- (37) Marsh, E. N. G. (1995) A radical approach to enzyme catalysis. *Bioessays* 17, 431-441.
- (38) Sawers, G. (1999) Biochemistry, physiology and molecular biology of glycy radical enzymes. *FEMS Microbiol. Rev.* 22, 543-551.
- (39) Frey, P. A., and Reed, G. H. (2000) Radical mechanisms in adenosylmethionine- and adenosylcobalamin-dependent enzymatic reactions. *Arch. Biochem. Biophys.* 382, 6-14.
- (40) Fontecave, M., Mulliez, E., and Ollagnier-de-Choudens, S. (2001) Adenosylmethionine as a source of 5'-deoxyadenosyl radicals. *Curr. Opin. Chem. Biol.* 5, 506-511.
- (41) Frey, P. A. (2001) Radical mechanisms of enzymatic catalysis. *Annu. Rev. Biochem.* 70, 121-148.
- (42) Hoganson, C. W., and Tommos, C. (2004) The function and characteristics of tyrosyl radical cofactors. *Biochim. Biophys. Acta* 1655, 116-122.
- (43) Layer, G., Jahn, D. W. H. D., and Schubert, W.-D. (2004) Structure and function of radical SAM enzymes. *Curr. Opin. Chem. Biol.* 8, 468-476.
- (44) Reed, G. H. (2004) Radical mechanisms in adenosylcobalamin-dependent enzymes. *Curr. Opin. Chem. Biol.* 8, 477-483.
- (45) Selmer, T., Pierik, A. J., and Heider, J. (2005) New glycy radical enzymes catalysing key metabolic steps in anaerobic bacteria. *Biol. Chem.* 386, 981-988.
- (46) Frey, P. A., and Magnusson, O. T. (2003) S-Adenosylmethionine: a wolf in sheep's clothing, or a rich man's adenosylcobalamin? *Chem. Rev.* 103, 2129-2148.
- (47) Jarrett, J. T. (2003) The generation of 5'-deoxyadenosyl radicals by adenosylmethionine-dependent radical enzymes. *Curr. Opin. Chem. Biol.* 7, 174-182.
- (48) Cheek, J., and Broderick, J. B. (2001) Adenosylmethionine-dependent iron-sulfur enzymes: versatile clusters in a radical new role. *J. Biol. Inorg. Chem.* 6, 209-226.
- (49) Banerjee, R., and Ragsdale, S. W. (2003) The many faces of vitamin B₁₂: catalysis by cobalamin-dependent enzymes. *Annu. Rev. Biochem.* 72, 209-247.
- (50) Lawrence, C. C., and Stubbe, J. (1998) The function of adenosylcobalamin in the mechanism of ribonucleoside triphosphate reductase from *Lactobacillus leichmannii*. *Curr. Opin. Chem. Biol.* 2, 650-655.
- (51) Westerlund, K., Berry, B. W., Privett, H. K., and Tommos, C. (2005) Exploring amino-acid radical chemistry: protein engineering and de novo design. *Biochim. Biophys. Acta* 1707, 103-116.
- (52) Stubbe, J. (1998) Ribonucleotide reductases in the twenty-first century. *Proc. Natl. Acad. Sci. U. S. A.* 95, 2723-2724.

- (53) Sjöberg, B.-M. (1997) Ribonucleotide reductases - a group of enzymes with different metallosites and a similar reaction mechanism. *Struct. Bond.* 88, 139-173.
- (54) Fontecave, M. (1998) Ribonucleotide reductases and radical reactions. *Cell. Mol. Life Sci.* 54 684-695.
- (55) Fernandez-Sarabia, M. J., and Fantes, P. A. (1990) Ribonucleotide reductase and its regulation during the cell cycle. *Trends Genet.* 6, 275-276.
- (56) Elledge, S. J., Zhou, Z., Allen, J. B., and Navas, T. A. (1992) DNA damage and cell cycle regulation of ribonucleotide reductase. *Bioessays* 15, 333-339.
- (57) Greenberg, G. R., and Hilfinger, J. M. (1996) Regulation of synthesis of ribonucleotide reductase and relationship to DNA replication in various systems. *Prog. Nucleic Acid Res.* 53, 345-395.
- (58) Graff, P., Åmellem, Ø., Andersson, K. K., and Pettersen, E. O. (2002) Role of ribonucleotide reductase in regulation of cell cycle progression during and after exposure to moderate hypoxia. *Anticancer Res.* 22, 59-68.
- (59) Elledge, S. J., Zhou, Z., and Allen, J. B. (1992) Ribonucleotide reductase: regulation, regulation, regulation. *Trends Biochem. Sci.* 17, 119-123.
- (60) Eliasson, R., Pontis, E., Sun, X., and Reichard, P. (1994) Allosteric control of the substrate specificity of the anaerobic ribonucleotide reductase from *Escherichia coli*. *J. Biol. Chem.* 269, 26052-26057.
- (61) Larsson, K.-M., Jordan, A., Eliasson, R., Reichard, P., Logan, D. T., and Nordlund, P. (2004) Structural mechanism of allosteric substrate specificity regulation in a ribonucleotide reductase. *Nature Struct. Mol. Biol.* 11, 1142-1149.
- (62) Kashlan, O. B., and Cooperman, B. S. (2003) Comprehensive model for allosteric regulation of mammalian ribonucleotide reductase: refinements and consequences. *Biochemistry* 42, 1696-1706.
- (63) Harder, J. (1993) Ribonucleotide reductases and their occurrence in microorganisms: a link to the RNA/DNA transition. *FEMS Microbiol. Rev.* 12, 273-292.
- (64) Reichard, P. (1993) From RNA to DNA, why so many ribonucleotide reductases? *Science* 260, 1773-1777.
- (65) Stubbe, J. (2000) Ribonucleotide reductases: the link between an RNA and a DNA world? *Curr. Opin. Struct. Biol.* 10, 731-736.
- (66) Stubbe, J., Ge, J., and Yee, C. S. (2001) The evolution of ribonucleotide reductase. *Trends Biochem. Sci.* 26, 93-99.
- (67) Poole, A. M., Logan, D. T., and Sjöberg, B.-M. (2002) The evolution of the ribonucleotide reductases: much ado about oxygen. *J. Mol. Evol.* 55, 180-196.
- (68) Torrents, E., Aloy, P., Gibert, I., and Rodríguez-Trelles, F. (2002) Ribonucleotide reductases: divergent evolution of an ancient enzyme. *J. Mol. Evol.* 55, 138-152.
- (69) Whitfield, J. F., Sikorska, M., Youdale, T., Brewer, L., Richards, R., and Walker, P. R. (1989) Ribonucleotide reductase - new twists in an old tale. *Adv. Enzyme Regul.* 28, 113-123.
- (70) Thelander, L., and Gräslund, A. (1994) Ribonucleotide reductase in mammalian systems. *Met. Ions Biol. Syst.* 30, 110-129.
- (71) Eklund, H., Eriksson, M., Uhlin, U., and Nordlund, P. (1997) Ribonucleotide reductase—structural studies of a radical enzyme. *Biol. Chem.* 378, 821-825.
- (72) Kolberg, M., Strand, K. R., Graff, P., and Andersson, K. K. (2004) Structure, function, and mechanism of ribonucleotide reductases. *Biochim. Biophys. Acta* 1699, 1-34.

- (73) Sjöberg, B.-M., and Sahlin, M. (2002) Thiols in redox mechanism of ribonucleotide reductase. *Methods Enzymol.* 348, 1-21.
- (74) Mao, S. S., Holler, T. P., Yu, G. X., Bollinger Jr., J. M., Booker, S., Johnston, M. I., and Stubbe, J. (1992) A model for the role of multiple cysteine residues involved in ribonucleotide reduction: amazing and still confusing. *Biochemistry* 31, 9733-9743.
- (75) Högbom, M., Stenmark, P., Voevodskaya, N., McClarty, G., Gräslund, A., and Nordlund, P. (2004) The radical site in chlamydial ribonucleotide reductase defines a new R2 subclass. *Science* 76, 245-248.
- (76) Panagou, D., Orr, M. D., Dunstone, J. R., and Blakley, R. L. (1972) A monomeric, allosteric enzyme with a single polypeptide chain. Ribonucleotide reductase of *Lactobacillus leichmannii*. *Biochemistry* 11, 2378-2388.
- (77) Knappe, J., and Wagner, A. F. V. (2001) Stable glycy radical from pyruvate formate-lyase and ribonucleotide reductase. *Adv. Prot. Chem.* 58, 277-309.
- (78) Ollagnier, S., Mulliez, E., Gaillard, J., Eliasson, R., Fontecave, M., and Reichard, P. (1996) The anaerobic *Escherichia coli* ribonucleotide reductase: subunit structure and iron sulfur center. *J. Biol. Chem.* 271, 9410-9416.
- (79) Uhlin, U., and Eklund, H. (1994) Structure of ribonucleotide reductase protein R1. *Nature* 370, 533-539.
- (80) Sintchak, M. D., Arjara, G., Kellogg, B. A., Stubbe, J., and Drennan, C. L. (2002) The crystal structure of class II ribonucleotide reductase reveals how an allosterically regulated monomer mimics a dimer. *Nature Struct. Biol.* 9, 293-300.
- (81) Uppsten, M., Färnegårdh, M., Domkin, V., and Uhlin, U. (2006) The first holocomplex structure of ribonucleotide reductase gives new insight into its mechanism of action. *J. Mol. Biol.* 359, 365-377.
- (82) Logan, D. T., Andersson, J., Sjöberg, B.-M., and Nordlund, P. (1999) A glycy radical site in the crystal structure of a class III ribonucleotide reductase. *Science* 283, 1499-1504.
- (83) Sommerhalter, M., Saleh, L., Bollinger Jr., J. M., and Rosenzweig, A. C. (2005) Structure of *Escherichia coli* ribonucleotide reductase R2 in space group P6122. *Acta Cryst. D* 61, 1649-1654.
- (84) Stenmark, P., Högbom, M., Roshick, C., McClarty, G., and Nordlund, P. (2004) Crystals of the ribonucleotide reductase R2 protein from *Chlamydia trachomatis* obtained by heavy-atom co-crystallization. *Acta Cryst. D* 60, 376-378.
- (85) Sommerhalter, M., Voegtli, W. C., Perlstein, D. L., Ge, J., Stubbe, J., and Rosenzweig, A. C. (2004) Structures of the yeast ribonucleotide reductase Rnr2 and Rnr4 homodimers. *Biochemistry* 43, 7736-7742.
- (86) Uppsten, M., Färnegårdh, M., Jordan, A., Eliasson, R., Eklund, H., and Uhlin, U. (2003) Structure of the large subunit of class Ib ribonucleotide reductase from *Salmonella typhimurium* and its complexes with allosteric effectors. *J. Mol. Biol.* 330, 87-97.
- (87) Stubbe, J., Ge, J., Perlstein, D. L., Nguyena, H.-H., Voegtli, W. C., and Rosenzweig, A. (2001) Structure and function of Y2, Y4, and a Y2Y4 heterodimer of the R2 subunit of yeast ribonucleotide reductase. *J. Inorg. Biochem.* 86, 101.
- (88) Uhlin, U., and Eklund, H. (1996) The ten-stranded β/α barrel in ribonucleotide reductase protein R1. *J. Mol. Biol.* 262, 358-369.
- (89) Nordlund, P., and Eklund, H. (1993) Structure and function of the *Escherichia coli* ribonucleotide reductase protein R2. *J. Mol. Biol.* 232, 123-164.

- (90) Booker, S., Licht, S., Broderick, J., and Stubbe, J. (1994) Coenzyme B₁₂-dependent ribonucleotide reductase: evidence for the participation of five cysteine residues in ribonucleotide reduction. *Biochemistry* 33, 12676-12685.
- (91) Persson, A. L., Sahlin, M., and Sjöberg, B.-M. (1998) Cysteinyl and substrate radical formation in active site mutant E441Q of *Escherichia coli* class I ribonucleotide reductase. *J. Biol. Chem.* 273, 31016-31020.
- (92) Persson, A. L., Eriksson, M., Katterle, B., Pötschi, S., Sahlin, M., and Sjöberg, B.-M. (1997) A new mechanism-based radical intermediate in a mutant R1 protein affecting the catalytically essential Glu441 in *Escherichia coli* ribonucleotide reductase. *J. Biol. Chem.* 272, 31533-31541.
- (93) Xu, H., Faber, C., Uchiki, T., Fairman, J. W., Racca, J., and Dealwis, C. (2006) Structures of eukaryotic ribonucleotide reductase I provide insights into dNTP regulation. *Proc. Natl. Acad. Sci. U. S. A.* 103, 4022-4027.
- (94) Bollinger Jr., J. M., Edmondson, D. E., Huyuh, B. H., Filley, J., Norton, J. R., and Stubbe, J. (1991) Mechanism of assembly of the tyrosyl radical-dinuclear iron cluster cofactor of ribonucleotide reductase. *Science* 253, 292-298.
- (95) Han, W.-G., Lovell, T., Liu, T., and Noodleman, L. (2003) A density functional evaluation of an Fe(III)-Fe(IV) model diiron cluster: comparisons with ribonucleotide reductase intermediate X. *Inorg. Chem.* 42, 2751-2758.
- (96) Stubbe, J. (2003) Radicals with a controlled lifestyle. *Chem. Commun.*, 2511-2513.
- (97) Siegbahn, P. E. M., Eriksson, L., and Pavlov, F. H. M. (1998) Hydrogen atom transfer in ribonucleotide reductase (RNR). *J. Phys. Chem. B* 102, 10622-10629.
- (98) Stubbe, J., Nocera, D. G., Yee, C. S., and Chang, M. C. Y. (2003) Radical initiation in the class I ribonucleotide reductase: long-range proton-coupled electron transfer? *Chem. Rev.* 103, 2167-2201.
- (99) Mayer, J. M. (2004) Proton-coupled electron transfer: a reaction chemist's view. *Annu. Rev. Phys. Chem.* 55, 363-390.
- (100) Chang, C. J., Chang, M. C. Y., Damrauer, N. H., and Nocera, D. G. (2004) Proton-coupled electron transfer: a unifying mechanism for biological charge transport, amino acid radical initiation and propagation, and bond making/breaking reactions of water and oxygen. *Biochim. Biophys. Acta* 1655, 13-28.
- (101) Schwarzer, D., and Cole, P. A. (2005) Protein semisynthesis and expressed protein ligation: chasing a protein's tail. *Curr. Opin. Chem. Biol.* 9, 561-569.
- (102) Winkler, J. R. (2000) Electron tunneling pathways in proteins. *Curr. Opin. Chem. Biol.* 4, 192-198.
- (103) Gräslund, A. (2002) Ribonucleotide reductase: kinetic methods for demonstrating radical transfer pathway in protein R2 of mouse enzyme in generation of tyrosyl free radical. *Methods Enzymol.* 354, 399-414.
- (104) Seyedsayamdost, M. R., and Stubbe, J. (2006) Site-specific replacement of Y₃₅₆ with 3,4-dihydroxyphenylalanine in the β_2 subunit of *E. coli* ribonucleotide reductase. *J. Am. Chem. Soc.* 128, 2522-2523.
- (105) Seyedsayamdost, M. R., Yee, C. S., Reece, S. Y., Nocera, D. G., and Stubbe, J. (2006) pH rate profiles of F_nY₃₅₆-R2s (n = 2, 3, 4) in *Escherichia coli* ribonucleotide reductase: evidence that Y₃₅₆ is a redox-active amino acid along the radical propagation pathway. *J. Am. Chem. Soc.* 128, 1562-1568.

- (106) Seyedsayamdost, M. R., Reece, S. Y., Nocera, D. G., and Stubbe, J. (2006) Mono-, di-, tri-, and tetra-substituted fluorotyrosines: new probes for enzymes that use tyrosyl radicals in catalysis. *J. Am. Chem. Soc.* *128*, 1569-1579.
- (107) Licht, S. S., Booker, S., and Stubbe, J. (1999) Studies on the catalysis of carbon-cobalt bond homolysis by ribonucleoside triphosphate reductase: evidence for concerted carbon-cobalt bond homolysis and thiyl radical formation. *Biochemistry* *38*, 1221-1233.
- (108) Chen, D., Abend, A., Stubbe, J., and Frey, P. A. (2003) Epimerization at carbon-5' of (5'R)-[5'-²H]adenosylcobalamin by ribonucleoside triphosphate reductase: cysteine 408-independent cleavage of the Co-C5' bond. *Biochemistry* *42*, 4578-4584.
- (109) Robins, M. J. (2003) Ribonucleotide reductase: radical chemistry and inhibition at the active site. *Nucleosides, Nucleotides Nucleic Acids* *22*, 519-534.
- (110) Himo, F., and Siegbahn, P. E. M. (2003) Quantum chemical studies of radical-containing enzymes. *Chem. Rev.* *103*, 2421-2456.
- (111) Stubbe, J., Ator, M., and Krenitsky, T. (1983) Mechanism of ribonucleoside diphosphate reductase from *Escherichia coli*: evidence for 3'-C—H bond cleavage. *J. Biol. Chem.* *258*, 1625-1630.
- (112) Licht, S., Gerfen, G. G., and Stubbe, J. (1996) Thiyl radicals in ribonucleotide reductases. *Science* *271*, 477-481.
- (113) Ashley, G. W., Harris, G., and Stubbe, J. (1986) The mechanism of *Lactobacillus leichmannii* ribonucleotide reductase: evidence for 3' carbon-hydrogen bond cleavage and a unique role for coenzyme B₁₂. *J. Biol. Chem.* *261*, 3958-3964.
- (114) Stubbe, J., Ackles, D., and Segal, R. (1981) On the mechanism of ribonucleoside triphosphate reductase from *Lactobacillus leichmannii*. *J. Biol. Chem.* *256*, 4843-4846.
- (115) Stubbe, J., and Ackles, D. (1980) On the mechanism of ribonucleoside diphosphate reductase from *Escherichia coli*: evidence for 3'-C—H bond cleavage. *J. Biol. Chem.* *255*, 8027-8030.
- (116) Zipse, H. (1995) The addition of water to ethylene and *trans*-butene radical cation. Model systems for the reaction of alkene radical cations with nucleophiles. *J. Am. Chem. Soc.* *117*, 11798-11806.
- (117) Buley, A. L., Norman, R. O. C., and Pritchett, R. J. (1966) Electron spin resonance studies of oxidation. Part VIII. Elimination reactions of some hydroxyalkyl radicals. *J. Chem. Soc. B*, 849-852.
- (118) Gilbert, C., Larkin, J. P., and R. O. C. Norman. (1972) Electron spin resonance studies. Part XXXIII. Evidence for heterolytic and homolytic transformations of radicals from 1,2-diols and related compounds. *J. Chem. Soc., Perkin Trans. 2*, 794-802.
- (119) Lenz, R., and Giese, B. (1997) Studies on the mechanism of ribonucleotide reductases. *J. Am. Chem. Soc.* *119*, 2784-2794.
- (120) Steenken, S. (1979) Oxidation of phenolates and phenylenediamines by 2-alkanonyl radicals produced from 1,2-dihydroxy- and 1-hydroxy-2-alkoxyalkyl radicals. *J. Phys. Chem.* *83*, 595-599.
- (121) Bansal, K. M., Gratzel, M., Henglein, A., and Janata, E. (1973) Polarographic and optical absorption studies of radicals produced in the pulse radiolysis of aqueous solutions of ethylene glycol. *J. Phys. Chem.* *77*, 16-19.
- (122) van der Donk, W. A., Yu, G., Silva, D. J., and Stubbe, J. (1996) Inactivation of ribonucleotide reductase by (*E*)-2'-fluoromethylene-2'-deoxycytidine 5'-diphosphate: a paradigm for nucleotide mechanism-based inhibitors. *Biochemistry* *35*, 8381-8391.

- (123) Åberg, A., Hahne, S., Karlsson, M., Larsson, Å., Ormö, M., Åhgren, A., and Sjöberg, B.-M. (1989) Evidence for two different classes of redox-active cysteines in ribonucleotide reductase of *Escherichia coli*. *J. Biol. Chem.* **264**, 12249-12252.
- (124) Akhlaq, M. S., Al-Baghdadi, S., and von Sonntag, C. (1987) On the attack of hydroxyl radicals on polyhydric alcohols and sugars and the reduction of the so-formed radicals by 1,4-dithiothreitol. *Carbohydr. Res.* **164**, 71-83.
- (125) Lawrence, C. C., Bennati, M., Obias, H. V., Bar, G., Griffin, R. G., and Stubbe, J. (1999) High-field EPR detection of a disulfide radical anion in the reduction of cytidine 5'-diphosphate by the E441Q R1 mutant of *Escherichia coli* ribonucleotide reductase. *Proc. Natl. Acad. Sci. U. S. A.* **96**, 8979-8984.
- (126) Alberty, R. A. (2004) Thermodynamic properties of nucleotide reductase reactions. *Biochemistry* **43**, 9840-9845.
- (127) Fernandes, P. A., and Ramos, M. J. (2004) Theoretical insights into the mechanism for thiol/disulfide exchange. *Chem. Euro. J.* **10**, 257-266.
- (128) Licht, S. S., Lawrence, C. C., and Stubbe, J. (1999) Class II ribonucleotide reductases catalyze carbon-cobalt bond reformation on every turnover. *J. Am. Chem. Soc.* **121**, 7463-7468.
- (129) Cho, K.-B., Himo, F., Gräslund, A., and Siegbahn, P. E. M. (2001) The substrate reaction mechanism of class III anaerobic ribonucleotide reductase. *J. Phys. Chem. B* **105**, 6445-6452.
- (130) Mulliez, E., Ollagnier, S., Fontecave, M., Eliasson, R., and Reichard, P. (1995) Formate is the hydrogen donor for the anaerobic ribonucleotide reductase from *Escherichia coli*. *Proc. Natl. Acad. Sci. U. S. A.* **92**, 8759-8762.
- (131) Plunkett, W., Huang, P., and Gandhi, V. (1997) Gemcitabine: actions and interactions. *Nucleosides Nucleotides* **16**, 1261-1270.
- (132) Silva, D. J., Stubbe, J., Samano, V., and Robins, M. J. (1998) Gemcitabine 5'-triphosphate is a stoichiometric mechanism-based inhibitor of *Lactobacillus leichmannii* ribonucleoside triphosphate reductase: evidence for thiyl radical-mediated nucleotide radical formation. *Biochemistry* **37**, 5528-5535.
- (133) van der Donk, W. A., Yu, G., Pérez, L., Sanchez, R. J., and Stubbe, J. (1998) Detection of a new substrate-derived radical during inactivation of ribonucleotide reductase from *Escherichia coli* by gemcitabine 5'-diphosphate. *Biochemistry* **37**, 6419-6426.
- (134) van der Donk, W. A., Gerfen, G. G., and Stubbe, J. (1998) Direct EPR spectroscopic evidence for an allylic radical generated from (*E*)-2'-fluoromethylene-2'-deoxycytidine 5'-diphosphate by *E. coli* ribonucleotide reductase. *J. Am. Chem. Soc.* **120**, 4252-4253.
- (135) Kanazawa, J., Takahashi, T., Akinaga, S., Tamaoki, T., and Okabe, M. (1998) The relationship between the antitumor activity and the ribonucleotide reductase inhibitory activity of (*E*)-2'-deoxy-2'-(fluoromethylene) cytidine, MDL 101,731. *Anti-Cancer Drugs* **9**, 653-657.
- (136) Mayhew, C. N., Sumpter, R., Inayat, M., Cibull, M., Phillips, J. D., Elford, H. L., and Gallicchio, V. S. (2005) Combination of inhibitors of lymphocyte activation (hydroxyurea, trimidox, and didox) and reverse transcriptase (didanosine) suppresses development of murine retrovirus-induced lymphoproliferative disease. *Antiviral Res.* **65**, 13-22.
- (137) King, S. B. (2005) *N*-Hydroxyurea and acyl nitroso compounds as nitroxyl (HNO) and nitric oxide (NO) donors. *Curr. Med. Chem.* **5**, 665-573.

- (138) Sumpter, L. R., Inayat, M. S., Yost, E. E., Duvall, W., Hagan, E., Mayhew, C. N., Elford, H. L., and Gallicchio, V. S. (2004) *In vivo* examination of hydroxyurea and the novel ribonucleotide reductase inhibitors trimidox and didox in combination with the reverse transcriptase inhibitor abacavir: suppression of retrovirus-induced immunodeficiency disease. *Antiviral Res.* **62**, 111-120.
- (139) Hendricks, S. P., and Mathews, C. K. (1998) Differential effects of hydroxyurea upon deoxyribonucleoside triphosphate pools, analyzed with vaccinia virus ribonucleotide reductase. *J. Biol. Chem.* **273**, 29519029523.
- (140) Gwilt, P. R., and Tracewell, W. G. (1998) Pharmacokinetics and pharmacodynamics of hydroxyurea. *Clin. Pharmacokinet.* **34**, 347-358.
- (141) Finch, R. A., Liu, M.-C., Cory, A. H., Cory, J. G., and Sartorelli, A. C. (1999) Triapine (3-aminopyridine-2-carboxaldehyde thiosemicarbazone; 3-AP): an inhibitor of ribonucleotide reductase with antineoplastic activity. *Adv. Enzyme Regul.* **39**, 3-12.
- (142) Finch, R. A., Liu, M.-C., Grill, S. P., Rose, W. C., Loomis, R., Vasquez, K. M., Cheng, Y.-C., and Sartorelli, A. C. (2000) Triapine (3-aminopyridine-2-carboxaldehydethiosemicarbazone): a potent inhibitor of ribonucleotide reductase activity with broad spectrum antitumor activity. *Biochem. Pharmacol.* **59**, 983-991.
- (143) Thelander, L., Larsson, B., Hobbs, J., and Eckstein, F. (1976) Active site of ribonucleoside diphosphate reductase from *Escherichia coli*: inactivation of the enzyme by 2'-substituted ribonucleoside diphosphates. *J. Biol. Chem.* **251**, 1398-1405.
- (144) Stubbe, J., and Kozarich, J. W. (1980) Inorganic pyrophosphate is released from 2'-chloro-2'-deoxyuridine 5'-diphosphate by ribonucleoside diphosphate reductase. *J. Am. Chem. Soc.* **102**, 2505-2507.
- (145) Stubbe, J., and Kozarich, J. W. (1980) Fluoride, pyrophosphate, and base release from 2'-deoxy-2'-fluoronucleoside 5'-diphosphates by ribonucleoside-diphosphate reductase. *J. Biol. Chem.* **255**, 5511-5513.
- (146) Harris, G., Ashley, G. W., Robins, M. J., Tolman, R. L., and Stubbe, J. (1987) 2'-Deoxy-2'-halonucleotides as alternate substrates and mechanism-based inactivators of *Lactobacillus leichmannii* ribonucleotide reductase. *Biochemistry* **26**, 1895-1902.
- (147) Ashley, G. W., Harris, G., and Stubbe, J. (1988) Inactivation of the *Lactobacillus leichmannii* ribonucleoside triphosphate reductase by 2'-chloro-2'-deoxyuridine 5'-triphosphate: stoichiometry of inactivation, site of inactivation, and mechanism of the protein chromophore formation. *Biochemistry* **27**, 4305-4310.
- (148) Ator, M. A., and Stubbe, J. (1985) Mechanism of inactivation of *Escherichia coli* ribonucleotide reductase by 2'-chloro-2'-deoxyuridine 5'-diphosphate: evidence for generation of 2'-deoxy-3'-ketonucleotide via a net 1,2 hydrogen shift. *Biochemistry* **24**, 7214-7221.
- (149) Kräutler, B. (2005) Vitamin B₁₂: chemistry and biochemistry. *Biochem. Soc. Trans.* **33**, 806-810.
- (150) Brown, K. L. (2005) Chemistry and enzymology of vitamin B₁₂. *Chem. Rev.* **105**, 2075-2149.
- (151) Banerjee, R. (2001) Radical peregrinations catalyzed by coenzyme B₁₂-dependent enzymes. *Biochemistry* **40**, 6191-6198.
- (152) Toraya, T. (2000) The structure and the mechanism of action of coenzyme B₁₂-dependent diol dehydratases. *J. Mol. Catal. B: Enzym.* **10**, 87-106.

- (153) Yamanishi, M., Ide, H., Murakami, Y., and Toraya, T. (2005) Identification of the 1,2-propanediol-1-yl radical as an intermediate in adenosylcobalamin-dependent diol dehydratase reaction. *Biochemistry* 44, 2113-2118.
- (154) Sandala, G. M., Smith, D. M., Coote, M. L., Golding, B. T., and Radom, L. (2006) Insights into the hydrogen-abstraction reactions of diol dehydratase: relevance to the catalytic mechanism and suicide inactivation. *J. Am. Chem. Soc.* 128, 3433-3444.
- (155) Harris, G., Ator, M., and Stubbe, J. (1984) Mechanism of inactivation of *Escherichia coli* and *Lactobacillus leichmannii* ribonucleotide reductases by 2'-chloro-2'-deoxynucleotides: evidence for generation of 2-methylene-3(2H)-furanone. *Biochemistry* 23, 5214-5225.
- (156) Ashley, G. W., Harris, G., and Stubbe, J. (1988) Inactivation of the ribonucleoside triphosphate reductase from *Lactobacillus leichmannii* by 2'-chloro-2'-deoxyuridine 5'-triphosphate: a 3'-2' hydrogen transfer during the formation of 3'-keto-2'-deoxyuridine 5'-triphosphate. *Biochemistry* 27, 7841-7845.
- (157) Stubbe, J., Smith, G., and Blakley, R. L. (1983) Interaction of 3'-[³H]2'-chloro-2'-deoxyuridine 5'-triphosphate with ribonucleotide reductase from *Lactobacillus leichmannii*. *J. Biol. Chem.* 258, 1619-1624.
- (158) Cerqueira, N. M. F. S. A., Fernandes, P. A., and Ramos, M. J. (2006) Enzyme ribonucleotide reductase: unraveling an enigmatic paradigm of enzyme inhibition by furanone derivatives. *J. Phys. Chem. B.* 110, 21272-21281.
- (159) Baker, C. H., Banzon, J., Bollinger Jr., J. M., Stubbe, J., Samano, V., Robins, M. J., Lippert, B., Jarvi, E., and Resvick, R. (1991) 2'-Deoxy-2'-methylenecytidine and 2'-Deoxy-2',2'-difluorocytidine 5'-diphosphates: Potent mechanism-based inhibitors of ribonucleotide reductase. *J. Med. Chem.* 34, 1879-1884.
- (160) Heinemann, V., Xu, Y.-Z., Chubb, S., Sen, A., Hertel, L. W., Grindey, G. B., and Plunkett, W. (1990) Inhibition of ribonucleotide reduction in CCRF-CEM cells by 2',2'-difluorodeoxycytidine. *Mol. Pharmacol.* 38, 567-572.
- (161) Sunkara, P. S., Lippert, B. J., Snyder, R. D., Jarvi, E. T., and Farr, R. A. (1988) Antitumor-activity of 2'-deoxy-2',2'-difluorocytidine, a novel inhibitor of ribonucleotide reductase. *Proceedings of the American Association for Cancer Research* 29, 324-324.
- (162) Artin, E., Thesis. (2006) in *Chemistry*, Massachusetts Institute of Technology, Cambridge, MA.
- (163) Silva, D. and Stubbe, J. Unpublished results, 1998.
- (164) Pereira, S., Fernandes, P. A., and Ramos, M. J. (2004) Mechanism for ribonucleotide reductase inactivation by the anticancer drug gemcitabine. *J. Comput. Chem.* 25, 1286-1294.
- (165) Xu, H., Faber, C., Uchiki, T., Racca, J., and Dealwis, C. (2006) Structures of eukaryotic ribonucleotide reductase I define gemcitabine diphosphate binding and subunit assembly. *Proc. Natl. Acad. Sci. U. S. A.* 103, 4028-4033.
- (166) Ator, M., Salowe, S. P., and Stubbe, J. (1984) 2'-Azido-2'-deoxynucleotide interaction with *E. coli* ribonucleotide reductase: generation of a new radical species. *J. Am. Chem. Soc.* 106, 1886-1887.
- (167) Salowe, S. P., Ator, M. A., and Stubbe, J. (1987) Products of the inactivation of ribonucleoside diphosphate reductase from *Escherichia coli* with 2'-azido-2'-deoxyuridine 5'-diphosphate. *Biochemistry* 26, 3408-3416.

- (168) Sjöberg, B.-M., Gräslund, A., and Eckstein, F. (1983) A substrate radical intermediate in the reaction between ribonucleotide reductase from *Escherichia coli* and 2'-azido-2'-deoxynucleoside diphosphates. *J. Biol. Chem.* 258, 8060-8067.
- (169) Fritscher, J., Artin, E., Wnuk, S., Bar, G., Robblee, J. H., Kacprzak, S., Kaupp, M., Griffin, R. G., Bennati, M., and Stubbe, J. (2005) Structure of the nitrogen-centered radical formed during inactivation of *E. coli* ribonucleotide reductase by 2'-azido-2'-deoxyuridine-5'-diphosphate: trapping of the 3'-ketonucleotide. *J. Am. Chem. Soc.* 127, 7729-7728.
- (170) Eriksson, L. A. (1998) Sulfinylimine radical in azido-CDP- and azido-UDP-inhibited ribonucleotide reductase. *J. Am. Chem. Soc.* 120, 8051-8054.
- (171) Salowe, S., Bollinger Jr., J. M., Ator, M., and Stubbe, J. (1993) Alternative model for mechanism-based inhibition of *Escherichia coli* ribonucleotide reductase by 2'-azido-2'-deoxyuridine 5'-diphosphate. *Biochemistry* 32, 12749-12760.
- (172) van der Donk, W. A., Stubbe, J., Gerfen, G. G., Bellew, B. F., and Griffin, R. G. (1995) EPR investigations of the inactivation of *E. coli* ribonucleotide reductase with 2'-azido-2'-deoxyuridine 5'-diphosphate: evidence for the involvement of the thiyl radical of C225-R1. *J. Am. Chem. Soc.* 117, 8909-8916.
- (173) Pereira, S., Fernandes, P. A., and Ramos, M. J. (2004) Theoretical study of ribonucleotide reductase mechanism-based inhibition by 2'-azido-2'-deoxyribonucleoside 5'-diphosphates. *J. Comput. Chem.* 25, 227-237.
- (174) Wright, P. S., Cross-Doersen, D., Th'ng, J. P. H., Guo, X.-W., Crissman, H. A., Bradbury, E. M., Montgomery, L. R., Thompson, F. Y., Loudy, D. E., Johnston, J. O., and Bitonti, A. J. (1996) A ribonucleotide reductase inhibitor, MDL 101,731, induces apoptosis and elevates TRPM-2 mRNA levels in human prostate tumor xenografts. *Exp. Cell. Res.*, 54-60.
- (175) Zhou, Y., Achanta, G., Pelicano, H., Gandhi, V., Plunkett, W., and Huang, P. (2002) Action of (*E*)-2'-deoxy-2'-(fluoromethylene)cytidine on DNA metabolism: incorporation, excision, and cellular response. *Mol. Pharmacol.* 61, 222-229.
- (176) Bridges, C. G., Ahmed, S. P., Sunkara, P. S., McCarthy, J. R., and Tyms, A. S. (1995) The ribonucleotide reductase inhibitor (*E*)-2'-fluoromethylene-2'-deoxycytidine (MDL 101,731) a potential topical therapy for herpes simplex virus infection. *Antiviral Res.* 27, 325-334.
- (177) Gerfen, G. G., van der Donk, W. A., Yu, G., McCarthy, J. R., Jarvi, E. T., Matthews, D. P., Farrar, C., Griffin, R. G., and Stubbe, J. (1998) Characterization of a substrate-derived radical detected during the inactivation of ribonucleotide reductase from *Escherichia coli* by 2'-fluoromethylene-2'-deoxycytidine 5'-diphosphate. *J. Am. Chem. Soc.* 120, 3823-3835.
- (178) Covès, J., Le Hir de Fallois, L., Le Pape, L., Décout, J.-L., and Fontecave, M. (1996) Inactivation of *Escherichia coli* ribonucleotide reductase by 2'-deoxy-2'-mercaptouridine 5'-diphosphate. Electron paramagnetic resonance evidence for a transient protein perthiyl radical. *Biochemistry* 35, 8595-8602.
- (179) Pereira, S., Fernandes, P. A., and Ramos, M. J. (2005) Theoretical study on the inhibition of ribonucleotide reductase by 2'-mercapto-2'-deoxyribonucleoside-5'-diphosphates. *J. Am. Chem. Soc.* 127, 5174-5179.

- (180) Roy, B., Chambert, S., Lepoivre, M., and Décout, J.-L. (2003) Thionucleotides as inhibitors of ribonucleotide reductase. *Nucleosides, Nucleotides Nucleic Acids* 22, 883-885.
- (181) Line, J. P., and Larson, R. A. (2005) Cloarabine in the treatment of acute myeloid leukaemia and acute lymphoblastic leukaemia: a review. *Expert Opin.* 6, 2711-2718.
- (182) Gandhi, V., and Plunkett, W. (2002) Cellular and clinical pharmacology of fludarabine. *Clin. Pharmacokinet.* 41, 93-103.
- (183) Harrington, J. A., and Spector, T. (1991) Human ribonucleotide reductase: activation and inhibition by analogs of ATP. *Biochem. Pharmacol.* 42, 759-763.
- (184) Parker, W. B., Bapat, A. A., Shen, J.-X., Townsend, A. J., and Cheng, Y.-C. (1988) Interaction of 2-halogenated dATP analogs (F, Cl, and Br) with human DNA polymerases, DNA primase, and ribonucleotide reductase. *Mol. Pharmacol.* 34, 485-491.
- (185) Parker, W. B., Shaddix, S. C., Chang, C. H., White, E. L., Rose, L. M., Brockman, R. W., Shortnacy, A. T., Montgomery, J. A., Secrist, J. A., and Bennett, L. L. (1991) Effects of 2-chloro-9-(2-deoxy-2-fluoro- β -D-arabinofuranosyl)adenine on K562 cellular-metabolism and the inhibition of human ribonucleotide reductase and DNA-polymerases by its 5'-triphosphate. *Cancer Res.* 51, 2386-2394.
- (186) Shao, J., Zhou, B., Zhu, L., Bilio, A. J. D., Su, L., Yuan, Y.-C., Ren, S., Lien, E. J., Shih, J., and Yen, Y. (2005) Determination of the potency and subunit-selectivity of ribonucleotide reductase inhibitors with a recombinant-holoenzyme-based *in vitro* assay. *Biochem. Pharmacol.* 69, 627-634.
- (187) Yeh, Y.-C., and Tessman, I. (1978) Differential effect of hydroxyurea on a ribonucleotide reductase system. *J. Biol. Chem.* 253, 1323-1324.
- (188) Berglund, O., and Sjöberg, B.-M. (1979) Effect of hydroxyurea on T4 ribonucleotide reductase. *J. Biol. Chem.* 254, 253-354.
- (189) Moore, E. C., and Hurlbert, R. B. (1985) The inhibition of ribonucleotide diphosphate reductase by hydroxyurea, guanazole and pyrazoloimidazole (IMPY). *Pharmac. Ther.* 27, 167-196.
- (190) Lam, K., Fortier, D. G., Thomson, J. B., and Sykes, A. G. (1990) Kinetics of inactivation of the tyrosine radical of the B2 subunit of *E. coli* ribonucleotide reductase. *Chem. Commun.*, 658-660.
- (191) Karlsson, M., Sahlin, M., and Sjöberg, B.-M. (1992) *Escherichia coli* ribonucleotide reductase: radical susceptibility to hydroxyurea is dependent on the regulatory state of the enzyme. *J. Biol. Chem.* 267, 12622-12626.
- (192) Nyholm, S., Thelander, L., and Gräslund, A. (1993) Reduction and loss of the iron center in the reaction of the small subunit of mouse ribonucleotide reductase with hydroxyurea. *Biochemistry* 32, 11569-11574.
- (193) Koç, A., Wheeler, L. J., Mathews, C. K., and Merrill, G. F. (2004) Hydroxyurea arrests DNA replication by a mechanism that preserves basal dNTP pools. *J. Biol. Chem.* 279, 223-230.
- (194) Moore, E. C., and Sartorelli, A. C. (1984) Inhibition of ribonucleotide reductase by α -(N)-heterocyclic carboxaldehyde thiosemicarbazones. *Pharmac. Ther.* 24, 439-447.
- (195) Li, J., Zheng, L., King, I., Doyle, T. W., and Chen, S.-H. (2001) Syntheses and antitumor activities of potent inhibitors of ribonucleotide reductase: 3-amino-4-methylpyridine-2-carboxaldehyde-thiosemicarbazone (3-Amp), 3-amino-pyridine-2-carboxaldehyde-thiosemicarbazone (3-Ap) and its water soluble prodrugs. *Curr. Med. Chem.* 8, 121-133.

- (196) Spector, T., Harrington, J. A., and Porter, D. J. T. (1991) Herpes and human ribonucleotide reductases - inhibition by 2-acetylpyridine 5-[(2-chloroanilino)-thiocarbonyl]-thiocarbonohydrazone (348U87). *Biochem. Pharm.* **42**, 91-96.
- (197) Porter, D. J. T., Harrington, J. A., and Spector, T. (1990) Herpes-simplex virus type-1 ribonucleotide reductase - selective and synergistic inactivation by A1110U and its iron complex. *Biochem. Pharm.* **39**, 639-646.
- (198) Richardson, D. R. (2005) Molecular mechanisms of iron uptake by cells and the use of iron chelators for the treatment of cancer. *Curr. Med. Chem.* **12**, 2711-2729.
- (199) Beraldo, H., and Gambino, D. (2004) The wide pharmacological versatility of semicarbazones, thiosemicarbazones and their metal complexes. *Mini-Rev. Med. Chem.* **4**, 31-39.
- (200) Li, J., Chela, S.-H., Li, X., Niu, C., and Doyle, T. W. (1998) Efficient synthesis of ribonucleotide reductase inhibitors 3-aminopyridine-2-carboxaldehyde thiosemicarbazone 3-AP) and 3-amino-4-methylpyridine-2-carboxaldehyde thiosemicarbazone 3-AMP) via palladium mediated cross-coupling reactions. *Tetrahedron* **54**, 393-400.
- (201) Cooper, C. E., Lynagh, G. R., Hoyes, K. P., Hider, R. C., Cammack, R., and Porter, J. B. (1996) The relationship of intracellular iron chelation to the inhibition and regeneration of human ribonucleotide reductase. *J. Biol. Chem.* **271**, 20291-20299.
- (202) Gao, Y., Kashlan, O. B., Kaur, J., Tan, C., and Cooperman, B. S. (2005) Mechanisms of action of peptide inhibitors of mammalian ribonucleotide reductase targeting quaternary structure. *Biopolymers* **80**, 9-17.
- (203) Pellegrini, M., Liehr, S., Fisher, A. L., Laub, P. B., Cooperman, B. S., and Mierke, D. F. (2000) Structure-based optimization of peptide inhibitors of mammalian ribonucleotide reductase. *Biochemistry* **39**, 12210-12215.
- (204) Pender, B. A., Wu, X., Axelsen, P. H., and Cooperman, B. S. (2001) Toward a rational design of peptide inhibitors of ribonucleotide reductase: structure-function and modeling studies. *J. Med. Chem.* **44**, 36-46.
- (205) Hamann, C. S., Lentainge, S., Li, L.-S., Salem, J. S., Yang, F.-D., and Cooperman, B. S. (1998) Chimeric small subunit inhibitors of mammalian ribonucleotide reductase: a dual function for the R2 C-terminus? *Protein Eng.* **11**, 219-224.
- (206) Fisher, A., Yang, F.-D., Rubin, J. H., and Cooperman, B. S. (1993) R2 C-terminal peptide inhibition of mammalian and yeast ribonucleotide reductase. *J. Med. Chem.* **36**, 3859-3862.
- (207) Duan, J., Liuzzi, M., Paris, W., Lambert, M., Lawetz, C., Moss, N., Jaramillo, J., Gauthier, J., DéZiel, R., and Cordingley, M. G. (1998) Antiviral activity of a selective ribonucleotide reductase inhibitor against acyclovir-resistant herpes simplex virus type 1 *in vivo*. *Antimicrob. Agents Chemother.* **42**, 1629-1635.
- (208) Moss, N., Beaulieu, P., Duceppe, J.-S., Ferland, J.-M., Garneau, M., Gauthier, J., Ghio, E., Goulet, S., Guse, I., Jaramillo, J., Llinas-Brune, M., Malenfant, É., Plante, R., Poirier, M., Soucy, F., Wernic, D., Yoakim, C., and Déziel, R. (1996) Peptidomimetic inhibitors of herpes simplex virus ribonucleotide reductase with improved *in vivo* antiviral activity. *J. Med. Chem.* **39**, 4173-4180.
- (209) Moss, N., Beaulieu, P., Duceppe, J.-S., Ferland, J.-M., Gauthier, J., Ghio, E., Goulet, S., Grenier, L., Llinas-Brunet, M., Plante, R., Wernic, D., and Déziel, R. (1995)

- Peptidomimetic inhibitors of herpes simplex virus ribonucleotide reductase: a new class of antiviral agents. *J. Med. Chem.* **38**, 3617-3623.
- (210) Moss, N., Beaulieu, P., Duceppe, J.-S., Ferland, J.-M., Gauthier, J., Ghio, E., Goulet, S., Guse, I., Llinàs-Brunet, M., Plante, R., Plamondon, L., Wernic, D., and Déziel, R. (1996) Ureido-based peptidomimetic inhibitors of herpes simplex virus ribonucleotide reductase: an investigation of inhibitor bioactive conformation. *J. Med. Chem.* **39**, 2178-2187.
- (211) Moss, N., Dbziel, R., Adams, J., Aubry, N., Bailey, M., Baillet, M., Beaulieu, P., DiMaio, J., Duceppe, J.-S., Ferland, J.-M., Gauthier, J., Ghio, E., Goulet, S., Grenier, L., Lavallbe, P., Upine-Frenette, C., Plante, R., Rakhit, S., Soucy, F., Wernic, D., and Guindon, Y. (1993) Inhibition of herpes simplex virus type 1 ribonucleotide reductase by substituted tetrapeptide derivatives. *J. Med. Chem.* **36**, 3005-3009.
- (212) Dutia, B. M., Frame, M. C., Subak-Sharpe, J. H., Clark, W. N., and Marsden, H. S. (1986) Specific inhibition of herpesvirus ribonucleotide reductase by synthetic peptides. *Nature* **321**, 439-441.
- (213) Cohen, E. A., Gaudreau, P., Brazeau, P., and Langelier, Y. (1986) Specific inhibition of herpes virus ribonucleotide reductase by a nonapeptide derived from the carboxy terminus of subunit 2. *Nature* **321**, 441-443.
- (214) Liuzzi, M., Déziel, R., Moss, N., Beaulieu, P., Bonneau, A.-M., Bousquet, C., Chafouleas, J. G., Garneau, M., Jaramillo, J., Krogsrud, R. L., Lagacé, L., McCollum, R. S., Nawoot, S., and Guindon, Y. (1994) A potent peptidomimetic inhibitor of HSV ribonucleotide reductase with antiviral activity *in vivo*. *Nature* **372**, 695-698.
- (215) Gao, Y., Liehry, S., and Cooperman, B. S. (2002) Affinity-driven selection of tripeptide inhibitors of ribonucleotide reductase. *Bioorg. Med. Chem. Lett.* **12**, 513-515.
- (216) Climent, I., and Sjöberg, B.-M. (1991) Carboxyl-terminal peptides as probes for *Escherichia coli* ribonucleotide reductase subunit interaction: kinetic analysis of inhibition studies. *Biochemistry* **30**, 5164-5171.
- (217) Fuertes, M. J., Kaur, J., Deb, P., Cooperman, B. S., and Smith III, A. B. (2005) Design, synthesis, and evaluation of octahydropyranopyrrole-based inhibitors of mammalian ribonucleotide reductase. *Bioorg. Med. Chem. Lett.* **15**, 5146-5149.
- (218) Liehr, S., Barbosa, J., Smith III, A. B., and Cooperman, B. S. (1999) Synthesis and biological activity of cyclic peptide inhibitors of ribonucleotide reductase. *Org. Lett.* **1**, 1201-1204.
- (219) Smith III, A. B., Sasho, S., Barwis, B. A., Sprengeler, P., Barbosa, J., Hirschmann, R., and Cooperman, B. S. (1998) Design and synthesis of a tetrahydropyran-based inhibitor of mammalian ribonucleotide reductase. *Bioorg. Med. Chem. Lett.* **8**, 3133-3136.
- (220) Brandt, C. R., Spencer, B., Imesch, P., Garneau, M., and Déziel, R. (1996) Evaluation of a peptidomimetic ribonucleotide reductase inhibitor with a murine model of herpes simplex virus type 1 ocular disease. *Antimicrob. Agents Chemother.* **40**, 1078-1084.
- (221) Lawetz, C., and Liuzzi, M. (1998) The antiviral activity of the ribonucleotide reductase inhibitor BILD 1351 SE in combination with acyclovir against HSV type-1 in cell culture. *Antiviral Res.* **39**, 35-46.

Chapter 5

Synthesis of Isotopically-Labeled Gemcitabine (F₂C) 5'-Phosphates

5.1 Introduction

F₂C and ribonucleotide reductase

The nucleoside analogue 2'-deoxy-2',2'-difluoro-cytidine (F₂C, Gemzar™, 5-1) is a clinically used anti-cancer drug, believed to target both ribonucleotide reductase and DNA polymerases *in vivo*.(1-6) F₂C was initially synthesized at Merrell Dow Pharmaceuticals(6) and Eli Lilly Research Laboratory(7) as part of an effort to determine the usefulness of nucleoside analogues as potential anti-viral and anti-tumor agents. F₂C itself showed strong activity against a broad spectrum of RNA and DNA viruses, but was deemed unsuitable for use as an antiviral due to its narrow therapeutic window.(3) Subsequent studies found F₂C was also a potent antitumor agent, whose activity could be maintained while reducing side-effects to tolerable levels.(8) F₂C has since seen broad application to a range of cancers.(1, 9-27)

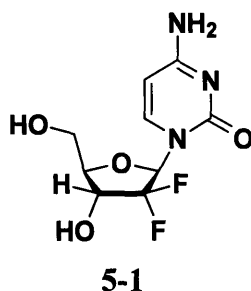


Figure 5-1. Gemcitabine (F₂C).

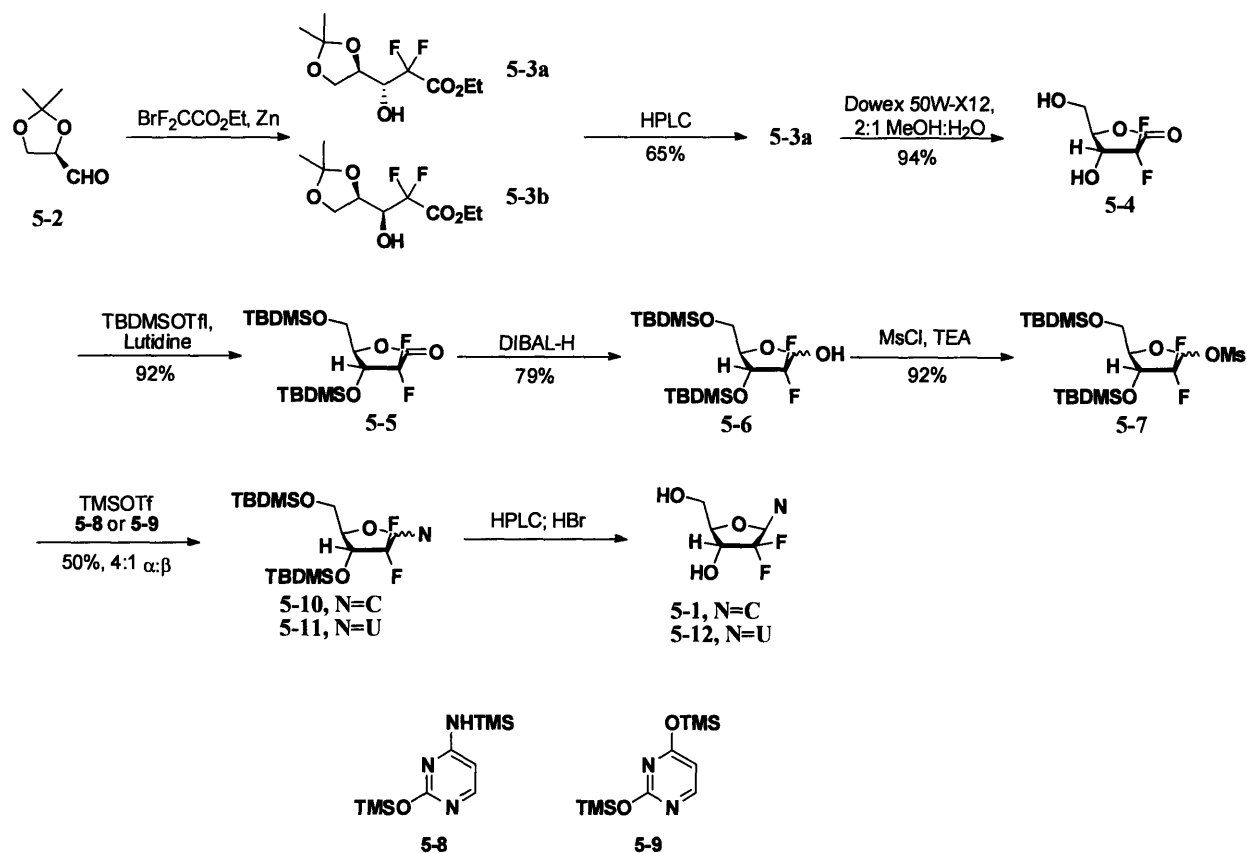
The mechanism by which F₂C inactivates ribonucleotide reductase (RNR) has been the subject of a number of investigations(28-31) modeled on the detailed understanding of the mechanism by which 2'-substituted nucleotides inhibit RNR.(32) These studies revealed that gemcitabine 5'-diphosphate (F₂CDP) (or -triphosphate (F₂CTP) in the case of RTPR) is a stoichiometric, mechanism-based inhibitor. Inactivation is irreversible, and accompanied by the loss of two equiv. of fluoride. This inactivation behavior has been observed for both *E. coli* RDPR(30) and *L. leichmannii* RTPR.(31) As with most nucleotide mechanism-based inhibitors,

base release was detected in the case of RDPR. In the case of RTPR, however, no cytosine release was detected. The lack of radiolabeled F₂C analogs made monitoring the fate of the nucleotide, both base and sugar, challenging. In order to gain new insights into the mechanism of inactivation, the synthesis of isotopically labeled derivatives of F₂C was required.

This chapter reports the synthesis of 1'-[²H], 1'-[³H], 5-[³H], and 3'-[²H] labeled F₂CDP and F₂CTP. The radiolabeled compounds have allowed us to track the fate of the nucleotide base and sugar moieties during the inactivation of RNR. The deuterated compounds have facilitated identification of peptides modified during the inactivation, provided insight into the structure of the nucleotide radical generated during inactivation, and provided the potential to examine effects on 3' C-H bond cleavage on rate and mechanism.

Syntheses of F₂C in the literature

The original synthesis of F₂C is outlined in Scheme 5-1.(7) Traditional methods of inserting a gem-difluoro moiety, such as (diethylamino)sulfur trifluoride (DAST), work poorly on five-membered sugar ring systems, due to competitive elimination and, for the 2-ketones, migration of the anomeric group, instead of addition of the second fluorine.(33) To avoid this problem, the group is installed as part of a total synthesis of the sugar ring. The D-stereochemistry desired in the final ribose analogue is first introduced as (*R*)-2,3-*O*-isopropylidene-glyceraldehyde (**5-2**), itself prepared from D-mannitol by the method of Baer and Fischer. This compound was coupled under Reformatsky conditions with ethyl bromodifluoroacetate to give a 3:1 mixture of the diastereomeric products **5-3a** and **5-3b**. These isomers were separated by HPLC to give the desired isomer **5-3a** in 65% yield.

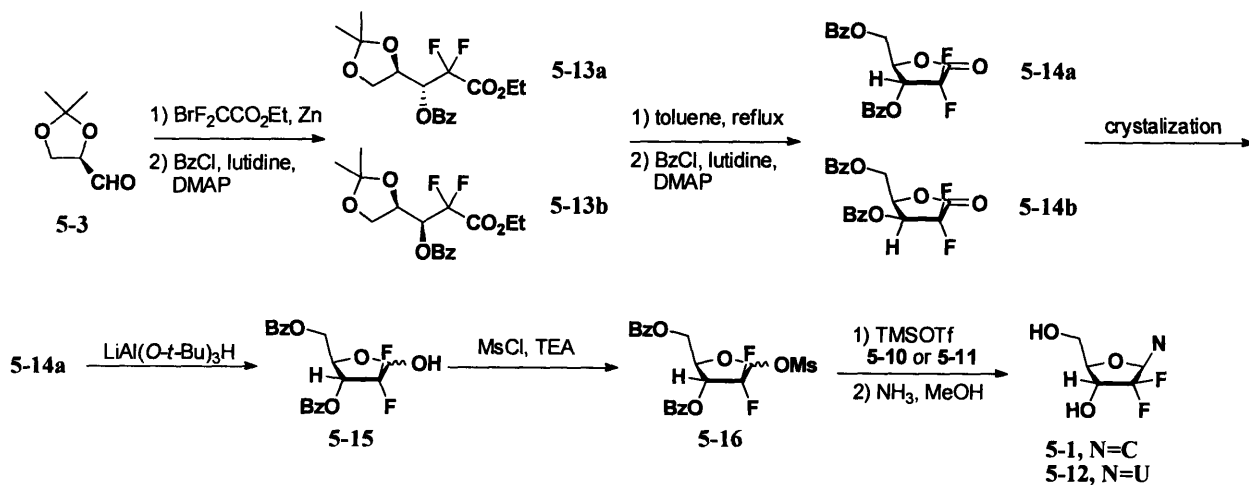


Scheme 5-1. First reported synthesis of F₂C.

The isopropylidene group of compound **5-3a** was cleaved under hydrolytic conditions with DOWEX 50W-X12 resin (acidic form) in 2:1 methanol: water, simultaneously closing the ring to the lactone product **5-4** in 94% yield. This compound was protected with TBDMS-ethers through reaction with TBDMS-triflate and lutidine to give **5-5** in 92% yield. The lactone could then be reduced by treatment with DIBAL-H to give the lactol **5-6** in 79% yield. The protected lactol **5-6** was converted to the anomeric mesylate **5-7** by treatment with methanesulfonyl chloride. The mesylate was used in this case due to the enhanced stability of anomeric leaving groups on 2,2-difluororibose derivatives, caused by the presence of the *gem*-difluoro moiety.⁽³⁴⁾ The presumed coupling mechanism using anomeric leaving groups such as mesyl is a S_N1-like Lewis-acid catalyzed loss of mesyl alcohol. The generation of the carbocationic species is highly disfavored by the electronegative *gem*-difluoro group. Coupling of the mesylate to *bis*-

trimethylsilyl-cytosine **5-8** or -uracil **5-9** could be achieved by extended reflux in the presence of trimethylsilyl triflate to give the product protected nucleosides **5-10** and **5-11** in 50% yield as a 4:1 α : β mixture. The desired β anomer could be separated by HPLC and deprotected by acidic hydrolysis to give **5-1** or its uracil analogue **5-12**.

A later refinement of this synthesis by Lilly researchers is outlined in Scheme 5-2.(34) The goal of this group was to produce a synthesis suitable for kilogram scale production. They thus needed to eliminate the HPLC purification steps and improve the yield of the desired β anomer. These goals were accomplished by use of the benzoyl ester protecting group in place of the TBDMS ethers used in the original synthesis. Here, the products of the initial coupling were esterified with benzoyl chloride in good yield to give **5-13a** and **5-13b**; the benzoyl group was introduced at this stage solely to provide a convenient chromophore for reaction monitoring by HPLC or TLC.(34) The isopropylidene group was removed by acid hydrolysis, and the deprotected compound converted to the furanose lactone derivatives through azeotropic distillation in toluene, then esterified with benzoyl chloride to give the isomers **5-14a** and **5-14b**. A selective crystallization from the crude reaction mixture provided the desired *ribo* isomer **5-14a** in good yields even on very large (thousand-gallon) scale.



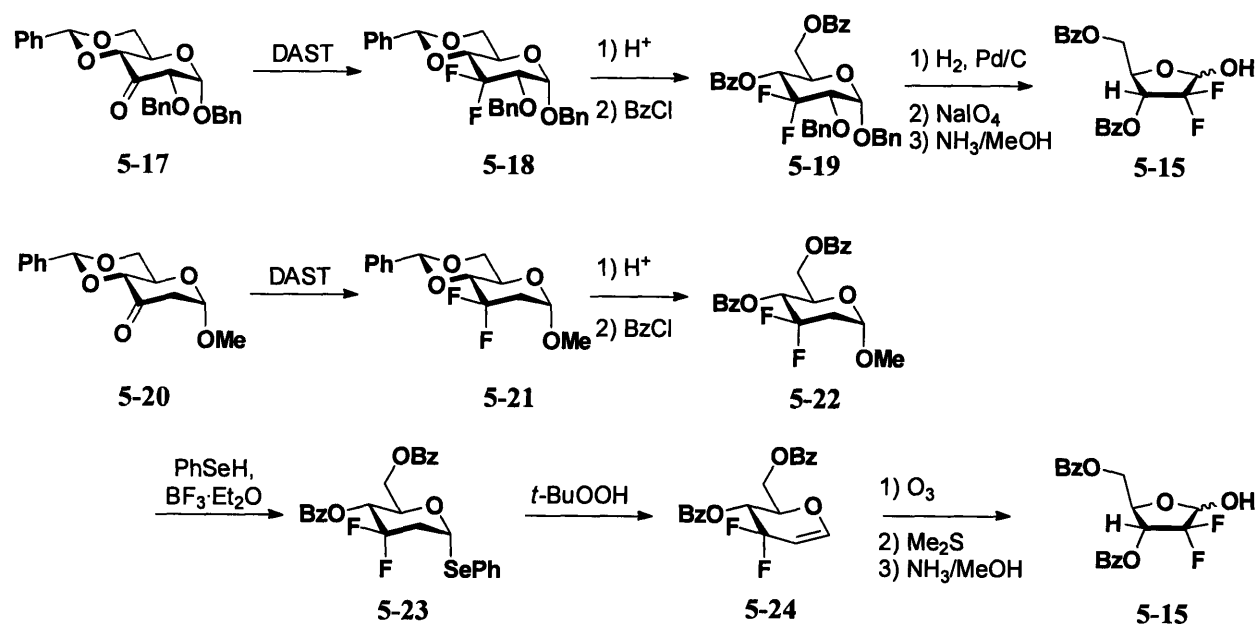
Scheme 5-2. Second generation F₂C synthesis.

The lactone **5-14a** was reduced to the lactol **5-15** through treatment with lithium tri-*tert*-butoxy aluminum hydride and converted to the mesylate **5-16** (1:1 mixture of anomers). The presence of the *gem*-difluoro group was found to render these mesylates very stable in inert solvents, even at elevated temperatures. Through the procedure outlined in the original publication, the mesylates could be coupled with the TMS derivatives of cytosine or uracil to give the protected nucleosides as 1:1 anomeric mixtures, a significant improvement over the original method. The desired β anomer could be separated from the α anomer through crystallization, either before or after cleavage of the benzoate esters by treatment with methanolic ammonia.

Other variations on the syntheses of 2,2-difluoro ribose have been published. Yatsuda and coworkers⁽³⁵⁾ described optimized coupling conditions for the condensation under Reformatsky conditions of chiral aldehydes and halodifluoroacetates. They surveyed a range of Lewis acids and concluded that use of Cp_2TiCl_2 gave the best results, with yields near 90% and enantioselectivities of 10-20:1 for the desired isomer when coupling (*R*)-2,3-*O*-cyclohexylidene-glyceraldehyde and ethyl difluoroiodoacetate in the synthesis of 2,2-difluororibose.

Using a different approach to installing the *gem*-difluoro moiety, Castellón and coworkers devised a route to 2,2-difluororibose that allowed the insertion of the fluorines using the reagent DAST (Scheme 5-3). By starting from D-glucose or D-mannose, the problem of diastereoselectivity is entirely avoided, as all stereocenters that will be in the 2,2-difluororibose are already set in the starting material. In preliminary work, the authors confirmed that attempts to react ribo-2-keto sugar with DAST produced only degradation products, while glucose 2- and 3-keto sugars reacted to produce the *gem*-difluoro moiety (though some products from

competitive reactions were observed).(33) A protected glucose derivative was oxidized to the corresponding keto sugar **5-17** using pyridinium chlorochromate (PCC) in 90% yield. This keto sugar was treated with DAST in refluxing benzene to yield the difluoro derivative **5-18** in 60% yield. The benzylidene was hydrolyzed with acid and the free hydroxyls were esterified with benzoyl chloride to give **5-19** in 85% yield. The benzyl ethers were removed by hydrogenation over Pd/C in 59% yield, and the resultant diol was converted to the *ribo* derivative by NaIO₄ cleavage followed by treatment with methanolic ammonia to give the lactol **5-15** in 43% yield.



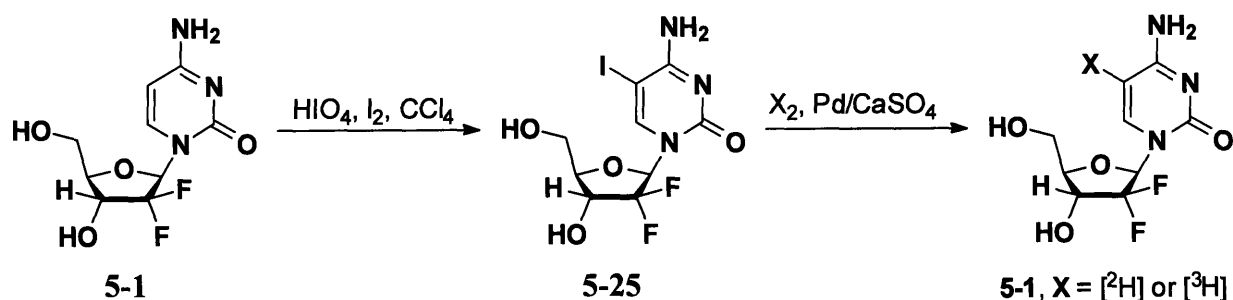
Scheme 5-3. Alternative synthesis of protected difluororibose.

Similarly, the authors synthesized **5-15** beginning from the D-mannose-derivative **5-20**. Treatment of this keto sugar with DAST gave **5-21** in 70% yield; the increased yield relative to the reaction of **5-17** is likely due to the less hindered nature of this keto sugar. Cleavage of the benzylidene followed by esterification with benzoyl chloride gave **5-22** in 85% yield. Reaction of this methyl glycoside with PhSeH and BF₃·Et₂O resulted in the seleno glycoside **5-23** in 72% yield; reaction with the radical initiator *t*-BuOOH gave the 1,2-anhydro sugar **5-24** in 72% yield. Ozonolysis of this compound, followed by treatment with Me₂S, then methanolic ammonia gave

5-15 in 42% yield. While approaches beginning with hexoses have the advantage of eliminating the separation of stereoisomers, the increased length and lower yields prevent them from displacing the Lilly synthesis (Scheme 5-2) as the method of choice for production of 2,2-difluororibose.

Synthesis of 2-[¹⁴C] and 5-[³H] F₂C

An early report from Eli Lilly(36) describes preparation of several radio-labeled versions of F₂C. The 2-[¹⁴C] derivative was prepared by substitution of 2-[¹⁴C]-cytosine in the normal reaction scheme (Scheme 5-2). Substitution of [²H] or [³H] at C5 was accomplished as shown in Scheme 5-4: F₂C was treated with HIO₄ and I₂ in CCl₄ in a procedure analogous to that used previously on cytidine(37) to give the 5-iodo derivative 5-25, then treated with deuterium or tritium gas in the presence of Pd/CaSO₄ in 1:1 dioxane:D₂O.

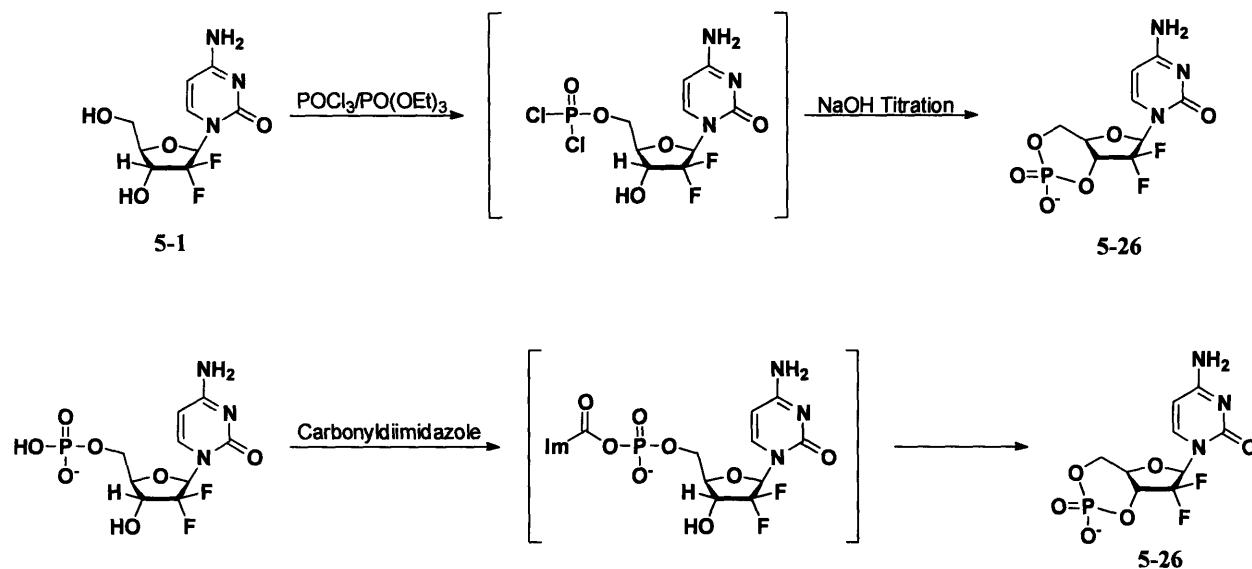


Scheme 5-4. Isotopic labeling of F₂C.

Phosphorylation of F₂C

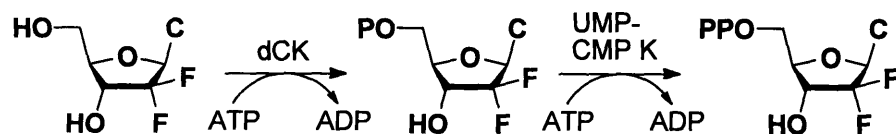
The synthesis of the F₂C di- and triphosphate substrates for RDPR and RTPR have also been challenging. In the early studies,(28, 29) the F₂C phosphates used were reported to have been prepared by the standard chemical methods (Scheme 5-5).(38-41) However, early studies in the McCarthy, Robins, and Stubbe groups (unpublished results) revealed that the primary

product of this chemistry was the 3',5' cyclic phosphate **5-26**. In retrospect, this result was not surprising due to the high acidity of the 3' hydroxyl group caused by the nearby fluorines; the desired 5'-phosphates can only be accessed in very low yield through these methods.



Scheme 5-5. Chemical phosphorylation of F₂C.

Several researchers have been able to circumvent this problem through the use of enzymatic phosphorylation methods. Early work at Merrell Dow,(29, 42) and later investigations have explored the use of human deoxycytidine kinase (dCK)(43-45) and human UMP/CMP kinase (UMP-CMP K)(46-48) as tools for the production of F₂CMP and F₂CDP.(43, 47, 48) The availability of large quantities of these proteins has been made possible through recombinant technology, and recent studies in the Stubbe laboratory have allowed the use of these enzymes for the production of large quantities of F₂C mono- and diphosphates (Scheme 5-6).(49)



Scheme 5-6. Enzymatic phosphorylation of F₂C.

Goals of current work

The primary limiting factors in the continued elucidation of the mechanism of action of F₂C has been the lack of derivatives isotopically labeled on the sugar ring, and a lack of a simple, generally applicable method for the production of F₂C 5'-phosphates. The current work describes syntheses that allow for the incorporation of [²H] or [³H] at the 1'- and 3'-positions of F₂C. Refinements to the enzymatic synthesis of F₂C 5'-phosphates are described, allowing easy production of significant quantities of F₂CDP and the extension of these methods to the production of F₂CTP, phosphorylation of isotopically-labeled derivatives of F₂C, and to the phosphorylation of 2'-deoxy-2'-fluorocytidine. The deuterated and tritiated compounds have been used for the mechanistic studies described in Chapter 6.

5.2 Experimental

General Procedures. Pyridine and triethylamine were dried by distillation from KOH. All other organic solvents were dried by distillation from CaH or purchased anhydrous, unless otherwise noted. Analytical thin-layer chromatography (TLC) was performed on E. Merck silica gel 60 F254 plate (≤0.25 mm). Compounds were visualized by cerium sulfate-ammonium molybdate stain and heating or by exposure to UV light. Triethyl ammonium bicarbonate (TEAB) buffers, pH 6.8 were prepared by bubbling CO₂ through 1M triethylamine in water on ice for 30 min; dilutions were made from 1 M stocks and CO₂ bubbled through for 15 min on ice. Human dCK expression plasmids were a gift of Dr. Staffan Eriksson,(45) and the protein was expressed and purified as described previously(49) and stored in 20 mM Tris pH 7.9, 0.5 M NaCl, 10 mM DTT, 20% glycerol, with a SA of 150 nmol mg⁻¹min⁻¹. UMP/CMP kinase plasmids were a kind gift of Dr. Anna Karlsson,(47) and was expressed and purified as described

previously(49) and stored in 50 mM TRIS pH 8.0 containing 10 mM reduced glutathione, with a SA of 2.1-4.8 $\mu\text{mol mg}^{-1}\text{min}^{-1}$. UMP-CMP K concentration was determined by Bradford assay with a BSA standard. 2-Deoxy-3,5-di-*O*-benzoly-2,2-difluororibonolactone was a gift of Eli Lilly & Co. Inorganic pyrophosphatase (baker's yeast), SA 868 U/mg, was obtained from Sigma as a lyophilized powder and taken up in 165 mM Tris pH 7.2 immediately prior to use. Pyruvate kinase (rabbit muscle), SA 450 U/mg, was obtained from Sigma as a lyophilized powder and prepared as a 1200 U/mL stock in 50 mM Tris pH 7.5, 80 mM KCl, 20 mM MgCl₂. Extinction coefficients used were: dCK ($\epsilon_{2808} = 56755$ at pH 7.0); F₂C, ($\epsilon_{268} = 9360$ at pH 7.0);(34) cytidine ($\epsilon_{271} = 9100$ at pH 7.0), cytosine ($\epsilon_{267} = 6100$ at pH 7.0), adenosine ($\epsilon_{259} = 15400$ at pH 7.0).(50) Solutions of BSA were quantified assuming an A(280) of 0.67 for a 1 mg/mL solution. (50) UV-vis spectra were taken on a Cary-3 spectrometer. Anion exchange column fractions were assayed using a Ultramark Bio-RAD fixed wavelength plate reader. Scintillation counting was performed using Emulsifier-Safe liquid scintillation counting cocktail (Perkin Elmer) on a Beckman LS6500 multipurpose scintillation counter.

Purification of 2-deoxy-3,5-di-*O*-benzoly-2,2-difluororibonolactone (5-14a)(34) Compound **5-14a** was purified before use by suspension in CH₂Cl₂ (5 mL/g of material) followed by filtration to remove the insoluble hydrolyzed lactone (**5-27**) The solvent was removed via rotary evaporator to give purified **5-14a**. To convert the hydrolyzed lactone back to **5-14a**, the compound (**5-27**, 2g, 5.29 mmol) was suspended in toluene (80 mL) in a round bottom flask. A Dean-Stark trap and condenser were attached and the trap filled with additional toluene (20 mL). The reaction was heated to reflux for 24 h. All solids went into solution upon boiling. The reaction was cooled to room temperature, filtered through a pad of celite, and the solvent

removed *in vacuo*. The product (1.9 g, 5.05 mmol, 95%) was a white powder fully soluble in CH₂Cl₂. The proton NMR spectrum was consistent with authentic **5-14a**.⁽³⁴⁾

2-Deoxy-3,5-di-O-benzoyl-2,2-difluoro-1-O-methanesulfonyl-D-ribofuranoside (5-16).

Procedure A:⁽³⁴⁾ All solvents and liquid reagents were distilled from CaH before use, except methanesulfonyl chloride, which was distilled from P₂O₅. Lactone **5-14a** (276 mg, 0.72 mmol) was dissolved in Et₂O (5.8 mL) and THF (1.4 mL). The reaction was cooled to 0°C in an ice/water bath, LiAl(*O-t*-Bu)₃H (218 mg, 0.86 mmol) was added as a solid, and the reaction was stirred 90 min at 0°C under N₂. The mixture was diluted to 100 mL with ethyl acetate and washed with 50 mL each of 1N HCl, brine, and saturated NaHCO₃. The organic layer was dried over MgSO₄, filtered, and the solvent removed *in vacuo*. The residue was dried by co-evaporation with toluene, dissolved in CH₂Cl₂ (7 mL), and cooled to 0°C. Triethylamine (350 μL, 2.5 mmol) and methanesulfonyl chloride (111 μL, 1.44 mmol) were added and the reaction stirred 1.5 h at room temperature. The reaction was diluted to 100 mL with CH₂Cl₂, washed with 50 mL each of 1N HCl, water, and saturated NaHCO₃. The organic layer was dried over MgSO₄, filtered, and the solvent removed *in vacuo*. The residue was purified on silica gel (1 cm x 15 cm column, 4:1 hexanes:ethyl acetate elutant) to yield **5-16** (279 mg, 0.61 mmol, 85%) as a clear oil. The ¹H NMR spectrum was consistent with previously reported data.⁽³⁴⁾

Procedure B:^(51, 52) All solid reagents were dried over P₂O₅ under vacuum overnight. All solvents and liquid reagents were distilled from CaH immediately before use, except mesyl chloride, which was distilled from P₂O₅. NaBH₄ (152 mg, 4 mmol) was dissolved in diglyme (4 mL) under N₂ to make a 1.0 M solution. The apparatus was assembled as pictured (Figure 5-2) under N₂ flow with flame drying. When the apparatus had cooled to room temperature, the cold finger attached to the three-necked flask was filled with dry ice/acetone (this was to prevent

solvents, particularly Et₂O, from exiting the three-necked flask and condensing in the pear shaped flask. The NaBH₄ solution was added to the dropping funnel and boron trifluoride diethyl etherate (1.25 mL, 10 mmol, 2.5 eq.) was added to the three-necked flask. The three-necked flask was placed in an oil bath initially at room temperature. The conical flask was immersed in a dry ice/acetone bath and THF (2 mL) added. The needle was immersed in the THF and the N₂ flow turned to a minimum. Dropwise addition of the borohydride solution was begun, adding the solution over 1 h. The evolution of gas was immediately evident and a white precipitate (NaBF₄)(53) formed over the course of the reaction. The oil bath was heated to 70°C for 30 min to distill off any remaining diborane. The apparatus was disassembled, leaving the THF flask under N₂ in the dry ice/acetone bath.

The concentration of BH₃:THF was established by titration.(51, 52) A 50 μL aliquot was removed from the THF solution of borane and added slowly to 3 mL acetone containing a trace of phenolphthalein (audible hissing occurred). To this solution was added water (3 mL) and mannitol (0.1g). The solution was titrated with 0.10 M NaOH to the phenolphthalein endpoint (1.12 mL added, 2.4 M concentration of the original solution). The yield of BH₃:THF was 4.8 mmol, 90%. (the maximum theoretical yield is 5.33 mmol, as one equivalent of BF₃ can also be converted to borane for every three equiv. NaBH₄ reacted).(53)

The solution of BH₃:THF was transferred to a ice/salt bath (-15°C) and 2-methyl-2-butene (1.03 mL, 9.6 mmol) added slowly dropwise via syringe over 1 h. The reaction mixture was stirred an additional 1 h at -15°C. The solution of disiamyl borane was transferred to an ice bath (0°C) and a solution of **5-14a** (188 mg, 0.5 mmol) in 1 mL THF was added dropwise via syringe over 30 min. The reaction was stirred 1 h at 0°C followed by 16h at room temperature. Water (1 mL) was added slowly. Foaming occurred as H₂ gas evolved. The flask was equipped

with a reflux condenser and the mixture was refluxed 30 min, then cooled to 0°C and the reflux condenser removed. Hydrogen peroxide (1 mL, 30% solution) was added dropwise over 5 min, along with enough 2N NaOH to keep the pH at 7.5-8.0 (monitored by microelectrode, ~200 μ L over the course of the quench). The mixture was poured into EtOAc (100 mL) and washed with water (2 x 50 mL). The organic layer was dried over MgSO₄, filtered, and the solvent removed *in vacuo*.

The residue was dried over P₂O₅ and dissolved in CH₂Cl₂ (5 mL). The reaction was cooled to 0°C and triethyl amine (0.5 mL) and mesyl chloride (0.39 mL, 5 mmol) were added. The ice bath was removed and the reaction stirred 3 h at room temperature. The reaction was diluted to 100 mL with CH₂Cl₂ and the organic layer washed with 1N HCl, water, saturated NaHCO₃, and water. The organic layer was dried over MgSO₄, filtered, and the solvent removed *in vacuo*. Purification using silica gel chromatography (1 cm x 15 cm column, 4:1 hexanes:ethyl acetate elutant) yielded **5-16** (143 mg, 0.313 mmol, 63%) as a clear oil. The ¹H-NMR spectrum was consistent with previously reported data.⁽³⁴⁾

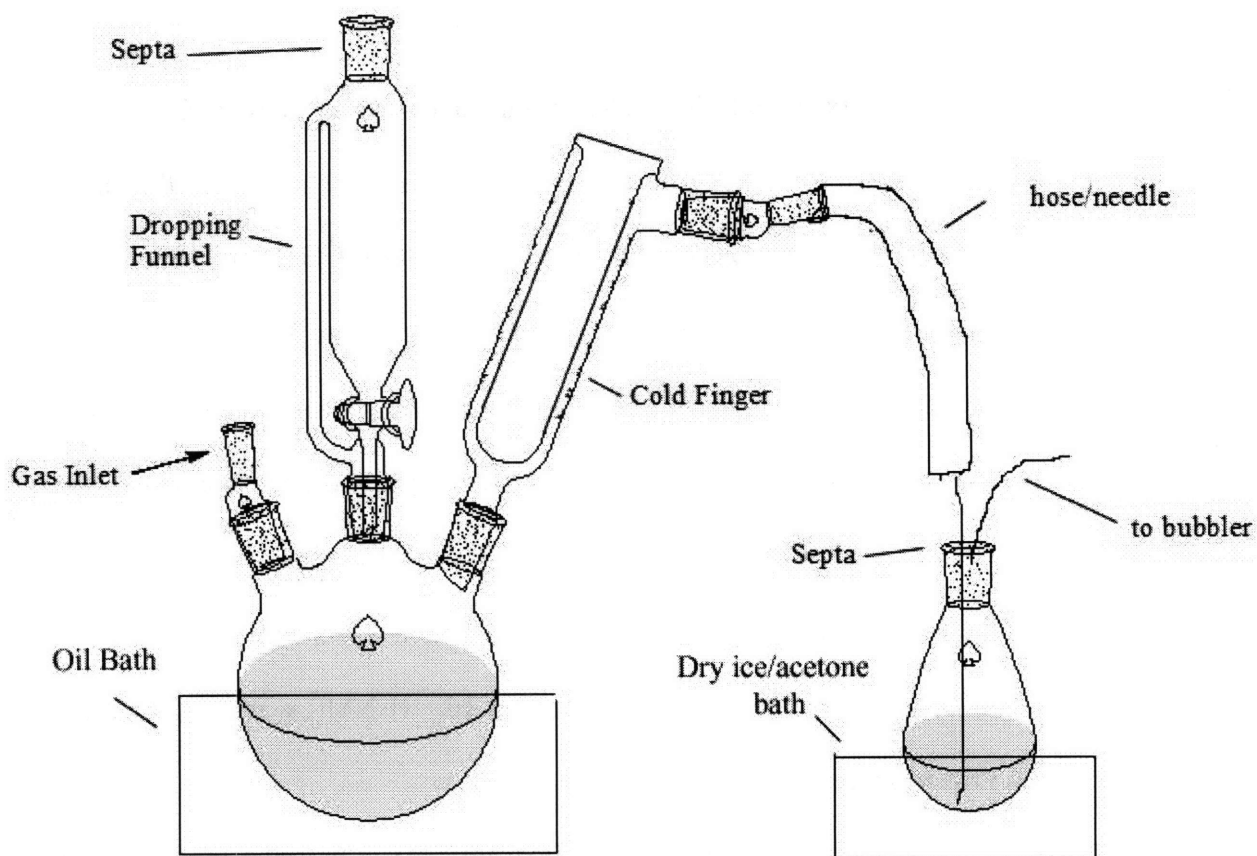


Figure 5-2. Apparatus for production of $\text{BH}_3:\text{THF}$.

Bis(trimethylsilyl)cytosine (5-8).⁽⁵⁴⁾ Cytosine (44.5 mg, 0.4 mmol) was dried overnight over P_2O_5 and suspended in hexamethyldisilazane (HMDS) (4 mL) and trimethylsilyl chloride (TMSCl) (0.4 mL) in a three-necked flask equipped with a reflux condenser. The solution was heated to reflux under N_2 for 2 h. The solvent was removed by distillation *in vacuo* with heating and the white crystalline solid **5-8** dried on a vacuum line for 15 min.

2'-Deoxy-2',2'-difluorocytidine α/β mixture (5-1 α/β). The **5-8** (0.4 mmol) produced in the previous step was dissolved in xylenes (1.5 mL) in the three-necked flask in which it was synthesized. Trimethylsilyl trifluoromethanesulfonate (72.5 μL , 0.4 mmol) was added and the reaction stirred 30 min at room temperature under N_2 . A solution of **5-16** (114 mg, 0.25 mmol)

in anhydrous xylenes (1 mL) was added via cannula and the reaction heated to reflux for 5 h. The reaction was cooled to room temperature and diluted to 100 mL with ethyl acetate, washed with 50 mL each water and saturated NaHCO₃. The organic layer was dried over MgSO₄, filtered, and the solvent removed *in vacuo*. The crude material was suspended in methanol (2.5 mL). Sodium metal (25mg, 1.1 mmol) was dissolved in methanol (1 mL) and 100 μL of this solution added to the reaction mixture. All solids dissolved within 5 min. The reaction was stirred for 1 h at room temperature, then Dowex 50W-X8 acidic resin (~1 mL) added until the pH was ~6. The reaction was filtered and the solvent removed *in vacuo*. The residue was taken up in water (50 mL) and extracted with Et₂O (2 x 20 mL). The aqueous phase was collected and the water removed *in vacuo* to yield **5-1** as a 6:4 α:β mixture, which was quantified by UV absorbance ($\epsilon_{268} = 9360$ at pH 7.0), 190.5 μmol, 76% from **5-16**. ¹H-NMR was consistent with reported data(34) and the product was >95% pure by NMR.

2'-Deoxy-2',2'-difluorocytidine -5'-monophosphate (F₂CMP).(45, 49) F₂C was converted to its monophosphate directly from the α/β mixture. The reaction contained in a final volume of 1 mL: 5 mM β F₂C (assuming a 6:4 α:β ratio as measured by NMR), 10 mM ATP, 2 mM DTT, 0.5 mg/mL BSA, 1.4 mg/mL human dCK, 50 mM Tris pH 7.6, 100 mM KCl, and 10 mM MgCl₂. The reaction was initiated by addition of dCK and incubated at 37°C for 45 min. The reaction mixture was loaded on a DEAE Sephadex A25 column (20 mL, 20 cm x 1 cm) equilibrated in 5 mM TEAB pH 6.8 and then column washed with 50 mL 5 mM TEAB. The product was eluted using a 100 mL x 100 mL linear gradient from 5 mM → 400 mM TEAB gradient. Fractions (5 mL) were assayed for A260 nm and the nucleotide containing fractions were combined and the solvent was removed *in vacuo*. The product was co-evaporated with 50% ethanol in water (5 x 20 mL). ¹H-NMR analysis of the flow-through from the initial wash

showed only the presence of the α anomer, (34) with no unphosphorylated β detectable. F₂CMP eluted at 250 mM TEAB (4.45 μ mol, 90%). ¹H-NMR (500 MHz, D₂O), selected peaks, δ 7.83 (d, J = 7.5 Hz, 1H), 6.15 (t, J = 6.4 1H), 6.05 (d, J = 7.5 Hz, 1H), 4.36 (dd, J = 12.4, 21.1 Hz, 1H), 4.02-4.09 (m, 2H), 3.91-3.96 (m, 1H). ³¹P-NMR (121.5 MHz, D₂O, phosphoric acid external reference) δ 4.6.

2'-Deoxy-2',2'-difluorocytidine -5'-diphosphate (F₂CDP).(47, 49, 55) The reaction mixture contained in a final volume of 5 mL: 2 mM F₂CMP, 8 mM ATP, 2 mM DTT, 50 mM Tris pH 8, and 25 mM MgCl₂, 66.5 μ g/mL UMP-CMP kinase. The reaction was incubated 30 min at 37°C, diluted to 50 mL with cold water and loaded onto a DEAE-Sephadex A-25 column (30 mL, 18 cm x 1.5 cm). The column was washed with water (100 mL) and the product eluted with a 400 mL x 400 mL linear gradient from 0 \rightarrow 600 mM TEAB. The fractions (7.5 mL) were assayed by A260 nm, with F₂CDP eluting along with ADP at 450 mM TEAB. The fractions were combined and the solvent removed *in vacuo*. The product was co-evaporated with 50% ethanol in water (5x20 mL) to remove excess TEAB. This material was dissolved in water (24 mL) and NaIO₄ (0.5 mmol, 1 mL of a 0.5 M solution) was added. The reaction was incubated 10 min at 37°C, then methyl amine (2.5 mmol, 640 μ L of 3.9 M solution in water, pH adjusted to 7.5 with phosphoric acid) added and the reaction incubated an additional 20 min. The reaction was quenched by addition of rhamnose (1 mmol, 1 mL of a 1M solution). To this mixture was added 6.6 mL of 8 mM MgCl₂, 165 mM Tris pH 7.2 and yeast inorganic pyrophosphatase (165 μ L of a 50 U/mL stock in 165 mM Tris pH 7.2) to give final concentrations of 2 mM MgCl₂, 55 mM Tris pH 7.2 and 0.25 U/mL inorganic pyrophosphatase. This mixture was incubated 45 min at 37°C, diluted to 300 mL with cold water, and loaded onto a DEAE Sephadex A25 column (30 mL, 18 cm x 1.5 cm). The column was washed with water (100 mL) and the product eluted with a 400

mL x 400 mL linear gradient from 0 → 600 mM TEAB. The fractions (7.5 mL) were assayed by A260 and the F₂CDP containing fractions eluting at 450 mM TEAB were combined and the solvent was removed *in vacuo*. The product was co-evaporated with 50% ethanol in water (5 x 20 mL). The product was lyophilized to dryness and resuspended in water (1 mL) giving 5.6 μmol, 56% yield. ¹H-NMR (500 MHz, D₂O) δ 7.71 (d, *J* = 7.7 Hz, 1H), 6.09 (t, *J* = 7.2 Hz, 1H), 5.96 (d, *J* = 7.7 Hz, 1H), 4.40 (dd, *J* = 13.3, 22.2 Hz, 1H), 4.05-4.21 (m, 2H), 3.99-4.03 (m, 1H). ³¹P-NMR (121.5 MHz, D₂O) δ (phosphoric acid external reference) -9.5 (d, *J* = 22.1 Hz), -10.6 (d, *J* = 22.1 Hz). The ³¹P NMR showed no contamination by inorganic pyrophosphate.

2'-Deoxy-2',2'-difluorocytidine -5'-triphosphate (F₂CTP). The reaction (20 mL) contained 2 mM F₂CDP, 4 mM phosphoenolpyruvate (PEP), 50 mM Tris pH 7.5, 80 mM KCl, 20 mM MgCl₂, and 120 U/mL pyruvate kinase. The reaction was incubated at 37°C for 1 h. The reaction was then diluted with cold water (50 mL) and loaded on a DEAE-Sephadex A-25 column (60 mL, 20 cm x 2 cm), the column was washed with water (100 mL), and the product eluted with a 400 mL x 400 mL linear gradient from 0→750 mM TEAB. The fractions (10 mL) were assayed for A260 nm. The triphosphate containing fractions eluting at 550 mM TEAB were combined and the solvent removed *in vacuo*. The product was co-evaporated with 50% ethanol in water (5 x 20 mL). The product was lyophilized to dryness and dissolved in 5 mL ddH₂O to give 35 μmol, 88% yield. ¹H-NMR (500 MHz, D₂O), selected peaks, δ 7.75 (d, *J* = 7.7 Hz, 1H), 6.09 (t, *J* = 7.2 Hz, 1H), 6.02 (d, *J* = 7.3 Hz, 1H), 4.33-4.40 (m, 1H), 4.21-4.26 (m, 1H), 4.10-4.14 (m, 1H), 4.03-4.06 (m, 1H). ³¹P-NMR (121.5 MHz, D₂O) δ (phosphoric acid external reference) -9.3, -10.5, -21.4.

1'-[²H]-F₂C. The synthesis of **5-16** was repeated (procedure B) with the substitution of NaBD₄ (98% [²H], Sigma) for NaBH₄. The **5-16** produced was carried on to **5-1** using the procedure for

the cold material to yield 1'-[²H]-F₂C, 274 μmol, 64%. [²H] incorporation was 93% by ¹H-NMR and ESI-MS.

1'-[²H]-F₂C-5'-diphosphate (1'-[²H]-F₂CMP). α/β 1'-[²H]-F₂C (5 μmol β) was converted to the monophosphate by the human dCk procedure described for the unlabeled compound. Yield 4.3 μmol, 86%.

1'-[²H]-F₂C-5'-diphosphate (1'-[²H]-F₂CDP). 1'-[²H]-F₂CMP (15 μmol) was converted to the diphosphate by the UMP-CMP kinase procedure described for the unlabeled compound. Yield 10 μmol, 60%.

1'-[²H]-F₂C-5'-triphosphate (1'-[²H]-F₂CTP). 1'-[²H]-F₂CDP (10 μmol) was converted to the triphosphate by the PEP/pyruvate kinase procedure described for the unlabeled compound. Yield 7.75 μmol, 77.5%.

1'-[³H]-F₂C. The synthesis of **5-16** was repeated (procedure B) with the addition of 500 mCi NaB[³H]₄ (SA 14.22 Ci/mM, Perkin Elmer) to the cold NaBH₄ used in the preparation of the Sia₂BH. The **5-16** produced was carried on to **5-1** using the procedure for the cold material to yield 1'-[³H]-**5-1**, 306 μmol, 71%. SA could not be determined at this stage due to [³H] containing impurities.

1'-[³H]-F₂C-5'-monophosphate (1'-[³H]-F₂CMP). The enzymatic phosphorylation was carried out on 25 μmol 1'-[³H]-β-F₂C (from the 6:4 anomeric mixture) using the procedure described for the unlabeled compound. Yield 21.25 μmol, 85 %, SA 8700 cpm/nmol.

1'-[³H]-F₂C-5'-diphosphate (1'-[³H]-F₂CDP). The enzymatic phosphorylation was carried out on 21 μmol 1'-[³H]-F₂CTP using the procedure described for the unlabeled compound. Yield 12.8 μmol, 60%, SA 8620 cpm/nmol.

1'-[³H]-F₂C-5'-triphosphate (1'-[³H]-F₂CTP). 1'-[³H]-F₂CDP (5 μmol) was converted to the triphosphate using the procedure described for the unlabeled compound. Yield 4.44 μmol , 88%, SA 8620 cpm/nmol. This material (1 nmol) was combined with 50 nmol unlabelled F₂CTP and treated with 2 U alkaline phosphatase in 100 mM Tris pH 8.6, 0.2 mM EDTA for 2 h at 37°C and purified by HPLC (Rainin SD-200) using a Adsorbosphere Nucleotide Nucleoside, Alltech (250mm x 4.6mm) with a flow rate of 1 mL/min. The solvent system was Buffer A, 10 mM NH₄OAc, pH 6.8; Buffer B: 100% methanol. The flow program was 100% A until 10 min, then a linear gradient to 40% B over 25 min, then to 100% B over 5 min, collecting 1 mL fractions. The fractions were assayed for radioactivity; 97% of the radioactivity co-eluted with the F₂C peak.

5-[³H]-F₂C-5'-triphosphate (5-[³H]-F₂CTP). 5-[³H]-F₂CDP was synthesized by E. Artin from 5-[³H]-F₂C provided by Eli Lilly.(49) 5-[³H]-F₂CDP (2.2 μmol) was converted to the triphosphate by the PEP/pyruvate kinase procedure described for the unlabeled compound. Yield 1.85 μmol , 85%, SA 10060 cpm/nmol.

Synthesis of 3'-[²H]-F₂C

2-Deoxy-2,2-difluoro-1-thexyldimethylsilyl-D-ribofuranoside (5-28).(56) 3,5-Di-*O*-benzoyl-2-deoxy-2,2-difluoro-ribonolactone (5-14a)(34) (1.33 g, 3.53 mmol) was dissolved in THF (7 mL) and ether (28 mL). The reaction was cooled to 0°C and LiAl(O-*t*-Bu)₃H (1.08 g, 4.29 mmol) was added slowly. The ice bath was removed and the reaction stirred 2.5 h at room temperature. The reaction was diluted with ethyl acetate (250 mL), washed with 100 mL each 1N HCl, brine, and saturated sodium bicarbonate. The organic layer was dried over Na₂SO₄, filtered, and the solvent evaporated *in vacuo*. The crude product was dried by co-evaporation

twice with toluene, then dissolved in CH₂Cl₂ (35 mL). Imidazole (477 mg, 7 mmol) and hexyldimethylsilyl chloride (TDSCl, 757 μL, 3.85 mmol) were added. The reaction was stirred 16 h at room temperature; a white precipitate was observed after 15 min. The reaction was diluted with ethyl acetate (250 mL), washed with 100 mL each 1N HCl, brine, and saturated sodium bicarbonate. The organic layer was dried over Na₂SO₄, filtered, and the solvent evaporated *in vacuo*. The crude product was dissolved in methanol (35 mL) and sodium methoxide (320 μL of a 25% solution in methanol, 1.4 mmol) was added. The reaction was stirred 1.5 h and Dowex 50W-X8 resin (acidic form) added until the pH was ~6 (~2 mL). The reaction was filtered and the solvent removed *in vacuo*. The crude product was purified by silica gel chromatography (1 cm x 15 cm column, 9:1 (2 cv) then 7:3 hexanes:ethyl acetate (5 cv) elutant) to yield **5-28** (760 mg, 2.43 mmol, 69%, 3:1 mixture of anomers) as a clear oil. Rf. 0.36 (2:1 hexanes:ethyl acetate). FT-IR (thin film, NaCl plate) 3397, 2960 cm⁻¹. ¹H-NMR (500 MHz, CDCl₃) δ 5.25 (d, *J* = 5.7 Hz, 0.25H), 5.15 (t, *J* = 6.7 Hz, 0.75H), 4.48 (m, 0.75H), 4.19 (m, 0.25H), 4.05 (dd, *J* = 4.8, 17.3 Hz, 0.25H), 3.96 (m, 0.75H), 3.76-3.90 (m, 1.25H), 3.69 (dd, *J* = 3.1, 12.2 Hz, 0.75 H), 2.3 (bs, 2H), 1.60-1.66 (m, 1H), 0.86-0.90 (m, 12H), 0.21 (s, 0.75H), 0.205 (s, 2.25H), 0.20 (s, 0.75H), 0.195 (s, 2.25H). ¹³C-NMR (125 MHz, CDCl₃) major isomer: δ 122.2 (dd, *J* = 248, 265 Hz), 95.4 (dd, *J* = 24.8, 39.4 Hz), 81.5 (d, *J* = 9.2 Hz), 69.1 (dd, *J* = 8.2, 13.8 Hz), 61.8, 34.1, 25.1, 20.1, 20.0, 18.7, 18.6, -2.3, -2.9; minor isomer: δ 122.0 (dd, *J* = 250, 268 Hz), 96.5 (dd, *J* = 23.8, 39.2 Hz), 84.3 (dd, *J* = 3, 4 Hz), 71.5 (dd, *J* = 10.3, 11.9 Hz), 61.8, 34.2, 25.3, 25.1, 20.1, 18.6, -2.3, -3.2. ESI MS (C₁₃H₂₆F₂O₄Si) *m/z* (M + Na⁺) calcd 335.1461, obsd 335.1470.

1-Thexyldimethylsilyl-2-deoxy-2,2-difluoro-5-(di-phenyl-mono-*p*-methoxyphenyl)methyl-D-ribofuranoside(5-29). Compound **5-28** (360 mg, 1.15 mmol), dried by co-evaporation with

toluene (3 x 5 mL), and monomethoxytrityl chloride (MMTCl, 292 mg, 1.27 mmol), were dissolved in anhydrous pyridine (5 mL). The reaction was stirred 2 d at room temperature under N₂, diluted with CH₂Cl₂ (50 mL), and washed with 25 mL each saturated NaHCO₃ and water. The organic layer was dried over Na₂SO₄, filtered and the solvent removed *in vacuo*. The crude product was purified by silica gel chromatography (1 cm x 15 cm column, 100% toluene (2 cv) then 30:1 toluene:ethyl acetate (5 cv) elutant) yielded **5-29** (715 mg, contaminated with 0.2 eq. of MMTOH based on ¹H-NMR, 95% yield of **5-29**) Further purification did not allow separation of the MMTOH and showed decomposition of the product through loss of the MMT group. The product was partially characterized as this mixture. Rf. 0.23, 0.29 (9:1 hexanes:ethyl acetate). ¹H-NMR (500 MHz, CDCl₃) Major isomer δ: 7.48 (d, *J* = 7.9 Hz, 2H), 7.18-7.37 (m, 10H), 6.84-6.87 (m, 2H), 5.13 (d, *J* = 7.3 Hz, 1H), 4.31-4.37 (m, 1H), 4.00 (m, 1H), 3.81 (s, 3H), 3.35 (dd, *J* = 9.6, 5 Hz, 1H), 3.26 (dd, *J* = 5.8, 9.6 Hz, 1H), 2.05 (d, *J* = 1.5 Hz, 1H), 1.55-1.6 (m, 1H), 0.82-0.88 (m, 12H), 0.08 (s, 3H), 0.17 (s, 3H). Minor isomer: δ 7.48 (d, *J* = 7.7 Hz, 4H), 7.23-7.37 (m, 8H), 6.85 (d, *J* = 8.7 Hz, 2H), 5.29 (d, *J* = 5.3 Hz, 1H), 4.23 (dd, *J* = 4.8, 9.4 Hz, 1H), 4.04 (m, 1H), 3.82 (s, 3H), 3.32 (d, *J* = 4.9 Hz, 2H), 2.24 (d, *J* = 8.8 Hz, 1H), 1.59-1.69 (m, 1H), 0.93 (s, 3H), 0.92 (s, 3H), 0.91 (s, 3H), 0.90 (s, 3H), 0.25 (s, 3H), 0.24 (s, 3H). ESI MS (C₃₃H₄₂F₂O₅Si) *m/z* (M + Na⁺) calcd 607.2662, obsd 607.2685.

Preparation of 5-28 from 5-29.(57, 58) Compound **5-29** (103 mg, 0.176 mmol) was dried by co-evaporation with toluene then dissolved in CH₂Cl₂ (1.75 mL). The solution was cooled to 0°C and Dess-Martin periodinane (187 mg, 0.44 mmol) was added. The solution was warmed to room temperature and stirred 16 h. The reaction was filtered through a pad of Celite, diluted to 50 mL with ethyl acetate and stirred with an equal volume of saturated NaHCO₃. Na₂S₂O₃ (2 g) was added, and the mixture was stirred 10 min. The layers were separated, the organic layer was

washed with 100 mL brine, dried over Na₂SO₄, filtered and the solvent removed *in vacuo*. The crude material was dried by co-evaporation with toluene and used in further steps without purification. The product was prone to decomposition, but a small amount was partially characterized to confirm the presence of a carbonyl. FT-IR (thin film, NaCl plate) 1799 (C=O), 1726 (C=O) cm⁻¹. ¹³C-NMR 200.1 (C=O).

This crude material was dissolved in acetic acid (2 mL) and water (0.5 mL) and stirred 2 h. The reaction was diluted with ethyl acetate (100 mL) and washed with saturated NaHCO₃ and brine (100 mL). The organic layer was separated, dried over Na₂SO₄, filtered, and the solvent removed. The crude material was dried with coevaporation toluene (5 x 2 mL) and carried on to the reduction step without further purification. Acetic acid (2 mL) and NaBH₄ (66 mg, 1.75 mmol) were combined at 0°C. When all solids were dissolved, this mixture was added to the crude material (~0.175 mmol), warmed to room temperature and the reaction stirred 16 h. The reaction was diluted with ethyl acetate (100 mL) and washed with saturated NaHCO₃ (100 mL). The organic layer was separated, dried over Na₂SO₄, filtered, and the solvent removed. The crude product was purified by silica gel chromatography (0.5 cm x 15 cm column, 3:1 hexanes:ethyl acetate elutant) to yield **5-28** (22 mg, 70 μmol, 40% from **5-29**). Spectra were consistent with those reported above.

3-[²H]-1-Thenyldimethylsilyl-2-deoxy-2,2-difluoro-1-O- D-ribofuranoside (3-[²H]-5-28) The synthesis of **5-28** from **5-29** was repeated substituting AcOD and NaBD₄ in the reduction step, Reacting 140 mg, 0.45 mmol **5-28** to yield 3-[²H]-**5-28** (53 mg, 0.175 mmol, 38% from **5-29**). The ¹H-NMR showed >99% [²H] incorporation.

3'-[²H]-2-Deoxy-3,5-di-O-benzoyl-2,2-difluoro-1-O-methanesulfonyl-D-ribofuranoside (3'-[²H]-5-16). Compound 3-[²H]-**5-28** (52 mg, 0.166 mmol) was dried by co-evaporation with

toluene then dissolved in pyridine (1.7 mL). Dimethylaminopyridine (2mg, 0.017 mmol) and benzoyl chloride (77 μ L, 0.66 mmol) were added and the reaction stirred 16 h under N₂. The reaction was diluted with ethyl acetate (100 mL) and washed with 100 mL each saturated NaHCO₃ and brine. The organic layer was dried over Na₂SO₄, filtered and the solvent removed *in vacuo*. The crude product was purified by silica gel chromatography (0.5 cm x 15 cm column, 25:1 hexanes:ethyl acetate (2 cv), then 10:1 hexanes:ethyl acetate (5 cv) elutant) to yield the dibenzoyl ester derivative (72 mg, 0.139 mmol, 84%). This product was dried by co-evaporation with toluene then dissolved in THF (1.2 mL). The reaction was cooled to 0°C and acetic acid (9.1 μ L, 0.16 mmol) was added, followed by tetrabutylammonium fluoride (152 μ L of a 1.0 M solution in THF, 0.152 mmol) and the reaction stirred 1 h under N₂. The reaction was diluted with ethyl acetate (50 mL) and washed with 25 mL each saturated NH₄Cl and water. The organic layer was dried over Na₂SO₄, filtered, and the solvent removed *in vacuo*.

The crude material was dried by co-evaporation with toluene then dissolved in CH₂Cl₂ (1.2 mL). The reaction was cooled to 0°C and triethyl amine (120 μ L, 1.63 mmol) and mesyl chloride (53.4 μ L, 0.69 mmol) were added. The ice bath was removed and the reaction stirred 3 h at room temperature under N₂. The crude product was purified by silica gel chromatography (0.5 cm x 15 cm column, 9:1 hexanes:ethyl acetate elutant) to yield 3'-[²H]-5-16 (48.5 mg, 0.105 mmol, 77%). [²H] incorporation was >99% by NMR. [²H] incorporation was shown to be >99% by ESI MS: (C₂₀H₁₇DF₂O₈S) *m/z* (M + Na⁺) calcd 480.0645, obsd 480.0636.

3'-[²H]-F₂C. Compound 3'-[²H]-5-16 (48 mg, 0.105 mmol) was converted to α/β 3'-[²H]-F₂C (65 μ mol, 62%, 6/4 α/β) through the procedure described for the unlabeled compound.

3'-[²H]-F₂CMP. The enzymatic phosphorylation was carried out on 17.25 μmol β 3'-[²H]-F₂C (from a 6:4 anomeric mixture) using the procedure described for the unlabeled compound. Yield 15 μmol, 87%.

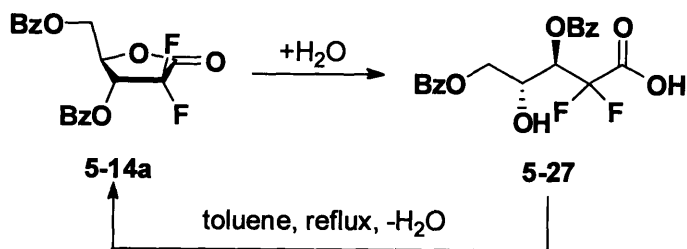
3'-[²H]-F₂CDP. The enzymatic phosphorylation was carried out on 15 μmol 3'-[²H]-F₂CMP using the procedure described for the unlabeled compound. Yield 10.2 μmol, 68%.

3'-[²H]-F₂CTP. The enzymatic phosphorylation was carried out on 5 μmol 3'-[²H]-F₂CDP using the procedure described for the unlabeled compound. Yield 3.4 μmol, 68%.

5.3 Results and Discussion

Refinements to published synthesis of F₂C for synthesis of isotopically labeled derivatives

For all syntheses described in this chapter, the starting material used was the 2,2-difluororibose precursor **5-14a**.⁽³⁴⁾ Compound **5-14a** is very prone to hydrolysis due to the enhancement of lactone electrophilicity by the vicinal *gem*-difluoro group (Scheme 5-7), and the starting material was found to be ~40% hydrolyzed by NMR. The lactone could be separated from its hydrolyzed form **5-27** readily by dissolution in CH₂Cl₂; the hydrolyzed lactone is sparingly soluble in this solvent and can be filtered off. Further, the hydrolyzed lactone can be recovered by dehydrative ring closure through azeotropic distillation of the H₂O in refluxing toluene, allowing **5-27** to be converted back to the lactone **5-14a** in 95% yield.

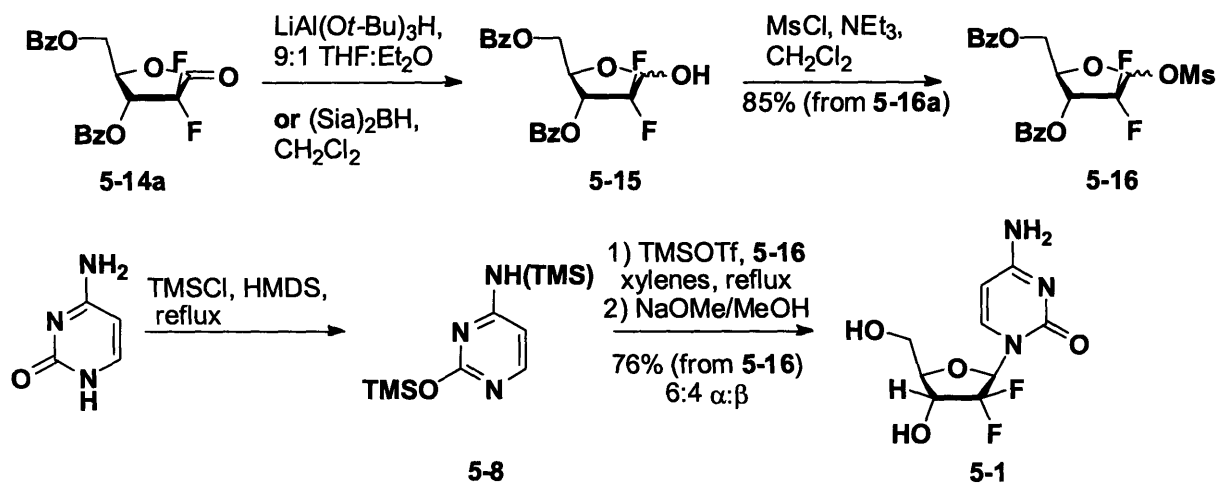


Scheme 5-7. Purification and recovery of 5-14a.

The synthesis of F₂C from **5-14a** through a modification of the previous synthesis is outlined in Scheme 5-8. The reduction of the lactol using LiAl(*O-t*-Bu)₃H was performed as previously described;⁽³⁴⁾ conversion to the mesylate **5-16** by treatment with mesyl chloride and triethylamine was done on the crude reduction product, producing **5-16** in 85% yield from **5-14a**. This mesylate was coupled to *bis*-trimethylsilylcytosine **5-8** as described in the original publication, however, a different method for production of **5-8** from cytosine was employed. The previously described procedure used a “catalytic” amount of ammonium sulfate, added as dry crystals, to a mixture of cytosine suspended in HMDS. The mixture is heated to reflux, effecting the reaction of cytosine to **5-8** by proton catalyzed transfer of TMS groups from the HMDS. The HMDS was then distilled off, leaving **5-8** and the non-volatile ammonium sulfate behind. This product was dissolved in xylenes, and **5-16** added. While suitable for large scale synthesis, on small scale the difficulty of adding a consistent amount of ammonium sulfate caused problems in the later coupling reaction. Ammonium sulfate is only slightly soluble in HMDS at room temperature, and thus could only be added to the reaction as individual crystals. On the hundred- μ mol scale typically employed in production of isotopically labeled F₂C, a small crystal often represented a significant molar fraction of **5-16**. The ammonium sulfate remaining in the reaction led to variable coupling yields (in one case, no product was detected at all).

More reproducible results were obtained using an alternative procedure.⁽⁵⁴⁾ Here, **5-8** was produced by the reflux of cytosine in 10:1 HMDS:TMSCl. In this case, TMS is the catalyst, and no proton source or salts are present. After reaction, both the HMDS and TMSCl are distilled off, leaving only **5-8**. Addition of **5-16** dissolved in xylenes and refluxing in the presence of TMSOTf resulted in the protected nucleoside as a 6:4 α : β mixture. This crude

mixture can be deprotected by treatment with methanolic sodium methoxide to give $\alpha:\beta$ 5-1 in 74% yield from 5-16.



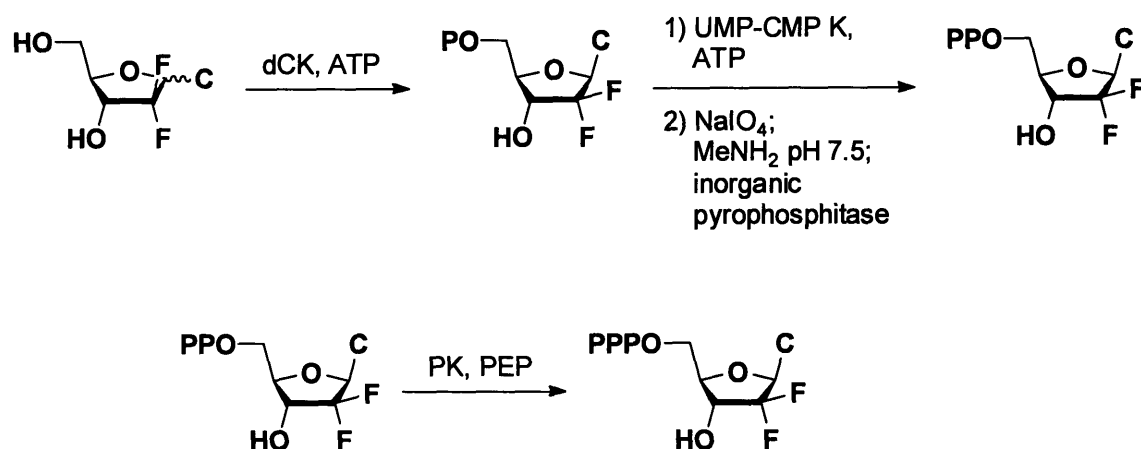
Scheme 5-8. Synthesis of F₂C.

The published procedure separated the F₂C anomers by crystallization at either the benzoate protected or fully deprotected stages. However, the much smaller scale used here (generally < 100 mg) with labeled F₂C derivatives was not conducive to high recoveries of pure product from crystallization. Thus, other methods for separating the anomers were explored. It was initially thought that the best place to remove the undesired α anomer was at the stage of the protected compounds prior to treatment with NaOMe. The mobility of this mixture on silica gel TLC plates indicated that silica gel chromatography using dichloromethane/methanol systems might allow separation of the anomers. Silica gel columns run in a variety of solvent systems partially separated the anomers, but they were time intensive, resulted in material loss, and never gave clean separation. Difficulty was encountered with compound solubility in the solvent systems used, but even dry loading did not result in good separation. In order to improve solubility in CH₂Cl₂/methanol, the *N*-acetyl derivatives⁽³⁴⁾ were synthesized by substitution of trimethylsilyl *N*-acetyl cytosine in the coupling to 5-16 (data not shown). Though this compound was isolated as an oil and was easily soluble in CH₂Cl₂, both anomers co-ran in all solvent

systems tried and proved no easier to purify. While the deprotected F₂C anomers could be separated by HPLC as described in the original publication, ultimately, it was found to be most convenient to resolve the α : β mixture enzymatically during the conversion of F₂C to F₂CMP.

Conversion of F₂C \rightarrow F₂CMP

In order to circumvent the problems associated with chemical phosphorylation of F₂C a procedure involving nucleoside kinases(59-61) was desired. Initial work on the development of the enzymatic synthesis of F₂C 5'-mono- and diphosphates was performed at Merrell-Dow(6, 42) and by Momparler,(43) Eriksson,(45, 61-63) and Karlsson(47). Modifications to the procedures allowing access to F₂C nucleotides on 100 μ mol scale were performed by Artin in the Stubbe group.(49) The phosphorylation procedures used for the synthesis of F₂C nucleotides described in this chapter are outlined in Scheme 5-9. Treatment of α / β -F₂C with human deoxycytidine kinase (dCK) using ATP as a phosphate donor allowed selective conversion of the β anomer to the 5'-monophosphate (F₂CMP) in 85% yield. The desired product was purified by anion exchange chromatography. The non-phosphorylated α anomer eluted in the void volume of the column; assignment of this product as the α anomer was made by comparison of the ¹H-NMR of this fraction to the previously reported spectrum.(34) The dCk proved 100% selective for the desired anomer, and thus could be used to resolve the anomeric mixture.



Scheme 5-9. Enzymatic phosphorylation of F_2C .

Conversion of $F_2CMP \rightarrow F_2CDP$

F_2CDP was also produced enzymatically using human UMP-CMP kinase (UMP-CMP K).^(47, 49) In the version of the procedure described here, the concentration of enzyme was dropped 20-fold over previous conditions, without affecting yield (Scheme 5-9). Reaction of F_2CMP with UMP-CMP kinase equilibrates the mono-phosphate and ATP to a mixture of F_2CDP and ADP. The diphosphate fraction was isolated by anion exchange chromatography. In contrast to results using UMP-CMP kinase to produce diphosphates of isotopically labeled cytidines,⁽⁴⁹⁾ where the CDP elutes just before the ADP and can be separated through two anion-exchange columns, the F_2CDP co-elutes with ADP (Figure 5-3). In order to separate F_2CDP , a periodate cleavage step is included to destroy contaminating ADP (Scheme 5-10).^(49, 55) Treatment of the F_2CDP/ADP mixture with $NaIO_4$ (aq) selectively reacts with the *syn*-diol of the ADP to cleave the 2'-3' bond generating a dialdehyde. The F_2CDP is unreactive due to the replacement of the 2' hydroxyl with the *gem*-difluoro moiety. The remaining periodate is reacted by the addition of an excess of rhamnose. $MeNH_2$ phosphate (pH 7.5) was added to catalyze elimination of pyrophosphate from the 5' position of the dialdehyde. Final treatment with

inorganic pyrophosphatase converts the inorganic pyrophosphate to inorganic phosphate, but does not react with the F_2CDP . Anion exchange chromatography of this reaction mixture allowed separation of F_2CDP in 56% yield.

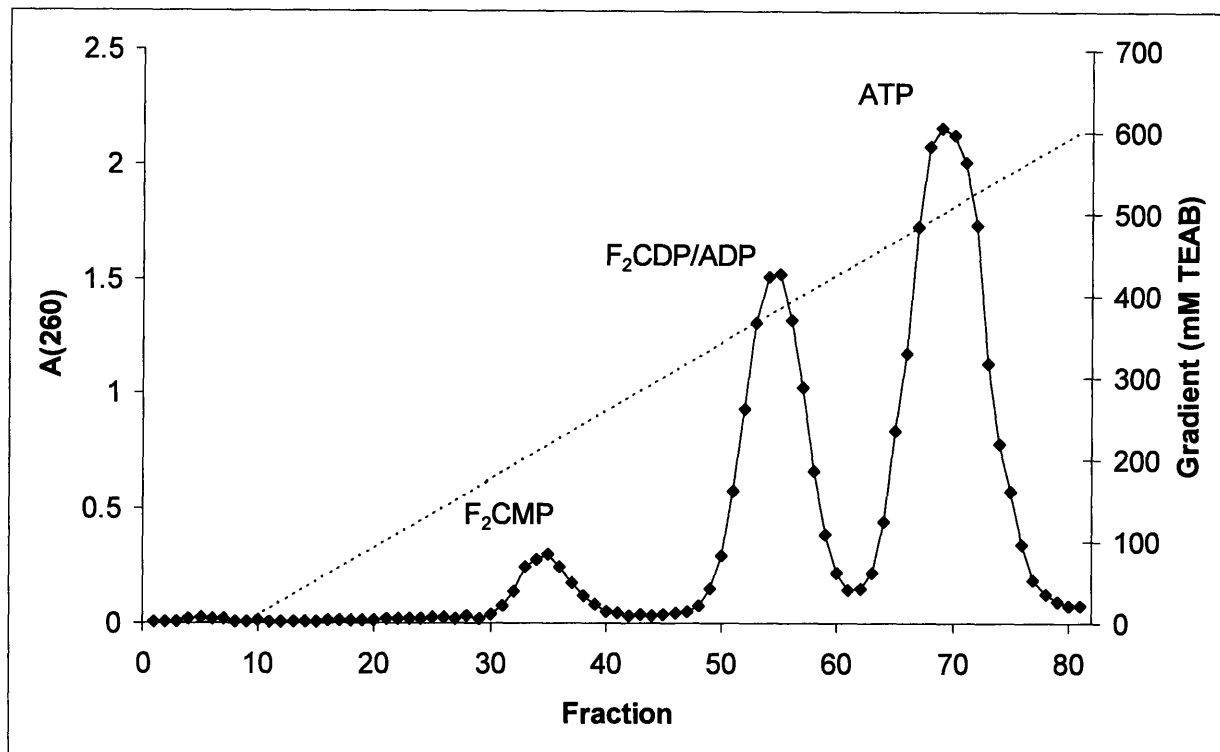


Figure 5-3. Anion exchange chromatography (DEAE-Sephadex) of the reaction of F_2CMP with UMP-CMP K and ATP. F_2CDP and ADP elute as one peak.



Scheme 5-10. Destruction of ADP by periodate cleavage.

Conversion of $F_2CDP \rightarrow F_2CTP$

In the development of the UMP-CMP kinase procedure for production of F_2CDP , attempts were made to include pyruvate kinase (PK) and phosphoenolpyruvate (PEP) in order to recycle the ADP to ATP.(49) Such a strategy would have removed the need for the periodate

cleavage of the ADP that is produced by the reaction. However, HPLC analysis indicated that the F₂CDP was being phosphorylated as well. This observation led us to believe F₂CDP could replace ADP in the PK reaction, converting it to F₂CTP (Scheme 5-9). Test reactions at 2mM F₂CTP, using variable concentrations of PEP (2mM, 4mM, 16mM), and pyruvate kinase (6 U/mL, 12 U/mL, 60 U/mL, and 120 U/mL) were carried out. PEP was saturating at all concentrations, but high concentrations of pyruvate kinase were needed to effect complete conversion to the triphosphate. Two equiv. of PEP and 120 U/mL pyruvate kinase could effect high (88%) conversion of F₂CDP to F₂CTP in 1 h. The enzymatic phosphorylation methods described here were also used to prepare F₂CDP and F₂CTP in 10-100 μmol quantities, 5-[³H]-F₂CDP and 5-[³H]-F₂CTP from the previously reported 5-[³H]-F₂C(36) and the di- and triphosphates of the isotopically labeled derivatives described in the remainder of this chapter. The use of these products in biochemical experiments is described in Chapter 6.

Synthesis of 1'-[²H]- and 1'-[³H]-F₂C

The incorporation of a radiolabel into the sugar ring of F₂C nucleotides would allow convenient identification of the products of the inactivation of RNR derived from the ribose ring and the ability to accurately quantify covalent modification of the protein. Incorporation of radioactivity at the 1' position was chosen due to the available lactone **5-14a**, which could be reduced with an isotopically labeled reductant. In order to introduce [³H] into F₂C at the 1', a reduction involving commercially available NaB[³H]₄ as a starting material was desired. While the previously described reduction using LiAl(*O-t*-Bu)₃H is suitable for introduction of deuterium using the commercially available [²H] version of this reductant, no [³H] containing aluminum hydride reagents are commercially available. Of the previously reported

methodologies for the reductions of ribonolactones to lactols, the use of disiamylborane ((Sia)₂BH), a reagent conveniently prepared from NaBH₄, was chosen.(51) Similar methodology has been applied by the Stubbe group in the production of radiolabeled nucleotides for studies on the chemistry of bleomycin interaction with DNA.(64)

The preparation of this reagent has been previously described.(51, 52) Briefly, a solution of NaBH₄ in anhydrous diglyme was added slowly dropwise to BF₃·Et₂O with gentle heating. Diborane gas (B₂H₆) evolved from this mixture and was bubbled into THF cooled to -78°C to generate a solution of BH₃·THF. The concentration of borane was determined by titration, and 2 equiv. of 2-methyl-2-butene were added slowly dropwise at -15°C over 1 h and the reaction stirred and additional 1 h to ensure complete reaction to (Sia)₂BH. Immediate use of the reagent gave the best results. The prepared (Sia)₂BH could be used in place of the LiAl(*O-t*-Bu)₃H in the reduction of lactone **5-14a** (Scheme 5-8). In this procedure, the lactone in THF (0.5 M) was added directly to the solution of (Sia)₂BH solution at 0°C, followed by stirring overnight at room temperature. While 3-4 equiv. of (Sia)₂BH was enough for complete reaction of dibenzoylribonolactone,(51) 8-10 equiv. (Sia)₂BH were required for complete reaction of **5-14a**. After workup to destroy remaining (Sia)₂BH, the crude lactol produced was converted directly to the mesylate **5-16** without purification. In order to get good conversion, 10 equiv. of mesyl chloride were required, allowing isolation of **5-16** in 88% yield starting from 500 μmol **5-14a**, a convenient scale for the isotopic synthesis. This mesylate was converted to F₂C and its phosphates through the procedures described above.

The above reaction sequence was also performed using NaBD₄ to quantify isotope incorporation by NMR and ESI-MS. ESI-MS revealed [²H] incorporation to be 93%. This material was carried forward to the di and tri phosphates by the procedure described above.

Given the success of this method, the reaction was repeated using $\text{NaB}[^3\text{H}]_4$ (SA 14.2 Ci/mmol) to give 1- $[\text{}^3\text{H}]$ -5-16. Through extension of the previous methodologies, 1'- $[\text{}^3\text{H}]$ - F_2CDP and 1'- $[\text{}^3\text{H}]$ - F_2CTP were produced with SA of 8620 cpm/nmol.

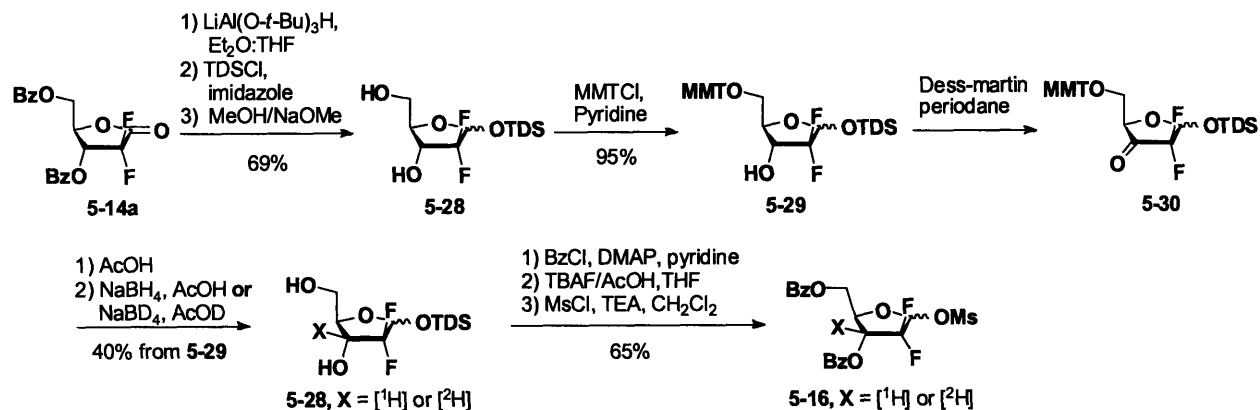
Synthesis of 3'- $[\text{}^3\text{H}]$ - F_2C

3'- $[\text{}^2\text{H}]$ labeled F_2C was synthesized for use in EPR experiments, and as a potential probe for isotope effects on the kinetics of inactivation of ribonucleotide reductases by F_2C nucleotides. Other mechanism-based inhibitors have shown a 3', 2' shift during reaction with RNR,(65) and 3'- $[\text{}^2\text{H}]$ - F_2C nucleotides were thus desired to investigate cleavage of this bond and potential rearrangements of the nucleotide during inactivation. A modification of the procedure used by Robins and coworkers(57, 58) to produce 2'- and 3'- isotopically labeled adenosines was selected to generate this compound. Incorporation was attempted on a 2,2-difluororibose, 3-ketone protected as the anomeric hexyldimethylsilyl (TDS) ether derivative, rather than F_2C itself, as previous results on cytidine derivatives indicate that the presence of the cytosine base can interfere with this chemistry.(66) Working with the ribose also eliminates the need for protection of the 4-amino group of the cytosine which is often required when working with cytidine derivatives.(67)

The initial synthetic plan sought to take advantage of the reported high stability of the 2,2-difluororibo anomeric mesylates(34) and to simply use the mesylate to block the 1-hydroxy group. However, the anomeric mesylate was not stable to the alkaline cleavage conditions used to remove benzoyl esters. Thus, a silyl protecting group (TDS) was employed to block the 1-hydroxyl (Scheme 5-11). Starting from difluorolactone 5-14a, the lactone was reduced with $\text{LiAl}(\text{O}-t\text{-Bu})_3\text{H}$ in $\text{THF}:\text{Et}_2\text{O}$, followed by protection of the lactol with (TDS) chloride.(56) The

hexyl group was chosen as the more common TBDMS group was too labile in subsequent reactions. It appears that the presence of the *gem*-difluoro group increases the liability of silyl ethers at this position. The crude product from the silyl ether formation was treated with sodium methoxide in methanol to cleave the benzoyl esters to give **5-28** in 69% yield from **5-14a**. Compound **5-28** was converted to the monomethoxytrityl (MMT) ether by reaction with MMTCI in pyridine over 2 days, yielding **5-29** in excellent yield, although the product was contaminated with MMT alcohol.(68, 69) MMT was chosen over related ethers as the trityl group was found to be too difficult to cleave in subsequent steps, and dimethoxytrityl (DMT) was not completely selective for the 5'-OH. The product **5-29** was oxidized to the 3-keto compound **5-30** by treatment with the Dess-Martin periodane in CH₂Cl₂ at neutral pH.(57, 58) The MMT was cleaved from the crude ketone by treatment with AcOH, and the crude product of this reaction was reduced with AcOH/NaBH₄ to regenerate **5-28** (40% from **5-29**) with no other isomers detected by ¹H-NMR.

Substitution of AcOD and NaBD₄ in this step yielded 3-[²H]-**5-28** (38% from **5-29**). The deuterated product was esterified with benzoyl chloride to yield the dibenzoyl derivative, and further converted to the anomeric mesylate by cleavage of the TDS ether through treatment with TBAF/AcOH in THF, followed by reaction of the crude lactol with mesyl chloride in CH₂Cl₂/pyridine. The mesylate 3-[²H]-**5-16** was isolated in 65% yield from **5-28**. This mesylate was converted to the α/β -3'-[²H]-F₂C by the procedure used for the unlabeled compound, and atom incorporation confirmed to be >99% by NMR and ESI MS at this stage (Appendix 2). This compound was transformed into the corresponding 5'-mono-, di- and triphosphates by procedures described above.



Scheme 5-11. Synthesis of 3'-[^2H]-F₂C.

Conclusions

The synthetic procedures described allow rapid production of large quantities of F₂C 5'-di- and tri- phosphates for use in a variety of biochemical studies. The enzymatic phosphorylation procedures described circumvent difficulties with the standard chemical phosphorylation methods and permit convenient and completely selective separation of the desired β -anomer from the α/β mixture produced in the coupling reaction. Routes are described to produce F₂C di- and triphosphates with isotopes of hydrogen incorporated selectively at the 1'- and 3'- positions, allowing production of [^2H] derivatives for EPR and kinetic studies and for use as a tracer in mass spectrometry experiments. F₂C phosphates labeled with [^3H] at the 1' position was produced as a tracer for detecting end products of the inactivation of RNR by gemcitabine.

5.4 References

- (1) Hui, Y. F., and Reitz, J. (1997) Gemcitabine: A cytidine analogue active against solid tumors. *Am. J. Health-Syst. Pharm.* 54, 162-170.
- (2) Matsuda, A., and Sasaki, T. (2004) Antitumor activity of sugar-modified cytosine nucleosides. *Cancer Sci.* 95, 105-111.
- (3) Hertel, L. W., Kroin, J. S., Grossman, C. S., Grindey, G. B., Door, A. F., Storinolo, A. M. V., Plunkett, W., Gandhi, V., and Huang, P. (1996) Synthesis and biological activity of

- 2',2'-difluorodeoxycytidine (gemcitabine), in *Biomedical Frontiers of Fluorine Chemistry* (Ojima, I., McCarthy, J. R., and Welch, J. T., Eds.), American Chemical Society, Washington, D. C.
- (4) Plunkett, W., Huang, P., and Gandhi, V. (1997) Gemcitabine: actions and interactions. *Nucleosides Nucleotides* 16, 1261-1270.
 - (5) Plunkett, W., Huang, P., Xu, Y.-Z., Heinemann, V., Grunewald, R., and Gandhi, V. (1995) Gemcitabine: metabolism, mechanisms of action, and self-potential. *Sem. Oncol.* 2, 3-10.
 - (6) Sunkara, P. S., Lippert, B. J., Snyder, R. D., Jarvi, E. T., and Farr, R. A. (1988) Antitumor-activity of 2'-deoxy-2',2'-difluorocytidine, a novel inhibitor of ribonucleotide reductase. *Proceedings of the American Association for Cancer Research* 29, 324-324.
 - (7) Hertel, L. W., Kroin, J. S., Misner, J. W., and Tustin, J. M. (1988) Synthesis of 2-deoxy-2,2-difluoro-D-ribose and 2-deoxy-2,2-difluoro-D-ribofuranosyl nucleosides. *J. Org. Chem.* 53, 2406-2409.
 - (8) Plunkett, W., Gandhi, V., Chubb, S., Nowak, B., Heinemann, V., Mineishi, S., Sen, A., Hertel, L. W., and Grindey, G. B. (1989) 2',2'-Difluorodeoxycytidine metabolism and mechanism of action in human leukemia cells. *Nucleosides Nucleotides* 8, 775-785.
 - (9) Bergenfeldt, M. (2006) Current state of adjuvant therapy in resected pancreatic adenocarcinoma. *Acta Oncol.* 45, 124-135.
 - (10) Cersosimo, R. J. (2002) Lung cancer: A review. *Am. J. Health-Syst. Pharm.* 59, 611-642.
 - (11) Lidestahl, A. (2006) Efficacy of systemic therapy in advance pancreatic carcinoma. *Acta Oncol.* 45, 136-143.
 - (12) Shore, S., Raraty, M. G. T., Ghaneh, P., and Neoptolemos, J. P. (2003) Chemotherapy for pancreatic cancer. *Aliment Pharmacol. Ther.* 18, 1049-1069.
 - (13) Barniaas, A. (2006) Systemic chemotherapy in inoperable or metastatic bladder cancer. *Annal. Oncol.* 17, 553-561.
 - (14) Rosti, G. (2006) Small cell lung cancer. *Annal. Oncol.* 17, 5-10.
 - (15) Oettle, H., Arnold, D., Hempel, C., and Riess, H. (2000) The role of gemcitabine alone and in combination in the treatment of pancreatic cancer. *Anti-Cancer Drugs* 11, 771-786.
 - (16) de Braud, F., Maffezzini, M., Vitale, V., Bruzzi, P., Gatta, G., Hendry, W. F., and Sternberg, C. N. (2002) Bladder cancer. *Crit. Rev. Oncol. Hematol.* 41, 89-106.
 - (17) Nabhan, C., Krett, N., Gandhi, V., and Rosen, S. (2001) Gemcitabine in hematologic malignancies. *Curr. Opin. Oncol.* 13, 514-521.
 - (18) Colomer, R. (2005) Gemcitabine plus taxane combination in metastatic breast cancer: a comprehensive review. *EJC Suppl.* 3, 9-16.
 - (19) Akerele, C. E., Rybalova, I., Kaufman, H. L., and Mani, S. (2003) Current approaches to novel therapeutics in pancreatic cancer. *Invest. New Drugs* 21, 113-129.
 - (20) Schrader, A. J., Varga, Z., Hegele, A., Pfoertner, S., Olbert, P., and Hofmann, R. (2006) Second-line strategies for metastatic renal cell carcinoma: classics and novel approaches. *J. Cancer Res. Clin. Oncol.* 132, 137-149.
 - (21) Barlési, F., and Pujola, J.-L. (2005) Combination of chemotherapy without platinum compounds in the treatment of advanced non-small cell lung cancer: a systematic review of phase III trials. *Lung Cancer* 49, 289-298.
 - (22) Barlési, F., Jacot, W., Astoul, P., and Pujol, J.-L. (2006) Second-line treatment for advanced non-small cell lung cancer: a systematic review. *Lung Cancer* 51, 159-172.

- (23) Juffs, H. G., Moore, M. J., and Tannock, I. F. (2002) The role of systemic chemotherapy in the management of muscle-invasive bladder cancer. *Lancet Oncol.* 3, 738-747.
- (24) Hussain, S. A., and James, N. D. (2003) The systemic treatment of advanced and metastatic bladder cancer. *Lancet Oncol.* 4, 489-487.
- (25) Donghui Li, K. X., Wolff, R., and Abbruzzese, J. L. (2004) Pancreatic cancer. *Lancet* 63, 1049-1057.
- (26) Rosenberg, J. E., Carroll, P. R., and Small, E. J. (2005) Update on chemotherapy for advanced bladder cancer. *J. Urol.* 174, 14-20.
- (27) Pauwels, B., Korst, A. E. C., Lardon, F., and Vermorken, J. B. (2005) Combined modality therapy of gemcitabine and radiation. *Oncologist* 10, 34-51.
- (28) Heinemann, V., Xu, Y.-Z., Chubb, S., Sen, A., Hertel, L. W., Grindey, G. B., and Plunkett, W. (1990) Inhibition of ribonucleotide reduction in CCRF-CEM cells by 2',2'-difluorodeoxycytidine. *Mol. Pharmacol.* 38, 567-572.
- (29) Baker, C. H., Banzon, J., Bollinger Jr., J. M., Stubbe, J., Samano, V., Robins, M. J., Lippert, B., Jarvi, E., and Resvick, R. (1991) 2'-Deoxy-2'-methylenecytidine and 2'-Deoxy-2',2'-difluorocytidine 5'-diphosphates: Potent mechanism-based inhibitors of ribonucleotide reductase. *J. Med. Chem.* 34, 1879-1884.
- (30) van der Donk, W. A., Yu, G., Pérez, L., Sanchez, R. J., and Stubbe, J. (1998) Detection of a new substrate-derived radical during inactivation of ribonucleotide reductase from *Escherichia coli* by gemcitabine 5'-diphosphate. *Biochemistry* 37, 6419-6426.
- (31) Silva, D. J., Stubbe, J., Samano, V., and Robins, M. J. (1998) Gemcitabine 5'-triphosphate is a stoichiometric mechanism-based inhibitor of *Lactobacillus leichmannii* ribonucleoside triphosphate reductase: evidence for thyl radical-mediated nucleotide radical formation. *Biochemistry* 37, 5528-5535.
- (32) Licht, S., and Stubbe, J. (1999) Mechanistic investigations of ribonucleotide reductases, in *Comprehensive Natural Products Chemistry* (Barton, S. D., Nakanishi, K., Meth-Cohn, O., and Poulter, C. D., Eds.) pp 163-203, Elsevier Science, New York.
- (33) El-Laghdach, A., Echarri, R., Matheu, M. I., Barrena, M. I., and Castellón, S. (1991) gem-Difluorination versus 1,2-migration and fragmentation in the reaction of 2- and 3-uloses with DAST. Influence of stereochemistry at the anomeric carbon atom. *J. Org. Chem.* 56, 4556-4559.
- (34) Chou, T. S., Heath, P. C., Patterson, L. E., Poteet, L. M., Lakin, R. E., and Hunt, A. H. (1992) Stereospecific synthesis of 2-deoxy-2,2-difluororibonolactone and its use in the preparation of 2'-deoxy-2',2'-difluoro-β-D-ribofuranosyl pyrimidine nucleosides: the key role of selective crystallization. *Synthesis*, 565-570.
- (35) Matsumura, Y., Fujin, H., Nakayama, T., Morizawa, Y., and Yasuda, A. (1992) Titanium-promoted highly stereoselective synthesis of α,α-difluoro-β,γ-dihydroxyester. Simple route to 2-deoxy-2,2-difluororibose. *J. Fluorine Chem.* 57, 203-207.
- (36) Wheeler, W. J., Mabry, T. E., and Jones, C. D. (1991) The synthesis of the ²H, ³H, and ¹⁴C-isotopomers of 2'-deoxy-2',2'-difluorocytidine hydrochloride, an anti-tumor compound. *J. Labelled Compd. Radiopharm.* 29, 583-561.
- (37) Bobek, M., Kawai, I., Sharma, R. A., Grill, S., Dutschman, G., and Cheng, Y.-C. (1987) Acetylenic nucleosides. 4. 1-β-D-Arabinofuranosyl-5-ethynylcytosine. Improved synthesis and evaluation of biochemical and antiviral properties. *J. Med. Chem.* 30, 2154-2157.

- (38) Yoshikawa, M., Kato, T., and Takenishi, T. (1967) A novel method for phosphorylation of nucleosides to 5'-nucleotides. *Tetrahedron Lett.* 8, 5065-5068.
- (39) Schendel, F. J., and Stubbe, J. (1986) Substrate specificity of formylglycinamide synthetase. *Biochemistry* 25, 2256-2264.
- (40) Hoard, D. E., and Ott, D. G. (1965) Conversion of mono- and oligodeoxyribonucleotides to 5'-triphosphates. *J. Am. Chem. Soc.* 87, 1785-1788.
- (41) Kozarich, J. W., Chinaiuk, A. C., and Hecht, S. M. (1973) Ribonucleoside phosphates via phosphorimidazolidate intermediates. Synthesis of pseudoadenosine 5'-triphosphate. *Biochemistry* 12, 4458-4463.
- (42) Stubbe, J. Personal communications, Merrell Dow Pharmaceuticals.
- (43) Bouffard, D. Y., Laliberté, J., and Momparker, R. L. (1993) Kinetic Studies on 2',2'-difluorodeoxycytidine (gemcitabine) with purified human deoxycytidine kinase and cytidine deaminase. *Biochem. Pharmacol.* 45, 1857-1861.
- (44) Hughes, T. L., Hahn, T. M., Reynolds, K. K., and Shewach, D. S. (1997) Kinetic analysis of human deoxycytidine kinase with the true phosphate donor uridine triphosphate. *Biochemistry* 36, 7540-7547.
- (45) Usova, E. V., and Eriksson, S. (1997) The effects of high salt concentrations on the regulation of the substrate specificity of human recombinant deoxycytidine kinase. *Eur. J. Biochem* 248, 762-766.
- (46) Liou, J.-Y., Dutschman, G. E., Lam, W., Jiang, Z., and Cheng, Y.-C. (2002) Characterization of human UMP/CMP kinase and its phosphorylation of D- and L-form deoxycytidine analogue monophosphates. *Cancer Res.* 62, 1624-1633.
- (47) van Rompay, A. R., Johansson, M., and Karlsson, A. (1999) Phosphorylation of deoxycytidine analog monophosphates by UMP-CMP kinase: molecular characterization of the human enzyme. *Mol. Pharmacol.* 56, 562-569.
- (48) Hsu, C.-H., Liou, J.-Y., Dutschman, G. E., and Cheng, Y.-C. (2005) Phosphorylation of cytidine, deoxycytidine, and their analog monophosphates by human UMP/CMP kinase is differentially regulated by ATP and magnesium. *Mol. Pharmacol.* 67, 806-814.
- (49) Artin, E., Thesis. (2006) in *Chemistry*, Massachusetts Institute of Technology, Cambridge, MA.
- (50) Dawson, R. M. C., Elliot, D. C., Elliot, W. H., and Jones, K. M. (1986) *Data for biochemical research*, third ed., Clarendon Press, Oxford.
- (51) Kohn, P., Samaritano, R. H., and Lerner, L. M. (1965) A new method for the synthesis of furanose derivatives of aldohexoses. *J. Am. Chem. Soc.* 87, 5475-5480.
- (52) Brown, H. C. (1975) in *Organic Synthesis via Boranes* pp 18-21, 29-31, 51-55, John Wiley and Sons, New York.
- (53) Brown, H. C., and Tierney, P. A. (1958) The reaction of lewis acids of boron with sodium hydride and borohydride. *J. Am. Chem. Soc.* 80, 1552-1558.
- (54) Examples of this procedure: Kaulinya, L. T.; Lidak, M. Y.; *Chem. Heterocycl. Compd.* 1987, 23, 77-81.; Novikov, M. S.; Ozerov, A. A.; Brel, A. K.; Boreko, E. I.; Korobchenko, L. V.; Vladyko, G. V. *Pharm. Chem. J.* 1994, 28, 110-113.
- (55) Garrett, C., and Santi, D. V. (1979) Rapid and sensitive high-pressure liquid-chromatography assay for deoxyribonucleoside triphosphates in cell-extracts. *Anal. Biochem.* 99, 268-273.
- (56) Green, T. W., and Wuts, P. G. M. (1999) in *Protective Groups in Organic Synthesis* pp 127-130, John Wiley and Sons, New York.

- (57) Robins, M. J., Samano, V., and Johnson, M. D. (1990) Periodinane oxidation, selective primary deprotection, and remarkably stereoselective reduction of *tert*-butyldimethylsilyl-protected ribonucleosides. Synthesis of 9-(β -D-xylofuranosyl)adenine or 3'-deuterioadenosine from adenosine. *J. Org. Chem.* 55, 410-412.
- (58) Robins, M. J., Sarker, S., Samano, V., and Wnuk, S. F. (1997) Nucleic acid related compounds. 94. Remarkably high stereoselective reductions of 2'- and 3'-ketonucleoside derivatives to give arabino, ribo, and xylofuranosyl nucleosides with hydrogen isotopes at C2' and C3'. *Tetrahedron* 53, 447-456.
- (59) Lewkowicz, E. S., and Iribarren, A. M. (2006) Nucleoside phosphorylases. *Curr. Org. Chem.* 10, 1197-1215.
- (60) Burgess, K., and Cook, D. (2000) Syntheses of nucleoside triphosphates. *Chem. Rev.* 100, 2047-2059.
- (61) Arner, E. S. J., and Eriksson, S. (1995) Mammalian deoxyribonucleoside kinases. *Pharmac. Ther.* 67, 155-186.
- (62) Bohman, C., and Eriksson, S. (1988) Deoxycytidine Kinase from Human-Leukemic Spleen - Preparation and Characterization of the Homogeneous Enzyme. *Biochemistry* 27, 4258-4265.
- (63) Usova, E., Maltseva, T., Foldesi, A., Chattopadhyaya, J., and Eriksson, S. (2004) Human deoxycytidine kinase as a deoxyribonucleoside phosphorylase. *J. Mol. Biol.* 344, 1347-1358.
- (64) Wu, J. C., Kozarich, J. W., and Stubbe, J. (1983) The mechanism of free base formation from DNA by bleomycin - a proposal based on site specific tritium release from poly(dA-dU). *J. Biol. Chem.* 258, 4694-4697.
- (65) Ator, M. A., and Stubbe, J. (1985) Mechanism of inactivation of *Escherichia coli* ribonucleotide reductase by 2'-chloro-2'-deoxyuridine 5'-diphosphate: evidence for generation of 2'-deoxy-3'-ketonucleotide via a net 1,2 hydrogen shift. *Biochemistry* 24, 7214-7221.
- (66) Stubbe, J., and Erlacher, H. A. Approaches to the synthesis of 1'-deuterated-2'-deoxy nucleosides. Internal lab report. Unpublished data.
- (67) Földesi, A., Kundu, M. K., Dinya, Z., and Chattopadhyaya, J. (2004) Synthesis of [2'-²H₁]-ribonucleosides. *Helv. Chim. Acta* 87, 742-757.
- (68) Gadikota, R. R., Callam, C. S., Wagner, T., Fraino, B. D., and Lowary, T. L. (2003) 2,3-Anhydro sugars in glycoside bond synthesis. Highly stereoselective syntheses of oligosaccharides containing α - and β -arabinofuranosyl linkages. *J. Am. Chem. Soc.* 125, 4155-4165.
- (69) Nyilas, Á., Glemarec, C., and Chattopadhyaya, J. (1990) Synthesis of [3'(O) \rightarrow 5'(C)]-oxyacetamido linked nucleosides. *Tetrahedron* 46, 2149-2164.

Chapter 6

Products of the Inactivation of Ribonucleoside Triphosphate Reductase by Gemcitabine Triphosphate

6.1 Introduction

Development of gemcitabine

Gemcitabine (2'-deoxy-2',2'-difluoro-cytidine, Gemzar™, F₂C) was first produced by Eli Lilly Research Laboratory(1, 2) and at Merrell Dow Pharmaceuticals(3) in independent research efforts to produce nucleoside analogues as potential anti-viral(4) and anti-tumor agents.(4, 5) Nucleotide analogues have the potential to inhibit DNA polymerase as well as many enzymes involved in nucleoside metabolism, including ribonucleotide reductase (RNR).(5-10) Ultimately these inhibitors can lead to the alteration of DNA replication and repair and trigger a cascade ending in apoptotic cell death. F₂C is a prodrug, and must be phosphorylated to the 5'-diphosphate to inhibit the class I ribonucleoside diphosphate reductase (RDPR), and to the 5'-triphosphate to inhibit class II ribonucleoside triphosphate reductases (RTPR) or become inhibitors of or substrates for DNA polymerases.

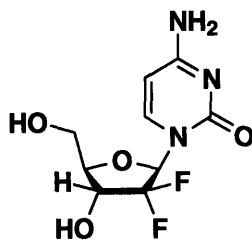


Figure 6-1. Gemcitabine (F₂C). The 5'-diphosphate and 5'-triphosphate are required for the inhibition of RDPR and RTPR, respectively.

The addition of fluorines to a potential inhibitor is a common substitution made by medicinal chemists. The van der Waals radius of fluorine (1.35 Å) is similar to that of hydrogen (1.2 Å).(11, 12) It is thus often considered to be a good isostere for hydrogen, though electronically the C-F group more closely resembles C-OH.(12-14) Replacement of a hydrogen or hydroxyl by fluorine can create a substrate analog with similar binding affinity to the natural

substrate, but with altered reactivity. Such compounds can be competitive inhibitors, binding preferentially over the natural substrate, or also mechanism-based inhibitors, taking advantage of enzyme chemistry to inactivate the enzyme.(15) Gemcitabine differs from the natural substrate cytidine only by the substitution of the CF₂ moiety for the CHOH at C2' (Figure 6-1), yet this simple change gives rise to potent cytotoxic activity *in vivo*.

Cytotoxicity and therapeutic potential

Gemcitabine now sees wide application as an anti-cancer therapeutic for a range of diseases.(16, 17) Alone, it has been approved as a treatment for non-small cell lung cancer(18-21) and advanced pancreatic cancer.(22-28) It is considered the first line treatment for advanced pancreatic cancer, though only 25% of patients benefit from F₂C therapy.(25) Gemcitabine has also been investigated as a single agent or in combination chemotherapy for the treatment of bladder cancer,(29-35) renal cancer,(36) leukemia and lymphoma,(37) ovarian cancer,(38, 39) and breast cancer.(40, 41)

It is well established that F₂CTP can be incorporated into both DNA and RNA. (42-48) The cytotoxic activity of F₂C correlates with the intracellular levels of F₂CTP.(49, 50) Incorporation of the nucleotide into DNA or RNA is believed to be followed by the insertion of an additional nucleotide before chain termination.(44, 45) This “masked” chain termination is resistant to exonuclease repair(44, 51) and begins a poorly-understood chain of events that lead to cell-cycle arrest in *S*-phase, DNA fragmentation, and cell death through apoptosis.(52-64) Treatment with F₂C has also been shown to result in inhibition of nucleotide reduction in cancer cell lines,(65, 66) resulting in depletion of intracellular deoxynucleotide pools.(67) Reduced dNTP pool sizes have been shown to be associated with the 5'-diphosphate (F₂CDP), a specific,

mechanism-based inhibitor of RDPR.(40, 66, 68-71) Inhibition of nucleotide reduction by F₂CDP primarily reduces the levels of intracellular dATP and dGTP and, more modestly, dCTP.(67) Depletion of dCTP pools is proposed to be an important self-potentiating mechanism of F₂C: reduction of dCTP alleviates dCTP inhibition of deoxycytidine kinase (dCk) thus increasing phosphorylation of F₂C, and increases the likelihood of F₂CTP entering DNA metabolism in place of dCTP.(2, 66) F₂CTP is also an inhibitor of CTP synthase, resulting in depleted CTP pools and, consequently, increased incorporation of F₂CTP into RNA.(2, 43)

Recently, it has been suggested that dNTPs, in particular dATP, play a role in inhibiting the apoptosome complex.(72) dNTPs bind to cytochrome *c*, preventing its interaction with Apaf-1 and the generation of the apoptosome. Depletion in dNTP pools may thus increase the likelihood of this apoptotic mechanism of occurring, and may explain why RNR inhibitors like F₂CDP enhance the cytotoxic activity of other DNA damaging agents.

Gemcitabine resistance

The phenotypes of resistant cell lines often grant insight into the mechanism, specificity and targets of a therapeutic agent. The determinants of resistance to F₂C in cancer cell lines have been well investigated.(73-75). Low expression levels of the human concentrative and equilibrative nucleoside transporters (hCNT and hENT) can lead to F₂C resistance.(76, 77) F₂C, like most nucleoside analogues, is too hydrophilic to passively diffuse across membranes. Gemcitabine uptake takes place through facilitated diffusion mediated by the human equilibrative nucleoside transporters hENT1 and hENT2, and through the sodium-coupled concentrative transporters hCNT1 and hCNT3.(75, 76, 78-84). Cells deficient in nucleoside transporters will avoid F₂C toxicity by excluding the drug from the cell.

The major mode of metabolic inactivation of F₂C is its deamination to difluorouridine (F₂U) by enzymes in the liver and plasma, and the deamination of F₂CMP to F₂UMP by intracellular dCMP-deaminase and its subsequent dephosphorylation. (34, 85-91) Typically, 77% of the F₂C injected is excreted by patients unchanged or as F₂U, never having entered intracellular metabolism.(86) While F₂UDP can still inhibit RNRs, the F₂U itself is not a good substrate for intracellular phosphorylation enzymes,(74, 89) and thus never becomes activated to the diphosphate, a requirement to be a substrate for RNR, or the triphosphate required for the cell's DNA/RNA synthesis and repair machinery. Intracellular F₂CMP deaminated to F₂UMP is also an inhibitor of thymidylate synthase, and can act to deplete TTP pools in the cell.

The most common mechanism of resistance stems from alterations in the expression or activity of deoxycytidine kinase (dCK).(65, 85, 92-94) Reduced expression of the protein is highly correlated with gemcitabine resistance.(22, 92, 94-98) Genetic mutation in the dCK genes themselves do not seem a common method of gemcitabine resistance.(36) Activity of dCK is also down-regulated by high dCTP pools, and cells maintaining high levels of dCTP have shown resistance to F₂C, likely by inhibition of dCK activity.(95)

Of primary interest to our research efforts is the contribution of RNR inactivation to F₂C cytotoxicity. Resistance related to nucleotide reduction enzymes provides some insight into the role of RNR as a target. Resistance in some cell lines appears to be related to increases in expression of either the RNR α subunit(99-102) or the radical-generating β subunit.(95, 103, 104) Further, patients with lower expression levels of the α subunit display longer survival times than those with high levels of expression.(105) Resistance through the over-expression of the active site subunit α is significantly more common than over-expression of β .

Several potential roles for the resultant resistance to F₂C have been proposed. By maintaining high nucleotide reduction activity, the pools of dCTP may be better maintained, reducing both incorporation of F₂CTP into DNA and reducing the phosphorylation of F₂C by dCK. It has also been proposed that the α -subunit is acting as a molecular sink, permanently associating with the F₂CDP and sequestering (or destroying) it, preventing the buildup of the F₂CTP critical for cytotoxic activity.(100) Interestingly, some cell lines which develop a resistance to hydroxyurea through up regulation of the β -subunit do not show cross resistance to gemcitabine,(106) and one hydroxyurea-resistant cell line actually displayed gemcitabine sensitivity.(107)

In recent years, attempts have been made to overcome problems of F₂C resistance(97, 108) and toxicity(109-111) through the synthesis of conjugates to a range of other molecules. F₂C was conjugated to folate through a succinate linker(109) to target and increase uptake by cancer cells which overexpress folate receptors. A F₂C-lipid conjugate synthesized as a phosphodiester has been shown to bypass several resistance mechanisms in cell culture.(108, 112) The lipid modification bypasses resistance due to reduced transport by increasing the rate of association with and passive diffusion across cell membranes. Once in cells, the lipid is believed to be hydrolyzed selectively, releasing F₂CMP and avoiding the need for phosphorylation by dCK.(97, 112)

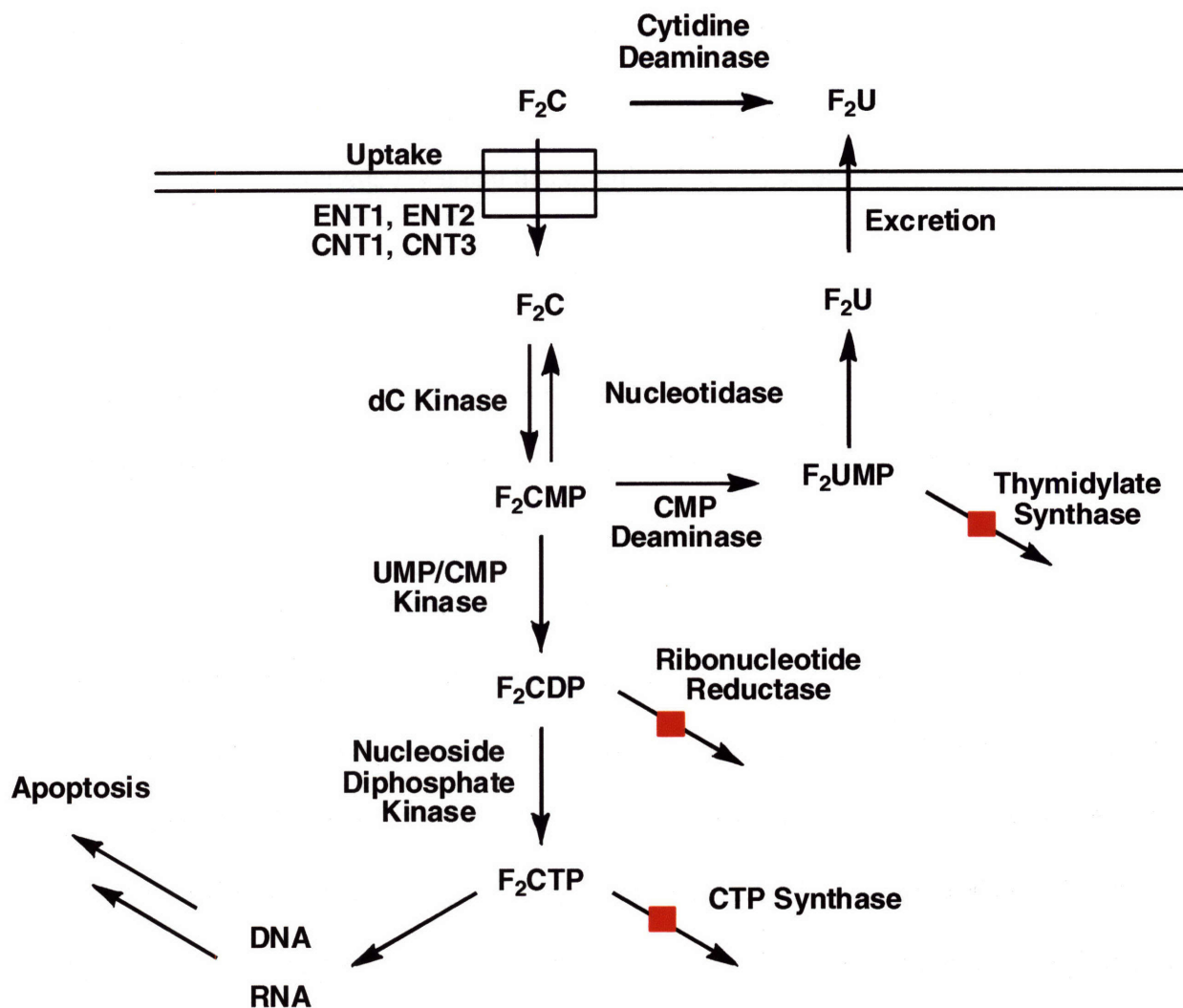


Figure 6-2. Cellular metabolism of F_2C . A red square indicates an enzyme inhibited by an F_2C metabolite.

From the many pharmacological studies of F_2C , a picture of its cellular metabolism has emerged (Figure 6-2).(75) The first step is uptake by the cell, mediated by the ENTs and CNTs. F_2C in the plasma can also be processed by the liver to F_2U , a poor substrate for the uptake system, which is excreted. F_2C within the cell is phosphorylated first by dCk. The monophosphate is further phosphorylated to F_2CDP by action of CMP/UMP kinase,(113-115) and to the triphosphate by the non-base specific enzyme nucleoside diphosphate kinase.(65) The monophosphate is also subject to deactivation by CMP deaminase activity, forming F_2UMP , which is dephosphorylated and excreted.(85) F_2UMP is also an inhibitor of thymidylate

synthase. The F₂CTP can then be incorporated in DNA and RNA through the normal synthetic machinery, and is an inhibitor of CTP synthase.(43-46) Strand breaks caused by this incorporation trigger a cascade of events leading to cell death via apoptosis.

Specific Aims

The focus of the current study is on further investigating the outcome and mechanism of inactivation of RNR by phosphorylated F₂C derivatives. This inactivation is of particular interest as F₂C is one of the few nucleoside analogues that can inactivate RNR *in vivo*. The closely structurally related 2'-monohalo-2'-deoxynucleotides inhibit RNR only *in vitro*, and it is surprising that the addition of a second fluorine transforms F₂C into a potent mechanism based inhibitor that is active in live cells. Additionally, F₂CDP and F₂CTP have proven to be stoichiometric inhibitors of *E. coli*, human, and yeast RDPR and *L. leichmannii* RTPR respectively. The investigation of the mechanism and end products of RNR inactivation by F₂C 5'-phosphates has been the subject of several prior studies, reviewed in Chapter 4.(3, 66, 68-70, 116)

The current work aims to further characterize the inactivation of RTPR by F₂CTP through the use of 1'- and 3'-[²H] and 1'- and 5'-[³H] labeled compounds. As described in Chapter 5, F₂CTP was synthesized containing [³H] at the 5-position of the base or at the 1'-position of the ribose ring. In this chapter, experiments are described utilizing these materials to track the fate of the base and the sugar ring and to quantify the products released. Small molecule products identified in this manner were characterized by NMR and mass spectrometry. The covalent modification of RTPR has also been investigated: labeled peptides have been identified through use of the sugar-[³H]-labeled inhibitor and structurally characterized through

the use of MALDI and post source decay (PSD) MS/MS. Deuterated derivatives of F₂CTP have been employed as mass labels to facilitate identification of MALDI peaks containing fragments derived from the inhibitor and for EPR studies in collaboration with Dr. Gary Gerfen (Albert Einstein College of Medicine).

Based on the results of these investigations, a working hypothesis for the mechanism of inactivation of RTPR by F₂CTP can be proposed (Figure 6-3 and Figure 6-4). In this model, the initial steps of reaction are analogous to the normal reaction mechanism. Initiation by the top face thio radical (**6-1**) proceeds by abstraction of the 3' hydrogen to give a 3' nucleotide-based radical (**6-2**). Deprotonation of the 3' hydroxyl by the glutamate residue catalyzes rearrangement to an α -keto radical with loss of fluoride (as HF, **6-3**). The mechanism then branches from this common intermediate into an "alkylative" pathway or a "non-alkylative pathway." Partitioning between these two is dependent on the manner in which fluoride is lost. If fluoride leaves as HF, resulting in deprotonation of the bottom-face thiol, the alkylative mechanism proceeds. If fluoride leaves as F⁻, the non-alkylative pathway proceeds instead. This idea is based on the past results with the monofluoro compounds, which show partitioning between dCDP formation or inactivation depending on whether or not fluoride removes this proton when it is eliminated.(117, 118)

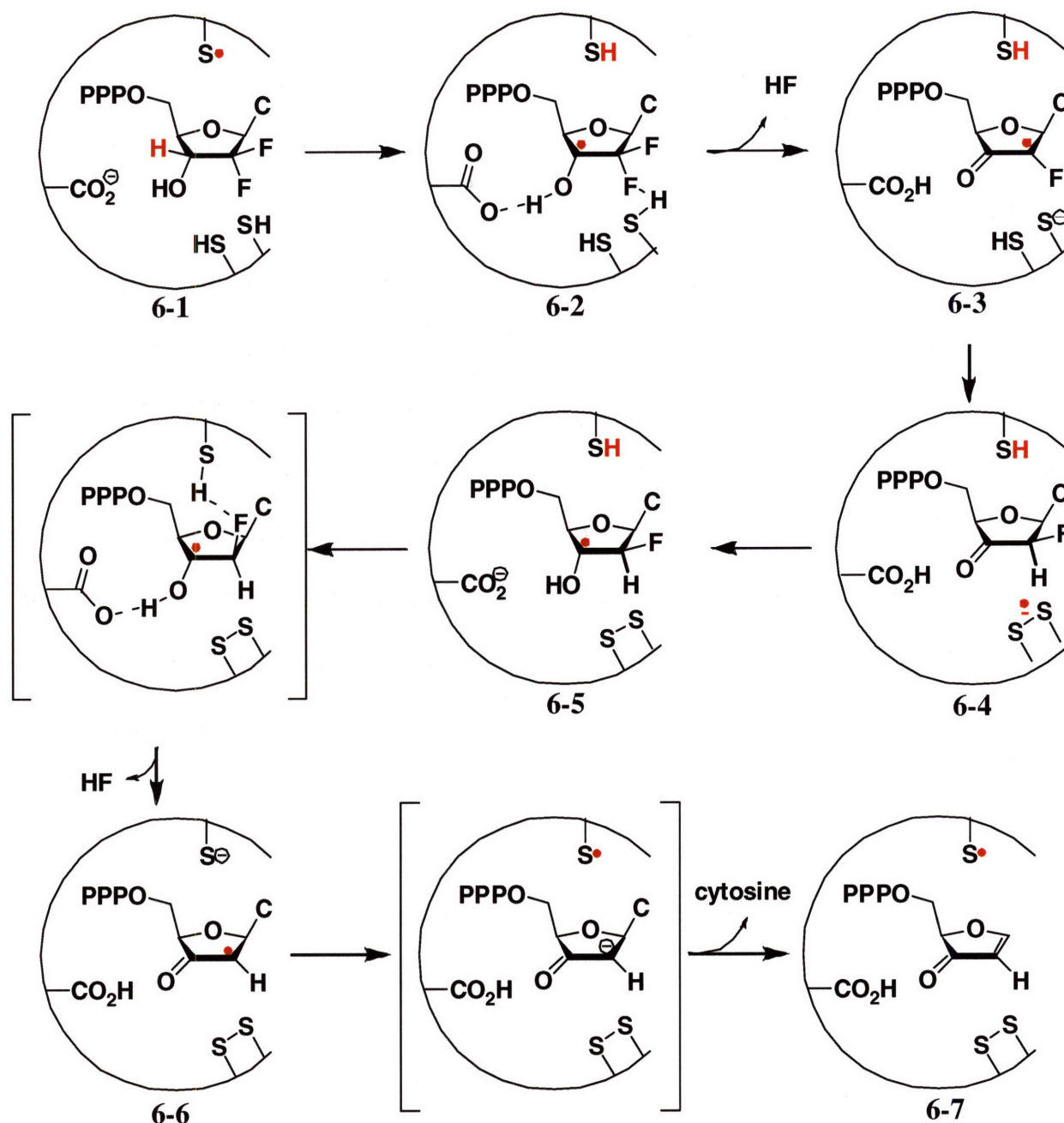


Figure 6-3. Proposed mechanism of F₂CTP inhibition of RTPR, "alkylative" pathway.

In the proposed alkylative pathway, fluoride leaves with deprotonation of the proximal bottom face cysteine (Figure 6-3). This results in a partial "turnover," very similar to the mechanism proposed by Ramos based on DFT calculations (described in Chapter 4).⁽¹¹⁶⁾ Here, the keto nucleotide radical may be reduced by proton-coupled electron transfer from the bottom face reducing equivalents with concomitant generation of a disulfide radical anion, producing a

3'-keto-2'-monofluoro nucleotide with the fluorine in the *ara* configuration (6-4). The disulfide radical anion may re-reduce the ketone with protonation from the glutamate to generate the 3' radical shown (6-5). Here, DFT calculations indicated that rearrangement to a second 3'-keto radical with loss of HF is more favorable than hydrogen abstraction to yield a fluoro ketone, and the first occurs with a much faster rate than reduction.(119) Thus, the top-face thiol is deprotonated by the leaving fluoride, generating a 3'-keto radical identical to that proposed for inhibition by monohalo nucleotides (6-6).(117, 118, 120-123) The key difference in this case is that there are no abstractable hydrogen atoms available on nearby cysteines. The most likely method of reduction for this keto-radical species would be by single-electron transfer from the top face thiolate,(124) regenerating the initial thio radical but placing a negative charge on the nucleotide. This intermediate would rapidly eliminate base, generating an α,β -ketone in the active site which could react with any nearby nucleophile to alkylate the protein by conjugate addition (6-7).

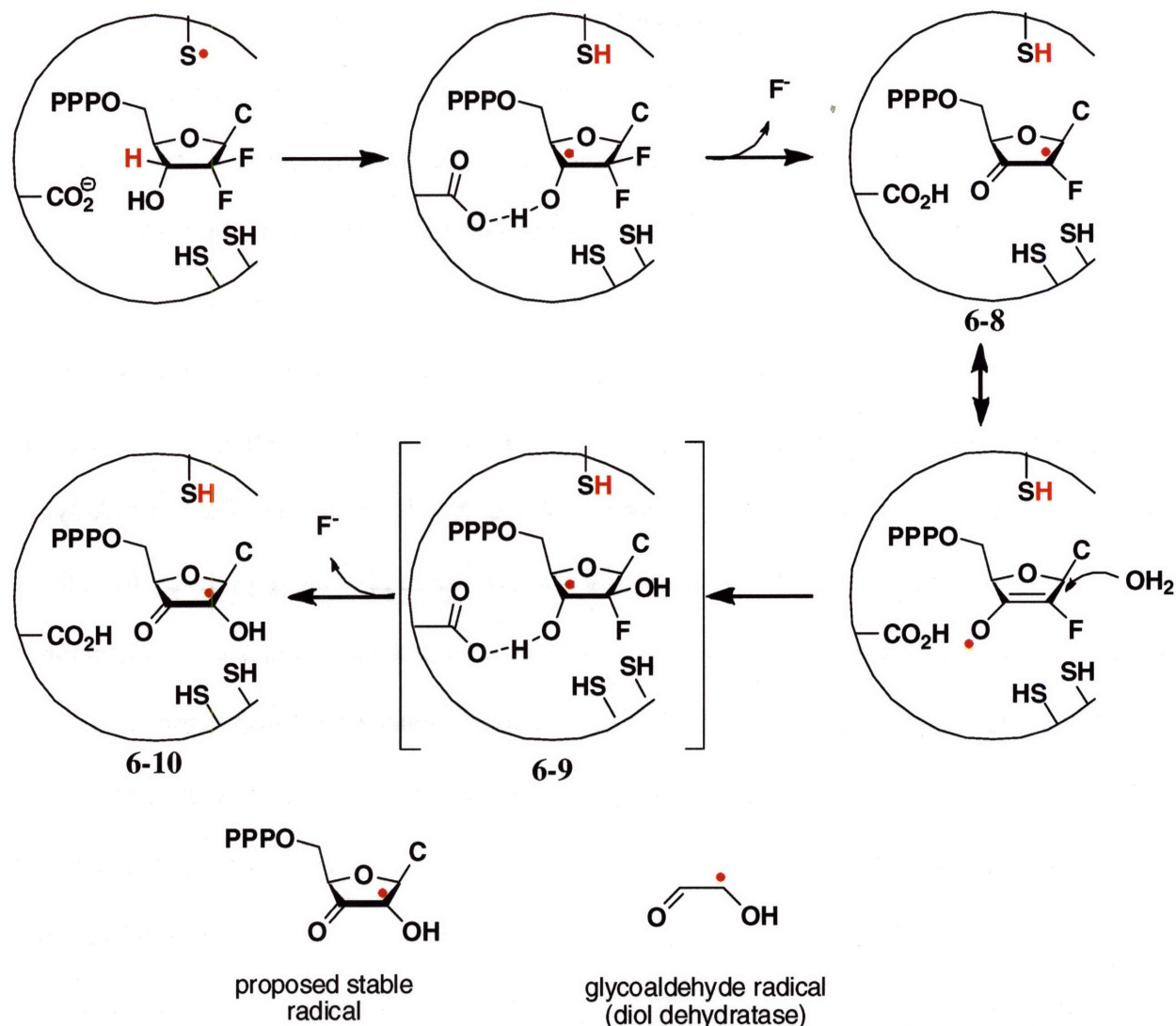


Figure 6-4. Proposed mechanism of F_2CTP inhibition of RTPR, “non-alkylative” pathway. The addition of water can be viewed as the reverse of the second step elimination of fluoride.

The non-alkylative pathway (Figure 6-4) results if the fluoride leaves without deprotonation of the proximal bottom-face cysteine (6-8). This loss of F^- might result if the ribose ring is bound too far away from the reducing equivalents to interact with them, as suggested by the recent yeast crystal structure.(125) It may simply be related to the leaving group ability of fluoride being intermediate between hydroxide, which must be protonated to leave at a reasonable rate, and the other halides, which can be lost without protonation.(118) In either case, reduction of the radical by proton-coupled electron transfer to generate a disulfide radical anion would not be possible. Further, if the F_2CTP was indeed bound too far from the

reducing equivalents to permit protonation, reduction by hydrogen atom transfer would also be impossible. A fluorine substituent has also been shown in some cases to provide stabilization to the radical(126) and may thus slow down the rate of hydrogen atom abstraction in **6-8** relative to the unfluorinated species. In particular fluorinated hydrocarbon radicals have been shown to abstract hydrogen atoms from benzene thiol more slowly than non-fluorinated analogs.(126-128)

In the absence of reduction, the radical would be long-lived enough to react with water at the 2' position, in what amounts to a reversal of the first two steps of the RNR reaction. The resulting 3' radical generated (**6-9**) could now lose the second fluoride, generating a 2'-hydroxy substituted radical (**6-10**). This radical would be expected to be much more stable than the 2' unsubstituted radical proposed in the alkylative pathway, and is a good candidate for the stable radical previously described in this system, seen at time scales of 20s and longer.(69) This radical is structurally very similar to the stable glycoaldehyde radical detected when diol dehydratase is inactivated by glycoaldehyde, a radical stable for days at room temperature under anaerobic conditions.(129, 130) This radical might disassociate from the active site and become reduced by solvent or be reduced within the active site by an amino acid to produce the 3'-keto nucleotide product which would decompose in a manner similar to the 2'-deoxy-3'-ketonucleotides generated in other systems (see Chapter 4). This radical might also decompose by a mechanism similar to that proposed for the 2' unsubstituted radical (Figure 6-3).

This proposal accounts for many of the previous experimental observations and is supported by the experiments described here. The alkylative pathway leads to the generation of an unsaturated ketone directly in the active site which could inactivate the α subunit by conjugate addition without ever releasing furanone into solution. Further, it explains how the alkylative pathway could return the radical to the top-face thiol, allowing regeneration of the tyrosyl radical

of the RDPR β subunit. The non-alkylative pathway shows a possible mechanism for loss of radical from the active site. In RDPR, this would result in inactivation of the β subunit but perhaps only partial inactivation of the α subunit through alkylation on a slow time scale. In the case of RTPR, the non-alkylative pathway could result in a Co(II) species tightly associated with the enzyme that may react on a slower timescale to inactivate the enzyme through the previously described alkylation of C419, though the mechanism of this process is currently unknown.⁽⁶⁹⁾ The differing results observed in RDPR and RTPR, and RDPR with and without reductants, may be explained as variations in partitioning between the two pathways described, influenced by variations in enzyme conformation and inhibitor binding. The model of inactivation proposed here is complex, but provides a useful framework for the consideration of the inactivation of RTPR by F₂CTP, and the specific experiments described here.

6.2 Experimental

Materials. 2-[¹⁴C]-CTP (250 μ Ci, 55 mCi/mmol, 99.2% pure) was purchased from Moravek Biochemicals, and diluted with cold CTP in 25 mM HEPES pH 7.5, 1 mM MgCl₂, 4 mM EDTA to a specific activity of 1000-3000 cpm/nmol. F₂CTP and isotopically labeled derivatives were produced as described in Chapter 5. All other reagents were purchased from Sigma or Mallinckrodt and used without further purification unless otherwise indicated. Silanized glassware was prepared by treatment with Sigmacote (Sigma), allowed to air dry, and washed with acetone, methanol and water before use. Calf intestine alkaline phosphatase was purchased from Roche as a 20U/ μ L stock in 100 mM Tris pH 8.5. *E. coli* thioredoxin (TR, SA of 40 units/mg) and *E. coli* thioredoxin reductase (TRR, SA of 1320 units/mg) were isolated as previously described.⁽¹³¹⁻¹³³⁾ RTPR (SA of 0.38-0.42 μ mol mg⁻¹ min⁻¹) was isolated using a

variant of a previously described procedure,⁽¹³⁴⁾ the second anion exchange column described in the original procedure was omitted. AdoCbl was handled with minimal exposure to light. All reactions including AdoCbl were kept wrapped in foil at all times. Transfer of AdoCbl solutions and other manipulations that required exposure to ambient lighting were performed under very dim or red light conditions.

Physical Measurements. ESI-MS was performed on a Bruker Daltonics APEXIV 4.7 Tesla Fourier Transform Ion Cyclotron Resonance Mass Spectrometer (FT-ICR-MS) at the MIT Department of Chemistry Instrumentation Facility. ¹H NMR spectra were recorded on a Varian 500 MHz NMR spectrometer at the MIT Department of Chemistry Instrumentation Facility. NMR samples were internally referenced to the solvent residual peak or to 3-(trimethylsilyl)propionic acid. Scintillation counting was performed using Emulsifier-Safe liquid scintillation counting cocktail (Perkin Elmer) on a Beckman LS6500 multipurpose scintillation counter. For [³H] samples, recoveries of radioactivity in all experiments were high (>95% for Sephadex columns, >80% for HPLC chromatography) and it was thus assumed no changes in quenching of the radioactivity were being observed. All spectrophotometric assays and UV-vis spectra were recorded on either a Cary 3 or a Cary 118-OLIS spectrophotometer. In both cases, the temperature was regulated using a Lauda water bath. Extinction coefficients at pH 7.0 (100 mM KP_i) used were: F₂C ($\epsilon_{268} = 9360 \text{ M}^{-1} \text{ cm}^{-1}$);⁽¹³⁵⁾ cytidine ($\epsilon_{271} = 9100 \text{ M}^{-1} \text{ cm}^{-1}$), cytosine ($\epsilon_{267} = 6100 \text{ M}^{-1} \text{ cm}^{-1}$), adenosine ($\epsilon_{259} = 15400 \text{ M}^{-1}$), adenosylcobalamin ($\epsilon_{524} = 8000 \text{ M}^{-1} \text{ cm}^{-1}$), NADPH ($\epsilon_{340} = 6200 \text{ M}^{-1} \text{ cm}^{-1}$);⁽¹³⁶⁾ RTPR ($\epsilon_{280} = 100960 \text{ M}^{-1}$).^(134, 137)

RTPR assay (Spectrophotometric assay 1). The assay mixture contained in a final volume of 500 μ L: RTPR (typically 0.25, 0.5 or 1 μ M), ATP (2 mM), NADPH (0.2 mM), TR (20 μ M), TRR (0.15 μ M), KP_i (50 mM, pH 7.5), EDTA (4 mM), and NaOAc (1 M). The background rate at

37°C was measured as the change in A 340 nm. AdoCbl (80 µM) was added to initiate the reaction. The change in A 340 nm at 37°C over time was measured. The SA of RTPR was typically 1.2-1.8 µmol mg⁻¹ min⁻¹.

RTPR assay (Spectrophotometric assay 2). The assay mixture contained in a final volume of 500µL: RTPR (typically 0.25, 0.5 or 1 µM), CTP (1 mM), dATP (100 µM), NADPH (0.2 mM), TR (20 µM), TRR (0.2 µM), HEPES (25 mM, pH 7.5), EDTA (4 mM), and MgCl₂ (1 mM). The reaction was initiated with AdoCbl (20 µM) at 37°C and monitored as in spectrophotometric assay 1. The SA of RTPR was typically 0.28-0.44 µmol mg⁻¹ min⁻¹.

RTPR assay ([¹⁴C-] dCTP monitoring). The assay mixture contained in a final volume of 300 µL: RTPR (1 µM), [¹⁴C-CTP] (specific activity used was typically 1500-2500 cpm/nmol, 1 mM), dATP (100 µM), NADPH (1 mM), TR (20 µM), TRR (0.2 µM), HEPES (25 mM, pH 7.5), EDTA (4 mM), and MgCl₂ (1 mM). The reaction was initiated by the addition of AdoCbl (20 µM) and incubated at 37°C; a control aliquot was removed before addition of AdoCbl. Four aliquots (50 µL) were removed at time points over five min, and the reaction quenched by addition of 2% perchloric acid (25 µL). The aliquots were neutralized with 0.4 M KOH (25 µL) after all time points were collected. Alternatively, for a single time point assay, the reaction (100 µL) was initiated by addition of RTPR, incubated 5 min at 37°C, quenched with 2% perchloric acid (50 µL) and neutralized with 0.4 M KOH (50 µL). Cytosine (50 nmol) and dC (50 nmol) were added to each aliquot, then 20 U alkaline phosphatase in 500 mM Tris pH 8.6, 1 mM EDTA (26.5 µL) was added and the aliquots were incubated 2h at 37°C. The aliquots were centrifuged (5 min at 5000 rpm) and 100 µL portions were loaded on 2 mL AG-1-X8 resin (borate form) columns, and the dC eluted with water (10 mL). The flow through (10 mL) was collected, mixed and 1 mL analyzed by scintillation counting. RTPR specific activity was

determined from a linear least-squares fit of activity versus time, and typically ranged from 0.20-0.40 $\mu\text{mol mg}^{-1} \text{min}^{-1}$.

Pre-reduction of RTPR. DTT was added to an aliquot of RTPR stock solution (~1 mM) to a final concentration of 30 mM. The solution was incubated 15 min at 37°C, then passed through a Sephadex G-25 size exclusion column (SEC) (1 cm x 20 cm, 20 mL for 0.5-1 mL of pre-reduction mixture), eluting with assay buffer (25 HEPES, pH 7.5, 4 mM EDTA 1 mM MgCl_2). The protein-containing fractions were combined and the concentration of RTPR determined by UV-vis spectroscopy.

Pre-reduction of RTPR with elimination of cytosine deaminase activity. RTPR stock solution (~1 mM, 250 μL) was mixed with 5 mM *o*-phenanthroline (750 μL) and DTT was added to a final concentration of 30 mM. The solution was incubated 20 min at 37°C, and the protein isolated and quantified as above.

Time dependent inactivation of RTPR with F_2CTP .(69, 70) The inactivation mixture contained in final volume of 100 μL : pre-reduced RTPR (5 μM), dATP (100 μM), NADPH (1 mM), TR (20 μM), TRR (0.2 μM), AdoCbl (20 μM), HEPES (25 mM, pH 7.5), EDTA (4 mM), and MgCl_2 (1 mM). NADPH, TR, and TRR were excluded from the inactivation mixture if the inactivation was to be assayed in the absence of reductants. The inactivation was initiated by addition of F_2CTP (or isotopically labeled derivative, 5 μM) and the reaction carried out at 37°C. At each time point (4 total over 5 min), 20 μL of the inactivation mixture was removed and assayed as described for the radioactive assay at an enzyme concentration of 1 μM . Control aliquots were removed before addition of F_2CTP . The $t = 0$ control was assayed immediately; the endpoint control was incubated at 37°C until the last inactivation time point was collected,

then assayed. A blank (20 μL ddH₂O) was also assayed as a control in place of an aliquot from the inactivation mixture.

SEC on RTPR inactivated with 1'-[³H]- or 5-[³H]-F₂CTP. Inactivation mixtures were prepared as described in the time dependent inactivation studies in a final volume of 500 μL . Experiments were run both in the presence and absence of reductants. Inactivations were initiated by addition of F₂CTP (1'-[³H], SA 7200 cpm/nmol or 5-[³H], SA 10800 cpm/nmol) and incubated for 2 min at 37°C. An aliquot was assayed for activity using spectrophotometric assay 2 before initiation and at the inactivation endpoint. After 2 min, an aliquot (200 μL) was loaded on Sephadex G-50 columns (1 cm x 20 cm, 20 mL), equilibrated with and eluting with assay buffer (25 mM HEPES pH 7.5, 1 mM MgCl₂, 4 mM EDTA) and 1 mL fractions were collected. A second aliquot (210 μL) was mixed with 630 μL 8 M guanidine, then loaded on a Sephadex G-50 column (1 cm x 20 cm, 20 mL) equilibrated in and eluted with 2M guanidine in assay buffer and 800 μL fractions were collected. Alternatively, the aliquot (200 μL) was combined with 50 μL of 250 mM NaBH₄, 500 mM Tris pH 8.5 in a 1.5 mL falcon tube and incubated 5 min at 37°C. The NaBH₄ solution was prepared by combining solid NaBH₄ with the buffer solution immediately before use; vigorous foaming occurred upon addition to the inactivation mixture. The mixture was then loaded on a Sephadex G-50 column (1 cm x 20 cm, 20 mL), equilibrated and eluted with assay buffer (25 mM HEPES pH 7.5, 1 mM MgCl₂, 4 mM EDTA) and 1 mL fractions were collected. In all cases, fractions were assayed for A260 nm and A280 nm and for radioactivity by scintillation counting (500 μL aliquots). Total cpm in each fraction were calculated as [(cpm measured)-(background)]*(fraction volume in μL)/(500 μL). Total recovery of radioactivity was typically >95%. Recovery of protein was determined from A280

nm and was typically >90%. The reported equiv. of nucleotide bound and in solution were adjusted for recovery and determined by (total cpm)/(F₂CTP SA)/(RTPR recovered (nmol)).

UV Detection of cytosine deaminase activity in the RTPR preparation. The conversion of cytosine ($\lambda_{\max} = 269$ nm) to uracil ($\lambda_{\max} = 258$ nm) was monitored by UV on a Cary-3 spectrometer. The reaction mixture contained in 500 μ L: 50 μ M cytosine, 5 μ M RTPR, 20 μ M AdoCbl, 5 mM DTT, 25 mM HEPES pH 7.5, 1 mM MgCl₂, and 4 mM EDTA. Three different preparations of RTPR were assayed: as isolated, purified by S-300 SEC, or pre-treated with 3 mM *o*-phenanthroline. The UV spectra were collected at t = 0, 30 min, 1 h, 6 h, and 1 day.

Purification of RTPR by SEC. RTPR (200 μ L of a 1.06 mM stock) was loaded onto a S-300 column (1.5 x 75 cm) equilibrated in 25 mM HEPES pH 7.5, 1 mM MgCl₂, 4 mM EDTA, 5% v/v glycerol and eluted in the same buffer at a rate of 1 mL/min. The center of the main peak was collected and tested for RTPR activity by the UV CTP/dATP assay (S.A. 0.41).

HPLC analysis of products generated on incubation of RTPR with F₂CTP. Inactivation mixtures, in a final volume of 220 μ L or 1020 μ L, contained pre-reduced RTPR (50 μ M), dATP (500 μ M), AdoCbl (50 μ M), HEPES (25 mM, pH 7.5), EDTA (4 mM), and MgCl₂ (1 mM). 1'-[³H]-F₂CTP (50 μ M, 7200 cpm/nmol), 5-[³H]-F₂CTP (50 μ M, 10,800 cpm/nmol) or unlabeled F₂CTP (50 μ M) was added to initiate the reaction which was then incubated 2 min at 37°C. Before initiation with F₂CTP and after the inactivation was complete, 10 μ L aliquots were removed and assayed for RTPR activity by spectrophotometric assay 2 (final assay volume 500 μ L). At 2 min the inactivation mixture was filtered through a YM-30 membrane (30,000 MWCO minicon), 10 min at 14,000 x g at 4°C. Alternatively, the reaction was first quenched with 50 μ L (250 μ L for the large scale reaction) of 250 mM NaBH₄, 500 mM Tris pH 8.5. The NaBH₄ solution was prepared by combining solid NaBH₄ with the buffer solution immediately

before use. In the case of NaBH₄ quench, the inactivation was run in a falcon tube of at least 4 times the volume of the inactivation mixture, due to vigorous foaming upon the addition of the NaBH₄ stock, and the inactivation/NaBH₄ mixture was incubated 5 min at 37°C and the reaction filtered through a YM-30 membrane (30,000 MWCO minicon) 10 min at 14,000 x g at 4°C. If radiolabeled F₂CTP was used, F₂C (50 nmol) and cytosine (50 nmol) were added as carrier before filtration. To the flow-through was added 20 U (100 U for large scale) alkaline phosphatase, the reaction incubated 3 h at 37°C, then filtered through a second YM-30 centricon. In the case of reactions quenched with NaBH₄, the sample was acidified by addition of glacial acetic acid (5% of the final volume) and the resulting mixture was lyophilized to dryness to hydrolyze borate esters.

In all cases, the entirety of the product mixture was purified by HPLC using a Rainin SD-200 HPLC and an Altech Adsorbosphere Nucleotide Nucleoside C-18 column (250 mm x 4.6 mm) with elution at a flow rate of 1 mL/min. The solvent system was: Buffer A, 10 mM NH₄OAc, pH 6.8; Buffer B: 100% methanol. The flow program was 100% A for 10 min followed by a linear gradient to 40% B over 25 min, then to 100% B over 5 min. Under these conditions, standards eluted as follows: cytosine, 5.7 min; uracil, 7.9 min; C, 12.6 min; *ara*-C-17.4 min; dC, 19.0 min; F₂C, 23.2 min. Fractions (1 mL) were collected; for samples with radiolabeled F₂CTP, 200 µL of each fraction was analyzed by scintillation counting. The cytosine peak was isolated and recovery (based on cytosine loaded as carrier) was calculated; recovery was also calculated based on the radioactivity eluted and agreed with the UV recovery to within 10%. The radioactivity in each fraction was adjusted for calculated recovery. To quantify base release on a fast time scale, the alkaline phosphatase step was omitted and the reaction injected on the HPLC after filtration through the first YM-30 membrane, using the same

purification conditions (injected 15 min after reaction initiated). Products produced during the inactivation were also examined using ion-pairing conditions, omitting the alkaline phosphatase step and injecting the reaction on the HPLC after filtration through the first YM-30 membrane. This purification was performed on a Rainin SD-200 HPLC and an Altech Adsorbosphere Nucleotide Nucleoside C-18 column (250 mm x 4.6 mm), eluted with a flow rate of 1 mL/min. The solvent system was Buffer A, 60 mM KPi pH 5, 5 mM tetrabutylammonium phosphate (TBAP), Buffer B, 100% methanol, 5 mM TBAP. The flow program was a linear gradient to 50% B over 20 min, then to 100% B over 10 min. Under these conditions, F₂CTP elutes at 27 min.

Characterization of major nucleoside product isolated from NaBH₄ quenched

RTPR/F₂CTP inactivation mixture. A large-scale inactivation reaction quenched with NaBH₄ was run as described above. In a final volume of 2 mL, the reaction mixture contained: RTPR (125 μM), dATP (500 μM), AdoCbl (125 μM), F₂CTP (125 μM), HEPES (25 mM, pH 7.5), EDTA (4 mM), and MgCl₂ (1 mM). The inactivation was quenched at 2 min with 500 μL of 250 mM NaBH₄, 500 mM Tris pH 8.5 as described above and filtered through a YM-30 membrane (30,000 MWCO minicon) 15 min at 14,000 x g at 4°C, and the flow through treated with 200 U alkaline phosphatase for 2 h at 37°C, followed by filtration through a second YM-30 membrane. The sample was acidified by addition of glacial acetic acid (5% of the final volume) and the resulting mixture was lyophilized to dryness to hydrolyze borate esters, then taken up in 1 mL 10 mM NH₄OAc. For the first chromatography step, the reaction was purified using identical equipment and buffer system to the smaller scale inactivation; the only difference was the use of a larger (2 mL) injection loop. Peaks displaying a cytosine UV-vis spectrum (diode-array detector equipped HPLC) were collected in each step directly. The peaks eluting between 16

min and 22 min were collected (estimated amount of cytosine-containing material in this region was ~60 nmol based on A 270). This material was lyophilized to dryness, taken up in 1 mM NH₄OAc, and repurified using the same elution program, substituting 1 mM NH₄OAc, pH 6.8, for buffer A and keeping buffer B 100% MeOH. The major cytosine-containing peak (diode-array UV spectrum) eluting at 16.2 min was collected (estimated quantity in this peak ~35 nmol, the remainder of the material in minor peaks that were not collected). Only silanized glassware was used for handling the repurified material. In order to collect material pure enough for NMR characterization, the product was again lyophilized and repurified by HPLC, and only the center of the major peak was isolated. Final recovery was typically 8-12 nmol of this product after three purifications. This product was characterized by NMR and ESI MS. ¹H-NMR (500 MHz, D₂O) δ: 7.71 (d, *J* = 7.5 Hz, 1H, H6), 5.99 (d, *J* = 6.1 Hz, 1H, H1'), 5.85 (d, *J* = 7.5 Hz, 1H, H5), 4.41 (dd, *J* = 5, 6 Hz, 1H, H2'), 4.24 (dd, *J* = 4.3 Hz, 4.9 Hz, 1H, H3'), 4.02 (m, 1H, H4'), 3.80 (dd, *J* = 4.0, 12 Hz, 1H, H5'), 3.75 (dd, *J* = 7.0, 12 Hz, 1H, H5''). ESI-MS (C₉H₁₃N₃O₅) *m/z* (M + Na⁺) calcd 266.0747, obsd 266.0743; (M + H⁺) calcd 244.0928, obsd 244.0921.

Characterization of major nucleoside product isolated from NaBD₄ quenched

RTPR/F₂CTP inactivation mixture. A reaction was run identically to the previous procedure, substituting NaBD₄ for NaBH₄. The purification protocol was the same, with the same region collected in the first purification. In the second chromatography step, the peak eluting at the same retention time as the compound characterized in the previous experiment was collected, and this compound repurified collecting only the center of the peak as described. The final recovery of this peak was ~5-8 nmol in this case. ¹H-NMR (500 MHz, D₂O) δ: 7.71 (d, *J* = 7.5 Hz, 1H, H6), 5.98 (s, 1H, H1'), 5.84 (d, *J* = 7.5 Hz, 1H, H5), 4.01 (dd, *J* = 4.0 Hz, 7.1 Hz, 1H, H4'), 3.80 (dd, *J* = 4.0, 12 Hz, 1H, H5'), 3.75 (dd, *J* = 7.0, 12 Hz, 1H, H5'').

Quantification and characterization of cobalamin, cytosine and protein labeling products

from RTPR inactivated with F₂CTP. The inactivation mixture in final volume of 1250 μ L contained: pre-reduced RTPR (50 μ M), dATP (500 μ M), AdoCbl (50 μ M), HEPES (25 mM, pH 7.5), EDTA (4 mM), and MgCl₂ (1 mM). After addition of AdoCbl, all aliquots were handled with minimal exposure to light (under red light and wrapped with foil). The inactivation was initiated by addition of either 1'-[³H]-F₂CTP (SA 1985 cpm/nmol) or 5-[³H]-F₂CTP (SA 1350 cpm/nmol) to a final concentration of 50 μ M. An aliquot was assayed for activity as described in the assay sections at t=0 and at the inactivation endpoint. The inactivation was incubated for either 2 min or 1 h at 37°C. An aliquots (100 μ L) was removed from each reaction at the endpoint, quenched by filtration through a YM-30 membrane, dephosphorylated and analyzed as described in the section HPLC analysis of products generated on incubation of RTPR with F₂CTP. A second aliquot (100 μ L) was removed and analyzed by HPLC directly after the initial filtration, as described in the same section. An aliquot (1000 μ L) from the inactivation mixture was loaded on a Sephadex G-50 column (1 x 20 cm, 20 mL) wrapped in foil, run at 4°C under dim red light at the inactivation endpoint. The column was equilibrated in and eluted with assay buffer (25 mM HEPES pH 7.5, 4 mM EDTA, and 1 mM MgCl₂), and 1 mL fractions were collected. Aliquots (200 μ L) were removed from each fraction and assayed for A260 nm A280 nm, and 100 μ L assayed for radioactivity. The amount of radioactivity eluting with the protein peak was used to determine the equiv. bound, as described in the section on the SEC of inactivated RTPR. Aliquots (750 μ L) from the protein containing fractions were combined and the UV-vis spectrum recorded. These fractions were then lyophilized to dryness (excluding light). Aliquots (750 μ L) from the small molecules fractions (determined by fractions where A260 >A280) were combined and lyophilized to dryness (excluding light). These samples were

dissolved in 500 μL water, and the UV-vis spectra recorded. The spectrometer baseline was determined by lyophilizing an equal volume of buffer identical to that used in the experimental samples, redissolving in 500 μL water. The spectra were deconvoluted by subtraction of linear combinations of standard spectra (AdoCbl, HOCbl).⁽¹³⁸⁾ For the solution phase products, combinations of AdoCbl and HOCbl were produced by adding the two standard spectra in proportions ranging from 1:0 AdoCbl:HOCbl to 0:1 AdoCbl HOCbl in 0.05 equiv. increments, scaled to match the A525 of the experimental sample, and subtracted.

Stability of [^3H]-RTPR generated by inactivation with 1'-[^3H]-F₂CTP. The mixture in final volume of 700 μL contained: pre-reduced RTPR (15 μM), dATP (100 μM), AdoCbl (22.5 μM), HEPES (25 mM, pH 7.5), EDTA (4 mM), and MgCl₂ (1 mM). The reaction was initiated by addition of 1'-[^3H]-F₂CTP (SA 7200) to a final concentration of 15 μM . The reaction was incubated 2 min at 37°C. The mixture was split into three 200 μL aliquots and passed through Sephadex G-50 columns (1 cm x 20 cm, 20 mL). Each column was equilibrated and eluted in a different buffer (0.1 M NH₄HCO₃, pH 8; 0.1 M NH₄HCO₃, pH 8, 2M urea; or 160 mM KPi, pH 5.6, 2M urea) and the protein containing fractions assayed for A280 and radioactivity. The samples (1.5 mL of each) were loaded into Slidalyzer dialysis cassettes (10,000 MWCO) and dialyzed against the same buffer in which the sample was eluted. Aliquots (250 μL) were removed at 1h, 2h, 4h, and 6h. The dialysis buffers were changed and the samples were dialyzed an additional 14h. A final aliquot was removed, and all aliquots were assayed for radioactivity by scintillation counting.

Trypsin Digestion of RTPR inactivated with 1'-[^3H]-F₂CTP. The reaction in a final volume of 220 μL contained: pre-reduced RTPR (50 μM), dATP (500 μM), AdoCbl (75 μM), HEPES (25 mM, pH 7.5), EDTA (4 mM), and MgCl₂ (1 mM). 1'-[^3H]-F₂CTP (50 μM , SA 7200

cpm/nmol) was added to initiate the reaction, and the reaction incubated for 2 min at 37°C. Before initiation with F₂CTP and after the inactivation was complete, 10 µL aliquots were removed and assayed for RTPR activity by spectrophotometric assay 2. At 2 min the inactivation mixture was quenched with 50 µL of 250 mM NaBH₄, 400 mM Tris pH 8.3 and incubated for an additional 5 min at 37°C. The NaBH₄ solution was prepared by combining solid NaBH₄ with the buffer solution immediately before use; vigorous foaming occurred upon addition to the inactivation mixture. To this mixture was added 750 µL 8M guanidine, 40 mM DTT, 5.33 mM EDTA, 400 mM Tris pH 8.3 and the reaction incubated 30 min at 37°C. Iodoacetamide was added to a final concentration of 250 mM (25000 equiv. per RTPR) and the reaction incubated an additional 1 h at 37°C. The protein was then separated from small molecules on a Sephadex G-50 column (1cm x 20 cm, 20 mL) equilibrated into 0.1 M NH₄HCO₃ pH 8.2 (or 0.1 M NH₄HCO₃ pH 8.2, 2M urea). The protein containing fractions (detected by A280) were combined (typically 2 mL total volume, 90% recovery of protein, >95% recovery of loaded radioactivity, 0.28 equiv. of radioactivity coeluting with protein). Trypsin (Worthington) was added from a freshly prepared stock solution to a final concentration of 4:1 RTPR:trypsin w/w, and incubated 2 h at 37°C. The reaction was quenched by addition of 25 µL TFA (to pH ~2), and the peptides were immediately separated using a Waters 2487 HPLC with a Phenomenex Jupiter C18 peptide column (150 x 4.6mm, 5 micron, 300 Å pore size) with a flow rate of 1 mL/min. The solvent system used was: Buffer A, 0.1% TFA in ddH₂O, Buffer B, 0.1% TFA in acetonitrile. A linear gradient of 0-45% B over 90 min was used. Fractions were collected (1 mL) and aliquots of each fraction (100 µL) were assayed for radioactivity by scintillation counting. The recovery of injected radioactivity was 70-85%, with a typical recovery of 80%. Four regions of radioactivity were observed: I, 48-50 min, a sharp peak

containing 17-20% of eluting radioactivity; II, 51-59 min, a broad region containing 20-30% of eluting radioactivity; III, 61-63 min, a sharp peak containing 13-17% of eluting radioactivity; and IV, 64-70 min, a broad, tailing peak containing 15-25% of eluting radioactivity. Very small quantities of radioactivity (< 2%) eluted in the dead volume. Fractions were pooled based on the observed peaks of radioactivity, concentrated to < 1 mL on a lyophilizer, and repurified using the same column with a flow rate of 1 mL/min. The solvent system used in repurifications was: Buffer A, 10 mM NH₄OAc, pH 6.8, buffer B, 100% acetonitrile with a gradient of 0-35% B over 90 min. Fractions (1 mL) were collected and aliquots of each fraction (250 μL) were assayed for radioactivity by scintillation counting. The major peaks of radioactivity were pooled from each run and submitted for peptide mass spectrometry without concentration. A summary of the recoveries at each stage is in Figure 6-5. In variants on this purification, the NaBH₄ treatment was omitted, or applied after digestion. Reactions were also run using this procedure substituting NaBD₄ or F₂CTP that was a mixture of 1'-[²H] and 1'-[³H], SA 7200 cpm/nmol, to give a stock with 60% 1'-[²H] with SA 2600 cpm/nmol.

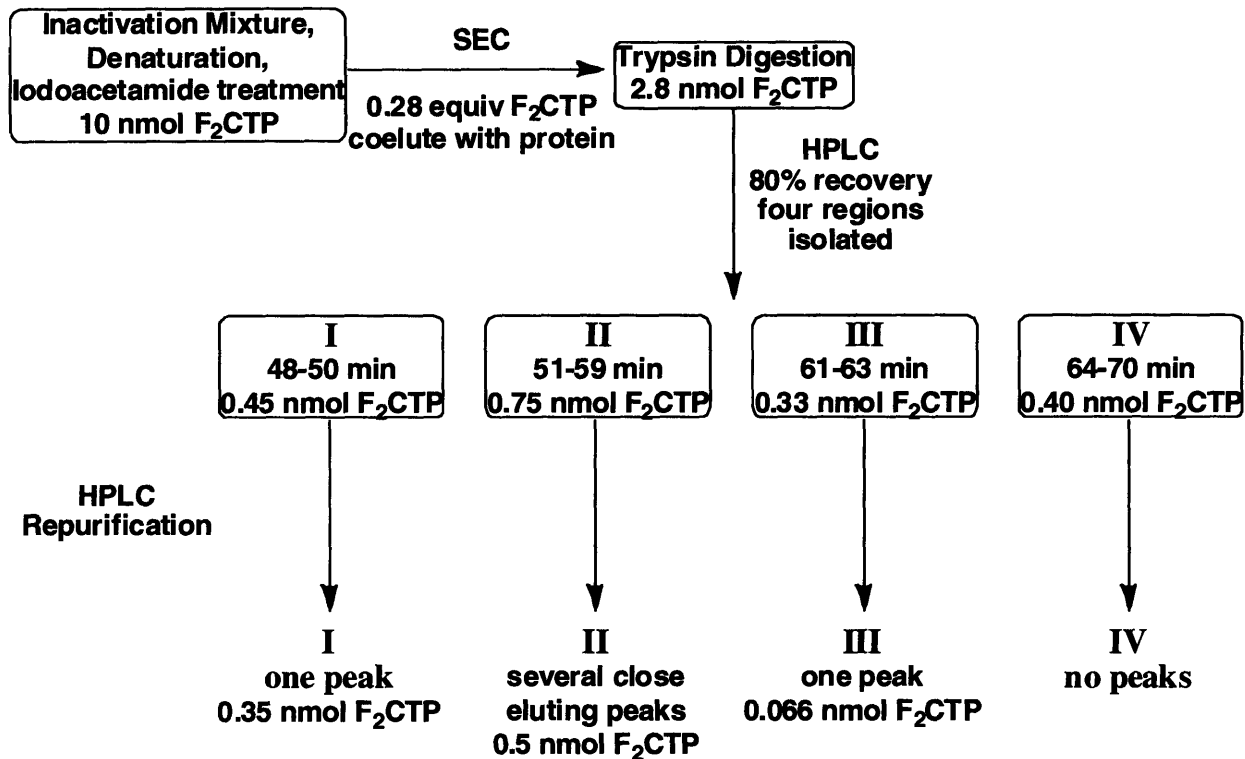


Figure 6-5. Outline of purification of labeled RTPR peptides and recoveries at each stage. The quantity of F₂CTP reported at each stage is estimated based on typical recoveries in these experiments.

Peptide mass spectrometry. (139) MALDI-TOF and tandem MS/MS mass spectrometry were performed by Dr. John Leszyk at UMass Medical School on a Kratos Axima CFR (Shimadzu Instruments) matrix-assisted-laser desorption/ionization (MALDI) mass spectrometer. Samples (0.5 μ L, containing 50-100 fmol of F₂CTP labeled peptide, determined by SA) were applied to the target and mixed with 0.5 μ l of matrix which was 2,5-dihydroxybenzoic acid at 15mg/ml in (CH₃CN:0.1%TFA 50:50). Samples were allowed to air dry prior to insertion into the mass spectrometer. Peptides were analyzed in positive ion mode in mid mass range (100-3000 Da) with an accuracy to within 100 ppm. The instrument was externally calibrated with bradykinin (757.40), P14R (MS mass standard, Sigma-Aldrich, 1533.86 Da), and adrenocorticotrophic hormone fragment 18-39 (Sigma-Aldrich, 2465.20 Da). Post-source decay (PSD) analysis were performed on the same instrument using a timed ion gate for precursor selection with a laser

power about 20% higher than for MS acquisition. PSD fragments were separated in a curved field reflectron which allowed for a seamless full mass range acquisition of the spectrum, with an accuracy of within 1000 ppm. All spectra were processed with Mascot Distiller (Matrix Sciences, Ltd.) prior to database searching.(140) Database searches were performed with Mascot (Matrix Sciences, Ltd.). For MS searches the Peptide Mass Fingerprint program was used with a peptide mass tolerance of 150 ppm. For MS/MS searching, the MS/MS Ion Search program was used with a Precursor tolerance of 150 ppm and a fragment tolerance of 1 Da.

6.3 Results

Time dependent inactivation of RTPR with F₂CTP

A brief study of the time dependant inactivation behavior of RTPR treated with F₂CTP prepared by the methods described in Chapter 5 was undertaken to establish that the same inactivation behavior was observed as previously described (Figure 6-6).(69) One equivalent of F₂CTP is sufficient to eliminate >90% of the activity within the first time point (20 s) in the presence of reductants (TR/TRR/NADPH), with >95% of activity eliminated by 2 min. Very similar results are seen in the absence of reductants using pre-reduced RTPR. It was typical to see >95% inactivation at 2 min in the presence of reductants, and 90-95% inactivation at 2 min in the absence of reductants. The results of these inactivations are very similar to those observed previously by Silva.(69)

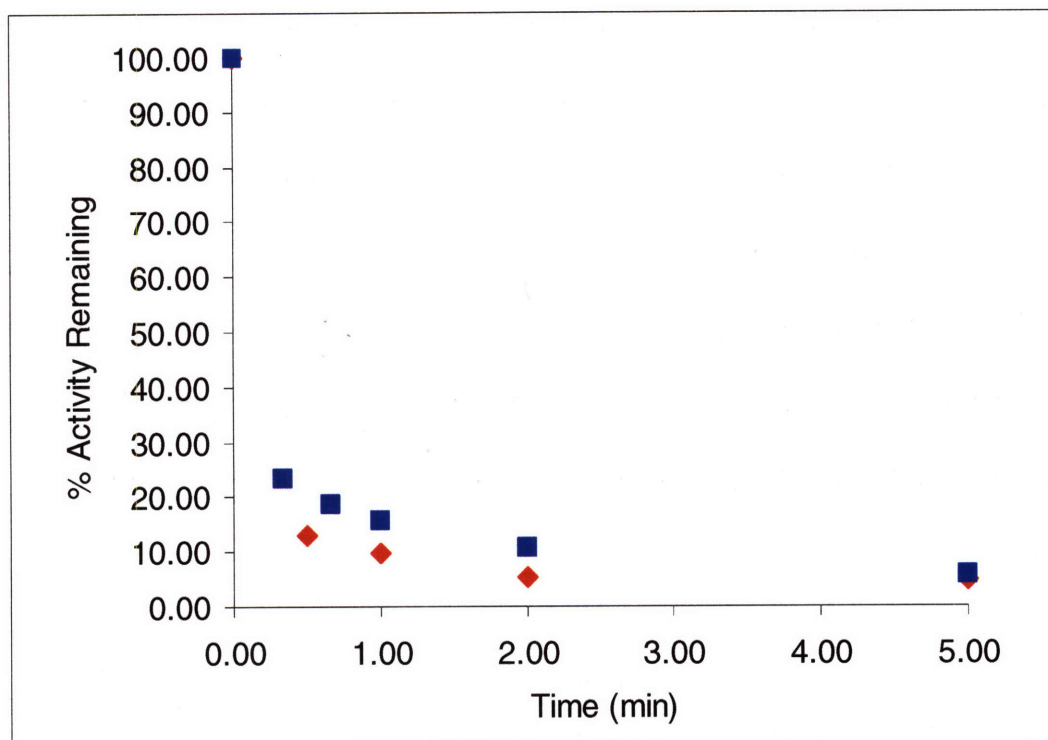


Figure 6-6. Time dependent inactivation of RTPR with F₂CTP (1 equiv.) in the presence of TR/TRR/NADPH (♦), the absence of reductants (■).

Determination of covalent labeling of RTPR inactivated by 1'-[³H]- and 5-[³H]-F₂CTP

Previous studies have shown that F₂CTP is a stoichiometric, mechanism-based inhibitor of RTPR, and have suggested that inactivation proceeds in part by alkylation of the enzyme, and in part by the covalent labeling of C419 by a cobalamin species.⁽⁶⁹⁾ Radiolabeled material was unavailable in these early studies. The synthesis of radiolabeled derivatives of F₂CTP has provided for the first time a method for quantifying alkylation of RTPR by F₂CTP. RTPR inactivated with 1'-[³H]- or 5-[³H]- F₂CTP was separated from small molecules by SEC in the presence or absence of denaturant. Radioactivity co-eluting with the protein is indicative of a covalent or tightly-bound non-covalent species. The results of a number of experiments are summarized in Table 6-1. In the case of 1'-[³H]-F₂CTP, 0.47 ± 0.02 equiv. co-elute with RTPR. The extent of labeling is the same in presence and absence of reductants. With 5-[³H]-F₂CTP,

0.16 equiv. co-elute with RTPR in the presence and absence of reductants, with a slight reduction in labeling under denaturing conditions. The substoichiometric labeling, combined with the >90% inactivation observed and the C419-Co bond observed by Silva together led to the initial proposal of a branching mechanism for this inactivation.(69)

Table 6-1. SEC of RTPR inactivated with 1'-[³H] and 5-[³H]-F₂CTP. (a) Under these conditions, the small molecules were analyzed by HPLC, and 0.71 equiv. of base and 0.18 equiv. of F₂C were found in the solution phase products after dephosphorylation and separation by reverse-phase HPLC.

Enzyme	F ₂ CTP Label	Reductants	Denaturing Column	Label eluting with protein (equiv./RTPR)
wt	1'-[³ H]	Y	N	0.46
wt	1'-[³ H]	Y	Y	0.47
wt	1'-[³ H]	N	N	0.49
wt	1'-[³ H]	N	Y	0.44
wt, NaBH ₄ @ 2min	1'-[³ H]	N	N	0.33
wt	5-[³ H]	Y	N	0.17
wt	5-[³ H]	Y	Y	0.13
wt	5-[³ H]	N	N	0.15 ^a
wt	5-[³ H]	N	Y	0.12
wt, NaBH ₄ @ 2min	5-[³ H]	N	N	0.03

Identification of cytosine release

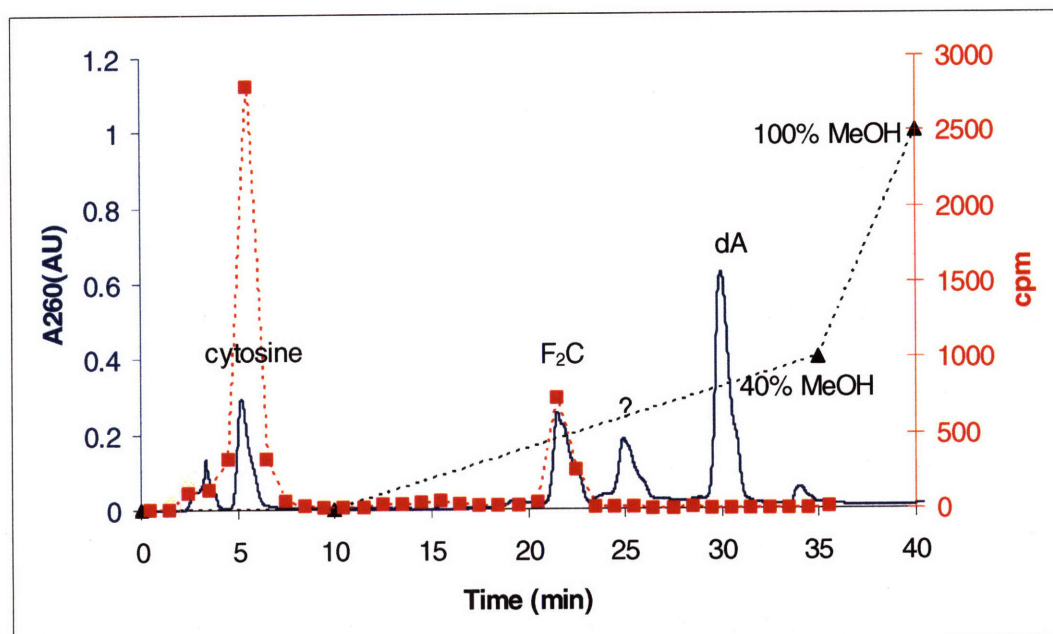
It was initially surprising that there was significantly less base bound to RTPR than ribose, as earlier studies failed to detect cytosine release during the inactivation.(69) Given the apparent loss of cytosine in these experiments and its previous loss observed when *E. coli* RDPR was inactivated with F₂CDP,(68) we refocused our efforts to determine if cytosine was being metabolized to uracil which would explain the apparent discrepancy. In order to confirm cytosine release, inactivations were run as described in the experimental section and the small molecule products were analyzed by HPLC. The retention time of 5-[³H]-labeled material was identical to a uracil standard at ~8 min (data not shown). Isolation of this material and examination by UV-vis and NMR confirmed its identity. To determine if a cytosine deaminase activity was present in RTPR preparations, cytosine was incubated with RTPR and was

completely converted to uracil within 2 h. This activity suggested RTPR was contaminated with *E. coli* cytosine deaminase.(141) This enzyme requires Fe^{2+} , and therefore 3mM *o*-phenanthroline was included in the RTRP pre-reduction mixture to chelate the iron and eliminate this activity. Alternatively, RTPR was further purified by SEC (S-300) chromatography to separate it from cytosine deaminase, expected to be a 300 kDa hexamer. In both cases, the contaminating activity was eliminated.

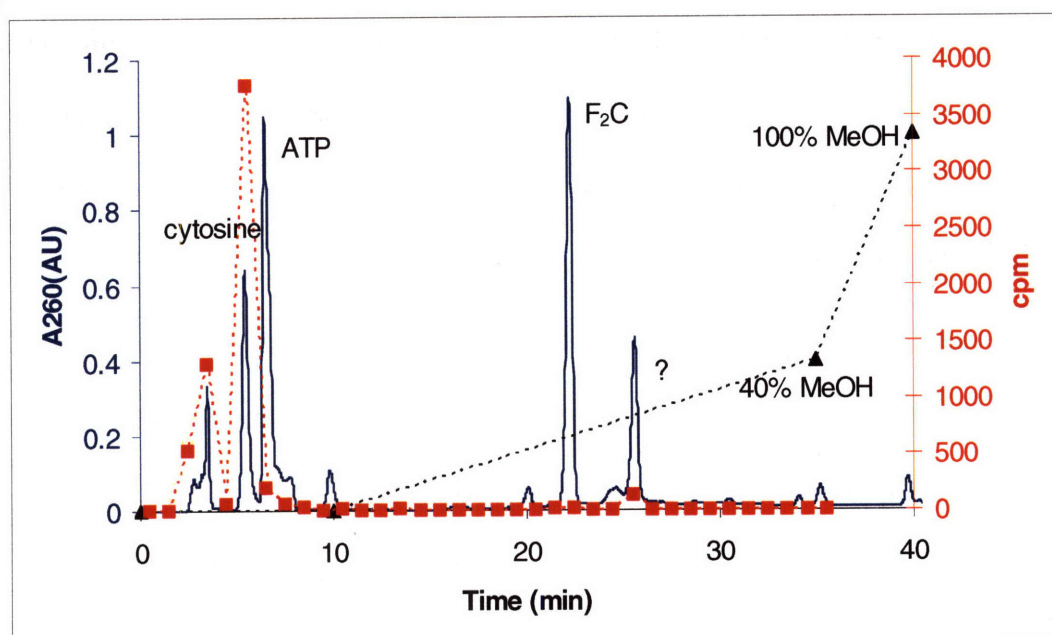
Removal of cytosine deaminase activity by inclusion of *o*-phenanthroline in the pre-reduction mixture allowed quantification of base release. Inactivations were performed using 5- $[\text{^3H}]$ - F_2CTP and the small molecules dephosphorylated and analyzed by HPLC (Figure 6-7 A). The majority (>95%) of radioactivity co-eluted with the cytosine and F_2C added as carrier. The other peaks visible in the absorbance spectrum are dA (30 min) and unknown products related to breakdown of AdoCbl. From this experiment, starting with a 1:1 ratio of F_2CTP :RTPR, 0.71 equiv. of cytosine were released and 0.19 equiv. of unreacted F_2C remained. As the previously described SEC showed 0.15 equiv. of cytosine co-elute with RTPR at 2 min, thus all the cytosine is accounted for.

To determine how rapidly cytosine is released, a reaction was performed where the products were not dephosphorylated, a process that takes several hours. Instead, the reaction mixture was filtered through a YM-30 membrane for 10 min at 14,000 x g at 4°C and injected directly onto the HPLC column (~15 min after the inactivation was initiated). In this case (Figure 6-7 B), 0.6 equiv. of cytosine were released, and the remainder eluted in the solvent front (most likely as F_2CTP and unknown phosphorylated nucleotide products). Thus, the majority of the nucleotide base (0.7 equiv. based on F_2CTP added, 0.87 equiv. of F_2CTP consumed) is released as cytosine, and most of this (0.6 equiv.) is released on timescales shorter than 15 min.

Previously-investigated mechanism-based inhibitors are always accompanied by base release. However, this base release was believed to be non-enzymatic, occurring in solution from 3'-keto-2'-deoxynucleotides on a minute time scale. Thus, results with F₂CTP indicate this inhibitor is unique with most cytosine eliminated from the RTPR-bound products by 2 min, and 0.6 equiv. present as free cytosine by 15 min. To gain more information on the timescale of cytosine release, the reaction mixtures were treated with NaBH₄ at the endpoint of inactivation (2 min). NaBH₄ can potentially reduce any 3'-ketonucleotides, preventing loss of base by β -elimination. The results of such an experiment show 0.33 equiv. of ribose coeluting with RTPR, and only 0.03 equiv. of cytosine. The depression in labeling is likely due to the base-catalyzed elimination of cytosine competing with the reduction of a ketone, or elimination of cytosine on a fast time scale. In either case, it is clear that most of the base is being eliminated from the labeled RTPR faster than a putative ketone can be reduced. This result suggested the loss of base was occurring during the course of the inactivation (Figure 6-3).



(A)



(B)

Figure 6-7. HPLC analysis of cytosine release from RTPR inactivated with 5- ^3H -F₂CTP, Absorbance (—), and cpm (■). Gradient (.....) Buffer A, 10 mM NH₄OAc, pH 6.8; Buffer B: 100% methanol, 100% A until 10 min, followed by a linear gradient to 40% B over 25 min, then to 100% B over 5 min. (A) Small molecule products dephosphorylated with alkaline phosphatase. Authentic cytosine and F₂C were included as carrier, and 95% of radioactivity co-elutes with these two peaks. 0.70 ± 0.03 equiv. of cytosine were detected, and 0.19 ± 0.02 equiv. of F₂C were observed. (B) Small molecule products not dephosphorylated. Authentic cytosine and F₂C were included as carrier, 0.6 equiv. of radioactivity elutes with cytosine.

Identification and quantification of products derived from the F₂CTP ribose ring.

With all of the cytosine accounted for, the next task was to establish the fate of the sugar moiety. From the SEC experiments, 0.47 equiv. were shown to co-elute with the protein, and the cytosine quantification experiments indicate ~0.2 equiv. remain in unreacted F₂C. Thus, ~0.3 equiv. of sugar are yet to be accounted for. To find this missing piece, inactivations were performed using 1'-[³H]-F₂CTP and the small molecules fraction, isolated by ultrafiltration and dephosphorylated with alkaline phosphatase, was analyzed by reverse-phase HPLC (Figure 6-8 A). Unreacted F₂C (0.15 equiv.) is again apparent. The majority of the radioactivity (0.28 equiv.) eluted with the solvent front, and the remainder (0.13 equiv.) is eluted as a broad region of radioactivity from 14-20 min. This elution profile suggests that the ribose-containing small molecules decompose over the course of the analysis.

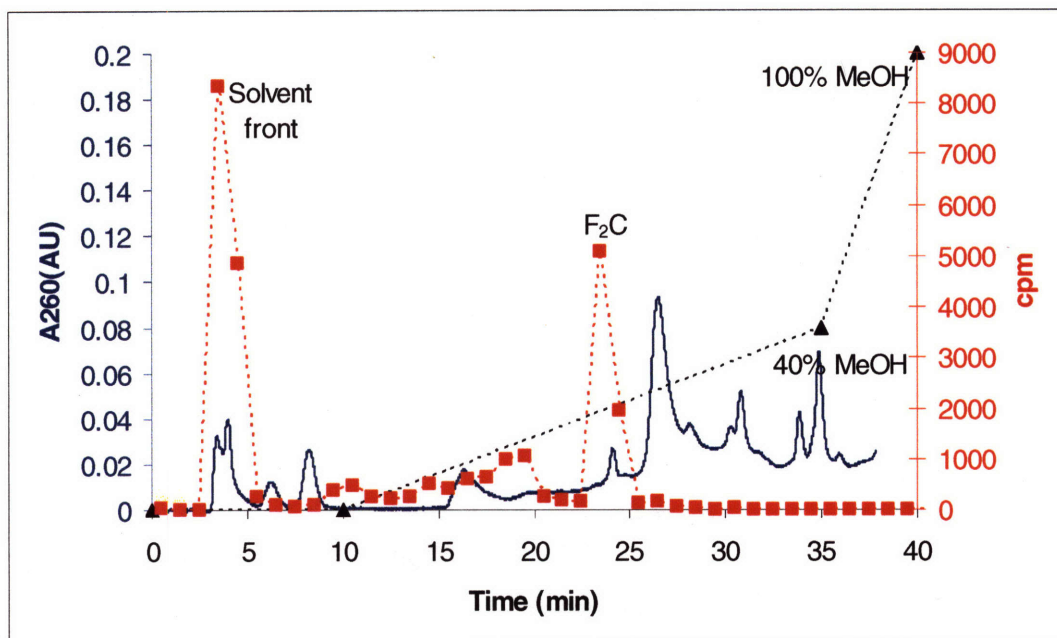
An examination of an identical reaction mixture under ion-pairing chromatography conditions gives the result shown in (Figure 6-8 B). In this case, the small molecule fraction was not subjected to alkaline phosphatase treatment and analyzed after filtration through one YM-30 membrane (10 min at 14,000 x g at 4°C) and injected onto the HPLC (~15 min after the inactivation was initiated). In this case, the HPLC trace shows some unreacted F₂CTP (0.12 equiv.), some material eluting in the solvent front (0.15 equiv.), and a third region of radioactivity (0.22 equiv.) eluting as a triphosphate (25.5 min), but earlier than F₂CTP. These results suggest that there is a solution phase nucleotide that can eliminate cytosine on a relatively slow timescale, in contrast to the peptide-bound species which seems to eliminate all cytosine very rapidly. If this nucleotide has been converted 3'-ketone as observed for other mechanism

based inhibitors (Chapter 4) it should be possible to reduce it with NaBH_4 , trapping this product before base and inorganic triphosphate can be eliminated.

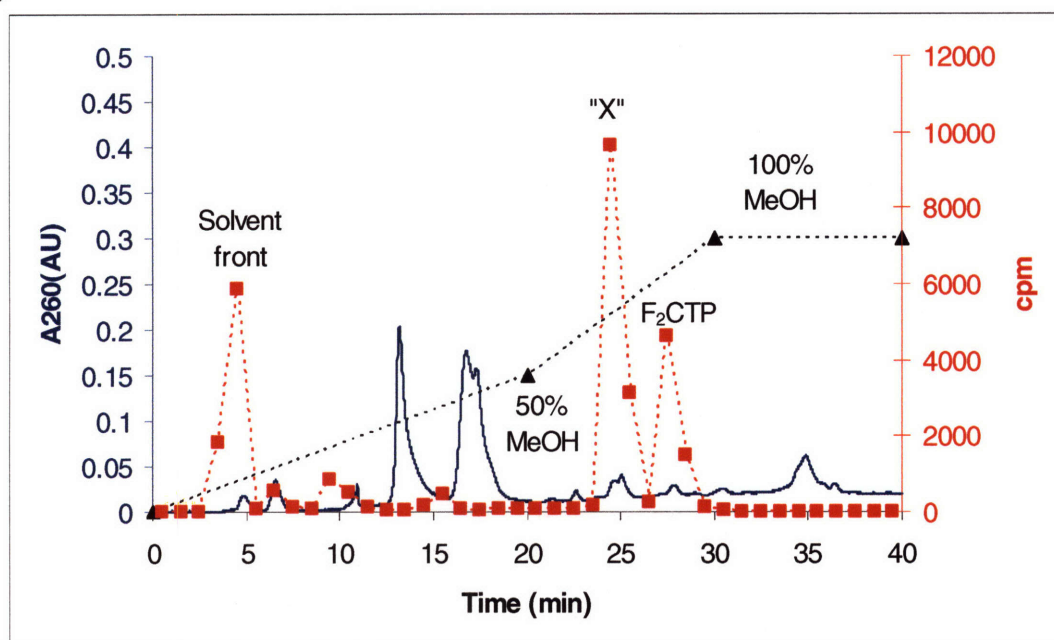
Figure 6-9 A shows the results of the HPLC analysis of an inactivation reaction with 1'- $[\text{}^3\text{H}]\text{-F}_2\text{CTP}$, treated with NaBH_4 at 2 min, followed by treatment with alkaline phosphatase. In this case, the trace shows unreacted F_2C (0.25 equiv.) but now only a small amount of radioactivity (<5%) elutes in the solvent front. A new, broad peak of radioactivity (0.28 equiv.) is observed at 13-17 min, a retention time consistent with cytosine nucleosides. The absorption is low as the peak appears to contain a number of compounds; the spectrum observed by the diode-array detector during elution appeared similar to cytosine throughout this region despite the low absolute absorbance. Repeats of these inactivation conditions found 0.24 equiv. and 0.41 equiv. of the new product; the latter case was accompanied by the presence of much less (<0.05 equiv.) unreacted F_2C than in the other two cases.

To test the hypothesis that the stable solution species was the 2'-OH radical proposed (Figure 6-4), 5 mM DTT was included in the reaction mixture in an effort to force reduction by hydrogen atom transfer before trapping by NaBH_4 reduction, and thus affect the number of hydrogen atoms delivered by NaBH_4 (see below). Interestingly, when the inactivation is run in the presence of 5 mM DTT, none of this new product is observed, and all radioactivity was seen eluting at the solvent front (Figure 6-9 B). Under these conditions almost all the F_2CTP was consumed; <2% of radioactivity is recovered as F_2C . The presence of DTT appears not only to facilitate complete reaction of the F_2CTP , but elimination of cytosine from the sugar ring as evidenced by the inability to trap any nucleotide products. No cytosine-containing peaks were observed by UV other than the free base. Note that cytosine release was not quantified under these conditions. It is possible that the DTT encouraged reduction to a ketone species that favors

elimination of cytosine over ketone reduction in the presence of NaBH₄. It is also possible that DTT does not reduce the glycoaldehyde-like radical directly; model systems have shown that the thiolate form of DTT reduces α -keto radicals (of acetaldehyde) several orders of magnitude faster than the thiol form.⁽¹²⁴⁾ Thus, the radical may persist in the presence of DTT, and the addition of NaBH₄ first deprotonated the DTT, and this thiolate rapidly reduces the radical by single electron transfer, generating a negative charge on C2' causing rapid elimination of base in a mechanism similar to that proposed in Figure 6-3.



(A)



(B)

Figure 6-8. (A) Reverse-phase HPLC analysis of small molecule products from RTPR inactivated with 1'-[³H]-F₂CTP, dephosphorylated with alkaline phosphatase, absorbance (—), and cpm (■). Gradient (·····) Buffer A, 10 mM NH₄OAc, pH 6.8; Buffer B: 100% methanol, 100% A for 10 min, followed by a linear gradient to 40% B over 25 min, then to 100% B over 5 min. The first peak of radioactivity elutes in the solvent front (0.28 equiv.); the second corresponds to unreacted gemcitabine (0.15 equiv.) and 0.13 equiv. elute in a broad region from 14-20 min. (B) Reverse-phase HPLC of small molecule products from RTPR inactivated with 1'-[³H]-F₂CTP, not dephosphorylated and eluted under ion-pairing HPLC conditions, Buffer A, 60 mM KPi pH 5, 5 mM TBAP, Buffer B, 100% methanol, 5 mM TBAP. The elution program used was a linear gradient to 50% B over 20 min, then to 100% B over 10 min. Here, 0.15 equiv. of radioactivity elute at the solvent front. 0.12 equiv. elute as F₂CTP (28 min), and 0.23 equiv. elute in a region consistent with a NTP (25.5 min) but earlier than F₂CTP.

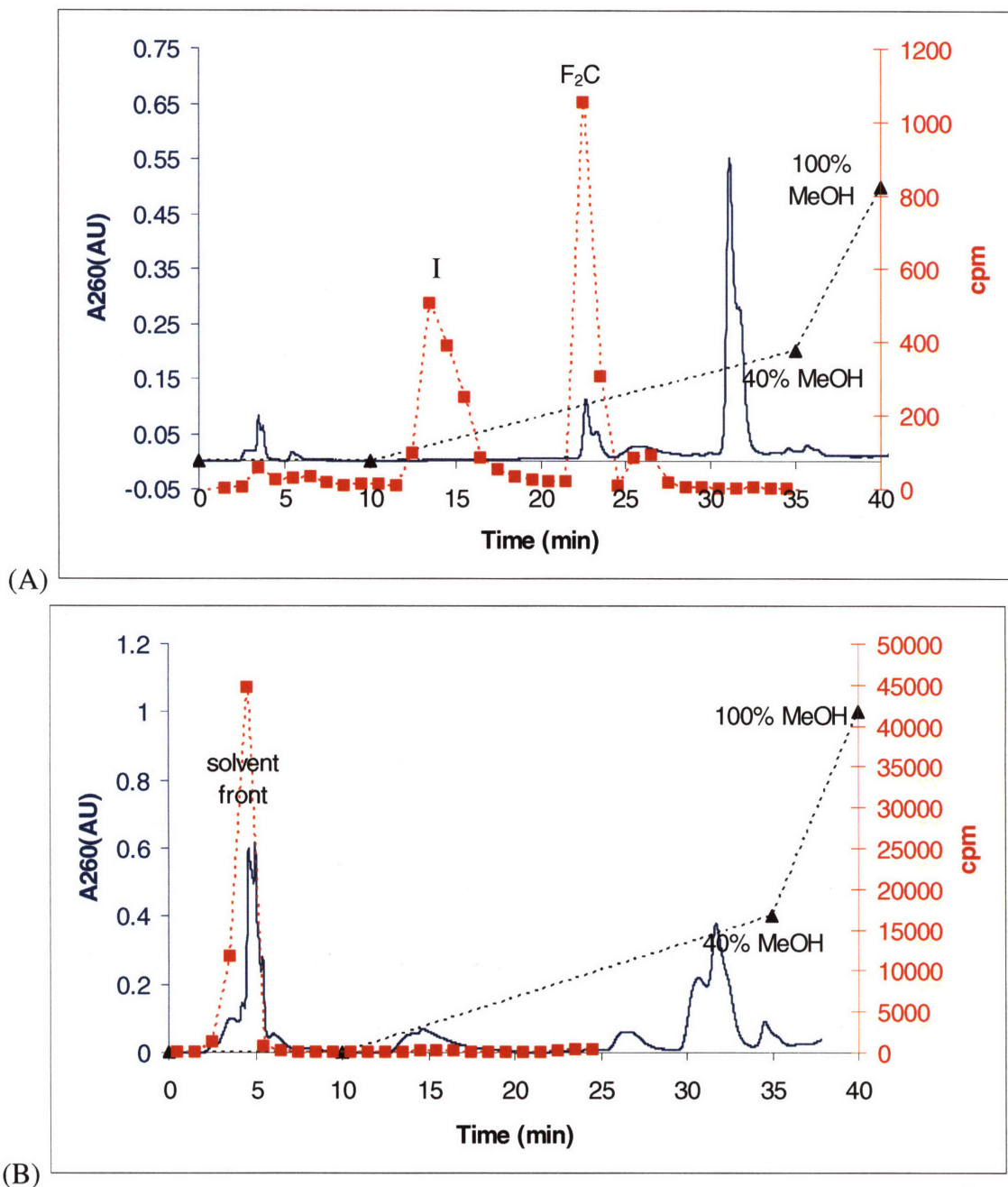
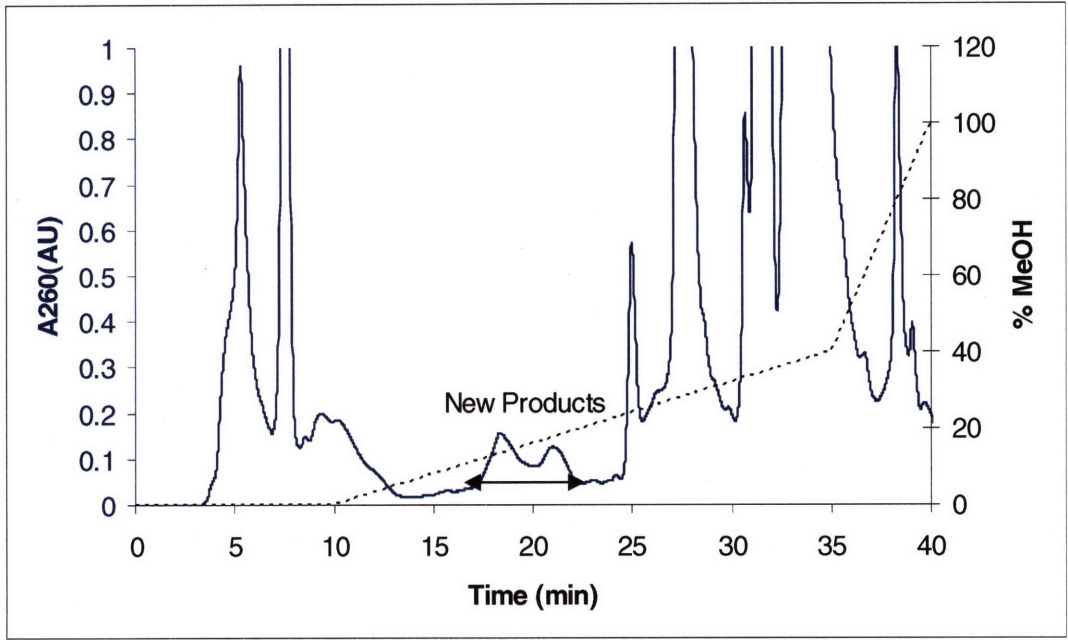


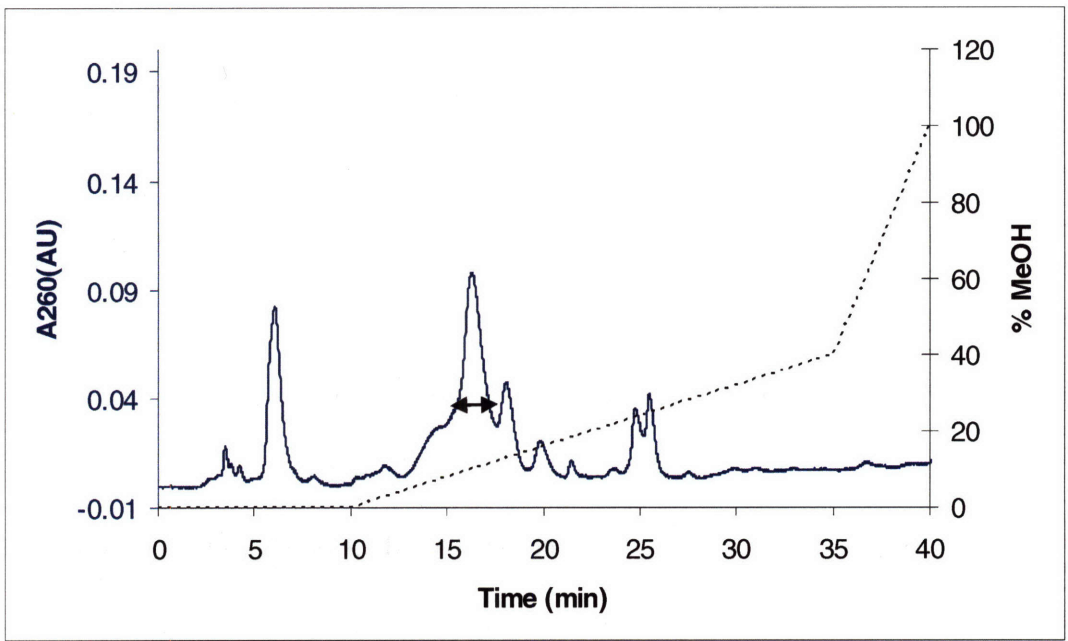
Figure 6-9. (A) Reverse-phase HPLC of small molecule products from RTPR inactivated with 1'-[³H]-F₂CTP treated with NaBH₄, and dephosphorylated with alkaline phosphatase, absorbance (—), cpm (■). Gradient (·····) Buffer A, 10 mM NH₄OAc, pH 6.8; Buffer B: 100% methanol, 100% A for 10 min, followed by a linear gradient to 40% B over 25 min, then to 100% B over 5 min. The new peak (I) represents 0.28 equiv. of ribose, and 0.25 equiv. of F₂C seen. (B) Reverse-phase HPLC of small molecule products from RTPR inactivated with 1'-[³H]-F₂CTP in the presence of DTT, treated with NaBH₄, and dephosphorylated with alkaline phosphatase, purified under the same conditions. All radioactivity eluted in the solvent front.

To identify the new products generated during the inactivation, the reaction was run on a large scale with unlabeled F₂CTP, and the new products isolated and characterized. The

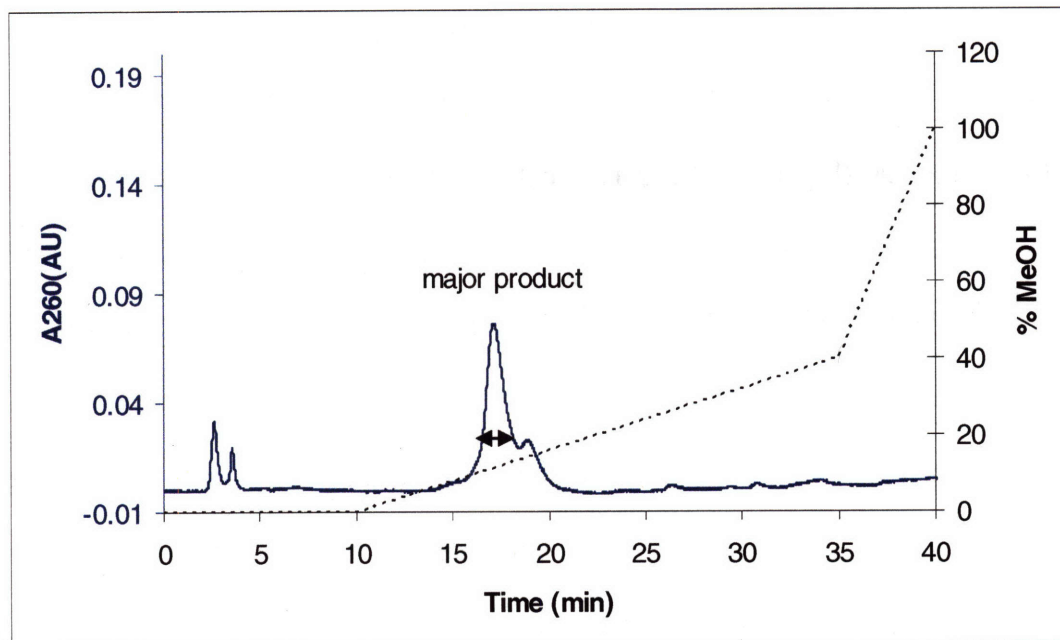
products were identified by their retention time and the similarity of their UV-vis spectrum to cytosine using a diode-array equipped HPLC. In the chromatogram of the initial purification, (Figure 6-10 A), several peaks eluted from 17-22 min, slightly later than the radioactive region seen in Figure 6-9 A. This effect is likely due to overloading of the column used for the purification (the same column was used for both scales) and the larger injection loop used (2 mL in this case vs. 200 μ L in the previous case) with the same flow rate. Examination of the peaks eluting between 17 min and 22 min showed that they possessed a UV-vis spectra consistent with cytosine, and contained ~ 0.25 equiv. of the F₂CTP in the initial reaction mixture quantified by A270. This is very similar to the equiv. calculated by radioactivity in the previous set of experiments. The initial repurification of this region (Figure 6-10 B) shows a sharpening of the peaks, an apparent decrease in the later-eluting peak, and a number of other contaminants, suggesting decomposition or the presence of multiple isomers of the product. It is suspected that the reason this initial peak was so broad is that borate esters are formed during the treatment with NaBH₄, and that these do not completely hydrolyze during workup, but decompose over the course of repurification and lyophilization in the presence of the NH₄OAc buffer after each isolation. Later attempts to isolate the second peak in the initial quench failed, and this peak appeared to decompose primarily to a species which matched the first eluting peak, supporting this hypothesis. Further, the reduction with NaBH₄ of ketone species may well result in more than one isomer, which may also explain the multiple peaks seen; only the major isomer was characterized.



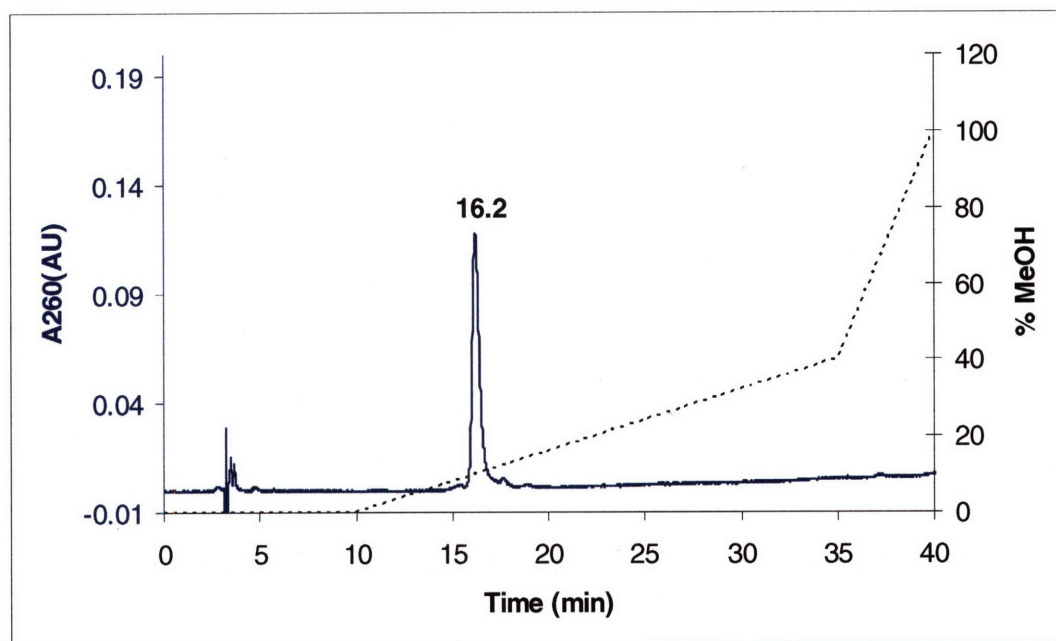
(A)



(B)



(C)



(D)

Figure 6-10. Reverse-phase HPLC of small molecule products from RTPR inactivated with F_2CTP treated with $NaBH_4$, and dephosphorylated with alkaline phosphatase. Absorbance (—), gradient (·····) Buffer A, 10 mM NH_4OAc , pH 6.8; Buffer B: 100% methanol, 100% A until 10 min, then a linear gradient to 40% B over 25 min, then to 100% B over 5 min. The double headed arrow indicates the region pooled in each step. (A) Initial purification: the material eluting from 17-22 min was collected. These products elute later than in the repurifications due primarily to the use of a larger injection loop. (B) Repurification of this region; in this and subsequent steps the elution program was identical, but Buffer A was changed to 1 mM NH_4OAc , pH 6.8. The major peak has sharpened, and was collected directly (15.5-17 min). (C) Final repurification of this region; only the major product was collected. This material was characterized after this purification. (D) Elution of the purified product, retention time of 16.2 min.

The major peak was collected, representing approximately half of the total material, and purified again using the same gradient, but with the concentration of NH_4OAc in Buffer A reduced to 1 mM (pH 6.8) (Figure 6-10 C). The center of the major peak was collected from this purification to ensure only a single isomer was isolated. The product now eluted as one peak by HPLC (Figure 6-10 D) and was of sufficient purity for characterization by NMR spectroscopy (Figure 6-11 A, Figure 6-12 A, and Figure 6-13 A; a peak list and coupling constants can be found in the experimental section). The product displays a spectrum consistent with that of a cytidine nucleotide (*ara-C* is shown for comparison, Figure 6-11 C). The use of gCOSY allowed confirmation of connectivity (full spectra can be found in Appendix 2), and ESI MS confirmed the mass is consistent with an isomer of cytidine. An expansion of the sugar ring region (Figure 6-12) shows the chemical shifts and splitting patterns are similar, but not identical to, *ara-C* (or cytidine, not shown). The compound has a different retention time from cytidine (12.6 min) or *ara-C* (17.4 min). These results suggest that the nucleoside is an isomer of cytidine differing in stereochemistry at one or more carbons. The major isomer formed is likely a consequence of NaBH_4 reduction of the precursor. The trapped nucleoside lead to the surprising conclusion that not only had both fluorines been eliminated from the F_2CTP , but that an oxygen had been *added*, proposed to occur through the addition of water to an intermediate radical (Figure 6-4).

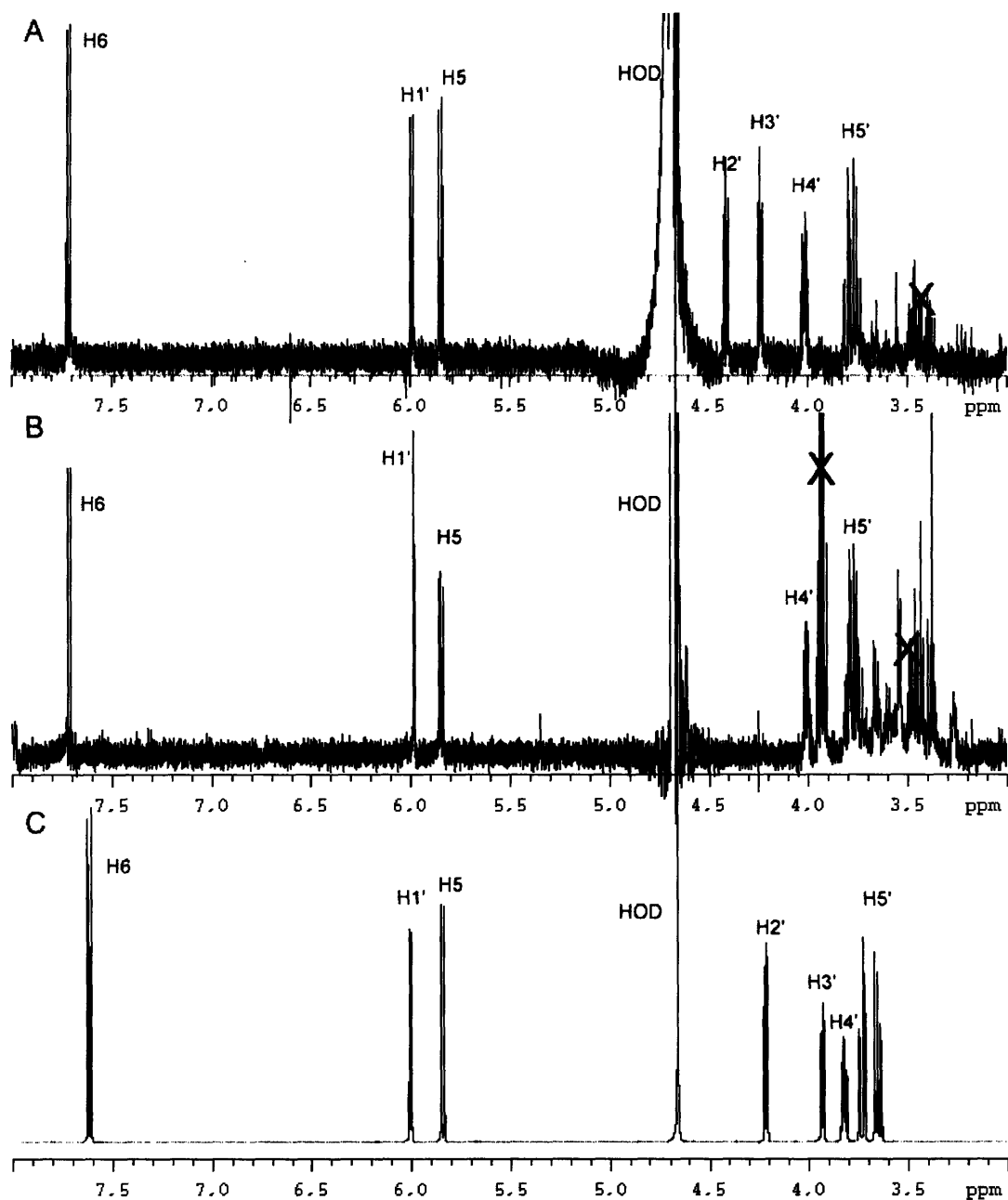


Figure 6-11. Comparison of $^1\text{H-NMR}$ (500 MHz, D_2O) spectra of new products isolated from NaBH_4 quench of RTRP inactivated with F_2CTP . (A) New product resulting from NaBH_4 quench; (B) new product resulting from NaBD_4 quench; (C) *ara-C* for comparison. The nucleoside proton resonances are labeled. In B and C, several impurity peaks can be seen; these are marked with X. In the spectrum for the NaBD_4 quenched material, it is clear that $\text{H1}'$ has collapsed to a singlet, $\text{H2}'$ and $\text{H3}'$ have disappeared. An expansion of the sugar region is found in Figure 6-12, and the downfield region in Figure 6-13.

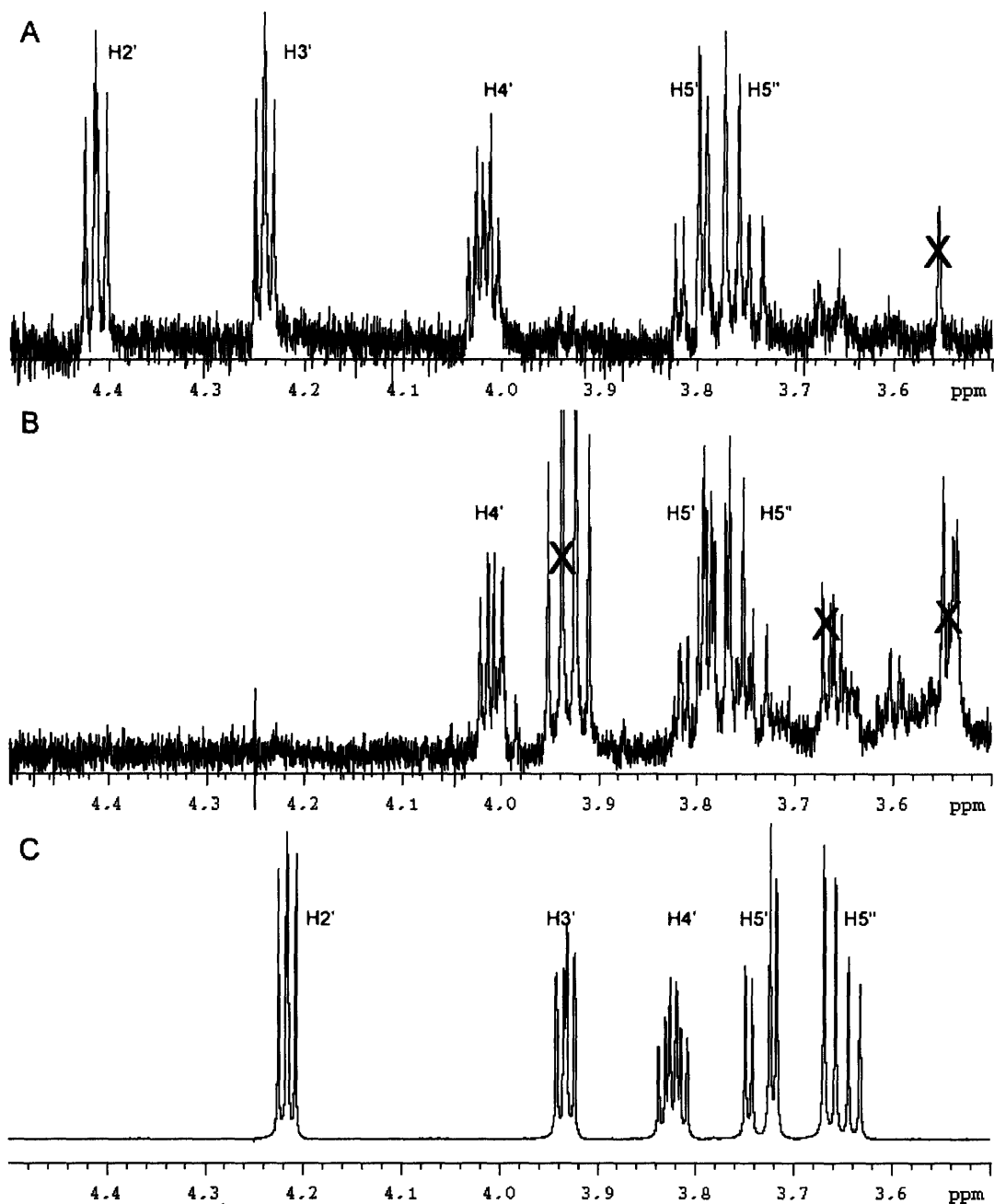


Figure 6-12. Comparison of ¹H-NMR (500 MHz, D₂O) spectra of new products isolated from NaBH₄ quench of RTRP inactivated with F₂CTP. (A) New product resulting from NaBH₄ quench; (B) new product resulting from NaBD₄ quench; (C) *ara*-C. Expansion of the region corresponding to 2', 3', 4' and 5' ribose ring protons. In B, signals from H2' and H3' are not visible, and H4' has simplified to a dd from a ddd in B. This indicates nearly complete [²H] incorporation at these positions. Several buffer-derived impurities are visible in C, marked with an X.

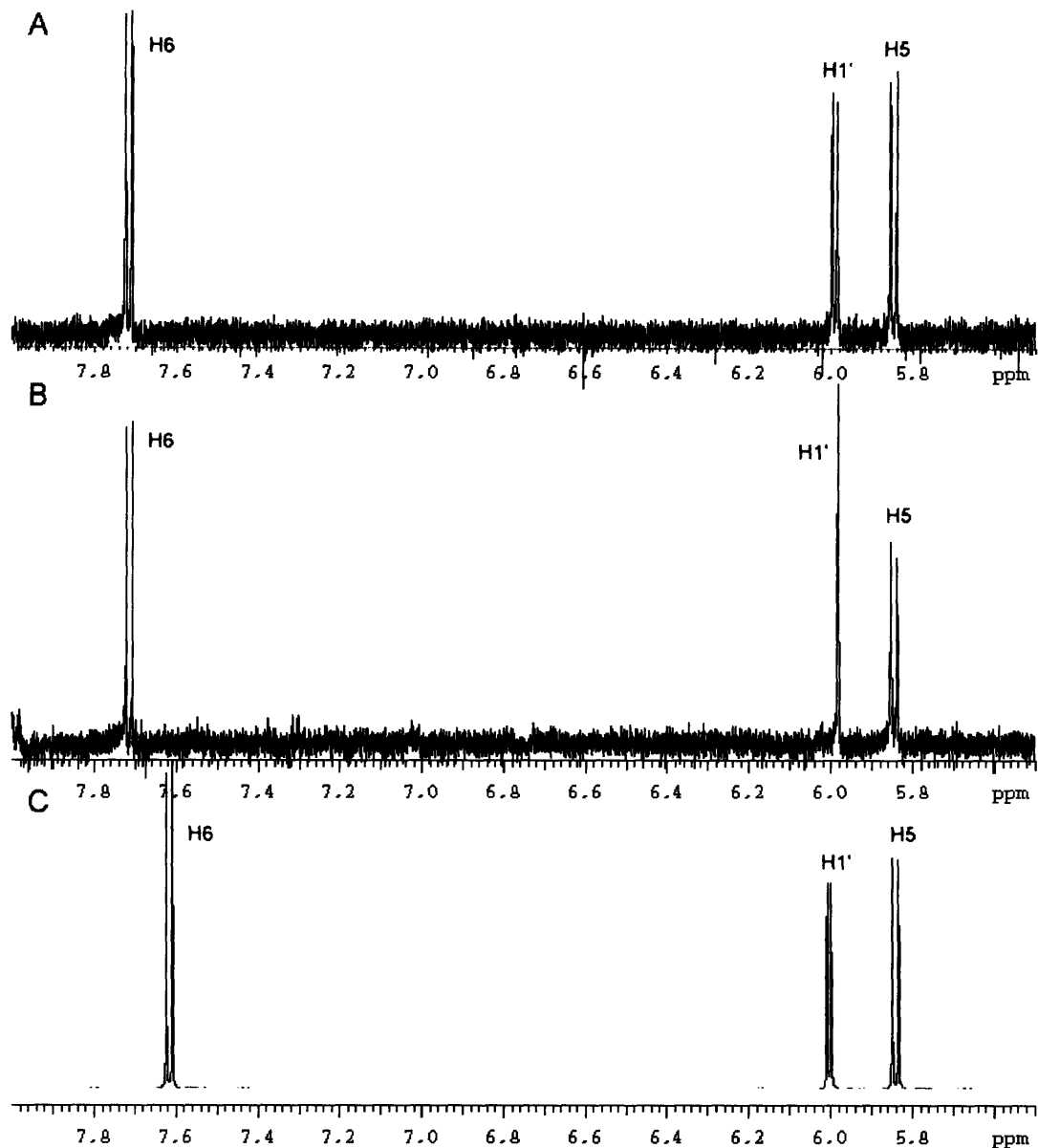
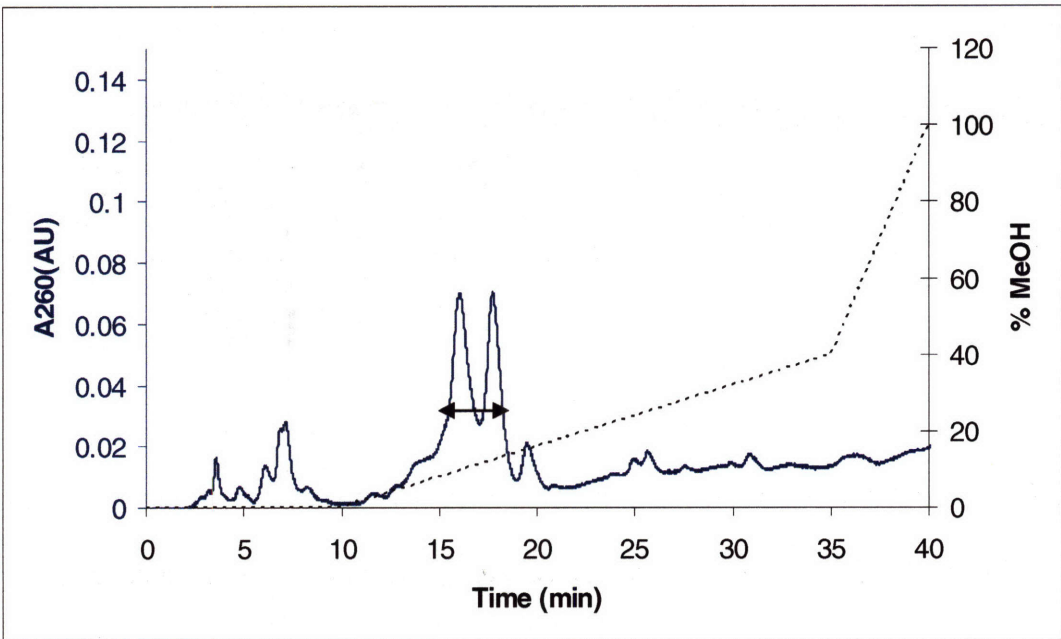
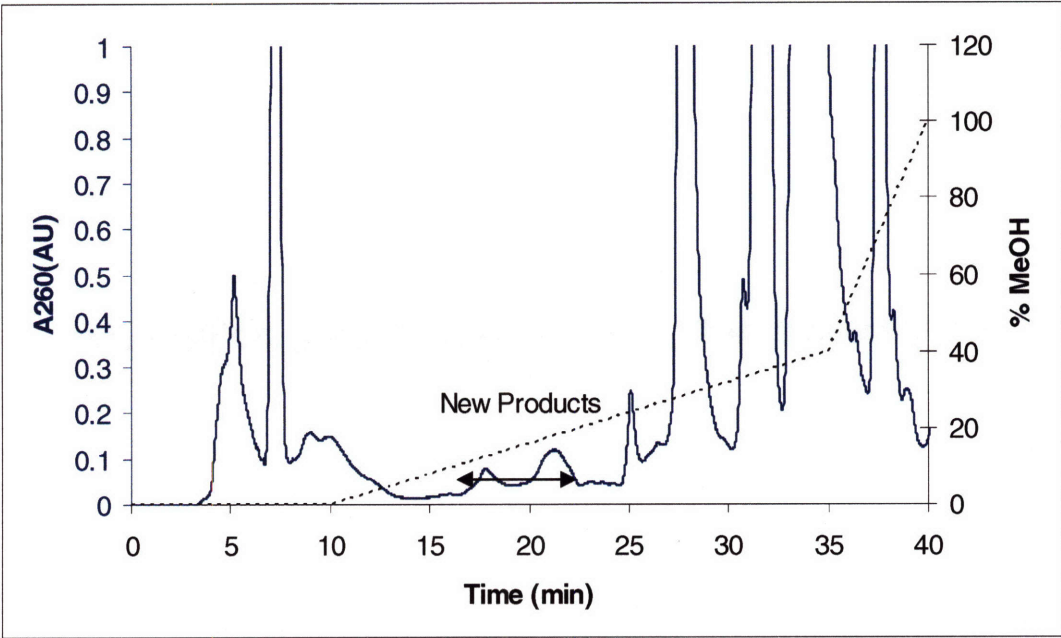


Figure 6-13. Comparison of ^1H -NMR (500 MHz, D_2O) spectra of new products isolated from NaBH_4 quench of RTRP inactivated with F_2CTP . (A) New product resulting from NaBH_4 quench; (B) new product resulting from NaBD_4 quench; (C) *ara-C*. Expansion of the region corresponding to 1' ribose ring proton and cytosine base protons. In B, the signal from $\text{H1}'$ has collapsed to a singlet.



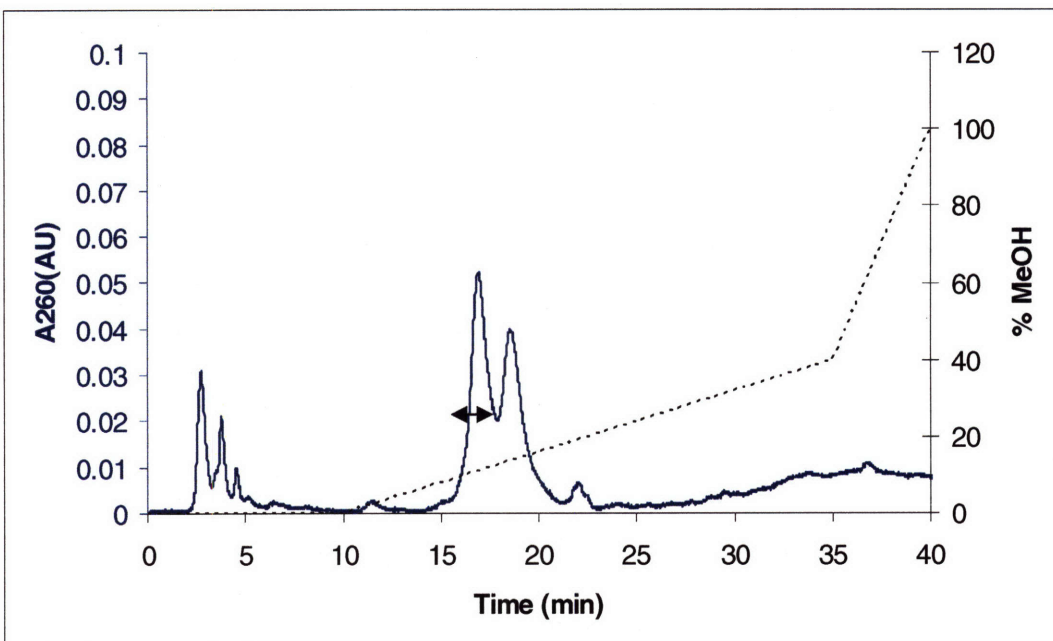


Figure 6-14. Reverse-phase HPLC of small molecule products from RTPR inactivated with F₂CTP treated with NaBD₄, and dephosphorylated with alkaline phosphatase. Absorbance (—), gradient (·····) Buffer A, 10 mM NH₄OAc, pH 6.8; Buffer B: 100% methanol, 100% A until 10 min, then a linear gradient to 40% B over 25 min, then to 100% B over 5 min. The double headed arrow indicates the region pooled in each step. (A) Initial purification: the material eluting from 17-22 min was collected. These products elute later than in the repurifications due primarily to the use of a larger injection loop. (B) Repurification of this region; in this and subsequent steps the elution program was identical, but Buffer A was changed to 1 mM NH₄OAc, pH 6.8. Two major peaks were seen, and collected directly based on absorbance (15.5-18 min). (C) Final repurification of this region; only the first product, which co-elutes with the material characterized in the NaBH₄ quench was collected. This material was characterized after this purification. Attempts to purify the second peak failed; it appeared to decompose into the first peak + minor contaminants with each attempted purification (data not shown).

To gain information on the precursor to this isolated structure, the inactivation was repeated, using NaBD₄ in place of NaBH₄. The same peak was isolated from this inactivation as in the previous experiment (Figure 6-14), and characterized by NMR. In this case an enhanced amount of one of the later running peaks was seen in the repurification; only the peak with the same retention time as the major peak in the first inactivation was purified for characterization. Later attempts to purify the second major peak found that the amount of this peak present varied from inactivation to inactivation, and seemed to decompose with each successive purification, primarily into the peak eluting at 16.2 minutes. The ¹H-NMR of the isolated species can be found in Figure 6-11 B, Figure 6-12 B, and Figure 6-13 B. Based on the model (Figure 6-4) and

precedent from the 2'-halo-2'-deoxynucleotides, a keto radical precursor would be expected to first be reduced by a hydrogen atom abstraction, and a single ketone would be reduced by NaBH₄, with the deuterium incorporation into the 3' position. Alternatively, the precursor radical proposed (Figure 6-4) might rearrange to the corresponding 2'-keto, 3' radical through a semidione intermediate (Figure 6-15). This isomerization would give rise to partial deuterium incorporation at C2' and C3' subsequent to initial reduction by hydrogen atom abstraction to generate the 2'- and 3'-keto sugars. Thus, the results of our spectroscopic analysis revealed another surprise, >99% [²H] incorporation was observed at both the 2' and 3' positions (Figure 6-11 B and Figure 6-12 B). In the compound resulting from trapping with NaBD₄, the chemical shifts are the same as in the NaBH₄ trapped material. However, the signals for the 2' and 3' hydrogens are absent, the signal for 1' has collapsed to a singlet, and the signal for the 4' to a dd.

This result suggests the direct precursor to reduction was not a monoketonucleotide as expected, but the 2',3'-diketonucleotide. This diketone would be unable to eliminate cytosine, which was detected and quantified as described in the previous section, providing insight into the timing of formation of this precursor. In the cytosine quantification experiments, it was found that after dephosphorylation of the product mixtures, the only cytosine-containing compounds were free cytosine and unreacted F₂C. The proposed stable radical intermediate radical (**6-10**, Figure 6-4) would be expected to be reduced by hydrogen atom transfer at long time scales, allowing elimination of the cytosine. If this radical is the precursor to the trapped nucleoside, however, it must be being oxidized under the NaBH₄ quench conditions.

A model for the observed deuterium incorporation during borohydride quenching is illustrated in Figure 6-15. Initial deprotonation of the hydroxyketone radical (**6-11**) would generate a semidione radical anion (**6-12**).⁽¹³⁰⁾ This compound might undergo reduction by

hydride transfer from NaBH₄, giving rise to a ketone radical-anion (**6-13**). This compound is a potent reductant, which could lose an electron to oxygen, or other oxidant to generate a second ketone, which would be itself reduced by NaBH₄.(142) Reduction of this new ketone by NaBD₄ would give the observed atom incorporation (**6-14**). Unfortunately no data on the trapping of semidione radicals exists in the literature, so it is currently unknown if this trapping pattern is what would be expected for this type of precursor radical.

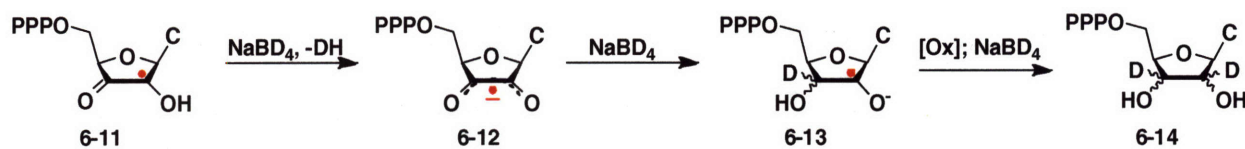


Figure 6-15. Deuterium incorporation at 2' and 3'. The proposed α -hydroxy keto radical is converted to a semidione radical anion by deprotonation. This species undergoes reduction by NaBH₄ to generate a ketone radical-anion, which loses an electron (potentially to oxygen) to form a second ketone. This ketone is in turn reduced by NaBH₄.

Identification and efforts to quantify cobalamin species accompanying F₂CTP inactivation of RTPR

Previous investigations showed that RTPR inactivation by F₂CTP was accompanied by the release of 0.84 equiv. of 5'-dA and the formation of a cobalamin species covalently linked to RTPR.(69) The UV-vis spectra of this species resembled the spectrum of glutathionyl cobalamin (GSCbl). Evidence from peptide digests and mass spectrometry indicated that this species was bound to C419 (one of the active site reducing equivalents) through a Co-S bond. Stopped-flow UV-vis spectroscopy at 525 nm of the inactivation on the ms time scale indicated the disappearance of 0.6-0.7 equiv. of cob(III)alamin, presumed to form a cob(II)alamin species. RFQ EPR experiments on the 22-250 ms timescale indicated the presence of a cob(II)alamin-thiyl radical coupled species which is converted to a cob(II)alamin-nucleotide radical coupled species. The cob(II)alamin precursor was hypothesized to react with a thiyl radical on RTPR (or a cob(III) species with a thiolate) to form the S-Co (III) species observed on the minute

timescale, determined to be to C419 by peptide mapping experiments. (69) To gain a better understanding of the partitioning between inactivation mechanisms and the relationship of the non-alkylative mechanism of inactivation to the formation of the Co-S bond to C419, the fate of AdoCbl was investigated.

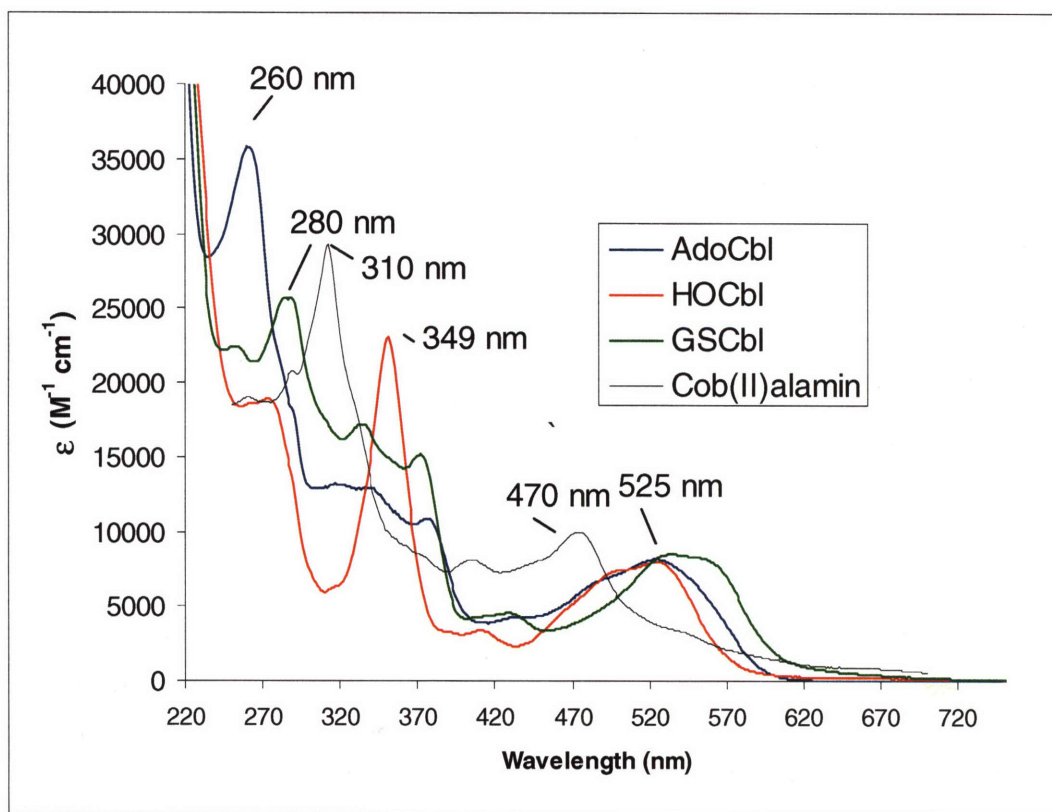


Figure 6-16. Standards of cobalamin compounds recorded at 25 μM . The spectrum of cob(II)alamin is at 21.5 μM and was recorded by J. Robblee.

In order to quantify the amount of cobalamin-protein adduct formed and determine the identity of the cobalamin products remaining in solution, several inactivations were carried out and the products analyzed by SEC. Inactivations were run with a 1:1:1 ratio of AdoCbl, RTPR, and F₂CTP and the products cobalamin bound to RTPR and remaining free in solution were characterized by UV-vis spectroscopy. The protein was separated from the small molecules by Sephadex G-50 chromatography in the dark and the protein-containing fractions combined and the UV-vis spectrum recorded. The combined protein-containing fractions were concentrated by

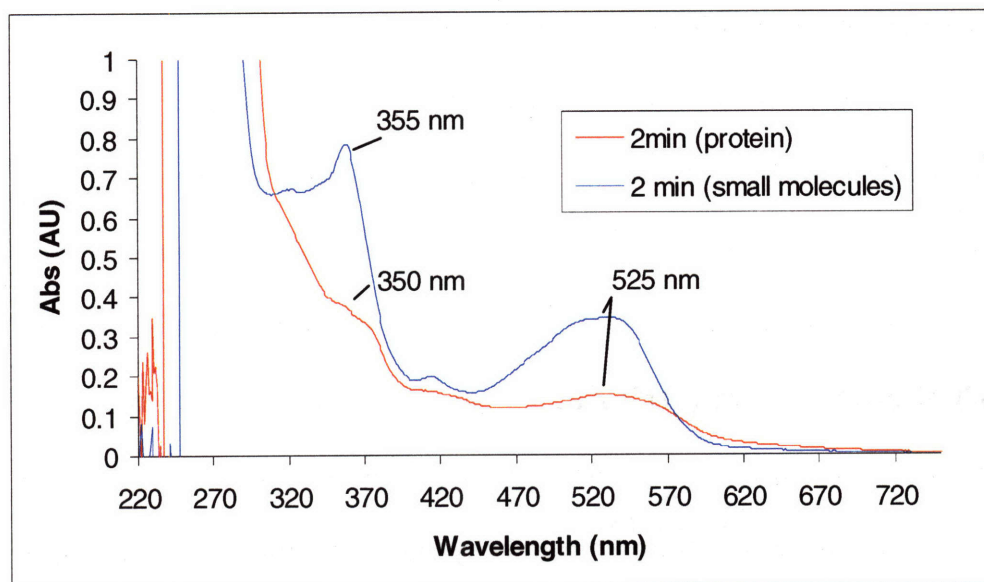
lyophilization in the dark (~16 h at room temperature), taken up in 0.5 mL water and the UV-vis spectrum recorded a second time. The small molecules-containing fractions were too dilute to observe a spectrum directly, so were simply combined and concentrated by lyophilization, then redissolved in 0.5 mL water and the UV-vis spectrum recorded. The experiments were run with inactivation endpoints of 2 min and 1 hr. This analysis was run once with 1'-[³H]-F₂CTP and once with 5-[³H]-F₂CTP, and the amount of alkylation by F₂CTP derived species and the amount of cytosine release also recorded; these values were consistent with the independent quantification experiments described above.

For quantification of the amounts of cobalamin species in solution, the products were assumed to be a mixture of AdoCbl, hydroxycobalamin (HOCbl) or other Co(III) species. No evidence of features associated with cob(II)alamin were observed in any of the described experiments timescale. The visible region of the Co(III) species associated with corrins are dominated by features related to the corrin ring.⁽¹⁴³⁾ Both AdoCbl and HOCbl possess an $\epsilon_{\max} = 8000 \text{ M}^{-1} \text{ cm}^{-1}$ in the red-visible region of the spectrum (523 nm), and this extinction coefficient was used to quantify the total amount of cobalamin. GSCbl is reported to possess an $\epsilon_{\max} = 8000 \text{ M}^{-1} \text{ cm}^{-1}$ at 525 nm,⁽⁶⁹⁾ and this extinction coefficient was used to quantify the protein-bound species, under the assumption that the cobalamin is bound to C419 as previously observed and thus has similar extinction coefficients.⁽⁶⁹⁾

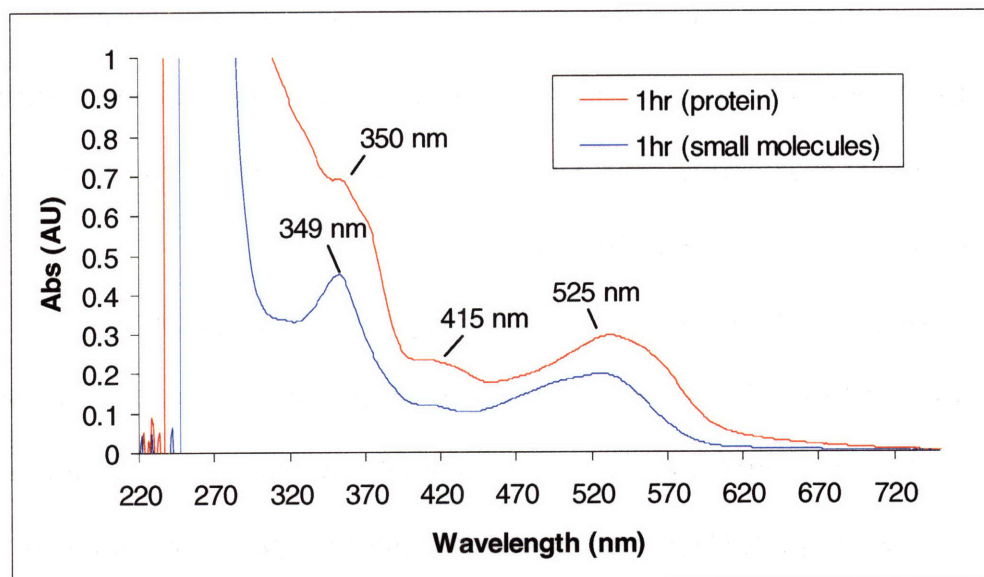
The UV-vis spectra of authentic AdoCbl, HOCbl, GSCbl and cob(II)alamin are shown in Figure 6-16.⁽¹⁴³⁾ All cob(III)alamin species possess features in the visible region (roughly 450 nm to 600 nm) which results from electronic and a series of C=C vibrational transitions in the corrin ring. Cob(III)alamins lacking a Co-C bond (such as HOCbl) also possess a sharp feature at 320-340 nm. AdoCbl itself has a strong absorbance feature at 260 nm from the adenosyl

moiety, but the transition that results in the intense near-UV species in HOCbl is distributed over a series of lower intensity transitions throughout the near UV.(143) GSCbl shows many features similar to AdoCbl, but is notably red shifted in the 450-600 nm feature, and has no absorption feature at 260 nm.

Figure 6-17 shows the UV-vis spectrum of the products of inactivation from SEC at 2 min (A) and 1 h (B), both protein-bound and in solution, recorded after lyophilization and resuspension. Using $\epsilon_{525\text{ nm}} = 8000\text{ M}^{-1}\text{cm}^{-1}$, 0.24 ± 0.3 equiv. were calculated to have co-eluted with RTPR at the 2 min time point, and 0.48 ± 0.03 equiv. for the 1 h time point (average of three experiments). The quantity of cob(III)alamin species remaining in solution at each time point (2 min and 1 hr) was also calculated, showing 0.65 ± 0.1 equiv. at 2 min, and 0.45 ± 0.1 equiv. at 1 h (average of three experiments). The total recovery of B₁₂ species was 85-95%, with the greatest variability seen in the solution phase products. The values of corrin coeluting with the protein were also determined for the spectra recorded before lyophilization (Figure 6-18 A). The 2 min RTPR was in a total volume of 3 mL, and showed 0.23 equiv. of cob(III)alamin with a A525/A280 of 0.021. The 1 h RTPR was in a total volume of 2 mL, showed 0.46 equiv. of cob(III)alamin and possessed an A525/A280 of 0.040. Assuming the A280 is due mostly to the RTPR ($\epsilon_{525\text{ nm}} = 101,000\text{ M}^{-1}\text{cm}^{-1}$) and A525 is due to the cobalamin species, RTPR that is labeled with 1 equiv. of the corrin would have an A525/A280 of ~0.08. In previous studies, it was reported that the RTPR isolated had an A525/A280 of 0.08, indicating nearly stoichiometric labeling.(69) It is not clear why the stoichiometry measured in these experiments is lower. The original study was run in degassed buffers, and used 2 equiv. of AdoCbl, while this study used 1 equiv. and was not degassed. A repeat run with degassed buffers gave nearly identical results (0.26 equiv. cobalamin species, 0.4 equiv. sugar ring coeluting with the protein at 2 min).



(A)



(B)

Figure 6-17. UV-vis spectra of peptide-bound (red line) and solution phase (blue line) products of inactivation of RTPR by F₂CTP in the presence of 1 equiv. of AdoCbl. (A) quench at 2 min. (B) quench at 1 h.

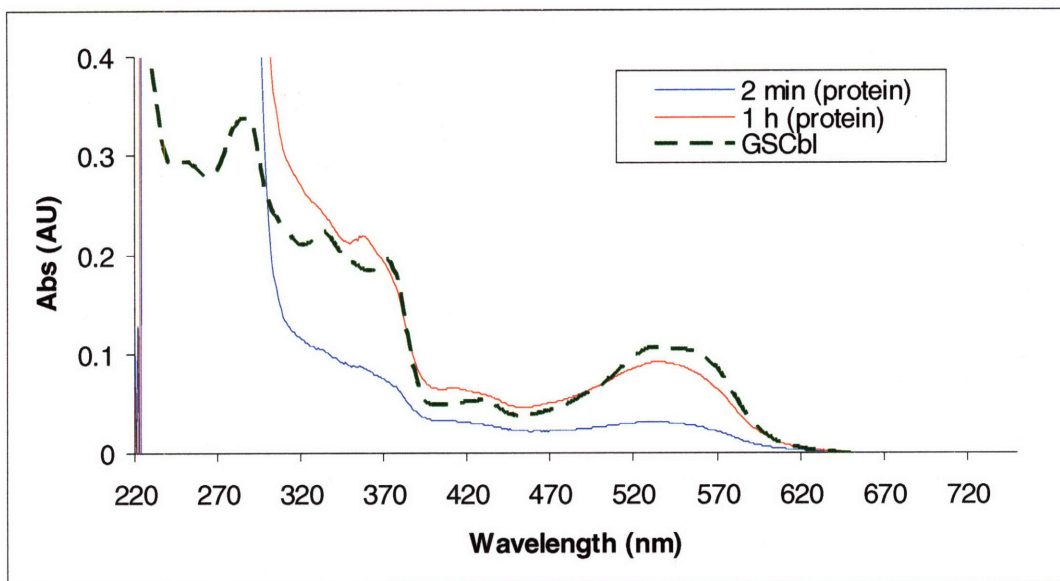
In both cases, the protein-bound species at 1 h resembled the GSCbl spectrum (Figure 6-18 A), though less so after lyophilization (Figure 6-18 B).⁽⁶⁹⁾ In the latter case, there are some differences in the ratios of the features, which may be due to absorption caused by protein that did not fully redissolve, or may be a cobalamin species which has cleaved from the protein during the lyophilization period (~16 h). Substantially more of this product is seen at 1 h than at 2 min, suggesting the covalent modification is occurring on a slow (minute) timescale, and

continues after inactivation is completed. Additionally, the product formed rapidly (by 2 minutes) is notably different from the GSCbl spectrum and the slow-forming product, lacking the feature at 350 nm and with an equal ratio between the 525 nm and 420 nm feature.

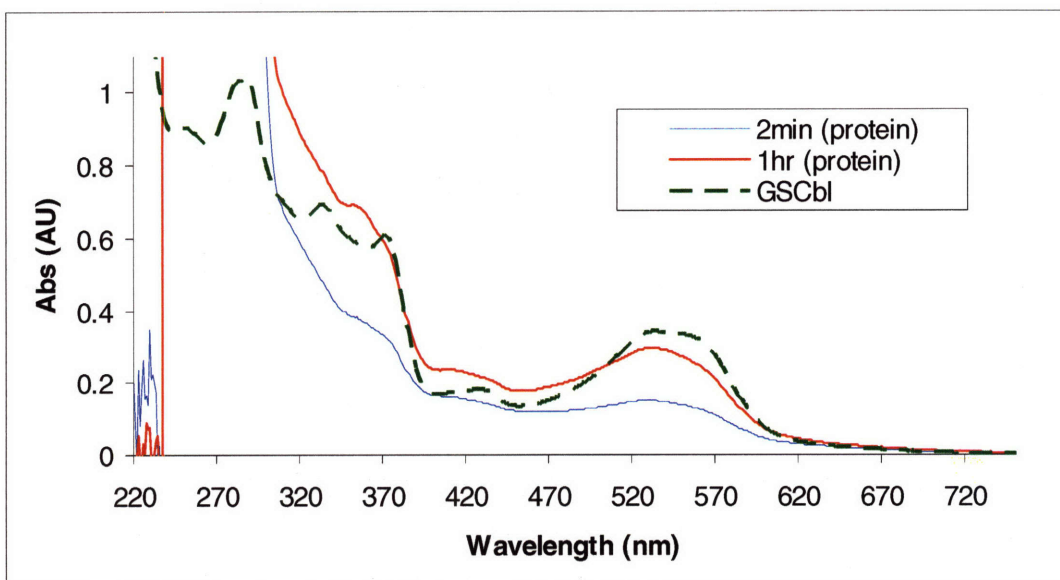
The spectra of the small molecule fraction products is markedly different between the two time points (Figure 6-17). Analysis of these spectra by subtracting linear combinations of the spectra of HOCbl and AdoCbl was performed, and showed an intriguing difference between the time points (Figure 6-19). The features in the spectrum of the small molecules fractions at 1 h (Figure 6-19 A) can be accounted for almost entirely by the combination of AdoCbl and HOCbl. Mixing the standard spectra of these compounds in a 1:1 proportion and scaling appropriately reproduces all the key features of this spectrum. Subtraction of this combination eliminates most absorption in the visible range. It is unclear if the residual features are related to another species, or simply result from imperfect subtraction.

The spectrum at 2 min (Figure 6-19 B) cannot be reproduced by the addition of the HOCbl or AdoCbl spectra in any proportion tried, and it appears that a third species is present. The small molecules fraction contained 0.6 equiv. of cob(III)alamin compounds at 2 min, and 0.4 equiv. at 1 h. The difference between these values is close to the observed increase in protein modification (0.25 equiv. of cob(III)alamin at 2 min, 0.5 equiv. at 1 hr), and thus may represent a third species which reacts during this period to form the Co-S bond. The subtraction of a 1:1 combination of HOCbl and AdoCbl scaled to 0.4 equiv. of cob(III)alamin species from the spectrum thus reveals the spectrum of the third component that makes up the difference (Figure 6-19 B, subtraction). A remarkably similar spectrum can also be produced by directly subtracting the spectrum of the small molecules fraction at 1 h from the spectrum at 2 min (Figure 6-20). Without knowing the identity of the third species present, it is impossible to

conclusively determine the relative proportions; the 1:1 ratio of AdoCbl to HOCbl represents a best approximation based on the appearance of the spectrum revealed by the subtraction. Since no combination could completely reproduce the spectrum, the combination which produced a cobalamin-type spectrum was chosen. The use of this specific combination was also chosen based on the presence of these species at 1 h, and the assumption that the unreacted AdoCbl should be present at the same proportion at 2 min.

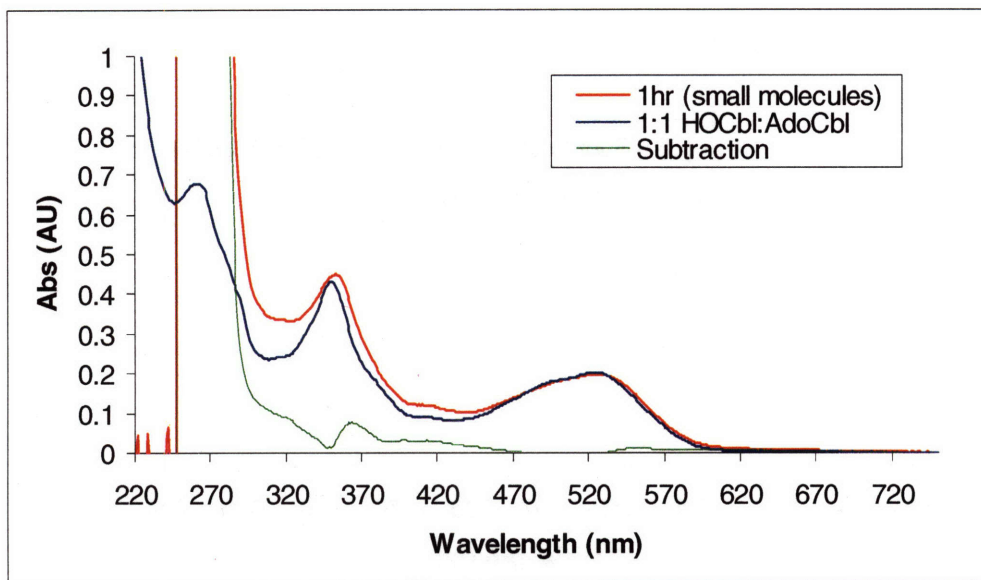


(A)

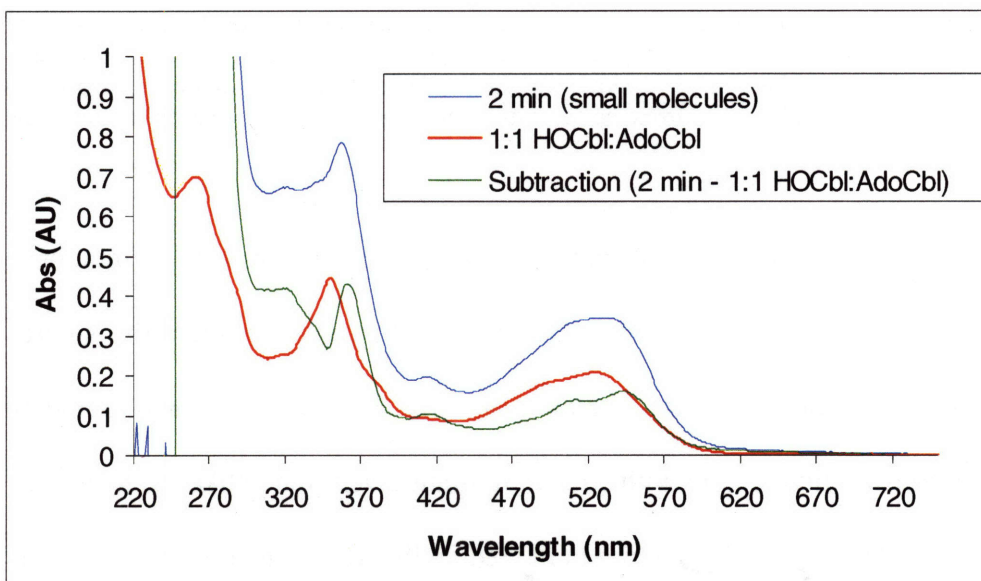


(B)

Figure 6-18. UV-vis spectra of peptide bound products at 2 min (blue line) and 1 h (red line). The spectra of GSCbl is shown for comparison (green line). (A) Spectra recorded directly off the SEC columns. The material at 2 min was in a total volume of 3 mL, and the material at 1 h was in a total volume of 2 mL. Found 0.23 equiv. cobalamin eluting with the protein at 2 min, 0.45 equiv. at 1 h, with A530/A280 ratios of 0.021 and 0.04 respectively. (B) Spectra recorded after lyophilization to dryness in the dark, followed by resuspension in 0.5 mL water. Found 0.25 equiv. cobalamin eluting with the protein at 2 min, 0.5 equiv. at 1 h.



(A)



(B)

Figure 6-19. UV-vis spectra of small molecules fraction from SEC of inactivation experiments. (A) Spectra of products at 1 h (red line) compared to the scaled spectra of HOCbl and AdoCbl standards, combined in a 1:1 proportion. The subtraction (green line) shows almost complete elimination of features in the visible region, leaving only a strong back absorption due to high salt concentrations. (B) Similar comparison of the solution- products at 2 min (blue line) to a standard spectrum of HOCbl and AdoCbl (red line). No linear combination of these two standards can eliminate the features in the visible region, and the subtraction (green line) indicates the presence of a third species.

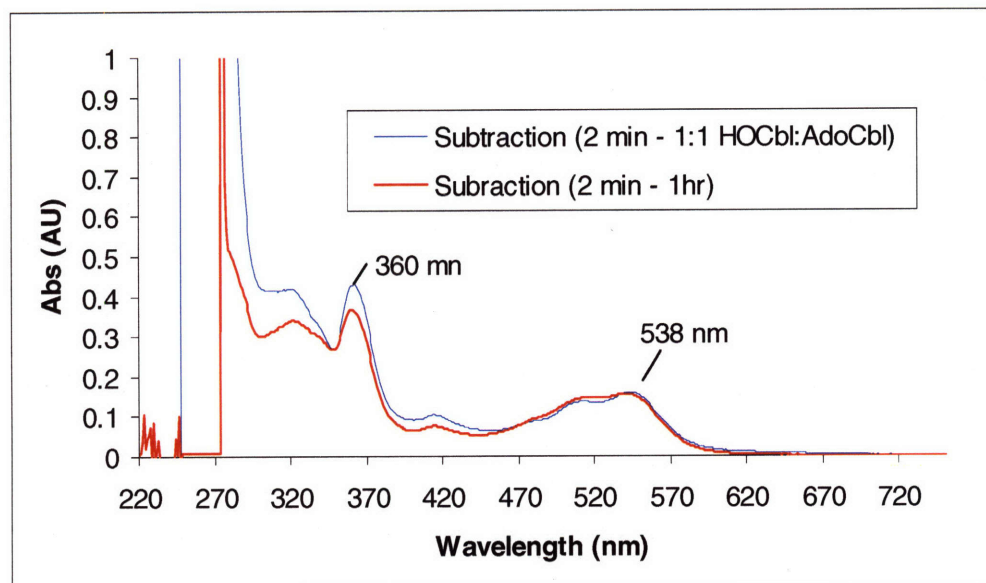


Figure 6-20. Comparison of subtraction spectra obtained from solution phase products of RTPR inactivation by F_2CTP in the presence of 1 equiv. of AdoCbl. The spectra of the small molecules fraction at 2 min minus the spectrum at 1 h (red line) reveals a third species. A similar spectrum can be obtained by subtracting appropriately scaled standard spectra of HOCbl and AdoCbl from the spectrum of the small molecule products at 2 min (blue line).

This spectrum represents a third cobalamin species present in solution at 2 min, but which has been consumed by 1 hr, presumably through covalent modification of the RTPR. This new spectrum closely resembles a Co(III) cobalamin species. The spectra in the 450-550 nm range shows a broad absorption feature with a local minimum, very much like the feature of HOCbl (Figure 6-16). The λ_{max} in this feature in the red-visible region is red shifted ~ 15 nm relative to HOCbl. There is also a distinct peak at 360 nm, again similar to HOCbl but red shifted ~ 10 nm, and not as sharp. This third species may represent a decomposition product (over the 16 h lyophilization period) of the precursor species that would normally react to form the Co-S bond to C419. This hypothesis would explain the disappearance of this species as the extent of alkylation increases. A Co(II) species may not be stable once separated from the protein by the SEC, and over the time scale of this experiment (30 min for the G-50 Sephadex

column, followed by ~16h of lyophilization) could well result in its oxidation to the observed species. The identity of this third species is unknown.

The analysis suggested that the small molecules fractions contained 0.2 equiv. of AdoCbl and 0.2 equiv. of HOCbl at the long timescale (1 h). At a shorter time point (2 min) the small molecules fraction contained ~0.2 equiv. of a third, unknown species in addition to 0.2 equiv. of AdoCbl and 0.2 equiv. of HOCbl. The amount of unreacted AdoCbl observed (0.2 equiv.) is consistent with earlier studies, which showed the release of 0.84 equiv. of 5'-dA when RTPR was inactivated with 1 equiv. F₂CTP in the presence of 1 equiv. of AdoCbl.(69) The direct analysis of the specific species present at 2 min and 1 h may bear further investigation. It is also unclear why this study showed only partial modification by cobalamin when the previous study suggested the RTPR was stoichiometrically modified.(69)

Summary of Inactivation Stoichiometry

The inactivation has been investigated with 1 equiv. RTPR and 1 equiv. F₂CTP with and without the use of a NaBH₄ quench at two minutes. A summary of the products characterized in each case, determined by use of 5-[³H]-F₂CTP and 1'-[³H]-F₂CTP, is outlined in Figure 6-21. In the absence of a NaBH₄ quench (Figure 6-21 A), 0.47 equiv. sugar, 0.16 equiv. of a nucleoside with cytosine attached, and 0.25 equiv. cobalamin are found coeluting with the protein after SEC. HPLC analysis after filtration, but before dephosphorylation, showed 0.6 equiv. of cytosine and 0.23 equiv. of an unknown phosphorylated sugar product. HPLC after dephosphorylation found 0.7 equiv. cytosine and 0.15-0.2 equiv. unreacted F₂C. When a NaBH₄ quench was employed at 2 min, (Figure 6-21 B) 0.33 equiv. of sugar and 0.03 equiv. of a nucleoside with cytosine attached were found coeluting with the protein. After

dephosphorylation, HPLC analysis showed 0.55 equiv. cytosine, 0.2-0.25 equiv F₂C, and 0.25 equiv. of a new nucleoside product.

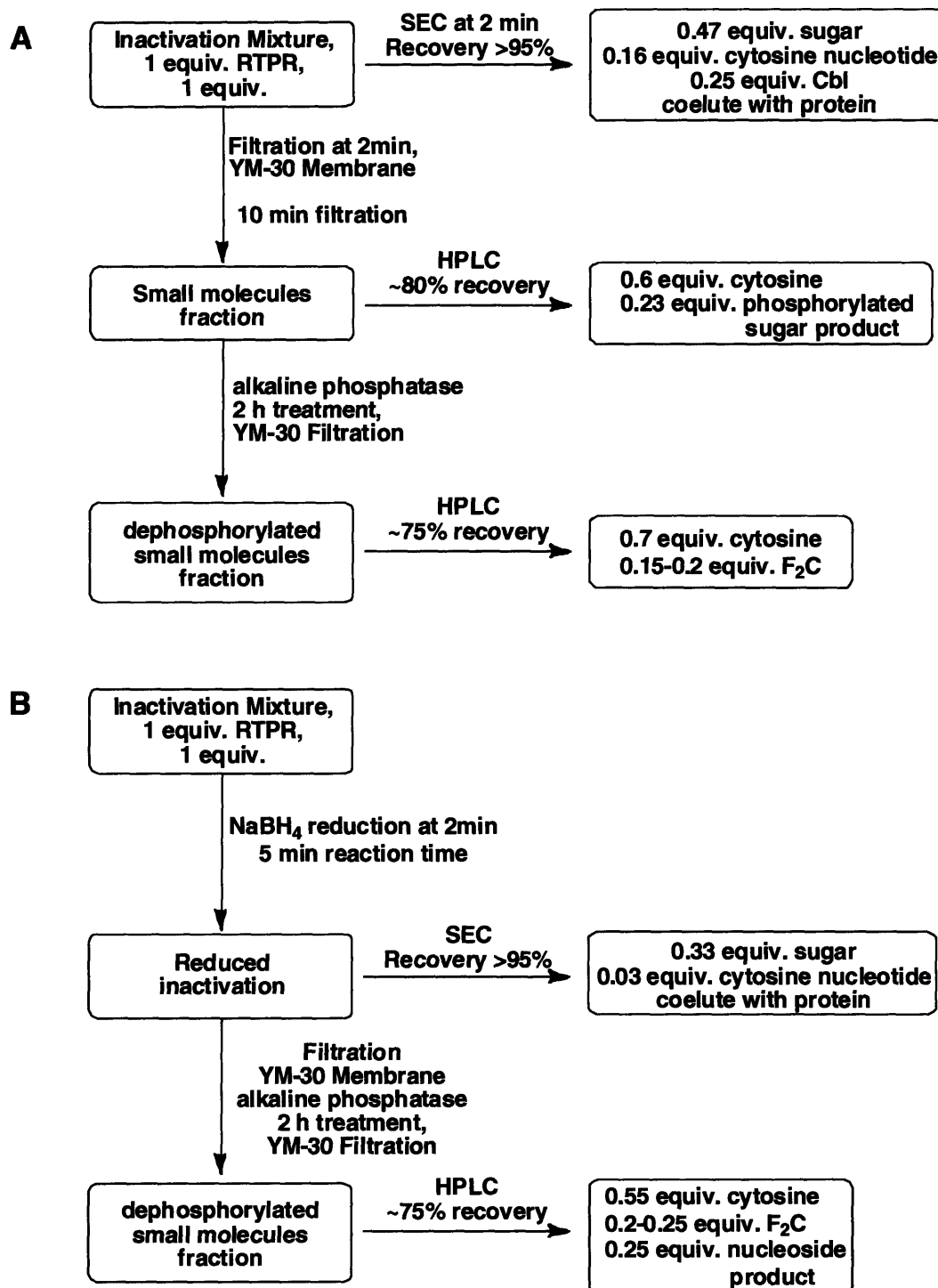


Figure 6-21. Summary of inactivation stoichiometry and recoveries with no quench (A) and with a NaBH₄ quench at 2 min (B). In all cases, the equiv. reported are adjusted for recovery.

Attempts to identify peptides of RTPR labeled during its inactivation with F₂CTP

The small molecule products of inactivation now characterized, our attention turned to the identification of peptide-bound fragments derived from the ribose ring of F₂CTP, and identification of the sites of labeling. To first test the stability of the sugar attached to RTPR, RTPR was inactivated with 1'-[³H]-F₂CTP and analyzed under conditions required for trypsin digestion of RTPR. The labeled RTPR was dialyzed against 0.1 M NH₄HCO₃, pH 8.2 with and without 2 M urea, typical conditions for trypsin digestion. A similar experiment was carried out in 160 mM KPi, pH 5.6, 2M urea, conditions used for digestion with endoproteinase C in a previous study.(69) The dialysis was carried out at 4°C over 20h, and aliquots were examined for the amount of radioactivity remaining inside the membrane. While there was some loss of label (20-25% lost by 20 h), the rate was slow enough that labeled peptides could be isolated (Figure 6-22).

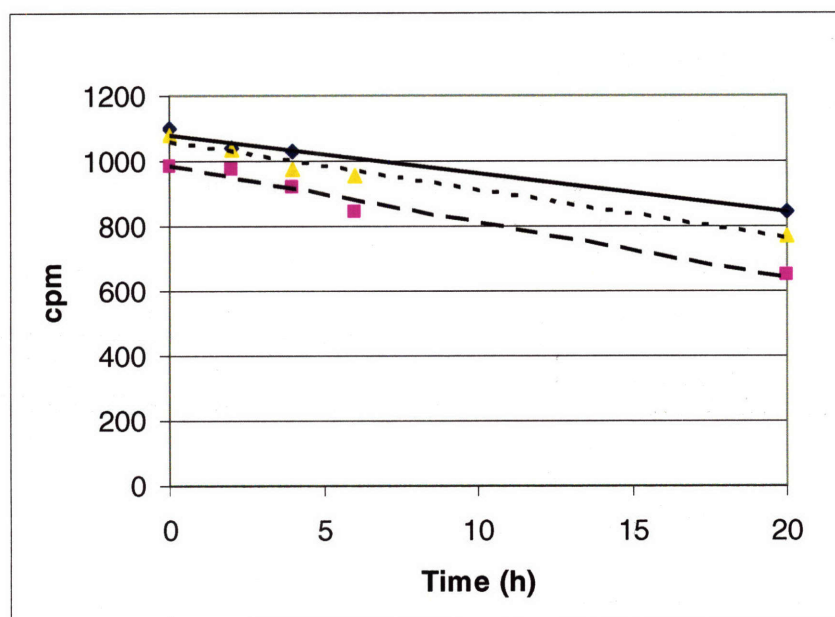


Figure 6-22. Loss of radioactivity over time from RTPR inactivated with 1'-[³H]-F₂CTP dialyzed against potential protein digestion buffers. (—) 0.1 M NH₄HCO₃, pH 8.2; (- -) 0.1 M NH₄HCO₃, pH 8.2, 2 M urea; (···) 160 mM KPi, pH 5.6, 2M urea. Aliquots (0.25 mL) were removed and assayed for cpm remaining at each time point.

These results suggested that RTPR could be successfully digested with trypsin without loss of the majority of the label. In order to minimize loss, digestion was performed over a short period of time with elevated levels of trypsin (1:4 vs 1:20). The inactivation was carried out with 1'-[³H]-F₂CTP and the inactivated protein was denatured in 8M guanidine then labeled with iodoacetamide. The alkylated RTPR was then exchanged into the trypsin digest buffer (0.1 M NH₄HCO₃, pH 8.2) by Sephadex G-50 chromatography and fractions were assayed for radioactivity. While recovery of protein off this column was good (~80% by A280), only 0.14 equiv. of radioactivity co-eluted with the protein of the expected 0.45 equiv. This result indicated substantial loss of the covalent label during the denaturation and iodoacetamide treatment.

The labeled RTPR was then digested with trypsin and the peptides were separated by reverse-phase HPLC. A typical HPLC trace is shown in Figure 6-23. Radioactivity eluted between 45 min and 75 min in a very broad peak. A sharper feature was contained within this region, eluting from 58-62 min. Loss of label from the protein was evident, as 10% of the radioactivity eluted in the void volume. The recovery off the column was 80%; 0.11 equiv. of the total initial radioactivity remained. The broad region of radioactivity suggests the inactivation process results in many sites of labeling, or potentially that one or more initial sites of label became redistributed to multiple residues during the workup and digestion of the RTPR.

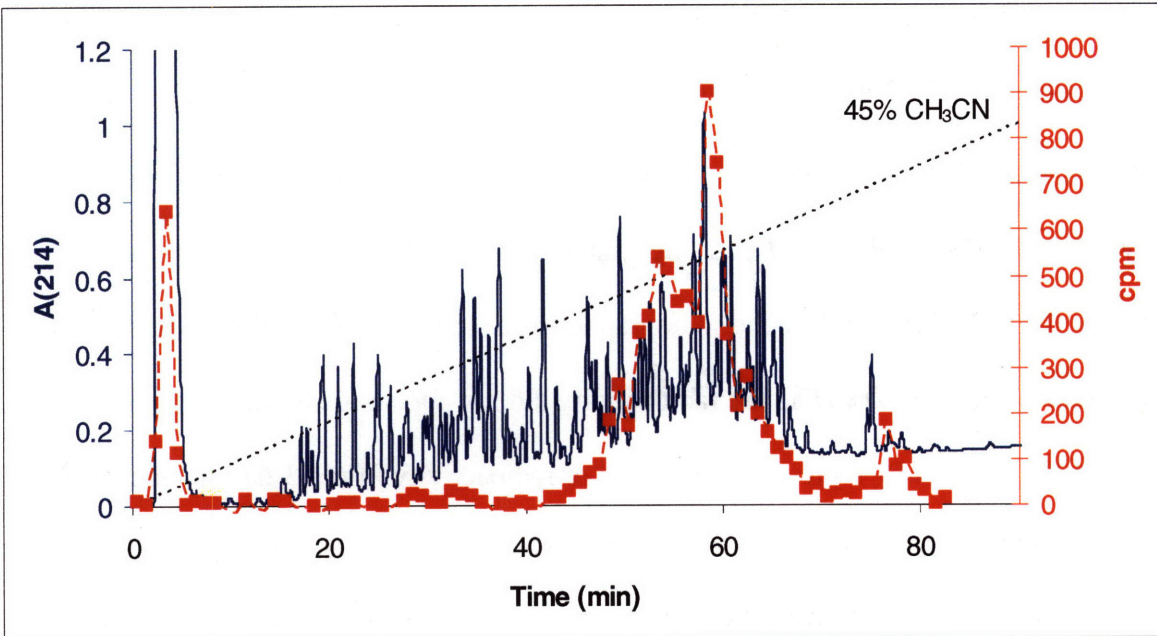


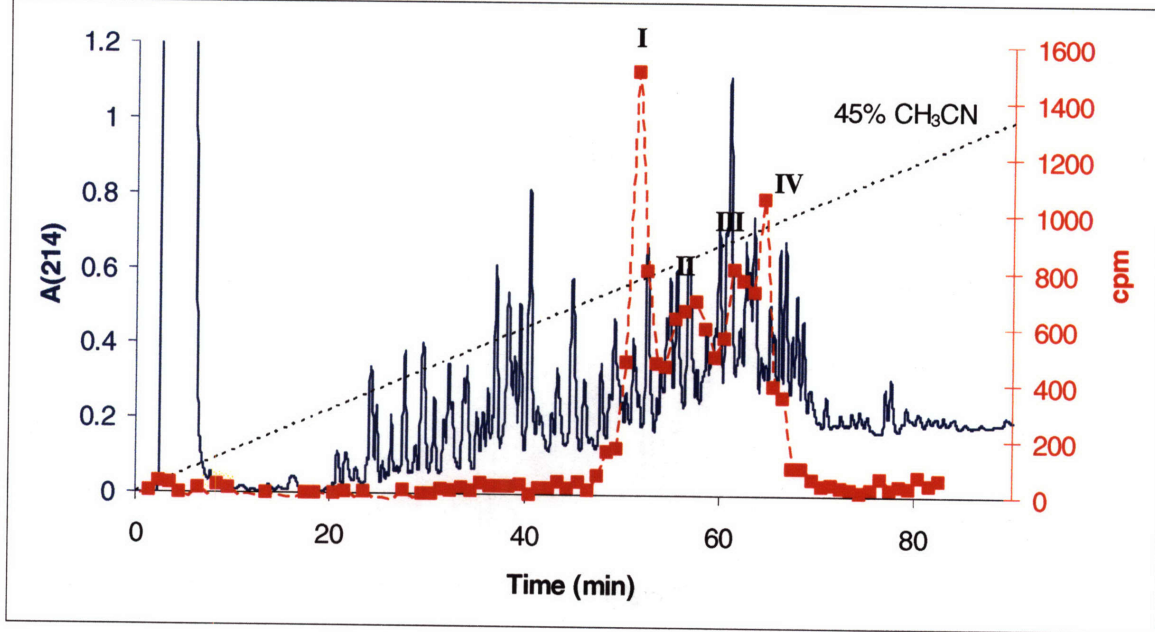
Figure 6-23. HPLC separation of peptides from RTPR inactivated with $1'-[^3\text{H}]\text{-F}_2\text{CTP}$, alkylated with iodoacetamide and digested with trypsin. Absorbance (—), cpm (■). Linear gradient (·····) 0.1% TFA, 0-45% CH_3CN over 90 min. 10% of the radioactivity eluted in the void volume. The remainder of radioactivity eluted from 45-70 min, with a sharper peak eluting from 58-62 min.

Given the substantial label loss during the denaturation, alkylation and digestion steps, a method of stabilizing the label was sought.⁽¹⁴⁴⁾ The inactivation and trypsin digestion were repeated, but prior to denaturation the inactivation mixture at 2 min was treated with 50 mM NaBH_4 . Previous experiments (Table 6-1) reveal a lower amount of labeled RTPR recovered in the case of NaBH_4 quenched reactions. Of the 0.33 equiv. of radioactivity expected to co-elute with the protein, 0.28 equiv. were observed in this experiment, indicating less loss of label during the denaturation and alkylation steps. Subsequent to trypsin digestion and acidification to pH ~2 with TFA to help break potential borate esters, the peptides were separated by HPLC as described above. Recovery from the chromatography was again 80% with no radioactivity eluting in the void volume. A typical chromatogram from a digestion of this type is found in Figure 6-24 A. Four main regions of radioactivity were seen. The first (Region I) was the sharpest peak, eluting from 50-53 min (25-26% acetonitrile) and accounted for 18% of the total

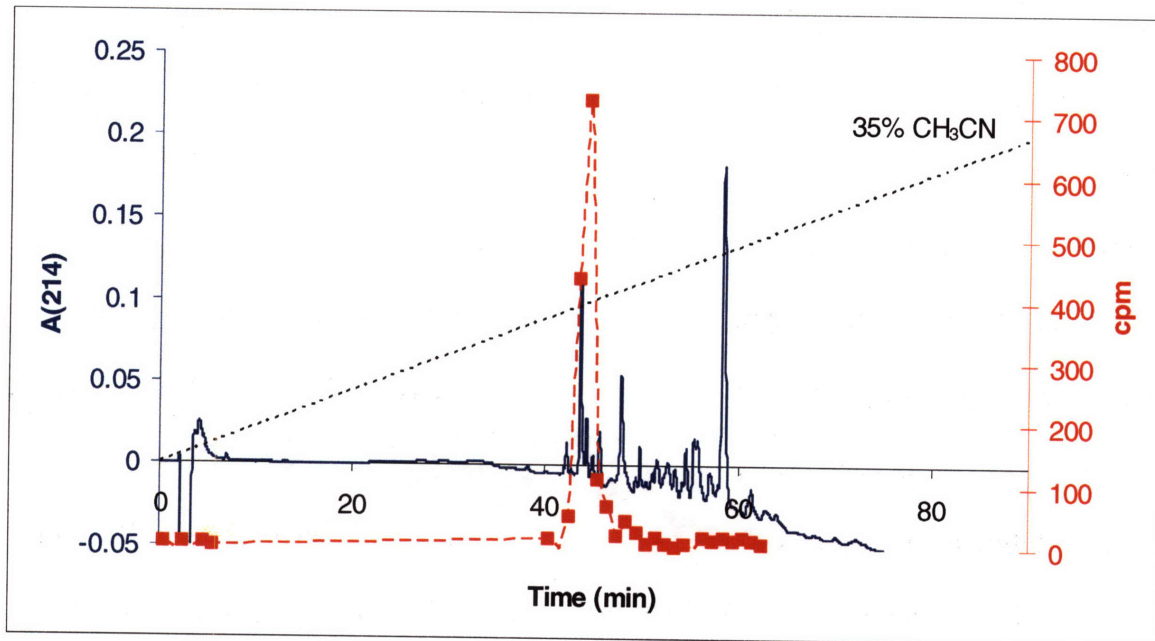
radioactivity. This peak rechromatographed as a single peak with 80% recovery (Figure 6-24 B). Region II, eluting from 54-59 min (27-29% acetonitrile) accounted for 19.7% of the radioactivity, and rechromatographed as several peaks with similar retention times with 70% recovery (Figure 6-24 C). Region III, eluting from 60-63 min (30-32% acetonitrile) accounted for 13.9% of the radioactivity. It rechromatographed as a single peak of radioactivity, but the recovery was very low (< 20%) and the radioactivity did not appear to co-elute with any peptides (Figure 6-24 D). Region IV represents the region of radioactivity from 63-67 min and accounts for 26% of the radioactivity. This region showed no peak of radioactivity in any attempts at repurification (Figure 6-24 E) and most radioactivity was lost. It is not clear what happened to these peptides, but it is possible they were not stable in solution after the initial purification. Over six experiments using these conditions, total recover off the column was $74 \pm 5 \%$. Of the eluting radioactivity, $20 \pm 2\%$ was found in region I, $26 \pm 4\%$ in region II, $20 \pm 5\%$ in region III and $21 \pm 4 \%$ in region IV.

Initial efforts for peptide identification by mass spectrometry focused on region I. In the rechromatogram, the radioactivity appeared associated with peptides and the recovery was excellent. The total recovery for this peak was $(.28 \text{ equiv. labeled RTPR}) \times (.8) \times (.18) \times (.8) = 0.032$ equiv. of radioactivity, representing ~10% of the alkylated RTPR, and the amount of radioactivity eluting in this region was consistent across experiments. Regions II and III were also investigated by similar methods. A discussion of the results of these experiments can be found in the next section.

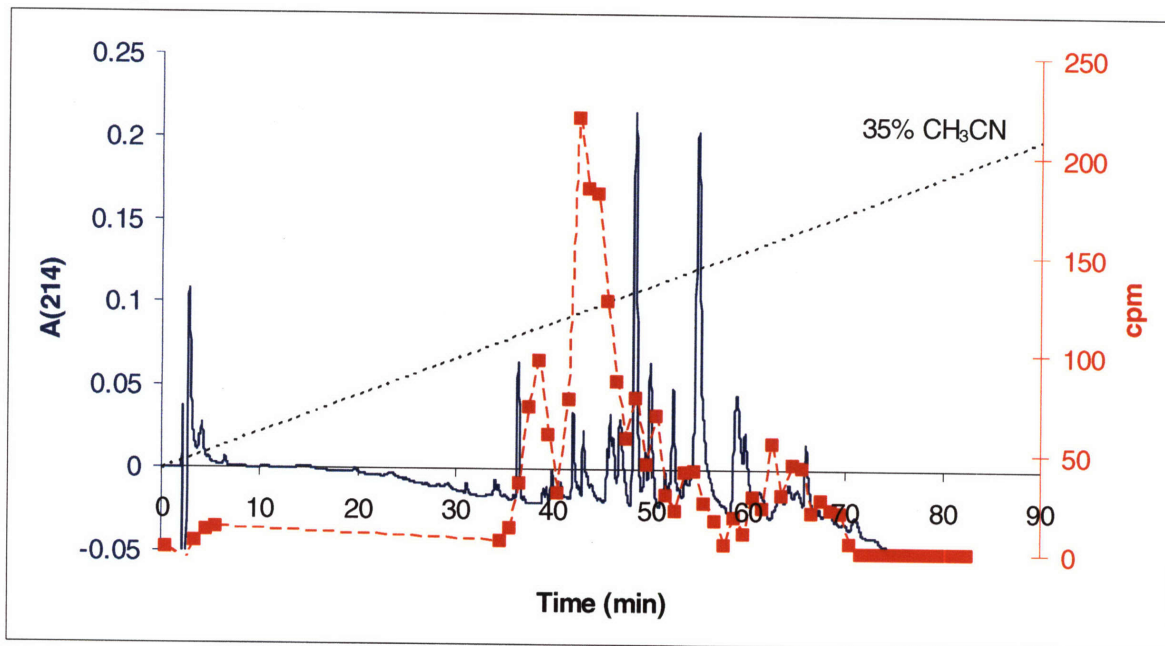
(A)



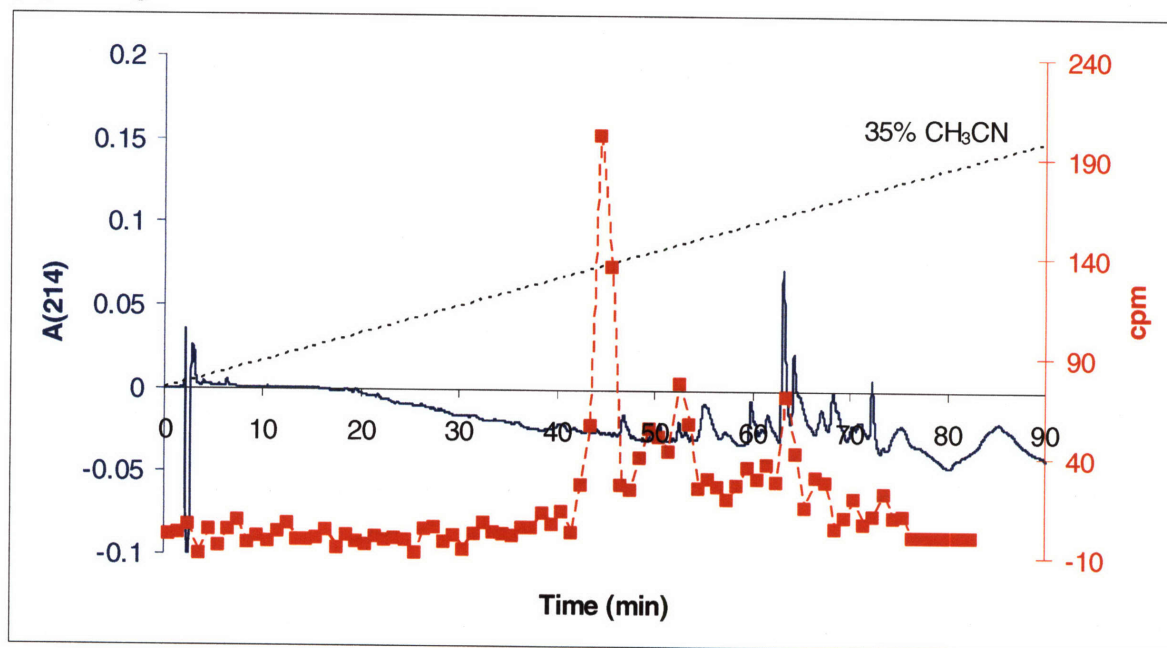
(B) Region I



(C) Region II



(D) Region III



(E) Region IV

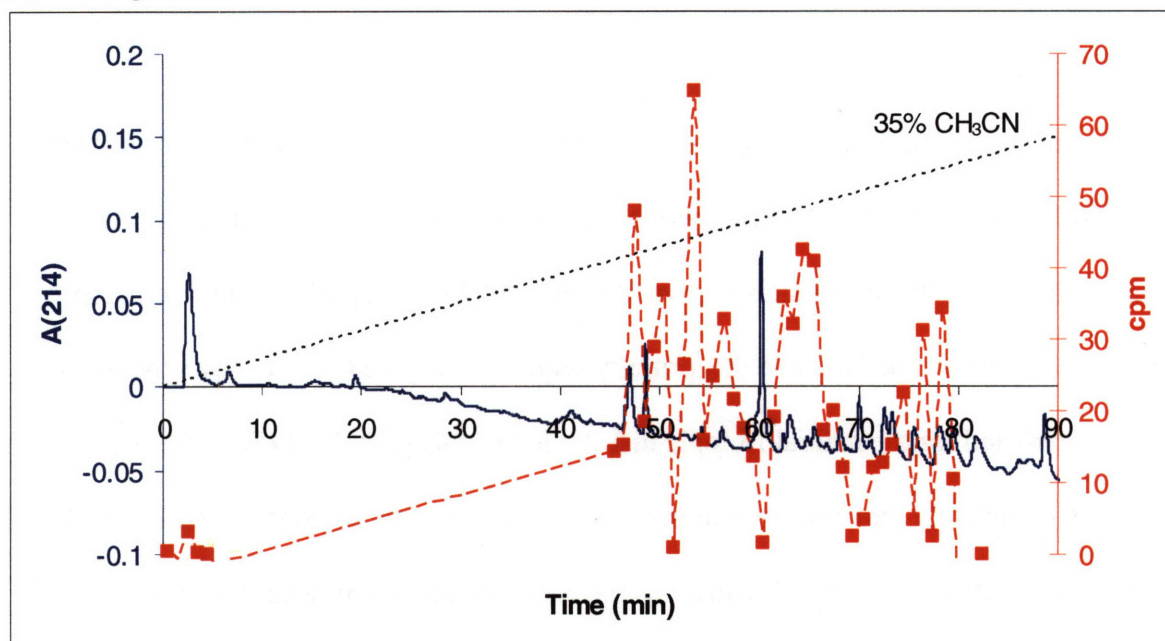


Figure 6-24. HPLC purification of peptides from RTPR inactivated with 1'-[³H]-F₂CTP, treated with NaBH₄ at 2 min, alkylated with iodoacetamide and digested with trypsin. Absorbance (—), cpm (■). (A) Initial purification, linear gradient (·····) 0.1% TFA, 0-45% CH₃CN over 90 min. Region I, 50-53 min, 18.1% of radioactivity. Region II, 54-59 min, 19.7% of radioactivity. Region III, 60-63 min, 13.9% of radioactivity. Region IV, 63-67 min, 26% of radioactivity. (B-E) Linear gradient (·····) 10 mM NH₄OAc, pH 6.8, 0-35% CH₃CN over 90 min. (B) repurification of I. (C) repurification of II. (D) repurification of III. (E) repurification of IV. For most of the repurifications, only regions showing peptide and the void volume were assayed for radioactivity.

Analysis of labeled peptides by mass spectrometry

MALDI analysis was performed on the peptides isolated regions I, II and III, described above (Figure 6-24 B-D). To provide a method for the identification of peaks containing a fragment derived from F₂CTP, a second inactivation was carried out under identical conditions, except the F₂CTP used was produced by combining 1'-[²H]-F₂CTP (93% ²H incorporation) with 1'-[³H]-F₂CTP (s. a. 7200 cpm/nmol). This F₂CTP stock contained ~60% ²H at the 1' position with a specific activity of 2600 cpm/nmol. Inactivations involving with this material would produce the same labeled peptides, except that 0.6 equiv. of a hydrogen will be replaced by deuterium. Isolated peptides will give the normal mass distribution with 1'-[³H]-F₂CTP (99.9% ¹H at the 1' position), but will show an increase in the +1 Da isotope with the partially [²H]

labeled F₂CTP. Thus, peptides modified by F₂CTP could be identified by a predictable change in mass distribution.

This concept is illustrated in Figure 6-25 for the C-terminal tryptic peptide from RTPR (722-739, DLELVDQTDCEGGACPIK) with both cysteines blocked with acetamide. This peptide was chosen for this discussion as several different labeled peptides identified in these experiments were determined to have this primary sequence. Figure 6-25 A shows the mass distribution predicted for the natural isotopic distribution of this peptide.⁽¹⁴⁵⁾ If the peptide had one hydrogen completely replaced by deuterium, the distribution would shift in its entirety by +1 Da. The mass distribution of a peptide that has 0.6 equiv. of deuterium would be the weighted average of the unlabeled distribution and the labeled distribution, and appear as in Figure 6-25 B.⁽¹⁴⁵⁾

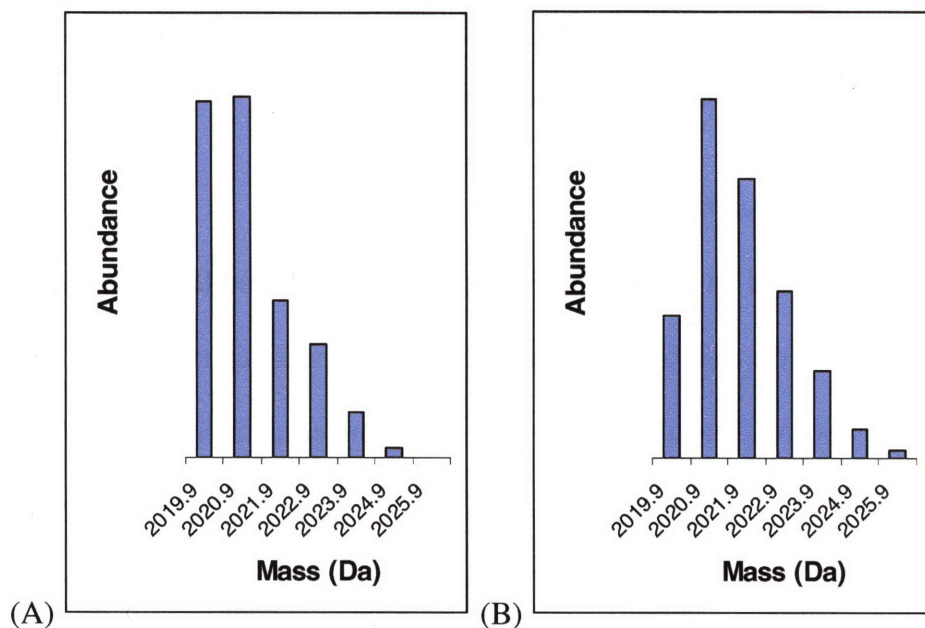


Figure 6-25. Predicted distribution of masses for the RTPR C-terminal peptide from trypsin digestion (DLELVDQTDCEGGACPIK, 2020 Da). (A) normal isotopic distribution and (B) with 0.6 equiv. of deuterium replacing 0.6 equiv. of hydrogen. C-terminal peptides modified with an inhibitor-derived fragment should have nearly identical distributions, shifted to the appropriate absolute mass.⁽¹⁴⁵⁾

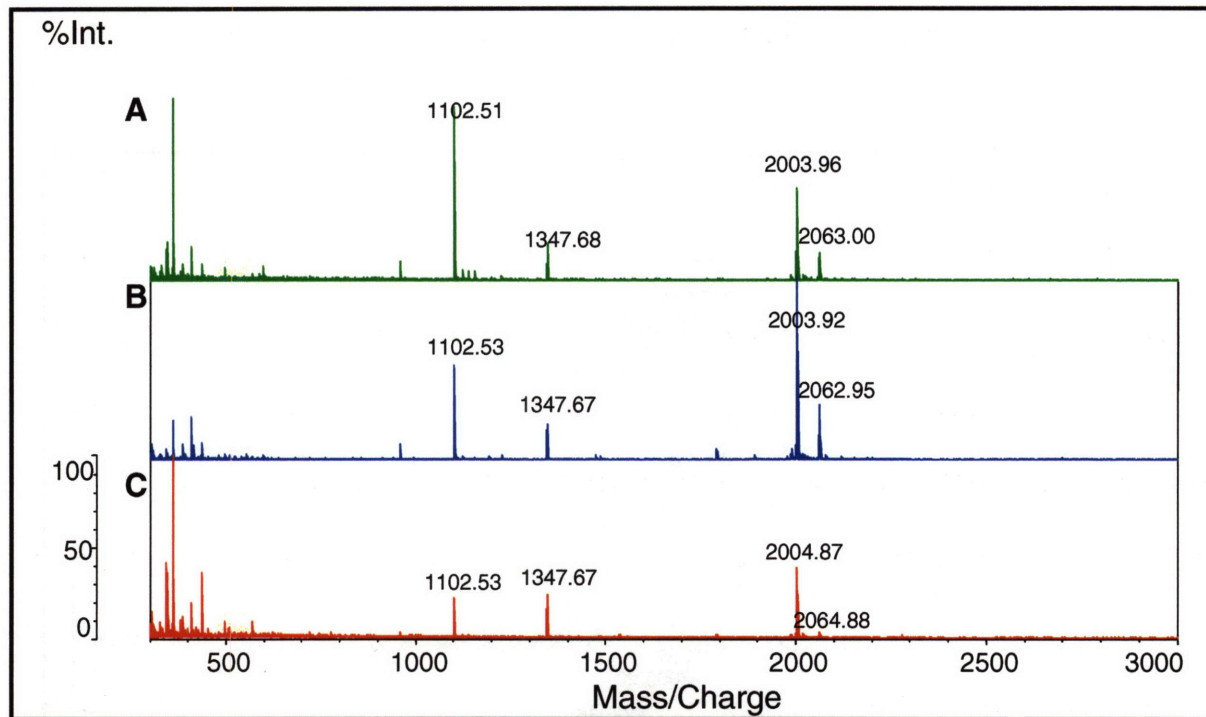


Figure 6-26. Full MALDI of peptides isolated in Region I from the trypsin digest of RTPR inactivated with F₂CTP and treated with NaBH₄ (Figure 6-24 B). (A) 1'-[³H]-F₂CTP, NaBH₄. (B) 1'-[²H,³H]-F₂CTP, NaBH₄. (C) 1'-[³H]-F₂CTP, NaBD₄. The features at 1102.5 Da and 1347.7 Da do not appear to be derived from RTPR, as they do not match any expected peptides from trypsin digestion and MS/MS fragmentation analysis showed no matches with sequences from RTPR.

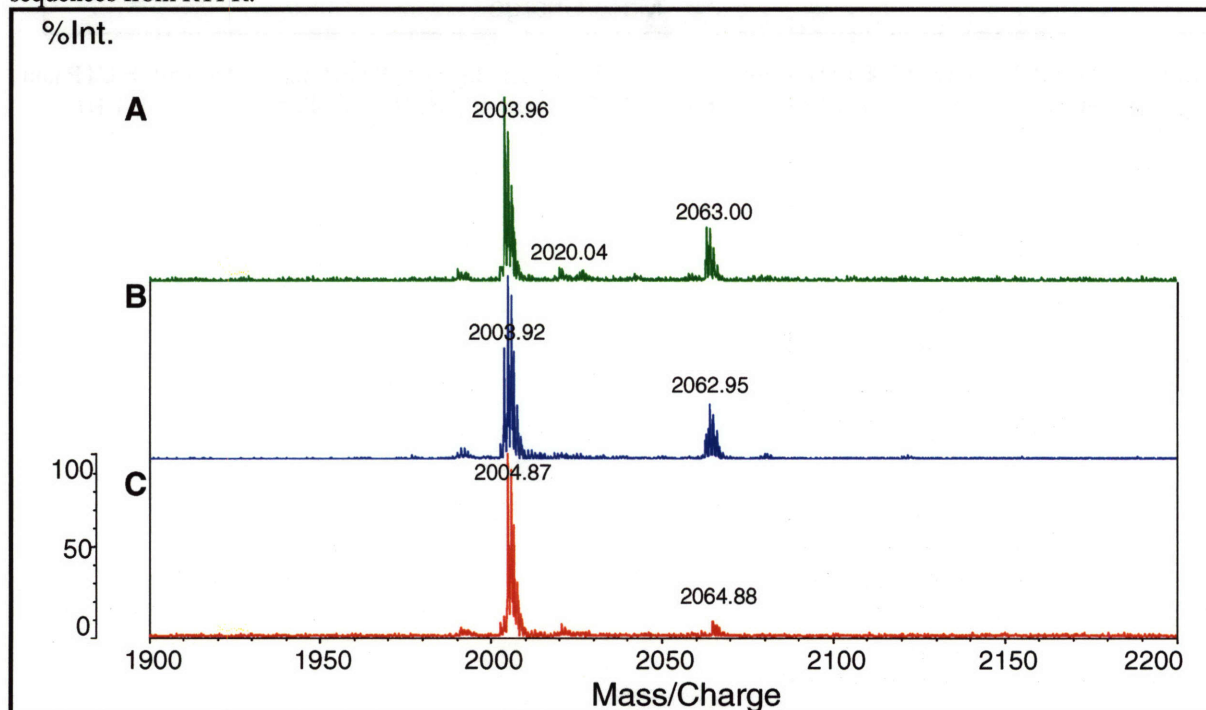


Figure 6-27. MALDI of peptides isolated in Region I from the trypsin digest of RTPR inactivated with F₂CTP and treated with NaBH₄, expansion on the region around the 2004 Da peak (Figure 6-24 B). (A) 1'-[³H]-F₂CTP, NaBH₄. (B) 1'-[²H,³H]-F₂CTP, NaBH₄. (C) 1'-[³H]-F₂CTP, NaBD₄.

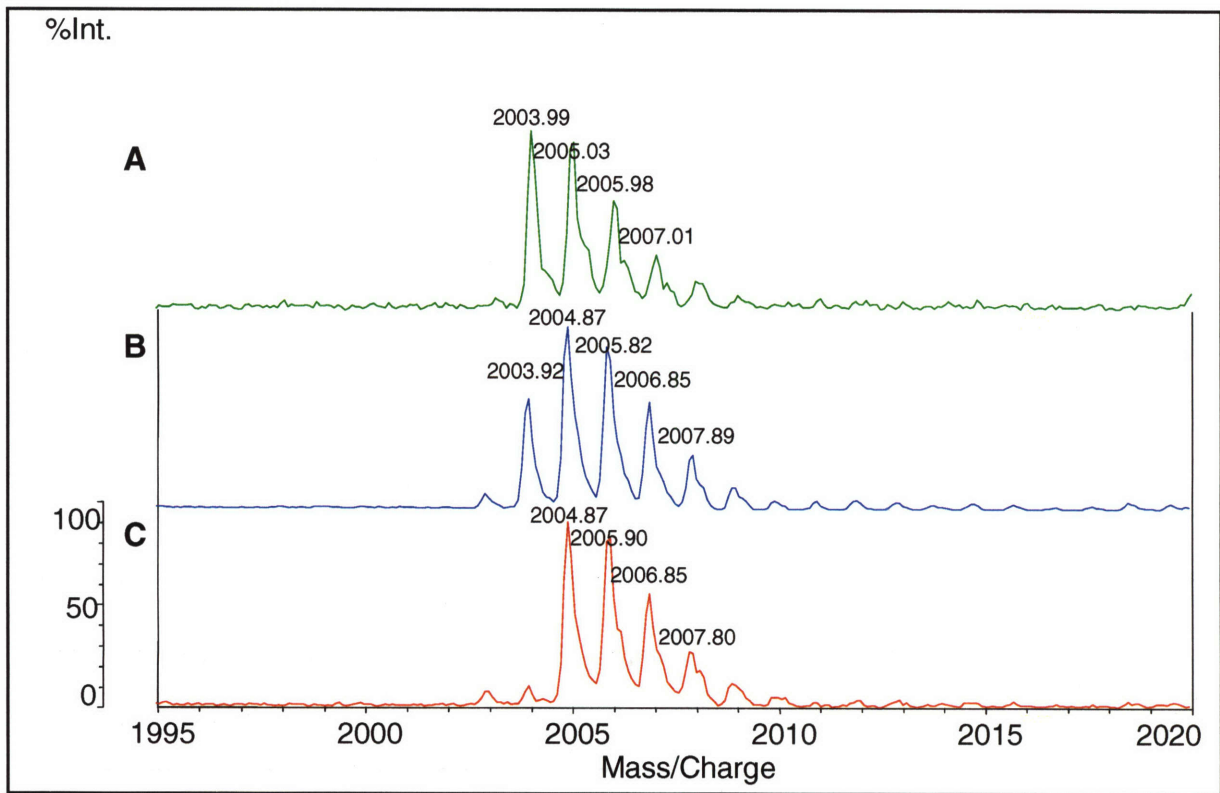


Figure 6-28. MALDI feature at 2004 Da, from Region I of the trypsin digest of RTPR inactivated with F₂CTP and treated with NaBH₄ (Figure 6-24 B). (A) 1'-[³H]-F₂CTP, NaBH₄. (B) 1'-[²H,³H]-F₂CTP, NaBH₄. (C) 1'-[³H]-F₂CTP, NaBD₄.

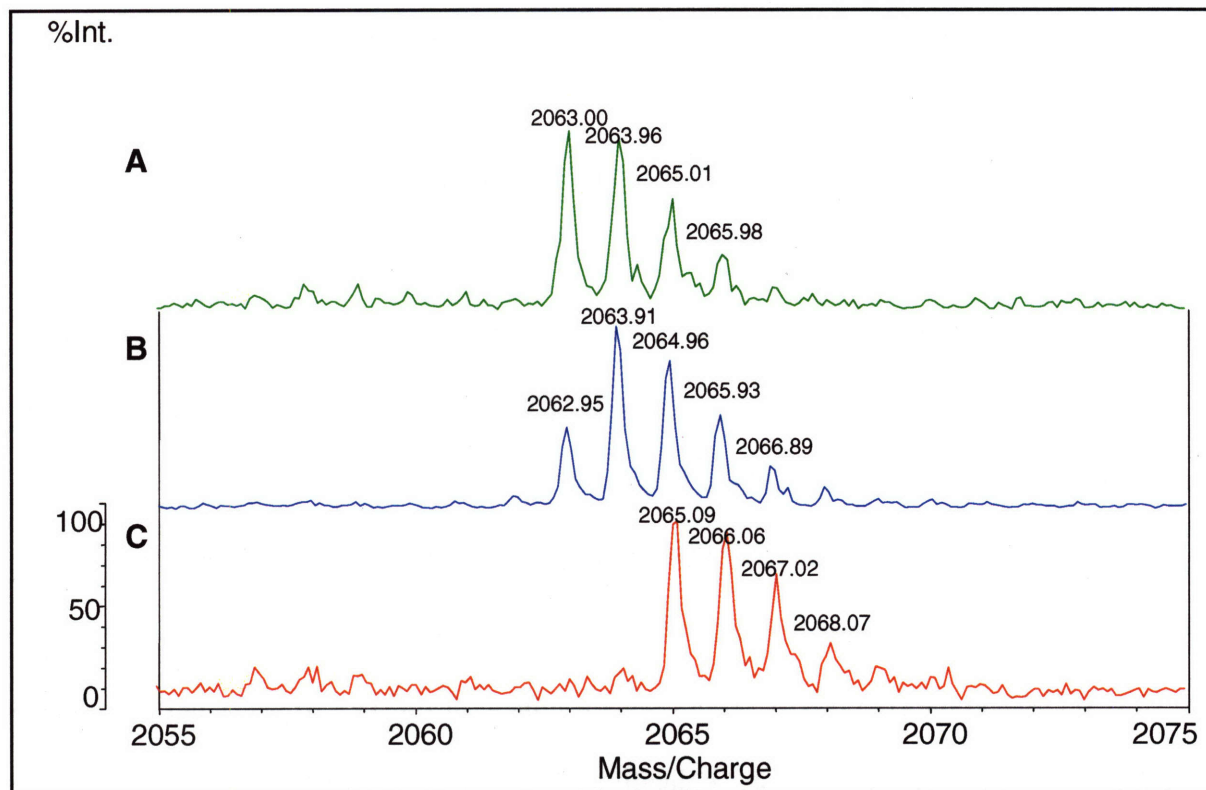


Figure 6-29. MALDI feature at 2063 Da, from Region I of the trypsin digest of RTPR inactivated with F₂CTP (Figure 6-24 B). (A) 1'-[³H]-F₂CTP, NaBH₄. (B) 1'-[²H,³H]-F₂CTP, NaBH₄. (C) 1'-[³H]-F₂CTP, NaBD₄.

Using this methodology, the MALDI spectra of the peptides isolated from the trypsin digest of RTPR inactivated with 1'-[³H]-F₂CTP were investigated (Figure 6-24). The fractions corresponding to the major peaks of radioactivity in each of Regions I, II and III (Figure 6-24 B-D) were analyzed for inactivation with the 1'-[³H]-F₂CTP and with 1'-[²H,³H]-F₂CTP. Two peptides of interest were identified in the MALDI spectra of region I (Figure 6-26 and Figure 6-27), at 2004 Da (Figure 6-28) and 2063 Da (Figure 6-29). These peaks show the predicted shift in isotopic distribution from the non deuterated (Figure 6-28 A and Figure 6-29 A) to the partially deuterated case (Figure 6-28 B and Figure 6-29 B). No peptides showing the shift in isotopic distribution predicted for peptides alkylated by a fragment of F₂CTP were detected in the MALDI for the region II and III peptides (Appendix 2). Regions II and III represent a substantial percentage of the radioactivity recovered from the trypsin digests, thus surprising that

no labeled peptides could be found. This negative result is discussed further below (see *Interpretation of MALDI and MS/MS data*).

Sequencing through post-source decay (PSD) MS/MS analysis (discussed in greater detail in the next section) revealed that the 2004 and 2063 Da peptides as being modified C-terminal peptides of RTPR. This peptide was previously observed in experiments with RTPR and CIUTP as a site of covalent modification using 2'-[³H]-CIUTP and NaBH₄ trapping, as well, apparently modified on the cysteines.(144) The expected mass of this C-terminal peptide with both cysteines acetamide blocked is 2019.90 (Table 6-2); this peptide can itself be seen as a minor peak in Figure 6-27 A (detected at 2020.04 Da). The differences in mass between this peptide (2020 Da) and the peptides incorporating a fragment of F₂CTP (2004 Da and 2063 Da) is -16 Da and +43 Da, respectively, and are indicative of the size of the covalent label.

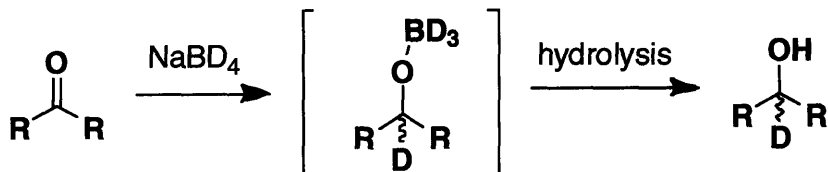
This appears to indicate a label with negative mass; however, as two cysteines within this peptide are a likely sites of alkylation (C731 and C736) and one must take into account the possibility of one or both acetamide groups being replaced by the covalent label derived from F₂CTP. Since the protein is treated with iodoacetamide after the inactivation is complete, any cysteines modified by the F₂CTP would not have reacted with iodoacetamide. Consequently, the labeled peptide would be missing one acetamide, which would be replaced by the F₂CTP derived label. The mass of one iodoacetamide unit is 58 Da (Table 6-2), and thus the peptide with unmodified cysteines is $2020 - 2(58) = 1904$ Da. If one considers possibilities for replacement of acetamides, the peak at 2004 can be seen to be a peptide missing *both* acetamides, alkylated by a group derived from F₂CTP of 100 Da. ($1904 + 100 = 2004$). Similarly, the peak at 2063 Da corresponds to the C-terminal peptide with *one* acetamide and a group derived from F₂CTP of 101 Da ($1904 + 58 + 101 = 2063$).

Table 6-2. Masses of the C-terminal tryptic peptide of RTPR, DLELVDQTD(C-R')EGGA(C-R'')PIK, with various cysteine modifications. X and Y represent the masses of hypothetical alkylations of unknown structure.

Cysteine modification	Mass of R (Da)	Mass of R' (Da)	Mass of Peptide (Da)
Oxidized (unmodified)	0	0	1904
Reduced: R' = R'' = H	1	1	1906
Acetamide labeled: R' = R'' = -CH ₂ (CO)NH ₂	58	58	2020
R' = -CH ₂ (CO)NH ₂ R'' = unknown	58	X	1962 + X
R' = unknown R'' = unknown	X	Y	1904 + X + Y
R' = R'' = unknown crosslink	X	N/A	1904 + X

The labeled structures observed were produced from reaction mixtures treated with NaBH₄. There is good evidence that the precursor structure contained a ketone or an α,β unsaturated ketone system, based on the nucleoside product isolated from the small molecule trapping experiments. Thus, one or more hydrogens in the label may originate from 1,2 or 1,4 reduction by NaBH₄ (Figure 6-30). In order to learn more about the structure of the labeled species and the precise number of hydrogen atoms derived from NaBH₄, the inactivation study was repeated a third time, using 1'-[³H]-F₂CTP, with NaBD₄ (98% D) in place of NaBH₄. Each hydrogen that originated from the borohydride will now be a deuterium, increasing the mass of the labeled peptides by 1 Da. Thus, the shift in mass indicates the number of hydrogens derived from the borohydride. The 1,2 reduction of a ketone or the 1,4 reduction of an unsaturated ketone would each result in the addition of one deuterium to the molecule. In addition, the ketone generated by 1,4 reduction would then be reduced, resulting in the incorporation of a second deuterium.

1,2 reduction



1,4 reduction

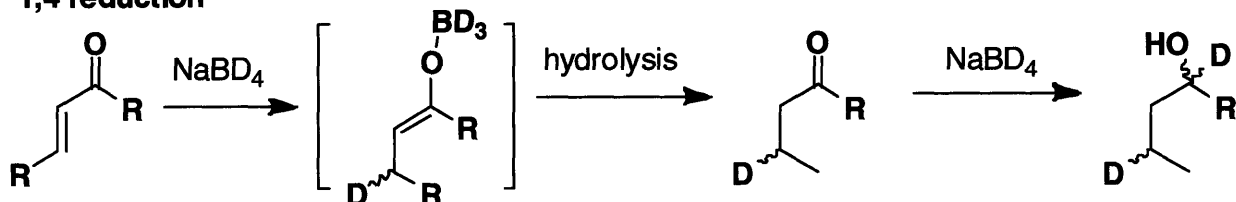


Figure 6-30. Reduction of ketones by NaBD₄.

Figure 6-26 C, Figure 6-27 C, Figure 6-28 C, and Figure 6-29 C show the MALDI trace from the samples quenched by NaBD₄. In the expansion on the 2004 Da peak (Figure 6-28 C), the mass of the peptide shifts from 2004 Da to 2005 Da. In the expansion on the 2063 Da peak (Figure 6-29 C), the mass was shifted by 2 Da to 2065 Da. This result indicates that one hydrogen in the 2004 Da and two hydrogens in the 2063 Da peptide came from NaBD₄, and has the structural implication that both contained ketones.

Analysis by MS/MS

In order to gain more information about the structure of the modification, the sequence of the peptide and the residues alkylated, MS/MS analysis was performed. As shown in Figure 6-27, a peptides of 2020 Da were detected. This mass matches that expected for the C-terminal peptide of RTPR (722-739, DLELVDQTDCEGGACPIK), when both cysteines are modified by acetamide (MW calcd 2019.90, Table 6-2). This assignment was confirmed by PSD fragmentation (Figure 6-31). In this method, additional energy is applied to the peptide of interest, initiating several predictable fragmentation modes. The major site of fragmentation using this method is at peptide bonds (Figure 6-32). This fragmentation gives two series of ions:

the y series in which charge is retained on the N-terminus, and the b series with charge retained on the C-terminus.(146, 147) Each mass peak within a given series is thus associated with a truncated peptide, and the difference in mass between each peak within a given series is the mass of one amino acid in the sequence. The relative abundance of each ion series detected is highly peptide dependent and, in the case of this peptide (Figure 6-31), the y series dominates the spectrum. A number of additional peaks can be seen that are -18 and -17 Da from the main y series. These are the y^0 and y^* series, representing loss of water or ammonia from the y series ions. The peaks from the major “y” series are marked, and the difference in mass indicates the amino acid lost, allowing sequencing of the peptide. Most remaining peaks visible in the spectrum are b series peptides. This spectra essentially allows N-terminal sequencing by viewing the y series. Fourteen y ions are observable, showing mass differences consistent with the C-terminal RTPR peptide, with both cysteines modified by acetamide.

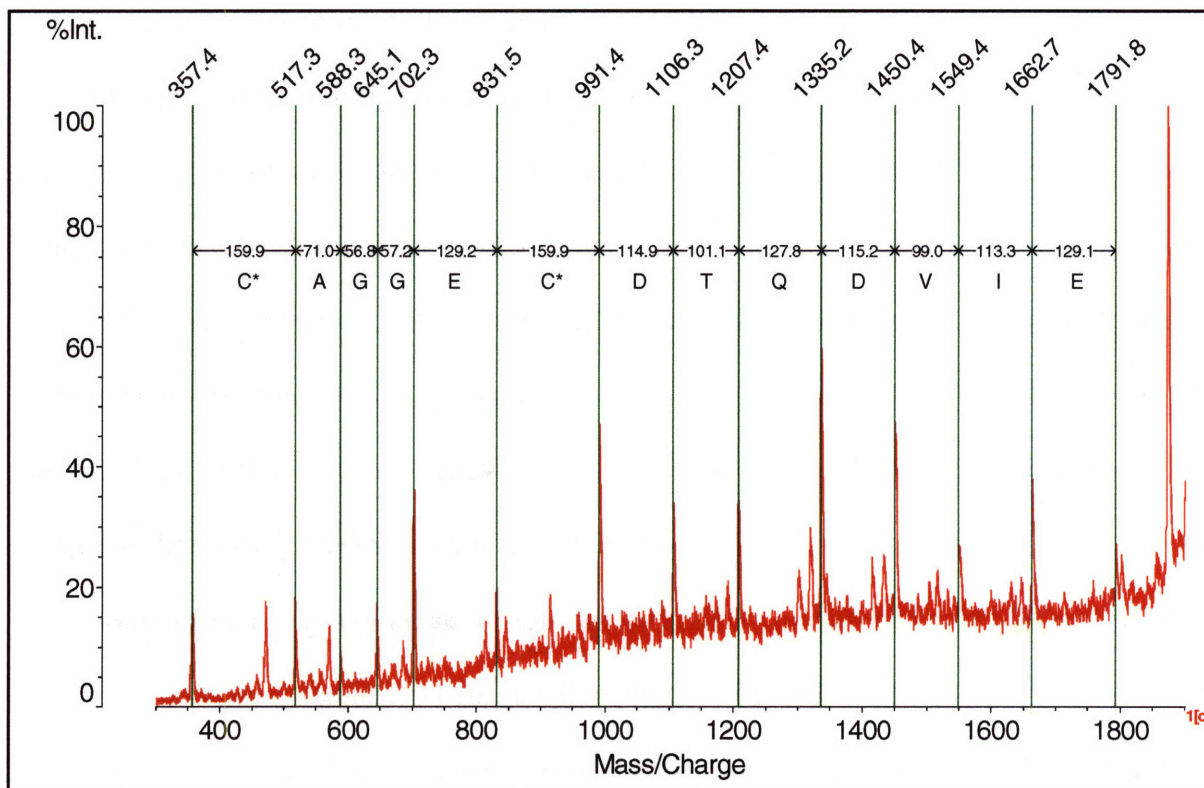


Figure 6-31. Annotated MS/MS spectrum of the 2020 Da peptide corresponding to the diacetamide labeled C-terminal RTPR peptide (DLELVDQTDCEGGACPIK). The y ion series is highlighted, representing fragmentation along the peptide bond with charge retention on the N-terminus. The difference in mass between each ion is the mass of the amino acid cleaved. C* = acetamide modified cysteine.

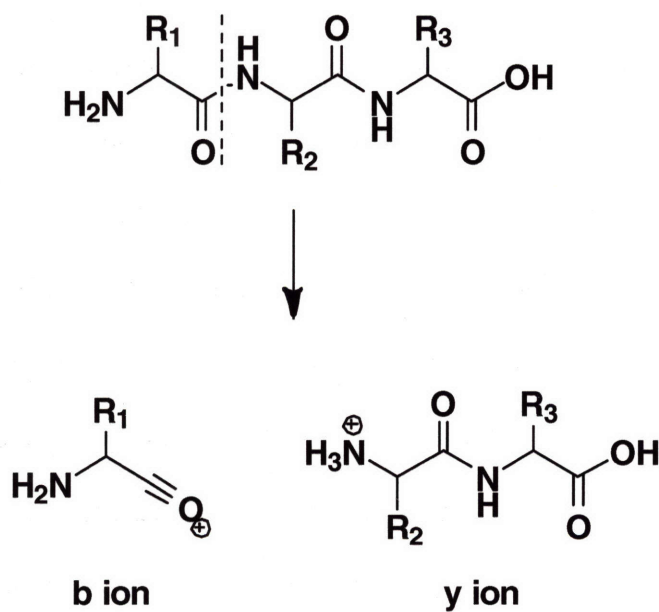


Figure 6-32. PSD fragmentation along the peptide-bonds to give b type and y type ions.

The MS/MS of the 2063 Da peptide shows the same series of ions, but shifted by +43 Da (Figure 6-33 A). The same series is visible in the 2065 Da peptide from the NaBD₄ quenched reaction, but at +45 Da relative to the y series in the 2020 Da peptide (Figure 6-33 B). Once the first cysteine is removed, both the normal series seen in the MS/MS for the acetamide modified peptide (generating the peaks at 831, 702, 645, 588 and 517 Da) and a series which remains at +43 Da (+45 Da in Figure 6-33 B) can be seen. After the cleavage of the second cysteine, only the normal mass peak remains (a fragment at 357 Da). The label derived from the inhibitor sugar fragment is thus attached to either C731 or C736. This method is not quantitative, and nothing concrete can be said about the relative extent of labeling at each site. As predicted by the MALDI, the sugar fragment has a mass of 101 Da (43 Da larger than acetamide) and incorporates two deuteriums when the inactivation is quenched with NaBD₄.

The MS/MS of the major labeled peak at 2004 Da is more complex (Figure 6-34 A). The expected y series for the C-terminal peptide is still evident, -16 Da relative to the diacetamide modified C-terminal peptide (Figure 6-31). Each of these peaks shows several closely related series, fragments that are -17 or -18 Da relative to each y ion (the y* series that has lost ammonia, and the y⁰ series that has lost water) and often one that is -35 Da, representing the loss of both water and ammonia (Figure 6-34 B). It is unclear why the intensities of these secondary fragments are enhanced relative to the corresponding series in the 2020 Da (Figure 6-31) and 2063 Da (Figure 6-33) peptides. Additionally, after the loss of the aspartate before C731 (giving the peak at 975), the peaks visible until the loss of the second cysteine do not correlate with any simple mass series. This result indicates some irregular fragmentation of the peptides in this mass range, and the nature of this fragmentation is not readily apparent. The final tripeptide peak after cleavage of C736 (PIK) appears the same in this spectra as in those for the 2020 and

2063 species. The PSD for the 2005 Da peak in the NaBD₄ spectra is similar, but shifted +1 Da relative to the 2004 Da spectra and the primary y series is of even lower abundance relative to the y⁰ and y* series (Appendix 2).

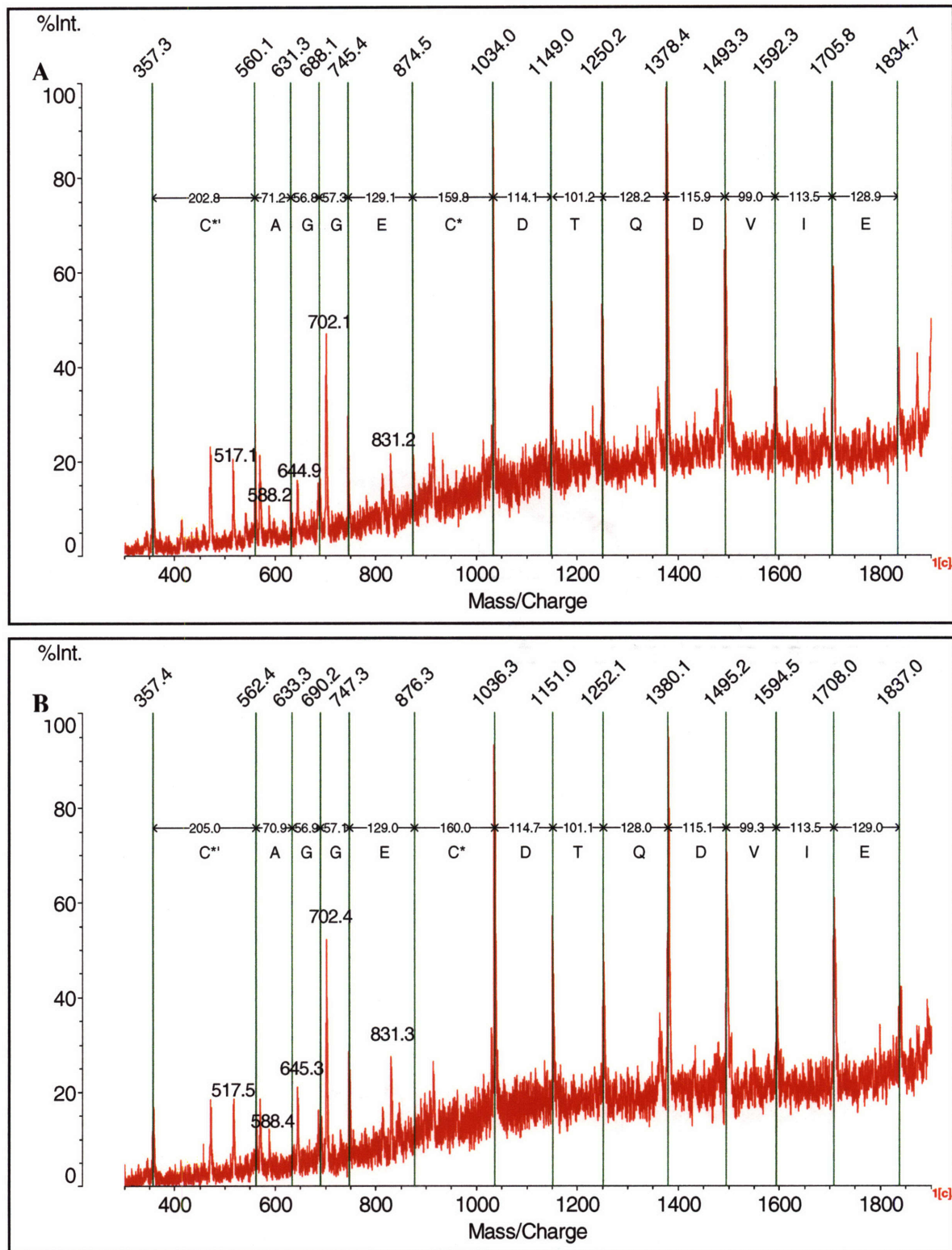


Figure 6-33. (A) MS/MS of peak at 2063 Da, containing a label derived from F₂CTP. (B) the same peptide, from the inactivation quenched with NaBD₄. The y series is indicated in each, shifted +43 Da in A and +45 Da in B relative to the acetamide labeled C-terminal peptide (DLELVDTQDCEGGACPIK). The final mass difference shows that the cysteine cleaved is modified with an alkylation 43 Da (45 Da in B) larger than acetamide. The modification is present to some extent on each cysteine, as indicated by the appearance of the y series of the normal peptide after C731 is cleaved (indicated at 831, 702, 645, 588 and 517 Da in both spectra).

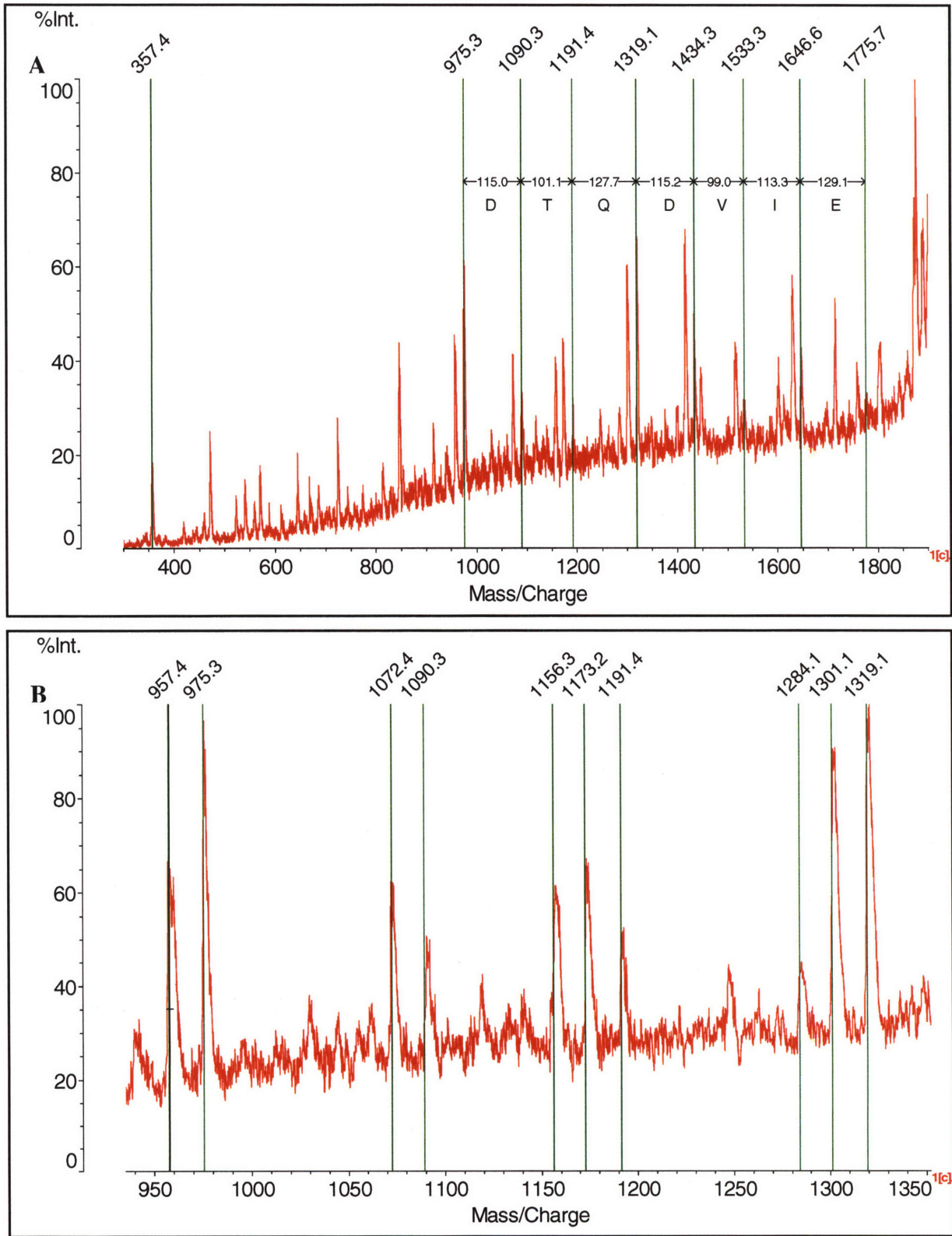


Figure 6-34. MS/MS of peak at 2004 Da, corresponding to the C-terminal peptide of RTPR (DLELVDTDCEGGACPIK) containing an internal cysteine-cysteine crosslink derived from F₂CTP. (A) Full PSD with y ion series marked. (B) Expansion, indicating primary y ions and the peaks representing the y⁰ and y* series (-18 Da and -17 Da, overlapped) and peaks -35 Da representing both the loss of a water and of an ammonia.

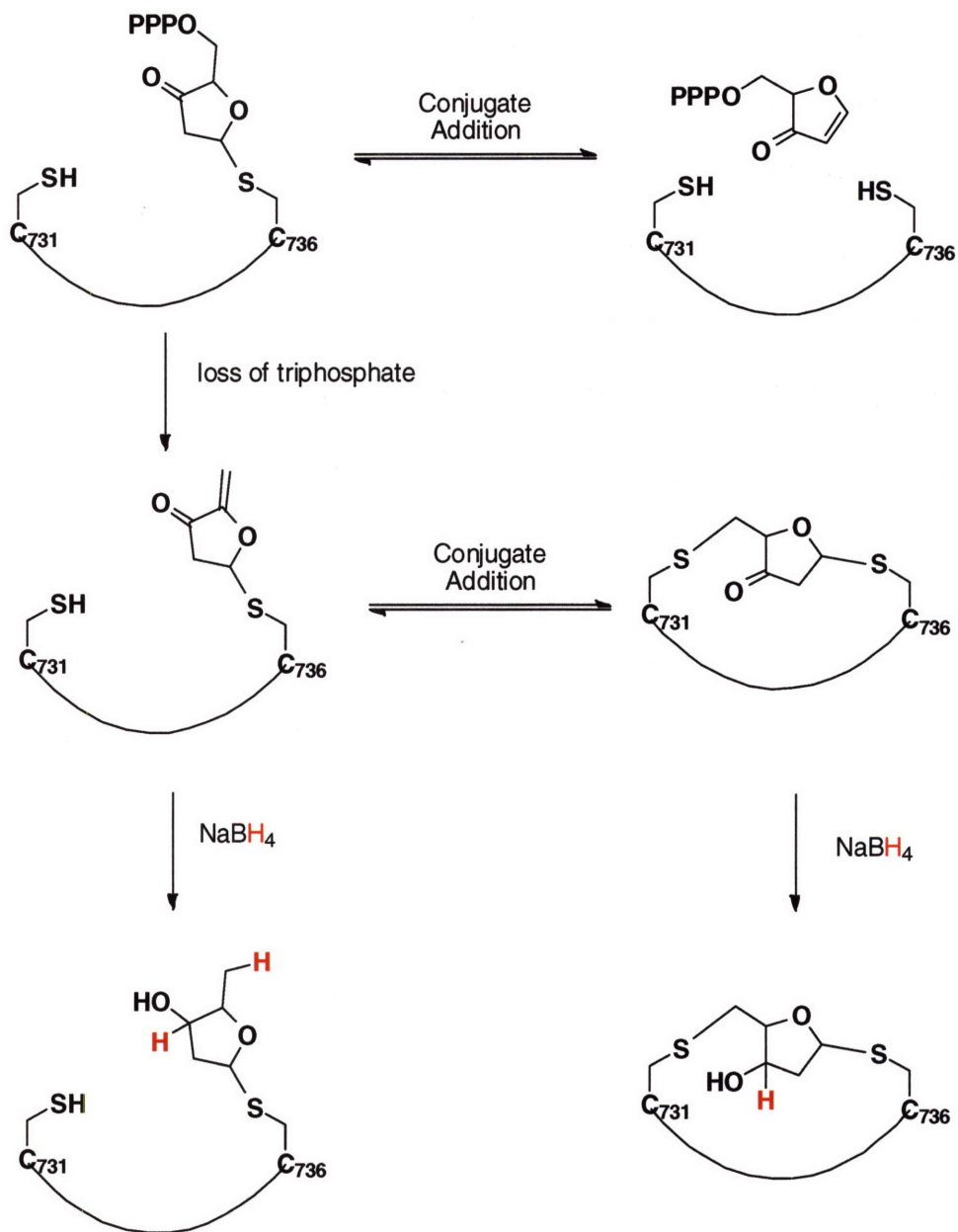
This data is consistent with modification at C731 and C736, and the apparent mass of the fragment derived from F₂CTP agrees with the MALDI data. If both acetamides are missing, a fragment of mass 100 derived from F₂CTP would account for the observed mass (2020 – 2*58 +100 = 2004). Based on the PSD spectra, this modification is unlikely to be two 50 Da fragments, one on each cysteine. Were this the case, we would expect to see a series of ions after the loss of C731 that was – 8 Da relative to the spectrum of the 2020 Da peptide. Instead, it seems likely this modification is a 100 Da fragment that is covalently modifying both cysteines, providing an internal crosslink. Cleavages in the backbone in between the two cysteines would not actually fragment the peptide if they were connected through a side-chain crosslink, and could account for the lack of regular fragments in this region.

Interpretation of MALDI and MS/MS data.

The peptides associated with masses at 2004 and 2063 Da represent cysteine-modified C-terminal peptides of RTPR. Modification is evident at both C731 and C736. The mass at 2004 Da is consistent with the replacement of both acetamides with a fragment of 100 Da that is covalently linked to both cysteines. The peptide at 2063 is consistent with the same tryptic peptide that has one cysteine labeled with acetamide and one with a sugar fragment label of 101 Da. The NaBD₄ quenched sample shows that one hydrogen on the 100 Da fragment comes from NaBH₄ and that two on the 101 Da fragment come from NaBH₄.

Figure 6-35 outlines a scheme consistent with this data. A furanone equivalent (see Figure 6-3) could react with the C-terminal cysteines through conjugate addition, either with one cysteine leaving a compound with an α,β unsaturated ketone, or with both cysteines giving rise to a saturated ketone. Reduction with NaBH₄ would provide the structure with the correct mass and

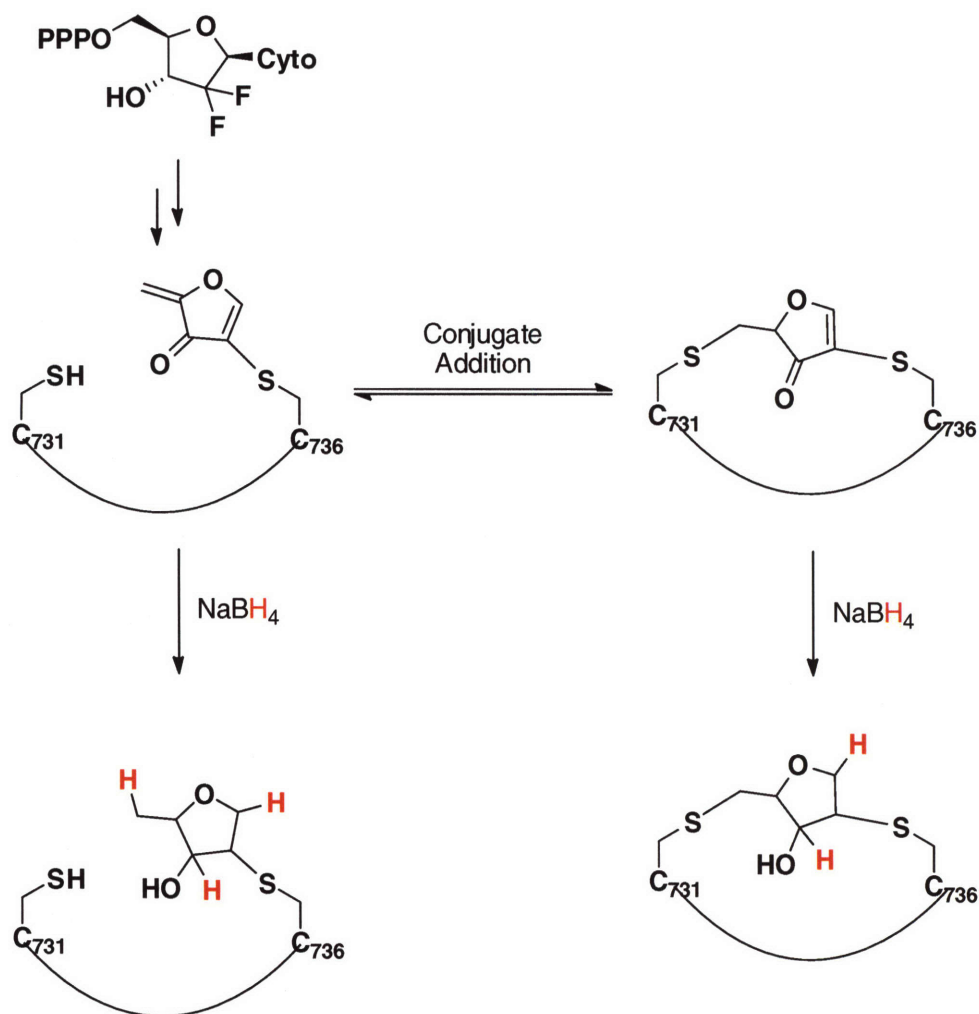
number of hydrogens delivered from NaBH_4 . An alternate proposal (Figure 6-36) can be drawn that gives the same masses associated with the sugar fragment. In this proposal, the first alkylation by cysteine would take place through a mechanism analogous to the addition of water proposed to explain the small molecule product (Figure 6-4). However, this mechanism would require an additional 1,4 reduction for each label, leading to expected incorporation of two deuteriums in the case of the 2004 Da peptide and three in the case of the 2063 Da peptide. Therefore, this second mechanism is eliminated by the results of the NaBD_4 reduction experiment.



Label mass 101 Da, 2H from NaBH₄

Label mass 100 Da, 1H from NaBH₄

Figure 6-35. Proposal for label structure and mechanism of formation.



Label mass 101 Da, 3H from NaBH₄

Label mass 100 Da, 2H from NaBH₄

Figure 6-36. Alternate proposal for label structure. This proposal is inconsistent with the data from the NaBD₄ quenched inactivations, requiring one more hydrogen in the label structures than is observed.

The site of the RTPR alkylation is on the C-terminal tail and not the active site cysteines, and is derived from a furanone-like precursor. This observation places strong constraints on the mechanism of adduct formation. This observation led to the “alkylative” mechanism proposed (Figure 6-3). The alkylation of RTPR by F₂CTP occurs within 2 min based on size exclusion chromatography experiments, with one equiv. of F₂CTP resulting in ~0.45 equiv. of labeled protein. Similar results were in fact previously observed in the inactivation of RTPR by 2'-[³H]-CIUTP.(144) In this case, the inactivation could be run with 13 equiv. of the inhibitor in the presence of NaBH₄, and one equiv. of alkylation was observed with the RTPR. Trypsin

digestion and purification by HPLC allowed isolation of three close-eluting peptides. Only one was of sufficient purity for identification by sequencing, found to be the C-terminal tail peptide with modifications on the cysteines. The mass measured was 2006, consistent with a furanone modified cysteine and the second cysteine unmodified, a surprise given that the RTPR was alkylated with iodoacetamide prior to digestion. No evidence of a species consistent with the characteristic chromophore formed in these systems was observed.

When furanone is generated in most other nucleotide analog inhibitors, the alkylation of the peptide occurs on the minute timescale, and requires multiple equivalents of the inhibitor to see significant amounts of alkylation, 2-100 depending on the inhibitor and the effector used.^(118, 121-123, 144, 148-151) In the case of the CIUTP/RTPR system described above,⁽¹⁴⁴⁾ alkylation and inactivation were high with only one equivalent of the inhibitor, with >0.8 equiv. bound and >80% inactivation by 10 min, and formation of the chromophore was observed to an extent determined only by the initial alkylation, and did not increase with increasing alkylation. In the case of these experiments, treatment with NaBH₄ rules out alkylation during the denaturation and iodoacetamide labeling steps. The NaBH₄ would reduce any ketone-containing species in solution, preventing modification through conjugate addition. Previous results support this assumption, as 13 equiv. of CIUTP resulted in only 1.3 equiv. or labeled RTPR as compared to >4 equiv. in the absence of NaBH₄. Finally, the characteristic chromophores that develop in RNRs alkylated by furanone have not been observed after inactivations using F₂CDP or F₂CTP, though in the case of RTPR observation of this potential chromophore is frustrated by the covalent modification by cobalamin, obscuring this region of the UV-vis spectrum.⁽⁶⁹⁾ However, it seems unlikely that F₂CTP is forming a free furanone species that can inactivate RTPR from reaction from solution; instead the primary source of

inactivation seems to be due to a specific alkylation, of a phenotype similar to that observed in the CIUTP/RTPR system.(144)

The mass spectrometry studies indicate a specific, rapid alkylation pathway, which we propose is associated with rapid loss of base, and provides the basis for the mechanism described in Figure 6-3. The mechanism likely involves rapid loss of cytosine to generate **6-7** (Figure 6-3) which is trapped by a nucleophile derived from RTPR (Figure 6-35). The loss of inorganic triphosphate is likely slow, but once released the product is set up for a second, rapid alkylation. The location of this label on the C-terminal tail rather than the active site, combined with the evidence against a non-specific alkylation from solution, suggests that the tail enters the active site, as it would during normal turnover to re-reduce the active site cysteine, while a reactive species is still bound. Reaction with C731 or C736 results in the modifications described. The proposed mechanism (Figure 6-3) provides an explanation for why the tail is the site of alkylation rather than the bottom-face active site cysteines. These cysteines (C119, C419) are proposed to be in an oxidized state and are thus unavailable for nucleophilic attack on the reactive sugar moiety.

The broad regions of radiolabeled peptides observed in HPLC analysis of the trypsin digests indicate multiple labeled peptides are present. However, no peptides could be identified in regions II or III by the MALDI methods described (Appendix 2). It is an important caveat that the label identified accounts for only ~18% of the total RTPR alkylated at 2 min. One possible explanation for the inability to detect additional peptides may be related to their size. If alkylation was occurring on C408 (the top-face active site cysteine) for example, the predicted peptide from trypsin digestion would be >6000 Da, too large to be visible using the MALDI method used here.(152) It is also possible that the label is crosslinking to other sites on the

protein, producing a mixture of peptides, many of which might also be too large to see by MALDI. Future experiments using electrospray ionization (ESI) methods may allow identification of additional sites of alkylation.

Additional Studies using 1'-[²H]-F₂CTP and 3'-[²H]-F₂CTP

The deuterated derivatives of F₂CTP produced as described in Chapter 5 have been used for several additional studies. The 3'-[²H]-F₂CTP has potential for giving information on the kinetics of this inactivation, and a preliminary experiment was done on the minute time scale. A time-dependant inactivation using the radioactive assay was performed as described above substituting 3'-[²H]-F₂CTP for F₂CTP. No difference in inactivation behavior was observed when using the 3'-[²H] inhibitor relative to F₂CTP.

Both 1'-[²H]-F₂CTP and 3'-[²H]-F₂CTP have been used in the investigation of the structure of the radical formed upon inactivation of RTPR through EPR methods. Inactivation studies were carried out using these compounds and quenched at 20 s in isopentane/liquid N₂ slurry. Analysis at 9 GHz showed no differences relative to each other and the EPR previously reported by Silva(69). These compounds were also used to prepare high-field (130 GHz) EPR samples by Gary Gerfen at the Albert Einstein College of Medicine at Yeshiva University. These samples were prepared at 300 μM RTPR, 450 μM AdoCbl, 1 mM dATP and 300 μM F₂CTP (either unlabeled, 1'-[²H], or 3'-[²H]). No differences were noted between the unlabeled inhibitor and the 3'-[²H]. The 1'-[²H]-F₂CTP/RTPR spectrum showed some differences which have not been fully deconvoluted at this stage. The differences suggested that D-ENDOR experiments might be informative to look for coupling of a deuteron to the radical. In this case, the sample prepared with 1'-[²H]-F₂CTP shows a clear 8.6 MHz coupling of the radical to a

deuteron, consistent with a radical at the 2'-position coupled to the 1' deuteron (Appendix 2).(153) This result provided the first direct evidence that the observed organic radical is indeed a nucleotide-based radical, and provides support for a mechanism that produces a stable, 2'-radical (Figure 6-4).

6.4 Discussion

Mechanistic implications of the inactivation products

The use of radiolabeled F₂CTP has allowed us to provide additional insight into the inactivation of RTPR by F₂CTP relative to our earlier studies.(69) Our studies with 5-[³H]-F₂CTP and 1'-[³H]-F₂CTP quantified the degree of RTPR alkylation by F₂CTP fragments derived from the base and the sugar ring, respectively, and of the quantity of each nucleotide fragment in solution. The analysis revealed that during the inactivation of RTPR, the majority of the cytosine is fairly rapidly cleaved from the inhibitor into solution. The kinetics of this release unfortunately cannot be measured, but 0.6 equiv. are observed to be lost from F₂CTP, in < 15 min. Further, SEC experiments showed that when quenched at 2 min by loading onto the Sephadex G-50 column, 0.45 equiv. of sugar ring co-eluted with the protein, but only 0.15 equiv. of cytosine, indicating cleavage of the cytosine in this short timeframe. The rate of loss is probably faster than seen in RNR inhibition by a variety of other nucleotide analogs, where reaction to a 3'-keto nucleotide results in loss of base through β elimination on a timescale of minutes.(117, 118, 121-123, 149, 154) This result suggests that loss of base is an integral part of the inactivation mechanism.

The SEC experiments indicated that although >90% of the RTPR was inactivated and 0.8-0.9 equiv. of F₂CTP was consumed, only 0.45 equiv. of F₂CTP was found covalently bound

to RTPR at the inactivation endpoint. This result was the first indication that the inactivation proceeded by multiple pathways, perhaps involving a common intermediate. One path involves F₂CTP alkylation of RTPR, while another results in F₂CTP consumption with all fragments of the inhibitor released into solution. The latter pathway suggests that the reaction with the AdoCbl cofactor previously characterized, resulting in the formation of a Co-S bond to C419, may be responsible for the remainder of the inactivation.⁽⁶⁹⁾ Our current studies found 0.25 equiv. of AdoCbl co-elute with RTPR in SEC experiments at 2 min, a value which rises to 0.5 equiv. on long (1 h) timescales. In the absence of modification by the F₂CTP, this adduct seems a likely suspect for the cause of the remaining activation. At 2 min, not enough has formed a covalent linkage with the protein to account for the remainder of the inactivation, but the increase to 0.5 equiv. suggests a tightly associated precursor may be present which forms the covalent species slowly, but leaves the RTPR unable to bind additional substrate at 2 min.

Several of the end products of the F₂CTP/RTPR reaction have been characterized as well, providing further mechanistic insight. One product of the alkylative pathway has been well characterized through the application of the MALDI and PSD techniques described in the previous section. The alkylation appears to result from a furanone-like precursor. The mechanism also must account for the site of alkylation observed (the C-terminal cysteines) and explain why multiple alkylated peptides are evident in the trypsin digests. The mechanism described in Figure 6-3 accounts for the features observed for this system. The loss of both fluorides occurs in a manner that also removes all abstractable protons from the active site, and leaves the bottom-face cysteines oxidized. Thus, the α -keto radical must be reduced by single-electron transfer, not hydrogen atom abstraction. The generation of a negative charge at the 2'-position would result in the rapid elimination of cytosine, explaining rapid base release and the

lack of peptide species isolated with a cytosine attached in the alkylating fragment and the low amount of radioactivity seen eluting with the protein in SEC experiments when 5- ^3H -F₂CTP was used. The product would be a furanone precursor generated in the active site rather than solution. The oxidized state of the bottom-face cysteines explains why these were not the site of alkylation—instead, the inhibitor fragment reacted with the C-terminal tail when it entered the active site to reduce the active site disulfide. It is interesting that this peptide is also observed when RTPR is inactivated by an excess of CIUTP in the presence of NaBH₄. This strongly suggests that a similar mechanism must account for at least a portion of the inactivation with 2'-monohalo-2'-deoxy analogs as well. (144)

The proposed mechanism suggests the other major site of alkylation should be the top-face cysteine, which has not been observed. It is important to note that only one region of radioactivity from the trypsin digest, accounting for ~18% of the total RTPR labeled during the reaction, has been well characterized, and no peptides have been identified from the remaining regions. This could mean that the peptide masses were too large to see by this method, such as is the case for peptides containing the top-face cysteine. The potential for the fragment to crosslink, and the reversible nature of alkylation through conjugate addition, may also explain the broad regions of radioactivity seen in the trypsin digests. Low abundance peptides consisting of the C-terminal tail cross linked to other side chain nucleophiles would be difficult to detect by MALDI methods.

However, the alkylation by F₂CTP accounts for only half of the inactivation. The small molecule products have been well characterized, but the formation of the proposed glycoaldehyde radical (Figure 6-4) and the resultant breakdown products cannot directly account for the inactivation of RTPR on a fast timescale. The working hypothesis is that the RTPR not

inactivated by alkylation by F₂CTP is inactivated through the covalent modification of C419 by cobalamin. This modification appears to be ~0.5 equiv., so could account for the difference between the total amount of RTPR inactivated (>90% inactivation observed at 2 min) and that alkylated by F₂CTP. It must be considered that the formation of the Co-S bond occurs on a slower timescale than inactivation: only ~0.25 equiv. co-elute with the protein at 2 min. The inactivation initially may result from the tight association of a precursor cob(II)alamin species, a nucleotide radical coupled to it, and RTPR. Further, previous studies gave a different result for this stoichiometry (1 equiv. at 20 min), and the reason for the discrepancy has not been elucidated. The relationship between inactivation and cobalamin alkylation bears further investigation.

A model for the overall inactivation taking into account both results could proceed from the initially generated cob(II)alamin-nucleotide radical species observed at 140 ms in previous studies.⁽⁶⁹⁾ This initial species may partition over time into the observed products. Reaction of the nucleotide radical terminating with one electron reduction of the nucleotide by a top face thiolate (**6-6** and **6-7**, Figure 6-3) would return the radical to C408 where it could exchange with the cob(II) species. This would generate could a terminal cob(III) species and an F₂CTP-derived electrophile that could alkylate the protein. Alternatively, if the nucleotide radical formed the proposed stable glycoaldehyde species **6-10** and was reduced by eventual hydrogen atom abstraction, a cob(II)alamin-protein thiyl radical coupled species could result. If the abstraction took place from the bottom face C419, this could lead to the formation of the protein S-Co bond. Thus, the partitioning between alkylation by F₂CTP and the formation of a stable protein-cobalamin species would account for the entirety of the inactivation.

Future Directions

Clearly, the current proposed model is open to further testing, and several specific issues may be resolved by future experiments. In particular, a kinetic analysis of this reaction would help elucidate many details of the mechanism. The release of cytosine is of particular interest. The model presented predicts rapid loss of cytosine from the alkylative pathway, and slower loss of cytosine from the non-alkylative pathway. The current model would assume a rapid loss of cytosine equal to the amount of alkylation measured. If the remainder of the cytosine is coming from the breakdown of the 2'-hydroxy radical, one would expect the remainder of the cytosine to be lost more slowly. Detection of cytosine at fast time points is complicated by the fact that chemical quenches to halt the reaction would catalyze breakdown of the nucleotide intermediates.

Revisiting the kinetics of AdoCbl consumption and formation of the Co(II) species is also warranted. The formation of an apparent steady-state of ~0.7 equiv. of cob(II)alamin species by 200 ms was observed in previous studies in this system by stopped-flow UV-vis spectroscopy, and 0.7 equiv. of a cob(II)alamin-nucleotide radical coupled species is observed by stopped flow EPR.⁽⁶⁹⁾ If the cob(II) species seen at this time is the species which forms a covalent linkage to C419, it should be possible to correlate the disappearance of this species on a s to min timescale to the formation of the peptide bound species.

Further characterization of the nucleotide radical species formed over the course of this reaction has the potential to give a great deal of information on the details of the mechanism. High-field EPR and the use of isotopically labeled derivatives of F₂CTP have the potential to give information beyond that already observed in this system.⁽⁶⁹⁾ Structural characterization of the radical formed on long time scales could confirm the presence of the proposed glycoaldehyde

radical product (Figure 6-4), and rapid freeze quench (RFQ) methods on the ms timescale have the further potential to identify radical intermediates generated early in the reaction pathway. The interpretation of these EPR spectra is complicated by exchange-coupling between cob(II)alamin and thiyl radicals and cob(II)alamin and nucleotide radicals. The distribution of radical species present at each time point has not been established.(69) Thus the ability to examine the radical at high field (130 GHz) on the ms and s timescales is also desired. Collaboration with the Gerfen laboratory (Albert Einstein College of Medicine) has begun to address these issues. His lab has developed a method for packing high-field EPR tubes from RFQ samples on the μ s to ms timescales(155) and is presently examining the radical species generated during the inactivation of F₂CTP with RTPR.(153) Preliminary results on the structure of the 20s radical using 1'-[²H]-F₂CTP indicates a coupling of the deuterium to the radical detected by D-ENDOR spectroscopy (Appendix 2). No coupling is observed using 3'-[²H]-F₂CTP. Analysis of the 130 GHz H-ENDOR spectrum shows hyperfine interactions of 20 G and 4 G to the radical. The 20 G coupling disappears when 1'-[²H]-F₂CTP is used, replaced by a 3.1 G deuterium coupling. The results are thus far consistent with the proposed glycoaldehyde-type radical **6-10**.(153) Work is underway to prepare high-field samples at different time points on the ms scale.

Finally, studies on model systems have the potential to provide insight on this mechanism. Rapid flow EPR studies similar to the original Gilbert and Norman investigations(156, 157) of radical formation upon the oxidation of ethylene glycol, β -chloroethanol, and related species by hydrogen peroxide/titanous ion could be repeated using commercially available β -difluoroethanol. EPR spectroscopy could be employed to monitor the formation of the glycoaldehyde radical, and GC-MS investigation of the end products could give

insight into the formation of the cytidine species trapped in the current studies. Additionally, generation of a semidione radical(158) and its trapping with NaBD₄ can determine whether such a radical precursor could give rise to the deuterium incorporation pattern observed in the small molecule trapping experiments. Further information on the mechanism could be gained from running the inactivation of RTPR with F₂CTP in the presence of [¹⁷O] water or oxygen gas and trapping with NaBH₄ as described above. These experiments would allow conclusive determination of the source of the oxygen at 2' of the trapped nucleotide: water as proposed in Figure 6-4, or oxygen as a result of the oxidation of the 2'-unsubstituted radical proposed to form in the alkylative mechanism (Figure 6-3) or another mechanism. EPR analysis and DFT calculations of the radical formed under these conditions would also give further evidence for the structure of the proposed stable radical, and its connection to the nucleoside product isolated after NaBH₄ quench.

Conclusions

The use of isotopically labeled F₂CTP has allowed the first quantitative analysis of the products of the inactivation of RTPR by this inhibitor. Use of 5-[³H]-F₂CTP allowed identification of cytosine release from the sugar ring on a rapid (s to min) timescale. Use of 1'-[³H]-F₂CTP revealed that inactivation is accompanied by only partial (0.45 equiv.) alkylation of RTPR by fragments derived from the ribose ring, supporting the proposal that multiple modes of inactivation are present. The 1'-[³H]-F₂CTP was further used to identify the soluble and protein-bound products generated during inactivation. The solution product trapped when the inactivation was quenched with NaBH₄ has provided evidence that not only are both fluorines rapidly eliminated from F₂CTP as previously observed,(69) but an oxygen, possibly from water,

is added to the 2' position. The protein-bound product shows a different result, proposed to be generated by alkylation with a furanone-like precursor on the C-terminal tail cysteines of RTPR. The alkylation by F₂CTP appears to account for only half the inactivation, indicating the covalent modification of C419S accounts for the remainder. An early intermediate may partition into two different pathways: one, the reduction of an initially formed nucleotide radical species which can alkylate RTPR by conjugate addition, or two, the release of the nucleotide species into the solution followed by the reaction of cob(II)alamin with a protein-based thiyl radical. The characterization of these products has for the first time allowed the proposal of a mechanistic model to describe this inactivation, paving the way for further studies into the details of the reaction.

6.5 References

- (1) Hertel, L. W., Kroin, J. S., Grossman, C. S., Grindey, G. B., Door, A. F., Storinolo, A. M. V., Plunkett, W., Gandhi, V., and Huang, P. (1996) Synthesis and biological activity of 2',2'-difluorodeoxycytidine (gemcitabine), in *Biomedical Frontiers of Fluorine Chemistry* (Ojima, I., McCarthy, J. R., and Welch, J. T., Eds.), American Chemical Society, Washington, D. C.
- (2) Plunkett, W., Huang, P., and Gandhi, V. (1997) Gemcitabine: actions and interactions. *Nucleosides Nucleotides* 16, 1261-1270.
- (3) Sunkara, P. S., Lippert, B. J., Snyder, R. D., Jarvi, E. T., and Farr, R. A. (1988) Antitumor-activity of 2'-deoxy-2',2'-difluorocytidine, a novel inhibitor of ribonucleotide reductase. *Proceedings of the American Association for Cancer Research* 29, 324-324.
- (4) Szekeres, T., Fritzer-Szekeras, M., and Elford, H. L. (1997) The enzyme ribonucleotide reductase and anti-HIV therapy. *Crit. Rev. Clin. Lab. Sci.* 34, 503-528.
- (5) Licht, S., and Stubbe, J. (1999) Mechanistic investigations of ribonucleotide reductases, in *Comprehensive Natural Products Chemistry* (Barton, S. D., Nakanishi, K., Meth-Cohn, O., and Poulter, C. D., Eds.) pp 163-203, Elsevier Science, New York.
- (6) Robertson, J. G. (2005) Mechanistic basis of enzyme-targeted drugs. *Biochemistry* 44, 5561-5571.
- (7) Cerqueira, N. M. F. S. A., Pereira, S., Fernandes, P. A., and Ramos, M. J. (2005) Overview of ribonucleotide reductase inhibitors: an appealing target in anti-tumor therapy. *Curr. Med. Chem.* 12, 1283-1294.

- (8) Robins, M. J., Samano, M. C., and Samano, V. (1995) Ribonucleotide reductase targets for chemotherapy: mechanistic aspects and biologically active agents. *Nucleosides Nucleotides* 14, 485-493.
- (9) Cory, J. G. (1988) Ribonucleotide reductase as a chemotherapeutic target. *Adv. Enzyme Regul.* 27, 437-455.
- (10) Shao, J., Zhou, B., Chu, B., and Yen, Y. (2006) Ribonucleotide reductase inhibitors and future drug design. *Curr. Drug Targets* 6, 409-431.
- (11) Hertel, L. W., Kroin, J. S., Misner, J. W., and Tustin, J. M. (1988) Synthesis of 2-deoxy-2,2-difluoro-D-ribose and 2-deoxy-2,2-difluoro-D-ribofuranosyl nucleosides. *J. Org. Chem.* 53, 2406-2409.
- (12) Frohlich, R., Rosen, T. C., Meyer, O. G. J., Rissanen, K., and Haufe, G. (2006) New indications for the potential involvement of C-F-bonds in hydrogen bonding. *Journal of Molecular Structure* 787, 50-62.
- (13) Bohm, H. J., Banner, D., Bendels, S., Kansy, M., Kuhn, B., Muller, K., Obst-Sander, U., and Stahl, M. (2004) Fluorine in medicinal chemistry. *Chembiochem* 5, 637-643.
- (14) Dunitz, J. D. (2004) Organic fluorine: Odd man out. *Chembiochem* 5, 614-621.
- (15) Walsh, C. (1982) Suicide substrates - mechanism-based enzyme inactivators. *Tetrahedron* 38, 871-909.
- (16) Matsuda, A., and Sasaki, T. (2004) Antitumor activity of sugar-modified cytosine nucleosides. *Cancer Sci.* 95, 105-111.
- (17) Hui, Y. F., and Reitz, J. (1997) Gemcitabine: A cytidine analogue active against solid tumors. *Am. J. Health-Syst. Pharm.* 54, 162-170.
- (18) Barlési, F., Jacot, W., Astoul, P., and Pujol, J.-L. (2006) Second-line treatment for advanced non-small cell lung cancer: a systematic review. *Lung Cancer* 51, 159-172.
- (19) Rosti, G. (2006) Small cell lung cancer. *Annal. Oncol.* 17, 5-10.
- (20) Barlési, F., and Pujola, J.-L. (2005) Combination of chemotherapy without platinum compounds in the treatment of advanced non-small cell lung cancer: a systematic review of phase III trials. *Lung Cancer* 49, 289-298.
- (21) Cersosimo, R. J. (2002) Lung cancer: A review. *Am. J. Health-Syst. Pharm.* 59, 611-642.
- (22) Sebastiani, V., Ricci, F., Rubio-Viquiera, B., Kulesza, P., Yeo, C. J., Hidalgo, M., Klein, A., Laheru, D., and Iacobuzio-Donahue, C. A. (2006) Immunohistochemical and genetic evaluation of deoxycytidine kinase in pancreatic cancer: relationship to molecular mechanisms of gemcitabine resistance and survival. *Clin. Cancer Res.* 12, 2492-2497.
- (23) Bergenfeldt, M. (2006) Current state of adjuvant therapy in resected pancreatic adenocarcinoma. *Acta Oncol.* 45, 124-135.
- (24) Lidestahl, A. (2006) Efficacy of systemic therapy in advance pancreatic carcinoma. *Acta Oncol.* 45, 136-143.
- (25) Akada, M., Crnogorac-Jurcevic, T., Lattimore, S., Mahon, P., Lopes, R., Sunamura, M., Matsuno, S., and Lemoine, N. R. (2005) Intrinsic chemoresistance to gemcitabine is associated with decreased expression of BNIP3 in pancreatic cancer. *Clin. Cancer Res.* 11, 3094-3101.
- (26) Shore, S., Raraty, M. G. T., Ghaneh, P., and Neoptolemos, J. P. (2003) Chemotherapy for pancreatic cancer. *Aliment Pharmacol. Ther.* 18, 1049-1069.
- (27) Donghui Li, K. X., Wolff, R., and Abbruzzese, J. L. (2004) Pancreatic cancer. *Lancet* 63, 1049-1057.

- (28) Akerele, C. E., Rybalova, I., Kaufman, H. L., and Mani, S. (2003) Current approaches to novel therapeutics in pancreatic cancer. *Invest. New Drugs* 21, 113-129.
- (29) de Braud, F., Maffezzini, M., Vitale, V., Bruzzi, P., Gatta, G., Hendry, W. F., and Sternberg, C. N. (2002) Bladder cancer. *Crit. Rev. Oncol. Hematol.* 41, 89-106.
- (30) Juffs, H. G., Moore, M. J., and Tannock, I. F. (2002) The role of systemic chemotherapy in the management of muscle-invasive bladder cancer. *Lancet Oncol.* 3, 738-747.
- (31) Witjes, J. A., Vriesema, J. L. J., van der Heijden, A. G., Peters, G. J., and Schalken, J. A. (2003) Pharmacokinetics of intravesical gemcitabine: a preclinical study in pigs. *Eur. Urol.* 44, 615-619.
- (32) Barniaas, A. (2006) Systemic chemotherapy in inoperable or metastatic bladder cancer. *Annal. Oncol.* 17, 553-561.
- (33) Rosenberg, J. E., Carroll, P. R., and Small, E. J. (2005) Update on chemotherapy for advanced bladder cancer. *J. Urol.* 174, 14-20.
- (34) Yılmaz, B., Kadioğlu, Y. Y., and Aksoy, Y. (2004) Investigation of the pharmacokinetics of gemcitabine and 2',2'-difluorodeoxyuridine in human plasma by liquid chromatography. *Anal. Biochem.* 332, 234-237.
- (35) Hussain, S. A., and James, N. D. (2003) The systemic treatment of advanced and metastatic bladder cancer. *Lancet Oncol.* 4, 489-487.
- (36) Schrader, A. J., Varga, Z., Hegele, A., Pfoertner, S., Olbert, P., and Hofmann, R. (2006) Second-line strategies for metastatic renal cell carcinoma: classics and novel approaches. *J. Cancer Res. Clin. Oncol.* 132, 137-149.
- (37) Nabhan, C., Krett, N., Gandhi, V., and Rosen, S. (2001) Gemcitabine in hematologic malignancies. *Curr. Opin. Oncol.* 13, 514-521.
- (38) Harries, M., and Gore, M. (2002) Part II: chemotherapy for epithelial ovarian cancer—treatment of recurrent disease. *Lancet Oncol.* 3, 537-545.
- (39) Fruscella, E., Gallo, D., Ferrandina, G., D'Agostino, G., and Scambia, G. (2003) Gemcitabine: current role and future options in the treatment of ovarian cancer. *Crit. Rev. Oncol. Hematol.* 48, 81-88.
- (40) Swaby, R. F., and Bhalla, K. N. (2005) Importance of rational pre-clinical development. *Cancer Biol. Ther.* 4, 872-873.
- (41) Colomer, R. (2005) Gemcitabine plus taxane combination in metastatic breast cancer: a comprehensive review. *EJC Suppl.* 3, 9-16.
- (42) Plunkett, W., Huang, P., Xu, Y.-Z., Heinemann, V., Grunewald, R., and Gandhi, V. (1995) Gemcitabine: metabolism, mechanisms of action, and self-potentiation. *Sem. Oncol.* 2, 3-10.
- (43) Ruiz van Haperen, V. W. T., Veerman, G., Vermorcken, J. B., and Peters, G. J. (1993) 2',2'-Difluoro-deoxycytidine (gemcitabine) incorporation into RNA and DNA of tumor cell lines. *Biochem. Pharmacol.* 46, 762-766.
- (44) Huang, P., Chubb, S., Hertel, L. W., Grindey, G. B., and Plunkett, W. (1991) Action of 2',2'-difluorodeoxycytidine on DNA synthesis. *Cancer Res.* 51, 6110-6117.
- (45) Ross, D. D., and Cuddy, D. P. (1994) Molecular effects of 2'-2'-difluorodeoxycytidine (gemcitabine) on DNA replication in intact HL-60 cells. *Biochem. Pharmacol.* 48, 1619-1630.
- (46) Richardson, K. A., Vega, T. P., Richardson, F. C., Moore, C. L., Rohloff, J. C., Tomkinson, B., Bendele, R. A., and Kuchta, R. D. (2004) Polymerization of the

- triphosphates of AraC, 2',2'-difluorodeoxycytidine (dFdC) and OSI-7836 (T-araC) by human DNA polymerase A and DNA primase. *Biochem. Pharmacol.* 68, 2337-2346.
- (47) Miura, S., and Izuta, S. (2004) DNA polymerases as targets of anticancer nucleosides. *Curr. Drug Targets* 5, 191-195.
- (48) Iwasaki, H., Huang, P., Keating, M. J., and Plunkett, W. (1997) Differential incorporation of ara-C, gemcitabine, and fludarabine into replicating and repairing DNA in proliferating human leukemia cells. *Blood* 90, 270-278.
- (49) Ruiz van Haperen, V. W., Veerman, G., Boven, E., Noordhuis, P., Vermorken, J. B., and Peters, G. J. (1994) Schedule dependence of sensitivity to 2',2'-difluorodeoxycytidine (gemcitabine) in relation to accumulation and retention of its triphosphate in solid tumour cell lines and solid tumours. *Biochem. Pharm.* 48, 1327-1339.
- (50) van Moorsel, C. J. A., Bergman, A. M., Veerman, G., Voorn, D. A., Ruiz van Haperen, V. W. T., Kroep, J. R., Pinedo, H. M., and Peters, G. J. (2000) Differential effects of gemcitabine on ribonucleotide pools of twenty-one solid tumour and leukaemia cell lines. *Biochim. Biophys. Acta* 1474, 5-12.
- (51) Gandhi, V., Legha, J., Chen, F., Hertel, L. W., and Plunkett, W. (1996) Excision of 2',2'-difluorodeoxycytidine (gemcitabine) monophosphate residues from DNA. *Cancer Res.* 56, 4453-4459.
- (52) Cappella, P., Tomasoni, D., Faretta, M., Lupi, M., Montalenti, F., Viale, F., Banzato, F., D'incalci, M., and Ubezio, P. (2001) Cell cycle effects of gemcitabine. *Int. J. Cancer* 93, 401-408.
- (53) Bandala, E., Espinosa, M., Maldonado, V., and Meléndez-Zajgla, J. (2001) Inhibitor of apoptosis-1 (IAP-1) expression and apoptosis in non-small-cell lung cancer cells exposed to gemcitabine. *Biochem. Pharmacol.* 62, 13-19.
- (54) Auer, H., Oehler, R., Lindner, R., Kowalski, H., Sliutz, G., Orel, L., Kucera, E., Simon, M. M., and Glossl, J. (1997) Characterization of genotoxic properties of 2',2'-difluorocytidine. *Mutat. Res.* 393, 165-173.
- (55) Huang, P., and Plunkett, W. (1995) Fludarabine- and gemcitabine-induced apoptosis: incorporation of analogues into DNA is a critical event. *Cancer Chemother. Pharmacol.* 36, 181-188.
- (56) Habiro, A., Tanno, S., Koizumi, K., Izawa, T., Nakano, Y., Osanai, M., Mizukami, Y., Okumura, T., and Kohgo, Y. (2004) Involvement of p38 mitogen-activated protein kinase in gemcitabine-induced apoptosis in human pancreatic cancer cells. *Biochem. Biophys. Res. Commun.* 316, 71-77.
- (57) Duxbury, M. S., Ito, H., Benoit, E., Waseem, T., Ashley, S. W., and Whang, E. E. (2004) A Novel Role for Carcinoembryonic Antigen-Related Cell Adhesion Molecule 6 as a Determinant of Gemcitabine Chemoresistance in Pancreatic Adenocarcinoma Cells. *Cancer Res.* 64, 3987-3993.
- (58) Pourquier, P., Gioffre, C., Kohlhagen, G., Urasaki, Y., Goldwasser, F., Hertel, L. W., Yu, S., Pon, R. T., Gmeiner, W. H., and Pommier, Y. (2002) Gemcitabine (2',2'-difluoro-2'-deoxycytidine), an antimetabolite that poisons topoisomerase I. *Clin. Cancer Res.* 8, 2499-2504.
- (59) Cory, A. H., and Cory, J. G. (2004) Gemcitabine-induced apoptosis in a drug-resistant mouse leukemia L1210 cell line that does not express p53. *Adv. Enzyme Regul.* 44, 11-25.

- (60) Chandler, N. M., Canete, J. J., and Callery, M. P. (2004) Caspase-3 drives apoptosis in pancreatic cancer cells after treatment with gemcitabine. *J. Gastrointest. Surgery* 8, 1072-1078.
- (61) Wachters, F. M., Putten, J. W. G. V., Maring, J. G., Zdzienicka, M. Z., Groen, H. J. M., and Kampinga, H. H. (2003) Selective targeting of homologous DNA recombination repair by gemcitabine. *Int. J. Radiat. Oncol. Biol. Phys.* 57, 553-562.
- (62) Crul, M., van Waardenburg, R. C. A. M., Boexe, S., van Eijndhoven, M. A. J., Pluim, D., Beijnen, J. H., and Schellens, J. H. M. (2003) DNA repair mechanisms involved in gemcitabine cytotoxicity and in the interaction between gemcitabine and cisplatin. *Biochem. Pharmacol.* 65, 275-282.
- (63) Sun, D., Urrabaz, R., Kelly, S., Nguyen, M., and Weitman, S. (2002) Enhancement of DNA ligase I level by gemcitabine in human cancer cells. *Clin. Cancer Res.* 8, 1189-1195.
- (64) Cartee, L., and Kucera, G. L. (1998) Gemcitabine induces programmed cell death and activates protein kinase C in BG-1 human ovarian cancer cells. *Cancer Chemother. Pharmacol.* 41, 403-412.
- (65) Heinemann, V., Hertel, L. W., Grindey, G. B., and Plunkett, W. (1988) Comparison of the cellular pharmacokinetics and toxicity of 2',2'-difluorocytidine and 1- β -D-arabinofuranosylcytidine. *Cancer Res.* 48, 4024-4031.
- (66) Heinemann, V., Xu, Y.-Z., Chubb, S., Sen, A., Hertel, L. W., Grindey, G. B., and Plunkett, W. (1990) Inhibition of ribonucleotide reduction in CCRF-CEM cells by 2',2'-difluorodeoxycytidine. *Mol. Pharmacol.* 38, 567-572.
- (67) Smid, K., van Moorsel, C. J. A., Noordhuis, P., Voorn, D. A., and Peters, G. J. (2001) Interference of gemcitabine triphosphate with the measurements of deoxynucleotides using an optimised DNA polymerase elongation assay. *Int. J. Oncol.* 19, 157-162.
- (68) van der Donk, W. A., Yu, G., Pérez, L., Sanchez, R. J., and Stubbe, J. (1998) Detection of a new substrate-derived radical during inactivation of ribonucleotide reductase from *Escherichia coli* by gemcitabine 5'-diphosphate. *Biochemistry* 37, 6419-6426.
- (69) Silva, D. J., Stubbe, J., Samano, V., and Robins, M. J. (1998) Gemcitabine 5'-triphosphate is a stoichiometric mechanism-based inhibitor of *Lactobacillus leichmannii* ribonucleoside triphosphate reductase: evidence for thiyl radical-mediated nucleotide radical formation. *Biochemistry* 37, 5528-5535.
- (70) Baker, C. H., Banzon, J., Bollinger Jr., J. M., Stubbe, J., Samano, V., Robins, M. J., Lippert, B., Jarvi, E., and Resvick, R. (1991) 2'-Deoxy-2'-methylencytidine and 2'-Deoxy-2',2'-difluorocytidine 5'-diphosphates: Potent mechanism-based inhibitors of ribonucleotide reductase. *J. Med. Chem.* 34, 1879-1884.
- (71) Artin, E., Thesis. (2006) in *Chemistry*, Massachusetts Institute of Technology, Cambridge, MA.
- (72) Chandra, D., Bratton, S. B., Person, M. D., Tian, Y., Martin, A. G., Ayres, M., Fearnhead, H. O., Gandhi, V., and Tang, D. G. (2006) Intracellular nucleotides act as critical prosurvival factors by binding to cytochrome C and inhibiting apoptosome. *Cell* 125, 1333-1346.
- (73) Galmarini, C. M., Mackey, J. R., and Dumontet, C. (2001) Nucleoside analogues: mechanisms of drug resistance and reversal strategies. *Leukemia* 15, 875-890.
- (74) Bergman, A. M., Pinedo, H. M., and Peters, G. J. (2002) Determinants of resistance to 2',2'-difluorocytidine (gemcitabine). *Drug Resist. Updat.* 5, 19-33.

- (75) Jordheim, L., Galmarini, C. M., and Dumontet, C. (2003) Drug resistance to cytotoxic nucleoside analogues. *Curr. Drug Targets* 4, 443-460.
- (76) Mackey, J. R., Mani, R. S., Selner, M., Mowles, D., Young, J. D., Belt, J. A., Crawford, C. R., and Cass, C. E. (1998) Functional nucleoside transporters are required for gemcitabine influx and manifestation of toxicity in cancer cell lines. *Cancer Res.* 58, 4349-4357.
- (77) Spratlin, J., Sangha, R., Glubrecht, D., Dabbagh, L., Young, J. D., Dumontet, C., Cass, C., Lai, R., and Mackey, J. R. (2004) The absence of human equilibrative nucleoside transporter 1 is associated with reduced survival in patients with gemcitabine-treated pancreas adenocarcinoma. *Clin. Cancer Res.* 10, 6956-6961.
- (78) Burke, T., Lee, S., Ferguson, P. J., and Hammond, J. R. (1998) Interaction of 2',2'-difluorodeoxycytidine (gemcitabine) and formycin B with the Na⁺-dependent and -independent nucleoside transporters of ehrlich ascites tumor cells. *J. Pharmacol. Exp. Ther.* 286, 1333-1340.
- (79) Lostao, M. P., Mata, J. F., Larrayoz, I. M., Inzillo, S. M., Casado, F. J., and Pastor-Anglada, M. (2000) Electrogenic uptake of nucleosides and nucleoside-derived drugs by the human nucleoside transporter 1 (hCNT1) expressed in *Xenopus laevis* oocytes. *FEBS Lett.* 481.
- (80) Mackey, J. R., Yao, S. Y. M., Smith, K. M., Karpinski, E., Baldwin, S. A., Cass, C. E., and Young, J. D. (1999) Gemcitabine transport in xenopus oocytes expressing recombinant plasma membrane mammalian nucleoside transporters. *J. Natl. Cancer Inst.* 91, 1876-1880.
- (81) Gray, J. H., Mangravite, L. M., Owen, R. P., Urban, T. J., Chan, W., Carlson, E. J., Huang, C. C., Kawamoto, M., Johns, S. J., Stryke, D., Ferrin, T. E., and Giacomini, K. M. (2004) Functional and genetic diversity in the concentrative nucleoside transporter, CNT1, in human populations. *Mol. Pharmacol.* 65, 512-519.
- (82) García-Manteiga, J., Molina-Arcas, M., Casado, F. J., Mazo, A., and Pastor-Anglada, M. (2003) Nucleoside transporter profiles in human pancreatic cancer cells: role of hCNT1 in 2',2'-difluorodeoxycytidine-induced cytotoxicity. *Clin. Cancer Res.* 9, 5000-5008.
- (83) Rauchwerger, D. R., Firby, P. S., Hedley, D. W., and Moore, M. J. (2000) Equilibrative-sensitive nucleoside transporter and its role in gemcitabine sensitivity. *Cancer Res.* 60, 6075-6079.
- (84) Graham, K. A., Leithoff, J., Coe, I. R., Mowles, D., Mackey, J. R., Young, J. D., and Cass, C. E. (2000) Differential transport of cytosine-containing nucleosides by recombinant human concentrative nucleoside transporter protein hCNT1. *Nucleosides, Nucleotides Nucleic Acids* 19, 415-434.
- (85) Bouffard, D. Y., Laliberté, J., and Momparler, R. L. (1993) Kinetic Studies on 2',2'-difluorodeoxycytidine (gemcitabine) with purified human deoxycytidine kinase and cytidine deaminase. *Biochem. Pharmacol.* 45, 1857-1861.
- (86) Kirstein, M. N., Hassan, I., Guire, D. E., Weller, D. R., Dagit, J. W., Fisher, J. E., and Remmel, R. P. (2006) High-performance liquid chromatographic method for the determination of gemcitabine and 2',2'-difluorodeoxyuridine in plasma and tissue culture media. *J. Chromatogr. B* 835, 136-142.
- (87) Pauwels, B., Korst, A. E. C., Lardon, F., and Vermorcken, J. B. (2005) Combined modality therapy of gemcitabine and radiation. *Oncologist* 10, 34-51.

- (88) Losaa, R., Sierraa, M. I., Guardadoa, C., Fernández, A., Gíona, M. O., Blancob, D., and Buesa, J. M. (2005) Development and validation of an ion pair HPLC method for gemcitabine and 2',2'-difluoro-2'-deoxyuridine determination. *Anal. Chim. Acta* 528 255-260.
- (89) Heinemann, V., Xu, Y.-Z., Chubb, S., Sen, A., Hertel, L. W., Grindey, G. B., and Plunkett, W. (1992) Cellular elimination of 2'-2'-difluorodeoxycytidine 5'-triphosphate: a mechanism of self-potential. *Cancer Res.* 52, 533-539.
- (90) Xu, Y., Keith, B., and Grem, J. L. (2004) Measurement of the anticancer agent gemcitabine and its deaminated metabolite at low concentrations in human plasma by liquid chromatography-mass spectrometry. *J. Chromatogr. B* 802, 263-270.
- (91) Yilmaz, B., Kadioğlu, Y. Y., and Aksoy, Y. (2003) Simultaneous determination of gemcitabine and its metabolite in human plasma by high-performance liquid chromatography. *J. Chromatogr. B* 791, 103-109.
- (92) van der Wilt, C. L., Kroep, J. R., Bergman, A. M., Loves, W. J. P., Alvarez, E., Talianidis, I., Wriksson, S., van Groeningen, C. J., Pinedo, H. M., and Peters, G. J. (2000) The role of deoxycytidine kinase in gemcitabine toxicity. *Adv. Exper. Med. Biol.* 486, 287-290.
- (93) Al-Madhouna, A. S., van der Wilt, C. L., Loves, W. J. P., Padron, J. M., Eriksson, S., Talianidis, I., and Peters, G. J. (2004) Detection of an alternatively spliced form of deoxycytidine kinase mRNA in the 2'-2'-difluorodeoxycytidine (gemcitabine)-resistant human ovarian cancer cell line AG6000. *Biochem. Pharmacol.* 68, 601-609.
- (94) Ruiz van Haperen, V. W. T., Veerman, G., Eriksson, S., Boven, E., Stegmann, A. P. A., Hermsen, M., Vermorken, J. B., Pinedo, H. M., and Peters, G. J. (1994) Development and molecular characterization of a 2',2'-difluorodeoxycytidine-resistant variant of the human ovarian carcinoma cell line A2780. *Cancer Res.* 54, 4138-4143.
- (95) Goan, Y.-G., Zhou, B., Hu, E., Mi, S., and Yen, Y. (1999) Overexpression of ribonucleotide reductase as a mechanism of resistance to 2,2-difluorodeoxycytidine in the human KB cancer cell line. *Cancer Res.* 59, 4204-4207.
- (96) Bergman, A. M., Pinedo, H. M., Jongsma, A. P. M., Brouwer, M., Ruiz van Haperen, V. W. T., Veerman, G., Leyva, A., Eriksson, L., and Peters, G. J. (1999) Decreased resistance to gemcitabine (2',2'-difluorodeoxycytidine) of cytosine arabinoside-resistant myeloblastic murine and rat leukemia cell lines: role of altered activity and substrate specificity of deoxycytidine kinase. *Biochem. Pharmacol.* 57, 397-406.
- (97) Jordheim, L. P., Cros, E., Gouy, M.-H., Galmarini, C. M., Peyrottes, S., Mackey, J., Perigaud, C., and Dumontet, C. (2004) Characterization of a gemcitabine-resistant murine leukemic cell line: reversion of *in vitro* resistance by a mononucleotide prodrug. *Clin. Cancer Res.* 10, 5614-5621.
- (98) Kroep, J. R., Loves, W. J. P., van der Wilt, C. L., Alvarez, E., Talianidis, I., Boven, E., Braakhuis, B. J. M., van Groeningen, C. J., Pinedo, H. M., and Peters, G. J. (2002) Pretreatment deoxycytidine kinase levels predict *in vivo* gemcitabine sensitivity. *Mol. Cancer Ther.* 1, 371-376.
- (99) Jordheim, L. P., Guittet, O., Lepoivre, M., Galmarini, C. M., and Dumontet, C. (2005) Increased expression of the large subunit of ribonucleotide reductase is involved in resistance to gemcitabine in human mammary adenocarcinoma cells. *Mol. Cancer Ther.* 4, 1268-1276.

- (100) Davidson, J. D., Ma, L., Flagella, M., Geeganage, S., Gelbert, L. M., and Slapak, C. A. (2004) An increase in the expression of ribonucleotide reductase large subunit 1 is associated with gemcitabine resistance in non-small cell lung cancer cell lines. *Cancer Res.* 64, 3761-3766.
- (101) Bergman, A. M., Eijk, P. P., Ruiz van Haperen, V. W. T., Smid, K., Veerman, G., Hubeek, I., van den IJssel, P., Ylstra, B., and Peters, G. J. (2005) *In vivo* induction of resistance to gemcitabine results in increased expression of ribonucleotide reductase subunit m1 as the major determinant. *Cancer Res.* 65, 9510-9516.
- (102) Beppler, G., Zheng, Z., Gautam, A., Sharma, S., Cantor, A., Sharma, A., Cress, W. D., Kim, Y.-C., Rosell, R., McBride, C., Robinson, L., Sommers, E., and Haura, E. (2005) Ribonucleotide reductase M1 gene promoter activity, polymorphisms, population frequencies, and clinical relevance. *Lung Cancer* 47, 183-192.
- (103) Duxbury, M. S., Ito, H., Zinner, M. J., Ashley, S. W., and Whang, E. E. (2004) RNA interference targeting the M2 subunit of ribonucleotide reductase enhances pancreatic adenocarcinoma chemosensitivity to gemcitabine. *Oncogene* 23, 1539-1548.
- (104) Zhou, B., Mo, X., Liu, X., Qiu, W., and Yen, Y. (2001) Human ribonucleotide reductase M2 subunit gene amplification and transcriptional regulation in a homogeneous staining chromosome region responsible for the mechanism of drug resistance. *Cytogenet. Cell Genet.* 95, 34-42.
- (105) Rosell, R., Danenberg, K. D., Alberola, V., Beppler, G., Sanchez, J. J., Camps, C., Provencio, M., Isla, D., Taron, M., Diz, P., and Artal, A. (2004) Ribonucleotide reductase messenger RNA expression and survival in gemcitabine/cisplatin-treated advanced non-small cell lung cancer patients. *Clin. Cancer Res.* 10, 1318-1325.
- (106) Cory, A. H., Hertel, L. W., Kroin, J. S., and Cory, J. G. (1993) Effects of 2',2'-difluorodeoxycytidine (gemcitabine) on wild type and variant mouse leukemia L1210 cells. *Oncol. Res.* 5, 59-63.
- (107) Wong, S. J., Myette, M. S., Wereley, J. P., and Chitambar, C. R. (1999) Increased sensitivity of hydroxyurea-resistant leukemic cells to gemcitabine. *Clin. Cancer Res.* 5, 439-443.
- (108) Alexander, R. L., Greene, B. T., Torti, S. V., and Kucera, G. L. (2005) A novel phospholipid gemcitabine conjugate is able to bypass three drug-resistance mechanisms. *Cancer Chemother. Pharmacol.* 56, 15-21.
- (109) Cavallaro, G., Mariano, L., Salmaso, S., Caliceti, P., and Gaetano, G. (2006) Folate-mediated targeting of polymeric conjugates of gemcitabine. *Int. J. Pharm.* 307, 258-269.
- (110) Ali, S. M., Khan, A. R., Ahmad, M. U., Chen, P., Sheikh, S., and Ahmad, I. (2005) Synthesis and biological evaluation of gemcitabine-lipid conjugate (NEO6002). *Bioorg. Med. Chem. Lett.* 15, 2571-2574.
- (111) Bergman, A. M., Kuiper, C. M., Noordhuis, P., Smid, K., Voorn, D. A., Comijn, E. M., Mÿhren, F., Sandvold, M. L., Hendriks, H. R., Fodstad, Ø., Breistøl, K., and Peters, G. J. (2004) Antiproliferative activity and mechanism of action of fatty acid derivatives of gemcitabine in leukemia and solid tumor cell lines and in human xenografts. *Nucleosides, Nucleotides Nucleic Acids* 23, 1329-1333.
- (112) Alexander, R. L., Morris-Natschke, S. L., Ishaq, K. S., Fleming, R. A., and Kucera, G. L. (2003) Synthesis and cytotoxic activity of two novel 1-dodecylthio-2-decyloxypropyl-3-phosphatidic acid conjugates with gemcitabine and cytosine arabinoside. *J. Med. Chem.* 46, 4205-4208.

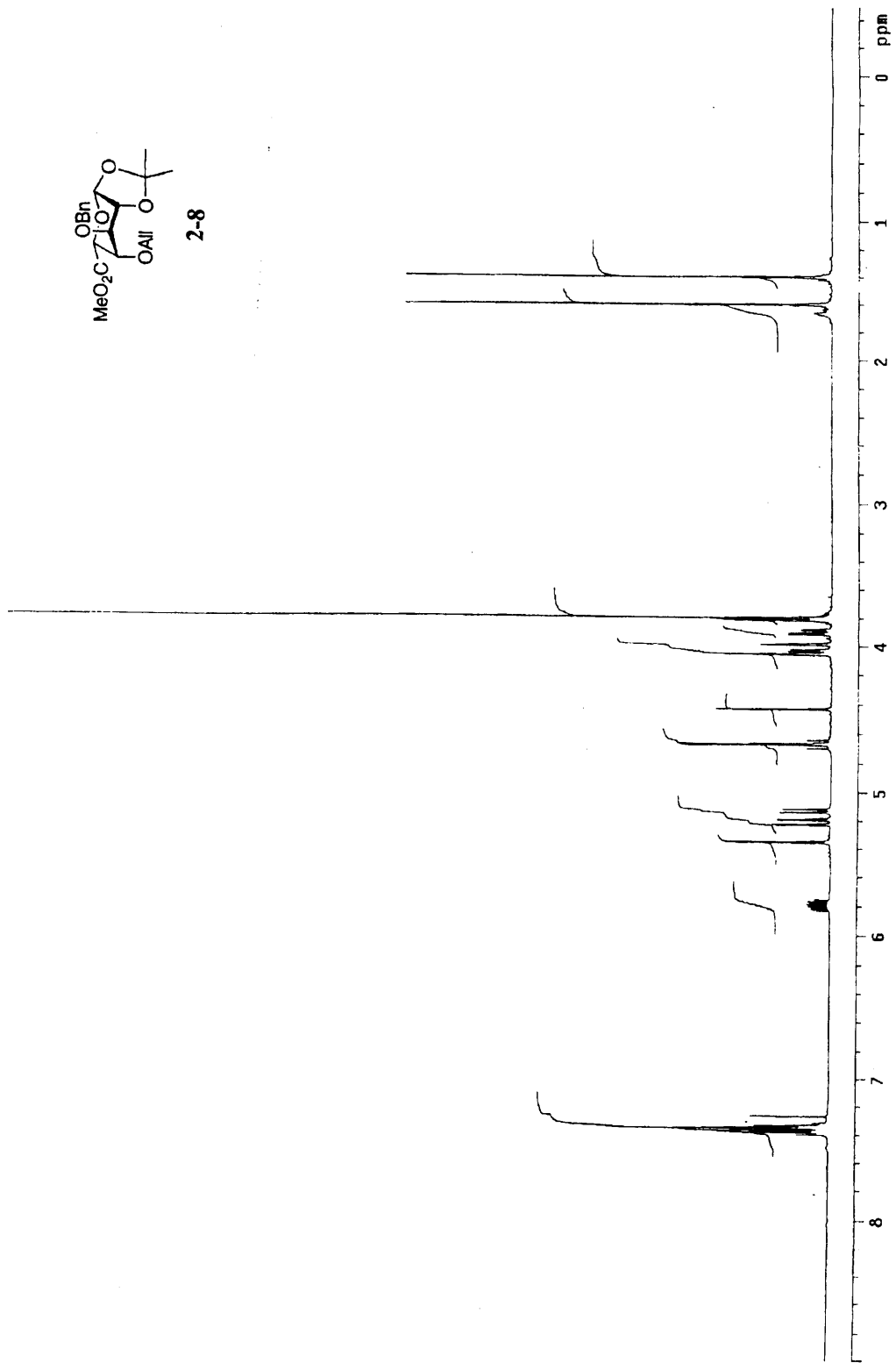
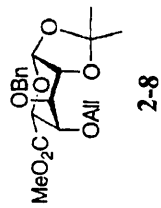
- (113) Liou, J.-Y., Dutschman, G. E., Lam, W., Jiang, Z., and Cheng, Y.-C. (2002) Characterization of human UMP/CMP kinase and its phosphorylation of D- and L-form deoxycytidine analogue monophosphates. *Cancer Res.* *62*, 1624-1633.
- (114) Hsu, C.-H., Liou, J.-Y., Dutschman, G. E., and Cheng, Y.-C. (2005) Phosphorylation of cytidine, deoxycytidine, and their analog monophosphates by human UMP/CMP kinase is differentially regulated by ATP and magnesium. *Mol. Pharmacol.* *67*, 806-814.
- (115) Segura-Peña, D., Sekulic, N., Ort, S., Konrad, M., and Lavie, A. (2004) Substrate-induced conformational changes in human UMP/CMP kinase. *J. Biol. Chem.* *279*, 33882-33889.
- (116) Pereira, S., Fernandes, P. A., and Ramos, M. J. (2004) Mechanism for ribonucleotide reductase inactivation by the anticancer drug gemcitabine. *J. Comput. Chem.* *25*, 1286-1294.
- (117) Stubbe, J., and Kozarich, J. W. (1980) Fluoride, pyrophosphate, and base release from 2'-deoxy-2'-fluoronucleoside 5'-diphosphates by ribonucleoside-diphosphate reductase. *J. Biol. Chem.* *255*, 5511-5513.
- (118) Harris, G., Ashley, G. W., Robins, M. J., Tolman, R. L., and Stubbe, J. (1987) 2'-Deoxy-2'-halonucleotides as alternate substrates and mechanism-based inactivators of *Lactobacillus leichmannii* ribonucleotide reductase. *Biochemistry* *26*, 1895-1902.
- (119) Fernandes, P. A., and Ramos, M. J. (2004) Theoretical insights into the mechanism for thiol/disulfide exchange. *Chem. Euro. J.* *10*, 257-266.
- (120) Thelander, L., Larsson, B., Hobbs, J., and Eckstein, F. (1976) Active site of ribonucleoside diphosphate reductase from *Escherichia coli*: inactivation of the enzyme by 2'-substituted ribonucleoside diphosphates. *J. Biol. Chem.* *251*, 1398-1405.
- (121) Stubbe, J., and Kozarich, J. W. (1980) Inorganic pyrophosphate is released from 2'-chloro-2'-deoxyuridine 5'-diphosphate by ribonucleoside diphosphate reductase. *J. Am. Chem. Soc.* *102*, 2505-2507.
- (122) Harris, G., Ator, M., and Stubbe, J. (1984) Mechanism of inactivation of *Escherichia coli* and *Lactobacillus leichmannii* ribonucleotide reductases by 2'-chloro-2'-deoxynucleotides: evidence for generation of 2-methylene-3(2H)-furanone. *Biochemistry* *23*, 5214-5225.
- (123) Ator, M. A., and Stubbe, J. (1985) Mechanism of inactivation of *Escherichia coli* ribonucleotide reductase by 2'-chloro-2'-deoxyuridine 5'-diphosphate: evidence for generation of 2'-deoxy-3'-ketonucleotide via a net 1,2 hydrogen shift. *Biochemistry* *24*, 7214-7221.
- (124) Akhlaq, M. S., Al-Baghdadi, S., and von Sonntag, C. (1987) On the attack of hydroxyl radicals on polyhydric alcohols and sugars and the reduction of the so-formed radicals by 1,4-dithiothreitol. *Carbohydr. Res.* *164*, 71-83.
- (125) Xu, H., Faber, C., Uchiki, T., Racca, J., and Dealwis, C. (2006) Structures of eukaryotic ribonucleotide reductase I define gemcitabine diphosphate binding and subunit assembly. *Proc. Natl. Acad. Sci. U. S. A.* *103*, 4028-4033.
- (126) Dolbier Jr., W. R. (1996) Structure, reactivity, and chemistry of fluoroalkyl radicals. *Chem. Rev.* *96*, 1557-1584.
- (127) Tedder, J. M. (1982) The importance of polarity, bond strength and steric effects in determining the site of attack and the rate of free radical substitution in aliphatic compounds. *Tetrahedron* *38*, 313-329.

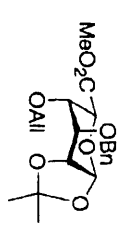
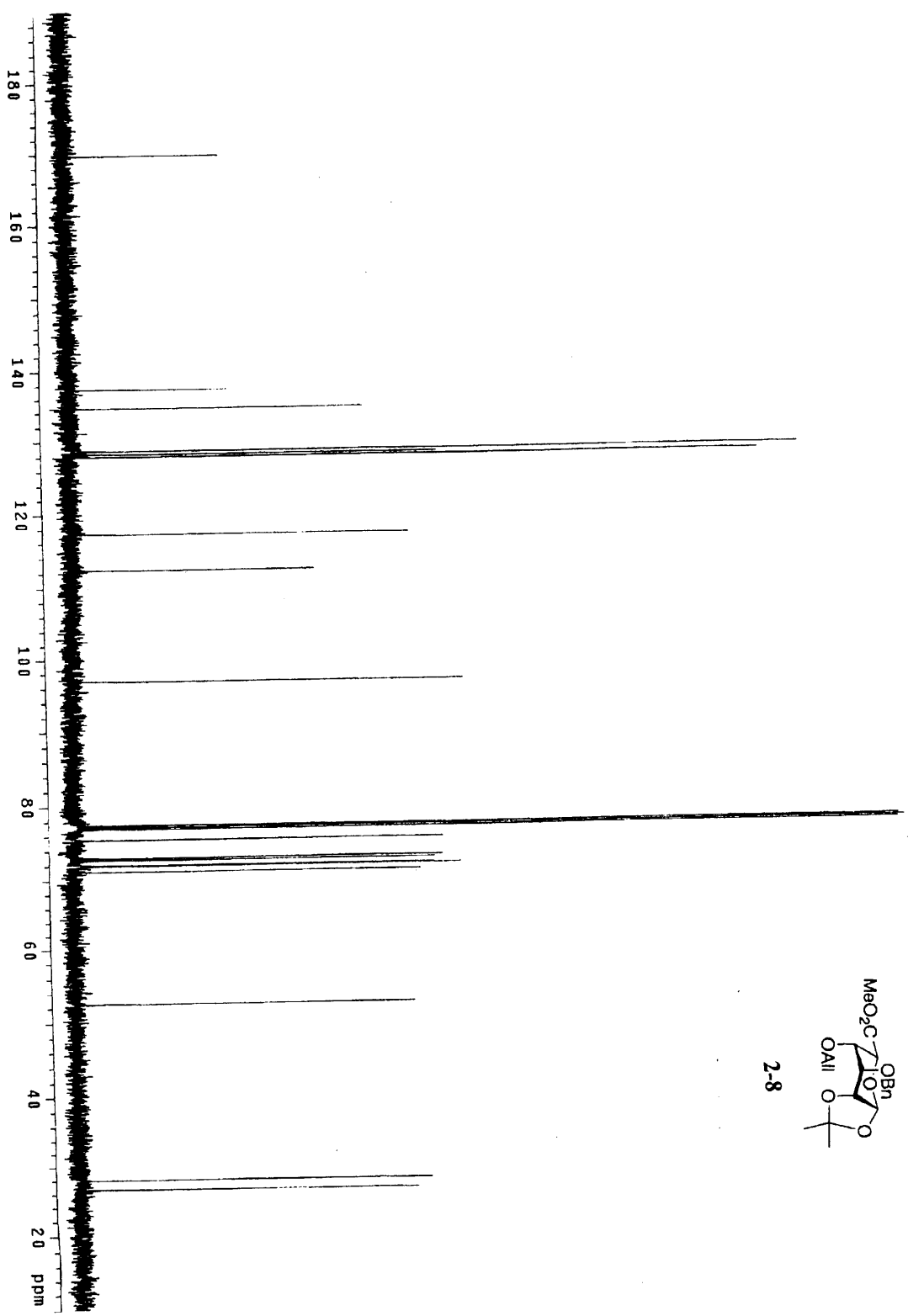
- (128) Chatgililoglu, C., Guerrini, A., and Lucarini, M. (1992) The trimethylsilyl substituent effect on the reactivity of silanes. Structural correlations between silyl radicals and their parent silanes. *J. Org. Chem.* 57, 3405-3409.
- (129) Abend, A., Bandarian, V., Reed, G. H., and Frey, P. A. (2000) Identification of *cis*-ethanesemidione as the organic radical derived from glycolaldehyde in the suicide inactivation of dioldehydrase and of ethanolamine ammonia-lyase. *Biochemistry* 39, 6250-6257.
- (130) Sandala, G. M., Smith, D. M., Coote, M. L., Golding, B. T., and Radom, L. (2006) Insights into the hydrogen-abstraction reactions of diol dehydratase: relevance to the catalytic mechanism and suicide inactivation. *J. Am. Chem. Soc.* 128, 3433-3444.
- (131) Lunn, C. A., Kathju, S., Wallace, B. J., Kushnern, S. R., and Pigiet, V. (1984) Amplification and purification of plasmid-encoded thioredoxin from *Escherichia coli* K12. *J. Biol. Chem.* 259, 10469-10474.
- (132) Russel, M., and Model, P. (1985) Direct cloning of the *trxB* gene that encodes thioredoxin reductase. *J. Bacteriol.* 163, 238-242.
- (133) Ge, J., Yu, G., Ator, M. A., and Stubbe, J. (2003) Pre-steady-state and steady-state kinetic analysis of *E. coli* class I ribonucleotide reductase. *Biochemistry* 42, 10071-10083.
- (134) Booker, S., and Stubbe, J. (1993) Cloning, sequencing and expression of the adenosylcobalamin-dependent ribonucleotide reductase from *Lactobacillus leichmannii*. *Proc. Natl. Acad. Sci. U. S. A.* 90, 8352-8356.
- (135) Chou, T. S., Heath, P. C., Patterson, L. E., Poteet, L. M., Lakin, R. E., and Hunt, A. H. (1992) Stereospecific synthesis of 2-deoxy-2,2-difluororibonolactone and its use in the preparation of 2'-deoxy-2',2'-difluoro- β -D-ribofuranosyl pyrimidine nucleosides: the key role of selective crystallization. *Synthesis*, 565-570.
- (136) Dawson, R. M. C., Elliot, D. C., Elliot, W. H., and Jones, K. M. (1986) *Data for biochemical research*, third ed., Clarendon Press, Oxford.
- (137) Licht, S. S., Lawrence, C. C., and Stubbe, J. (1999) Class II ribonucleotide reductases catalyze carbon-cobalt bond reformation on every turnover. *J. Am. Chem. Soc.* 121, 7463-7468.
- (138) Bandarian, V., Ludwig, M. L., and Matthews, R. G. (2003) Factors modulating conformational equilibria in large modular proteins: A case study with cobalamin-dependent methionine synthase. *Proc. Natl. Acad. Sci. U. S. A.* 100, 8156-8163.
- (139) Mass spectrometry described herein and the fragment analysis was performed by Dr. John Leszyk, UMass Medical School, Proteomic Mass Spectrometry Lab, Shrewsbury, MA.
- (140) Data processing was performed using Kompact V. 2.2.1, Kratos Analytical Ltd., Manchester, UK. Fragment searching and analysis was performed by Dr. John Leszyk using Mascot, Matrix Science Ltd., Boston, MA.
- (141) Ireton, G. C., McDermott, G., Black, M. E., and Stoddard, B. L. (2002) The structure of *Escherichia coli* cytosine deaminase. *J. Mol. Biol.* 315, 687-697.
- (142) Smith, D. (2006) Personal Communication.
- (143) Stich, T. A., Brooks, A. J., Buan, N. R., and Brunold, T. C. (2003) Spectroscopic and computational studies of Co^{3+} -corrinoids: spectral and electronic properties of the B-12 cofactors and biologically relevant precursors. *J. Am. Chem. Soc.* 125, 5897-5914.
- (144) Ashley, G. W., Harris, G., and Stubbe, J. (1988) Inactivation of the *Lactobacillus leichmannii* ribonucleoside triphosphate reductase by 2'-chloro-2'-deoxyuridine 5'-

- triphosphate: stoichiometry of inactivation, site of inactivation, and mechanism of the protein chromophore formation. *Biochemistry* 27, 4305-4310.
- (145) Prediction of isotopic distribution made using ChemDraw Ultra V 10.0, CambridgeSoft, 2005.
- (146) Ashcroft, A. E. An Introduction to Mass Spectrometry <http://www.astbury.leeds.ac.uk/facil/MStut/mstutorial.htm>.
- (147) Dass, C. (2004) *An Introduction to Biological Mass Spectrometry*, John Wiley & Sons, USA.
- (148) Stubbe, J., Ator, M., and Krenitsky, T. (1983) Mechanism of ribonucleoside diphosphate reductase from *Escherichia coli*: evidence for 3'-C—H bond cleavage. *J. Biol. Chem.* 258, 1625-1630.
- (149) Stubbe, J., Smith, G., and Blakley, R. L. (1983) Interaction of 3'-[³H]2'-chloro-2'-deoxyuridine 5'-triphosphate with ribonucleotide reductase from *Lactobacillus leichmannii*. *J. Biol. Chem.* 258, 1619-1624.
- (150) Ator, M. A., and Stubbe, J. (1986) Mechanism of ribonucleotide reductase from herpes simplex virus type 1: evidence for 3' carbon-hydrogen bond cleavage and inactivation by nucleotide analogs. *J. Biol. Chem.* 261, 3595-3599.
- (151) Ashley, G. W., Harris, G., and Stubbe, J. (1988) Inactivation of the ribonucleoside triphosphate reductase from *Lactobacillus leichmannii* by 2'-chloro-2'-deoxyuridine 5'-triphosphate: a 3'-2' hydrogen transfer during the formation of 3'-keto-2'-deoxyuridine 5'-triphosphate. *Biochemistry* 27, 7841-7845.
- (152) Dr. John Leszyk, personal communication, 2006.
- (153) Gerfen, G. J., and Manzerova, J. (2006) Unpublished data. Personal communication.
- (154) Ator, M., Salowe, S. P., and Stubbe, J. (1984) 2'-Azido-2'-deoxynucleotide interaction with *E. coli* ribonucleotide reductase: generation of a new radical species. *J. Am. Chem. Soc.* 106, 1886-1887.
- (155) Lin, Y., Gerfen, G. J., Rousseau, D. L., and Yeh, S. R. (2003) Ultrafast microfluidic mixer and freeze-quenching device. *Anal. Chem.* 75, 5381-5386.
- (156) Buley, A. L., Norman, R. O. C., and Pritchett, R. J. (1966) Electron spin resonance studies of oxidation. Part VIII. Elimination reactions of some hydroxyalkyl radicals. *J. Chem. Soc. B*, 849-852.
- (157) Gilbert, C., Larkin, J. P., and R. O. C. Norman. (1972) Electron spin resonance studies. Part XXXIII. Evidence for heterolytic and homolytic transformations of radicals from 1,2-diols and related compounds. *J. Chem. Soc., Perkin Trans. 2*, 794-802.
- (158) West, P. R., Schnarr, G. W., and Sitwell, L. (1977) Semidione radical ion formation in monosaccharide oxidation. An electron spin resonance study. *Tetrahedron Lett.* 44, 3869-3872.

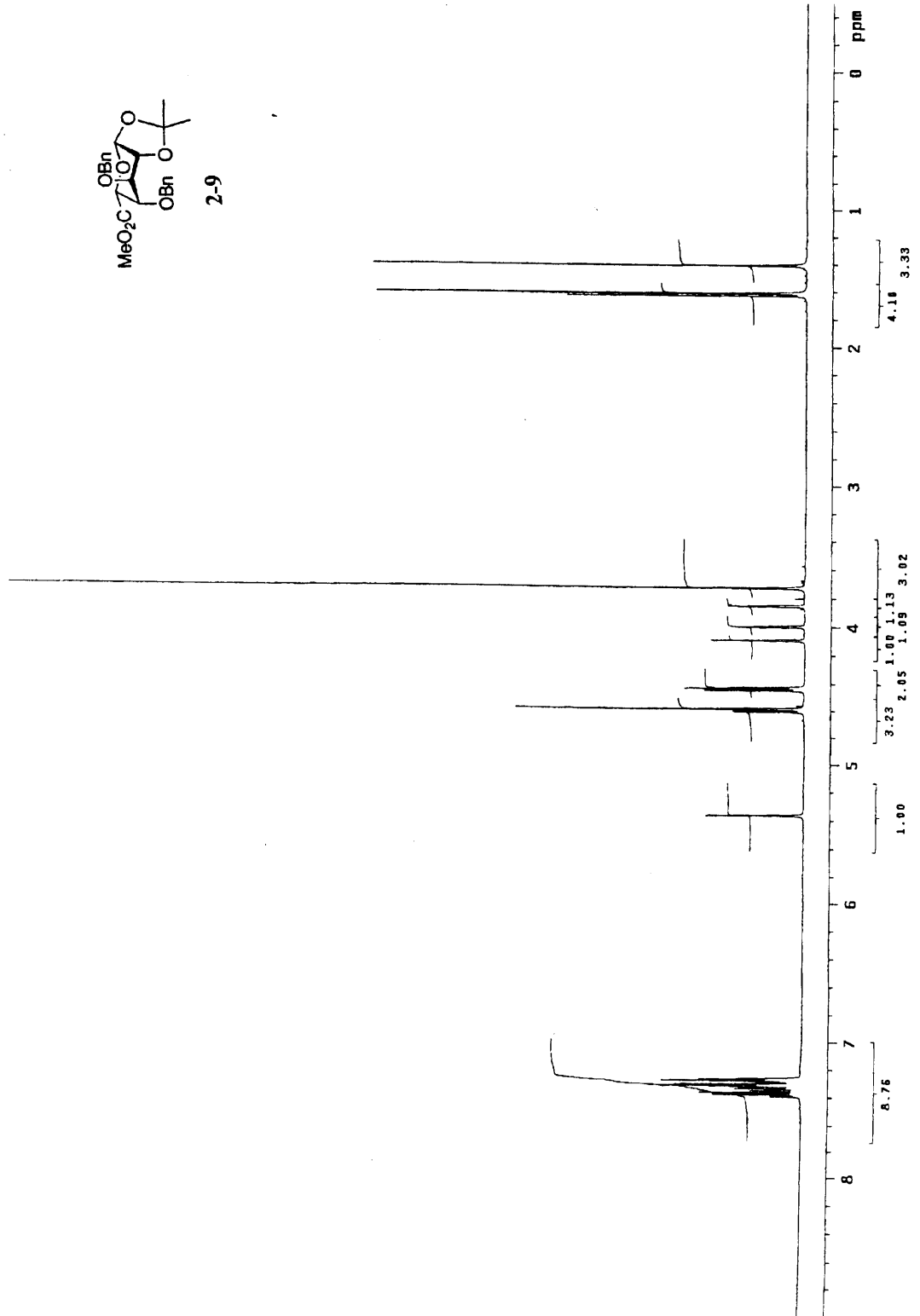
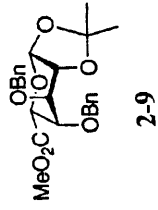
Appendix 1: Supporting Information from Part I

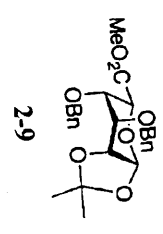
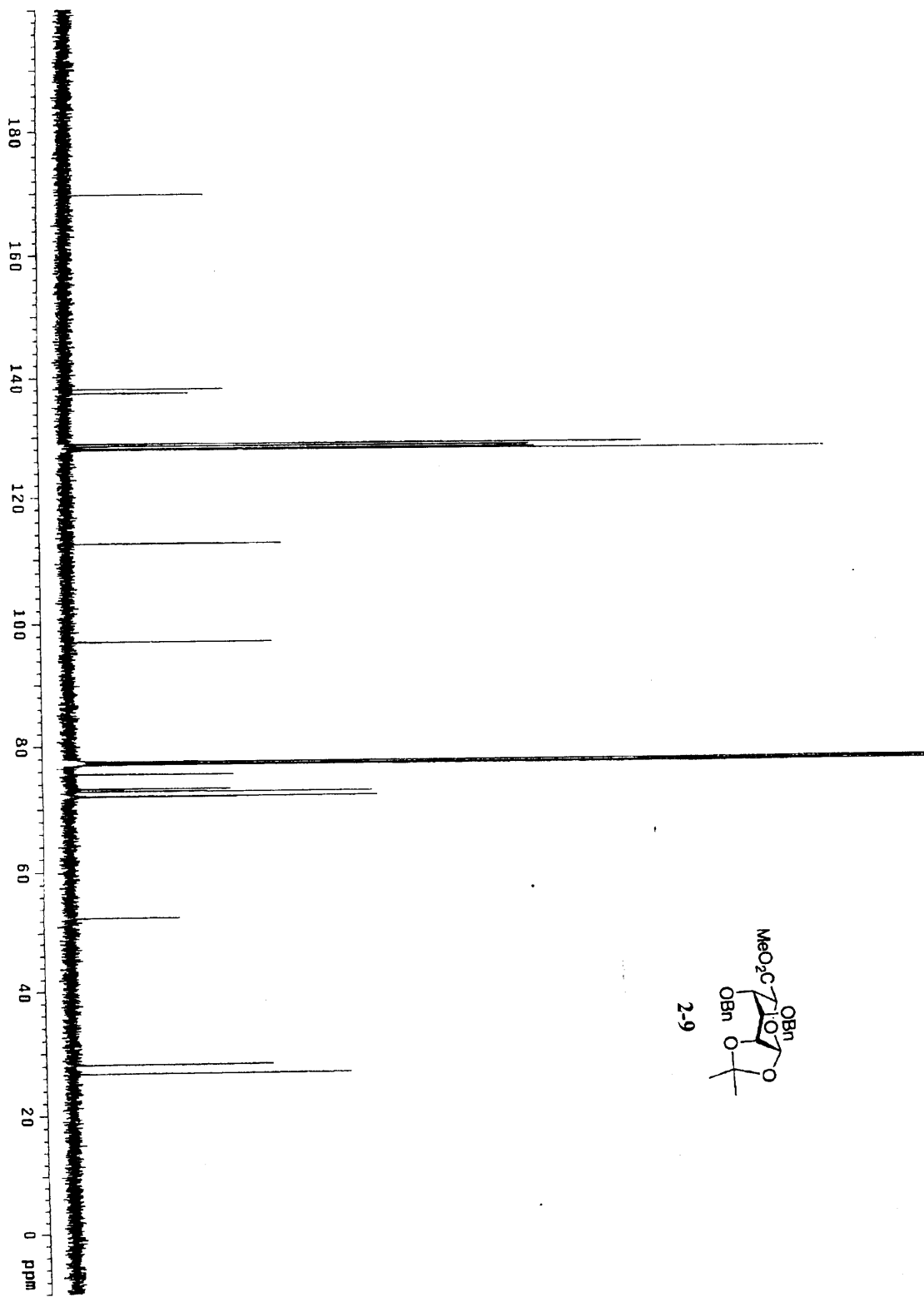
NMR Spectra for Chapter 2	369	NMR Spectra for Chapter 3	443
Compound 2-8	369	Compound 3-11	443
Compound 2-9	371	Compound 3-12	445
Compound 2-10	373	Compound 3-13	447
Compound 2-11a	375	Compound 3-3	453
Compound 2-11b	381	Compound 3-14	455
Compound 2-12	387	Compound 3-15	461
Compound 2-13	389	Compound 3-16	463
Compound 2-14	391	Compound 3-17	465
Compound 2-15	397	Compound 3-18	467
Compound 2-16	403	Compound 3-19	469
Compound 2-17	413	Compound 3-20	476
Compound 2-18	415	Compound 3-21	478
Compound 2-19	417	Compound 3-4	483
Compound 2-23a	419	Compound 3-10	485
Compound 2-23b	421	Compound 3-23	490
Compound 2-24a	423	Compound 3-5	492
Compound 2-24b	425	Compound 3-26	497
Compound 2-25a	427	Compound 3-27	499
Compound 2-25b	429	Compound 3-28	501
Compound 2-26b	431	Compound 3-30	503
Compound 2-27b	433	Compound 3-32	509
Compound 2-28a	435	Compound 3-34	515
Compound 2-28b	437	Compound 3-35	517
Compound 2-29b	439	Compound 3-36	519
Compound 2-30b	441	Compound 3-37	521
		Compound 3-38	527

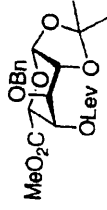




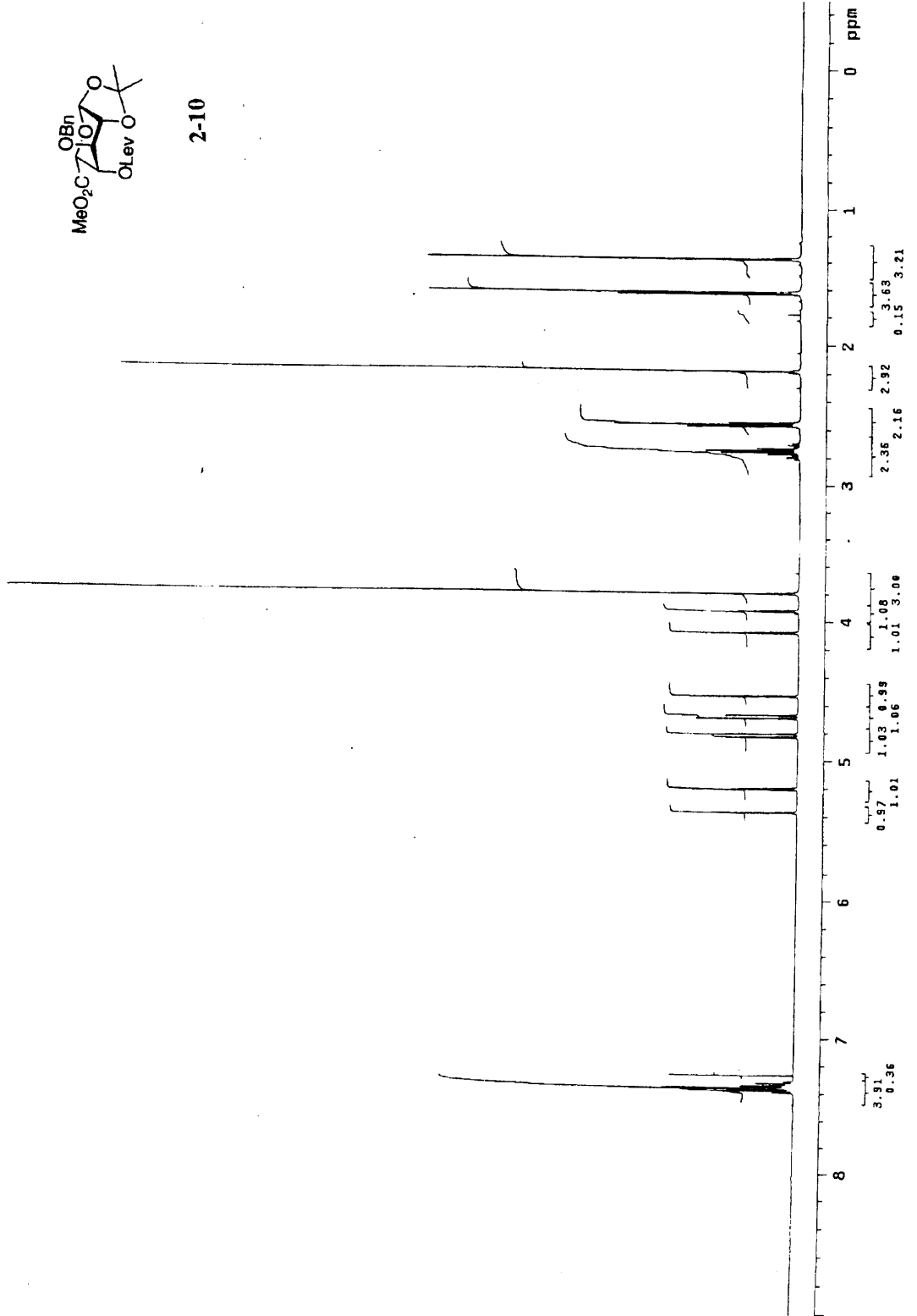
2-8

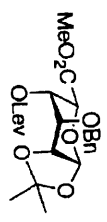
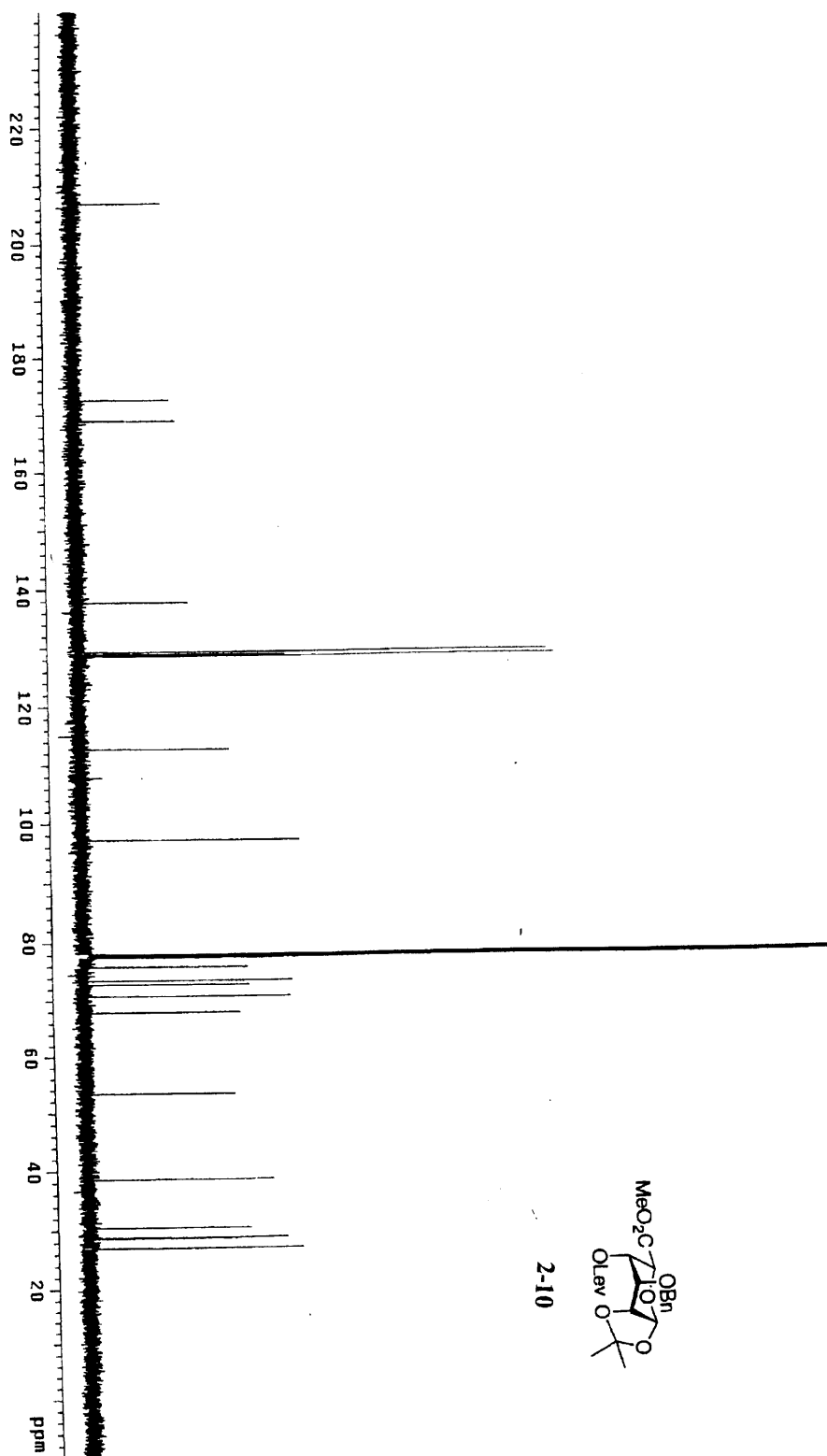




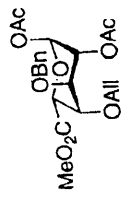


2-10

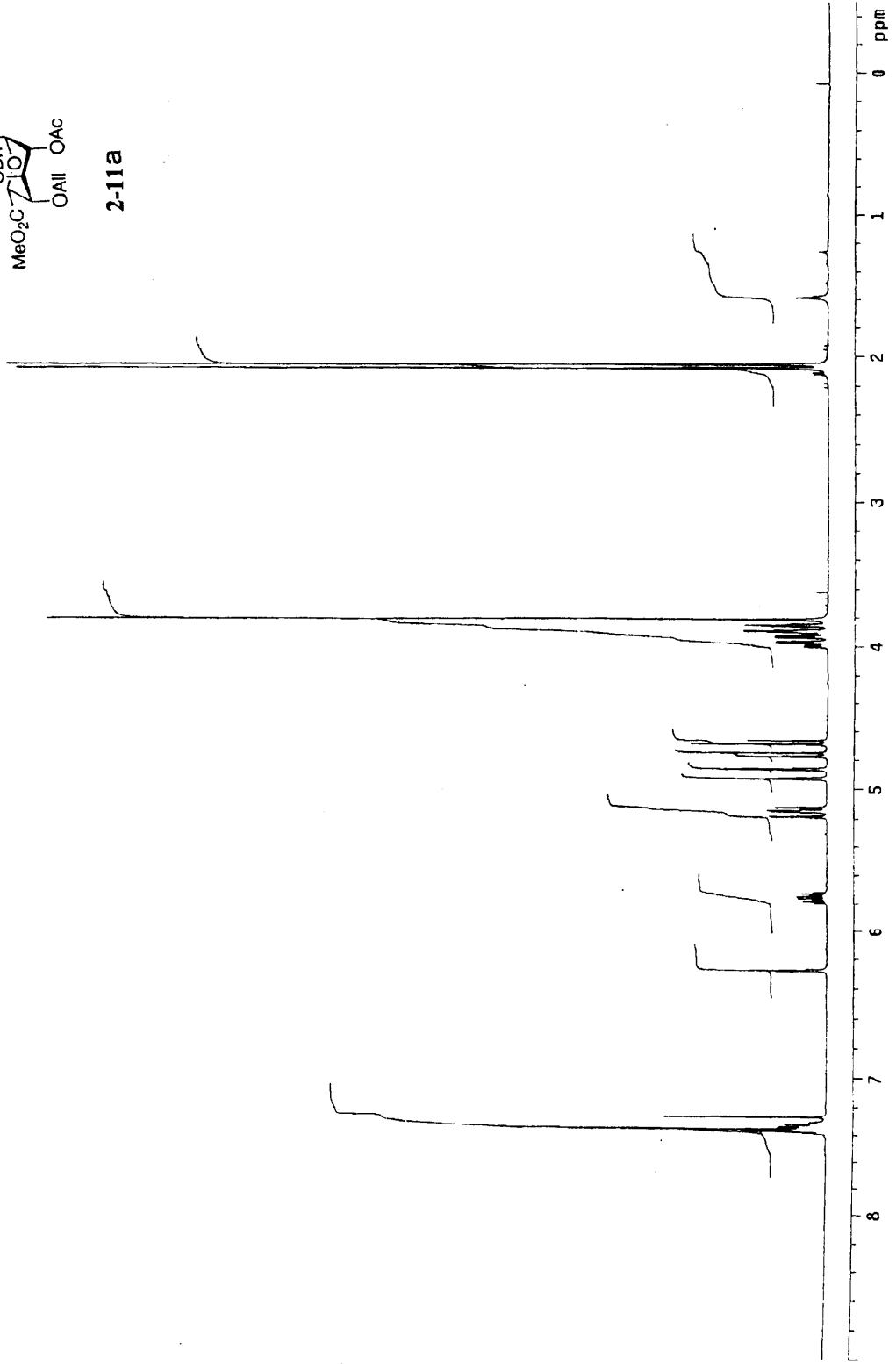


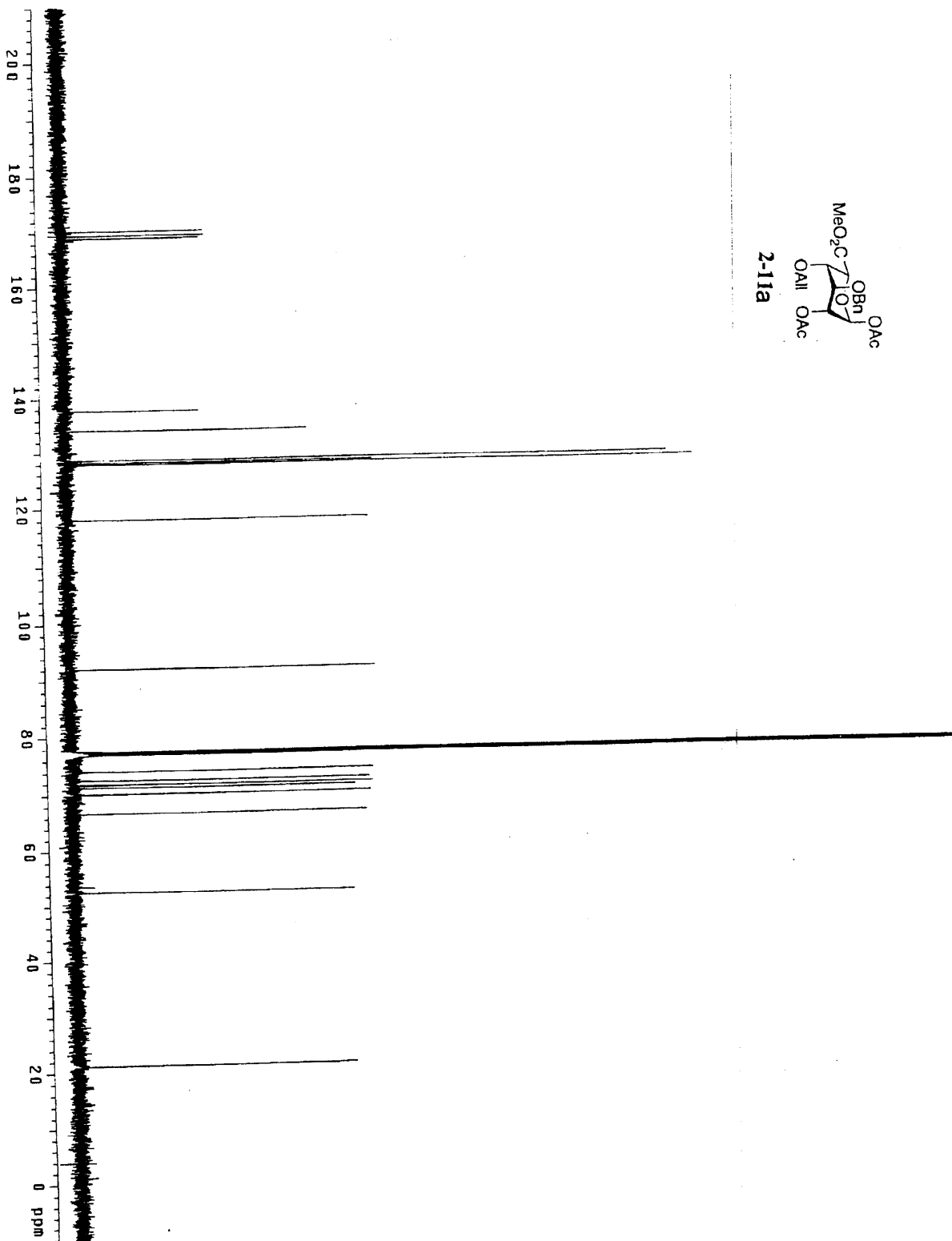
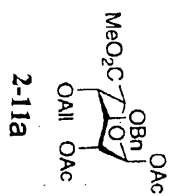


2-10



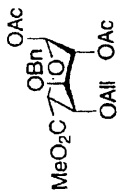
2-11a



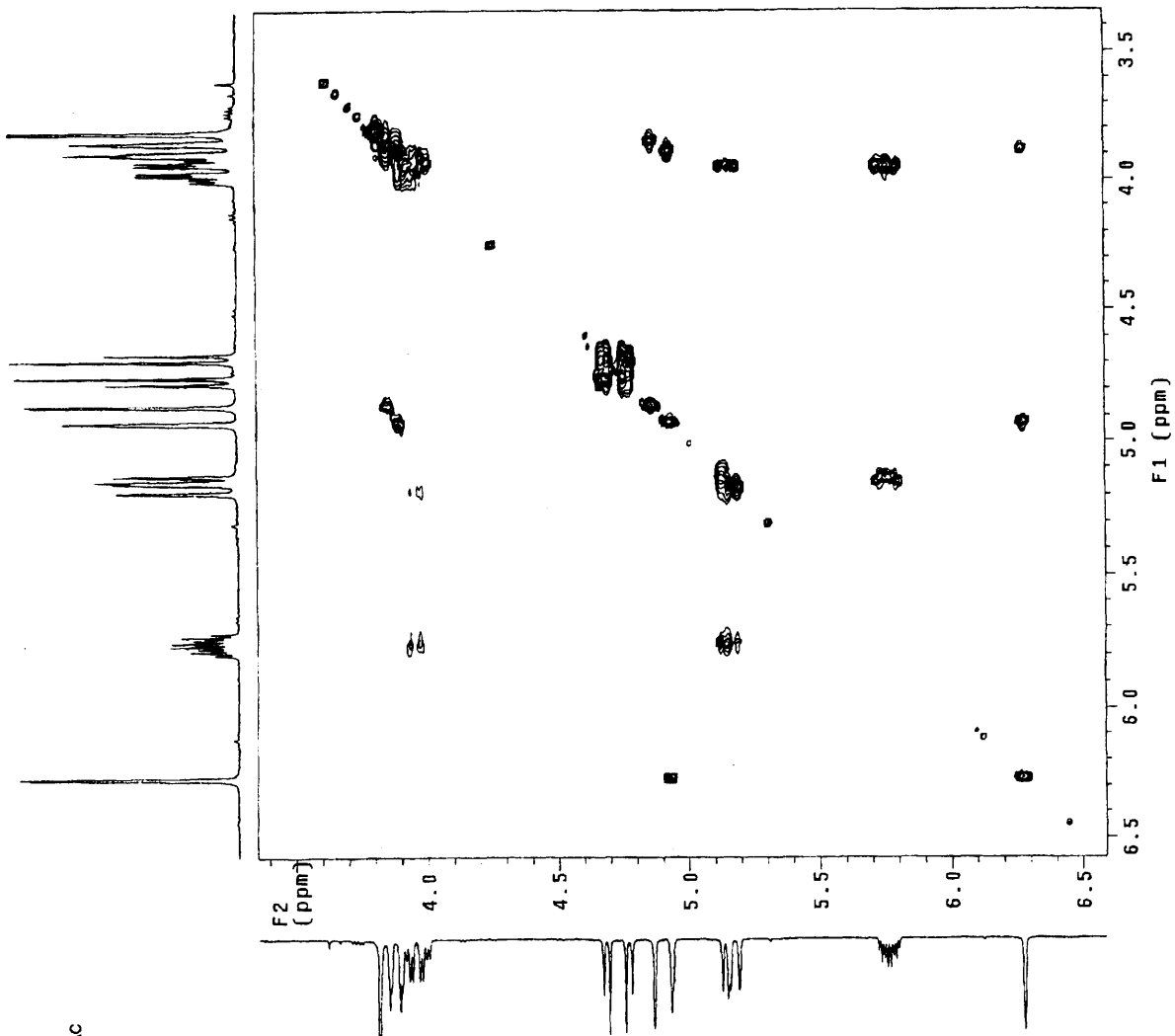


GL-1-157A gCOSY

Pulse Sequence: gCOSY
Solvent: CDCl₃ 295.1 K
Temp: 2. °C "but1rinkit"
INVA-500 "but1rinkit"
PULSE SEQUENCE: gCOSY
Relax. delay: 1.000 sec
Acq. time: 0.216 sec
Width: 4748.3 Hz
CD Width: 4748.3 Hz
256 scans
256 points
OBSERVED: 499.7537719 MHz
DATA PROCESSING
Sf. sine bell 0.108 sec
F1 DATA PROCESSING
Sf. sine bell 0.108 sec
F1 size: 2048 x 2048
Total time: 5 min, 41 sec



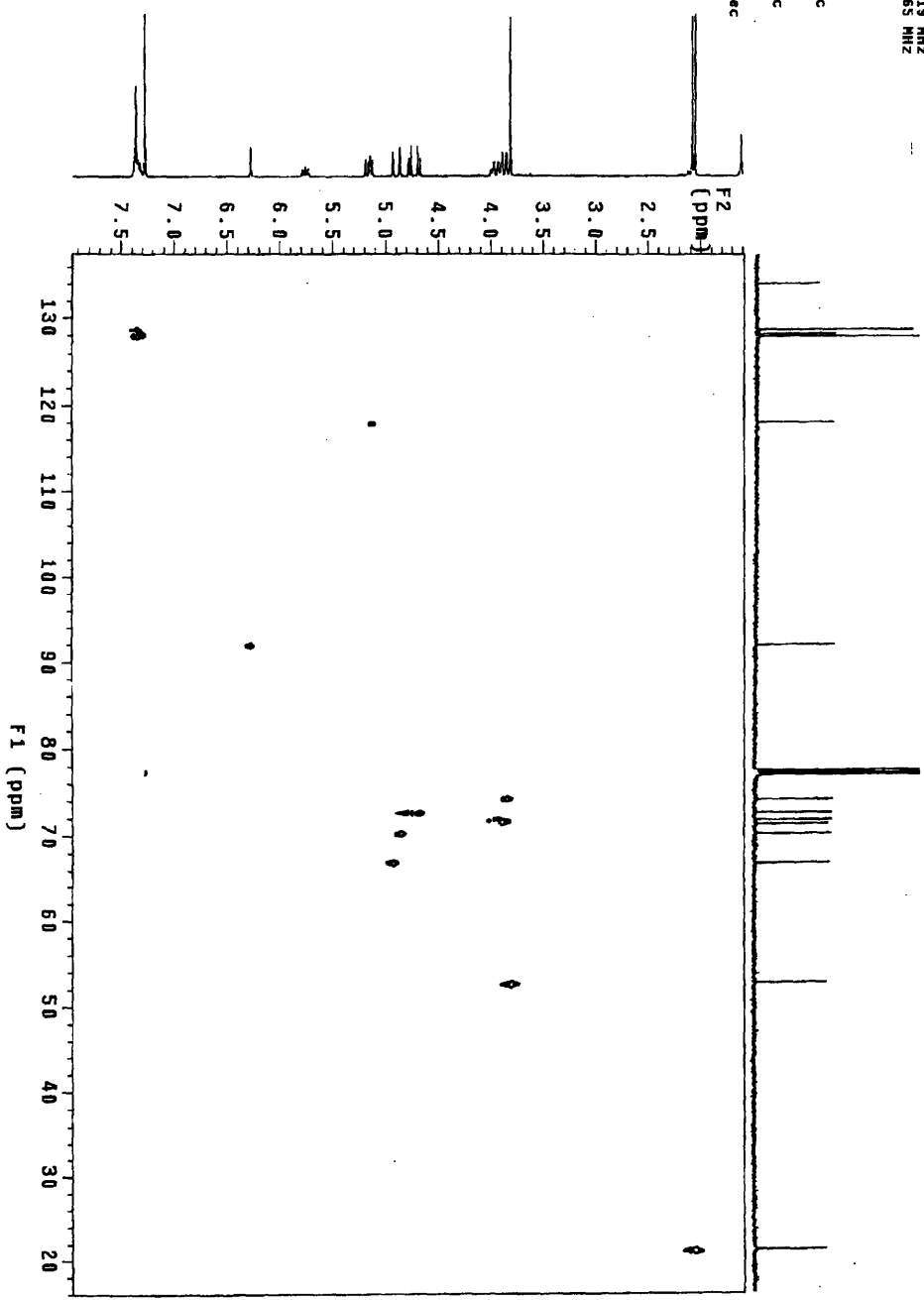
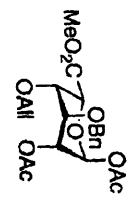
2-11a



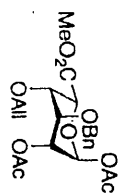
OL-1-167A HSQC

Pulse Sequence: HSQC

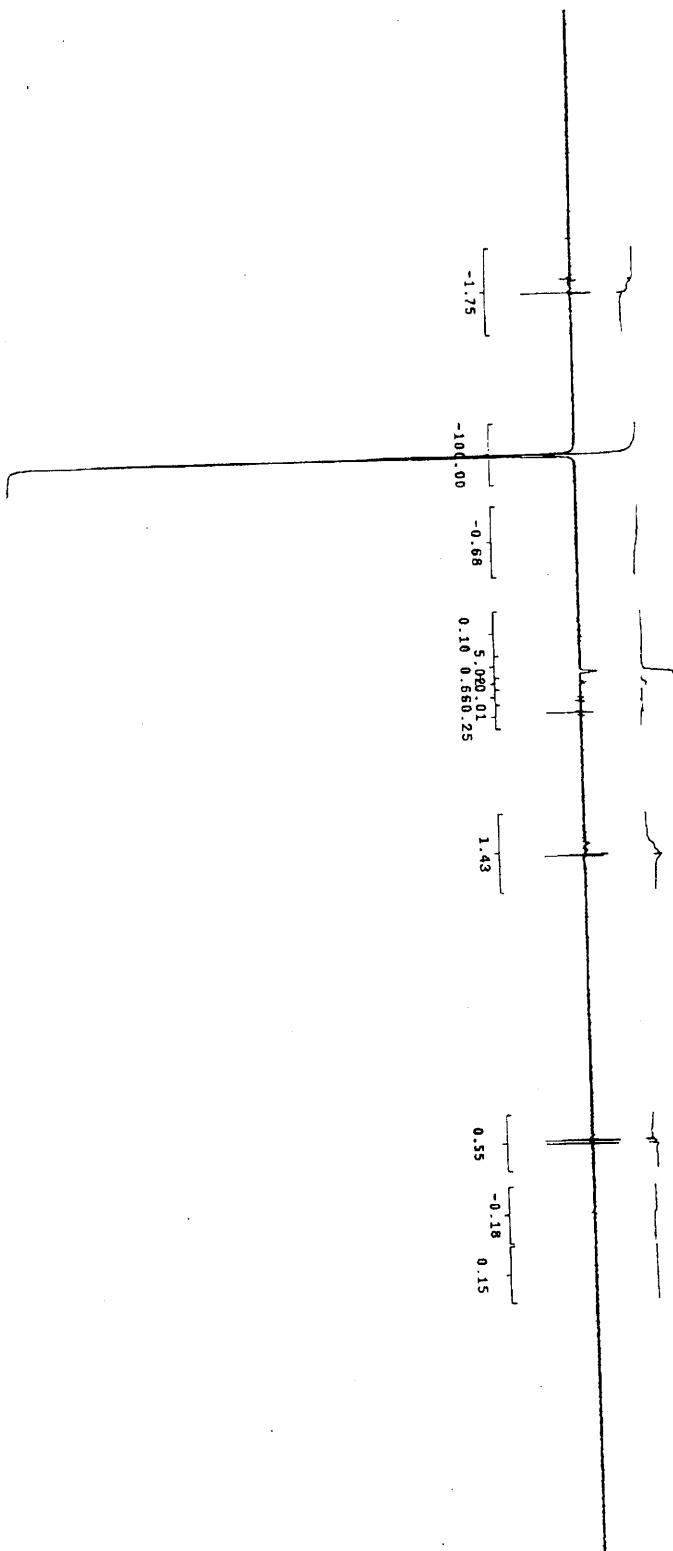
Solvent: GPC19
Temp: 12.14-57
INOVA-500 "but1winkle"
PULSE SEQUENCE: HSQC
Relax: delay: 1.000 sec
Acq: time: 47.101 sec
2D Width: 27881.7 Hz
4 repetitions
2 x 256 increments
OBSERVE: H1, 499.7537719 MHz
DECUPLE: C13, 125.6757265 MHz
Power: 52 dB
on during acquisition
off during delay
GARP-1 modulated
DATA PROCESSING
Sg: sine bell 0.101 sec
Sf: sine bell 0.111 sec
F1: DATA PROCESSING
Sg: sine bell 0.016 sec
Shifted by -0.016 sec
F1 size: 2048 x 2048
Total time: 42 min, 33 sec

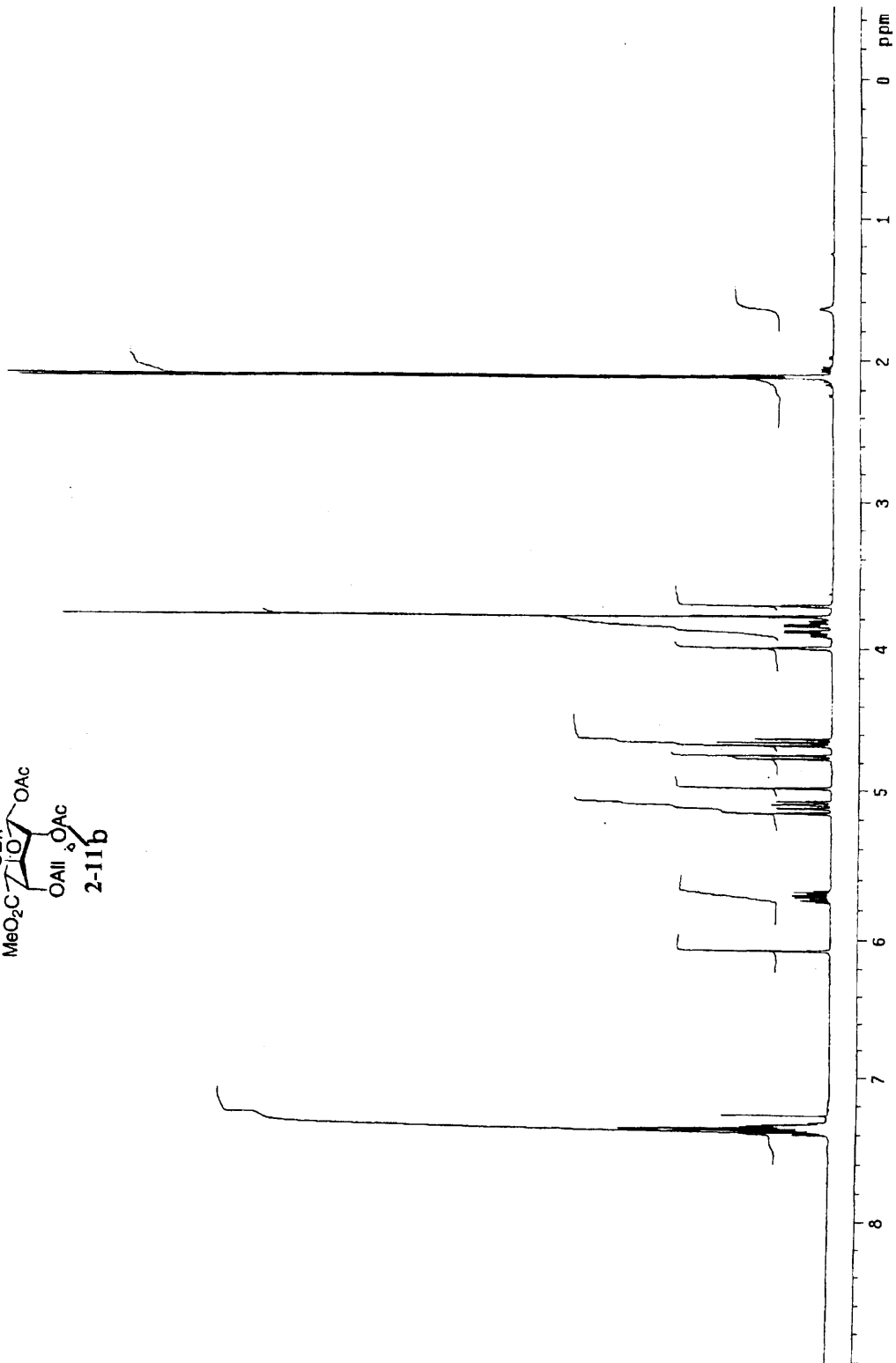
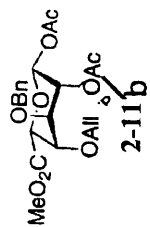


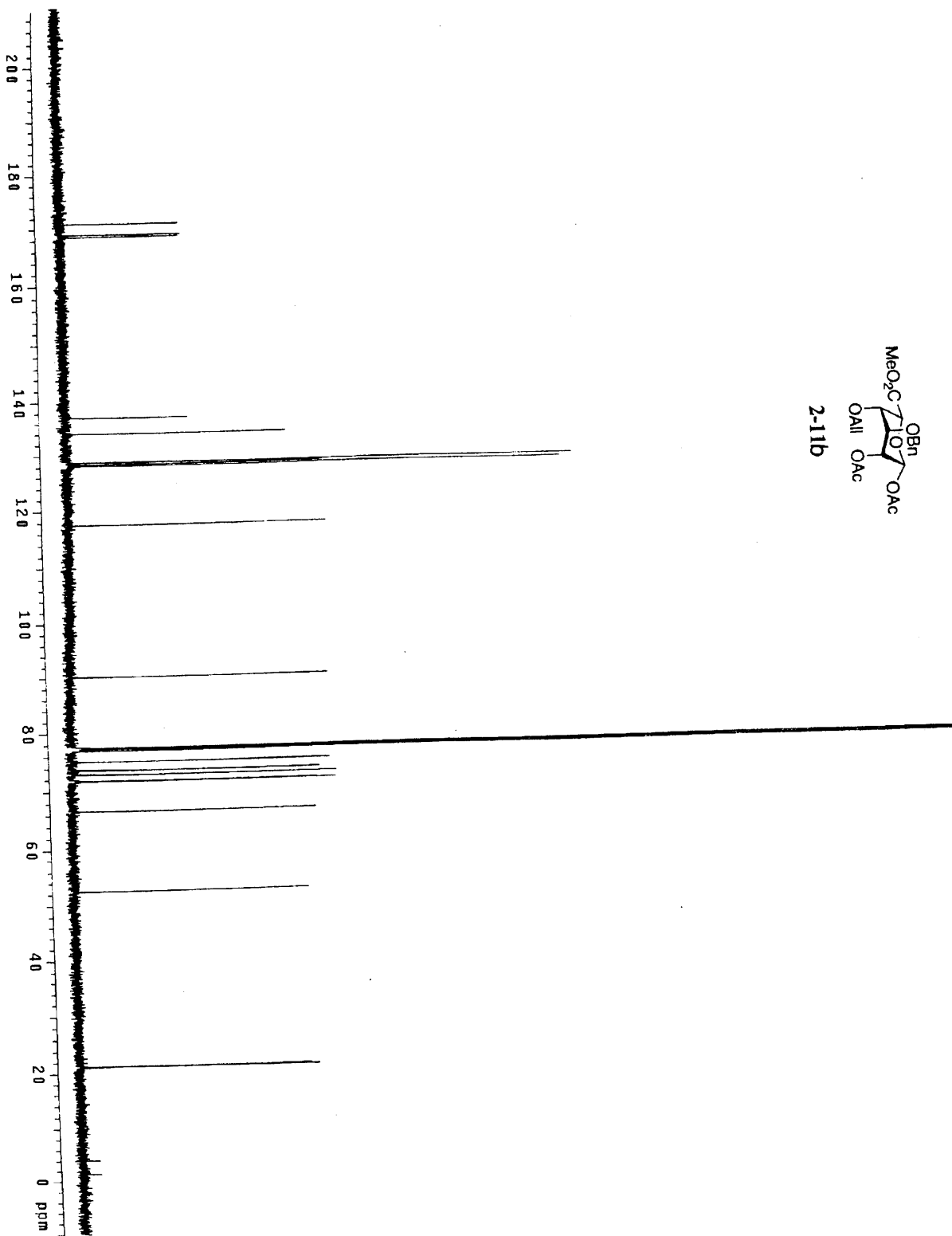
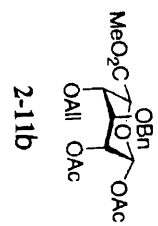
GL-1-167A NOE diff 6.27 satfrq
Pulse Sequence: presat



2-111a







GL-1-1676 gCOSY

Pulse Sequence: gCOSY

Solvent: CDC13

Temp: 22.0 C / 295.1 K

INSTR: 500 "Bullwinkle"

PULSE SEQUENCE: gCOSY

Relax. delay: 1.000 sec

Acq. time: 0.216 sec

Width: 4748.3 Hz

SF width: 4748.3 Hz

19F 16 scan

256 increments

OBSERVE: H1

DATA PROCESSING

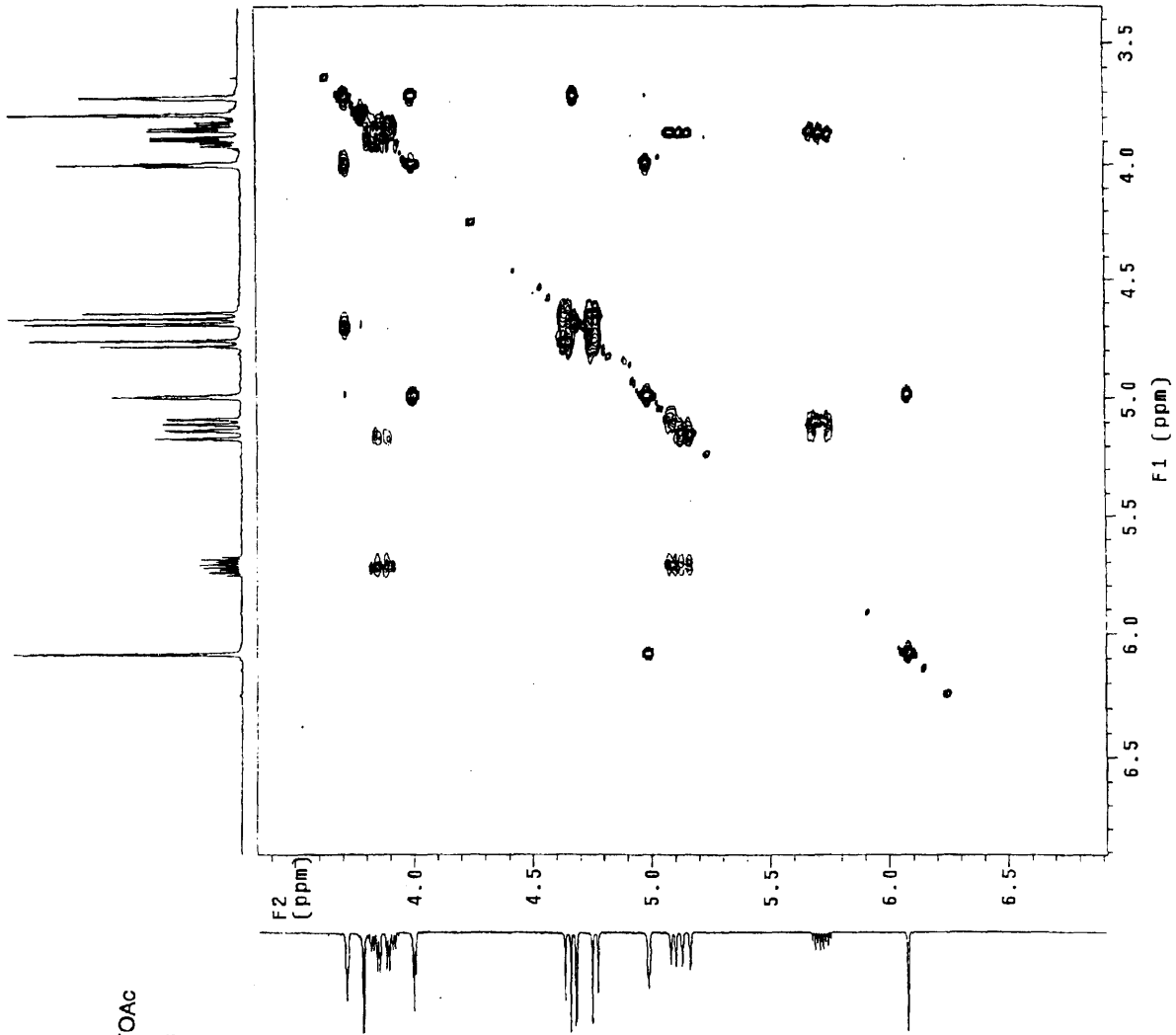
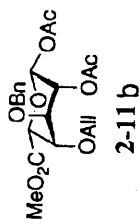
Sq. sine bell 0.108 sec

F1 DATA PROCESSING

Sq. sine bell 0.108 sec

FT size 2048 x 2048

Total time 5 min. 41 sec



DL-1-167B HSQC

Pulse Sequence: HSQC

Solvent: CDCl3

Temp: 22.0 C / 295.1 K

User: 1-16-87

INOVA-500 "nutlinkie"

PULSE SEQUENCE: HSQC

Relax. delay: 1.00 sec

Acq. time: 0.101 sec

Width: 4748.3 Hz

2D Width: 27881.7 Hz

4 F repetitions

2 X 256 increments

OBSERVE: H1, 498.7537216 MHz

DECOUPLE: C13, 125.8757288 MHz

Power: 52 db

on during acquisition

off during delay

DATA PROCESSING

Sq. sine bell: 0.101 sec

Shifted by: -0.101 sec

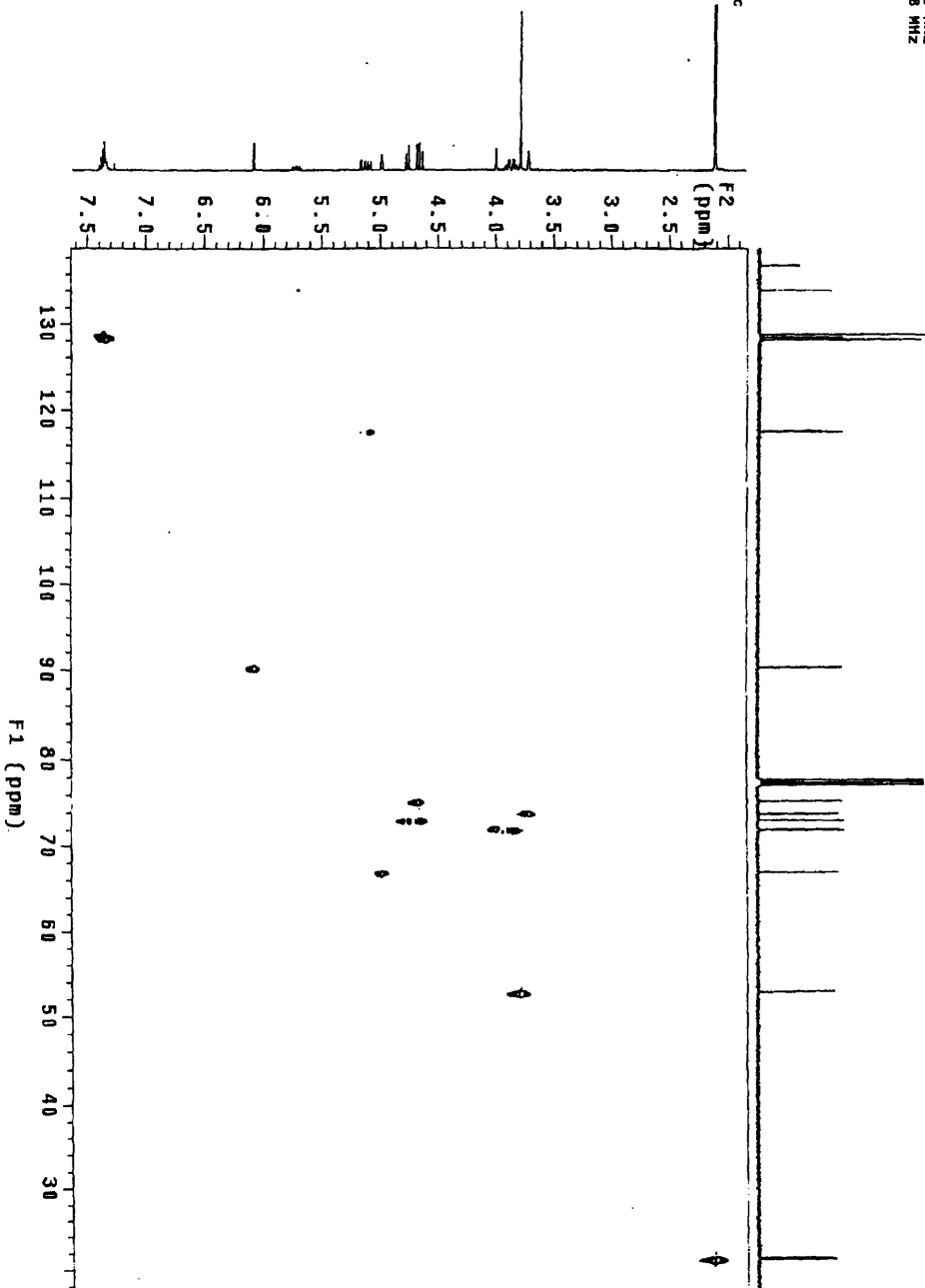
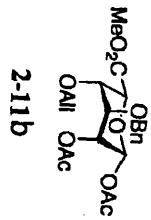
F1 DATA PROCESSING

Sq. sine bell: 0.018 sec

Shifted by: -0.018 sec

F1 size: 2048 x 2048

Total time: 42 min., 53 sec



GL-1-167B

Pulse Sequence: HMB

Solvent: CDCl₃

Temp: 22.0 C / 295.1 K

User: 1-14-87

INNOVA-500 "bulwinkle"

PULSE SEQUENCE: HMB

Relax. delay: 1.000 sec

Acq. time: 0.216 sec

Width: 4748.3 Hz

2D Width: 27681.7 Hz

B repetitions

2 x 256 increments

OBSERVE: H1, 499.7537716 MHz

DATA PROCESSING

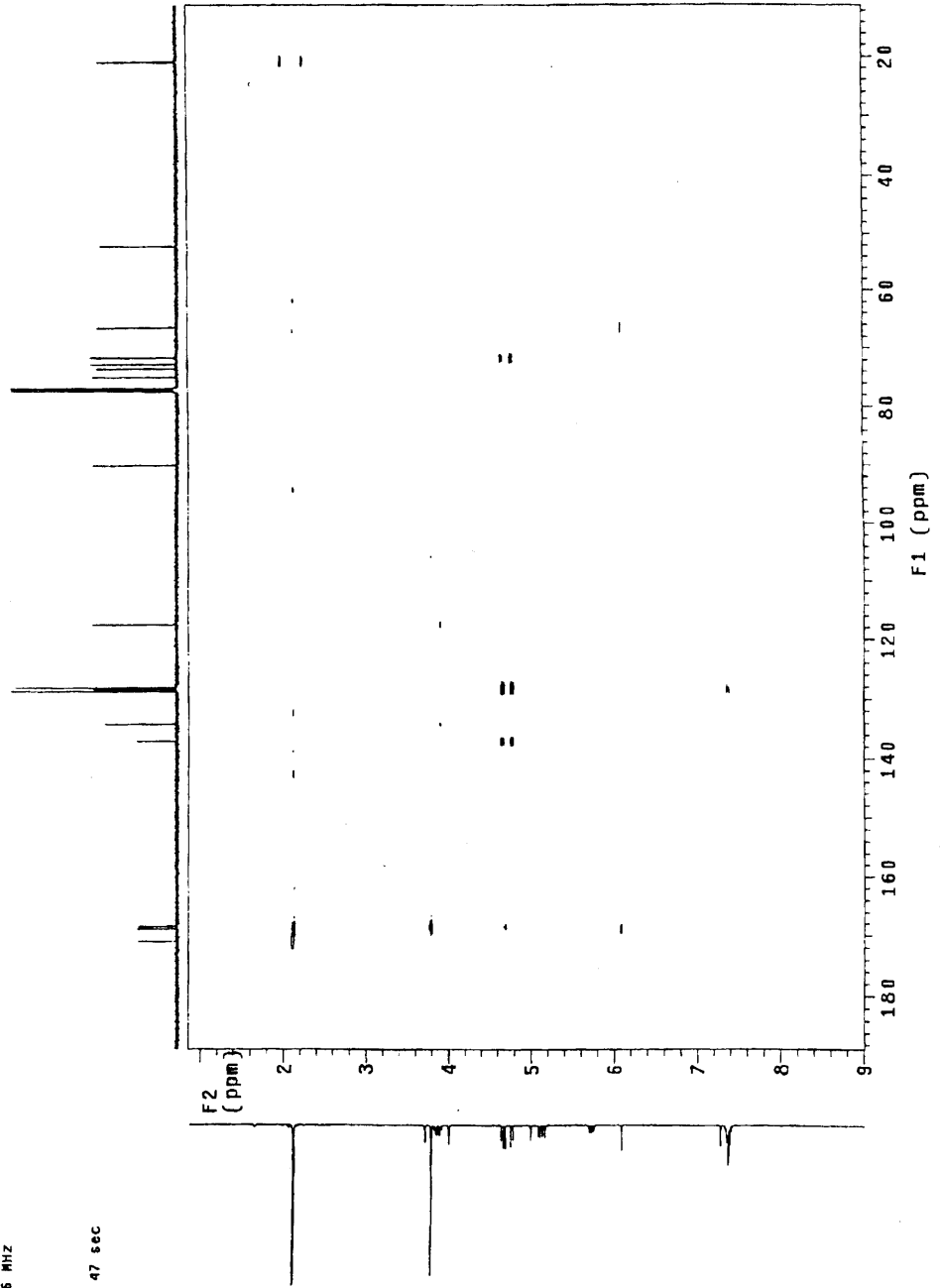
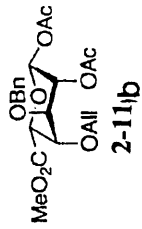
Sine bell: 0.108 sec

F1 DATA PROCESSING

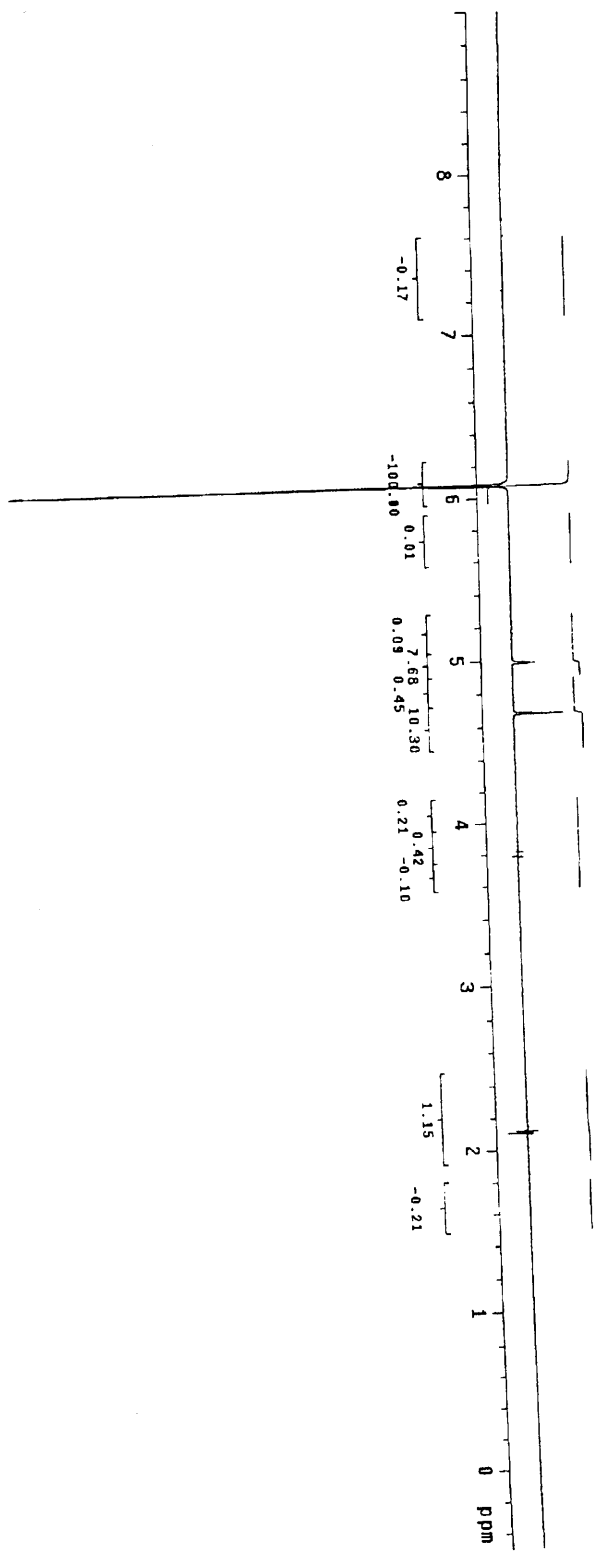
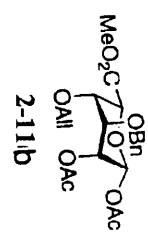
F1 delay: 0.004 sec

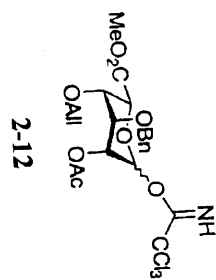
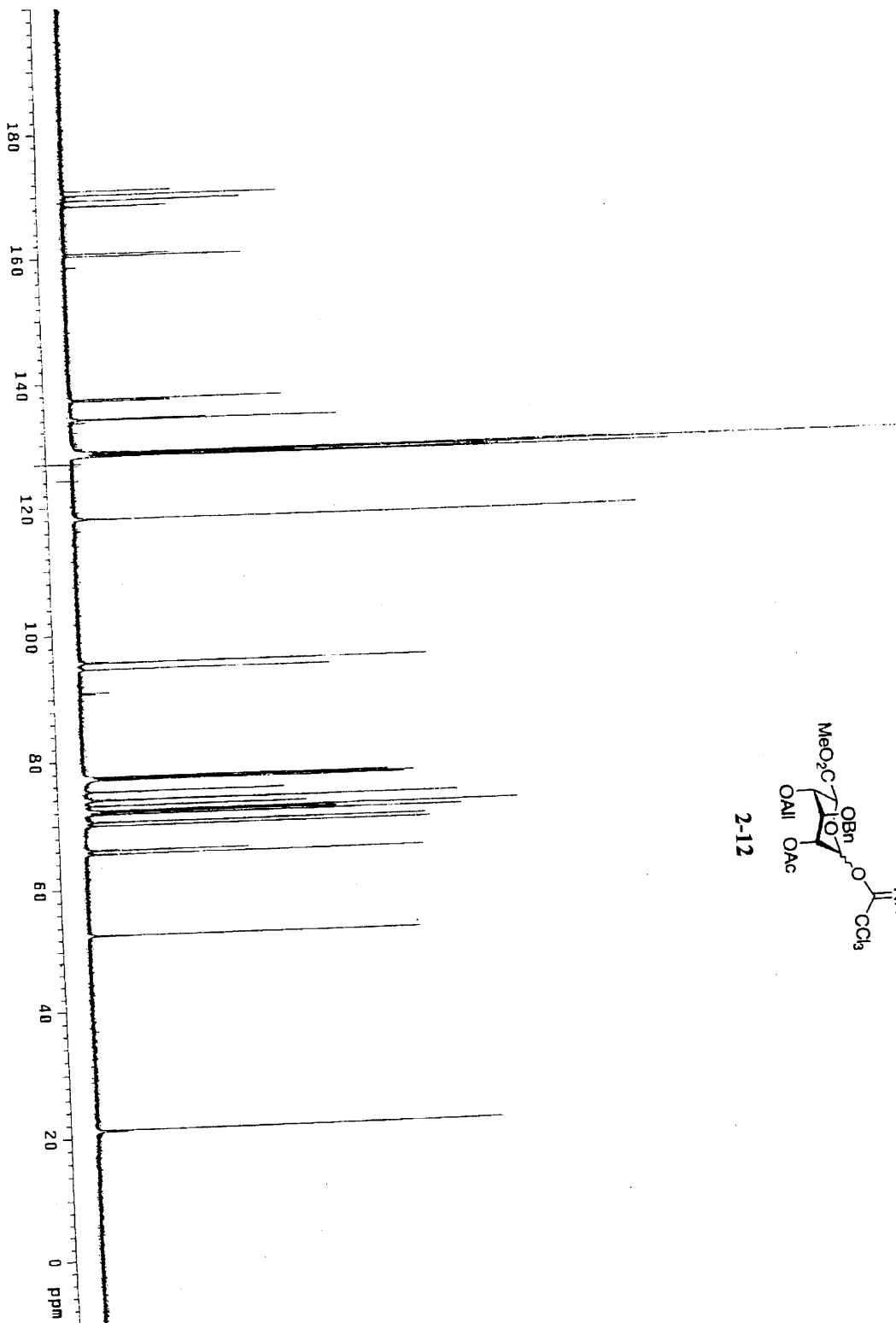
F1 size: 2048 K, 2560

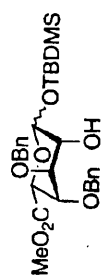
Total time: 1 hr, 32 min, 47 sec



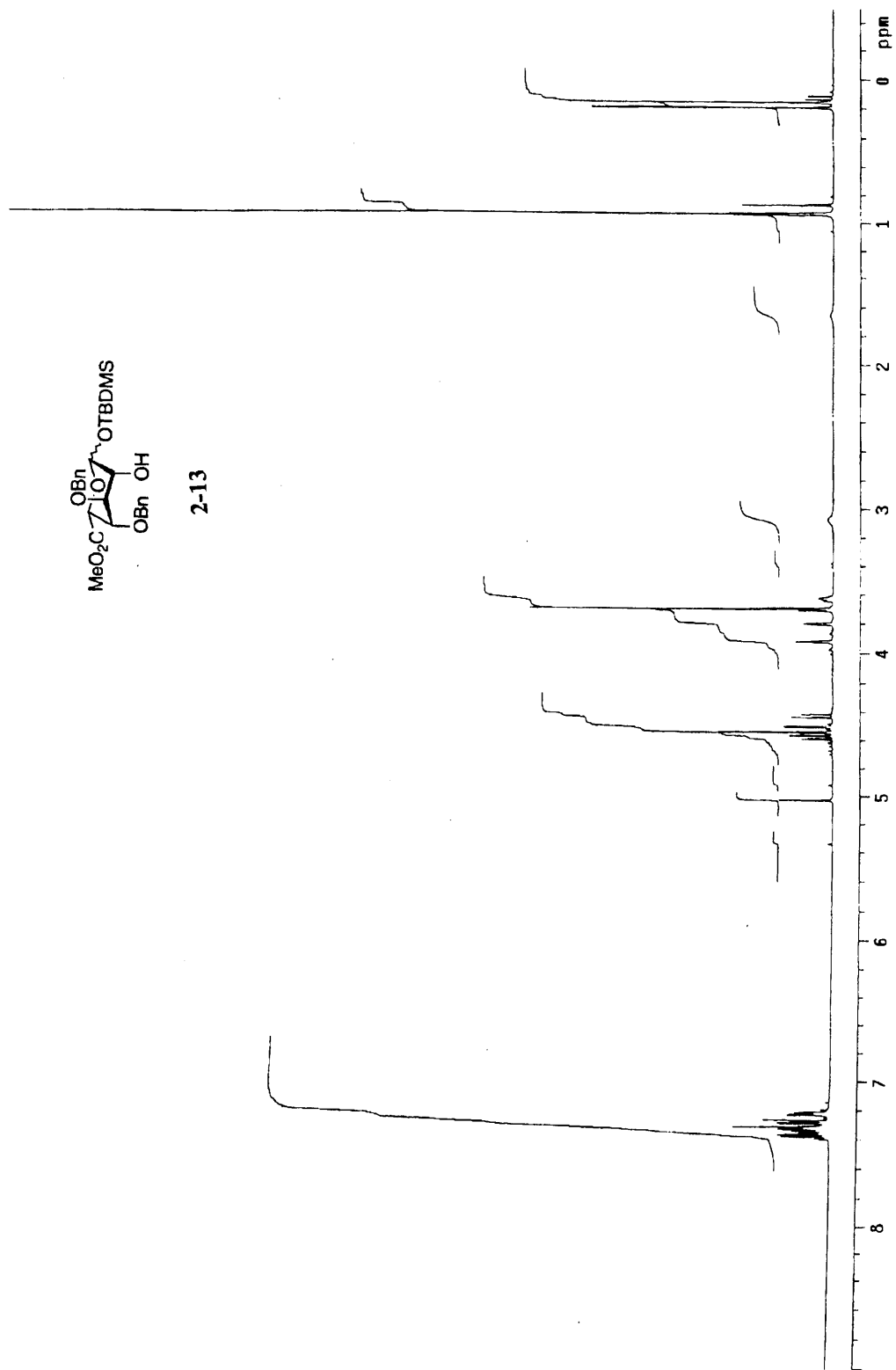
GL-1-1678 NOE diff, 6.08 startq
Pulse Sequence: preset

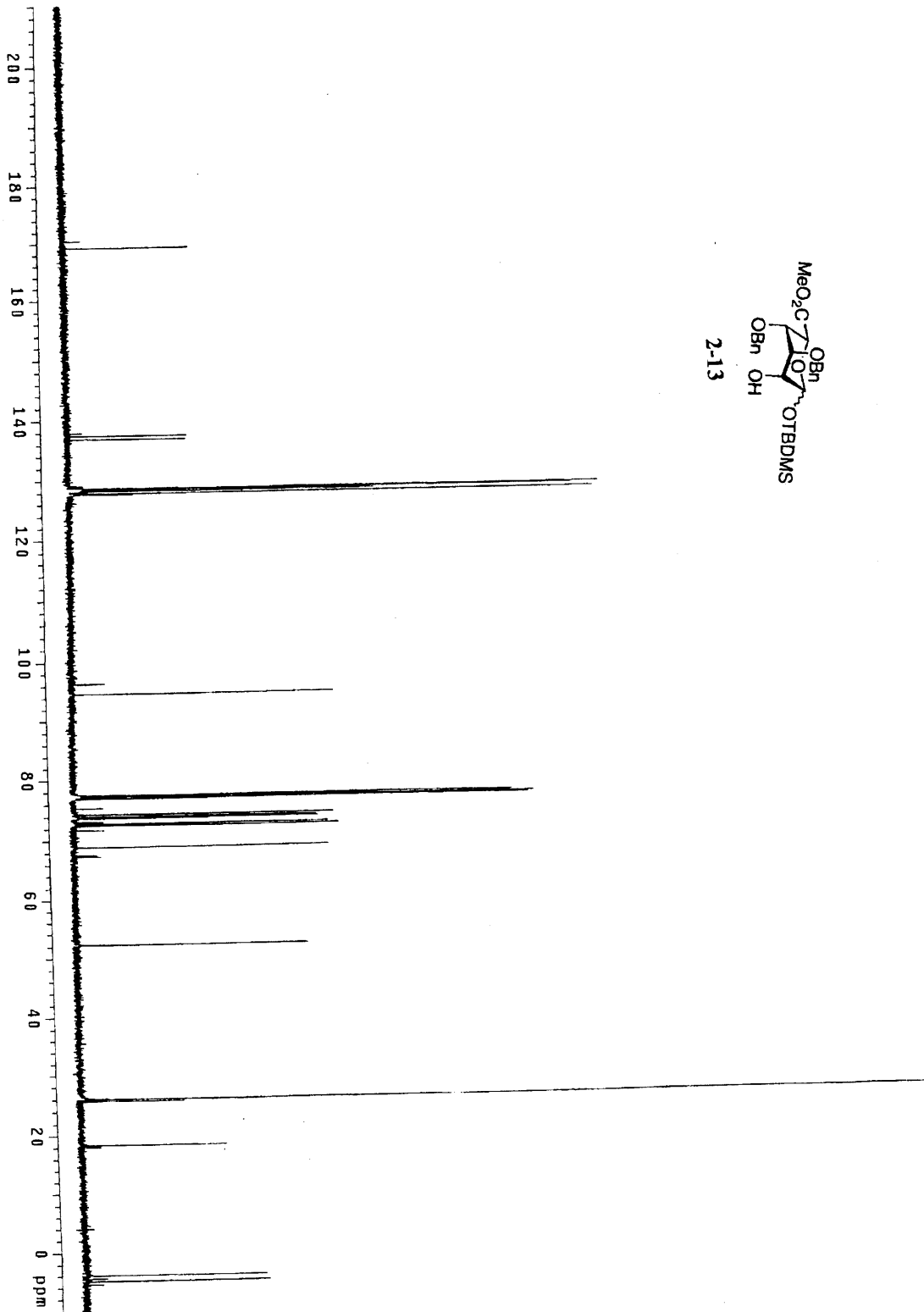
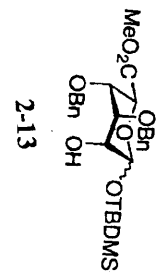


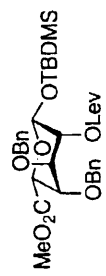




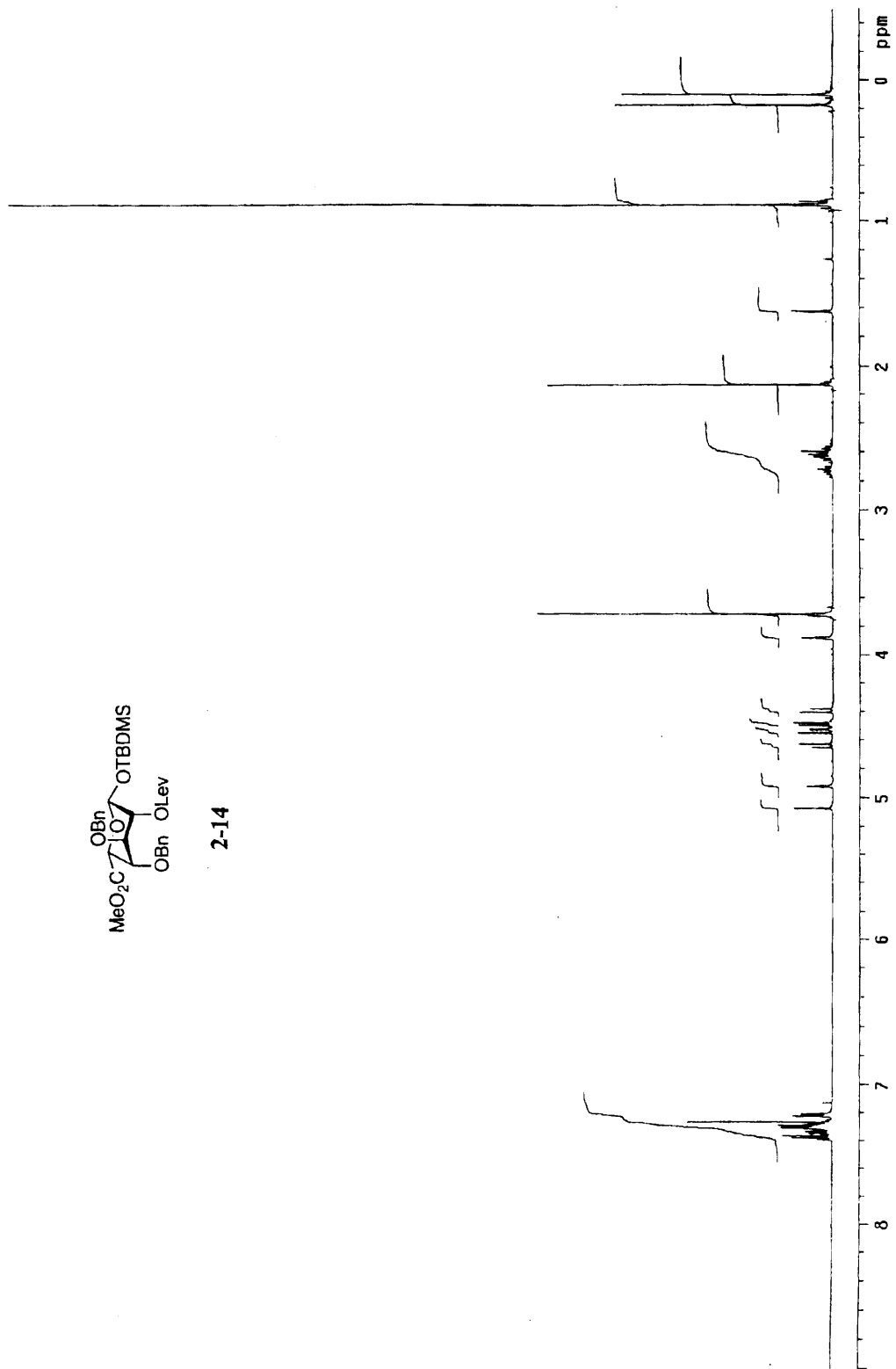
2-13

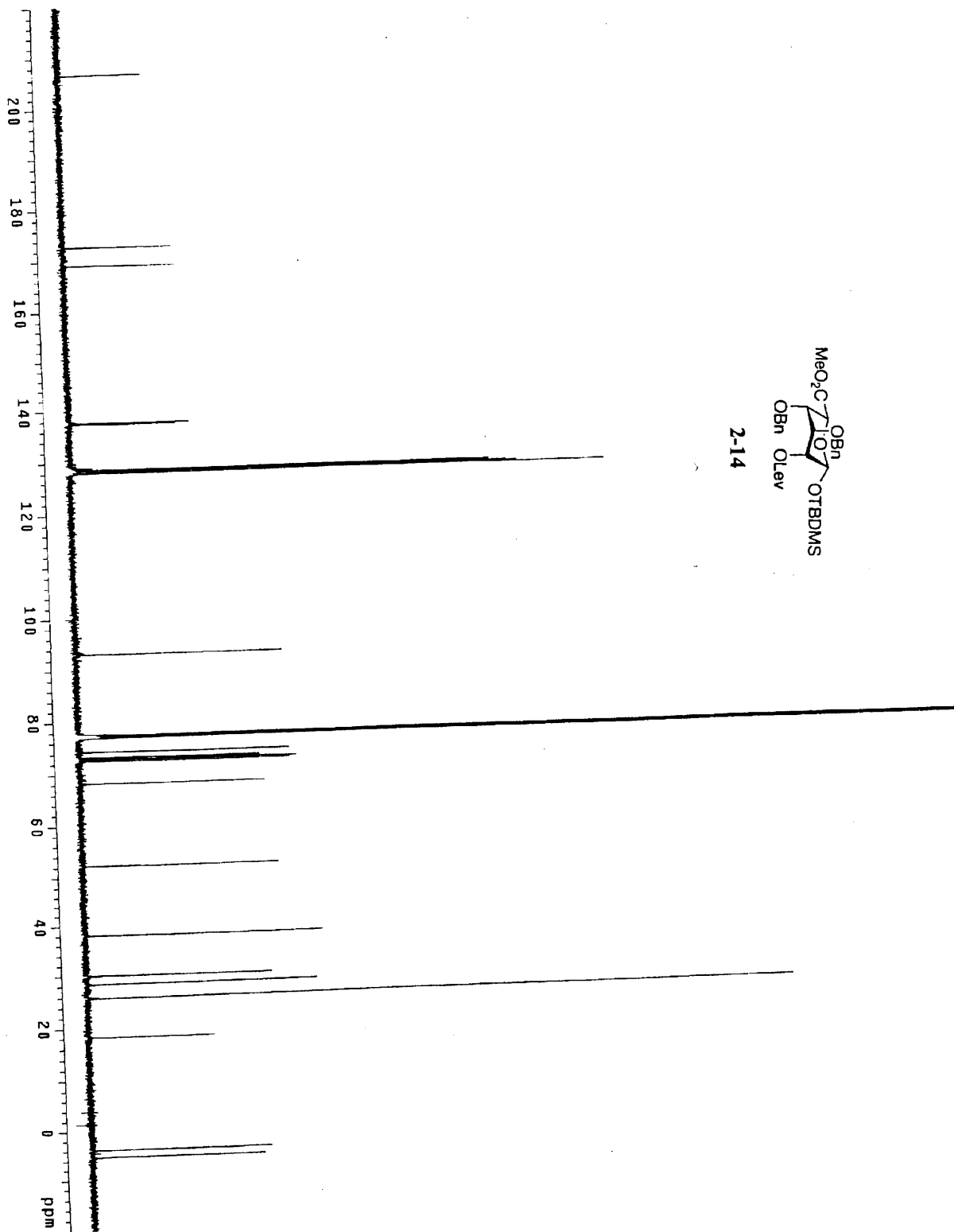
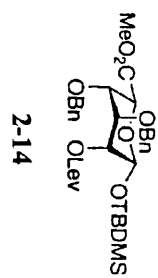






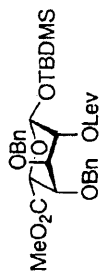
2-14



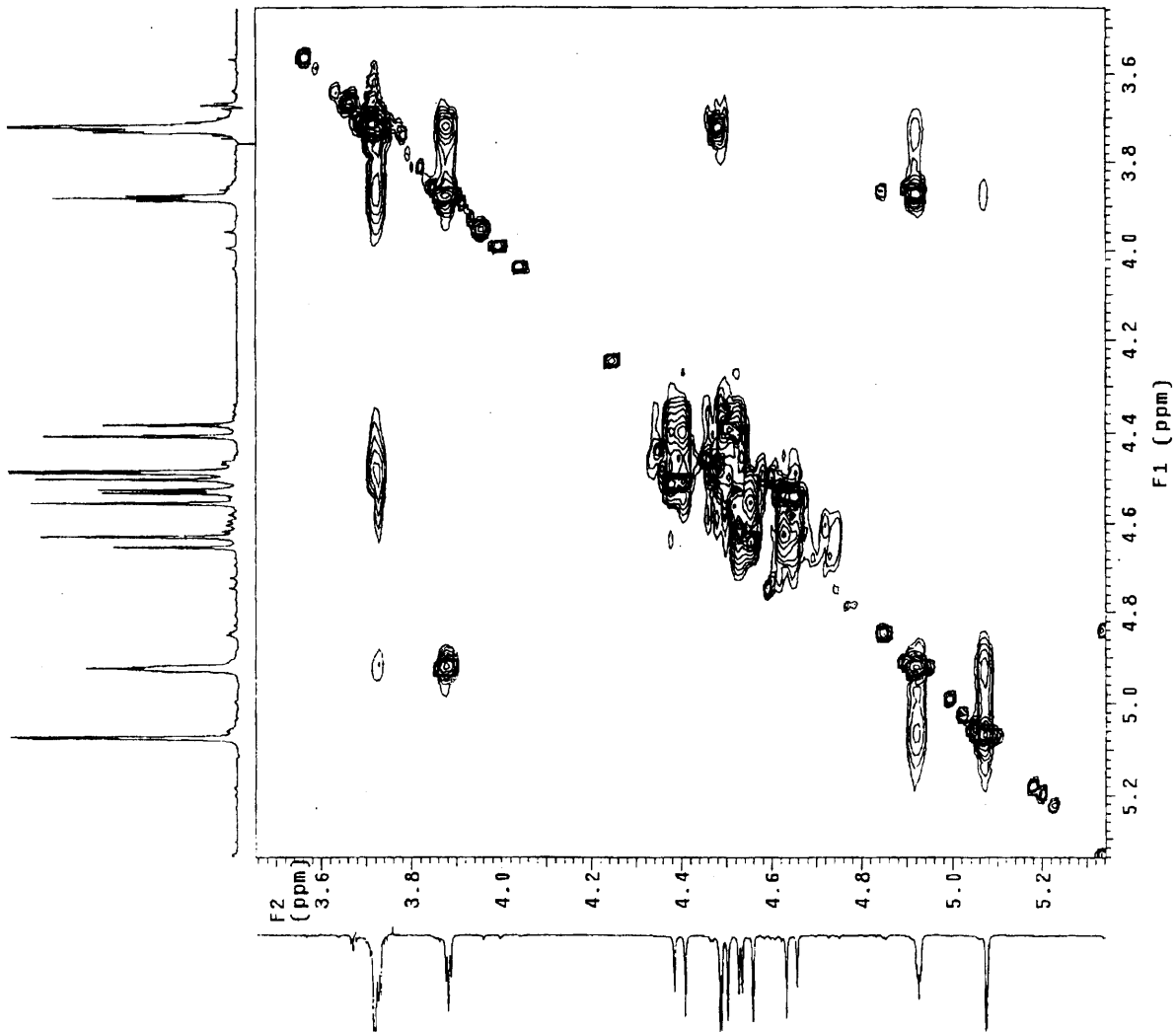


GL-2-27gCOSY

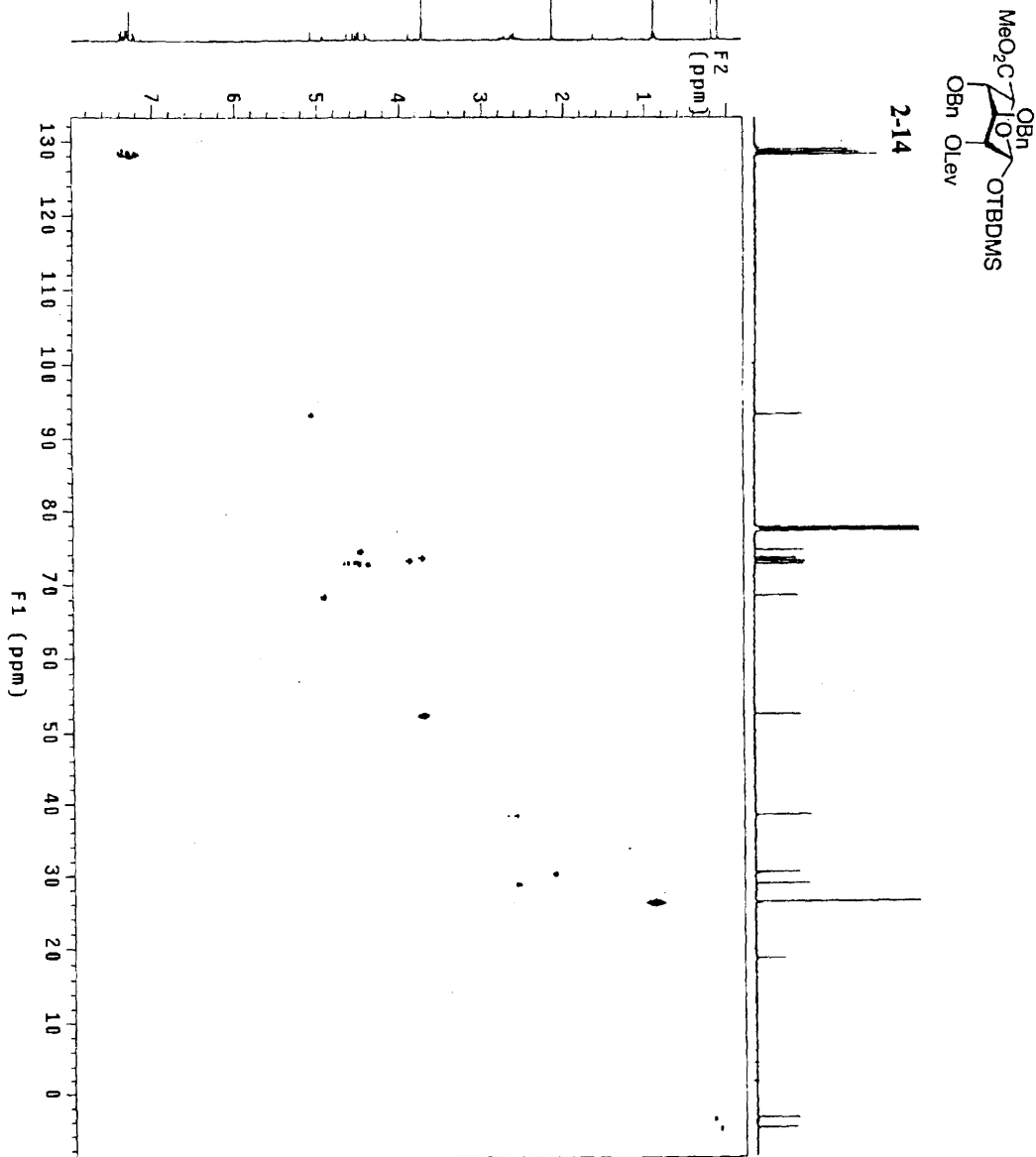
Pulse Sequence: gCOSY
Solvent: CDCl3
Temp: 22.0 C / 295.1 K
INOVA-506 "bulwinkle"
PULSE SEQUENCE: gCOSY
Relax. delay: 1.000 sec
Acq. time: 0.216 sec
F2 width: 4746.3 Hz
Single scan
256 increments
OBSERVE H1: 499.7537719 MHz
DATA PROCESSING
S4. sine bell 0.108 sec
F1 DATA PROCESSING
S4. sine bell 0.108 sec
FT size: 2048 x 2048
Total time: 5 min, 41 sec



2-14



QI-2-27 HSQC
 Pulse Sequence: HSQC
 Solvent: CDCl3
 Temp: 22.0 C / 295.1 K
 User: J-14-8111winkler
 INOVA-500 -b111winkler
 PULSE SEQUENCE: HSQC
 Relax. delay: 1.000 sec
 Acq. time: 0.101 sec
 Width: 9748.3 Hz
 ZD Width: 3188.7 Hz
 2 x 256 F2ions
 OBSERVE: H1 459.7537219 MHz
 DECOUPLE: C13 125.6757277 MHz
 Power: 52 dB
 on during acquisition
 off during delay
 GARP-1 modulated
 DATA PROCESSING
 Sg. sine bell: 0.101 sec
 F1 Shifted by: -0.101 sec
 S. DATA PROCESSING
 Shifted by: 0.071 sec
 FT size: 2048 x 2048
 Total time: 42 min, 32 sec



GL-2-27 HMBC

Pulse Sequence: HMBC

Solvent: CDCl3

Temp: 22.0 C / 295.1 K

User: 1-14-87 "bulwinkle"

INDVA-500 "bulwinkle"

PULSE SEQUENCE: HMBC

Relax. delay 1.000 sec

Acq. time 0.216 sec

Width 4748.3 Hz

ZD Width 30188.7 Hz

8 repetitions

0.5 sec increments

OSERVE 13C

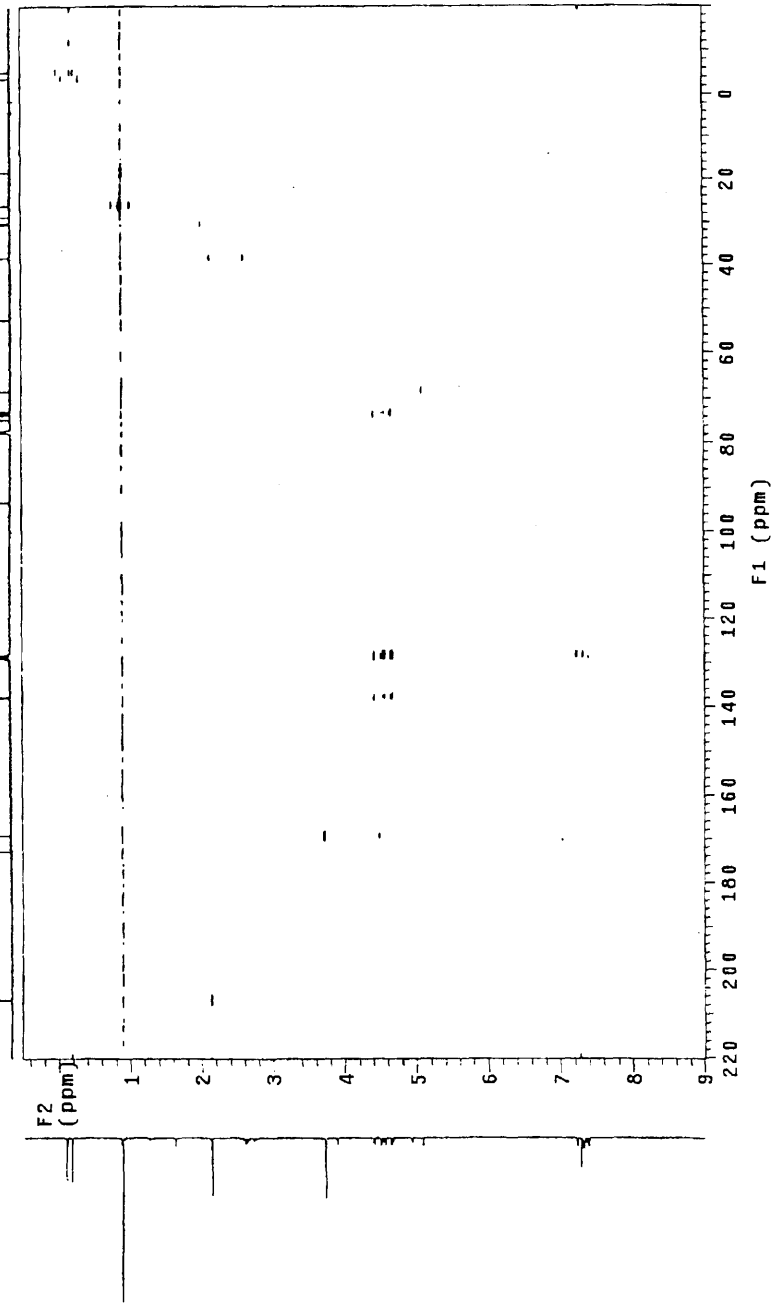
DATA PROCESSING

FT size 2048 x 2048

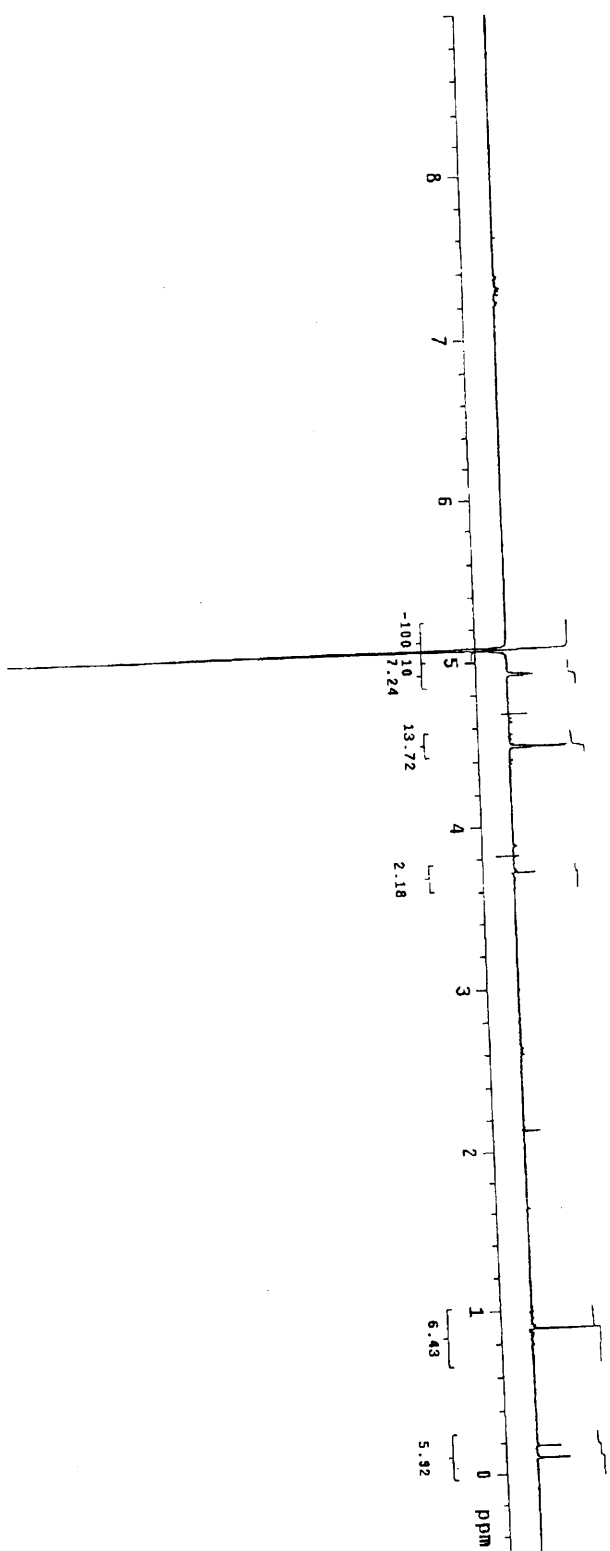
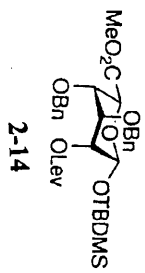
Total time 1 hr, 32 min, 46 sec

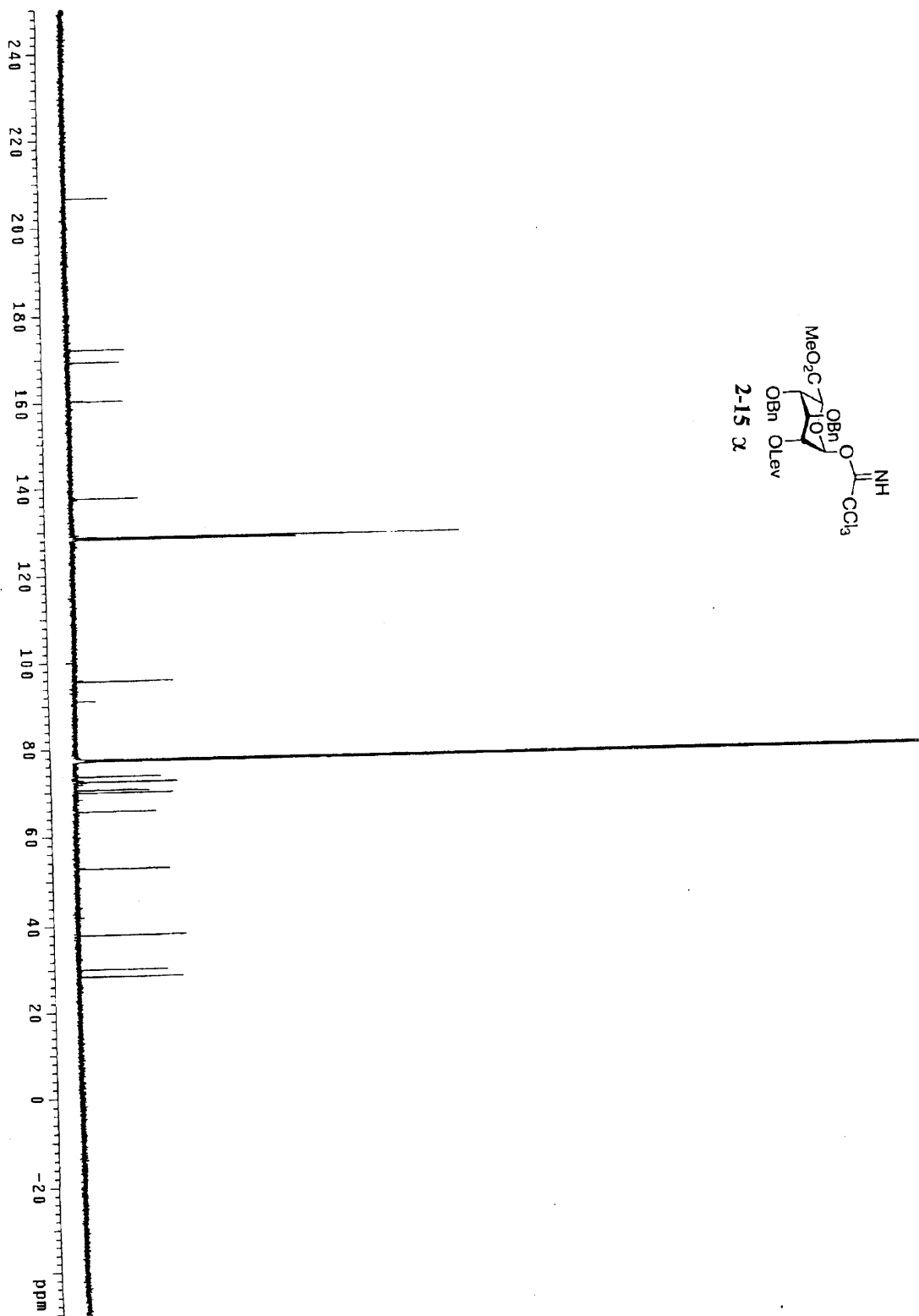


2-14

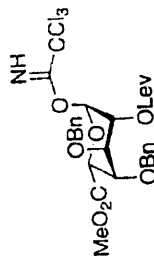


GL-2-27, NOE diff, satfrq=5.07
Pulse Sequence: preset

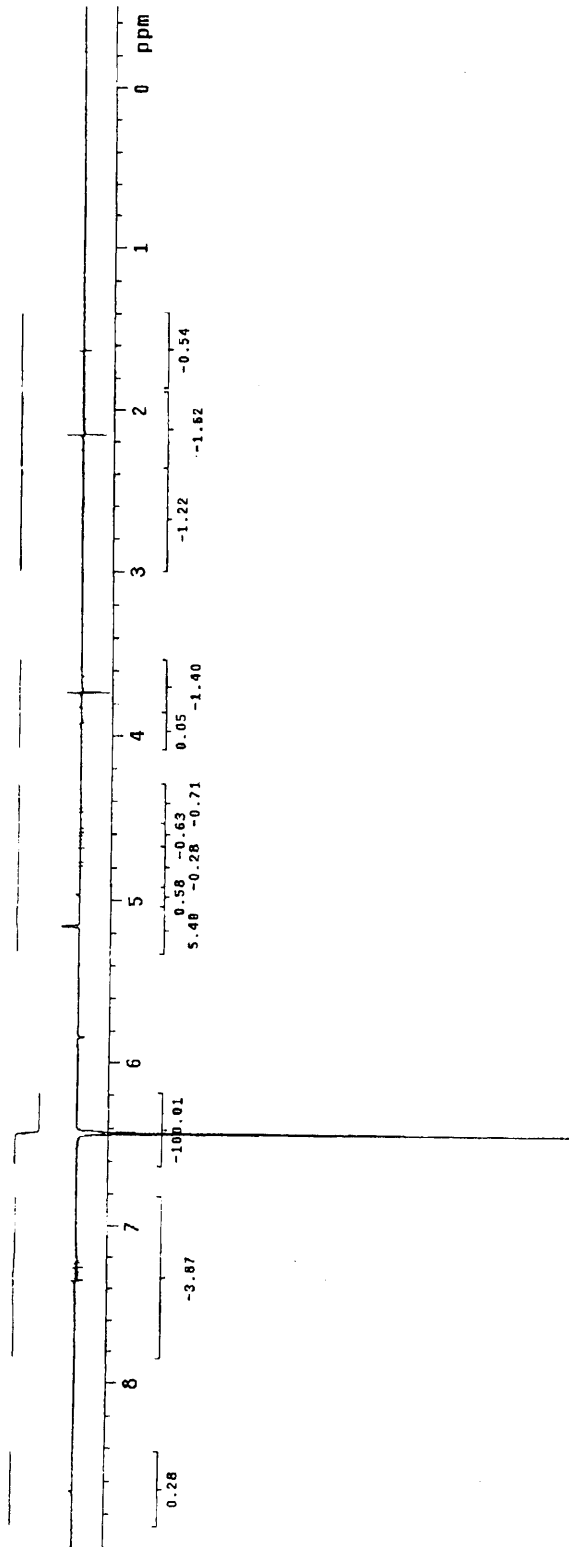


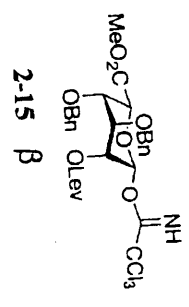


GL-2-11bottom NOEdiff sat=6.43
Pulse Sequence: presat

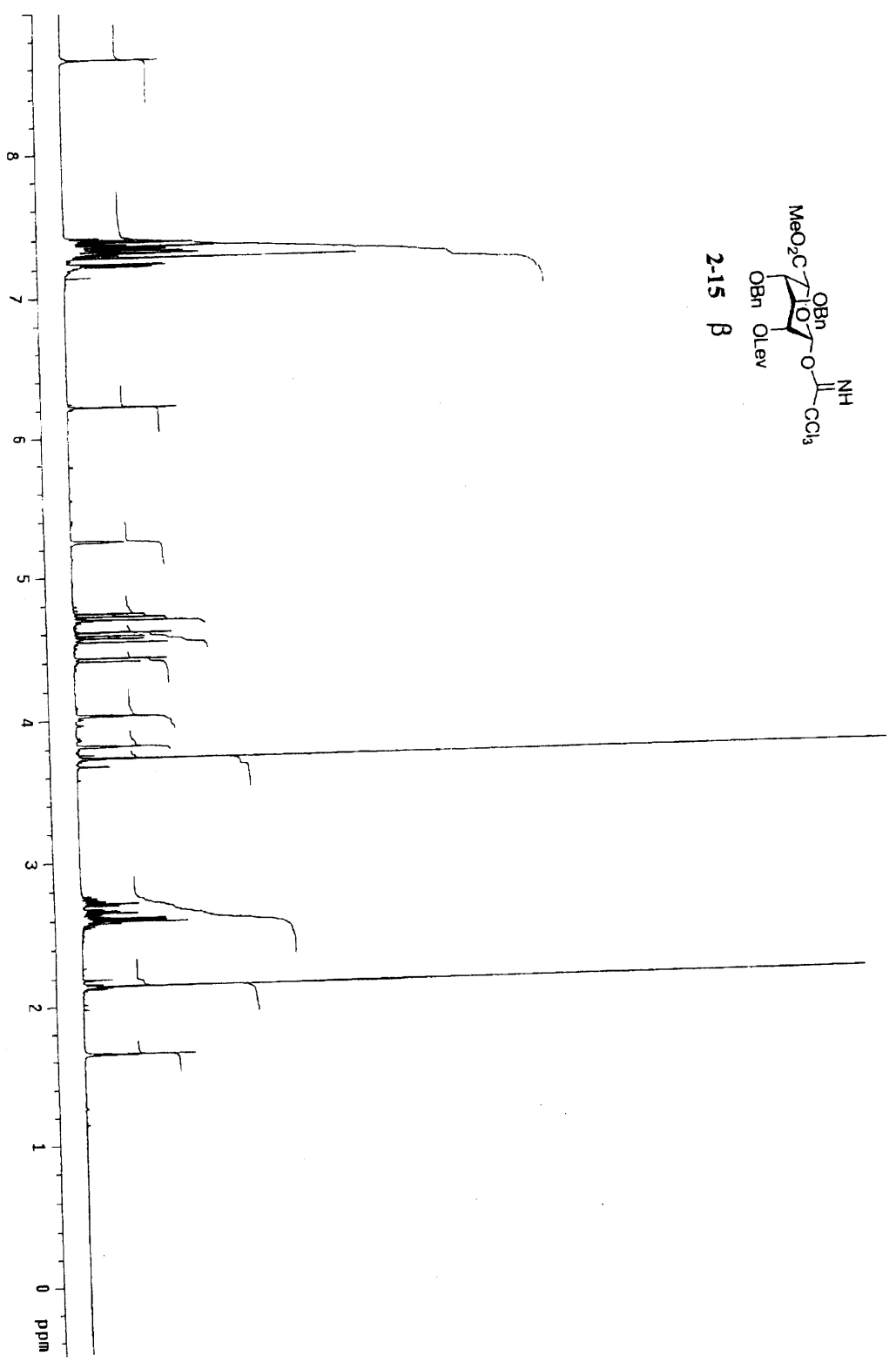


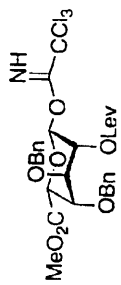
2-15 α



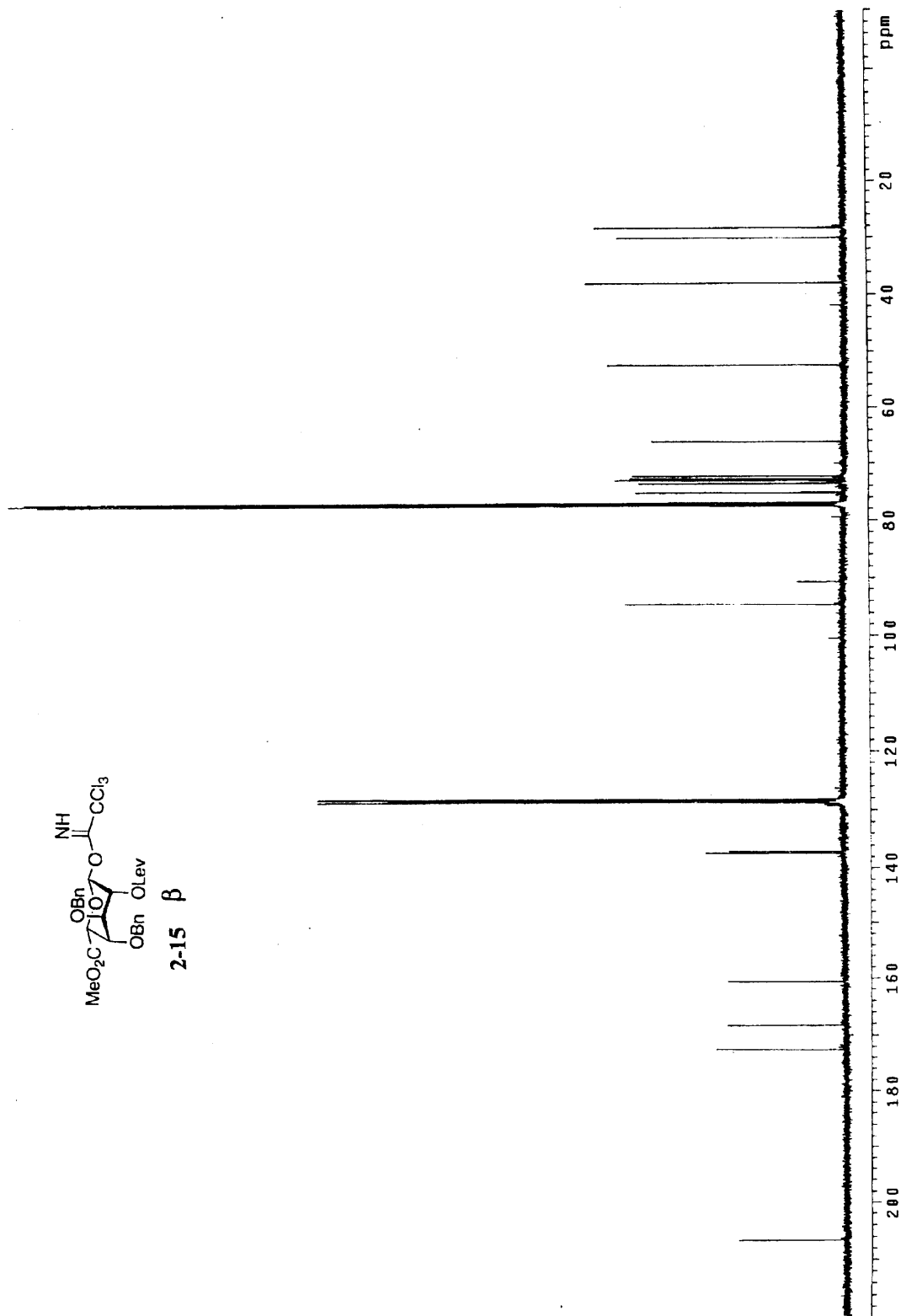


2-15 β

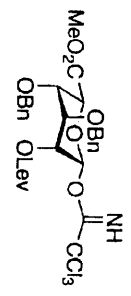




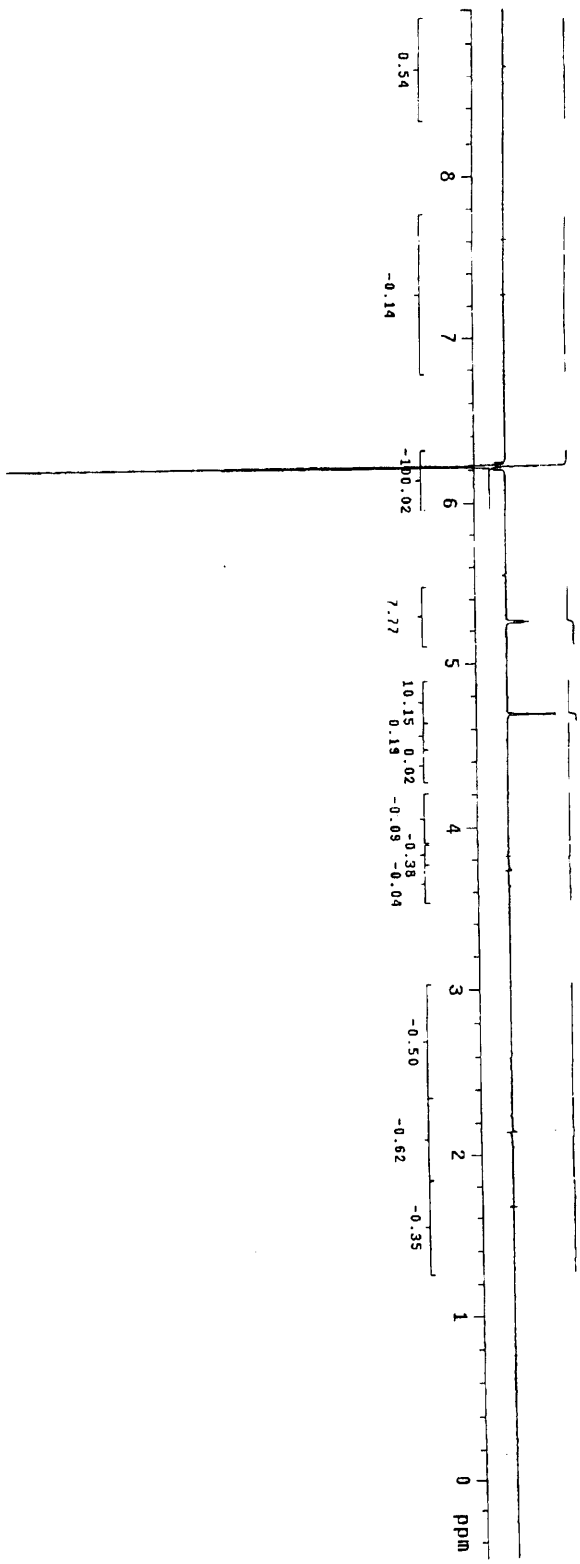
2-15 β

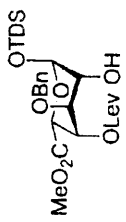


GL-2-110top MODdiff sat=6.22p
Pulse Sequence: presat

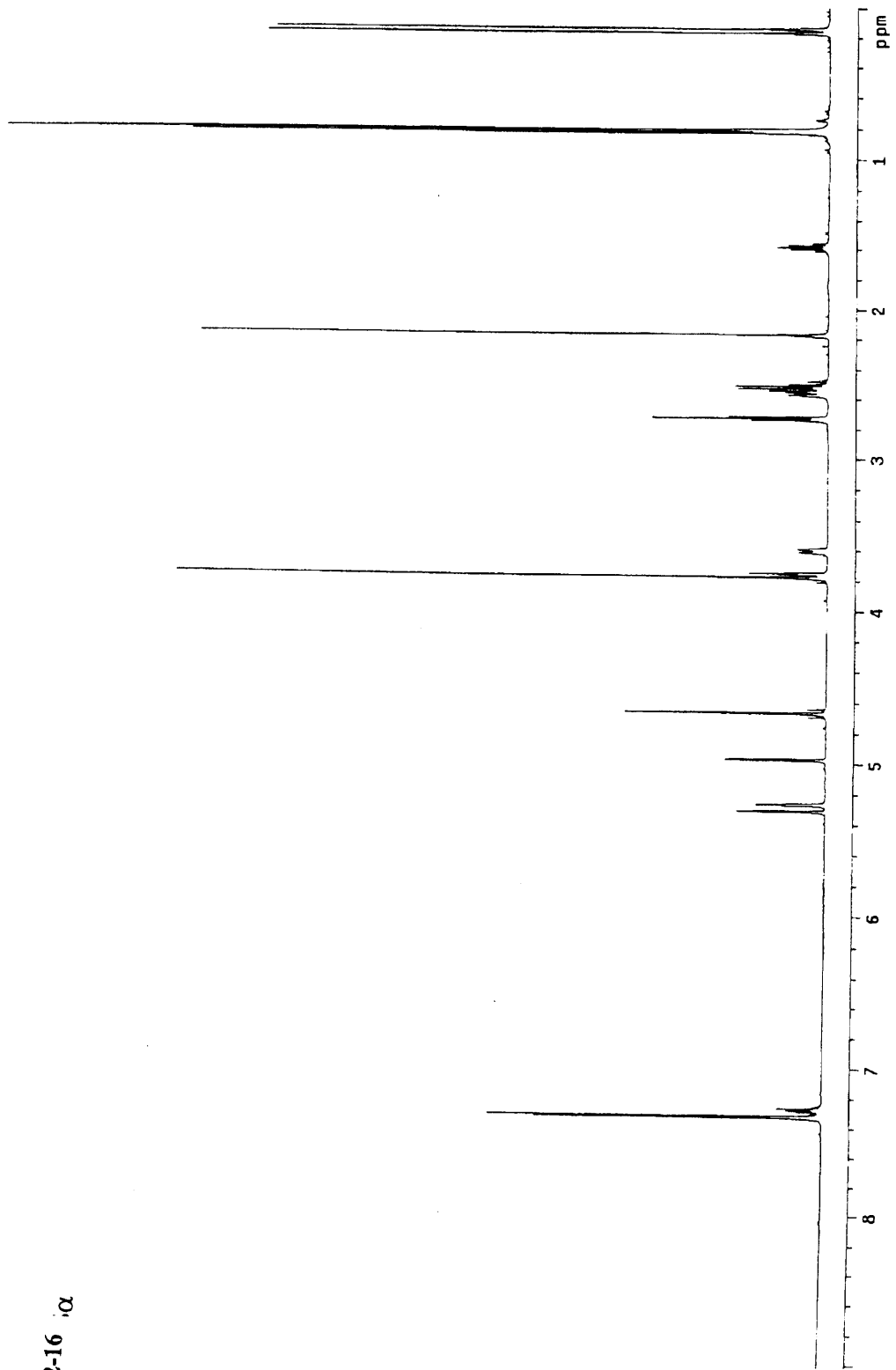


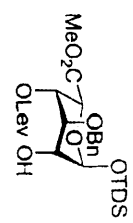
2-15 β



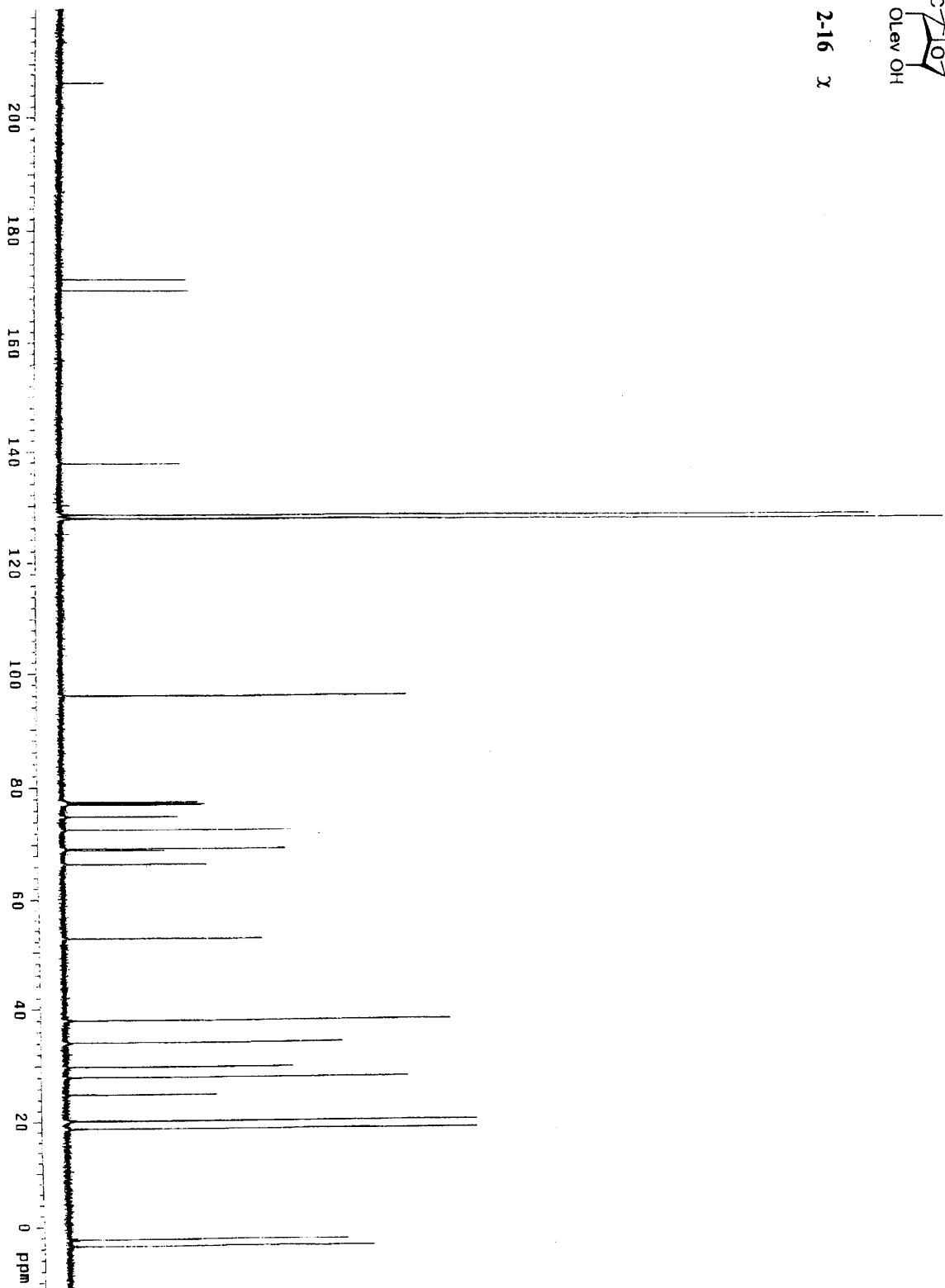


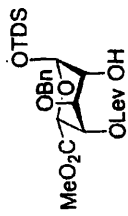
2-16 α





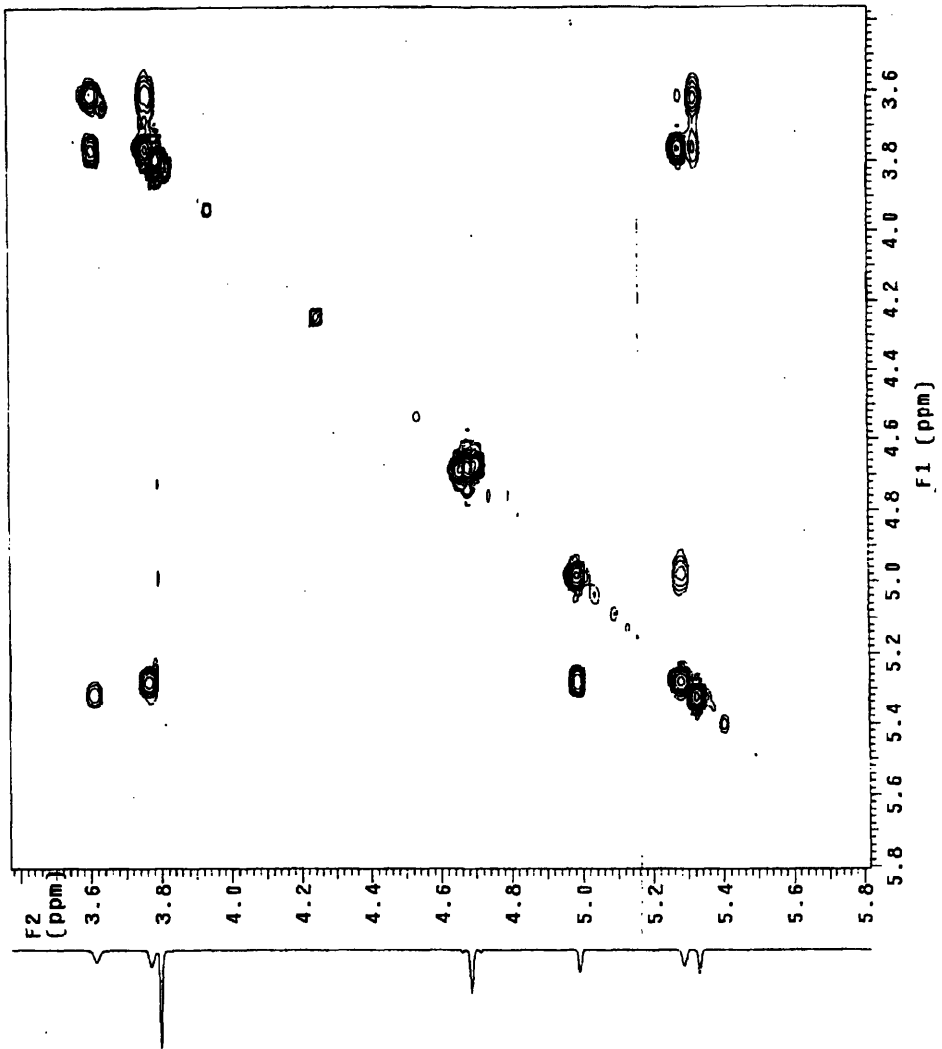
2-16 γ

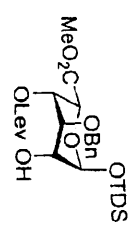




2-16 α

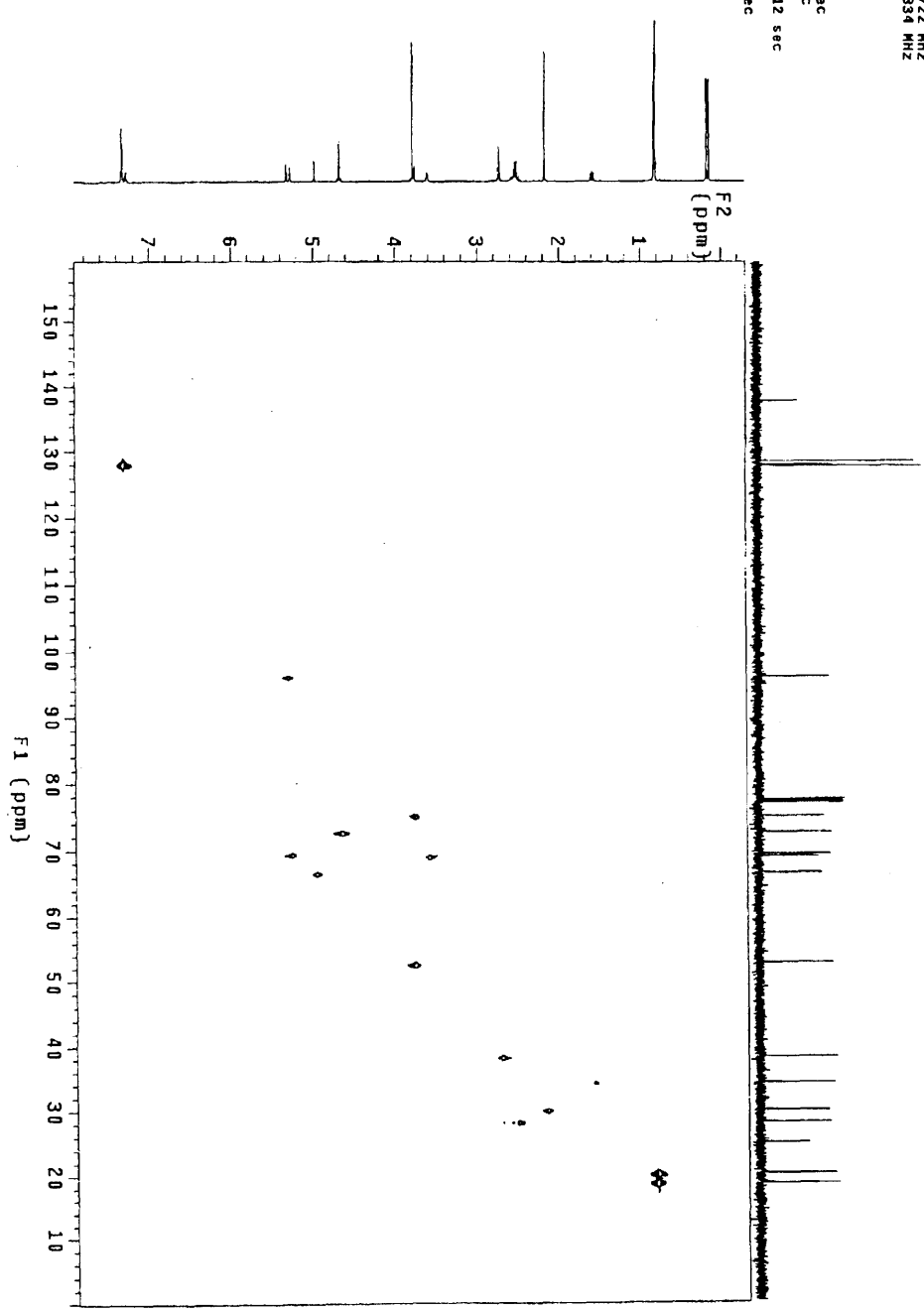
PULSE SEQUENCE: gCOSY
 Relax time 1.000 sec
 Acq. time 0.115 sec
 Width 4748.3 Hz
 2D Width 4748.3 Hz
 Single scan
 256 increments
 OBSERVE HI, 499.7537731 MHz
 DATA PROCESSING
 Sg. sine bell 0.100 sec
 F1 DATA PROCESSING
 Sg. sine bell 0.052 sec
 F1 size 2048 x 2048
 Total time 3 min, 41 sec

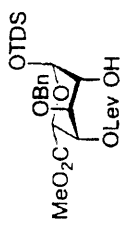




2-16 α

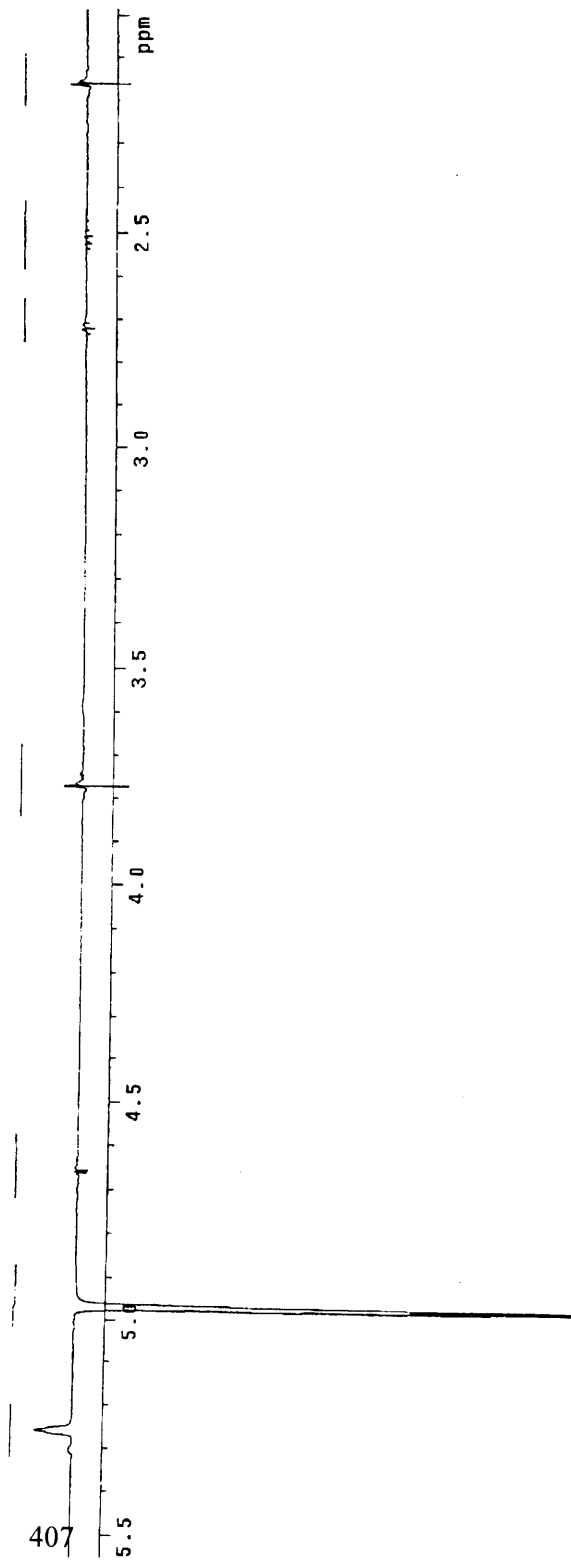
PULSE SEQUENCE: HSQC
 Relax. delay 1.000 sec
 Acq. time 0.101 sec
 2D Width 2322.0 Hz
 4 repetitions
 2 x 128 increments
 OBSERVE H1, 499.753722 MHz
 DECOUPLE C13, 125.6759334 MHz
 Power 53 dB
 on during acquisition
 off during delay
 GAMP-1 modulated
 DATA PROCESSING 0.101 sec
 Sg. sine bell 0.101 sec
 F1 DATA PROCESSING 0.101 sec
 Gauss apodization 0.012 sec
 FI size 2048 x 2048
 Total time 23 min, 8 sec

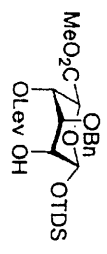




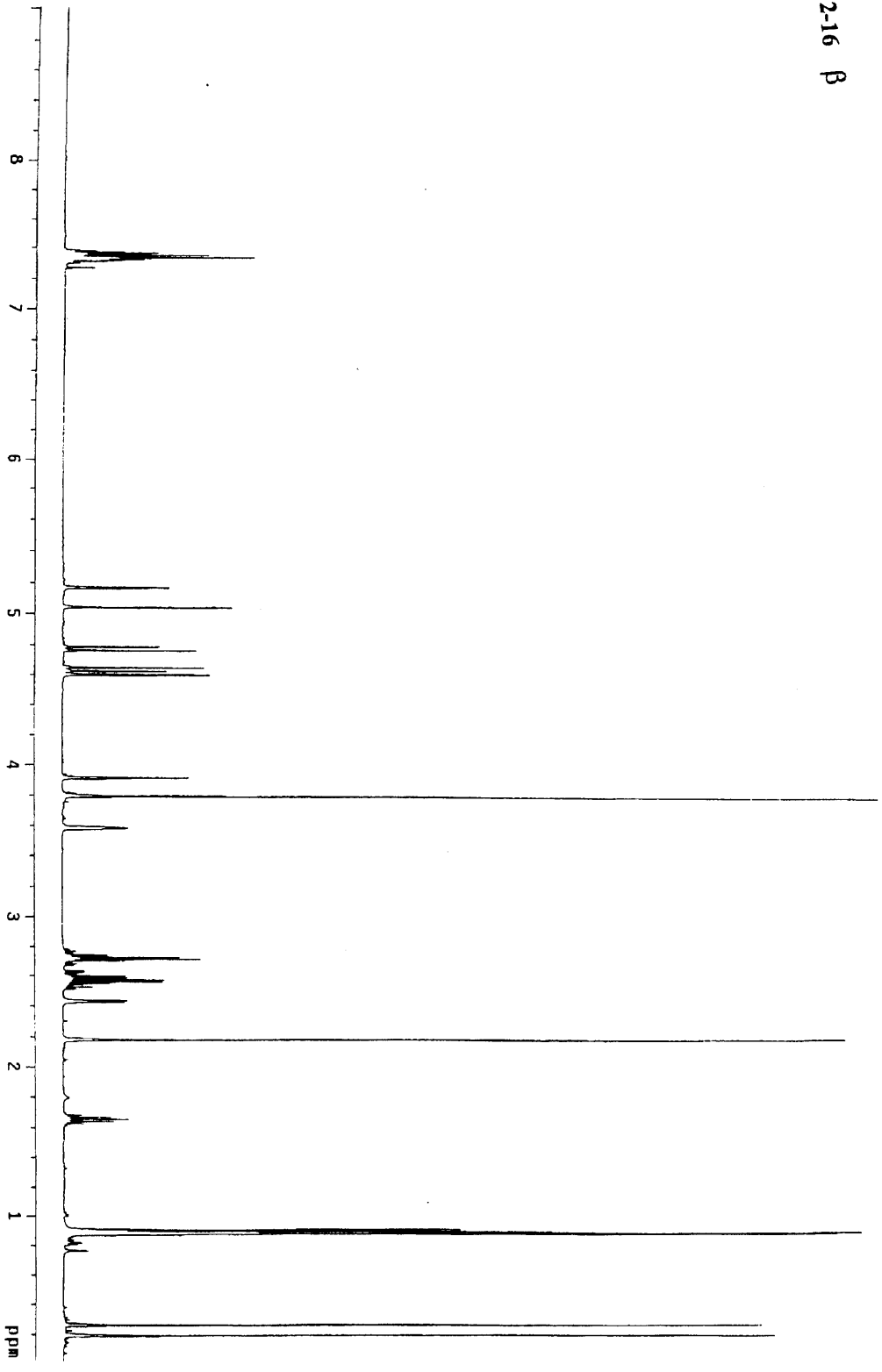
NOE saturation frequency 4.97 ppm

2-16 α



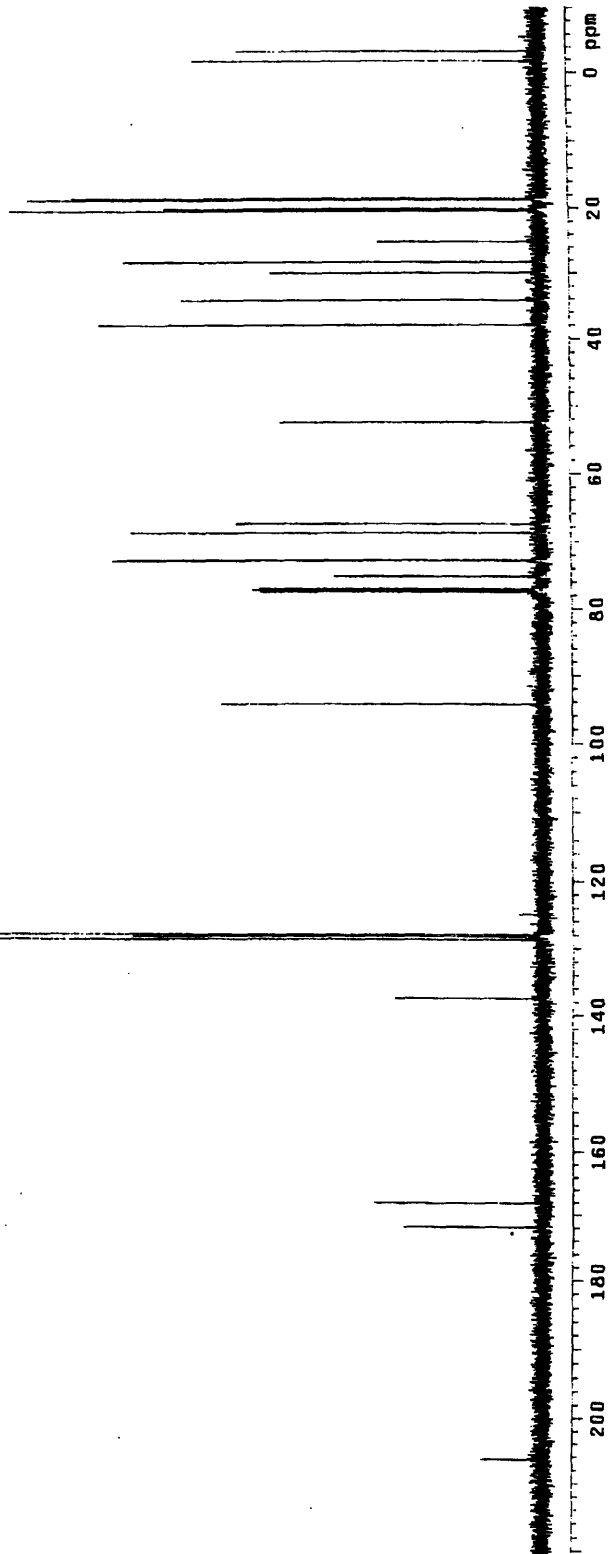


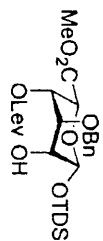
2-16 β





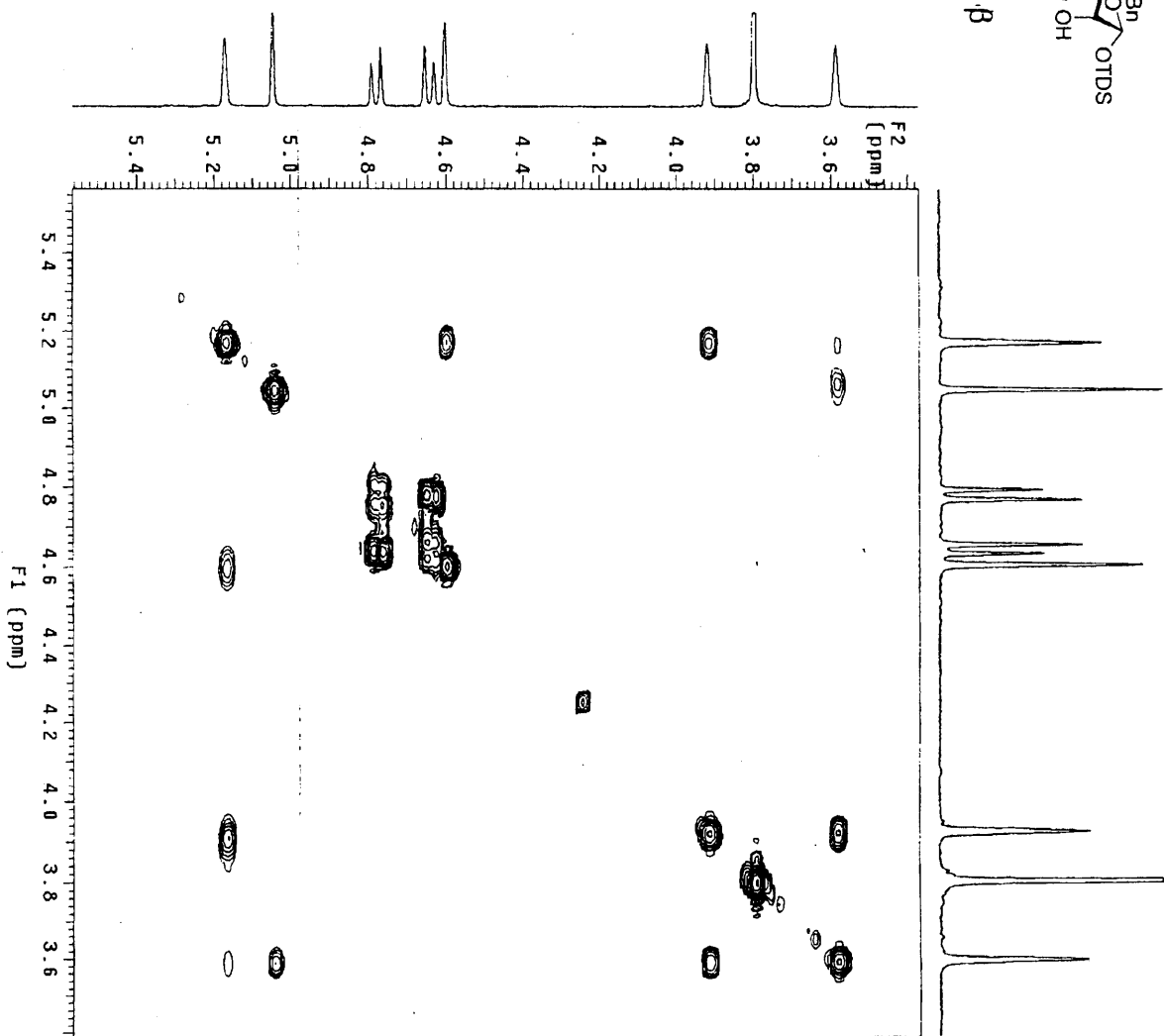
2-16 β





2-16 β

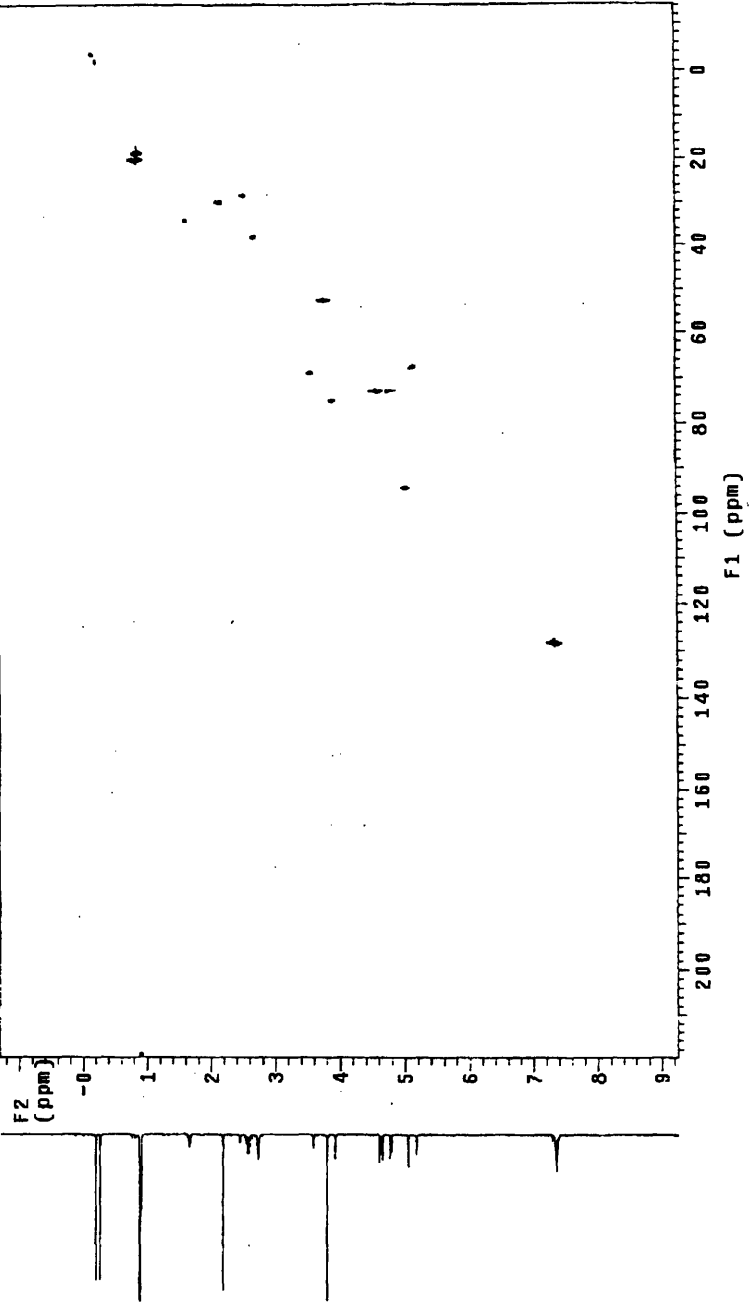
PULSE SEQUENCE: gCOSY
 Relax. delay: 1.000 sec
 Acq. time: 0.216 sec
 2D Width: 4748.3 Hz
 Single scan
 256 increments
 OBSERVE: H1, 499.753725 MHz
 DATA PROCESSING
 Sd. sine bell: 0.108 sec
 F1 DATA PROCESSING
 Sg. sine bell: 0.052 sec
 Ff. size: 2048 x 2048
 Total time: 5 min, 41 sec





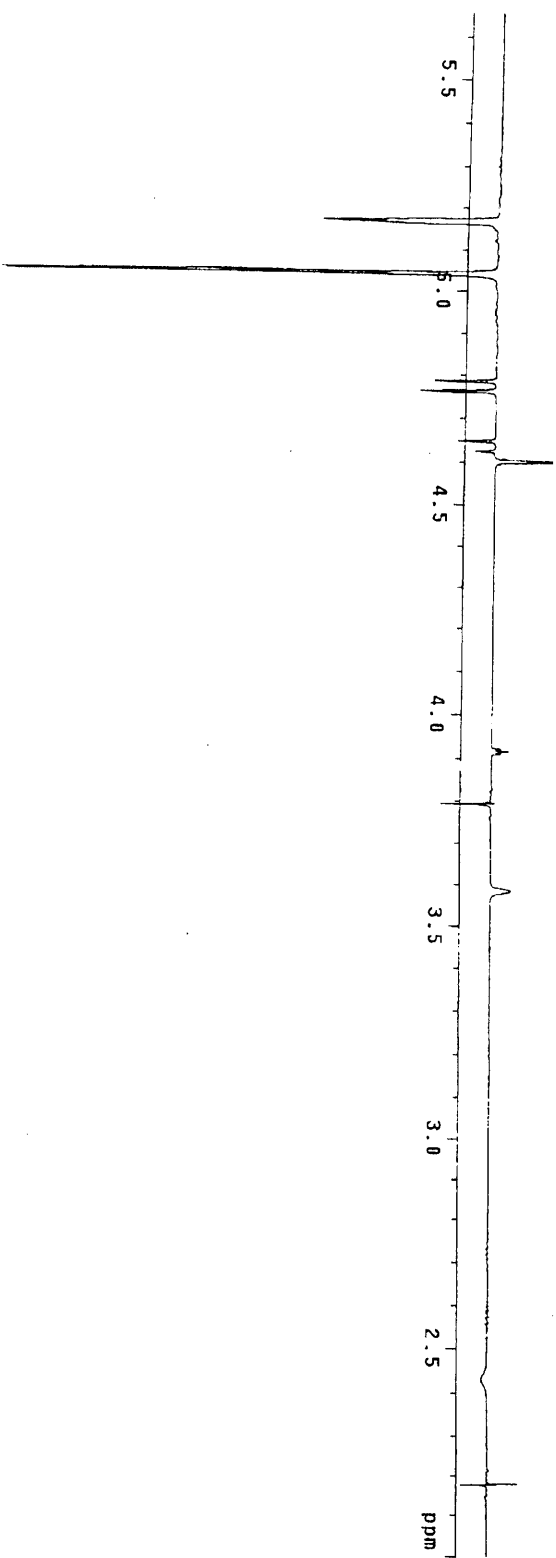
2-16 β

PULSE SEQUENCE: HSQC
 Relax delay 2.000 sec
 Width 5220.1 Hz
 2D Width 29411.5 Hz
 4 repetitions
 2 x 128 increments
 OBSERVE H1, 489.753722 MHz
 DECOUPLE C13, 125.6760827 MHz
 Power 59 dB
 on during acquisition
 off during delay
 GARP-1 modulated
 DATA PROCESSING
 Slicing 0.037 sec
 Slicing 0.037 sec
 F1 DATA PROCESSING
 Gauss apodization 0.012 sec
 FT size 2048 x 2048
 Total time 23 min, 2 sec



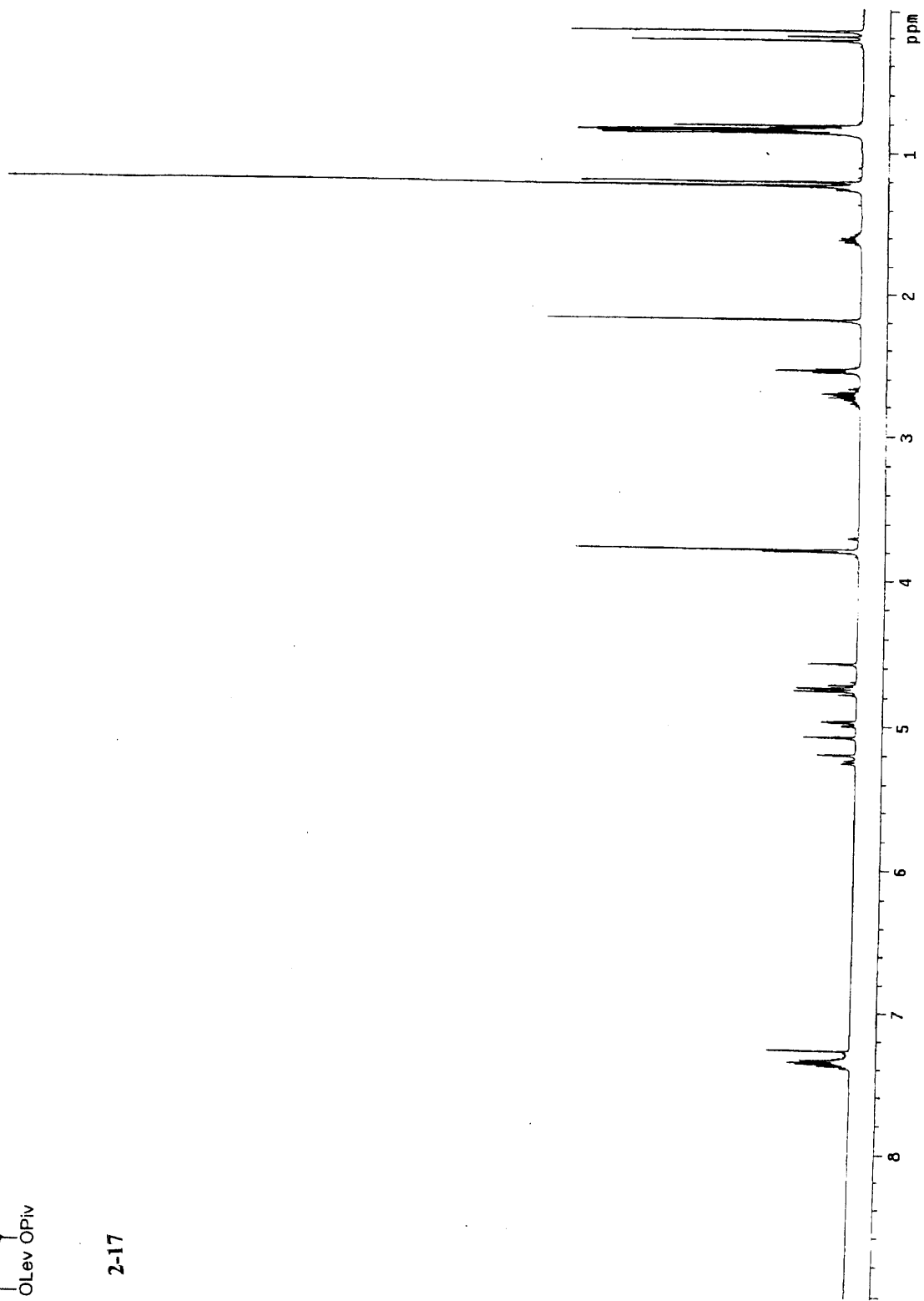
MeO₂C OBn
OTDS
OH ev
NOE saturation frequency 5.04 ppm

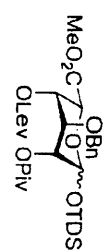
2-16 β



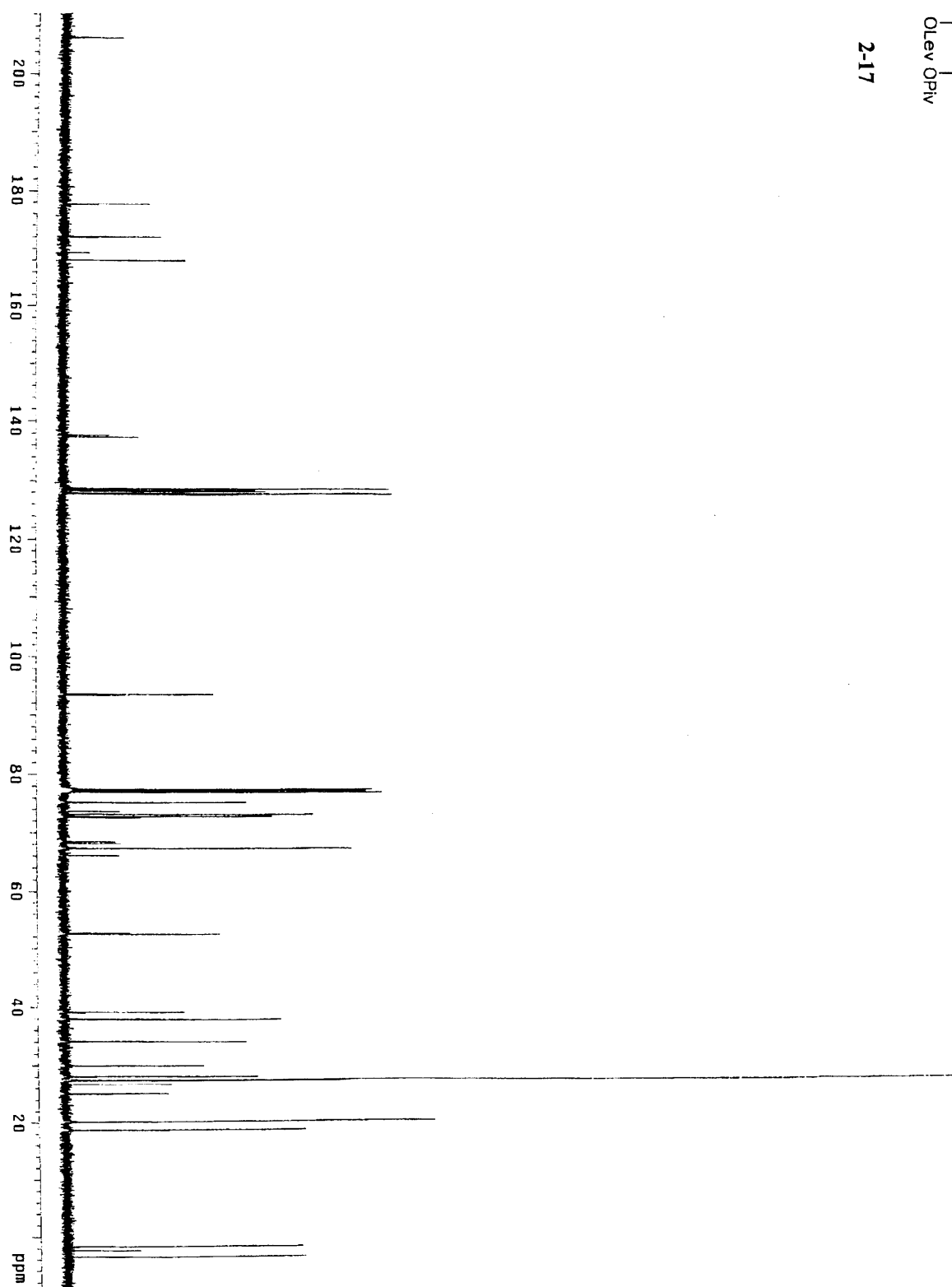


2-17



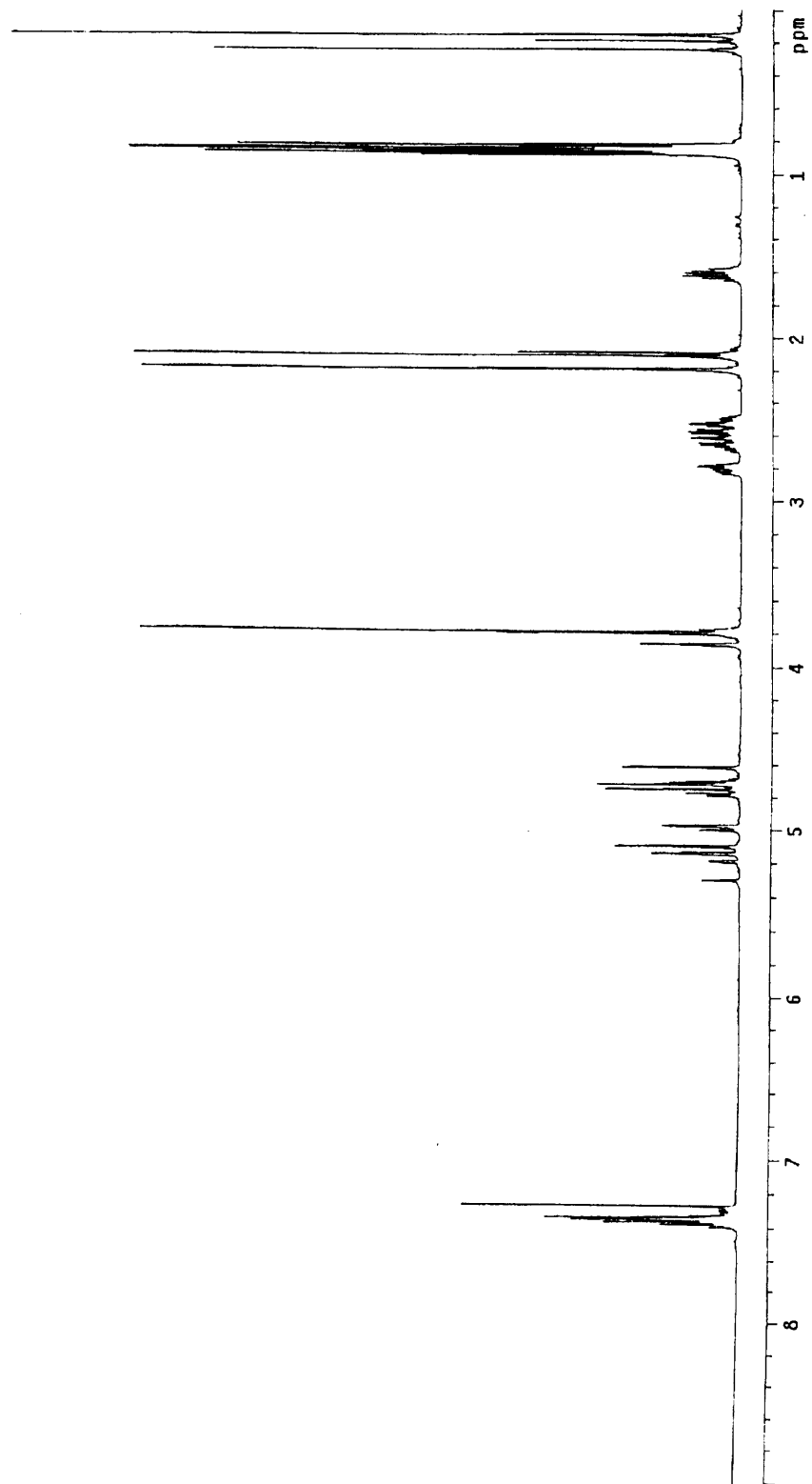


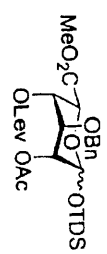
2-17



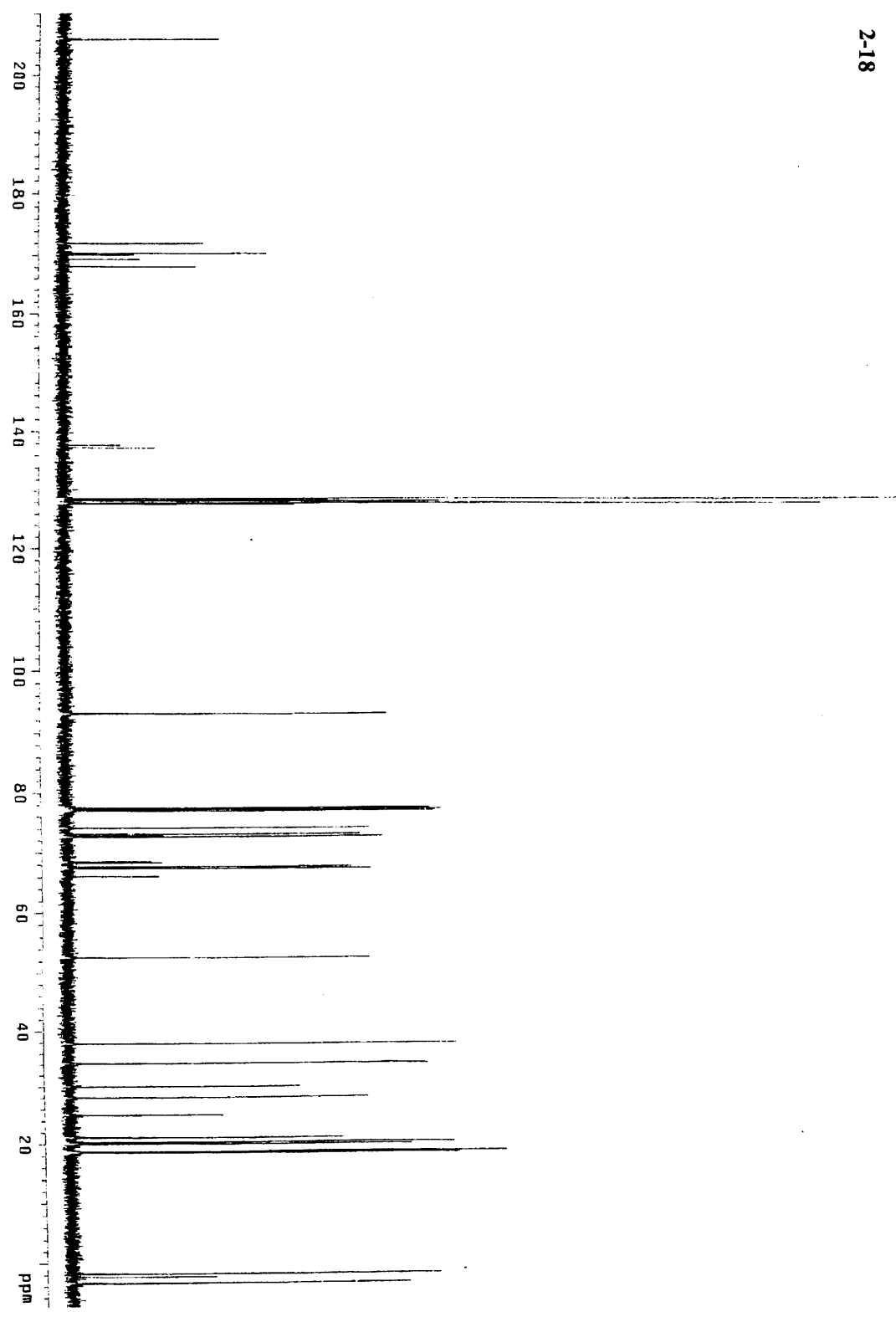


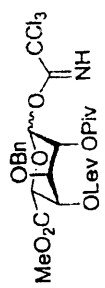
2-18



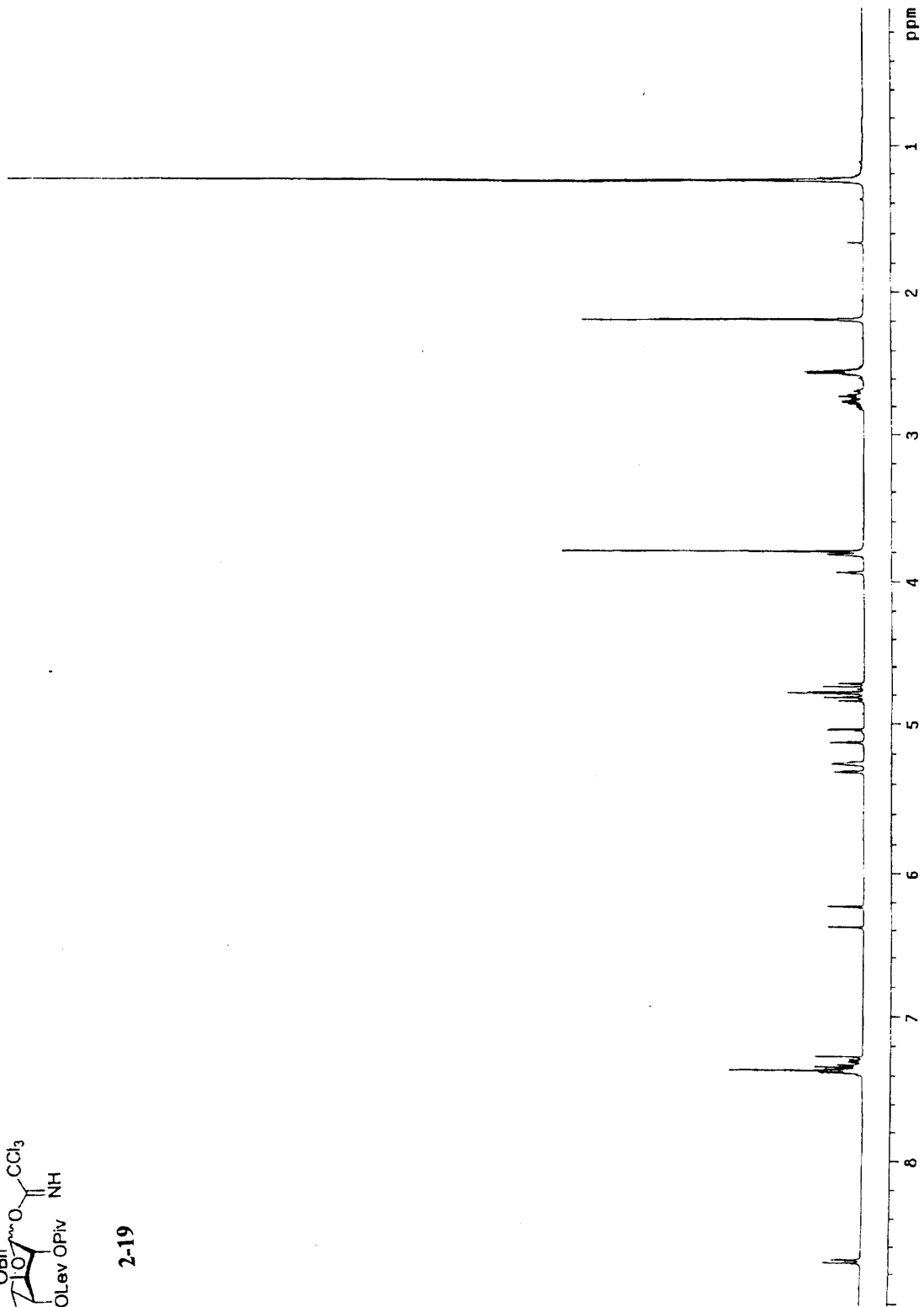


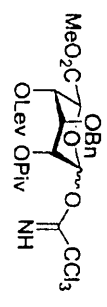
2-18



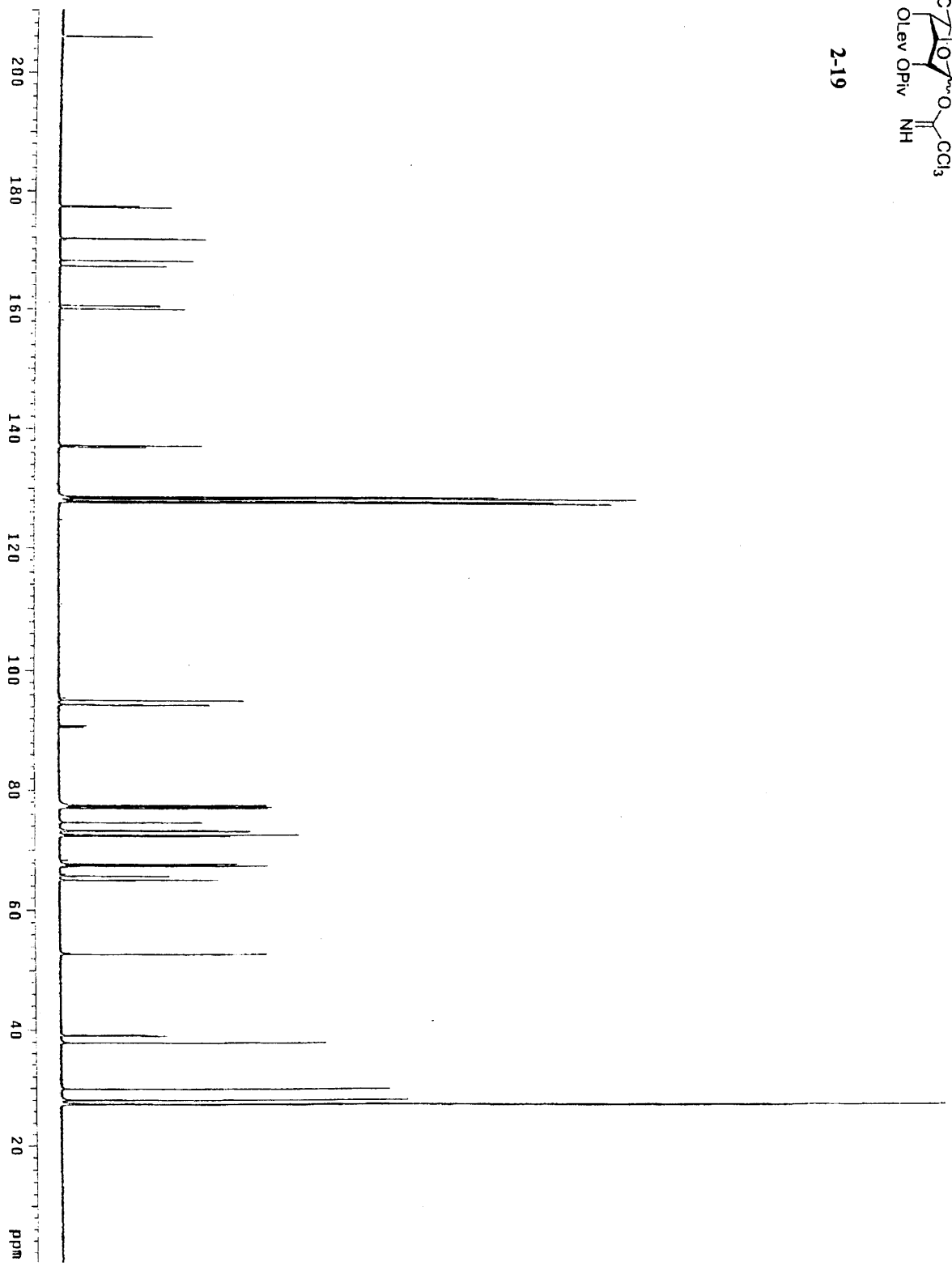


2-19



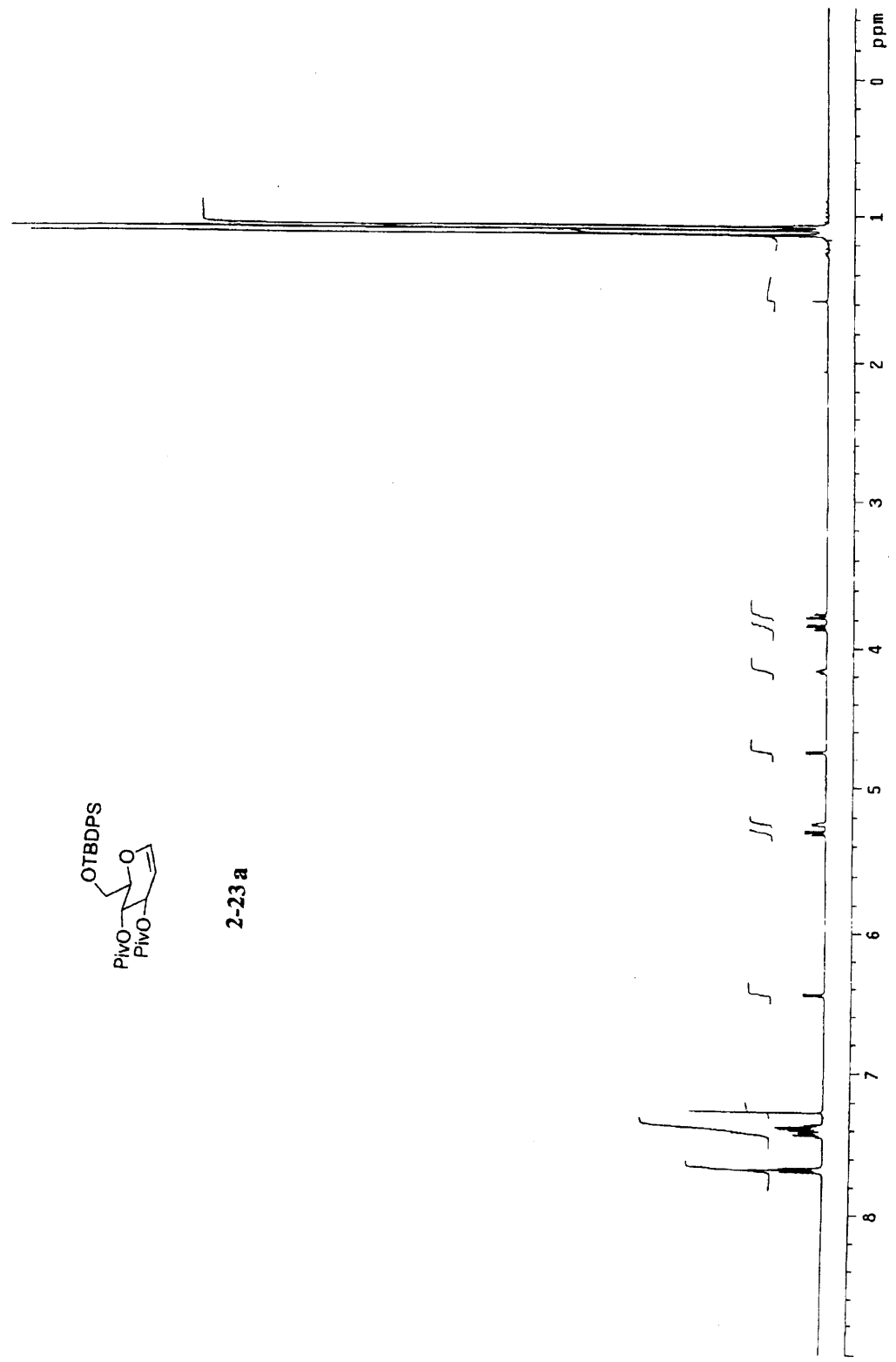


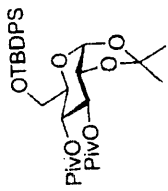
2-19



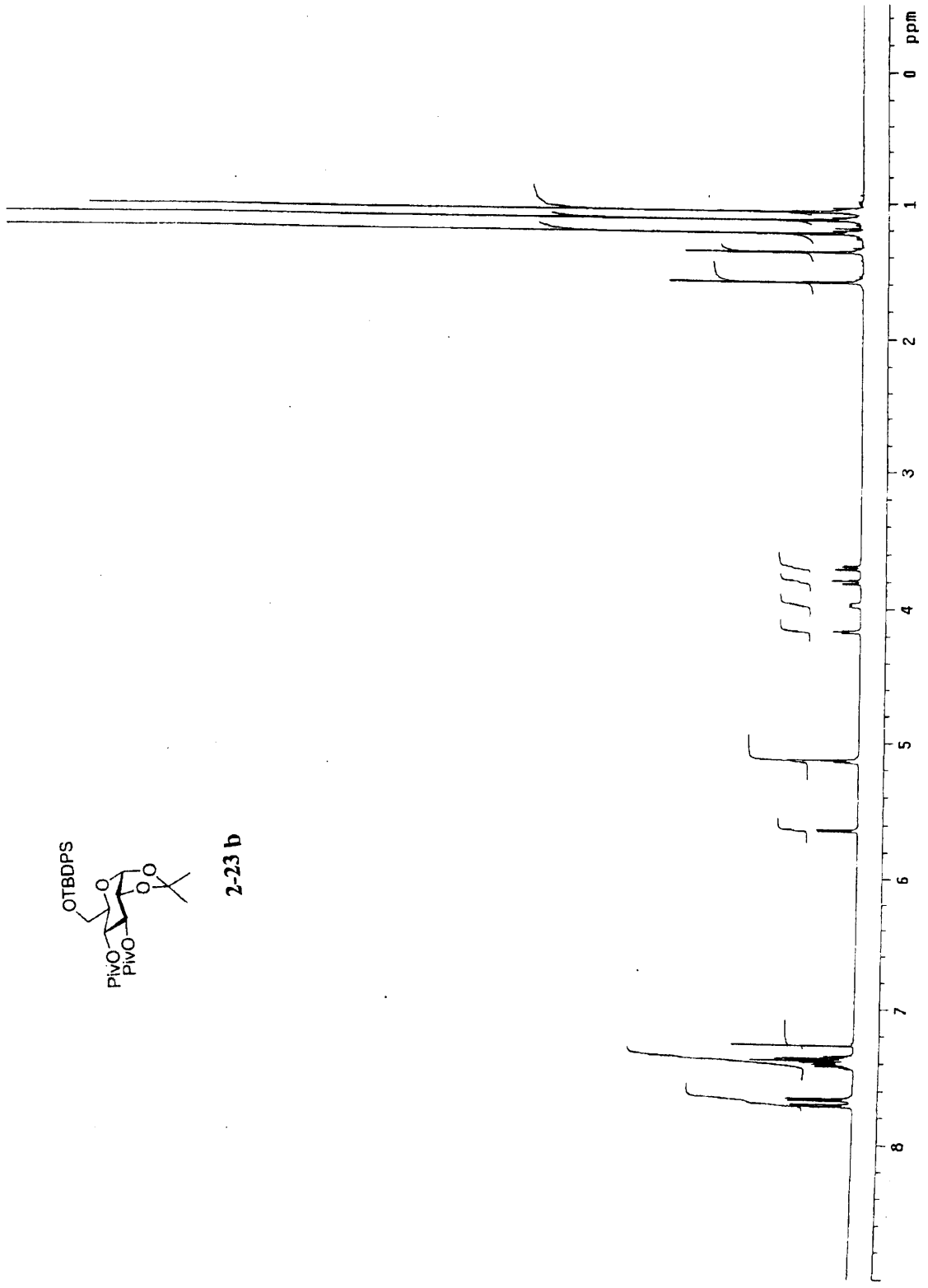


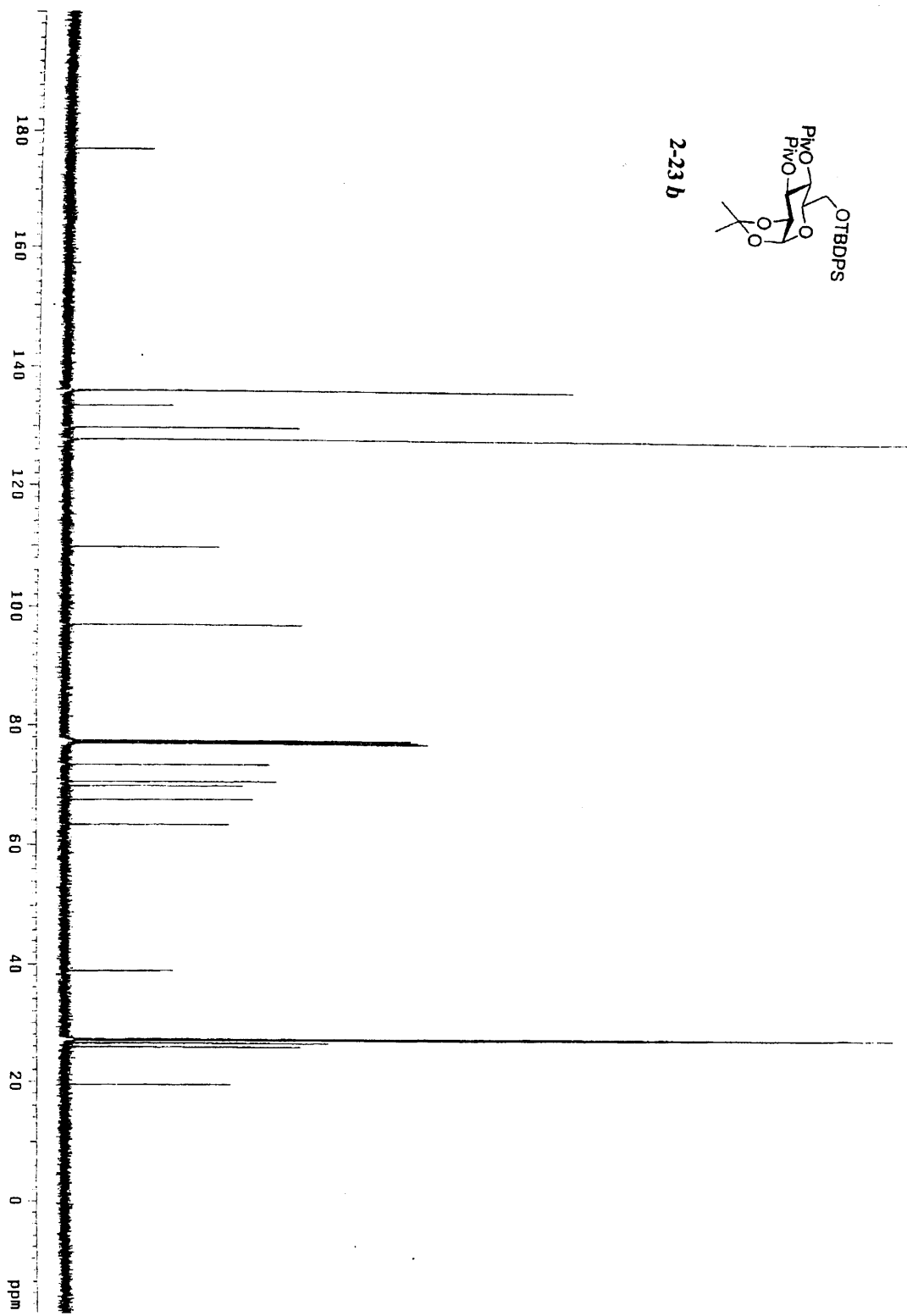
2-23 a



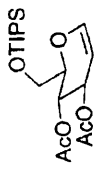


2-23 b

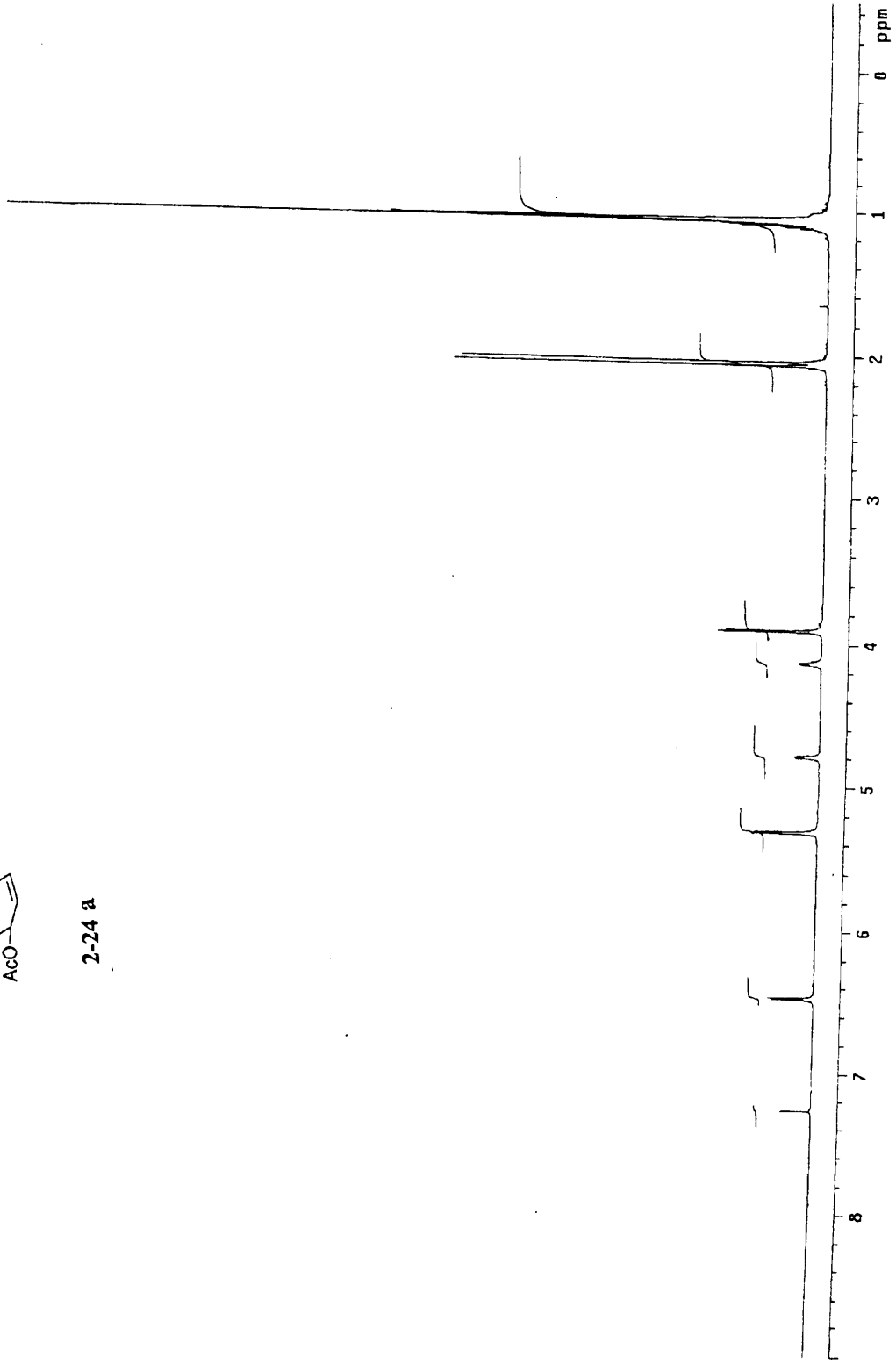


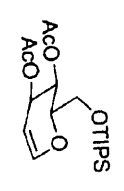
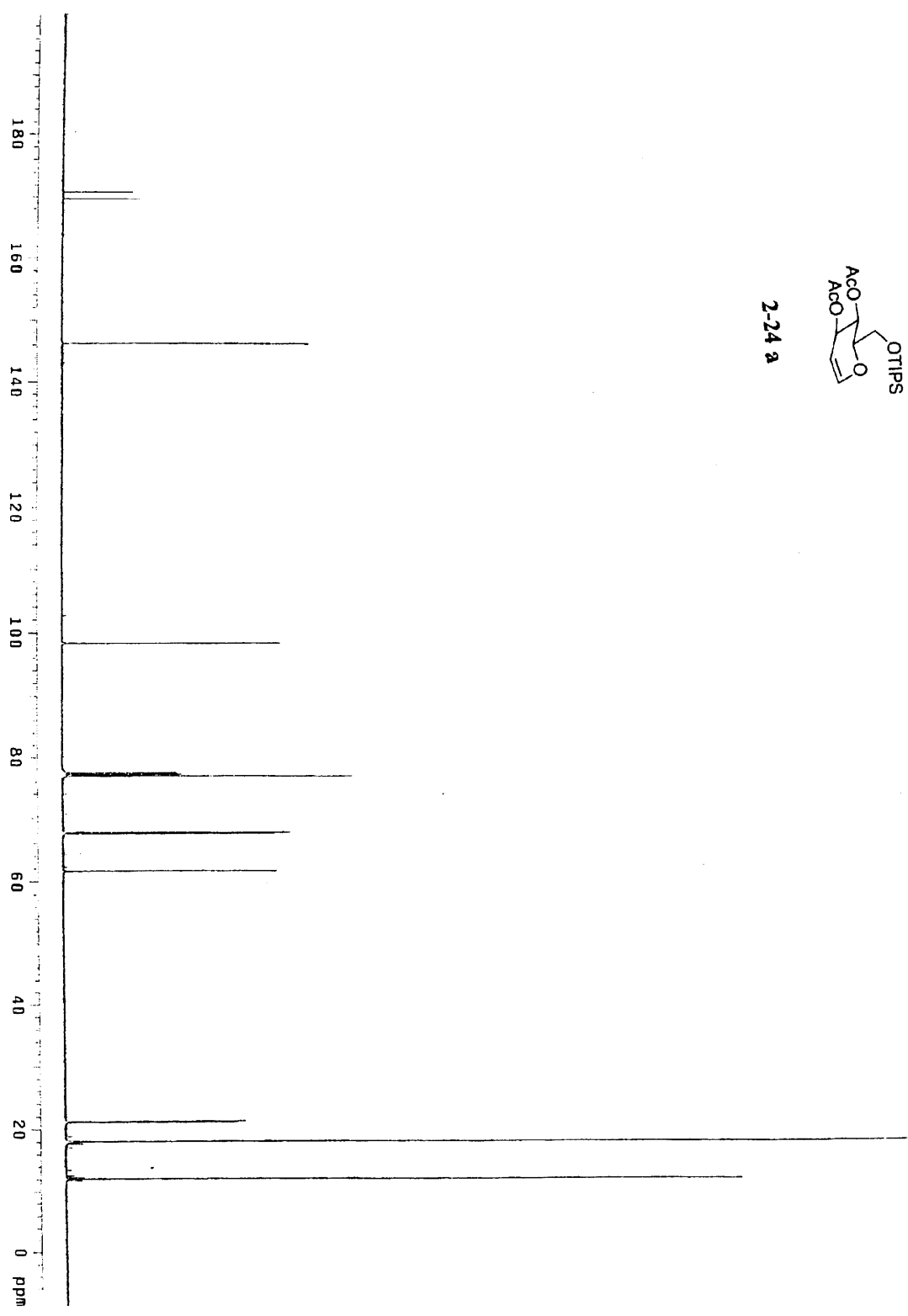


2-23 b

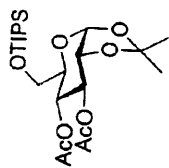


2-24 a

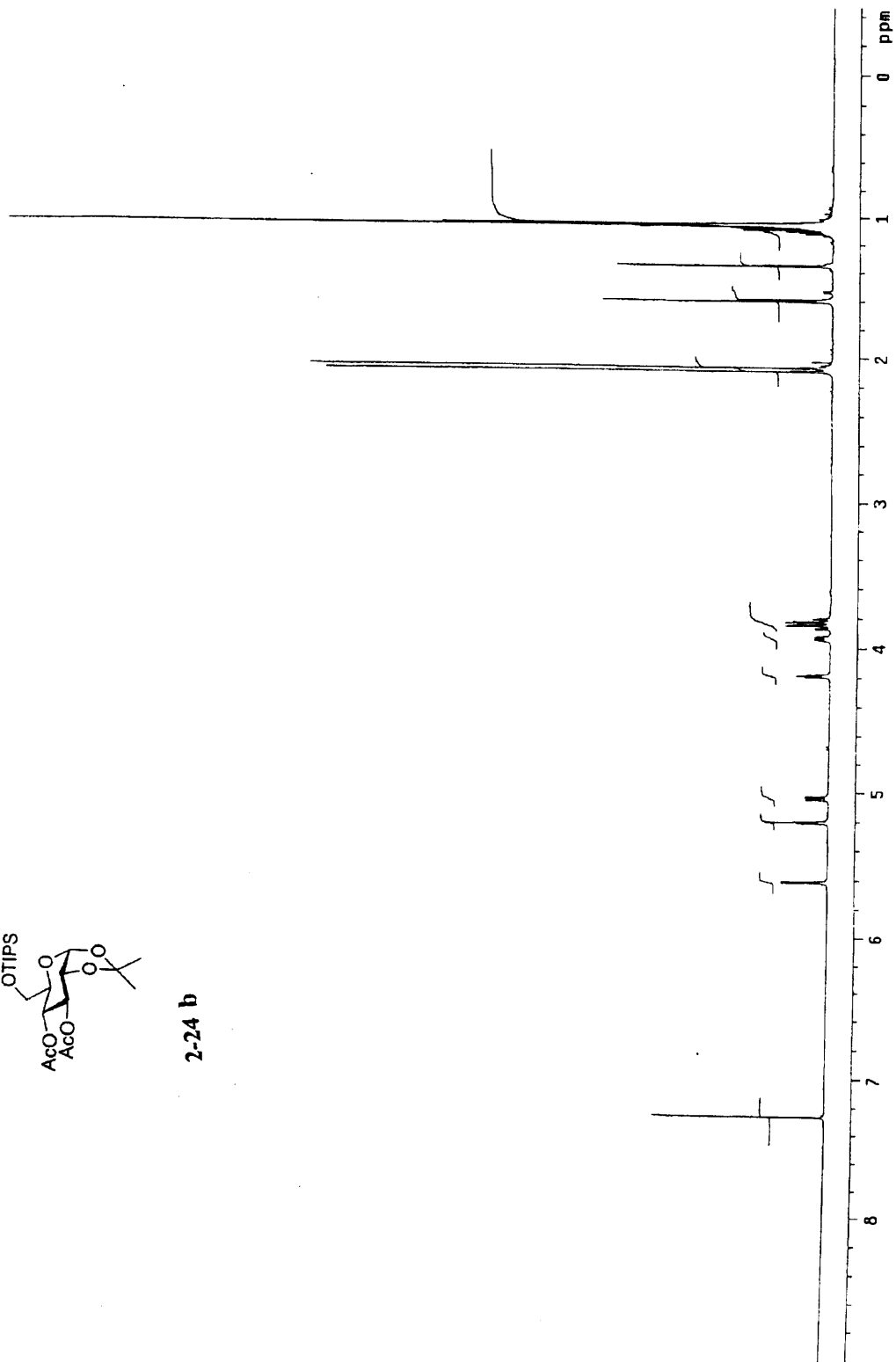


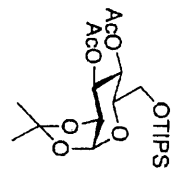
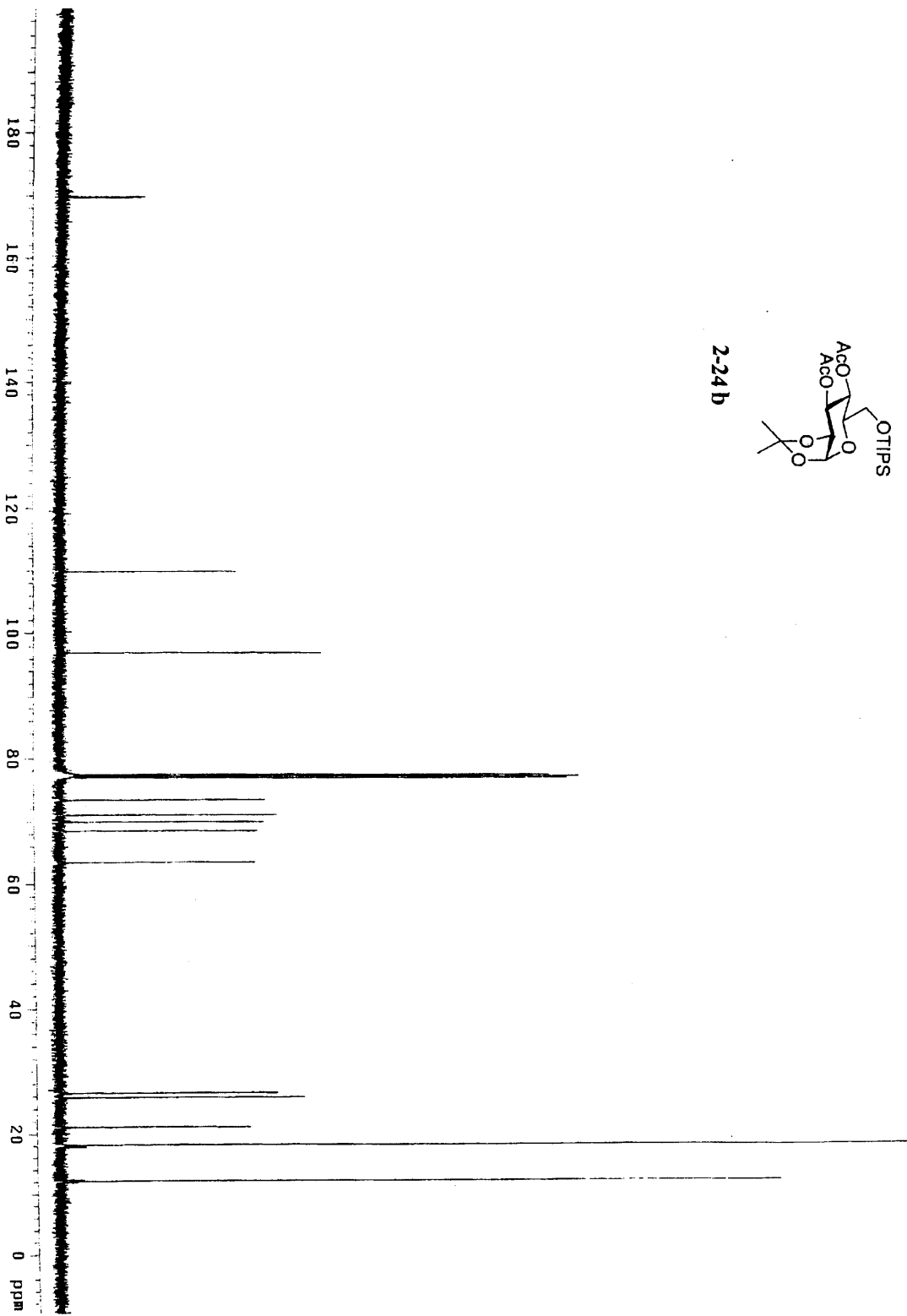


2-24 a

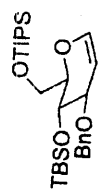


2-24 b

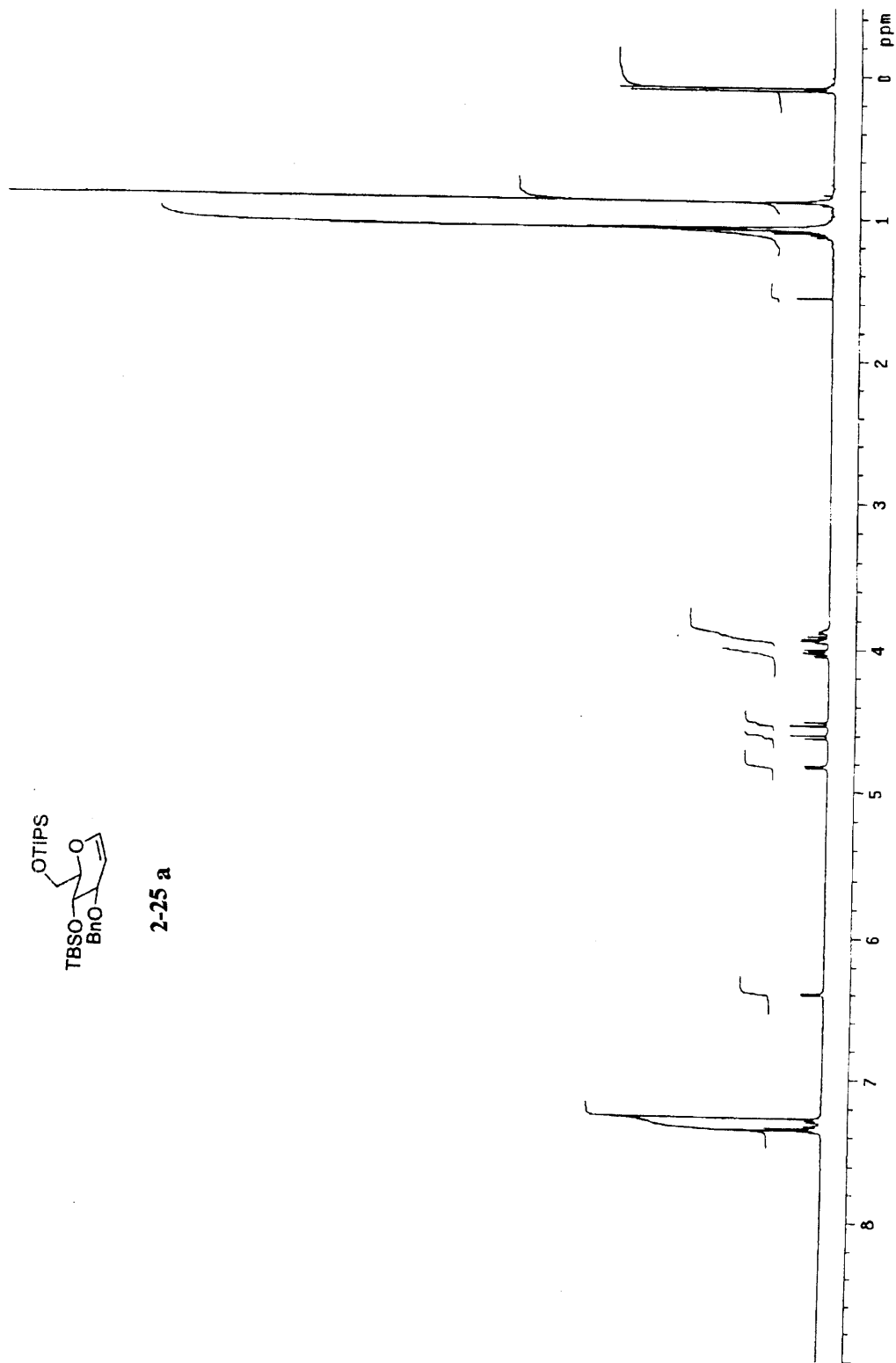


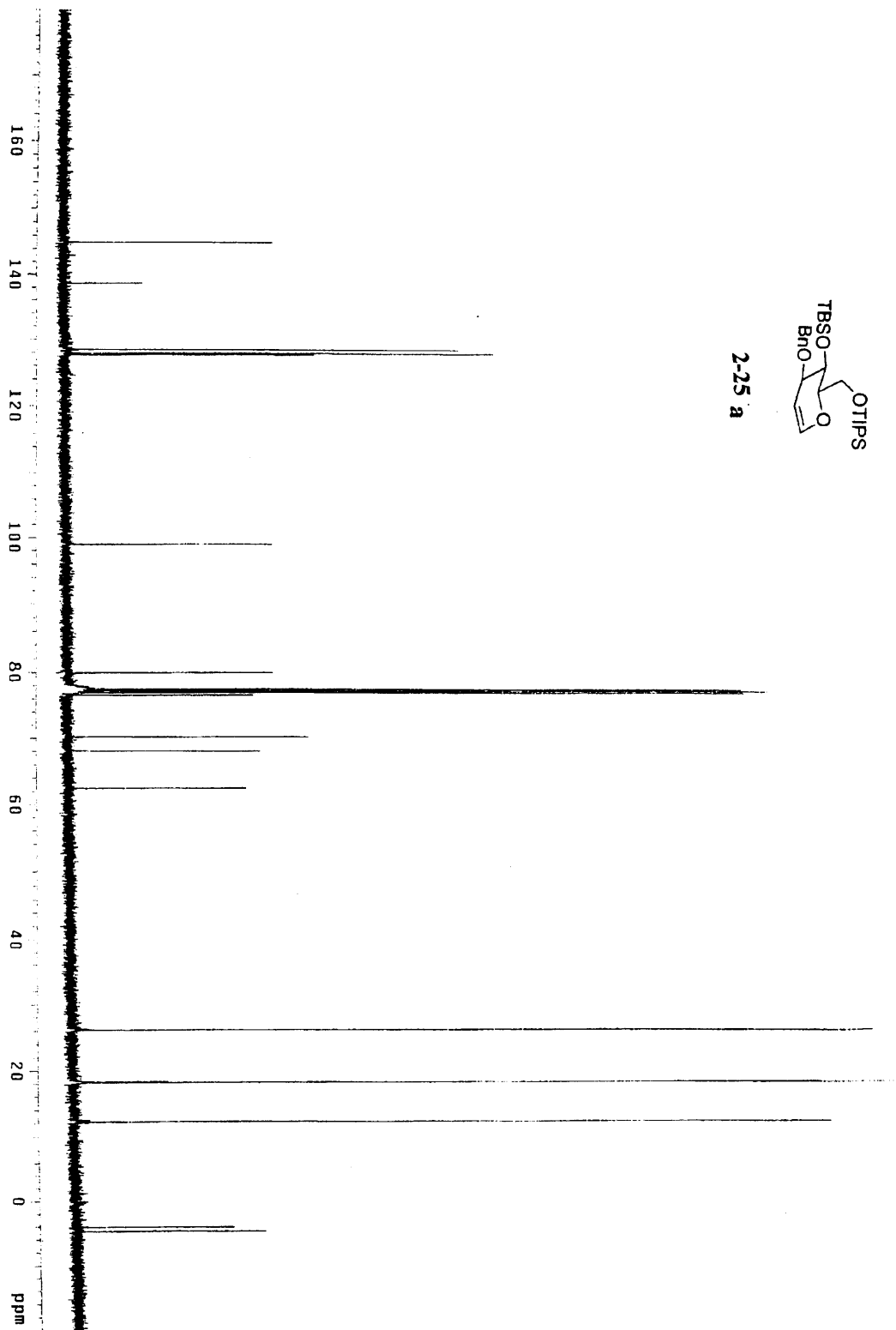


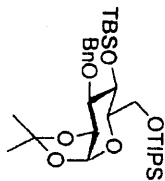
2-24b



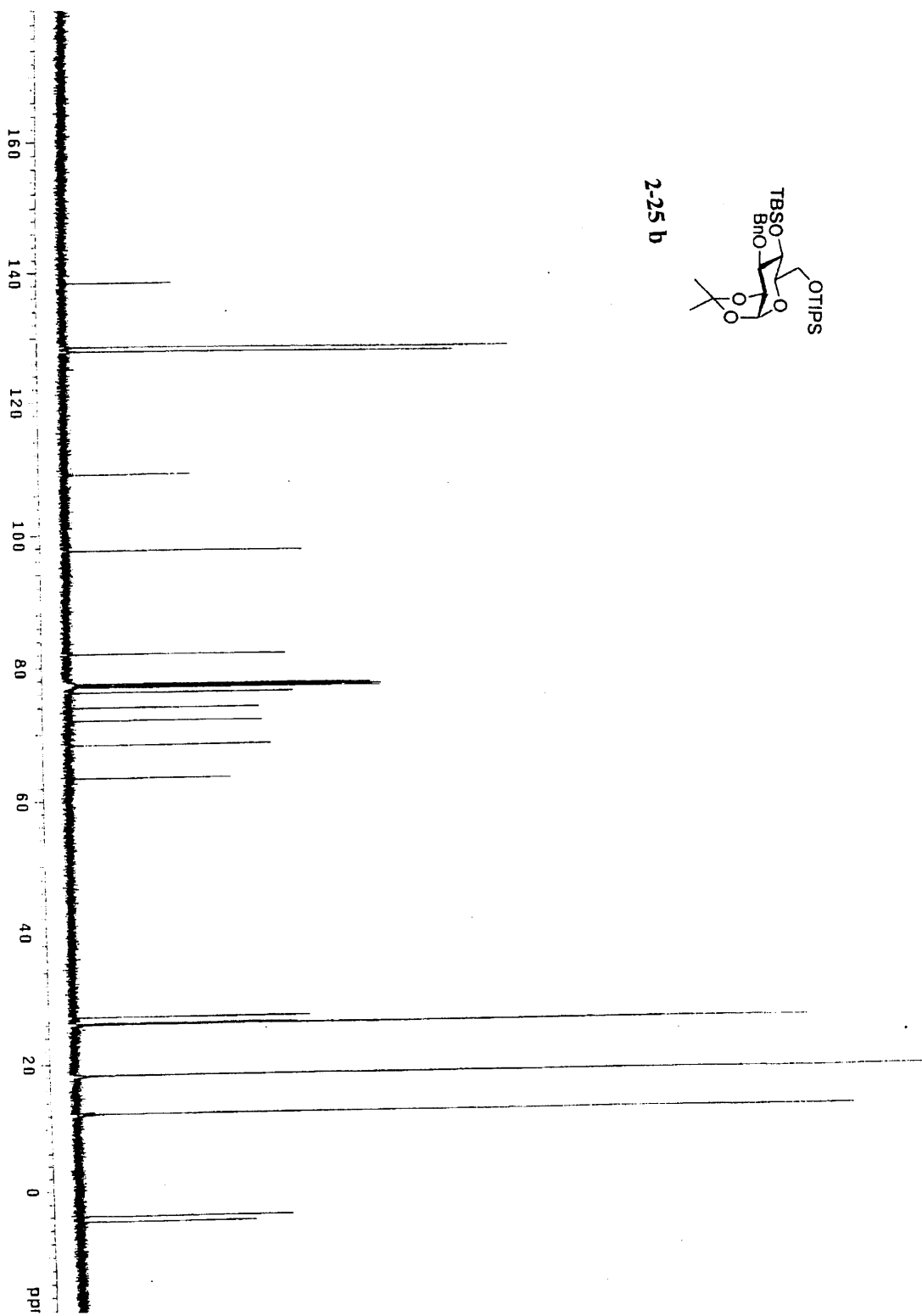
2-25 a

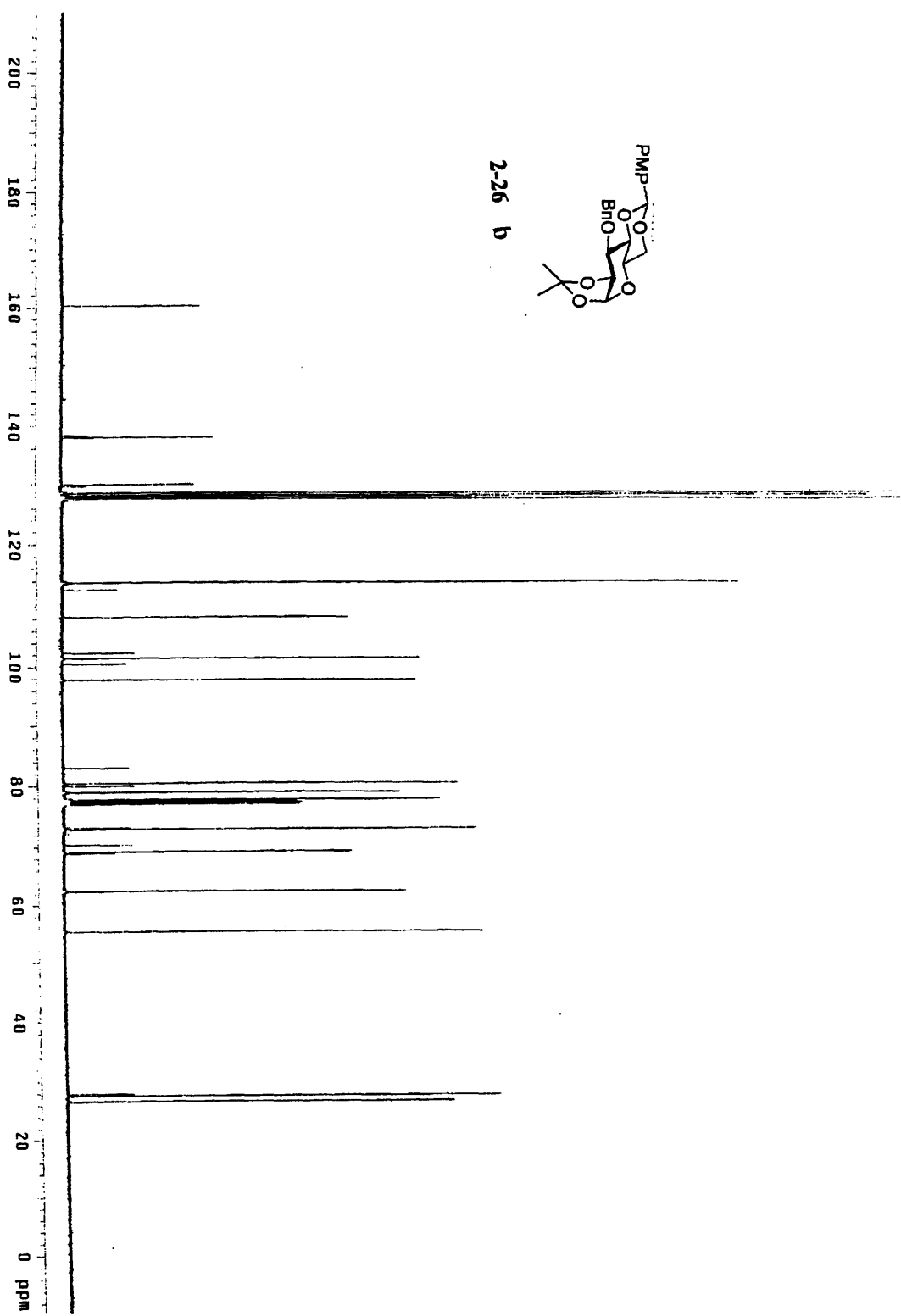


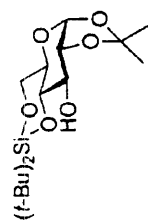




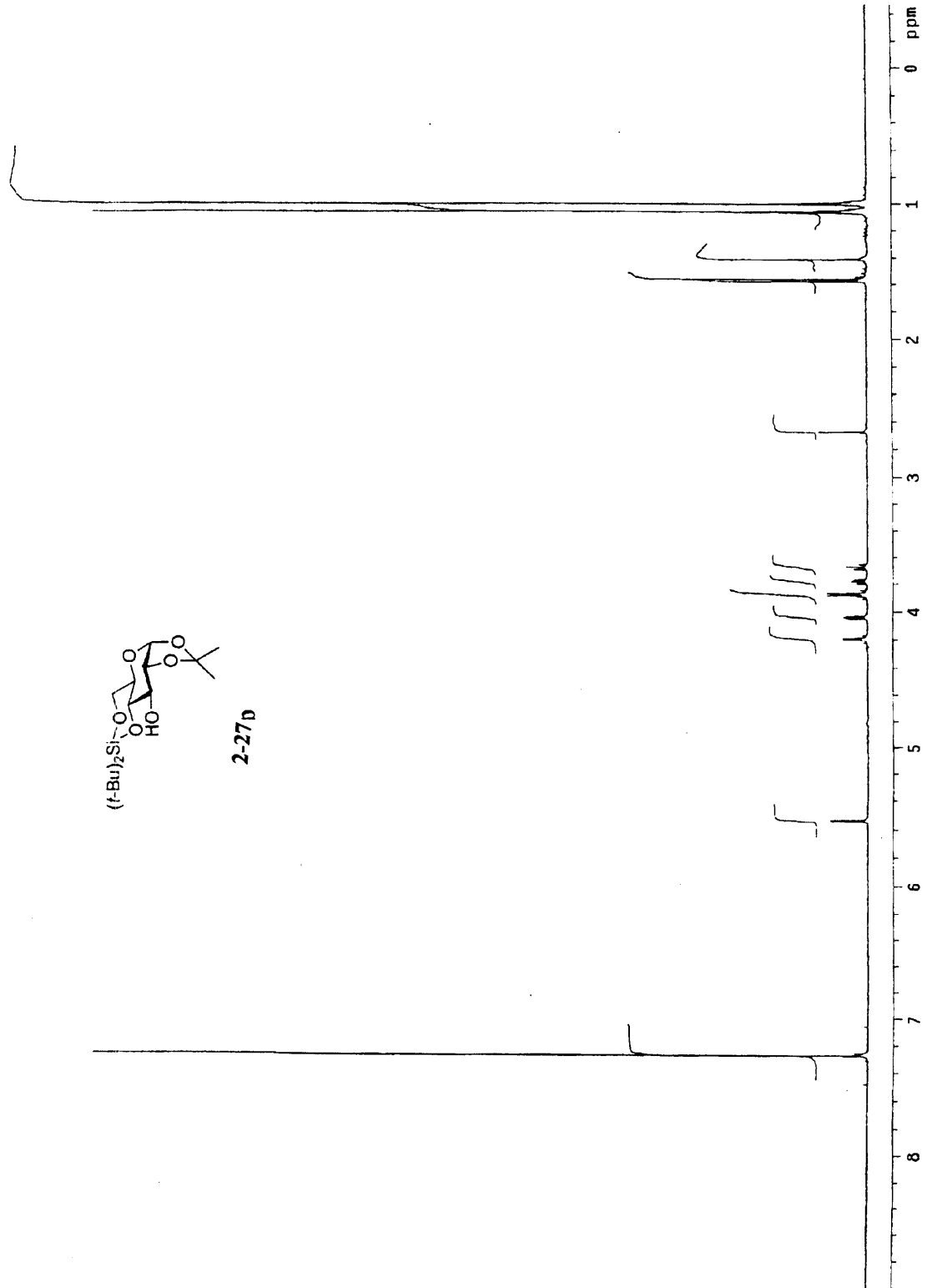
2-25 b

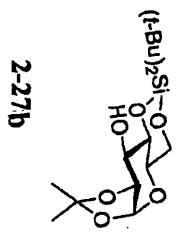
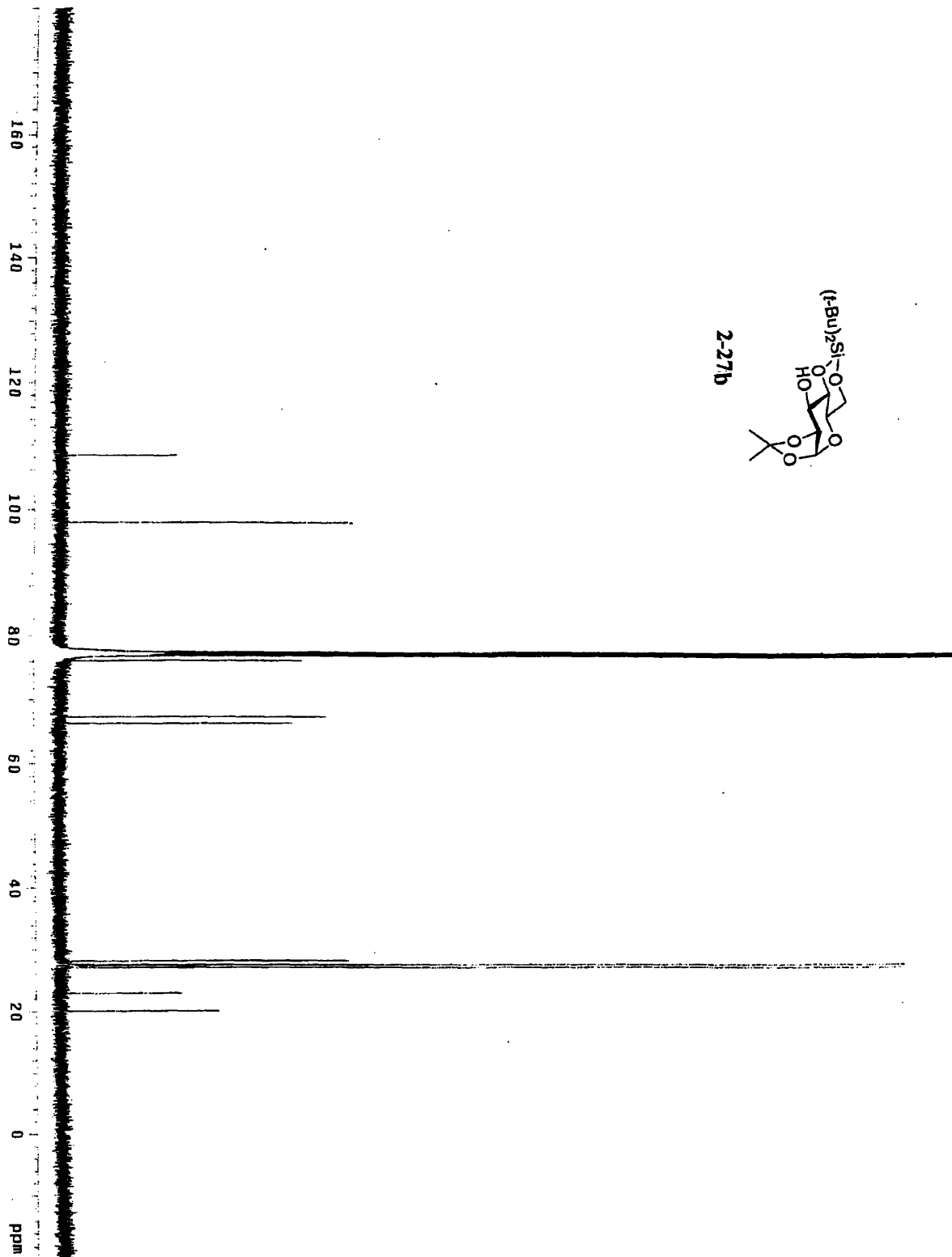


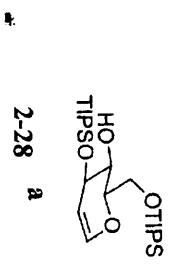
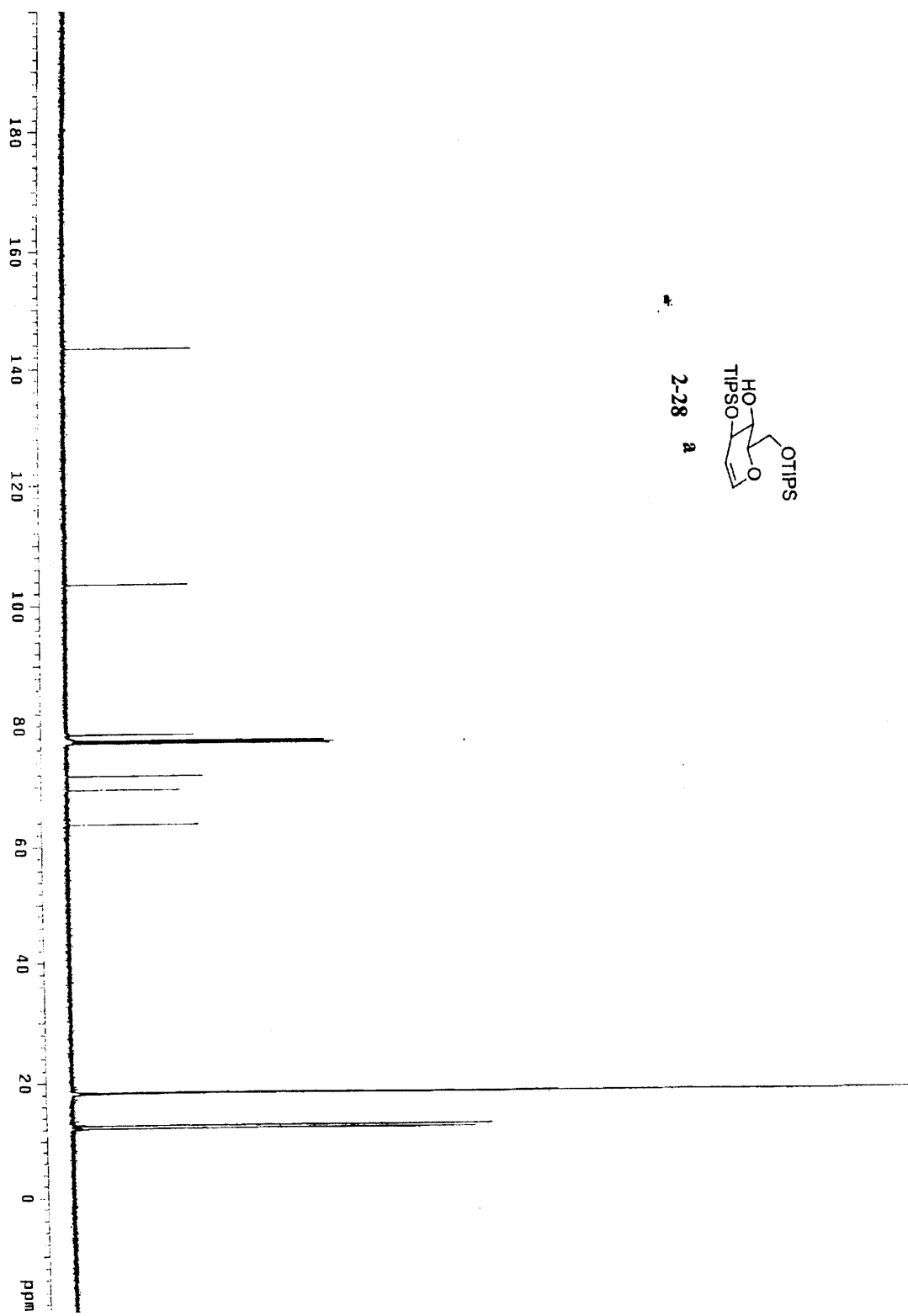


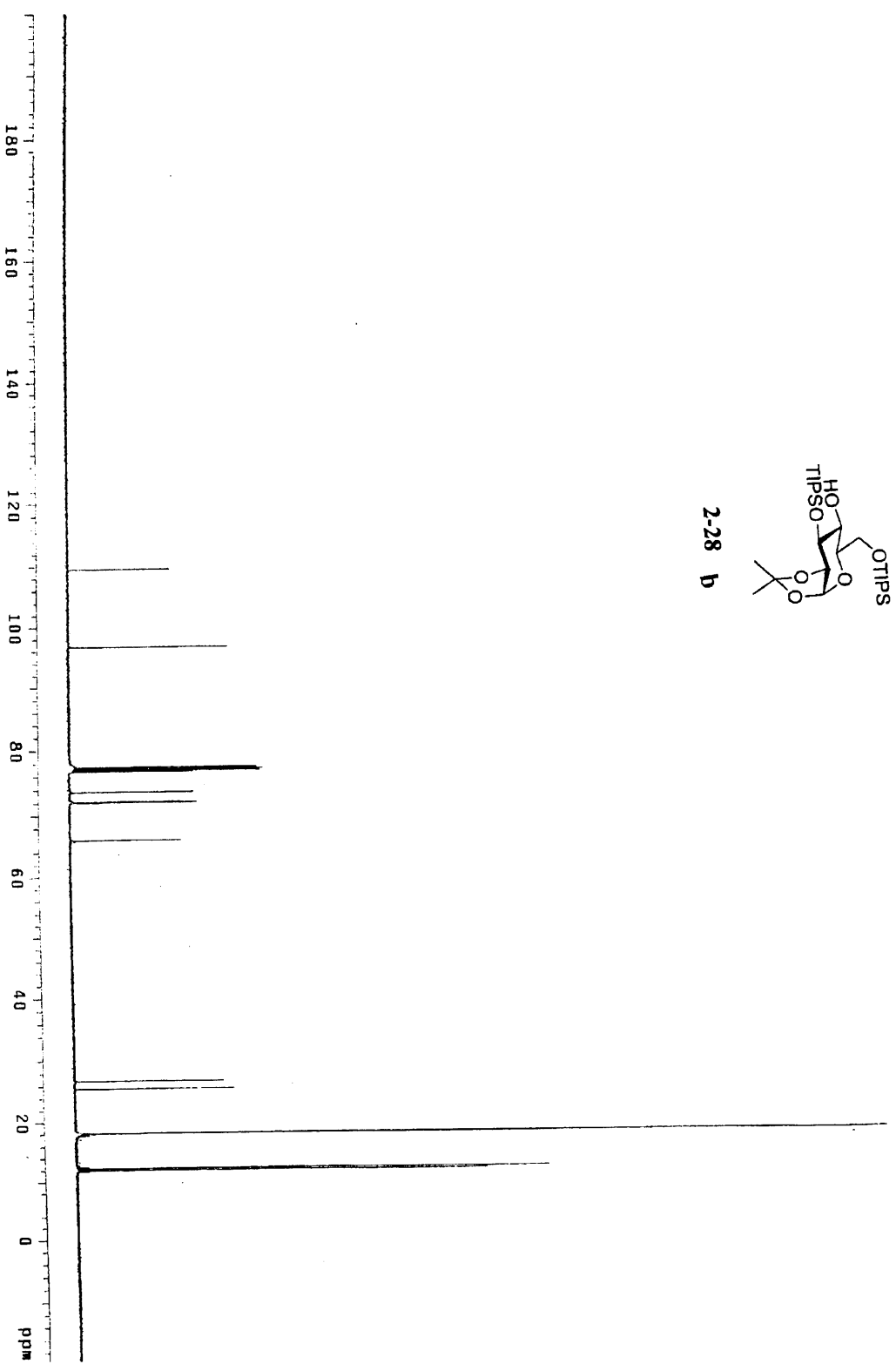


2-27D

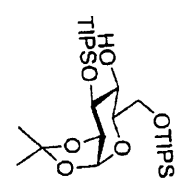


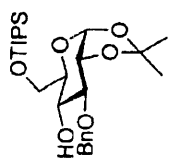




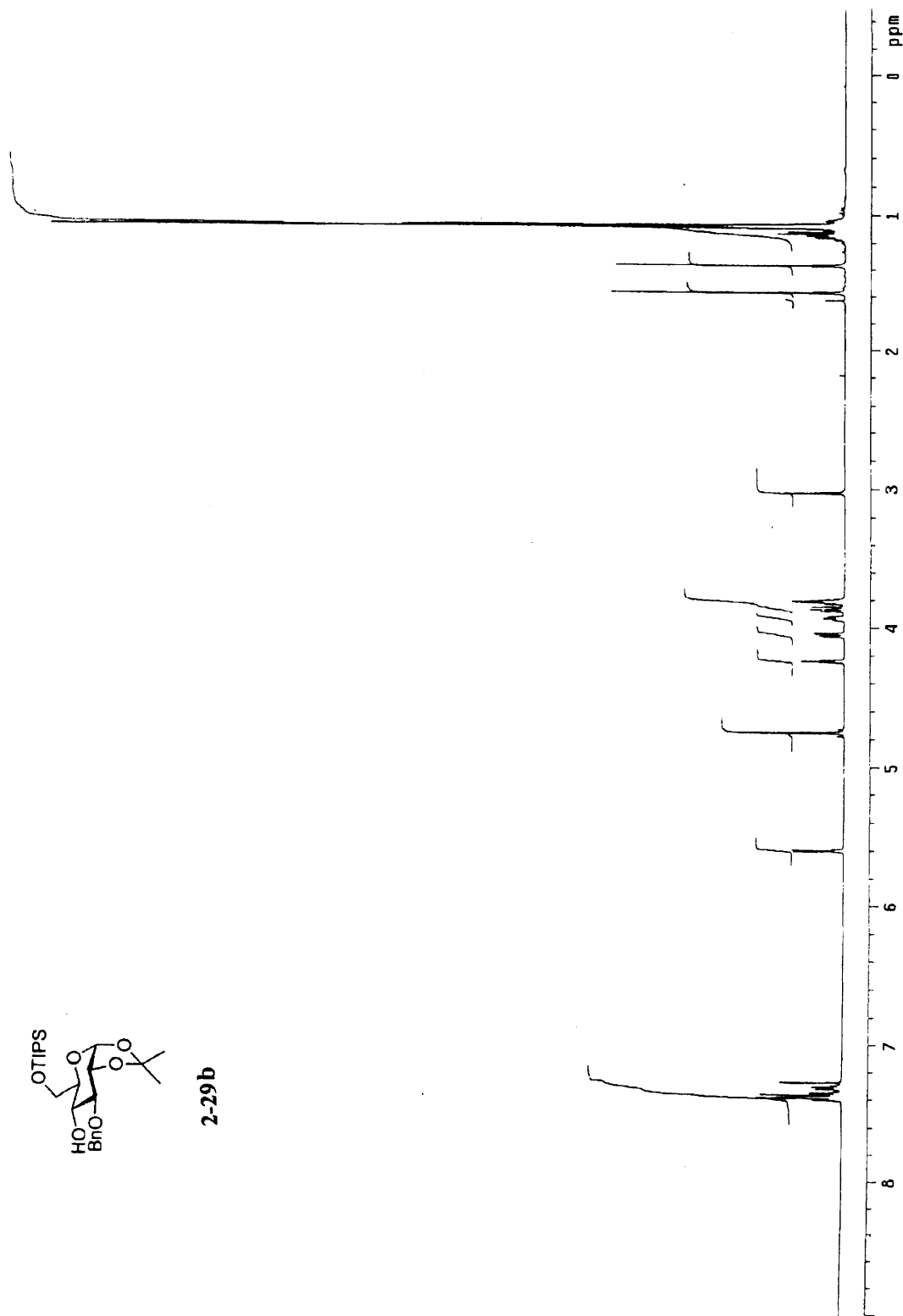


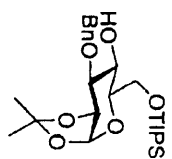
2-28 b



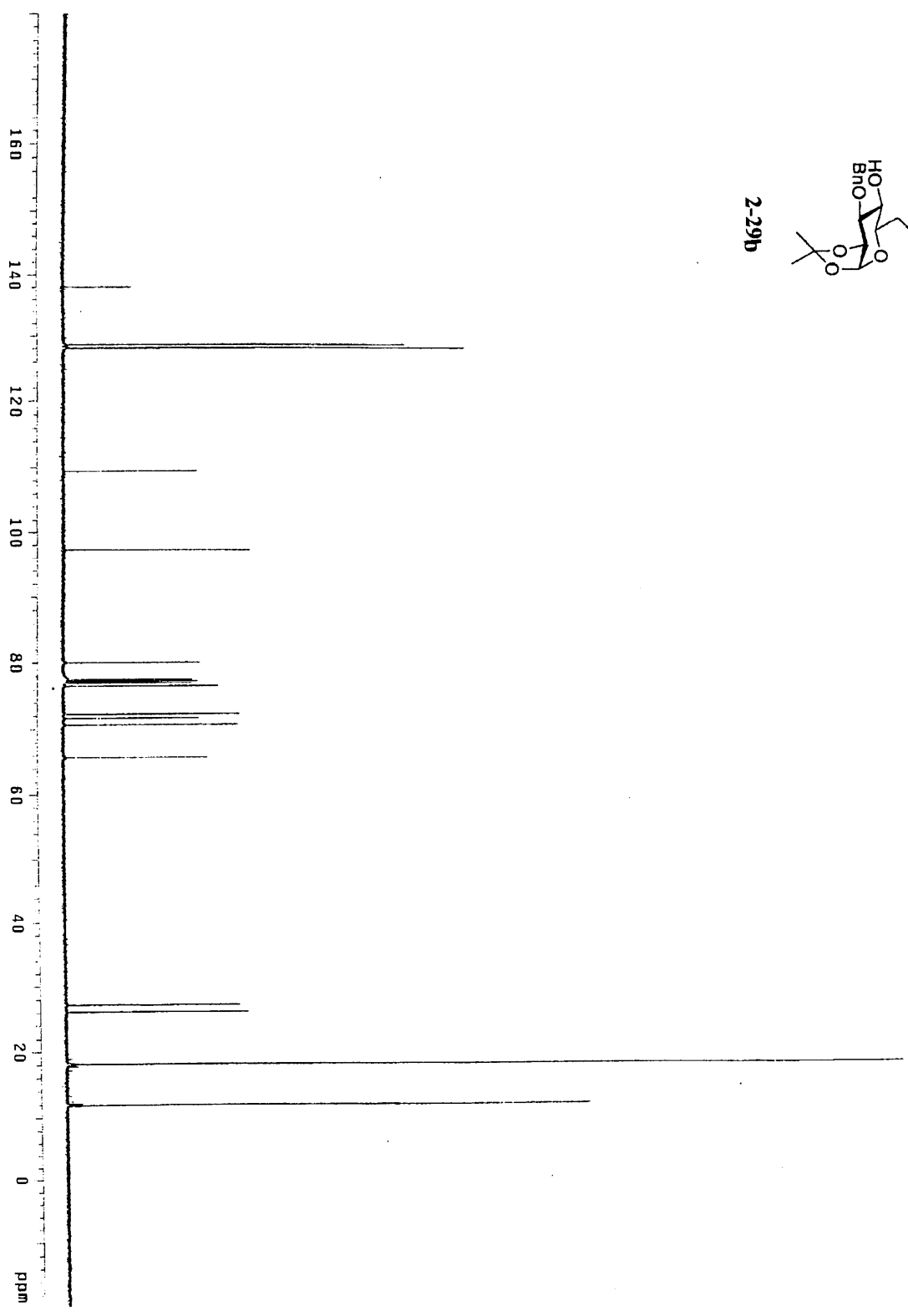


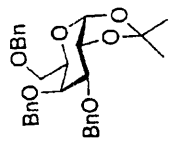
2-29b



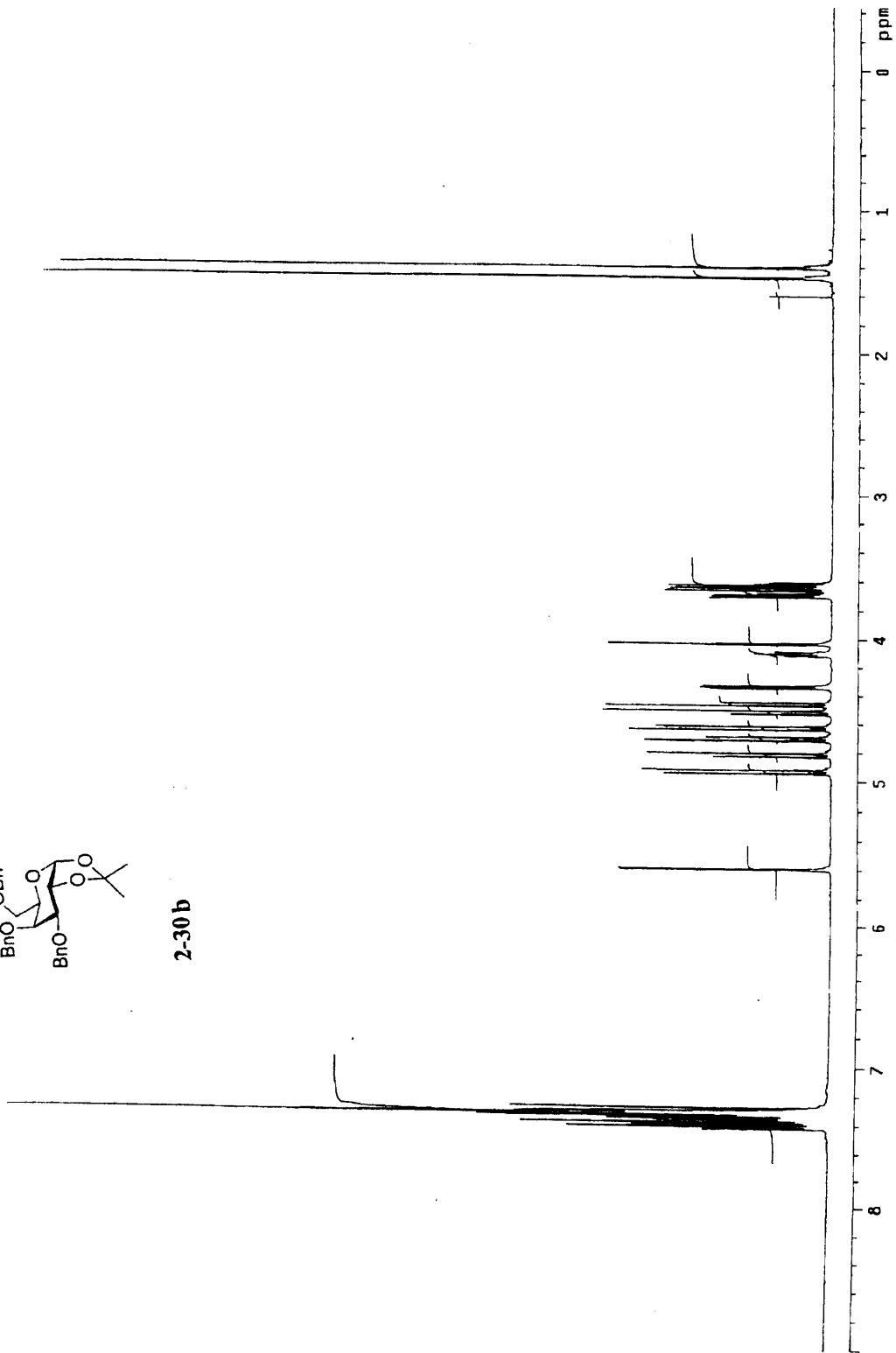


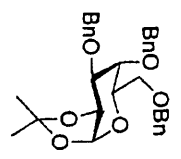
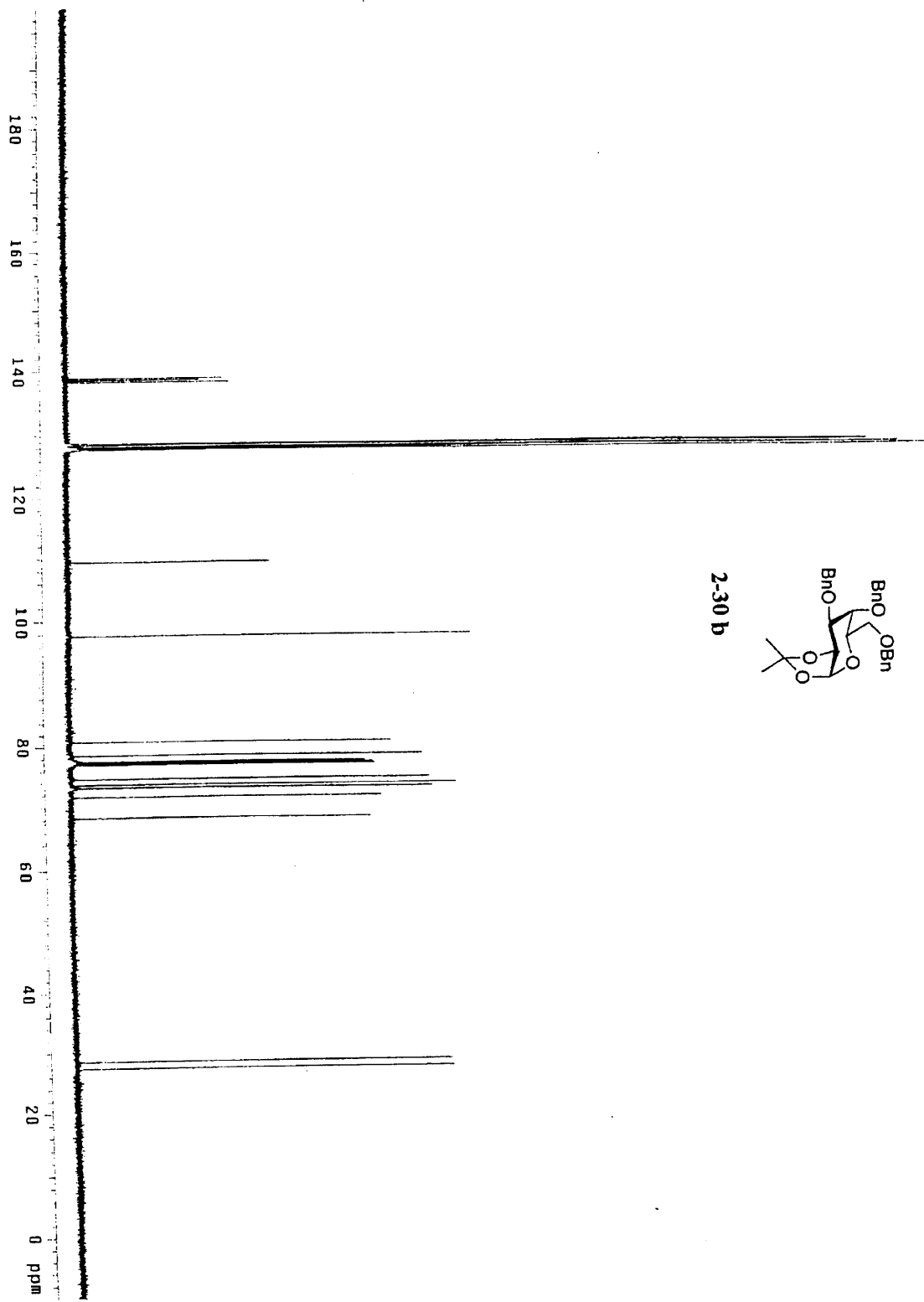
2-29b



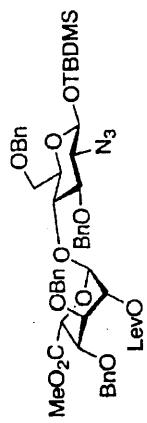


2-30b

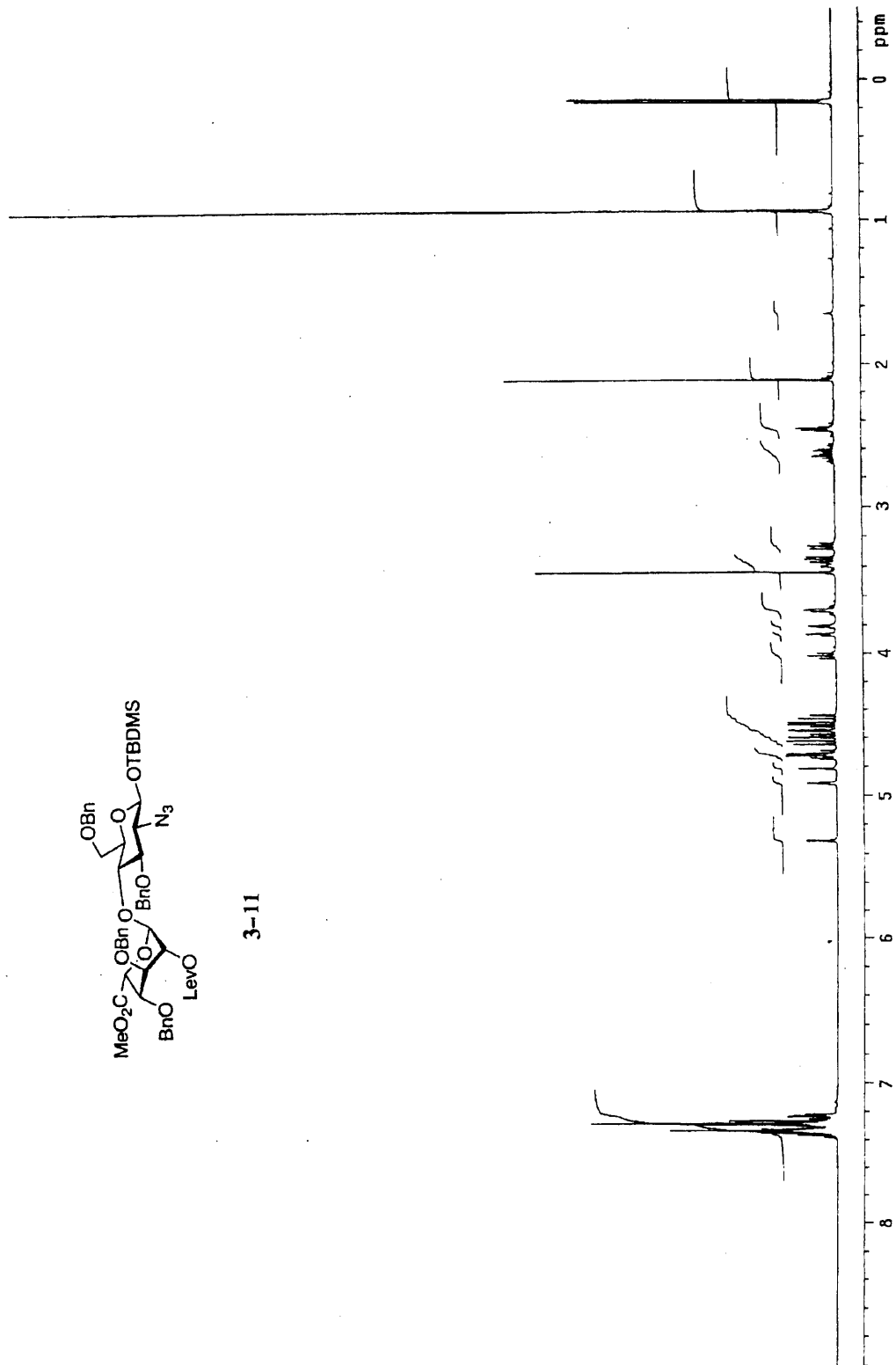


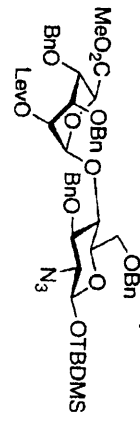


2-30 b

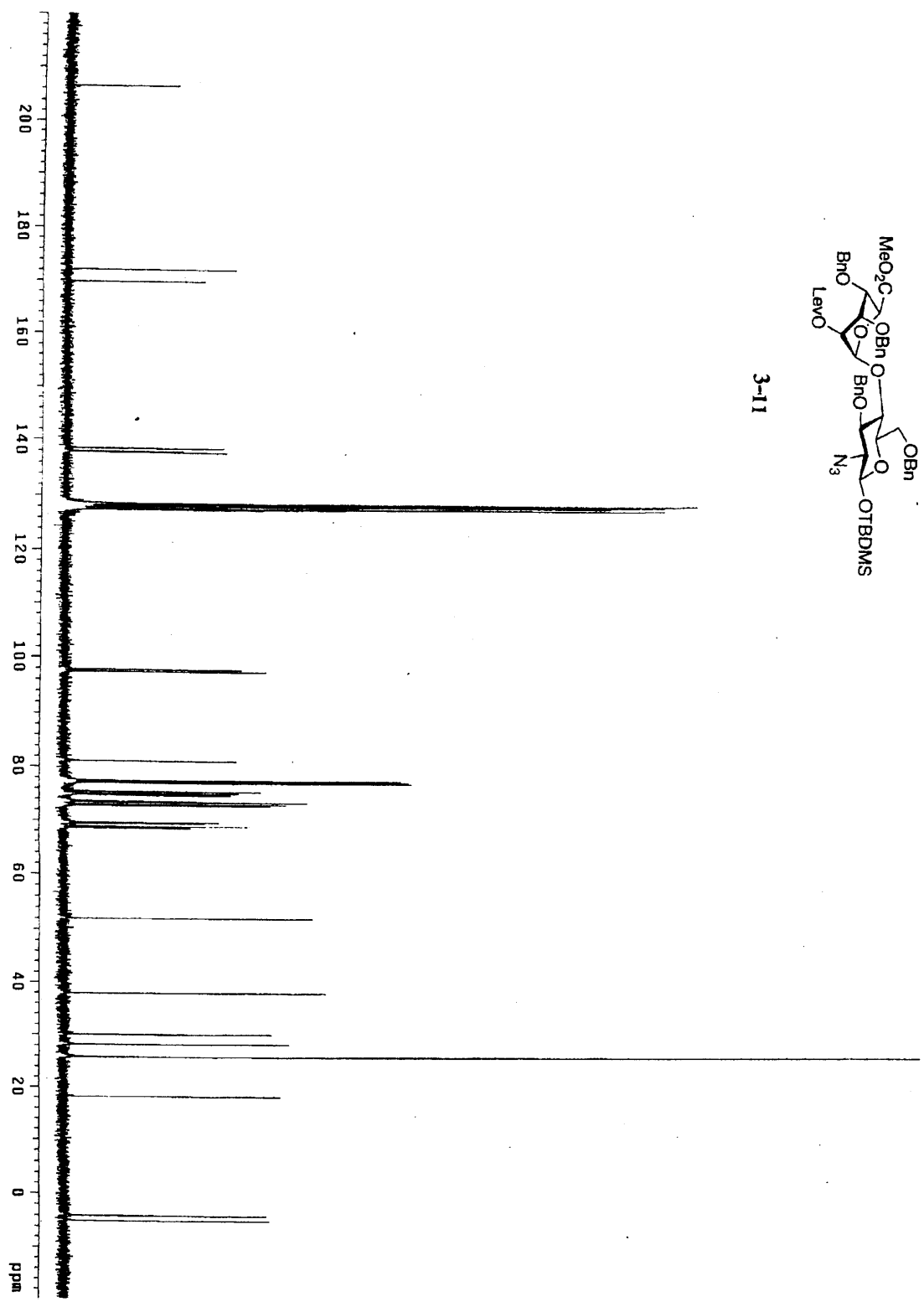


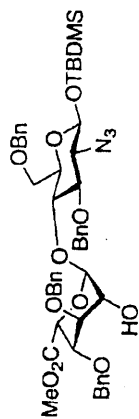
3-11



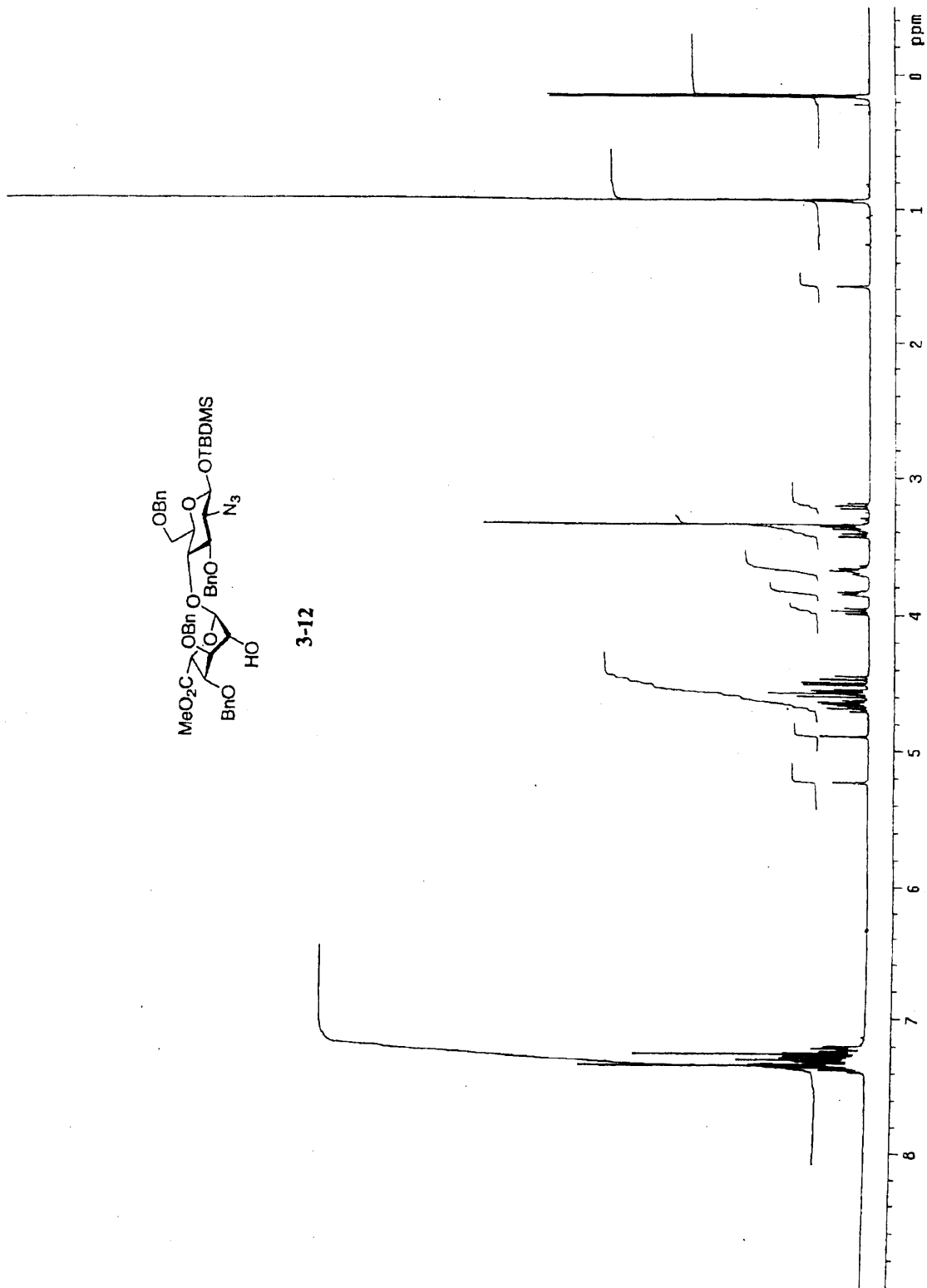


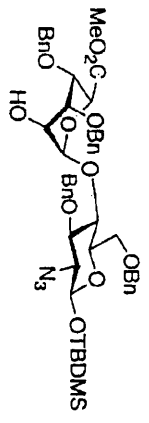
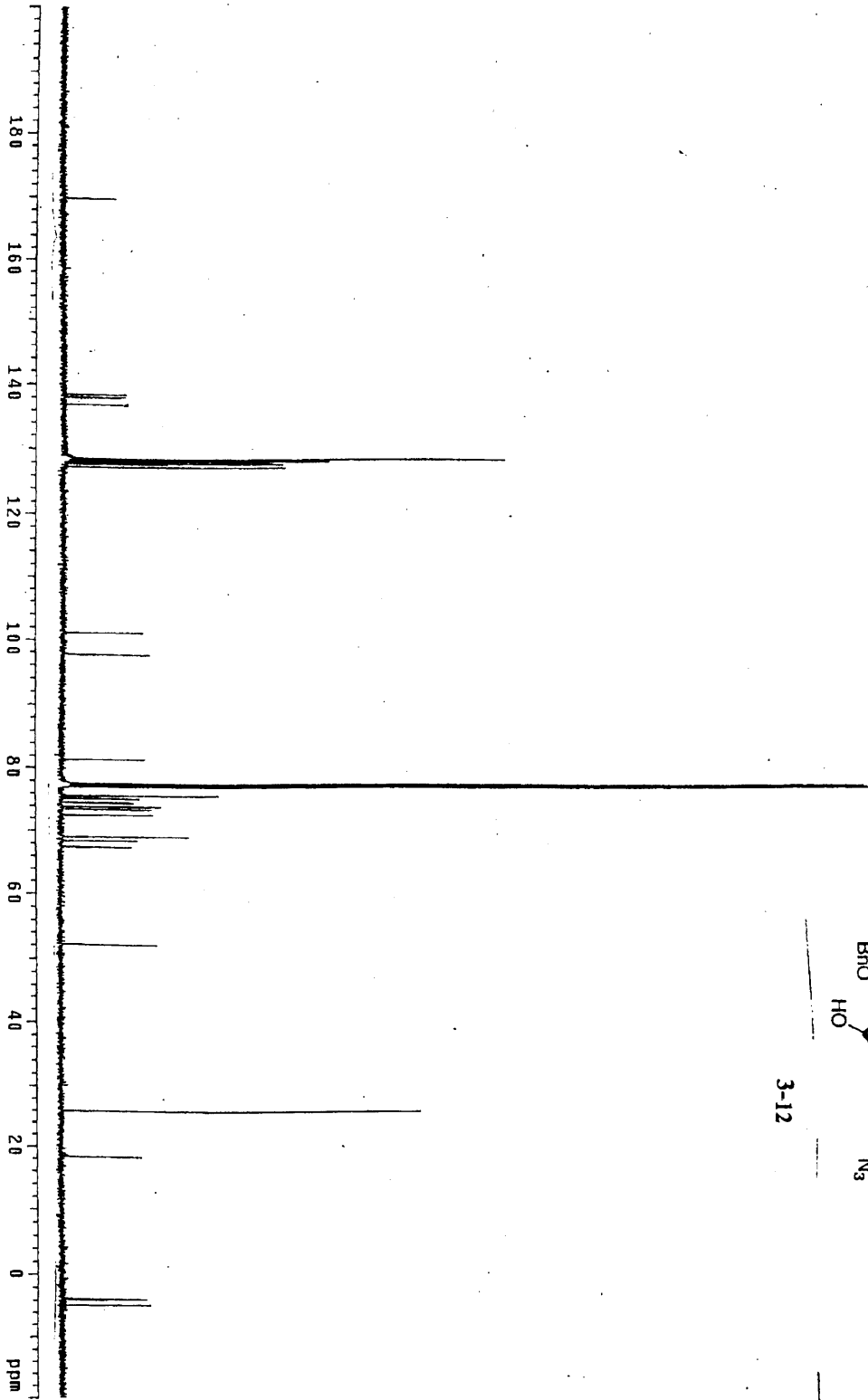
3-11



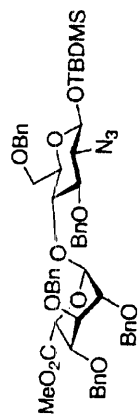


3-12

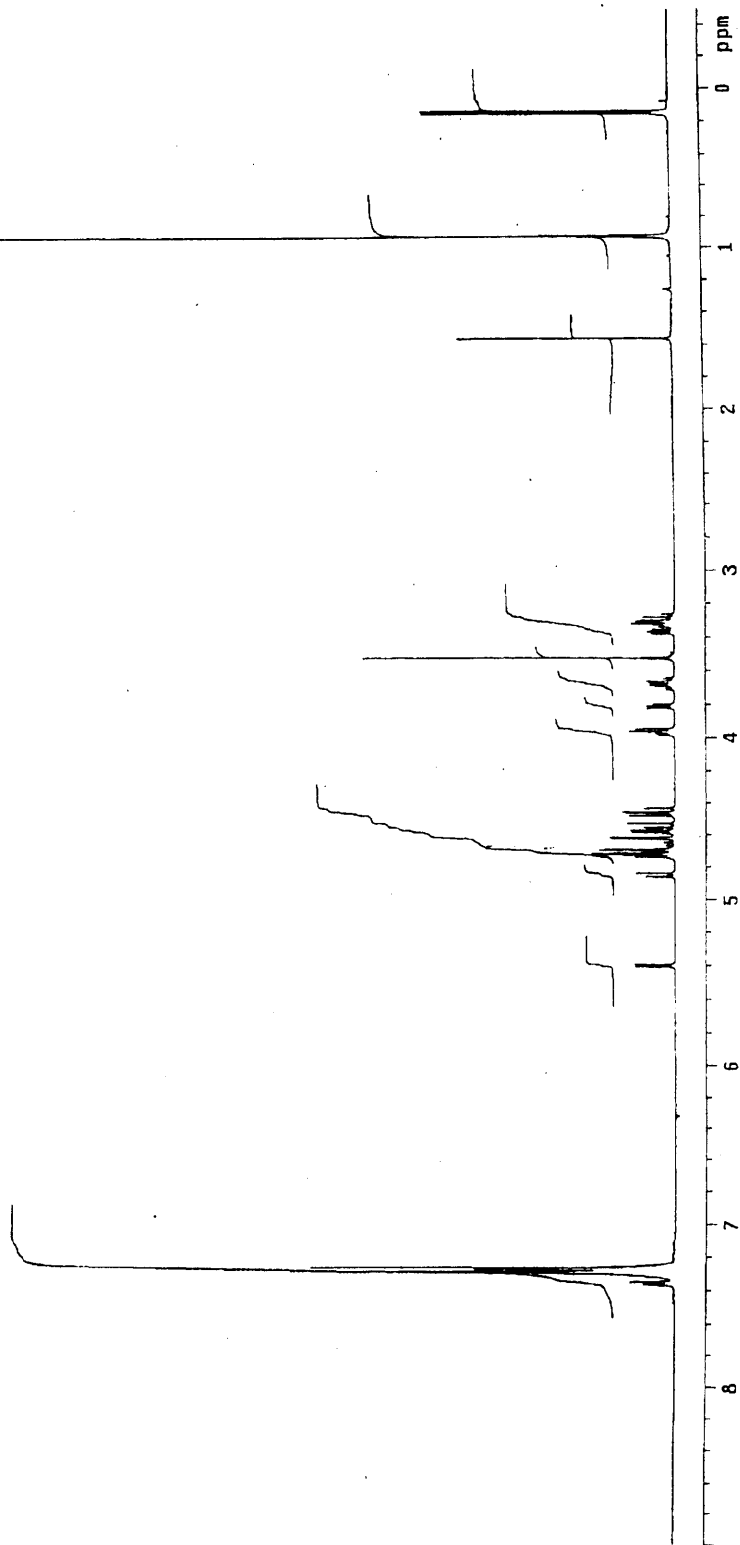


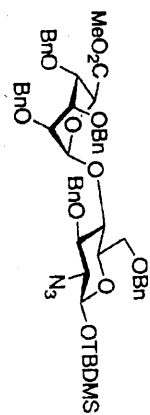


3-12

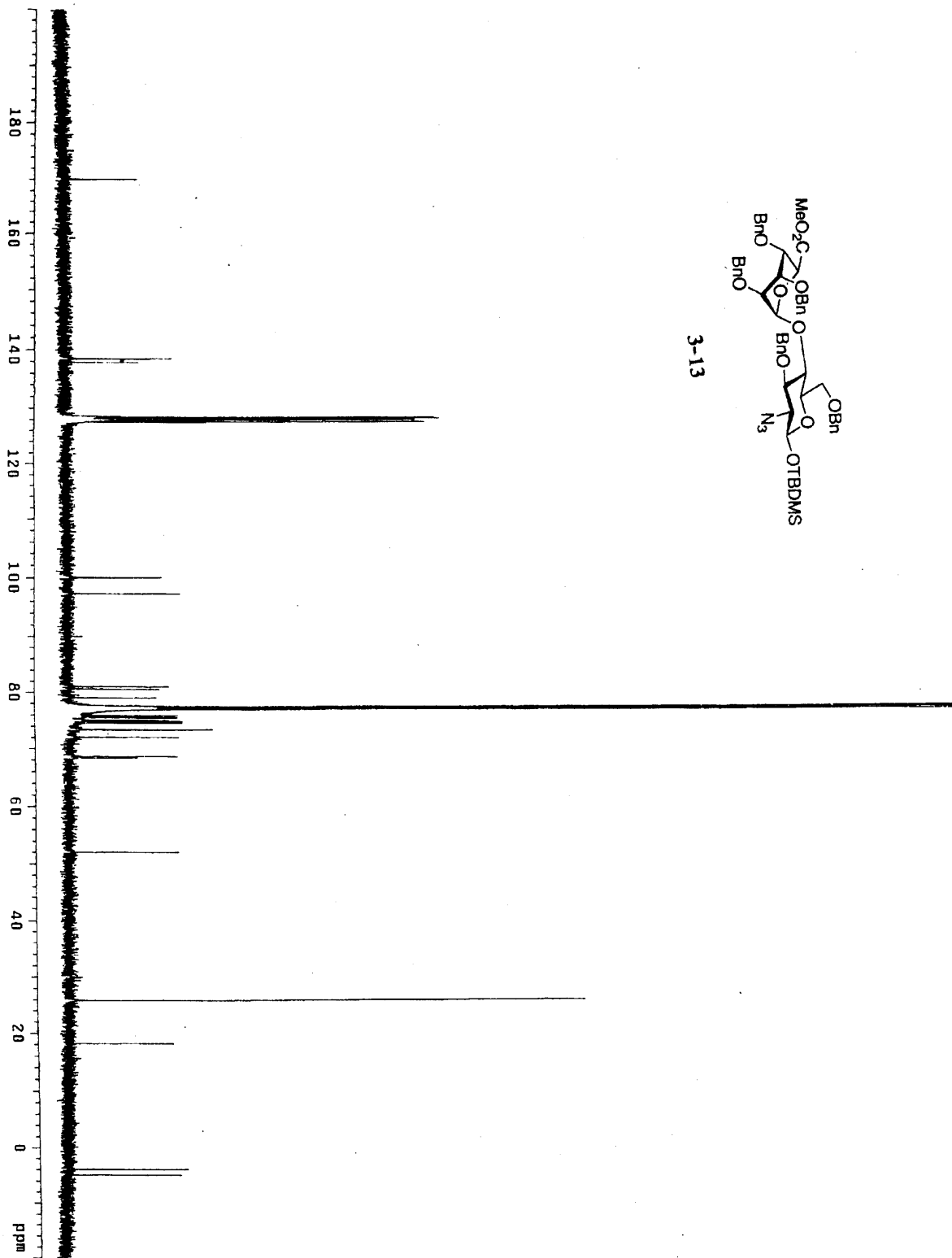


3-13



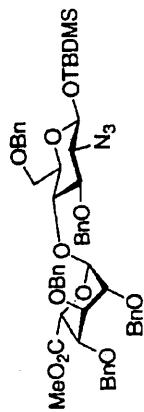


3-13

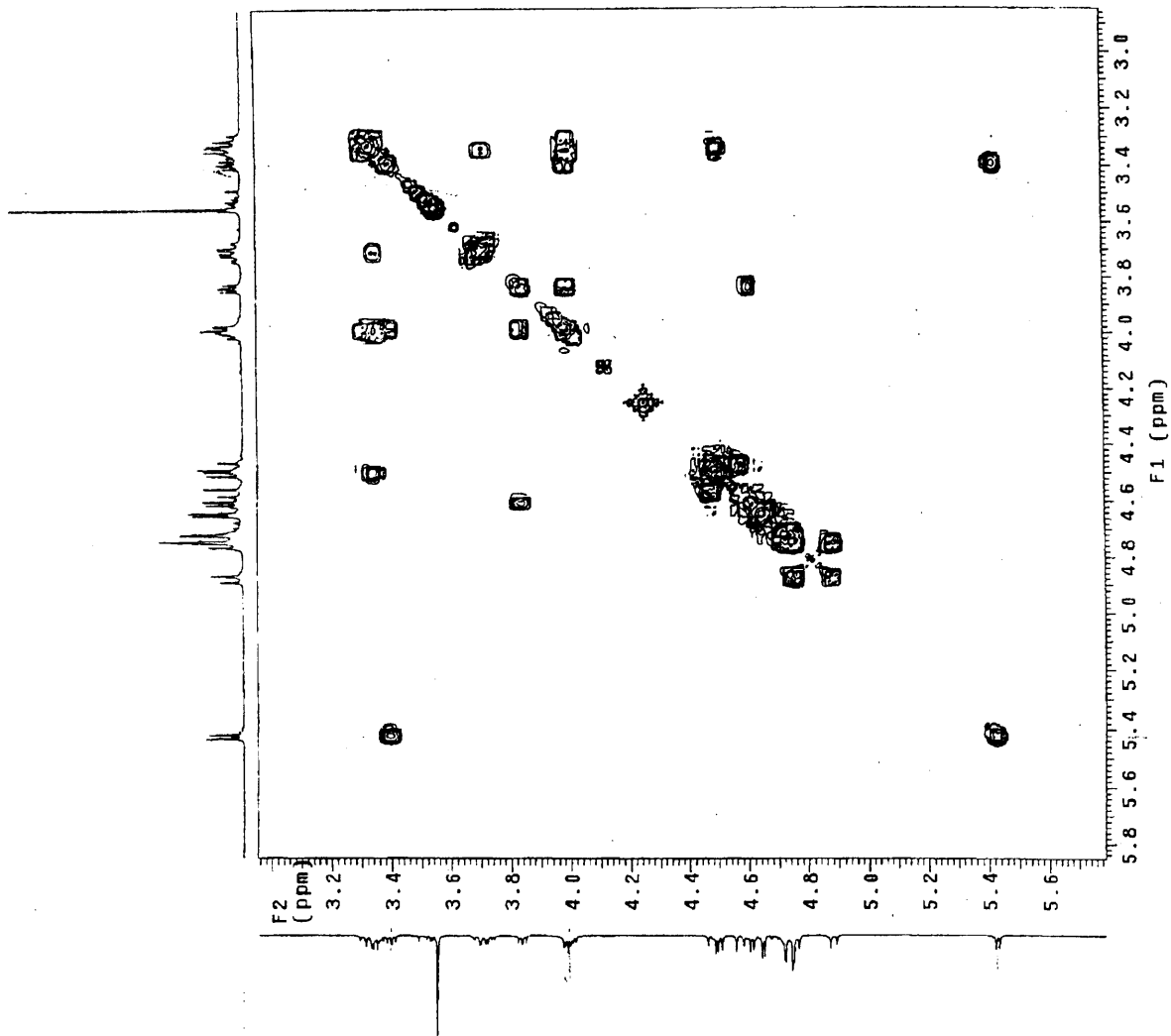


GL-2-53 gCOSY

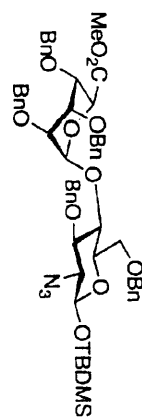
Pulse Sequence: gCOSY
Solvent: CDCl3
Temp: 22.0 C / 295.1 K
INVA-500 "butwinkle"
PULSE SEQUENCE: gCOSY
Relax time: 21.000 sec
Acq time: 0.215 sec
Width: 4748.3 Hz
2D Width: 4748.3 Hz
Single scan
256 increments
OBSERVE H1, 499.7537707 MHz
DATA PROCESSING
Sf. sine bell 0.108 sec
F1 DATA PROCESSING
Sf. sine bell 0.052 sec
F1 size 2048 x 2048
Total time 5 min, 41 sec



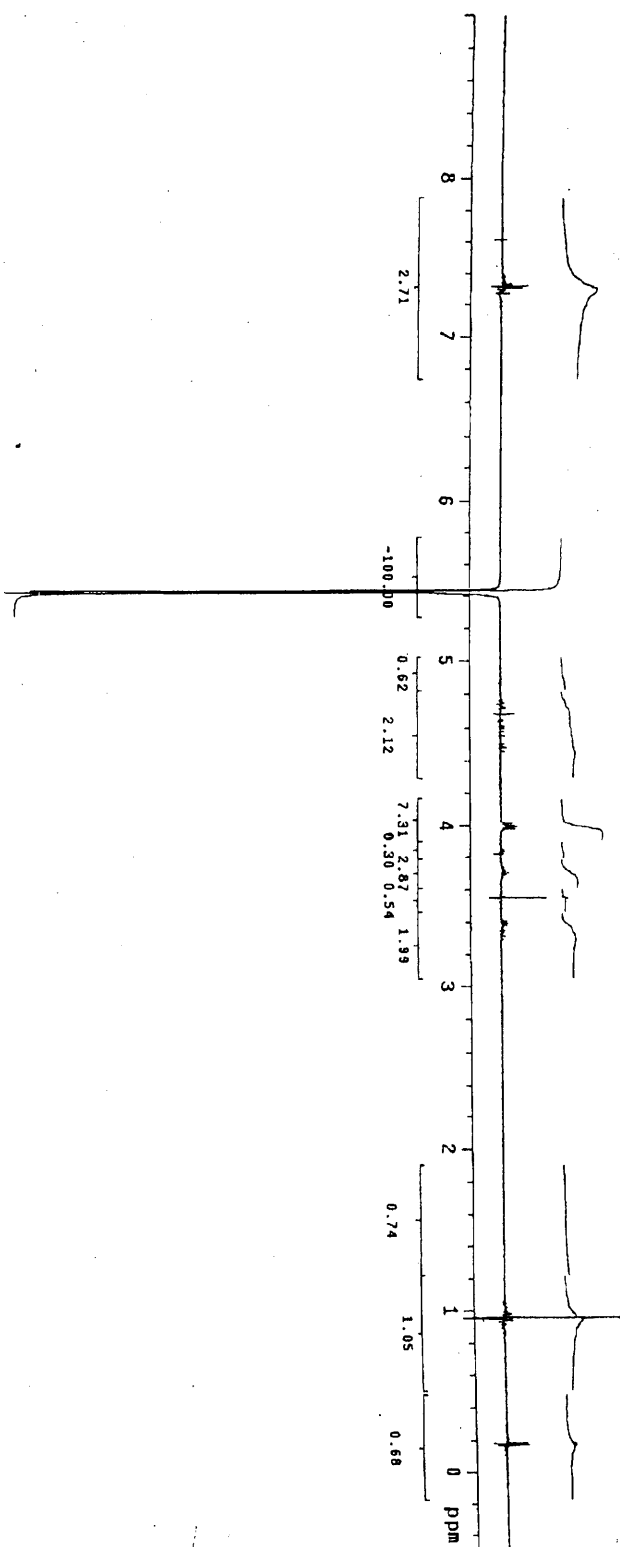
3-13



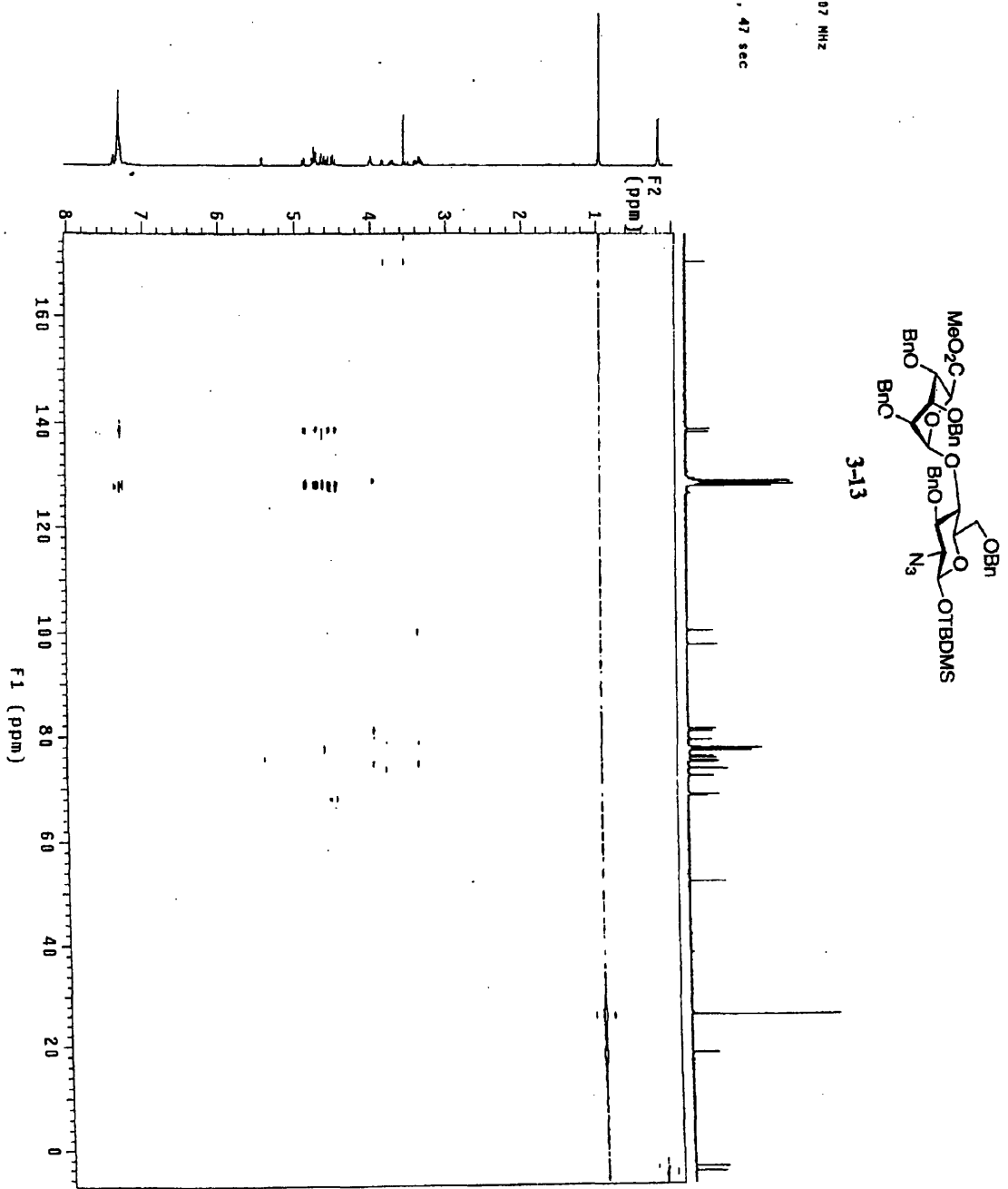
GL-2-53 NOE diff dof=5.43ppm
Pulse Sequence: presat1

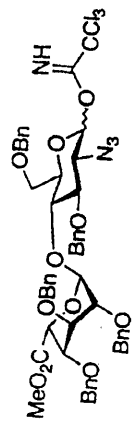


3-13

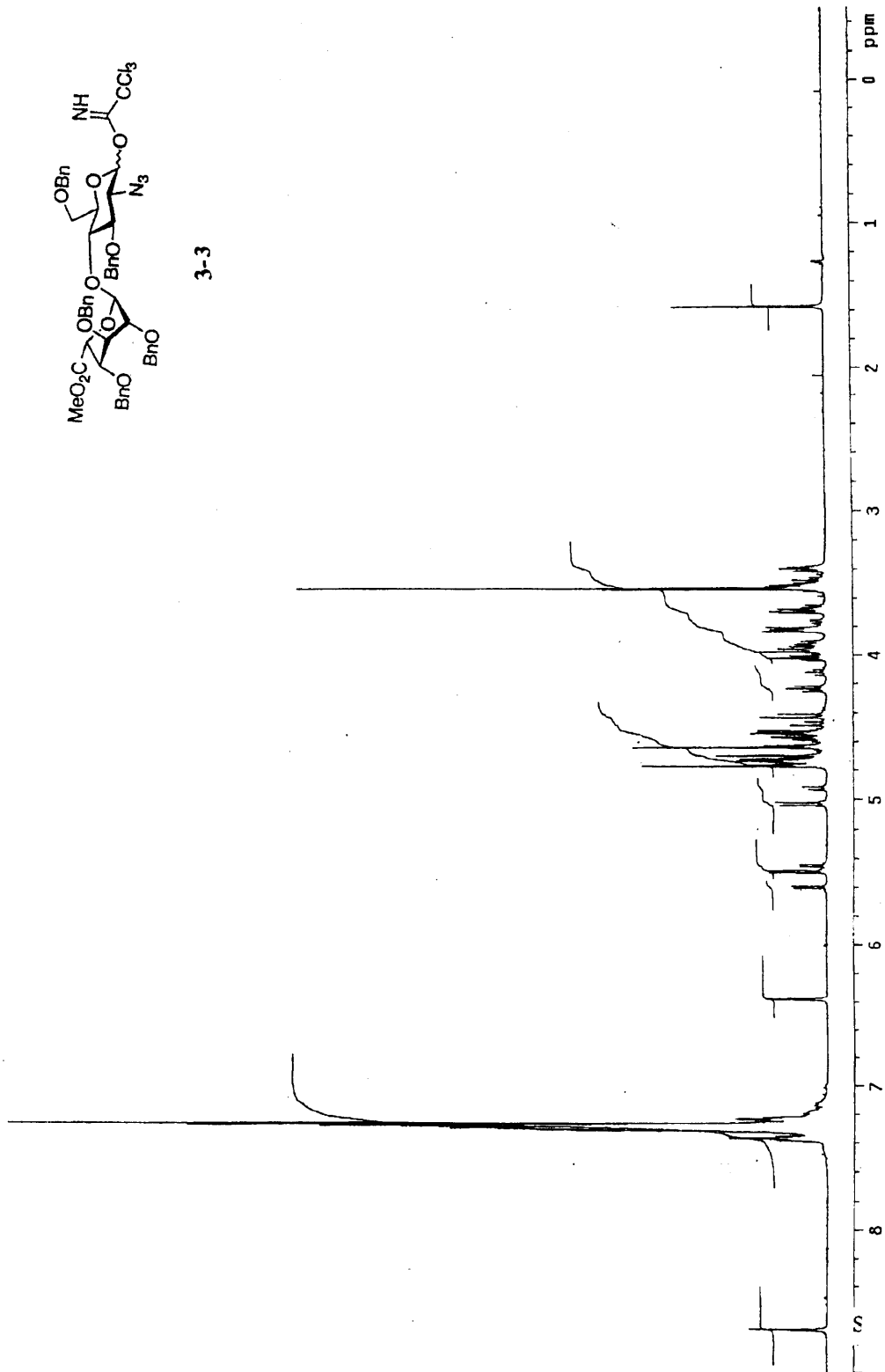


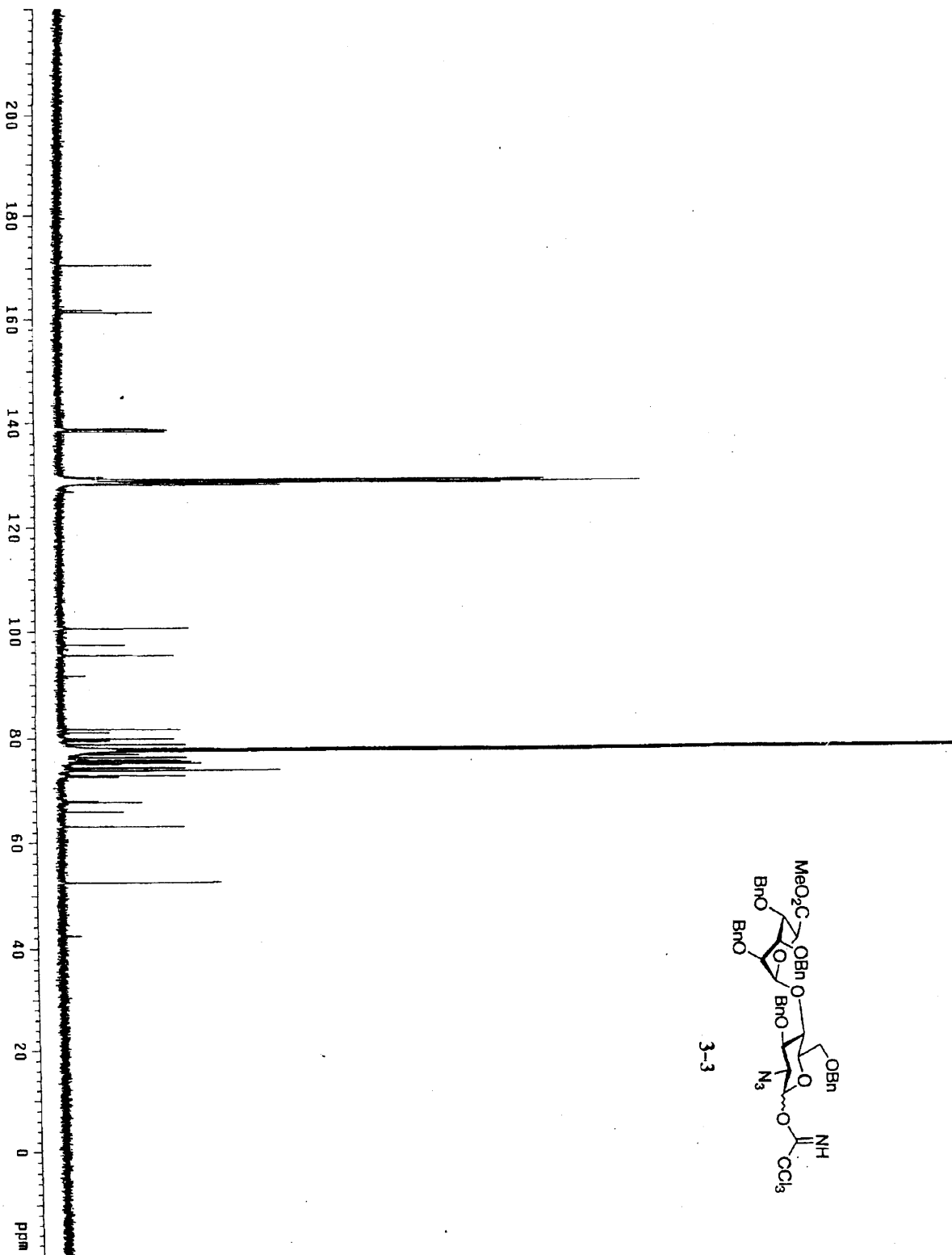
01-2-53H
 Pulse Sequence: HMQC
 Solvent: CDCl3
 Temp: 22.0 C / 295.1 K
 User: 1-14-87
 File name: 01-2-53HMQC
 INOVA-500 "21ppm"
 PULSE SEQUENCE: HMQC
 Relax. delay 1.000 sec
 Acq. time 0.216 sec
 Width 4740.3 Hz
 2D Width 27681.7 Hz
 8 repetitions
 2 K 256 increments
 DQ SINE: Hz 93.7537707 MHz
 DQ SINE: Hz 93.7537707 MHz
 Sine bell 1108 sec
 F1 DATA PROCESSING
 Sine bell 0.004 sec
 FT size 2048 x 2048
 Total time 1 hr, 32 min, 47 sec

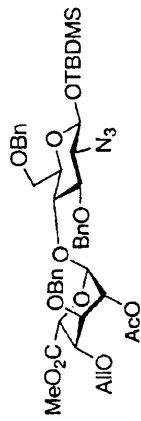




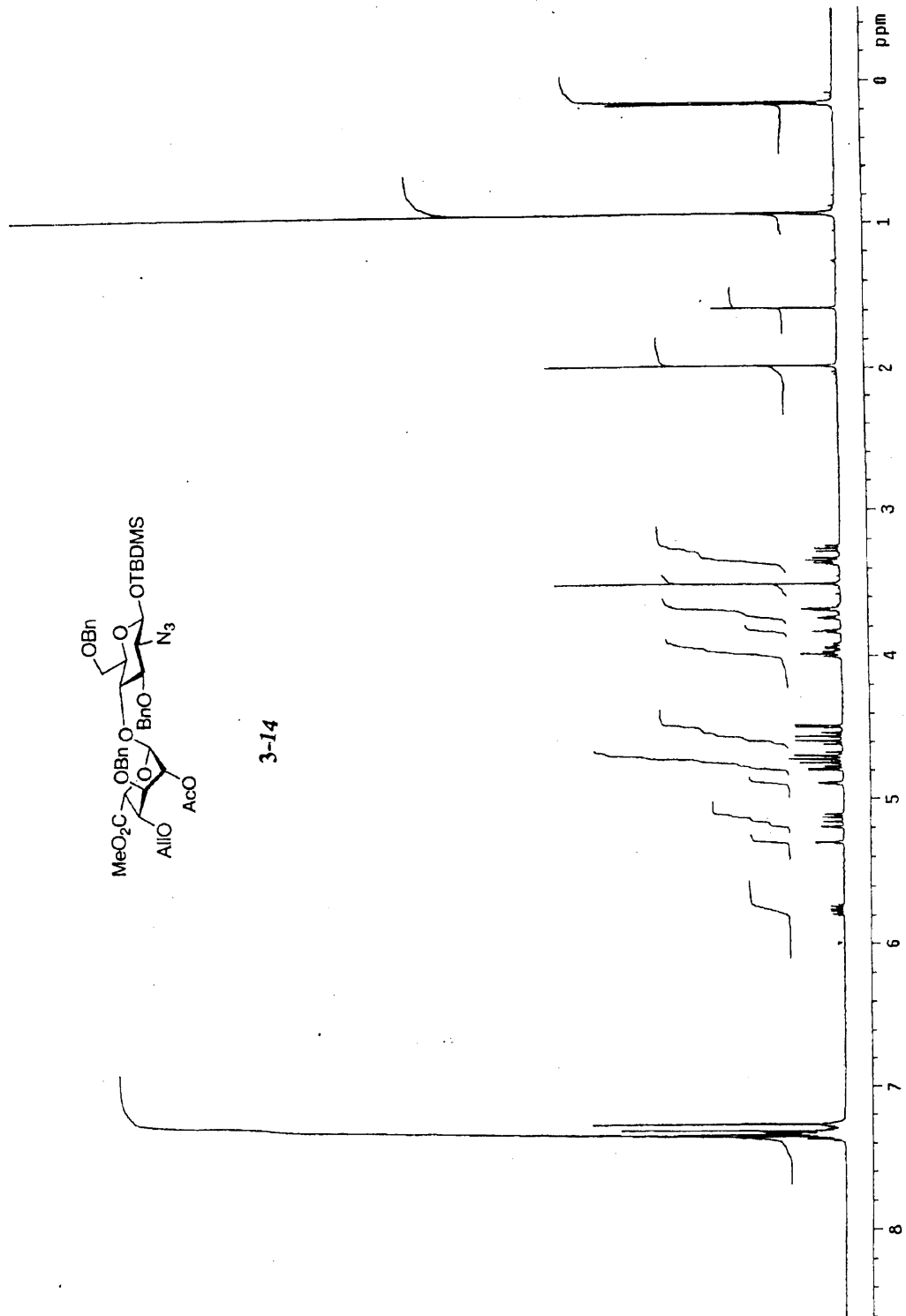
3-3

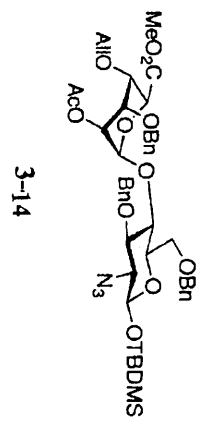




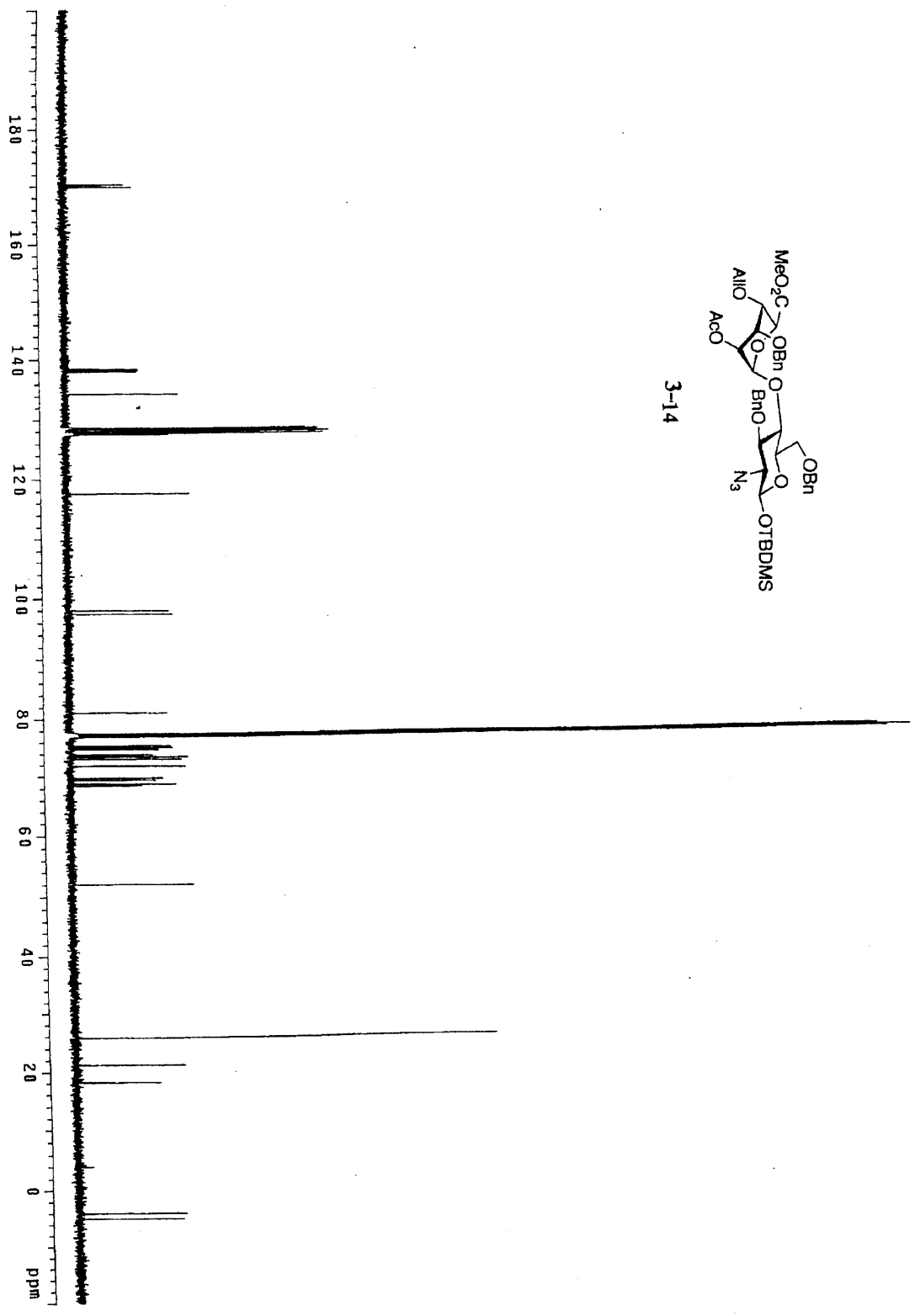


3-14



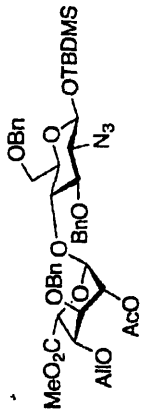


3-14



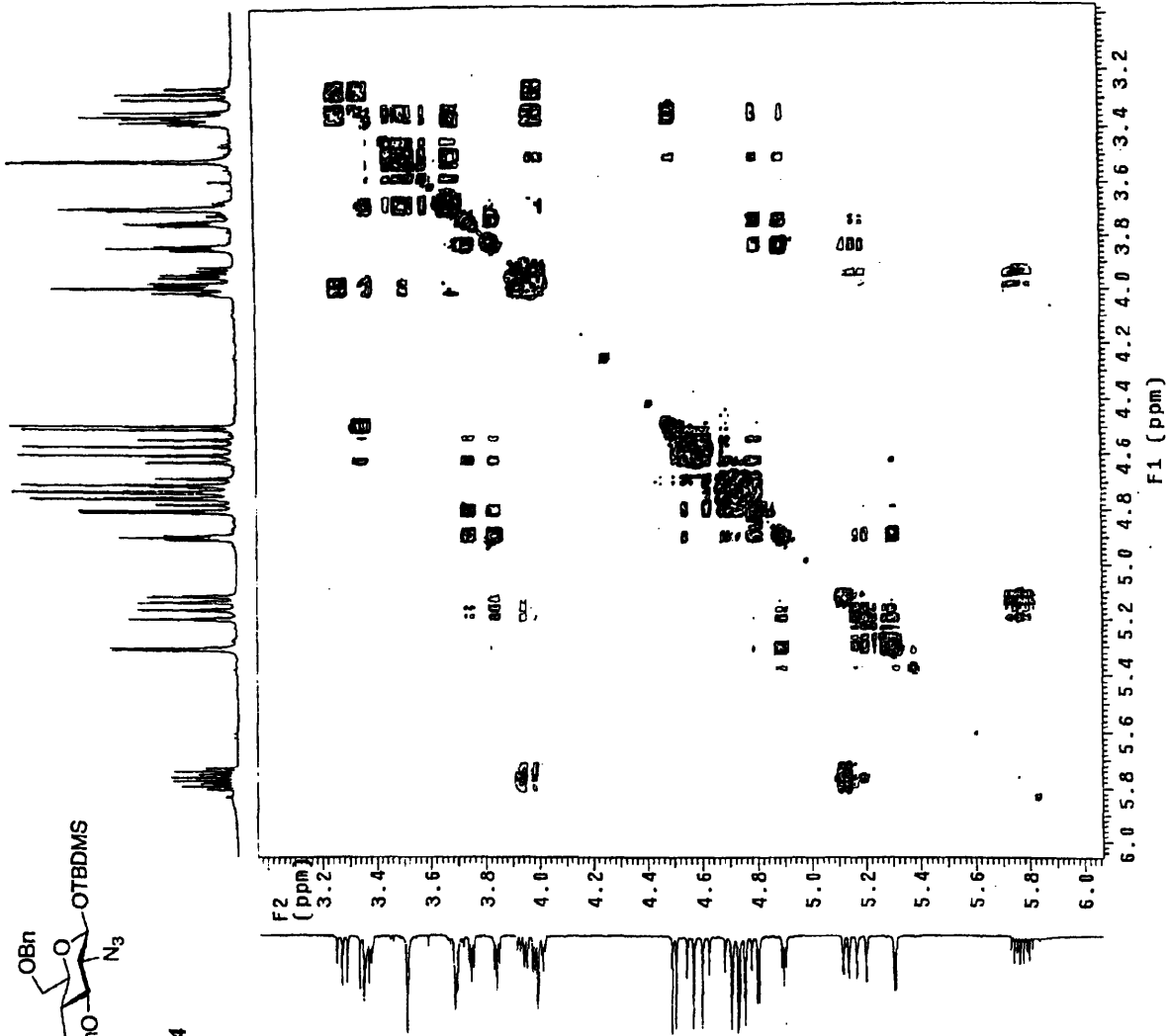
GL-2-34 gCOSY

Pulse Sequence: gCOSY
Solvent: CDCl3
Temp: 22.0 C / 95.1 K
File name: GL-2-34gCOSY
INOVA-500 "21ppm"
PULSE SEQUENCE: gCOSY
Relax: delay 1.000 sec
Acq: time 47.683 sec
Width 4768.3 Hz
20 Width 4768.3 Hz
Single scan
256 increments
OBSERVE H1 495.753725 MHz
DATA PROCESSING
Sg. sine ball 0.108 sec
F1 DATA PROCESSING
Sg. sine ball 0.200 sec
F1 size 2048 x 2048
total time 5 min, 40 sec

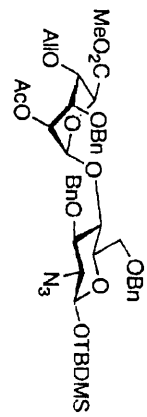


3-14

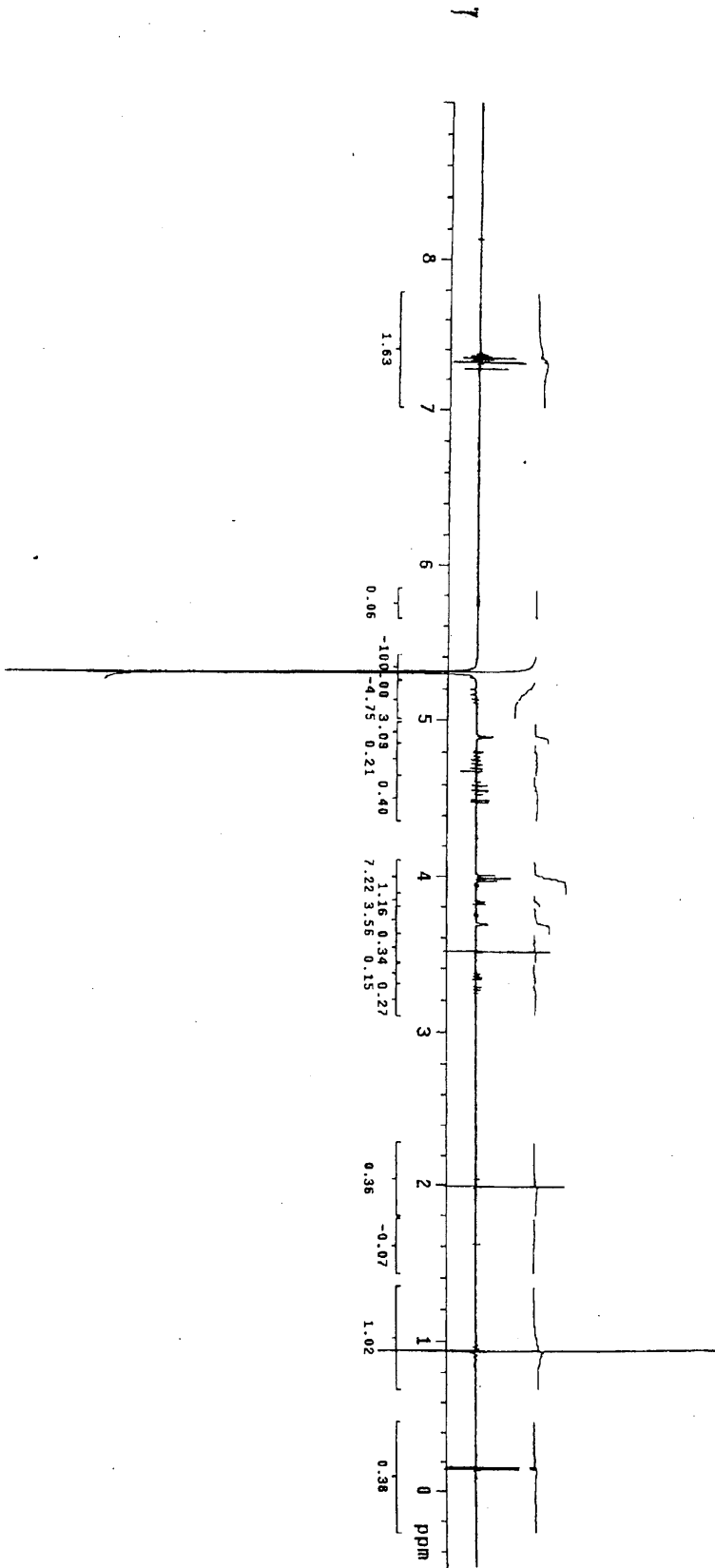
LP +
FOLD

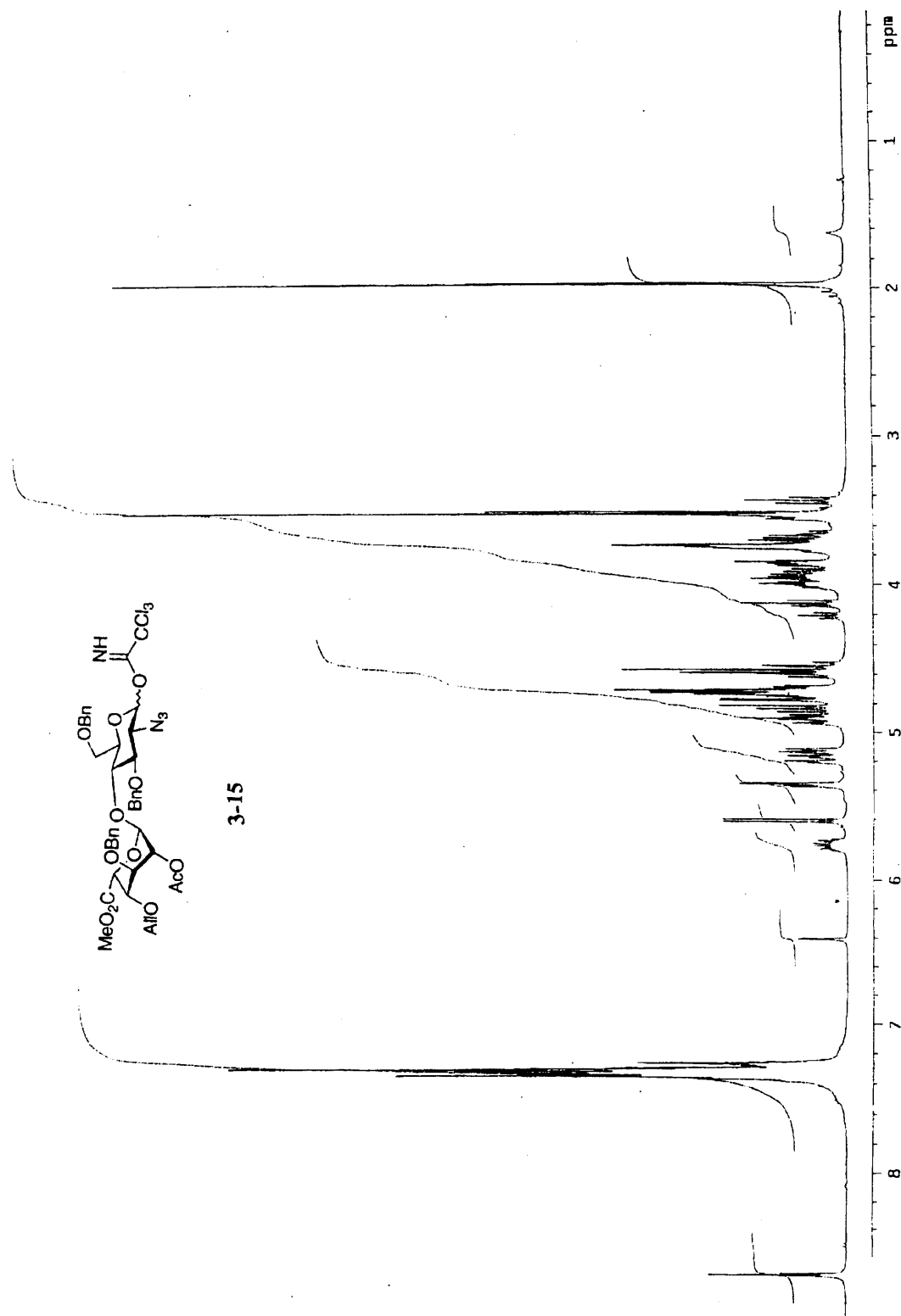


GL-2-34 1DMOE setfrrq=5.3p
Pulse Sequence: presat

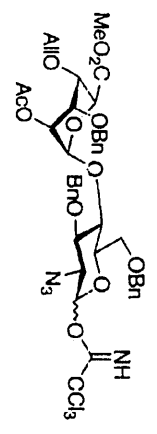
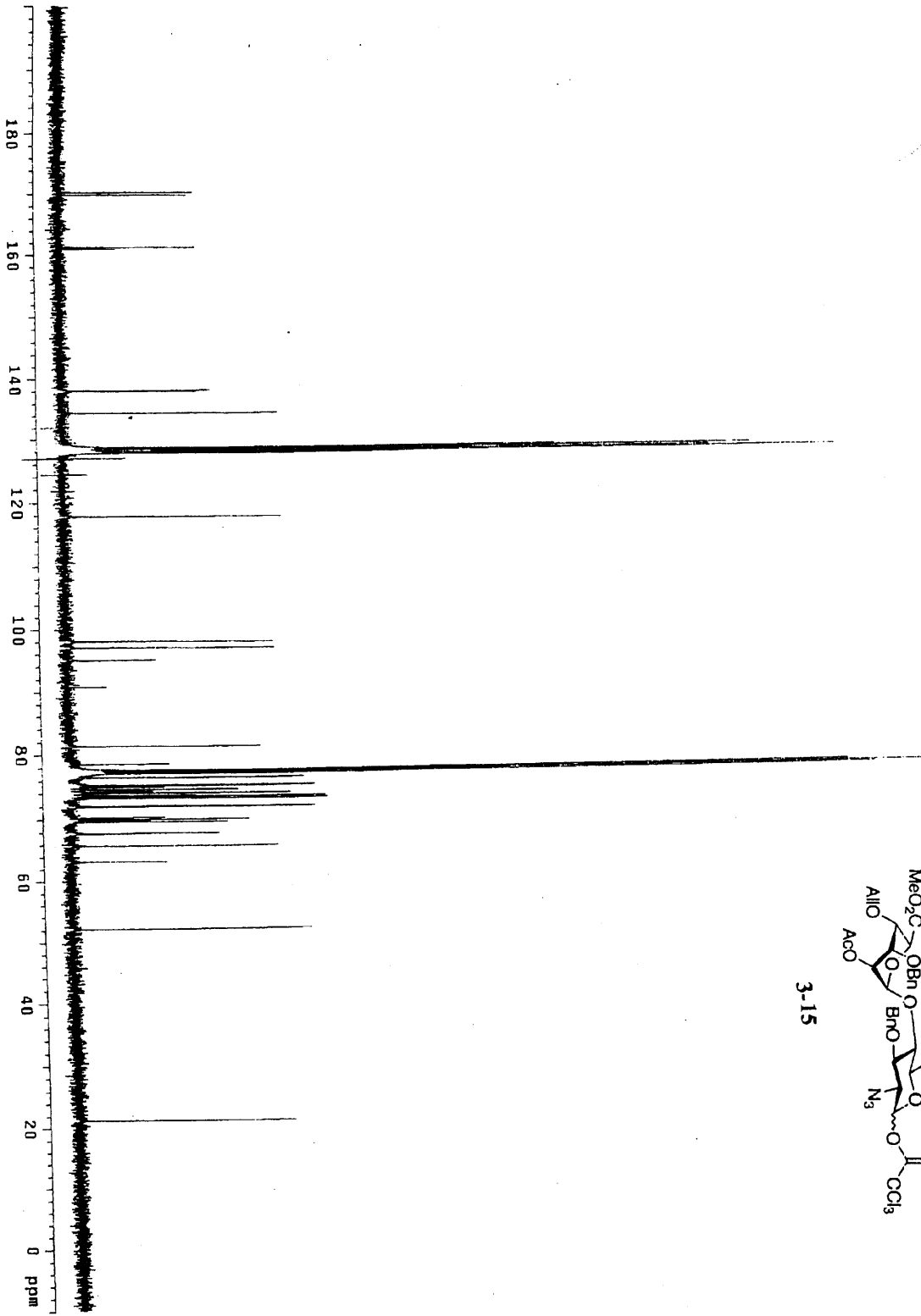


3-14

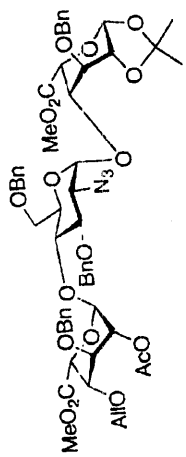




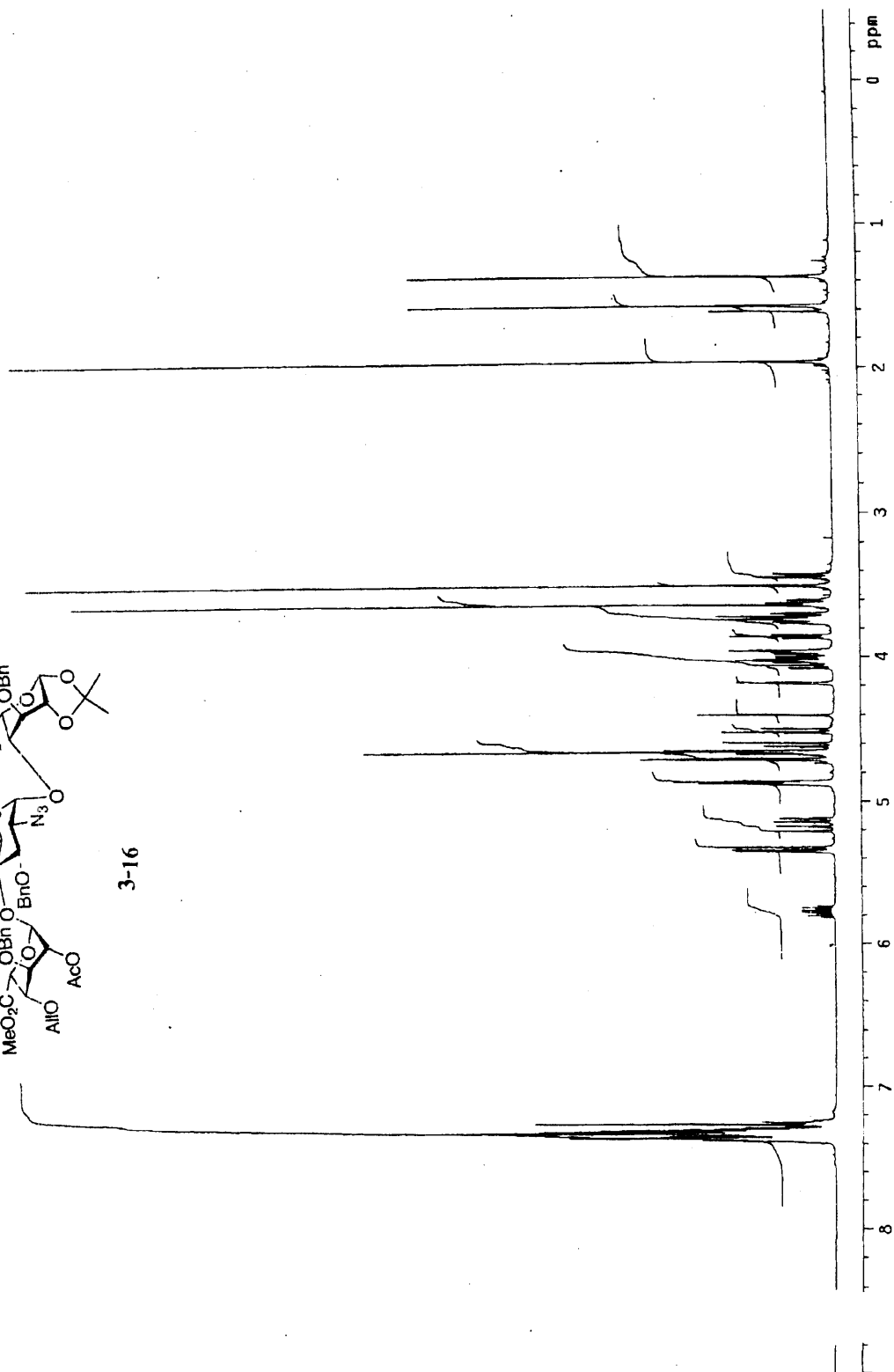
3-15



3-15

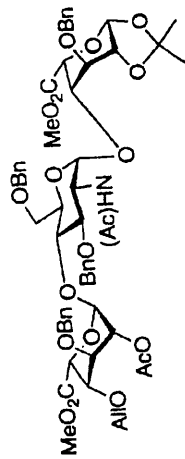


3-16

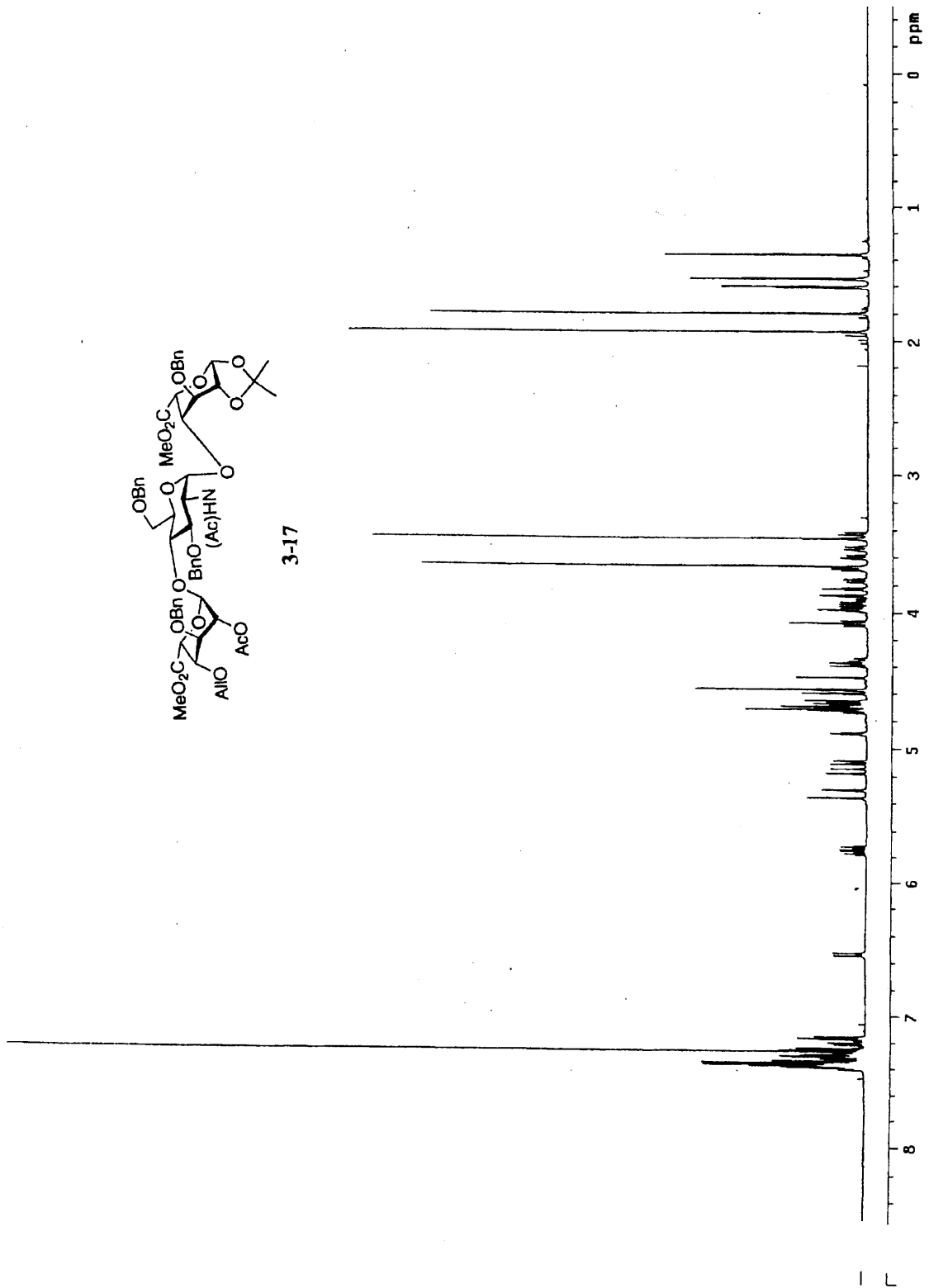


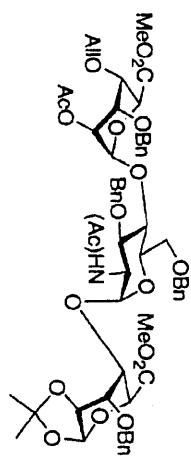


3-16

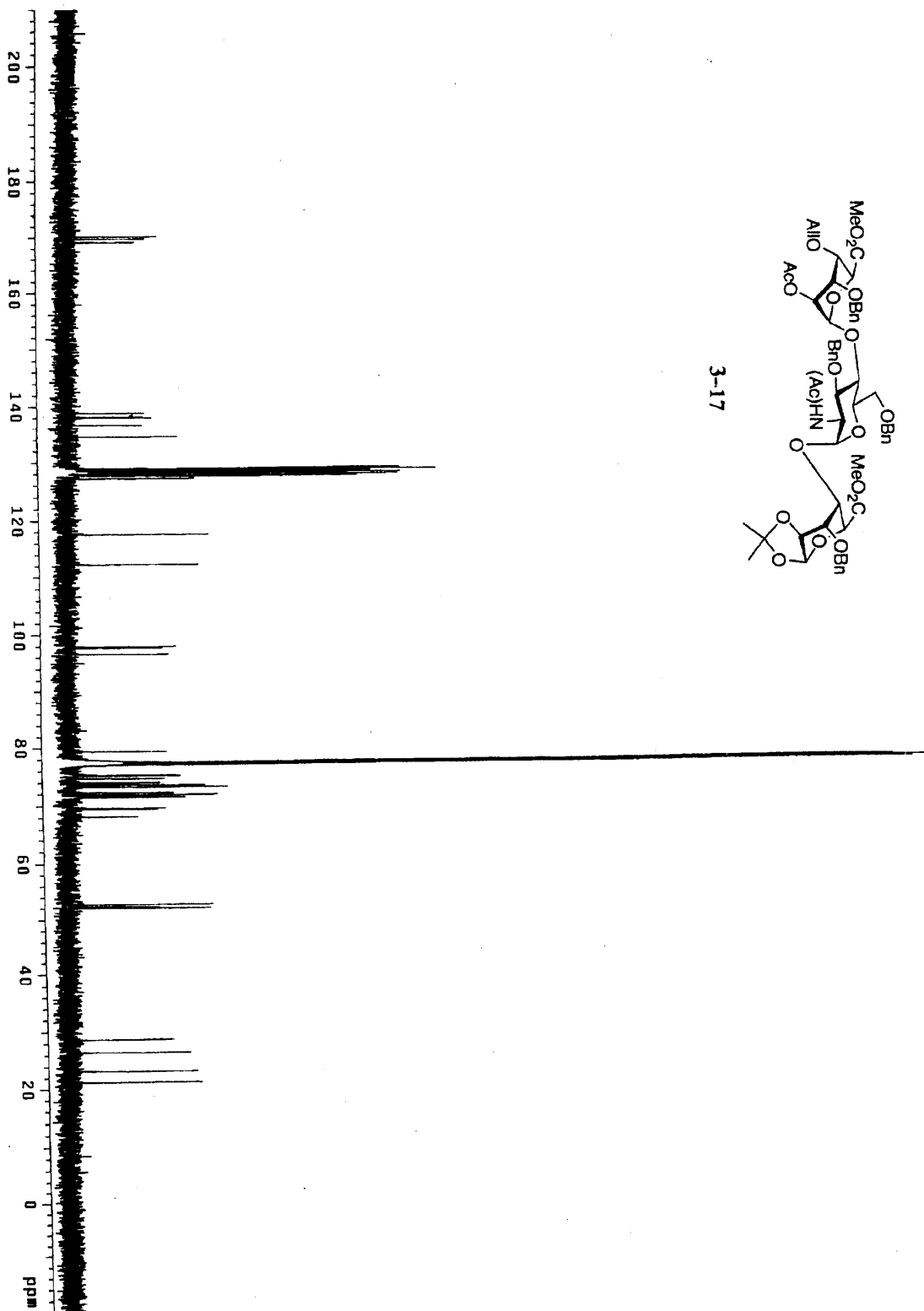


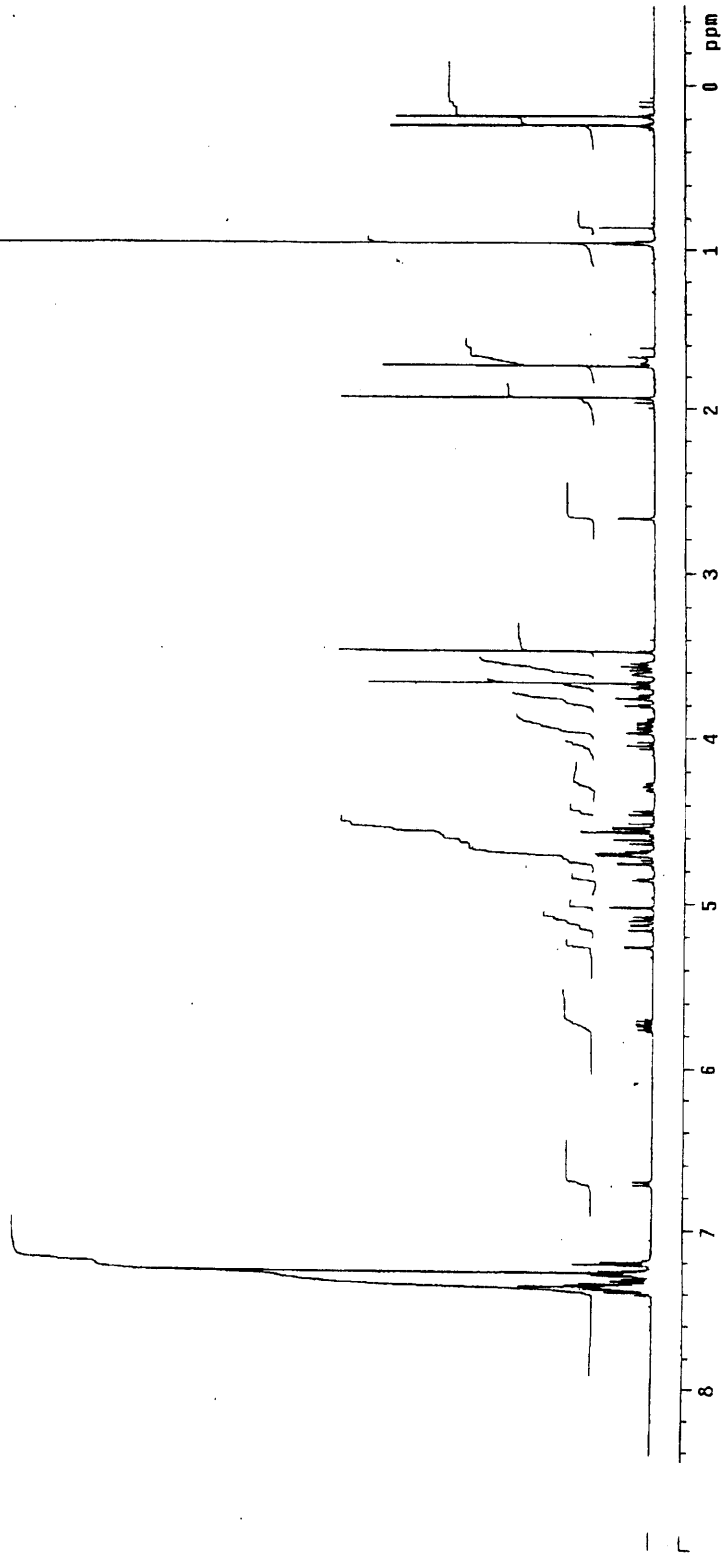
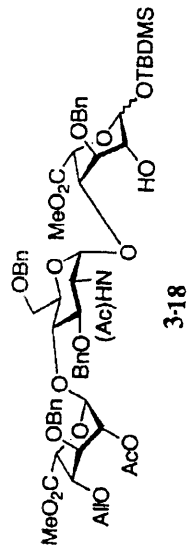
3-17

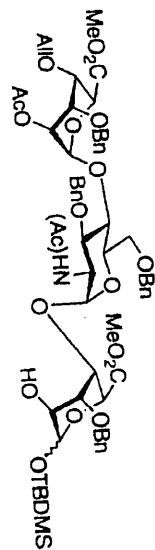




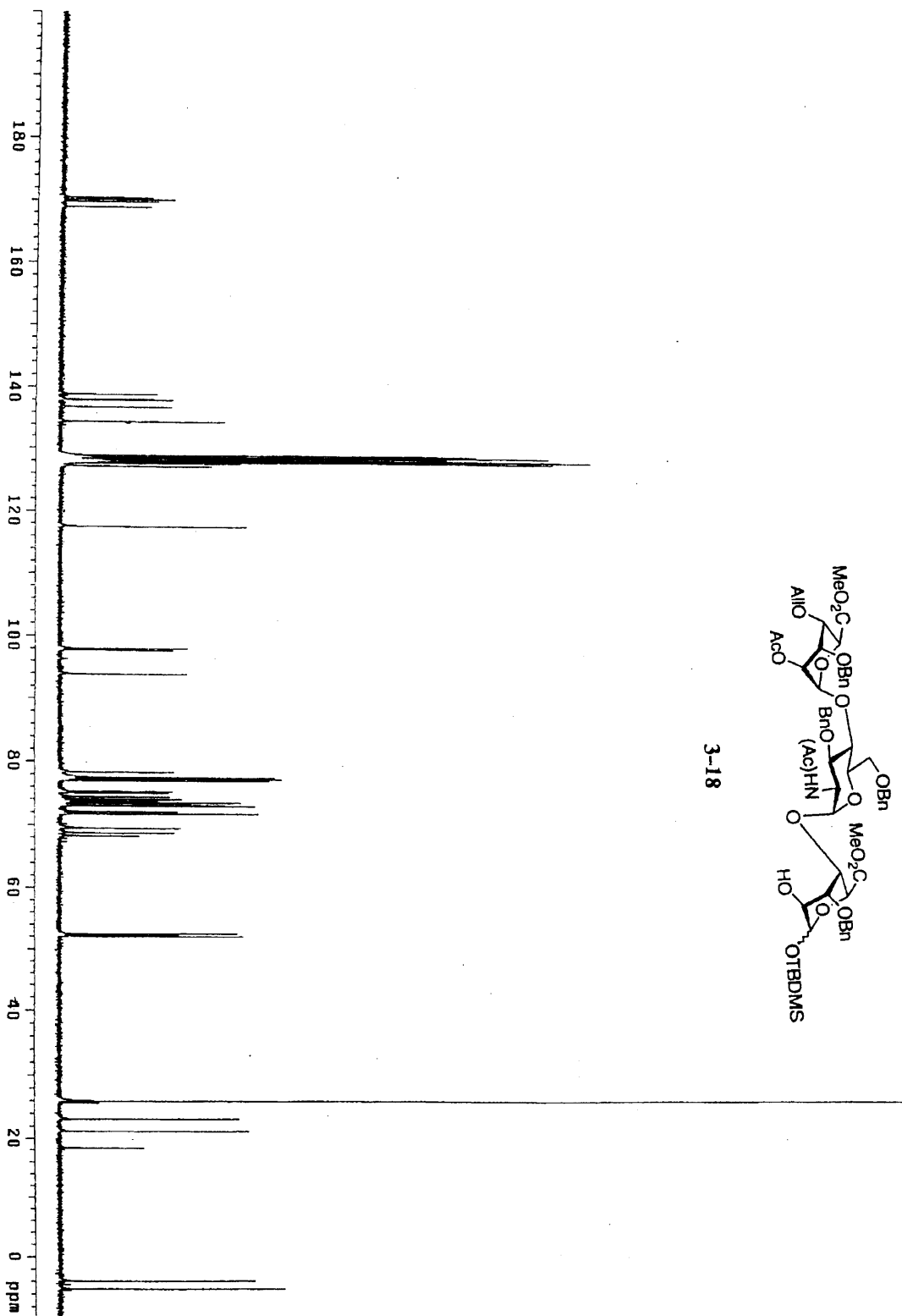
3-17

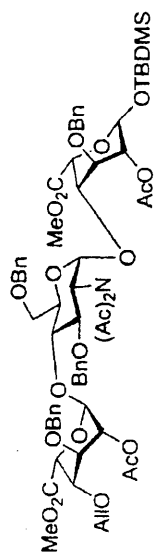




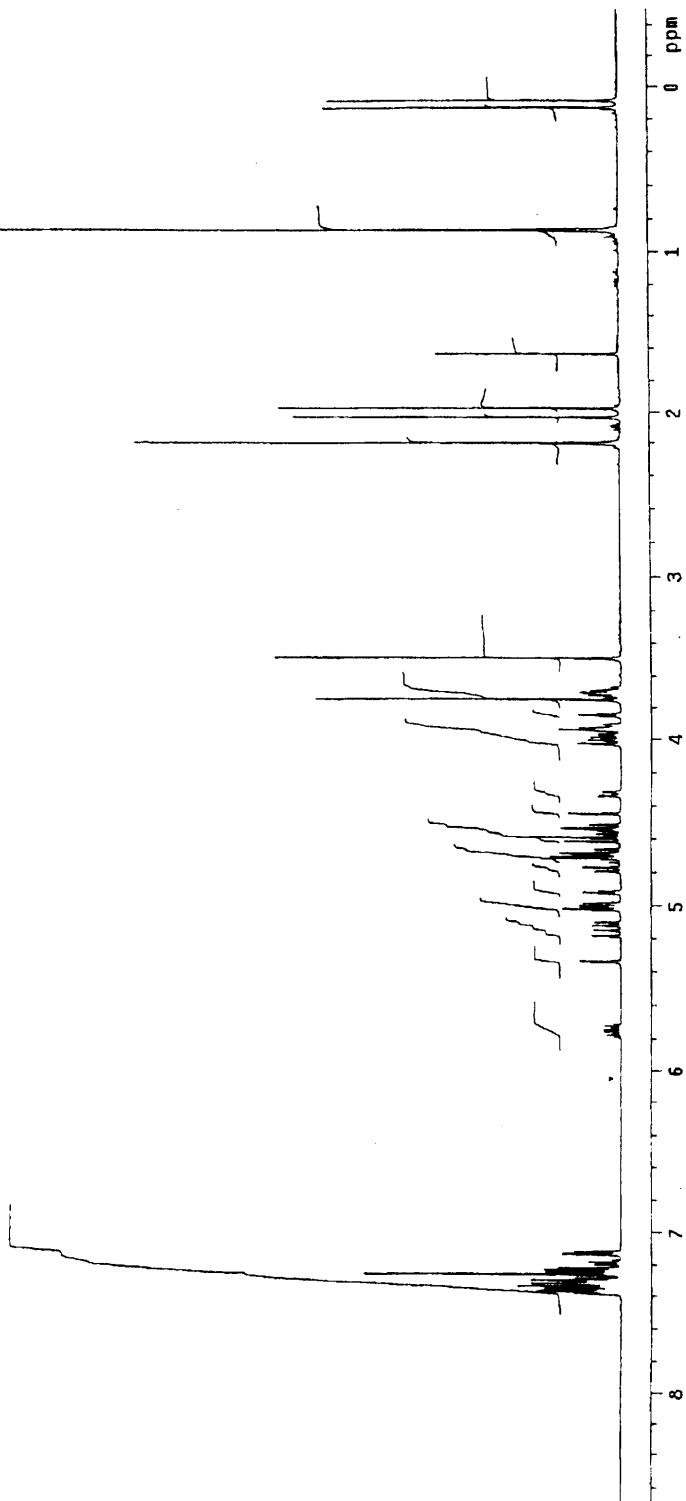


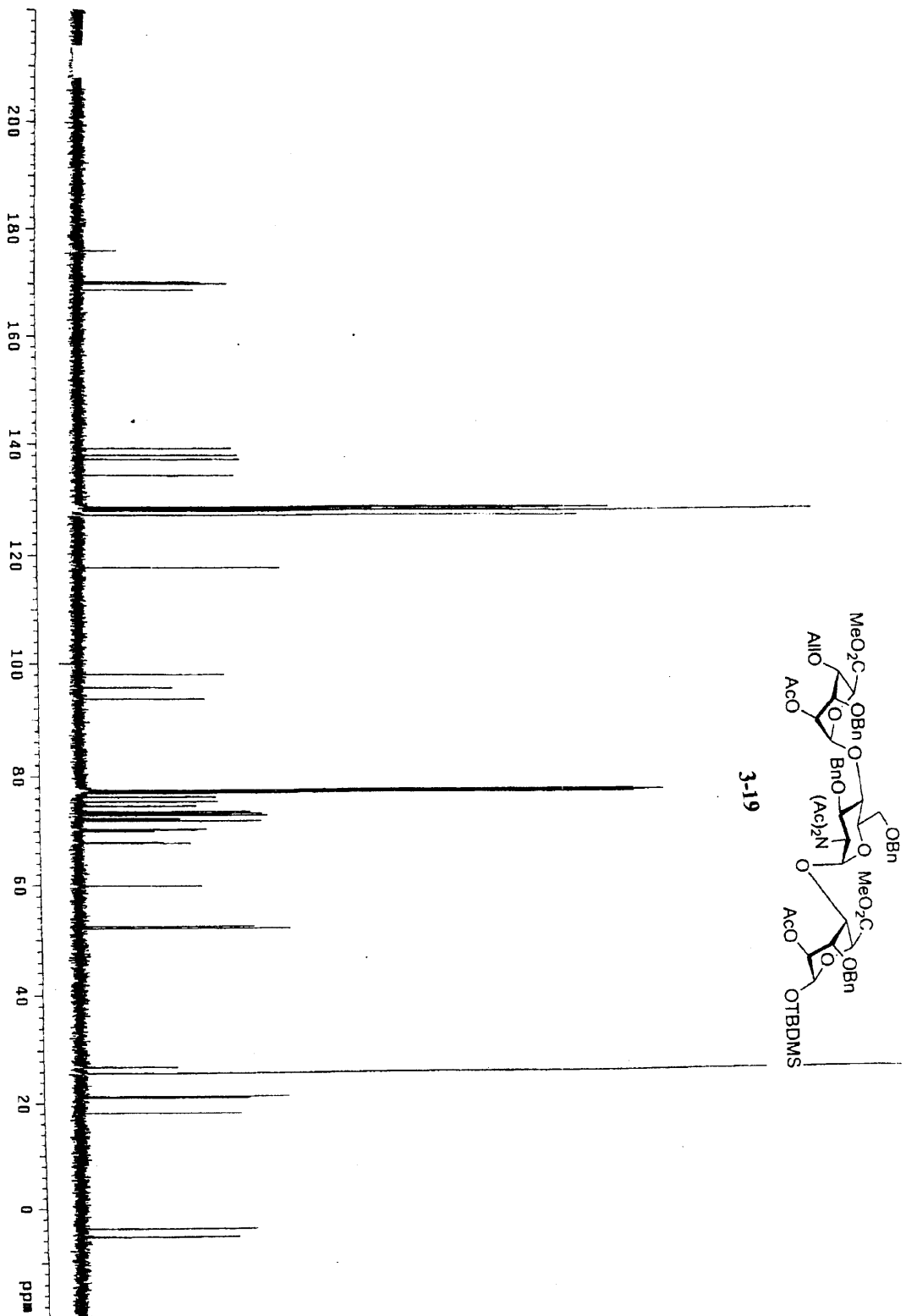
3-18



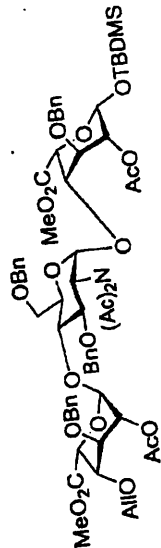


3-19

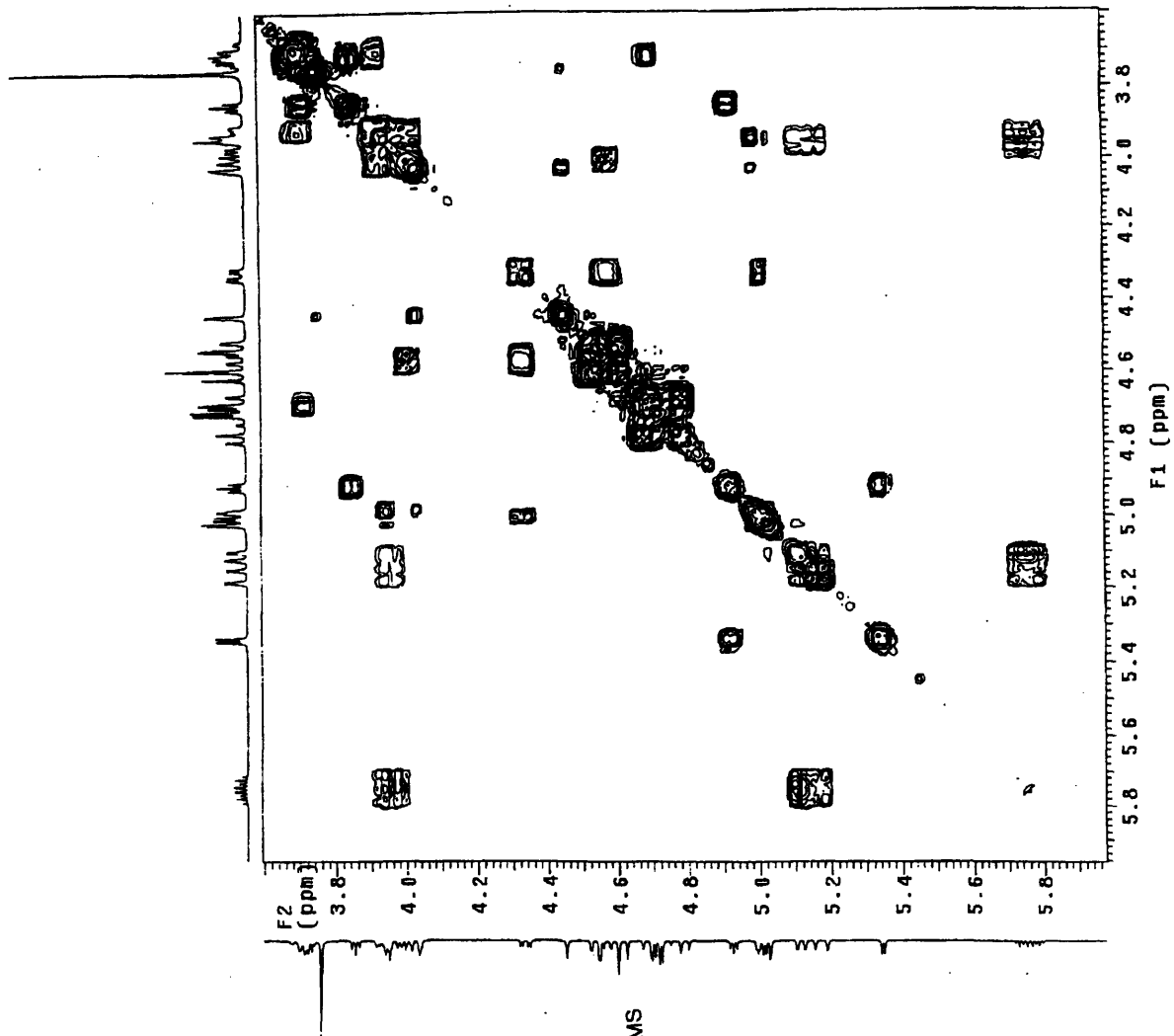




GL-2-247 H
 Pulse Sequence: gCOSY
 Solvent: CDCl3
 Temp. 22.0 C / 235.1 K
 File: GL-2-247gcosy
 INOVA-500 "zippy"
 PULSE SEQUENCE: gCOSY
 Relax delay 1.000 sec
 Acq. time 0.216 sec
 Width 4748.9 Hz
 2D Width 4748.9 Hz
 4 repetitions
 256 increments
 OBSERVE HI, 499.7537713 MHz
 DATA PROCESSING
 Sg. sine bell 0.108 sec
 F1 DATA PROCESSING
 Sg. sine bell 0.252 sec
 F1 size 2048 x 2048
 Total time 0 min., -1 sec



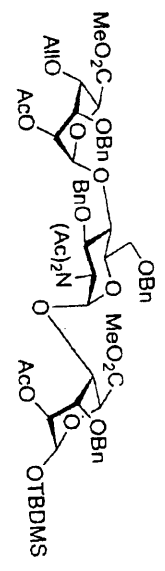
3-19



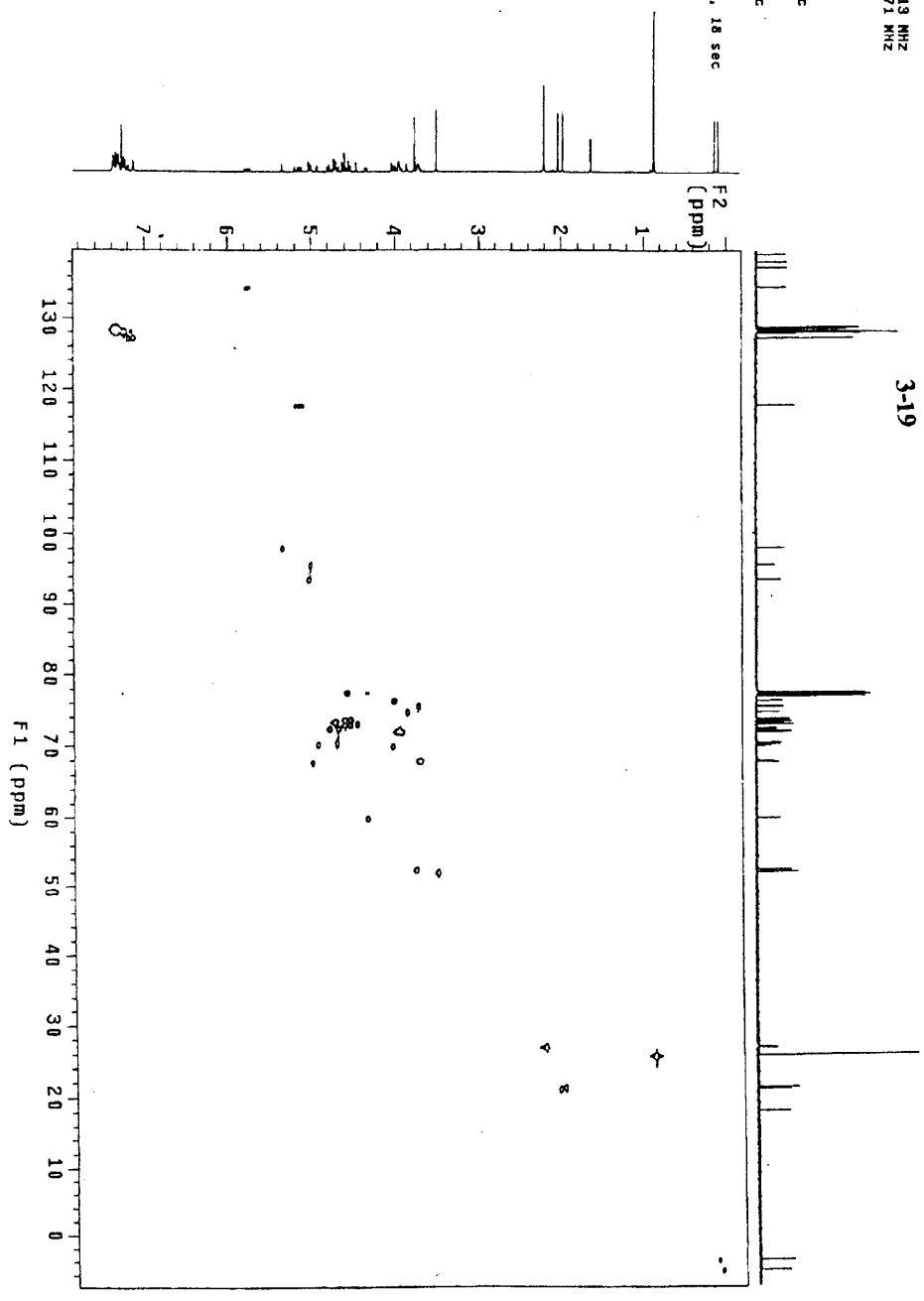
GL-2-247 HSQC

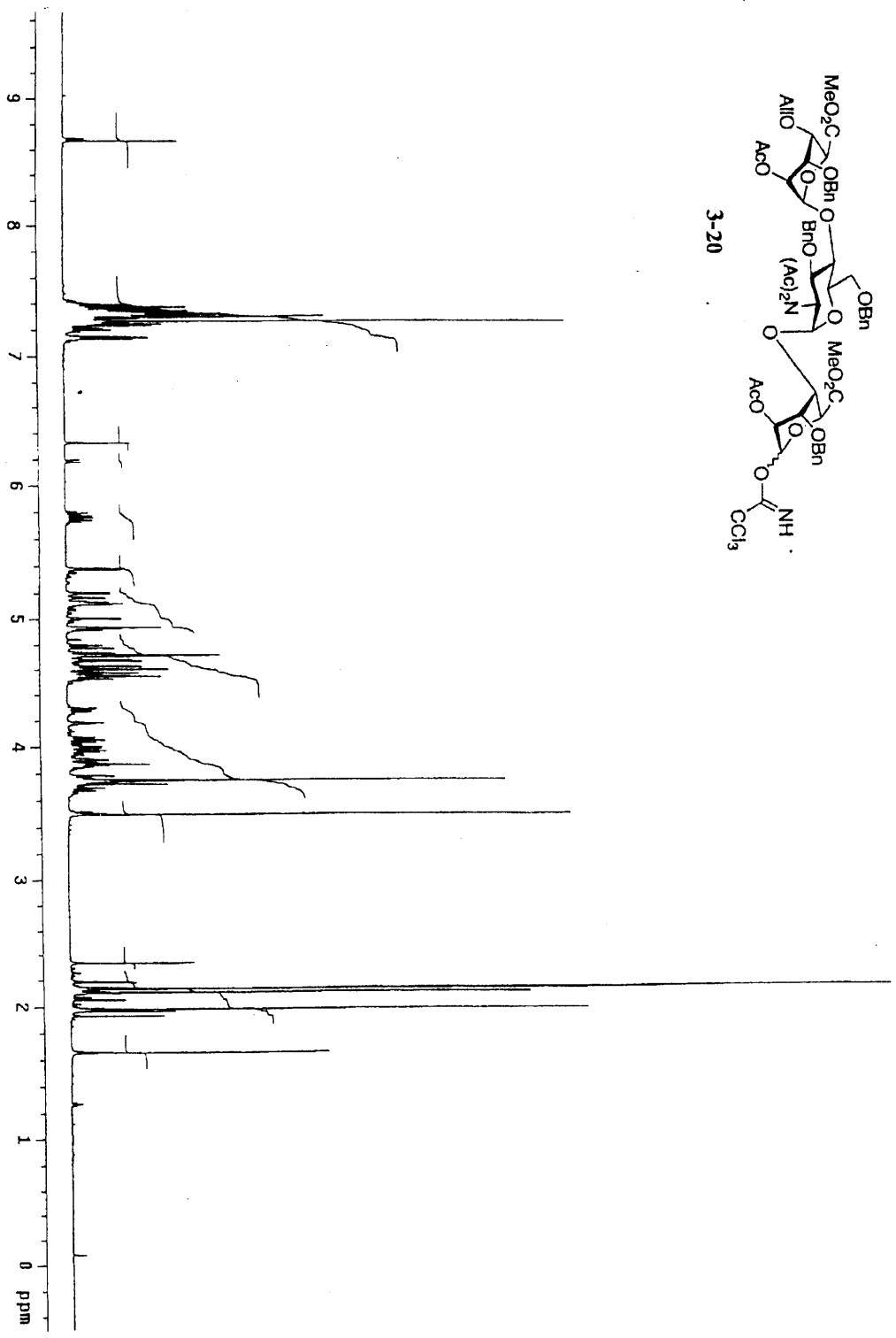
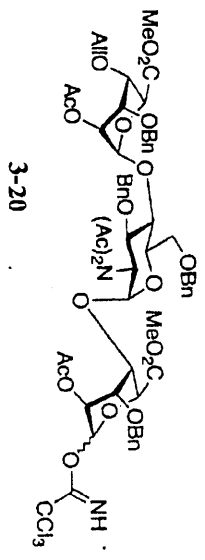
Pulse Sequence: HSQC

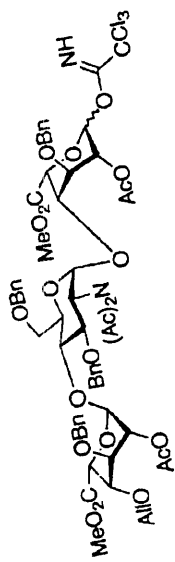
Solvent: CDCl3
Temp: 22.0 C / 285.1 K
User: J-14-87
File: GL-2-24/HSQC
INDVA-500 "zippy"
PULSE SEQUENCE: HSQC
Relax. delay: 1.000 sec
Acq. time: 0.101 sec
Width: 4748.3 Hz
ZD Width: 30188.7 Hz
9 repetitions
9 F2 increments
OBSERVE INCREMENTS: 5592719 MHz
DECUPLE C13: 125.675271 MHz
Power: S9 dB
on during acquisition
off during delay
GARP-1 modulated
DATA PROCESSING
Sg. sine bell: 0.101 sec
F1 Shifted by: 0.101 sec
F2 DATA PROCESSING
Sg. sine bell: 0.077 sec
Shifted by: 0.077 sec
FT size: 2048 x 2048
Total time: 1 hr, 21 min, 18 sec



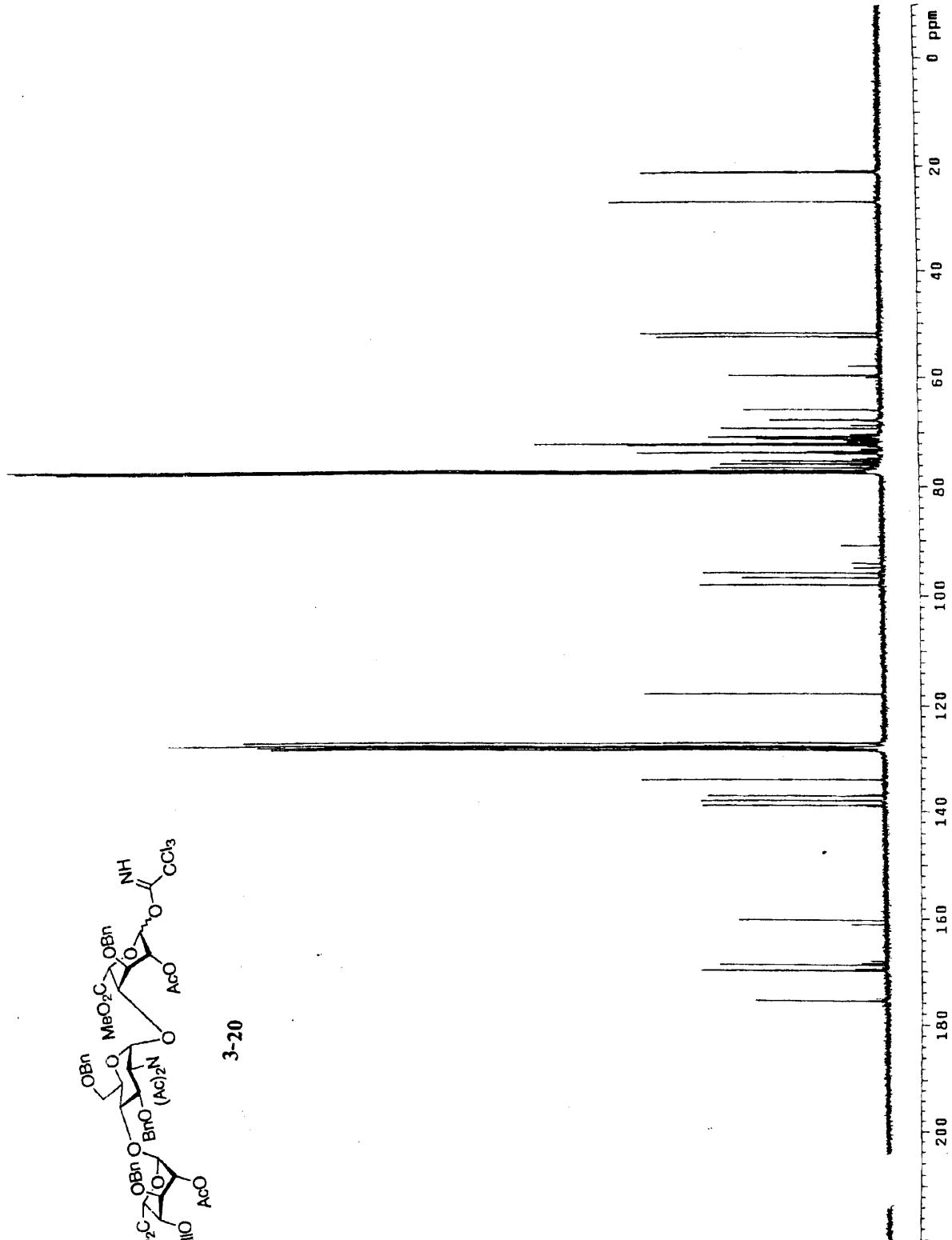
3-19

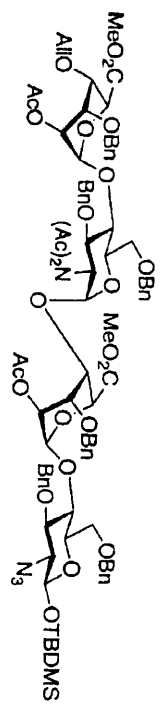




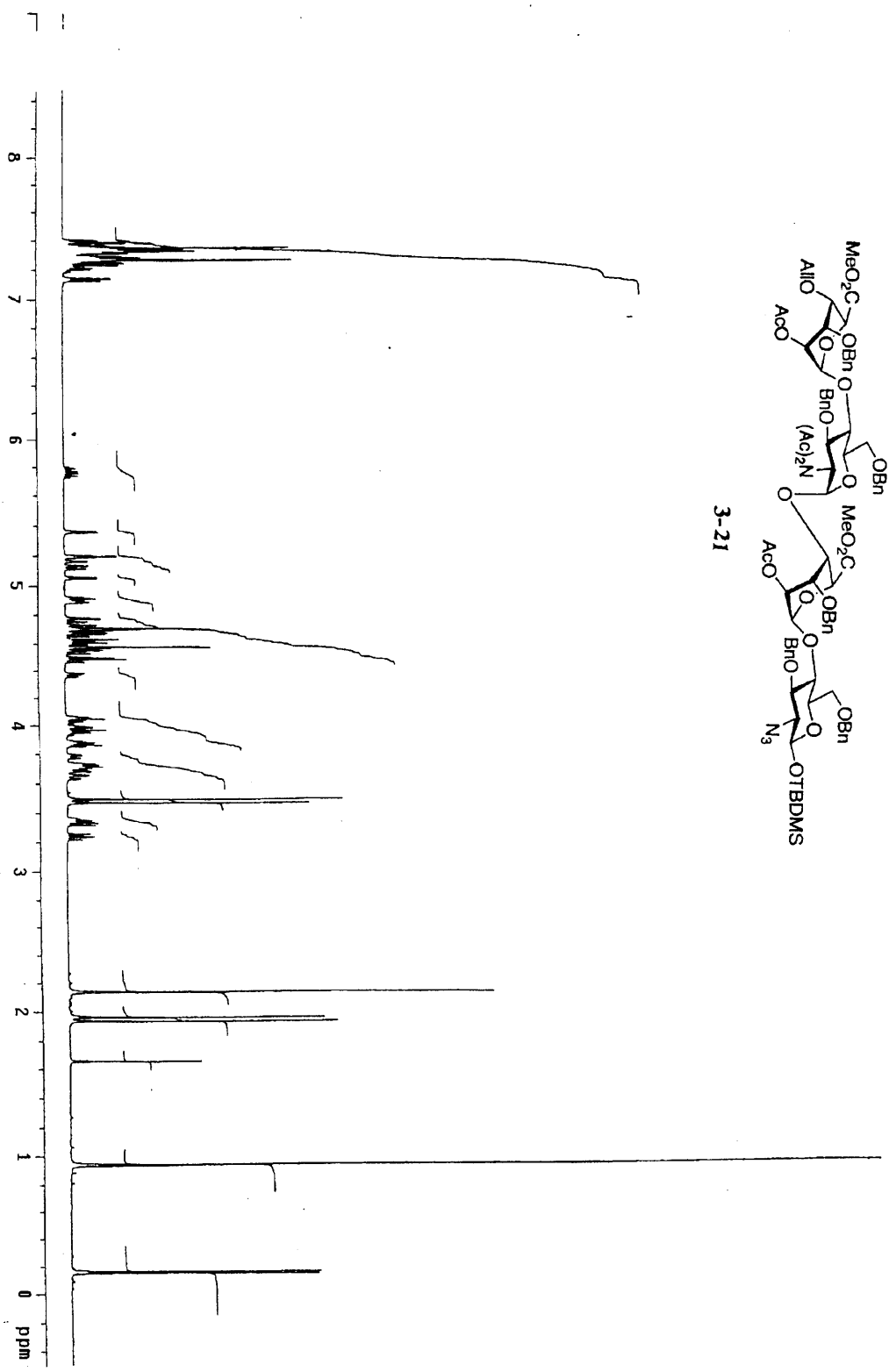


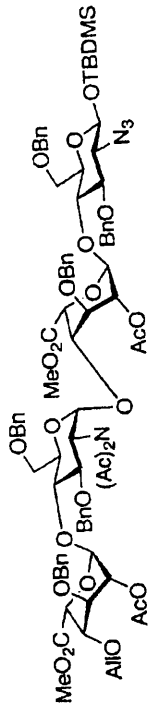
3-20



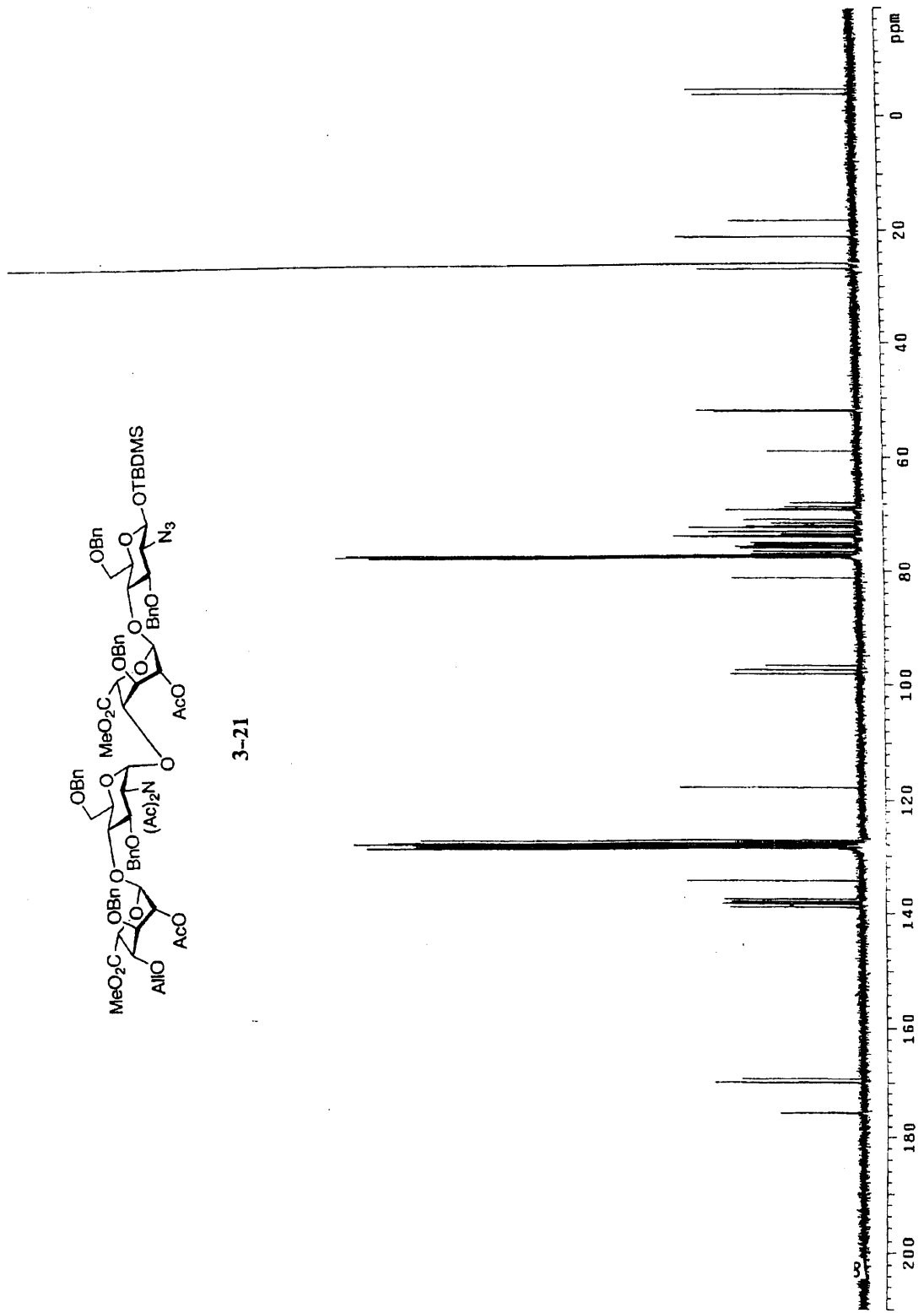


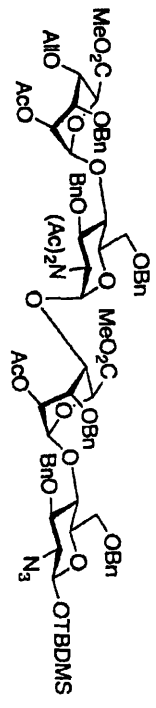
3-21



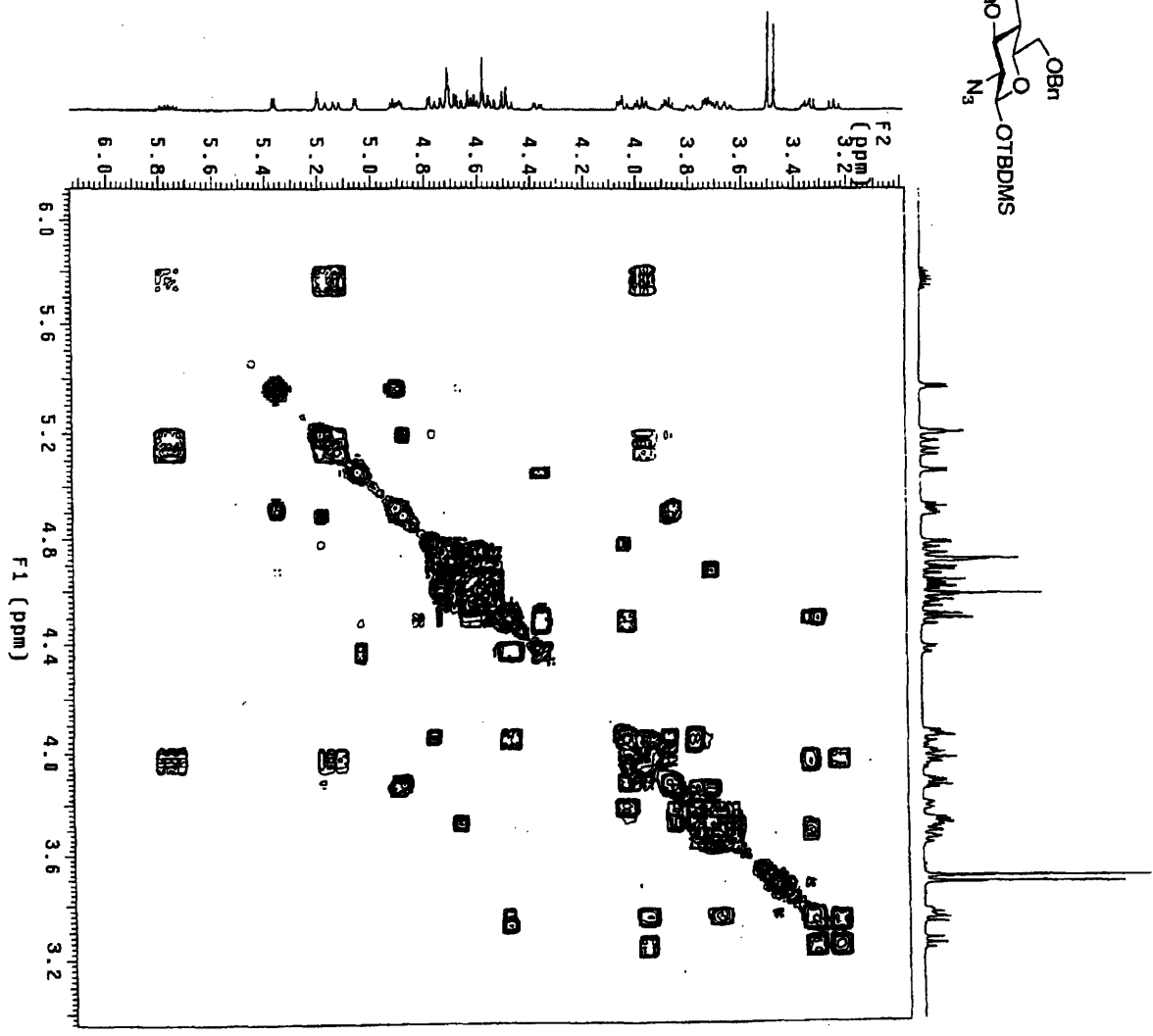


3-21



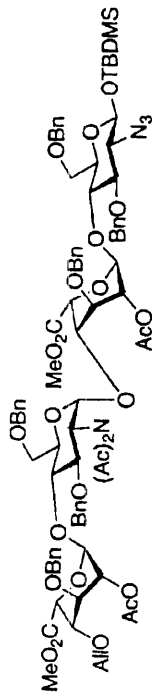


256 INCREMENTS
 OBSERVE: NI 499.7537719 MHz
 DATA PROCESSING: 3-21
 F1 DATA ACQUISITION: 108. sec
 F2 DATA ACQUISITION: 1052 sec
 Sp. size: 2048 X 2048
 Total time: 0 min., -1 sec

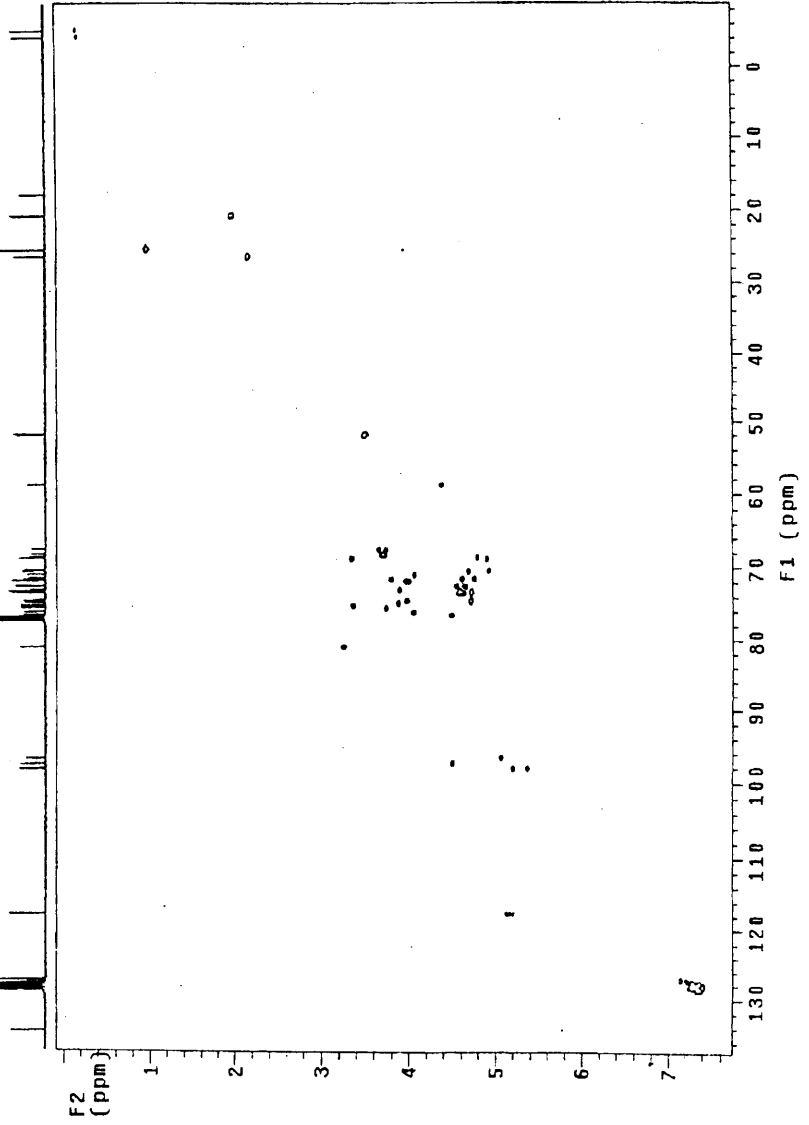


STANDARD PROTON PARAMETERS
 01-1-261

Pulse Sequence: HSQC
 Solvent: CDCl3
 Temp: 22.0 C / 295.1 K
 File: 01-2-261HSQC
 INOVA-500 "zippy"
 PULSE SEQUENCE: HSQC
 Relax. delay 1.000 sec
 Acq. time 9.101 sec
 F1 width 2400.3 Hz
 200 MHz 25000.9 Hz
 4 repetitions
 2 x 256 increments
 OBSERVE H1, 499.753713 MHz
 DECOUPLE C13, 125.6750940 MHz
 Power 53 dB
 on during acquisition
 off during delay
 GARP-1 modulated
 DATA PROCESSING
 Sg. time bell 0.101 sec
 Sh. time bell 0.101 sec
 F1 DATA PROCESSING
 Sg. time bell 0.018 sec
 Sh. time bell 0.018 sec
 Shifted by -0.018 sec
 FT size 2048 x 2048
 Total time 42 min, 33 sec



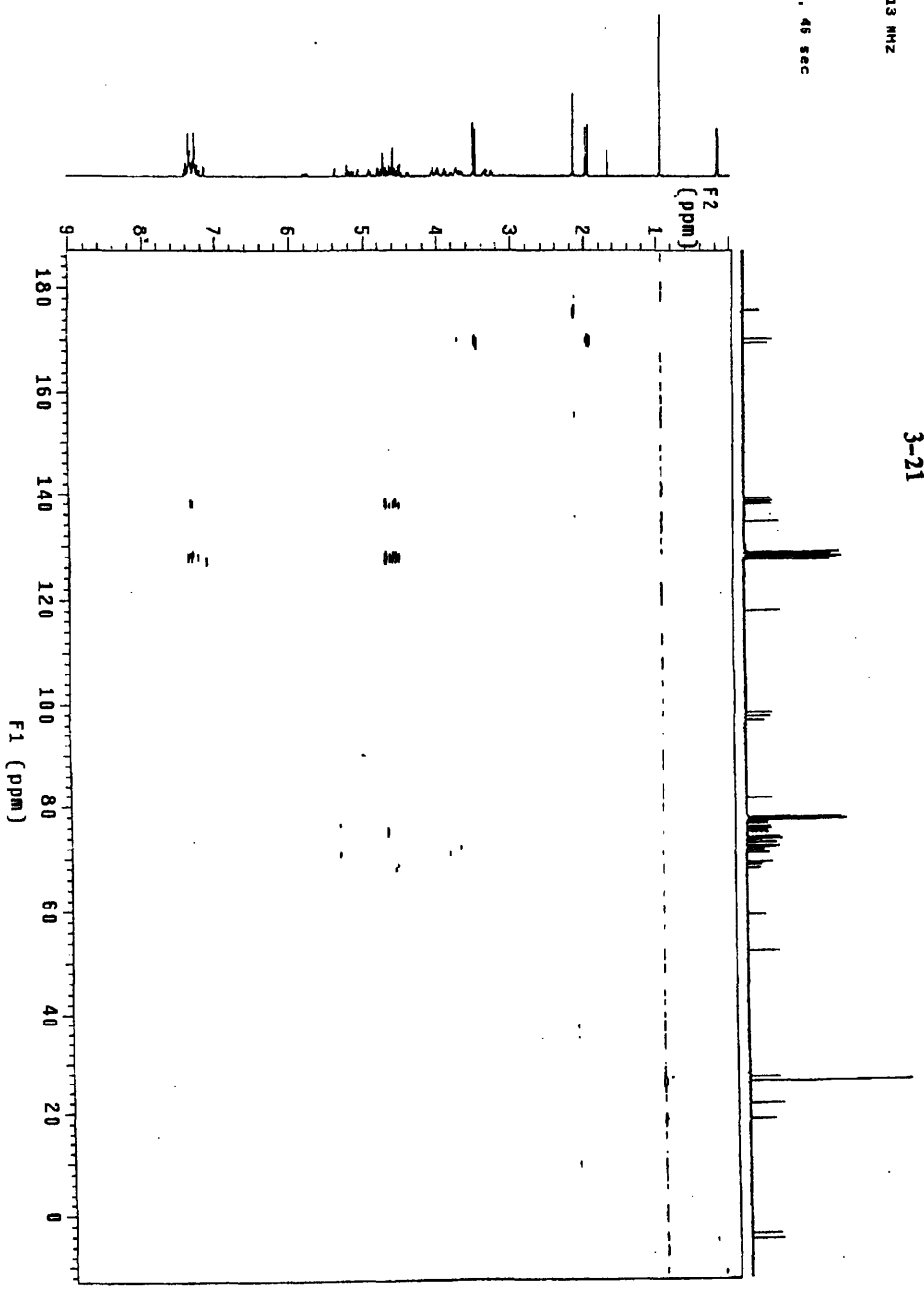
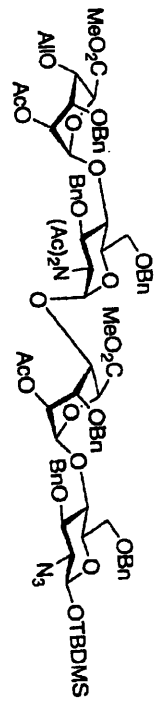
3-21

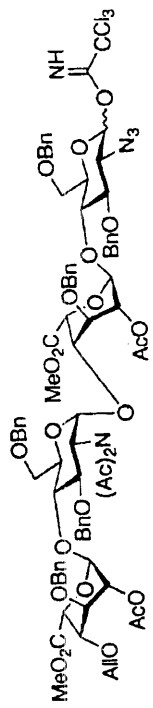


STANDARD PROTON PARAMETERS

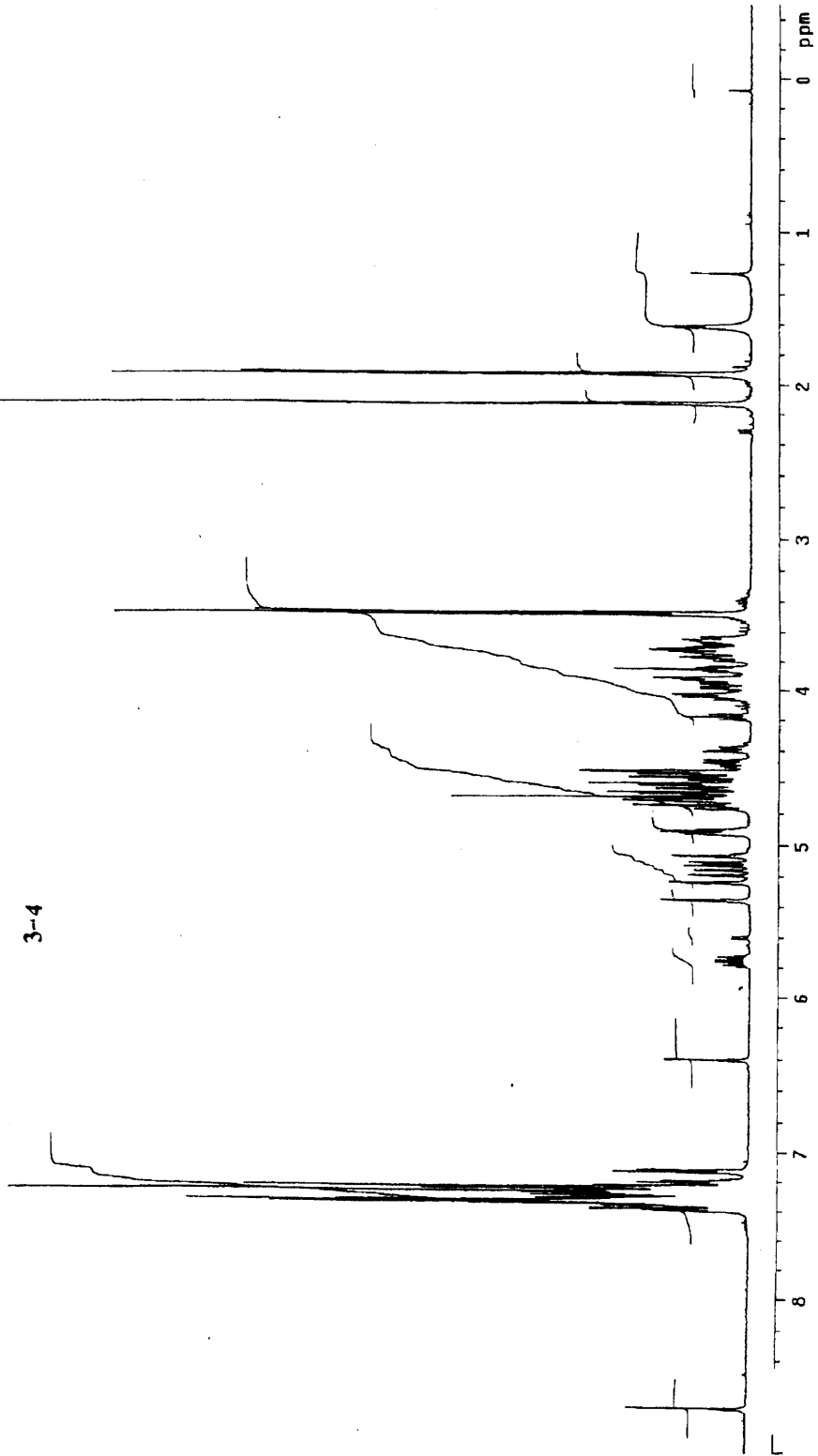
6-1-167

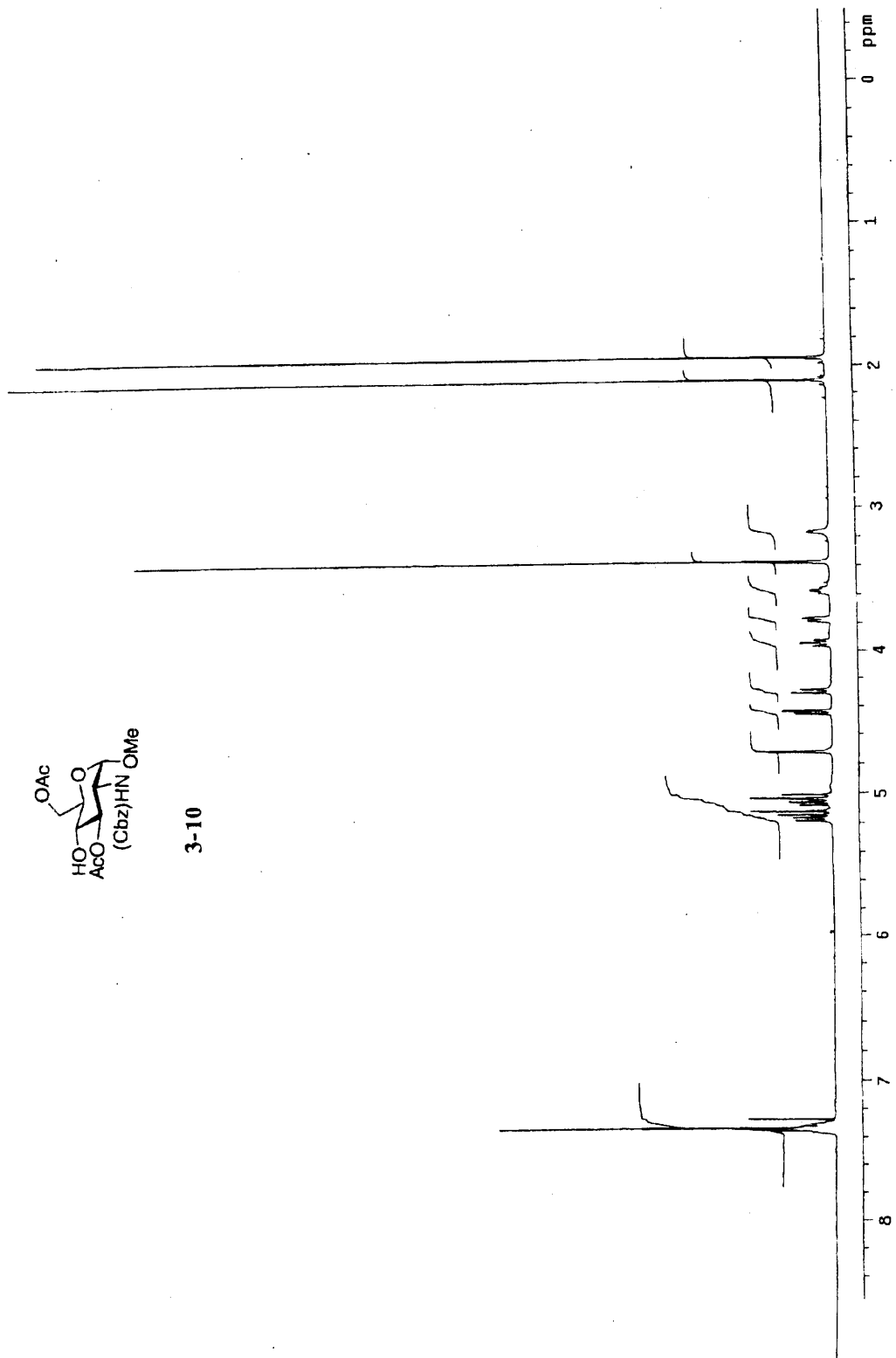
Pulse Sequence: HMQC
 Solvent: CDCl3
 Temp: 42.9 C / 295.1 K
 User: jk
 F2: 125.761 MHz
 INOVA-500 "zippy"
 PULSE SEQUENCE: HMQC
 Relax. delay: 1.000 sec
 Acq. time: 2.218 sec
 F2 (1H): 499.818 MHz
 F2 (13C): 200.131 MHz
 # Repetitions: 2 x 256 increments
 OBSERVE: H1, 499.7537719 MHz
 DATA PROCESSING
 Sine bal 1 0.108 sec
 F1 DATA PROCESSING
 Sine bal 1 0.004 sec
 FT size 2048 x 2048
 Total time 1 hr, 32 min, 46 sec



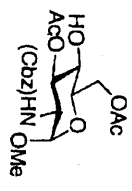
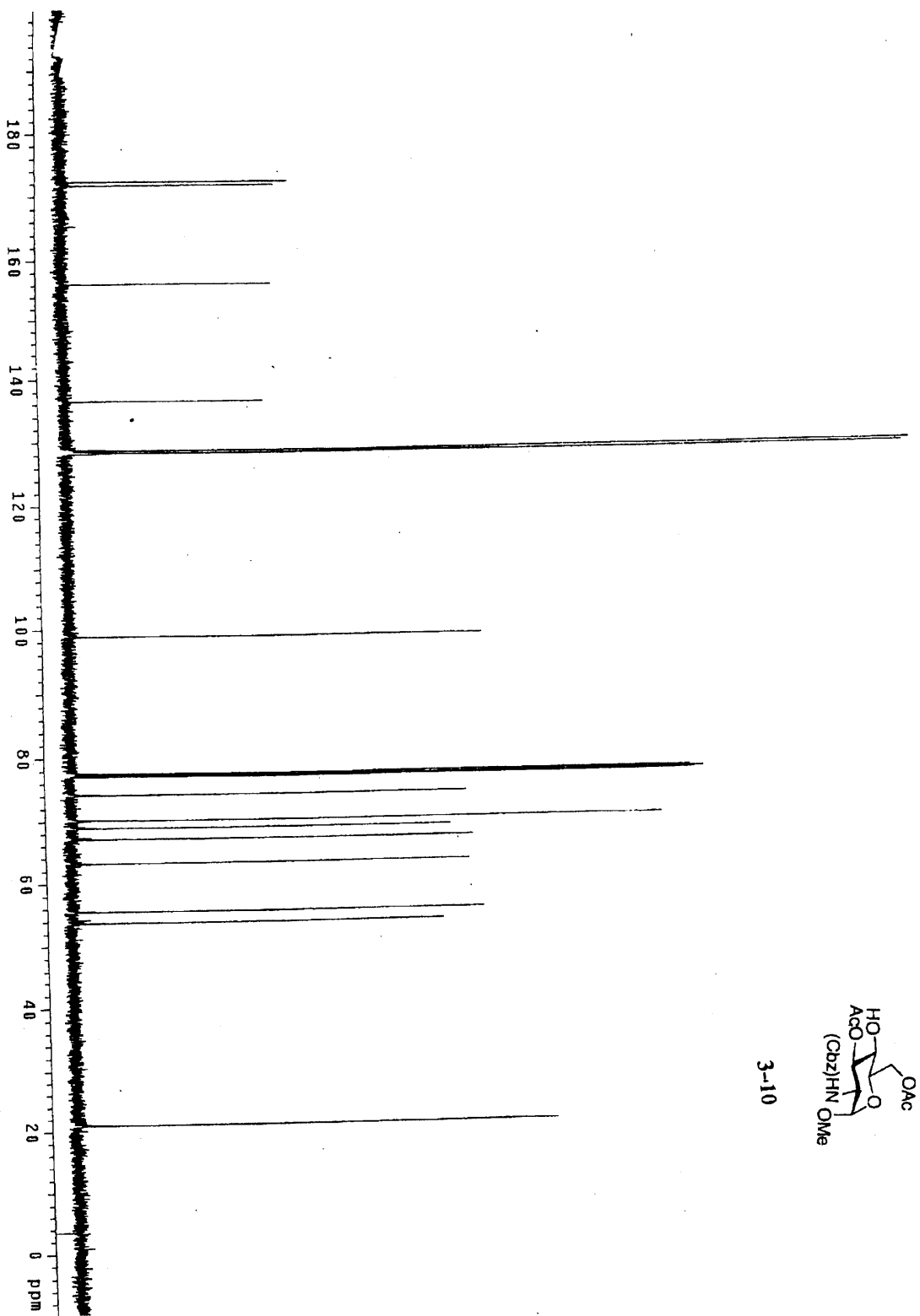


3-4





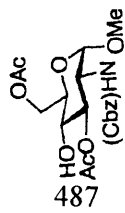
3-10



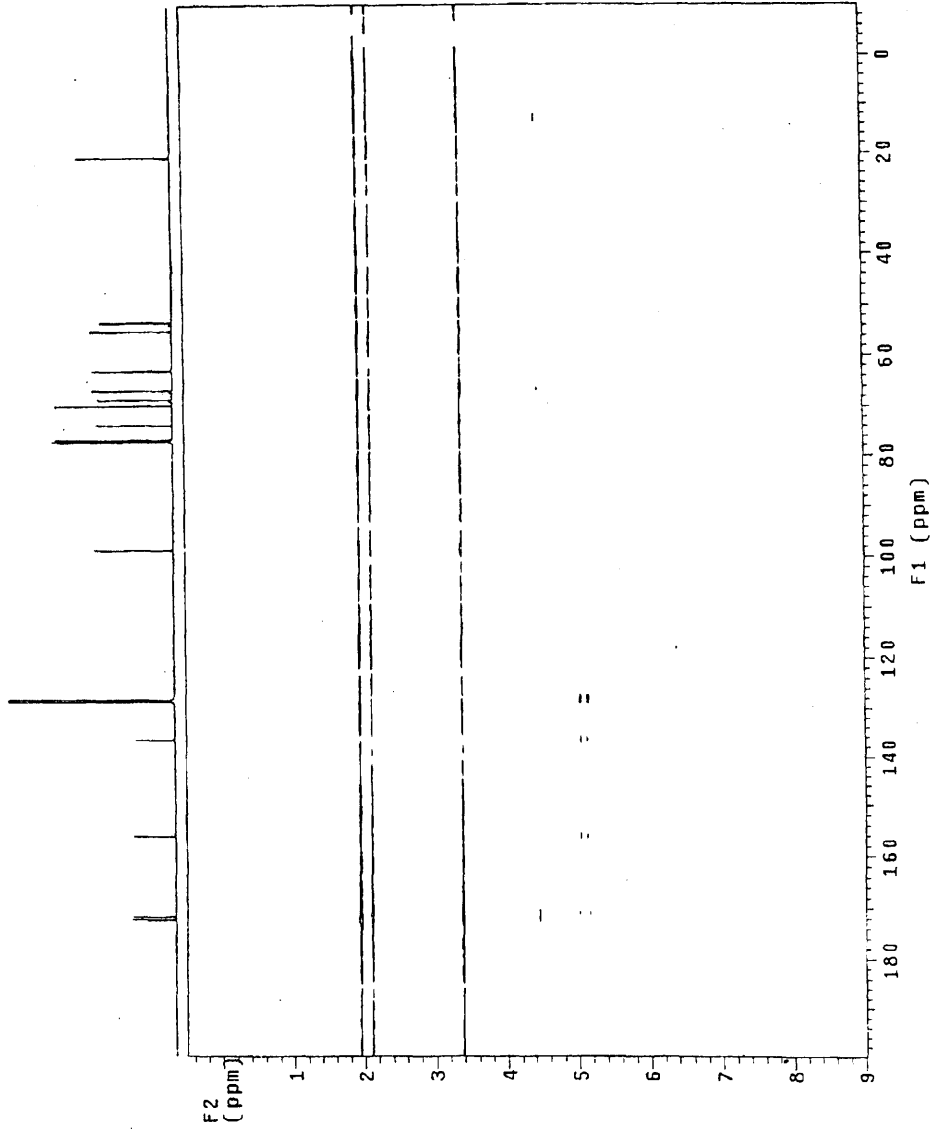
3-10

GL-2-71 H

Pulse Sequence: HMBC
Solvent: CDCl₃
Temp. 22.0 C / 295.1 K
User: 1-14-87
File name: GL-2-71HMBC
INOVA-500 "zippy"
PULSE SEQUENCE: HMBC
Relax. delay 1.000 sec
Acq. time 0.216 sec
Width 4748.3 Hz
2D Width 26350.5 Hz
8 repetitions
2 x 256 increments
OBSERVE: H1, 499.7537722 MHz
DETAILED PROCESSING
F1: 125.761 MHz
F2: 500.136 MHz
F3: 500.136 MHz
F4: 500.136 MHz
F5: 500.136 MHz
Sine bell 0.804 sec
FI size 2048 x 2048
Total time 1 hr, 32 min, 48 sec



3-10



GL-2-71 H

Pulse Sequence: HSQC

Solvent: CDCl3

Temp: 22.0 C / 285.1 K

User: 1-14-87

File name: GL-2-71HSQC

INOVA-500 "zippy"

PULSE SEQUENCE: HSQC

Relax. delay: 1.000 sec

Acq. time: 0.101 sec

Width: 4748.3 Hz

20 Width: 28350.5 Hz

4 repetitions

2 x 256 increments

OBSERVE: H1, 451.7597722 MHz

DECOUPLE: C13, 125.6751874 MHz

Power: 35 dB

or during acquisition

QAP-1 mode used

DATA PROCESSING

Sq. sine bell: 0.101 sec

Shifted by: -0.101 sec

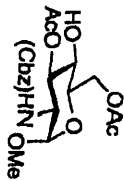
F1 DATA PROCESSING

Sq. sine bell: 0.018 sec

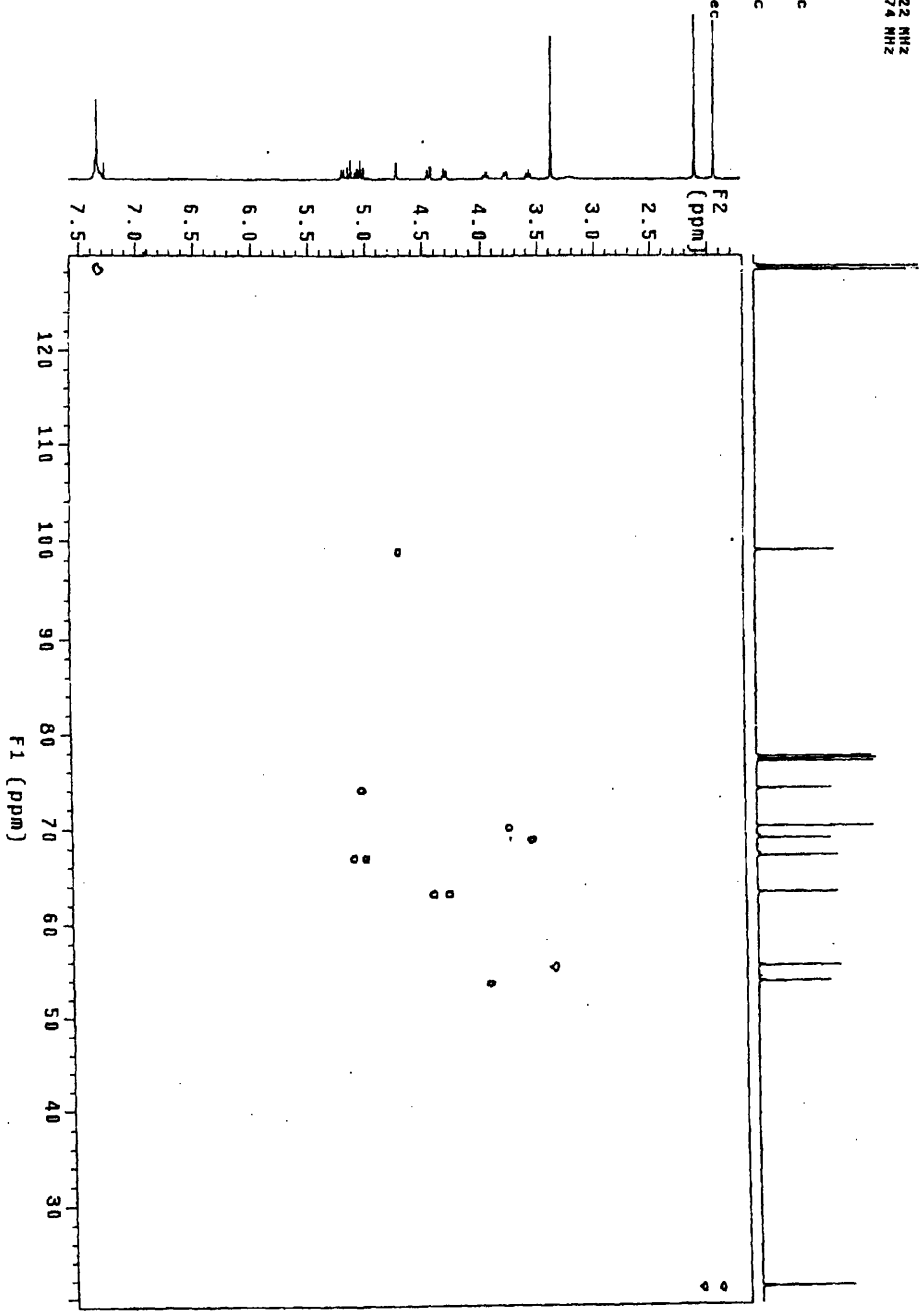
Shifted by: -0.018 sec

FT size: 2048 x 2048

Total time: 42 min, 39 sec

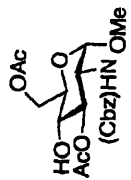


3-10
4

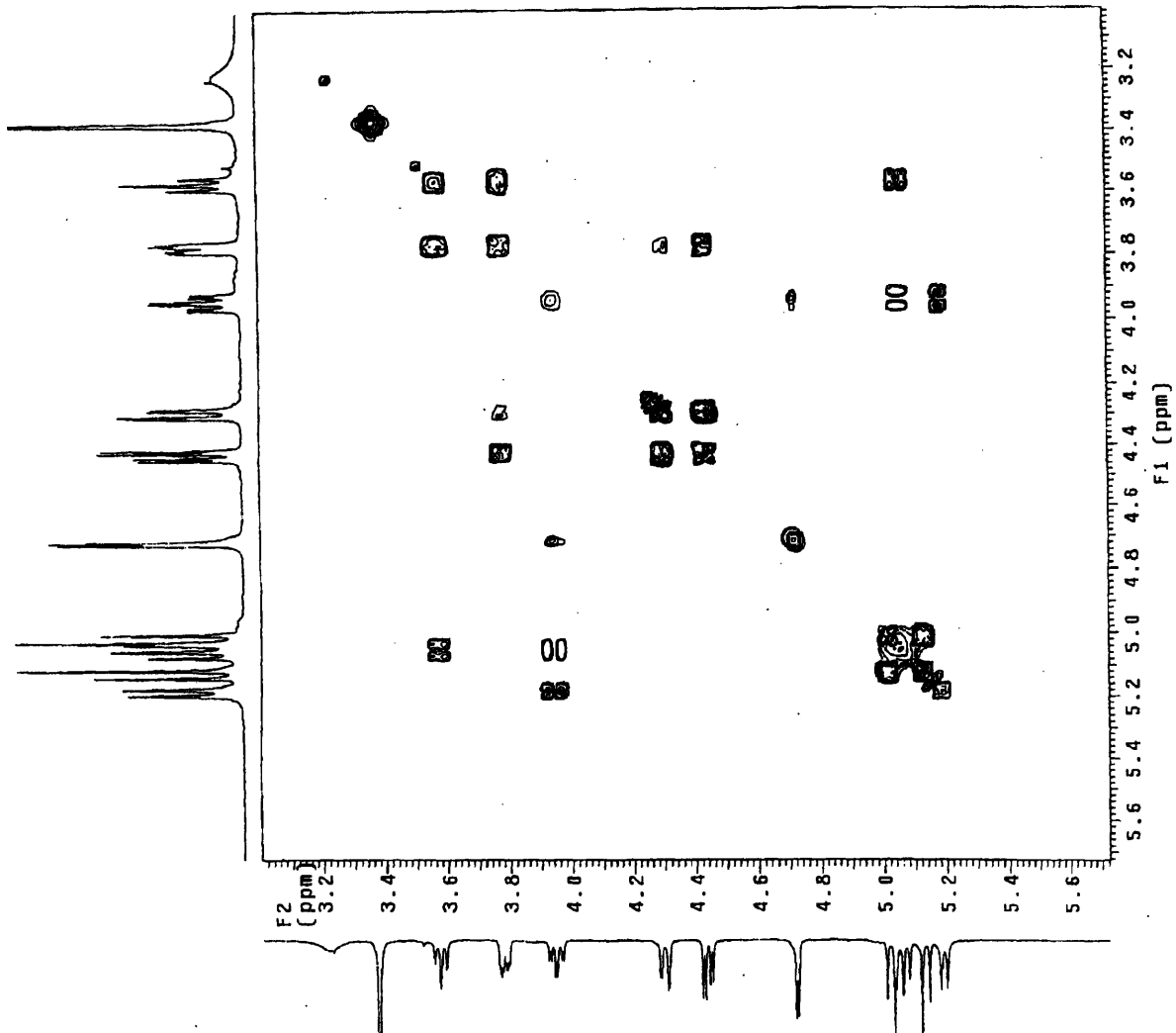


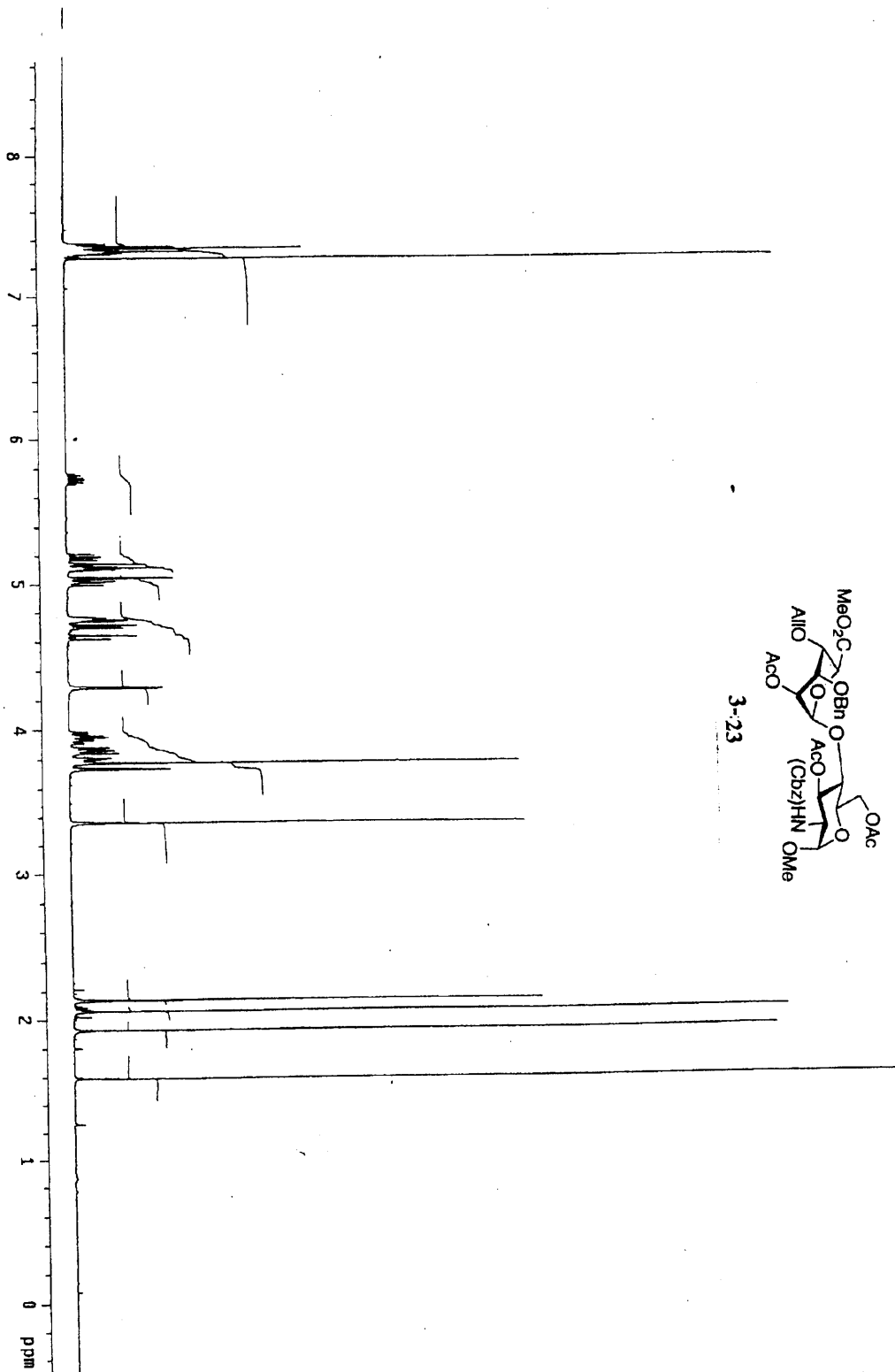
GL-2-71 H

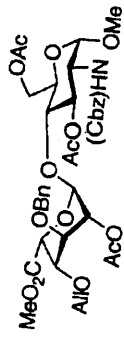
Pulse Sequence: gCOSY
Solvent: CMC13
Temp: 22.0 C / 215.1 K
File name: GL-2-71gcosy
INDVA-500 "zippy"
PULSE SEQUENCE: gCOSY
Relax. delay: 1.000 sec
Acq. time: 0.216 sec
Width: 4748.3 Hz
2D Width: 4748.3 Hz
Single scan
256 increments
OBSERVE: F1, 499.7537722 MHz
DATA PROCESSING
Sg. sine bell: 0.108 sec
F2 DATA PROCESSING
F2 sine bell: 0.052 sec
F2: 1.2000 X 2048
Total time: 5 min, 40 sec



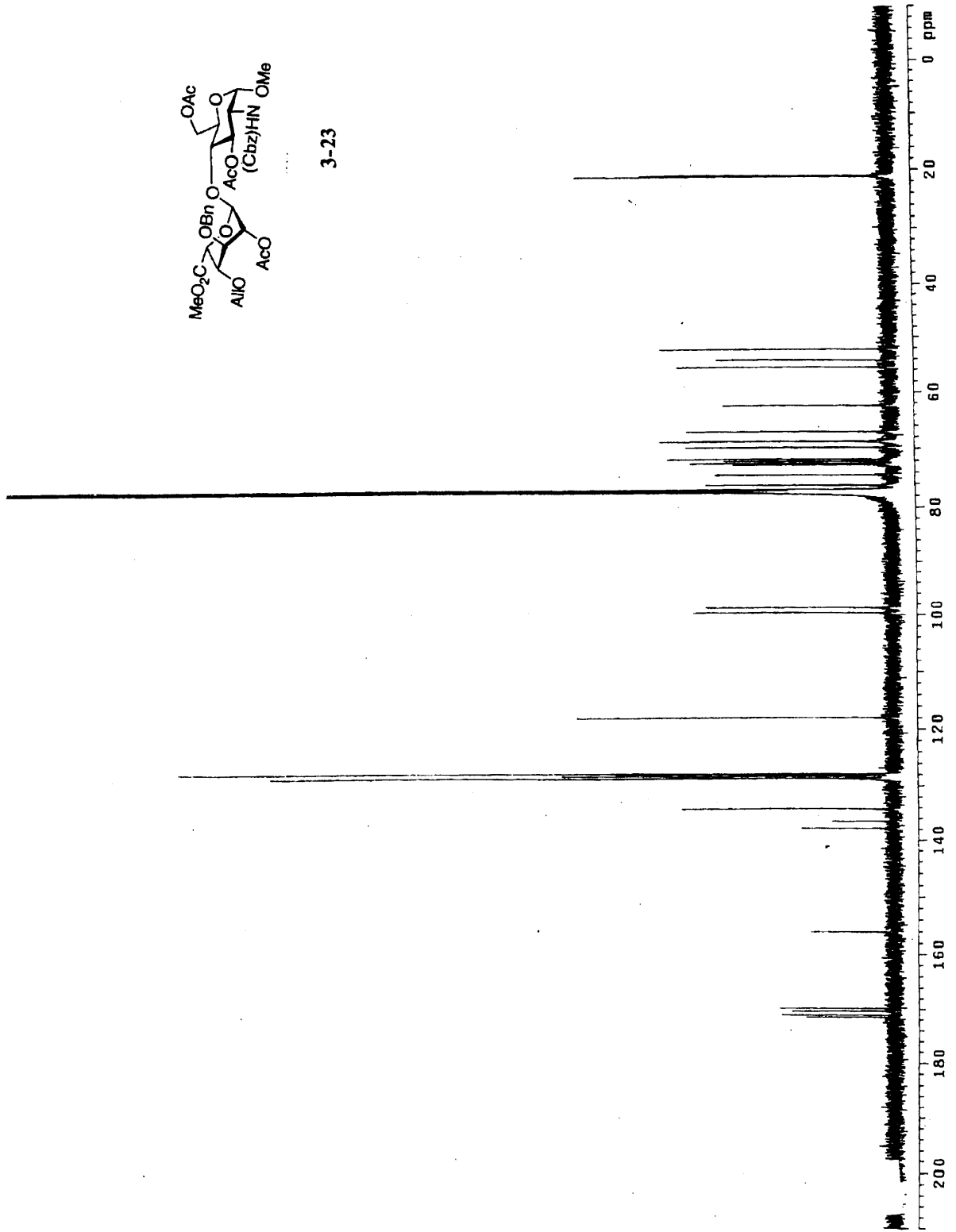
3-10

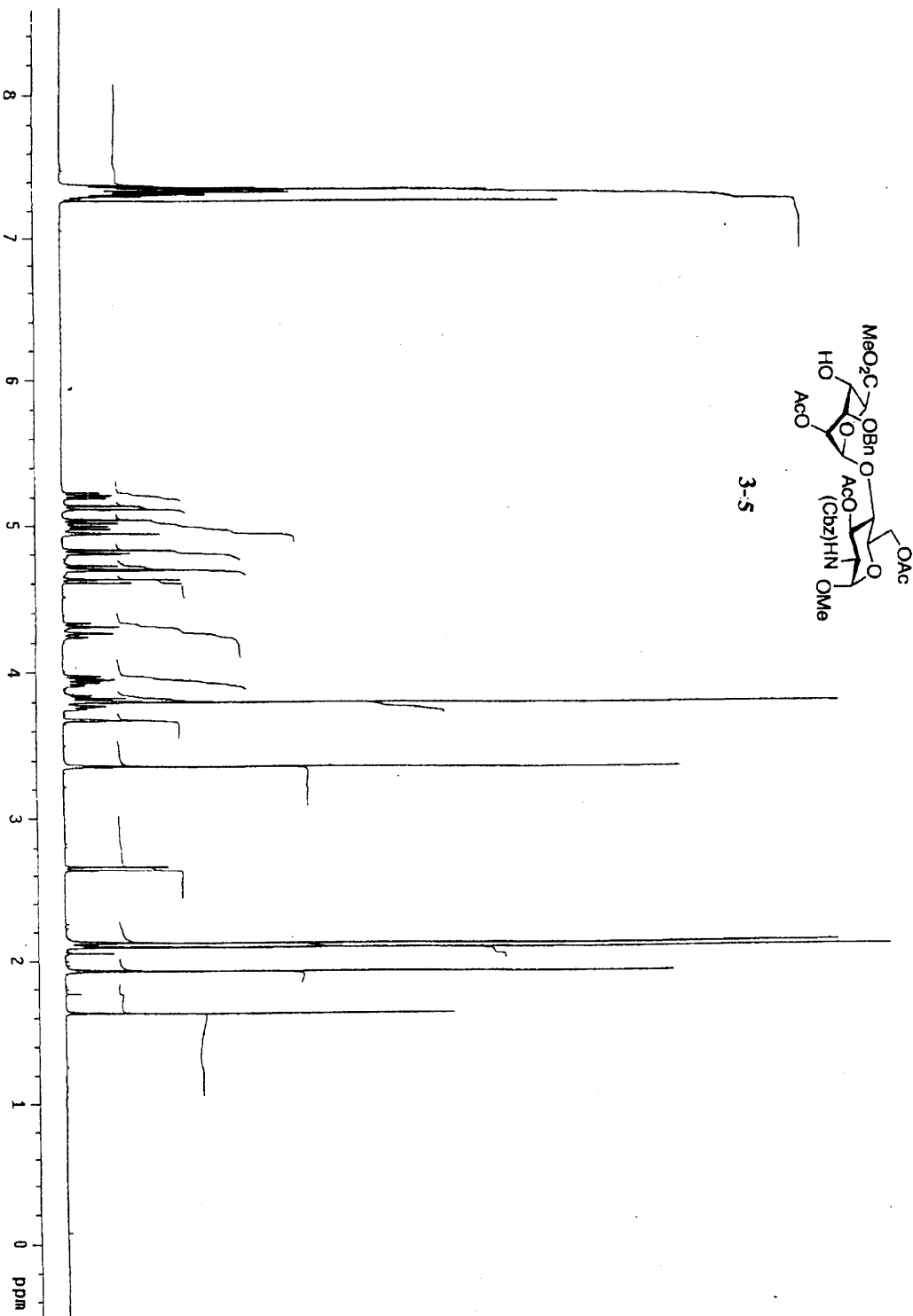


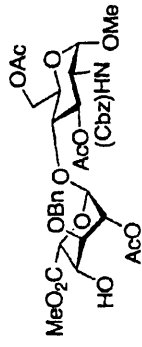




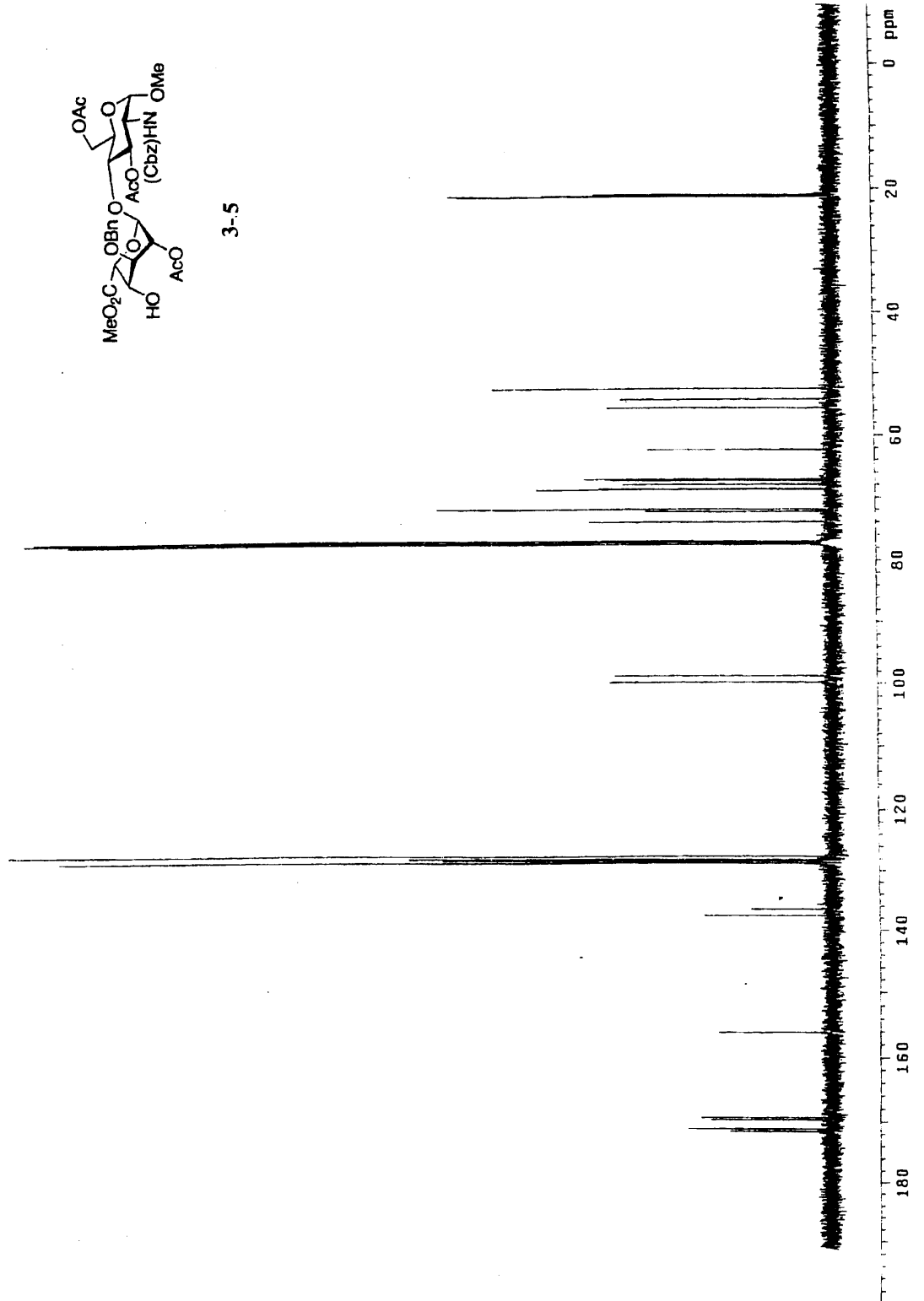
3-23





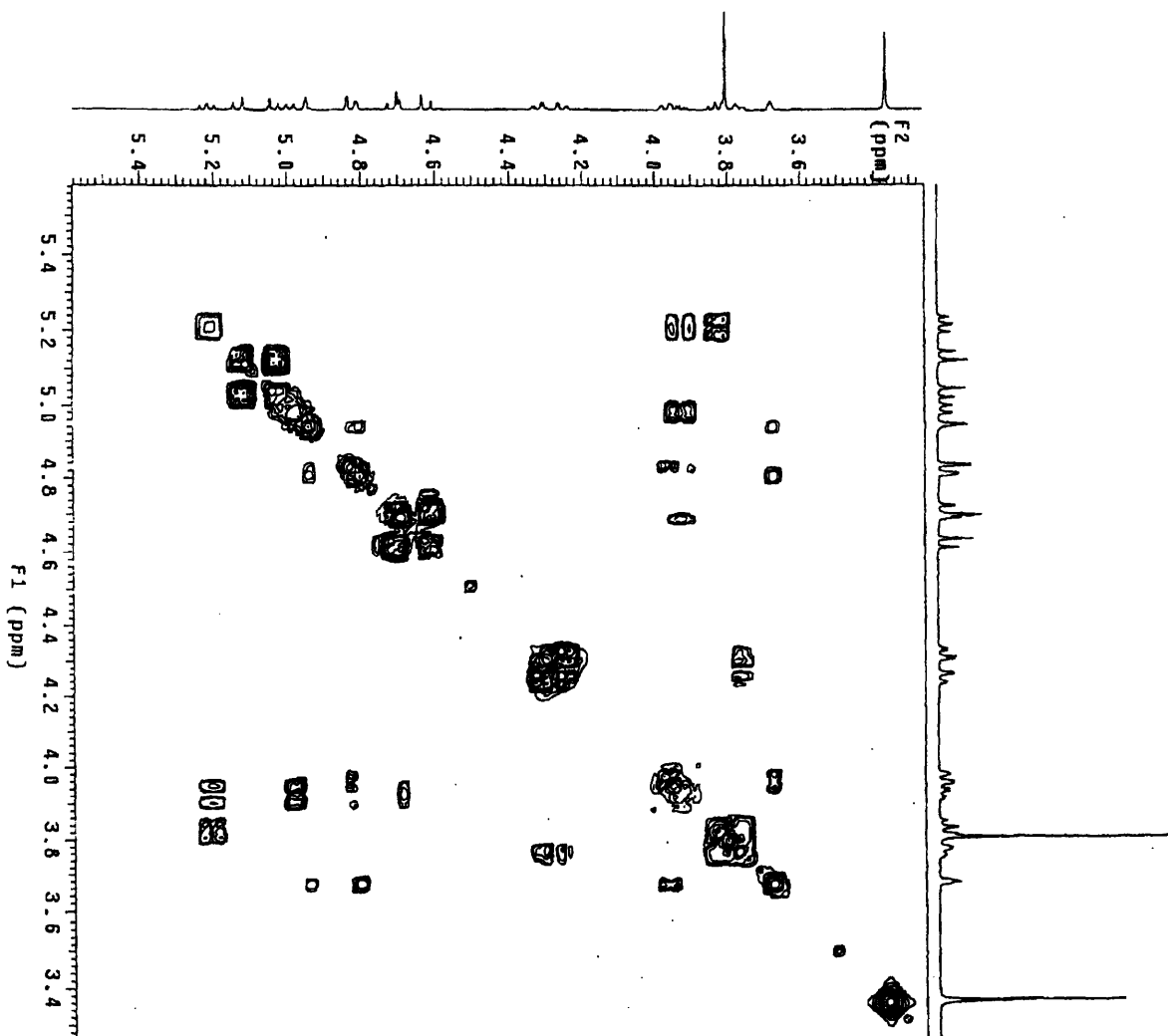
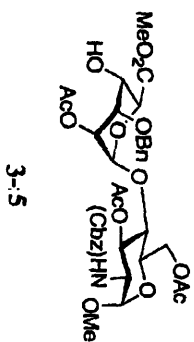


3-5



GL-2-243 gcossy

Pulse Sequence: gcossy
Solvent: CDCl3
TMR: 295.1 K
INSTR: spect
PULSE SEQUENCE: gcossy
Relax. delay: 1.000 sec
Acq. time: 0.215 sec
NUC1: 13C
NUC2: 1H
2 repetitions
256 increments
OBSERVE: H1, 499.753713 MHz
DATA PROCESSING
Sf. sine bell: 0.106 sec
F1 DATA PROCESSING
Sf. sine bell: 0.052 sec
F1 size: 2048 x 2048
Total time: 11 min, 2 sec



GL-2-243 HSQC

Pulse Sequence: HSQC

Solvent: CDCl₃

Temp: 22.0 C / 295.1 K

User: 1-14-87

File: GL-2-243HSQC

INNOVA-500 "zippy"

PULSE SEQUENCE: HSQC

Relax. delay 1.000 sec

Acq. time 0.101 sec

Width 4748.3 Hz

2D Width 28350.5 Hz

4 repetitions

2 x 256 increments

OBSERVE F1, 498.7537713 MHz

DECOUPLE C13, 125.8750988 MHz

Lowpass during acquisition

on during delay

off during delay

CARP-1 modulated

DATA PROCESSING

Sq. sine bell 0.101 sec

Shifted by -0.101 sec

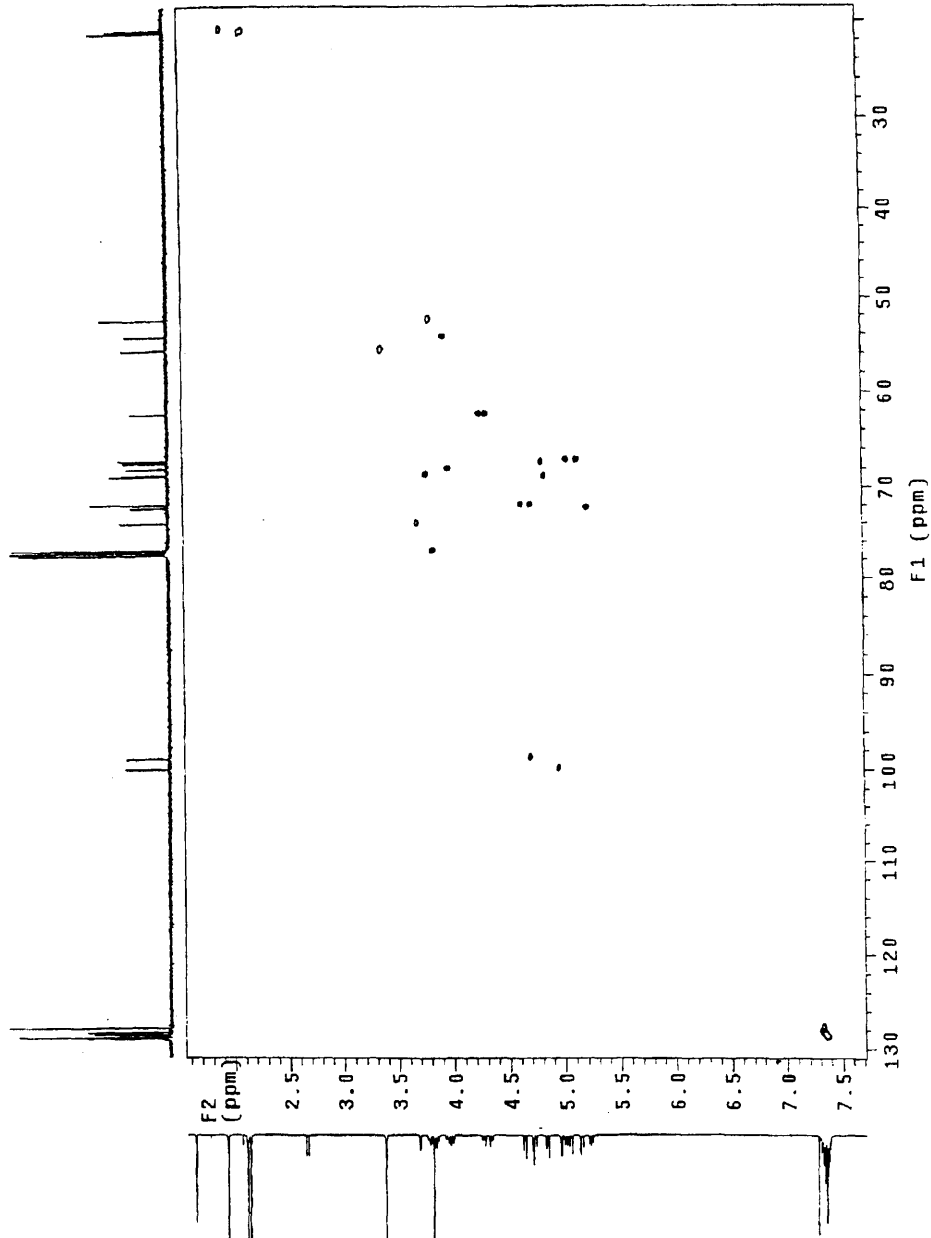
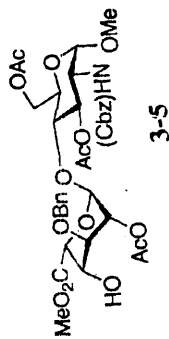
F1 DATA PROCESSING

Sq. sine bell 0.019 sec

Shifted by -0.019 sec

F1 size 2048 x 2048

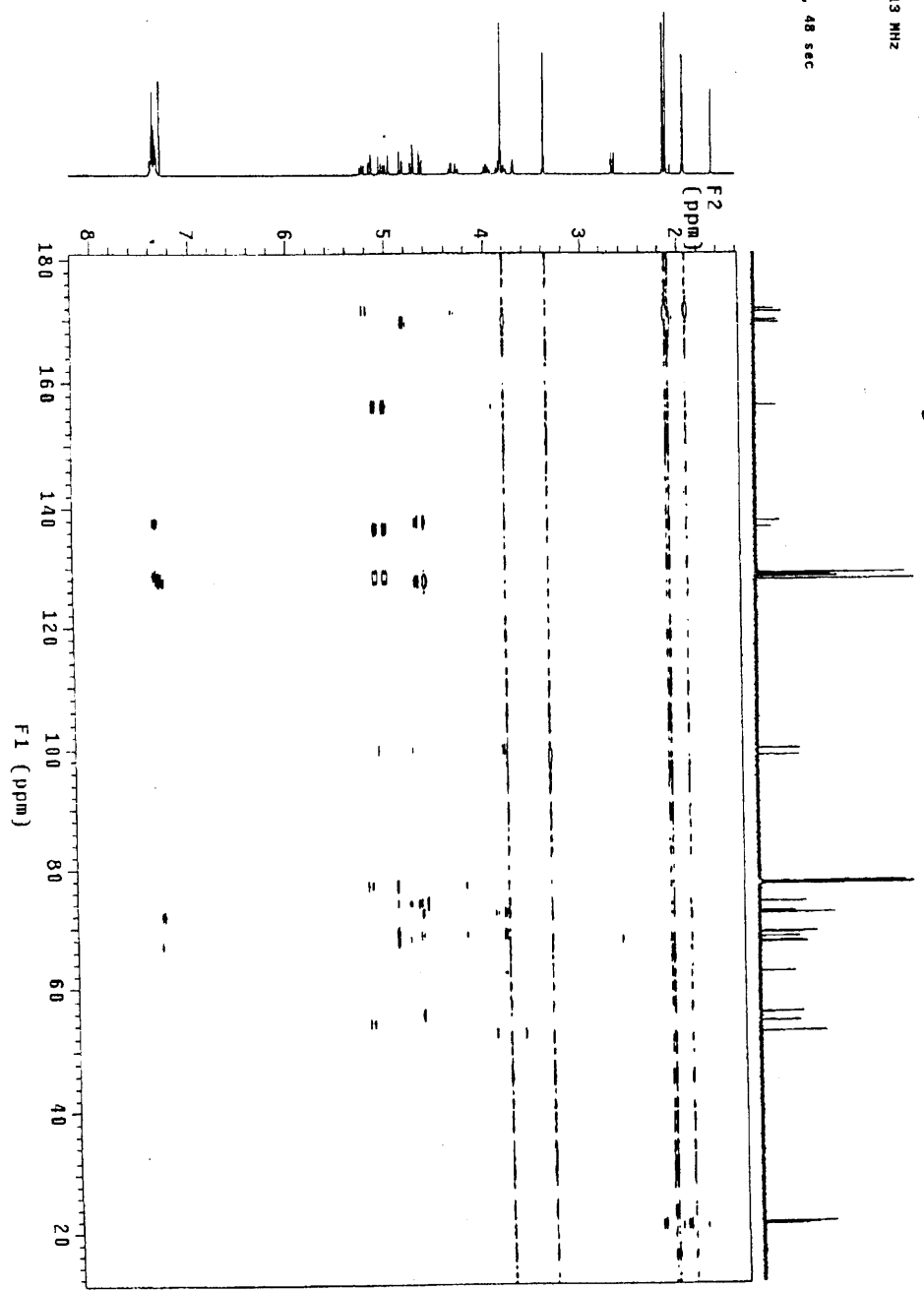
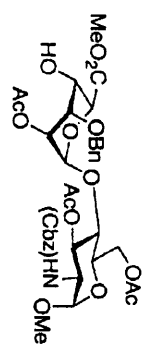
Total time 42 min, 33 sec

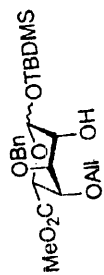


GL-2-243HMBC

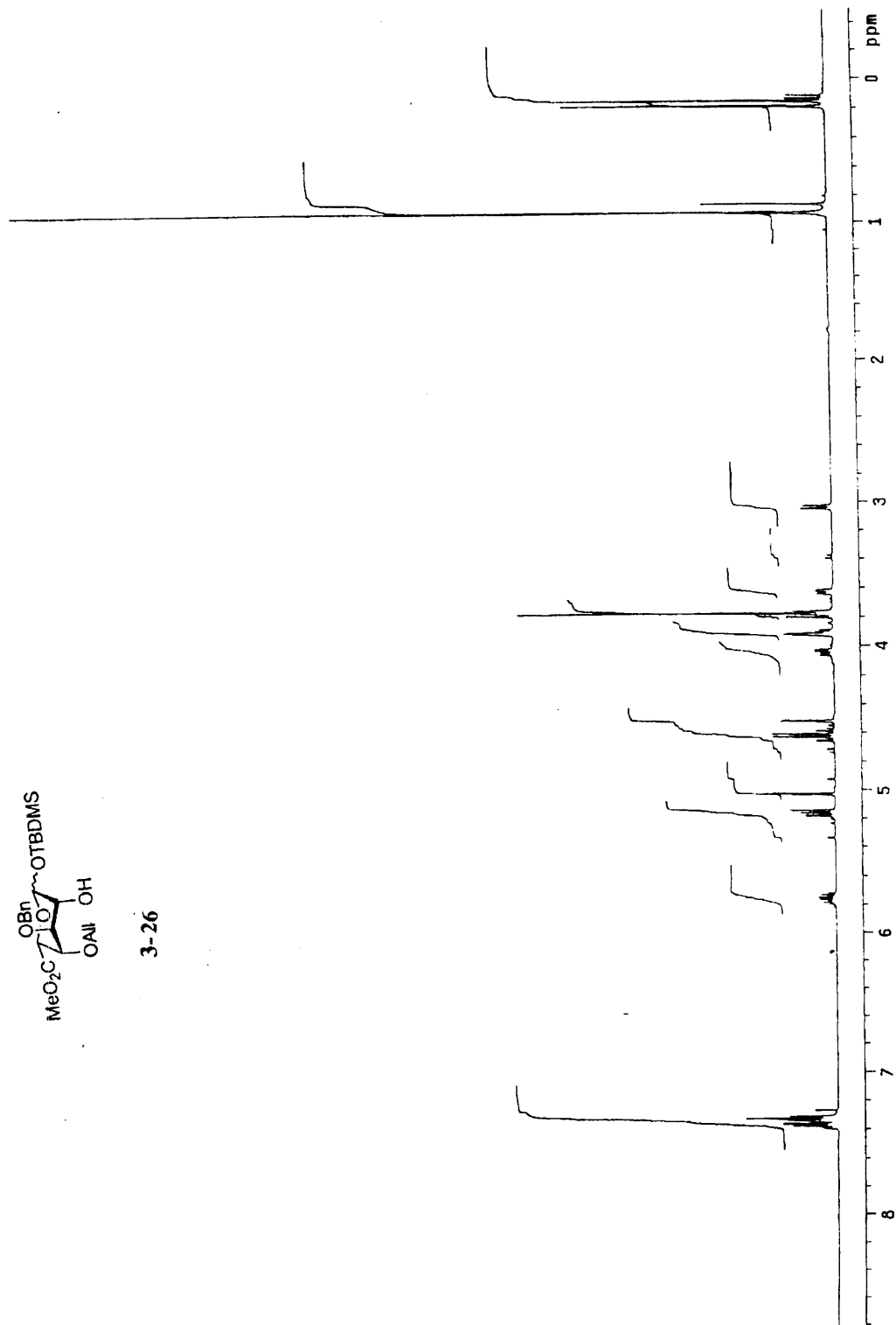
Pulse Sequence: HMBC

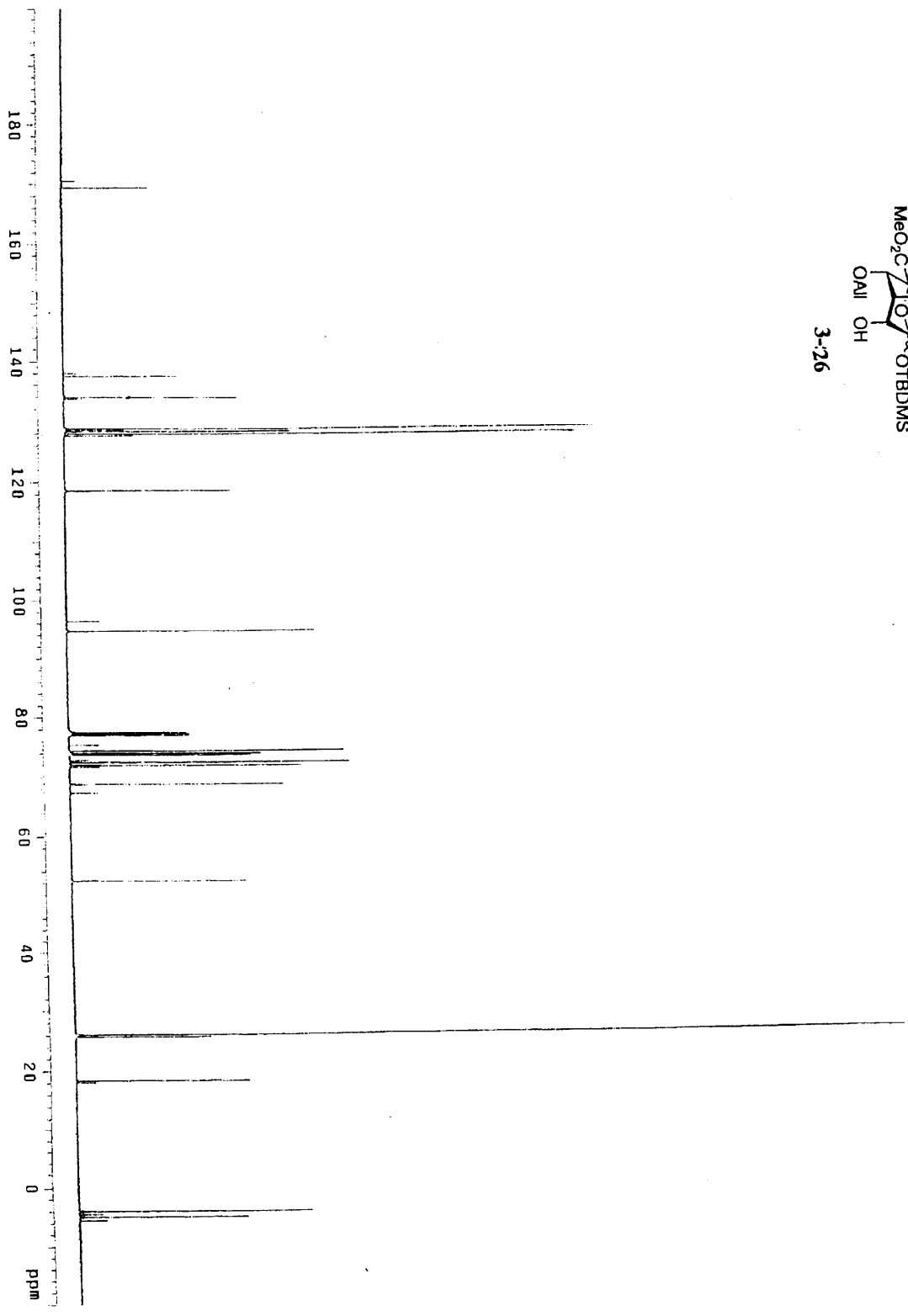
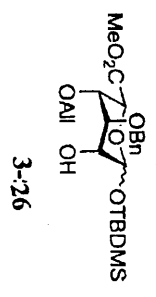
Solvent: CDCl3
Temp: 22.9 C / 295.1 K
User: 1-14-87
File: GL-2-243HMBC
INOVA-500 "zippy"
PULSE SEQUENCE: HMBC
Relax. delay 1.000 sec
Acq. time 0.216 sec
Width 4748.3 Hz
2D Width 25350.5 Hz
Repetitions
X 256 increments
OBSERVED F2 F1
F2 (ppm) 99.7537713 MHz
SIN SINE BEAT
SIN BEAT 0.188 sec
F1 DATA PROCESSING
SINE BEAT 0.004 sec
F1 size 2048 x 2048
Total time 1 hr, 32 min, 48 sec

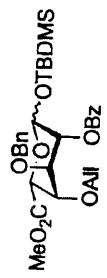




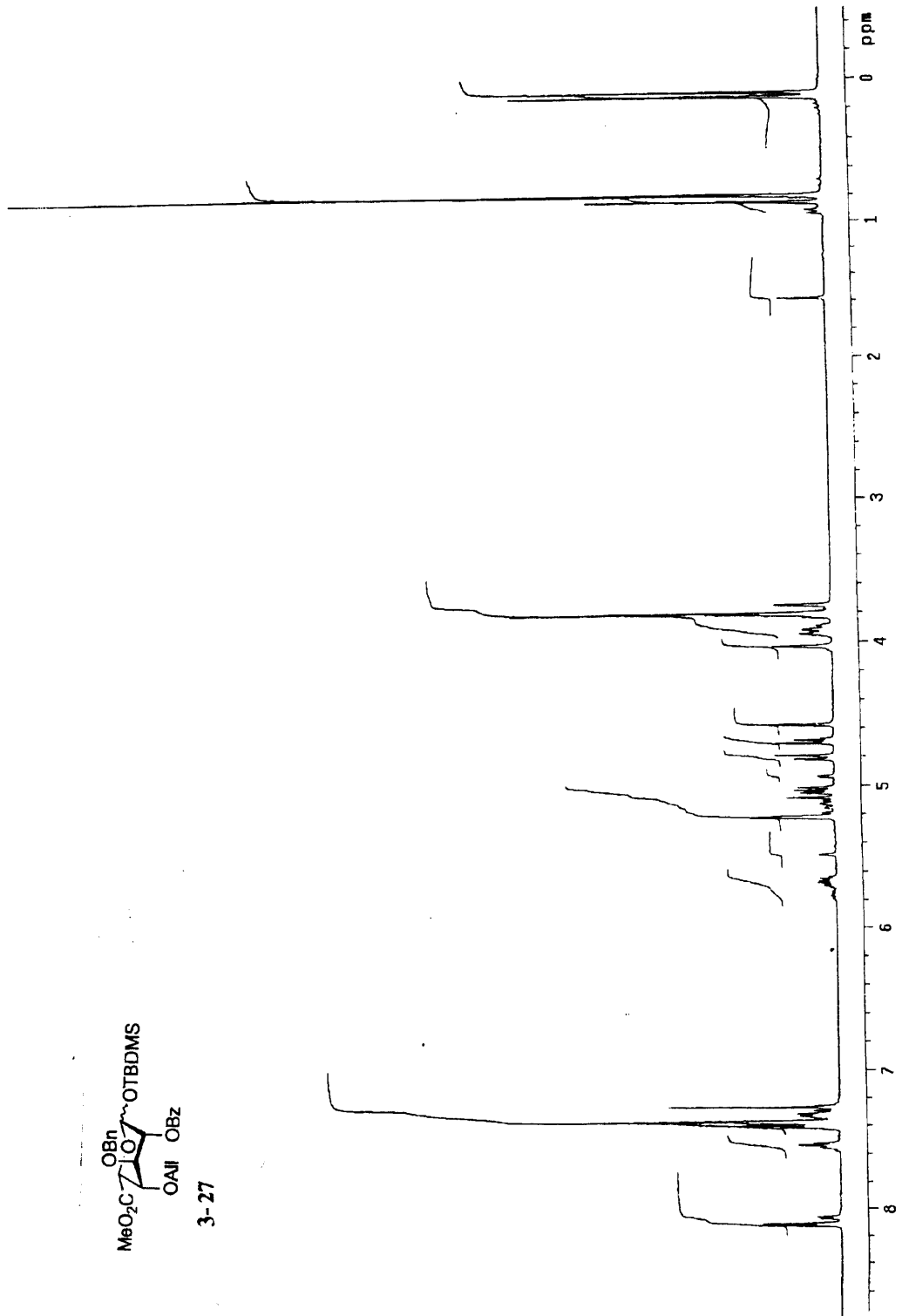
3-26

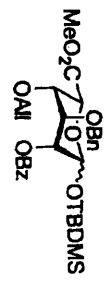




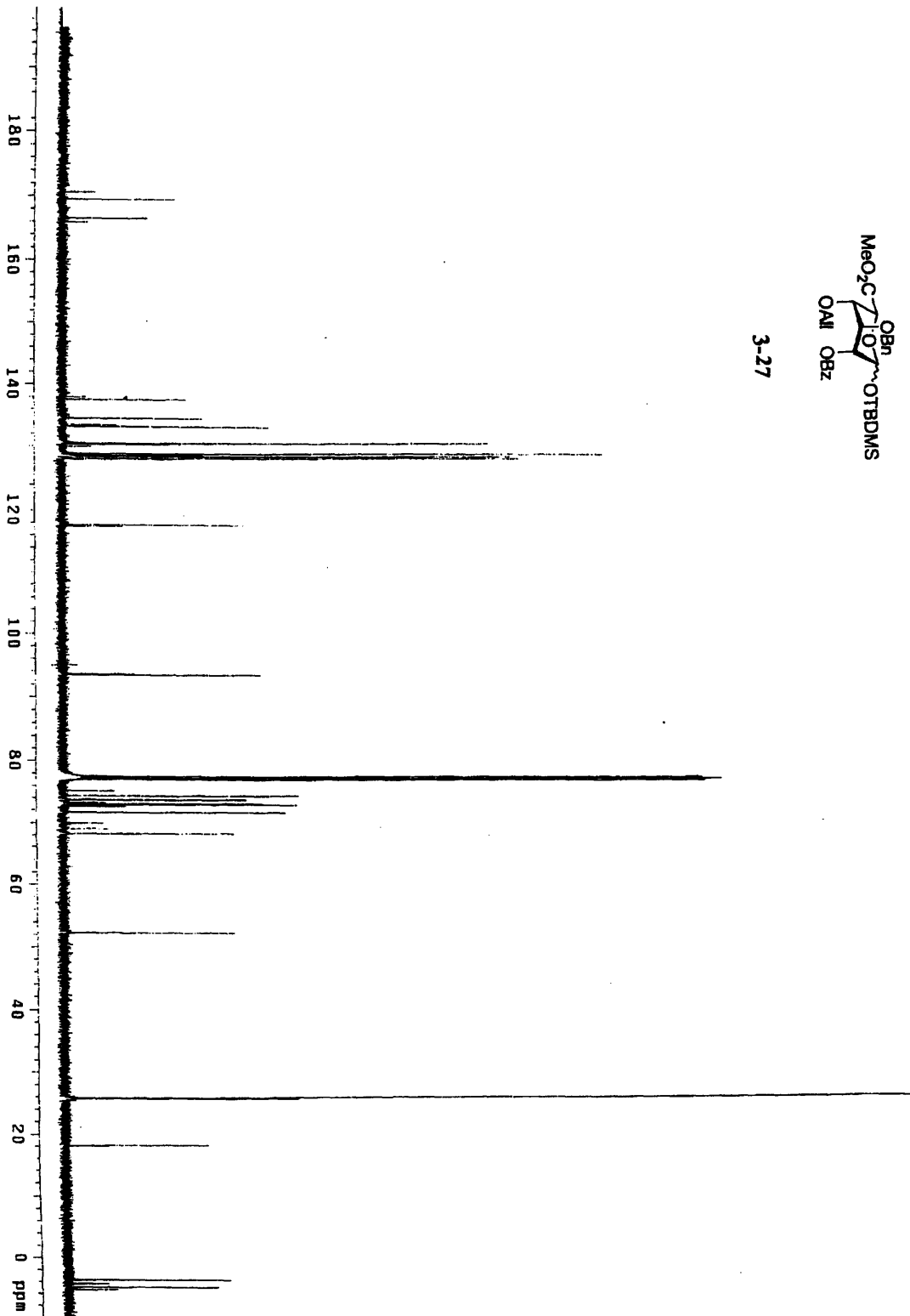


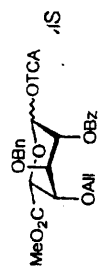
3-27



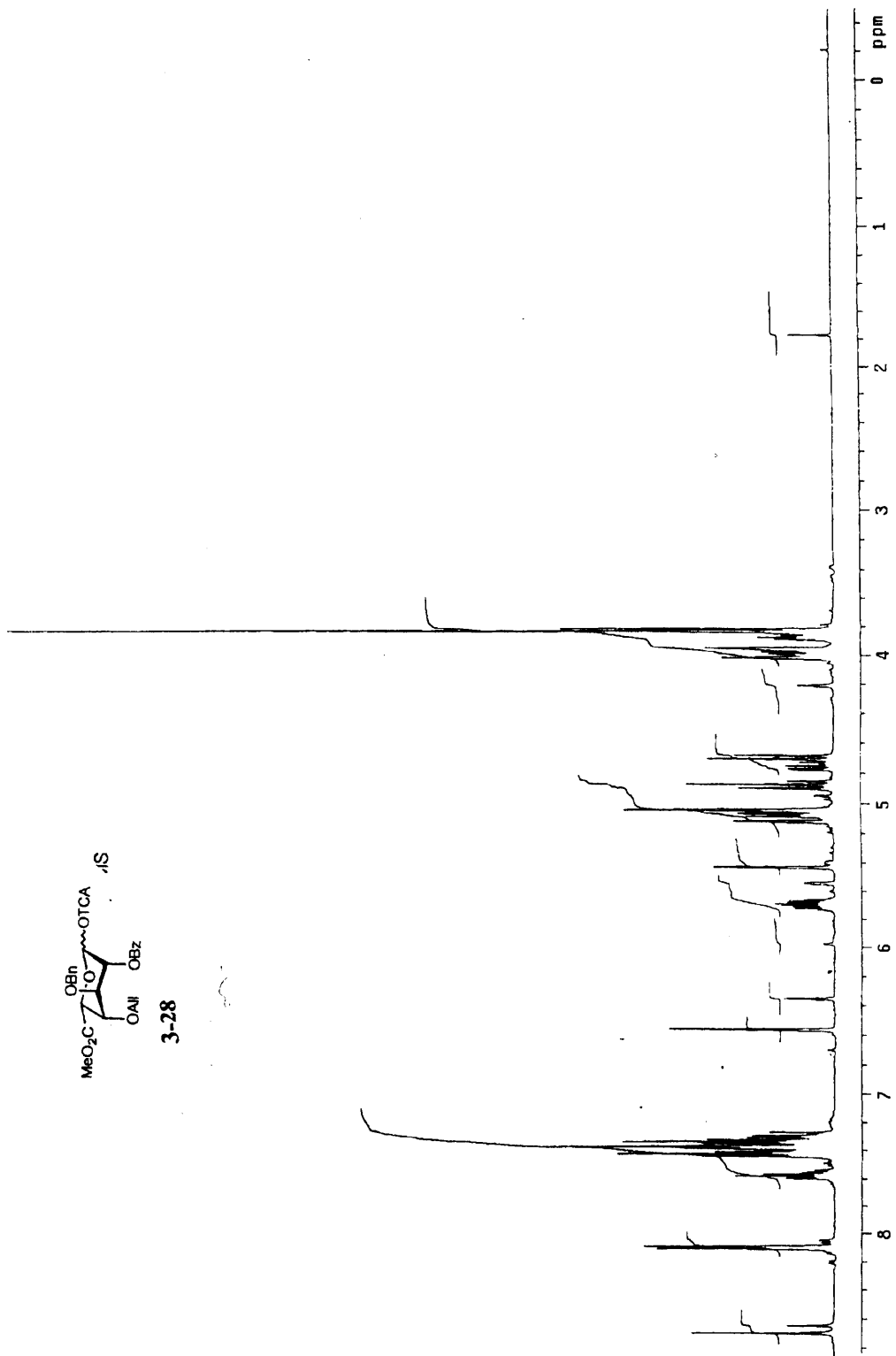


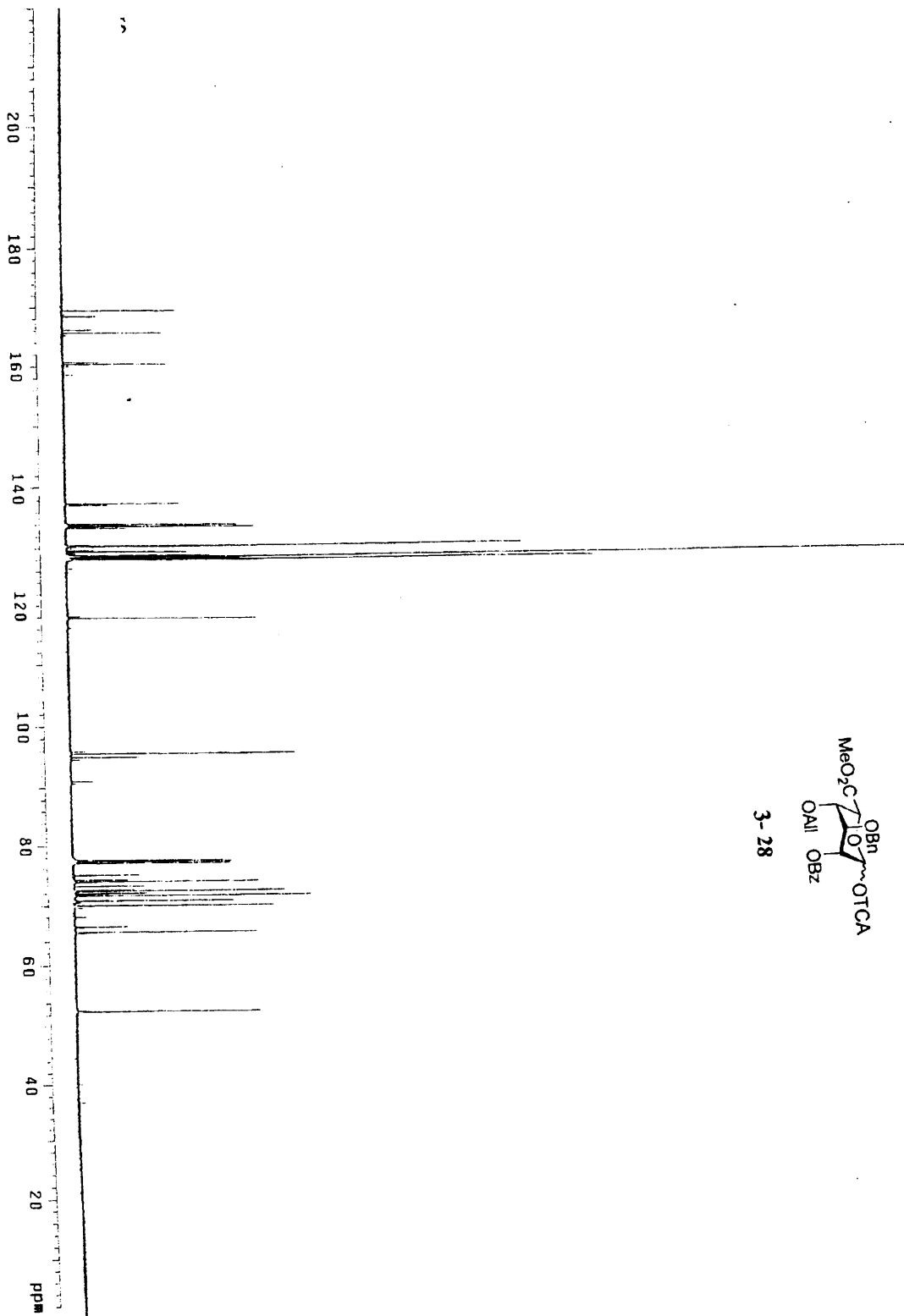
3-27

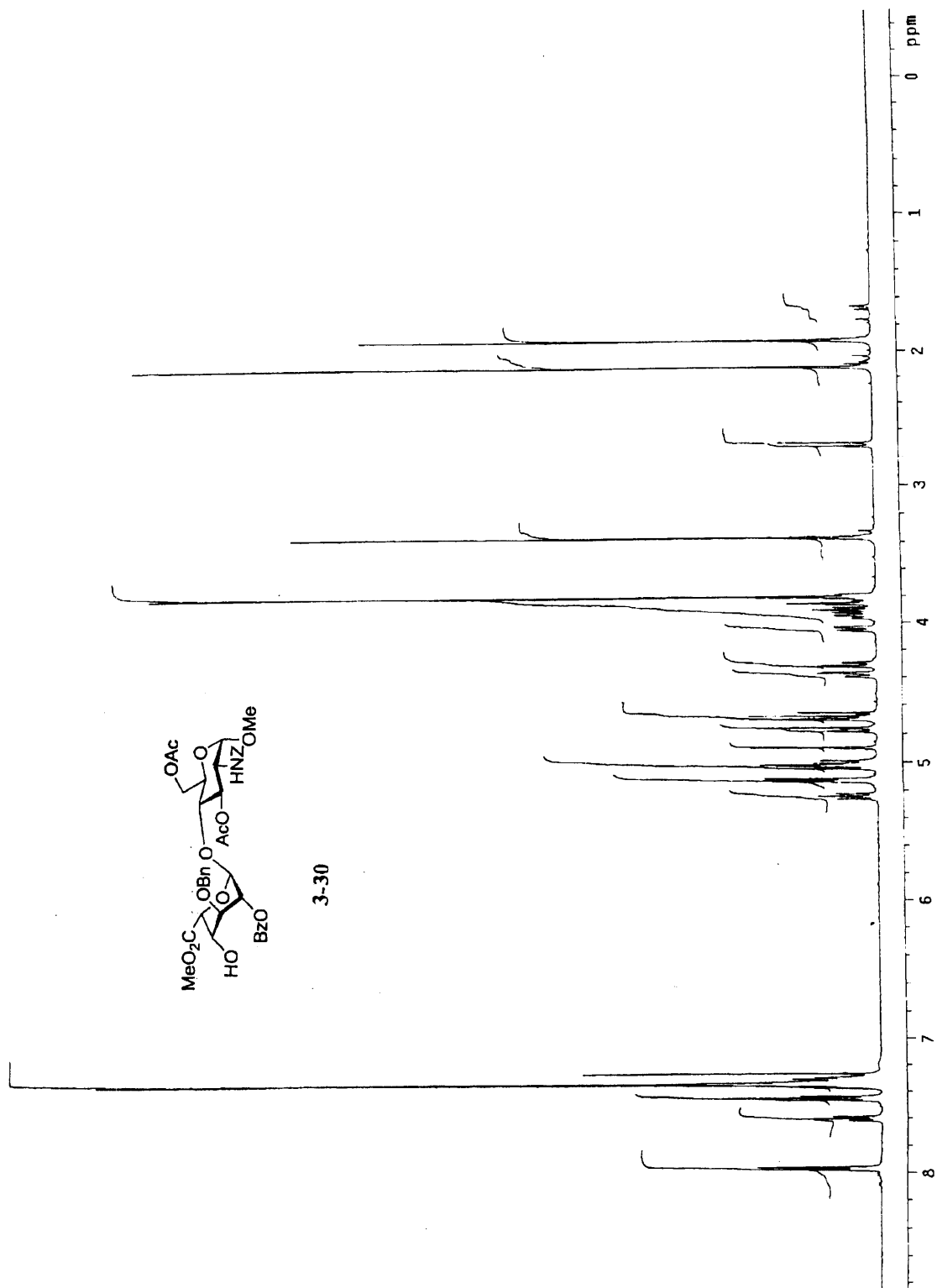


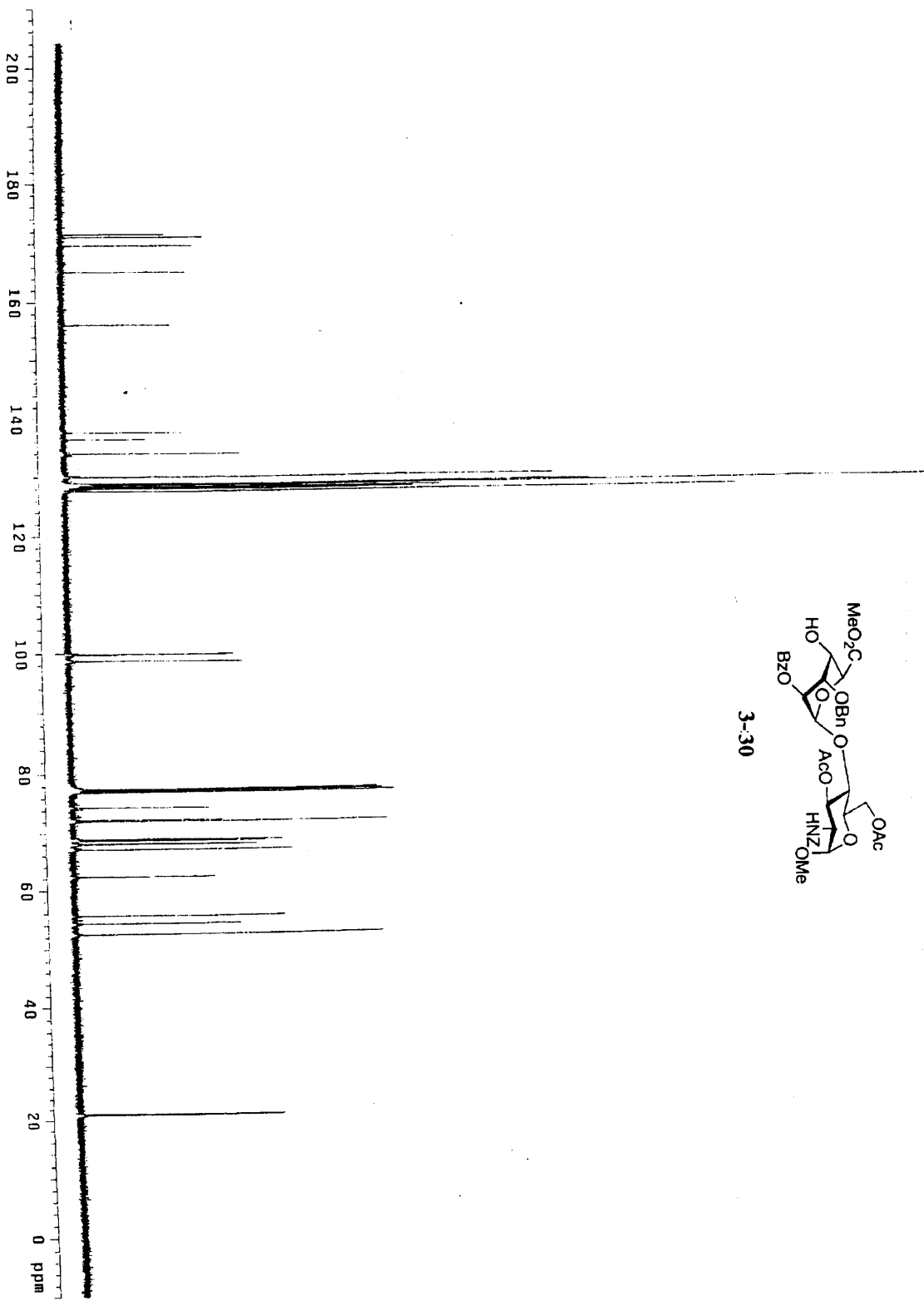


3-28





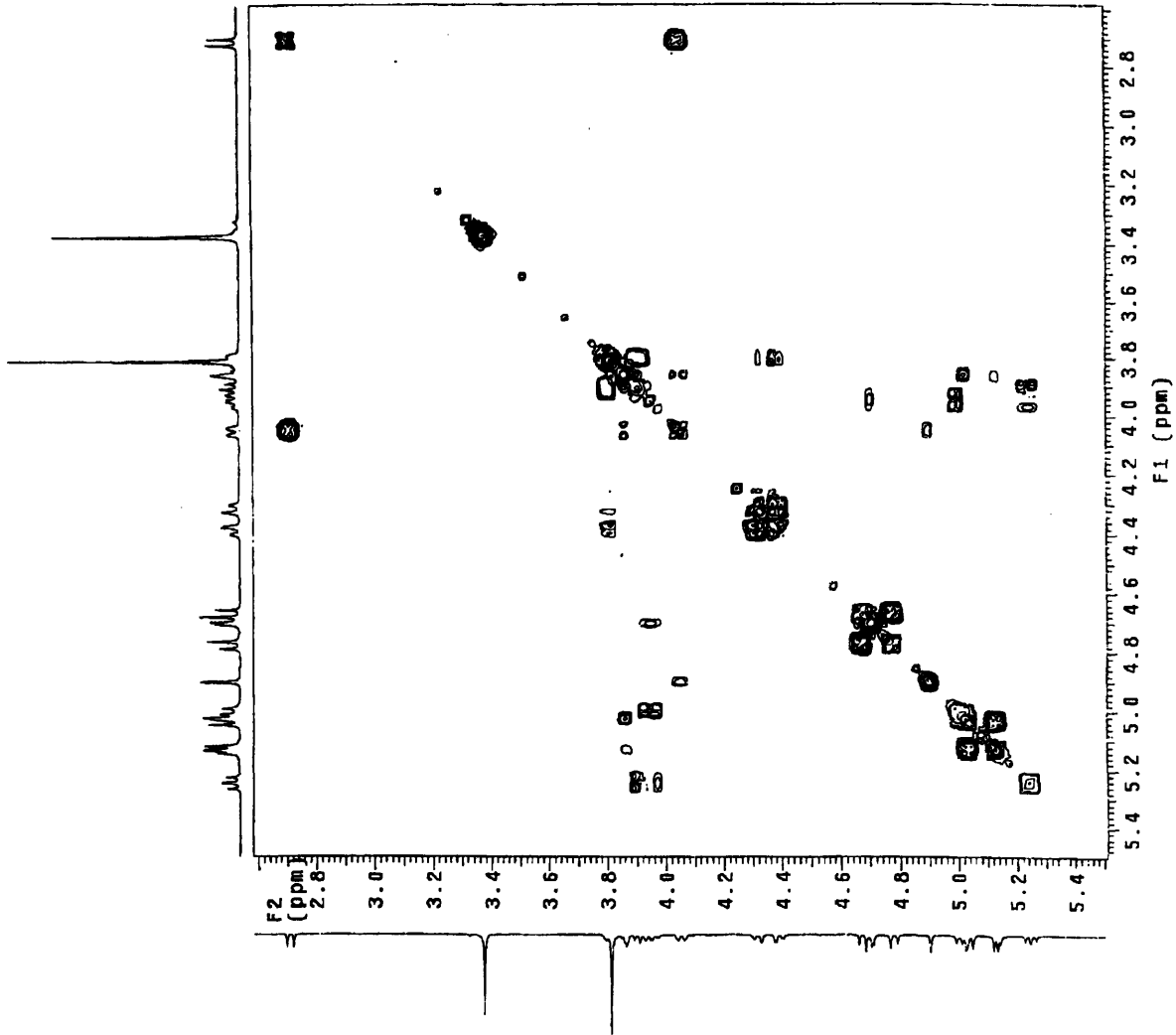




DL-3-245 gcusy
 Pulse Sequence: gcusy
 Solvent: CDC13
 Temp: 22.0 C / 285.1 K
 INOVA-500 "bulwinkle"
 PULSE SEQUENCE: gcusy
 Relax. delay 1.000 sec
 Acq. time 0.216 sec
 Width 4748.9 Hz
 2D Width 4748.9 Hz
 Single scan
 256 increments
 OBSERVE F1 499.7537719 MHz
 DATA PROCESSING
 F1 DATA PROCESSING
 S4. sine bell 0.052 sec
 FT size 2048 x 2048
 Total time 5 min, 41 sec



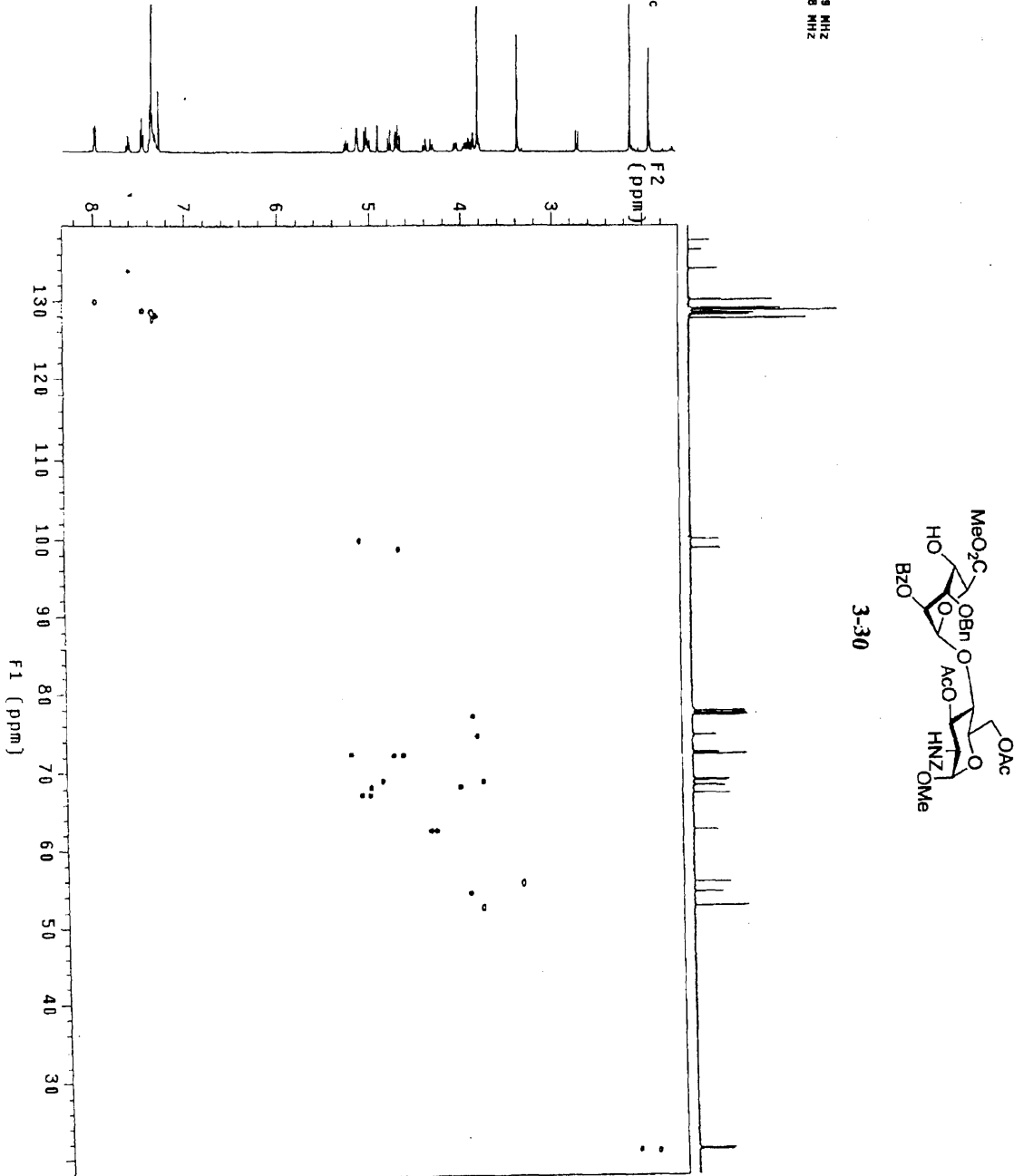
3-30



OL-9-245H

Pulse Sequence: HSQC

Solvent: CDCl3 / 295.1 K
Temp: 22.9 C / 295.1 K
User: J-L-S
File: G-3-21HSQC
INVA-500 "z1ppp"
PULSE SEQUENCE: HSQC
Relax. delay: 1.000 sec
Acq. time: 0.101 sec
Acq. date: 04.13.97
2D Width: 27681.7 Hz
4 repetitions
2 x 256 increments
OBSERVE M1, 499.753719 MHz
DECOUPLE C13, 125.6757288 MHz
Power: 53 dB
on during acquisition
off during delay
GAP-1 modulated
DATA PROCESSING: 0.101 sec
Shifting by: 0.101 sec
F1 DATA PROCESSING:
Sg. sine bell: 0.018 sec
Shifted by: -0.018 sec
FT size: 2048 x 2048
Total time: 42 min, 33 sec



GL-2-245HSQC

Pulse Sequence: HSQC

Solvent: CDCl3

Temp: 22.0 C / 285.1 K

User: 1-14-87

File: GL-3-245HSQC

INNOVA-500 "zippy"

PULSE SEQUENCE: HSQC

Relax. delay 1.000 sec

Acq. time 0.101 sec

Width 4748.3 Hz

2D Width 27851.7 Hz

4 repetitions

2 x 256 increments

OBSERVE F1, 488.7597718 MHz

DECOUPLE C13, 125.6757288 MHz

Power is on during

acq. during

ORF during

GASP-1 modulated

DATA PROCESSING

Sq. sine bell 0.101 sec

Shifted by -0.101 sec

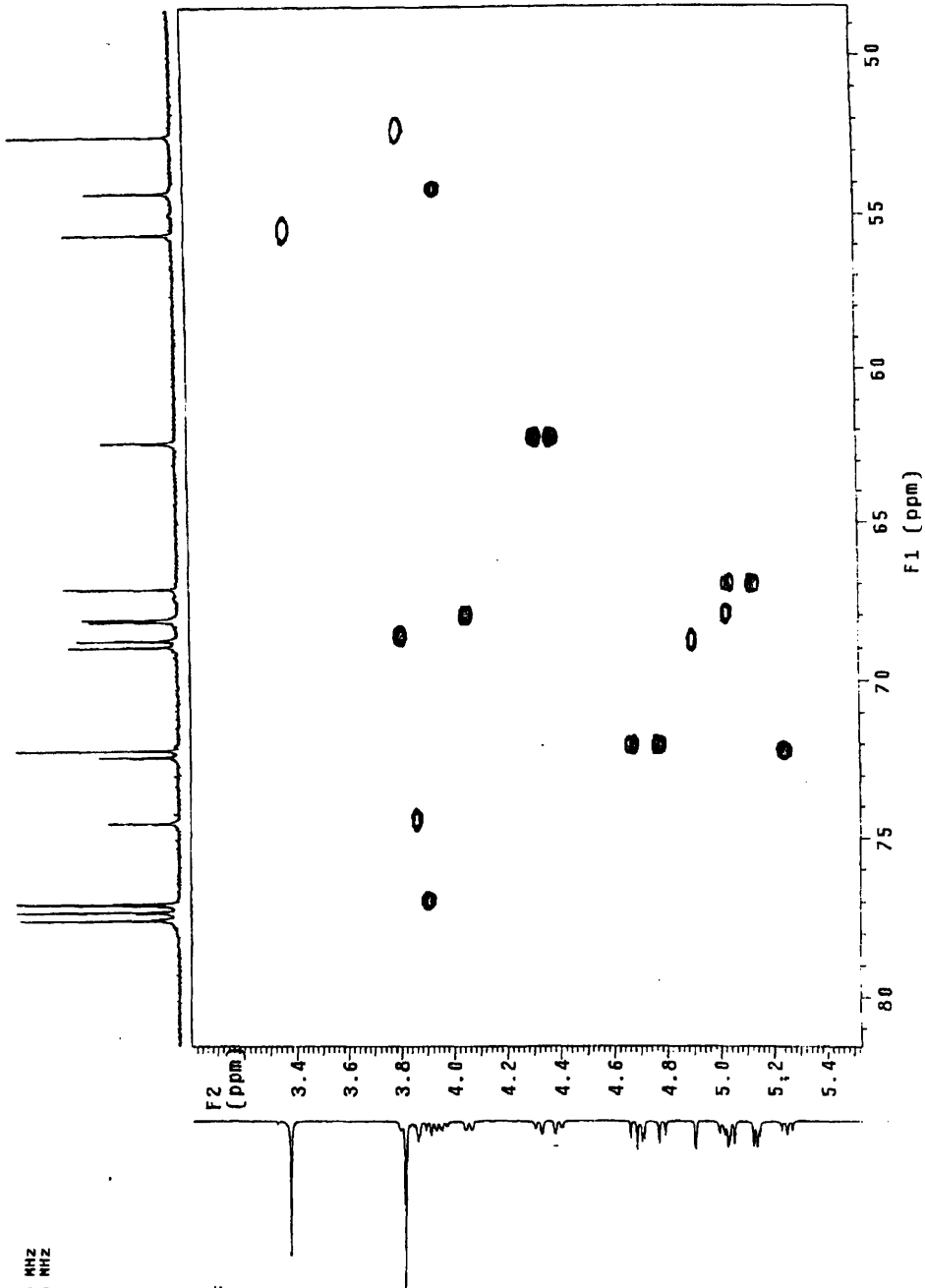
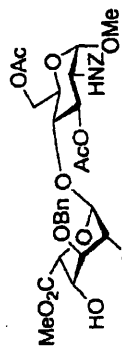
F1 DATA PROCESSING

Sq. sine bell 0.018 sec

Shifted by -0.018 sec

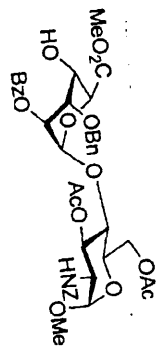
FT size 2048 x 2048

Total time 42 min, 33 sec

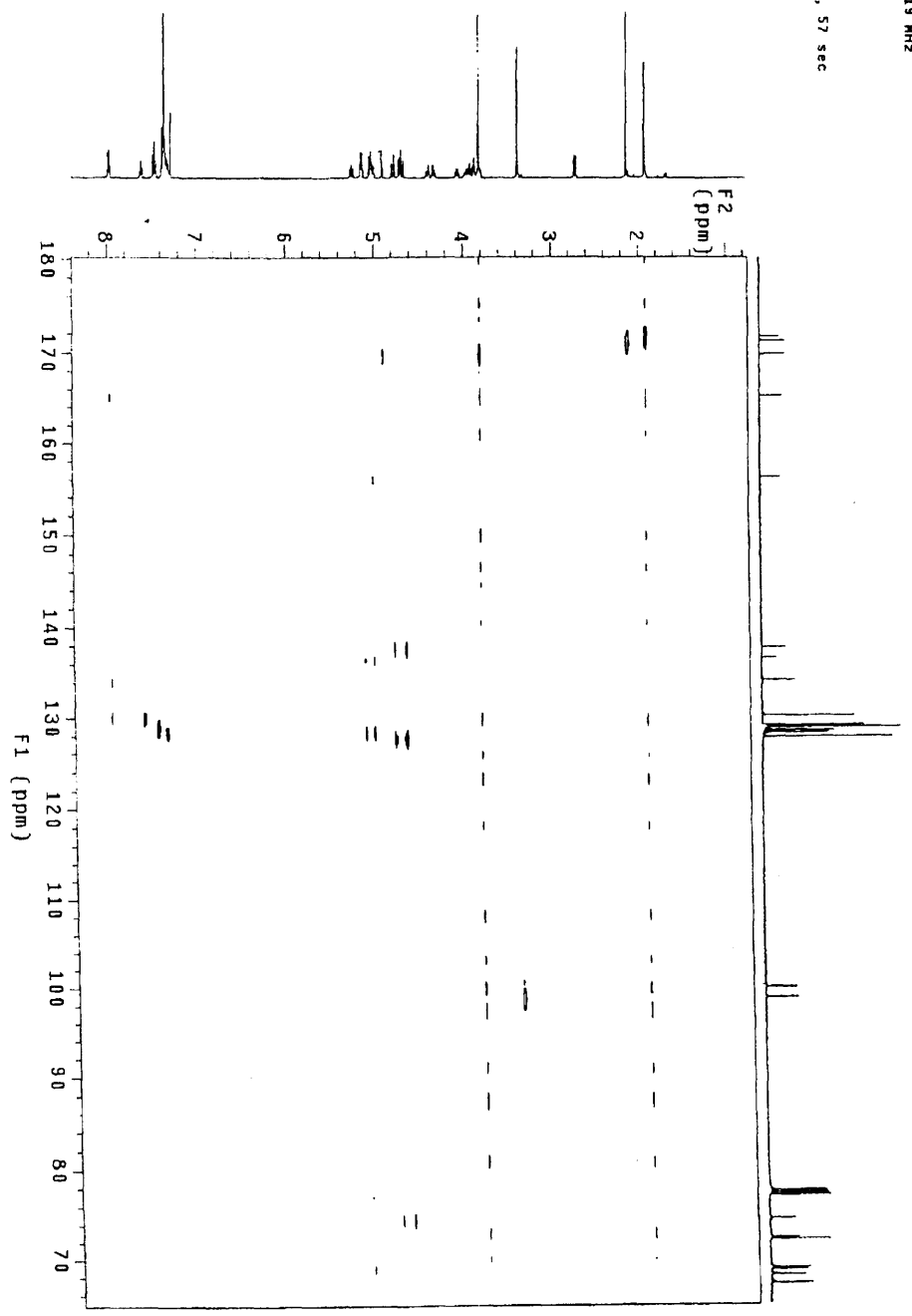


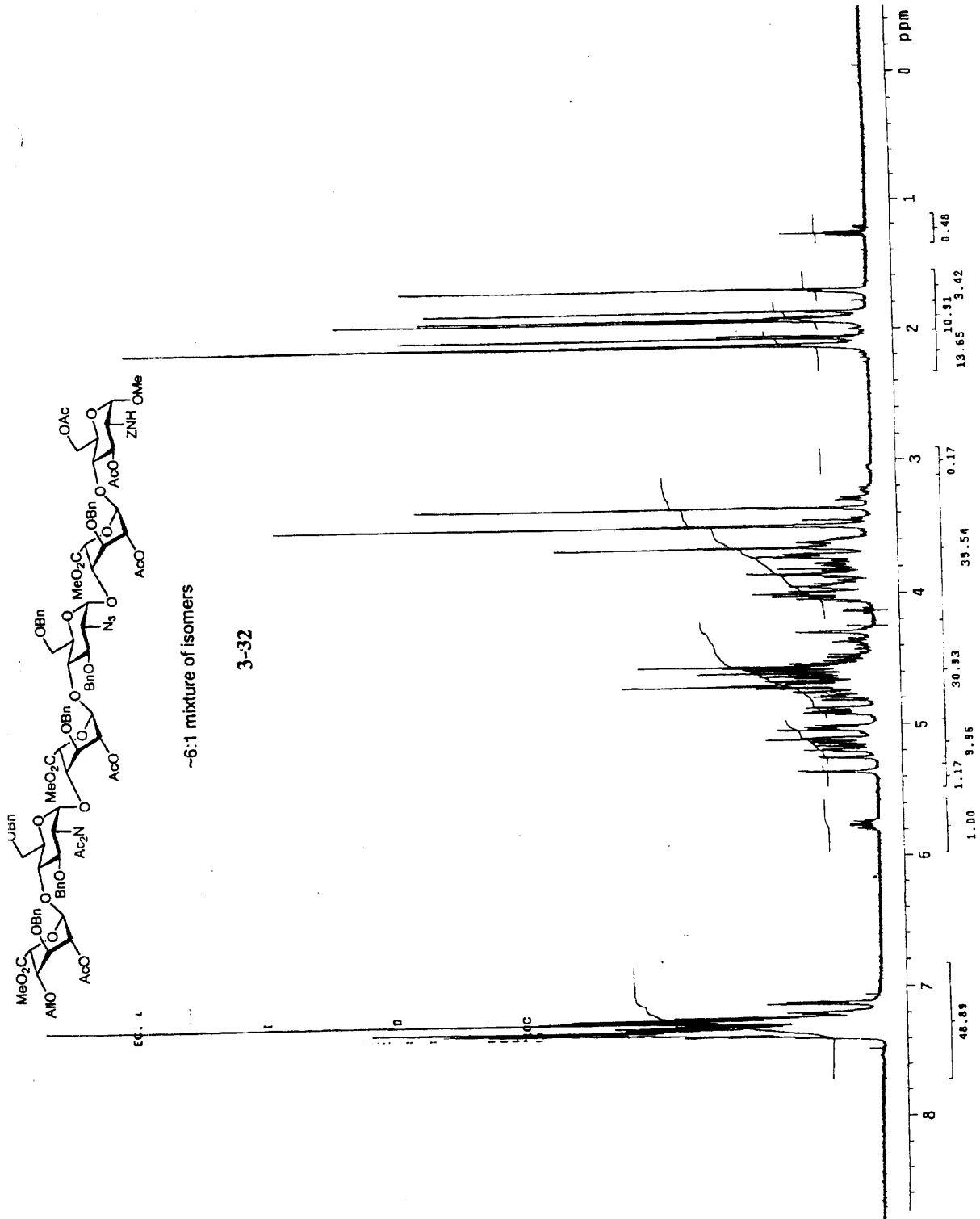
GL-9-245H

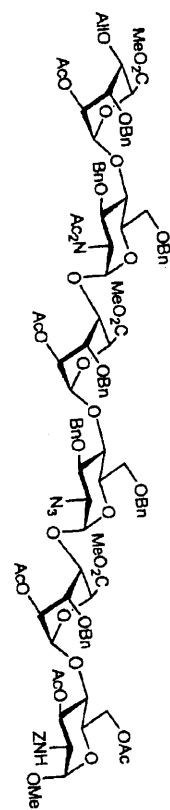
Pulse Sequence: HMQC
Solvent: CDCl3
Temp: 22.0 C / 295.1 K
User: 1-14-87
File: GL-9-245HMQC
INOVA-500 "z1ppy"
PULSE_SEQUENCE: HMQC
Relax_delay: 1.000 sec
Acq_time: 0.216 sec
Width: 4746.9 Hz
2D_Width: 27681.7 Hz
8 repetitions
2 x 256 increments
OBSERVE_HI: 499.753719 MHz
DATA_PROCESSING
Sine Bell: 0.108 sec
F1 Dir: PROCSSING
Sine Bell: 0.108 sec
FT size: 2048 x 2048
Total time: 1 hr, 29 min, 57 sec



3-30

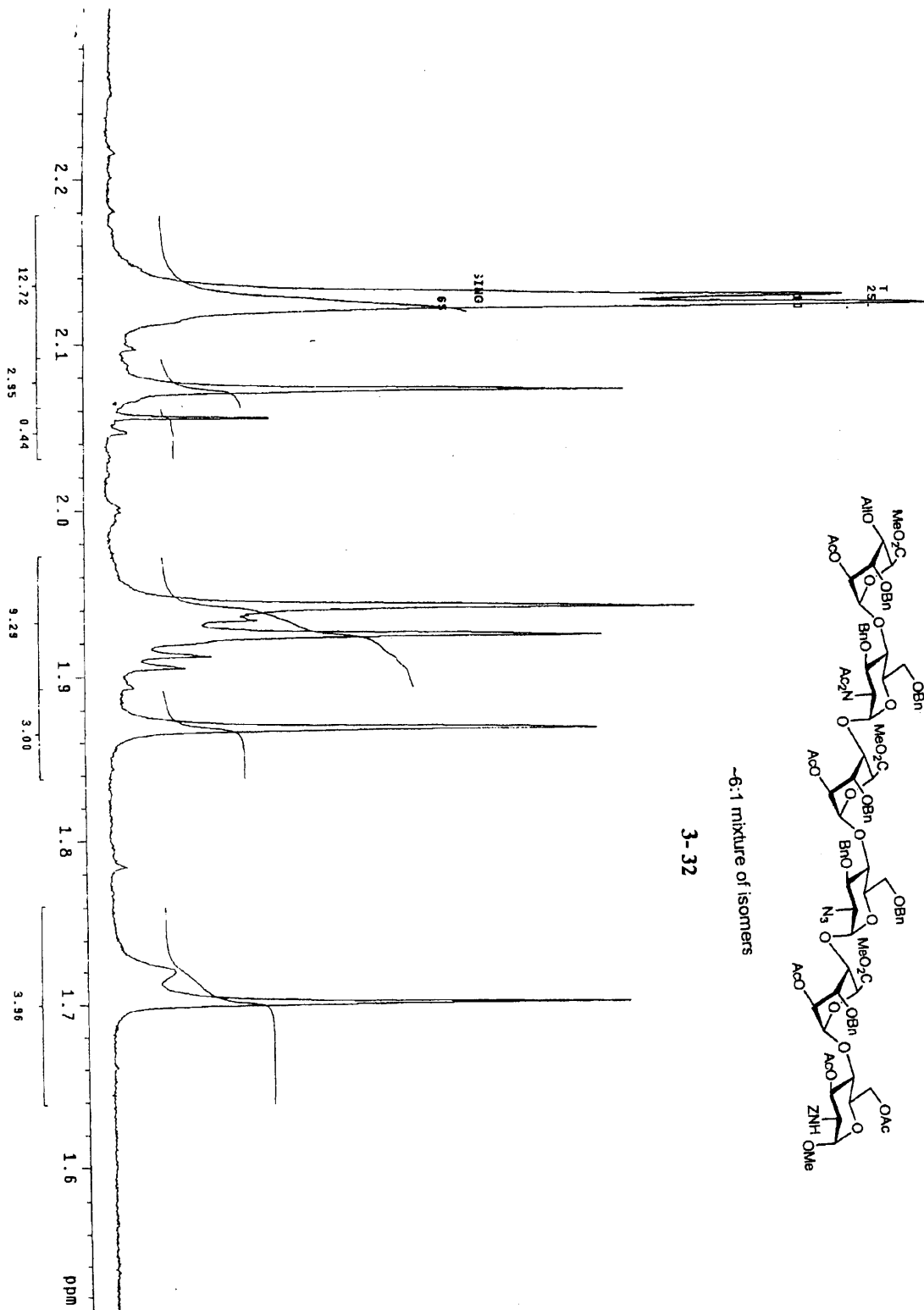


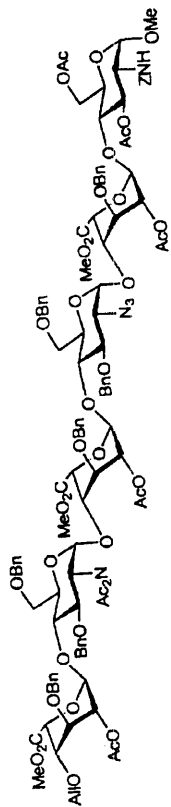




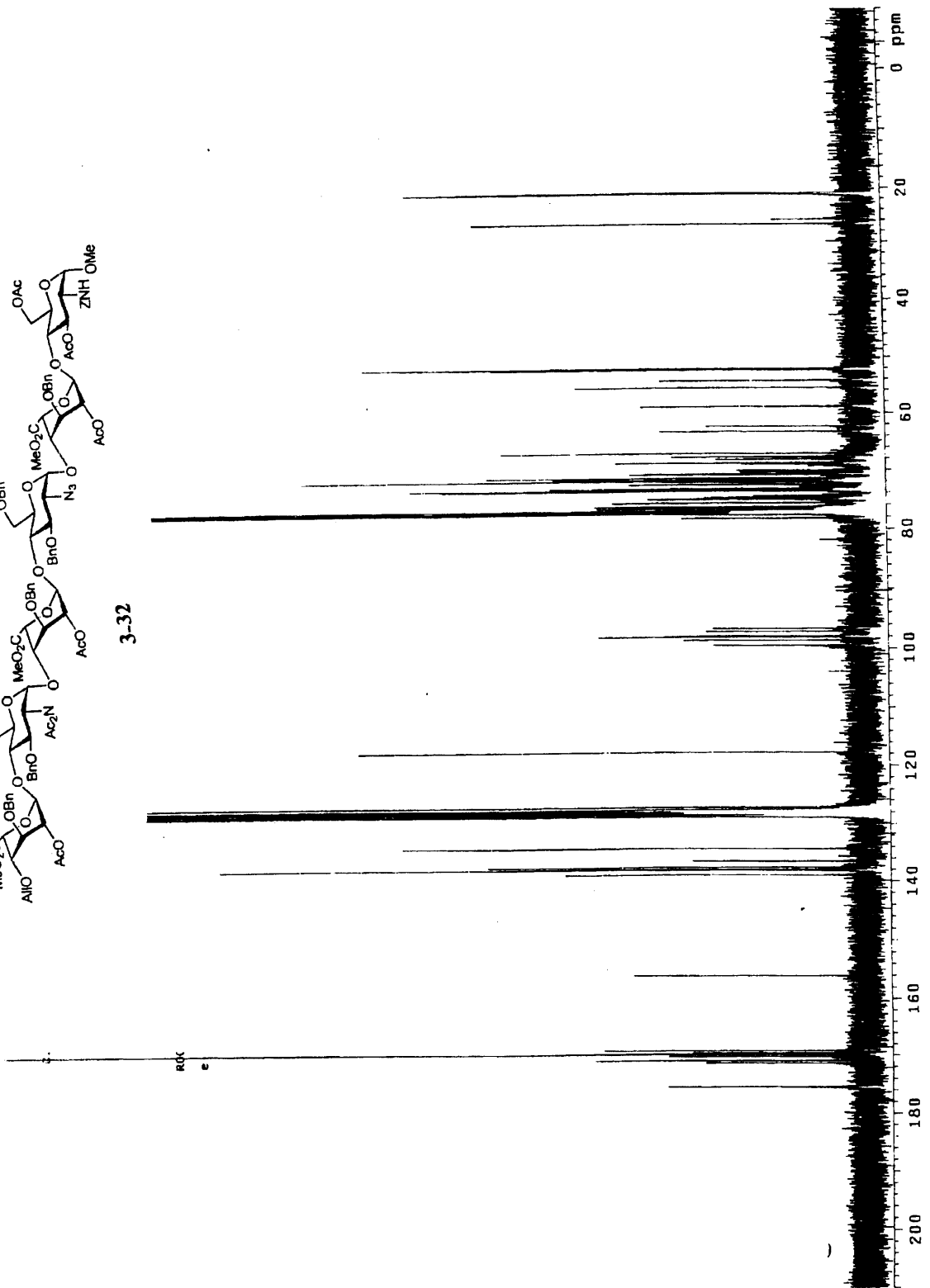
-6:1 mixture of isomers

3-32

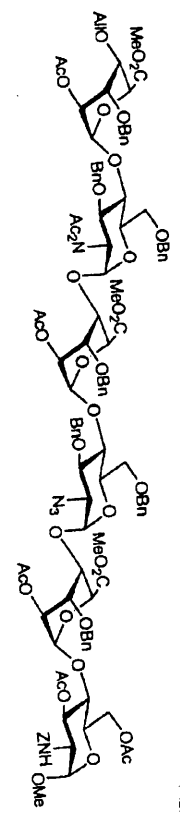




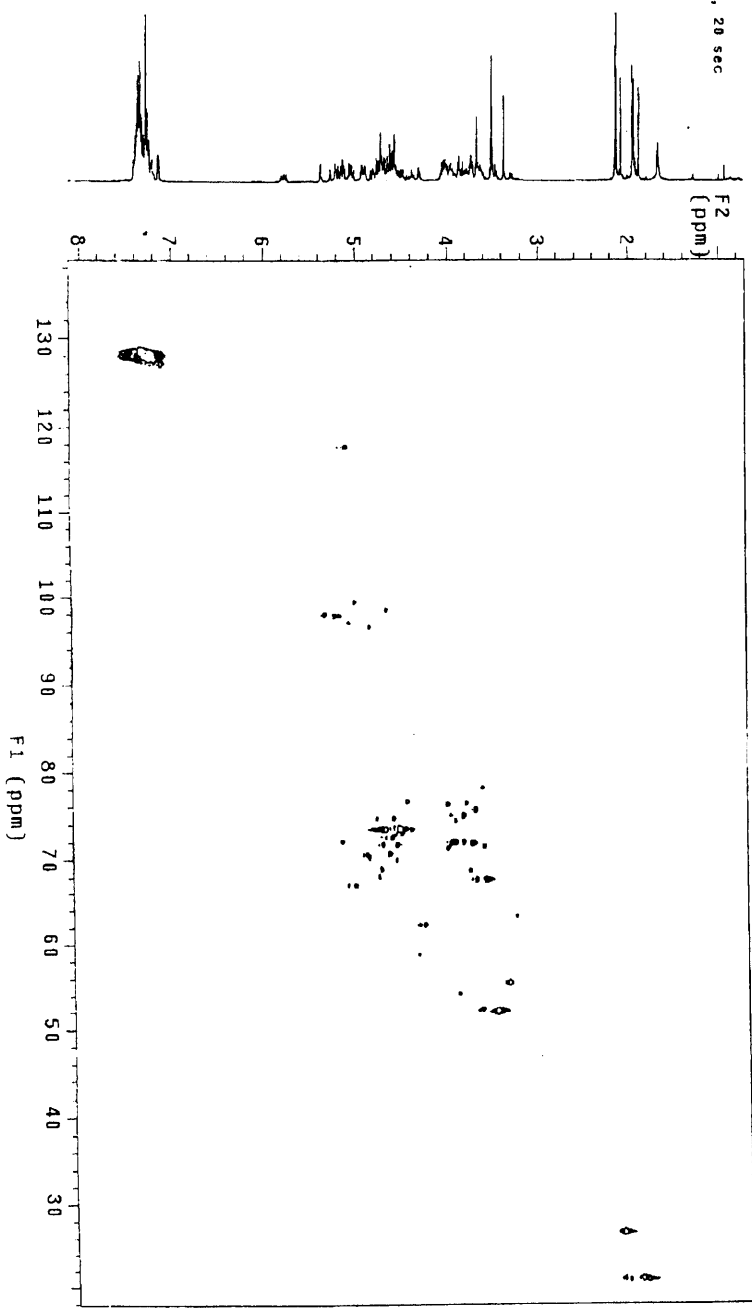
3-32



GL-3-123, hexa
 Pulse Sequence: HSQC
 Solvent: CDCl3
 Temp: 22.0 C / 295.1 K
 User: 1-14-87
 File: GL-3-123HSQC
 INOVA-500 *21ppm*
 PULSE SEQUENCE: HSQC
 Relax. delay 1.000 sec
 Acq. time 0.101 sec
 Width 4748.3 Hz
 2D Width 27681.7 Hz
 8 repetitions
 2 K 256 increments
 DESIRVE H1, 499.75972716 MHz
 DESIRVE C13, 125.6797277 MHz
 Power 5.9
 on during acquisition
 off during delay
 GARP-1 modulated
 DATA PROCESSING
 Sg. sine bell 0.101 sec
 Shifted by -0.101 sec
 F1 DATA PROCESSING
 Sg. sine bell 0.018 sec
 Shifted by -0.018 sec
 FT Size 64K x 2095
 Total time 1 hr, 21 min, 20 sec



3-32

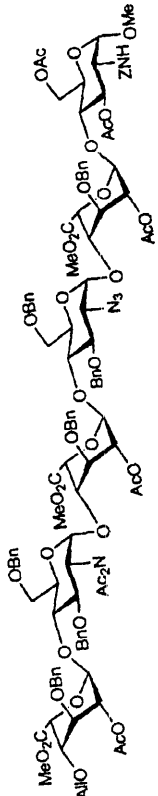


GI-3-123, hexa
 Pulse Sequence: HSQC
 Solvent: CDCl3
 Temp: 121.57 / 295.1 K
 Width: 12.67
 File: GI-3-123HSQC
 INOVA-500 "zipp"

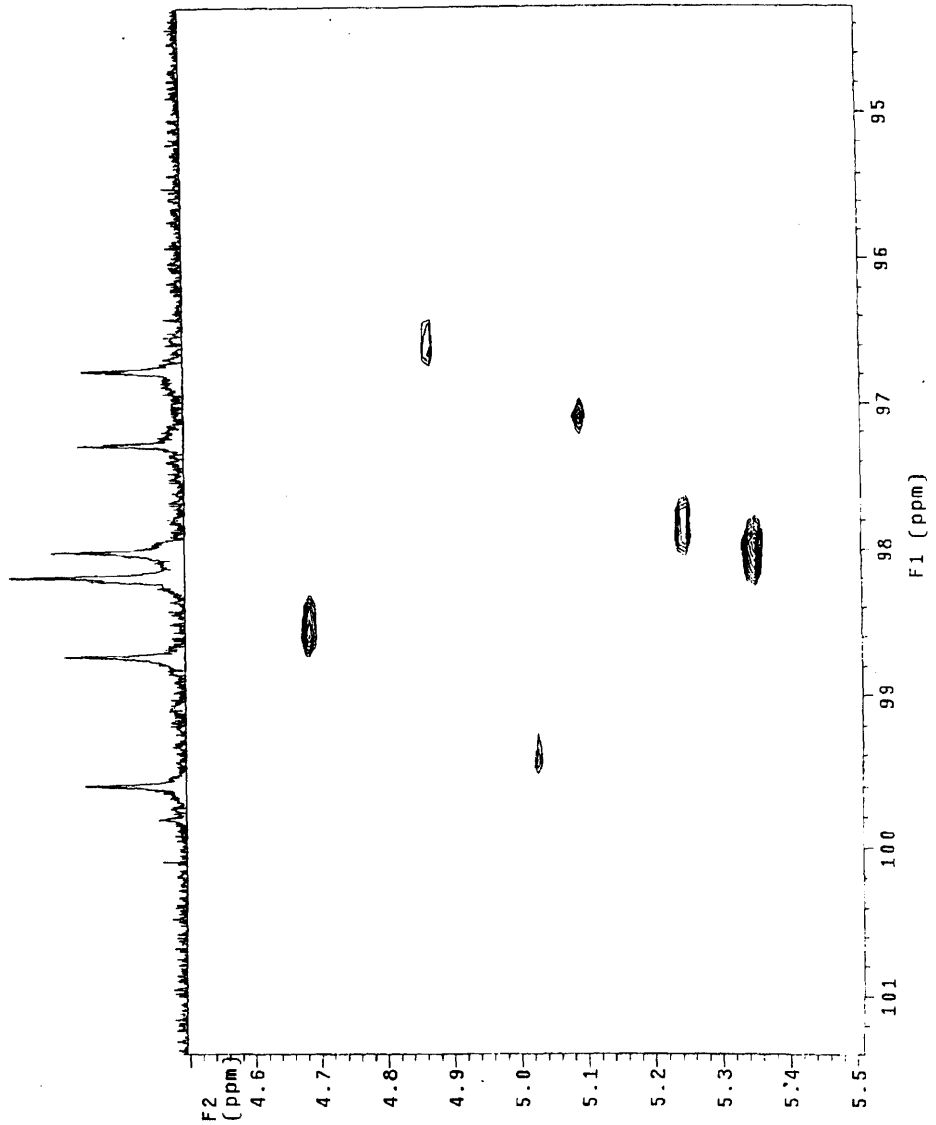
PULSC SEQUENCE: HSQC
 Relax: delay 1.000 sec
 Pre: time 1.000 sec
 Width: 12.67 Hz
 2D Width 27681.7 Hz
 8 repetitions
 2 x 256 increments

OBSERVE H1, 499.753716 MHz
 DECOUPLE C13, 125.675277 MHz
 Power 53 dB
 on during acquisition
 off during delay

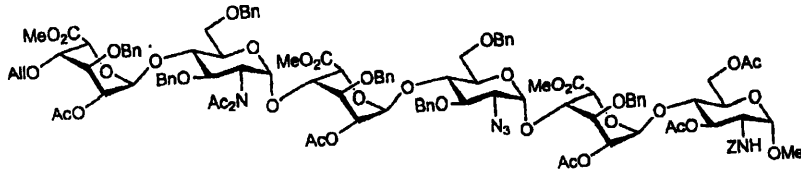
GARP-I modulated
 DATA PROCESSING
 Sg: time bel 0.101 sec
 S: Shifted bel -0.101 sec
 F1 DATA PROCESSING
 Sg: sine bel 0.018 sec
 Shifted by -0.018 sec
 FT size 2048 x 2048
 Total time 1 hr, 21 min, 20 sec



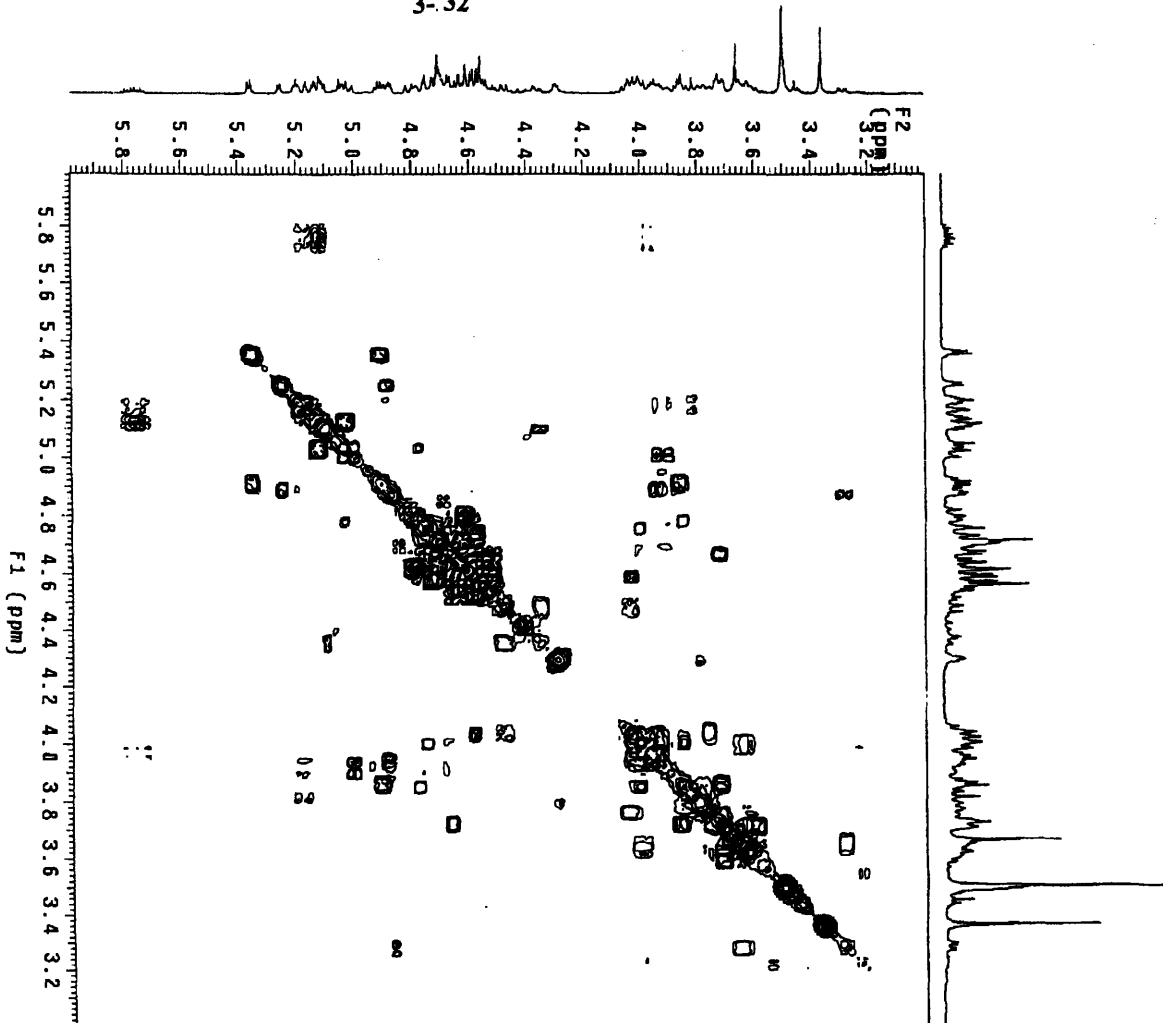
3-32

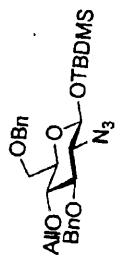


OL-9-129, hexa
 Pulse Sequence: gcosy
 Solvent: CDCl3
 Temp.: 22.0 C / 295.1 K
 INOVA-500 "butylvinyle"
 PULSE SEQUENCE: gcosy
 Relax. delay: 1.000 sec
 Acq. time: 0.218 sec
 Width: 4748.3 Hz
 2D Width: 4748.3 Hz
 2. Repetitions
 ASSEMBLY PARAMETERS
 DATA PROCESSING
 Sg. sine bell: 0.108 sec
 F1 DATA PROCESSING
 Sg. sine bell: 0.052 sec
 FT size: 2048 x 2048
 Total time: 11 min., 2 sec

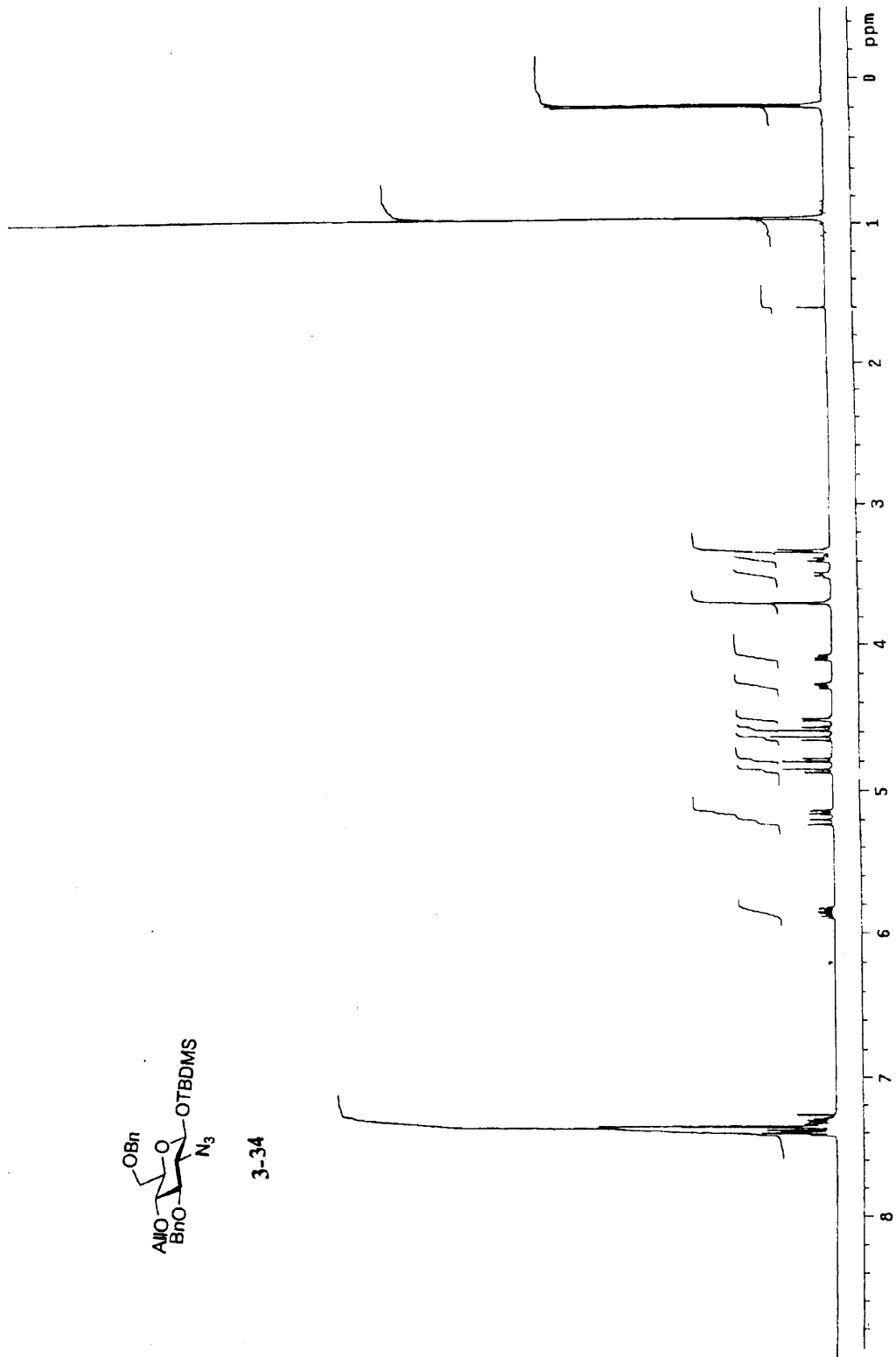


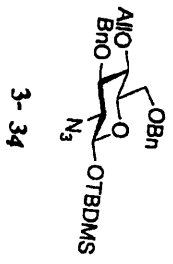
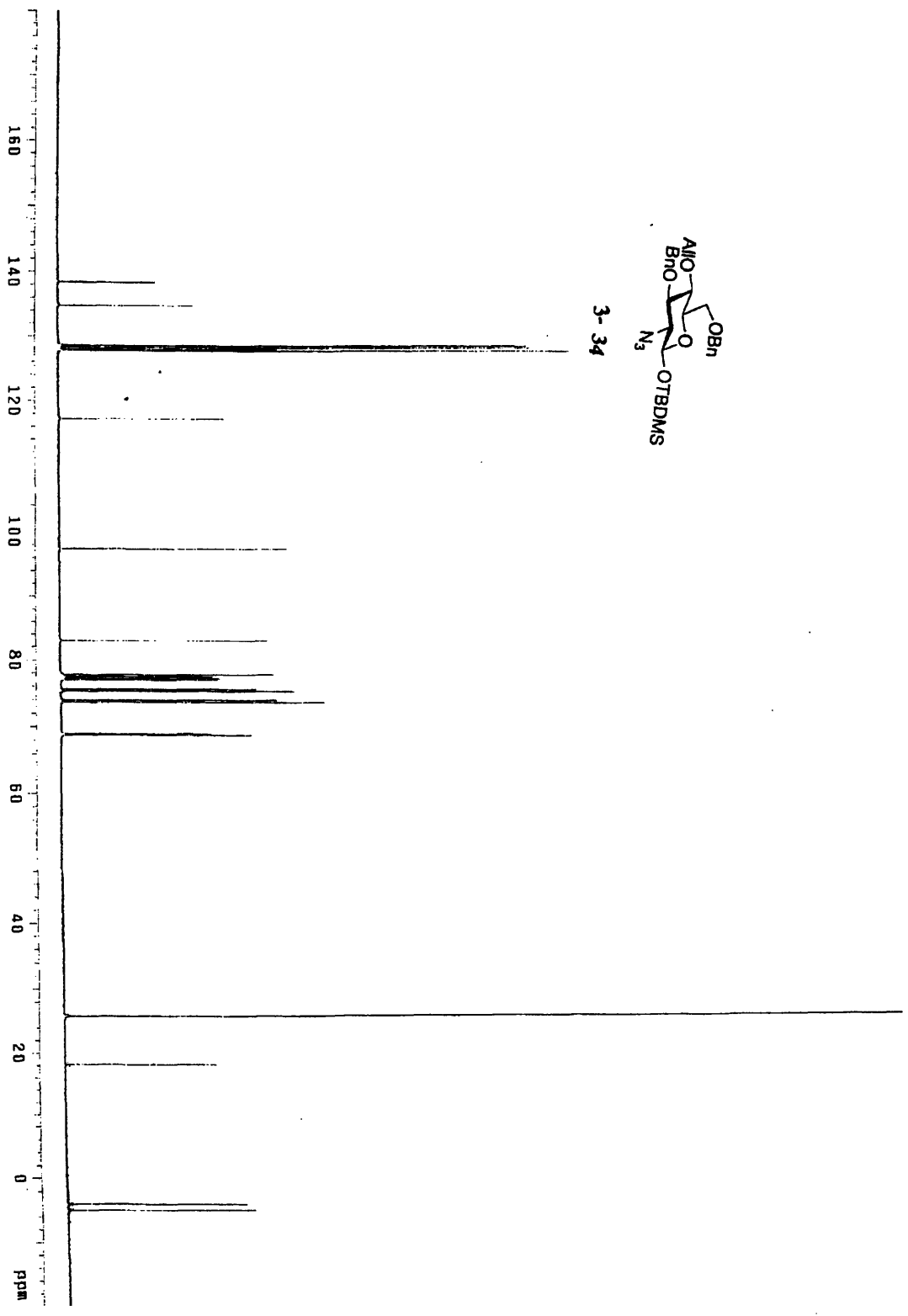
3-32

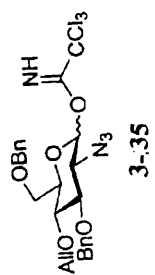
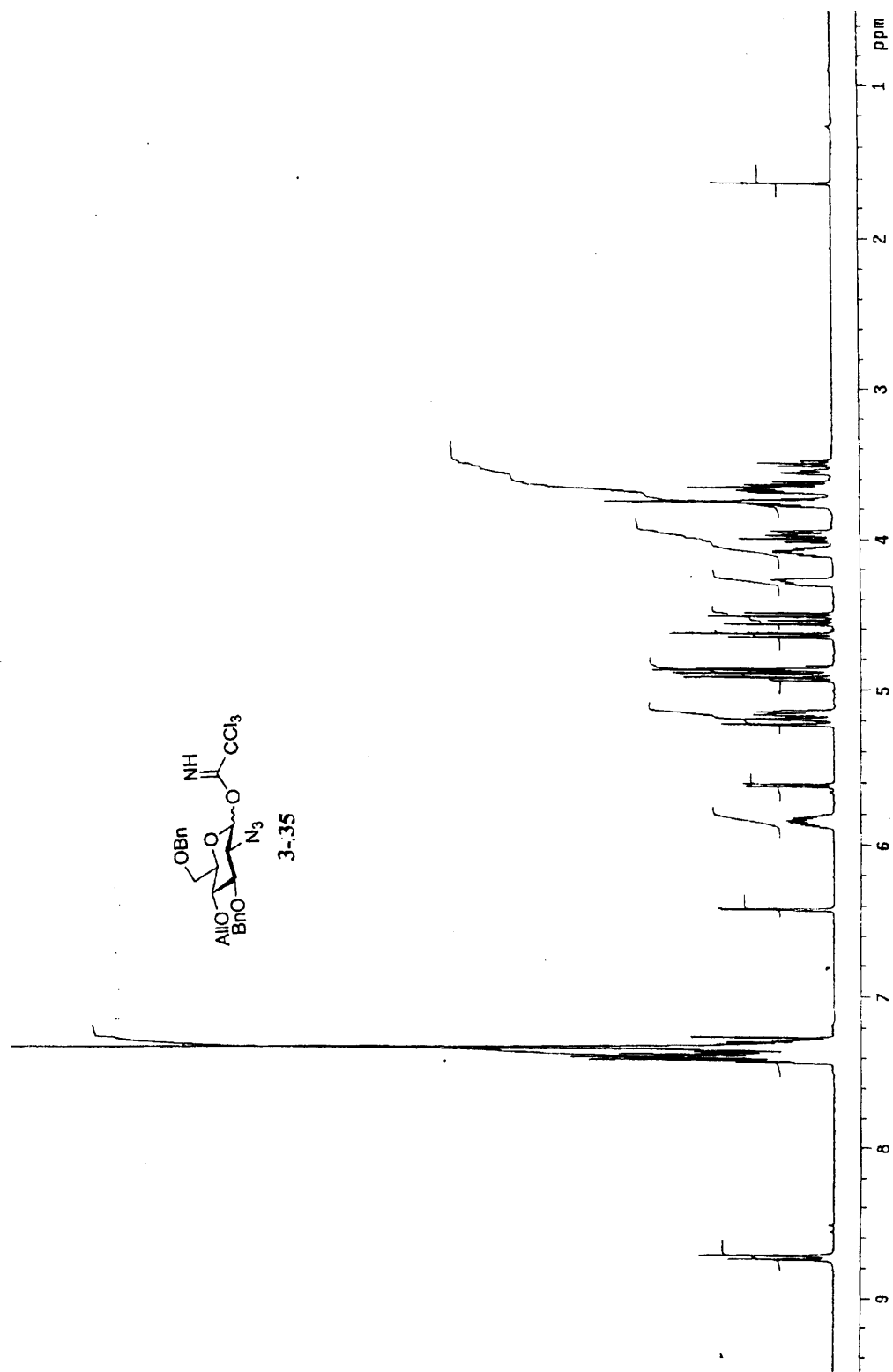


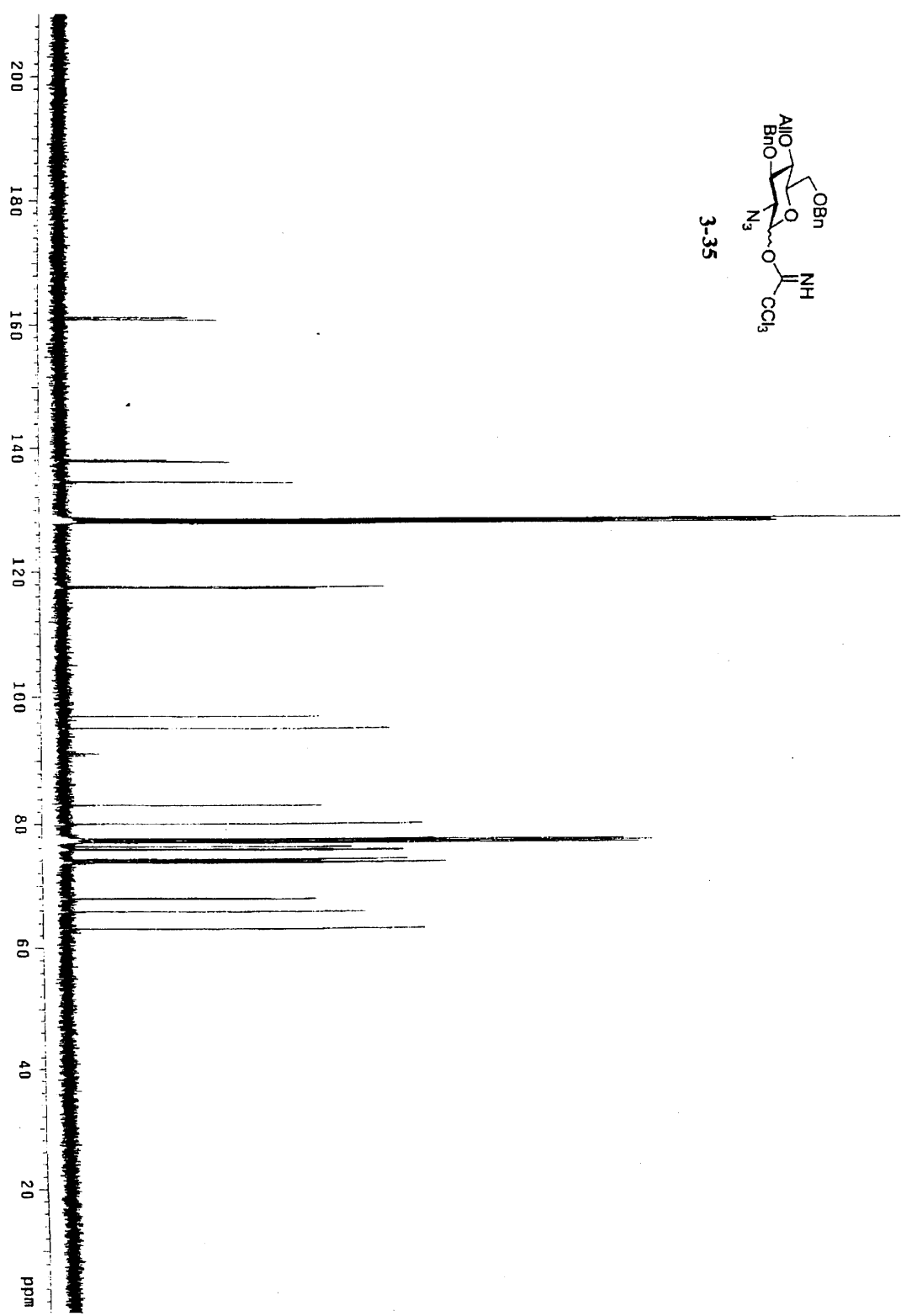
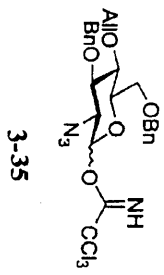


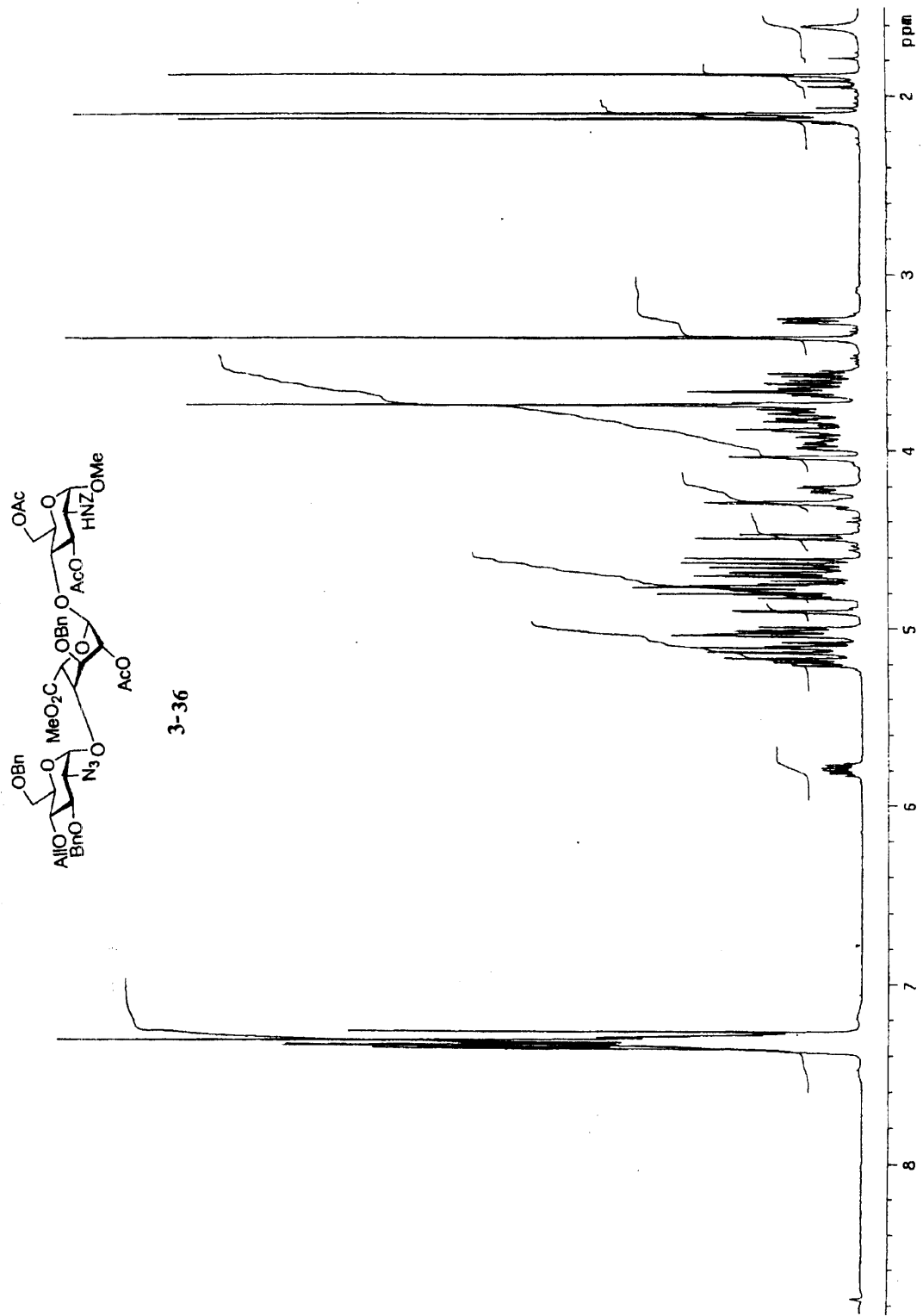
3-34

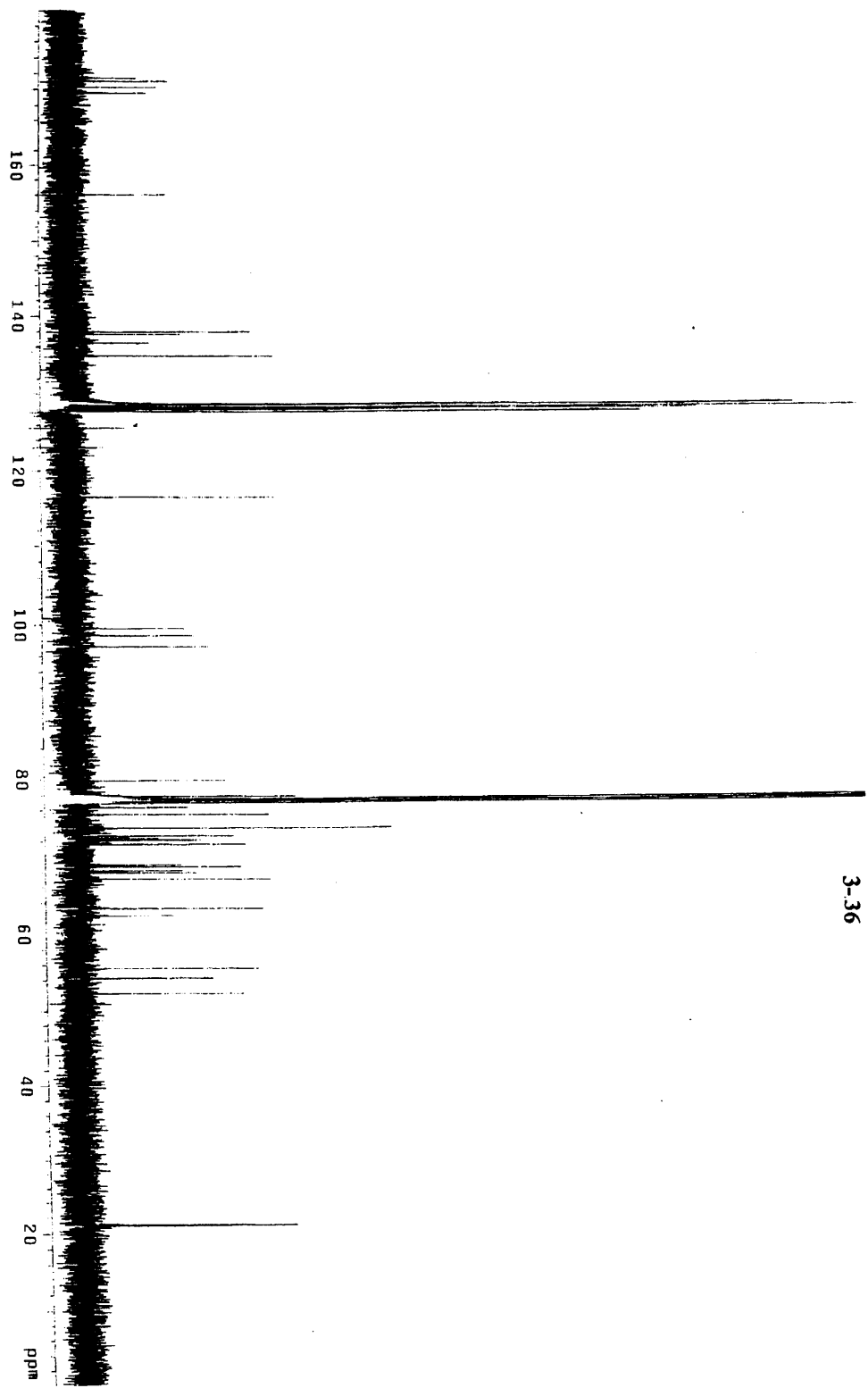




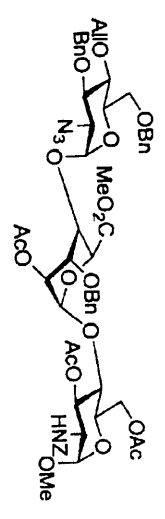


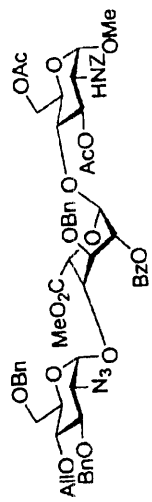




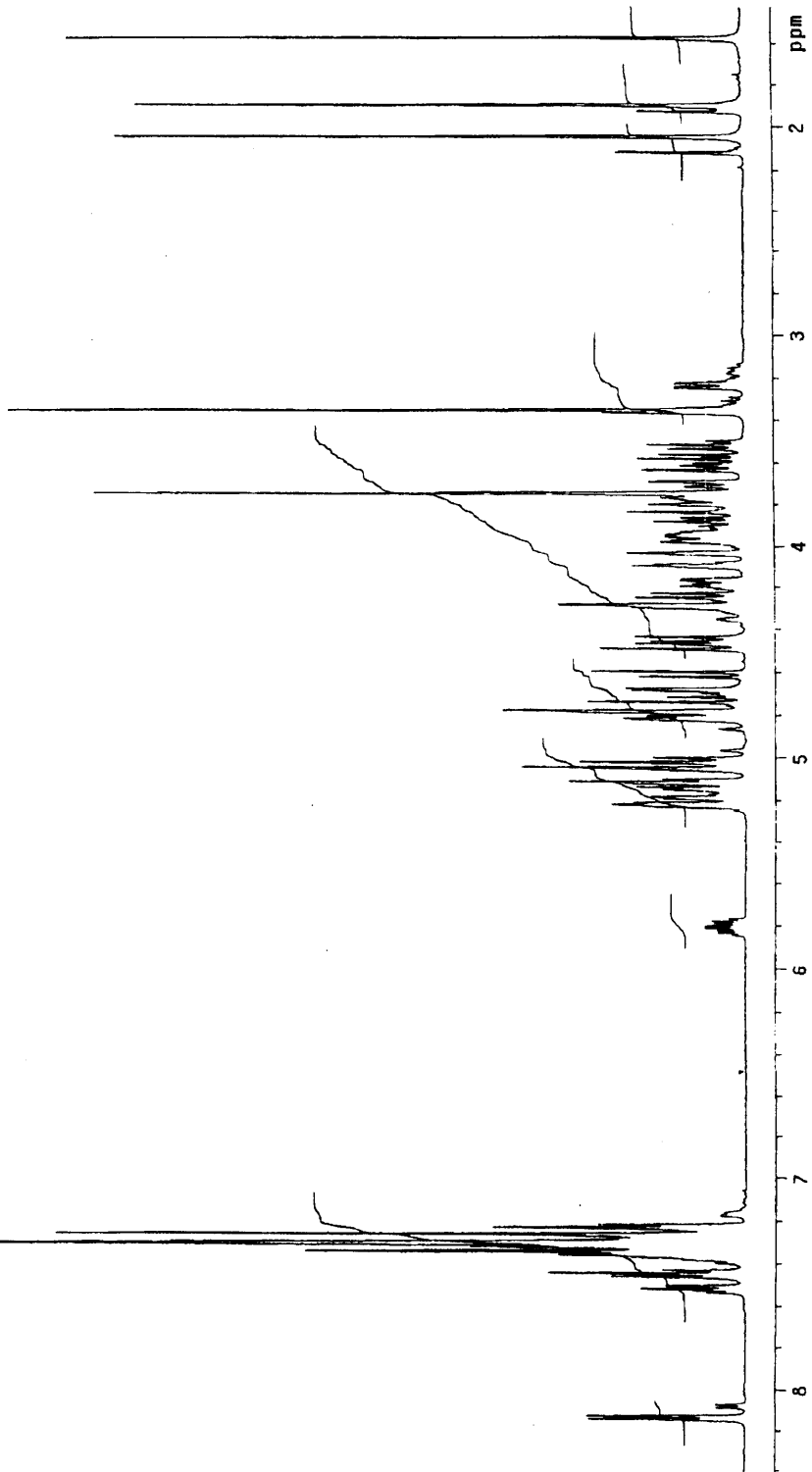


3-36

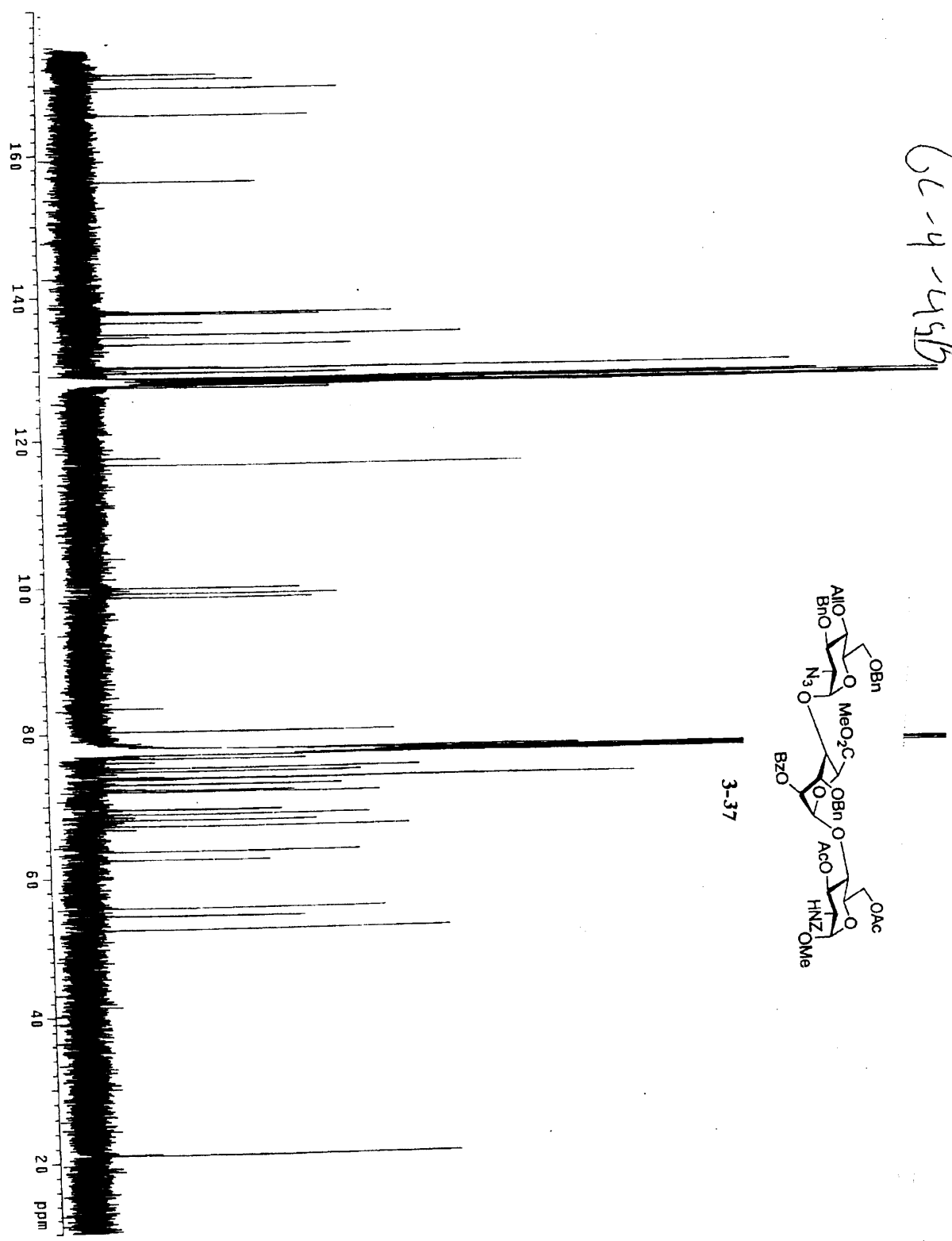




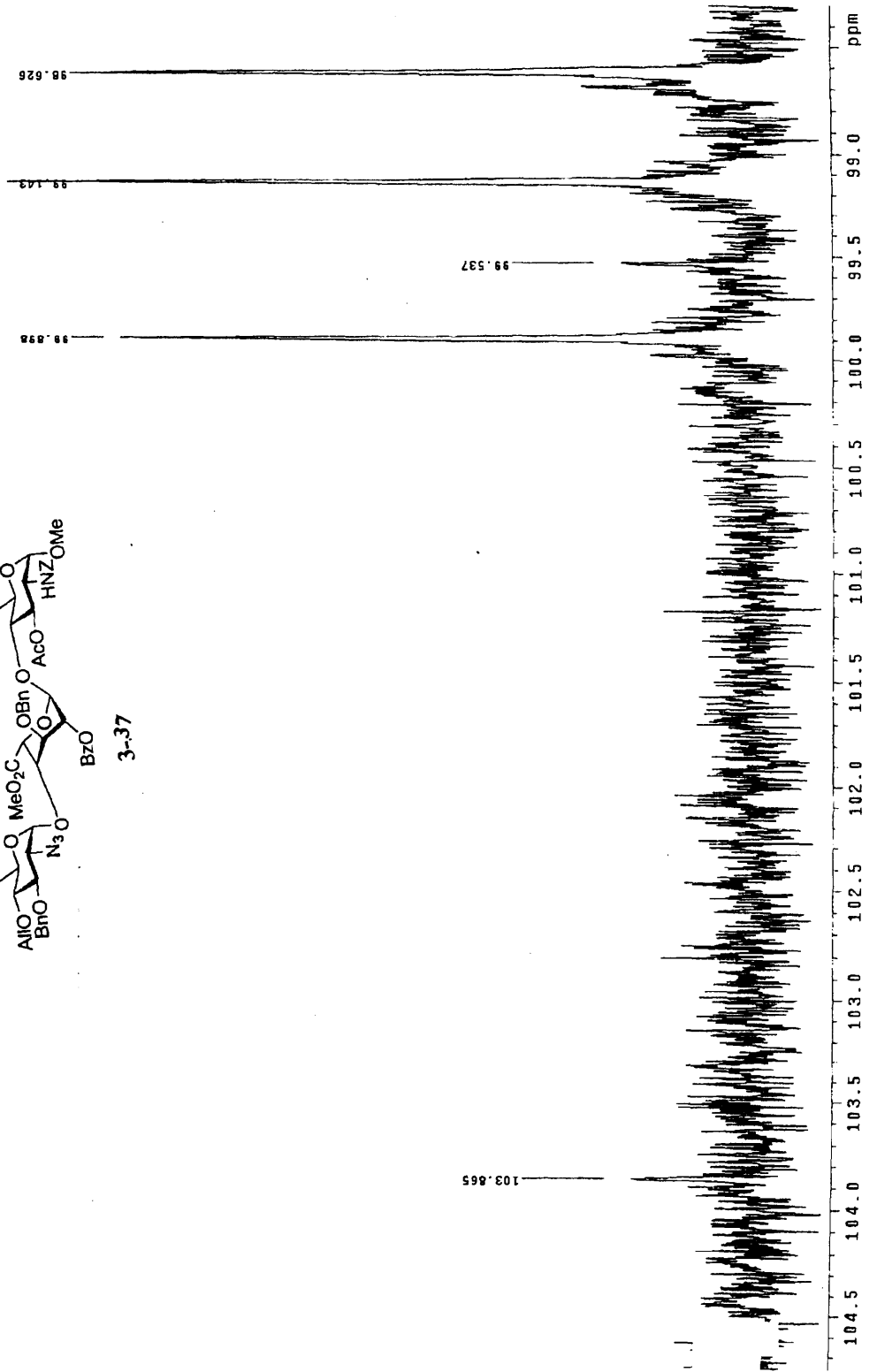
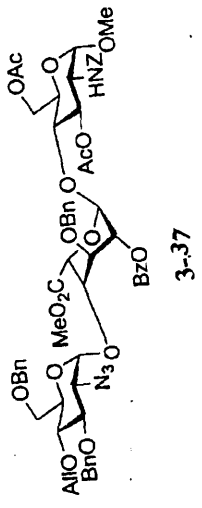
3-37



6c-4-45B



GL-4-488 C
Pulse Sequence: szput



GL-4-498 H

Pulse Sequence: NSQC

Solvent: CDCl3

Temp: 28.0 C / 283.1 K

User: J14-87

Prgr: g14-87

INNOV-550 *2IPY

PULSE SEQUENCE: NSQC

Relax. delay: 1.000 sec

Acq. time: 0.096 sec

File: 21322.0 Hz

20 v/dth: 21322.0 Hz

8 repetitions

2 x 512 increments

OBSERVE: H1, 499.7537725 MHz

DECUPLE: C13, 125.6750883 MHz

Power: 52 dB

on during acquisition

off during delay

QASP-1 modulated

DATA PROCESSING

SF: 499.7537725 MHz

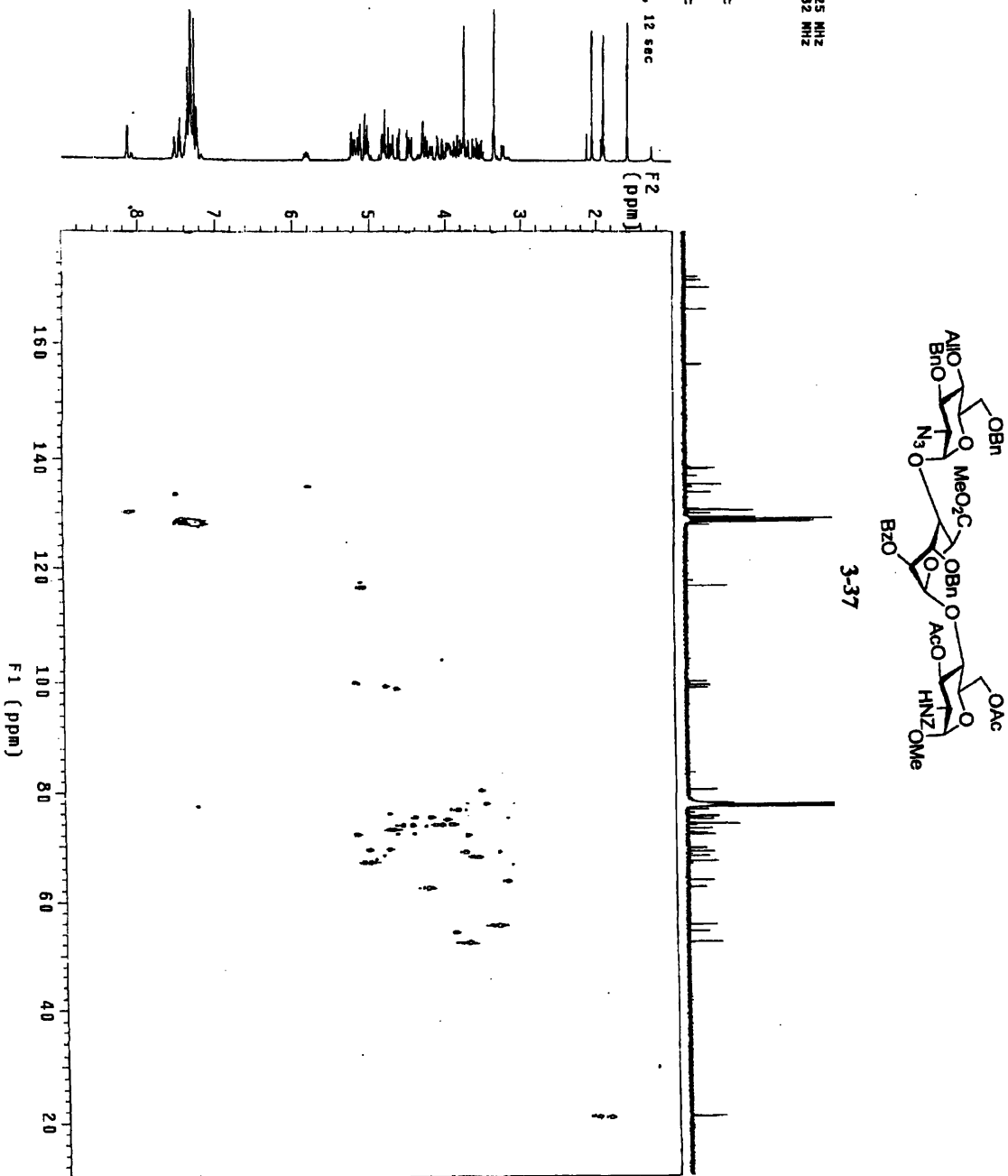
SF: 125.6750883 MHz

Sq. sine bell: 0.824 sec

Shifted by: -0.024 sec

FT size: 1024 x 2048

Total time: 2 hr, 39 min, 12 sec



GL-4-488 H

Pulse Sequence: HSQC

Solvent: CDCl₃

Temp: 20.0 C / 293.1 K

User: 1-14-87

File: GL-4-488HSQC

INOVA-500 "zippy"

PULSE SEQUENCE: HSQC

Relax. delay 1.000 sec

Acq. time 0.095 sec

Width 3198.0 Hz

2D Width 21322.0 Hz

8 repetitions

2 x 512 increments

OBSERVE M1, 499.7597785 MHz

DECOUPLE C13, 125.6750862 MHz

Reverse decoupling

on during acquisition

off during delay

GARP-1 modulated

DATA PROCESSING

Sq. sine bell 0.086 sec

Shifted by -0.085 sec

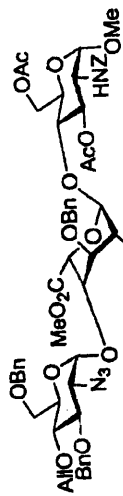
F1 DATA PROCESSING

Sq. sine bell 0.024 sec

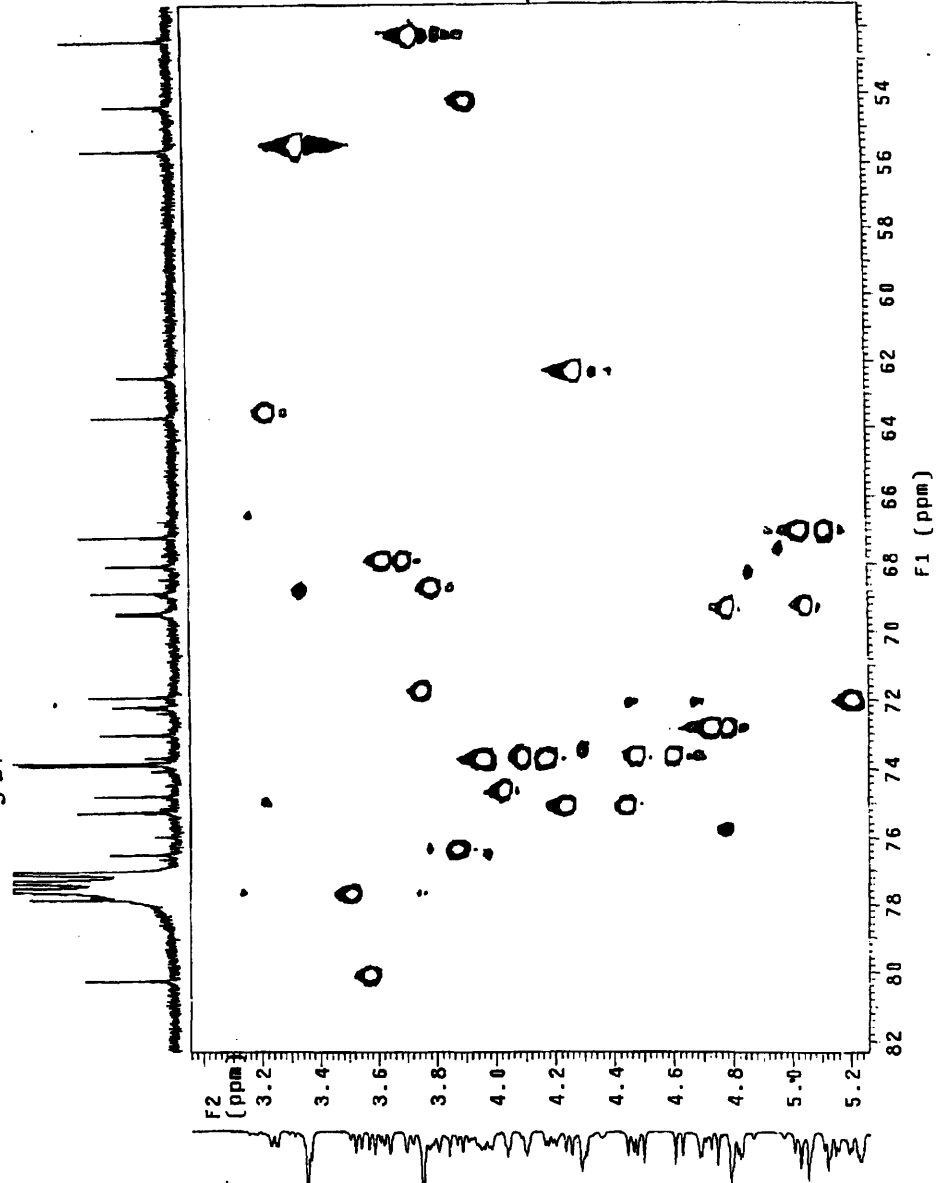
Shifted by -0.024 sec

FT size 1024 x 2048

Total time 2 hr, 35 min, 12 sec



3-37



GL-4-498 H

Pulse Sequence: HSQC

Solvent: CDCl3

Temp: 29.0 C / 293.1 K

USER: 1-18-87

File: GL-4-498HSQC

INSTR: 500 ZIPPY

PULSE SEQUENCE: HSQC

Relax. delay: 1.000 sec

Acq. time: 0.095 sec

NUC1: 13C 101.326 MHz

NUC2: 1H 500.136260 MHz

2 X 512 FID/REALTIME

OBSERVE: H1 499.753725 MHz

DECOUPLE: C13 125.6250882 MHz

Power: 52 dB

on during acquisition

off during delay

GARP-1 modulated

DATA PROCESSING:

SF: sine bell 0.095 sec

SH: sine bell 0.095 sec

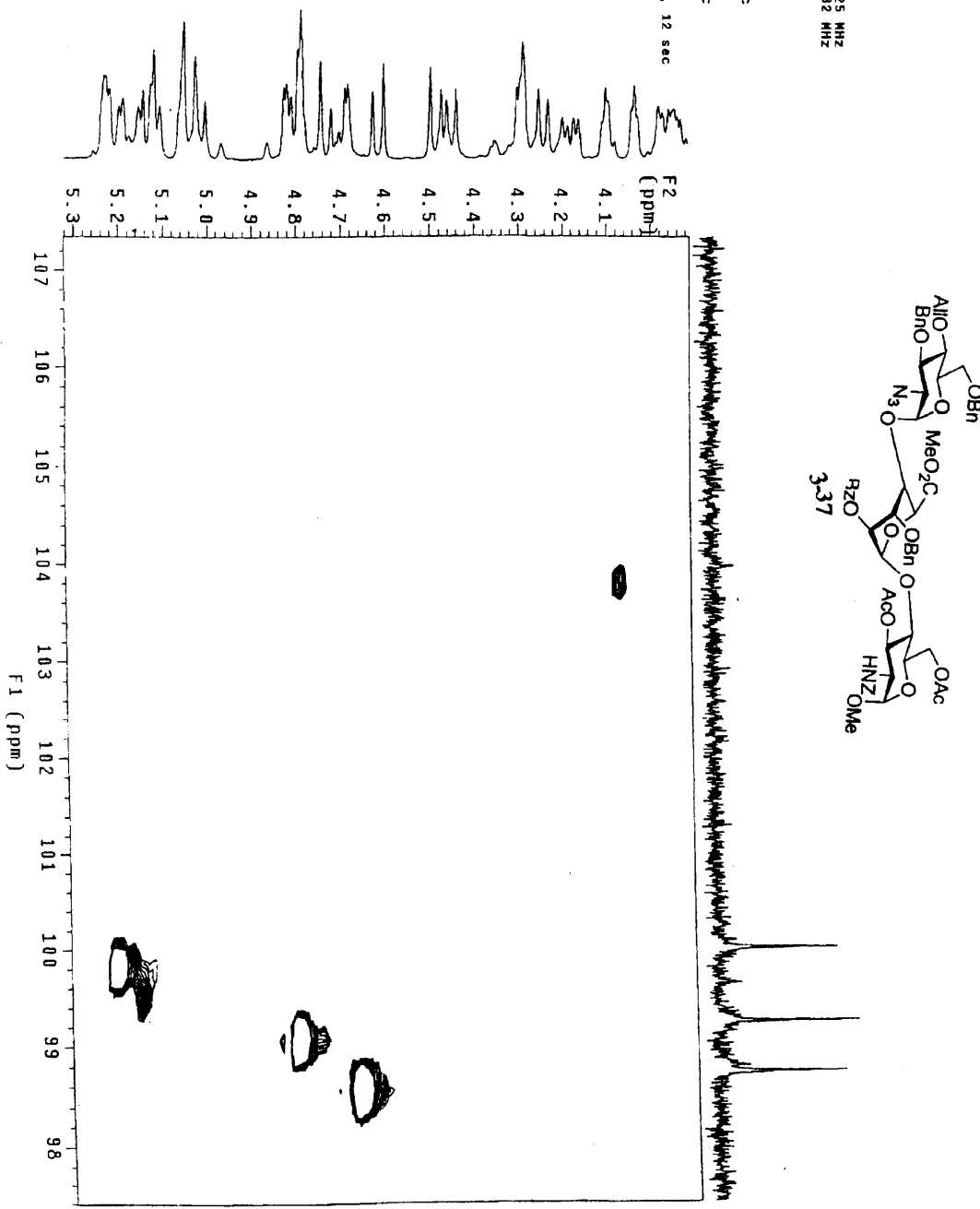
F1: sine bell 0.0924 sec

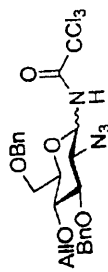
Sq: sine bell 0.0924 sec

Shifted by -0.024 sec

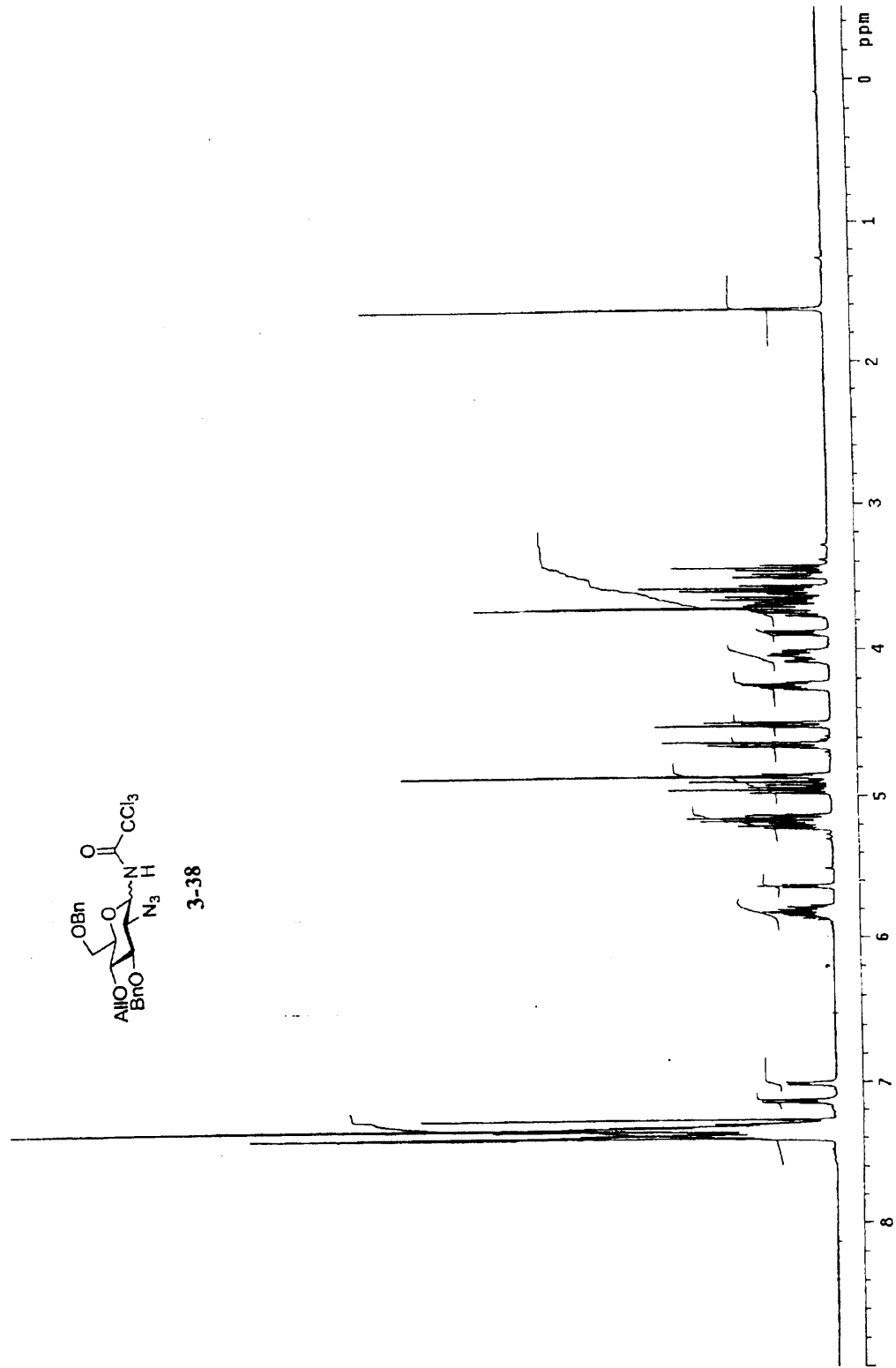
FT size 1024 x 2048

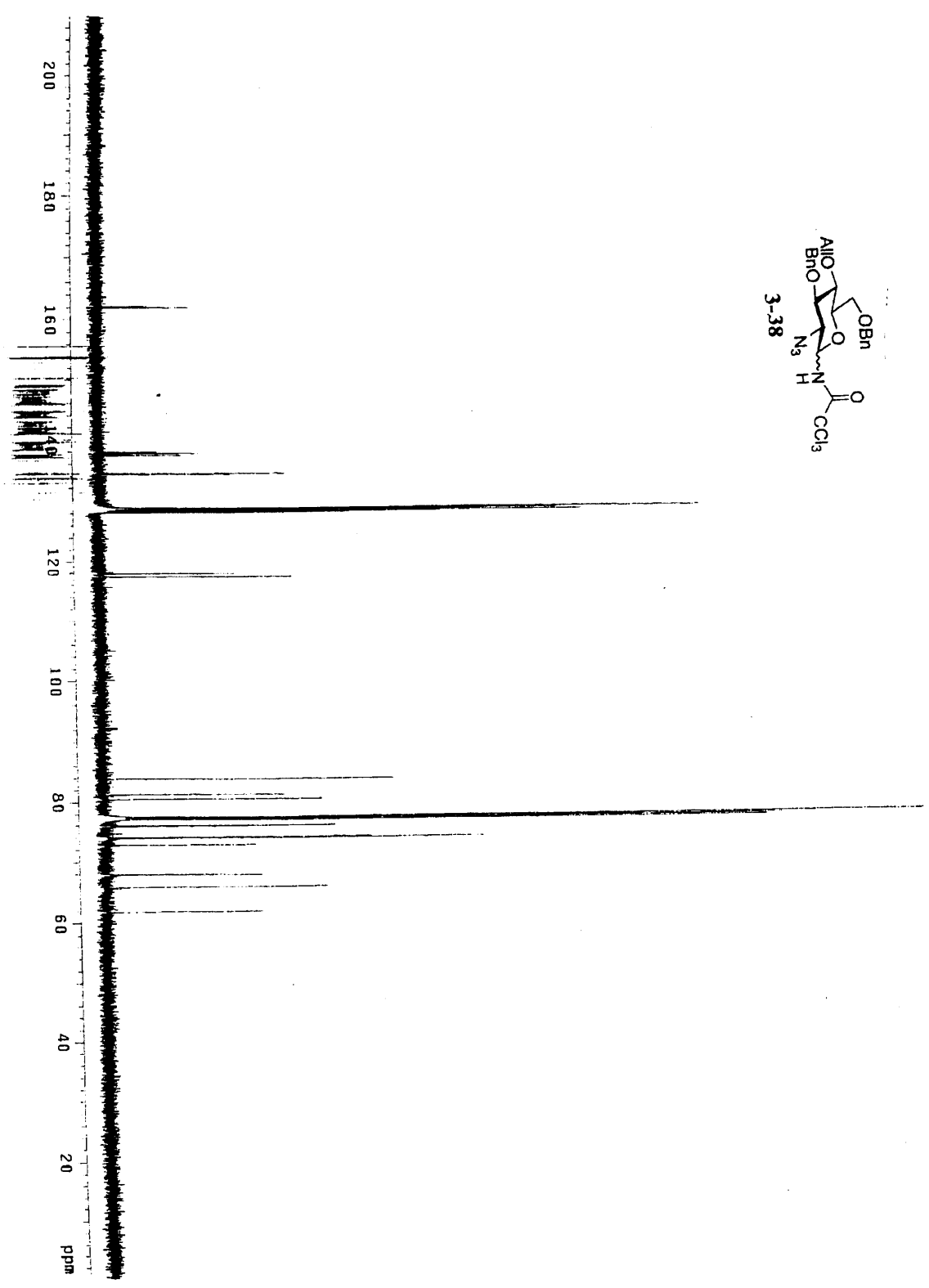
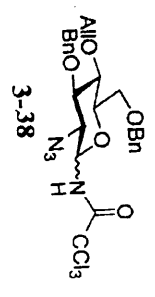
Total time 2 hr, 39 min, 12 sec





3-38





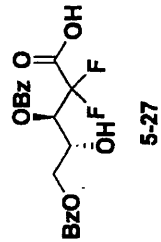
Appendix 2: Supporting Information from Part II

Supporting information for Chapter 5	531	Supporting information for Chapter 6	567
Compound 5-27	531	NMR of <i>ara-C</i>	567
Compound 5-14a	532	NMR of small molecule product of inactivation. NaBD ₄ quench	570
Compound 5-16	535	NMR of small molecule product of inactivation, NaBD ₄ quench	574
1'-[² H]-F ₂ C	539		
F ₂ CMP	540		
F ₂ CDP	543		
F ₂ CTP	546	MALDI of region II peptides	577
1'-[² H]- 5-14a	549	MALDI of region III peptides	584
Compound 5-28	553	MS/MS of 2005 Da peptide	587
Compound 5-29	555		
Compound 5-30	556	H-ENDOR of RTPR/F ₂ CTP	588
1'-[² H]- 5-28	559	D-ENDOR of RTPR/1'-[² H]-F ₂ CTP	589
3'-[² H]- 5-14a	560	130 GHz EPR of RTPR/F ₂ CTP	590
3'-[² H]-F ₂ C	565		
3'-[² H]-F ₂ CMP	566		

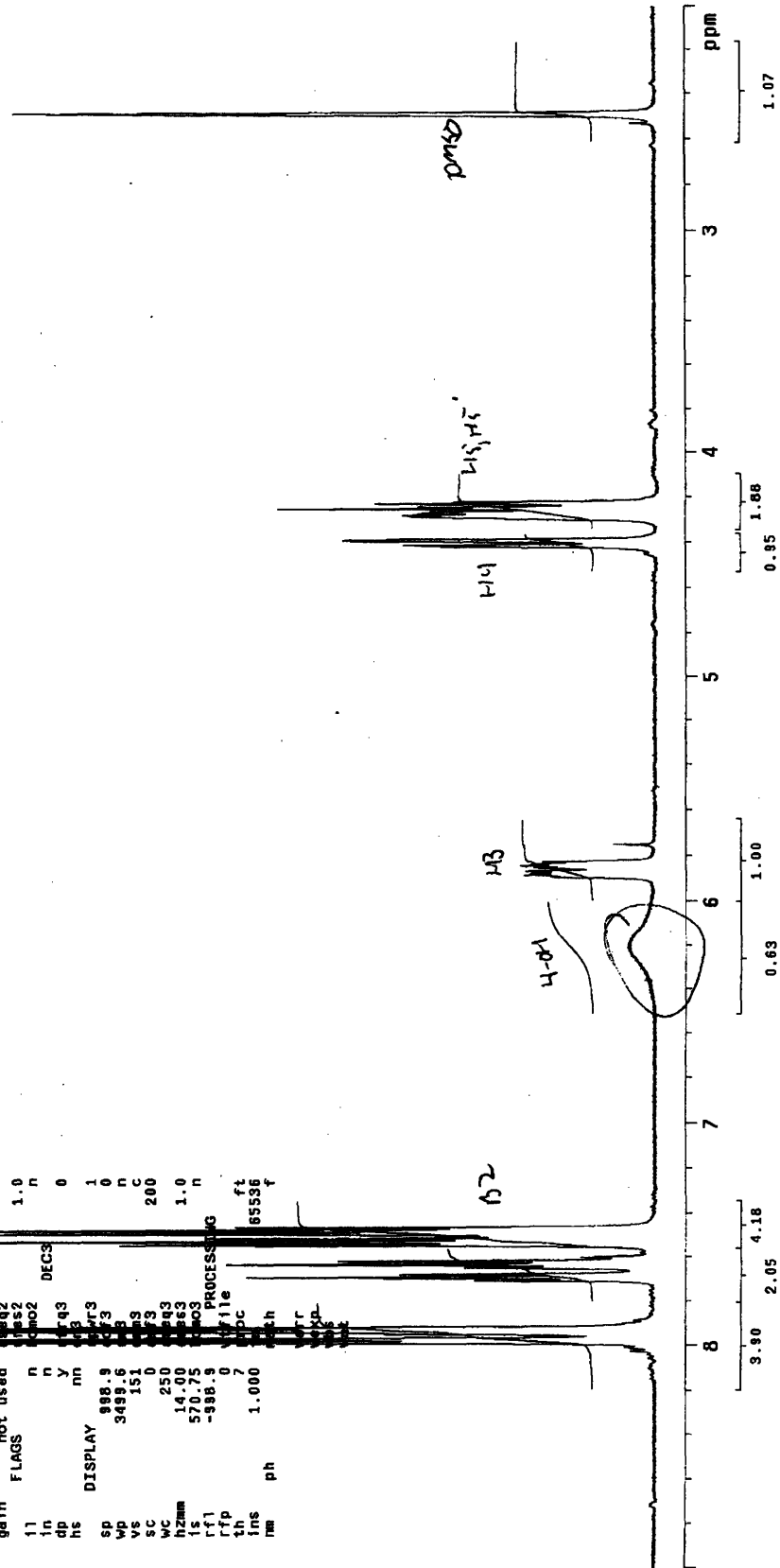
GL-1-21, leftover, dessication

exp2 szpu1

SAMPLE	date	Jun 5 2003	DEC. & Vt	dfrq	125.677
solvent	DMSD		an	C13	
file	ACQUISITION	exp szpu1	gpcw	1498.1	
freq	488.758	dm	mm	10000	
at	3.274	dayf	w		
sh	22612	dayg			
sb	3498.6	dayh			
fb	not used	days	1.0	n	
bs	16	inquo	DEC2		
tpwr	56	qfqr2	0		
pw	8.2	qfqr2	1		
di	250.0	qfqr2	0		
nt	8	qfqr2	n		
ct	8	qfqr2	C		
elock	n	qfqr2	200		
gain	not used	qfqr2	1.0	n	
flags	n	qfqr2	0	n	
ll	n	qfqr3	0		
in	y	qfqr3	1		
ds	nn	qfqr3	0		
hs	3498.6	qfqr3	n		
sp	988.9	qfqr3	C		
wp	151	qfqr3	200		
vs	250	qfqr3	1.0		
sc	14.00	qfqr3	n		
vc	570.75	qfqr3	ft		
hzm	-988.9	qfqr3	f		
ls	1.000	qfqr3	f		
rf1		qfqr3			
rfp		qfqr3			
th		qfqr3			
ins		qfqr3			
nm		qfqr3			

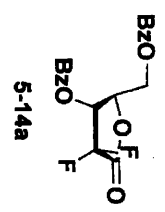
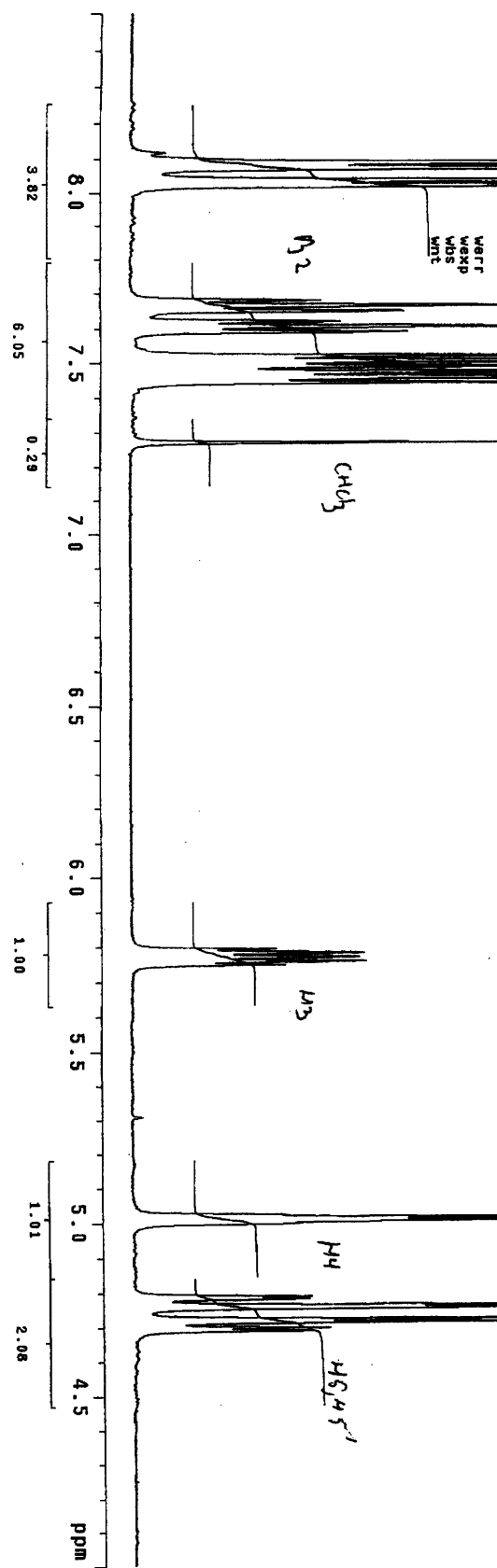


(CH₂Cl₂ insoluble contaminant of 5-14a)



recovered lactone
exp2 s2pu1

SAMPLE Dec 15 2003
 date Dec 15 2003
 solvent CDC13
 file exp
 ACQUISITION
 srrq 498.756
 tn H1
 at 3.275
 mp 381.04
 sw 878.3
 fb not used
 bs 16
 tpwr 56
 pw 8.2
 di 0
 tof 75.0
 nt 1
 ct 1
 alock n
 gain 38
 flags n
 11 n
 in n
 dp n
 hs n
 DISPLAY
 SD 129.0
 WD 129.0
 VS 151
 SC 250
 VC 250
 WZ 250
 IS 250
 ffr 250
 rfp 250
 th 250
 lns 250
 pha 250

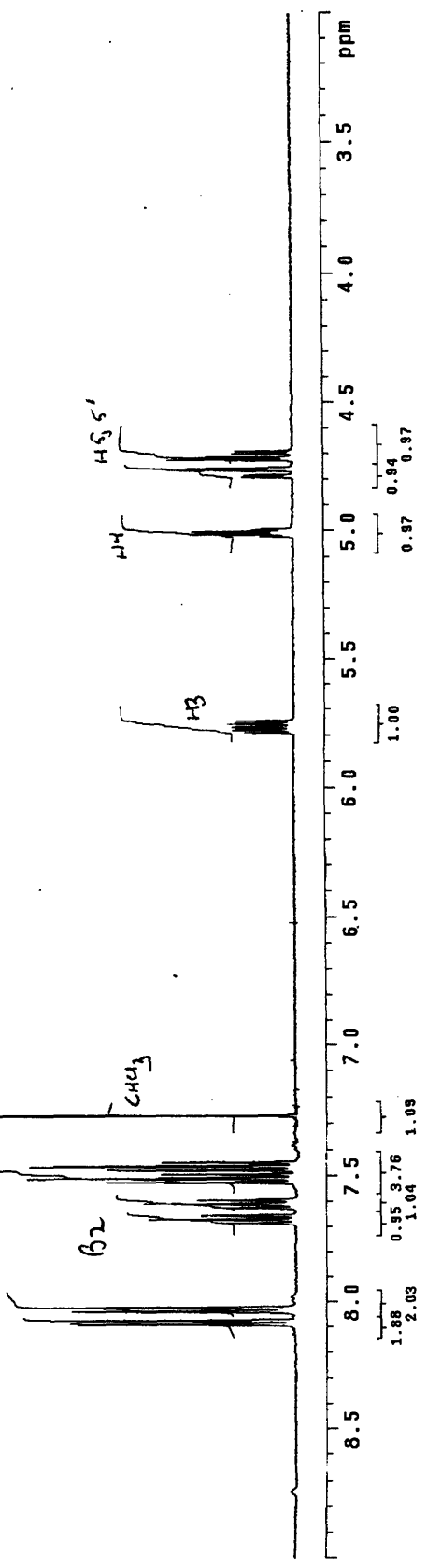
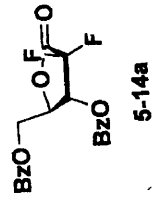


Product
from
5-23

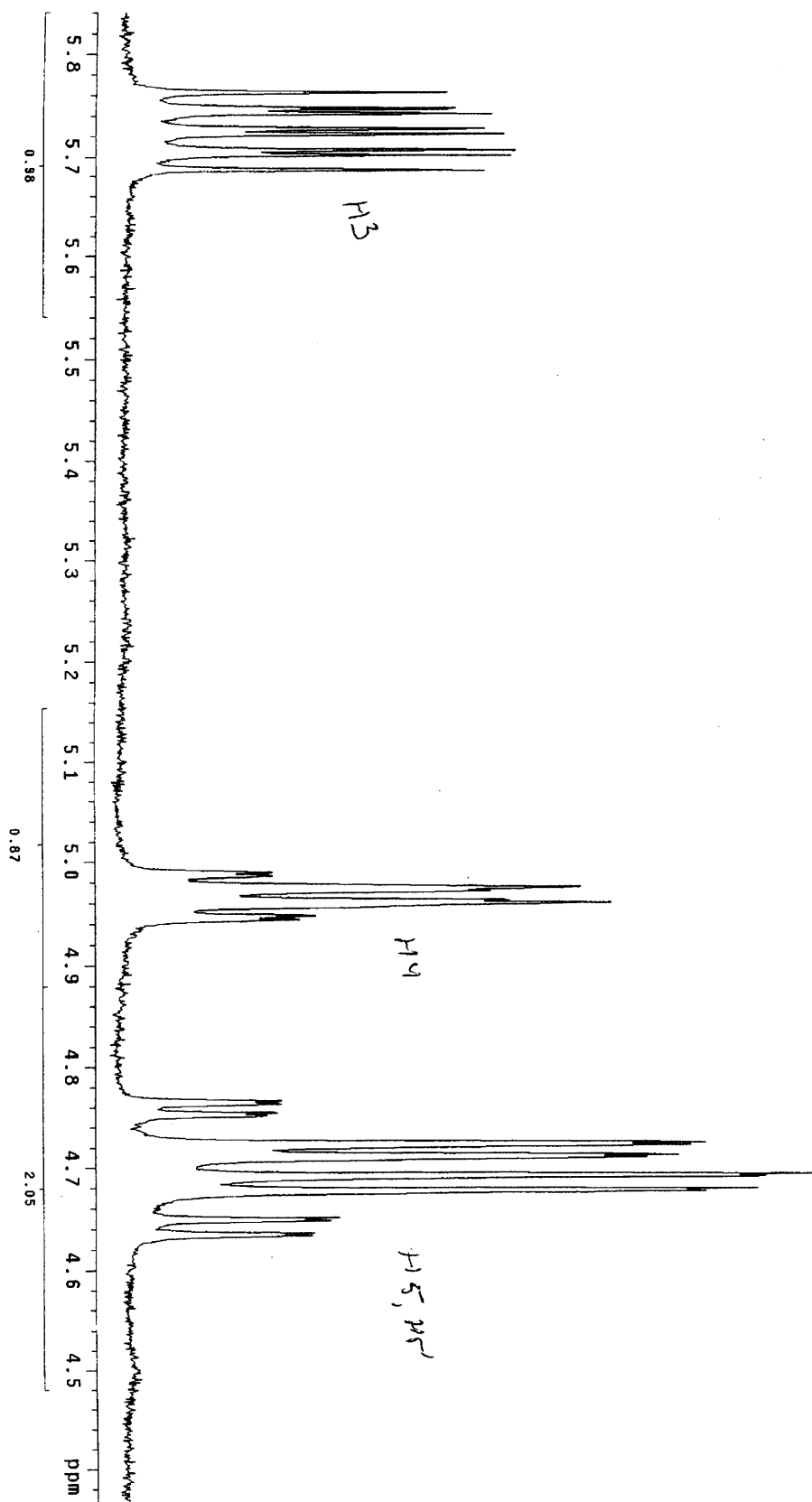
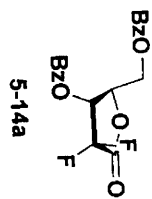
sm, filtered
exp3 s2pu1

SAMPLE DEC. & VT
 date May 29 2003 dfrq 125.677
 solvent CDC13 en C13
 file ACQUISITION exp 34 dpwr 1488.1
 493.756 dm rnm
 tr 10000 w
 at 3.273 dmf
 up 3110.4 dseq
 pw 4748.3 dres
 fb not used homo DEC2
 bs 56 dfrq2 0
 tprw 8.2 dn2 1
 dt 8.0 dpr2 0
 tof -375.7 qof2 0
 nt 1 dm2 C
 ct 1 dm2 C
 alock 200
 gain 52 dres2 1.0
 flags n homo2 DEC3
 ll n
 ln n
 dp y dfrq3 0
 hs nm dpr3 1
 DISPLAY 1488.1 dpr3 0
 2888.5 dm3 n
 vs 151 dm3 C
 sc 6 dm3 200
 wc 250 dseq3
 hznm 11.99 dres3 1.0
 ls 979.63 homo3 n
 rffl 250.3 wfile
 th 0
 ins 2 proc ft
 nm 1.000 fn 65536 f
 math
 werr
 wexp
 wbs
 wnt

purified by filtration



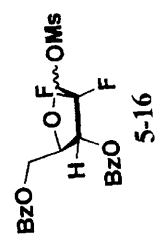
Starting material, filtered
Pulse Sequence: szpu1



$CDCl_3$ ref to solvent peak

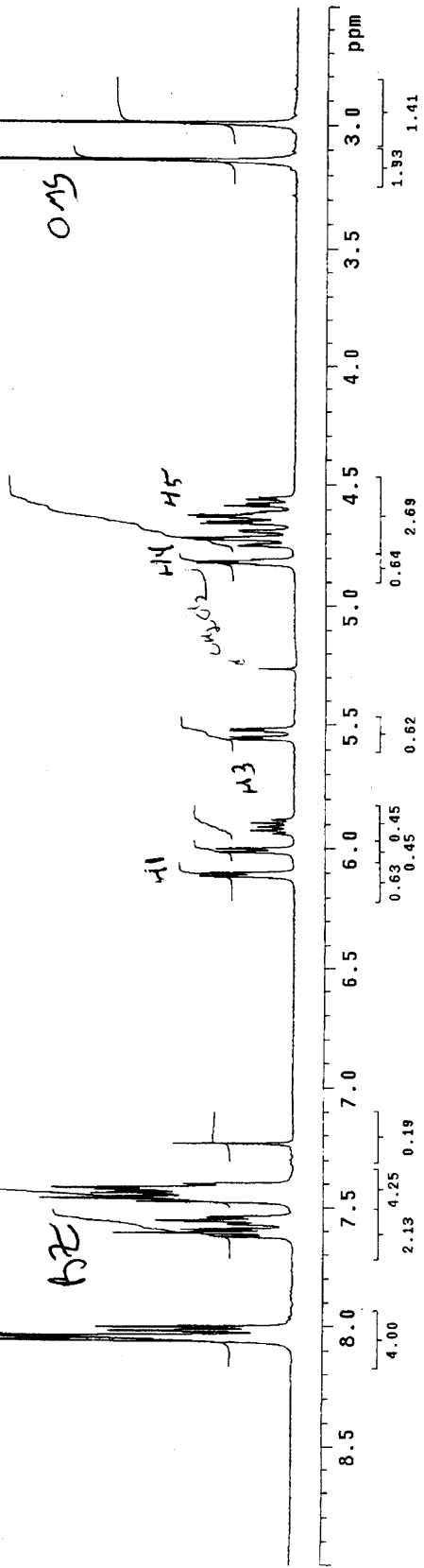
δ 's matched to lit. values of previously prepared compound.

from compound label, test scale ppm

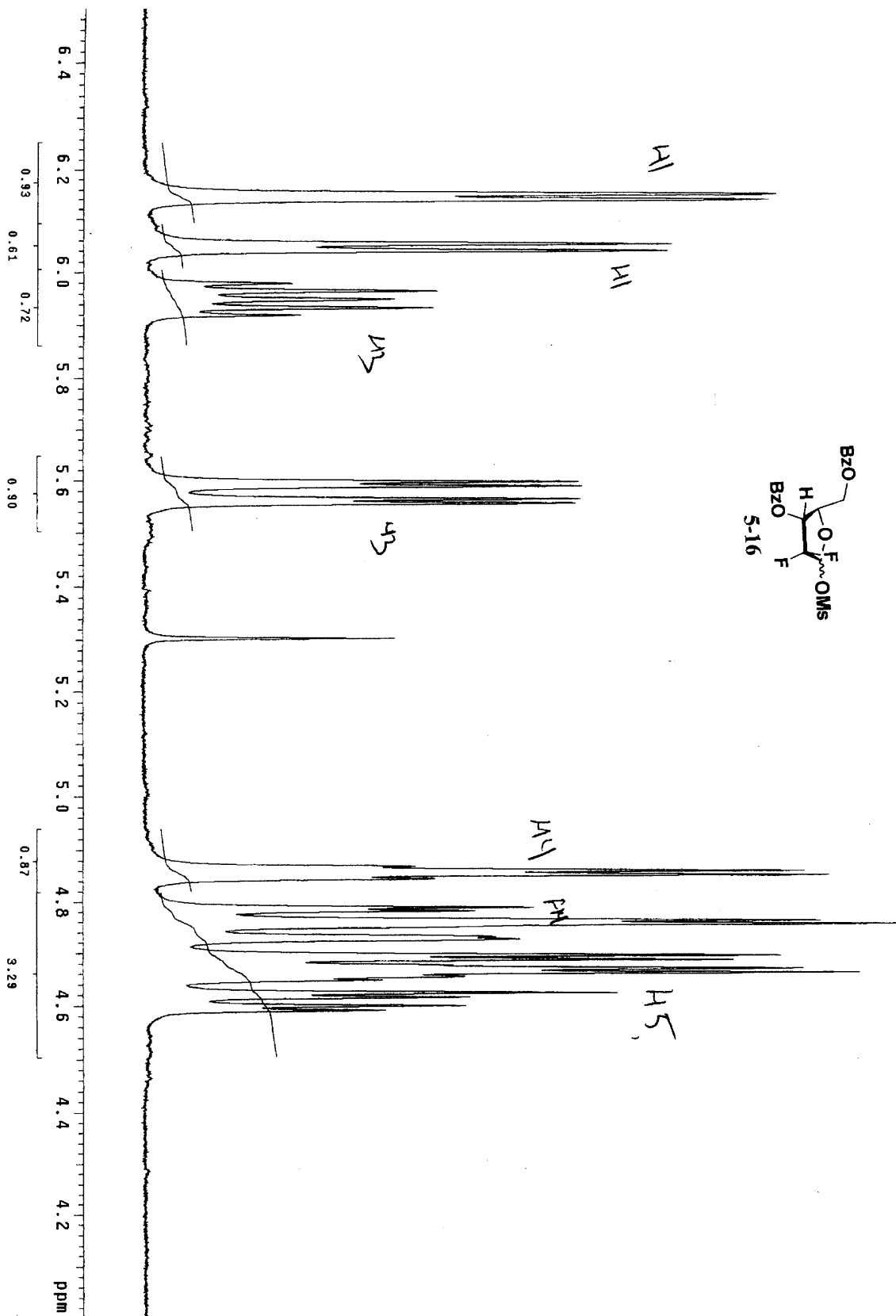
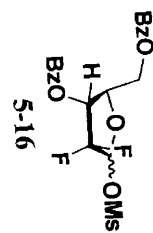


```

mesylate
exp2 s2pu1
SAMPLE
date Sep 29 2003
solvent CDC13
file CDC13
ACQUISITION
sfreq 499.756
tn H1
at 3.275
np 31104
sw 4748.3
fb not used
bs 16
tpwr 56
pw 8.2
di 0
tof -354.7
nt 1
ct 1
alock n
gain 34
FLAGS
il n
in n
dp y
hs nn
sp 1249.3
wp 3248.4
vs 151
sc 0
wc 250
hzmm 12.98
ls 1007.20
rfi 250.3
rfp 0
th 0
ins 4.000
nm ph
DEC. & VT
dfrq 125.677
dn C13
dpmr 34
dof 1498.1
dm n
dmm nn
dmf H1
dseq 10000
dres 1.0
homo n
dfrq2 0
dn2 8.2
dpmr2 0
dof2 0
dm2 n
dmm2 C
dmf2 n
dseq2 200
dres2 1.0
homo2 n
dfrq3 0
dn3 n
dpmr3 1
dof3 0
dm3 n
dmm3 C
dmf3 200
dseq3 0
dres3 1.0
homo3 n
PROCESSING
wf file
proc 65536
math f
werr
wexp
wps
wint
  
```



mesylate
Pulse Sequence: szpu1



GL-1-31TH

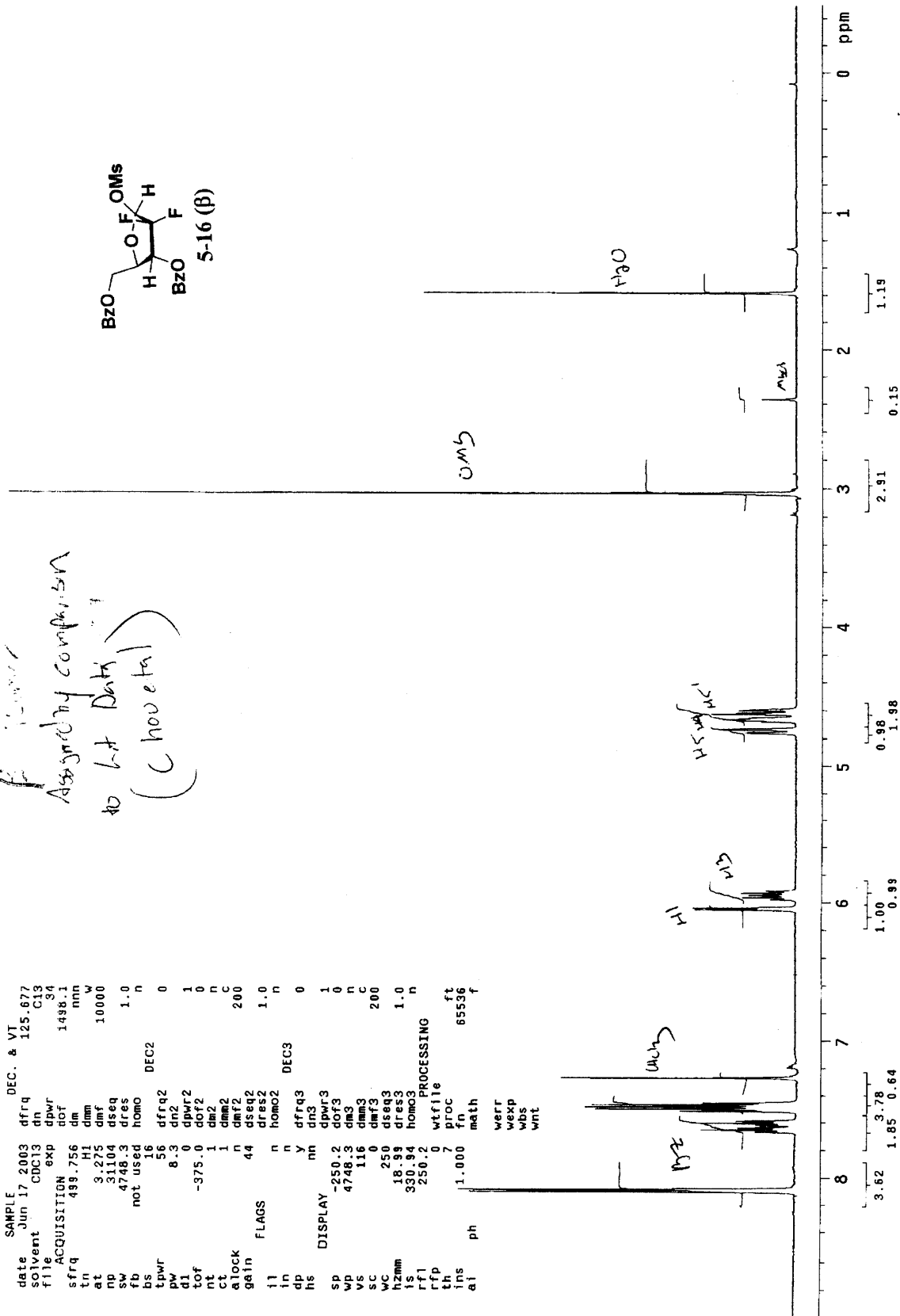
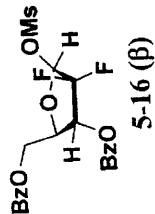
exp2 s2pu)

```

SAMPLE
date Jun 17 2003
solvent CDC13
file
ACQUISITION
sfrq 499.756
tn H1
at 3.275
np 31104
sw 4748.3
fb not used
bs 16
tpwr 56
pw 8.3
d1 0
tof -375.0
nt 1
ct 1
alock n
gain 44
FLAGS
ll n
ln n
dp n
hs nn
sp -250.2
wp 4748.3
vs 116
sc 0
wc 250
nzmm 330.94
rs 250.2
rf1
rfp
tn
ins
al ph
DEC. & VT
dfrq 125.677
dn C13
dpwr 34
nof 1498.1
dmm n
dmf 10000
dseq 1.0
dres 1.0
homo n
DEC2
dfrq2 0
dn2 0
dpwr2 1
dof2 0
dm2 n
dmm2 C
dmf2 200
dseq2 1.0
dres2 1.0
homo2 n
DEC3
dfrq3 0
dn3 0
dpwr3 1
dof3 0
dmm3 C
dmf3 200
dseq3 1.0
homo3 n
PROCESSING
wtfile 0
proc 7
fn 65536
math f
werr
wexp
wds
wnt

```

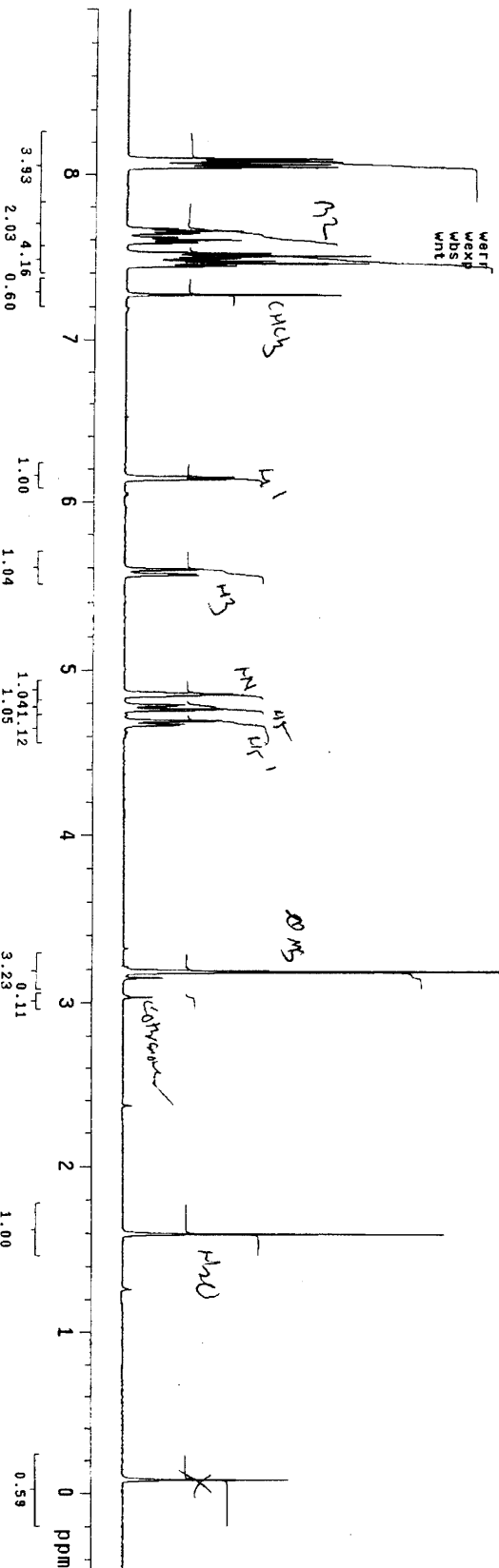
f *linear*
Assigning comparison
to lit Data
(Chou et al)



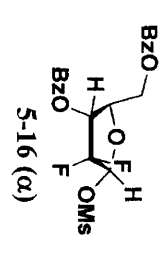
GL-1-31 bottom

exp2 s2pul

SAMPLE Jun 17 2003 DEC. & VT
 date Jun 17 2003 dfrq 125.877
 solvent CDC13 dn 013
 file ACQUISITION exp dpr 34
 ln 499.756 dt 1498.1
 tn H1 dm 10000
 at 3.275 dseq
 np 31104 dres
 sw 4748.3
 fb not used
 bs 16 homo 1.0
 tpwr 56 dfrq2 DEC2 0
 pw 8.2 dn2
 di 0 dpr2 1
 lof -375.7 dof2 0
 nt 1 dm2 n
 ct 1 dm2 c
 atlock 40 dseq2 200
 gain 40 dres2 1.0
 11 n homo2
 in n DECS 0
 dp y dfrq3
 hs mn dn3
 DISPLAY
 sp -250.3 dpr3 1
 wp 4748.3 dof3 0
 vs 147 dm3 n
 sc 250 dm3 c
 wc 0 dm3 200
 hzmm 18.99 dseq3
 ls 755.48 dres3 1.0
 ftl 250.3 homo3
 FTI 0 wifile
 th 7 proc
 ms 1.000 ft
 al ph 65536 f

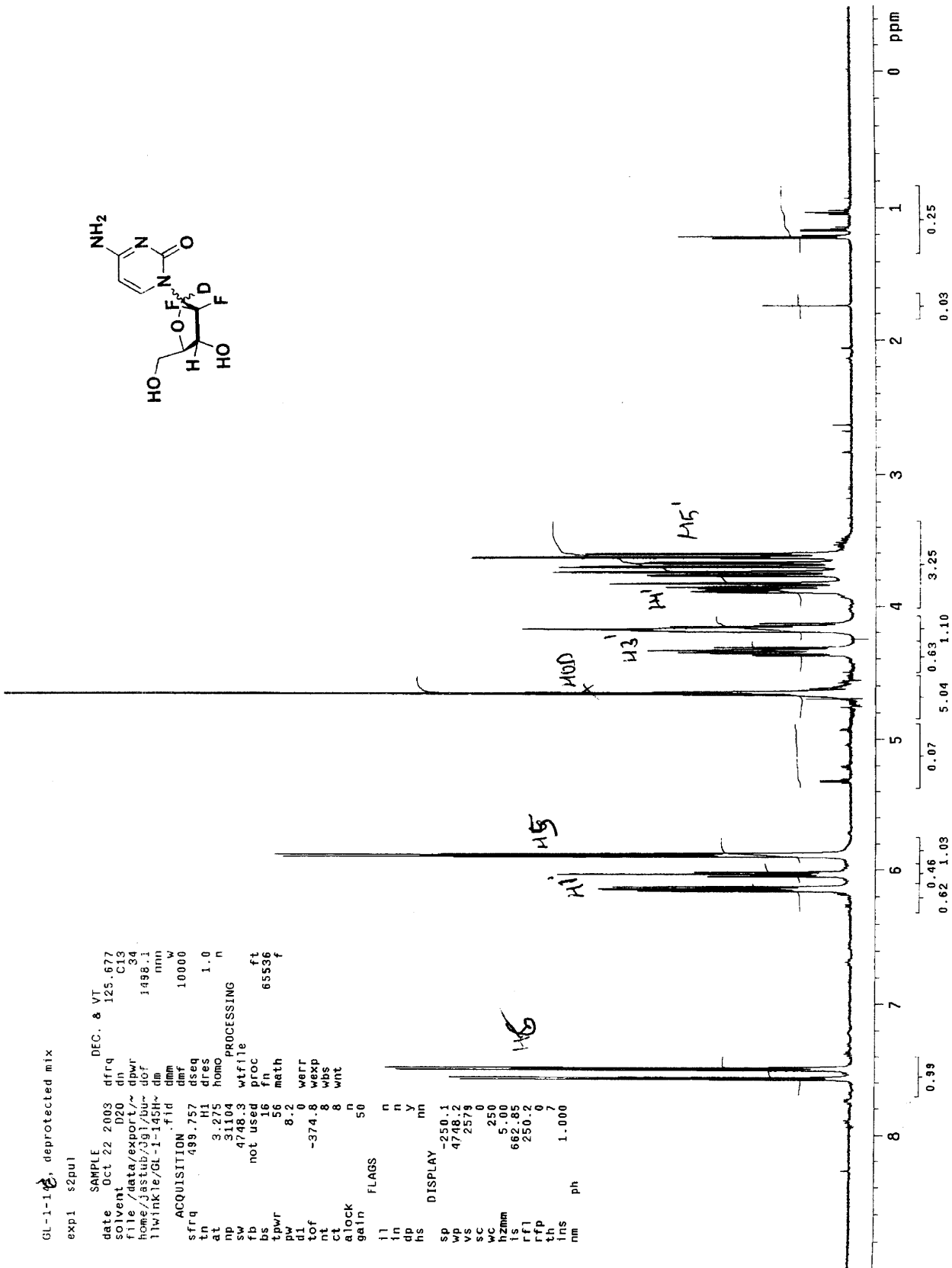
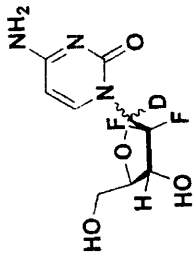


Assigned by
 Comparison table
 (Chow et al, 1992)



GL-1-1-1, deprotected mix
exp1 s2pul

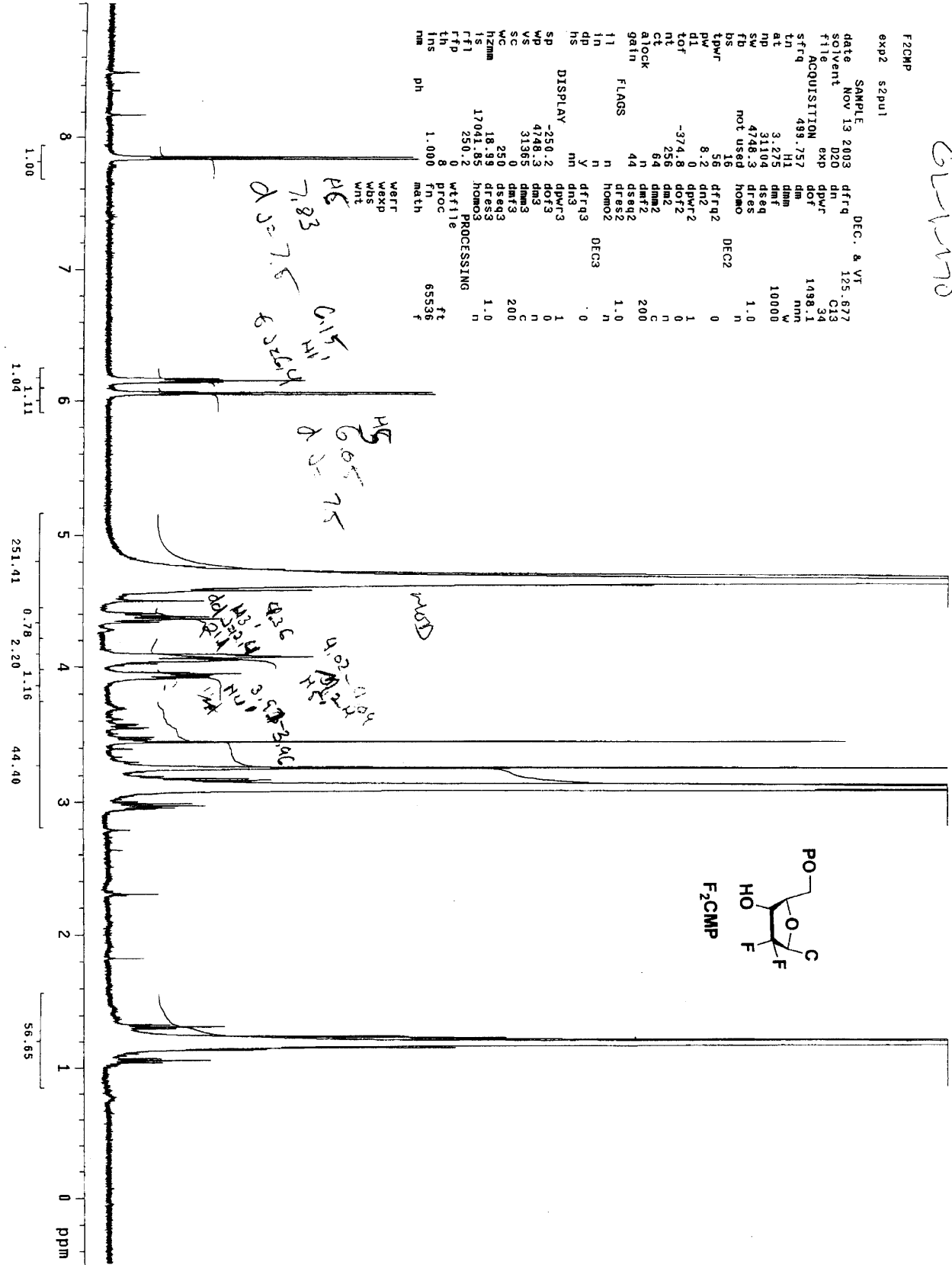
SAMPLE DEC. & VT
 date Oct 22 2003 dfrq 125.677
 solvent D2O dn C13
 file /data/export/~ dpwr 34
 home/jastub/391/bu~ dof 1498.1
 llwinkle/GL-1-145H~ dm nm
 .fid w
 ACQUISITION
 sfrq 499.757 dseq 10000
 tn H1 dres 1.0
 at 3.275 homo n
 np 31104
 sw 4748.3 wfile
 fb not used proc ft
 bs 16 fn 65536 f
 tpwr 56 math
 pw 8.2
 dl 0 werr
 tof -374.8 wexp
 nt 8 wbs
 ct 8 wnt
 alock n
 gain 50
 FLAGS
 ll n
 ln n
 dp y
 hs mn
 sp -250.1
 wp 4748.2
 vs 2578
 sc 0
 w 250
 hzmm 5.88
 fl 68.88
 rfl 250.2
 th 7
 ins 1.000
 nm ph



GL-1170

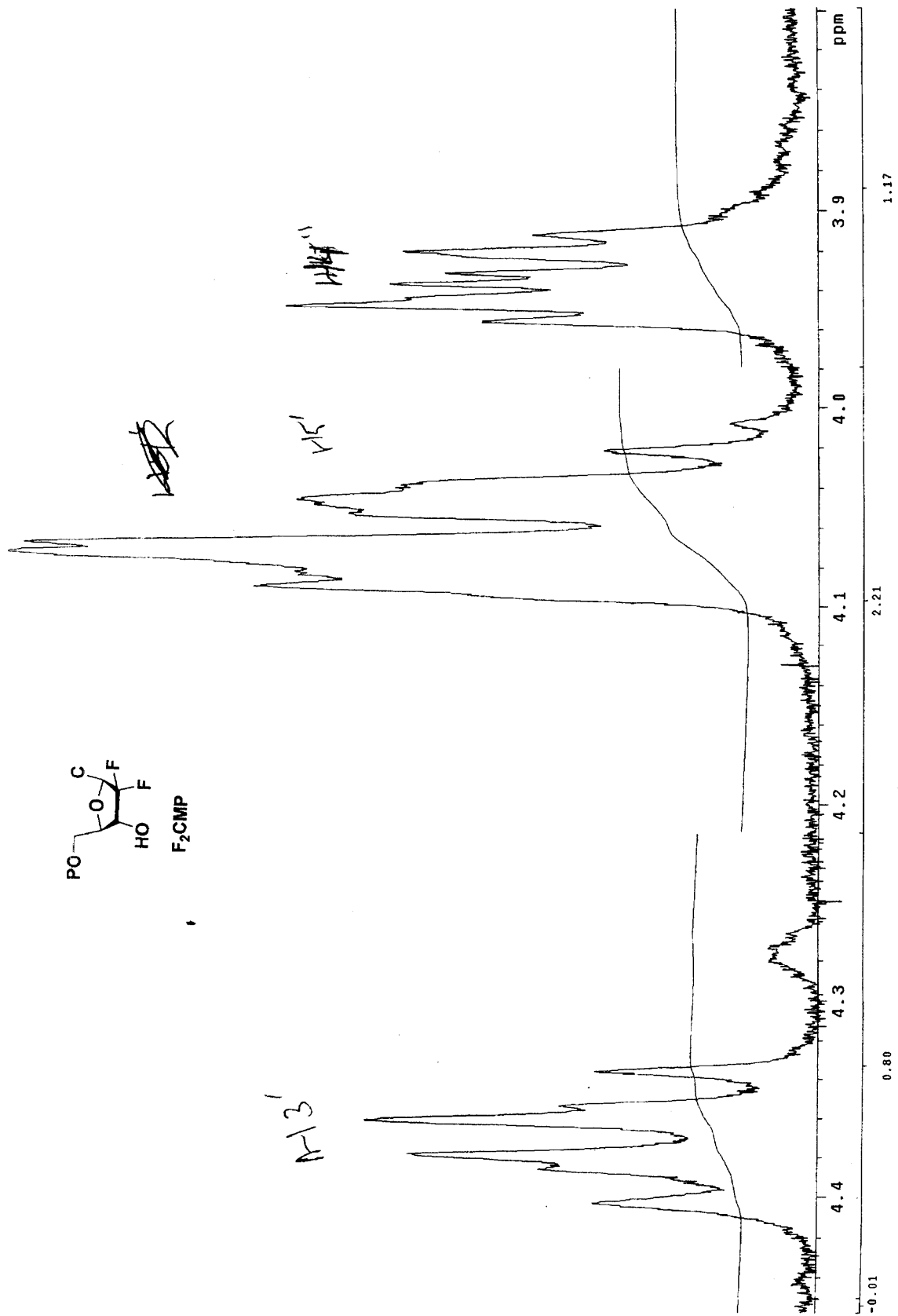
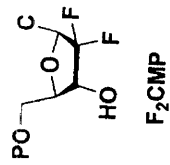
F2CMP
exp2 s2pul1

date	Nov 13 2003	DEC. & VI	125.877
solvent	D2O	dn	C13
file	exp	dpwr	34
ACQUISITION	499.757	dof	1498.1
sfreq	H1	dm	nm
tn	3.275	dmm	10000
at	3104	dmt	W
np	4748.3	dseq	1.0
sw	not used	dres	1.0
lb	16	homo	0
us	16	dfrq2	DEC2
tdwrt	8.2	dn2	0
rv	0	dpwr2	1
llf	-374.8	dot2	0
to	256	dm2	0
ct	84	dmm2	0
stlock	n	dmt2	200
galt	44	dseq2	1.0
ll	n	dres2	1.0
in	n	homo2	0
id	n	dfrq3	DEC3
dd	y	dn3	0
hs	nm	dpwr3	1
DISPLAY	-250.2	dot3	0
sp	4748.3	dms	0
vp	31365	dmm3	0
vs	0	dmt3	200
sc	250	dseq3	1.0
wc	18.99	dres3	1.0
hzmh	17041.85	homo3	0
is	250.2	wtfile	0
rf1	8	proc	65536
th	8	fn	f
ins	1.000	math	0
nm			



F2CMP

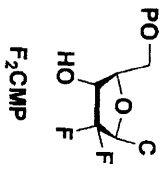
Pulse Sequence: s2pu1



6-1-154, MP

F2CMP 31P
exp2 s2pu1

SAMPLE		DEC. & VT	
date	Oct 30 2003	dfreq	300.101
solvent	D2O	dn	H1
file		dpwr	39
file		dof	0
ACQUISITION			
sfreq	121.485	dm	YY
tn	P31	dmm	W
at	1.261	dmf	11000
np	61204	td	PROCESsing
sw	24271.8	wf11e	1.00
fb	13400	proc	not used
bs	16	fn	ft
tpwr	62		
pw	10.0	werr	
dl	0.250	wexp	
tof	2337.3	wbs	
nt	1024	wnt	
ct	443		
alock	n		
gain	not used		
FLAGS			
i1	n		
in	n		
dp	Y		
DISPLAY			
sp	-99507.1		
wp	24271.1		
vs	121		
sc	0		
wc	250		
hzmm	20.16		
fs	354.40		
rf1	3507.5		
rfp	0		
th	0		
ins	116		
nm	100.000		
no	ph		



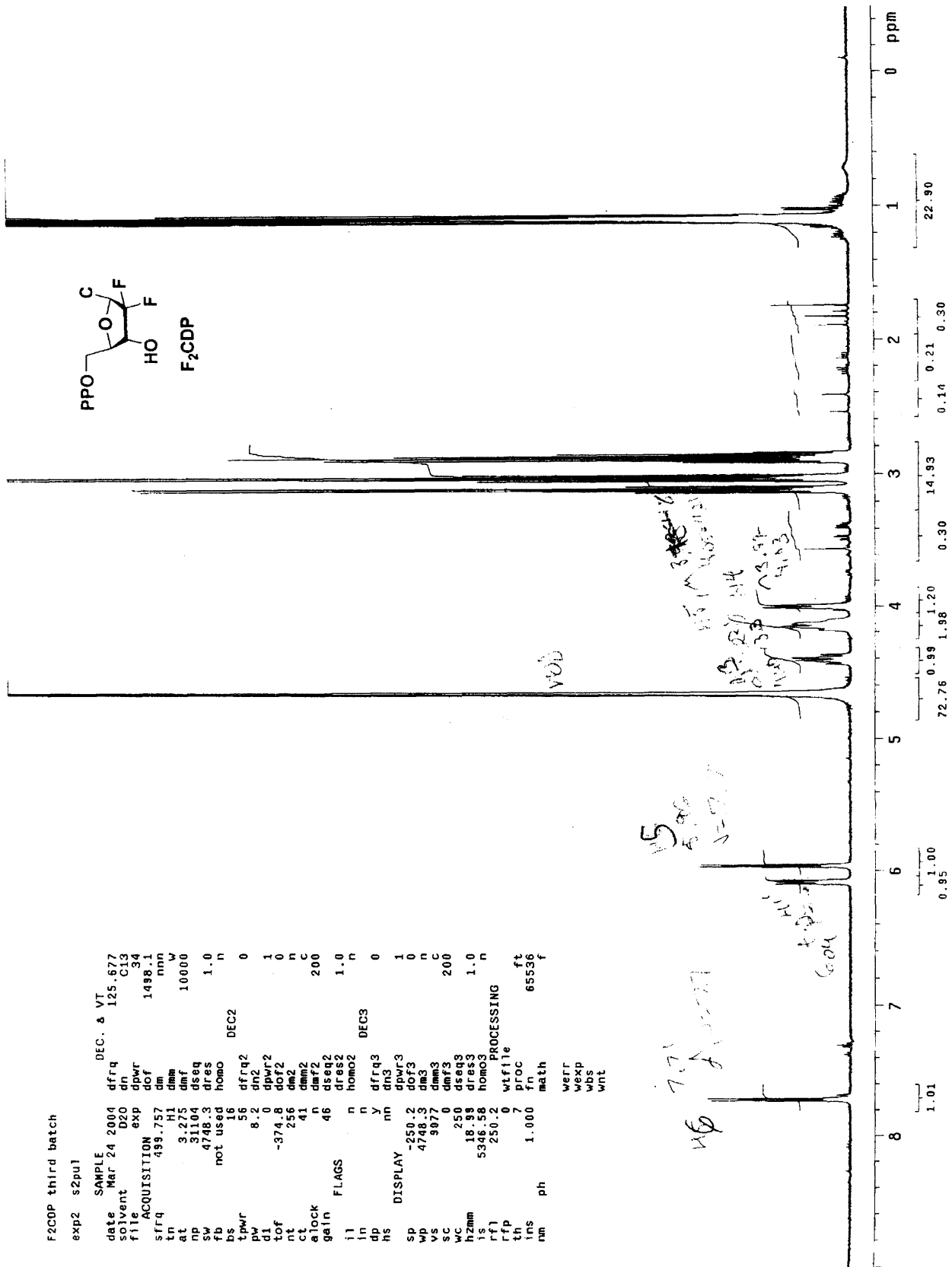
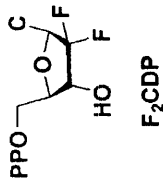
F2CDP third batch

exp2 s2pu1

```

SAMPLE DEC. & VT
date Mar 24 2004 dfrq 125.677
solvent D2O dn C13
file ACQUISITION exp 34 dpwr 1498.1
sfrq 499.757 dm nnn
tn HI W
dm 10000
at 3.275 dnf
np 31104 dseq
pw 4746.3 dres 1.0
fb not used homo DEC2
ts 56 dfrq2 0
tpwr 5.2 dn2
dw 8.2 dn3
df -374.8 dpr2 1
tf 256 dpr3 0
ct 41 dm2 n
slck 41 dm3 n
gain 46 dfr2 200
flags n homo2 1.0
il n dfrq3 0
in y dn3
hs nm dnw3 1
SP -250.2 dof3 0
WD 4748.3 dm3 n
VS 9977 dm3 C
SC 0 dm3 200
WC 250 dseq 1.0
hzmm 18.99 dres9
is 5346.58 homo3 n
rfl 250.2 wfile
rfp 7 proc ft
th 7 fn 65536 f
ins ph math
nm werr
wexp
wbs
wnt

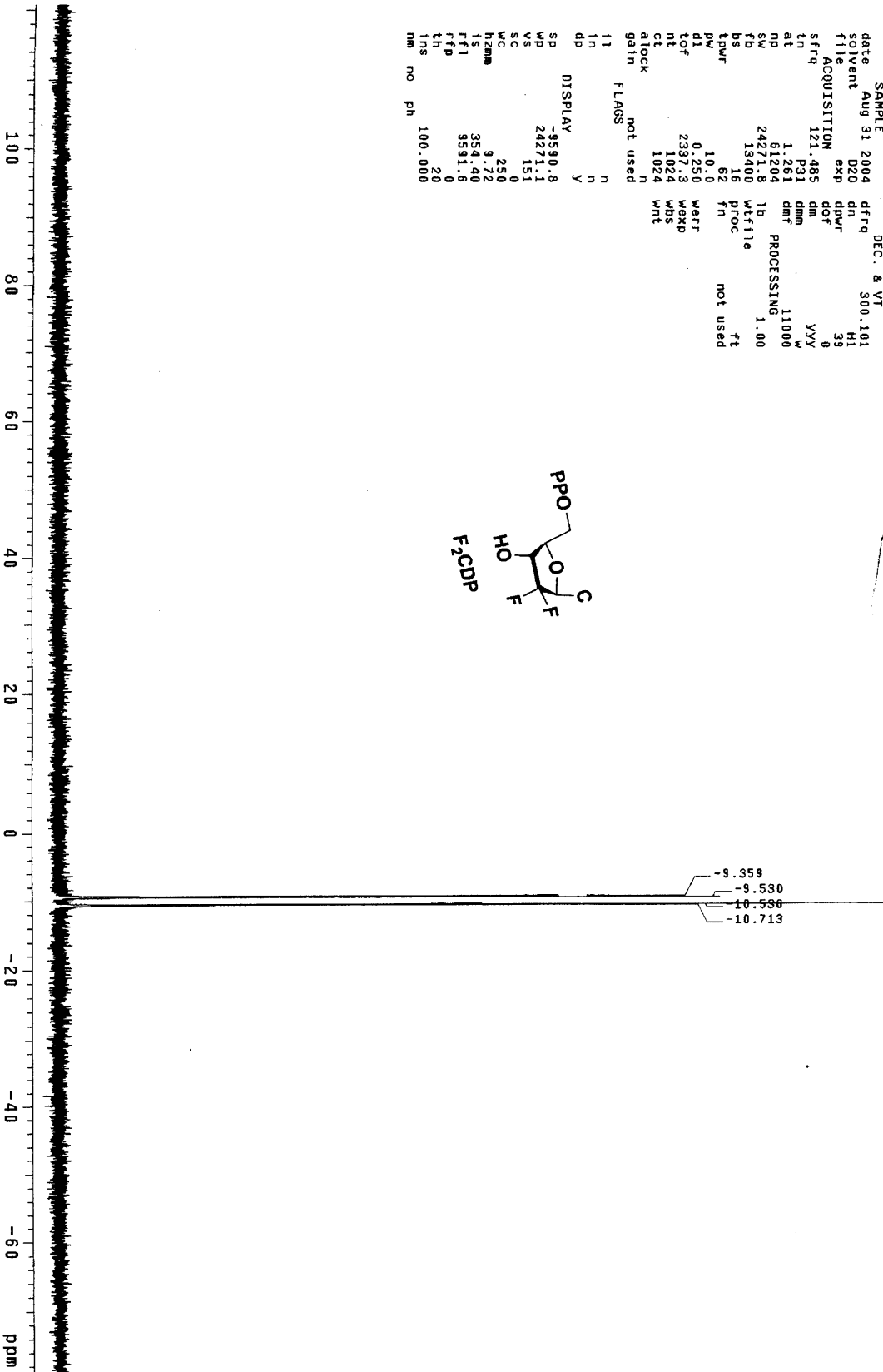
```



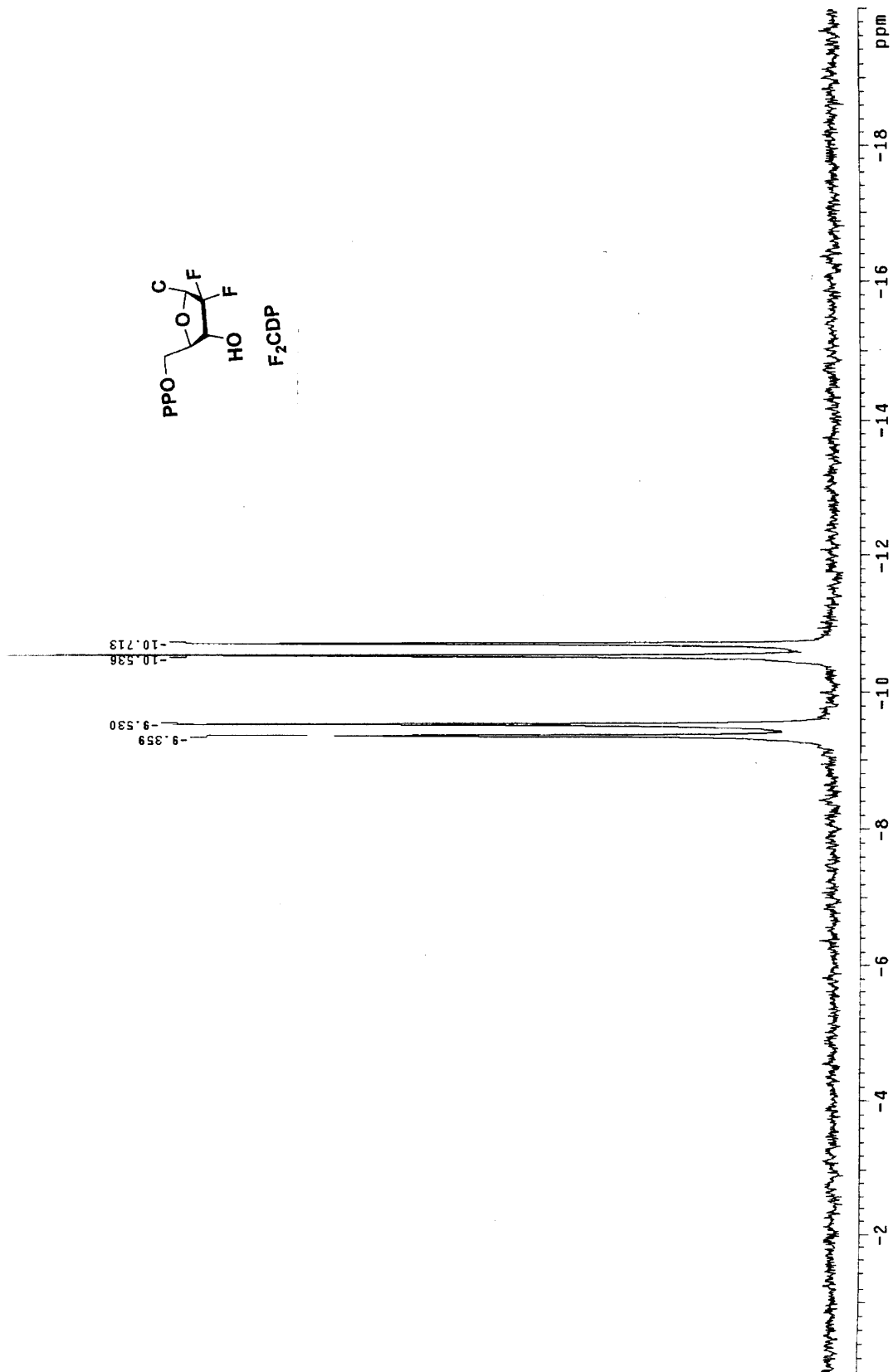
F2CDP. ref to H3P04, 8/31/04

exp2 s2pu1

SAMPLE DEC. 8 VT
date Aug 31 2004 dfrq 300.101
solvent D2O dn 51
file exp dpuw 51
ACQUISITION exp dof 32
sfrq 121.485 dm yyy
tn p31 dmm
at 1.281 dmf PROCESSING 1.00
np 61204 lb
sw 24271.8 wfile
fb 13400 wproc
bs 15 fn not used
tpwr 62 ft
pw 10.0 werr
d1 0.250 wexp
tof 2397.3 wbs
nt 1024 wnt
ct 1024
atlock not used
gain not used
flags not used
11 n
1n n
dp y
DISPLAY
sp -9590.8
wp 24271.1
vs 151
sc 0
wc 250
hzmm 9.72
ls 354.90
ftf 3591.6
th 0
rms 100.000
nm no ph

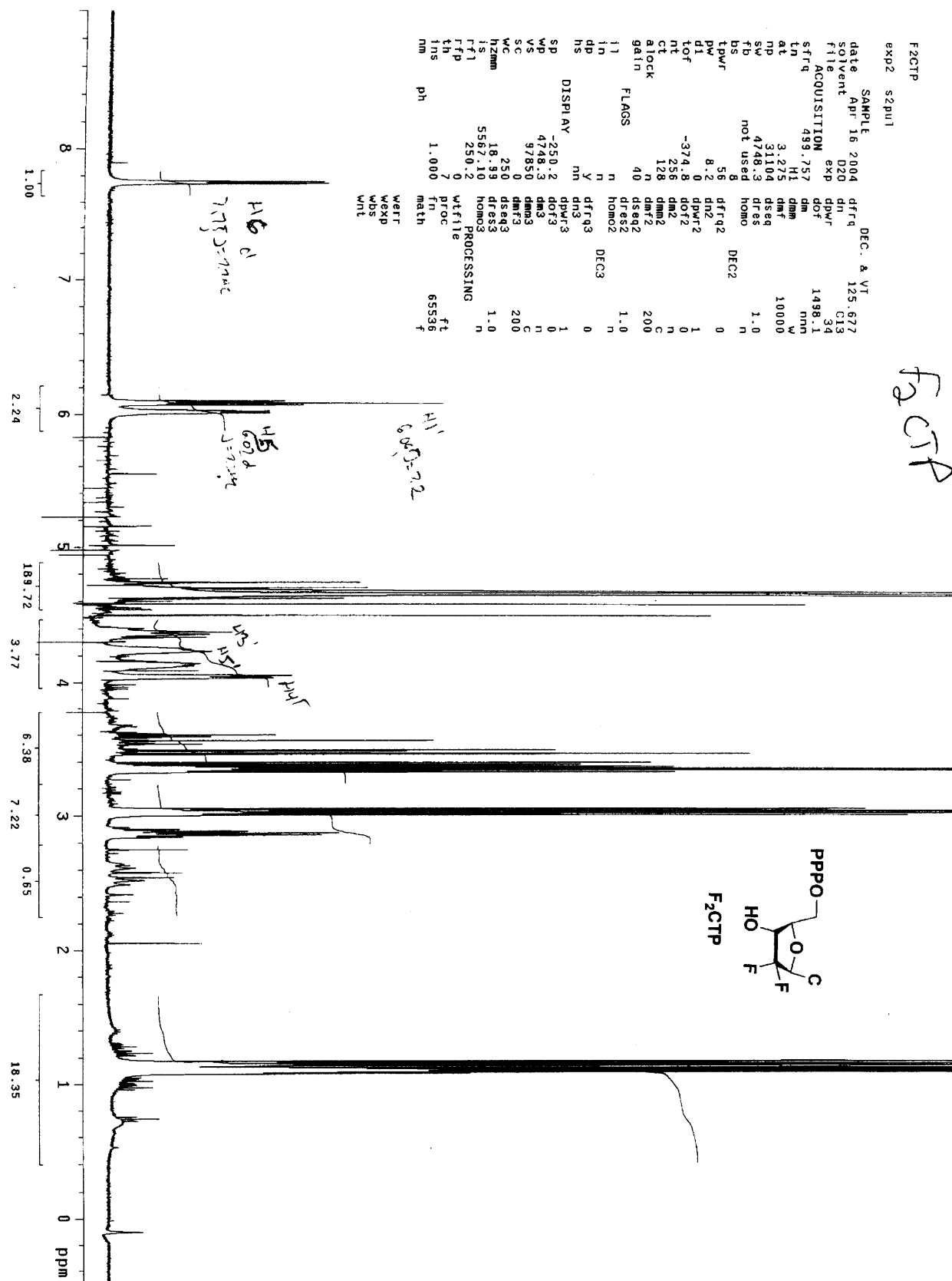
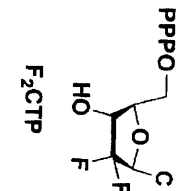


F2CDP. ref to H3P04, 8/31/04
Pulse Sequence: s2put

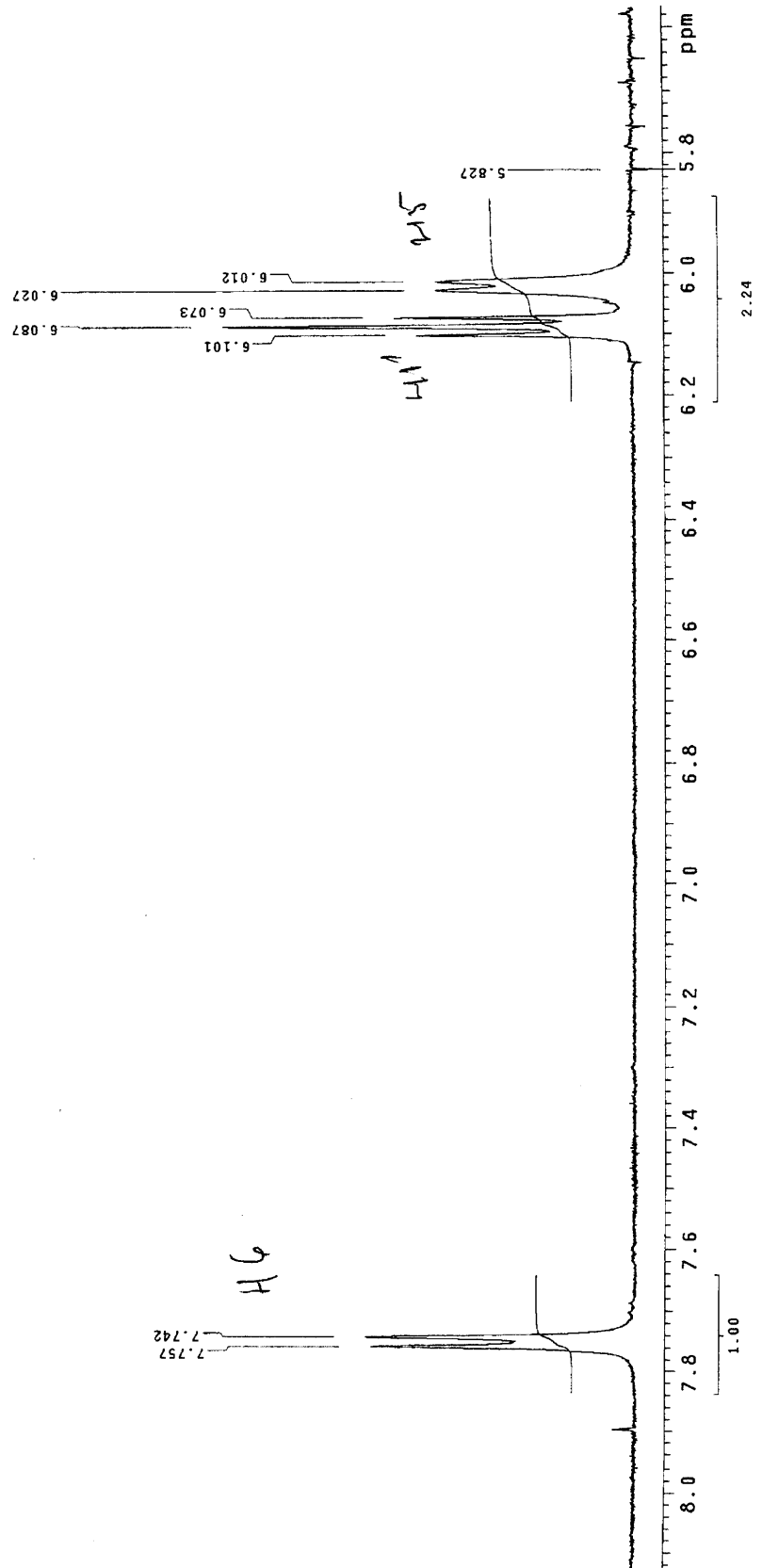
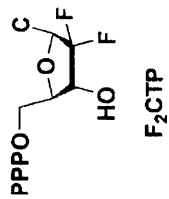


F2CTP

FaCTP



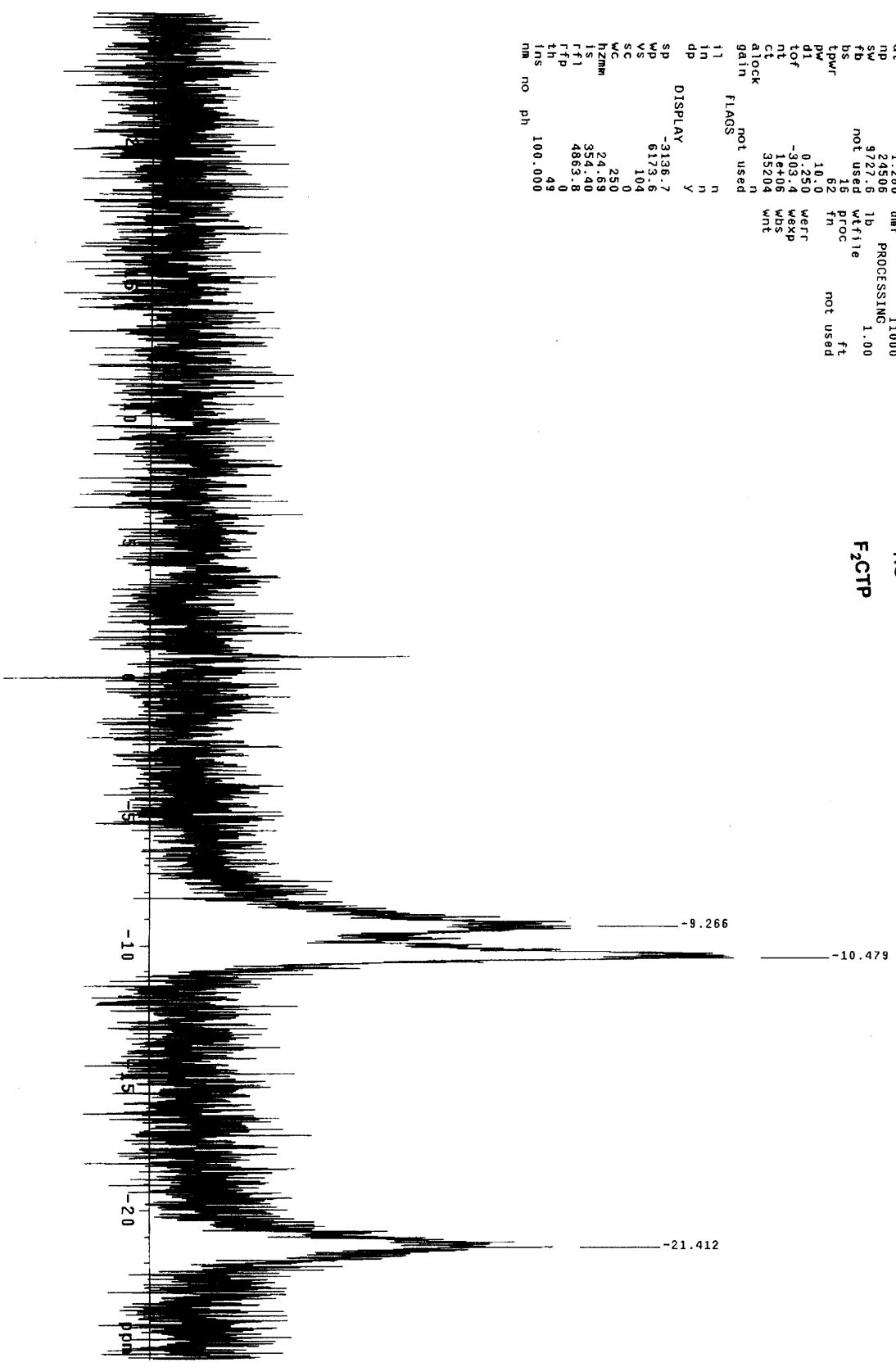
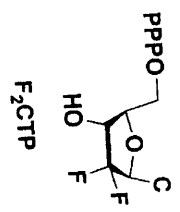
F2CTP
Pulse Sequence: s2pul



319

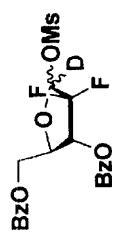
FACITP
exp2 s2pu1
SAMPLE DEC. & VT
date Apr 16 2004 dfreq 300.101
solvent D2O dn H1
file exp dpwr 39
ACQUISITION dof 0
sfrq 121.482 dm dmm yyy
tn P31 dmm w
at 1.260 dmf 11000
np 24506 PROCESSING 1.00
sw 9727.6 lb wfile
fb not used wtfile
bs not used proc ft
tpwr 62 fn
pw 10.0 werr not used
d1 0.250 wexp
tof -303.4 wbs
nt 1e+06 wnt
ct 35204
alock n
gain not used
flags n
i1 n
i2 n
dp DISPLAY y

DISPLAY
SP -3136.7
WP 6173.6
WS 104
SC 0
SC 250
h2mm 24.68
IS 324.40
rfi 4883.8
th 49
ins 100.000
nm no ph

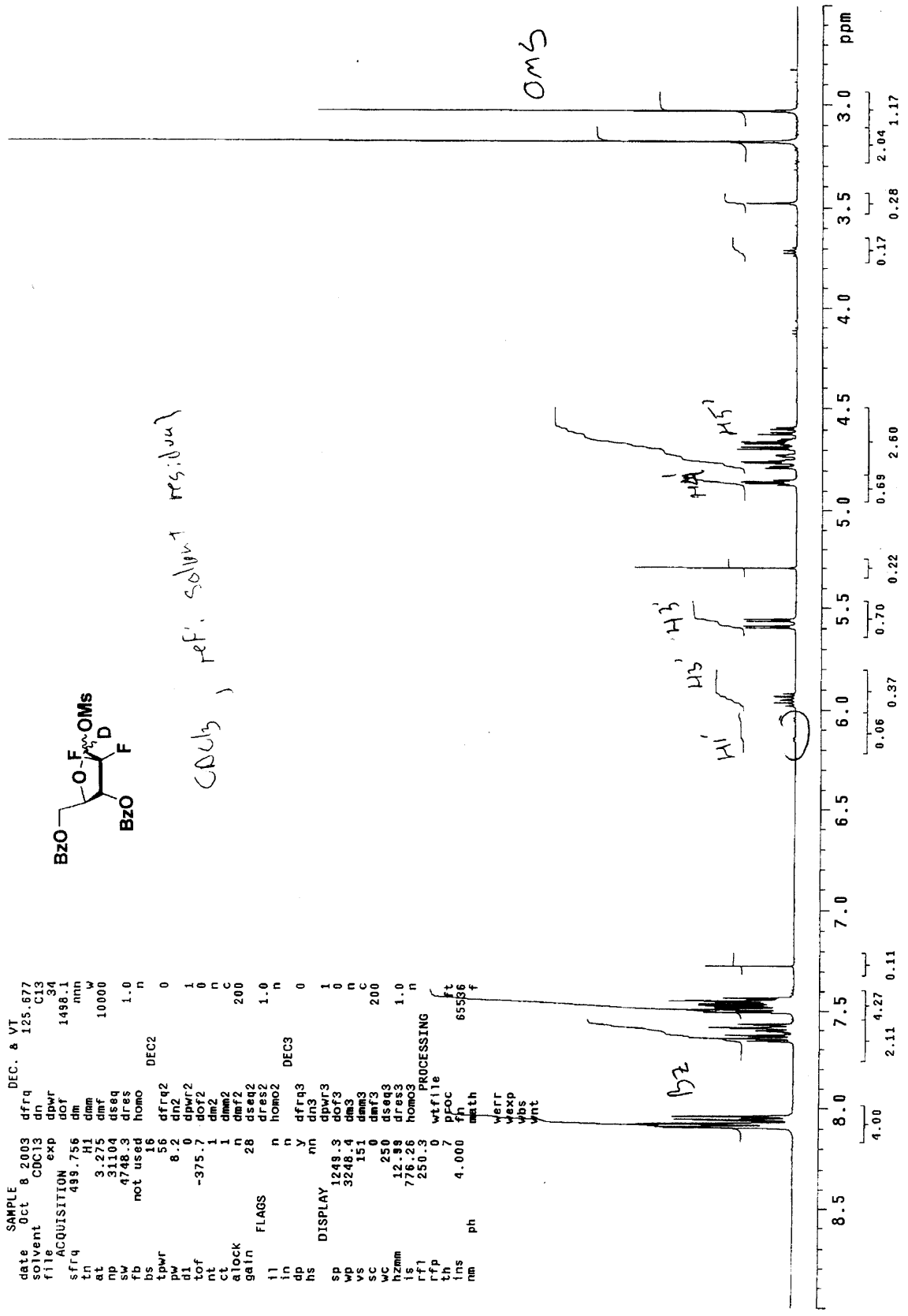


GL-1-1315, 1-D mesylate
exp2 s2pu1

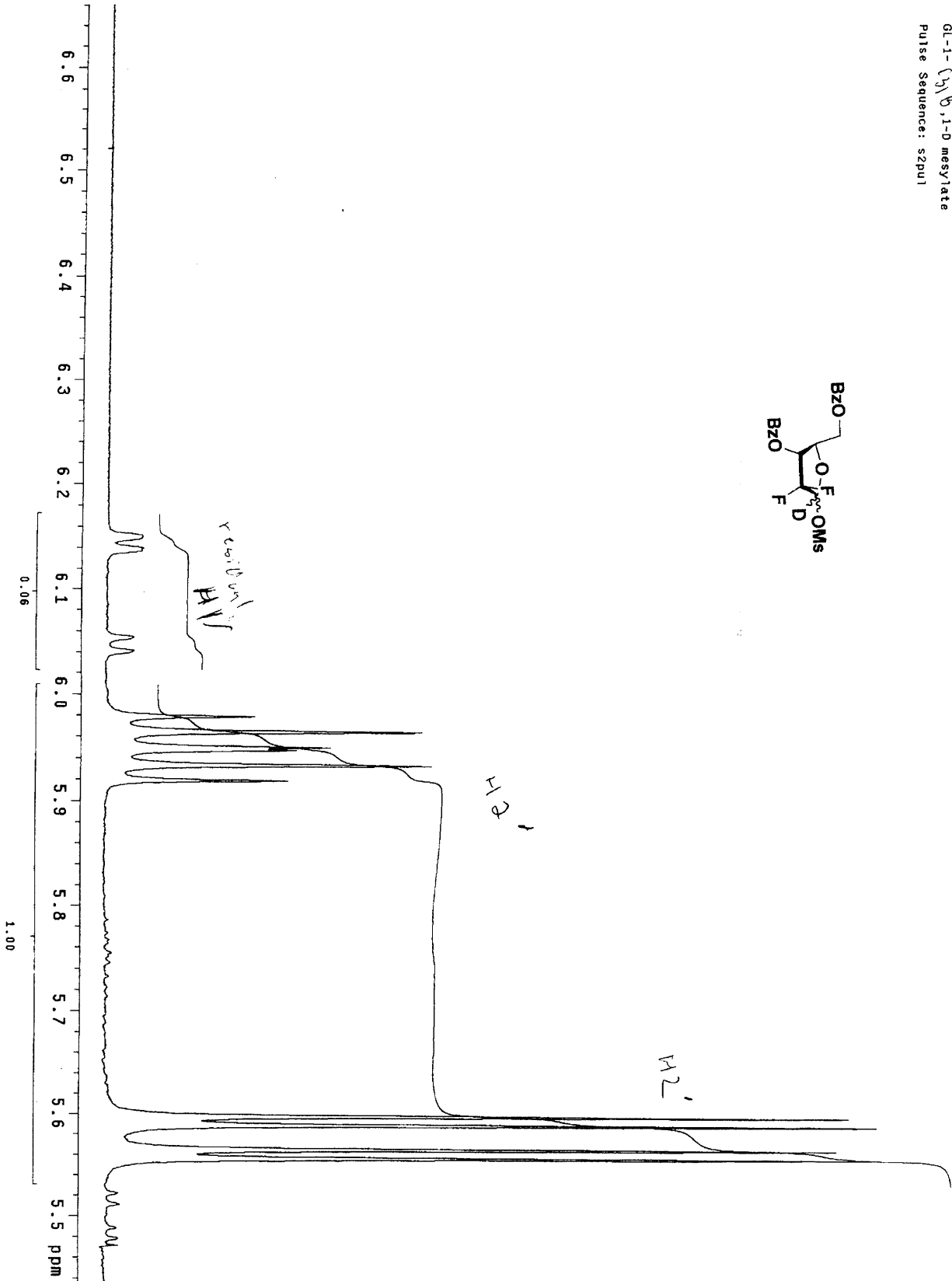
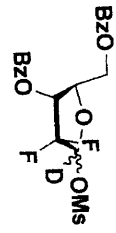
DEC. & VI
 SAMPLE date 8.2003 dfrq 125.677
 solvent Oct CDC13 dn C13
 file 34
 ACQUISITION exp dpr 1498.1
 dof 34
 tfrq 499.756 dm rnh
 tn H1 dnm W
 at 3.275 dmf 10000
 np 31104 dseq
 sw 4748.3 dres
 fb not used homo 1.0
 bs 16 DE2
 i6
 tpwr 56 dfrq2 0
 pw 8.2 dn2
 dl 0 dpwr2 1
 tof -375.7 dof2 0
 nt 1 dm2 n
 ct 1 dnm2 C
 alock n dmf2 200
 gain 28 dseq2
 dres2 1.0
 homo2 n
 homo3 DE2
 flags n
 in n dfrq3 0
 dp y dn3
 hs nn
 DISPLAY
 sp 1249.3 dpwr3 1
 wp 3248.4 dof3 0
 vs 151 dm3 n
 sc 151 dnm3 C
 wc 0 dmf3 200
 hzmm 250 dseq3
 ls 12.98 dres3
 rfl 776.26 homo3 1.0
 rfp 250.3
 PROCESSING
 wifile ft
 fh 65586
 math f
 ph
 verr
 maxp
 vbs
 vnt



CDCl3, ref. solvent residual

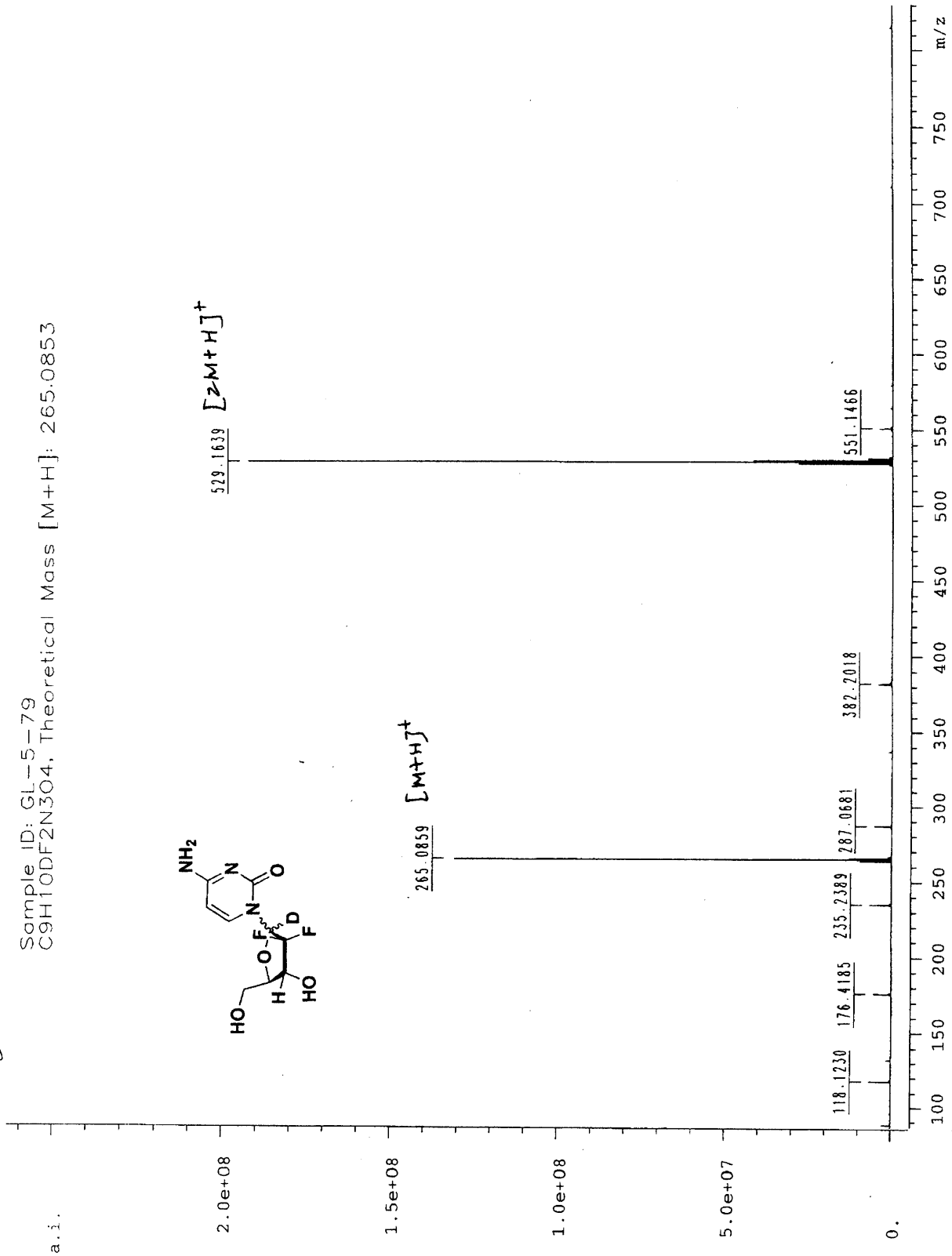
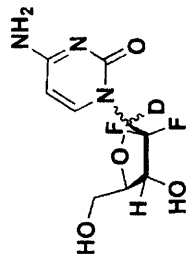


GL-1- (2) 6,1-D mesylate
Pulse Sequence: szpu1



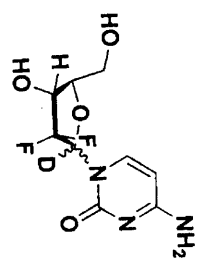
Greg Lohman (Stubbbe) x3-0084

Sample ID: GL-5-79
C9H10DF2N3O4, Theoretical Mass [M+H]⁺: 265.0853

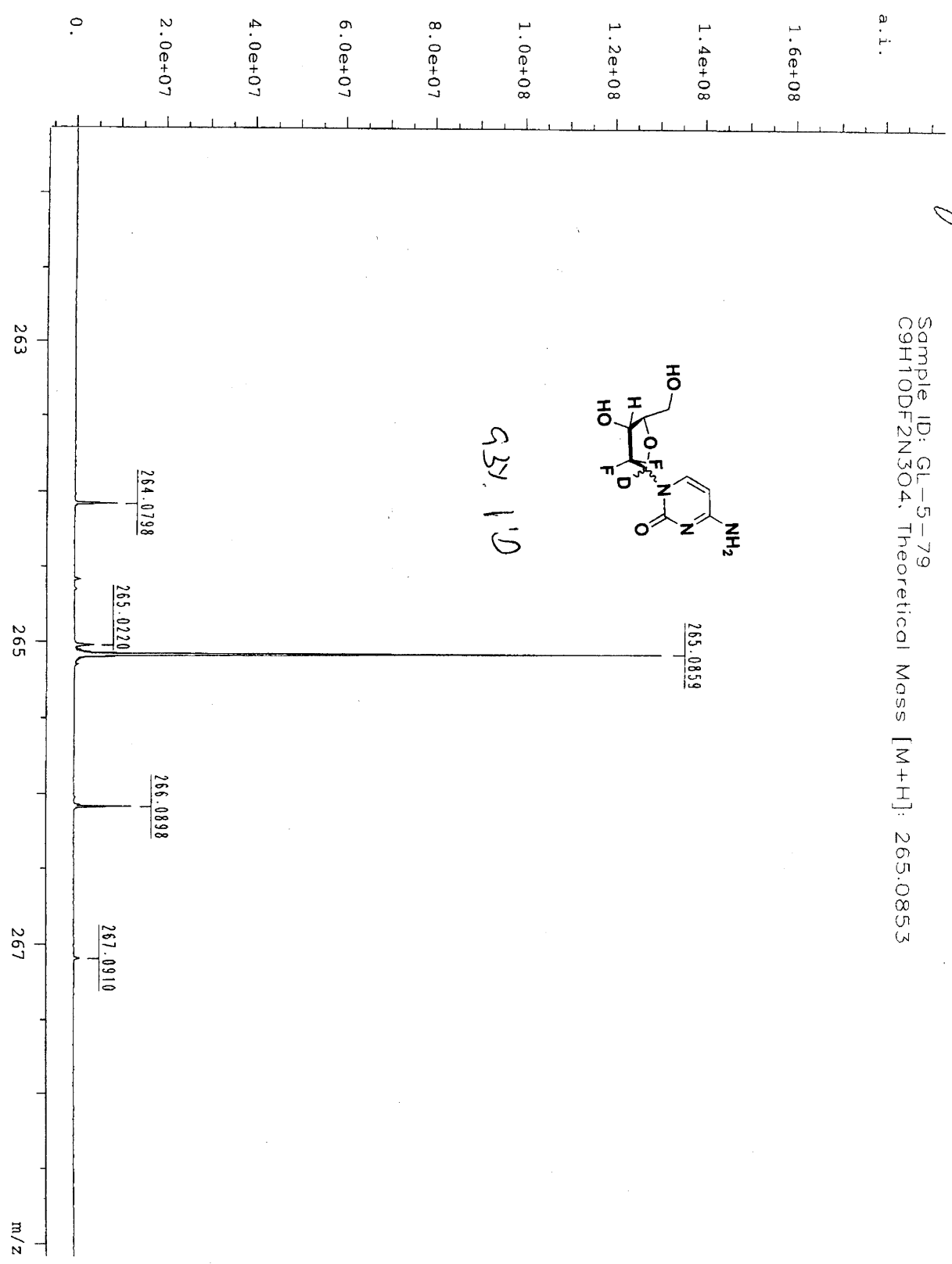


Greg Lehman

Sample ID: GL-5-79
C9H10DF2N3O4, Theoretical Mass [M+H]: 265.0853

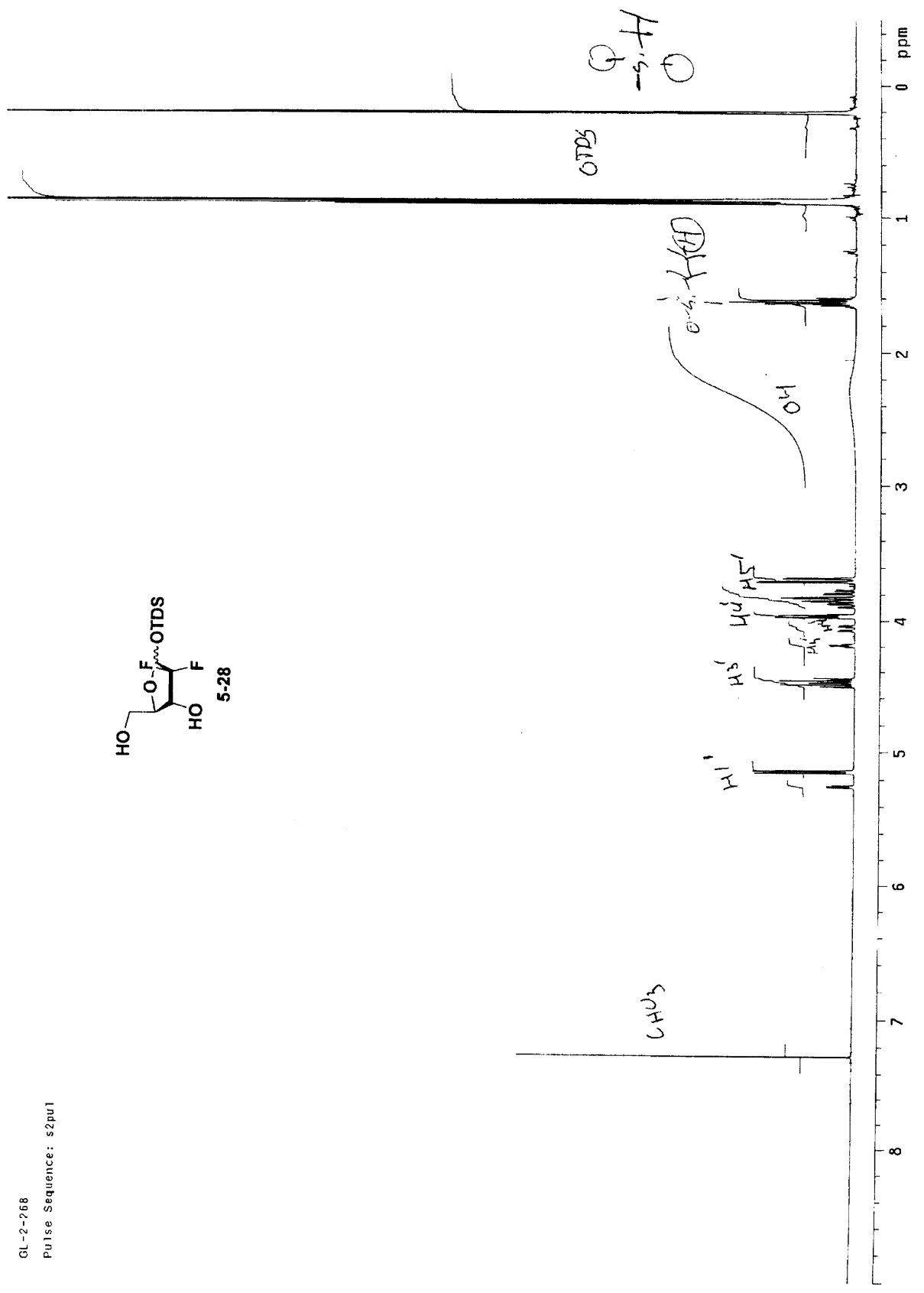
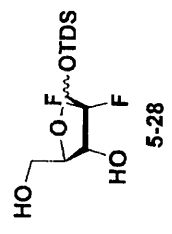


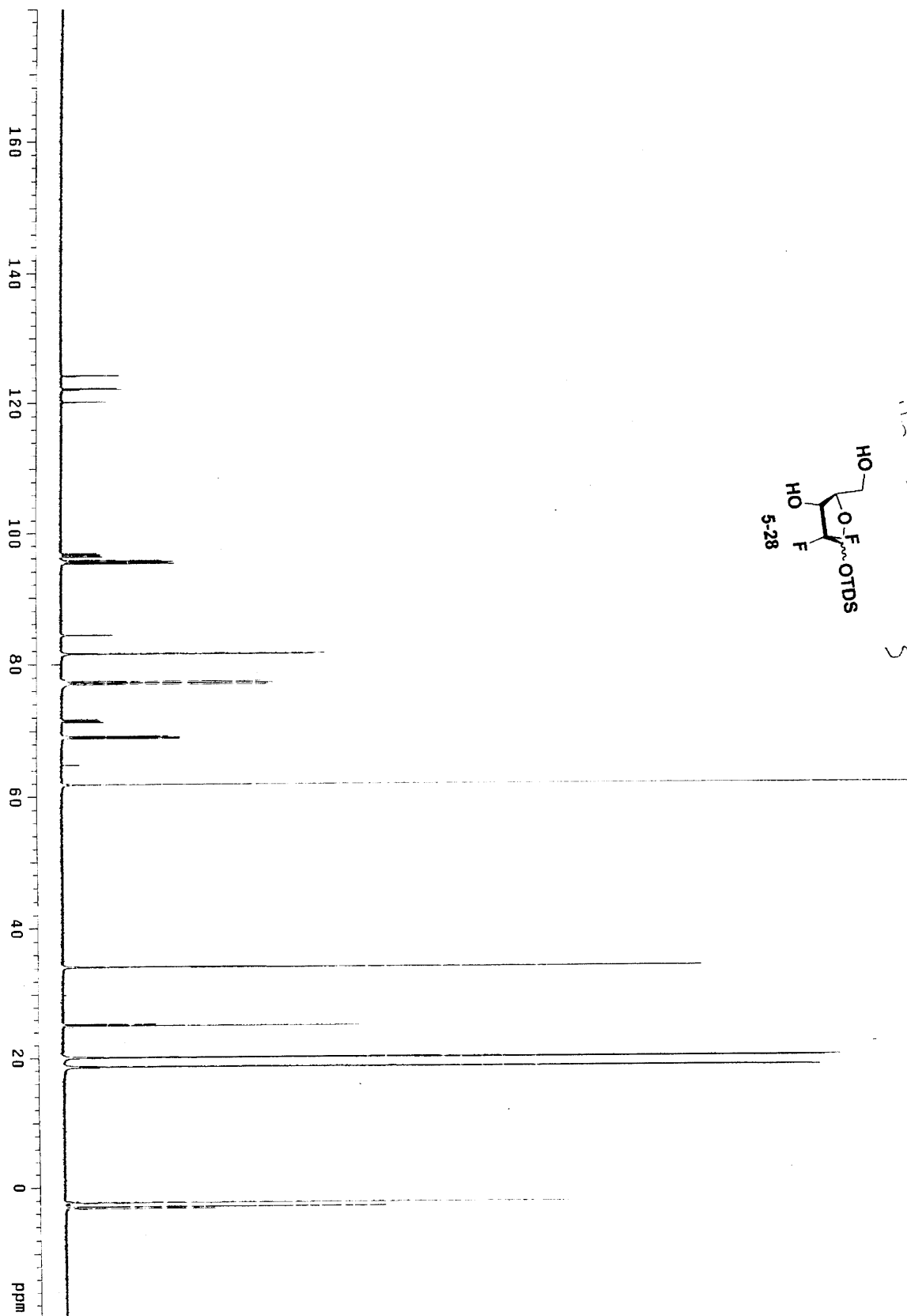
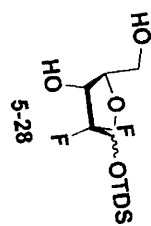
93% 1'D



/Bruker/data/2006/ST/STgl0h_ESI/GL-5-79/pdata/1 FTMSuser Thu Oct 5 11:28:38 2006

GL-2-268
Pulse Sequence: s2pu1



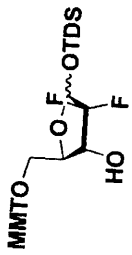


GL-3-20

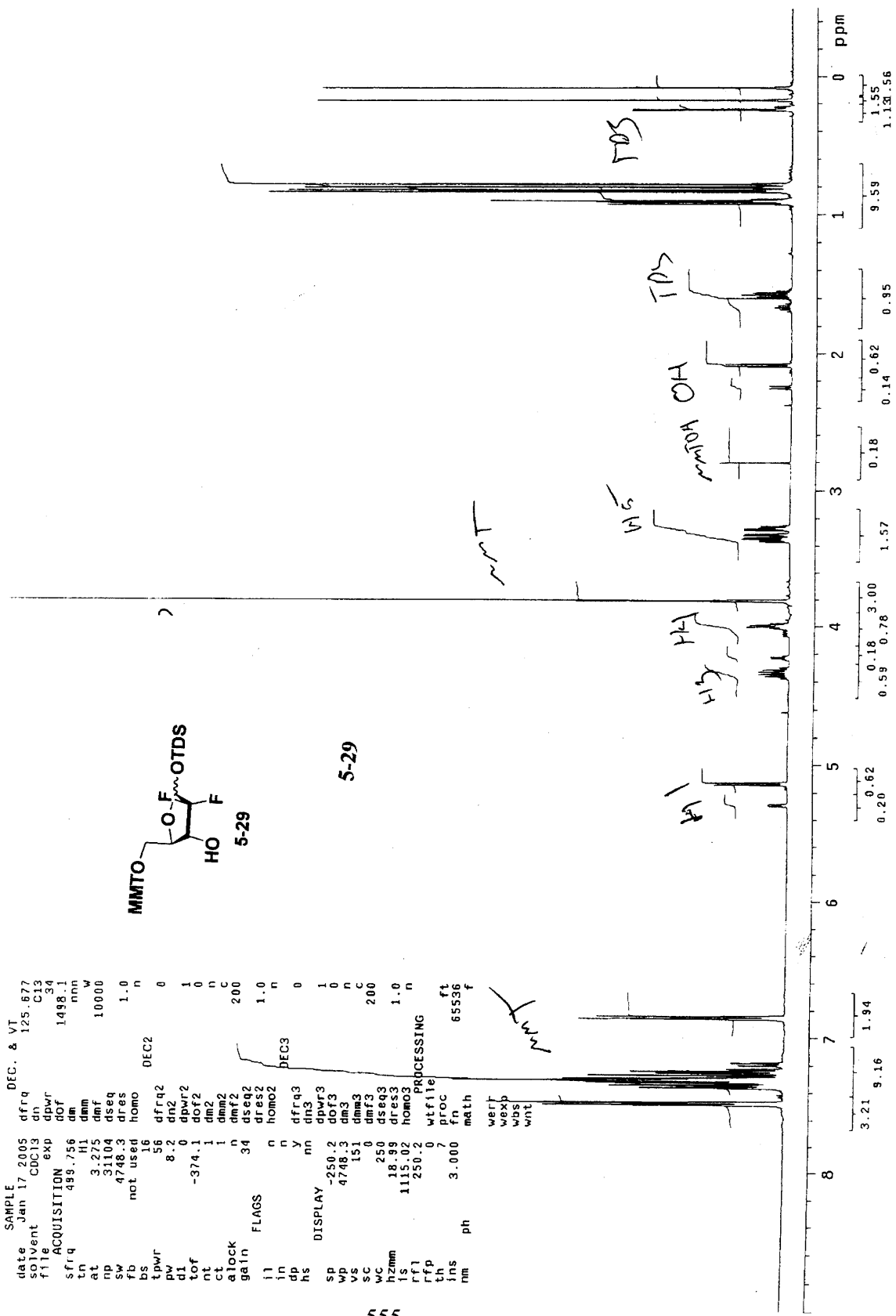
exp2 s2pu1

```

SAMPLE          DEC. & VT
date            Jan 17 2005   dfrq 125.677
solvent         CDC13        ah   C13
file           1498.1       apwr 34
ACQUISITION    499.756     aq  1498.1
sfrq           499.756     dm   nnn
tn            3.275        dmw  10000
at            31104        dmf  W
np            4748.3       dseq
sw            not used     dres 1.0
fb            16          homo  n
bs            56          DECE2
tpwr         8.2         dfrq2 0
pw           374.1       dfr2  1
d1           -374.1       ddf2  0
nt            1         dm2   n
ct            1         dmf2  n
alock        34         dseq2 200
gain         n          dres2 1.0
FLAGS        n          homo2 n
il           Y          dfrq3 0
in           Y          dm3   1
dp           Y          ddf3  0
hs           Y          dmms  n
          mn          dmf3  n
          nn          dseq3 200
          nn          dres3 1.0
          nn          homo3  n
DISPLAY      -250.2      wfile  ft
          4748.3         wproc  85536
          151          math   f
          250          wexb
          18.99         wbs
          1115.02       wnt
          250.2
          3.000
          7
          85536
          fn
          math
          wexb
          wbs
          wnt
          ph
  
```



5-29

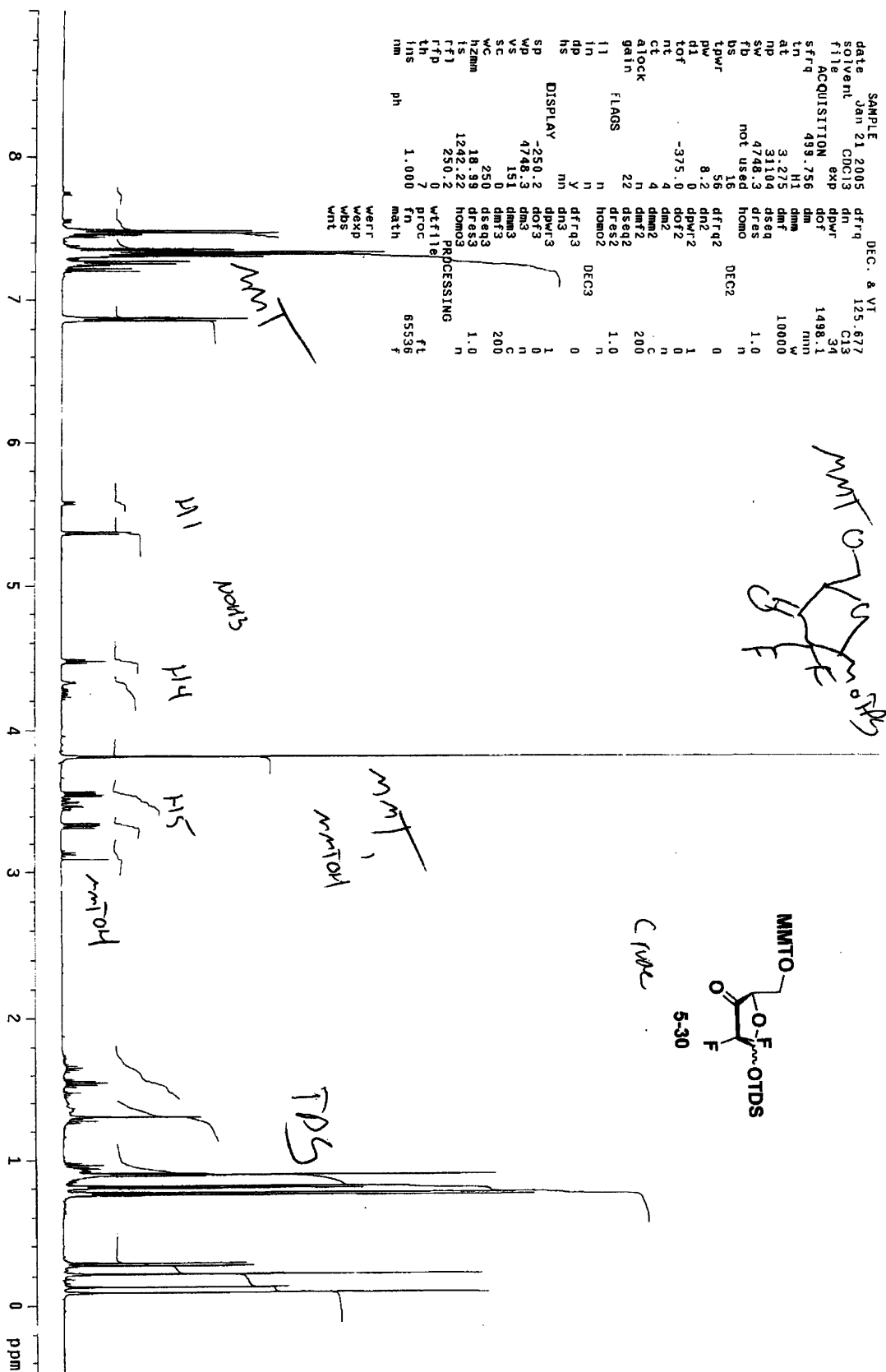


GL-3-24, 5-MMT, 3-ketone

exp2 s2pui

SAMPLE Jan 21 2005 DEC. & VI
 solvent CDC13 dn 125.677
 file exp dpwr C13
 ACQUISITION 499.756 dm 34
 sfreq H1 dmf 1498.1
 ln H1 dma 10000
 at 3.275 dmt w
 mp 31104 dseq
 SW 4748.3 dres 1.0
 FB not used homo
 US 16
 LPWR 56 dfrq2 DEC2 0
 PW 8.2 dnr2
 Q1 0 dpwr2 1
 LOF -375.0 dorf 3
 TC 4 dm2 n
 CL 4 dm2 C
 atlock n dmr2
 gain 22 dseq2 200
 11 dres2
 in n homo2 1.0
 dp n
 hs y dfrq3 DEC3 0
 DISPLAY -250.2 dm3 1
 SP 4748.3 dnr3 0
 VS 151 dms 0
 SC 0 dmf3 200
 WC 250 dseq3
 hzmm 18.99 dres3 1.0
 IS 1242.22 homo3
 rffl 250.2
 rfp
 th
 ins
 nm ph 1.000 math

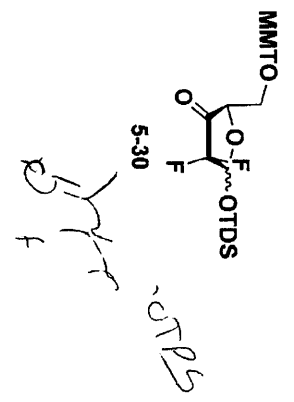
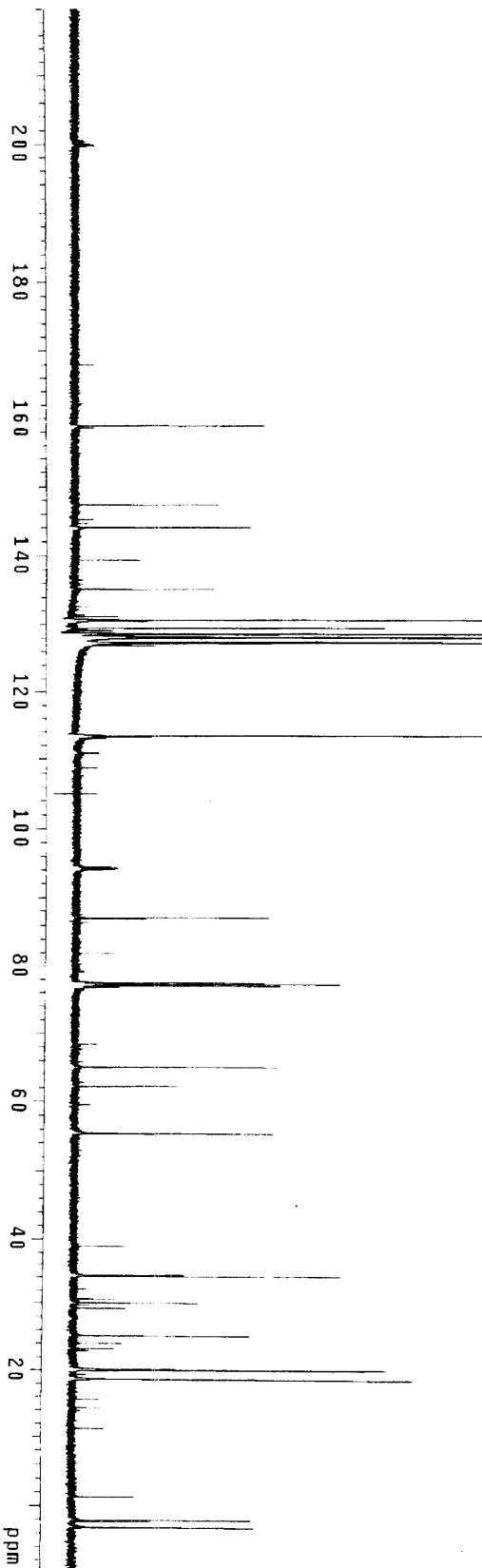
PROCESSING
 wfile ft
 proc 65536
 fn
 verr
 wexp
 wds
 wnt



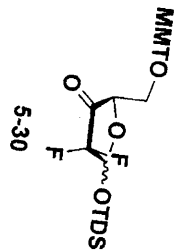
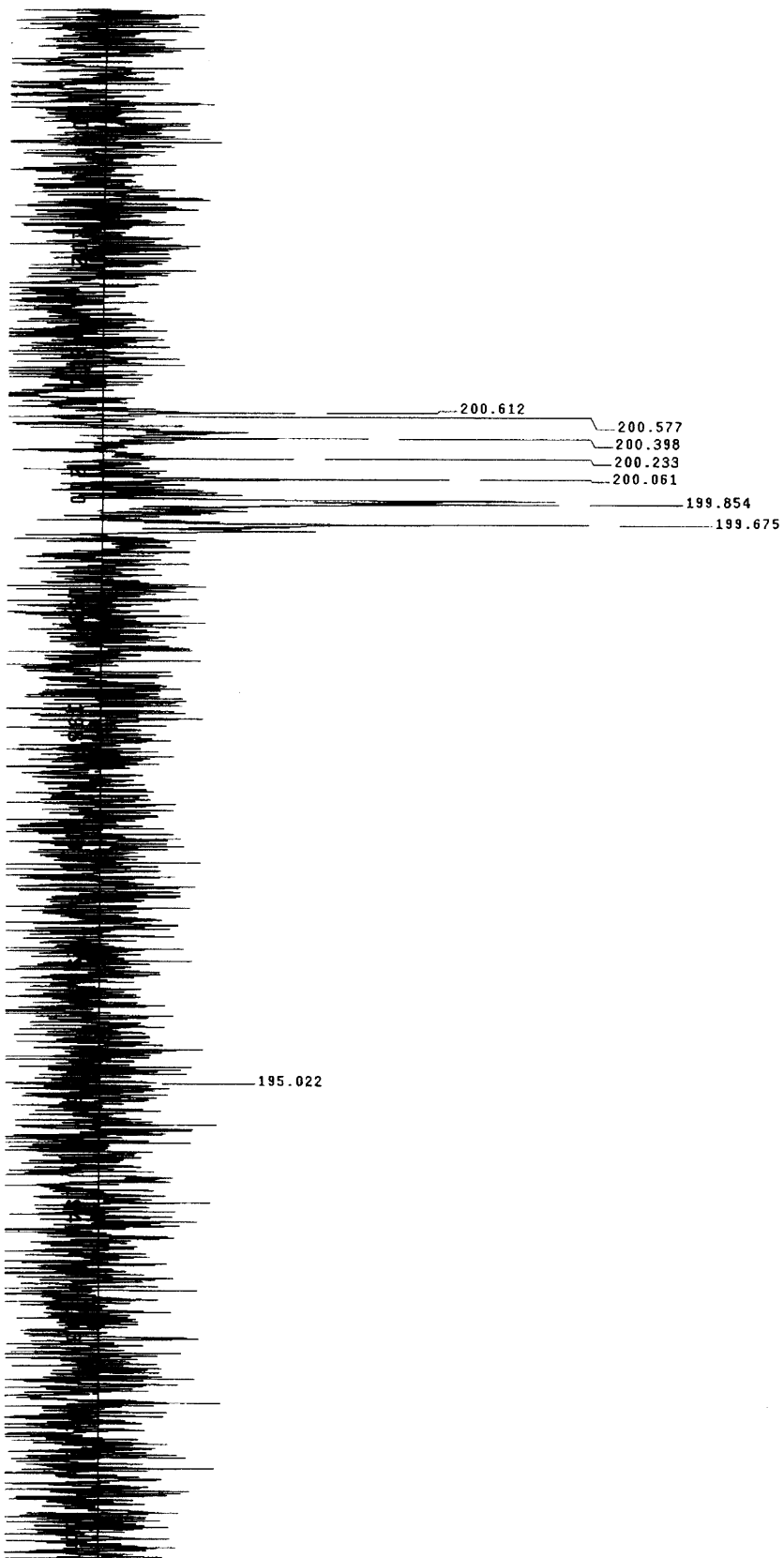
GL-2-24, 5-mm, 3-keto

expi szput1

SAMPLE DEC. 8 VT
 date Jan 22 2005 dfreq 500.233
 solvent CDCl3 dn H1
 file /data/export/~ dpwr 37
 home/jastub/jg1/fr0- dof -500.0
 CKY/GL-3-24C.fid dm
 ACQUISITION dmm
 sfreq 125.796 dmf 10000
 tn C13 dres
 et 1.736 dseq 1.0
 np 100448 homo
 sw 28933.1 PROCESSING 0.30
 fb not used 1b wtfile ft
 bs 8 wtfile 131072 f
 ss 1 pproc
 tdwr 53 fn math
 pw 6.9
 dl 0.763
 tof 1265.5 werr
 nt 1e+06 wexp
 ct 1821 wbs
 alock n wnt
 gain not used
 flags
 i1 n
 in n
 dp y
 hs nn
 DISPLAY
 sp -1257.8
 wp 28932.7
 vs 8954
 sc 0
 wc 250
 hzmm 115.73
 ls 500.00
 rfl 10973.3
 rfp 9715.0
 th 9
 at 1.000
 al ph



GL-2-24, 5-mmT, 3-Keto
Pulse Sequence: szpu1



GI-3-36

```

exp2  s2pu1
SAMPLE
date   Feb 2 2005
solvent CDC13
file   CDC13
ACQUISITION
sfrq   488.756
at     9.275
np     31104
sw     4748.3
fb     not used
bs     16
tpwr   56
pw     8.2
d1     0
tof    -375.3
nt     1
ct     1
alock  n
gain   32
FLAGS  n
i1     n
in     n
dp     n
hs     n
SP     -250.3
VS     4748.3
WC     487
h2mm  0
is     18.99
rfl    1449.86
rfp    250.3
th     0
ins    7
rm     1.000
ph     65536
werr   wexp
wbs    wbs
wnt    wnt

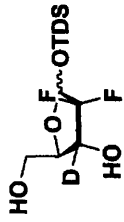
```

DEC. & VT

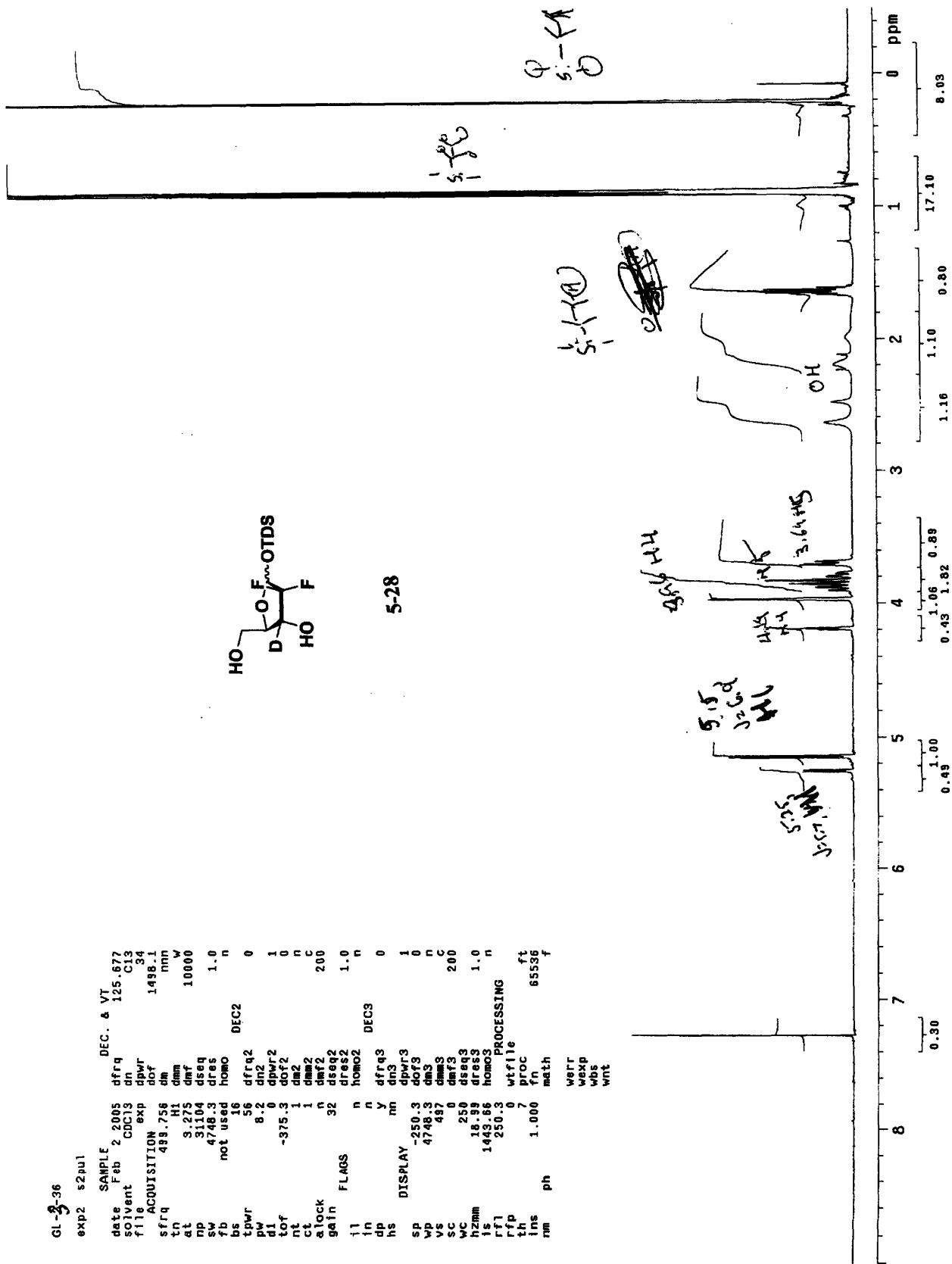
```

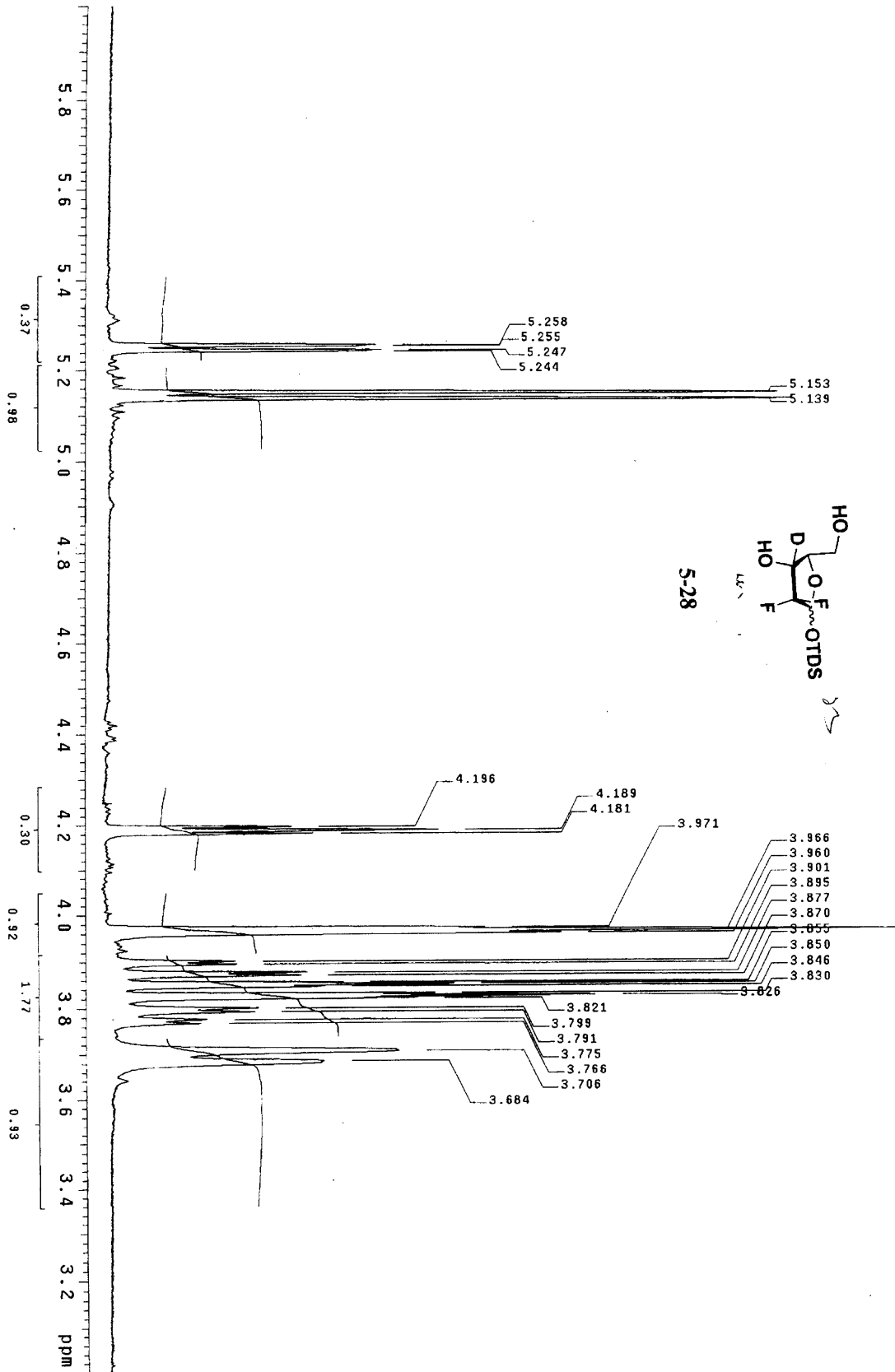
dfrq   125.877
dn     C13
dpr    34
dof    1498.1
dm     mmn
dm2    W
dms    10000
dres   1.0
dres2  n
dres3  DEC2
dfrq2  0
dn2    8-2
dpr2   0
dof2   0
dm2    0
dm2    1
dm2    n
dm2    C
dms2   200
dres2  1.0
dres3  DEC3
dn3    0
dpr3   1
dof3   0
dm3    n
dm3    C
dm3    C
dms3   200
dres3  1.0
dres3  n

```

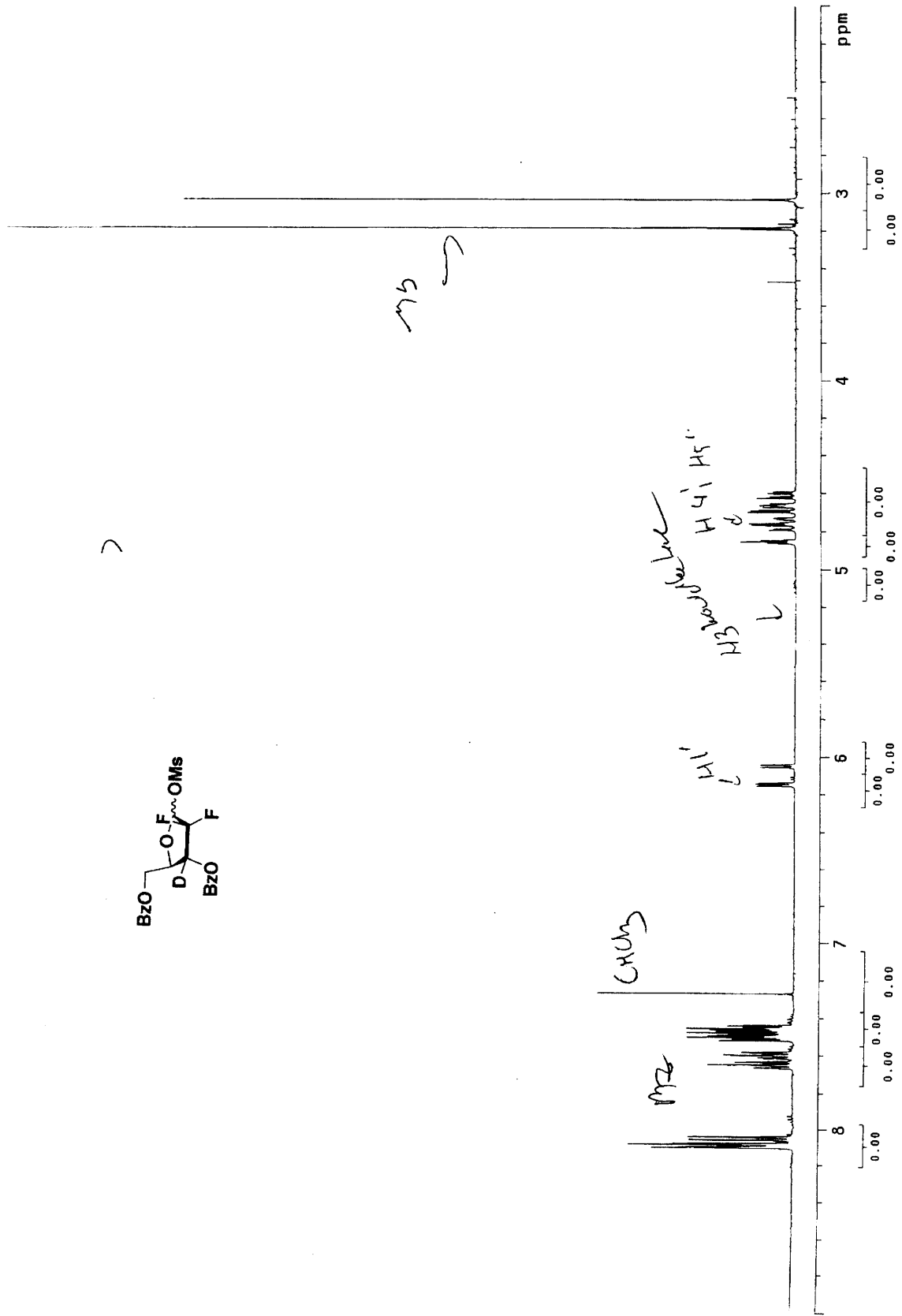


5-28

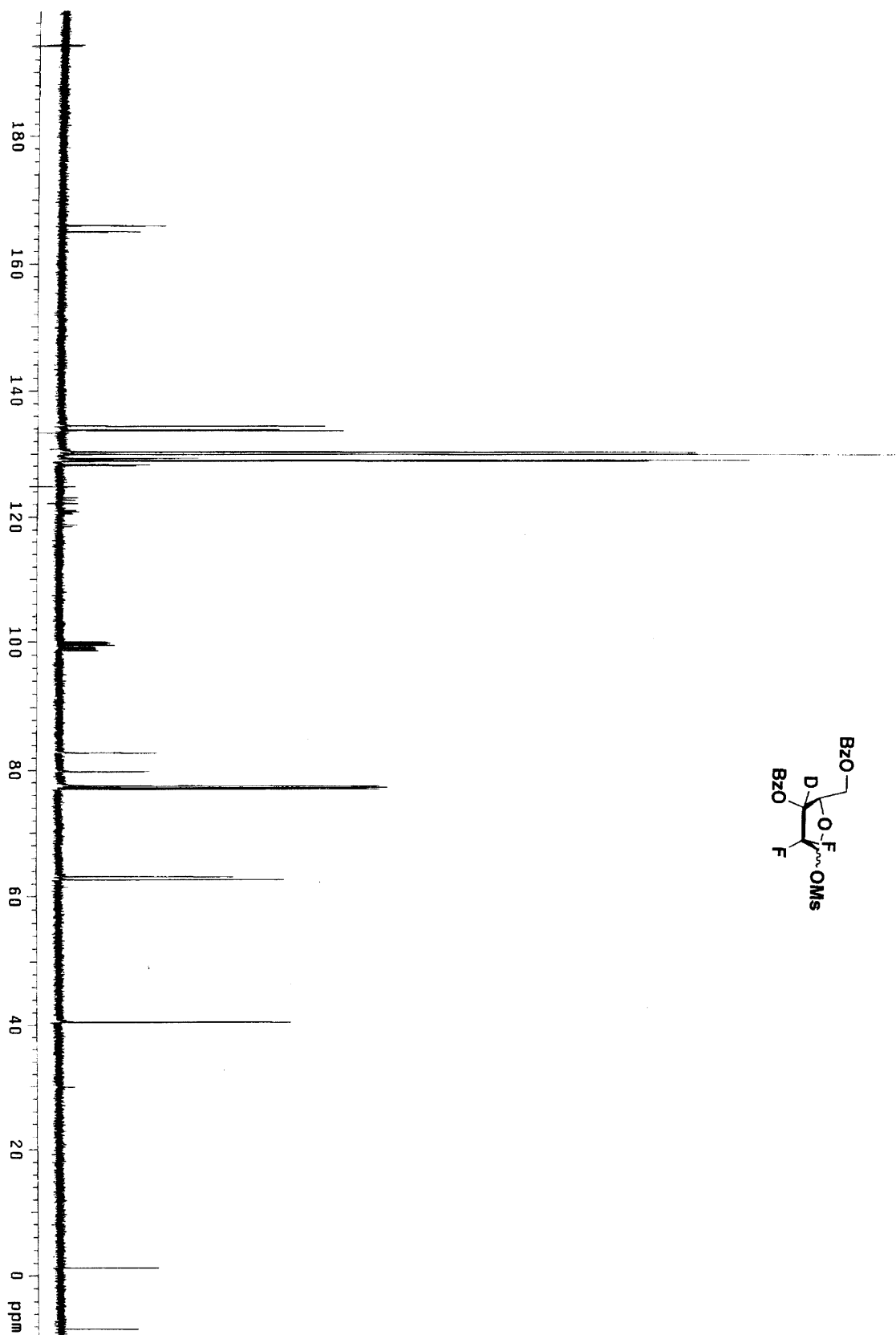
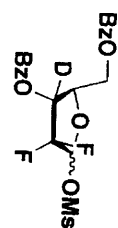




3-deutero-mesylyate
Pulse Sequence: s2pul

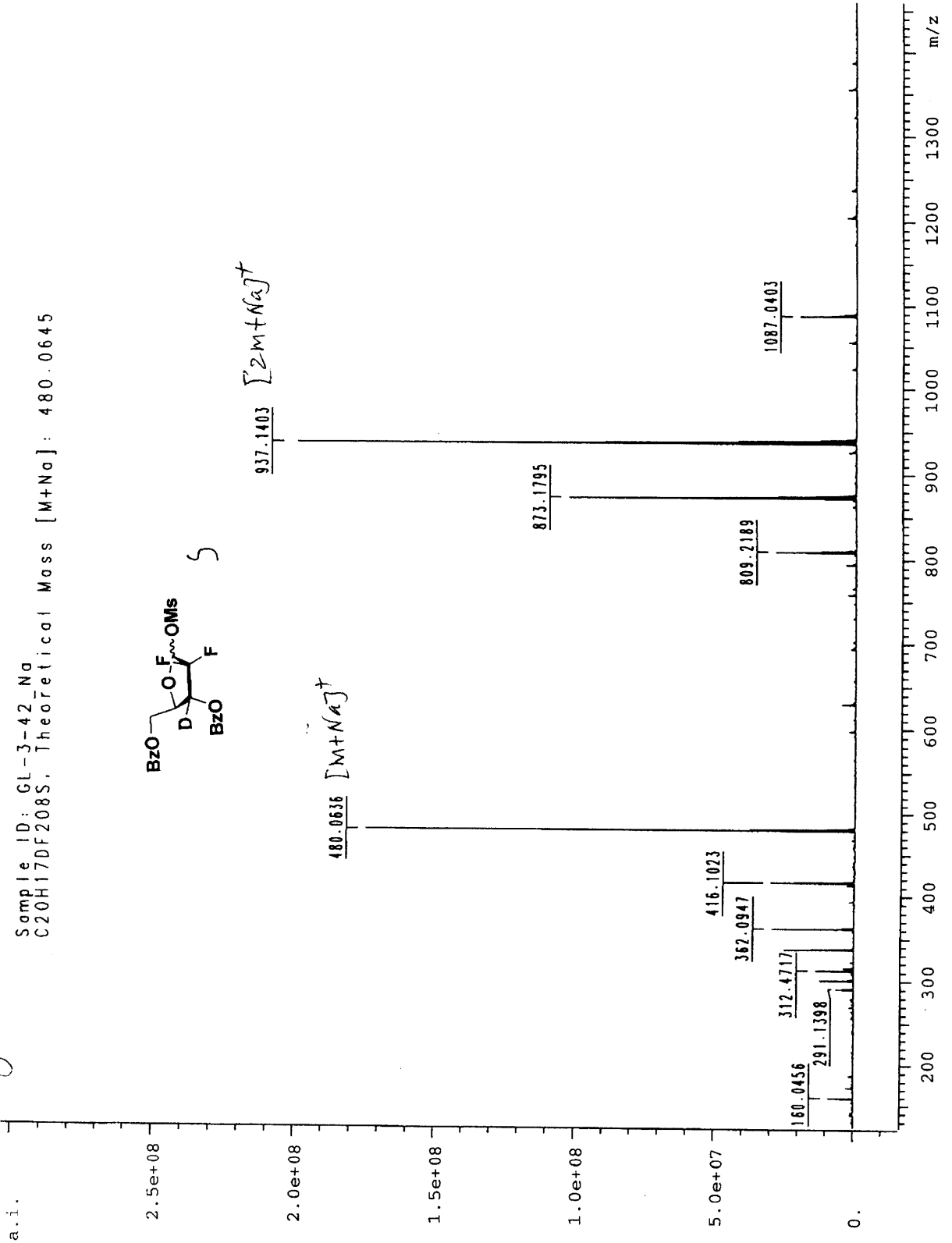
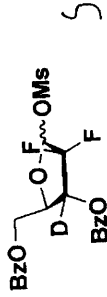


01-3-42-mesy1ate



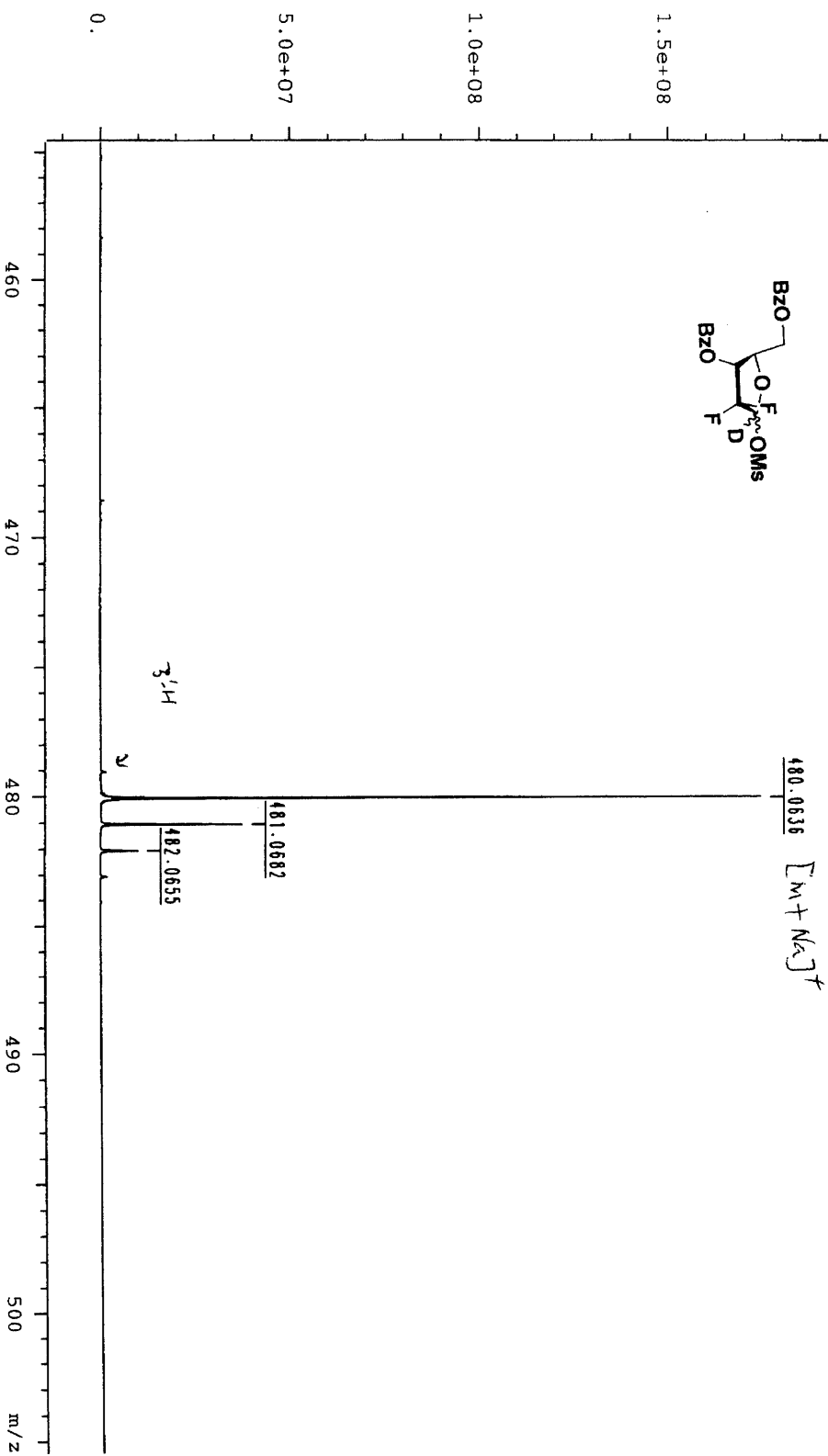
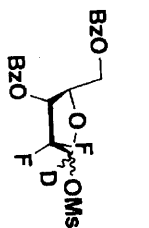
Greg Lohman (Stubbe) X3-0084

Sample ID: GL-3-42_Na
C20H17DF2O8S. Theoretical Mass [M+Na]: 480.0645



a.i.

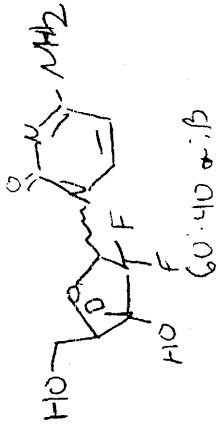
Sample ID: GL-3-42_No
C20H17DF2O8S, Theoretical Mass [M+Na]: 480.0645



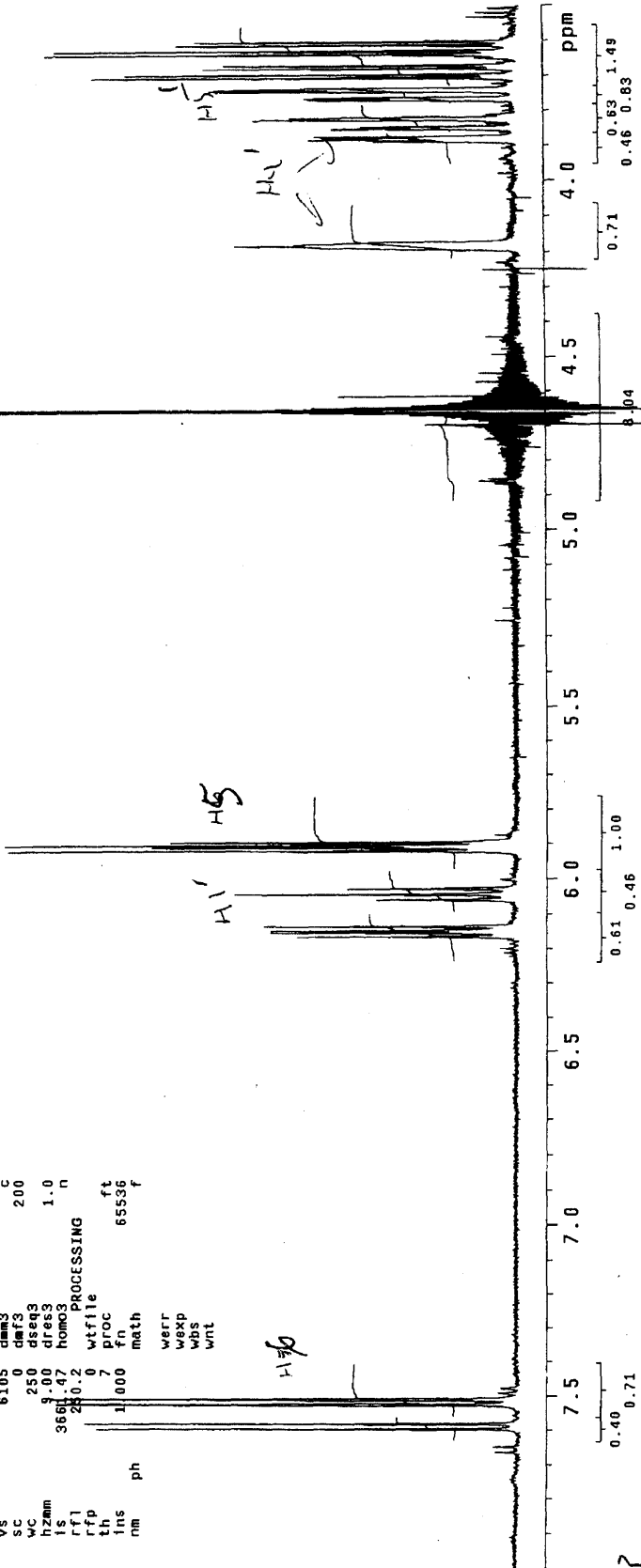
/Bruker/data/stubbe/ESI_Lohman/GL-3-42_Na/pdata/1 FTMUser Tue Apr 12 15:31:46 2005

3-0-gemzar
exp2 s2pul

date	Feb 24 2005	dfrq	125.677	DEC. & VI
solvent	D2O	dn	C13	
file	ACQUISITION	exp	34	
sfrq	499.757	dof	1488.1	
tn	HI	dm	nmn	
at	3.275	dmi	10000	
ap	31104	dseq		
aw	4748.3	dres	1.0	
fb	not used	homo	n	
bs	8			DEC2
tpwr	56	dfrq2	0	
pw	8.2	dn2		
pl		dpwr2	1	
prof	-374.8	dof2	0	
cl	32	dm2	n	
cl	32	dm2	n	
clock		dm2	200	
gain	52	dfr2		
flags		dseq2	1.0	
il	n	dres2	n	
in	y	homo2	0	
dp		dfrq3	DEC3	
hs	nm	dn3	0	
display		dpwr3	1	
sp	1748.8	dof3	0	
wp	2248.8	dm3	n	
vs	6105	dm3	n	
sc	0	dfr3	200	
wc	250	dseq3		
hzam	9.00	dres3	1.0	
is	3681.47	homo3	n	
rfl	280.2			PROCESSING
rff		wfille	ft	
th	7	fn	65536	
ins	1.000	math		
nm	ph	werr		
		wexp		
		wbs		
		wnt		

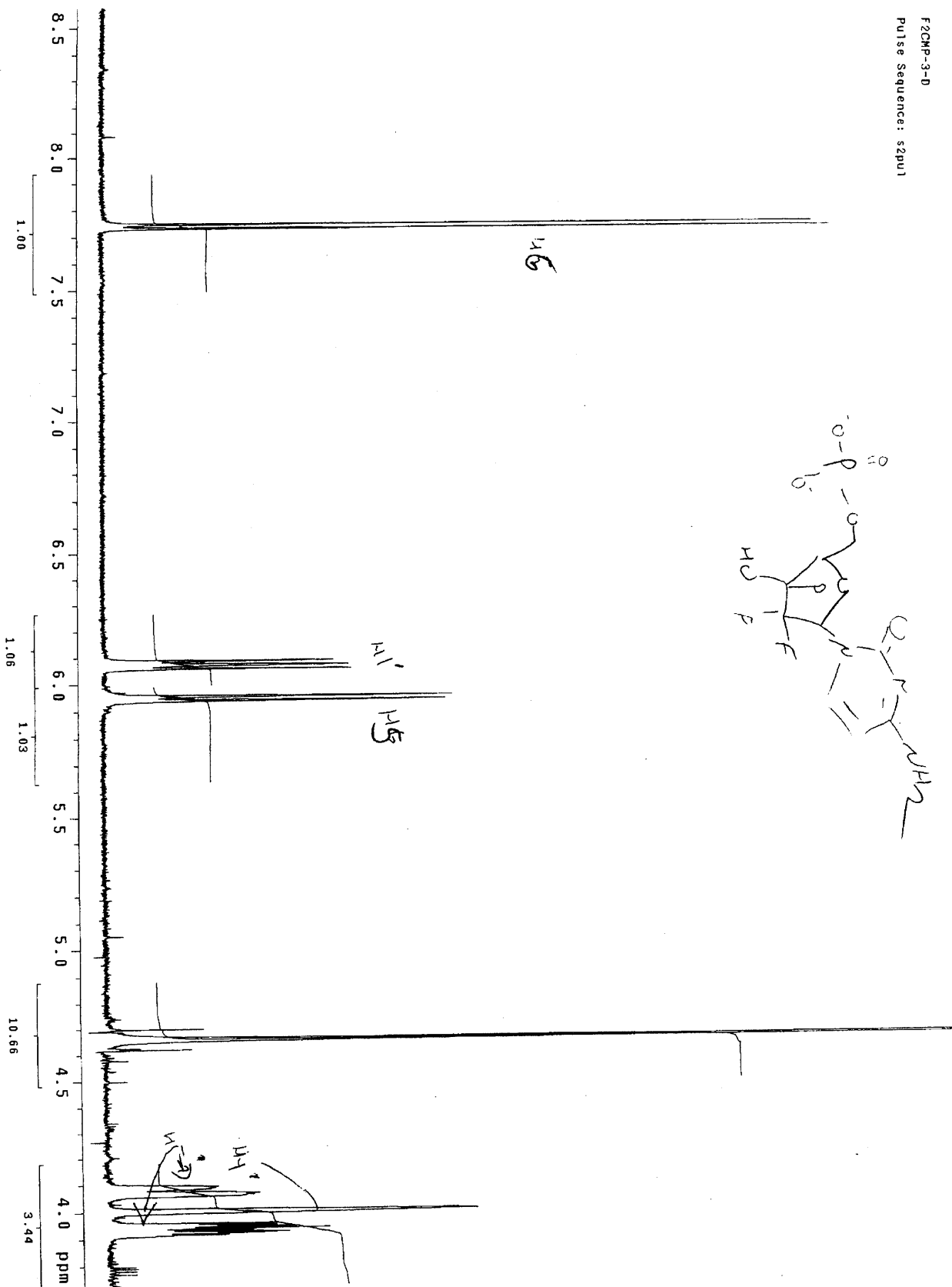
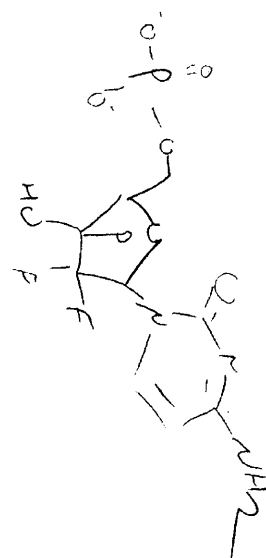


60:40 a:b



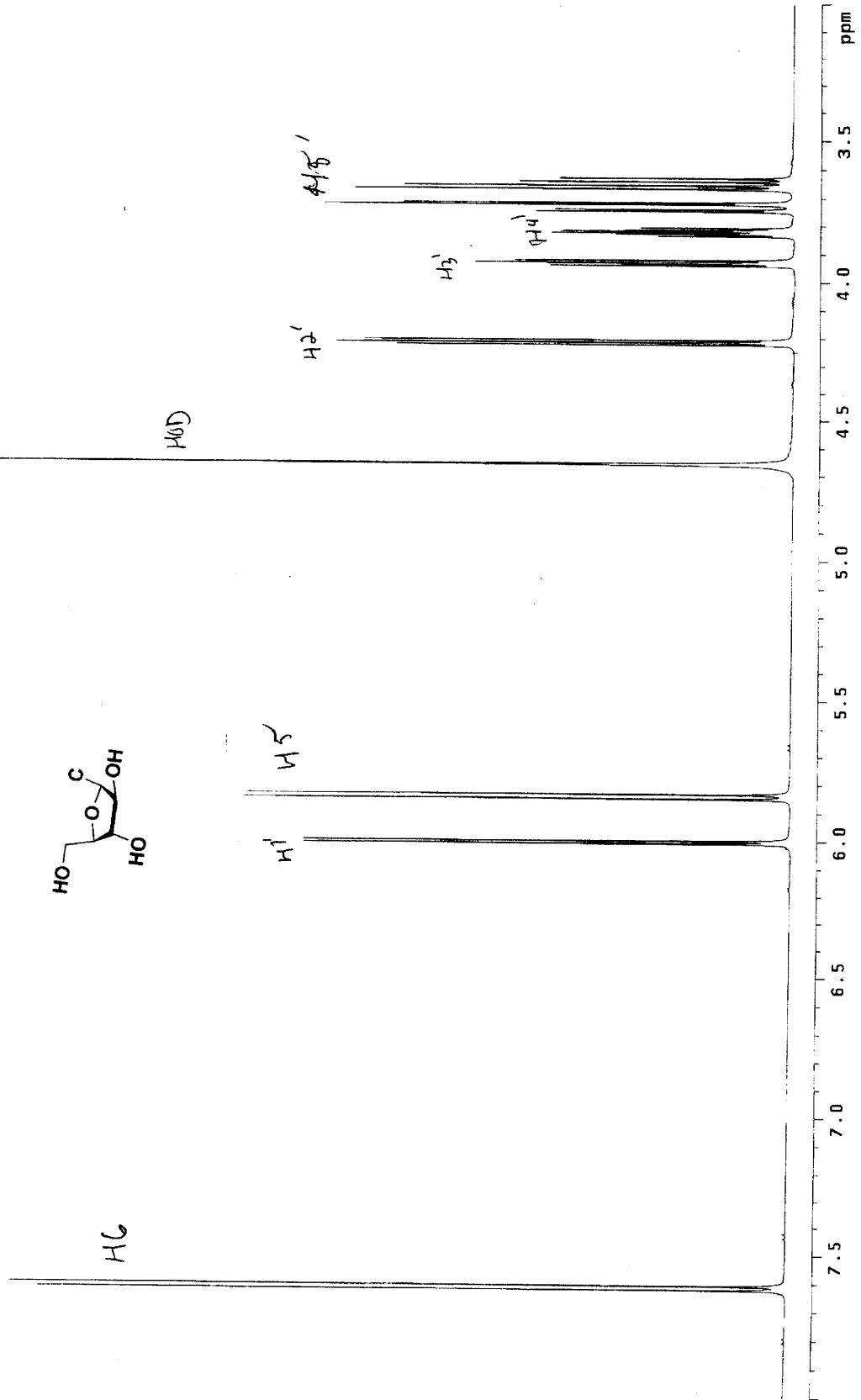
4059

F2CMP-3-D
Pulse Sequence: sqpu1

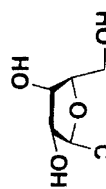


STANDARD PROTON PARAMETERS
Pulse Sequence: s2pu1

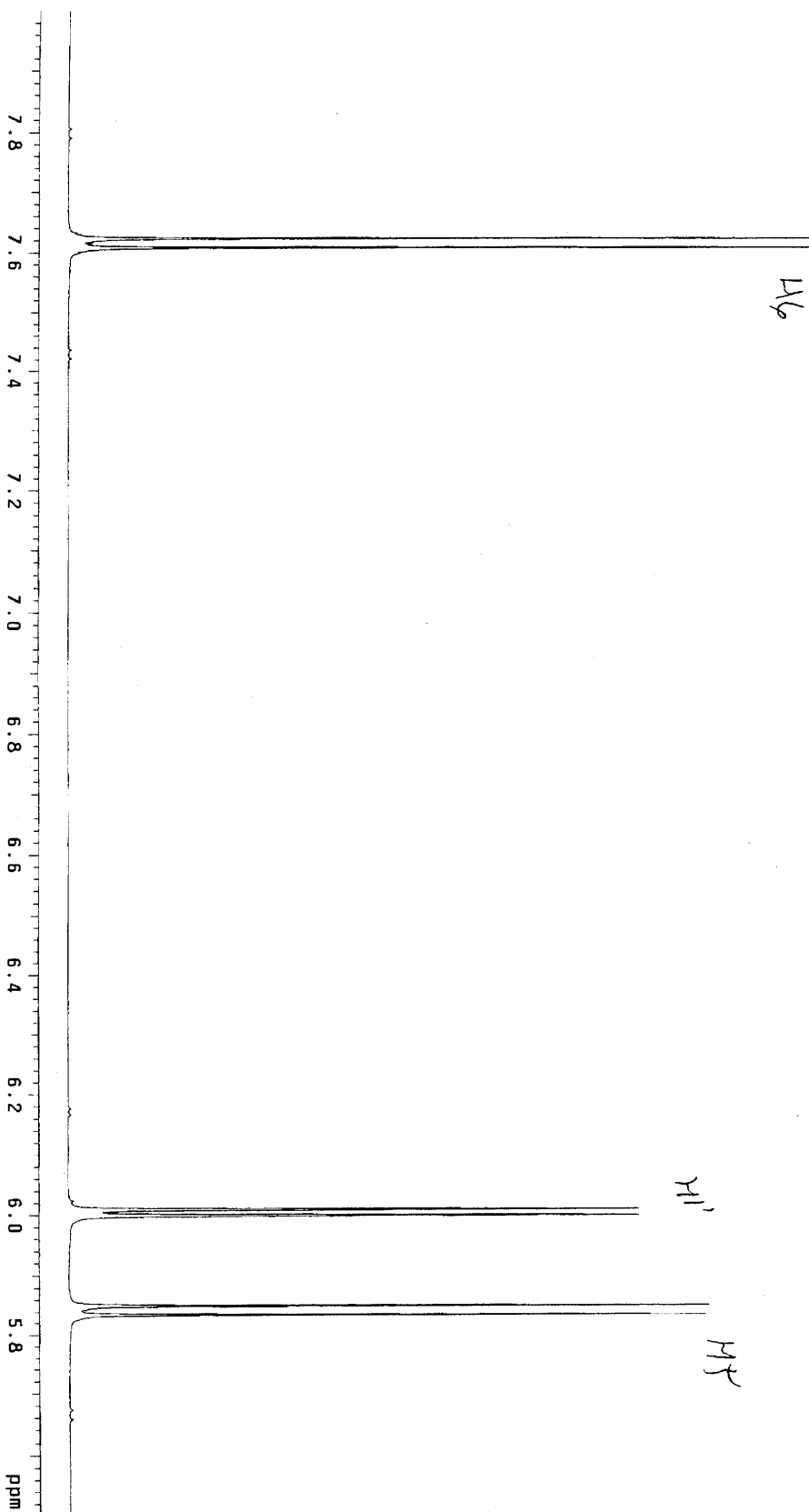
¹H-NMR, 500 MHz, D₂O



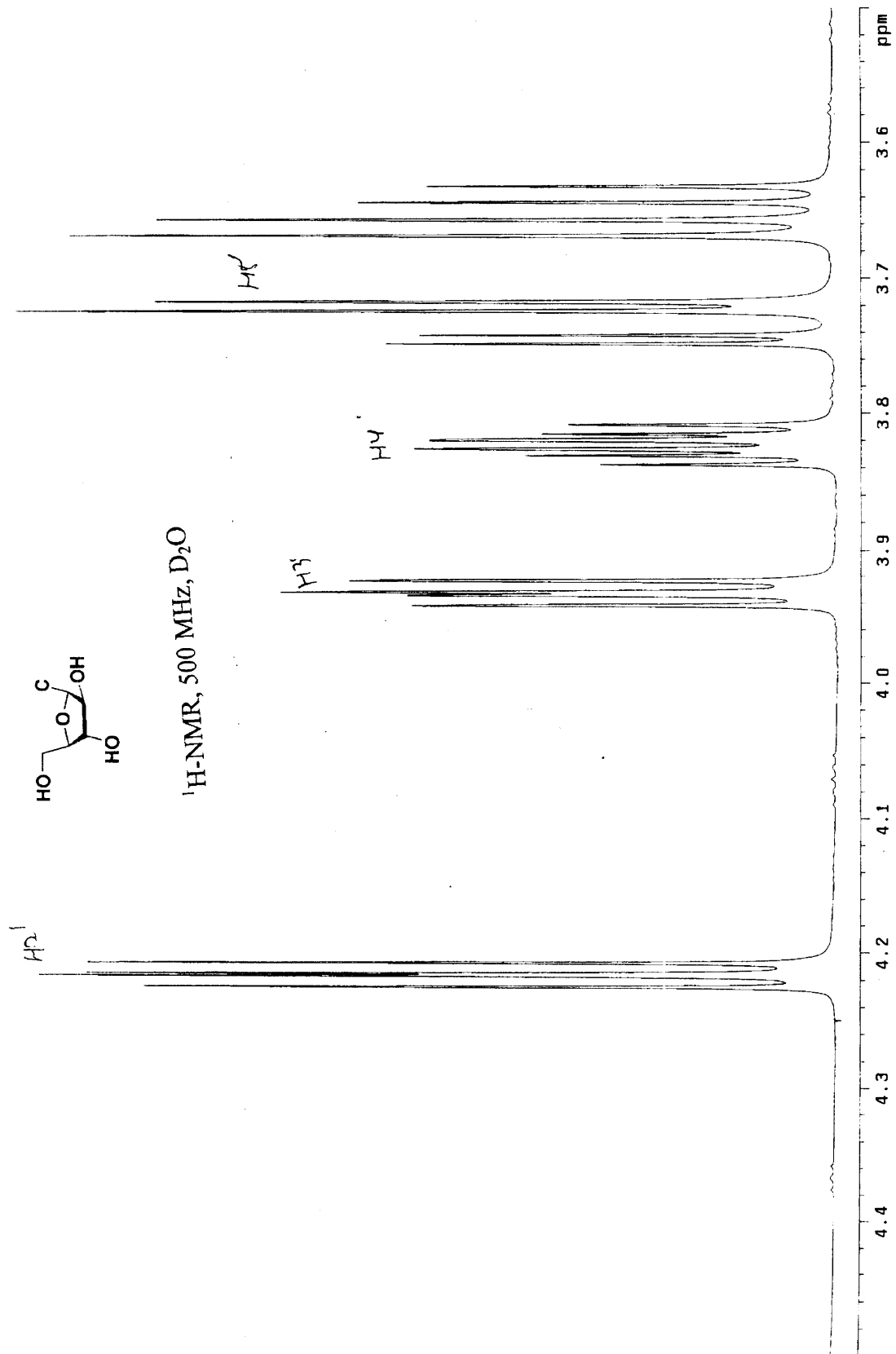
STANDARD PROTON PARAMETERS
Pulse Sequence: szpu1



$^1\text{H-NMR}$, 500 MHz, D_2O

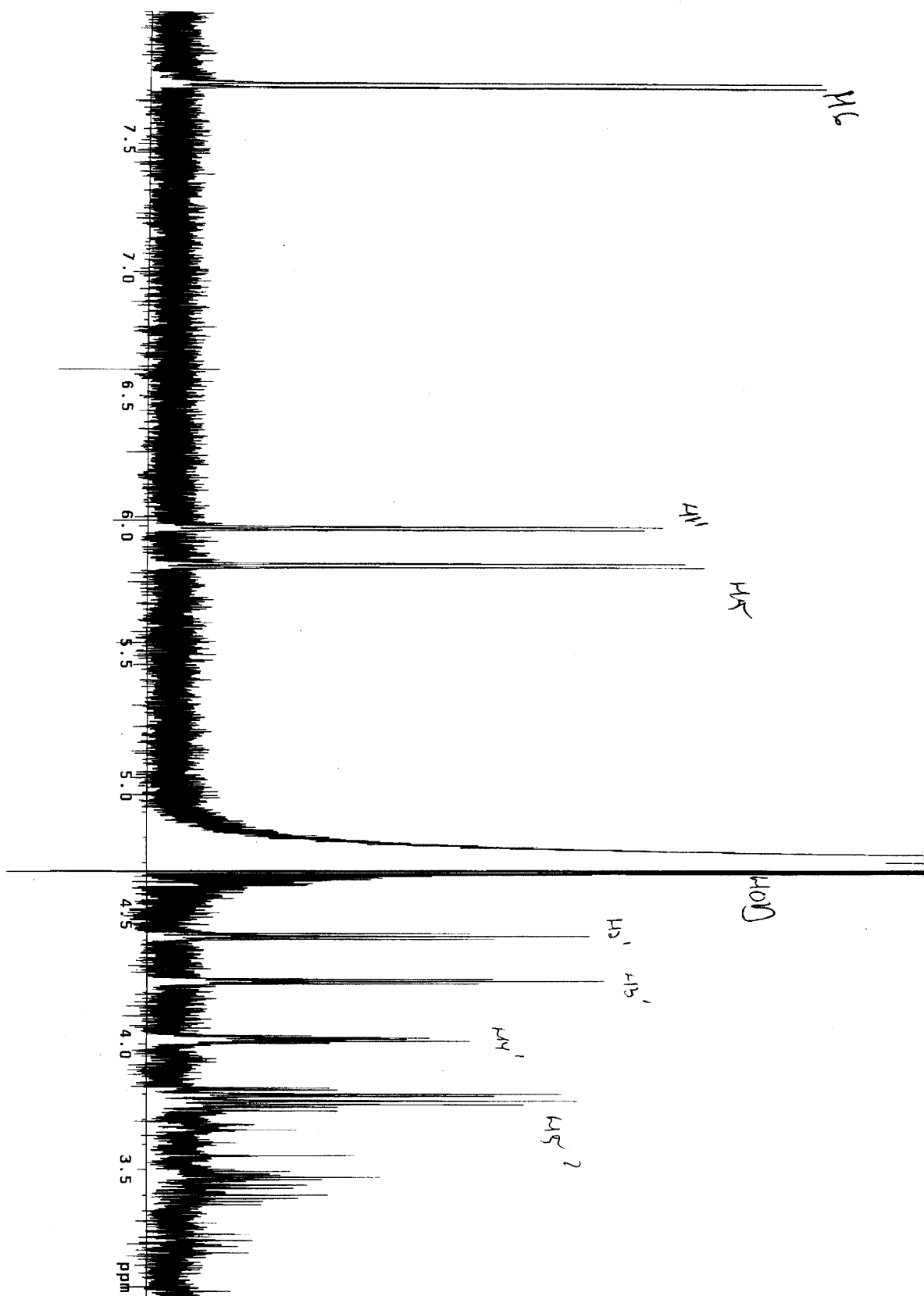


STANDARD PROTON PARAMETERS
Pulse Sequence: s2pu1



NABH4 quench 7-3-05
Pulse Sequence: presat

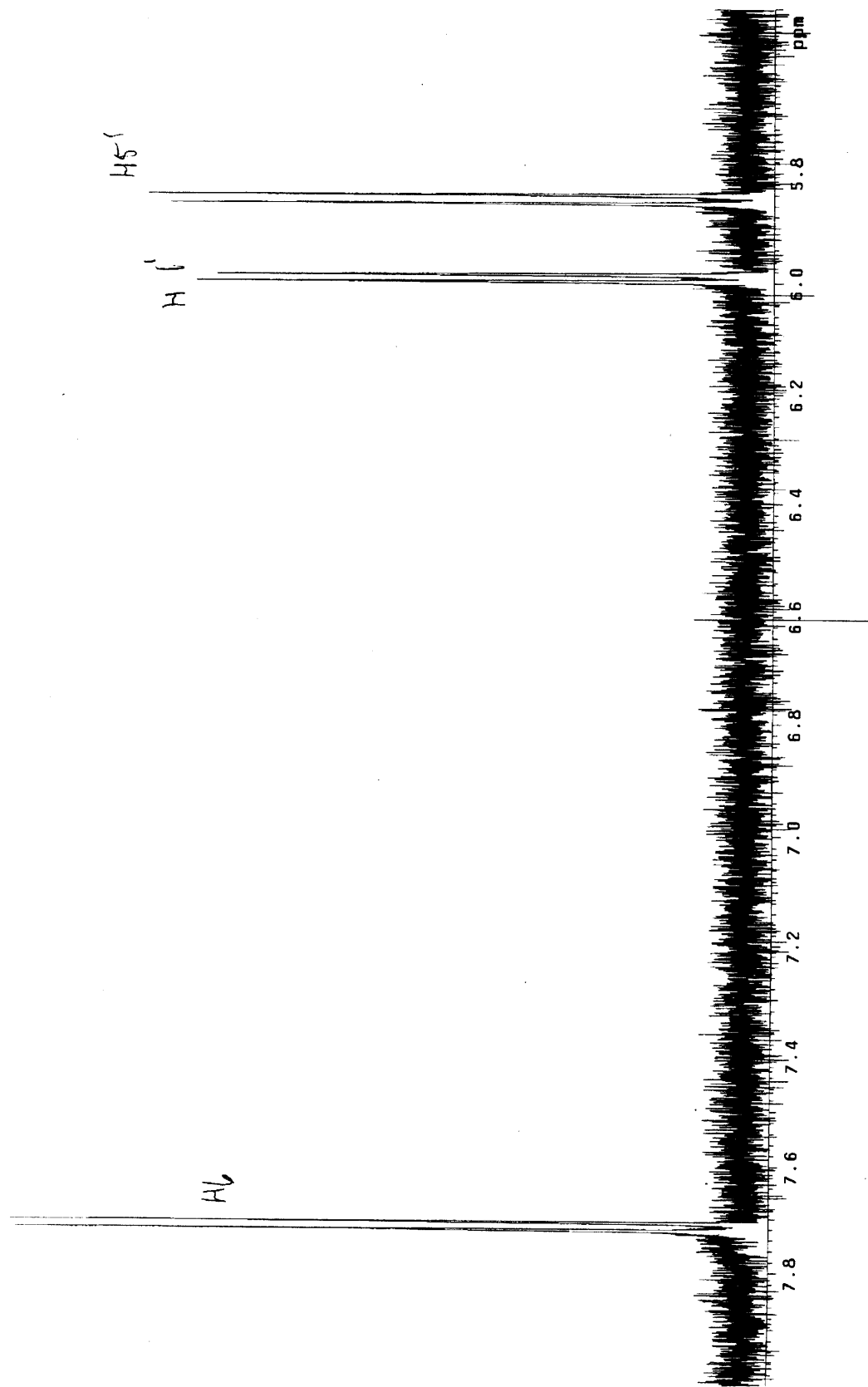
Small molecule product isolated from the inactivation of RTPR with F₂CTP, NaBH₄ quench.
¹H-NMR, 500 MHz, D₂O



NaBH4 quench 7-3-05
Pulse Sequence: presat

Small molecule product isolated from the inactivation of RTPR with F₂CTP, NaBH₄ quench.

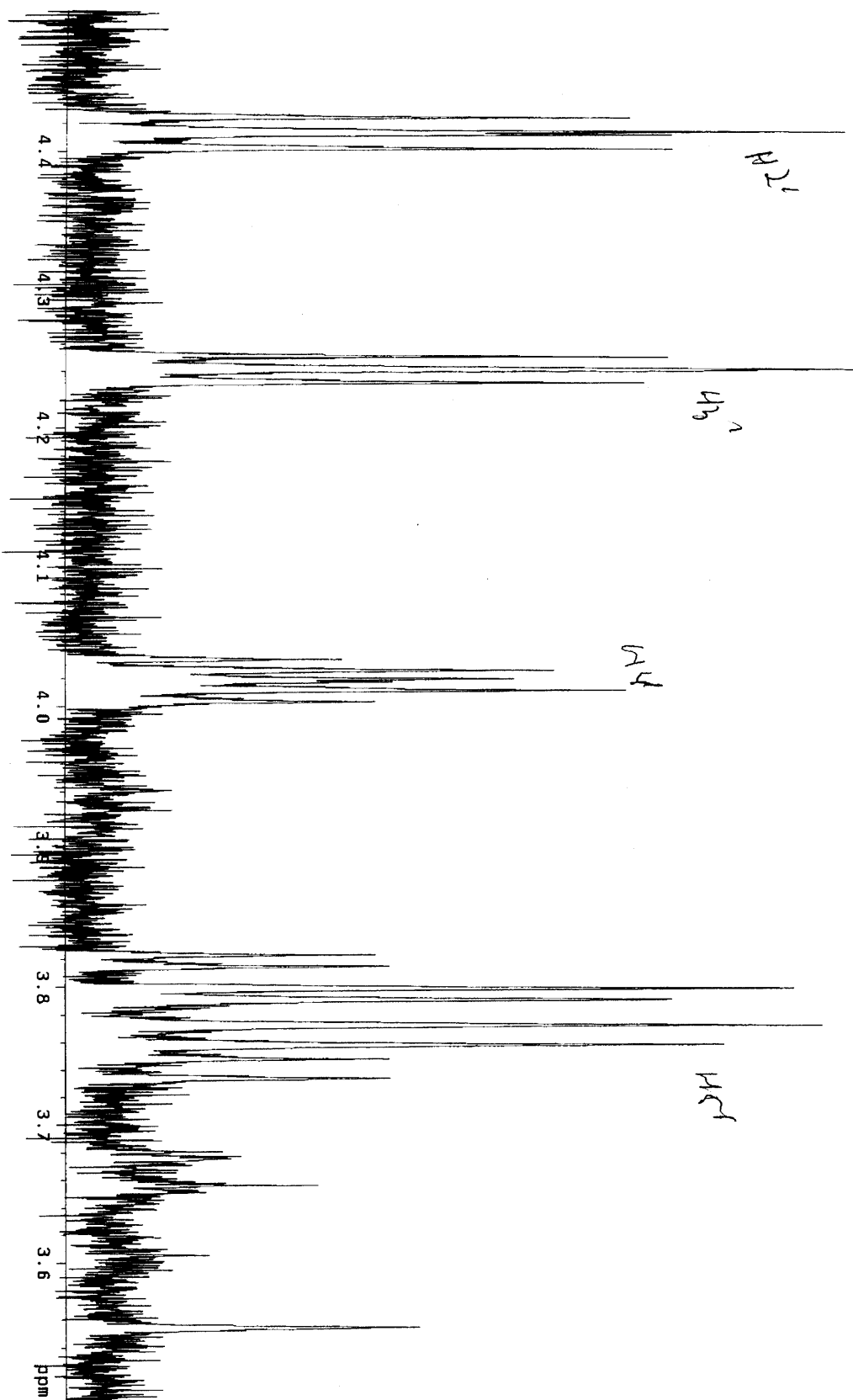
¹H-NMR, 500 MHz, D₂O



NaBH4 quench 7-3-05
pulse sequence: presat

Small molecule product isolated from the inactivation of RTPPR with F₂CTP, NaBH₄ quench.

¹H-NMR, 500 MHz, D₂O



NaBH4 quench 7-3-05

Pulse Sequence: gCOSY

Solvent: D2O

Temp: 22.0 C / 295.1 K

INOVA-500 "bulwinkle"

PULSE SEQUENCE: gCOSY

Relax delay: 1.000 sec

Acq. time: 0.216 sec

Width: 4743.8 Hz

2D Width: 4743.8 Hz

64 repetitions

128 increments

OBSERVE: H1 499.7459364 MHz

DATA PROCESSING

Sq. sine bell 0.108 sec

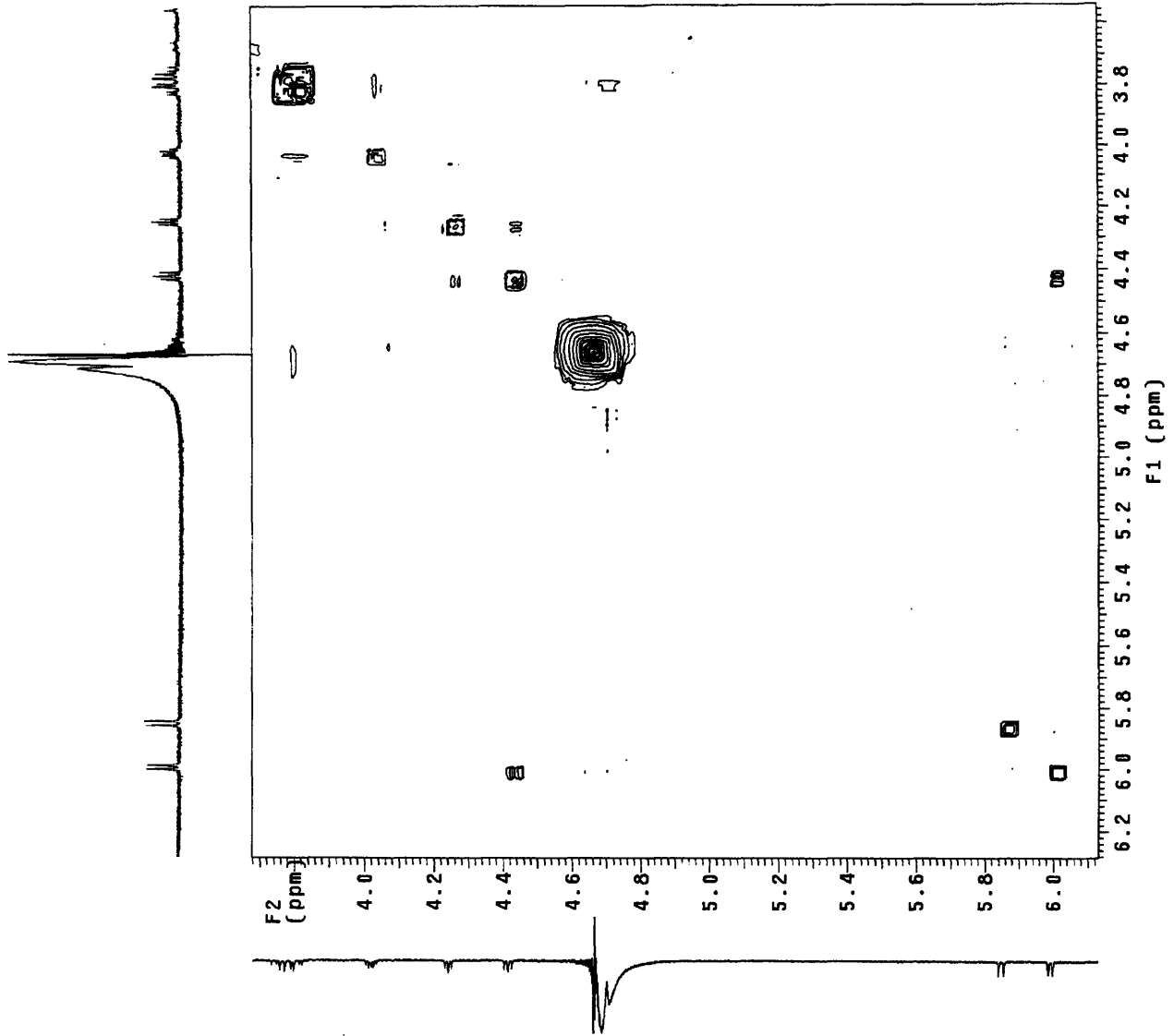
F1 DATA PROCESSING

Sq. sine bell 0.026 sec

FT size 2048 x 2048

Total time 2 hr, 49 min, 56 sec

gCOSY, 500 MHz, D₂O



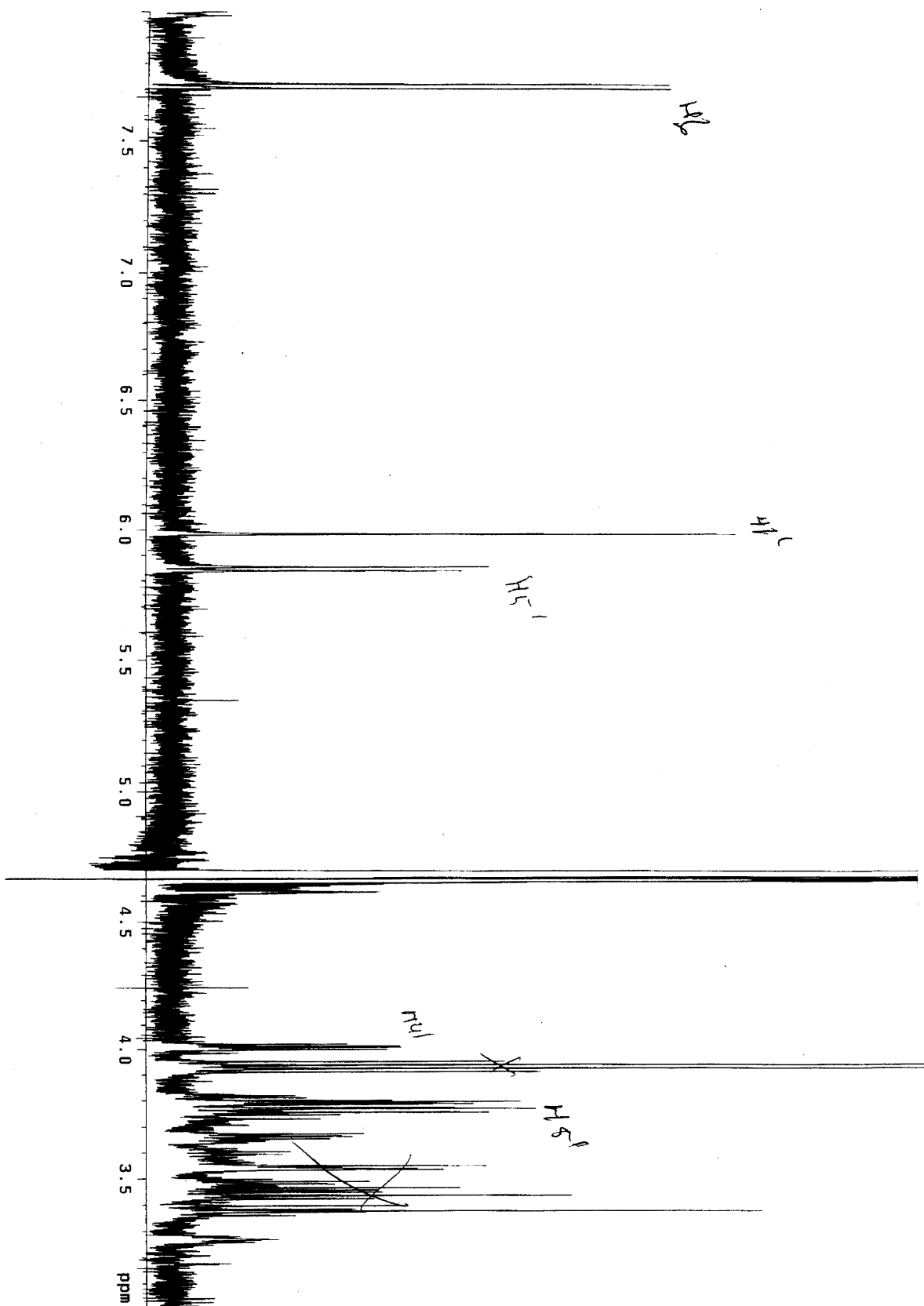
Small molecule product

isolated from the inactivation

of RTPR with F₂CTP, NaBH₄ quench.

NaBD4 quench 7/3/05
Pulse Sequence: presat

Small molecule product isolated from the inactivation of RTPPR with F₂CTP, NaBD₄ quench.
¹H-NMR, 500 MHz, D₂O



Small molecule product isolated from the inactivation of RTPR with F₂CTP, NaBD₄ quench.

NaBD₄ quench 7/3/05

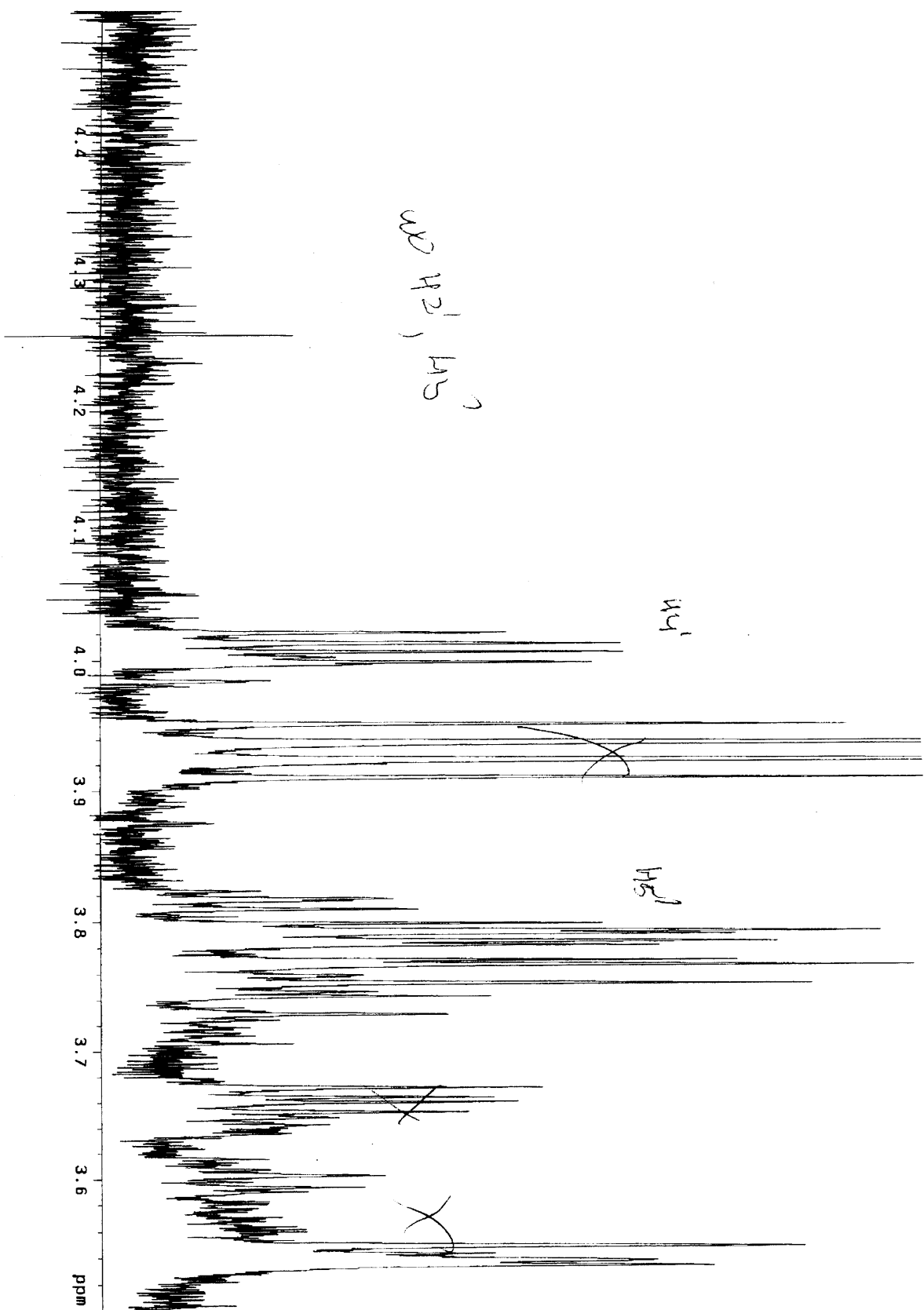
Pulse Sequence: presat

¹H-NMR, 500 MHz, D₂O

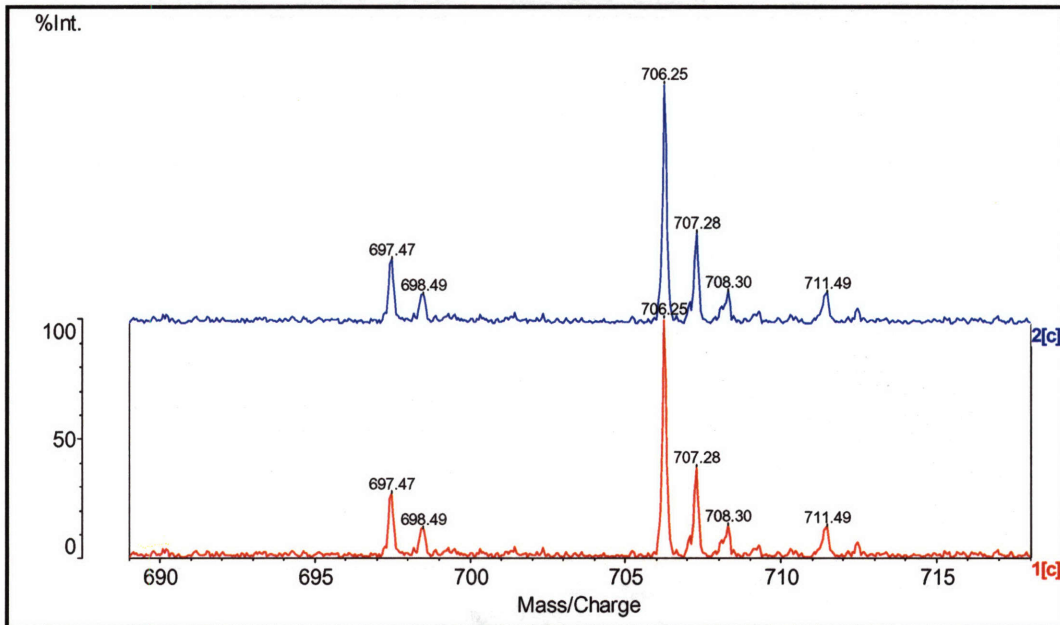
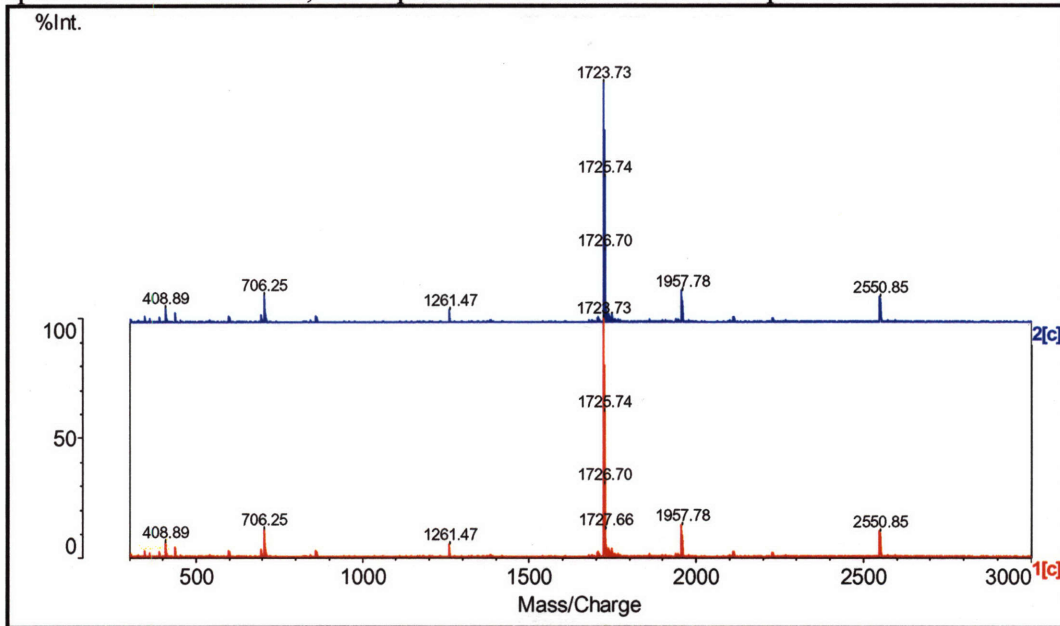


NaBD₄ quench 7/3/05
pulse Sequence: presat

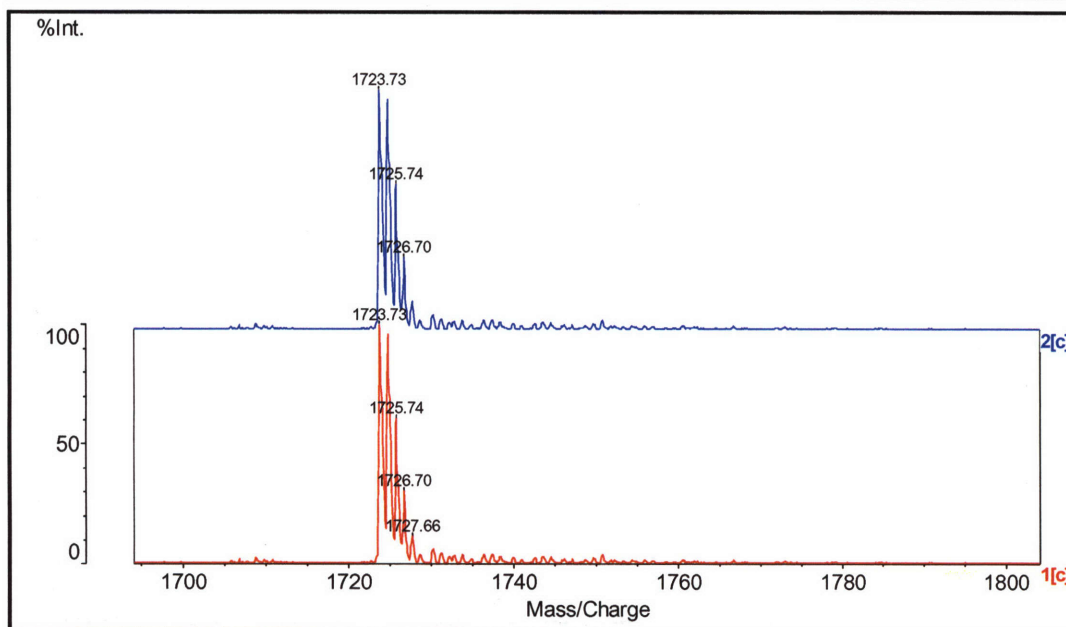
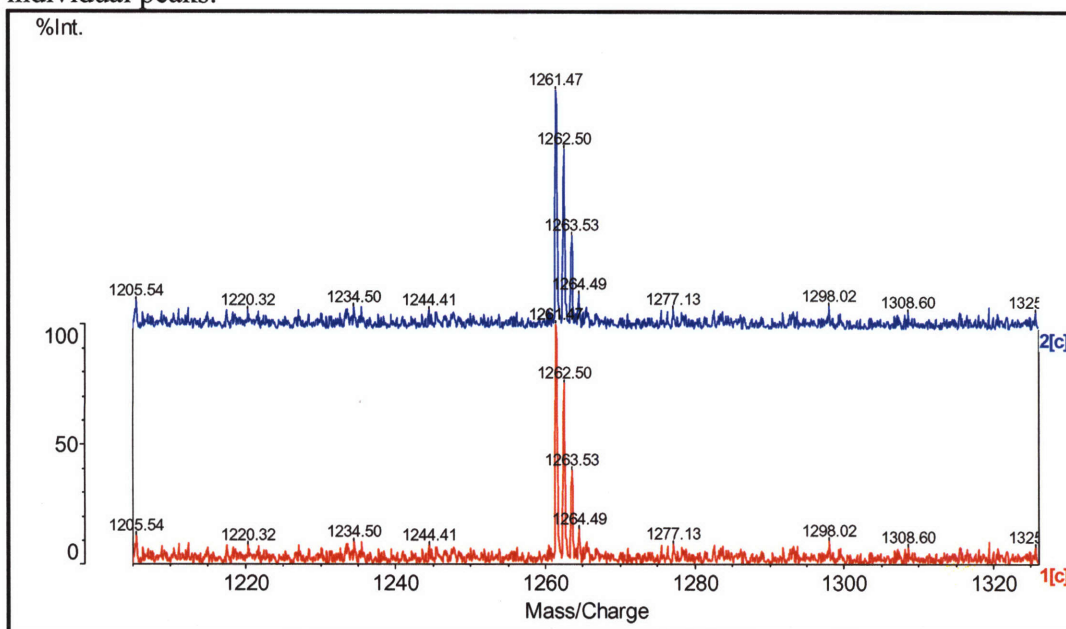
Small molecule product isolated from the inactivation of RTPPR with F₂CTP, NaBD₄ quench.
¹H-NMR, 500 MHz, D₂O



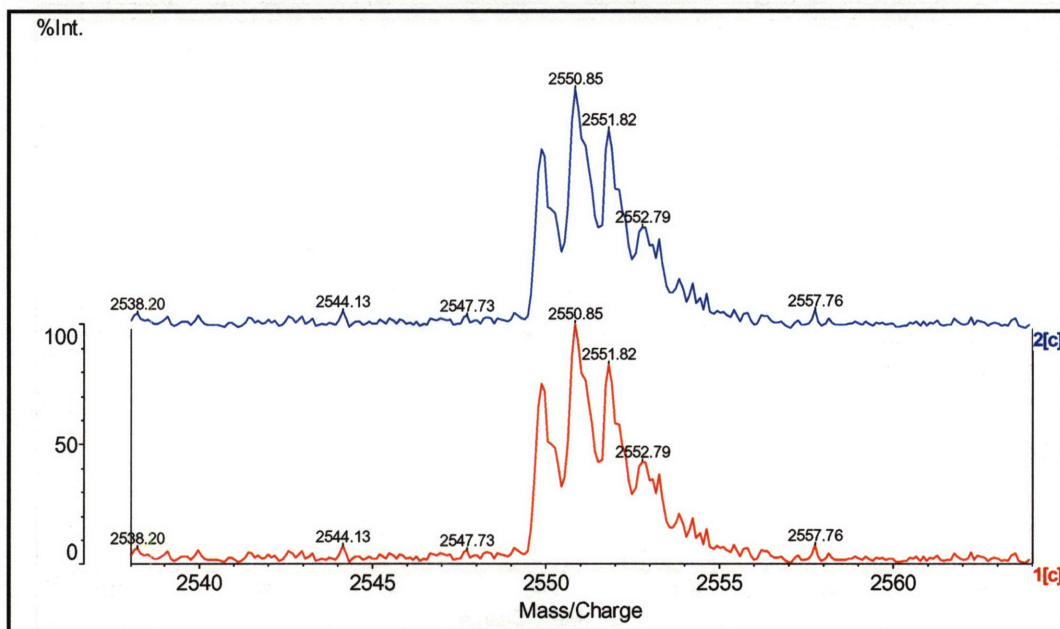
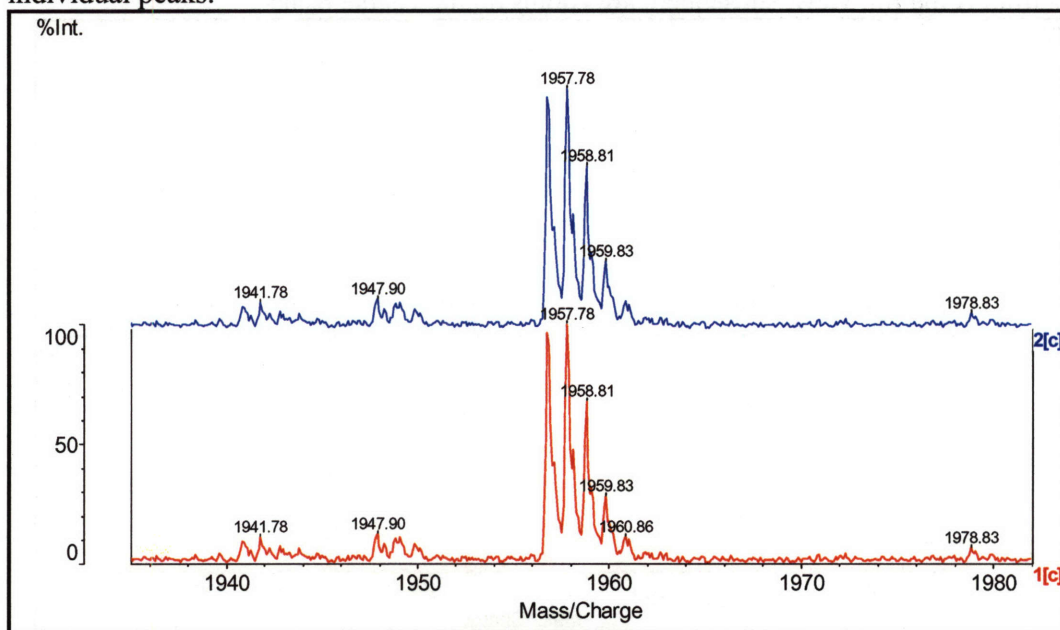
MALDI of R II peptides from trypsin digest of inactivation of RTPR with 1'-[³H]-F₂CTP, NaBH₄ quench a 2 min. From rechromatographed samples, first part of the peak of radioactivity. In all spectra, the top (blue) is from an inactivation using 1'-[³H]-F₂CTP, the bottom (red) from an inactivation using 1'-[²H, ³H]-F₂CTP, ~60% D. The first spectrum is the full view, subsequent are zooms on the visible peaks.



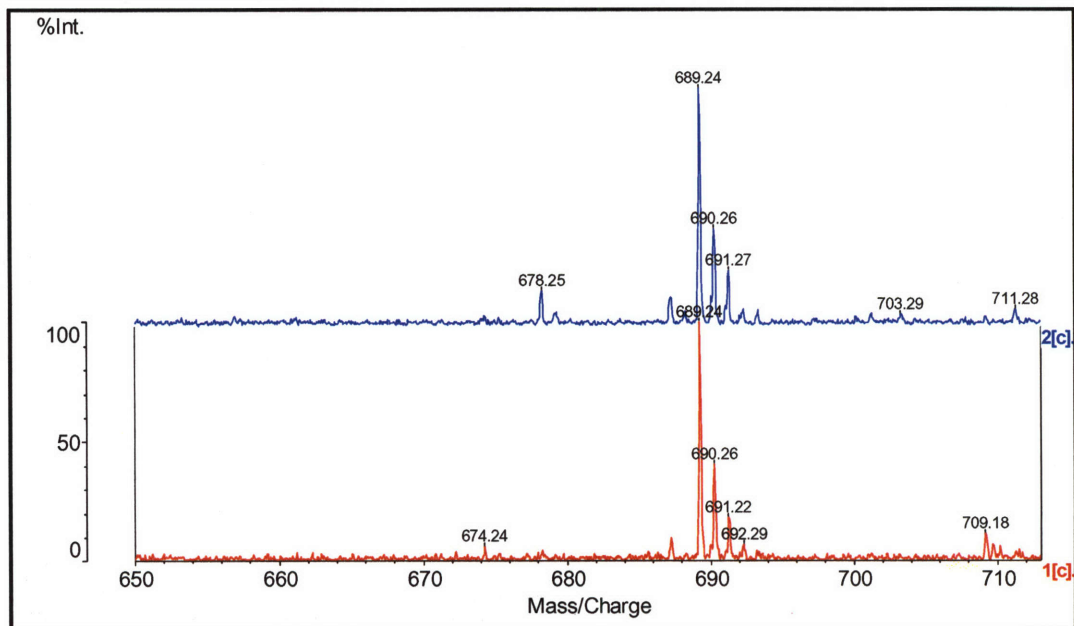
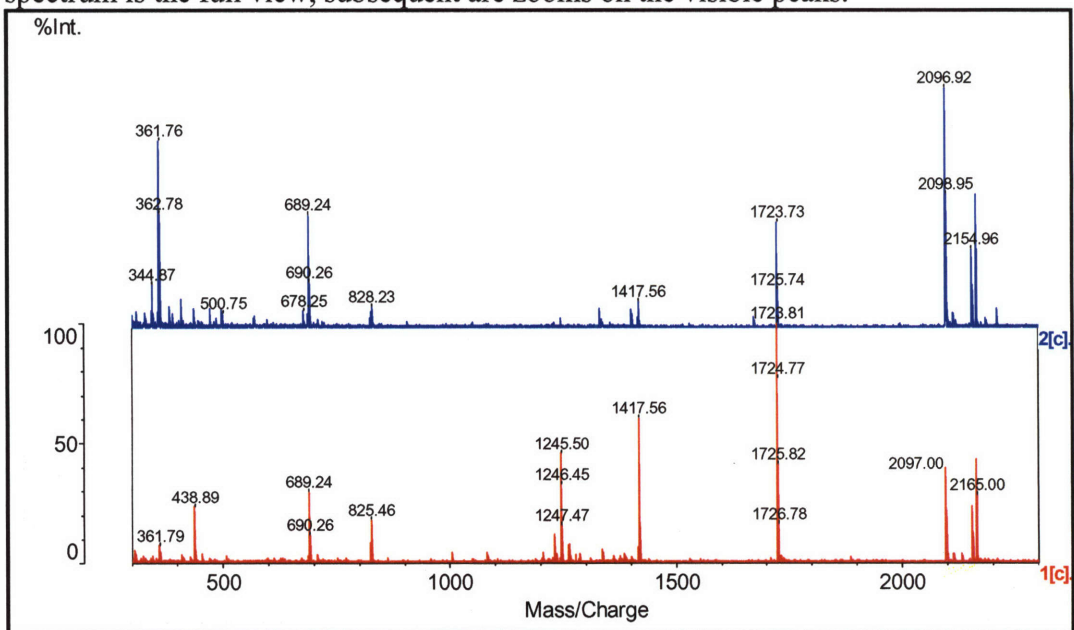
MALDI of R II peptides from trypsin digest of inactivation of RTPR with 1'-[³H]-F₂CTP, NaBH₄ quench a 2 min. From rechromatographed samples, first part of the peak of radioactivity. In all spectra, the top (blue) is from an inactivation using 1'-[³H]-F₂CTP, the bottom (red) from an inactivation using 1'-[²H, ³H]-F₂CTP, ~60% D. Expansions on individual peaks.



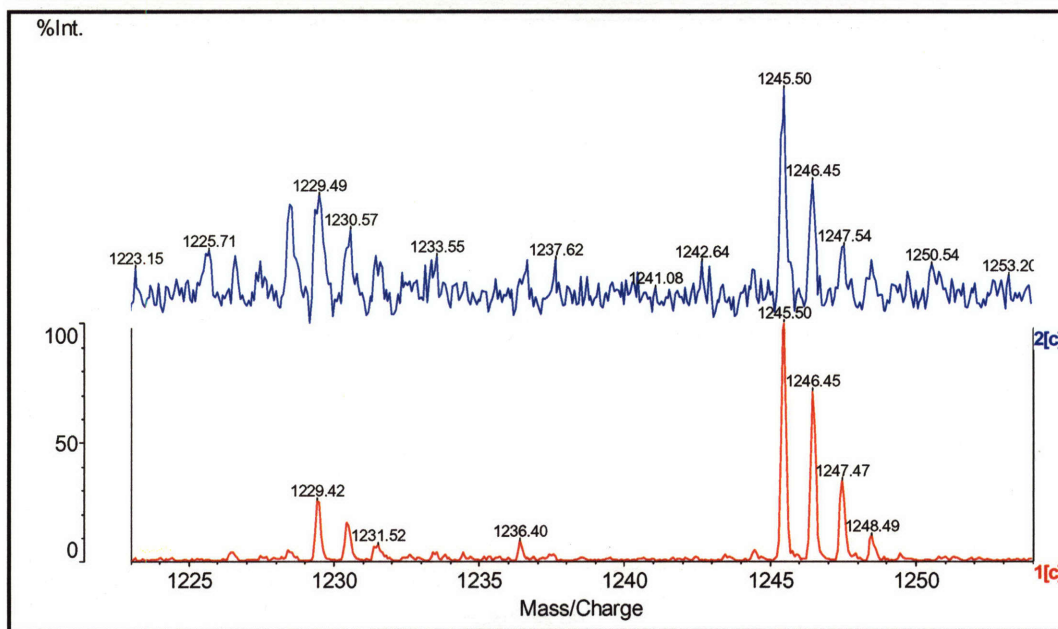
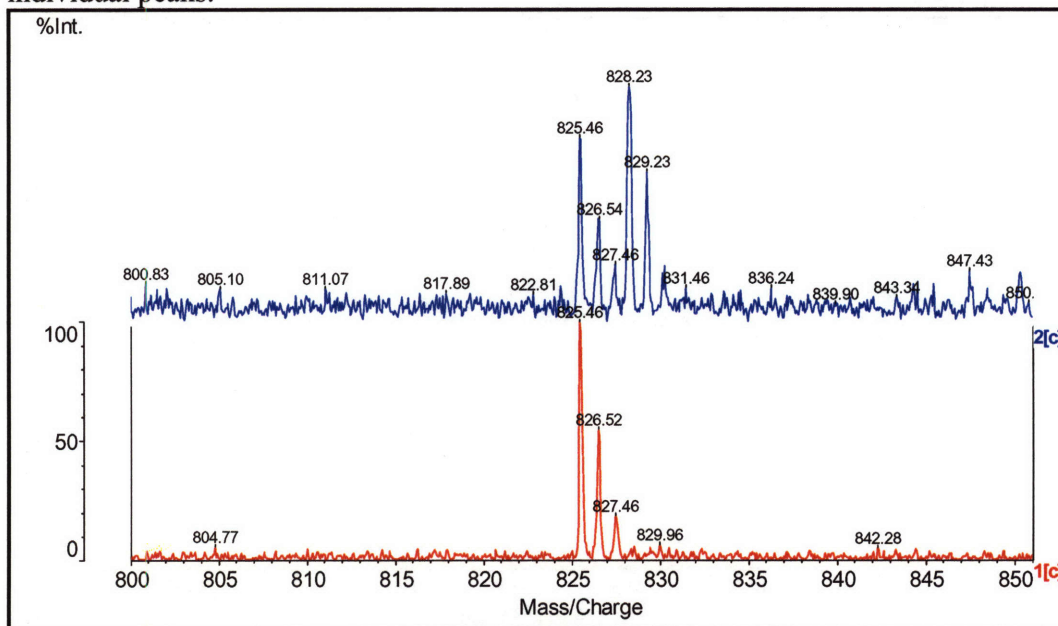
MALDI of R II peptides from trypsin digest of inactivation of RTPR with 1'-[³H]-F₂CTP, NaBH₄ quench a 2 min. From rechromatographed samples, first part of the peak of radioactivity. In all spectra, the top (blue) is from an inactivation using 1'-[³H]-F₂CTP, the bottom (red) from an inactivation using 1'-[²H, ³H]-F₂CTP, ~60% D. Expansions on individual peaks.



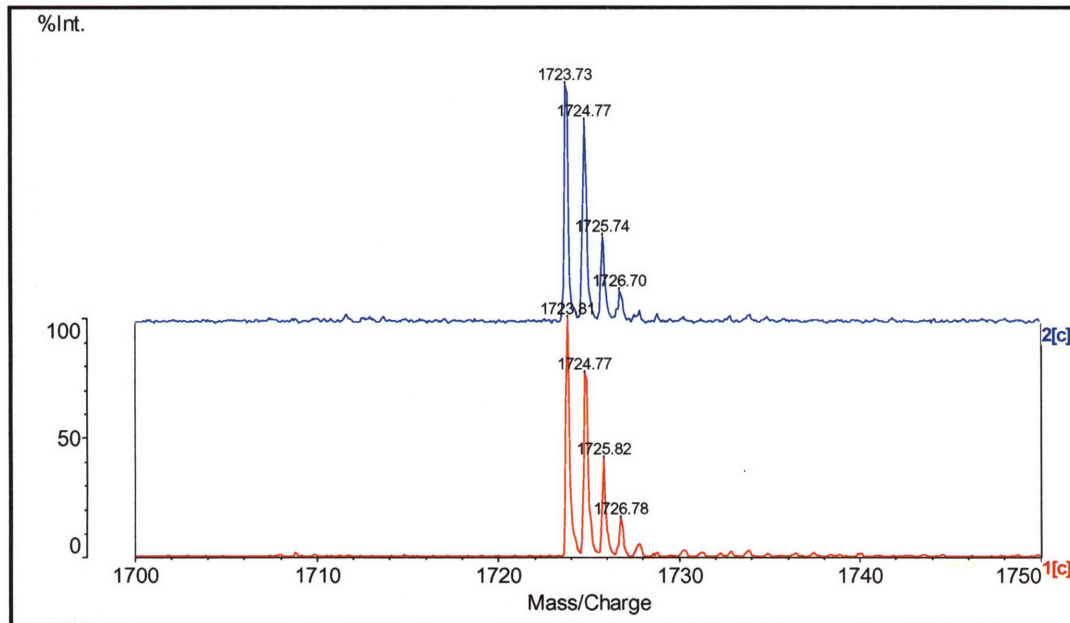
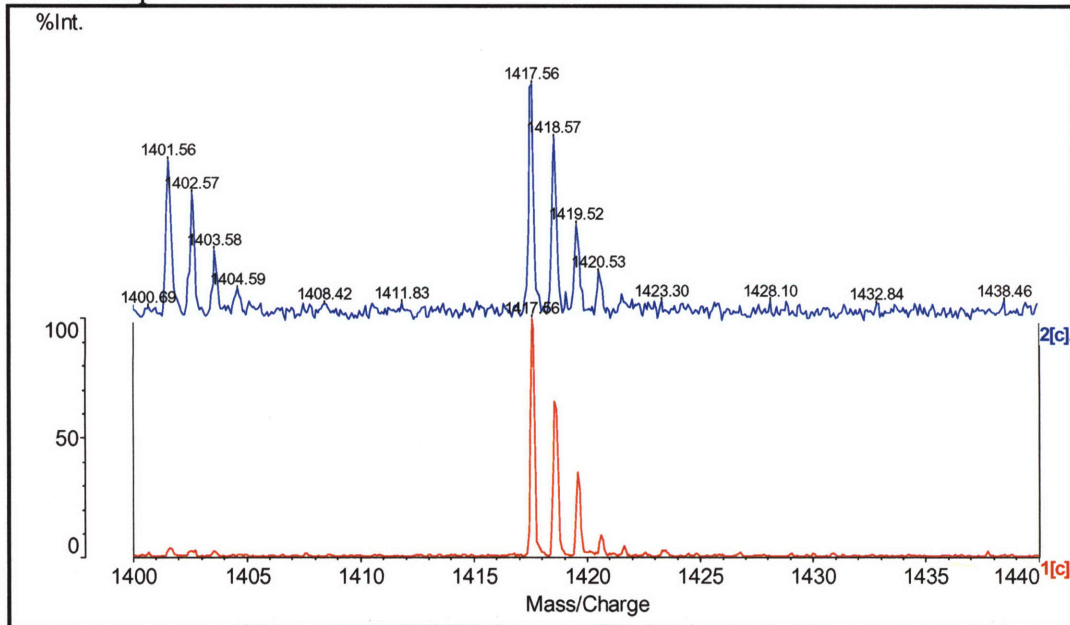
MALDI of R II peptides from trypsin digest of inactivation of RTPR with 1'-[³H]-F₂CTP, NaBH₄ quench a 2 min. From rechromatographed samples, second part of the peak of radioactivity. In all spectra, the top (blue) is from an inactivation using 1'-[³H]-F₂CTP, the bottom (red) from an inactivation using 1'-[²H, ³H]-F₂CTP, ~60% D. The first spectrum is the full view, subsequent are zooms on the visible peaks.



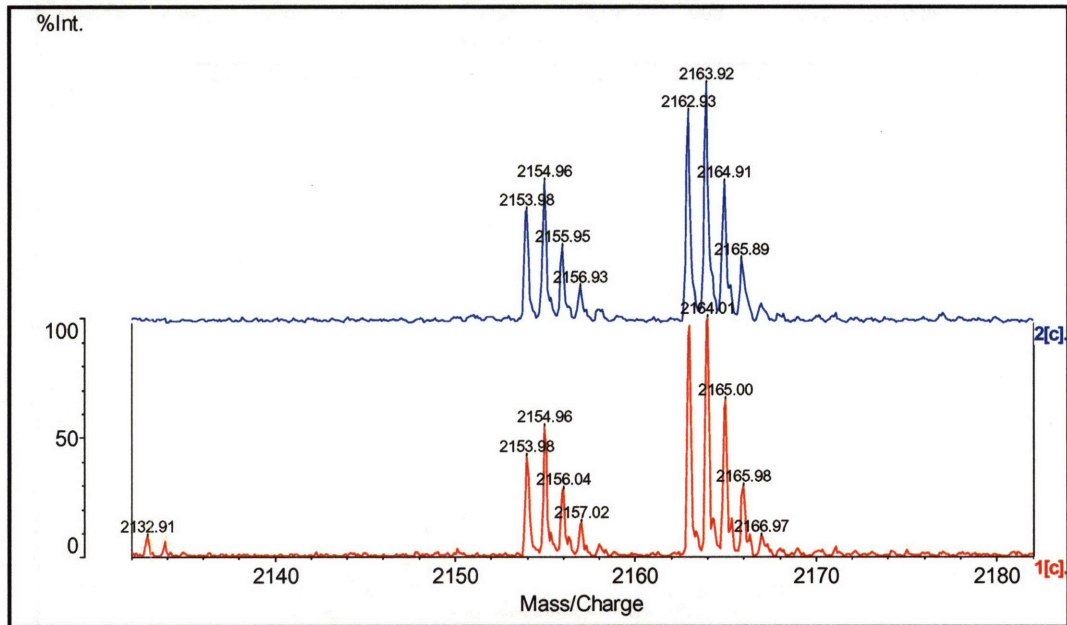
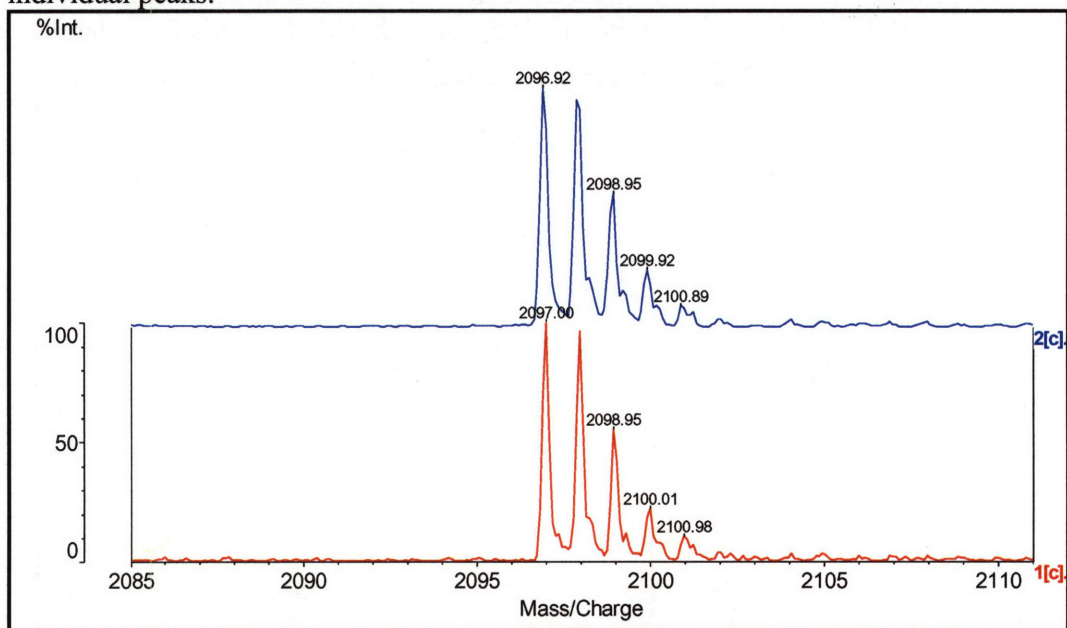
MALDI of R II peptides from trypsin digest of inactivation of RTPR with 1'-[³H]-F₂CTP, NaBH₄ quench a 2 min. From rechromatographed samples, second part of the peak of radioactivity. In all spectra, the top (blue) is from an inactivation using 1'-[³H]-F₂CTP, the bottom (red) from an inactivation using 1'-[²H, ³H]-F₂CTP, ~60% D. Expansions on individual peaks.



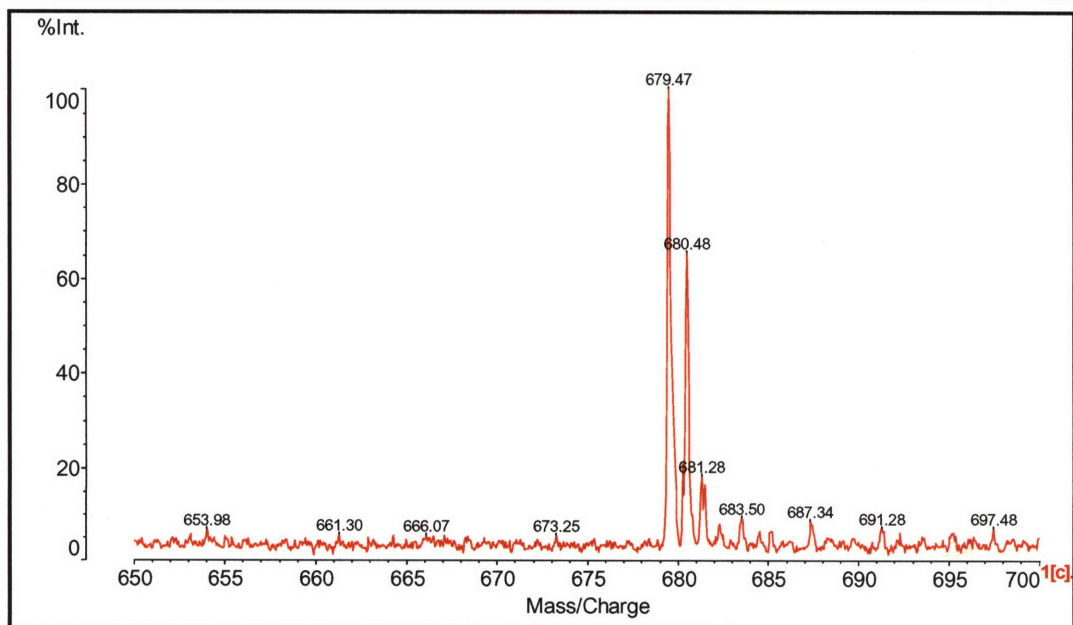
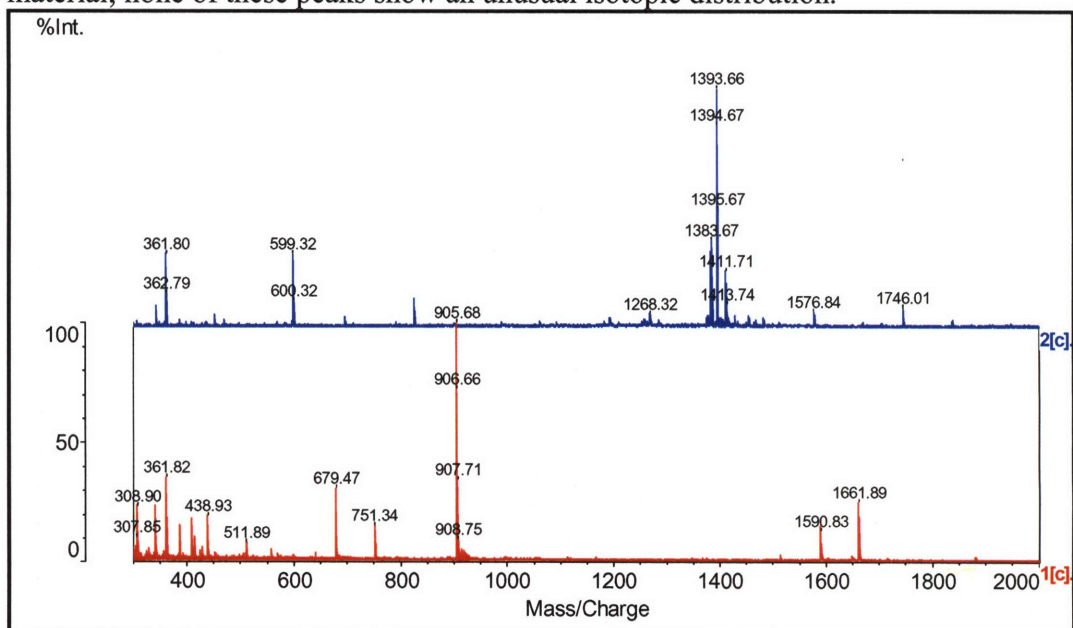
MALDI of R II peptides from trypsin digest of inactivation of RTPR with 1'-[³H]-F₂CTP, NaBH₄ quench a 2 min. From rechromatographed samples, second part of the peak of radioactivity. In all spectra, the top (blue) is from an inactivation using 1'-[³H]-F₂CTP, the bottom (red) from an inactivation using 1'-[²H, ³H]-F₂CTP, ~60% D. Expansions on individual peaks.



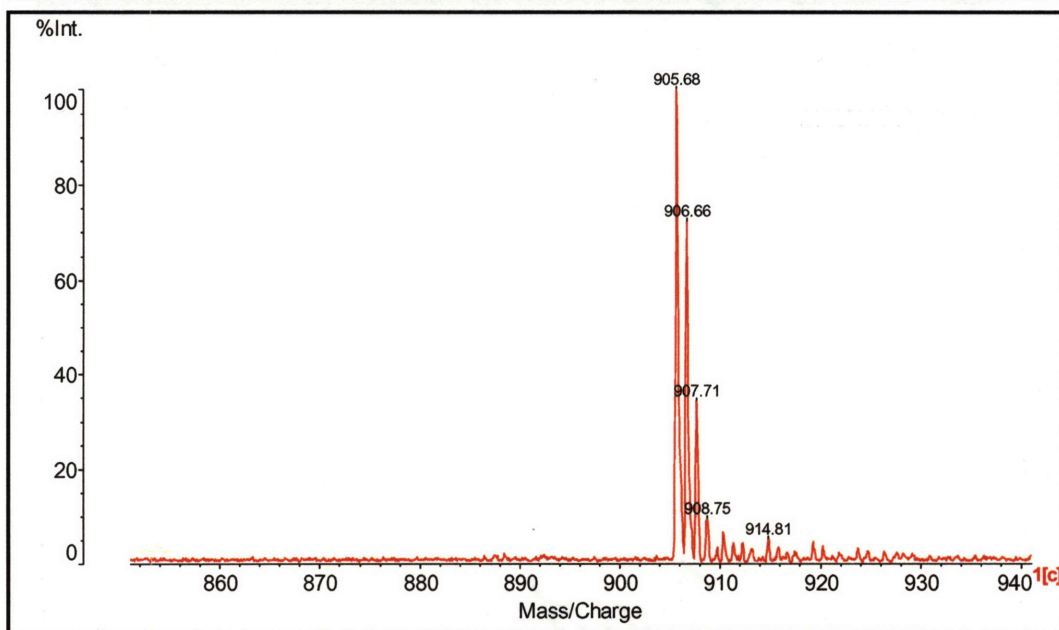
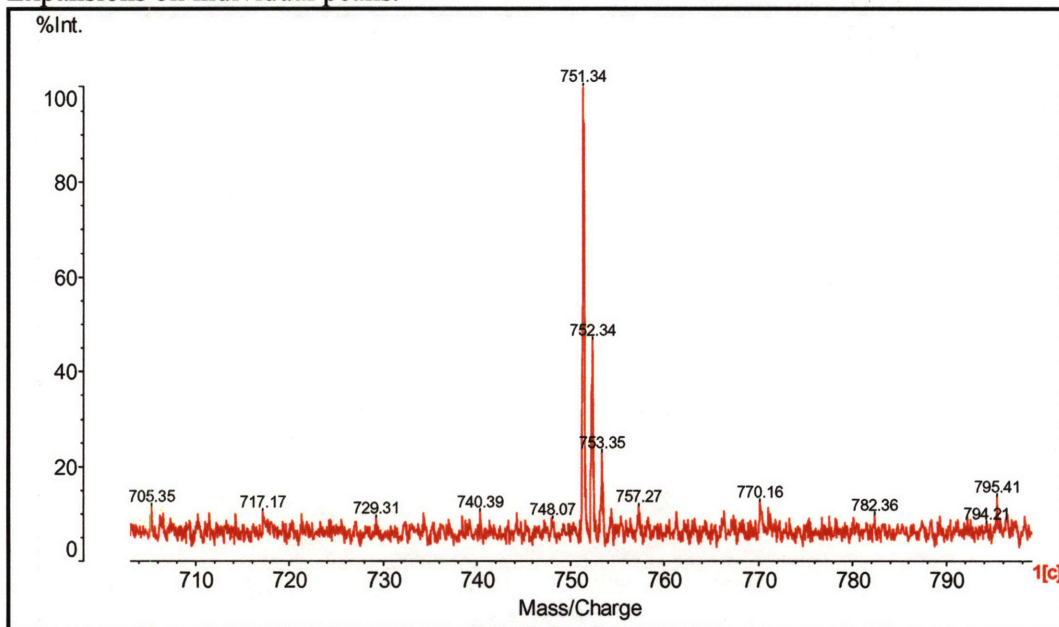
MALDI of R II peptides from trypsin digest of inactivation of RTPR with 1'-[³H]-F₂CTP, NaBH₄ quench a 2 min. From rechromatographed samples, second part of the peak of radioactivity. In all spectra, the top (blue) is from an inactivation using 1'-[³H]-F₂CTP, the bottom (red) from an inactivation using 1'-[²H, ³H]-F₂CTP, ~60% D. Expansions on individual peaks.



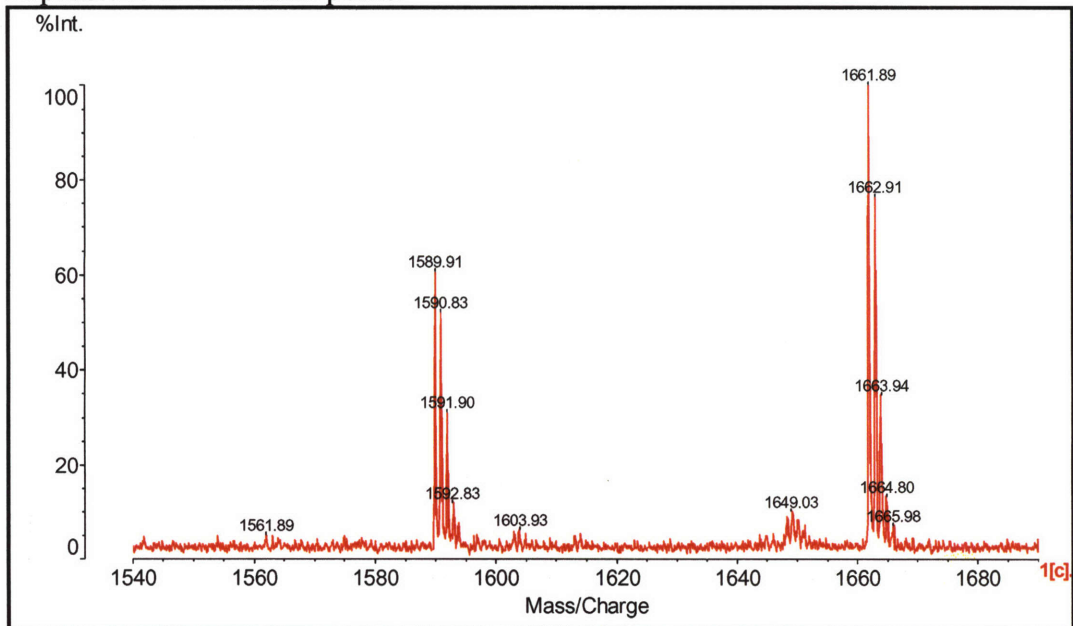
MALDI of R III peptides from trypsin digest of inactivation of RTPR with 1'-[³H]-F₂CTP, NaBH₄ quench a 2 min. In all spectra, the top (blue) is from an inactivation using 1'-[³H]-F₂CTP, the bottom (red) from an inactivation using 1'-[²H, ³H]-F₂CTP, ~60% D. This region did not appear to have any peptide running with the radioactivity in the rechromatograph, and the MALDI do not show consistent peaks from sample to sample as the RI and RII do. Expansions are shown for the quench with the partially deuterated material; none of these peaks show an unusual isotopic distribution.

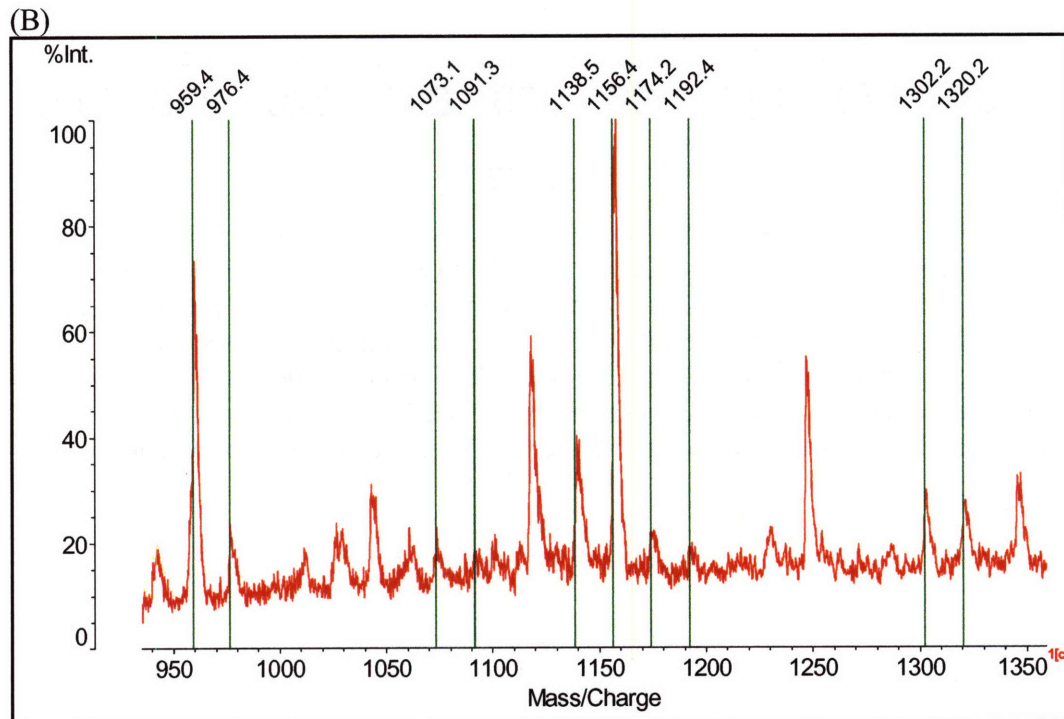
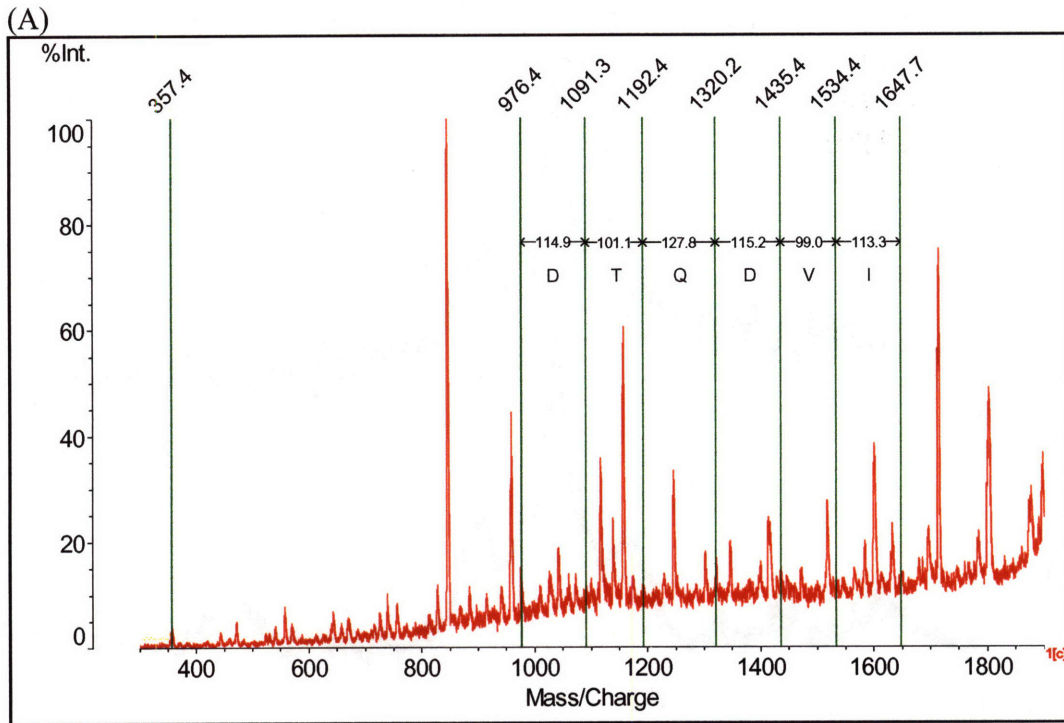


MALDI of R III peptides from trypsin digest of inactivation of RTPR with 1'-[³H]-F₂CTP, NaBH₄ quench a 2 min. From rechromatographed samples, first part of the peak of radioactivity. All spectra are from an inactivation using 1'-[²H, ³H]-F₂CTP, ~60% D. Expansions on individual peaks.

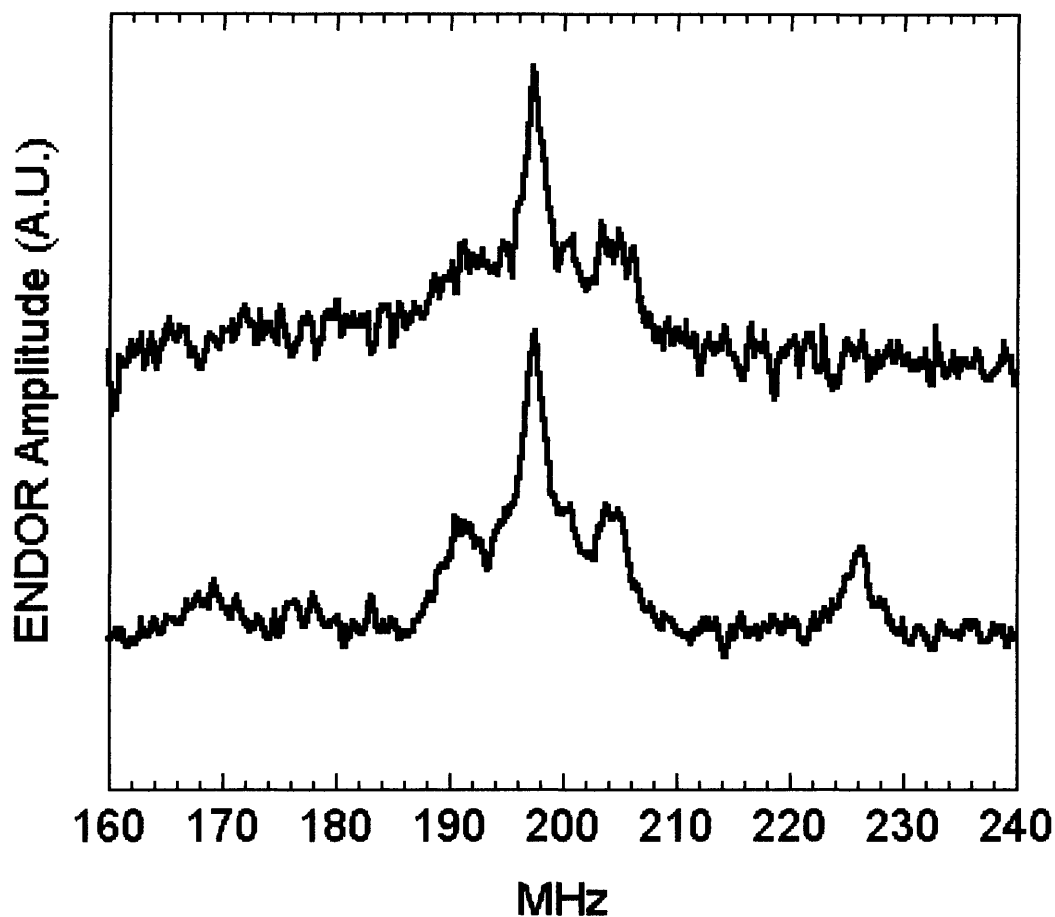


MALDI of R III peptides from trypsin digest of inactivation of RTPR with 1'-[³H]-F₂CTP, NaBH₄ quench a 2 min. From rechromatographed samples, first part of the peak of radioactivity. All spectra are from an inactivation using 1'-[²H, ³H]-F₂CTP, ~60% D. Expansions on individual peaks.

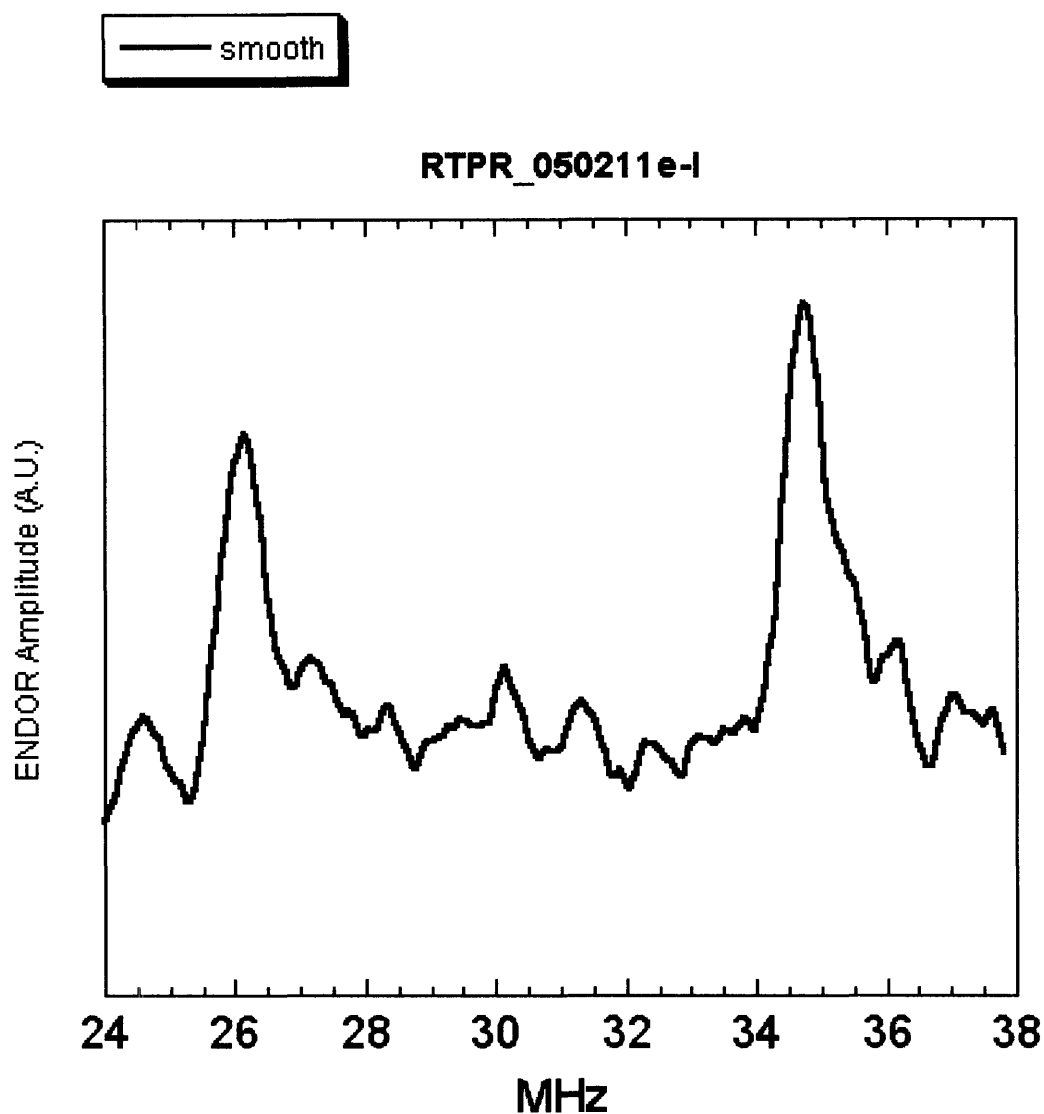




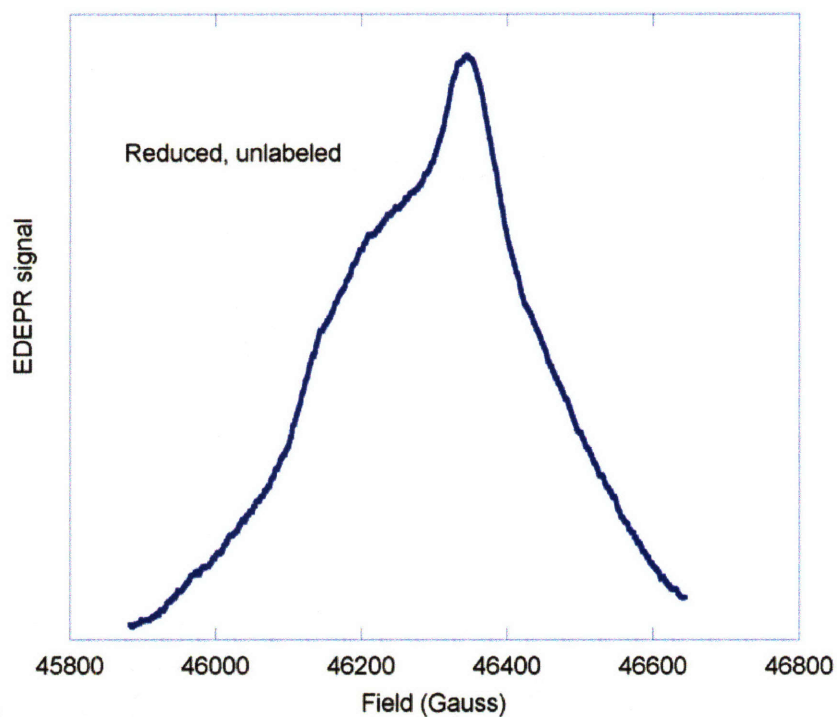
MS/MS of peak at 2005 Da, corresponding to the C-terminal peptide of RTPR (DLELVDTDCEGGACPIK) containing an internal cysteine-cysteine crosslink derived from F₂CTP, from NaBD₄ quench. (A) Full PSD with y ion series marked; this series is of low intensity in this sample compared to the y⁰ and y*. (B) Expansion, indicating primary y ions and the peaks representing the y⁰ and y* series (-18 Da and -17 Da, overlapped) and peaks -35 Da representing both the loss of a water and of an ammonia.



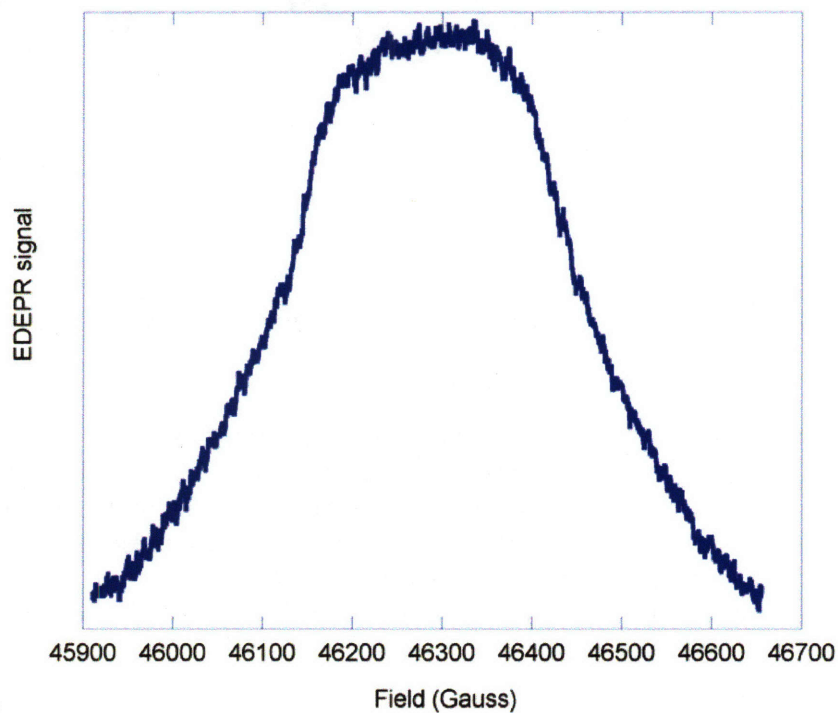
Davies H-ENDOR of RTPR/F₂CTP, 300 μ M in each, 450 μ M AdoCbl, 1 mM dATP, hand freeze-quench at 20s. Temperature: 7 K; RF pulse width: 6.8 microseconds; Microwave pulse widths: 70 ns, 35 ns, 70 ns; time between 2nd and 3rd pulse: 200 ns; 800 averages per point; Repetition rate: 100 Hz; RF pulse toggled for baseline subtraction; RF frequency increment: 200 KHz; RF Power: \sim 300 W. Top sample: 1'D; Bottom sample: wild type. Experiment performed by Gary Gerfen and Julia Manzerova, Albert Einstein College of Medicine, Yeshiva University, New York.



Davies D-ENDOR of RTPR/1'-[²H]-F₂CTP, 300 μM in each, 450 μM AdoCbl, 1 mM dATP, hand freeze-quench at 20s. Parameters were: Temperature: 7 K; RF pulse width: 20 microseconds; Microwave pulse widths: 80 ns, 40 ns, 80 ns; time between 2nd and 3rd pulse: 200 ns; 8000 averages per point; Repetition rate: 100 Hz; RF pulse toggled for baseline subtraction; RF frequency increment: 50 KHz; RF Power: ~ 300 W. Experiment performed by Gary Gerfen and Julia Manzerova, Albert Einstein College of Medicine, Yeshiva University, New York.



(A)



(B)

High Field (130 GHz) RTPR/F₂CTP, 300 μ M in each, 450 μ M AdoCbl, 1 mM dATP, hand freeze-quench at 20s. (A) Unlabeled. (B) 1'-[²H]-F₂CTP. Experiment performed by Gary Gerfen and Julia Manzerova, Albert Einstein College of Medicine, Yeshiva University, New York.

Gregory J. S. Lohman

EDUCATION

- Massachusetts Institute of Technology** Cambridge, MA
Doctoral candidate in Organic Chemistry (Dec 2006)
- Case Western Reserve University** Cleveland, OH
Bachelor of Science degrees in Chemistry and Biology (2000, *summa cum laude*)

RESEARCH EXPERIENCE

- Massachusetts Institute of Technology, Stubbe Laboratory** Cambridge, MA
(May 2003-Dec 2006) *Ribonucleotide Reductase/Gemcitabine*
- Massachusetts Institute of Technology, Seeberger Laboratory** Cambridge, MA
Predoctoral Fellow (November 2000-May 2003) *Heparin Synthesis*
- BFGoodrich Co., Electronic Materials Division** Brecksville, OH
Research Assistant (Summer internships, 1998, 1999, 2000) *Polymer Chemistry*
- Case Western Reserve University, Protasiewicz Laboratory** Cleveland, OH
Research Assistant (August 1999-May 2000) *Organophosphorous Synthesis*
- Case Western Reserve University, Cullis Laboratory** Cleveland, OH
Research Assistant (September 1998-May 1999) *Banana Molecular Genetics*

AWARDS

- NDSEG predoctoral fellowship (2001-2004)
- DuPont/MIT Alliance predoctoral fellowship (2000)
- Phi Beta Kappa (2000)
- Daniel Burke Prize for excellence in both chemistry and biology (2000)
- Hypercube Scholar Award in chemistry (2000)
- Carl F. Prutton Prize to an outstanding chemistry major pursuing the B.S. degree (1999)
- Case Alumni Association Scholarship (1998)

PUBLICATIONS AND CONFERENCES

- Lohman, G. J. S.; Stubbe, J. S. "Efforts Towards Understanding the Mechanism of Inactivation of Ribonucleoside Triphosphate Reductase by Gemcitabine Triphosphate." MIT Biochemistry Seminar Series, Cambridge, MA, December 2005.
- Lohman, G. J. S.; Seeberger, P. H. "A Stereochemical Surprise at the Late Stage of the Synthesis of Fully *N*-Differentiated Heparin Oligosaccharides Containing Amino, Acetamido, and *N*-Sulfate Groups." *J. Org. Chem.* **2004**, *69*, 4081-4093.
- Lohman, G. J. S.; Seeberger, P. H. "The One Pot Conversion of Glycals to *cis*-1,2-isopropylidene- α -glycosides." *J. Org. Chem.* **2003**, *68*, 7541-7543.
- Lohman, G. J. S.; Hunt, D. K.; Högermeier, J. A.; Seeberger, P. H. "Synthesis of Iduronic Acid Building Blocks for the Modular Assembly of Glycosaminoglycans." *J. Org. Chem.* **2003**, *68*, 7559-7561.
- Lohman, G. J. S.; Seeberger, P. H. "Synthesis of a Herpes Simplex Virus Binding Heparin Octasaccharide." American Chemical Society Meeting, Carbohydrate Chemistry Section, Boston, MA, August 2002.
- Padovani, A. M.; Rhodes, L.; Riester, L.; Lohman, G.; Tsuie, B.; Conner, J.; Allen, S. A. B.; Kohl, P. A. "Porous Methylsilsesquioxane for Low-*k* Dielectric Applications." *Electrochemical and Solid State Lett.* **2001**, *4*, F25-F28.